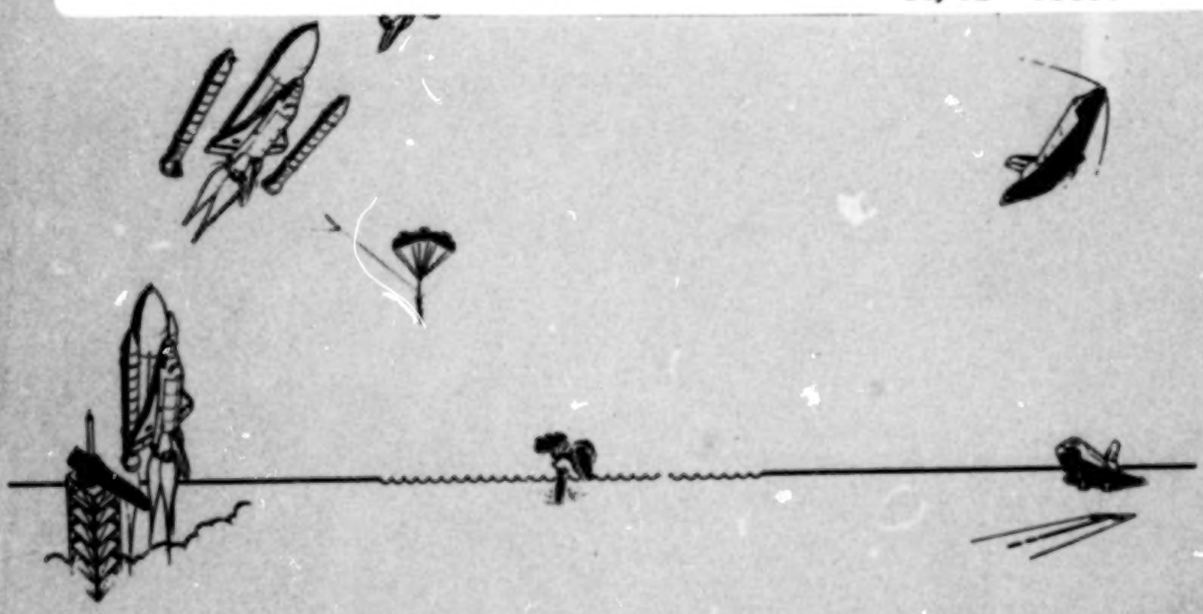
STAR (1+47)

NASA Conference Publication 2342
Part 1

Space Shuttle Technical Conference

(NASA-CP-2342-Pt-1) SPACE SHUTTLE TECHNICAL CONFERENCE, PART 1 (NASA) 598 p HC A25/MF A01 CSCL 22A
N85-16889 THRU N85-16936 Unclas G3/12 13550



Papers prepared for a conference held at
Lyndon B. Johnson Space Center
Houston, Texas
June 28-30, 1983



NASA

NASA Conference Publication 2342
Part 1

Space Shuttle Technical Conference

Norman Chaffee, *Compiler*
Lyndon B. Johnson Space Center
Houston, Texas

Papers prepared for a conference sponsored by the National Aeronautics and Space Administration and held at Lyndon B. Johnson Space Center
Houston, Texas
June 28–30, 1983

NASA
National Aeronautics and Space Administration

Scientific and Technical Information Branch

1985

PREFACE

This publication is a compilation of the papers prepared for the Space Shuttle Technical Conference held at the NASA Lyndon B. Johnson Space Center, Houston, Texas, June 28-30, 1983. The purpose of this conference was to provide an archival publication for the retrospective presentation and documentation of the key scientific and engineering achievements of the Space Shuttle Program following the attainment of full operational status by the National Space Transportation System.

To provide technical disciplinary focus, the conference was organized around 10 technical topic areas: (1) Integrated Avionics, (2) Guidance, Navigation, and Control, (3) Aerodynamics, (4) Structures, (5) Life Support, Environmental Control, and Crew Station, (6) Ground Operations, (7) Propulsion and Power, (8) Communications and Tracking, (9) Mechanisms and Mechanical Systems, and (10) Thermal and Contamination Environments and Protection Systems.

The papers in each technical topic which were presented over the 3-day conference period provide a historical overview of the key technical problems and challenges which were met and overcome during the development phase of the Space Shuttle Program. Taken as a whole, these papers provide a valuable archival reference to the magnitude and scope of this major national achievement.

Because of the large volume of material prepared for the conference, this publication is divided into two parts.

This publication was prepared through the efforts of the staff of the Technical Information Branch, Management Services Division, Johnson Space Center.

PRECEDING PAGE BLANK NOT FILMED

FOREWORD

The achievement of operational status of the National Space Transportation System represented a historic accomplishment for the National Aeronautics and Space Administration (NASA), its contractors, and for the United States. To recognize this accomplishment, NASA organized a technical conference focusing on the design and development phase of the Space Shuttle Program. The purpose of the conference was to permit a presentation by key members of the NASA-Industry-Department of Defense team of the outstanding achievements of the program. Toward this end, the conference theme "The Space Shuttle Program: From Challenge to Achievement" was selected.

To provide a comprehensive and balanced program for the conference, the Conference Organizing Committee selected 10 broad, technical topic areas for which papers were invited from individuals who played key technical roles in the success of the design and development program. An extraordinarily fine selection of 91 papers was submitted for the conference representing the contributions of 6 NASA field centers, the Department of Defense, 2 universities, and 27 industrial organizations. Over the 3-day period of June 28-30, 1983, these papers were presented at the Lyndon B. Johnson Space Center in a format of multiple, parallel technical sessions, fully satisfying the "Achievement" portion of the conference theme.

The "Challenge" aspect of the conference theme was provided by Lieutenant General James A. Abrahamson, NASA Associate Administrator for Space Flight, who presented the conference keynote address; and by Dr. Maxime A. Faget, President of Space Industries Incorporated and former Director of Engineering and Development at the Johnson Space Center, who organized and moderated the discussions of a panel of distinguished government and industry executives who presided over the early days of the program. Excellent retrospective presentations were also made by Dr. Glynn S. Lunney, Manager of the National Space Transportation System Program, and by Donald K. (Deke) Slayton, President and Vice Chairman of Space Services Incorporated of America and former NASA astronaut and management official. The complementary combination of technical papers, addresses, and panel discussions provided a satisfying, synergistic package for the more than 1200 conference attendees.

As former Manager of the Orbiter Project, it was my privilege to serve as General Chairman of the Space Shuttle Technical Conference and to recognize and honor the team of men and women responsible for this historic accomplishment.

I am grateful for the help and support of the other members of the Conference Organizing Committee: Elwood W. Land, Jr. (NASA Headquarters); James E. Kingsbury (Marshall Space Flight Center); and Peter A. Minderman (Kennedy Space Center); and to Norman H. Chaffee (Johnson Space Center) who served as Conference Arrangements Chairman.

Aaron Cohen
General Chairman

PRECEDING PAGE BLANK NOT FILMED

CONTENTS

Page

PART 1

SESSION 1: INTEGRATED AVIONICS

Cochairmen: H. E. Smith, Johnson Space Center
W. C. Bradford, Marshall Space Flight Center
J. A. Anderson, Kennedy Space Center

EVOLUTION OF SHUTTLE AVIONICS REDUNDANCY MANAGEMENT/FAULT TOLERANCE 1
Jack C. Boykin, Joseph R. Thibodeau, and Henry E. Schneider

SHUTTLE AVIONICS SOFTWARE -- TRIALS, TRIBULATIONS AND SUCCESSES . . . 19
O. L. Henderson

SHUTTLE AVIONICS SOFTWARE DEVELOPMENT -- TRIALS, TRIBULATIONS, AND SUCCESSES: THE BACKUP FLIGHT SYSTEM 30
Edward S. Chevers

FLIGHT SOFTWARE FAULT TOLERANCE VIA THE BACKUP FLIGHT SYSTEM 35
Terry D. Humphrey and Charles R. Price

SSME DIGITAL CONTROL DESIGN CHARACTERISTICS 38
Walter T. Mitchell and Richard F. Searle

MAN-MACHINE INTERFACE AND CONTROL OF THE SHUTTLE DIGITAL FLIGHT SYSTEM 47
Richard D. Burghduff and James L. Lewis, Jr.

SPACE SHUTTLE MAIN ENGINE HARDWARE SIMULATION 54
H. G. Vick and P. W. Hampton

DEVELOPMENT AND IMPLEMENTATION OF THE VERIFICATION PROCESS FOR THE SHUTTLE AVIONICS SYSTEM 64
H. E. Smith, W. B. Fouts, and J. Mesmer

GROUND/MAN-MACHINE INTERFACES FOR ORBITER CHECKOUT 76
F. Herb Blackmon

INTEGRATION OF GROUND AND ON-BOARD SYSTEM FOR TERMINAL COUNT 81
Charles A. Abner and Don H. Townsend

INTEGRATED DESIGN CHECKOUT OF SHUTTLE PAYLOAD AVIONICS INTERFACES 87
John F. Muratore and Kathy K. Whitcomb

PRECEDING PAGE BLANK NOT FILMED

Page

AUTOMATION OF CHECKOUT FOR THE SHUTTLE OPERATIONS ERA 97
Judith A. Anderson and Kenneth O. Hendrickson

SESSION 2: GUIDANCE, NAVIGATION, AND CONTROL

Cochairmen: Dr. K. J. Cox, Johnson Space Center
K. J. Szalai, Ames Research Center/
Dryden Flight Research Facility

SHUTTLE NAVIGATION STATUS 102
Emil R. Schiesser

DESCENT GUIDANCE AND MISSION PLANNING FOR SPACE SHUTTLE 113
B. Kent Joosten

SOME EFFECTS OF DIGITAL SAMPLING ON ORBITER FLIGHT CONTROL
SYSTEM OPERATION 125
S. V. Murray

SPACE SHUTTLE HANDLING QUALITIES 137
David W. Gilbert

LOW-SPEED LONGITUDINAL ORBITER FLYING QUALITIES 143
Bruce G. Powers

SESSION 3: AERODYNAMICS

Cochairmen: B. G. Jackson, Johnson Space Center
C. D. Andrews, Marshall Space
Flight Center
W. I. Scallion, Langley Research
Center

THE SPACE SHUTTLE ASCENT VEHICLE AERODYNAMIC CHALLENGES --
CONFIGURATION DESIGN AND DATA BASE DEVELOPMENT 151
Charlie C. Dill, J. C. Young, B. B. Roberts,
M. K. Craig, J. T. Hamilton, and W. W. Boyle

THE SPACE SHUTTLE LAUNCH VEHICLE AERODYNAMIC VERIFICATION
CHALLENGES 177
R. O. Wallace, L. D. Austin, J. G. Hondros,
T. E. Surber, L. M. Gaines, and J. T. Hamilton

THE AERODYNAMIC CHALLENGES OF SRB RECOVERY 189
D. L. Bacchus, D. A. Kross, and R. D. Moog

Page

THE AERODYNAMIC CHALLENGES OF THE DESIGN AND DEVELOPMENT OF THE SPACE SHUTTLE ORBITER 209
James C. Young, Jimmy M. Underwood, Ernest R. Hillje, Arthur M. Whitnah, Paul O. Romere, Joe D. Gamble, Barney B. Roberts, George M. Ware, William I. Scallion, Bernard Spencer, Jr., James P. Arrington, and Deloy C. Olsen

THE DEVELOPMENT AND APPLICATION OF AERODYNAMIC UNCERTAINTIES; AND FLIGHT TEST VERIFICATION FOR THE SPACE SHUTTLE ORBITER 264
Joe D. Gamble, Douglas R. Cooke, Jimmy M. Underwood, Howard W. Stone, Jr., and Donald C. Schlosser

AERODYNAMIC CHALLENGES OF ALT 295
Ivy Hooks, David Homan, and Paul Romere

THE ORBITER AIR DATA SYSTEM 313
Ernest R. Hillje

SESSION 4: STRUCTURES

Cochairmen: D. C. Wade, Johnson Space Center
R. S. Ryan, Marshall Space Flight Center

SHUTTLE STRUCTURAL DYNAMICS CHARACTERISTICS -- THE ANALYSIS VERIFICATION 325
C. Thomas Modlin, Jr., and George A. Zupp, Jr.

STRUCTURAL LOAD CHALLENGES DURING SPACE SHUTTLE DEVELOPMENT 335
Alden C. Mackey and Ralph E. Gatto

ORBITER STRUCTURAL DESIGN AND VERIFICATION 345
Philip C. Glynn and Thomas L. Moser

SPACE SHUTTLE EXTERNAL TANK PERFORMANCE IMPROVEMENTS -- THE CHALLENGE 357
Harold R. Coldwater, Richard R. Foll, Gayle J. Howell, and Jon A. Dutton

STRUCTURAL AND MECHANICAL DESIGN CHALLENGES OF SPACE SHUTTLE SOLID ROCKET BOOSTERS SEPARATION AND RECOVERY SUBSYSTEMS 365
William R. Woodis and Roy E. Runkle

SSME LIFETIME PREDICTION AND VERIFICATION, INTEGRATING ENVIRONMENTS, STRUCTURES, MATERIALS; THE CHALLENGE 386
Robert S. Ryan, Larry D. Salter, George M. Young III, and Paul M. Munafo

Page

THE CHALLENGING "SCALES OF THE BIRD" (SHUTTLE TILE STRUCTURAL INTEGRITY) 403
William C. Schneider and Glenn J. Miller

SESSION 5: LIFE SUPPORT, ENVIRONMENTAL CONTROL, AND CREW STATION

Cochairmen: H. W. Guy, Johnson Space Center
P. D. Quattrone, Ames Research Center

CHALLENGES IN THE DEVELOPMENT OF THE ORBITER ATMOSPHERIC REVITALIZATION SUBSYSTEM 414
R. Norman Prince, Joe Swider, John Wojnarowski, Angelo Decrisantis, George R. Ord, James J. Walleshauser, and John W. Gibb

CHALLENGES OF DEVELOPING AN ELECTRO-OPTICAL SYSTEM FOR MEASURING MAN'S OPERATIONAL ENVELOPE 426
Barbara Woolford

CHALLENGES IN THE DEVELOPMENT OF THE SHUTTLE EXTRAVEHICULAR MOBILITY UNIT 435
Harold J. McMann and James W. McBarron II

CHALLENGES IN THE DEVELOPMENT OF THE ORBITER ACTIVE THERMAL CONTROL SUBSYSTEM 450
John R. Nason, Frederic A. Wierum, and James L. Yanosy

OTHER CHALLENGES IN THE DEVELOPMENT OF THE ORBITER ENVIRONMENTAL CONTROL HARDWARE 465
John W. Gibb, M. E. McIntosh, Steven R. Heinrich, Franz Schubert, E. P. Koszenski, R. A. Wynveen, Emory Thomas, Mike Steele, R. W. Murray, J. D. Schelkopf, and J. K. Mangialardi

CHALLENGES IN THE DEVELOPMENT OF THE ORBITER RADIATOR SYSTEM 480
J. L. Williams, J. A. Oren, H. R. Howell, and M. F. Modest

Page

SESSION 6: GROUND OPERATIONS

Cochairmen: D. E. Phillips, Kennedy Space Center
W. C. Fischer, Johnson Space Center

OVERVIEW OF STS GROUND OPERATIONS/ORBITER TURNAROUND: STS-1 THROUGH STS-7 490
Richard Schwartz

EXTERNAL TANK PROCESSING FROM BARGE TO PAD 498
J. E. Carpenter

SOLID ROCKET BOOSTER RETRIEVAL OPERATIONS 505
Anker M. Rasmussen

SPACE SHUTTLE FLIGHT READINESS FIRING -- DRESS REHEARSAL FOR STS-1 510
Lt. Col. Warren L. Riles

TRANSITION TO THE SPACE SHUTTLE OPERATIONS ERA 525
William F. Edson, Jr.

LAUNCH PROCESSING SYSTEM -- CONCEPT TO REALITY 532
William W. Bailey

AUTOMATIC SOFTWARE FOR CONTROLLING CRYOGENIC SYSTEMS 539
James W. Rudolph

MATHEMATICAL MODELS FOR SPACE SHUTTLE GROUND SYSTEMS 550
Edward G. Tory

MANAGING COMPUTER-CONTROLLED OPERATIONS 558
John B. Plowden

SUPPORT SYSTEMS DESIGN AND ANALYSIS 565
Robert M. Ferguson

HISTORY, DESIGN, AND PERFORMANCE OF THE SPACE SHUTTLE HAZARDOUS GAS DETECTION SYSTEM 573
William R. Helms

PART 2

Page

SESSION 7: PROPULSION AND POWER

Cochairmen: H. O. Pohl, Johnson Space Center
J. A. Lombardo, Marshall Space Flight Center

PROPULSION AND POWER SYSTEMS PERSPECTIVE 581
Joseph G. Thibodaux, Jr.

CRYOGENIC PROPELLANT MANAGEMENT -- INTEGRATION OF DESIGN, PERFORMANCE, AND OPERATIONAL REQUIREMENTS 585
Armis L. Worlund, John R. Jamieson, Jr., Timothy W. Cole, and Tibor I. Lak

SPACE SHUTTLE MAIN ENGINE -- INTERACTIVE DESIGN CHALLENGES 600
John P. McCarty and Byron K. Wood

SOLID ROCKET MOTOR CERTIFICATION TO MEET SPACE SHUTTLE REQUIREMENTS: FROM CHALLENGE TO ACHIEVEMENT 618
John Q. Miller and Joe C. Kilminster

DEBRIS CONTROL DESIGN ACHIEVEMENTS OF THE BOOSTER SEPARATION MOTORS 628
Gerald W. Smith and Charles A. Chase

ORBITAL MANEUVERING SYSTEM DESIGN EVOLUTION 639
Cecil Gibson and Clarence Humphries

DESIGN EVOLUTION OF THE ORBITER REACTION CONTROL SUBSYSTEM 656
Ralph J. Taeuber, W. Karakulko, Don Blevins, Carl Hohmann, and John Henderson

SPACE SHUTTLE ORBITER AUXILIARY POWER UNIT DEVELOPMENT CHALLENGES 673
Renee Lance and Dwayne Weary

THE SOLID ROCKET BOOSTER AUXILIARY POWER UNIT -- MEETING THE CHALLENGE 690
Robert W. Hughes

SPACE SHUTTLE ELECTRICAL POWER GENERATION AND REACTANT SUPPLY SYSTEM 702
William E. Simon

Page

SESSION 8: COMMUNICATIONS AND TRACKING

Cochairmen: R. S. Sawyer, Johnson Space Center
R. L. Owen, Goddard Space Flight Center

SHUTTLE S-BAND COMMUNICATIONS TECHNICAL CONCEPTS 720
J. W. Seyl, W. W. Seibert, J. A. Porter, D. S. Eggers, S. W. Novosad, H. A. Vang, S. D. Lenett, W. A. Lewton, and J. F. Pawlowski

SHUTTLE Ku-BAND COMMUNICATIONS/RADAR TECHNICAL CONCEPTS 757
J. W. Griffin, J. S. Kelley, A. W. Steiner, H. A. Vang, W. E. Zrubek, and G. K. Huth

SHUTTLE PAYLOAD S-BAND COMMUNICATIONS SYSTEM 767
Bartus H. Batson, William E. Teasdale, James F. Pawlowski, and Oron L. Schmidt

TDRSS S-SHUTTLE UNIQUE RECEIVER EQUIPMENT 777
John J. Schwartz, Robert Spearing, and Aaron Weinberg

THE COMMUNICATIONS LINK ANALYSIS AND SIMULATION SYSTEM (CLASS) 787
Robert D. Godfrey

MODELING TECHNIQUES USED IN THE COMMUNICATIONS LINK ANALYSIS AND SIMULATION SYSTEM (CLASS) 798
Walter R. Braun and Teresa M. McKenzie

VALIDATION OF THE COMMUNICATIONS LINK ANALYSIS AND SIMULATION SYSTEM (CLASS) 804
Walter R. Braun and Teresa M. McKenzie

THE STATISTICAL LOOP ANALYZER (SLA) 810
William C. Lindsey

DIGITAL SCRAMBLING FOR SHUTTLE COMMUNICATION LINKS: DO DRAWBACKS OUTWEIGH ADVANTAGES? 815
Khaled Dessouky

NOVEL APPLICATIONS OF THE NASA/GSFC VITERBI DECODER HARDWARE SIMULATOR 821
Denver W. Herr, John J. Schwartz, Dirk J. M. Walvis, and Aaron Weinberg

ELECTRONICS SYSTEMS TEST LABORATORY TESTING OF SHUTTLE COMMUNICATIONS SYSTEMS 831
C. Jack Stoker and Linda K. Bromley

Page

SESSION 9: MECHANISMS AND MECHANICAL SYSTEMS

Cochairmen: W. K. Creasy, Johnson Space Center
J. D. Phillips, Kennedy Space Center

ORBITER WHEEL AND TIRE CERTIFICATION 850
Carlisle C. Campbell, Jr.

SPACE EXPLORATION ROLLING ON TIRES 857
G. L. Felder

SPACE SHUTTLE ELEVON SEAL PANEL MECHANISM 861
John G. Ripley

SPACE SHUTTLE WHEELS AND BRAKES 872
Renton B. Carsley

THE SPACE SHUTTLE ORBITER REMOTE MANIPULATOR POSITIONING MECHANISM 883
J. H. Hardee

AN OVERVIEW OF THE SHUTTLE REMOTE MANIPULATOR SYSTEM 892
T. H. Ussher and K. H. Doetsch

SPACE SHUTTLE RUDDER/SPEEDBRAKE ACTUATION SUBSYSTEM 905
Ruth A. Naber

DEVELOPMENT OF THE SPACE SHUTTLE BODY FLAP ACTUATION SUBSYSTEM . . . 910
Clifton R. Boggs

MECHANICAL FEATURES OF THE SHUTTLE ROTATING SERVICE STRUCTURE . . . 920
John M. Crump

ORBITER PROCESSING FACILITY: ACCESS PLATORMS 935
Michael Haratunian

EXTERNAL TANK GH_2 VENT ARM. 942
Garland E. Reichle and Charles W. Glassburn

PAYLOAD TRANSPORTATION AT KSC. 952
Michael E. Donahue

STS PAYLOAD GROUND HANDLING MECHANISM AT JOHN F. KENNEDY SPACE CENTER 961
Vincent Cassisi and Bemis C. Tatem, Jr.

THE ORBITER MATE/DEMATE DEVICE 972
Arthur J. Miller and William H. Binkley

Page

COMPUTER AIDED PROCESSING USING LASER MEASUREMENTS 986
Richard M. Davis and John C. Koch

SESSION 10: THERMAL AND CONTAMINATION ENVIRONMENTS AND PROTECTION SYSTEMS

Cochairmen: D. H. Greenshields, Johnson Space Center
Dr. J. W. Littles, Marshall Space Flight Center

IN-FLIGHT TESTING OF THE SPACE SHUTTLE ORBITER THERMAL CONTROL SYSTEM 995
J. Thomas Taylor

SHUTTLE SYSTEM ASCENT AERODYNAMIC AND PLUME HEATING 1022
Lee D. Foster, Terry F. Greenwood, and Dorothy B. Lee

THERMAL DESIGN OF THE SPACE SHUTTLE SOLID ROCKET BOOSTER 1030
Robert R. Fisher, Jerold L. Vaniman, and William J. Patterson

THERMAL DESIGN OF THE SPACE SHUTTLE EXTERNAL TANK 1041
Frederick D. Bechtel, Jerold L. Vaniman, James M. Stuckey, Carroll Gray, and Bernard Widofsky

ORBITER ENTRY AEROTHERMODYNAMICS 1051
Robert C. Ried

ORBITER THERMAL PROTECTION SYSTEM 1062
Robert L. Dotts, Donald M. Curry, and Donald J. Tillian

SHUTTLE ON-ORBIT CONTAMINATION AND ENVIRONMENTAL EFFECTS 1082
L. J. Leger, S. Jacobs, H. K. F. Ehlers, and E. Miller

N85
16890

UNCLAS

N85-16890

EVOLUTION OF SHUTTLE AVIONICS REDUNDANCY MANAGEMENT/FAULT TOLERANCE

Jack C. Boykin and Joseph R. Thibodeau
NASA Lyndon B. Johnson Space Center
Houston, Texas

and

Henry E. Schneider
McDonnell-Douglas Technical Services Company
Houston, Texas

ABSTRACT

The challenge of providing redundancy management (RM) and fault tolerance to meet the Shuttle Program requirements of fail operational/fail safe for the avionics systems was complicated by the critical program constraints of weight, cost, and schedule. This paper addresses the basic and sometimes false effectivity of less than pure RM designs. Evolution of the multiple input selection filter (the heart of the RM function) is discussed with emphasis on the subtle interactions of the flight control system that were found to be potentially catastrophic. Several other general RM development problems are discussed, with particular emphasis on the inertial measurement unit RM, indicative of the complexity of managing that three-string system and its critical interfaces with the guidance and control systems.

PROGRAM REQUIREMENTS AFFECTING FAULT TOLERANCE/RM

Space Shuttle Program requirements dictate fault tolerance in all systems other than primary structure, thermal protection, and pressure vessels. In the case of avionics systems, those requirements are specified to be two-fault tolerant, or fail operational/fail safe (FO/FS) (ref. 1) as commonly referred to in Shuttle terms. Considering the design life goals of 100 missions and 10 years or more operational span, this FO/FS requirement not only appears reasonable but almost minimally mandatory. Given a free hand in hardware provisioning, meeting the FO/FS requirement may have been obtainable. As would be expected in a program heavily pressed with cost and weight constraints, the avionics designers' hands were not so free.

Providing FO/FS fault tolerance with no holes or subtle escapes would most easily be accomplished by providing independent five-string operation with independent data inputs to each of the five strings and command functions requiring three out of five votes before execution. This approach would obviously be costly in weight and cost of wiring and avionics components but does offer an FO/FS design approach that could be void of in-flight failure effects concerns for two failures. It would also eliminate the historically complex hardware/software requirements for fault detection and isolation since the first two failures would be transparent. This five-string approach is indeed being implemented in the flight-critical interfaces of the Centaur payloads with the Orbiter. The approach was never seriously considered for Shuttle/Orbiter design because of the obvious systems weight and cost impacts, yet the FO/FS requirement was maintained.

The first step down from the five-string design to meet FO/FS is to provide four-string operation with fault detection and isolation of at least the first fault. Various schemes can be implemented at the four-string level to choose proper data or perform the proper command function, but the susceptibility to the second failure requires a fault detection and isolation scheme to eliminate the first failure before occurrence of the second failure in order to be FO/FS. Two simultaneous or near-simultaneous (within the timespan required to detect and isolate the first failure) failures will defeat this approach; however, Shuttle Program management has granted detection and reconfiguration time in its FO/FS requirement provided the detection is reasonably assured of working. In this scheme, the second failure is then tolerated by selecting the middle valued data of the remaining three inputs and voting two of three for command functions or providing enough muscle in the two good command channels to override the second failure channel. This four-level approach was selected for a major portion of the Shuttle avionics and has fared well with the possible exception of null failures in sensors normally operating about their null, thereby hindering the fault detection of either the first or the second null failure.

The next step down in redundancy while maintaining FO/FS fault tolerance is to provide three-string operation in conjunction with fault detection and isolation of both the first and second failures in the system. Detecting and isolating the first failure in a three-string system is not overly complex and detecting the second failure through two-level comparison of inputs or outputs is straightforward. The difficulty in this approach comes in isolating the second failure. Disagreement between only two inputs requires a decisionmaking vote that is often costly and still not 100 percent

certain, such as built-in test equipment (BITE), self-tests, or reasonableness tests. In the cases where isolation is still lacking, a crew "guesstimate" and manual reconfiguration may be used to supplement the auto RM. This approach can also be costly and leaves room for errors. This second fault isolation problem was a primary factor in the basic four-string avionics design in the Shuttle with the Orbiter inertial measurement units (IMU's) being the most notable exception. The basis for this exception, as with the other three-string systems, included weight and cost, reliability background and history of similar hardware, and projected BITE capabilities to cover second failure isolation. Treatment of the second failure detection and isolation of the IMU's has involved such extensive efforts in analysis, verification, software changes, and flight procedures development that the possibility of adding a fourth IMU to the Orbiter is still under consideration. Indeed, the complexities of timely detection and isolation of two-level IMU faults and the capabilities and limitations of the IMU BITE design are sufficient to warrant treatment as an individual paper, accounting for the large portion of this paper being dedicated to IMU RM. A considerable amount of the IMU RM design change activity deals with fine tuning of the data to minimize errors passed to the guidance and control systems; however, the final fault tolerance assessment accounting for the two-level isolation problems results in no capability to isolate approximately 0.7 percent of the second faults and an even more disconcerting 0.15 percent of the second faults which can result in selection of the failed IMU (ref. 2).

Any further reduction in redundancy level below three strings obviously fails to meet the avionics FO/FS requirement unless, of course, the function itself is not required and is then by definition FS after the second failure. The net result is that Shuttle avionics basically evolved as a three- and four-string design attempting to provide fault detection and isolation capability to make these redundancy levels equal to the five-string design required to be purely FO/FS. The success of this design is not easily measured; however, there are several key data points to recount when considering Shuttle redundancy design versus a blanket FO/FS requirement. First, the Orbiter avionics alone has officially documented some 255 critical-items lists (CIL) exceptions to the FO/FS requirement. Secondly, in striving to meet the blanket FO/FS requirement, the less than pure approach has resulted in an analysis and verification program of staggering proportions. As former astronaut and Orbital Flight Test Manager Donald K. Slayton stated (ref. 3), though possibly too late to influence the Shuttle Program direction, there is an unpredictable but "high cost of worrying improbable possibilities." Because of the second fault tolerance requirement and the fault detection and isolation deficiencies (delays in isolation and/or various degrees of escapes), every combination of failures, however improbable, must be analyzed and verified as acceptable. This is then magnified by reconfiguration actions planned to optimize the postfailure system configuration, each of these obviously requiring verification. In this process, as is its objective, escapes from the FO/FS requirement are sometimes discovered, leading to software, hardware, and/or procedural changes which, of course, add to the verification work. Quantification of such changes is nearly impossible but some understanding of the problem can be evidenced by the ever-present hardware and software change boards, the approximately 700 pages of crew malfunction procedures, the more than 1000 pages of off-nominal crew procedures, the libraries full of off-nominal verification procedures and test reports, and the more than 250 software change requests which have currently been approved to the RM Flight System Software Requirements (FSSR) alone (ref. 4).

Mr. Slayton's approach to the problem was proposed basically as drawing a line in the sand defining some failure criticality not based on a blanket FO/FS requirement but rather based on the probability of that failure (or combination of failures) to occur. If the failure probability is determined to be lower than that line, the design would not have to accommodate changes to meet the FO/FS requirement. The obvious problems of choosing the acceptable failure probability and the mechanization of determining the probability of potential failures are admittedly nontrivial; however, Mr. Slayton cites the success of the Saturn 5 program as a working example of this approach.

An alternate approach that has essentially been described earlier is to provide a five-string operation with data and command selection, based on the middle value of the five or voted to require three of the five data or command statuses to produce a functional response. The aforementioned weight and cost penalties of such a system are understandably undesirable and easily considered unjustified in the preliminary stages of system design. Considering the historically costly change traffic and verification activities that go with the attempted development of less than pure redundancy matching requirements, the initial acceptance of the additional string weight and cost may have been an effective overall decision for the Shuttle/Orbiter Program.

IMPACTS OF SUBSYSTEM PERFORMANCE CHARACTERISTICS ON RM

The Shuttle RM involves both hardware and software functional implementations, the extent of each determined by the design and response characteristics of the individual subsystem element. As with any development program on the level of sophistication and gross technical expansion of functional capabilities such as in the Shuttle Program, the potentials for hardware and software design

deficiencies are not few. Adding the scheduling demands typically forced on NASA programs complicates the situation by requiring parallel development of subsystem hardware and the associated applications and RM software. This parallel RM design does not then allow for an individual line replaceable unit (LRU) performance understanding beyond that established as design requirements in the procurement specifications. Additionally, the benefits of failure modes and effects analyses on the LRU's cannot be utilized in initial designs, since these analyses are not completed sufficiently until final design and/or design verification testing has been completed. Finally, the performance of the LRU's within the system as a whole cannot be adequately anticipated until integrated systems simulations and/or verification programs are underway involving flight hardware/software designs and sophisticated models of environments, aerodynamic effects, and vehicle dynamic models. Development of the RM schemes under these handicaps can and did result in many initial assumptions that turned out to be invalid or at least not sufficient to provide totally acceptable RM.

A primary example of this programmatic dilemma occurred in the Orbiter flight control system (FCS) interface with the redundant FCS sensor systems. Providing the FCS with the best available rate and acceleration data from a quad redundant sensor set at first glance appeared trivial. The program had provided the fourth sensor set after only three had been initially proposed because it was recognized that isolation of the second failure in dynamic periods of flight could not be guaranteed within FCS control limits. The formulation and use of a software-derived fourth input was too complex and laced with its own shortcomings.

The selection of the "best" data input from this set was considered to be a simple extension of the three-sensor method; i.e., provide a software selection filter (SF) which dealt with the first three inputs by simply selecting the middle valued input for use by the FCS, substituting the fourth sensor input only after one of the original three had been determined to be failed (fig. 1). This SF design was baselined and implemented in the software RM along with a fault detection, isolation, and reconfiguration (FDIR) scheme that used a unit-to-unit comparison test to determine whether a unit had failed. On the surface, this approach was simple and foolproof; in final application, it was not so simple and indeed inadequate. Two key conditions combined to defeat this original approach: (1) to eliminate or limit false alarm exposure, the magnitude of the differences between units had to be significantly large enough to account for unfailed unit normal deviations (3σ), system noise, and transients; and (2) the FCS control laws and vehicle responses aimed toward and generally achieved stable flight conditions within the limits of times and/or magnitudes established to prevent the false alarms. The interaction of these two factors resulted in a general inability to detect and isolate a null failed sensor (fig. 2).

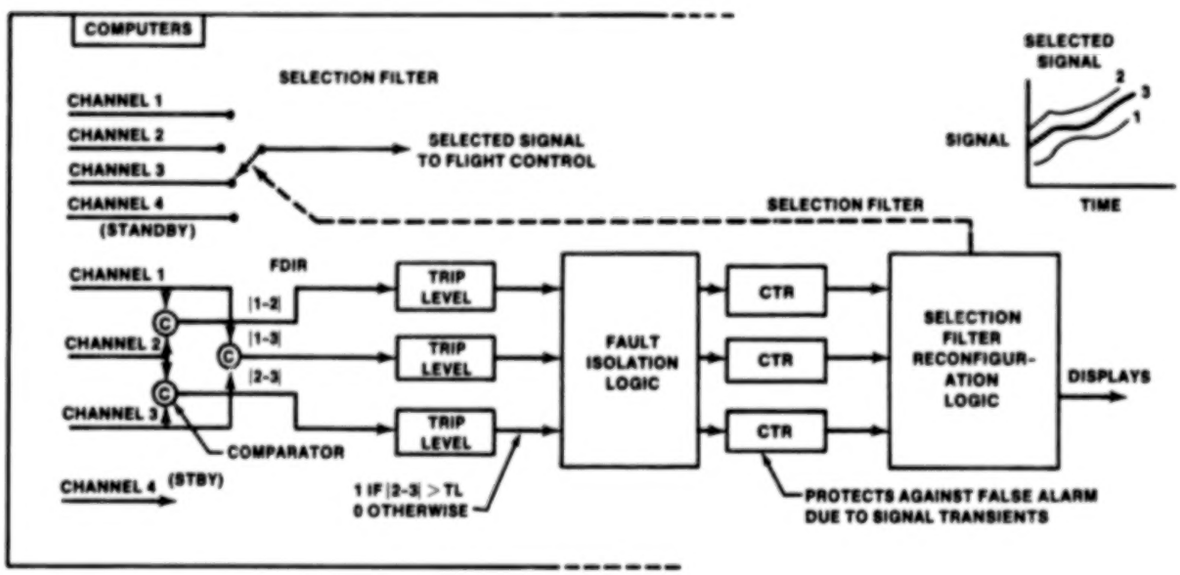


FIGURE 1.- INITIAL SOFTWARE QUAD RM APPROACH.

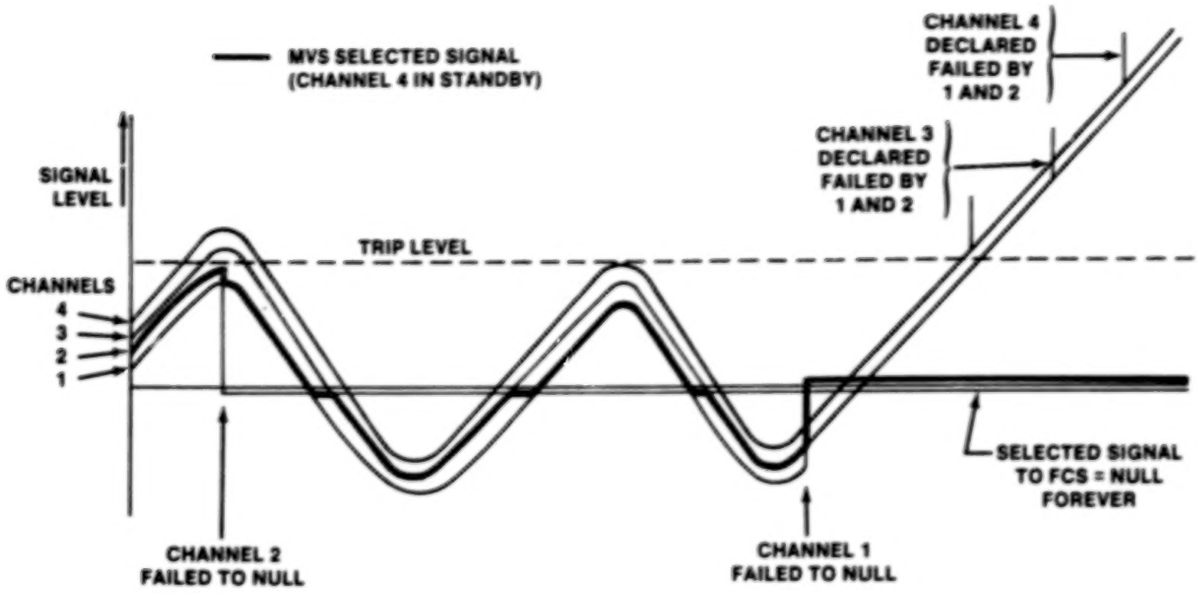


FIGURE 2.- MVS NULL FAILURE SCENARIO.

For the first null failure experienced, this was an insignificant event since the SF still provided a good output in the form of the smaller of the two remaining good units or the null if the two remaining good units were operating near to and bracketing the null failure. With the first null failure included in the SF set, however, the effects of the second null failure became catastrophic. With a second null failure in the set, the middle value in the SF will always obviously be a null. As vehicle stability deviates from this point, the FCS will not see the change and quickly becomes unstable. An additional irony is that the RM will actually declare a failure against the only good sensor input in the SF as its output builds, deselect that sensor, and replace it with the fourth (good) sensor, only to have it defeated just as the first good sensor was. The recognition of the inability of the baselined RM to deal with this dual null scenario was not possible until the hardware and systems models were completed and evaluation and verification test facilities could be used. Verification analyses showed the dual null system effects to be an unstable vehicle in ascent and entry mission phases for the pitch, roll, or yaw rate gyros and severe violation of the load relief and g limits for such loss of the normal or lateral accelerometers.

The risk associated with the dual null deficiency in the RM was considered to be extremely small considering the relatively short period of use of the rate gyros and accelerometers. This could be further minimized by performing stim tests just before lift-off and again just before entry, thereby detecting nulls and allowing proper reconfiguration. The risk was not zero, however, and a proposed fix to obtain the highly desirable FO/FS status which involved a software modification only was developed. The impact of this software change was evaluated as an increase in CPU requirements for the SF from 0.875 to 1.46 percent, an increase in memory requirements for the SF from 75 to 90 words, and a decrease in memory requirements for the FDIR from 229 to 200 words. At this point in the program, the new quad midvalue select (QMVS) SF was accepted as the resolution of the dual null failure concerns for the rate gyros and accelerometers. Since that time, the body flap position feedbacks and the solid rocket booster (SRB) rate-gyro assemblies (RGA's) have also been improved by application of the four active inputs SF (QMVS) in place of the three active with a standby.

For flight control and dynamic response limitations, the QMVS eventually proved to be adequate. However, the verification analyses with dynamic flight models discovered yet another sophisticated escape. The QMVS SF was observed in these verification activities as meeting the flight control stability requirements with dual nulls present. However, an unexpected increase in reaction control system (RCS) jet activity was resulting in significant increases in RCS propellant consumption. Refinement of these cases determined that with the dual null failures and reasonable biases on the remaining two sensors, RCS propellant consumption could increase by as much as a factor of four (ref. 5). The contribution of the QMVS SF to this phenomenon is illustrated in figure 3.

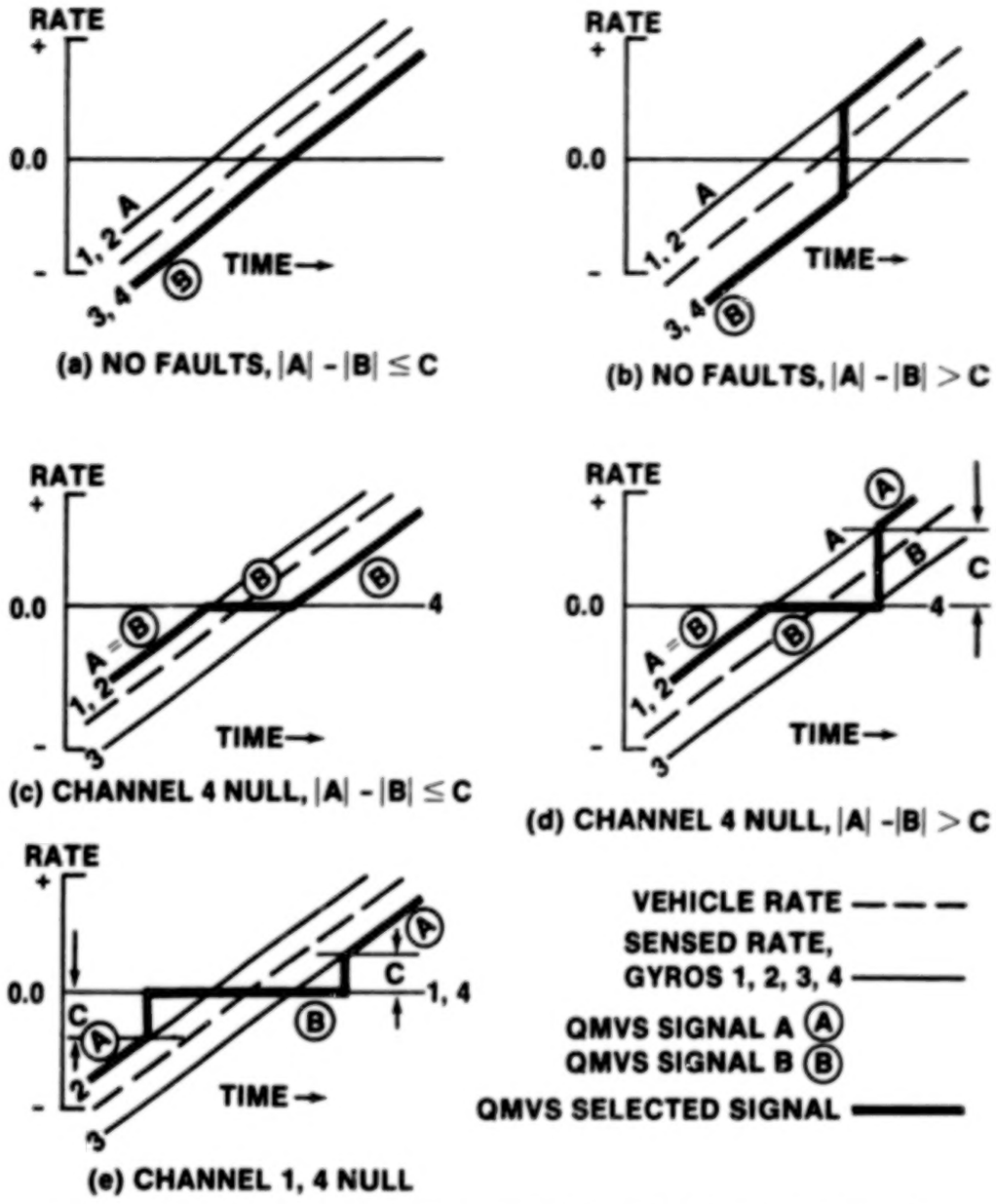


FIGURE 3.- QMVS SELECTION FILTER OUTPUT COMPARED TO VEHICLE RATE AND SENSED RATE.

The QMVS basically works as illustrated in figures 3(a) and 3(b) in that the SF logic evaluates all four inputs, determines the two middle valued inputs, and selects one of them based on a test of their difference between each other (the "C" value). The "C" value is fixed based on the reasonably expected null offsets between good gyros, null offsets between good multiplexer/demultiplexer (MDM) channels, and MDM nonlinearity. It is designed to prevent discontinuous SF outputs caused by switching between signal A and signal B for the no-fault case and yet provide satisfactory rate outputs with undetected single or dual null failures. Figures 3(c), 3(d), and 3(e) illustrate the QMVS performance with single and dual undetected null features. Because of the fine-tuned FCS and vehicle responses and the typical operation at near null vehicle rates, the illustrated nonlinearities in the sensed vehicle rates can result in residual oscillations and attendant RCS propellant consumption as previously described. Evaluation test cases indicated that under the dual null conditions, sufficient propellant consumption could result in depletion and loss of control unless the condition was recognized and crew intervention was timely.

As another escape from the FO/FS design requirement, however limited in probability, changes were developed as candidate solutions and evaluated in flight performance simulators to eliminate this last caveat from the FCS RM verification status. With the weakness of the QMVS being the deficiency of the FDIR to detect and isolate null failures in the Shuttle FCS environment, one obvious approach was to bias the SF to choose the more active midvalue parameter and stay with it until fault conditions indicated that the other midvalue parameter was significantly more active. The term used to describe this SF approach is interchangeable midvalue selection (IMVS). The IMVS operation under nominal, single, and dual null failure conditions is presented in figure 4. The primary difference in the IMVS and the QMVS is that once the two middle valued parameters of the four-parameter set have been determined (identically in both approaches), the SF chooses the largest of these two values and sticks with that selection until fault conditions are detected and then switches one time only to the other midvalued parameter. Remember that the QMVS selected the highest of the middle valued parameters for dispersions greater than a present value "C" and the smaller middle value for dispersions less than "C," resulting in undesirable discontinuities being provided to the SF user. As previously described, the discontinuities and nonlinearities of the QMVS SF in the presence of dual undetected null failures results in unacceptable propellant consumption. As shown in figure 4, the IMVS eliminates these discontinuities and reduces the nonlinearities, thereby improving FCS efficiency. Evaluation test cases showed propellant consumption reduction compared to the QMVS ranging from 62 to 1100 pounds, depending on the axis containing the null faults, the point of fault insertion, and the biases assigned to the remaining two good parameters.

The IMVS has been approved for Shuttle implementation, providing resolution to the current RM design caveat. It will likewise serve as a verified approach in future four-string design activities. One can only wonder again whether the costs of the changes from MVS to QMVS to IMVS and the associated analysis and verification activities might have compared to initial design implementation of a five-string system.

FAULT TOLERANCE ASSESSMENT OF INTEGRATED SYSTEMS

It has already been pointed out that design of the Shuttle avionics systems to the FO/FS program requirement under the weight and cost constraints which drove designers to not demand the pure five-string approach is at best a complex and difficult task. Several of the major exceptions to full-up redundancy in the Shuttle avionics interfaces are especially noteworthy, specifically the universal servicing systems such as electrical power distribution, cooling, and instrumentation. Of these, possibly the key factor in concern for integrated systems failure tolerance turned out to be the three-string electrical power distribution system. Obviously, with only three sources of power to spread to up to four user interfaces, cross-strapping of power to some or all of the components in critical functions was a necessity. Providing the visibility and assessment of the effects of this and other cross-strapping proved to be the weakness of the avionic fault tolerance assessment.

The typical programmatic tools to assess failure modes and effects were employed, including individual subsystem analyses and some level of integrated systems fault testing in facilities such as the Flight Systems Laboratory (FSL) and the Shuttle Avionics Integration Laboratory (SAIL). Some fault tolerance escapes were discovered through the subsystem analysis, and test programs periodically resulted in unexpected problems under fault or off-nominal conditions which could be catastrophic if occurring in flight. These escapes, though almost all attributable to the less than total redundancy design, were basically the result of the overall system complexity and subtleties, which could hardly be expected to be foreseen by the individual subsystem designer performing his failure modes and effects analysis (FMEA). Some of these factors include understanding the timing of the failures with respect to each other and to the mission phase, understanding the software mechanization and its dependence on time homogeneous data, understanding the normal and malfunction procedures which might be used by the crew to operate the systems and control configuration, and finally, understanding the individual subsystem functional impacts caused by failures in the universal service subsystems.

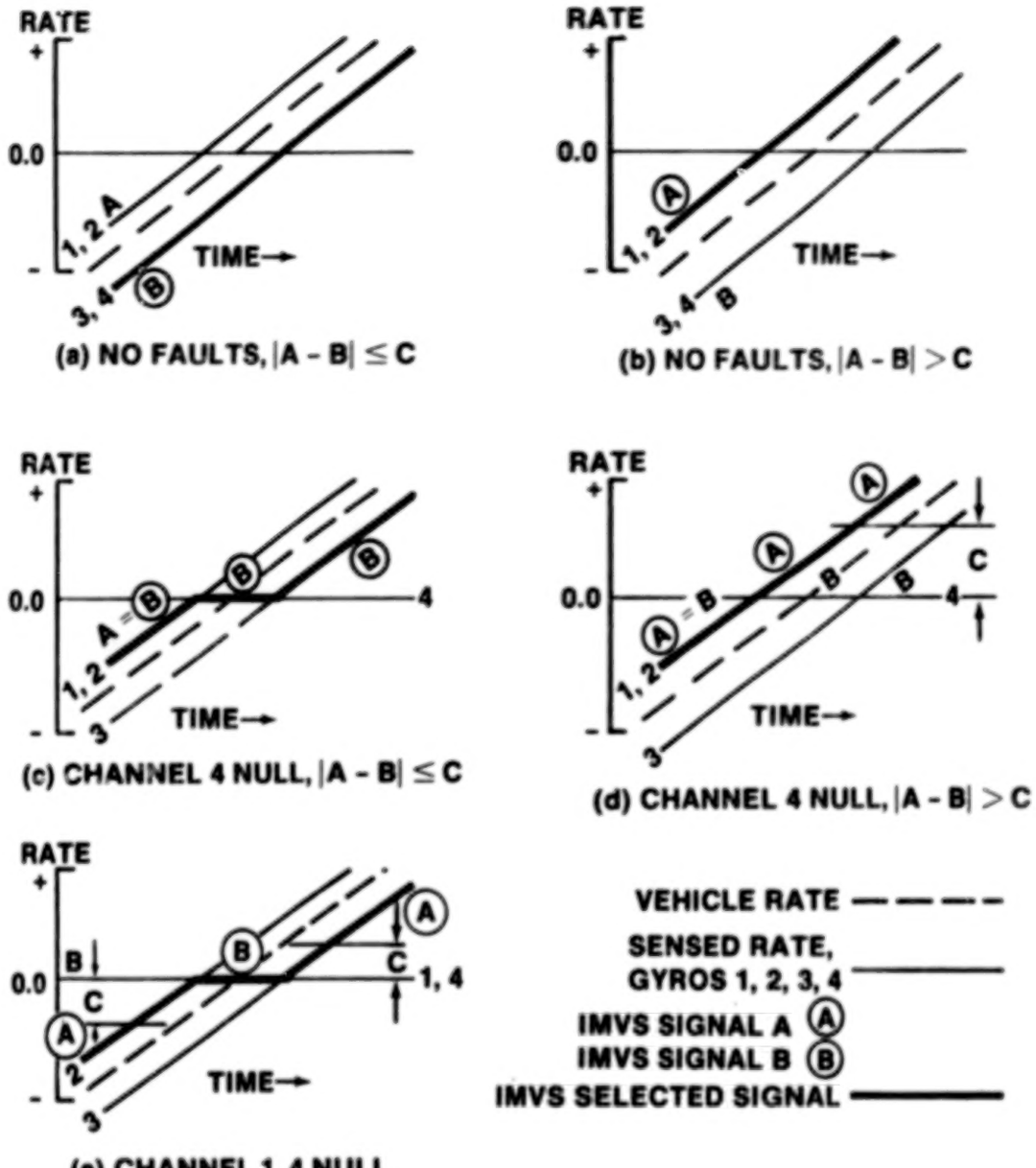


FIGURE 4.- IMVS SELECTION FILTER OUTPUT COMPARED TO VEHICLE RATE AND SENSED RATE.

This integrated fault tolerance assessment escape mechanism can be demonstrated by the example in figure 5. The FCS muscle for control during early entry stages is provided by the aft RCS jets. These jets, unlike other flight control effectors, employ single-string authority for jet firing, relying on the quantity of jets to satisfy the FO/FS requirement. The FCS avionic interface to fire these jets is provided by the reaction jet driver (RJD) circuits, which are divided into four channels with each channel receiving dual power inputs from the three-string EPD system such that any two failures can disable only two of the four RJD channels. The instrumentation monitoring of the RJD/jet system is provided in only two signal conditioning units; however, each one contains isolated internal modules and each box receives dual power inputs from the three-string EPD system such that any two failures can disable only half of the instrumentation system. In like manner, the data management/command interface is a four-channel system with identical redundancy to the serviced RJD's (including power redundancy). Taken piece by piece, the flight-critical function of RCS jet control appears to be FO/FS and each subsystem-level FMEA would support that conclusion. On closer inspection from an integrated, functional end-to-end viewpoint, with software performance considered, it becomes obvious

that the fault tolerance is not completely FO/FS, because of the channelization of the EPD inputs to each subsystem element. As can be seen in figure 5, if the aft local power buses A and C were lost, the total power to half of the RCS control circuitry would be lost (RJD's 1A and 2A), along with their respective data management interfaces (MDM's FA3 and FA4). Through cross-strapping, the remaining half of the RCS jets would be normally sufficient to control the vehicle. The total system reaction to the loss of buses A and C, however, includes loss of the instrumentation subsystem's signal conditioner OL2, which happens to provide service to the RCS jets controlled by RJD 2B, resulting in unresponsive data monitoring of those jets. The RM software will respond to this situation by recognizing the communications fault in strings 3 and 4 and suspending processing of those strings. The signal conditioning fault in string 2, however, is not discernible from actual low value data response to the RM, thereby leading to a failed "leaking" and/or failed "OFF" conclusion by the RM. Either of these events results in a deselection of the affected jets, with the final result being that the FCS muscle for the two bus failures is cut to a single set of jets which cannot maintain vehicle control.

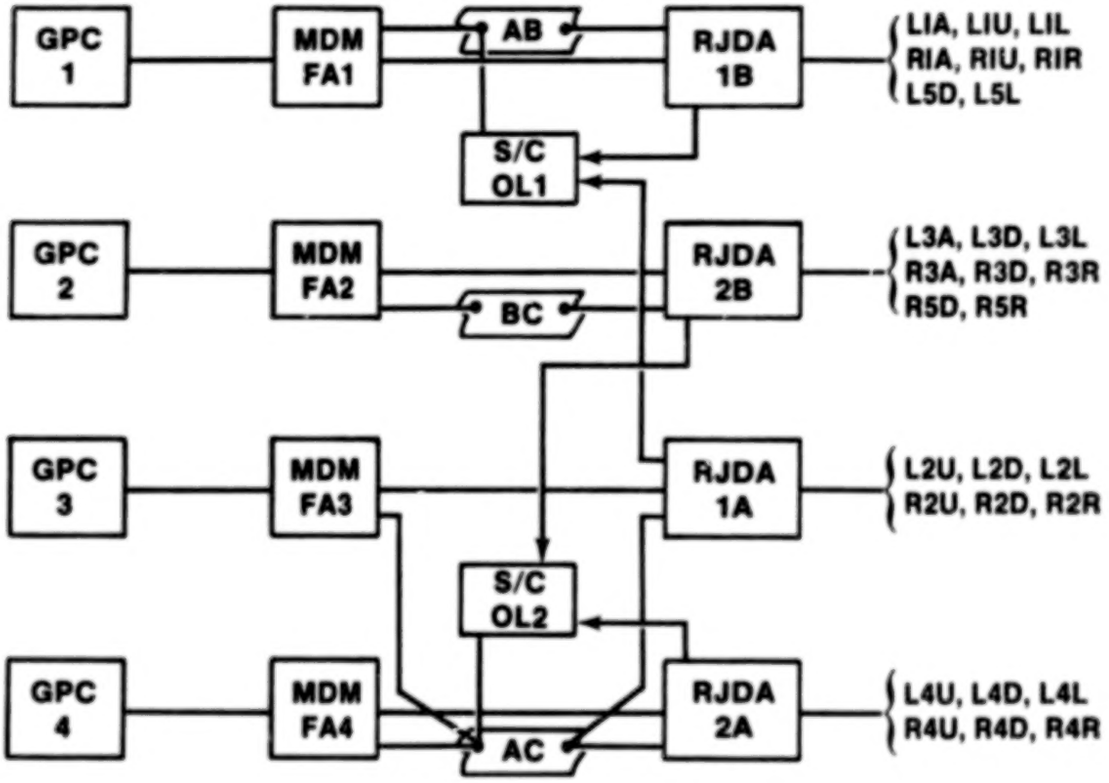


FIGURE 5.- AFT RCS CHANNELIZATION ESCAPE.

The loss of two power buses in a basic three-bus system is obviously a low-probability situation. It is, however, required to be addressed in assessment of an FO/FS requirement and is the reason for the multiple cross-strapping schemes on the Shuttle. As this and other specific escapes from the FO/FS requirement were discovered in test facilities and flight environments with failures actually present, the potential for further unknown escapes in a system as complex as the Shuttle hardware/software system became painfully obvious. The limitations of resources to perform actual verification tests for every combination of failures, under every critical mission phase, with every version of hardware and software to be flown, with every reasonable crew procedural response, and with every reasonable variation of flight environments are equally as painful. Recognizing this problem, the Shuttle Program established an "Avionics Audit" task to "perform a study and analysis that

identifies the fault tolerance capability of the integrated Orbiter avionics with respect to functional authority or influence derived from hardware channelization, hardware cross-strapping, software cross-strapping, control points, crew procedures, and external environments."[1] This ongoing task has been funded for more than $1 000 000 directly with unestimable program costs associated with study management and review and hardware and software changes resulting to date.

As previously implied, FO/FS implementation through a five-string approach would architecturally eliminate essentially all of this type of escape. Lacking that luxury, programs as complex as the Shuttle avionics must establish high-priority activities, such as FMEA's and sneak circuit analyses, and integrated end-to-end functional fault analysis, such as the avionics audit, early in the design phases of the program to develop a confident position from which to claim conformance with that program's fault-tolerance requirements.

OTHER LESSONS LEARNED IN RM EVOLUTION

Similar to the painful evolution experienced with the RM SF interaction with the FCS performance, a major area of potentially avoidable RM change activity resulted because of hardware performance definitions not being mature early enough to allow adequate RM design. A primary example of this problem is the RCS RM. Propellant leaks in an RCS jet can result in hazardous operation, thereby requiring fault monitoring and reconfiguration by RM to preclude further use of a leaking jet. RCS hardware design provided for a temperature measurement on the oxidizer and fuel valves on each jet and an initially proposed RM algorithm which would declare a jet as leaking when either temperature fell below 48° F. Vacuum chamber testing of actual hardware later provided a better definition of the jet thermal responses to various leak conditions and allowed the RM thresholds to be adjusted in software to 30° F to minimize false alarms and still provide adequate hazard protection. Flight experiences in the early STS missions provided the final environmental operation assessment, which revealed still another hardware performance sensitivity and required further RM software adjustments. It was determined that the upfiring primary jets experienced a significant cooling effect in the early stages of entry where the "g" field holds the postfiring "dribble" propellant in the jet and the near-vacuum environment enhances the cold-inducing evaporation/sublimation of that propellant. This phenomenon actually resulted in several false alarm/deselects on early missions where jets were relatively cool before reentry, resulting in a software change to provide an even lower fault detection limit and minimize the false alarms. Another erroneous original assumption which guided RCS RM design was that the large primary jets would respond to leaks in the same fashion as the smaller vernier jets. Again, vacuum testing of actual hardware under leak conditions provided the surprise that the vernier jets could not leak enough to provide for sufficient cooling effects to ever reach the limits established for the primary jets. The resulting RM change to account for this hardware performance characteristic included RM software mods, heater thermostat setting changes, crew procedural impacts, and flight usage restrictions based on vernier jet warmup sufficient to ensure RM leak protection. The problems evidenced by experiences such as these, although not totally avoidable, do point out the need to develop as completely as possible the hardware performance characteristics under true flight conditions before fixing the associated RM schemes. Lacking that luxury, modification impact could be minimized by implementation schemes which include as much flexibility as can be afforded, such as separate I-loadable limits for each data input to an algorithm.

A second area of continuing RM design modification and assessment is the dilemma of providing the best fault protection thresholds possible while not allowing any significant chance of a false alarm. A key factor in this dilemma is the 3σ program-established variation to be allowed in hardware and system performance. This implies that RM should not declare an LRU failed that is within 3σ of the "normal" performance, and further that, since -3σ is as good as +3σ, actual differences between usable LRU's must allow for somewhat more than 3σ (statistically reasonable to assume $\sqrt{2}$ x 3σ). Accounting for this type of variation and arbitrarily selecting a design goal to have no more than one false alarm in 500 missions (the approximate original number of missions in the Shuttle Program), the fault detection thresholds can be significantly large so as to mask some LRU failures and/or result in system errors or transients that can jeopardize mission performance. Determination of the smallest acceptable thresholds to minimize false alarms while providing adequate fault detection is another late-blooming product due to the necessity to have statistically accurate performance assessments. This involves not only certifiable LRU standard deviation data but also development of accurate vehicle systems and flight profile environments. Although this development task is not easily hurried or readily avoidable, some potential areas for minimizing the dilemma do exist. Premium dollars in the LRU design and production phase could result in the guaranteed 3σ variation of some LRU's being significantly smaller. Indeed, the exact same hardware design could sometimes be

---

[1]Contract Change Authorizations 892 and 1032 to NASA Contract 9-14000, Schedule A.

"improved upon" by simply paying for screening and documentation of its quality. A variation of this theme could be to establish a set of thresholds based on periodic monitoring and verification of the actual variation of the flight hardware. One-sigma deviations are considerably more normal in the Shuttle hardware performance to date, and thresholds based on more realistic variations could obviously be tighter so as to improve system performance while maintaining the same realistic false alarm sensitivity. The final solution is, of course, to provide five-string operation as previously described, thereby eliminating the requirement for fault detection and the dilemma of protection thresholds versus false alarms.

EVOLUTION OF SHUTTLE AVIONICS FAULT TOLERANCE - LESSONS LEARNED

IMU REDUNDANCY MANAGEMENT

The lessons learned for IMU RM have occurred mainly in three areas: (1) understanding the hardware and its failure modes and error characteristics; (2) understanding the design of the software and its ability to attenuate errors and protect against transients; and (3) making the software conformable to variations in mission plans, flight rules, or crew procedures. Key facets of these problem areas are summarized in table 1.

TABLE 1.- LESSONS LEARNED - IMU REDUNDANCY MANAGEMENT OVERVIEW

Area	Problem
Hardware	• Error modeling, failure modes • Warmup transients, trending, aging • Heading sensitivity • Single-point failures • BITE use, performance, sensitivity
Software	• Threshold formulation, queuing, resetting • Dilemma resolution, lack of FD/FS • IMU redundant gyro BITE use • Strapdown rate-gyro use • Transient protection, velocity and attitude selection filter design • Velocity downmode transients • Attitude dithering
Flight operations	• Extended launch holds • Early alinement/delayed entry • Computer/LRU reconfiguration • Freeze-dried GPC • Commfaulted LRU's

Three gimbaled IMU's supply velocity and attitude data to the airborne computers, which have the ability to automatically detect and isolate up to two mission-critical failures. Setting thresholds as bounds for normal or acceptable performance has been one of the critical software design tasks. Setting thresholds below the envelope of normal measurement error can lead to nuisance false alarms and premature loss of an IMU. Allowing for normal or expected divergence in measurement error can lead to transients when changing from the use of one IMU to another, as well as to degraded system performance before isolation of the second failure.

To avoid or minimize these difficulties, selection filters (operating at either 6.25 or 1 hertz, according to need) are used to protect against hardover failures, to control switching transients, and to inhibit or attenuate error growth before isolation of the second failure. Tracking tests are used for failure detection and isolation (FDI) at a background rate of 0.0625 hertz to protect against soft performance failures. To guard against a wrong identification in the event of a transient error condition, an IMU can be permanently failed only after a number (n-count) of successive identical fault identifications occur in consecutive passes of the fault identification logic.

USE OF BITE

Without adequate failure-to-noise margins, it is unreasonable to expect failure isolation by means of software tests. To avoid this difficulty, BITE is used as the first-priority discrimination after detection of a failure in a pair of IMU's. If BITE does not discriminate, the software isolation tests are used to identify the failed IMU. Use of BITE in this manner avoids the possibility of BITE false alarms causing premature loss of an IMU whose attitude and velocity measurements continue to be good. Also, software tests are vulnerable to wrong isolation decisions when exposed to simultaneous multiaxis failures - failures of the kind most often isolatable by BITE (a tumbling platform, for example).

If a fault remains unidentified after a given number of consecutive fault detections, an IMU dilemma is signaled to the crew to indicate the need for manual intervention.

FAILURE MODES

The software design was conceived to detect and identify soft bias shifts in attitude or velocity outputs. One of the great fears was to falsely detect errors and downmode good units, which was recognized as an easy way to catastrophe. Part of this fear was also detection, identification, and reconfiguration which could occur for a transient error condition which was conceivable for a lightning strike or temporary communications failures in a data bus link between the IMU's and the general-purpose computers (GPC's), hence the use of an n-counter logic.

These concerns basically have led to a design that is tolerant of system noise. During STS-6, 5000μg noise was evident on the IMU 3 z-axis accelerometer during the entire flight. The noise was as high as 30 000μg, evidenced by the velocity underlimit (VUL) BITE alarms during entry. This IMU was a good navigator and was used almost exclusively for attitude reference during STS-6.

Because the noise was contained only on the one z-axis accelerometer, IMU 3 would have been most likely deselected for a threshold violation. If the noise were correlated to other axes, the resulting error could resemble a simultaneous multiaxis failure. The danger here is that, for the two-level IMU case, a unit could be deselected based on random error with a small but real risk that a good unit could be removed and the noisy unit could remain in candidacy. Although an observant crew could manually deselect the offending unit, procedures for trapping a noisy unit are being investigated.

SOFTWARE

Although we had confidence software could be designed to handle failures in two IMU's and obtain FO/FS performance in three IMU's, the coverage of failure rate is not 100 percent in a pair of IMU's. The BITE coverage is on the order of 90 percent of the failure rate. Of the remaining 10 percent, the software coverage is on the order of 60 to 80 percent at best, giving a total coverage of 96 to 98 percent of the failure rate for the hardware/software system. Although, in theory, we could achieve 99.8 percent of the mission-critical failure rate of 300.4×10^{-6} failures per operating hour, operational considerations such as extended holds or delayed entry can reduce coverage.

Lack of 100-percent FO/FS coverage in IMU RM has led to reliance on other available sensors especially for attitude during entry where a two-case dilemma could be catastrophic for a hard-failure condition. A body-mounted RGA supplying instantaneous body rate to flight control is used to integrate and maintain an inertial body-attitude state during a two-case IMU attitude dilemma, thus creating an artificial fourth IMU for attitude. The maintenance of the integrated fourth IMU attitude state from RGA data does not result in an inertial quality attitude reference. Although the RGA's produce a good instantaneous body rate, noise and quantization result in an inferior integrated attitude state (e.g., approximately 70° per hour effective drift rate). The addition of a fourth IMU could eliminate the risk of the IMU RM system defaulting to the RGA's forever dilemma as well as simplify the design of the IMU attitude selection filter and attitude processor.

Differentiating IMU attitude data to supply a quality body rate to flight control could potentially eliminate the need for the rate-gyro assembly and the complexities of selection filtering of the body rate data. Refinements in the software area include integrating and maintaining a separate quaternion of body attitude from each IMU for flight control. Quaternion averaging could eliminate attitude dithering between prime selected IMU's. Averaging could also provide performance enhancement and open up the tight margins that now exist between mission performance requirement and instrument capability.

Because performance of the guidance, navigation, and control (GN&C) system is degraded when errors escape detection, the propagation of second failure errors has received considerable attention. Everyone is aware that the effects of a first failure in three IMU's can be avoided. Everyone

knows performance degradation cannot easily be avoided when one IMU in a pair fails. Although prime selecting a unit in a pair for measurement can avoid ill effect in half the failure cases, there exists the intolerable risk of having selected a failing unit and having to absorb the full impact of a failure in the GN&C system. Averaging measurements in a pair can cut the error exposure in half between the time of inception of a failure and the time of final system reconfiguration. For threshold violations, immediate deselection of an element of the pair based on BITE status can further reduce failure effects, leaving a residual problem of error propagation for a failed unit tracking just below the threshold. To do a good job, the RM designer must be given an error allowance or margin between normal measurement error and system performance requirements. The alternatives are to accept the degraded performance or to have more IMU's.

The lesson learned here is that FO/FS in three strings requires tightening up on instrument error specifications so that, even in the degraded mode before isolation of the second failure, the worst performance is still within the acceptable system performance envelope. This lesson would be an important consideration for an autonomous onboard navigation system where three or four high-accuracy IMU's could limit error without the need for outside manual intervention by the crew or flight controllers.

One-hundred-percent FO/FS probably cannot be achieved in three IMU's. The problem with three strings is after losing one, there are only two left. No matter how much thought is given to failure, a new, unanticipated and unmodeled failure lurks around the next corner. That failure is the next two-string dilemma: the next dragon to be slain.

THRESHOLD FORMULATION

In most instances, values for the isolation threshold are set at 20 percent above the noise envelope generated by the McDonnell-Douglas Monte Carlo studies. The detection thresholds are set at the highest value which still protects the GN&C system from IMU errors that cause violation of mission ground rules, operational constraints, or vehicle safety limits. Sensitivity studies by Rockwell International-Downey were used to set the detection thresholds.

ASCENT THRESHOLDS

The onboard IMU RM software in combination with the IMU hardware BITE will detect and identify the first IMU failure during ascent. It will allow up to a 50-ft/sec velocity error at main engine cutoff (MECO) before detection of a second IMU failure but it may not be able to identify the failed IMU.

Ground-based flight control personnel will be prepared to identify a second failure by comparing the IMU navigation states against the navigation state derived from ground-based radar tracking data. An onboard state vector update is planned during ascent if the predicted onboard velocity error should violate a 40-ft/sec MECO constraint, which is the orbital maneuvering system (OMS) fuel budget for an abort-to-orbit in event of a MECO underspeed.

During ascent, there is no margin between detection requirements and instrument performance at the two-level. An adequate margin for 100-percent probability of isolation of a second failure requires a ratio of 2 for VCONS2/VCONS6 for optimal skewing. The ratio is only slightly greater than one for the I-load values. Onboard dilemmas will occur for accelerometer failures between 5000μg and 16 500μg.

A mean acceleration error of 6000μg will violate the 50-ft/sec MECO velocity accuracy targeting constraint for jettison of the external tank. Delta-V averaging at the two-level will attenuate a velocity bias by one-half so the range of failure dilemmas that potentially must be isolatable by ground-based personnel is from 12 000μg to 16 500μg.

ON-ORBIT THRESHOLDS

Normal instrument performance for platform alinement and drift will not support mission accuracy requirements without frequent IMU realinements, yet there is a necessity to allow extended periods for the crew to sleep. The I-load values for the on-orbit attitude detection thresholds are set to allow a 10-hour sleep period before potential false alarms can occur at the three-level (8 hours for two IMU's). The detection threshold will ramp above the attitude requirement for a safe entry 2.5 hours after alinement. After this time, ground personnel must be prepared to call for a realinement (if the actual IMU attitude divergence should exceed the attitude error constraint for a safe entry) to maintain capability for a safe return in event of a contingency deorbit.

For a protected entry, IMU realinement must occur no earlier than 2 hours before entry interface or 2.5 hours before TACAN acquisition. Earlier alinements result in loss of second failure coverage during entry.

The 100-ft/sec altitude rate error requirement at TACAN acquisition requires that velocity tilt error transmitted to navigation be no more than 1350 arc-seconds during entry. The two-IMU detection threshold ceiling (VCONS8) is set to protect this requirement.

ENTRY THRESHOLDS

IMU RM can detect and isolate both a first and a second IMU failure during entry, allowing errors up to 100 ft/sec in altitude rate at TACAN acquisition for the second failure with one notable exception: if the second IMU failure is a dual-axis failure in the ambiguous direction and not covered by BITE, then there is potential for dilemma at the two-level.

The velocity isolation threshold (VRAMP2) is queued by a manual operation by the crew. The value of VRAMP2 assumes the crew will PRO to MM 304 5 minutes before entry interface (EI). If the crew delays the PRO until EI, the 20-percent margin over instrument noise disappears. If the PRO occurs later than EI, there is a danger of false isolation during entry.

The altitude rate uncertainty should not exceed 100 ft/sec during blackout. The 3σ altitude rate error due to navigation, atmosphere, and winds is 48 ft/sec. The RM community chose to allow approximately 85 ft/sec error in altitude rate due to IMU failures. There are two ways to look at this error:

1. The budget is the requirement minus 3σ Nav in RSS sense.

   $$\dot{h} = \left[100^2 - 48^2\right]^{1/2} = 87 \text{ ft/sec}$$

2. The budget is the requirement minus 1σ Nav in an additive sense.

   $$\dot{h} = \left[100 - 16\right] = 84 \text{ ft/sec}$$

IMU RM LAUNCH HOLD CONSTRAINTS

A greater launch hold capability is needed to avoid potential launch delays resulting from IMU alinement accuracy limitations. Present baseline flight software and I-loads were designed to support a safe entry for an abort once around (AOA) given a 3σ vendor specification IMU for which the preflight gyrocompass alinement was completed 50 minutes before lift-off.

Present flight rules result in a nominal countdown time line with 30 minutes between completion of the alinement and lift-off. The nominal time line provides a 10-minute planned hold at T-20 (just before the OPS 9/1 transition). This hold does not affect the IMU's because the preflight alinement programs are scheduled so that the alinement process continues during the hold. Platform release occurs at the OPS 9/1 transition at T-20 minutes in the count. A second planned hold of 10 minutes is scheduled at T-9 minutes, yielding the 30 minutes between platform release and lift-off.

For the case of 3σ IMU's, the Shuttle flight software IMU RM I-loads allow a maximum time of 110 minutes between platform release and lift-off. Because 30 minutes of this time is spent in the nominal count, 80 minutes are available for unplanned holds. Because flight IMU's are rarely 3σ and their relative performance can be monitored by flight controllers, much longer holds may be possible based on the real-time prelaunch performance. Up to 4 hours may be available between platform release and lift-off based on past performance.

In any event, beginning 100 minutes from platform release, flight controllers are required to identify all IMU failures at the two-level because the flight software no longer has this capability. Second failure identification capability is not restored again until the first on-orbit alinement.

Platform misalinement can be predicted analytically based on expected initial misalinement and nominal gyro drift at platform release:

Equation (1) Up error = RSS (60, 0.02915 T_1) arc-seconds

Equation (2) North or West error = RSS (20, 0.0094 T_2) arc-seconds

where T_1 is time in seconds from completion of gyrocompassing and T_2 is the time in seconds from completion of the VEL_TILT subroutine.

Here, the North, West, and Up coordinates are topodetic and are frozen at the instant of platform release. This epoch North, West, Up frame is labeled (N_0, W_0, U_0). After platform release, the true topodetic North, West, Up frame (N, W, U) will be rotating at Earth rate compared to the inertial IMU frame or the epoch (N_0, W_0, U_0) frame. To find the expected IMU misalinement about North, West, Up at lift-off, it is first necessary to calculate the expected IMU error in N_0, W_0, U_0 coordinates and then to transform this result to the N, W, U frame at lift-off. Table 2 shows the final launch misalinement as transformed for the effect of Earth rotation rate. The earth rotation rate carries the vertical axis error into the West axis. (For a level IMU on the Equator, the vertical axis would point West 6 hours after platform release.) Knowledge of platform misalinement at lift-off allows the use of nominal dispersion analysis sensitivities for predicting navigation state error at MECO or at points of interest along the AOA reference mission profile.

TABLE 2.- IMU MISALINEMENT AT LAUNCH FOR INCREASING HOLD TIME IN OPS 101 (1σ)

Time		North, sec	West, sec	Up, sec	RSS, sec	LEVEL, sec
Hr	Min					
0	0	20	20	63	69	28
	20	24	28	79	86	37
	40	33	43	99	113	54
1	60	45	64	124	146	78
	80	61	88	147	182	107
	100	79	117	167	219	141
2	120	99	148	184	256	178
	140	120	179	196	292	216
	160	145	213	205	330	258
3	180	172	247	209	366	301
	200	203	381	208	405	347
	220	236	314	204	443	393
4	240	270	348	194	481	440

The analytically derived IMU misalinement can be used to predict the time of violation of the IMU RM attitude threshold, thereby estimating the available unplanned hold time. Table 2 shows the misalinement of a single 1σ IMU for the first 4 hours after completion of the preflight alinement. The table shows the misalinement about North, West, and Up, the RSS of the three misalinements (labeled RSS), and the RSS of the two-level errors (LEVEL). At 2 hours, the RSS misalinement is 256 arc-seconds 1σ. For a pairwise IMU tracking test, the parity equation residual would be expected to be $\sqrt{2}$ x 256 or 362 arc-seconds 1σ. The 3σ misalinement would be expected to be 1086 arc-seconds.

The two-level attitude fault detection threshold is 1138 arc-seconds as defined in the current flight software I-loads. (The threshold half-angle of 2.76×10^{-3} radian is stored in ACONS5, MSID V97U4215C.) A 3σ IMU pair would be expected to violate the two-level fault detection threshold just beyond 2 hours from platform release. These data are plotted in figure 6, which shows the expected pairwise tracking test errors for 1σ, 2σ, and 3σ IMU pairs compared to the two-level attitude fault detection threshold. A 3σ IMU pair would intercept the threshold 126 minutes after platform release.

It should be noted that IMU misalinements are not completely observable by ground monitoring. Flight controllers observe total relative misalinement between pairs of IMU's and azimuth misalinement is not observable by ground navigation performance analysis. Hence, launch hold performance constraints must be based in part on results of premission simulations.

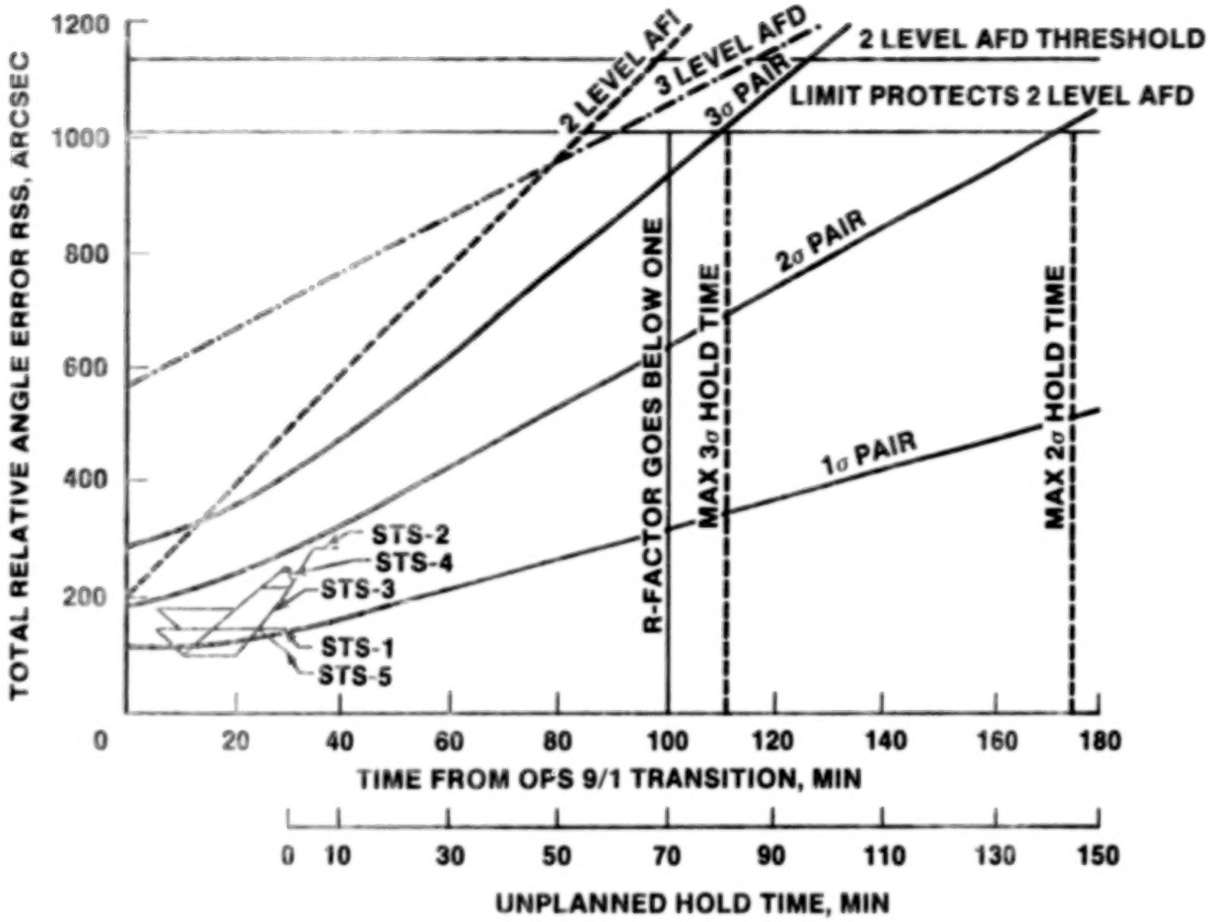


FIGURE 6.- PRELAUNCH IMU DRIFT MISALINEMENTS.

MEASUREMENT REDLINE

Protecting the threshold against false alarms implies the observed instrument error is below the threshold after making allowance for observation errors. The measurement error bound can be estimated analytically. The granularity of the display is 0.01 deg/axis and the measurement error can be no more than 0.01 deg/axis about three axes or 0.017^{o}. The Mission Control Center algorithms compute pairwise IMU errors using functions of gimbal angles the readout quantization of which is 20 arc-seconds per axis, and the expected measurement error would be no less than 20 arc-seconds about eight axes of two four-gimbal platforms or 0.0157^{o} (RSS of 20 taken eight times). An additional error of 65 arc-seconds is budgeted for the resolved errors and gimbal pivot misalinement which shows up during the post-lift-off tower-clear roll maneuver as observed in Monte Carlo simulations of the ascent flight profile.

An IMU performance redline is established as follows:

The threshold	0.316^{o}
Less measurement error	0.017^{o}
Less tower-clear roll error	0.018^{o}
Limit line	0.281^{o}

This limit line, plotted in figure 6, is violated by a 3σ IMU pair 111 minutes after platform release.

MCC MONITORING OF EXTENDED HOLDS

Because the RM threshold could possibly be violated at 80 minutes into a hold, the Flight Operations Directorate decided to monitor relative performance to protect the threshold knowing they could terminate an unplanned hold earlier; otherwise, the program would continue the present baseline which allows 90 minutes of unplanned hold.

VELOCITY UNDERLIMIT BITE

The loss of IMU velocity output is one area of software transient protection that is not adequately covered. The current understanding of the failure mode is that all three accelerometer counters freeze. The IMU SOP will then output the accelerometer bias calibration terms only. Therefore, wrong isolations or dilemma can occur.

The VUL BITE was designed to detect the loss of velocity output. The VUL BITE is the only BITE that compares one IMU against another in order to make a decision. The VUL BITE uses the compensated delta velocities to perform the test so the frozen counters are masked by the compensation terms. This test works only in acceleration environments greater than 60 000μg (i.e., not during OPS 2) and the test is limited to IMU's having accelerometer bias calibration terms less than 50 000μg. Commfaulted IMU's are not excluded from this test. The crew select/deselect switch determines the test candidacy. If a loss of velocity output occurs when the VUL BITE is disabled, a dilemma or wrong isolation will occur because of the large accelerometer bias compensations.

A solution to this problem is to check the uncompensated velocity counts for each IMU. The revised VUL BITE test would then be performed at a rate such that the smallest accelerometer bias compensation term yields at least one count.

If the sum of the squares of the velocity counts for all three axes is less than three, the counters have frozen and that IMU has a VUL failure. This test assumes that the velocity counter bit toggling will cause at most one count per axis during the period of consideration. This proposed VUL BITE test is valid during all flight phases. The only problem with the revised BITE is that transient BITE false alarms can occur if the environment exactly matches the accelerometer bias compensation terms. The revised VUL BITE test was felt to be an expensive software change and the community was willing to accept the loss of failure coverage (ref. 6).

VELOCITY SELECTION FILTER RECTIFICATION TRANSIENTS

Another area of inadequate software transients protection is in the velocity selection filter. The velocity-data-good logic was designed to protect navigation from large constant IMU failures. However, during STS-3 on-orbit, a new IMU failure mode was observed (ref. 7). IMU 3 experienced a large transient bias shift (34 750μg) followed by a smaller constant accelerometer bias (500μg). If this failure had occurred at the two-IMU level, the selection filter would have correctly performed the temporary downmode to the one-IMU level for the duration of the transient. If the transient had occurred between rectification cycles, navigation would have experienced the full effect of the transient (ref. 8).

One solution to the problem of transients polluting navigation is to exclude temporarily deselected IMU's from the selection filter until a new set of rectification biases has been computed. Deselected IMU's refer to commfaulted IMU's or any temporarily downmoded IMU due to a velocity-data-good violation. This procedure will prevent the transient from polluting the selected velocity and thus the single-string navigation. Currently, a crew-reselected IMU is treated in this manner. However, this solution does not protect the entry three-string navigation since it does not use the selected velocity. The ground support console operators will have to monitor the three navigated states to protect navigation from transients.

This solution has been approved for software implementation as CR 59308A on release 2X/XX.

FLIGHT TIME-LINE IMU RM EFFECTS

The values of the IMU RM fault detection and isolation thresholds are a function of certain mission events. The attitude thresholds ramp from either OPS 9/1 transition (platform release) or on-orbit alinements. The velocity thresholds are constant before lift-off, jump to a higher value during ascent, and drop to a low value until MM 304 (entry interface minus 5 minutes). At MM 304, the velocity thresholds begin to ramp until a high constant value is reached. The threshold values were determined by instrument performance, guidance constraints, and IMU platform skewing geometry.

The velocity thresholds are insensitive to mission time-line changes since the triggering events always occur at roughly the same times. However, time-line changes are critical to the attitude thresholds since they are reset at each on-orbit alinement. The attitude fault detection threshold ramps to a constant value while the fault isolation threshold continues to ramp. Consequently, after about 5 hours, all two-IMU level attitude failure coverage is lost (fig. 7). The attitude thresholds were set based on the last onboard alinement occurring approximately 70 minutes before the deorbit burn. The attitude RM covered about 60 percent of all failures not covered by BITE. (BITE covers about 90 percent.)

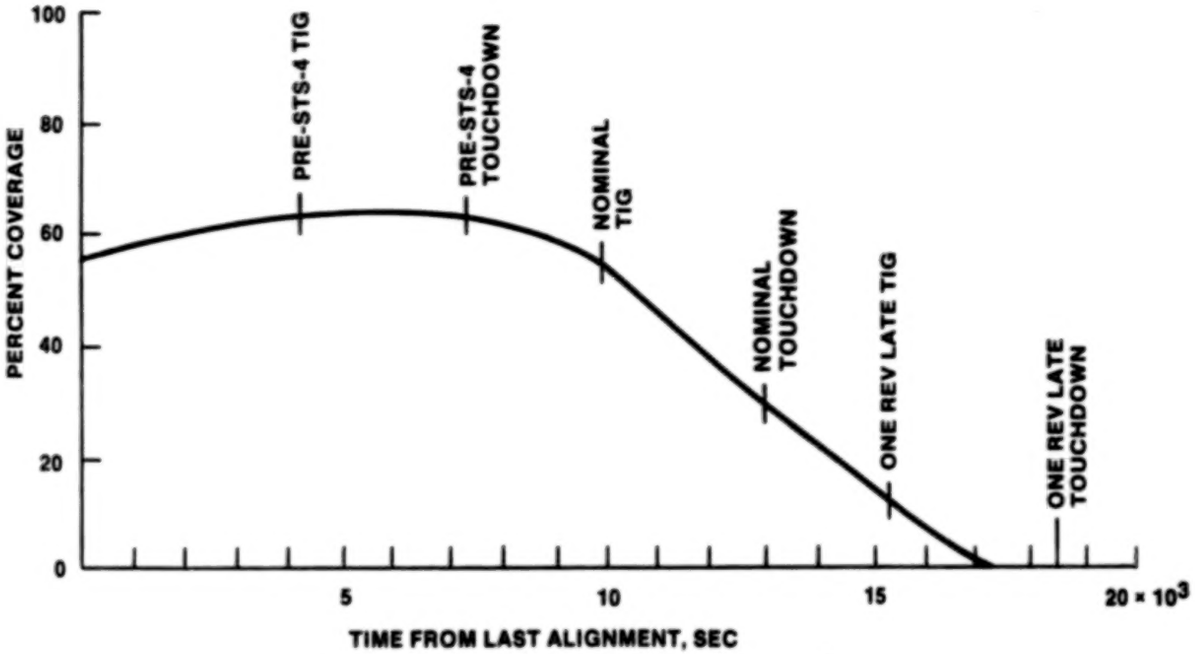


FIGURE 7.- TWO-IMU LEVEL ATTITUDE FAILURE COVERAGE.

Before STS-4, it was decided to perform the last onboard alinement one revolution earlier than on previous flights (165 minutes before the deorbit burn) to ease the crew workload. Unfortunately, this decision caused a degradation of the two-IMU level attitude failure coverage. (See fig. 1.) The Entry Flight Techniques Panel decided to leave the time line alone if there are three good IMU's. If there are only two good IMU's in the system, the last onboard alinement will be performed 70 minutes before the deorbit burn, as it was done previously (ref. 9).

The other flight time-line attitude threshold concern is for a one-revolution-late deorbit. All two-IMU level attitude failure coverage will be lost before touchdown (ref. 10). In this case, an IMU-to-IMU alinement should be performed about 70 minutes before the deorbit burn.

The entry attitude threshold criteria preclude changing the values without degrading the RM coverage even further. Since the IMU's have been behaving well on orbit and during entry for the first six flights, it may be possible to reevaluate the 1σ drifts and lower the thresholds, thus regaining RM attitude coverage.

REFERENCES

1. Space Shuttle Flight and Ground Systems Specification. JSC-07700, Vol. X, Rev. C, Para. 3.3.1.2.3.1.2.

2. Thibodeau, J. R.; and Bauer, Steven R.: Redundancy Management of the Space Shuttle Inertial Measurement Units. AIAA Guidance and Control Conference, Aug. 9, 1982.

3. The High Cost of Worrying Improbable Possibilities. JSC Memorandum LA15(81-518), Sept. 28, 1981.

4. Redundancy Management Flight Systems Software Requirements. STS 83-0010, NASA Lyndon B. Johnson Space Center, 1983.

5. Bennett, D. E.: QMVS Evaluation at SES. Rockwell International, Internal Letter No. 283-210-82-019, June 14, 1982.

6. Schneider, H. E.: Velocity-Under-Limit BITE Proposed Fix. MDTSCO Transmittal Memorandum 1.4-TM-D2630-380, Feb. 12, 1982.

7. Gibbs, R. G.: IMU 3 Accelerometer Error During STS-3 On-Orbit. MDTSCO Transmittal Memorandum 1.4-TM-D1730-72, June 22, 1982.

8. Schneider, H. E.: Velocity Data Good Logic. MDTSCO Transmittal Memorandum 1.4-TM-D1730-660, July 21, 1982.

9. Schneider, H. E.: IMU-RM Impact of Early Entry Alignment. MDTSCO Transmittal Memorandum 1.4-D1730-681, Aug. 6, 1982.

10. Schneider, H. E.: IMU-RM Impact of One Rev Late Deorbit. MDTSCO Transmittal Memorandum 1.2-TM-FM53A01-457, Mar. 29, 1983.

N85
16891

UNCLAS

D2

N85-16891

SHUTTLE AVIONICS SOFTWARE
TRIALS, TRIBULATIONS AND SUCCESSES

O. L. Henderson
HONEYWELL INC.

ABSTRACT

The decision to use a programmable digital control system on the Space Shuttle engine was a new application of digital control in the early 1970's. The use of digital control was primarily based upon the need for a flexible control system capable of supporting the total engine mission on a large complex pump fed engine. The mission definition included all control phases from ground checkout through post shutdown propellant dumping.

The flexibility of the controller through reprogrammable software allowed the system to respond to the technical challenges and innovation required to develop both the engine and controller hardware. This same flexibility, however, placed a severe strain on the capability of the software development and verification organization. The overall development program required that the software facility accomodate significant growth in both the software requirements and the number of software packages delivered.

The above requirements became a serious challenge to the software development facility. This challenge was met by reorganization and evolution in the process of developing and verifying software. The resulting process consistently provided high quality software on schedule throughout the balance of the shuttle program.

INTRODUCTION

In March, 1972, NASA selected the Rocketdyne Division of Rockwell International to design and develop the Space Shuttle Main Engine (SSME) for the reusable Space Shuttle. The engine development program was managed by NASA/Marshall Space Flight Center (MSFC) and was supported by various engineering laboratories within the Science and Engineering Directorate.

A digital computer control concept was selected as the basis of the engine control system. Digital control was selected over the more classical engine control concepts of valve sequencing or analog computer control because of the following advantages.

The engine was still in the early stages of development and the digital controller allowed modified operational sequences and functional changes through software updates. Time consuming and costly controller hardware modification could be avoided as the engine matured. The concept of software modification provided flexibility and adaptability during all stages of the engine development and use.

The digitally based systems also demonstrated the most economic means of providing fast and flexible control and sophisticated monitoring and redundancy management schemes for the complex operational sequence of the engine.

The above attributes of the system were reflected in the requirements for a software development and test facility which could respond quickly and accurately to the needs of a dynamic engine development program. The initial organization defined for this facility had previously demonstrated iteself as being effective for the typical embedded software program in a digital controller. The magnitude and scale of software development required for the Main Engine Program soon made it evident that the "classical" organization was not up to the task.

The following paragraphs describe the early problems and the solutions developed to provide the required quality software needed to support the engine development program.

DISCUSSION

EARLY HISTORY AND CHALLENGES

The initial organization defined for the software development was as shown in Figure 1. This organization was typical for an embedded software program delivered with a hardware unit in the early 1970's.

The software group had a vertical organization for design coding and testing of software programs. Requirements were from two sources: the controller hardware/software relationships from the project systems group; and the engine system software needs from the customers software requirements specification. The organization had a strong knit team approach and was staffed with experienced software designers who had the background to efficiently develop and test a software program. This approach had generally worked and was cost effective on the embedded software programs delivered in previous control system applications.

The organization appeared to fit the program. The initial design definition was going to lead to the Flight Configuration. The controller hardware being developed was the projected flight control configuration and there was only one defined deliverable software configuration.

The major challenges recognized relative to the controller software at this time were:

1. The engine being developed was the most complex high performance engine ever built. Due to its high operating pressures, temperatures and turbopump speeds very precise and rapid control of critical engine functions were of prime importance.

2. Failure of a control function during engine hot fire development testing could result in catastrophic damage. The system hardware was redundant to provide safety against failure. The software, however, was identical in the redundant channels of the controller. A software error that was fatal in the first channel would also be present in the second channel.

The above requirements dictated a conservative software design with significant amounts of selfchecking and the ability to respond rapidly to a control perturbation. It was also recognized that this software would require extensive testing and verification prior to use in an engine hot fire situation.

The philosophy on the testing was to do three levels of test. The first at the software module level using a host machine. The second at the software system verification level in the controller hardware while the hardware was linked to a hybrid simulation of the engine and vehicle interfaces. The final testing was to be performed at the NASA Marshall Hardware Simulation Laboratory where the software again in the controller hardware was verified with an engine simulation containing the actual engine control sensors and actuators.

This overall test philosophy proved to be correct and remained throughout the software program development stages.

There was a third and significant challenge to the software development. This challenge was not initially recognized for either its scope or magnitude. The problem evolved from one of the significant advantages of using the programmable digital controller. The control system allowed relative inexpensive flexibility in accomodating changes in the engine and associated control scheme. This led to a staged evolution of the overall system development. Innovative changes to the engine system could be planned and implemented without schedule loss due to controller modifications.

The difficulty was in the demand this placed on the software development and verification operations. The changes and evoluation required ever increasing software growth in program size and sophistication. This had been anticipated but the actual growth was between 100 to 200% over early projections. The growth was primarily due to the fact that as the engine/controller system matured it was recognized that a more efficient and sophisticated control capability could be accomodated by the basic digital control concept. The most severe demand on the software development, however, was due to the fact that engine development dictated a controller and associated

software be available from the earliest stages. The early availability need resulted in a semi-hardened controller hardware design and placed the rapid change requirements on the software. This was further aggrevated as both the engine systems and the controller hardware definition changed as the engine matured. The above created an incremental or multilevel approach to the engine testing and resulting controller software needs.

Reasonable progress on the program dictated that there would be several iterations of both the engines configuration and engine controllers as we progressed to the final operational stage. These iterations had changing and or conflicting software requirements. Also several versions of the software configurations were required simultaneously to service the various engine test stands and development laboratories.

The above scenario resulted in the requirement of simultaneous development, testing and maintenance of two to three basic versions of the operational software in the same facility with the same technical staff. Each basic version of the software had 20 to 30 revisions which required verification, certification and shipment.

The realities of the situation soon made it evident that the software organization was not meeting the immediate or long term needs of the controller program or the engine development program.

The initial concept of software development could not handle the environment. We saw a degradation of the quality of the software documentation and numerous errors in the shipped versions of software. Serious cost overruns and schedule slips developed. There was a growing concern we would provide software that could result in a catastrophic engine failure.

DEVELOPED SOLUTION

The basic problem with the existing organization was that it had not been structured to handle the large software development operation required to deliver and maintain simultaneously several software definitions for a single target control system.

The problem was reviewed and broken down into the following elements:

1. Organization: The software design, development and test responsibilities had been organized as a tight knit team with overlapping and fuzzy responsibilities. The group worked well on a typical single string embedded software development but was inefficient for the large embedded program requiring multiple simultaneous program design cycle iterations.

   Their was a need for a better definition of the responsibilities and interface between the Systems group and the Software Design group. Software Design was accepting direction from both the customer through the Customer Software Requirements Specification and from Systems through the Controller Systems Requirements Specification. This direction at times conflicted or overlapped due to the different stages of engine system and controller development.

2. Change Control: Software requirements were changing rapidly. Change and problem control were not rigidly documented and became suspect when the volume of changes and problems increased. The test plan or test tracking system defined could not handle the heavy volume of test and retest that was building up on the program. The software design documentation specification structure was formalized and specific but the above problems caused this documentation to degrade significantly in both its accuracy and the ability to meet shipping schedules.

3. Quality Control: There was a need for an independent group identified to review and pass on the accuracy or quality of the software or its progress throughout the design process. Quality was left to the individual designers for their portion of the effort. Although the individual effort was good, the continuity across the program was missing and overall quality suffered.

4. Management: The design process had grown so complex and large that even though individuals in the organization felt that they were accomplishing their tasks currently and reporting to be on schedule, the overall development was missing all of the major milestones. The problem was isolated to the fact that intermediate check points or gates in the design process were non-existant. The designers did not understand they had a problem until the last step which was to test their design, against a program requirement, in the verification test facility.

The above reviews and problem identification resulted in a reorganization of the software development groups and the development process. The reviews identified that the environment of the project required multiple software programs in various stages of maturity to be in the development pipeline simultaneously.

The software development was reorganized by borrowing from the structures and documentation requirements that had been proven for multiple phase hardware development cycles. Specifically the development was changed to break the overall process up into smaller operations which could be identified and managed independant of the proceeding or following operation. Completion criteria and control documentation was then identified for each of the operations. These changes allowed the tracking and management of the multiple programs in process.

The software development was reorganized as shown in Figures 1 and 3. This organization provided solutions to the specific problems we had identified in the previous paragraphs. Originally it was felt that the change in organization and added controls would significantly increase the cost of the operation, however, after some evolution and refinement this organization proved to be able to deliver higher quality software and software documentation at a comparable cost and always on schedule.

Referring to Figure 2, it can be seen that the new organization contained two new groups, Test and Reliability. Also the roles of Systems and Software Design were modified to fit the concept of the software development facility operating as a software factory or production line.

The reorganization and the addition of several procedures and methods did not significantly change the overall functions performed during the software development. The changes were intended to break the overall development of the process into manageable and traceable subunits with definitive completion criteria. Each subunit process had a controlled source of incoming information and in turn became the controller source of incoming information for the next step of the process.

The following paragraphs will describe the changes that were made and the problems that were solved by these changes.

Systems Design

The Systems design group was identified as the primary customer interface. All customer direction and software design requirements flowed through the systems group. This provided a focal point for the design requirements definition for the various software packages being developed. The above procedures provided a unified and controlled interface between the software process and the customer and hardware needs and revisions.

The second significant change relative to the system group was that they were given the responsibility for the generation of the Verification Test Requirements for the software. This document defined the test or retest required for a base program or for a revision. Generation of these documents significantly improved the quality of the software testing. The software was not tested against a design requirement and not the software design interpretation of the requirement.

Systems was also given the responsibility of defining the retest required against a given operational program if that program was revised and updated. The organization now had all external interfaces and software requirement documentation, both design and test,focused in one group. This change eliminated the earlier conflicting requirements and definitions from reaching the design floor. The Systems group integrated all design and test requirements into documents they controlled and maintained, the

software designers and software testers could work to a single consistent source of direction.

Software Design

The Software Design group was also reorganized to provide a process which had small identifiable design steps that the process development could progress through. These steps were designed such that completion of a given step or function was identifiable and had a testable criteria for completion. The Software Design process now included the detail design, code and walk through of the design, testing of the design module and integration of the module into the operational program as independant functions.

The functional and detail design were provided by the software design engineers and the changes were documented via a software change memo. This memo identified the module being designed in response to the specific design requirements and also incorporated the new and/or modified software documentation required for the change.

The change memo was then used as the design print for coding of the changes. It was also used as the document that directed change of both the source code for the operational program and the program design documentation.

The software change memo provided a definite reviewable traceable definition of a piece of the software design. Although it required considerable time and detailing by the designer it allowed the use of junior grade engineers and/or technicians to do the coding, the production of the software source change and the update of the source configuration library. It also provided a document that could be reviewed against the design requirement for correctness by the reliability group. After review and completion of coding and mark-up of the redline source configuration, the design walk through was completed. Members of software design, software production, verification and systems group used the walk-through as a vehicle to verify the code, met the design and the design met the intent of the requirements.

The code was then incorporated into the source and the module was tested as an entity by the software group. It was then incorporated in the source being prepared for the test floor and the software designer and coders would use abbreviated test documentation to perform integration testing of the change. This integration testing was the final debugging of the particular change by the software group and determined if the module was ready to be handed over to the test team for verification. After completion of integration testing the new test source program was presented to the Verification Test Group. They would perform a standard verification acceptance test of the new program. This standard test checked the critical paths and timing of the operational programs nad was the criteria for acceptance of a new software version for detailed testing on the test floor.

Verification Test

The verification testing group was one of the two new sections created in the software organization. Their responsibilities included the generation of detailed cookbook type test procedures to be used in the testing of the software. The verification test group was also responsible for identification, scheduling and control of all equipment and documentation required to create and control the test facility. Their primary function, however, was to perform the actual verification of the software program and revisions.

The verification was completed as a two step process. The first testing of a new software program was called the dry run. The dry run test purpose was to identify any problems with the software update code and test procedure or test implementation. Problem resolution or debugging was not allowed during Dry Run Test. When a problem was encountered an Internal Software Note (ISN) was generated and the testing continued through the procedure. The identified problems were then assigned to the responsible groups and worked off without interrupting the test flow.

After completion of Dry Run Testing and correction of all identified problems, the formal verification testing was initiated. This formal testing did not allow deviation from procedures or expected results. Problems that occurred during this test would require a formal review and retest after correction. No outstanding problem was allowed after formal verification test completion unless it had been accepted via the customer through a Software Waiver.

The verification test group solved three problems that had plagued the earlier development. These were:

1. Under the original organization Software Design was to do their own verification testing of the software. Experience with that organization showed that the designers were not generating their test procedures to verify that the software met the design requirements. The procedures were generated to test that the software worked the way the software designer had designed it. The new organization utilized test personnel to generate detailed test procedures from test requirements documentation. These detailed cookbook procedures were purposely generated with a minimum knowledge of the actual software design. The procedure writer used the software design documentation only to find the names of subroutines or data words required for a particular test sequence.

2. The second problem solved was the original organization put an unreasonable amount of schedule pressure on the software designer. The designer had to design, code and debug his programs. He was then required to generate a formal test procedure and accomplish the verification testing. This effort did not utilize the software designers major talent in the most efficient manner. He spent too much time generating test procedure and performing verification testing of the software. The new organization solved the problem by allowing the test group to develop test procedures in parallel with the software design and also relieved the software designer of test responsibility. The software design group could go on to the next design cycle while the test group verified the current design.

3. The third problem solved was the parallel operation significantly collapsed the amount of time required to process a change. Paralleling the design operation and the generation of test procedures provided adequate margin to allow the consistent delivery of software updates to the Marshall Simulation Laboratories and the Engine Test Stands.

Software Reliability

The final group in the new organization was a small group of reliability engineers who functioned as a product assurance organization for the software operation. Their duties included review and approval of the software change memos against the design requirments. They reviewed all test procedure generation against the test requirements. Verified that all required documentation updates and design walk throughs had been completed prior to release of software to a source update. Verified that all test paragraphs had been completed and the data was acceptable. Identified and tracked all open problems against a source update through the use of Internal Software Notes (ISN) and the ISN log.

The Internal Software Note was the key document in the tracking of the entire software development effort, including the testing. While many of the ISNs are generated by the test teams, they may be written by any member of any of the four groups who detects a potential problem in a specification, the program, a test procedure, a flow chart, test equipment or anything else that may affect the software or its verification. Groundrules are that only one problem is documented on each ISN and that every problem, proposed software change, procedure chance, etc., must be documented in an ISN. New ISNs are collected each day and are reviewed by the ISN board.

The board is chaired by Reliability and includes members of the other three groups. They determine the most likely cause of the problem and assign the ISN to one of the four groups for action. At these daily board meetings all other outstanding ISNs are reviewed to determine if any are completely resolved and can be closed or should be transferred to another group for further action. Approval of all four groups is required to close an ISN.

Following the meeting, the additions, changes and closures are entered into a computer program and an ISN log is printed showing all open ISNs and the groups responsible for

action. The reports highlight the number of known problems requiring resolution prior to a shipment and any group that is developing a significant backlog.

Reliability was tasked with maintaining the ISN log and a log on the status of open and completed testing. Software update could not be shipped from the facility until these two logs had been closed through resolution of the open problems or a request for outstanding problem waivers from Rocketdyne.

CONCLUSIONS

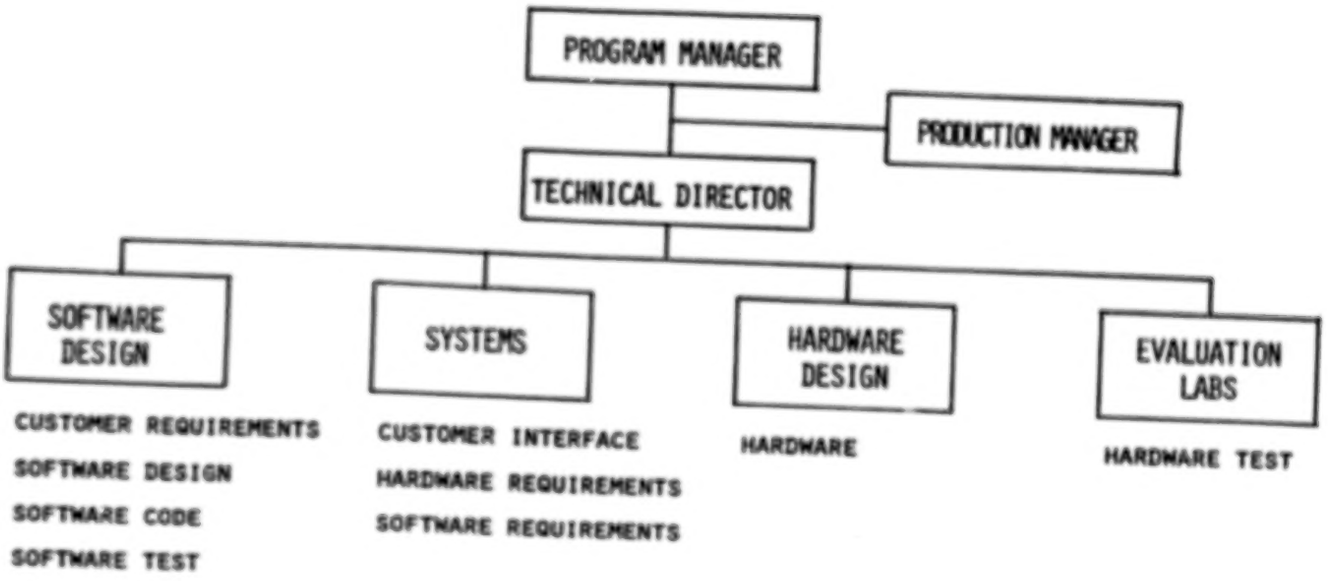
The process described above evolved from a need for extremely reliable software as a part of a critical shuttle control system and early difficulties with this software development effort. A significant measure of the success of the developed process is that the earlier experienced problems did not exist through the balance of the development program. Since implementing the process, each software update and accompanying documentation was delivered on or ahead of schedule.

The vast amount of engine hot fire time that the controllers and the associated software have successfully supported demonstrate that the developed process has consistently provided high quality operational programs. Successful completion of the Shuttle launches further confirms that the software development program is sound.

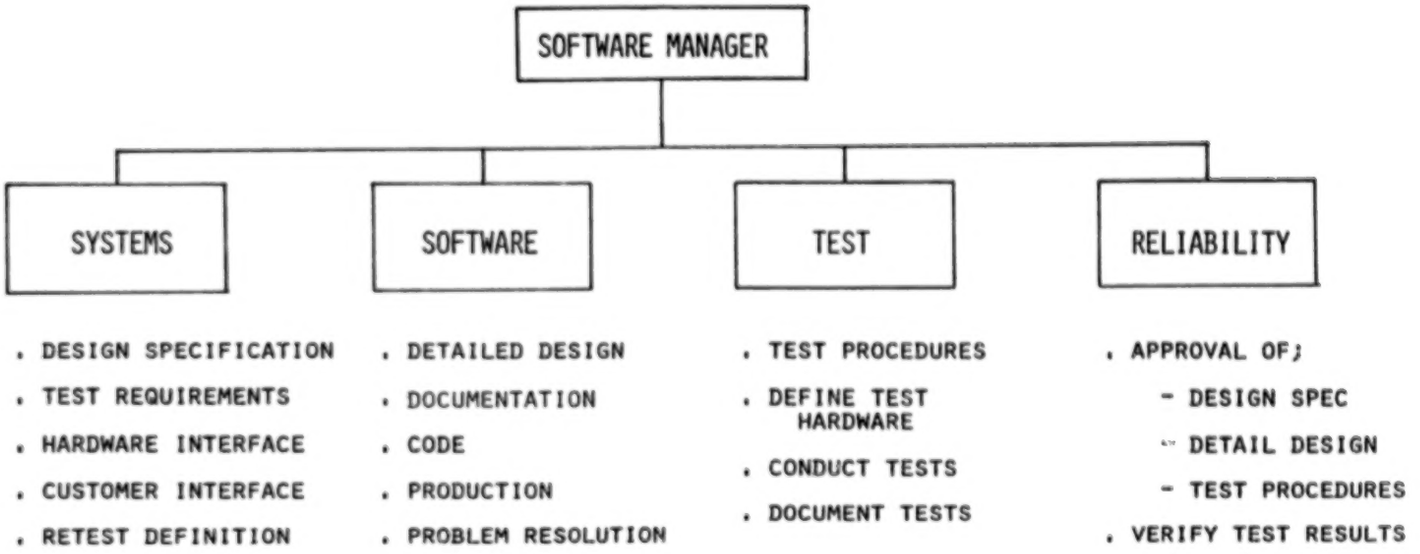
It has been said that the real benefit of our exploration of space is not the exploration itself, but the development of techniques needed to manage large, complex processes where success is a must rather than a goal. The development of this software design system is a case in point of the above statement. The key elements of this success -- planning, organization, tracking and discipline are applicable to all software processes. The concept of distinct groups with well defined responsibilities, periodic status reviews, documentation control approvals and reviews, a formal tracking procedure and, providing authority consistent with responsibility, are not unique in their application to the SSMEC program. The need for these elements of their effective implementation was learned through experience on the program. The real benefit from this experience is the continued use of these concepts on future software development and verification programs.

MAIN ENGINE CONTROLLER
INITIAL ORGANIZATION

FIGURE 1

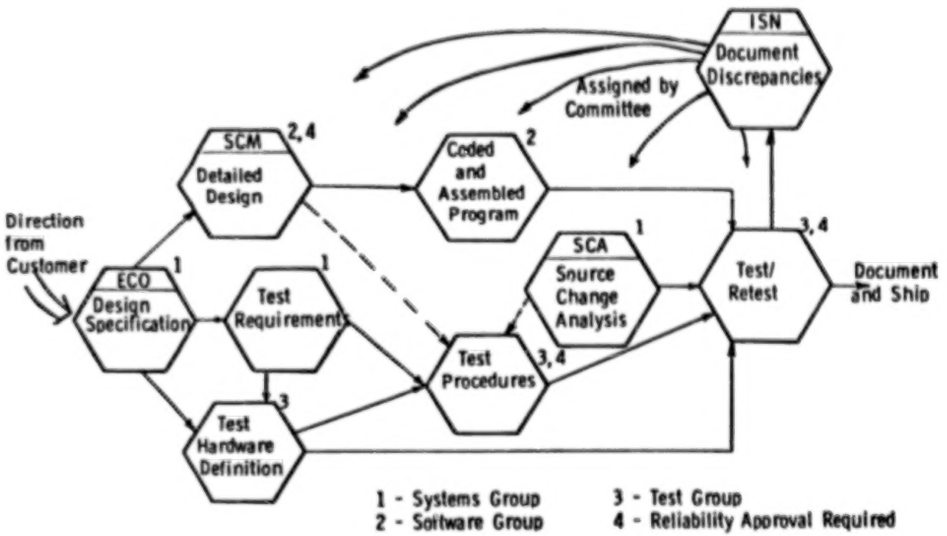


SOFTWARE DEVELOPMENT ORGANIZATION FIGURE 2



PROJECT WORK FLOW

FIGURE 3



REFERENCES

1. W. T. Mitchell, "Space Shuttle Main Engine Digital Controller", Conference on Advanced Control Systems for Aircraft Powerplants, Proceedings No. 274, North Atlantic Treaty Organization, 1979.

2. R. M. Mattox, J. B. White, "Space Shuttle Main Engine Controller", NASA Technical Paper 1932, November 1981.

3. W. T. Mitchell, R. F. Searle, "SSME Digital Control Design Characteristics", Space Shuttle Technical Conference, NASA, JSC, June 28-30, 1983.

N85
16892

UNCLAS

D3 N85-16892

SHUTTLE AVIONICS SOFTWARE DEVELOPMENT TRIALS, TRIBULATIONS, AND SUCCESSES: THE BACKUP FLIGHT SYSTEM

Edward S. Chevers
NASA Lyndon B. Johnson Space Center
Houston, Texas 77058

THE BACKUP FLIGHT SYSTEM REQUIREMENT

The initial design of the Orbiter flight control system was limited to the quad-redundant computer complex. Systems management and nonavionic functions were contained in a fifth computer, which was not considered flight critical. This concept was well into development when a blue ribbon panel was asked to review all aspects of the Approach and Landing Test (ALT) phase of the Space Shuttle Program to verify that the design was proper. One of the conclusions reached by the panel was that an unnecessary risk was being taken by not providing a backup flight control system for the first flight. This decision was based on the relative complexity of the computer synchronization scheme being implemented and the lack of a direct manual flight control capability.

It must be remembered that the ALT development occurred during the early seventies when microprocessors as such did not exist, only four-bit arithmetic chips were available, and software consisted mostly of punched cards implemented in batch mode on a ground computer. Of course, man had gone to the Moon in an Apollo spacecraft and used a digital computer for navigation and guidance, but there was also an analog flight control system onboard with both automatic and manual modes available. Beyond that, a manual direct mode enabled bypassing all the electronics and powering the reaction jets directly. Thus, the step forward to a total computer-controlled flight system was very significant and risky according to the blue ribbon panel. Therefore, they recommended a backup mode for ALT.

That was the background behind the decision to add the backup flight system (BFS). Initially, it was to be a very simple system installed for ALT only and deleted once confidence had been developed in the primary flight system. The word simple is very important because one of the main concerns was the NASA capability to properly verify the large software programs being developed for the Orbiter. The development of the primary flight system software is addressed in a companion paper; therefore, that area is not discussed further here.

THE BFS IN THE APPROACH AND LANDING TEST PHASE

The approach taken for the BFS was to develop a very simple and straightforward software program and then test it in every conceivable manner. The result was a program that contained approximately 12 000 full words including ground checkout and the built-in test program for the computer. The flight control portion of the software consisted of approximately 6000 words. The remainder was for the systems management functions, which still had to be performed in the fifth computer along with the backup autopilot functions. The BFS ALT configuration is shown in figure 1.

Because of the relatively simple program involved, several decisions were made that had major impact later in the Space Shuttle Program. First, Rockwell was given the contract for the BFS and the contract was an amendment to the vehicle contract. Technically, this arrangement meant that the BFS was delivered to NASA as part of the vehicle and not as an independent entity like the primary flight system software. This difference was not significant in ALT since the BFS had a unique set of hardware, the software program was small, and much of the testing was done on the vehicle. During the Orbital Flight Test (OFT) phase, when the BFS software grew to almost 100 000 words, it became very difficult to equate the primary and backup software verification efforts and to break out the BFS software as an independent deliverable product. Second, and even more significant with time, was the decision to not provide a BFS software development and verification facility at Rockwell. Here again, it was a logical and proper choice for the ALT BFS but unsatisfactory from the standpoint of long-term programmatic effects. This subject is addressed later in discussions concerning the BFS in the OFT phase of the program.

To perform verification, a series of tests was defined using the actual flight-type hardware and simulated flight conditions. Then, literally hundreds of simulated flights were flown and detailed performance analysis was conducted. The intent of most BFS tests was to demonstrate that a stable flightpath could be obtained after engagement from an anomalous initial condition. In fact, the early ground rule for BFS was to stabilize the vehicle long enough for the crew to bail out. Later, the importance of completing the mission was stressed. Since the tests did not have to run from separation to touchdown every time and the ALT flights lasted less than 30 minutes, quite often it was

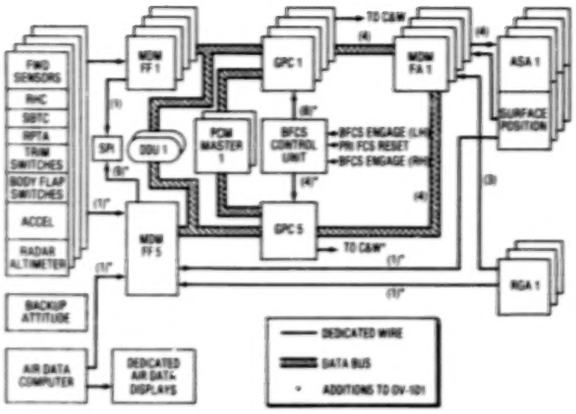


FIGURE 1.- BACKUP FLIGHT SYSTEM CONFIGURATION.

- CERTIFICATION PLAN
- SCHEDULE
- CSDL TESTING
  - STATIC
  - DYNAMIC
- ADL TESTING
  - OFP CHECKOUT
  - SOFTWARE/HARDWARE INTEGRATION
  - PARALLEL SYSTEM OPERATION
  - SYSTEM DEMONSTRATION
- SAIL TESTING
  - SOFTWARE/HARDWARE INTEGRATION
  - SOFTWARE VALIDATION
  - SYSTEM VERIFICATION
- OV-101
  - GROUND
  - TAXI
  - FLIGHT

FIGURE 2.- BACKUP FLIGHT SYSTEM TESTING.

possible to run five or six tests per hour by merely changing the initial conditions. Figure 2 contains an overview of the tests performed on the BFS.

With a well-documented set of requirements, a software program that was easy to understand, a dedicated set of hardware for performing tests, and a combined Rockwell/NASA team of less than 50 compatible people, the ALT BFS could be called "the ideal program." Any proposed changes from either Rockwell or the NASA Lyndon B. Johnson Space Center (JSC) had to be justified. Changes were not allowed just because they made things easier or took less code or ran faster in the computer. A significant improvement in system capability and a requirement for the improvement had to be demonstrated before a modification was allowed.

One change that was made before the first ALT flight was the technique for acceptance testing of the software. As stated earlier, the BFS was delivered as part of the vehicle, but it was always recognized that separation of the software from the total system was desirable from a contractual standpoint. To accomplish this separation, Rockwell combined with Intermetrics in development of a FORTRAN simulation of the BFS that would run on a ground-based computer. The program emulated the AP-101 flight computer and executed the programs one minor cycle at a time. The input data being used in the emulator and output commands computed from these data were collected each minor cycle along with cycle counts, error logs, status words, and other pertinent internal computer parameters. These data were then fed into buffers in multiplexer-demultiplexer (MDM) simulators in a Shuttle Avionics Test Set (SATS), which could be connected directly to a flight computer. The flight computer then accessed the data buffers by using actual MDM address codes and did computations based on the data acquired. The general-purpose computer (GPC) outputs were collected each minor cycle and stored for comparison with the precalculated results from the Intermetrics emulation program.

Many will recognize this technique as being the equivalent of the flight equipment interface device (FEID) used with the flight computers in the JSC Software Development Laboratory (SDL). The primary difference was that the BFS technique was used for final tape verification rather than for software development. Every parameter in the emulation program and in the calculated answers was carried out to the full 32-bit word size in the ground processing computer. The flight computer results were also dumped as 32-bit words, and complete bit-for-bit comparison was made during postprocessing. Only the last 2 bits of each 32-bit word were allowed to be different before a failure was noted. This technique was the precursor to the captive simulation (CAPSIM) procedure used by the BFS for verification during the OFT flight phase.

THE BFS IN THE ORBITAL FLIGHT TEST PHASE

As the ALT phase of the program neared completion and attention was turned to the OFT phase, several conditions became apparent. First, a large portion of the primary flight system software development for ALT was unique to that portion of the Space Shuttle Program and could not be used during OFT. Second, a backup flight system was going to be required and it would have to operate during both the ascent and the descent portions of the mission. Since some abort options required a once around the Earth abort or an abort to orbit before reentry, navigation and guidance would have to be added to the BFS. Suddenly, the BFS had matured to a full guidance, navigation, and control (GN&C) system and some of the early ALT decisions became very important. As indicated by figure 3, the BFS no longer is limited to a small subset of dedicated hardware. The BFS GPC is in parallel with

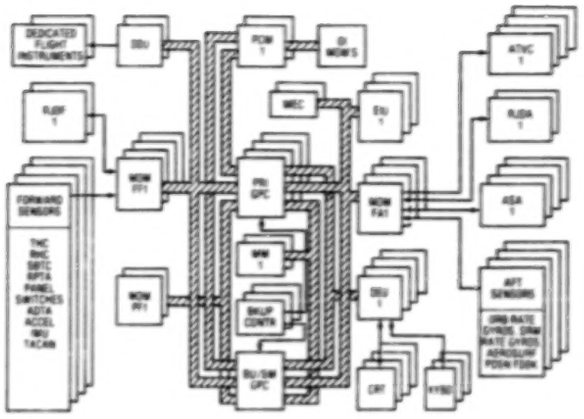


FIGURE 3.- ORBITER 102 PRIMARY/BACKUP FLIGHT SYSTEM.

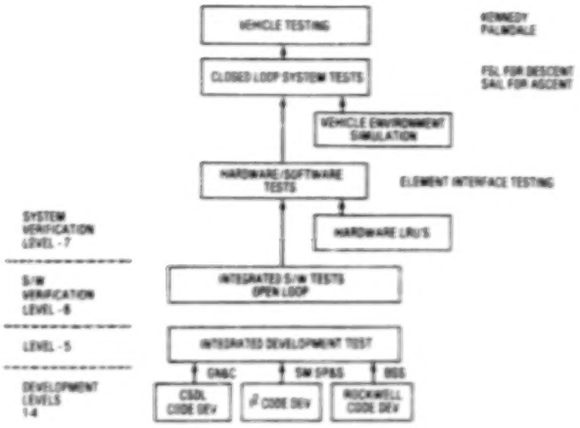


FIGURE 4.- BFS DEVELOPMENT AND VERIFICATION TEST LEVELS.

the primary flight system computers and has full access to all sensor inputs and effector output changes after engagement.

As mentioned previously, there was an early decision by both Rockwell and NASA program management to not provide a software development facility at Rockwell for the BFS. When couched in the context of BFS being used only for ALT and never again, that decision was certainly proper. However, for OFT, there was a requirement to develop a full-blown BFS with GN&C, systems management (SM), sequencing, and display capability. Experience with the primary flight system during ALT had shown that developing the primary flight system software and the SDL simultaneously was almost an unmanageable effort. Each task was major in regard to the number of highly trained specialists necessary, and the level of management ability needed was not available at the beginning of the ALT phase.

Now, the BFS was faced with the same dilemma: how to bring together the massive resources required to develop some of the most sophisticated software ever attempted while imposing the most stringent safety and reliability specifications ever conceived. Although the decision may have been based more on ALT problems than on pure logical reasoning, it was decided that having one contractor do all programing was not the best choice. Therefore, C. S. Draper Laboratories (CSDL) was selected to program the GN&C, Intermetrics would program the SM, sequencing, uplink, and ground checkout functions, and Rockwell would program the operating system, the displays, and the overall integration. As prime contractor, Rockwell was also responsible for total system verification. The various levels of integration and verification required by the BFS are shown in figure 4. With the software tasks broken into three approximately equal sized portions, everything should have gone along in parallel until it came together again at the end in a nice, neat package. The first indication of trouble appeared when CSDL had to spend a considerable amount of time developing their best guess of how the backup system software (BSS) would work. This research was necessary since much of the GN&C is input/output (I/O) oriented and depends on the timing established by the BSS. Intermetrics developed preliminary sequencing codes but could not perform any dynamic verification because most of the sequences were dependent on guidance and navigation events for which programing had not been done by CSDL. Rockwell could not spend full time on the BSS because most of their time was spent resolving integration problems among all three sections of the software. In addition, JSC began asking Rockwell for their system integration and verification plan and the issue of software validation was drawing increased attention.

It was in this time frame that the CAPSIM technique became a predominant feature in BFS verification. The technique was similar to the emulation program used in ALT but was revised to use actual code to generate the output data for the comparison program. Precalculated inputs were used as drivers and placed in the input compools or buffer areas of the computer. The GN&C and sequencing code accessed these inputs and performed their minor cycle computations. Output results including actuator commands and display signals were then put into output compools, where the data were collected and stored on tape. All of this was done at CSDL using actual GN&C, sequencing, and, later, SM flight code, but still with the CSDL version of the operating system. The other limitation was in use of the CSDL statement level simulator (SLS), which is a non-real-time development tool and thus would not detect marginal timing conditions or dynamic interactive timing problems between different software modules. The CAPSIM data generator procedure is depicted in schematic form in figure 5.

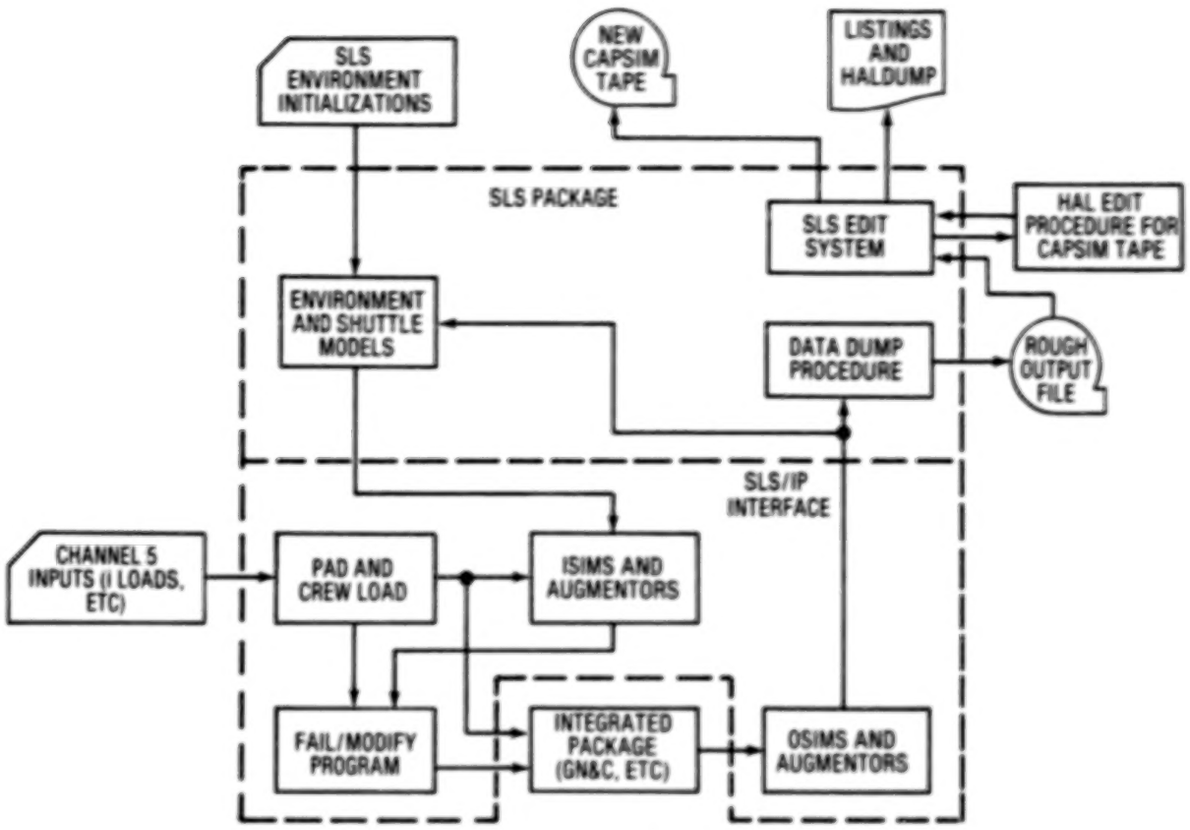


FIGURE 5.- CAPSIM DATA GENERATION.

The next step was to integrate the Draper, Intermetrics, and Rockwell portions of software into a single load tape for verification at Downey. Computer test sets and mass memory units were not available for general-purpose use; therefore, a test set tape was made that could be loaded into the flight computer from a SATS unit. The tape format was tailored to the requirements of the specific computer in the SATS; therefore, the test set tape was different from the final mass memory load tape which would be required at JSC. With the flight computer loaded and cabled to the SATS, the operational BFS was ready for the simulated input data from the CAPSIM program, and, as anticipated, operation was not smooth initially. The evaluation procedure involved collecting the output buffer data each minor cycle from the flight computer and then comparing the tabulated data with equivalent data sets from the CSDL tests.

Approximately 25 test points in ascent and 20 in descent were selected for comparison. Continuous comparison was not possible at first because no automated plotting programs were available. These programs were developed after 6 to 8 months of the effort and later included dual comparison on the same plot. If all of this history seems archaic, remember that the BFS started from scratch and had to compete with the primary system for resources and time on any existing facilities. During the first 6 months of CAPSIM testing, the BFS was a virtual basket case. When output data were compared, there were times when it was impossible to determine whether they were from the same program. One of the main problems consisted of the initial condition values used at CSDL and Rockwell. The guidance and navigation programs were very sensitive to the data-base parameters, and as many as five or six different versions could exist at any given time in the various JSC, CSDL, and Rockwell facilities. The problem is not major in terms of gross performance of the flight system, but when two different facility tests were overlayed and every discrepancy had to be accounted for, a considerable amount of time was wasted in trying to explain away what could be a minor difference. Of course, in the beginning, no one was sure whether a minor difference was insignificant or an indication of a potential major software coding problem.

With time, as everyone began to get a better feeling for the differences in output results and more of the process became automated, dual comparisons between the BFS and the primary flight system also were begun. One of the cost-saving features of BFS verification was the so-called "piggyback"

mode of operation, in which the BFS was to use all applicable data from the primary flight system and eliminate duplication. The results of one test case showed very close correlation between the primary and the backup systems and both were found to be wrong. The problem would not have had a major impact on the flight but did serve to show the danger in not performing total independent analysis. Afterwards, the BFS people were careful to spot check more test cases and to perform some independent analysis.

Although the CAPSIM technique was the primary verification tool for the BFS, it did have one serious shortcoming. The test case scenarios were from a cataloged set of runs at CSDL which had been based on primary flight system testing. Again, this procedure was in accordance with direction to control development cost and maximize use of existing primary flight system information. The concern that arose was based on the fact that the BFS would only be engaged after a massive primary flight system failure. Therefore, the initial conditions could quite possibly be at the limits of the normal primary GN&C boundary conditions and very few BFS test runs were made from these very abnormal conditions. Therefore, approximately 100 additional "stress cases" were developed to be run in the Flight Simulation Laboratory (FSL) in Downey and the Shuttle Avionics Integration Laboratory (SAIL) at JSC. By combining multiple objectives into one test run, the final number of individual test runs was refined to 37. Every one of these tests was unique and required special downlist data formats for additional visibility, and all data analysis was manual. Since these tests were to be performed one time as a final safety verification check before the first OFT flight, automated data processing could not be justified. All but a few of these tests were performed successfully, and failure of the few was due to procedural errors or to a misunderstanding of the intent of the stress condition. However, adequate data were collected to give the Shuttle community a high level of confidence in the capability of the BFS to meet its intended objectives for the first orbital flight.

Some of this confidence waned on launch day, when the BFS failed to synchronize with the primary flight system a few hours before lift-off. However, the shock to the BFS developers quickly disappeared when it was determined that the problem was due to a timing error in the priuary system and that, in fact, the BFS recognized the problem and was trying to inform the launch team that an anomaly existed. When the problem was identified and fully analyzed, it was shown that the mission could have been flown successfully even with the interface timing error. The BFS would have bypassed the data being sent in the wrong time slot and corrected itself after engagement had that been necessary. However, those facts were not available for several days after the launch. A modification was made, the flight was highly successful, and considerable relief was expressed by all involved. The primary flight system people said they knew all along the BFS would not be needed but were glad it was there. The BFS people said they knew they were ready to take over and save the mission but were glad they did not have to do it.

CONCLUDING REMARKS

The BFS has never been required to demonstrate its capability. A proposed on-orbit engagement and orbital maneuvering system (OMS) engine burn has now been deleted from the list of flight test requirements. This change is partly the result of a very full and busy flight plan and partly of the high confidence level which exists in the capability of the BFS to perform when required. Although most of the people who worked on the backup flight system would like to see it used, I consider it a supreme compliment from the Program Office and the Flight Directors to accept the system on the faith of the development and verification program. This acceptance is a tribute to the people and organizations who put so much of themselves into the project for many years.

SUMMARY

In retrospect, several factors or lessons learned in the BFS evolution stand out prominently. Neither the NASA nor anyone else should ever attempt to develop a software program approaching 100 000 words in size without having the development facilities in place, especially when the requirement is for zero-defect software code. In addition to the basic facility, the software analysis and support tools should be available throughout the project, not near the end. It will always be difficult to convince a program manager that he should put a sizable amount of his money into a facility initially for the purpose of saving money several years downstream. But no NASA or contractor program manager should again have to experience the trials and tribulations that existed for the primary flight system in ALT and the backup flight system in OFT. In the end, the only glory is in success.

FLIGHT SOFTWARE FAULT TOLERANCE VIA THE BACKUP FLIGHT SYSTEM

Terry D. Humphrey and Charles R. Price
NASA Lyndon B. Johnson Space Center
Houston, Texas 77058

ABSTRACT

A generic software error in the quadruply redundant primary flight system could result in the catastrophic loss of Space Shuttle vehicle control in the hostile environment of ascent or reentry. The Space Shuttle backup flight system was designed to protect the crew and vehicle in this eventuality. The significant challenges met in the design and development of this state-of-the-art protective system is the subject of this paper.

INTRODUCTION

Implementation of the backup flight system (BFS) for the Space Shuttle is a major advance in state-of-the-art fault-tolerant software in general and in Space Shuttle fault-tolerant flight software in particular. The BFS was chartered to protect against a software fault in the most sophisticated flight software system ever implemented: the Space Shuttle primary flight software (PFS). The PFS is designed to operate a redundant set of general-purpose computers (GPC) to control an innovative, multiple-element, reusable, manned spacecraft through an ensemble of flight regimes never before encountered by a single vehicle. For STS-1, the PFS consisted of more than 400 000 computer words of flight code, a complete test of every possible combination of branch instruction or decision point of which would take more than 10 000 years of computer time on today's fastest computers.

To protect against a latent programing error (software fault) existing in an untried branch combination that would render the Space Shuttle out of control in a critical flight phase, the BFS was chartered to provide a safety alternative. The BFS is designed to operate in critical flight phases (ascent and descent) by monitoring the activities of the Space Shuttle flight subsystems that are under control of the PFS (e.g., navigation, crew interface, propulsion), then, upon manual command by the flightcrew, to assume control of the Space Shuttle and deliver it to a noncritical flight condition (safe orbit or touchdown). Many technical, managerial, and operational challenges were experienced by the development team of NASA and its contractors in bringing the BFS from a concept to a working operational system. The challenges addressed herein are those associated with the selection of the PFS/BFS system architecture, the internal BFS architecture, the fault-tolerant software mechanisms, and the long-term BFS utility.

CHALLENGE 1: A MANAGEABLE SYSTEM ARCHITECTURE

Central to any concept of a reusable spacecraft is the theme of higher system reliability through redundancy of finite-lived components. In the Space Shuttle avionics, the availability of a properly functioning flight computer is assured through the wiring of five identical GPC's in parallel. Since the memory available for state-of-the-art GPC's at the beginning of the Space Shuttle development cycle was much less than the flight software requirements dictated, an early partitioning scheme was established. For each of three flight phases (ascent, on-orbit, descent), a redundant copy of all critical functions was loaded in each of four GPC's and the fifth GPC was loaded with a complement of useful functions the loss of which could be tolerated. This strategy assured protection from multiple, sequential computer hardware failures, but did not address the possibility of a software fault generic to the set of four redundantly programed GPC's causing loss of control of the Space Shuttle. Concern for such a software fault is valid in that regardless of the number of checks and balances that are put in place to find and eliminate specification and coding errors in major software developments, there can be no 100-percent assurance that latent, potentially dangerous software errors do not exist in the delivered product.

The obvious strategy for increasing the software reliability of the Space Shuttle was through software redundancy, but the challenge of the problem was the form of the redundancy to implement within time and cost constraints. Three redundancy alternatives were available: (1) increasing the internal PFS redundancy; (2) duplicating the PFS in another software version programed by a different set of programers completely isolated from the PFS programer, or (3) implementing a reduced-capability backup system by a semi-isolated set of programers. The first alternative was not pursued because it was felt that every practical internal measure was already being pursued by the PFS designers. The second alternative was considered too costly and fraught with duplication of functions not essential for a secondary system. The third alternative was selected since it afforded an additional measure of protection that was achievable within cost and schedule constraints. The reduced capability was

set by a single memory load for both ascent and descent in a single GPC. The BFS also assumed the non-flight-critical functions that had been scheduled for the nonredundant fifth GPC for ascent and descent. The semi-isolation of the programers was achieved by having the BFS programed by a contractor geographically separated from the PFS contractor.

THE BFS FAULT-TOLERANT ARCHITECTURE

Significant challenges were faced by the designers to develop a BFS which would closely track the PFS, protect itself and the PFS from data pollution from each other, and also be ready at any point in the ascent, abort, or descent profile to take over control of the vehicle safely when manually engaged by the crew. To provide this capability, a technique had to be developed that would provide for tight synchronization of the BFS to the PFS in order to prevent divergence, but that would also protect both from inducing faults in the other. A more pollution-protective technique than that used for PFS redundant-set synchronization had to be developed. To protect the PFS from faulty BFS data or timing, this technique would permit no transfer of data from the BFS to the PFS.

An innovative technique for synchronization of the BFS and the PFS was developed using flight-critical data bus input profile tracking of the PFS that involves use of the input/output processor (IOP) input data bus listen capability and the transfer of input profile and minor cycle data from the PFS to the BFS. The BFS protects itself from pollution by erroneous input profile data by voting on the redundant data sent to it by the individual PFS GPC's. In addition, the BFS protects itself from input profile timing faults of the PFS by the use of its own data bus timing window thresholds for each of the individual groups of input profile data.

To protect the BFS and PFS from pollution by erroneous data received from one another, an interface design policy was established which allowed no transfer of software-generated data from the BFS to the PFS but did allow data absolutely essential to the proper tracking of the PFS to be transferred and used by the BFS. The absence of data transfer to the PFS prevents any pollution of the redundant PFS by the BFS. The BFS was designed to protect itself from pollution from erroneous PFS data first, by being limited to the use of a small amount of absolutely essential transfer data; second, by performing a vote on the redundant sets of data obtained from the redundant PFS GPC's; and third, by performing reasonableness checks on the voted data.

Another challenge faced in the development of the fault-tolerant BFS was the design of a safe method of taking control of the vehicle at any point in the flight profile without inducing control effector transients which might endanger the crew and the vehicle. The design developed to provide this protection required the input of engage initialization data from the subsystems via the flight-critical data buses immediately after BFS engagement. These data were then used to ensure that subsequent BFS control commands did not overstress or generate significant transients on the control effector subsystem.

One of the foremost innovative techniques used in the BFS fault-tolerant design was developed to provide for recovery from the loss of PFS-generated master events controller (MEC) sequencing as well as for attempting recovery from BFS GPC hardware or software errors. The loss of MEC sequencing commands might occur either as a result of a generic PFS software failure or as a result of the abrupt termination of all PFS-controlled flight-critical data buses at BFS engagement. Recovery from these types of errors is provided by the BFS software restart technique. A software restart is initiated upon BFS engagement, and, in the event that critical MEC command sequences are found not to have been properly performed, the BFS reinitiates the full MEC sequence of commands for the appropriate mission event.

The use of the restart technique to attempt recovery from BFS GPC hardware or software errors was developed to protect the BFS from transient errors and, in the case of hard errors, to continue attempts at recovery in hopes that the error will not persist. This restart recovery involves reinitialization of input/output (I/O) and restarting of BFS application processing at the beginning of a new GPC major processing cycle. The restart recovery technique provides this protection for both the preengaged and engaged modes of BFS operation.

A MOVING TARGET: MAINTAINING TRACK OF SOFTWARE CHANGES

Unlike the Approach and Landing Test (ALT) PFS, the BFS for ALT could not be used as a base upon which to build Orbital Flight Test (OFT) software. The BFS software for ALT was designed and developed by Charles Stark Draper Laboratories and provided backup for flight control functions only, provided no CRT/crew interface, and provided only a very minimal task-list-type executive. Rockwell was selected to develop the BFS for OFT and essentially started anew about 2 years behind the PFS

software development. A new operating system had to be designed and developed, all existing PFS requirements and change requests (CR's) had to be reviewed for applicability to the BFS, and an overall BFS software design had to be developed. The BFS not only had to catch up with the PFS level of maturity very quickly, but then had to maintain pace with a very large amount of PFS requirements development and software change activity. A significant amount of effort and manpower was required to accomplish this goal.

POST-OFT UTILITY OF THE BACKUP FLIGHT SYSTEM

The BFS was initially envisioned to be used only through the Shuttle OFT flights. The expectation was that after OFT, the entire Shuttle system design, including PFS software, would be proven safe for operational use and, therefore, the BFS would no longer be needed. Close to the end of OFT, an examination was undertaken to assess the need for continuing the use of the BFS. Assessments of the PFS software discrepancy report (DR) traffic showed it to correlate proportionally to the level of PFS software change traffic but, even in cases in which software change traffic was small, the number of DR's appeared to decay exponentially rather than to drop abruptly. These data indicated that latent software errors had high levels of persistence. This information was used in conjunction with the projections of PFS software change traffic for future flights. It was determined that for a significant time in the future, the PFS software change traffic would continue to remain at significant levels and therefore the risks would remain high for latent PFS software errors. Therefore, it was concluded that for at least a significant time in the future, the BFS would be needed to protect against generic PFS software faults.

BIBLIOGRAPHY

Rockwell International Specification: Backup Flight System Program Requirements Document Overview. Rockwell International MG038100, 1979.

Rockwell International Specification: Primary Avionics Software System (PASS) and Backup Flight System (BFS) Software Interface. Rockwell International ICD-3-0068-03, 1981.

Rockwell International Specification: Backup System Services Program Requirements Document. Rockwell International MG038101, 1982.

N85
16893

UNCLAS

D4

N85-16893

SSME DIGITAL CONTROL DESIGN CHARACTERISTICS

Walter T. Mitchell/Richard F. Searle
NASA/Rocketdyne

National Aeronautics and Space Administration
Marshall Space Flight Center, AL

ABSTRACT

The Space Shuttle Main Engine (SSME) presented new requirements in the design of controls for large pump-fed liquid rocket engine systems. These requirements were the need for built-in full mission support capability, and complexity and flexibility of function not previously needed in this type of application.

An engine mounted programmable digital control system was developed to meet these requirements. The engine system and controller and their function are described. Design challenges encountered during the course of development included accommodation for a very severe engine environment, the implementation of redundancy and redundancy management to provide fail-operational/fail-safe capability, removal of heat from the package, and significant constraints on computer memory size and processing time.

The flexibility offered by programmable control reshaped the approach to engine design and development and set the pattern for future controls development in these types of applications.

INTRODUCTION

Development of controls for the Space Shuttle Main Engine (SSME) presented many new engineering challenges which had not been previously faced in the design of controls for large pump-fed liquid rocket engine systems. Notable among these challenges were:

1. A requirement for built-in full mission support capability from the early checkout phases through main engine cutoff and propellant dump during flight.

2. A need for flexibility and complexity of function not previously attained in any liquid rocket engine system.

Most of these challenges were the direct result of a new orientation in control system requirements for rocket engines brought about by the unique requirement of the Space Shuttle for a reusable and maintainable man-rated system.

The following sections, review requirements and give a general description of the control system. Some of the major alternatives considered are discussed along with reasons for selecting the final configuration. Development problems are reviewed and development experience evaluated.

DISCUSSION

CONTROL SYSTEM REQUIREMENTS

The SSME control system must support engine utilization during all phases of the mission sequence from checkout through propellant loading, liftoff, flight and shutdown in orbit. It is required to have the capability of self-contained checkout in the assembly area, and at the launch area prior to flight. The control system must also support engine start preparations, provide repeatable start, mainstage control, and shutdown upon vehicle command. In addition, it must have the ability to monitor engine critical operating parameters (redlines), provide fault detection, manage redundancy and report engine status conditions during all phases of operation.

The control system is required to vary engine thrust upon vehicle command between 65 and 109% of Rated Power Level in 1% increments while maintaining mixture ratio within specification. Rated Power Level (RPL) is 100%, while Full Power Level (FPL) at 109% can be commanded when vehicle conditions require it.

Require[d] thrust precision is +-6000 lb (3 sigma) during steady-state operation. Thrust must be within ste[p] size limits within 1 second after a commanded change without rate of change exceeding 7000 lb/[s]. Mixture ratio accuracy is required to be within +-1%. The engine must be capable of accel[erating] from start signal to RPL in 3.9 seconds with mixture ratio within tolerance in less th[an] seconds.

Requirements include on-board checkout capability, redundancy verification, and status monitoring for systems verification during ground and flight operations. Rapid fault isolation techniques are required which activate or deactivate redundant components without unduly disturbing engine operation. The control system is also required to provide automatic checkout of engine functional components with fault isolation to Line Replaceable Units (LRU) during ground checkout to minimize vehicle turnaround time, and to be capable of subsystem replacement without engine recalibration.

All critical electrical elements of the control system must be redundant for a fail-operational/ fail-safe design.

ENGINE AND CONTROL SYSTEM DESCRIPTION

The SSME is a reusable, high performance, Liquid Hydrogen/Oxygen, rocket engine designed and produced by the Rocketdyne Division of Rockwell International under contract with Marshall Space Flight Center. It has four turbopumps (two low-pressure and two high-pressure), two preburners, a main combustion chamber, five hydraulically actuated propellant control valves, sensors, and an engine mounted electronic digital controller. The staged-combustion cycle burns low mixture ratio propellants in the preburners first. These fuel-rich gases are used to drive the high-pressure turbopumps and are then routed to the main combustion chamber where they are burned with additional oxidizer to obtain maximum performance.

Performance control is closed-loop feedback control with full authority over the engine operating range. The control block diagram is illustrated in Fig. 1. Thrust and mixture ratio control are provided by adjusting the power to the two high-pressure turbopump turbines through control of the oxidizer flow to the preburners with modulating preburner oxidizer valves. Thrust control is provided by modulation of the oxidizer preburner oxidizer valve, and mixture ratio control is accomplished by modulation of the fuel preburner valve. Cross-feed compensation from the oxidizer preburner valve command to the fuel preburner valve is used to minimize the effects of thrust transient changes on engine mixture ratio. In addition to the two preburner valves used in performance control, three other propellant valves are scheduled to initiate propellant flow during start and to assist in control of shutdown. In addition the chamber coolant valve is scheduled as a function of thrust to prevent overheating in the nozzle and combustion cooling circuit as the engine is throttled. More detailed descriptions of the control logic and hardware are contained in Ref. 1 and 2.

The controller, which was designed and manufactured by Honeywell, Incorporated, is mounted on the side of the main combustion chamber. It is a single, integral electronics package containing dual programmable digital computers, each with 16384 words of memory. The Honeywell HDC-601 digital computer with 2 mil plated wire memory is used in the controller. Input electronics, computers, power supplies, and output electronics are dual redundant, Fig. 2, with cross-strapping at the input and output of the computer electronics. Installation characteristics are listed in Table 1. The controller interfaces (Fig. 3) with 67 sensor inputs and 43 output device channels. Controller to vehicle interfaces include 3 redundant vehicle command channels, 2 status recorder output channels, 2 redundant power channels, and a 28 vdc input for heater operation in orbit. The status recorder channels transmit 128 data words every 40 milliseconds to the vehicle data bus.

DESIGN ALTERNATIVES AND DEVELOPMENT CONSIDERATIONS

Controller Location and Mounting

Both mechanical and electrical problems were experienced during the design and development. Early studies clearly showed the controller should be engine mounted to provide an integral complete engine system and to avoid routing in excess of four hundred wires across the gimballed engine interface. Presently there are a total of twenty three wires across the interface for power, commands, memory loading, status data, controller heater power, and analog temperature measurement.

The controller was initially designed to be hard mounted vertically against the thrust chamber with a requirement to meet a 22.5 grms vibration environment. This was a very severe constraint on controller mechanical design so the controller mounting was subsequently changed to use rubber inserts which reduced the vibration environment to approximately 4 grms.

Digital Versus Analog and Hardware Software Partitioning

Although the selection of digital versus analog implementation of control logic would be heavily weighted in favor of programmable digital today, the case was not so clear-cut in 1970 when decisions of this nature were being made. However, the complexity of functions and need for ease of change in logic during the early phases of engine development weighted the decision towards digital programmable controls. The valve positioning curves of Fig. 4 are an illustration of the case in point. All five engine propellant valves are commanded to multiple positions during the start sequence. Up to seven different positions and rates are commanded to each propellant valve during the 3.9 second engine start sequence. The parameters for these valve positioning commands were changed many times during the engine development program in order to obtain the desired start characteristics.

Complexity and immaturity of the control algorithms and checkout functions also required the flexibility of a programmable system. In addition, calibration factors unique to each engine were required to be stored and utilized by the controller.

Packaging and Heat Removal

The controller electronics are mounted on conventional printed circuit cards. The printed circuit cards are retained in the controller chassis by a rigid foam packaging system which further isolates the electronics from the vibro-acoustic environment of the engine. In this packaging system, the chassis is divided into cavities, each of which accepts two cards. Each card has an open foam grid attached to the component mounting side and a foam half-wedge attached to the back side.

The cards are retained in the chassis cavity by loading a foam wedge between the two cards. This provides for very tight card retention as well as isolation from vibration transmitted through the chassis and it detunes the printed circuit card/chassis structure system. This protected the modules from vibration but created a problem in dissipating the heat from the cards. A design change was made so that the foam grids, which are in contact with both the printed circuit cards and chassis walls, have an aluminum foil surface which provides heat transfer from the electronic parts. Cooling is accomplished by conductive heat transfer through the chassis and convection heat transfer from the chassis surface to the atmosphere. Additional chassis surface area is obtained by extensive use of pin fins machined into the chassis.

Electrical and Memory Problems

Other notable problems were the memory system and power supply. Plated wire was selected for the memory based on speed, power, non-volatility, and non-destructive readout. At the time of design, five mil diameter wire was being used on several programs. However, two mil wire was selected for the controller to reduce size and power. Many problems were encountered in the development of the memory system until a "coupled film" plating was developed and used on both the SSME and Viking programs.

Input power to the controller was selected to be 115 volt, 400 Hz three-phase in preference to 28 vdc. A small transformer on the input provides power for operating the power supply. The primary load is three-phase full-wave rectified resulting in 270 vdc to be switched by the switching regulator. Potential faults on the input bus from other users resulted in a requirement to be able to operate down to 95 volts rms for up to one second. A boost stage regulator was employed to accommodate this requirement. A problem of high current demand of engine solenoid loads during power recovery and engine start operation was solved by dividing the solenoids into banks. The biggest problem of all in the power supply was packaging the unit in the space available.

Software Design

Software program organization as it finally evolved is illustrated in Fig. 5. Because of computer memory size constraints three types of program configurations are resident in memory at different times depending upon the phase of mission operations. Changes in configuration are accomplished by use of "roll-in" modules of code which overlay pre-existing code and change controller function. All coding is in DAP-16 assembly language.

The ground checkout configuration is used during component checkouts. This configuration has five sub-configurations, each designed to facilitate automated checkout of different elements of the engine and controller such as actuators, pneumatic solenoid valves, sensors, ignitors and redundancy.

The flight readiness test (FRT) configuration is used to perform an extensive system test of the engine and controller without initiating powered operation of the engine. This test configuration includes a simplified digital dynamic model of the engine which produces simulated pressures, temperatures and flows in response to measured engine valve positions. These simulated parameter values are substituted for actual sensor readings and used by the controller to "run" the engine with the same logic as used in powered operation during flight.

The flight configuration is used for engine start preparation, start, and all flight operational phases.

Dominant constraints on software design were process time and memory size. Dynamic simulation studies of the engine system early in the program demonstrated that a major cycle (control iteration) time of .02 seconds or less was necessary in order to provide adequate control response capability in the event of certain types of oxidizer preburner oxidizer valve actuator failures. Worst case major computation cycle time grew rapidly in the early years of the program, reaching .018 seconds in the first few years. An on-going effort was necessary to hold the line on this parameter.

Program size grew much faster and larger than ever seemed reasonable to anticipate given the requirements as they were understood at the beginning of the project. At the very beginning it was estimated that 8000 words would be sufficient for all program requirements, so 12000 words memory capacity was proposed. Requirements to vote variable commands from the orbiter with software rather than hardware, requirements to do an FRT, and other changes necessitated expanding the memory to 16000 words. Fig. 6 documents memory requirement estimates over the 11 year life of the program.

Early phases of program size growth were, to a great extent, the result of maturing of system requirements as detailed engine hardware design and development progressed. Program size initially grew rapidly as the complexity of checkout requirements increased. This early rapid growth resulted in a decision in mid-1973 to separate checkout functions from the flight portion of the program and to implement the roll-in module concept. The roll-in concept was further implemented late in 1974 with the conversion of the sample problem element of the software to a roll-in module.

Since 1976 there has been a continuous effort to work within the memory size constraint. Design scrubs are necessary in order to allow implementation of new requirements. In the course of development 12 major software program versions have been issued with many more interim revisions. Maximum resident code today is 15696 16 bit plus parity words. Total program code including roll-in modules is 23349 words. Over 200,000 words of code have been implemented or rearranged in the course of the software effort.

A more detailed discussion of avionics software development is presented in Ref. 3.

Control System Integration

The SSME control system is a complex hardware/software system. Extensive analysis and testing was necessary to develop and verify the control system hardware/software implementation. Detailed digital and analog modeling studies were performed at Rocketdyne to characterize engine control characteristics. These studies were extended at Honeywell in detailing the controller design. Extensive simulation testing of the control system was performed at Honeywell using an analog model of the engine and a Command and Data Simulator to simulate the orbiter interface. More recently the majority of the control system testing has been accomplished at the Huntsville Simulation Laboratory (Ref. 4). This laboratory employs actual flight configuration control system hardware (controller, sensors, actuators, etc.) interfaced to a hybrid analog/digital real-time engine system simulator.

The Simulation Laboratory provides a high fidelity test bed which allowed detailed integration testing of the control system prior to use in actual SSME test firings. Since the initiation of engine test firings, the Simulation Laboratory has continued to be extensively used for software verification and engine test support and more recently for flight support.

EVALUATION OF DEVELOPMENT EXPERIENCE

The SSME Digital Control System has been utilized for all engine test firings. As of this writing, 40 different SSME's have accumulated a total of over 1000 test firings, including 6 orbital flights, and over 50 hours of powered operation.

As the SSME system has matured through this program, many control system requirement additions and changes have been made. The flexibility provided by use of a fully programmable digital computer has allowed the majority of these changes to be accomplished by software modification. This has facilitated rapid change incorporation and verification (through use of the Simulation Laboratory) with only minor perturbation to engine test schedules.

Development of the SSME would not have been possible in a practical sense without the use of programmable digital control. Even though the introduction of operational software added a significant new cost element to rocket engine development, and cost saving benefits far outweighed the software costs. The very flexibility offered by programmable control, from the beginning of the program reshaped the approach to engine design and development. It is unlikely any pump-fed throttleable and reusable liquid rocket engine of the future will be designed without this approach.

The importance of good simulation of the engine system, fault insertion capability, the use of prototype hardware which can be easily modified, and the capability for memory history tracking cannot be over emphasized. These capabilities will be essential to cost effective and timely development of any future system of this nature.

There is never enough memory or, conversely, the program always expands to fill the space available. This situation is not necessarily bad. As the hardware aspects of a program mature the number of practical options to fix problems diminish. Software, as it matures, still retains the ability to absorb small changes on a short turn-around time basis. This factor should be given more weight at the beginning of a program. In the case of the SSME the nearly 300 percent increase in program size from original estimates was largely the result of immaturity of system requirements at the program onset. Unless the software requirements are well defined and mature from prototype system testing, program size estimate increases of 100 to 200 percent should not be surprising.

The existing controller program is, of necessity, in assembly language because of processing speed and memory size limitations. Recent developments in microprocessors and memories have made practical significantly faster processing speeds and greater memory capacity at no expense in size or power relative to the existing controller. If software requirements can be maintained within bounds these increased capacities may enable the use of higher order languages in future engine controllers, thus reducing the cost of producing software and increasing its reliability.

CONCLUSIONS

The requirements for the Space Shuttle Main Engine dictated a control system design that was unique to large pump-fed rocket engines. The digital programmable full-authority control implemented has demonstrated its ability to meet or exceed all mission requirements. The very flexibility offered by programmable control reshaped the approach to engine design and development. The success and benefits of this approach, demonstrated with the Shuttle Main Engines, have set the pattern for the future in development of controls for this type of application.

ACKNOWLEDGMENT

Appreciation is expressed for the assistance of Kenneth Hildreth, Project Engineer for the SSME Controller, in preparing this paper by providing written material and comments which contributed significantly to its content and value.

REFERENCES

1. W. T. Mitchell, "Space Shuttle Main Engine Digital Controller", Conference on Advanced Control Systems For Aircraft Powerplants, Proceedings No. 274, North Atlantic Treaty Organization, 1979.

2. R. M. Mattox, J. B. White, "Space Shuttle Main Engine Controller", NASA Technical Paper 1932, November 1981.

3. E. S. Chevers, "Shuttle Avionics Software Development--Trials, Tribulations, and Successes: The Backup Flight System", Space Shuttle Technical Conference, NASA-JSC, June 28-30, 1983.

4. H. G. Vick, P. Hampton, "SSME Hardware Simulation", Space Shuttle Technical Conference, NASA-JSC, June 28-30, 1983.

TABLE I CONTROLLER INSTALLATION CHARACTERISTICS

SIZE	23.5 X 14.5 X 17.0 INCHES	
WEIGHT	211 POUNDS	
INPUT POWER	490 WATTS (STANDBY) 600 WATTS (MAINSTAGE)	
HEAT TRANSFER	FORCED AIR COOLING (GROUND) CONVECTIVE COOLING (FLIGHT)	
MOUNTING	FOUR POINT VIBRATION ISOLATORS	
VIBRATION ENVIRONMENT	SINE RANDOM	24 G's PEAK 22.5 G's RMS
TEMPERATURE ENVIRONMENT	OPERATIONAL NON-OPERATIONAL	-50 TO +95F -200 TO +200F

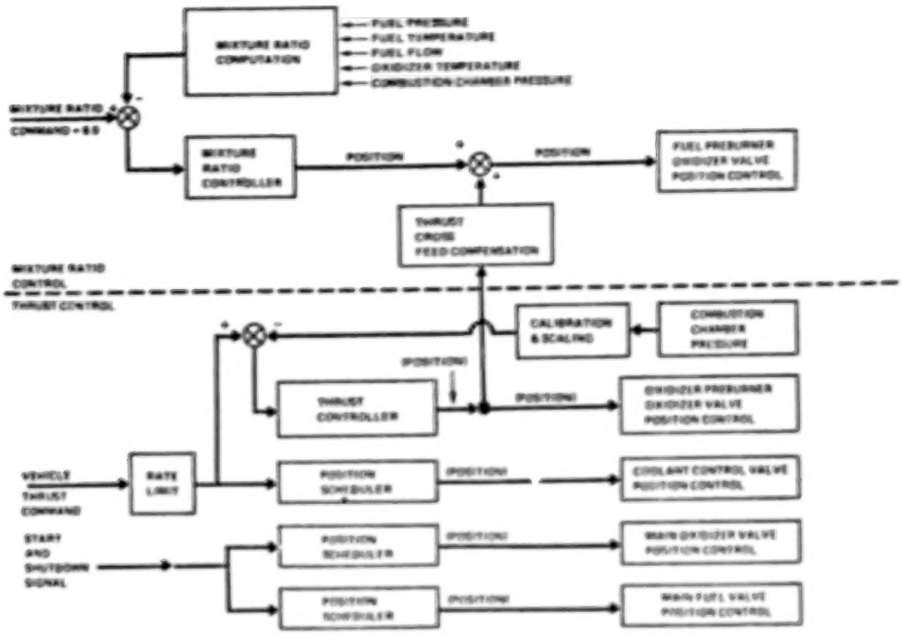


FIGURE 1 PERFORMANCE CONTROL DIAGRAM

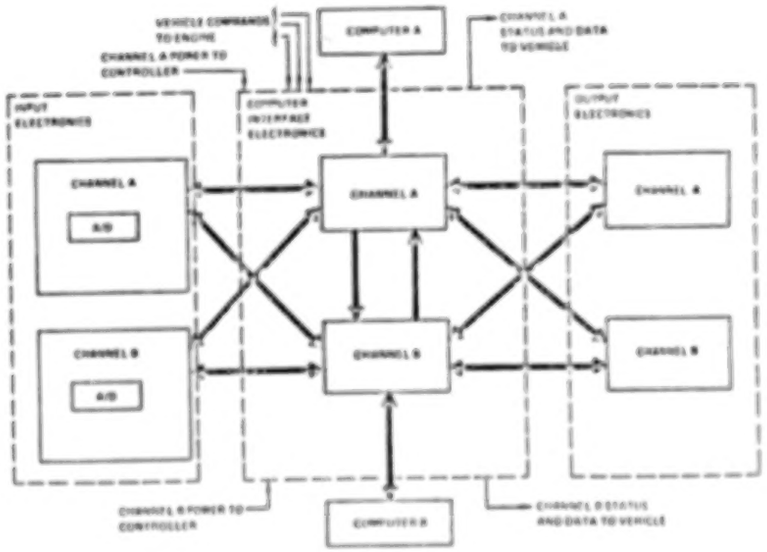


FIGURE 2 SIMPLIFIED REDUNDANCY DIAGRAM

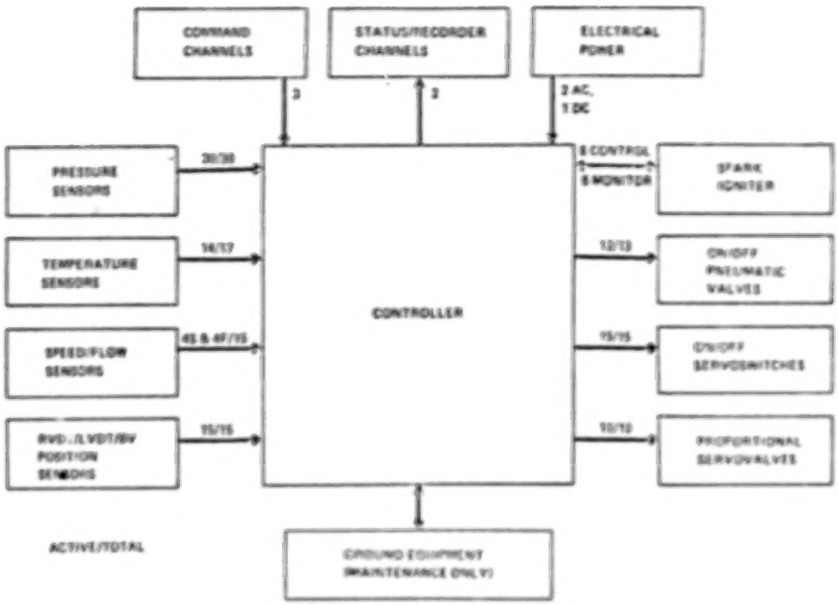


FIGURE 3 CONTROLLER INTERFACES

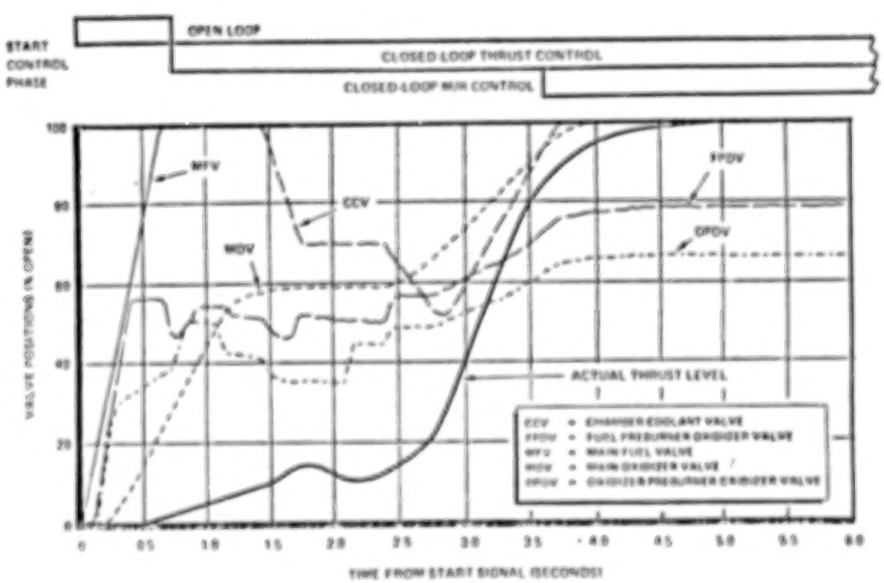


FIGURE 4 TYPICAL ENGINE START SEQUENCE TO RPL

ORIGINAL PAGE IS
OF POOR QUALITY

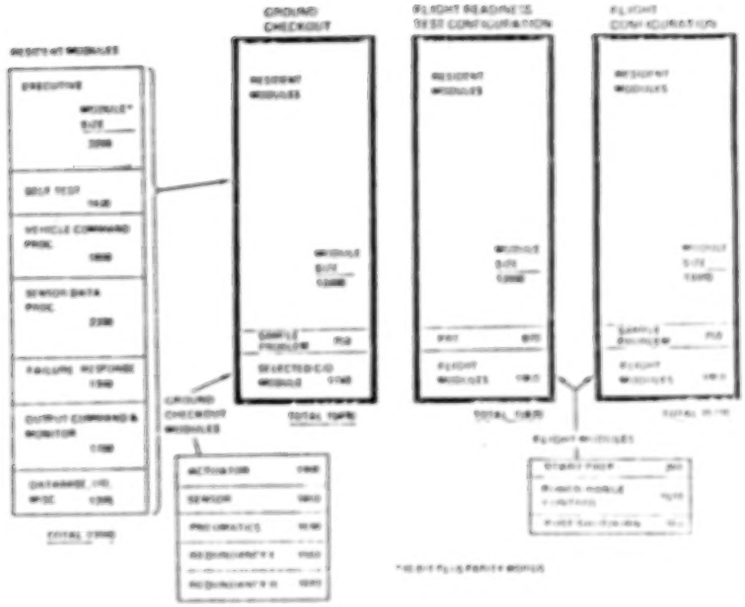


FIGURE 5 SOFTWARE PROGRAM COMPONENTS AND CONFIGURATIONS

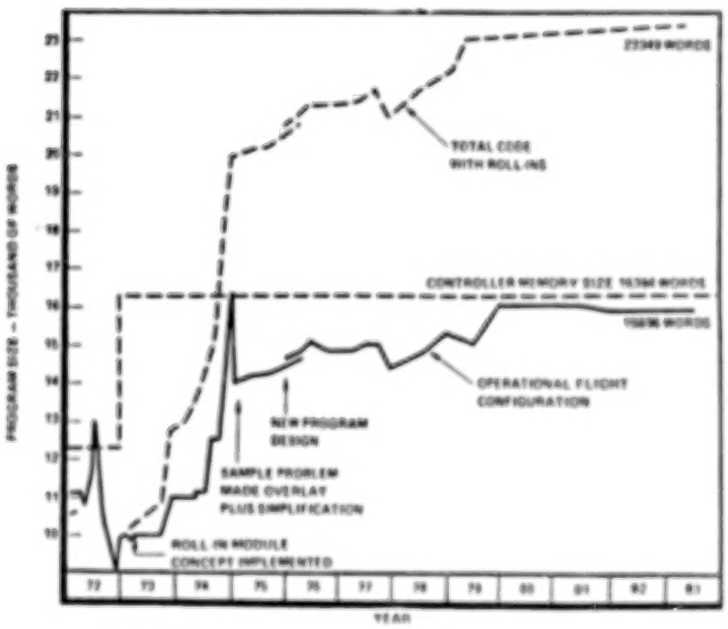


FIGURE 6 CONTROLLER MEMORY REQUIREMENT ESTIMATES

N85
16894

UNCLAS

D5

N85-16894

MAN-MACHINE INTERFACE AND CONTROL OF THE SHUTTLE DIGITAL FLIGHT SYSTEM

Richard D. Burghduff and James L. Lewis, Jr.
NASA Lyndon B. Johnson Space Center
Houston, Texas 77058

The challenge in designing the Orbiter displays and controls (D&C) system was to integrate the required aircraft and spacecraft D&C in the space available within the pilot's reach and vision. Some of the basic requirements for the D&C system were as follows:

1. A safe return with a single crewman from either forward crew station

2. Normal operation (exclusive of payload management) of all mission phases using a flightcrew of two

3. Accessibility to the flightcrew from the flight seats of D&C required for vehicle or subsystem management during ascent and entry

4. D&C to provide for crew override of automated critical command functions

5. Crew selection of automatic or manual flight guidance and control

6. The means to annunciate and command safing of hazardous systems

7. Interior and exterior illumination consistent in type and quality for crew operations

In early 1970, the D&C system was evolving into an integrated, multipurpose data bus connected system (fig. 1). Front station concepts were to use five or six cathode-ray tubes (CRT's) for most of the display requirements and reformattable control panels and keyboards for most of the controls. Some dedicated switches were used for system initialization and where immediate crew access was required. Circuit breakers were used for power control. A head-up display (HUD) was used for out-the-window display presentation. The HUD is an electronic/optical device that presents essential flight information in the pilot's head-up field of view. The information is projected from a small CRT onto a combiner glass and collimated at "infinity" to overlay the out-the-window, "real world" scene.

During the phase B contract studies, conventional and integrated avionics systems were compared for weight, power, cost, and technology risk. With involvement of flight crewmen and flight operation engineers, many studies of electronic attitude direction indicators (EADI's) versus conventional attitude direction indicators (ADI's) and multipurpose data bus versus hardwired D&C were conducted. The Orbiter program management then chose a low-risk off-the-shelf technology approach. This choice eliminated the EADI's, the HUD's, and the multipurpose displays and controls. Dedicated D&C components with electromechanical displays and hardwired switches were used, although four multifunction displays with keyboards were retained for the digital system interface.

The Orbiter contract was awarded to Rockwell International and the subsystem engineers at both Rockwell and the NASA Lyndon B. Johnson Space Center (JSC) started working together to complete the detail design of the D&C system. One agreement that proved to be very valuable was to initiate a series of formal D&C reviews at Rockwell chaired by the Rockwell and JSC D&C Work Breakdown Structure (WBS) managers. There were 13 of these major reviews during which representatives from the flightcrew, flight operations, engineering, reliability, safety, program office, payloads, software, NASA John F. Kennedy Space Center, Rockwell, and the U.S. Air Force were present. The reviews averaged 46 people including 4 astronauts. The reviews were 2 to 3 weeks long with the first week consisting of the Rockwell subsystem engineers describing their subsystem and the D&C engineers presenting the D&C concept for the subsystem. This procedure allowed NASA to ask questions of the subsystem engineers to understand the system and the Rockwell concept of the operation. Many times, a subsystem engineer desired more D&C for his subsystem than was required for operational use. This method of review also provided consistency between the different subsystems D&C requirements. Rockwell produced a comprehensive blue book handout for these reviews, and review item dispositions (RID's) could be written for consideration by the formal board chaired by the JSC Orbiter Project Manager a week later.

By the end of the first week, the subsystem information for the review was completed and the RID's were written. A few JSC people would stay for the second week with the flightcrew and determine subsystem by subsystem the D&C required and the appropriate nomenclature. Full-size drawings were used to arrange the D&C panel configuration. A full-size foam core mockup was made of the

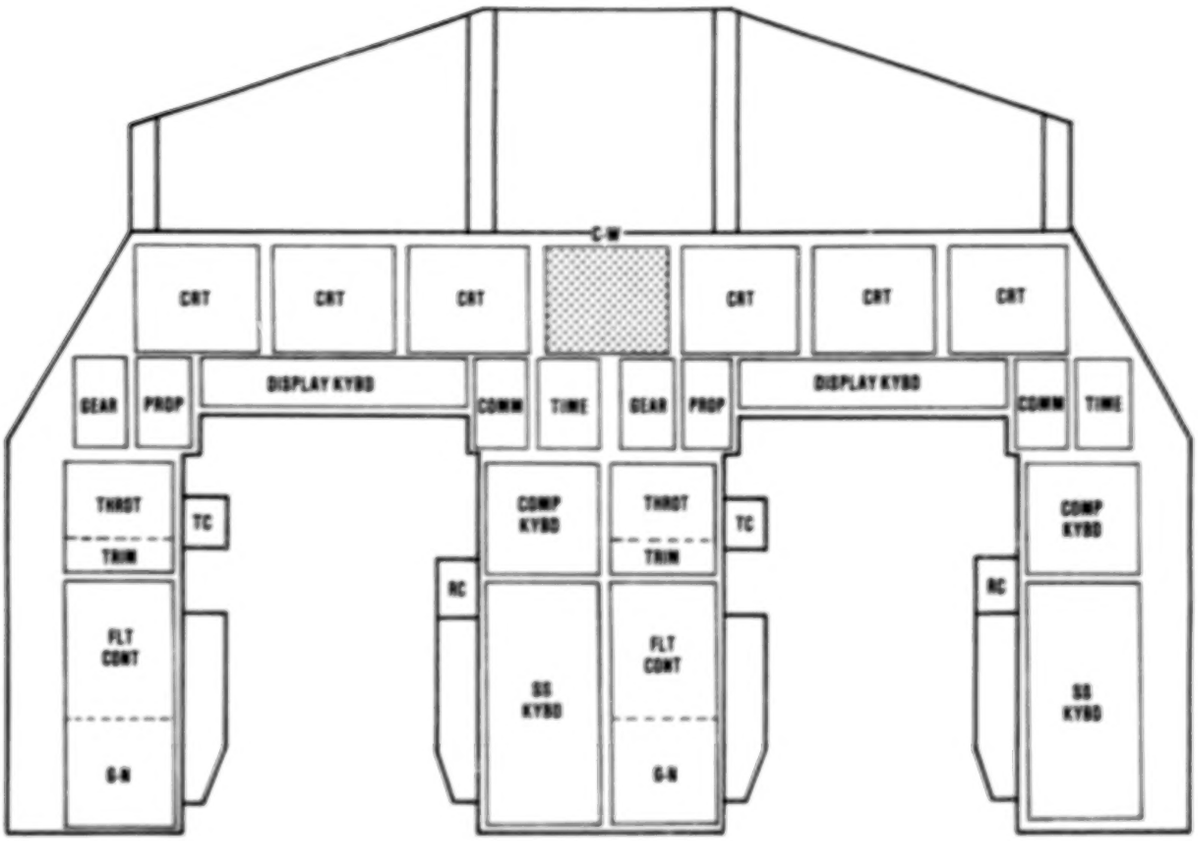


FIGURE 1.- EARLY D&C SYSTEM.

cabin area, and cutouts of the D&C were used to determine the proper location within the reach and visibility requirements derived from other studies. The flightcrew's support was invaluable during these design sessions. At the end of each review, Rockwell produced a D&C configuration drawing and updated the cabin mockup to be ready for the next D&C review, where the process would be repeated. As the subsystems became firm, the D&C panel layout and nomenclature were baselined and put under configuration control. Panel components were selected, meter scaling was chosen, and caution and warning (C&W) parameters were baselined.

The D&C reviews were progressive as a function of Orbiter system maturity, where, in general, D&C reviews 1 through 5 designed the OV-101 system, D&C reviews 5 through 11 designed the OV-102 system, and D&C reviews 12 and 13 completed the OV-099 or operational system. Between the formal reviews, a series of change package teleconferences was held between JSC and Rockwell to get JSC engineering and flightcrew participation in parallel with the Rockwell design process. These teleconferences are continuing much less frequently, to discuss D&C changes required in response to subsystem design changes. These teleconferences greatly reduced the quantity of D&C items that would otherwise go to the JSC Configuration Control Board (CCB). All change package teleconferences were documented with a set of minutes.

Early in the D&C design process, it was discovered that existing human factors D&C requirements documents should be used as design guides and not firm design requirements. With JSC crew station engineers and flightcrew participation in the design process, many of the human factors requirements were modified to produce a much better D&C system design. One example of this approach was the yellow pointers now used on the flight control electromechanical displays, especially the surface position indicator (SPI). Rockwell made a mockup of an SPI (which contains nine scales) using the standard white pointers. The crew, after determining the pointers were not visible enough, recommended yellow. Another good example was the background lighting specification for the pushbutton switches and the annunciators. Using the recommended specification light levels, the annunciator lighting was satisfactory in the laboratory. To be certain the annunciator lighting was readable in sunlight, sample devices were installed in the JSC one-g trainer and it was towed outside. The trainer was positioned so that the sunrise would shine through the cockpit windows. It was discovered that the

annunciator status could not be determined because the resulting Sun shafting washed out the lighted annunciation. The annunciation was changed from lighted background to lighted legend, and optical elements were added to concentrate the light. This change raised the intensity and contrast sufficiently to provide annunciator legibility in full sunlight.

Early in the D&C panel configuration design, it was decided to group subsystem controls by function. However, associated circuit breakers were separated because of a concern that if the higher power circuits behind the circuit breakers did have an electrical fault or mechanical damage in a particular location, the entire subsystem could be affected. To lessen the training impact on the crew, the circuit breakers for each system were positioned at the same relative location on different panels or section of panels.

A numbering system for every panel surface was provided by the crew station engineers. This system is necessary when referring to a control location, especially on test and operational procedures or schematics. The panels are numbered from left to right or front to aft in the cabin. Letters are used for locations such as R for right side, O for overhead, L for left side, C for center console, A for aft, and M for middeck.

The foam core evaluator was a valuable tool for D&C panel component location. The D&C components were located by priority with the systems that need to be reached and viewed during maximum ascent acceleration positioned first. Other controls that require operation during periods in which the crew is strapped in the seats were positioned next, then lower order subsystem D&C components were positioned in the aft flight deck and the middeck. A more advanced analysis capability was used later in the program to assess crew accessibility to various displays and controls. Specifically, a three-dimensional graphics computer-aided design modeling package was used to depict a crewman's access to various D&C components under negative-g conditions during a contingency two-engine-out abort maneuver. The access depicted by the reach modeling program was then verified in a mockup. By increasing use of such modeling and simulation techniques, front-end mockup costs are reduced. Such techniques will not replace mockups, but will permit rapid evaluations of many configuration alternatives during conceptual and preliminary phases before the construction of mockups.

The aft flight deck was divided into three zones designated mission station, on-orbit station, and payload station. The mission station was assigned the D&C to manage flight-critical payload subsystem controls and non-flight-critical Orbiter subsystem controls. A CRT and keyboard is at this station to display subsystem information. The on-orbit station is separated into the on-orbit and the remote manipulator system (RMS) functions. The on-orbit station has an overhead window and a payload bay window; D&C for the functions of rendezvous, docking, TV, lighting, and communications are located here. The RMS station contains D&C for manipulator arm operations and an overhead and aft view. The RMS operator shares D&C for TV, lighting, and communications with the on-orbit station; RMS operations require the simultaneous use of two three-degree-of-freedom hand controllers. The operator also must set up views from as many as seven TV cameras in the payload bay on two monitors, both of which have a split-screen capability. During some payload deployment and retrieval operations, a crewman would be well served to have four arms to accomplish all the required tasks in the necessary timeframe. As it is, the operational configuration of the RMS station contains only about one-third of the D&C originally proposed and evaluated for that function. The payload station was reserved for payload-provided D&C except for an audio and station lighting panel. The middeck panel areas were designated for circuit breakers, housekeeping functions, middeck audio and lighting controls, and airlock controls.

Maintainability of the D&C panels and the line replaceable units (LRU's) was a strong driver in the D&C design. The D&C panels were designed to be small enough to be removed individually. There are more than 80 panels in the Orbiter and many include hinges to allow the panels to be swung out for access behind them. Each LRU is mounted from the front of the panel and can be installed and replaced without removing the panel.

The Orbiter operates in a zero-g environment while on orbit; therefore, any contaminants or extraneous materials are free to migrate. These materials can be conductive and of sufficient length to bridge terminals on such devices as switches, circuit breakers, and meters. To prevent this eventuality, all exposed electrical terminations on the panels are protected with a conformal coat of resilient insulating material, which also provides a humidity barrier. As with the external terminations on the D&C equipment items, the internal terminations are also treated to eliminate the possibility of floating conductive particles causing failures.

All Orbiter equipment and particularly items in the crew compartment are required to meet very stringent flammability and toxicity requirements. This requirement means that all exposed materials (not contained within at least an environmentally sealed enclosure) must be reviewed by materials and processing specialists for approval before use. In numerous cases in which existing hardware was used, special testing was required to determine the flammability, toxicity, and outgassing characteristics of specific materials for which these data were not available. When an unacceptable material

could not be changed, it was overcoated or otherwise protected, and, in some cases, waivers were granted after analysis indicated acceptability because of configuration, quantity, etc.

One early problem was a means of complying with the NASA design standards that included a prohibition on the use of frangible materials. Most of the existing display devices such as CRT's and meters used a glass window as a means of providing visual access and sealing the instrument case. To circumvent this problem, most display devices with glass were provided with a Lexan cover over the window to protect the glass and contain the glass in the eventuality of a fracture. These Lexan covers were easily removable for maintenance. The protective covers were coated with antireflective material for correct optical properties and have proven very practical in actual usage. Other protective devices were designed to protect the D&C from a crewman possibly causing damage to the D&C hardware while floating around the cabin. Wickets were placed around the switches on most of the panels, and on the panels the crew was most likely to step on, the switches were recessed into the panel.

Lighting, both internal and external, would appear to be a straightforward area; however, much design effort went into the Orbiter lighting. Lighting in the cabin consists of fluorescent lights for general area illumination, incandescent floodlights for spot illumination, and integral lighting for meters and panel nomenclature illumination. A good full-size cabin lighting mockup or evaluation would have been desirable. Most of the lighting evaluation was done by area or analysis, and the results were confirmed in the Orbiter cabin built for the Shuttle Avionics Integration Laboratory. The external lighting consists of metal halide lights for the payload bay and incandescent floodlights for overhead and manipulator illumination. One area of design difficulty with the external lights is the rejection of heat from the lights. Conductive cooling and innovative lamp design were required.

As the D&C requirements for the various subsystems continued to grow, the crew workload and knowledge required of each subsystem grew. Much effort went into the nomenclature designation to give the best operational understanding of the use of each control. This task must have crew or operations involvement because subsystem engineers tend to use engineering rather than operational nomenclature.

The flightcrew suggested that schematic layouts on the panels be considered for some of the subsystems to help understand their operation. Schematic panel layouts were done for panel R1 (power distribution and control), panel L1 (environmental control), panel L2 (atmospheric pressure control), panels O7 and O8 (fig. 2) (reaction control and orbital maneuvering systems), panel A1 (communications), panel R12 (supply water), and panel ML31C (wastewater). The use of schematic layouts should be implemented only when the subsystems are mature because once a panel is built, it is very difficult to add a switch in the correct place of the schematic.

The HUD was brought back into the program as an approach and landing aid and flown for the first time on STS-6. From the point of program approval to hardware delivery, a little more than 2 years elapsed, a very tight time frame for hardware development, qualification, and delivery. One area that proved to be a difficult problem was the format development. Simulations are required using both fixed- and motion-base simulators. The simulators had to represent the Orbiter software as closely as possible. One problem area with the HUD display format design effort was that it came in the program with a ground rule to impact the Orbiter general-purpose computers (GPC's) as little as possible. The HUD used the data bus information going to the dedicated electromechanical displays, but the data update rates were too slow. Therefore, data smoothing had to be done in the HUD and, where possible, faster data rates within the GPC were brought to the HUD. The moving-base simulator at the NASA Ames Research Center was not available to evaluate the HUD format, except for a few hours, before the software programable read only memories (PROM's) had to be burned for the hardware. The format that was used at this time had a large amount of information displayed with the capability of decluttering seven levels. The crew was involved during all the format design effort and, as more simulations were conducted, it was obvious the format had too much information. A large effort using fixed- and motion-base simulators and the Shuttle training aircraft (STA) was made and an updated, simpler format was designed for first use on STS-8. Since the hardware PROM's had to be built to deliver hardware on schedule, a retrofit program is now in process to update the HUD. One of the reasons the HUD development went as well as it did was a series of teleconferences held every other week with JSC, Rockwell, Kaiser Electronics (HUD supplier), Sperry (autopilot supplier), and Draper Labs (early systems support). These teleconferences are documented in a comprehensive set of minutes. Astronauts and software, simulator, program, hardware, and flight control engineers attend these teleconferences and help provide integration of the total HUD community.

As the Orbiter became operational, it also became obvious that the cockpit contains the most complicated assortment of D&C ever developed for an aerodynamic vehicle. There is a large variety of D&C devices. For control, there are toggle, pushbutton, thumbwheel, and rotary switches; potentiometers; keyboards; circuit breakers; and hand controllers. Display devices include circular and vertical meters, tape meters, mechanical talkbacks, annunciators, flight control meters, digital readouts, and CRT's. There are more than 2100 D&C devices in the Orbiter cockpit (fig. 3).

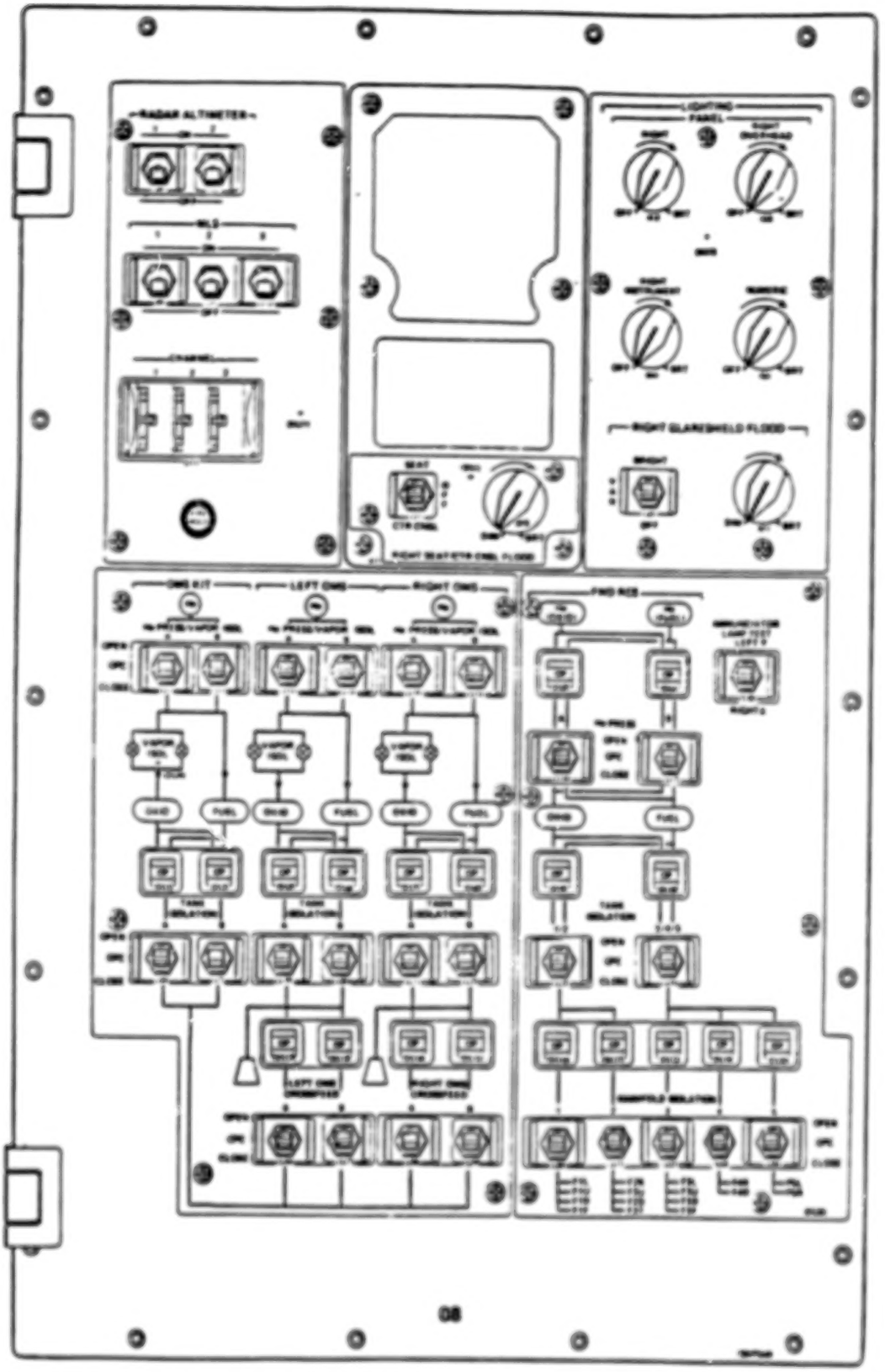
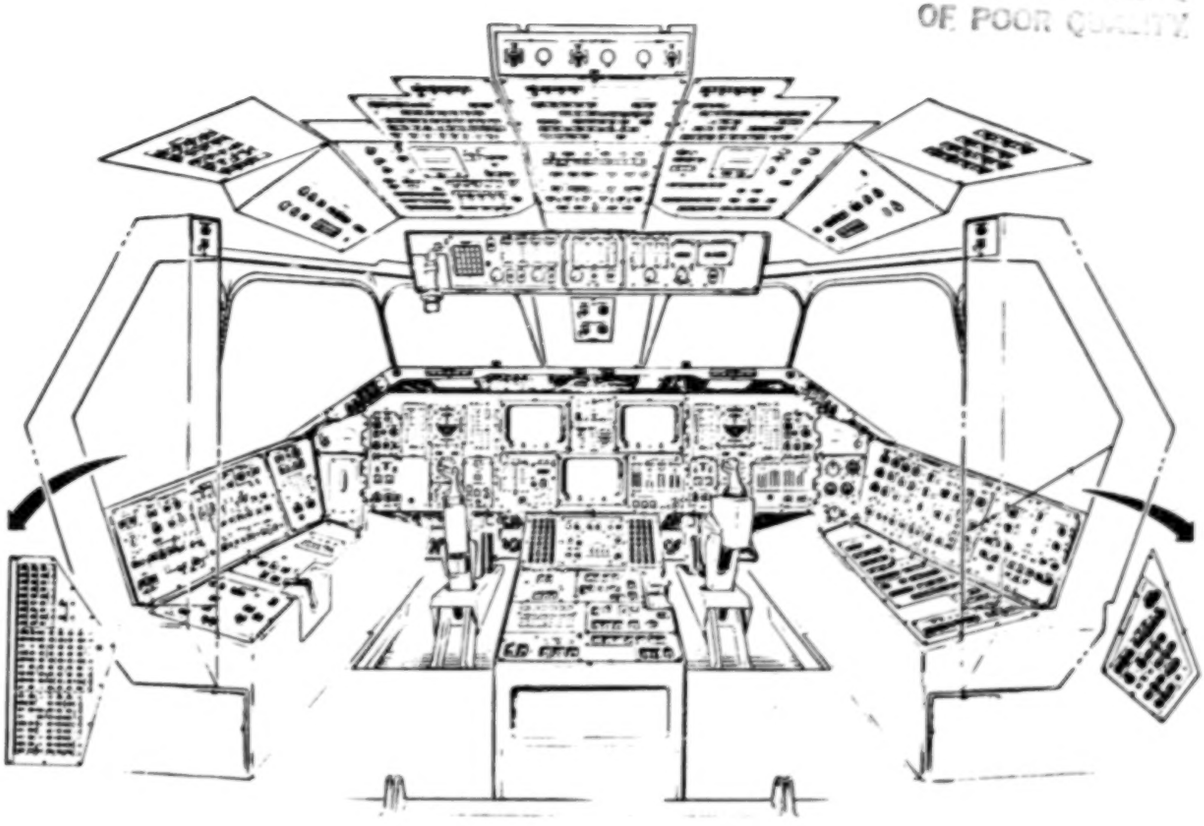
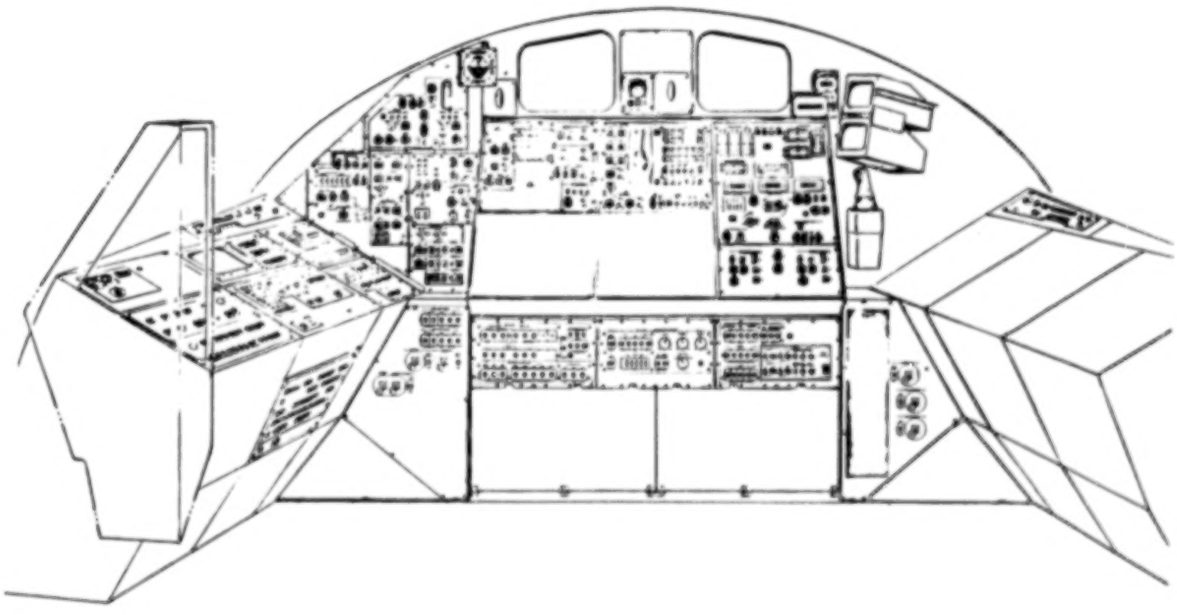


FIGURE 2.- PANEL O8.

ORIGINAL PAGE IS
OF POOR QUALITY



(a) VIEW LOOKING FORWARD.



(b) VIEW LOOKING AFT.

FIGURE 3.- ORBITER COCKPIT.

ORIGINAL PAGE IS
OF POOR QUALITY

Orbiter enhancement D&C studies conducted recently have all gone back to the multifunctional cockpit (fig. 4). To get the systems operations to a more automated and simpler level will greatly reduce crew workload. Multifunction CRT's and flat panel displays could replace the electromechanical displays and annunciators. Programable keyboards or CRT overlays could replace most of the 1300 control devices. Remote power switching could eliminate many of the 400 circuit breakers. Voice control and synthesis could be used as an added input/output channel to more efficiently use the crew during peak workload periods. A study was conducted in the Manipulator Development Facility (MDF) to assess the feasibility of using voice control of the many switching functions associated with the closed-circuit television system supporting the RMS. It was found that identical tasks (berthing and deployment) were completed in virtually identical times using manual switching (standard Orbiter operation) as a comparison for voice-controlled switching having a recognition accuracy between 85 and 95 percent. Using state-of-the-art voice recognition equipment should allow a marked improvement in the overall RMS operations.

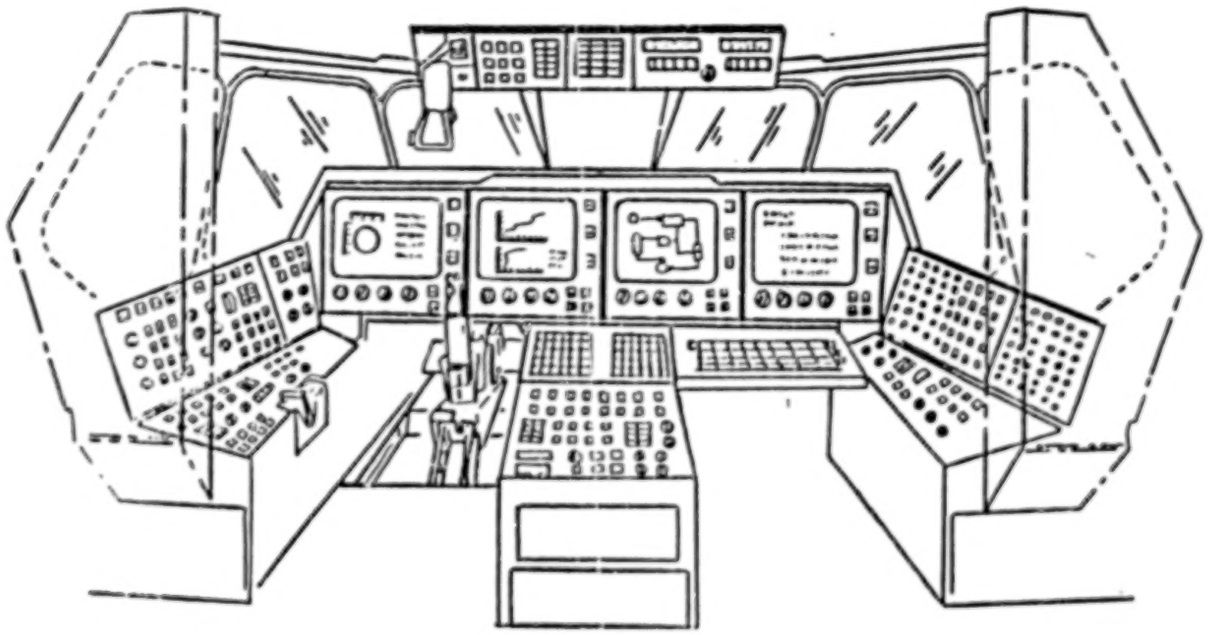


FIGURE 4.- MULTIFUNCTIONAL COCKPIT.

In summary, some of the most important lessons learned during the Orbiter D&C program are repeated here.

1. The formal D&C reviews held at Rockwell were necessary. The total Orbiter systems community needs to be involved; participation by the flightcrew and engineering personnel is very important. The reviews should be well documented.

2. The change package teleconferences are valuable to provide continuous JSC input into the Rockwell D&C design effort.

3. D&C engineers with crew and human factors engineering support should provide a consistent D&C panel layout and nomenclature configuration.

4. The early availability of the foam core cabin mockup was very important for D&C placement within reach and visibility constraints.

5. The HUD integration teleconferences were necessary, and comprehensive documentation of these teleconferences is important. Formal simulations should be done early in the program using high-fidelity simulators.

6. With large numbers of redundant subsystems, the use of dedicated D&C devices can rapidly grow into a large, complex system. Multipurpose D&C should be encouraged with local processing to help offload the central computer system and to improve crew efficiency.

N85
16895

UNCLAS

D/0

N85-16895

SPACE SHUTTLE MAIN ENGINE

HARDWARE SIMULATION

H. G. Vick/P. W. Hampton

NASA/Rocketdyne

National Aeronautics and Space Administration
Marshall Space Flight Center

ABSTRACT

The Huntsville Simulation Laboratory (HSL) provides a simulation facility to test and verify the Space Shuttle Main Engine (SSME) avionics and software system using a maximum complement of flight-type hardware. The HSL will permit evaluations and analyses of the SSME avionics hardware, software, control system, and mathematical models. It is a unique facility in its authenticity as well as in the complexity and scope of simulation. The laboratory has performed a wide spectrum of tests and verified operational procedures to ensure system component compatibility under all operating conditions. It is a test bed for integration of hardware/software/hydraulics. The HSL is and has been an invaluable tool in the design and development of the SSME.

INTRODUCTION

Simulation has been an invaluable tool in design and development of the SSME. Usages of simulation techniques are numerous and range from component design parameter definition and digital control design to operating software design, development, and verification.

The SSME, three of which provide primary thrust for the NASA Orbiter vehicles, incorporates many advanced features including a programmable digital control system (1). Control is accomplished with an engine-mounted electronic digital control system packaged in a single assembly called the controller. The controller contains dual programmable computers with 16,000 memory words for each computer. The controller, in conjunction with five hydraulically actuated propellant valves, 43 performance, limit, position and maintenance sensor inputs and six solenoid control valves, accepts vehicle commands for the SSME operational phases, positions the appropriate valves, monitors the engine for performance conditions and provides redundancy management (2 and 3). The relationship of the engine avionics to the Orbiter vehicle is shown in a simplified manner in Figure 1.

The SSME control system provides checkout, start, mainstage operation and shutdown in response to vehicle commands. The control system also has the capability to check out and monitor its own status and to monitor and report engine status conditions while maintaining full redundancy management. The software used by the controller to accomplish the noted functions must be designed, tested and verified to satisfy the system requirements. It is extremely important that software discrepancies or errors be identified and corrected before the software is used by the SSME to avoid engine or vehicle damage.

The HSL located at Marshall Space Flight Center (MSFC) provides a program-unique capability of simulating SSME system operation at nominal and off-nominal conditions. The simulation provides the capability of perturbating variables of software, hardware or internal engine operations to determine the SSME system response in all modes of operation.

The present primary usage of the HSL is the design, development, and verification of the SSME controller software. Other program uses of the facility include systems integration, system characteristics definition, control system dynamic response definition and verification, and problem resolution support to Kennedy Space Center (KSC) and engine test sites. The operational software that is used for SSME single engine testing, Main Propulsion Test Article (MPTA) testing and KSC flight vehicle operation is verified at the HSL prior to usage. Thus errors or conflicts are identified in a benign environment without program impact. The SSME software is flown tens of times at the HSL before usage is authorized for flight operation.

SPACE SHUTTLE MAIN ENGINE

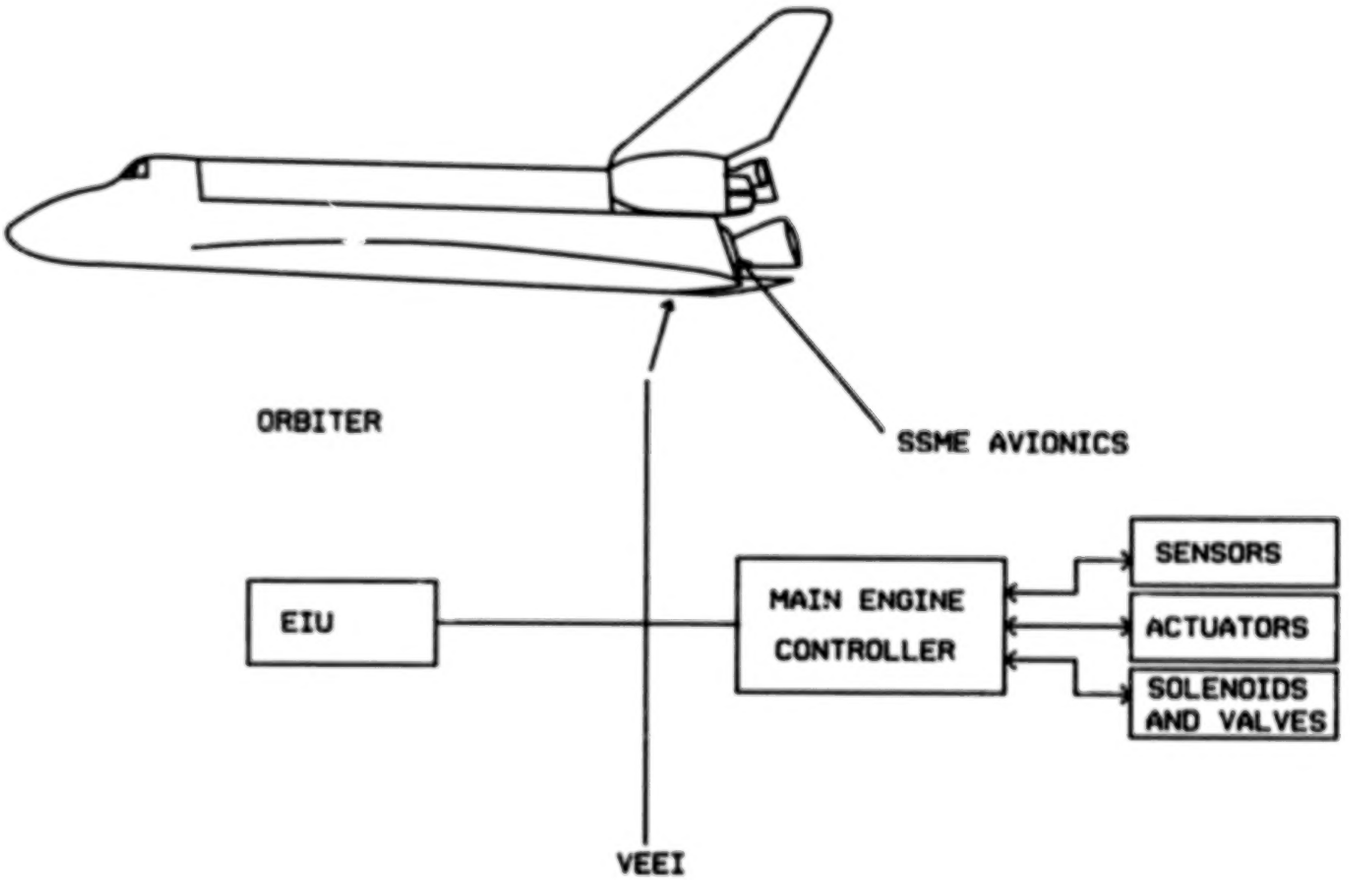


FIGURE 1

SIMULATION FACILITY

The need for a hardware simulation facility which incorporated a maximum complement of avionics hardware was recognized early in the SSME program. NASA/MSFC started the initial facility design efforts in the early 1970's, and the HSL was declared operational in 1975.

The hardware simulation incorporates as many flight components and functional stimuli as are practical for the extensive testing required for system and subsystem analysis, validation, and verification. A maximum hardware complement is used in conjunction with the hybrid simulation to perform the following system tests:

a. Hardware Integration
b. Software Integration
c. Failure Mode and Parameter Anomaly Evaluation
d. System Dynamic Validation
e. Sensitivity Analysis
f. Special Effects Analysis
g. Live Engine Correlation

The hardware simulation must be capable of cycling all phases of engine operation, including purge sequences, startup, mainstage, shutdown, and post-shutdown.

The HSL can be divided into three major elements as shown in Figure 2. The elements are the engine dynamic model, a complement of flight configuration hardware, and a simulation control center.

Engine Dynamic Model - Hybrid Computer

A hybrid simulation of the SSME is programmed on two CI5000 analog computers and one SEL 840 MP digital computer. This simulation was developed from the mathematical models specified in the Engine Balance and Dynamic Model Specification (RL00001) and the Engine Control Design Document (RSS-8551). This simulator is programmed such that it will operate independent of or with any subset of the flight-type hardware contained in the Simulation Laboratory Control Room. The engine, actuators, and sensors are simulated on the analog computers. The digital computer is used to simulate the main engine controller and to handle initialization and timing functions. In the all-software mode, the simulation is used to evaluate and validate the mathematical models. In the standard operating mode, the hybrid simulation supplies the engine internal pressure and temperature parameter values to the Simulation Control Room where they are interfaced with the SSME Controller, Figure 3. A new dual AD-10 digital simulator using a DEC host will be brought on-line to replace the classic Hybrid.

An engine simulation model of lower fidelity has been programmed on a PDP 11/34 computer to provide a backup to the hybrid simulation. This backup enables continuation of HSL testing during hybrid computer maintenance operations.

Flight Configuration Hardware

Flight configuration SSME avionics hardware usage is maximized at the HSL to gain simulation fidelity. The major elements are a flight configuration SSME controller and propellant valve hydraulic actuators. The SSME has five propellant control valves which are hydraulically actuated These five hydraulic actuators are incorporated into the simulation facility and integrated into the control system in the same manner as they are used by the SSME.

The HSL also includes spark igniters, instrumentation sensors, control solenoids, propellant bleed valves and a pneumatic control assembly. A detailed list of SSME avionics hardware is included in Figure 4.

Simulation Control Center

The simulation control center interfaces the HSL elements and acts as the command center for testing. The center contains a Command and Data Simulator (CADS), test consoles, hydraulic actuator load system, and a support system consisting of data recording/display and diagnostic tools (Figure 3).

SSME HSL

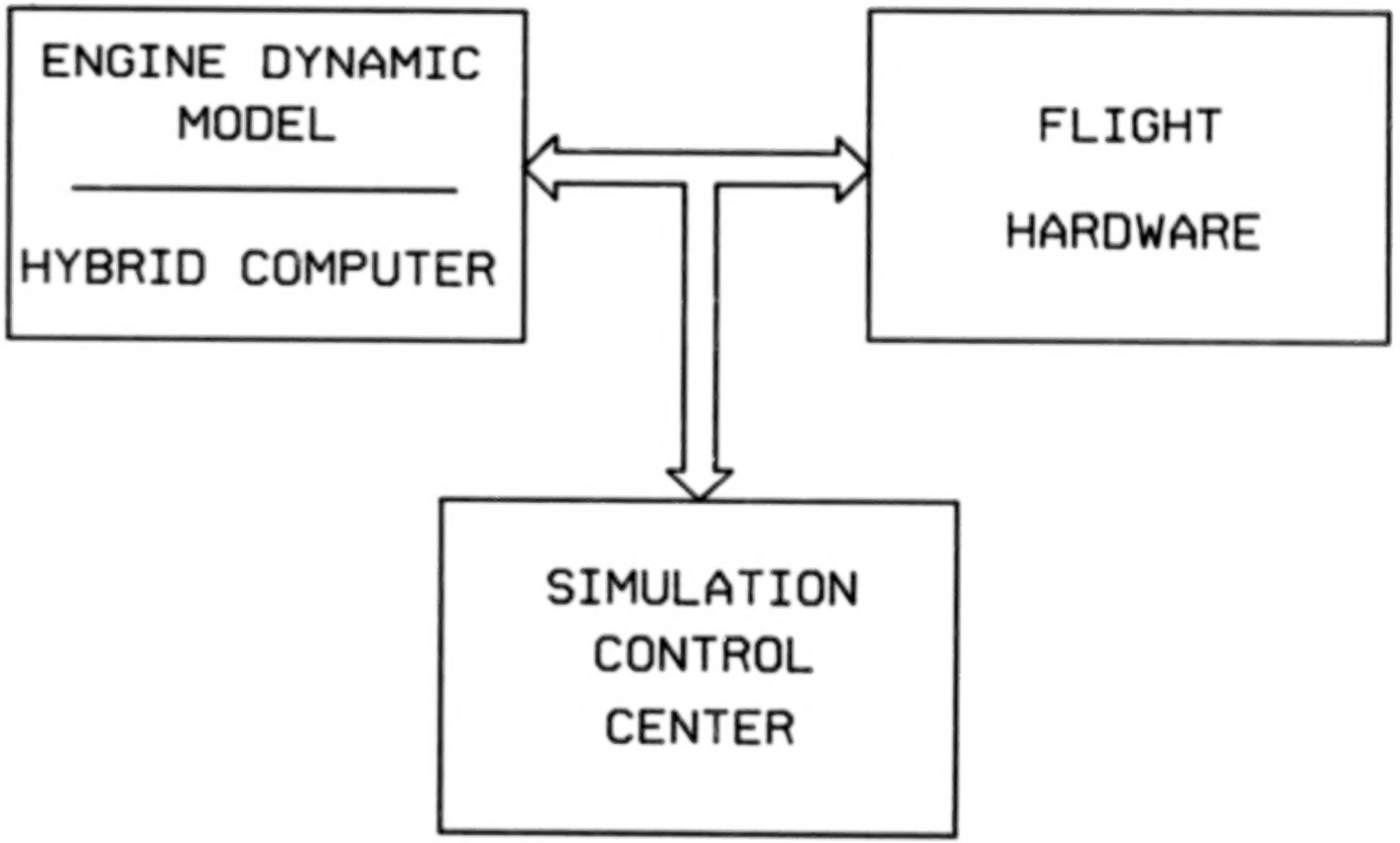


FIGURE 2

SSME HSL

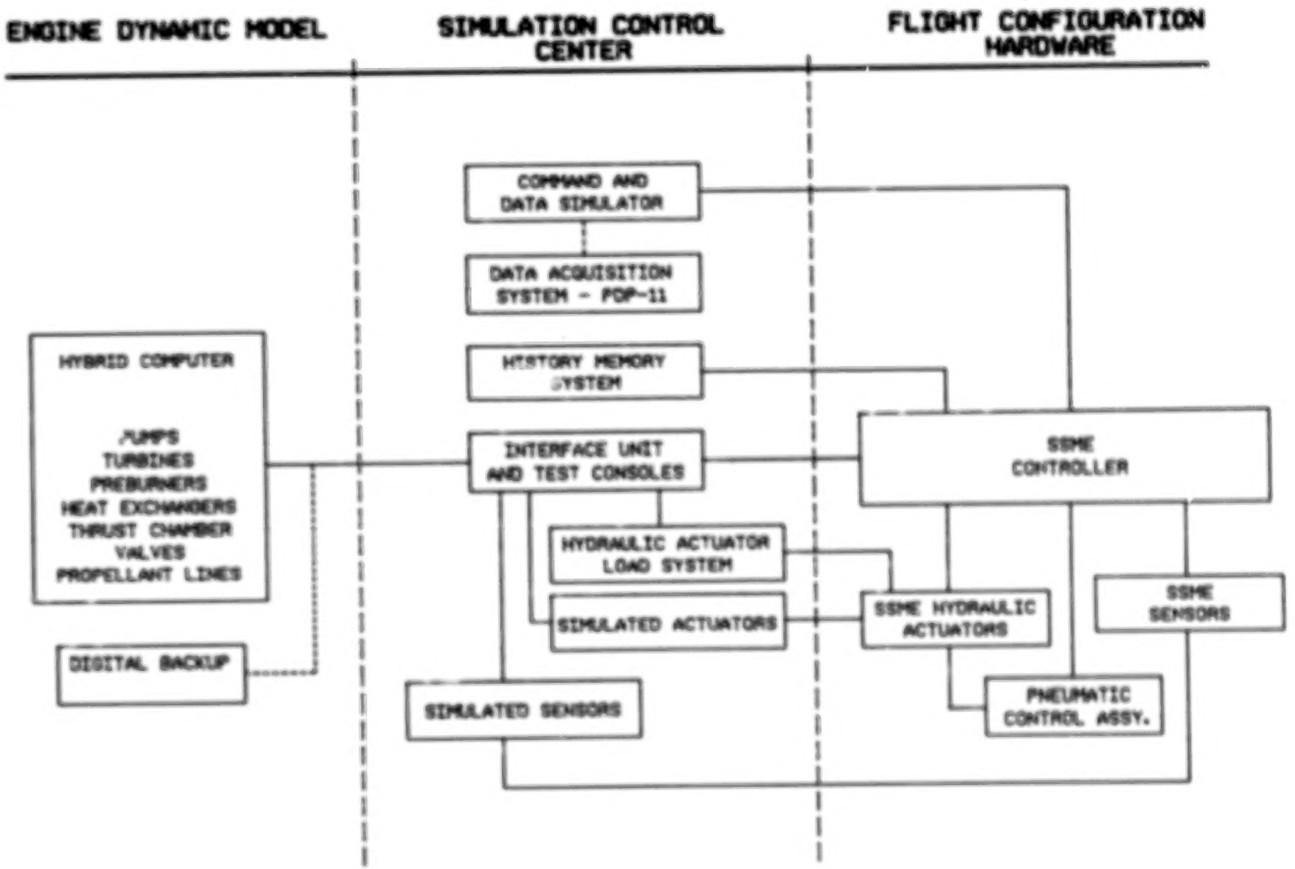


FIGURE 3

CONTROLLER

MAIN FUEL VALVE HYDRAULIC ACTUATOR

MAIN OXIDIZER PREBURNER VALVE HYDRAULIC ACTUATOR

OXIDIZER PREBURNER VALVE HYDRAULIC ACTUATOR

FUEL PREBURNER VALVE HYDRAULIC ACTUATOR

CHAMBER COOLANT VALVE HYDRAULIC ACTUATOR

SPARK IGNITERS (6)

PRESSURE SENSORS (20)

TEMPERATURE SENSORS (10)

SPEED SENSORS (4)

FLOW SENSORS (2)

OXIDIZER BLEED VALVE

FUEL BLEED VALVE

PNEUMATIC CONTROL ASSEMBLY

- SOLENOID VALVES (5)
- PRESSURE ACTUATED VALVES (8)
- PRESSURE SENSORS (5)

RECIRCULATION ISOLATION VALVE

GOX FLOW CONTROL VALVE

HELIUM PRECHARGE VALVE

FIGURE 4

HSL SSME FLIGHT HARDWARE

A test is initiated with commands from the CADS to the SSME controller, SSME actuator positions are sent to the Engine Dynamic Model which then supplies the sensor stimuli representing engine internal parameters to the SSME controller. The controller outputs data and status to the CADS and data recordings are made for further analysis.

Command and Data Simulator

The Command and Data Simulator (CADS) contains a digital computer that interfaces directly with the main engine controller. It is used to simulate the Orbiter vehicle interface. The two primary functions of the CADS are to send commands to the controller and receive and record from the controller.

Test Consoles

Power-up, testing, and monitoring of all simulation flight hardware are controlled from the consoles located in the Simulation Laboratory Control Room. The consoles include the capability of fault insertion. Manual switch control is provided for SSME controller input and output lines. Thus, in the case of engine control parameters, such as thrust chamber pressure where multiple sensor inputs are used, failure insertion can be accomplished to fail maximum, fail minimum, fail mid-range, or insert a bias between sensor inputs. In the case of propellant valve actuators, the fault insertion can be loss of command signal to the actuator or loss of position signal from the actuator.

Hydraulic/Actuator Load System

The five primary propellant valves on the SSME are controlled by hydraulic actuators. The facility hydraulic system provides 3,000 psi pressure at the SSME required flowrate. Hydraulic supply and return lines are sized to simulate the engine lumped line inertia to enable testing of fluid system transients. During mainstage operation, the actuators are under dynamic stress due to the flow of fuel or oxidizer through their respective valves. In order to simulate this loading, a load actuator is coupled to each primary valve actuator. The load actuators are controlled by the hybrid computer and can apply a physical load to the primary valve actuators that is representative of the dynamic loading that will be experienced during actual engine operation.

Simulation Support System

The HSL includes the following Simulation Support System to accomplish data recordings, simulator (program) handling, input features, and diagnostic tools:

a. Data Recording

   (1) Strip-Chart Recorders
   (2) Real-Time Printer
   (3) Magnetic Tape

b. Data Display CRT
c. Predetermined Initialization Input
d. Diagnostic Software
e. PDP/11-34 Computer for Data Analysis
f. History Memory System
g. Power Transient Generator

MAJOR PROGRAMMATIC BENEFITS

Avionics and Systems Integration

A facility such as the HSL enables the first-time integration of controls and system in a supportive test environment. The HSL has served as the site for initial integration of the SSME controller to the the control system sensors, hydraulic actuators, pneumatic solenoids, the Orbiter Engine Interface Unit (EIU), and the Flight Accelerometer Safety Cutoff System (FASCOS).

The FASCOS development effort is an excellent example of maximum utilization of simulation facilities for systems integration. The first FASCOS unit built was a rack-mounted breadboard. Following build and laboratory checkout, the FASCOS breadboard was connected to a SSME controller for the first time at the HSL. Initial testing verified interfaces and FASCOS hardware function. The breadboard was then used for development and initial verification of the controller software. A prototype FASCOS unit of the engine-mounted configuration was built and that unit was also integrated with the SSME controller at the HSL. Formal verification of the controller software was conducted at the HSL using the prototype unit. The prototype, together with the verified software, were then exposed to single engine hot-fire testing. Usage of simulation facilities resulted in of the FASCOS configuration into the SSME with avoidance of any delay at the test site due to hardware or software integration problems.

Integration tests have also been conducted at the HSL to define engine hydraulic system pressure transients for the Orbiter system. These simulations of the SSME hydraulic system operation verified engine/orbiter interface pressure level limits and worse-case surge pressure transient response with maximum propellant valve excursion rates.

Software Change Verification

The SSME control system provides flexibility due to the programmable digital logic. Thus changes in operational sequence, function, limits, and redundancy management can be readily incorporated as knowledge is gained throughout the engine testing and flight operation program.

These software changes are all subjected to verification testing at the HSL prior to engine usage. The philosophy of change verification is to expose the avionics hardware and software systems to a simulation of the expected as well as possible conditions. For example, if a change were to be desired in combustion chamber pressure data processing to enhance redundancy management, verification would require off-nominal and malfunction conditions as well as the expected operating profiles. The HSL verification of such a change would entail normal start, mainstage, throttle up and down, and shutdown operating mode simulations. Off-nominal testing would involve simulating bias of sensor outputs and evaluation of control system discrimination. Malfunction testing would involve simulation of single and multiple sensor input failures. This testing would be accomplished using the change in conjunction with the operational software configuration. Results of these simulations are evaluated to ensure that operating characteristics and requirements of the SSME are satisfactory. Satisfactory results can be incorporated into engine testing and flight operations. Conversely, if undesirable results are obtained, the software design can be corrected without having endangered engine or vehicle operation.

Launch Support and Problem Resolution

The HSL has proven a valuable resource in the prompt resolution of problems experienced at KSC. Use of the facility for this purpose allows simulation and resolution of the problem and development and proofing of backout procedures or corrections with minimum impact on the operational site.

An example of this was the supplementing of the Huntsville Operational Support Center (HOSC) during the initial launch attempt for STS-1. During that operation, improper positioning of an Orbiter cockpit switch resulted in generation of SSME Failure Identifications (FID's). Discussion of FID's between the HOSC and HSL personnel resulted in identification of the probable cause as a SSME input power failure. The HSL simulated a power failure and produced the identical FID's experienced at KSC. A procedure for restoration of power to the SSME controller was developed and verified at the HSL. HOSC reviewed HSL results and concurred with the procedure. HOSC communications with KSC confirmed the error in switch positioning, reported the HSL simulation results, and transmitted to KSC the verified power-up procedure. This entire scenario occurred in less than one hour and avoided launch delay.

Another typical example occurred during preparation for FRF-2 for STS-6. Engine position two experienced two HALT's and required usage of the ground support equipment memory loader to recover. The HSL simulation capabilities were used to duplicate the HALT condition and to aid site personnel in restoring SSME controller operation. Further simulation testing at the HSL resulted in identification of the cause of the HALT condition, a correction for the problem and a procedure for avoiding the condition. Usage of the HSL in this manner resulted in minimization of the time required to restore operating conditions at KSC and avoidance of a schedule delay which would have resulted if the launch site had been required for the extensive testing required to identify the problem cause and its resolution.

Engine System Malfunction Analysis

The fidelity of the HSL, including the engine model and hardware/software system response, enables usage of the facility for malfunction analyses of the SSME system. Examples of this usage include evaluation of thrust chamber coolant tube rupture and chamber pressure sensor port blockage effects upon engine system operation.

In the evaluation of the effect of a nozzle tube rupture, the hybrid computer analog model was changed to simulate an overboard bleed flowrate from the thrust chamber nozzle fluid circuit. The bleed flowrate could be varied from one to ten pounds per second. Flight simulation runs were then conducted using varying bleed flowrates to determine the engine control system response, with special emphasis on position changes of the preburner valve actuator position relative to operating limits.

The simulation of the effect of chamber pressure sensor port blockage was accomplished by using the test console features which allowed biasing a pair of sensor outputs. Flight simulation runs were then conducted using pre-set biases to determine the effect upon engine system operation.

FUTURE APPLICATIONS

The HSL will continue to be utilized in the SSME program in its current role, with emphasis on KSC launch support and software verification. Launch support responsibilities will be expanded as Vandenberg Air Force Base (VAFB) becomes operational as a Space Shuttle launch site.

SSME controller piece part obsolescence has resulted in the requirements for a Block II controller for future engine deliveries. This controller will require a different set of software. Formal validation and verification of the Block II software will be major HSL activity in the late 1980 time period. The flexibility of the HSL design will allow usage of the facility to support both sets of software with minimal facility modification.

REFERENCES

1. W. F. Wilhelm, "Space Shuttle Main Engine Design." SAE Transactions, Volume 81 (1972), paper 720807

2. P. F. Seitz and R. F. Searle, "Space Shuttle Main Engine Control System." SAE Transactions, (1973), paper 730927

3. W. T. Mitchell, "Space Shuttle Main Engine Digital Controller." Conference Proceedings No. 274, Advanced Control Systems for Aircraft Power Plants, Advisory Group for Aerospace Research and Development, North Atlantic Treaty Organization. October 1 and 2, 1979.

N85
16896

UNCLAS

D1

N85-16896

DEVELOPMENT AND IMPLEMENTATION OF THE VERIFICATION PROCESS FOR THE SHUTTLE AVIONICS SYSTEM

H. E. Smith
NASA Lyndon B. Johnson Space Center
Houston, Texas 77058

W. B. Fouts and J. Mesmer
Rockwell International
Downey, California 90241

ABSTRACT

The paper examines the background of the Shuttle avionics system design and the unique drivers associated with the redundant digital multiplexed data processing system. With flight software pervading to the lowest elements of the flight-critical subsystems, it was necessary to identify a unique and orderly approach of verifying the system as flight-ready for STS-1. The approach and implementation plan is discussed, and both technical problems and management issues are dealt with. A summary of "lessons learned" completes the presentation.

BACKGROUND

Before addressing the subject of this paper, it would be worthwhile to summarize the salient features of the Shuttle avionics system in preparation for the subsequent discussion (fig. 1).

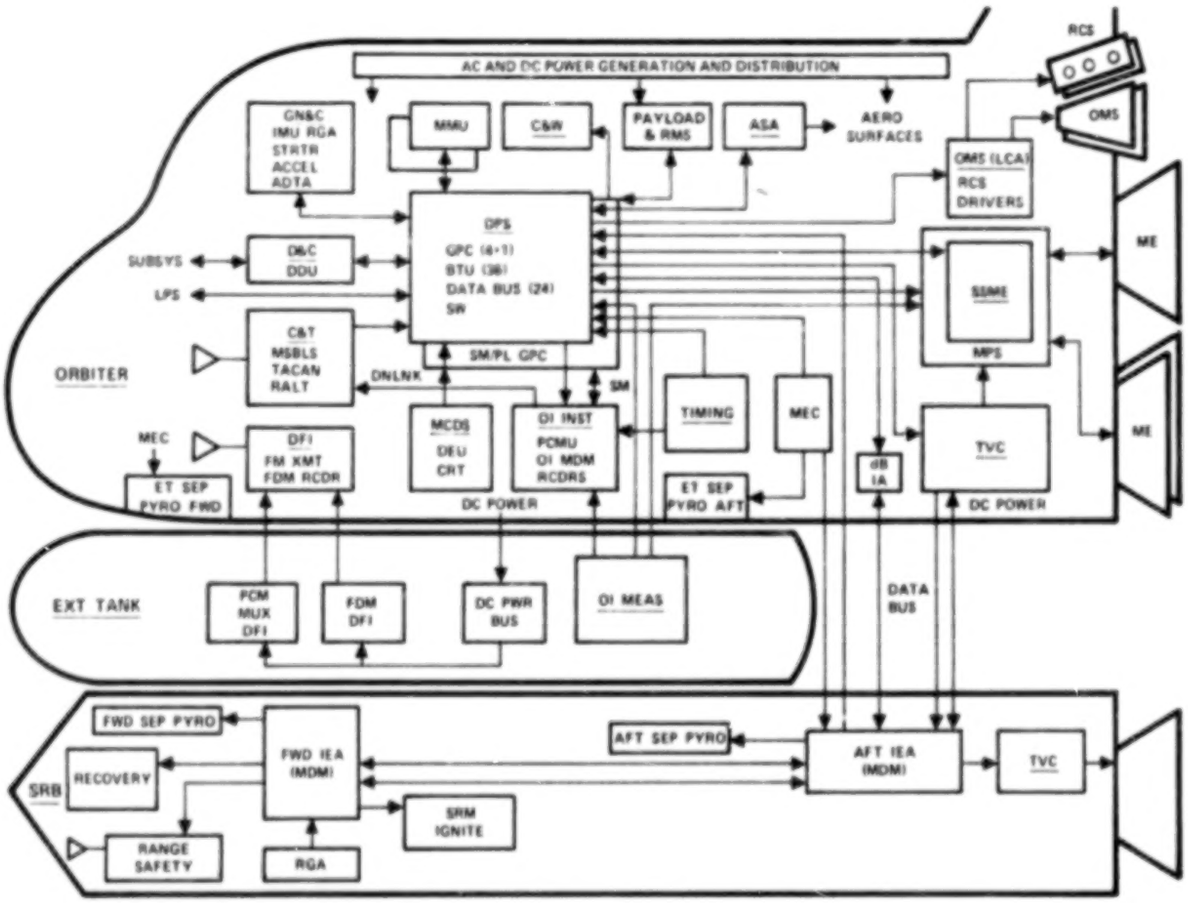


FIGURE 1.- AVIONICS SYSTEM FUNCTIONAL DIAGRAM.

1. The primary flight system (PFS) design is based on a centralized set of quad-redundant general-purpose computers (GPC's) within the data processing system (DPS) which provides the primary mode of acquiring flight-critical sensor data, processing the data, and, finally, generating and delivering guidance, navigation, and control (GN&C) commands to the various vehicle control elements (fig. 2).

2. Additionally, a single GPC with independently designed and coded flight software, called the backup flight system (BFS), is available to take over vehicle control through the primary bus structure from the PFS, if necessary.

3. The DPS bus structure contains 24 separate serial digital input/output (I/O) buses including 8 flight-critical (GN&C) and 5 intercomputer (ICC) buses, which provide for sensitive data communications and control through the GPC redundant set.

4. The various multiply redundant inertial navigation and flight control sensors and effectors must be in a constant state of readiness to perform the fault detection, isolation, and reconfiguration (FDIR) functions.

5. The avionics and nonavionics system management (SM) function is performed in conjunction with the operational instrumentation (OI).

6. A three-string electrical power distribution and control system provides single fault-tolerant power to non-flight-critical systems and dual fault-tolerant power to flight-critical systems (fig. 3).

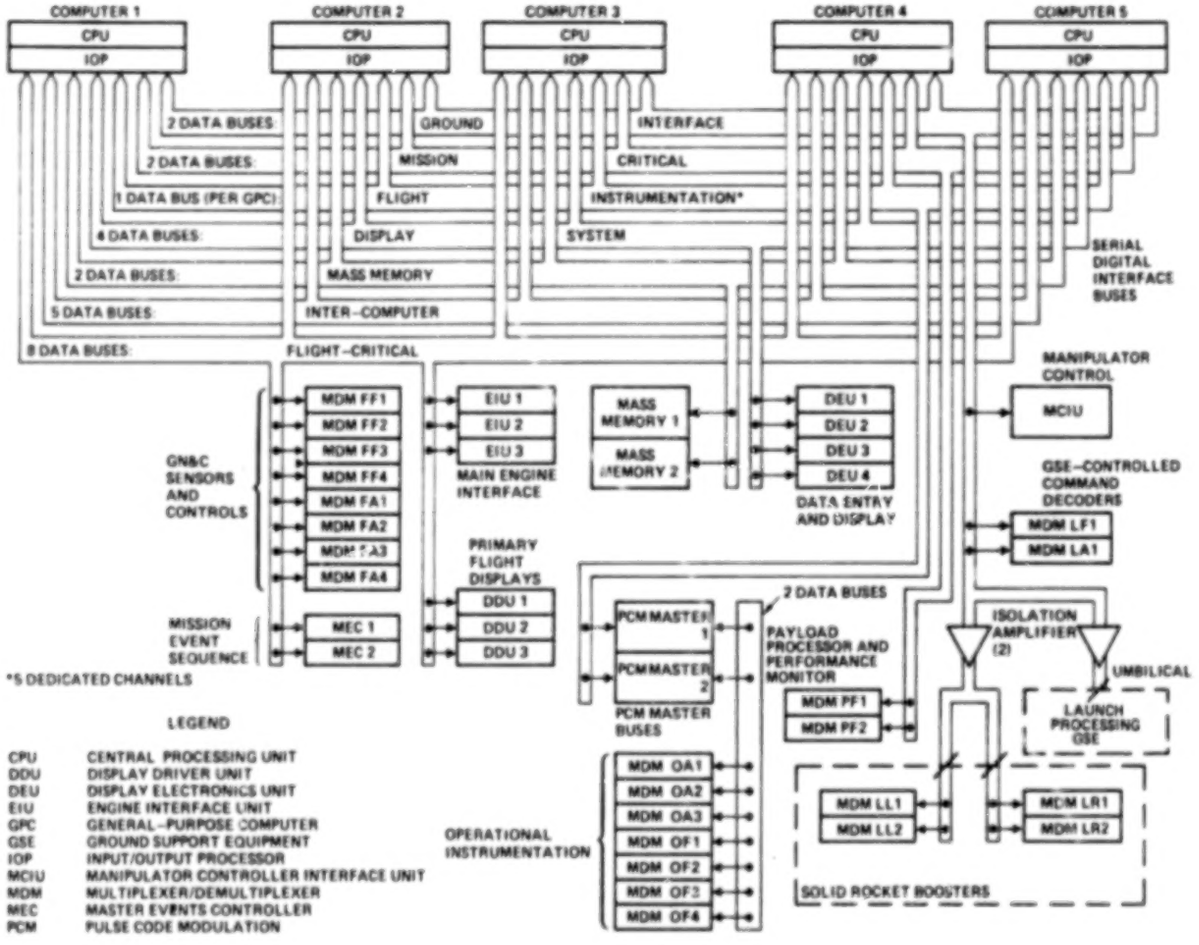


FIGURE 2.- ORBITER DATA PROCESSING SYSTEM.

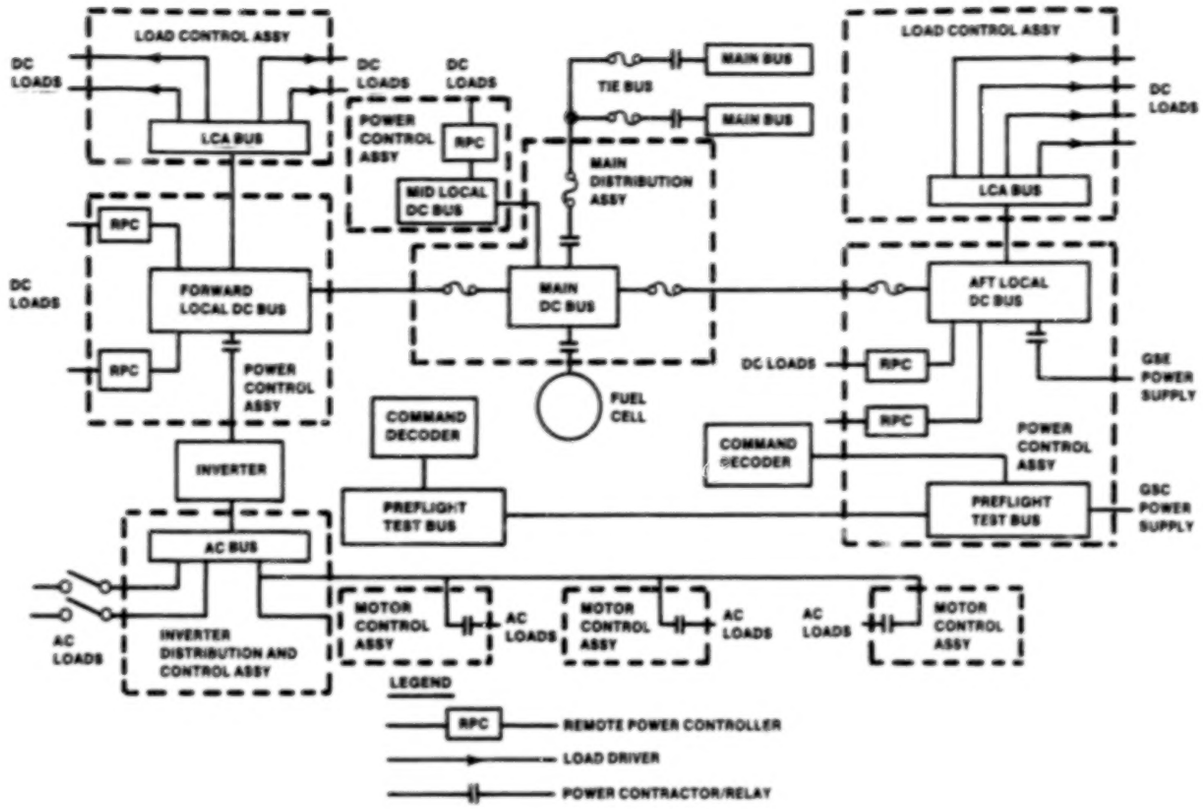


FIGURE 3.- ORBITER POWER DISTRIBUTION, SINGLE STRING.

During the early years of the Space Shuttle Program, the avionics system was defined and understood with regard to design requirements from the top downward, and it was assumed that the methods used for system certification during the Apollo Program would suffice for the Shuttle. However, it became apparent, as the various subsystem designs matured, that software would be increasingly dominant in the system functions. In fact, the flight software would pervade throughout multiple levels of the various elements as evidenced in the GN&C system (fig. 4).

With the significant improvements in capability of digital flight computers, the increasing importance of software within a hardware design was not unexpected. The unexpected factor was the time phasing of the software code design and development, which, because of the need to understand first the hardware design and operating characteristics, lagged behind the hardware in subsystem test readiness. A significant dilemma that emerged was a means of testing and certifying the lower level subsystem elements in a reasonable time phase in the program with already developed hardware and immature flight software.

The complexity of the problem became apparent during laboratory testing of the various avionics subsystems which were to be employed in the Orbiter 101 (Enterprise) Approach and Landing Test (ALT) Program at Edwards Air Force Base in 1977. During the laboratory test period, which preceded the flights by a year, concern was generated because of confusion arising in the following areas.

1. The scope of hardware certification, which generally was thought to be stand-alone line replaceable unit (LRU) (i.e., black box) testing, and its relationship with subsystem- and system-level function and performance testing, usually requiring some of the flight software elements in combination with hardware LRU's

2. The scope of testing necessary to declare the system ready to fly as compared to the test and analysis necessary to provide specification compliance

3. Visibility of the requirements to meet both flight-readiness and specification compliance

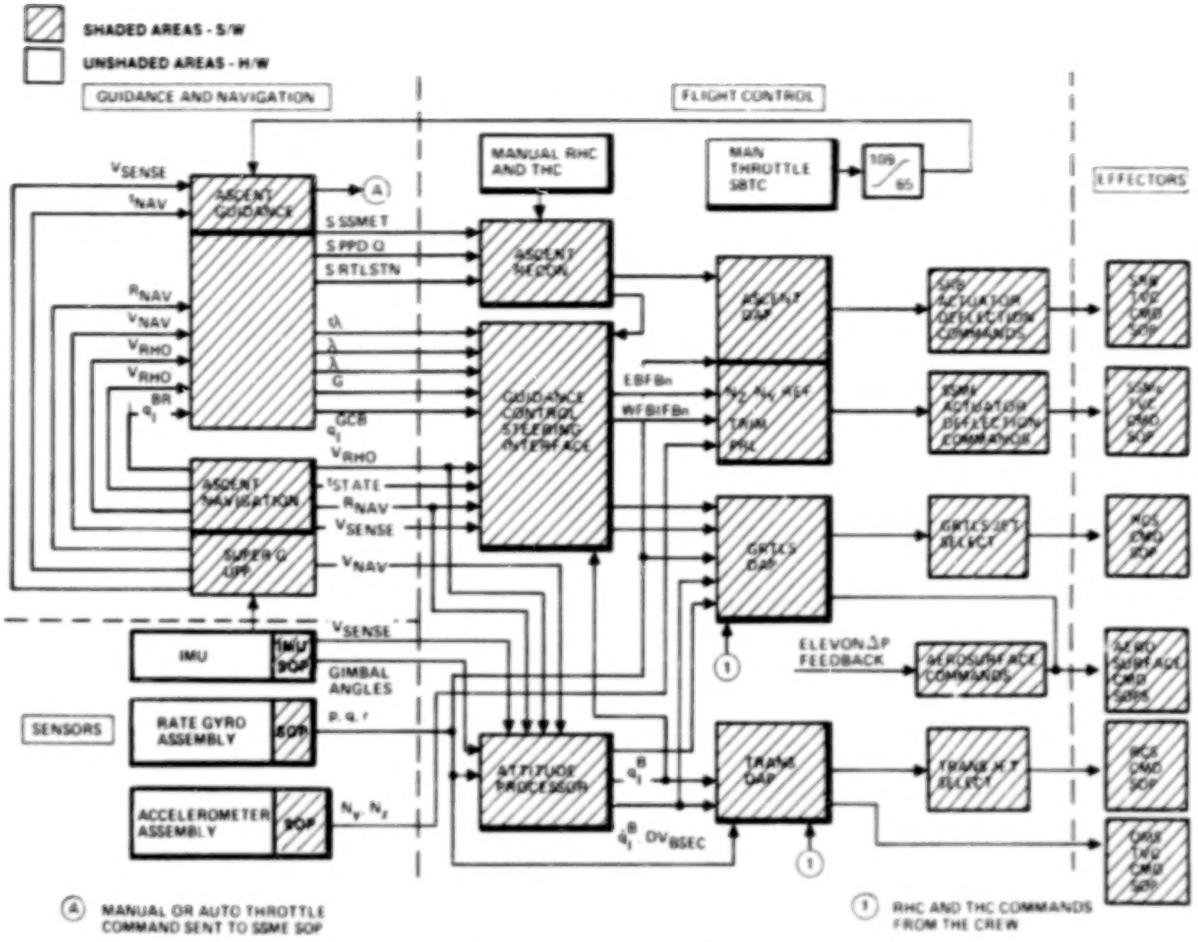


FIGURE 4.- ORBITER GUIDANCE AND CONTROL ELEMENTS.

In 1978, following the ALT Program, several members of Rockwell and NASA engineering management met for the purpose of addressing the previously mentioned problems before the onset of Orbital Flight Test (OFT) preparations. At the meeting, it was decided (1) to modify the scope and relationship of the Orbiter LRU certification and necessary subsystem- and system-level avionics tests and analyses, hereinafter called verification, (2) to differentiate between mission-to-mission flight readiness during OFT and operational readiness indicated by specification compliance, and (3) to develop a mission-to-mission verification process with adequate rigor and visibility necessary to identify the specific requirements to meet flight readiness during OFT.

GENERAL APPROACH

To establish a verification process, it was first necessary to establish the relationship between hardware and software. In the case of the Orbiter DPS, flight software elements which were commonly resident in the GPC's supported the lowest level hardware LRU's. To treat these software elements, which effectively stand alone in function, and their hardware LRU counterparts as functioning subsystems, the software elements were also called LRU's. Simply stated, verification may be defined as higher level tests and analyses above the LRU certification level necessary for compliance with predefined requirements. For purposes of Shuttle avionics verification, the various levels range from the lowest stand-alone functional element (actuation subsystem) to the highest level of integrated vehicle elements (mated Shuttle vehicle), as shown in figure 5. This definition also infers that the avionics verification process would transcend project-level boundaries between the various vehicle elements and would, indeed, be an integrated avionics verification process.

As a result of the 1978 discussions, it became apparent that it was neither necessary nor possible to complete all verification tests and analyses required to achieve specification compliance before the first OFT flight (STS-1). Instead, it was decided to address flight-readiness verification on a mission-by-mission basis. The cumulative mission verification effort coupled with a defined analytical effort became the building blocks to complete specification compliance verification (fig. 6). Finally, it was evident, because of the system complexity, that a highly visible and rigorous process must be in place to assure that the necessary tests and analyses had been completed to provide confidence in declaring system flight readiness.

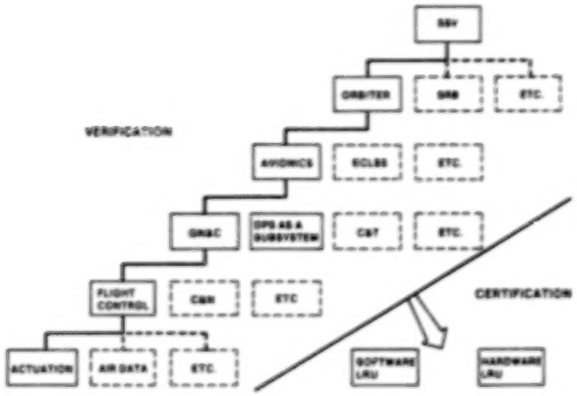


FIGURE 5.- SHUTTLE LRU CERTIFICATION AND SUBSYSTEM- AND SYSTEM-LEVEL VERIFICATION.

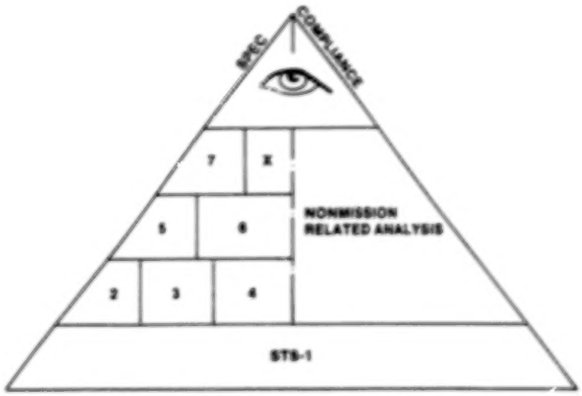


FIGURE 6.- RELATIONSHIP OF FLIGHT-READINESS VERIFICATION TO TOTAL VEHICLE SPECIFICATION COMPLIANCE VERIFICATION.

In the case of the DPS and the GN&C system, the design teams were in place and were sensitive to the relationship of their respective technical disciplines with the integrated avionics system. This was not necessarily the case for the nonavionics disciplines, for which sequencing, control, and system management functions for power generation, mechanical, and propulsion systems were provided as a service by the DPS. To provide verification requirements visibility within the nonavionics systems, three-man subsystem teams, consisting of one each software, hardware, and test specialist familiar with each of the subsystem designs, were formed. They were responsible for using the various subsystem specification and design documents to define a bottom-upward approach to the verification requirements.

In the case of all systems, as the requirements were identified, they were mapped, using as a reference hardware, drawings, software specifications, certification, qualification test, acceptance test plans, and designer insight. The resulting "roadmap" identified the type of analysis, laboratory, and/or flight vehicle test necessary to accomplish verification for that specific element, function, or subsystem. Each roadmap stood alone but provided the foundation for higher level elements in the verification tree (fig. 7). Each roadmap evolved into a verification plan which was jointly negotiated between the Rockwell sponsor responsible for design and acceptance in the respective technical discipline and the NASA counterpart. Tests and analyses were conducted and results jointly reviewed by the sponsors. The final conclusions were documented in a Verification Completion Notice (VCN), which was signed by the sponsor counterparts. The resulting documentation (verification plan, VCN, and associated test and data requirements documents) provided the desired rigor and traceability to the process.

In summary, the role of the technical sponsors was the keystone to the verification process. Each was charged with the responsibility of defining the verification requirements, determining the method of test or analysis to meet requirements, defining the criteria for test site acceptance, determining the data requirements for the tests, determining the pass-fail criteria for those data, resolving test anomalies, reporting the test results, and, finally, determining the flight readiness of his function or element. It is now appropriate to describe the technical and management tools necessary to make the verification process work.

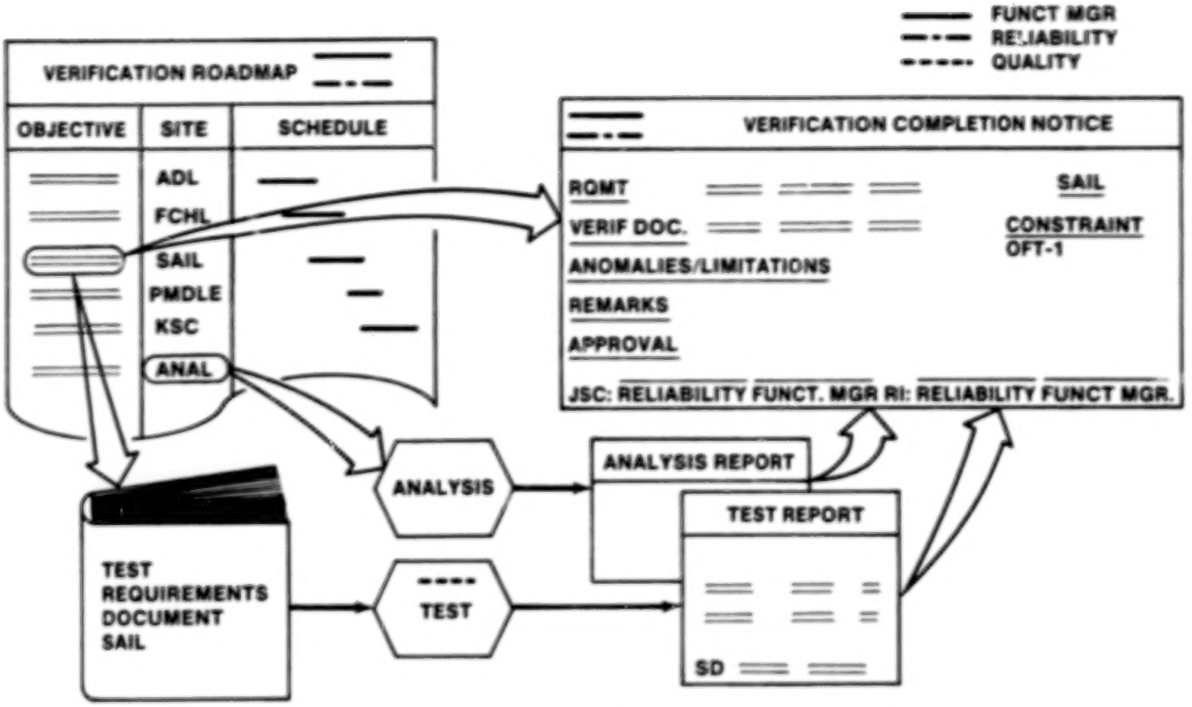


FIGURE 7.- OFT FLIGHT-READINESS VERIFICATION PROCESS.

DESIGN VERIFICATION APPROACH

The avionics design verification approach employed the following methodology.

1. Divide the total avionics system into technical disciplines.

2. Utilize the best technical resources for verification; i.e., assign the best technical personnel as verification sponsors for each technical discipline and determine the best combination of test and analysis tools for the job.

3. Establish a framework for avionics integration.

Figure 5 shows the application of this logic tree process to the lowest levels. As a basis for the verification, the sponsors treated both the hardware and the software LRU's as flightworthy elements; i.e., the hardware LRU's were certified to withstand the flight environments, and software was independently tested to show requirements compliance.

The sponsor's challenge was to demonstrate the flightworthiness of his respective hardware or software element to accomplish the mission. The following tools were used as appropriate.

1. Hardware and software laboratories and test facilities

2. Analysis programs

3. Airborne test articles

4. Shuttle flight vehicle prelaunch testing

The use of the flight vehicle was very restricted. The strategy was to perform the bulk of verification through laboratory testing and analysis.

HARDWARE AND SOFTWARE LABORATORIES AND TEST FACILITIES

The Flight Systems Laboratory (FSL) at Downey, California (fig. 8), and the Shuttle Avionics Integration Laboratory (SAIL) at the NASA Lyndon B. Johnson Space Center (JSC), Houston, Texas (fig. 9), had been developed as the primary test facilities for avionics verification. Because of avionics system complexity and for schedule considerations, the SAIL was developed for the ascent flight phase and the FSL was developed for the descent flight phase. The FSL and the SAIL shared the on-orbit verification. Both facilities provided system-level open- and closed-loop capability, and SAIL possessed a complete set of flight-type avionics hardware and cable harnesses.

Other hardware test facilities included the Flight Control Hydraulic Laboratory (FCHL), the JSC Electronics Systems Test Laboratory (ESTL), Thiokol, the Main Propulsion Test Article (MPTA), and the NASA George C. Marshall Space Flight Center (MSFC) Main Engine Simulator. Using these facilities, the sponsor would typically develop and validate math models, establish open- and closed-loop function and performance, and confirm hardware-to-hardware and hardware-to-software compatibility. Before a facility was used for formal verification, the sponsors performed site acceptance testing using off-line analytical data as a reference. Site acceptance provided sponsor confidence in facility representation of the flight article.

ANALYSIS PROGRAMS

The sponsors used analysis programs to confirm stability and to verify dynamic performance considering nominal and off-nominal conditions. The sponsors developed the analysis programs in parallel with the system design, development, and verification testing. The fidelity of the analysis programs was updated by correlating their performance with test results. Eventually, the analysis programs became key off-line analysis tools that could repeat test results and expand operating conditions by parametric changes to establish envelopes about the design nominal. These analysis tools effectively supplemented the hardware test articles for complete system verification.

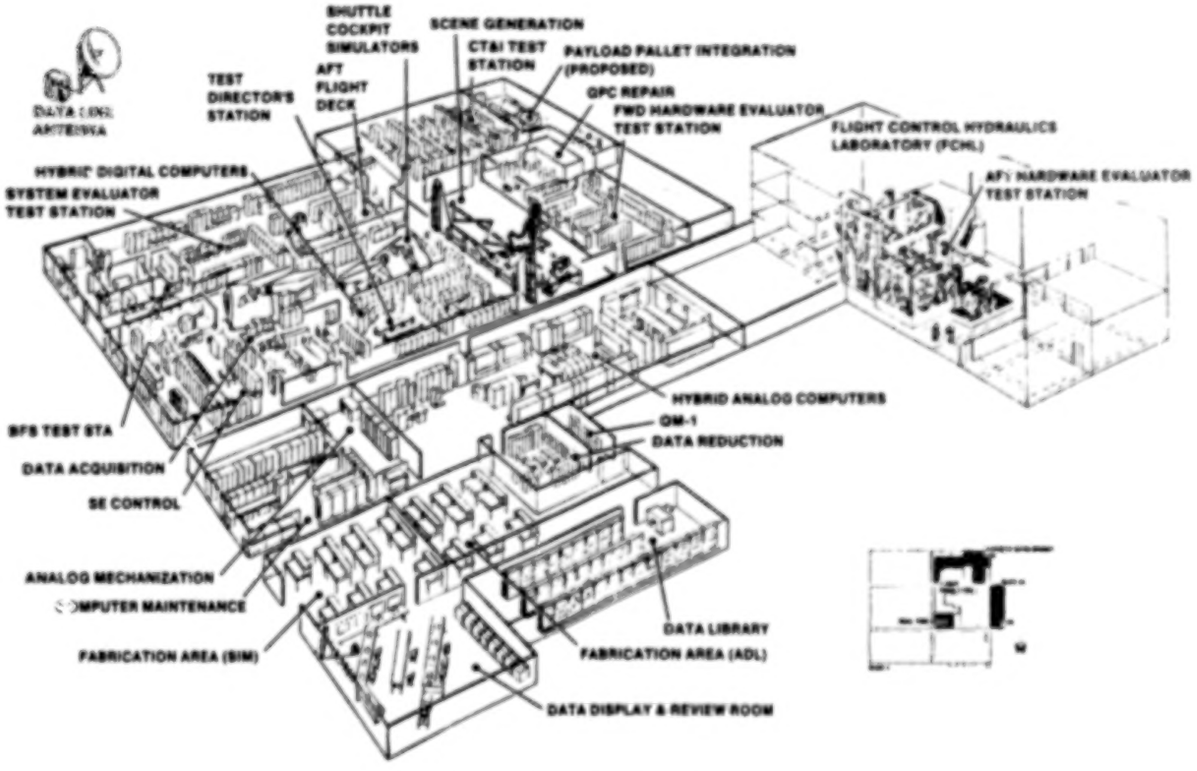


FIGURE 8.- FLIGHT SYSTEMS LABORATORIES.

ORIGINAL PAGE IS
OF POOR QUALITY

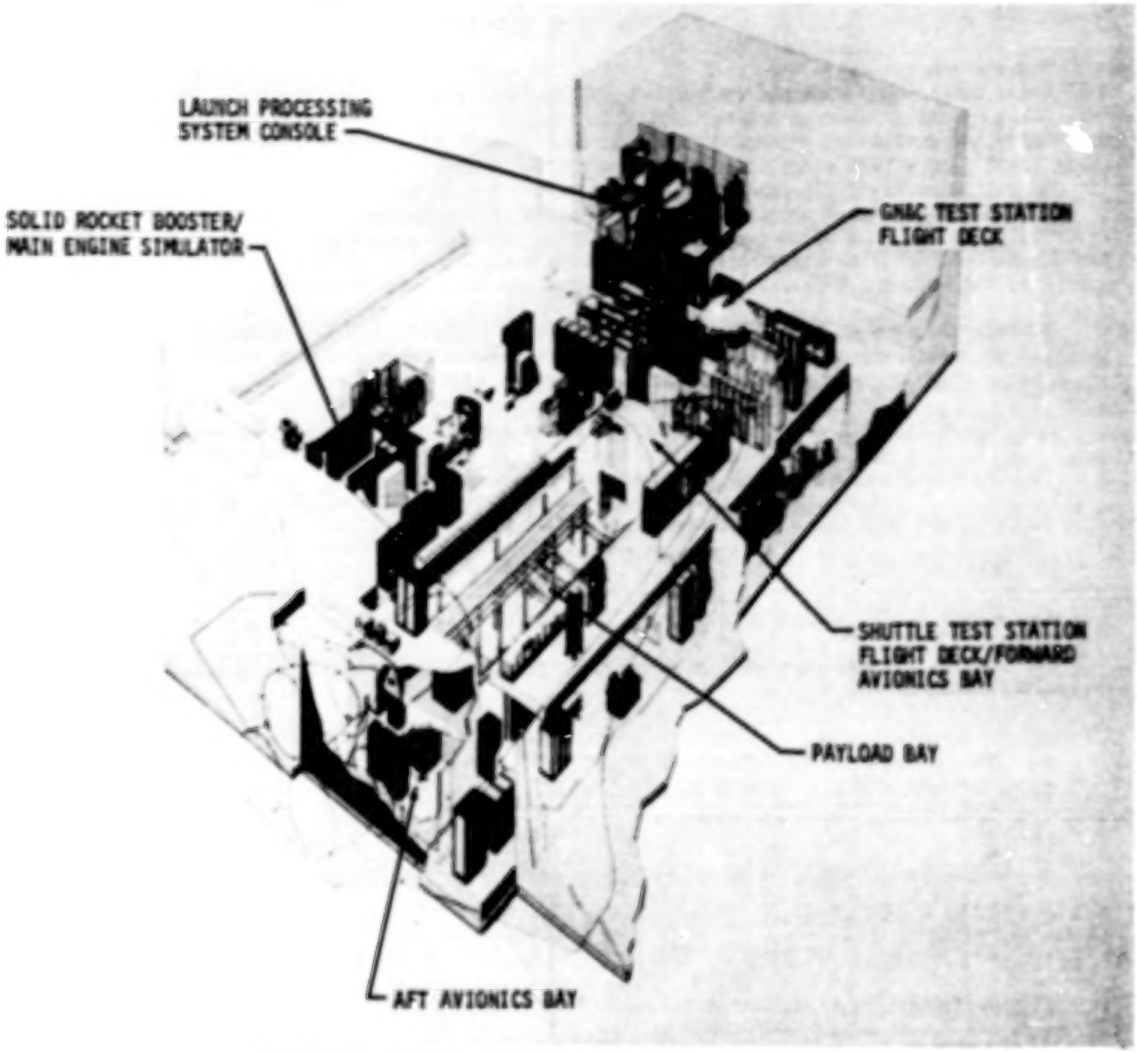


FIGURE 9.- SHUTTLE AVIONICS INTEGRATION LABORATORY.

AIRBORNE TEST ARTICLES

The Shuttle Training Aircraft (STA) and the SR71 flight test program supplemented avionics verification by providing in-flight characteristics to enhance sponsor understanding. Limited but valuable flight insights were derived through use of this technique.

SHUTTLE FLIGHT VEHICLE PRELAUNCH TESTING

Ground testing of the actual vehicle to be flown provided an extremely beneficial understanding of specific flight vehicle characteristics. In addition to the rigorous ground checkout process, which was an independent key element for committing to flight, specific verification ground tests were accomplished on the flight vehicle. These tests required a higher level of assembly and integration than could prudently be accomplished in a laboratory. End-to-end flight control tests, dynamic stability verification, and simulated integrated mission runs were typical types of tests. Because these tests used both flight hardware and flight software, extremely high preflight confidence in the integrity of the flight article was obtained.

To complete the framework for the avionics integration, a challenge emerged which required the NASA and contractor institutional managers to coordinate their various technical resources and meet a time-critical flight-readiness schedule.

MANAGEMENT CHALLENGE

Because the various elements of the integrated avionics system were being developed by three NASA field centers and numerous contractors, it was necessary to provide some means of unified control. The myriad of diverse program elements (fig. 10) had to be integrated by a process capable of developing the confidence necessary to ensure that the avionics hardware and software system was ready for flight within a defined time schedule. The control mechanism had to be capable of providing communication among the various program elements, system technical areas, and program management. It also had to be capable of controlling all aspects of the avionics verification process without restricting the feeling of personal accountability. In addition to providing for program biases, the management function also had to be responsible for assuring availability of the tools necessary for providing the test and the analysis data base required for proof of system flight readiness.

Taking into account these fragmented but critical activities, the complexity of the avionics system, and the magnitude of verification requirements, it was necessary that specific management controls be provided. These included the following.

1. Obtain and maintain the commitment from the technical sponsors to do the verification job.

2. Provide interface between the program elements.

3. Allocate test facility resources.

4. Resolve issues.

5. Secure flight-readiness commitment from the sponsors.

6. Provide program management with focused visibility of verification progress and bring forth unresolved issues.

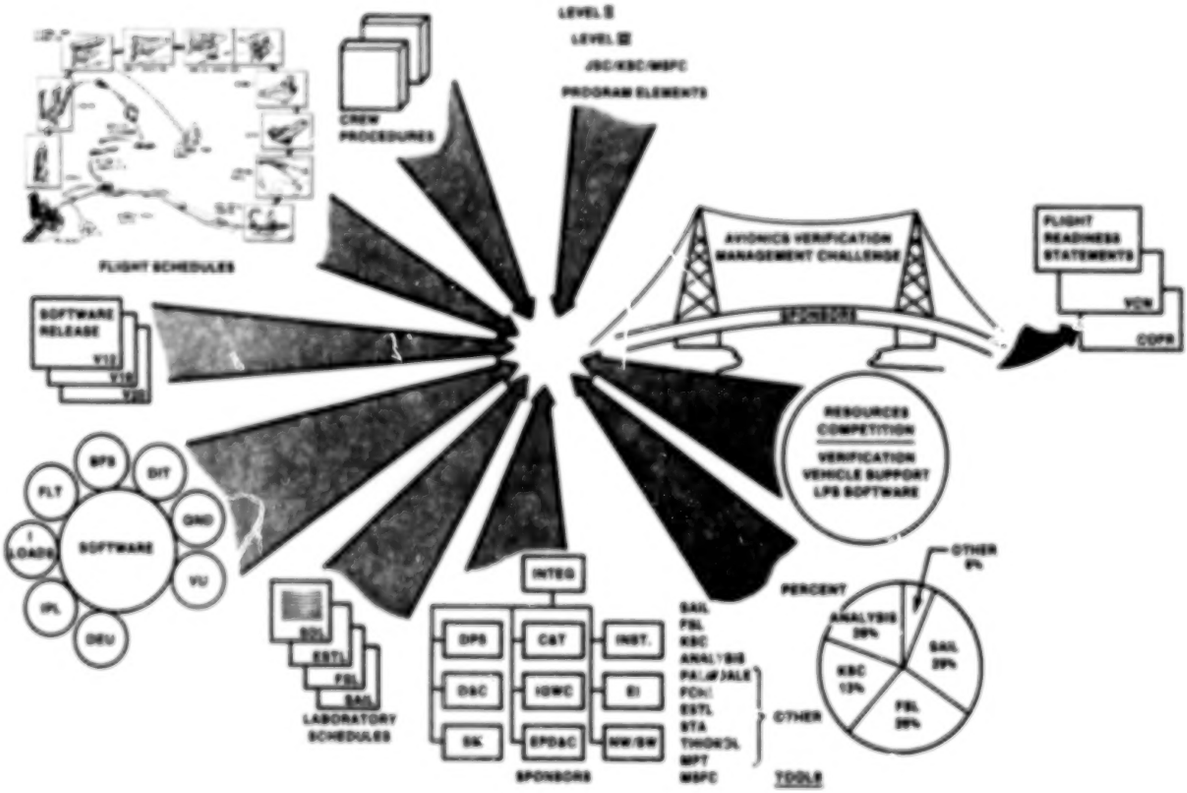


FIGURE 10.- MANAGEMENT CHALLENGES.

ORIGINAL PAGE IS
OF POOR QUALITY

Early in 1978, the avionics verification management was established to provide these controls. It encompassed all aspects of avionics verification and was focused through a management review team, which presided over and administered the avionics verification activities. The team consisted of managers from each aspect of avionics verification, as follows.

Management Working Group (MWG) Membership

NASA	Rockwell
Systems Engineering	Systems Engineering
SAIL	FSL
NASA John F. Kennedy Space Center (KSC) Engineering	SAIL
GN&C Engineering	KSC Engineering
Flight Software Engineering	

The MWG was provided with tools to assure their ability to control the process. These tools consisted of the following.

VERIFICATION LOGIC TREE

The verification logic tree (fig. 11) defined the scope of avionics verification. It provided a single source to relate the individual subsystem function to other elements in the integrated avionics system. Each subsystem function is depicted in a block on the tree; relationships of subfunctions are listed below each block. The tree provides a "bottom-up" hierarchy of subsystem functions (such as flight control) to the higher functions (such as descent GN&C) and then to the top function (integrated avionics). The verification logic tree provided a reference tool with which to measure the verification progress, to establish priorities, and to determine areas requiring additional emphasis.



FIGURE 11.- AVIONICS VERIFICATION LOGIC NETWORK.

INDIVIDUAL ACCOUNTABILITY MATRIX

Related to the verification tree was the matrix of sponsor accountability. As previously mentioned, success of the verification process depended on the involvement of the avionics system design personnel. This involvement was assured by developing an accountability matrix based on the verification logic tree and assigning the appropriate NASA and Rockwell counterparts to each subsystem or function and by obtaining commitments from line management that avionics verification sponsorship was truly the individual's assigned task. In other words, the process was totally reliant on the design community for the technical effectiveness of avionics verification. Without the commitment of the proper personnel to the process and the backing of the process by program management, it would not have been possible to integrate and manage the effort required for commitment to flight readiness.

MANAGEMENT WORKING GROUP

The MWG was the forum for administering the avionics verification process. It met weekly by teleconference to review progress of avionics hardware and software system verification and to resolve issues impacting the process as shown in figure 12. Specifically, the functions of the MWG were as follows.

1. Review and baseline the verification tests for each flight.

2. Review and approve changes to the baseline for new requirements (mission changes, software changes, or delivery schedules).

3. Establish test priorities.

4. Review laboratory schedules.

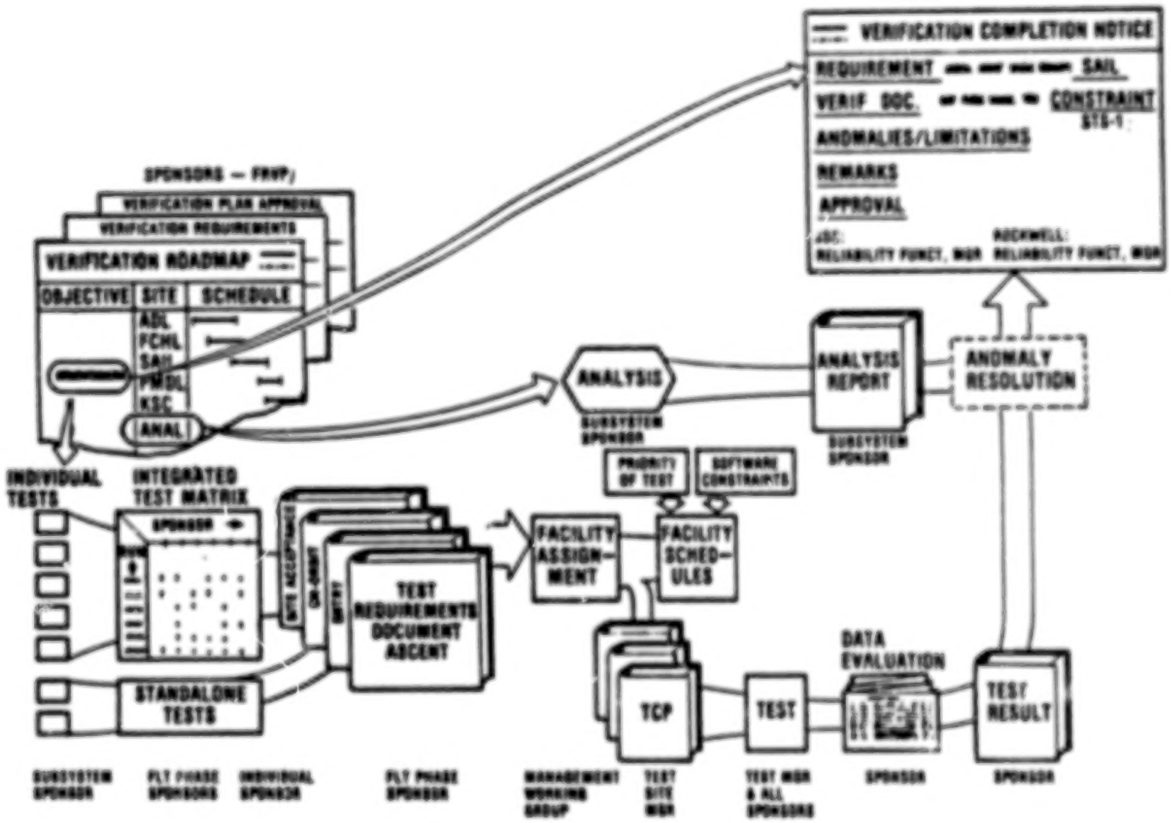


FIGURE 12.- VERIFICATION PROCESS FLOW AND DOCUMENTATION SUMMARY.

5. Identify laboratory problems, hardware availability issues, and manpower assignments that must be taken to program management for resolution.

6. Review verification issues.

The M&G provided the medium for sponsor interface with the laboratories, JSC, KSC, and MSFC. The M&G was co-chaired by Rockwell and NASA, and decisions of the M&G Board constituted direction to the verification community to proceed. Any issues which carried impacts beyond the verification community were taken forward to program management for disposition.

FLIGHT READINESS VERIFICATION PLANS

The Flight Readiness Verification Plans (FRVP's) provided traceability to the sponsor's verification requirements and consisted of three parts: (1) verification roadmaps, (2) verification requirements, and (3) an approval sheet. The verification roadmap identified the verification tasks, the test site, and the planned schedule for the tests. The verification requirements sheet defined each verification task in general terms and assigned a tracking number to each task. The tracking number was used to provide traceability from the VCN back to the FRVP. The approval sheet was signed by Rockwell and NASA counterparts after the plan and the details had been coordinated. The FRVP, in conjunction with the verification logic tree, defined the total task, which, when completed, would provide a data base sufficient to permit signoff at each level of the commit-to-flight process. These two documents provided the M&G with the necessary criteria for evaluation of the criticality of remaining effort.

SUMMARY - WITH REFLECTIONS

The resulting verification process culminated in an intense but orderly effort which provided the necessary confidence in the Space Shuttle avionics system to perform the STS-1 mission. The process remains in place today and is providing the necessary incremental verification to determine flight readiness for subsequent flights.

Throughout the effort leading to the first flight, the process provided the means for successfully resolving the conflicts which occurred during the integration of this complex system. Typical were the significant problems discovered within the Orbiter entry flight control system during initial verification testing. A resulting major redesign within the flight software required major replanning and schedule changes. During this period, the working relationships among the verification sponsors (designers), the laboratory test teams, and the flight software design and test personnel led to mutual respect for the common objective: "Get the avionics system ready to fly!" Their commitment to that objective minimized the conflicts that had to be resolved. Had management, early in the program, understood the impacts of software involvement throughout the avionics system, the logjam of concurrent subsystem- and system-level testing resulting from late release of flight software might have been minimized. As it was, the process lessened the logjam by integrating subsystem requirements into system-level test runs. The message, however, remains: "In future programs, the subsystem designs should acknowledge the need for an up-front verification strategy which minimizes the labor-intensive laboratory test effort."

Finally, the need to involve the designer personally in the flight-readiness verification process for future programs needs to be acknowledged. This involvement includes not only the planning phases of the verification but also the final decisions of system flight readiness. With the increased interaction of future flight systems, the individual designers must be accountable for the readiness of their respective elements for flight.

N85
16897

UNCLAS

N85-16897

GROUND/MAN-MACHINE INTERFACES FOR ORBITER CHECKOUT

F. Herb Blackmon
IBM Test & Operations
Kennedy Space Center

ABSTRACT

This paper discusses the challenges presented by the concept of a reusable, cargo carrying space vehicle, and how those challenges were met for the Space Shuttle. Areas discussed here include the complexity of the vehicle, the ground support system, the onboard computer system, ramifications of a reusable vehicle, and the turn-around objectives for Shuttle flights.

After six successful flights at the time of this writing, it can be safely said that the challenges presented here have been basically met.

INTRODUCTION

Adjacent to the Vertical Assembly Building (VAB) at Kennedy Space Center (KSC) is an APOLLO vehicle, complete with all the stages required to orbit the Moon and return. The long, sleek and sharply pointed configuration could be imagined to be a spear used by some mythological god to fling into the heavens to bring down a passing star.

In the VAB, in preparation for a Space Transportation System (STS) flight is a configuration of two Solid Rocket Boosters (SRBs), an External Tank (ET), and an Orbiter. Unlike the APOLLO launch configuration, the STS looks bumpy, unsymmetrical, and no god would have any use for it. Indeed, the STS configuration could be thought of as the bumblebee of space flight - it appears to be an ill-conceived design, but does its job beautifully.

Although the appearance of the two vehicles is remarkably different, the technical aspects of preparing each for, and accomplishing a launch are even more different. This article will present some comparisons in vehicle complexity, ground support systems, objectives, and turn-around requirements to demonstrate how the STS challenges were responded to.

VEHICLE COMPLEXITY

As stated earlier, the appearance of STS is very different from its predecessors in America's space ventures. The STS is several orders of magnitude more complex than earlier launch vehicles. Indeed, STS is the first vehicle conceived, designed, and implemented strictly as a space transportation system. Earlier vehicles used to put payloads into space were, at best, quasi-military in concept and design, and in some cases such as Thor, Atlas, Delta, etc. were military vehicles adapted for use by NASA.

Several items may be compared between APOLLO and STS to demonstrate the increased complexity of the vehicle: engines, control capability, computers, payloads, and landings.

Engines

The APOLLO vehicle, although consisting of three stages, can be thought of as a single engine vehicle, since only one type of engine was ignited at a time. Even in the Saturn V first stage with its five engines, the engines were arranged symmetrically about the center of the vehicle with the middle engine fixed.

The STS, in a nominal launch, also has five engines ignited. However, two of these are SRBs, while three are the Space Shuttle Main Engines (SSME); and the engines are not symmetrical about the centerline of the total vehicle.

The SSME's are liquid fueled from the ET and controlled by their own computer (Engine Controller) which interfaces with the onboard computer system, while the SRBs are solid fueled and controlled directly by the onboard computer system.

In some non-nominal situations, the STS can also utilize the two Orbital Maneuvering System (OMS) engines to assist in later stages of the launch. These engines are liquid fueled from tanks onboard the Orbiter.

Control Capability

In APOLLO, the astronauts were "along for the ride" - that is, the launch and ascent were automatically controlled by the ground and onboard computer. The crew had very few options if trouble developed during the ascent into Earth orbit.

The STS has both automatic control and manual control. The automatic control is similar to APOLLO. The manual control allows the pilot to manually steer the vehicle using the Rotational Hand Controller (RHC) from SRB ignition through SSME shutdown.

The STS also has the capability, for non-nominal situations, of several abort modes: a Return-to-Launch-Site (RTLS), a Trans-Atlantic Landing (TAL), an Abort-Once-Around (AOA), and an Abort-to-Orbit (ATO).

Computers

The APOLLO configuration contained a single computer in the Instrumentation Unit which controlled the vehicle's flight. The computer was preloaded with the flight profile, data, etc. and, for ascent, had no crew interface capability.

STS, on the other hand, has five General Purpose Computers (GPCs) which control the vehicle's flight and provide interfaces to the crew to allow them to make inputs during ascent. Four of the computers run in a "redundant set" using the Primary Avionics Software System (PASS), while the fifth is loaded with the Back-up Flight System (BFS). During ascent the four PASS computers synchronize themselves over 300 times per second and pass data to the BFS computer to allow it to track the flight. Should the PASS set fail, the crew can order the BFS computer to take command and provide for a safe flight to either continue or return.

Payloads

APOLLO was designed to put a single payload into space - the crew compartment (and Lunar Excursion Module) and its contents. It was strictly an exploration program to increase our knowledge of near space through manned exploration.

STS is a service system designed to put many types of payloads into space. With its Remote Manipulator System (RMS), or "arm", STS can deploy and retrieve payloads, shuttle them back and forth, and perhaps even effect repairs on faulty payloads in orbit.

Landings

The APOLLO crew compartment effected a ballistic reentry with a water landing where it was plucked from the water by a ship stationed in the landing zone, then transported back to the USA for display.

The STS lands in a conventional aircraft manner on a landing strip using conventional areosurface controls such as elevons, rudder, and speedbrake, with retractable landing gear. It can then be readied for the next launch.

GROUND SUPPORT SYSTEMS

The ground support systems of APOLLO and STS are as different in nature and complexity as the vehicles themselves are. Indeed, the consoles of the STS ground system are said to be inverted APOLLO ground system consoles!

Apollo Ground Support System

The APOLLO ground support system was composed of two ground computers which were transistorized, large scale, serial, digital computers. One computer was located in the Launch Control Center (LCC) and communicated via a data link with the other computer in the Mobile Launcher.

The two computers were required to be on-line and operational for checkout and launch so there was very little redundant or backup hardware. There were numerous single-point failures, and nearly 50 percent of the hardware was located within a few hundred feet of the vehicle, creating hazardous areas for maintenance.

More than two hundred people were required to monitor the meters, lights, plotters, etc. used in the launch complex to checkout and launch the vehicle. Data was obtained through fixed telemetry streams and fed into the LCC for interpretation by the individual engineers.

Testing of the launch configuration was largely a serial operation. A particular subsystem would have to be fully tested before the next subsystem could be started.

The net effect of this system was a long, tedious process to ready the launch vehicle for flight.

STS Ground Support System

The STS ground support system, termed the Launch Processing System (LPS), is designed to meet the rapid turn-around requirements for a reusable vehicle and to reduce the number of people involved in vehicle testing and launch. At the same time, the LPS preserves the test engineer's direct control over checkout and launch procedures.

The LPS is a network of minicomputers (up to 64) which share a common data buffer to pass data and commands between computers and the vehicle. Communications between the LPS in the LCC and the vehicle is accomplished via a Launch Data Bus (LDB) which is "attached" to the GPCs onboard.

Two key differences between APOLLO and STS have been realized through LPS: visibility through CRT displays (and thus digital display in engineering units of data) of status and data, and the ability to perform parallel testing.

Also realized through LPS, although not readily "seeable" to the user, is a high degree of flexibility and redundancy. Since the LPS is a distributed system, any minicomputer can be loaded from a master computer with a selected subsystem load. Thus, if a console and/or a computer fails, a spare console/computer can be quickly brought up in its place. Critical system functions are backed up in computers in such a manner that a switch can be made with minimum loss of data.

An overview of the LPS and its architecture is presented in "The Launch Processing System for STS and DoD Space Shuttle" by Don G. Satterfield (IBM), published in the IBM/FSD magazine Technical Directions, Fall/Winter 1981, Vol. 7, Number 3.

OBJECTIVES

The objectives to be met in producing the ground/man-machine interfaces for Orbiter checkout were:

* Rapid turn-around - Initial requirements for an operational STS called for a 160 hour turn-around (10 working days of two shifts each).

* Minimization of "fixed" software - The amount of software residing in the GPCs uniquely for checkout was to be minimized as well as minimizing the ground software which was "fixed", that is, tailored for a specific vehicle/payload configuration.

* Flexible capabilities - Provide engineers with "menu" selection of predefined tasks to be done and provide the capability to perform contingency tasks.

* Complete vehicle checkout - Provide the capability to test the Orbiter in the Orbiter Processing Facility (OPF), the STS (Orbiter, ET, and SRBs) in the VAB and at the pad, and the payload(s) at the Cargo Interface Test Equipment (CITE), OPF, and pad.

IMPLEMENTATION

The objectives spelled out have been met through implementation of computer programs in onboard GPCs in PASS and in the LPS computers, and procedures for engineers to use.

Onboard Capabilities

The primary interface between the LPS and the vehicle is the Launch Data Bus (LDB). While a direct mode between LPS and the command decoders onboard exists, we are primarily concerned here with the mode where the LPS and the GPCs communicate. In this mode, polling on the LDB occurs between the LPS and the GPCs every 40 milliseconds, with an established protocol being followed.

Commands from the LPS may be directed to one of six "functional destinations" in the GPC and may range from simply setting a discrete on in an MDM to initiating a series of commands to an actuator in a predefined pattern up to 100 times a second for a Frequency Response Test (FRT).

Single function commands are sent through "operators" in either the Test Control Supervisor (TCS) mode, or the System Avionics Command Support (SACS) mode, based on availability determined from the Operational Sequence the GPC is in.

Functions such as the FRT reside onboard in Explicitly Coded Programs (ECPs) which are designed to accomplish specific tasks. These are requested from the LPS via a single operator. The ECPs, once requested from LPS, will execute, based on parameters from LPS contained in the request, without further LPS intervention.

The PASS also uses the LDB to communicate with the LPS in the final phases of a launch countdown. The LPS Ground Launch Sequencer (GLS) uses the LDB to send control commands to the onboard Redundant Set Launch Sequencer (RSLS). LPS monitors Launch Commit Criteria (LCC) on the ground from the STS and RSLS to determine the status of the countdown.

Another key element of vehicle checkout is the securing of data from the various subsystems of STS. This is accomplished in PASS during vehicle checkout by the Housekeeping Data Acquisition (HDA) function which reads the various avionics related hardware and provides the data via downlist to LPS. The type of data and its format is selectable in predefined formats. So, unlike APOLLO with its fixed telemetry stream, STS has selectable telemetry streams with selectable downlist data imbedded in it.

Finally, the PASS has several autonomous vehicle checkout capabilities which are usable from the onboard keyboard/CRT system. These are called SPEC (Specialist) functions, and provide for predefined test and checkout capabilities.

Ground Capabilities

The LPS, as discussed earlier, is composed of a network of minicomputers. Each console/computer can support three operators who may be doing testing of different aspects within their subsystem in parallel.

In addition to the computers at each console, minicomputers are used to interface to the LDB and to receive data from the STS. These computers are called Front-End Processors (FEPs) and perform such functions as preconditioning data, formatting requested commands properly for the LDB, switching data formats, etc.

Engineers produce programs for the console computers using the Ground Operations Aerospace Language (GOAL), written by IBM for use in LPS. This language is oriented for engineering terminology and provides powerful, yet flexible capabilities.

In addition to the predefined capabilities generated through GOAL programs by the engineers, LPS contains a Command Processing system whereby an engineer can "build" commands to be sent to STS via the LDB. This capability allows the engineer to react to anomalous conditions and/or to accomplish a minor task which would not warrant generation and validation of a GOAL program.

ENHANCEMENTS

In large, complex computer systems, initial designs are seldom completely adequate or satisfactory. The STS checkout system is no exception to this. Many enhancements have been suggested and are either already implemented or planned.

Drivers for these enhancements, for the most part, have been the reduction of "special" considerations, greater flexibility, and increased visibility. For example, some enhancements that have already occurred are:

* The selection of aerosurface limits for movement when the Orbiter is in a horizontal position in the OPF or a vertical position at the pad. Initially these limits had to be "patched" in the PASS to change them. Now, an entry on a SPEC function display allows selection.

* Increased communication of TCS status between PASS and LPS. Additional status parameters have been added to ECPs to provide the LPS better visibility into reasons for rejection or failure of ECPs.

* Selection and saving of IMU parameters. Similar to the aerosurface limits, several IMU calibration parameters change when the Orbiter is in different locations. Originally, the only way to change these was via a patch to PASS. Now, on the IMU Calibration SPEC, the vehicle site can be selected prior to calibration. Also, the IMU checkpoint data can now be saved on all areas of each Mass Memory Unit (MMU) directly from the SPEC function.

The enhancement of ground/man-machine interface is not complete. Indeed, a task force of engineers from the Space Shuttle community still meets periodically to consider suggested enhancements which will make the system faster, more reliable, and easier to use.

SUMMARY

The STS is a very complex system which required a quantum step forward in the ground/man-machine interface system for checkout. This step has been made with the combination of the LPS and the PASS, so that the resulting system is:

* Flexible
* Powerful
* Conducive to parallel testing
* Highly visible
* Conducive to multi-vehicle flow testing.

ACKNOWLEDGEMENTS

The author wishes to express his thanks to Tom Santos, Elliot Burton, and Don Kleckner (all IBMers who were at KSC during the APOLLO era) for their support in producing this article. Also, to the IBM Test and Operations group at KSC for reviewing the article to make sure I didn't stray too far from the path.

N85
16898

UNCLAS

N85-16898

INTEGRATION OF GROUND AND ON-BOARD SYSTEM FOR TERMINAL COUNT

Charles A. Abner
Guidance, Digital & Software Systems Division
Kennedy Space Center

Don H. Townsend
Avionics Systems Division
Johnson Space Center

ABSTRACT

This paper discusses the challenge faced in the development of an integrated ground and on-board system for Space Shuttle terminal count management. The criteria considered in designing this system are outlined with some attention given to examples of problems encountered in the process of maturing the design.

INTRODUCTION

The integrated launch system developed in the Space Shuttle program requires a closely coordinated effort between the ground system and the on-board system. The system had to be structured so that it would be flexible enough for more rapid reconfiguration than in past programs. This was true not only for ground systems but also for the vehicle as well. This is a brief overview of the development of the Space Shuttle terminal count integrated monitor and control system.

SOFTWARE MANAGEMENT IS THE KEY

The Apollo launch support systems was composed of two computers, one located in the mobile launcher and directly locked to the vehicle, and one located in the Launch Control Center. These two computers were connected via a data link which provided fixed telemetry streams to the Launch Control Center for vehicle systems evaluation. The majority of the monitoring function was done by Firing Room personnel looking at meters, lights, and plotters driven by the Launch Control Center computer. Thus, the Apollo launch approach was essentially a fixed system which was structured to provide a single sequential flow for vehicle checkout and launch.

In contrast with the more restrictive approach for terminal count management as was used in Apollo, the challenge arose in the Shuttle era to allow a more flexible design which would be adaptable to the varied configurations of the launch vehicle. In order to achieve this flexibility a software architecture was designed for both on-board and ground systems to readily adapt to any requirement changes. This approach not only allowed for the initial development of the integrated launch system but also supports the basic concept of a multi-mission Space Shuttle Program.

SOFTWARE DESIGN STRUCTURE

The on-board systems management software structure was designed based on individual system inputs as to command/monitoring requirements. The terminal count and launch requirements were considered by the systems during the definition and design of this software structure.

The ground systems software structure was designed to meet total system checkout requirements. These include the requirements for terminal count capabilities.

CONTROLLING DOCUMENTS

During the process of defining these two software systems a interface definition document (CPDS-150) was developed. The primary purpose of this document was to baseline and establish configuration control of the Launch Data Bus (LDB) interface between the ground and on-board systems. This interface definition encompasses both day-to-day test and checkout requirements as well as specific terminal count requirements.

Various documents exist which control the requirements for terminal count activities. The on-board software requirements (for terminal count) were specified in the Functional Subsystem Software Requirements, Sequencing Requirements, STS 81-0026 (FSSR-26). The Launch Commit Criteria (LCC), JSC 16007 and KSC S00000-3, documents were established and are maintained by JSC and KSC. The Ground Launch Sequencer Description Document (GLSDD-OMI-S9005) establishes the parameter monitoring and sequencing requirements for ground systems and vehicle systems activities in support of terminal count and launch. The above documents not only relate software design requirements but also contain real-time anomaly guidelines such as hold/scrub situations.

SEQUENCE CONTROL

VEHICLE SOFTWARE

The flight GN&C software load supports all of the vehicle terminal count requirements. These requirements include both the on-board sequencing as well as the system software necessary to support ground initiated tasks. The on-board sequencing software has interfaces through the GN&C systems software with both the Backup Flight System (BFS) computer and the Space Shuttle Main Engine (SSME) computers. Through the use of these three software sets all Shuttle systems are managed/monitored for terminal count.

GROUND SOFTWARE

The Launch Processing System (LPS) application software supports all the terminal count requirements for ground systems and vehicle interfaces. Most of the terminal count activities are incorporated in the Ground Launch Sequencer (GLS) application software. The remaining terminal count activites are controlled/monitored by systems engineers via their own application software. The vehicle interface for these activities is supported by the on-board GN&C system software via the LDB and the PCM system. This interface provides the LPS access necessary to control all vehicle systems.

LIMITATIONS

It is now appropriate that a few software design limitations be discussed in order that the reader fully appreciates how the challenge of interfacing the ground to on-board systems with the required flexibility was achieved. Trade-offs of total software design capabilities were considered which resulted in today's limitations.

One of the primary limitations was that encountered with LDB structure. Design considerations were vehicle weight and hardware design flexibility in choosing a serial interface over parallel interfaces for the LDB. Additionally, software complexity and memory allocation were drivers in the decision process. The resulting LDB structure allows 240 msec to complete one ground to on-board transaction. This transaction may consist of a one-to-one task such as an operate valve request, a predetermined and stored sequence of one-to-one tasks, or a special coded flight software request for use in terminal count. A 120 msec timing may be achieved by the ground requesting to inhibit the on-board response available in the protocol. The serial data operation was designed with a redundant capability. This redundancy/design includes the necessary data bus hardware as well as the ground and on-board software.

Another limitation which affected the terminal count protocol was the design of ground software. Each firing room console (terminal count activities are controlled at the integration console in the firing room) has the capability of running six application tasks in addition to several other system software tasks. There are time critical functions in terminal count opera-

tions which require stringent control of these six application tasks in order to avert a console throughput (timing) problem. Increased console throughput activities result in delayed and inconsistent LDB operations.

Limitations for vehicle systems management arose as a result of constraining the number of systems parameters to be processed and monitored on-board. This limitation is taken care of by the ground system monitoring and processing of additional parameters.

The combination of the above limitations and several other factors led to the biggest challenge which was managing terminal count time critical events and time critical operations.

DESIGN CRITERIA

The design criteria of coordinating vehicle/ground clocks, performing retries of parameter statusing and command executions, real time data manipulations, and managing potential recycle/scrub activities greatly affected the integrated terminal count software structure.

TIME MANAGEMENT

Of prime importance in the integration of terminal count activities is the management and control of the ground and vehicle clocks. Greenwich Mean Time (GMT) is the reference used by both the ground and on-board software systems. By use of this reference the countdown clock is initialized and controlled by ground system commands. Countdown time is used to initiate all of the terminal count events required by the vehicle and ground. The primary challenge in this areas was the detailed analysis and coordination required to place each function at a specified time with relation to its associated terminal count events. An example of the need for integrated timing requirements was the disposition of the delta that existed between the ground and on-board time due to the on-board software delaying for main engine/vehicle structure stabilization prior to the Solid Rocket Booster (SRB) ignition. This integrated effort was required to achieve a common T-0 lift-off reference.

RETRIES

The initial design requirement was to provide retry logic for anomalous conditions prior to initiating corrective action or proceeding to the next countdown task. Due to previously mentioned LDB timing constraints in conjunction with the requirement for nominal terminal count tasks, the retry logic was found inappropriate and unachievable in most cases. Software verification and validation testing gave the confidence required to assure that retry logic was not mandatory for reasons of safety or for the high probability of an unsuccessful software/hardware transaction. The data transmission "glitch" problems experienced during the Apollo era which originally drove the retry design requirement were found to be non-existent with the Shuttle hardware. The vehicle application software was structured to provide retry capability for certain tasks based upon a systems analysis of potential problems which could be encountered. Even though the ground application software utilizes minimum retry logic, provisions do exist in the ground systems software to retry unsuccessful INPUT/OUTPUT transactions three times.

REAL-TIME OPERATIONS

The capability of manipulating all terminal count events to react to real time event and parameter deviations was another requirement consideration in software design. In keeping with this requirement, the software was designed to allow the bypassing of any terminal count task and to change the limits of any terminal count analog measurement. Provisions were made in the vehicle software for bypassing of certain vehicle monitor/command tasks in response to ground system inputs.

RECYCLE/SCRUB

Another criteria which influenced the integrated software design was capability to perform a recycle or scrub operation at any time during the terminal count. Vehicle safing requirements and ground/vehicle clock synchronization requirements were the primary drivers in implementing the recycle/scrub requirement. Consideration for the implementation must allow for a continually changing vehicle configuration and the need for both ground and vehicle software applications to track the current status. In the design of the recycle/scrub software logic an analysis of the independent on-board software to vehicle systems interface and ground systems management procedures was performed to assure that the vehicle could be placed in a safe configuration. For example the vehicle application software was programmed to go through its predetermined set of recycle/scrub safing commands and then terminate all activity to assure no interference with the ground systems tasks. The ground systems primarily manage the reconfiguration of the vehicle based on the countdown time at which a recycle/scrub was requested.

VERIFICATION AND VALIDATION

As previously mentioned, the primary integration effort required of the ground/vehicle for terminal count operations was the detailed timing analyses to verify time critical operations. In addition to the individual development center's analysis and verification processes, a highly integrated test activity was implemented at the Lyndon B. Johnson Space Center (JSC) Shuttle Avionics Integration Laboratory (SAIL) and at the John F. Kennedy Space Center (KSC) during actual integrated vehicle functional testing. The results of this testing were fed back into the ground and vehicle software design requirements. Software changes were made after analysis and trade-off studies were performed to determine whether adjustments could best be made on the ground or on the vehicle. Software change lead time constraints played an important part in this decision process. Numerous changes were implemented due to the timing analysis and testing results. Adjustments to Launch Commit Criteria also caused numerous changes. Any change always required additional analysis and a test program to insure that no unforeseen problems were created or compounded.

EXAMPLE PROBLEMS ENCOUNTERED

It would be appropriate at this point to discuss several situations which were confronted during the process of integrating the terminal count.

SRB LOCKOUT MANAGEMENT

At a specific point in the countdown sequence, T-40 seconds, the SRB Multiplexer-Demultipler's (MDM's) LL1/LR1 modules 0 and 4 are commanded to the lockout state in preparation for lift-off. At T-13 this same lockout function is performed for LL2/LR2. Initially, in order to achieve this, the ground system was required to issue 20 LDB one-to-one transactions. These commands required an unacceptable amount of time to accomplish at this point in terminal count. This situation was analyzed by JSC and KSC and the best practical solution was found to be a change to flight software. It provided an explicitly coded software function which would issue the necessary commands to accomplish the lockout of LL1/LR1 or LL2/LR2 based upon a single LDB transaction. This transaction provided a positive response to the ground system to assure each module was locked. The following is the list of commands for LL1/LR1 that was initially performed from the ground via one-to-one transactions which required approximately 2.5 seconds for each set of MDM's.

- READ LL1 MDM BITE
- ISSUE LOCK LH SRB MDM LL1 MOD 0
- READ LL1 MDM BITE
  IF BITE / 1000_{16} EXIT SEQUENCE AND SET RESPONSE TO VERIFY FAIL
- ISSUE LOCK LH SRB MDM LL1 MOD 4
- READ LL1 MDM BITE
  IF BITE / 1000_{16} EXIT SEQUENCE AND SET RESPONSE TO VERIFY FAIL

- READ LRl MDM BITE
- ISSUE LOCK RH SRB MDM LRl MOD 0
- READ LRl MDM BITE
  IF BITE / 1000_{16} EXIT SEQUENCE AND SET RESPONSE TO VERIFY FAIL
- ISSUE LOCK RH SRB MDM LRl MOD 4
- READ LRl MDM BITE
  IF BITE / 1000_{16} EXIT SEQUENCE AND SET RESPONSE TO VERIFY FAIL
  EXIT SEQUENCE AND SET RESPONSE TO VERIFY

The set of commands to perform the LL2/LR2 lockout would be identical to the above with the LL1's replaced by LL2's and LR1's replaced by LR2's. The flight software change reduced the ground system commands to one LDB transaction for each set of MDM lockouts.

It was also determined that in the case of a recycle/scrub in which the MDM's had been locked, the ground systems was unable to reliably time the unlock sequence using one-for-one commands (700 $\pm$ 100 msec). The difficulty was due to the unpredictability of LDB traffic and ground software activity. It was determined that an existing "pulse mode" option, available in a test and checkout configuration, would best provide the required capability in the prelaunch flight configuration. Flight software was changed to provide this capability.

With this integrated effort the SRB MDM's may be locked and unlocked in a highly efficient and reliable mode.

SRB HYDRAULIC POWER UNIT (HPU) START & GIMBAL PROFILE MONITOR

One of the most delicate tasks in the integrated terminal count sequence is the startup and monitor of the SRB HPU's which occurs inside of T-30 seconds. Many hours of design, testing, and data analysis were used to insure that the HPU's could be started in a timely manner without an overspeed condition and that the SRB gimbal profile which immediately follows the startup sequence would execute properly.

During the HPU startup sequence one GLS design requirement had to be waived in order to allow the numerous HPU prestart commands to be issued in the time available. The requirement was that any GLS command could be individually bypassed or have its command state altered during a real time firing room environment. For the HPU prestart sequence it was decided to use the software capability of issuing multiple commands via a single LDB transaction.

The potential inadvertant runaway overspeed at startup is monitored by the use of an LPS application software technique known as Control Logic. Control Logic design allows the monitoring of PCM parameters and an associated predetermined response independent of the actions required of the normal application software. The turbine speed monitored for startup is higher than the normal range of turbine speed. The normal GLS application software monitors the normal range of the HPU turbine speed after startup has occurred.

In the process of vehicle testing flow for the first Space Shuttle launch it was found that the enabling of this normal monitoring function was about 100 msec early and caused a shutdown of the HPU due to an overspeed condition. This anomoly, which was caused by a controlled higher initial speed in the start as requested by the HPU controller was not considered in GLS timing and resulted in another detailed analyses of the ground to vehicle timing for terminal count. The GLS enabling of overspeed monitoring was subsequently adjusted to correct this situation.

At T-21 seconds the SRB Gimbal profile is initiated by the ground software. This 4 second test of establishing a positive, negative, and null position of the SRB Tilt and Rock actuators required many hours of testing and analysis. Actual vehicle testing along with the SAIL facility produced the necessary data to provide the confidence of a good system checkout and a "go for launch" status.

RECYCLE AFTER SSME START ENABLE COMMAND

An example of an integrated task which included the SSME controller is the potential main engine shutdown initiated after the "start enable" command has been issued. Once the SSME con-

troller has received start enable, it must receive the "start" command within 5 seconds or "start enable" must be commanded again. The on-board application software is structured such that once "start enable" is commanded the only command that may be sent is "start". In the event that a recycle occurs after "start enable" has been commanded, the time out between the two commands in the SSME controller will occur but the on-board count cannot be resumed without a reload of the computer.

The decision was made to change the on-board application software to reinitialize upon recycle and thus allow a resumption of the count without reloading the on-board computer program.

STACKED RESUME

Whenever the on-board application software is requested by the ground or detects a limit violation which causes it to go into a "hold", the ground has to issue a "resume" count request. In the initial design, the on-board system software would accept and save a "resume" count request sent by the ground even though a "hold" was not in effect. Then, when the next hold condition occurred the stored "resume" would be executed immediately, which essentially would negate the hold. This condition was discovered in testing and changes to both on-board and ground software now precludes the possibility of the on-board inadvertantly resuming the count.

SUMMARY

The challenges of the Integrated Ground and On-board Terminal Count development may be summarized in three categories: task integration, software management, timing analysis. The many functions that must be considered and implemented into a terminal count sequence require a super integrated effort among many contractors and many disciplines. The incorporation of these functions into the software require a well managed software development organization. The verification/validation that all functions will be performed in an efficient and timely manner requires a dedicated test team approach.

The successful launch of STS-1 and subsequent flights is proof that the challenge of these three important functions have been met and are continuing to be met for each launch.

N85
16899

UNCLAS

D16

N85-16899

INTEGRATED DESIGN CHECKOUT OF SHUTTLE PAYLOAD AVIONICS INTERFACES

JOHN F. MURATORE, 1LT, USAF
6555th AEROSPACE TEST GROUP
SPACE LAUNCH VEHICLE SYSTEMS
CAPE CANAVERAL AFS, FL

KATHY K. WHITCOMB
NASA CARGO OPERATIONS
CITE AND SOFTWARE BRANCH
KENNEDY SPACE CENTER, FL

Orbiter/payload avionics integration testing is a relatively new activity in the shuttle program. Payloads flown to date have shown extensive orbiter interfaces. This paper describes the three modes of testing at Kennedy Space Center and Cape Canaveral Air Force Station used to verify orbiter/payload avionics interfaces. These modes consist of orbiter testing using generic payload simulators, payload testing utilizing the actual payload and a high fidelity orbiter simulator, and interface testing with the actual orbiter and payload. Several special avionics techniques, such as the split flight computer technique have been developed to accomplish this testing. Experience from the first six shuttle cargoes is reviewed with emphasis on problems found in testing that would have hampered mission success.

Opinions expressed by the authors are their own and not to be considered as official expression of the Department of the USAF or the National Aeronautics and Space Administration.

INTEGRATED DESIGN CHECKOUT OF SHUTTLE PAYLOAD AVIONICS INTERFACES

Many of the challenges that the Space Shuttle Program generated in integrated avionics have been met and conquered by a variety of sophisticated techniques. In this session we have seen presentations of the tremendous challenges associated with flight computer, ground computer, and simulator hardware and software development. The challenges which we are going to discuss in this presentation are very different from these previous areas. The challenges of these other areas have been substantially met and resolved. In the area of checkout of shuttle payload avionics, however, we are just beginning to understand the true nature of the challenge. In this presentation we will discuss our approaches at Kennedy Space Center (KSC) and Cape Canaveral Air Force Station (CCAFS) to perform checkout of the avionics interfaces between the orbiter and payloads. This presentation will not discuss classified defense payload processing. We will, however, discuss integration of the Inertial Upper Stage (IUS) with NASA payloads such as the Tracking and Data Relay Satellite (TDRS). Also, the discussion of Spacelab processing will be limited because we have not yet completed Spacelab processing.

The primary challenge that we face is how to test shuttle and payload avionics so that we have confidence that when the payload arrives on orbit it will successfully function. These interfaces are definitely substantial. Table 1 shows a list of payloads carried to date on-board shuttle missions. Several observations can be made from this table. First, even "simple" payloads like the OSTA and OSS-1 pallets carried on STS-2 and STS-3 have significant avionics interfaces. Second, the amount of interfaces between the orbiter and the payloads are growing as we fly more sophisticated payloads. This trend will probably continue for some time. The Centaur, for example, will have more extensive avionics interfaces than the IUS. Therefore, we have a significant challenge which is growing.

There are many factors which complicate this problem. Some of these are very unique to payload integration. For example, for many of these payloads, the first time the payload avionics is actually connected to orbiter avionics may be as late as 2 weeks before launch. A major part of the challenge of interface checkout has been to define testing to detect problems in the interfaces as early as possible. Another unique complicating factor is that in many cases we are dealing with organizations outside of the Shuttle Program. In some cases, the users have been extensively involved with the shuttle prior to arriving at the launch base; in others, they have not. In almost all cases, the payload users are used to flying expendable boosters where the interfaces between satellite and booster are very limited (e.g., separation indicators). The large involvement of shuttle hardware in payload mission success (providing power, telemetry, attitude control, pointing, commands, etc.) is a new phenomena to most users. Another major complicating factor is that the complex payload support services provided by shuttle are just beginning to mature. The S-Band Payload Communications System, for example, did not arrive at KSC much before its first use by a payload. This lack of experience with this hardware at the launch base has complicated interface verification between cargoes and the orbiter.

In order to meet the challenge of checkout of orbiter payload avionics interfaces, a system has evolved which is based on three modes of interface checkout. This system is still evolving and is very fluid depending on a specific payload user's needs. In general, these three modes are:

MODE A - CHECKOUT OF ORBITER SUPPLIED SERVICES UTILIZING ACTUAL ORBITER AND GENERIC PAYLOAD SIMULATORS

MODE B - CHECKOUT OF THE PAYLOAD TO ORBITER INTERFACES USING THE ACTUAL PAYLOAD AND A HIGH FIDELITY ORBITER SIMULATOR (CARGO INTEGRATION TEST EQUIPMENT (CITE)) AT KSC

MODE C - INTERFACE TESTING UTILIZING ACTUAL PAYLOAD AND ORBITER

This mode of terminology should not be confused with the "levels of integration" used by NASA Cargo at KSC. In using this "mode" terminology we hope to show how a cargo processing through the shuttle launch site really consists of three distinct phases with different techniques and objectives. This mode terminology will not be found in any formal documentation and is intended for clarity in this paper.

The main purpose of Mode A is to verify that the orbiter is properly configured for a given payload and that all of the orbiter support services are functioning.

Mode B verifies the functioning of the major avionics interfaces between the actual payload and an Orbiter Simulator (CITE). In addition to interface verification, several other types of testing are performed in Mode B. Most payloads contain ordnance devices such as separation pyrotechnics which are tested in this mode.

Most payloads have on-orbit control centers. For detached payloads these control centers are usually not at Shuttle Mission Control at JSC. For example during STS-6, the Tracking and Data Relay Satellite (TDRS) was controlled by a control center at White Sands, New Mexico. In order to verify these control centers interfaces to the payload, an "end to end" test is usually part of Mode B. In this test payload telemetry is sent to the control centers and commands are sent from the control centers to the payload.

The other major test that is performed in Mode B is Mission Sequence. Most payloads have extensive mission sequencing of events that involve the interfaces between the orbiter and the payload. A good example of this is the deploy sequencing of PAM Payloads or IUS Payloads. In most cases, it is impossible to test the interfaces involved in this sequencing after the payload has been installed in the orbiter. This is usually due to installation of ordnance or lack of access to test points. In order to test these interfaces, a Mission Simulation is run which includes launch countdown, on-orbit checkout, deploy and post deployment operations. Items that are included in this testing are simulated ordnance firing, power transfers, and umbilical separations.

Mode C checkout is the culmination of all previous testing. Mode C is the type of payload to booster interface testing that has traditionally been performed at the launch site, i.e., post mate testing. Test time for cargo after orbiter mate means consuming time in the orbiter schedule. This time is expensive in terms of support dollars and is becoming less available as we try to reduce turnaround time. Both of the previous modes can be conducted in parallel with other orbiter activities. Mode A testing (orbiter with payload simulator) is generally a low level effort and can be conducted in parallel with other orbiter servicing. Mode B testing (payload with CITE) does not affect the orbiter schedule. By conducting these two previous modes we greatly decrease the risk that in Mode C (post cargo mate) testing we will discover major problems that will delay launch schedule. This saves real dollars in terms of test time and in preventing delays to the shuttle schedule.

In Mode C testing, the major objectives are functional verification of interfaces between the cargo and the orbiter, "end to end" testing with spacecraft control centers, stray voltage verification, and terminal count demonstration. Many of these tests were performed in Mode B testing and experience from this testing is usually very applicable to Mode C. In fact, it is often possible to verify solutions to problems discovered in Mode B during Mode C.

Several unique techniques have been developed to implement these three modes of testing. These techniques are, out of necessity, very fluid and are constantly changing to meet individual payload needs. Some of the more common techniques are described in following paragraphs.

MODE A CHECKOUT

Mode A checkout is performed in the Orbiter Processing Facility (OPF). Mode A checkout is performed after the orbiter has been configured for the mission. Configuring the orbiter for a specific mission usually consists of the following:

Installing Shuttle Mixed Cargo Harnesses (SMCH) Cables for Specific Cargoes

Installing Aft Flight Deck (AFD) Panels

Installing Payload Retention Fittings

Configuring Payload Patch Panel

Installing Interface Electronics

Loading Orbiter Flight Software with Telemetry/Decom Format Loads

Install Remote Manipulator System (RMS), if required

In Mode A checkout generic payload simulators are used for the following tasks:

Sending simulated payload telemetry to Payload Signal Processor, (PSP)/ Payload Data Interleaver, (PDI)/Payload Interrogator, (PI)/Payload Recorder/Communications Interface Unit (CIU)

Sending commands via orbiter to simulated payload using PI/PSP/CIU/Multiplexer/Demultiplexer (MDM)

Verifying Payload timing buffer outputs to the simulated payload

Verifying Payload power voltage and current at Orbiter connect points

Exercise RMS electrical interface, if required

These generic payload simulators are basically racks of electronics capable of generating simulated payload telemetry streams and receiving payload commands and timing. They are programmable to generate/accept a wide variety of data types and rates. They are not designed as a specific payload simulator (e.g., a TDRS simulator) but rather are designed to checkout generic capabilities. These simulators are hooked into the orbiter at the same places that the payload will be connected. In this way, we are able to perform "copper path" verification of the mission specific cabling used to support the payload.

In addition to copper path testing, functional testing of orbiter support services is performed in the OPF. For example, functioning of the Payload Recorder is performed. Perhaps the most extensive functional testing performed is with the S-Band Payload RF System and the Payload Data Interleaver.

The OPF Communications and Tracking (C&T) Station is used to checkout the S-Band Payload System. Both command transmission via the S-Band Payload System and telemetry reception are checked out in this manner.

MODE B PAYLOAD TO ORBITER SIMULATOR - CITE

The foremost objective of testing a payload with an orbiter simulator like CITE is to minimize the number of surprises encountered by first time testing and mating of the payload and orbiter. To accomplish this objective, the Vertical Processing Facility, the Horizontal Processing Facility and the CITE Control Room were conceived. The major initial design considerations were to use the Orbiter to Payload interface control document in the design of the test stands, to use flight type avionics for the Pulse Code Modulation Master Unit (PCMMU), PDI, MDM, PSP, PI and to use a smaller Launch Processing Unit (LPS) type set for the CITE Control Room. These design considerations allowed procedures and software used to test the payload to be validated prior to orbiter to payload testing.

Since the original CITE did not have a General Purpose Computer (GPC), LPS was designed to include a "GPC Simulator" in CITE. This simulator controlled the acquisition of downlist, loading of the PCMMU, PDI, and the command interface to the payload for uplink and Launch Data Bus (LDB) commands. It in no way attempted to execute the GPC flight software. This design was more than adequate for OSTA, OSS and IUS pathfinder testing.

For OSTA processing, the original concept of processing a payload through CITE was to design an automated sequencer in the LPS which would be patterned after the mission scenario. This concept proved to be an error since the payload requirements and the mission scenario were very dynamic. The LPS software could not be modified as often as required or verified and validated in time for future payloads. A decision was made to return to more manual programs with simple display/command functions. Therefore, the Operation and Maintenance Instructions (OMI's) would control the testing and software redesign would not be necessary if the mission scenario changed. We also discovered the payload community and the flight crew wanted to use the GPC flight software to the maximum extent possible.

As payloads became more complicated and the role of the GPC flight software become more involved with the payload, it became apparent that a GPC, Display Electronics Unit (DEU) and Mass Memory Unit (MMU) were necessary to support payload testing in the CITE facility. A CITE Augmentation System was added which includes the GPC, DEU, MMU and an Eclipse Computer. The Eclipse computer simulates the GNC computer of the Orbiter (e.g., state vector and uplink command routing). By using a GPC in CITE, the CITE procedures could be transferred for use on the Orbiter. It was also determined that if flight software required modification as a result of CITE test, there would be enough time between CITE test and post orbiter/mate of the payload to incorporate the software change.

To support the payload for CITE test, the test stand is configured to support the payload in much the same manner as in preparing the Orbiter in Mode A. Concurrent with the hardware reconfiguration, the LPS Ground Software Development is performed. To validate the Ground Software and Flight Software compatibility, a test prior to payload installation is performed where the payload telemetry stream is simulated to match the Command and Data Annex. This is the first time all the software products are truly merged.

The major tests will be described under Mode C discussion since they are common to both CITE and post orbiter mate testing. The only unique payload test performed in CITE is the Mission Sequence Test. The purpose of this test is to perform a nominal mission flow using the flight data file and to the maximum extent possible exercise the GPC flight software. If no flight software problems are detected, this testing is not performed after the orbiter and payload are mated.

MODE C TESTING

Mode C testing is performed after cargo installation in the orbiter. For horizontally installed payloads, this activity is performed in the Orbiter Processing Facility (OPF). For vertically installed payloads, this activity is performed on the pad. This may be as late as two weeks before launch. Mode C testing consists primarily of functional interface testing, "end to end" testing with spacecraft control center, ordnance stray voltage testing, and terminal countdown demonstration.

After cargo installation and electrical connection to the orbiter, the first major activity is cargo/orbiter interface test. The major purpose of this test is to perform a functional test of the interfaces between the orbiter and cargo. The cabling which connects the orbiter equipment to the payload and the orbiter services should have been checked out in Mode A. The payload side of these interfaces should have been tested in Mode B. In Mode C, we basically perform the Mode B interface testing with the real orbiter.

We face a significant challenge in this area because most of the orbiter support to payloads is only available in on-orbit Orbiter flight software operational sequences (OPS). In some cases to test significant interfaces, the payload must also be moded to on-orbit flight software modes. The challenge we face is that the orbiter/cargo is still on the ground. Things that the orbiter/cargo are programmed to do on-orbit may not work on the ground or even worse may be hazardous to equipment and personnel. Consider the disastrous impacts if the orbiter decided to fire thrusters to correct its attitude or the upper stage decided it was time to separate.

In order to avoid this problem, we have developed several techniques. The central technique is called the split computer, Diagram 1. Under split computer technique, two orbiter computers are activated with different OPS. One computer is loaded with standard ground checkout software, designated GNC9. The other computer is loaded with on-orbit System Management software, designated SM2. The orbiter flight critical buses, which connect the orbiter computers to most of the flight control and other flight critical equipment, are assigned to the GNC9 computer. This effectively safes most of the orbiter because the GNC9 load will not perform autonomous subsystem commanding. The orbiter payload buses which connect the orbiter computers to the payload multiplexer-demultiplexer (MDM), PAM Sequence Control Assembly (SCA), PDI, and other payload equipment are assigned to the SM2 computer. The SM2 computer is thus able to communicate to the payload utilizing the on-orbit software.

There are several problems associated with this configuration. First, there is a significant amount of orbiter equipment attached to "payload" MDMs. Included in the SM2 Computer is "special processes" software. Special processes software consists of automated routines which perform housekeeping of flight systems. For example, the SM2 computer monitors temperatures in the hydraulic system and activates the hydraulic system and the hydraulic circulation pumps to keep the hydraulic fluid from freezing. These are definitely things which could cause havoc during ground test. In order to prevent this functioning, the applicable systems are safed by cockpit switches.

Another problem which occurs is that of downlink bandwidth. With normal vehicle control data being downlisted by the GNC computer, payload interface data being downlisted by the SM computer and Payload data being interleaved into the downlink by the PDI, we have several data sources all competing to fill the 128 kbit downlink bandwidth. The normal on-orbit downlink/downlist formats cannot be used because they do not have the kind of data required for ground operations. More specifically, most on-orbit formats have a very small window for the GNC downlist. The prelaunch checkout (GNC9) load has a large downlist (51.2 kbit) of data. At KSC, we like to monitor this data continuously because these systems are hazardous (e.g., hypergolic systems). The large prelaunch checkout downlist cannot fit into the small on-orbit window. In order to solve this problem, we have designed special downlink formats that have all of the critical downlink information but still have room for SM and the payload data. This is done mostly by decreasing sample rate of high frequency measurements and by specifically planning to drop certain kinds of special test measurements (e.g., range safety) in parallel with payload work.

The final challenge in developing this test configuration is to find a way to command both the orbiter and the payload. Some of the payloads have their own dedicated umbilicals through the orbiter T-0 umbilical (e.g., IUS/TDRS, PAM). This eases the command problems somewhat. Other payloads require use of the launch data bus (LDB) for command. This presents us with a dilemma. We need the launch data bus to control the orbiter flight critical systems as well as the payload. Normally at KSC we try to keep the two launch data buses assigned to only one computer at a time to prevent confusion in the

ground and flight systems. During STS-2 and 3 pallet checkout, we tried to pass the LDB between the GNC9 computer when we needed to command orbiter flight critical systems and the SM2 computer when we needed to command the payload. The result of this technique was a lot of confusion in the control room as to what computer was being sent commands. This is a bad situation.

To solve this problem for later flows, it was decided to split the launch data buses. One data bus is assigned to the GNC9 computer and the other to the SM2 computer. This presented us with some confusion in our ground system with regard to how to route commands. Rather than implement some routing software, it was decided to use two separate LPS sets in two different control rooms. Since the normal control room is designated Firing Room-1, the payload control room is designated Firing Room-X. This system has been used extensively for STS-5 and STS-6 with great success.

An additional fallout of this configuration is that the orbiter uplink can be used to command the payload - either by RF or hardwire. Destination codes of uplink messages can be set to the GNC or SM orbiter computer. The GNC machine receives the uplink messages from the Network Signal Processor (NSP) and sends the messages to the SM machine via the Inter-Computer Communication (ICC) bus, if required. At KSC, we normally use the LDB for most command purposes because it is more versatile than for the uplink for most ground testing. However, because the Orbiter community tends not to use the uplink for ground checkout, the payload community has begun to use it more and more. In hindsight, it makes more sense to use the uplink for payload checkout because payloads are designed to work on-orbit and there is extensive payload support in the orbiter uplink software. We still use the LDB for payload checkout but there is a definite trend to use more uplink commands by the payload community.

Stray Voltage Ordnance Testing simply consists of a demonstration that the orbiter systems do not induce voltages on cargo ordnance lines and vice versa. This is not an electromagnetic compatibility (EMC) test, since EMC testing is usually a design type test/analysis activity. We have performed some minor EMC testing in the Orbiter (Example: Wireless headset compatibility in crew cabin with IUS communications interface unit, CIU) but this is not normal. In stray voltage testing, we configure the orbiter and the payload into prelaunch and on-orbit conditions and perform voltage checks on ordnance lines. This usually involves activating a considerable amount of orbiter and payload equipment such as RF systems, payload bay floodlights, hydraulic circulation pumps, etc.

"End to end" testing is also performed after cargo mate. Initially (STS-2) this test was combined with Orbiter/Mission Control Center Compatibility Testing. As we have gained more experience with the orbiter, the degree of payload to payload control center testing has increased, however, MMC to orbiter testing has decreased. Thus, the payload control center "end to end" tests have been separated from the Orbiter/MCC testing.

These "end to end" tests have become extremely complex affairs. Diagram 2 shows the control center testing. No less than 11 separate centers were processing data. In fact, in one test we shipped data from the IUS to Sunnyvale, CA (SCF) to Greenbelt, MD (GSFC) to Houston, TX (JSC) and then to White Sands, NM (TDRS Control). This data criscrossed the country 3 times.

In "end to end" testing, we ship data from the payload to the user control center. The user control center also formats commands and ships them to the payload. This is a test of the payload, the data network, and the payload control centers.

The purpose of the terminal count demonstration test is to perform a dress rehearsal of the countdown. STS-6 was the first time the payload community was actively involved in the demonstration. This is because the IUS is very active in the terminal count. There are two critical command actions which must take place in the last 9 minutes before launch. AT T-5min30sec, the IUS Inertial Navigation System is commanded to free inertial mode (flight mode). This must be complete before Orbiter APU start at T-5min. It must be commanded as late as possible, however, because due to software/hardware limitations, the IUS navigation system has a limit of time on the ground in the free inertial state. At T-3min59sec, the IUS is switched from orbiter power to Airborne Support Equipment (ASE) batteries. This is to lower electrical power demand on orbiter main C power bus during ascent. The ASE batteries have a limited ground budget so it is important to go on these batteries as late as possible.

In order to properly integrate countdown activities with the orbiter and to train both the shuttle and payload launch teams, the payload functions were included into the STS-6 Terminal Countdown Demonstration Test. During this test, it was discovered that the time required to issue the IUS navigation to flight mode command and the delay until it was verified at the Checkout Station (COS) was very long. In fact, it was so long that the operator at the Checkout Station did not have enough time to call a hold prior to APU start. One of the most highly stressed rules at KSC is "You don't start APU's unless you're ready to go." This is because APU fuel is a limiting factor during any hold. Most important, if all of the APU fuel ground budget is used, it forces a several day reservicing and launch slip. Based directly on the Terminal Countdown Demonstration Test experience, we changed IUS ground software and procedures so that the IUS navigation command was moved back 30 seconds. This way, we

were assured that the IUS navigation mode was completed at T-5min30sec instead of just starting at T-5min30sec. This was a very important lesson to learn and it is possible that we avoided an inadvertent payload hold on the STS-6 launch.

We expect that the STS-6 cargo is the first of many cargoes to have terminal count involvement. Preliminary Centaur High Energy Upper Stage planning indicates the Centaur will have extensive terminal count involvement. The Terminal Countdown Demonstration Test will probably grow to be a very important payload/upper stage test in the future.

RESULTS

Now that we have presented a rather elaborate test program, the obvious question is "Is it worth it?" Based on experience so far, we have found that this program regularly detects problems that could cause launch or mission failures.

One of the major areas in which we have found problems in is flight software. In STS-5, 6 and 7 processing, we have found errors in the Command and Data Annex and the Master Measurement Data Bank (MMDB). Improper command or telemetry/decom formats were in the data base. This could have caused the wrong commands to be issued from MCCH/POCC or wrong interpretations of downlink telemetry. In STS-5 and 6, we also found that the flight software was improperly annunciating payload faults or displaying data improperly on the on-board CRT. In some of these cases, it was possible to make fixes to flight software before flight. In other cases, we were able to brief the crew to ignore certain alarms.

In a similar item, we discovered a CIU to Orbiter incompatibility during Mode A testing. The CIU rejected the GNC State Vector transfer from the orbiter the first time it was enabled. This caused the CIU to turn on a "GPC error" light on the CIU display panel. We found that if the crew simply cleared the first time alarm (by pushing a clear pushbutton) that it caused no further problems.

During STS-5 pad testing of a PAM, a Sequence Control Assembly (SCA) failed. It issued several inadvertent commands to the PAM and satellite. If this had happened in flight we might have damaged flight hardware. The unit was replaced with a redesigned unit to preclude the failure mode.

During the terminal countdown test for STS-6, we found an incompatibility between Shuttle launch procedures and the IUS. At T-11min,, the payload bay purge flow rate is lowered to lower the delta pressure across the quick disconnect on the T-0 umbilical. This is in preparation for "popping" the umbilical at liftoff. In terminal count demonstration test we found that the lower flow rate altered the thermal environment of the IUS Redundant Inertial Measurement Unit (RIMU). This alteration was sufficient to cause large drift in the calculated azimuth of the RIMU. If the first time this had happened had been launch countdown, we certainly would have scrubbed the launch. Having observed this in countdown demonstration test, we were able to research and explain it so it was not a concern on launch day.

A similar item was observed regarding the Orbiter to IUS timing interface. At approximately T-1hour, a final update of the on-board Greenwich Mean Time (GMT) in the Orbiter Master Timing Unit (MTU) is made. During Orbiter to Cargo interface testing (Mode C), we found that an update of the MTU caused the IUS to declare a timing fault and go onto its own internal time. The IUS reset back to orbiter time within a second of the update. This, however, caused a Launch Commit Criteria failure in the IUS ground computer. This would have caused significant problems on launch day if we had not been expecting it, perhaps even a scrub.

There are many other examples of problems we have found that have had an affect on mission success. The above examples are "typical" problems we find.

SUMMARY

We have described the three modes of checkout that have evolved at KSC and CCAFS for Payload to Orbiter Interface Checkout. Mode A consists of copper path checks of mission unique wiring and functional checks of orbiter supplied payload services such as the payload recorder and the S-Band Payload system on the orbiter. Mode B consists of checkout with the real payload and a high fidelity orbiter simulator. Typical testing that occurs in Mode B is CITE/Cargo interface test, "end to end" test with control centers, ordnance test and mission sequence test. Mode C testing is performed after cargo installation in the orbiter. This is similar to traditional booster to spacecraft integration testing, but much more extensive. A full Cargo/Orbiter Interface test, and "end to end" test, Ordnance test and a Terminal Countdown Demonstration test is performed.

These testing modes have found numerous problems with spacecraft processed at KSC and CCAFS to date. This system will continue to evolve as more complex payloads arrive at the launch base with increasingly compressed processing schedules.

PAYLOAD/MISSION	INTERFACE SUMMARY
STS-1/DFI PALLET INTEGRATED ENVIRONMENT CONTAMINATION MONITOR (IECM)	PAYLOAD MDM COMMAND INTERFACE
STS-2/OFFICE OF SPACE AND TERRESTRIAL APPLICATIONS (OSTA-1) PALLET	FLEX MDM INTERFACE FLIGHT SOFTWARE/ON-BOARD CRT DISPLAY ORBITER POWER DATA IN GPC DOWNLIST (SM GPC)/COMMAND BY S BAND PM
STS-3/OFFICE OF SPACE SCIENCE (OSS-1) PALLET	FLEX MDM INTERFACE FLIGHT SOFTWARE/ON-BOARD CRT DISPLAY ORBITER POWER DATA IN GPC DOWNLIST (SM GPC)/COMMAND BY S BAND PM PAYLOAD TELEMETRY BY S BAND PM RMS POWER/DATA INTERFACE
STS-4/DOD 82-1	CLASSIFIED
STS-5/TELESAT ANIK ON PAYLOAD ASSIST MODULE (PAM) AND SATELLITE BUSINESS SYTEM (SBS) ON PAM	SEQUENCE CONTROL ASSEMBLY (SCA) ON PAYLOAD DATA BUS PAYLOAD DATA INTERLEAVER (PDI) S BAND PAYLOAD SYSTEM (SIGNAL PROCESSOR/INTERROGATOR) ORBITER POWER FLIGHT SOFTWARE/AUTOMATIC SEQUENCING ON-BOARD CRT DISPLAY SUBSTANTIAL FUNCTION ON STANDARD SWITCH PANEL (SSP)
STS-6/TRACKING AND DATA RELAY SATELLITE (TDRS-a)/INERTIAL UPPER STAGE (IUS-1)	COMMUNICATIONS INTERFACE UNIT (CIU) TO PAYLOAD MDM ORBITER STATE VECTOR TRANSFER TO PAYLOAD FLIGHT SOFTWARE/ON-BOARD CRT PAYLOAD DATA INTERLEAVER (PDI) S BAND PAYLOAD SYSTEM (SIGNAL PROCESSOR/INTERROGATOR) ORBITER POWER POWER CONTROL PANEL AND STANDARD SWITCH PANEL TDRS COMMAND VIA ORBITER S BAND PM

ALL PAYLOADS HAD PAYLOAD RECORDER AND PAYLOAD TIMING BUFFER INTERFACE

TABLE 1 PAYLOAD INTERFACE SUMMARY

DIAGRAM 1 SPLIT COMPUTER TECHNIQUE

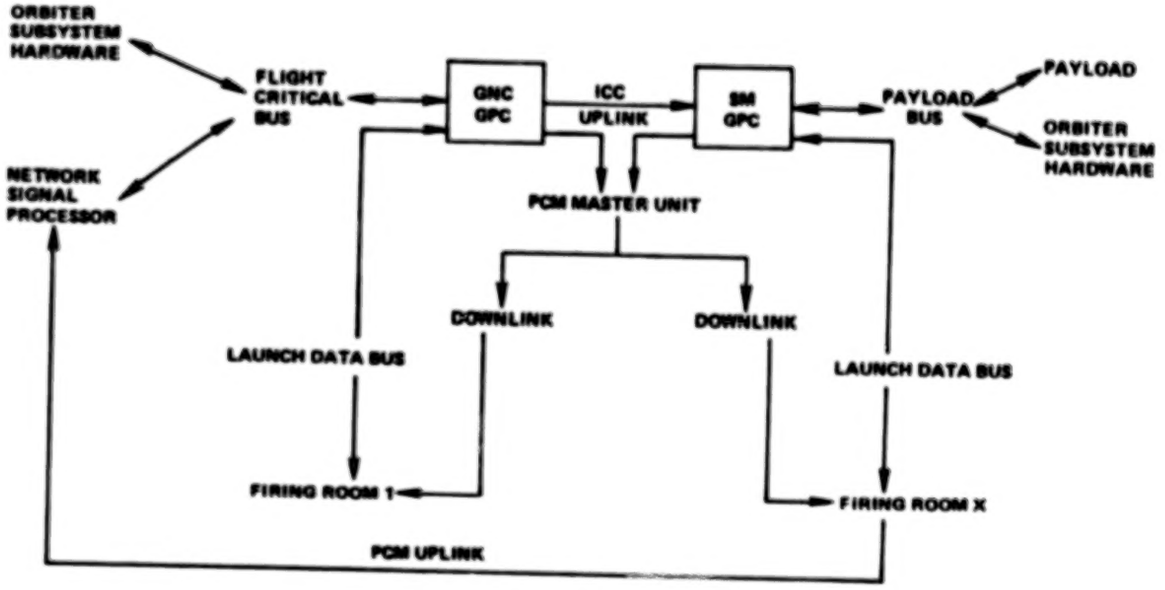
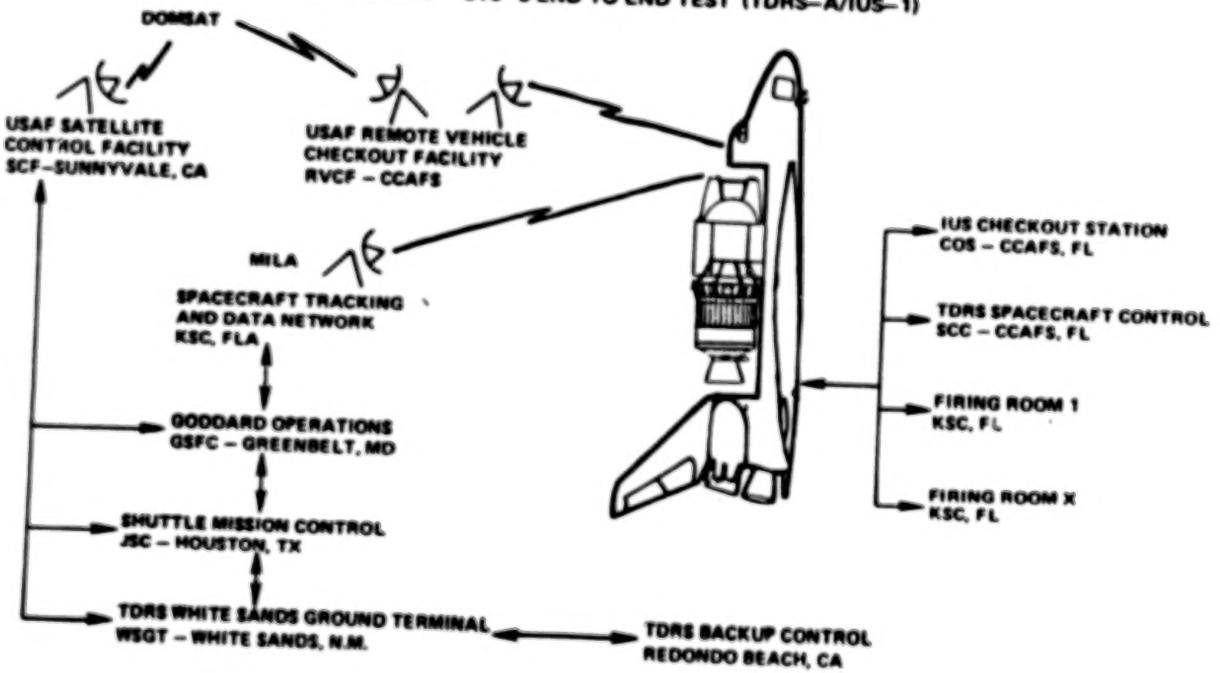


DIAGRAM 2 STS–6 END TO END TEST (TDRS–A/IUS–1)



N85
16900

UNCLAS

N85-16900

AUTOMATION OF CHECKOUT FOR THE SHUTTLE OPERATIONS ERA

Judith A. Anderson
Guidance, Digital & Software Systems Division
Kennedy Space Center

Kenneth O. Hendrickson
Applications & Integration Software Section
Kennedy Space Center

ABSTRACT

The Space Shuttle checkout is quite different from its Apollo predecessor. The complexity of the hardware, the shortened turnaround time, and the software that performs ground checkout have proven a challenging task to overcome.

Generating new techniques and standards for software development and the management structure to control it have been implemented. New challenges await those that have been solved.

INTRODUCTION

Testing of the Space Shuttle's many systems to assure that the Shuttle is ready to refly is a complex process. This paper will highlight some of the challenges in utilizing these computer systems in the testing of the vehicle in a timely fashion and how these challenges are being met.

HISTORY

During the Apollo program, the Saturn launch vehicle was heavily computer controlled (via the RCA 110A computers) and had virtually no cockpit control since the Apollo spacecraft was totally separate. The ground computer programs were primarily assembly language, with very low change rate. A very elementary user test language (ATOLL) was available for "linking" assembly language programs and to perform simple command verification sequences. This capability allowed KSC to automate the last nine hours of countdown to an almost hands-off point by the end of the Apollo program.

Where the Saturn automation was primarily a command-by-command serial sequencing function, the automation of the Shuttle checkout and launch preparation is a very complex scheduling exercise, with complex operations to be performed. The tools provided were: 1) the LPS system, with its GOAL user oriented language, capable of monitoring the measurements on the vehicle and in the ground systems, and (2) the on-board computer system (DPS), which provided the linkage to control, in a test environment, all the vehicle subsystem controllable during flight.

CHALLENGES

The complexity of the Space Shuttle has come to haunt us frequently in our efforts to automate our turnaround activities -- from the sheer numbers of measurements to be monitored and commands to be issued to the interrelationships of the subsystems. The flexibility of redundancy makes a highly reliable vehicle to fly, however, a difficult one to test. Our earliest efforts at automated testing were just to get the minimum amount of software written to get the job done -- we did not have time for any more. As we progressed thru the STS-1 flow, the need to do things faster, and more reliably became strong drivers. For manual operations, we found all the many ways one could do them -- many which would not work!

We also found during the early flows that we were spending large amounts of manpower sitting in the firing room waiting for a problem to occur. As problems decreased because of system maturity, we still needed the same number of people on console monitoring data. This was neither cost effective nor interesting. In order to have a cost effective system we had to reduce Firing Room manpower.

The shortening of the turnaround has been a constant driver to get things done faster and more efficiently. (Reference Table 1). The STS-7 turnaround was 63 days and our target for STS-30 is 28 days, a 60% reduction. This can be attacked several ways -- decrease test requirements, accomplish the same tests faster, and accomplish more testing in parallel.

TABLE I. FLIGHT vs. TURNAROUND FLOW LENGTH

FLIGHT	LENGTH
STS-1	2 years
STS-7	63 days
STS-8	49 days
STS-16	35 days (target)
STS-30	28 days (target)

SOLUTIONS

Our first approach at speeding operations up was to automate discrete activities. During early STS-1 it would take us over two hours to power up the Orbiter. This drove us to a 24 hour/day operation in just one week to avoid the overhead of the daily power-up time. We are currently powering up OV102 (STS-9) daily in less than 25 minutes. During this time period, approximately 500 commands are issued via computer and approximately 50 switches are thrown in the cockpit. How did we do it? First, each of the institutional support systems (EPDC, instrumentation, cooling and DPS) developed software to automatically perform each of their power up functions with a minimum of manual intervention. Control of these programs was then centralized at the integration console which cues each of the subsystem consoles when it is time to do a part of their activation. Procedural steps which must be run manually are tutorially presented to the console operator. This eliminates any unnecessary decision making in selecting the proper support LRU's for the day and "filling in the blanks". It also allowed all measurement/feedback information to be checked by the software.

Could these kinds of techniques be applied to other situations? Certainly, however, our normal testing situation is not as easily predefinable on a day to day basis as power up. Today we may want to test system A then B then C. Tomorrow we may need to test A in parallel with C and then do B. There are many drivers to the order of testing -- manpower available to do a job, Ground Support Equipment ready, compatibility of operations (downlist/downlink formats, GPC memory configuration, etc.) and the jobs scheduled due to unexpected drivers such as equipment failure and replacement.

In order to automate on a global firing room basis, we first have to automate individual subsystem functions. This is currently underway. To assure that these functions can then be integrated, a common set of groundrules (standards) have been developed to assure that subsystems can communicate with one another and with the integration console in a uniform manner.

STANDARDS

A set of groundrules were established to design the application software. Early efforts concentrated on standardizing the man-computer interface. Standards were developed for the use of color on the CRT's and on how the data was to be displayed. Standards were developed on how the engineer would use the CCMS keyboard to communicate to the application software. Later standards were developed that provided rules on how the software structure was to be designed. This standard identified program types and the relationship of each type to the overall design of the

software set. Application sets were defined along engineering subsystems, e.g., Hydraulics, Environmental Control and Life Support, Electrical Power Distribution and Control, Data Processing, etc. These Application Sets were assigned to a physical Firing Room console and teams were established by console to produce the documentation and software.

Each Console Set Working Team is comprised of contractor and NASA system engineers from each member Application Set, software specialist engineers, technical documentation, and quality control personnel. The teams are responsible for producing console application software requirements, software design specifications, and development and implementation of the software itself. The teams meet on a regular basis to coordinate requirements and implementation details. This highly organized activity is opposed to the methods used earlier where a system engineer had a broad, general set of requirements which he went off and coded to. Since most programs were simple, stand-alone programs, this method was satisfactory. The increased level of organization and coordination was driven by the increased complexity and interdependency of the software which was required. Because this software was now going to be used at multiple sites (VAFB), and because it would probably be with the Shuttle program longer than its designer, documentation became more important.

In addition to the console set working teams, someone had to assure the consoles would communicate properly with one another, and that subsystems required to support other subsystems were aware of it. This function is provided for by the Software Automation Subpanel. This group's primary responsibility is the integration of the automation effort within the Firing Room.

STRUCTURE STANDARD

The Software Structure Standard establishes a software design that separates the overall software function into primarily three groups. Display Driver programs are the primary man-machine interface. The operator uses these Display Driver programs to initiate software functions and also to view data on the engineering system. While looking at an overview display of a Shuttle system, the operator may move a cursor to a target on the CRT which causes the overview display to terminate and another Display Driver is to be performed which displays a particular subsystem in greater detail. This Display Driver may have cursor targets that, when selected, cause a particular command to be issued. The command feedback is displayed, allowing the operator visability into system response to the command.

Sequencer programs are designed to automate a particular function. There are Sequencer programs that power-up a particular hardware system on the Orbiter. There are sequencers that perform detailed LRU checkout. In general, a sequencer requires no manual control except to perhaps supply program options, or respond to errors. A sequencer provides only limited operator interface capability. Instead the sequencer interfaces with Display Driver programs to display messages or to present prompts to the operator. The Sequencer program is also responsible for recognizing and reacting to system anomalies.

The third class of programs are those that bind the other program types together and provide the continuity between one function and another. The main program in this type is called the System Scheduler. The purpose of this program is to validate all requests to perform a function against functions already in progress and the current hardware configuration. It also establishes a relative priority among functions and will interrupt one task to execute a task of a higher priority. The System Scheduler is the hub of inter and intra console software communication. When one program needs to communicate to another it sends the request to the System Scheduler which will validate the request and relay it to the proper receiving program. This same scheme works when one Application Set needs to send data to or request data from another Application Set. This standardized communication scheme provides the linkages that form an integrated Application Set and ultimately an integrated Firing Room software design.

CONSOLE STATIONKEEPING

In order to solve the problem of decreasing the number of engineers required on console during relatively quiet periods while other subsystems are testing, we developed a concept called

"Stationkeeping", (frequently referred to as "babysitting"). Depending upon the system being station-kept, the level of monitoring of functions and automatic response varies. All systems have a set of measurements which are monitored for anomalous conditions. In general, these measurements are monitored against limits in the Front End Processors. When a limit is violdated, an interrupt is sent to the GOAL program at the console. In response to this interrupt, the program then evaluates a set of related measurements to determine what, if any, the failure was. A message indicating the failure is then sent to the operator. In the case where no operator is present, the message is routed to the Integration console for display to the operator there.

What happens in response to an error? Here again, this is system dependent. In DPS, any failures which degraded the testing support (such as a GPC failure) caused data collection to be automatically initiated and a proposed plan for recovery to be displayed to the operator. If the console operator selects to perform the recovery plan, all steps which can are automatically executed. Any steps requiring manual actions are presented in a tutorial fashion. This software, in essence, is a canned "expert system engineer" who knows what to do ahead of time in all predictable failures. There undoubtably will be cases which the software was not designed to cover. When these occur they will be added into our software, thus teaching our "expect" something new.

The concept of stopping to provide the console operator with an option to perform the recovery sequence or not is not used in all cases. In many instances, because of possible hazards involved or potential hardware damage, recovery is invoked automatically. Loss of cooling is an example where steps are automatically taken to restore cooling to the vehicle without operator intervention.

Once we developed the concept of stationkeeping software for systems when engineers were not going to be on station, it was just an extension to also use this same software when the engineer was on station. This helps in assuring the appropriate data is taken when a problem occurs and that the correct steps are taken to correct a problem. This allows less experienced engineers to become console operators. The stationkeeping concept has also been extended to systems such as hydraulics to provide their "incident prevention" software which causes emergency hydraulics power down whenever anything is detected which indicates the system is incorrectly configured or something critical has failed which could result in hardware damage.

In the case of DPS, in order to have Integration console do their stationkeeping a number of support functions had to be performed from the Integration console (i.e., format changes, launch data bus switching, I/O resets, etc.). This was easily implemented using the communication techniques described above. As the system matures, additional capabilites will be added to the Integration console menu of DPS functions to increase the amount of time stationkeeping can be active from the Integration console.

Although our stationkeeping software is still under development, we have already begun to reap the rewards. DPS stationkeeping software went on station during STS-6. Approximately 80% of the flow is now done with no one at the DPS console. This solves many problems:

- o More cost effective utilization of manpower.
- o Improved morale by decreasing shift work.
- o Allow engineers to work more interesting tasks.

THE CHALLENGE IS NOT OVER

The solutions that have been outlined have a common denominator. They all require highly integrated and complex software. Early efforts at automation isolated top level functions from one another to minimize the amount of interaction between software elements. This methodology worked fine but it would not support an environment where multiple semi-independent operations

Firing Room environment is exactly what is needed to produce a turnaround concept that minimizes human intervention and decision making. Now that we have solutions for our past challenges, new ones confront us in our efforts to control this huge ball that has begun to roll called "automation". The software development tools that we have used in the past were fashioned after our level of sophisticated software which in most cases was crude. The new challenge that we face is to produce the software development tools and techniques that will keep the automating ball rolling in the right direction and speed so as not to swallow up those of us in its path.

For the most part, mathematical models of the various Shuttle and ground support systems were used to verify the checkout application software. Our simulation capability is called the SGOS (Shuttle Ground Operations Simulator) system. It consists of math models executing under a real-time operating system in one of our ground data processing computers and another computer that supports the Orbiter and ground data links, buffering, and data conditioning between the Firing Room and the real-time operating system. To the Firing Room personnel and their software executing in the consoles, a high fidelity math model will provide measurements and react to commands identically to its hardware counterpart. The math models would adequately allow the engineer to debug and verify his mostly manually controlled programs, but they were not to the level of fidelity to simulate a total system response to a stimuli. The need to have high fidelity integrated models of hardware was an obvious priority when we began our automation effort. Once high fidelity models were produced, we quickly ran into the limits of the real-time simulation capabilities. Unlike other NASA centers, we don't have dedicated computers for our math models to run in. Instead we designed a real-time simulation operating system that would time-share the computer resources with many other operations. Because of this constraint, the problem of increasing the simulation capability without taking over the whole computer and still maintaining real-time response proved quite challenging. The end result of this challenge is affectionately known as "Big Sim". The system has just been released for Firing Room use. It triples our model capacity while spreading out its operating system responsibilities so as not to significantly increase processor usage. With this increased capability, we are now able to integrate enough system models to simulate a total Shuttle at the Pad with the required ground support equipment. For the first time we will have the capability to provide launch countdown simulation with high fidelity math models. "Big Sim" is a necessary and welcome addition to our expanding collection of software development tools.

Software development is a lengthy and time consuming process. Requirements must be generated, software specifications must be developed, and the programs themselves have to be coded, debugged, and verified. Each of these steps have to be reviewed and approved. The whole process is complicated even more by our overall objectives to significantly increase the level of integration between systems. The automation effort requires a substantial committment by NASA and its contractors to supply the necessary manpower to implement these concepts that have been discussed. This software development effort coincides with our requirement to shorten Shuttle turnaround and to process multiple Orbiters, ET, and SRB's in parallel. All this must be done within the current manpower ceilings in order to remain cost-effective. How do we do it?

We are currently working on a software system that will take a software specification as input and generate an application program. The system is called LAP (Launch Processing System Automatic Programmer). The specification document written in a user oriented language is processed against the rules of our Application Software Structure Standard. The output will be an application program meeting the software specification requirements and also conforming to the Structure Standard. This automatically generated program should be much easier to debug because only high level logic needs to be checked instead of a module by module debug. This system is in the very early stages of implementation, so it is too early to tell how efficient the end product will be. Because few of our application programs have been optimized for speed, we do not expect the inherent degradation of performance usually associated with adding another layer of software between the programmer and computer to be much of a problem.

We have accomplished a lot in our automation efforts to date, but the job is far from complete and we continue to meet challenges on a daily basis.

N85
16901

UNCLAS

D12

N85-16901

SHUTTLE NAVIGATION STATUS

Emil R. Schiesser
NASA Lyndon B. Johnson Space Center
Houston, Texas 77058

INTRODUCTION

Shuttle navigation, for the purpose of this report, is defined as the determination of Orbiter position, velocity, and attitude and associated effort. This, together with guidance, flight control, consumables, and systems management, is required for classical navigation - successful movement of a craft from an initial to a final destination.

Position and velocity propagation (the extrapolation in time using an initial estimate) requires the measurement or modeling of the gravitational, aerodynamic, and rocket engine forces acting on the vehicle. Position and velocity determination is performed using observations such as the distance to external features, the rate of change of such a distance, and the direction toward the feature. Onboard state propagation is more often the mode of state knowledge maintenance, as is shown in table 1, since the ability to determine position and velocity using such observations is limited. An overview of Shuttle navigation is presented in reference 1.

TABLE 1.- SHUTTLE NAVIGATION SYSTEM

Navigation systems	Ascent	Descent	Orbit
Orbiter	State[a] propagation	Propagation and determination	State propagation, attitude determination
Ground	State determination	State determination	Orbit determination

[a]State: position and velocity.

By state is meant that set of parameters which adequately describes the translational and/or rotational situation of the Orbiter. The actual state parameter set maintained onboard sometimes includes acceleration and system biases; however, most of the time, it is limited to position and velocity.

CHALLENGING AREAS

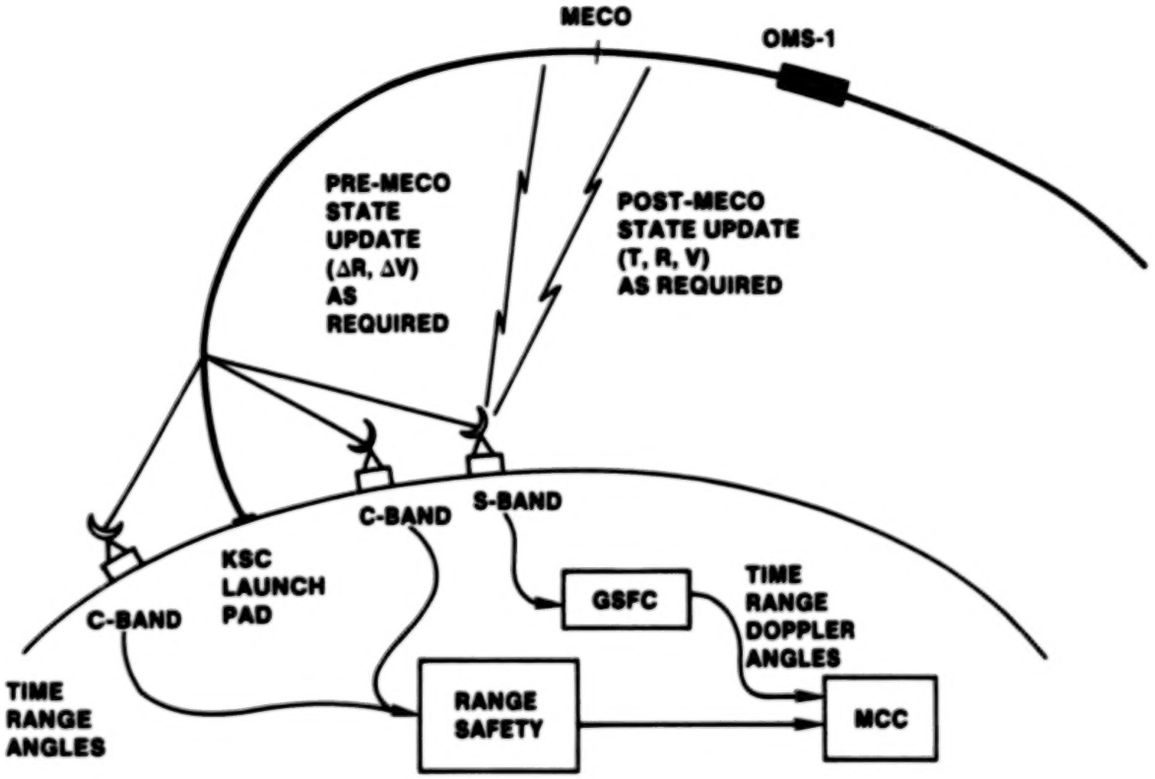
Shuttle navigation as accomplished during the initial flights was challenging in at least three respects: the use of off-the-shelf redundant conventional navigation equipment and the project goal to successfully return the vehicle and crew after two nonsimultaneous failures; the need for accurate, timely ground-determined position and velocity during ascent; and navigation during descent from orbit through rollout.

The management of redundant Inertial Measurement Units (IMU's), the use of redundant Tactical Air Navigation (TACAN) equipment, the use of triple state maintenance, and the details of descent navigation have been presented in reference 2. The following material contains a review of ascent ground state determination and selected descent navigation areas.

ASCENT GROUND NAVIGATION

A ground-based system (state calculation performed by a ground computer) was developed to support the ascent flight phase during the interval from lift-off through about 1 minute past main engine cutoff (MECO). This system provided the ground flight control team with a capability to monitor onboard navigation system performance and to protect engine cutoff conditions as necessary with an update to the onboard position and velocity. A capability to update the onboard state after MECO was provided to protect ascent abort options - primarily the ability to return to a landing site within one revolution.

Figure 1 shows these update opportunities. Both C-band (range and angle observations) and S-band (range, Doppler, and angle observations) tracker data were used in the Houston Mission Control Center (MCC) computers to determine position and velocity. The transfer of state information to the Orbiter is done in the form of a correction using differences between onboard and ground knowledge during powered flight. The onboard state vector is replaced as necessary with ground information during free flight.



OMS - ORBITAL MANEUVERING SYSTEM
KSC - KENNEDY SPACE CENTER
GSFC - GODDARD SPACE FLIGHT CENTER

FIGURE 1.- ASCENT STATE UPDATE OPPORTUNITIES.

The ground pre-MECO performance is shown in table 2. Position accuracy has been 300 to 1100 feet, well below a 6000-foot goal. The critical parameters, radial and downtrack velocity components, ranged from 3 to 20 ft/sec and 2 to 5 ft/sec, respectively, compared to a required accuracy of 50 and 40 ft/sec.

Figure 2 is a sketch of the post-MECO geometry. One minute of tracking data is available from which to determine the orbit. During this time, the vehicle covers about 4° of travel. The task is to determine the orbit semimajor axis (SMA) to 1 nautical mile or the perigee altitude to approximately 2 nautical miles. The insertion altitude (post-MECO) is approximately 60 nautical miles and the Orbiter skims the Earth to reach 150 to 160 nautical miles halfway around, at which time a maneuver is performed to circularize the orbit.

An accuracy in the semimajor axis of 0.3 nautical mile or better has been achieved as shown in table 3. The position was determined to a few hundred feet on most flights. Orbit plane was determined to about 0.01°. These accuracies were achieved through the use of a Kalman filter and measurements from multiple trackers, accurate atmospheric refraction models with constants reflecting launch day conditions, and by including measurement bias and vehicle thrusting as state elements. Interactive controls and displays allowed for some inflight ground user control such as the adjustment of the filter state noise for powered versus free flight and the assessment of the quality and validity of navigation results.

TABLE 2.- STS ASCENT DELTA STATE UPDATE ERRORS
(MECO MINUS 30 SEC)

Flight	Position errors,[a] ft				Velocity errors, ft/sec			
	U	V	W	Mag	U	V	W	Mag
STS-1	300	100	100	330	3	2	2	5
STS-2	100	50	50	120	5	3	2	7
STS-3	500	100	-300	590	10	-5	-5	13
STS-4	1000	500	300	1160	20	5	5	22
STS-5	-300	200	300	470	-10	5	7	14
STS-6	500	400	-200	670	10	5	-5	13
Predicted (3σ)					40	20		
Required (3σ)					50	40		

[a]U = radial, V = downtrack, W = crosstrack.

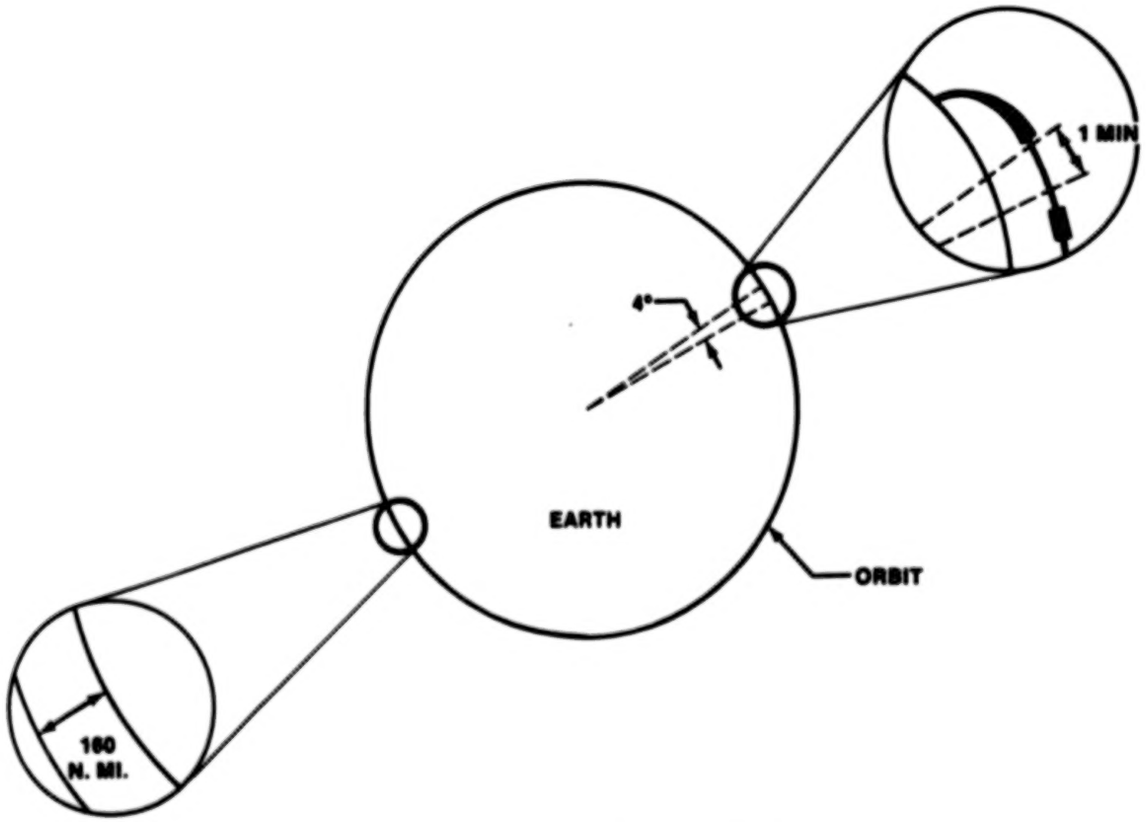


FIGURE 2.- POST-MECO ORBIT DETERMINATION.

TABLE 3.- STS ASCENT GROUND NAVIGATION ERRORS
(MECO PLUS 60 SEC)

Flight	Position, ft			SMA, n. mi.	Orbital plane, deg
	U	V	W		
STS-1	-100	100	40	0.3	0.007
STS-2	70	10	-50	-.1	-.012
STS-3	41	31	-58	-.2	.005
STS-4	220	65	30	-.2	.007
STS-5	-1350	300	-100	-.3	-.012
STS-6	40	50	40	0	-.005
Predicted (3σ)				0.5	
Required (3σ)				1.0	

Onboard post-MECO errors are shown in table 4. The onboard navigation state has never been updated by the ground because the errors are small.

TABLE 4.- STS ASCENT ONBOARD NAVIGATION ERRORS
(MECO PLUS 60 SEC)

Flight	Position, ft			SMA, n. mi.	Orbital plane, deg
	U	V	W		
STS-1	700	-300	-4200	0.1	-0.04
STS-2	700	-600	-3000	-.5	-.03
STS-3	600	-200	-3200	0	-.04
STS-4	300	300	-3200	.1	-.04
STS-5	200	-300	-1800	-.1	-.02
STS-6	-600	100	-2100	-.2	-.03

ENTRY NAVIGATION

The entry pre-deorbit activities include establishment of a knowledge of IMU orientation using star trackers and the transfer of an accurate state vector from the ground to the Orbiter. On some flights, there is provision for a downtrack position update between the deorbit maneuver and 400 000 feet altitude (entry interface).

Figure 3 shows events and altitudes. Use of altitude data derived from IMU measurements starts at 235 000 feet altitude and continues until barometric altimeter data are used at about 84 000 feet. TACAN range and bearing data are used from about 135 000 feet until microwave landing system data are used at 17 000 feet altitude.

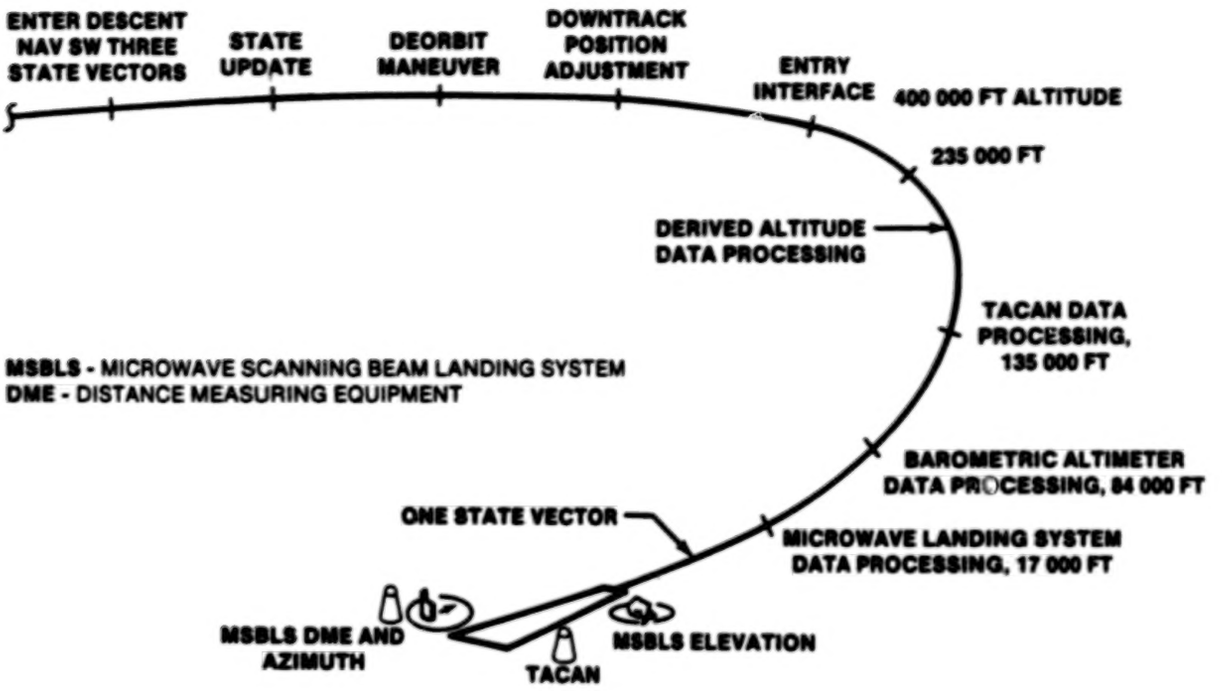


FIGURE 3.- DESCENT ONBOARD NAVIGATION.

BASE VECTOR

The accurate propagation of an initial state vector to entry interface is affected by translational effects from rotational maneuvers, drag, and vehicle outgassing or venting. These effects were reduced by procedures designed to minimize the time between ground state determination and entry interface, minimizing the rotational maneuvers, and use of attitude-dependent drag force models.

The position accuracy at entry interface has ranged from 0.2 to 0.8 nautical mile. This is small compared to a 5-nautical mile 3σ predicted accuracy because the propagation interval was greatly reduced from that originally expected.

DOWNTRACK ADJUSTMENT

A capability was developed to quickly determine downtrack position and adjust the onboard vector if necessary in the region between the deorbit maneuver and entry interface. The procedure is to use S-band range and Doppler data directly to determine the downtrack position error in the onboard state and then calculate the adjustment to the onboard vector timetag required to move the estimate of position forward or back along the orbit path. The timetag adjustment is voiced to the flightcrew for manual entry into the onboard computer.

The range measurement is used at vehicle acquisition near the horizon, at which point most of the downtrack position error is reflected in the differences between the observed range and the range computed using the onboard state vector (fig. 4).

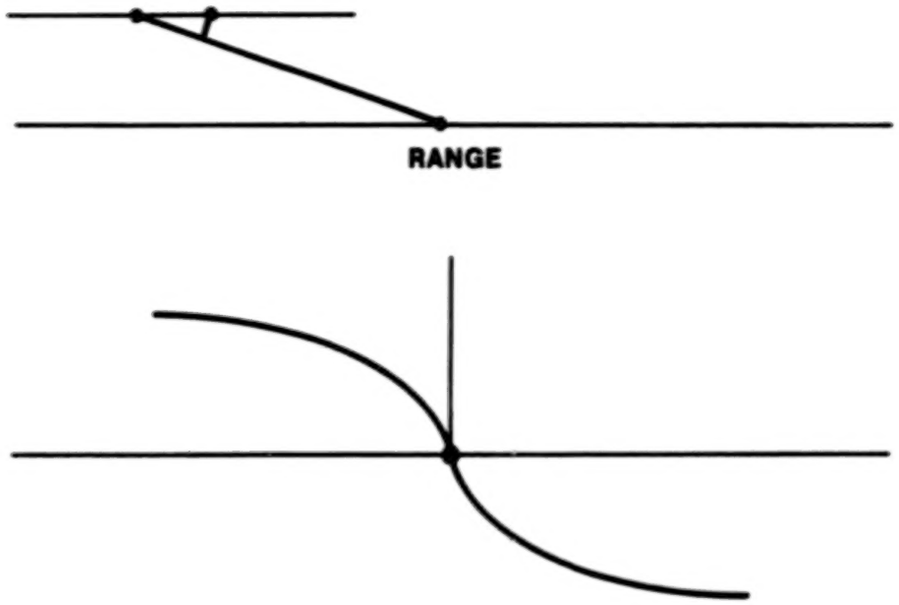


FIGURE 4.- DOWNTRACK POSITION ADJUSTMENT TECHNIQUE.

The Doppler measurement is zero as the vehicle passes by the site which, given good orbit shape and plane information, enables downtrack position to be easily determined. The two independent determinations of downtrack position are compared. No adjustment has been made on any of the flights to date because of the very small errors in the base vector. The adjustment technique has been accurate to at least 1000 feet (0.04 second).

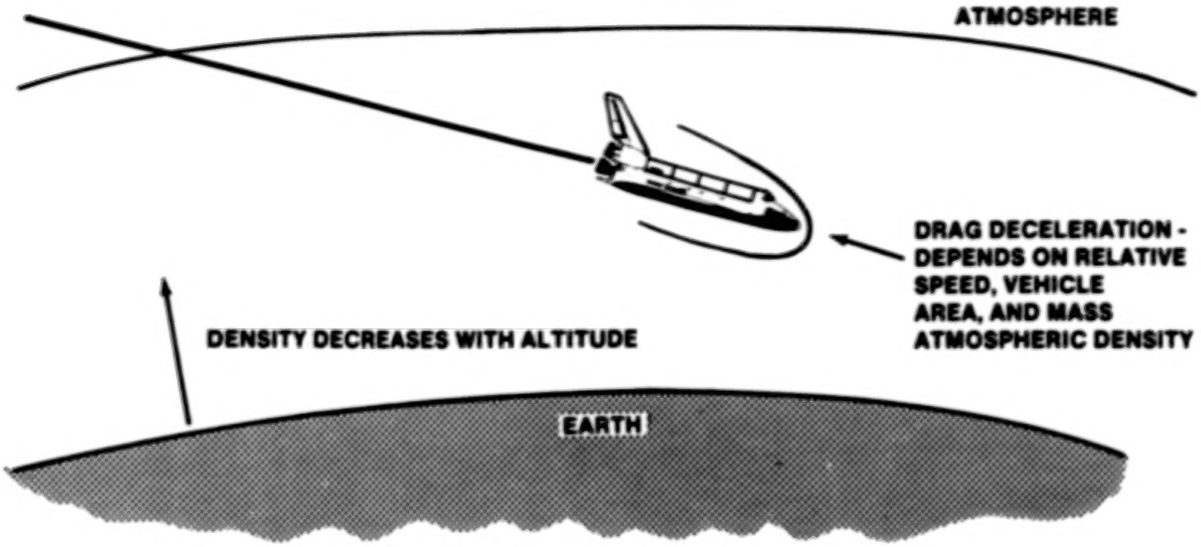
IMU ORIENTATION

The IMU orientation accuracy requirement for descent support is 0.53^{0} with a design goal to provide for desired system performance margins of 0.26 deg/axis. Orientation knowledge is accurate to about 0.06 deg/axis 1σ using the star tracker for initial determination and 0.08 deg/axis 1σ using a crew optical alinement system. These accuracies allow for 3.3 hours of IMU drift from the last alinement to entry interface. IMU drifts are calibrated in flight by the ground. Typical calibrated drift rate errors are about 0.02 deg/hr/axis. IMU alinement on Apollo was performed using a manually operated sextant. Use of the automatic star tracker has also been very successful.

DESCENT NAVIGATION

RADIAL POSITION ERROR AND IMU MEASUREMENTS

State propagation with the use of velocity change due to contact forces measured by the IMU and gravitational acceleration models was expected to result in large errors in radial position during descent. A method for constraining the size of the radial position and velocity error was desired to minimize position transients at TACAN acquisition and to provide good radial rate information for guidance. The approach taken is shown in figure 5. Drag acceleration, measured by the IMU, is a function of vehicle speed, mass, area, and atmospheric density. Atmospheric density decreases exponentially with altitude. Altitude was computed given the other parameters and provided to a navigation filter as an observation for state determination. This approach was expected to degrade IMU altitude knowledge for normal IMU performance at higher altitudes but to improve on it at lower altitudes. This prediction can be seen in figure 6. A shift in the predicted error (mean +3σ) in radial position occurs at initial use of the derived altitude at about 230 000 feet altitude. The predicted errors apply for all of the flights shown except flight 4. Flight 4 occurred in July and the uncertainty in atmospheric density is expected to be worse than for cooler seasons. Use of derived altitude worked as predicted. The altitude error is less than 1 nautical mile throughout descent.



DETERMINE ALTITUDE USING IMU MEASUREMENTS OF DECELERATION
PROCESS ALTITUDE INFORMATION IN NAVIGATION FILTER

FIGURE 5.- DESCENT ALTITUDE AND DOWNTRACK POSITION ERROR RESTRAINT TECHNIQUE.

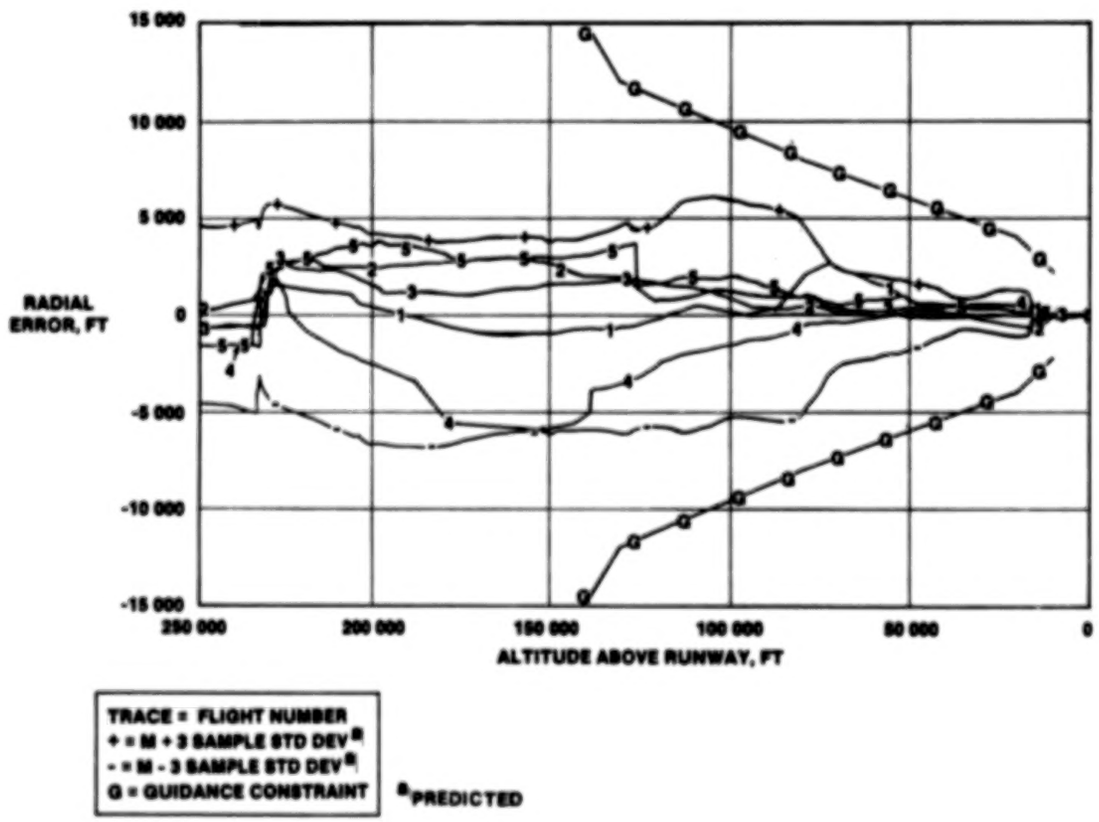


FIGURE 6.- ERROR IN RADIAL POSITION.

Some effect on radial position accuracy from the use of TACAN range data can be seen (fig. 6) in the 130 000-foot-altitude region. The TACAN ground site is near the runway and the line of sight between it and the Orbiter is more toward the horizontal than the vertical. The result is limited direct visibility of radial position and limited ability to correct it. Use of barometric altimeter data at about 84 000 feet altitude reduces radial position error to less than 500 feet by the time landing system measurements are available. Use of microwave landing system data at about 17 000 feet altitude reduces the position error to less than 100 feet. Radial position guidance requirements have been met with good margins.

The use of derived altitude affects downtrack position because radial and downtrack position errors are correlated (fig. 7). The use of TACAN observations easily reduces downrange position errors to less than 3000 by 120 000 feet altitude.

Crosstrack position error is shown in figure 8 as a function of altitude. A 1.2° TACAN bearing error on flight 1 led to an 8000-foot crosstrack error at about 115 000 feet altitude. The error decreased with decreasing range to the TACAN site. Otherwise, the crosstrack error was less than 1 nautical mile throughout descent.

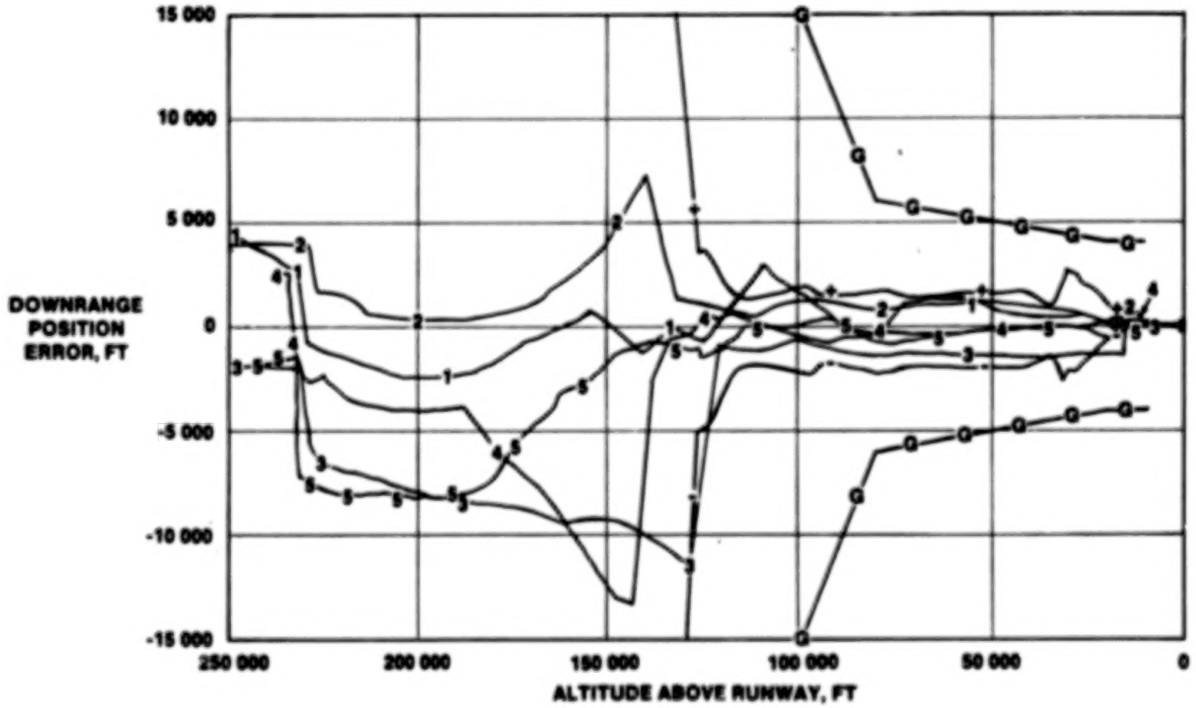


FIGURE 7.- ERROR IN DOWNRANGE POSITION.

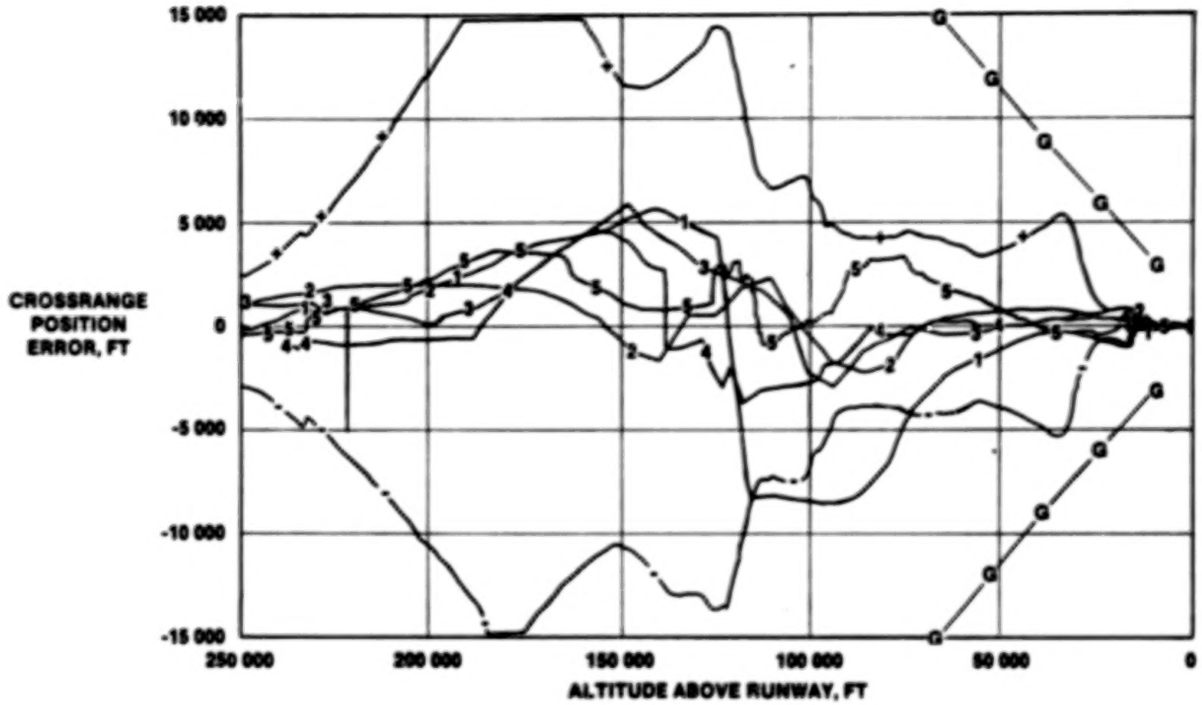


FIGURE 8.- ERROR IN CROSSRANGE POSITION.

The error information for selected times is provided in tables 5 to 7. Table 7 shows an improvement at touchdown on flight 6 due to the use of a microwave landing system ground antenna that was more compatible with the Orbiter antenna. The vertical error on flight 2 at touchdown is the result of using microwave landing system elevation data at too low an elevation so that multipath error effects deteriorated the state.

AIR RELATIVE DATA

Air relative parameters - Mach number, angle of attack, and dynamic pressure - are required for flight control prior to air data availability at about 84 000 feet altitude. There was a desire to have the vehicle control be independent of position and velocity error. Use of drag acceleration measured by the IMU's for the computation of air relative parameters resulted in relatively accurate parameters with only second-order dependence on position and velocity.

FUTURE NAVIGATION EFFORT

New capabilities planned include navigation for rendezvous and proximity operations and refined orbital onboard state propagation in 1984; flexibility ahd reduced onboard maintenance of runway, TACAN, and microwave site data in 1985; and autonomous orbital navigation by 1986. There will be three additional vehicles to check, a first KSC landing, a Vandenberg launch, a Vandenberg landing, and an automatic landing. The first use of the Tracking and Data Relay Satellite (TDRS) for ground-based orbital navigation will occur in 1983. Onboard descent autonomy requires autonomous orbital navigation, deorbit targeting, and independence from current ground management of the use of onboard descent navigation sensors.

TABLE 5.- ONBOARD NAVIGATION SUMMARY NEAR TACAN ACQUISITION

Pre-TACAN			Post-TACAN		
Flight	Position, ft		Flight	Position, ft	
	Horizontal	Vertical		Horizontal	Vertical
STS-1	5 822	-696	STS-1	4349	-467
STS-2	1 452	2021	STS-2	1230	998
STS-3	11 834	1831	STS-3	2460	728
STS-4	15 458	-5858	STS-4	2609	-3903
STS-5	4 050	3720	STS-5	2262	1625
STS-6	6 334	-1860	STS-6	1052	-1241
Mean +1σ[a]	10 602	2269	Mean +1σ	3326	2291
Mean +3σ	27 066	5903	Mean +3σ	9980	6134

[a]Expected.

TABLE 6.- ONBOARD NAVIGATION SUMMARY NEAR MSBLS ACQUISITION

Pre-MSBLS			Post-MSBLS		
Flight	Position, ft		Flight	Position, ft	
	Horizontal	Vertical		Horizontal	Vertical
STS-1	877	303	STS-1	36	51
STS-2	1113	-488	STS-2	120	51
STS-3	1386	-6	STS-3	14	-54
STS-4	320	411	STS-4	54	78
STS-5	750	194	STS-5	83	23
STS-6	1220	440	STS-6	102	74
Mean +1σ[a]	470	420	Mean +1σ	67	43
Mean +3σ	1230	1213	Mean +3σ	198	99

[a]Expected.

TABLE 7.- ONBOARD NAVIGATION SUMMARY AT TOUCHDOWN

Flight	Touchdown, ft		
	Downtrack	Crosstrack	Vertical
STS-1	-4	18	5
STS-2	36	50	15
STS-3	32	72	6
STS-4	19	48	6
STS-5	10	29	2
STS-6	20	4	4
Mean $+3\sigma$[a]	48	30	30

[a]Expected.

REFERENCES

1. Schiesser, Emil R.: Use of Radio Equipment for Space Shuttle Navigation. IEEE Transactions on Communications, Vol. Com-26, No. 11, Nov. 1978.

2. A Collection of Technical Papers. AIAA Guidance and Control Conference, San Diego, Calif., Aug. 9-11, 1982.

3. Edwards, Andrew, Jr.: Report on Space Shuttle Navigation. International Congress of Institutes of Navigation, Paris, France, Sept. 21-24, 1982.

4. Ewell, James J., Jr.: Orbiter Navigation During Entry Through Landing. Paper presented at the 39th Annual Meeting, The Institute of Navigation, NASA Lyndon B. Johnson Space Center, Houston, Tex., June 20-23, 1983.

5. Little, Michael J.: Space Shuttle Orbiter Onboard Rendezvous Navigation. Paper presented at the IEEE Position Location and Navigation Symposium (PLANS '82), Atlantic City, N.J., Dec. 7-9, 1982.

6. Pixley, Paul T.; Lowes, Flora B.; Williamson, Bruce; et al.: OFT High Speed Trajectory Determination for Launch and Landing Phases. NASA Lyndon B. Johnson Space Center, JSC-11709, July 1977.

N85
16902

UNCLAS

N85-16902

D13

DESCENT GUIDANCE AND MISSION PLANNING FOR SPACE SHUTTLE

B. Kent Joosten
NASA Lyndon B. Johnson Space Center
Houston, Texas

ABSTRACT

The Space Shuttle descent mission planning, mission design, deorbit targeting, and entry guidance have necessarily become interrelated because of the nature of the Orbiter's design and mission requirements. The desired descent trajectory has been formulated in a drag acceleration/relative velocity state space since nearly all of the vehicle's highly constraining flight limitations can be uniquely represented in this plane. This paper presents a description of these constraints along with the flight requirements that affect them, a discussion of the guidance logic which allows the Orbiter to follow the designed trajectory, and a summary of the impacts of contingency aborts and flightcrew interaction. The mission planning and guidance techniques have remained essentially unchanged through the Shuttle flight test program and subsequent operational flights. No problems or anomalies have been observed in these areas.

INTRODUCTION

The experience gained in developing the Gemini and Apollo entry mission plans, flight software, and trajectory monitoring procedures has provided insight into the problems encountered during the atmospheric descent of a manned spacecraft. The Shuttle Orbiter shares many requirements and constraints with these earlier vehicles. A flightpath must be maintained that causes no violations of the spacecraft's thermal or load limits yet ensures atmospheric capture and stable flight. Allowance must be made for uncertainties in atmospheric properties, navigational accuracies, and aerodynamic characteristics. The vehicle and crew must be able to function autonomously because of communication blackout and limited ground coverage. Finally, the spacecraft must be delivered to a specified location and energy state with the required precision.

Although the general nature of these requirements for manned reentry vehicles is similar, because of the Orbiter's basic design, nearly all of its flight constraints are significantly more limiting than those of previous spacecraft, and its mission is more complex. In addition to the normal end-of-mission functions, the Shuttle's entry system must support the needs of transoceanic abort landing (TAL) and abort once around (AOA) contingencies. These factors imply a wide range of vehicle weights and center-of-gravity (c.g.) locations and have made it necessary to implement a complex guidance scheme with greater flexibility than that of either the Gemini or the Apollo vehicle.

The development of the guidance logic and the selection of a basic flight profile are closely related through the Shuttle descent mission planning. Therefore, the effects of both mission requirements and guidance system characteristics are addressed.

ENTRY CONFIGURATION

During the early phases of entry (before active guidance), attitude control in all vehicle axes is maintained by the Orbiter reaction control system (RCS). To avoid unacceptable aerothermodynamic heating, especially on the upper surface and wing leading edge, a 40° angle of attack is flown during the high-speed flight regime (Mach > 14). Even though this value is far on the back side of the lift-to-drag ratio (L/D) curve, it still results in a much higher L/D than for previously flown manned reentry vehicles. Figure 1 shows the overall aerodynamic characteristics on a typical Orbiter entry trajectory (ref. 1).

When sufficient atmospheric dynamic pressure has been achieved, attitude control is transferred to the aerodynamic control surfaces (aerosurfaces). At a navigation-sensed dynamic pressure of 10 psf, the roll RCS jets are deactivated and differential elevon deflections control motion about that axis. When the dynamic pressure exceeds 20 psf, control by the elevator in the form of symmetric elevon deflections replaces the pitch jets. As is indicated later, the primary maneuvers performed during entry are rotations about the vehicle velocity vector. These maneuvers amount to coordinated roll and yaw rates about the spacecraft body axes. Because of the large angle of attack, the vertical stabilizer is not an effective aerosurface during high-speed flight; therefore, the maneuvers require a combination of aft yaw RCS jets and ailerons. The yaw jets operate throughout entry.

In addition to providing active vehicle control (i.e., the Orbiter is statically unstable during much of its flight), the flight control system must compensate for variations in pitching moment due

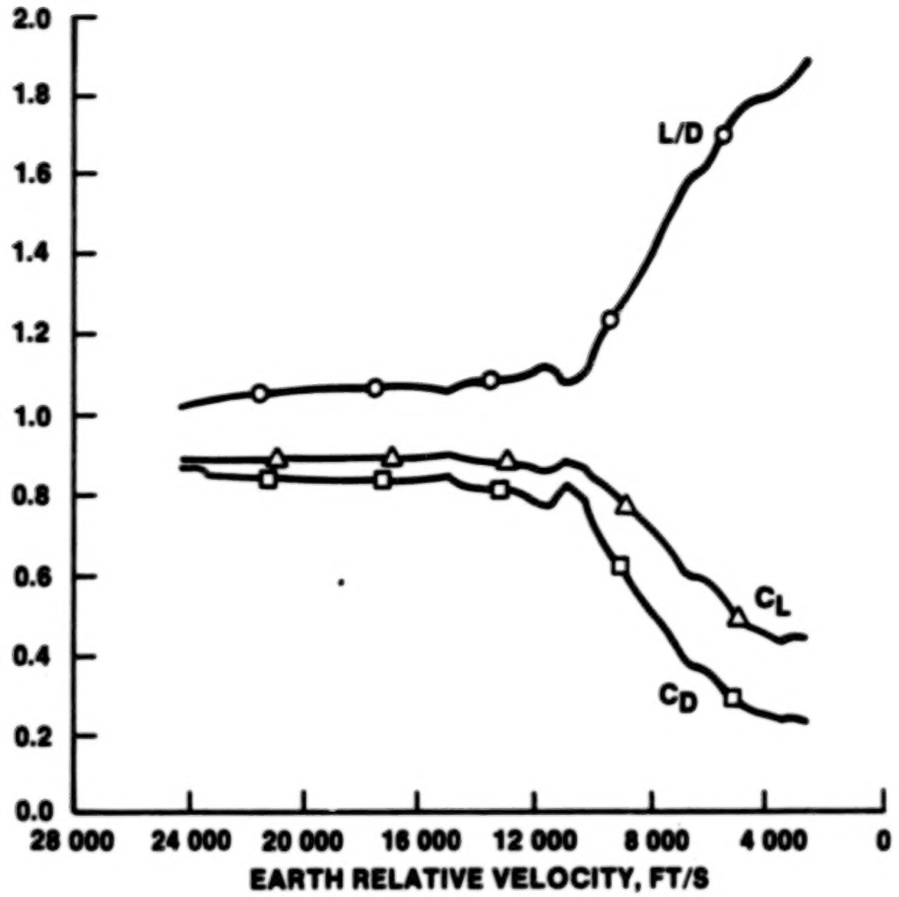


FIGURE 1.- TYPICAL ORBITER AERODYNAMIC CHARACTERISTICS.

to shifts in the spacecraft center of gravity and aerodynamic moments. To maintain the elevons in a thermally benign position where they are aerodynamically effective for lateral control, the large aft body flap is used for pitch trim. The ailerons trim out any lateral c.g. effects.

ENTRY CORRIDOR

Entry imposes on a returning vehicle certain physical conditions, the severity of which depends on the particular trajectory flown. In general, for a given entry velocity, a steep flightpath angle implies high surface temperatures and aerodynamic load factors, whereas a shallow flightpath angle can result in poor trajectory control (phugoids) or atmospheric skipout. The width of the entry corridor is a function of such vehicle capabilities as thermal and structural constraints and aerodynamic characteristics. Figure 2 shows the entry corridors for the Apollo command module (CM) and the Shuttle Orbiter (ref. 2). Both are defined by the flightpath angle and the inertial velocity at entry interface (400 000 feet altitude). It is apparent that the Shuttle thermal limits impose severe restrictions on the entry corridor and place stringent requirements on entry targeting and guidance.

DEORBIT TARGETING

The Shuttle orbital maneuvering system (OMS) performs a single deorbit burn to arrive at entry interface. The result is a specific combination of velocity, flightpath angle, and range to go, which depend on the orbital altitude and burn characteristics. To cover the range of Shuttle operational orbits (as high as 500 nautical miles), a target line is generated in the V-Y plane representing a set of acceptable entry interface (EI) conditions. The intersection of this target line with the appropriate deorbit curve defines the target state. The range to the target is controlled by properly

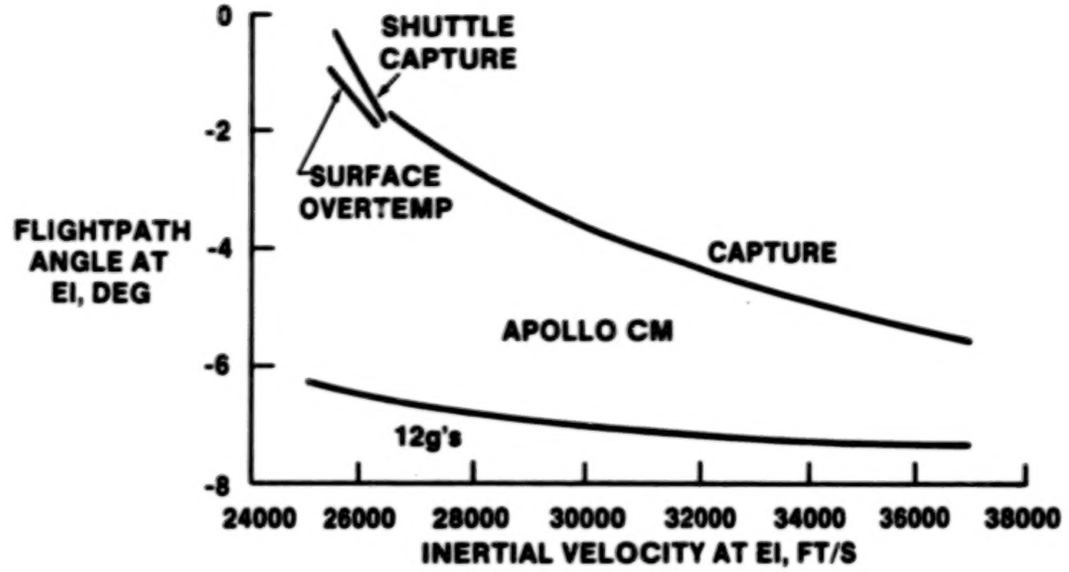


FIGURE 2.- APOLLO COMMAND MODULE AND SHUTTLE ORBITER ENTRY CORRIDORS.

timing the burn. The segment of the entry from EI to active guidance initiation is normally flown at a wings-level attitude (steep target). In the event of a fuel-critical deorbit or an OMS underburn, a bank angle as great as 90^{0} can be commanded (shallow target). This prebank has the effect of steepening the early trajectory by dumping lift. Typical steep and shallow target lines and the transfer-orbit curves are shown in figure 3. The onboard deorbit guidance actually targets the line rather than the intersection, so that any deviation from the ideal transfer still results in acceptable entry conditions. The target lines themselves represent EI states which allow the trajectory to converge to preplanned entry profiles (to be discussed later). For steep targets, the line is adjusted to optimally trade surface temperatures against high backface temperatures; the latter temperatures are caused by the large heat loads generated during long, shallow glides.

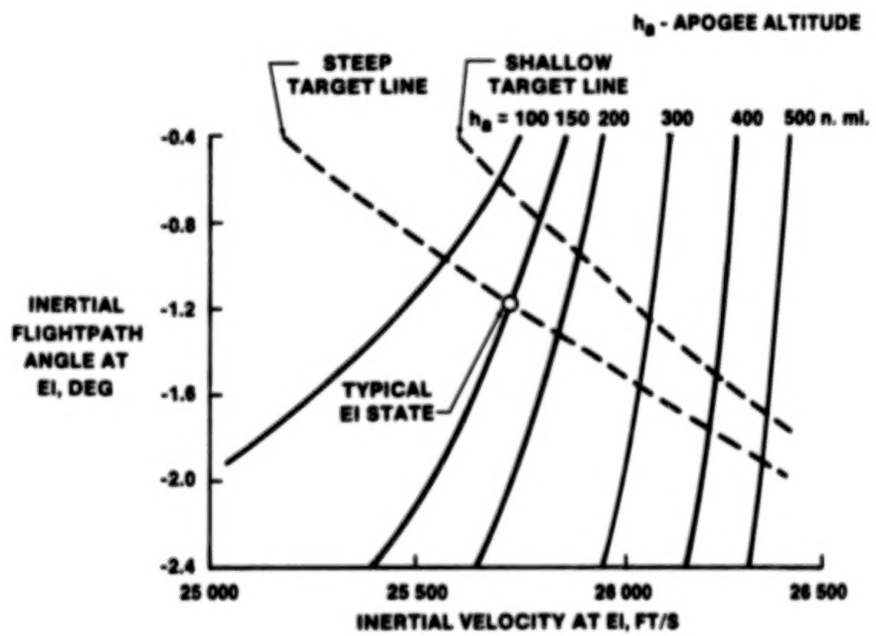


FIGURE 3.- STEEP AND SHALLOW TARGET LINES.

TRAJECTORY CONSTRAINTS

Once the Orbiter has achieved the desired EI state, it is still necessary to actively guide the vehicle to the landing site while remaining within trajectory and vehicle limits. The various constraint boundaries become binding at different flight conditions, and their interaction can be complex. To visualize the profile that must be flown, the constraints must be formulated as functions of the proper trajectory variables.

For thermal and flight control system considerations, the Orbiter angle of attack (and therefore its aerodynamic characteristics) has been scheduled as a function of Earth relative velocity. Figure 4 shows the profile used in the majority of Shuttle flights. The ramp beginning at a velocity of 14 500 ft/s delivers the Orbiter to the terminal area energy management (TAEM) interface (2500 ft/s) on the front side of the L/D curve, where more conventional aircraft-type control is employed.

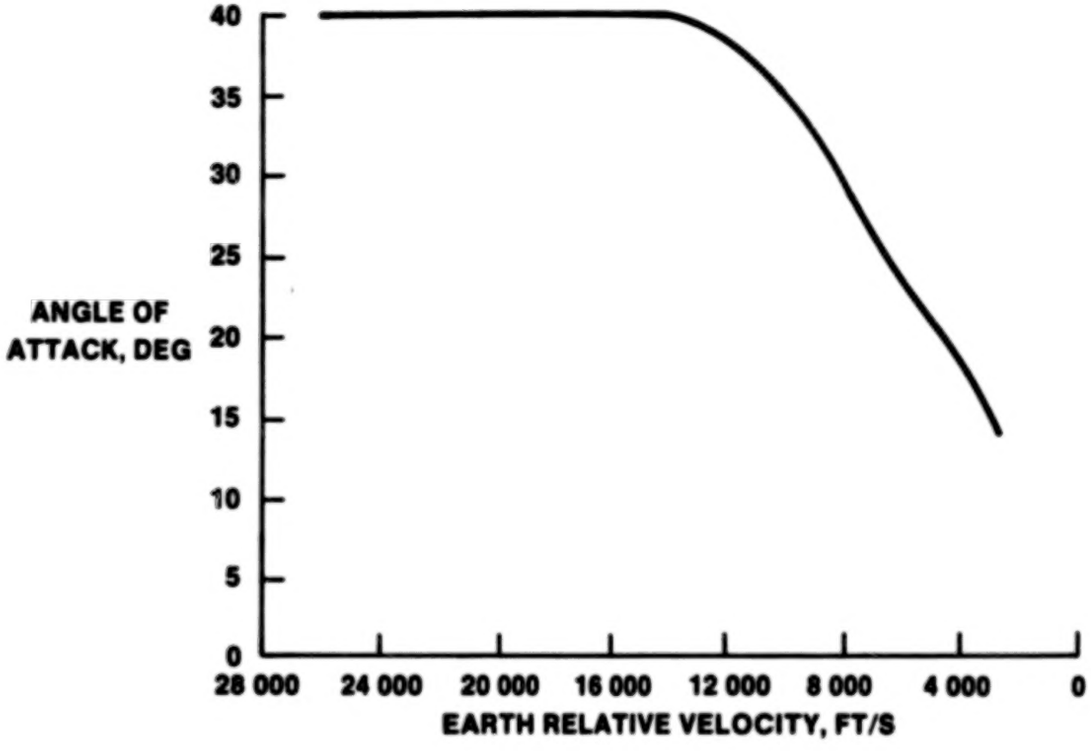


FIGURE 4.- ORBITER ANGLE OF ATTACK PROFILE.

The most critical constraints during early entry are the thermal protection system (TPS) surface temperatures. For a fixed angle-of-attack profile, large dynamic pressures and relative velocities will elevate surface temperatures. Since the aerodynamic flow field over the Orbiter's surface is complex, mathematical models representing heat rates on specific vehicle locations or control points are used for trajectory design (ref. 3). Figure 5 depicts the positions of several control points. Depending on the particular flight condition and the maximum allowable temperature at each point, any of these locations may represent the limiting constraint on the trajectory.

To ensure stable, nonoscillatory flight, a design requirement has been implemented to guarantee that the Orbiter flightpath angle is always decreasing, that is, that the trajectory is constantly becoming steeper. The limiting case, where $\dot{\gamma} = 0$, defines the equilibrium glide boundary. Physically, this value corresponds to the flight condition in which the vertical component of the vehicle lift acceleration plus the centripetal acceleration induced by the high velocity are balanced by gravity. For a given bank angle, the constraint can be expressed as a function of dynamic pressure and inertial velocity since they determine the magnitudes of lift and centripetal acceleration, respectively. The value of the minimum allowable bank angle resulted from trade studies evaluating the horizontal lift component necessary for Orbiter crossranging requirements.

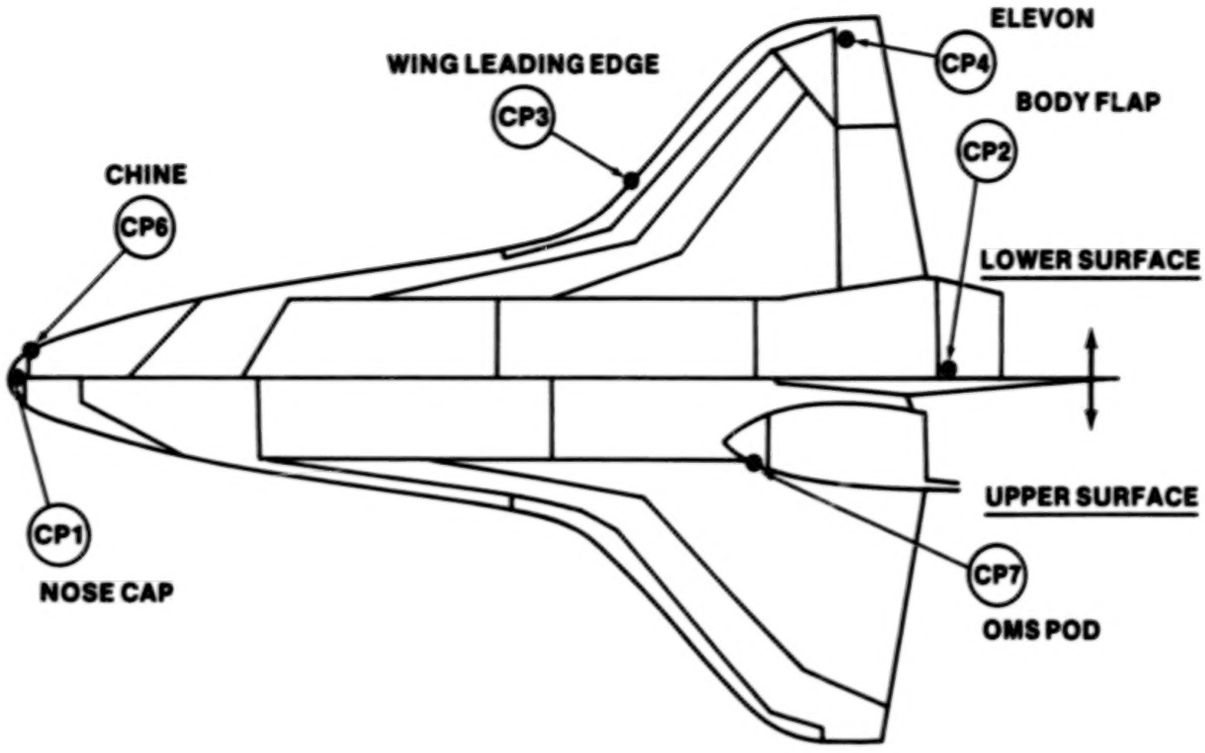


FIGURE 5.- CONTROL POINT GEOMETRY.

The Shuttle Orbiter is also much more limited in its maximum allowable load factor than were previous reentry vehicles. Gemini and Apollo spacecraft operated at 4g to 7g with a design limit of 12g on the Apollo CM (refs. 4 and 5). In contrast, the Orbiter was designed with a maximum normal load factor of 2.5g and a trajectory-shaping goal of 1.5g. The actual load factor encountered depends only on the normal acceleration magnitudes or, equivalently, on angle of attack and dynamic pressure. During lower speed portions of the entry (3500 to 2500 ft/s), dynamic pressure becomes a constraint because of its effects on wing loading and aerosurface hinge moments.

All of these constraints could be portrayed in a dynamic pressure/velocity state space. Use of dynamic pressure as a guidance control parameter would involve derivation from sensed vehicle accelerations and attitudes and would require lift and drag coefficient models for all valid angles of attack and Mach numbers. Since considerable uncertainties existed in the preflight predictions of these quantities, the constraint boundaries were reformulated into a drag acceleration/Earth relative velocity state space. This formulation requires only an estimate of the Orbiter lift-to-drag ratio, which is probably the most reliable aerodynamic parameter to predict and can also be directly measured during flight. In addition, a drag acceleration profile uniquely defines the range flown during entry. Figure 6 depicts the surface temperature, equilibrium glide, load factor, and dynamic pressure constraints in this plane for typical mission parameters. To accomplish a safe entry, the Orbiter must fly the corridor between these constraint boundaries.

The corridor width, and therefore the safety margins of the entry flightpath, depends on specific mission characteristics. The Space Shuttle must operate over large variations of orbital inclination, vehicle weight, and center-of-gravity location. Inclination affects the relationship between inertial and Earth relative velocity and shifts the equilibrium glide constraint in the D-V plane; the corridor narrows for increasing inclination. Vehicle weight is the driver on the location of all the surface temperature boundaries. An increase in weight narrows the corridor as the Orbiter must fly a trajectory consistent with larger aerodynamic forces to produce equivalent accelerations. The change in these constraint boundaries can be seen in figure 7. As the c.g. shifts, the body flap must deflect to trim the vehicle and thereby alters the airflow and thermal distribution on that surface. An aft c.g. deflects the body flap down into the airflow and increases the temperature of the associated control point as shown in figure 8. In practice, the elevon and predicted body flap positions are balanced so that neither surface temperature is excessively more restricting than the other.

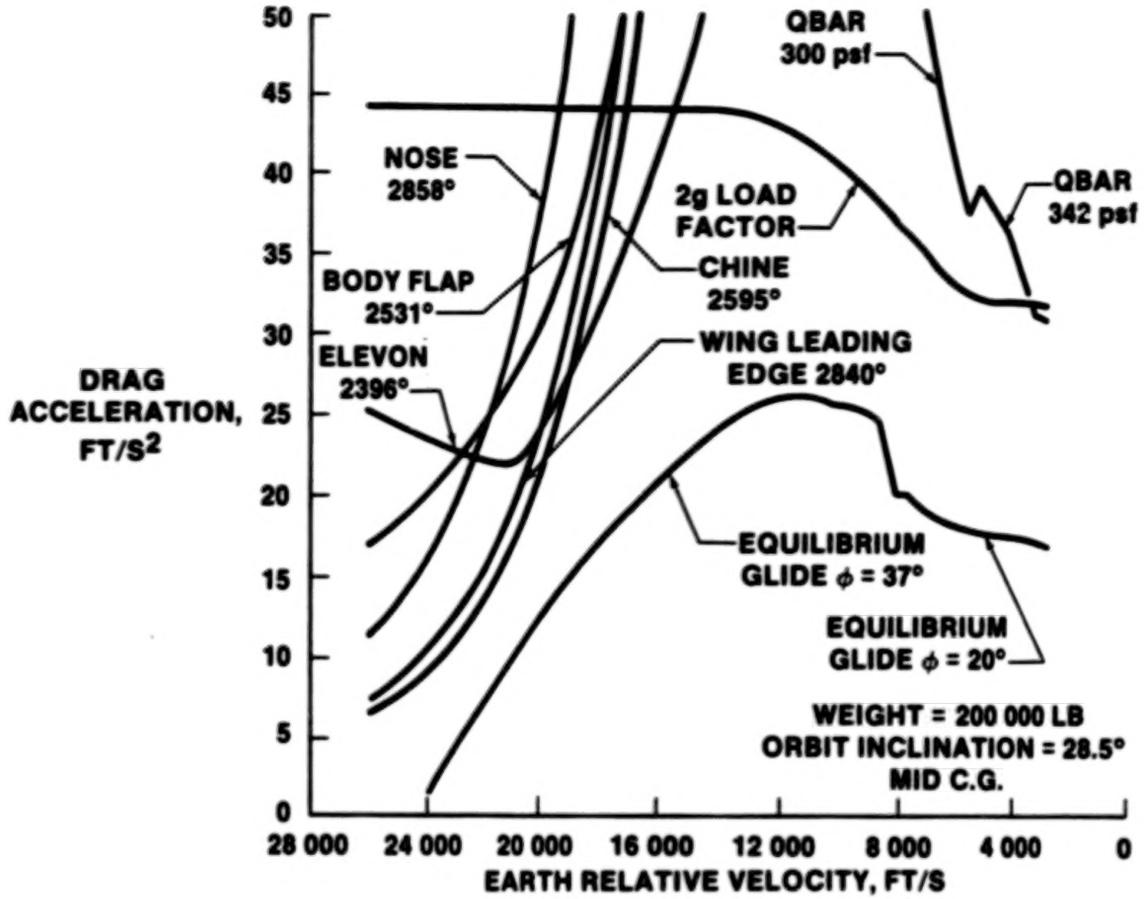


FIGURE 6.- REPRESENTATIVE CONSTRAINT BOUNDARIES.

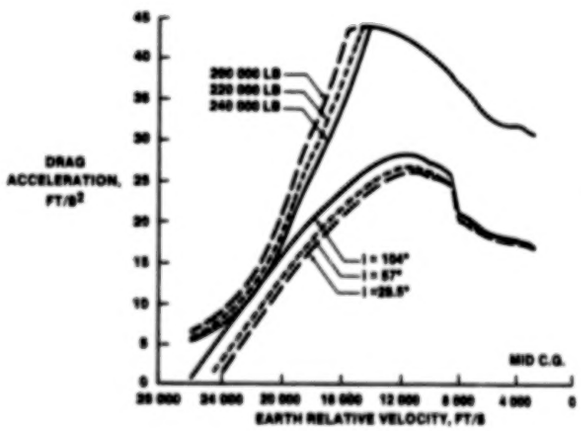


FIGURE 7.- EFFECTS OF WEIGHT AND INCLINATION ON CONSTRAINT BOUNDARIES.

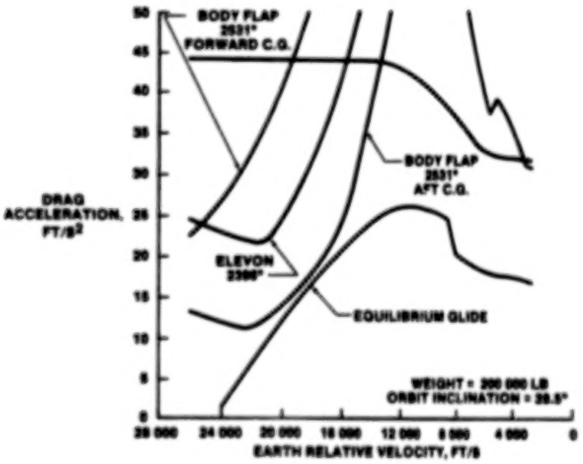


FIGURE 8.- EFFECT OF CENTER OF GRAVITY ON CONSTRAINT BOUNDARIES.

The combination of the effects of these mission parameters can be seen in the constraint boundaries of a "worst case" entry. As shown in figure 9, essentially no corridor remains.

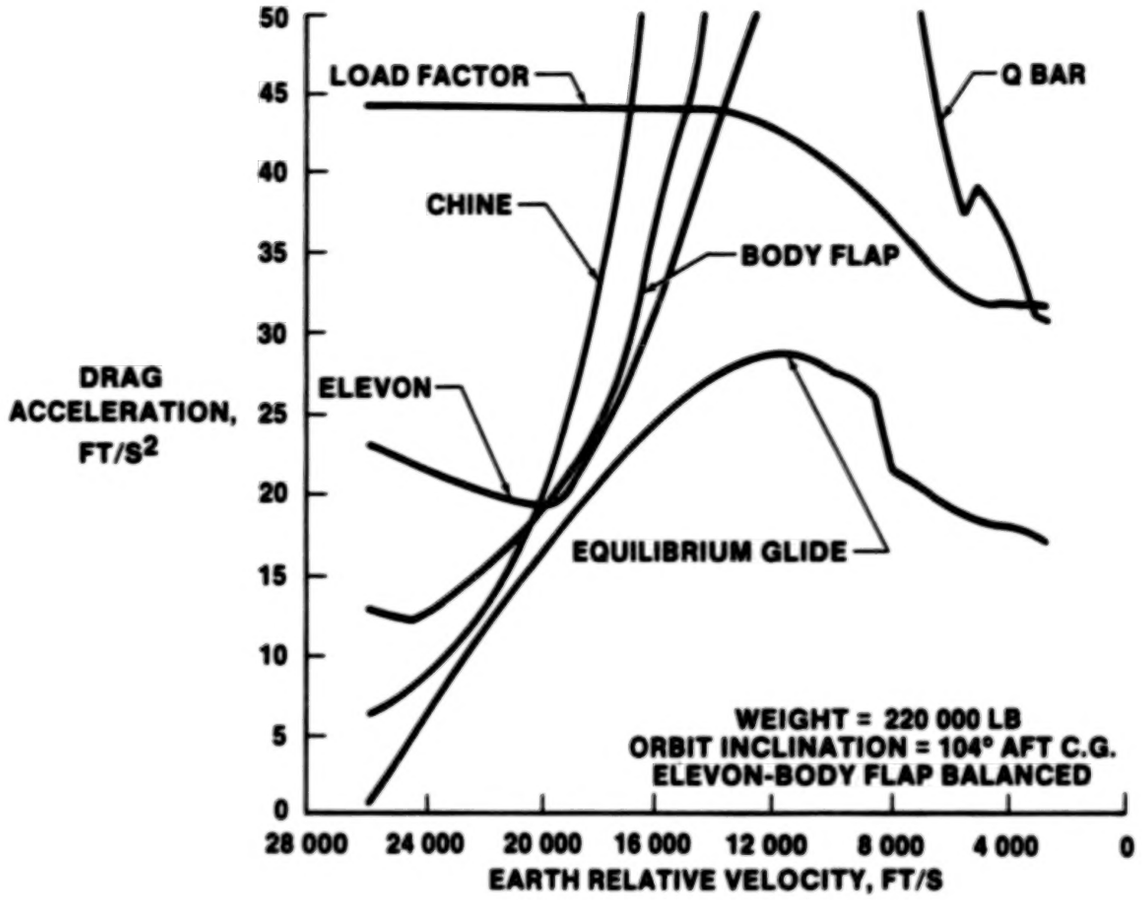


FIGURE 9.- "WORST CASE" CONSTRAINT BOUNDARIES.

GUIDANCE LOGIC

The engineering challenge addressed in designing the entry guidance was to devise a method for directing the Orbiter along a trajectory which remained within the highly confining constraint corridor using primarily the onboard navigation while still allowing enough flexibility to arrive at the landing site with the proper energy reserve. Achievement of this objective was made possible by the realization that the drag acceleration/relative velocity plane was the proper state space in which to view the constraints and define the entry range. It then became natural to implement the guidance logic in this plane also (ref. 6). Figure 10 depicts a typical drag profile, which represents the desired entry trajectory for the boundaries in figure 6.

ENTRY PROFILE

To remain within the constraint corridor, the guidance has been divided into four phases. The temperature control phase is initiated at a vehicle load factor of 0.176g and continues as long as surface temperatures are the binding constraints. At a relative velocity of 17 000 ft/s, a pseudo-equilibrium glide phase is entered for a short time to deliver the vehicle to the flight region in which load factor limits deceleration. A constant-drag phase designed to produce a 1.5g total load factor is then followed until the Orbiter pitch down and associated L/D increase requires a lower deceleration level. The transition phase completes the entry and delivers the spacecraft to the desired energy state at TAEM interface. All guidance phases are defined by simple geometry in the D-V plane, and 15 constraints mathematically describe the entire entry profile. It is the task of descent mission planning to select this profile based on its capability to accommodate nominal and all foreseen stress requirements.

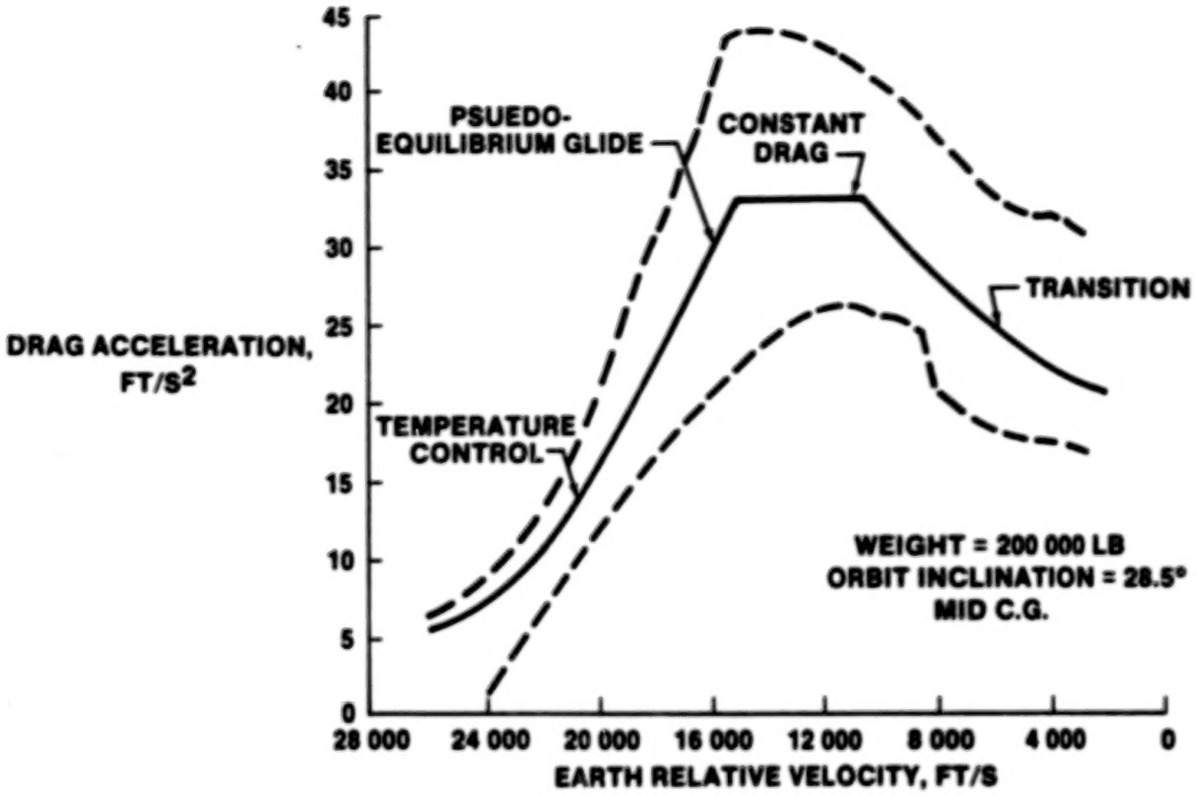


FIGURE 10.- DRAG PROFILE AND CONSTRAINTS.

The flightpath resulting from the profile of figure 10 is shown in figure 11 along with typical Apollo and Gemini descents (refs. 7 and 8). It is obvious that an extended high-altitude glide is the direct result of the thermal and load factor limitations. This long flight time produces a backface temperature constraint which is not uniquely defined in the D-V plane. The TPS was sized on the basis of a reference heat load, and any increase in this value has a direct bearing on the temperature of the Orbiter's aluminum structure. Procedures such as on-orbit shading of the lower surface before entry help alleviate this heat soak, but, in practice, the constraint on backface temperature is more binding than the equilibrium glide boundary.

TRAJECTORY CONTROL

Once a reference profile with the proper range potential has been designed, a method of commanding flight control and correcting for deviations must be devised. Recall that the only vehicle characteristic necessary to define a path in the D-V plane is the vertical component of the lift-to-drag ratio, L/D_V. Conversely, a reference L/D_V corresponding to the reference drag profile can be computed. Since the total vehicle L/D is scheduled with velocity (through angle of attack), this L/D_V is achieved by rotating the lift vector about the velocity vector through a stability bank angle with magnitude

$$\phi_S = \cos^{-1}\left[\frac{L/D_V}{L/D}\right].$$

Also, because the in-flight L/D can be measured directly by the onboard navigation, the vertical component can be precisely controlled.

To compensate for deviations from the drag profile, a drag error feedback term was introduced into the commanded L/D_V equation. It is usually desirable to include a lead term in a feedback control

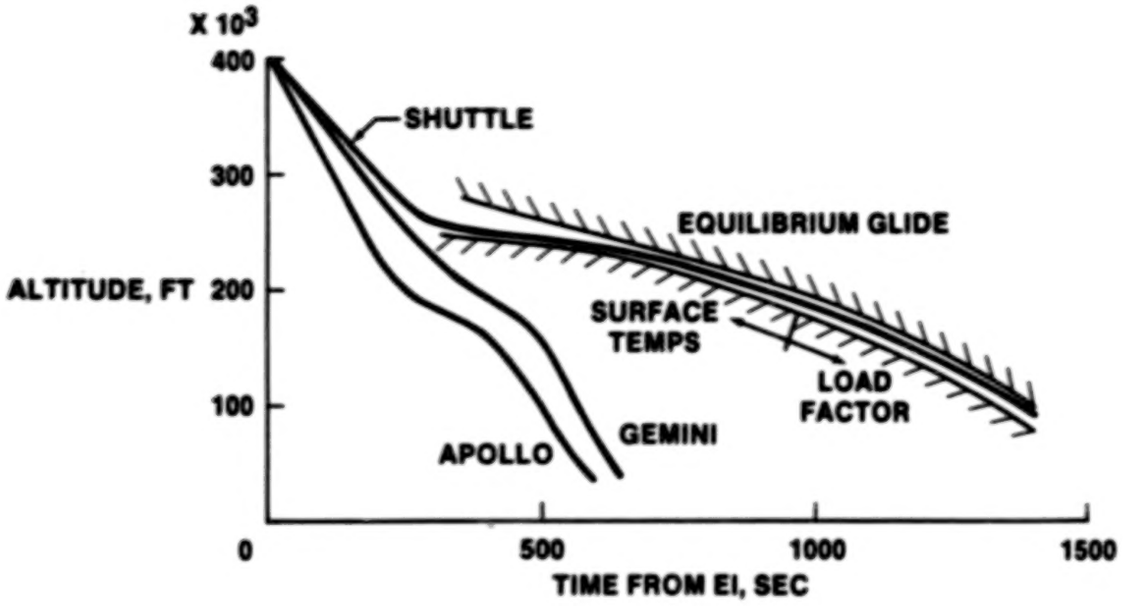


FIGURE 11.- FLIGHTPATH COMPARISIONS.

system, but accelerometer noise and small vehicle attitude changes make the time derivative of drag an unsuitable measurement without significant filtering. After appropriate manipulation, altitude rate ($\dot{h}$) can be used as a measure of the drag rate due to trajectory effects only, and a reference $\dot{h}$ profile can be analytically constructed from the reference drag profile. The final form of the vertical L/D command equation is

$$L/D_{V_{COMMAND}} = L/D_{V_{REF}} + k_D (D - D_{REF}) + k_{\dot{h}} (\dot{h} - \dot{h}_{REF})$$

where k_D and $k_{\dot{h}}$ are appropriate system gains. Again, this expression is implemented through a stability bank angle command.

RANGE PREDICTION

As has been stated earlier, the reference drag profile uniquely defines the range remaining to be flown from a given velocity. This range prediction, based on approximations to the equations of motion, is compared with the navigation-based range-to-go value to form an error term used to adjust the current drag profile as follows: increase it if the Orbiter is too close to the target, decrease it if it is too far. Thus, in effect, an outer feedback loop which continually updates the original reference profile is formed. Operationally, it is desirable to preserve as much ranging capability as possible late in the entry to allow for postblackout navigation updates and runway redesignations. Therefore, only the current guidance phase of the profile is adjusted for ranging and, consequently, the Orbiter is forced back toward the center of the ranging footprint (ref. 9).

CROSSRANGE CONTROL

Because a bank angle must be maintained to achieve the proper vertical trajectory, the horizontal component of lift can be used to turn the flightpath. The relatively high Orbiter L/D allows a much larger crossranging capability than with previous vehicles, approximately 750 nautical miles. This capability greatly aids operational factors such as the number of return opportunities into a given landing site and abort-once-around contingencies. To target for the proper crossrange, the guidance computes the azimuth error between the velocity vector and the line of sight to the runway. If this angle becomes greater than a stored deadband schedule, a bank reversal is commanded.

The trajectory is essentially uncontrolled during a reversal, and some lofting occurs because of the Orbiter's maximum roll rate of only 5 deg/s. This lofting would cause the drag level to drop

below the reference profile; consequently, compensation has been added to the guidance pitch channel by which the angle of attack and, therefore, the drag coefficient is allowed to increase for driving the vehicle back to the reference. This modulation also decreases the effect of any unforeseen atmospheric density gradients. Typical altitude rate, roll, and angle-of-attack histories are shown in figure 12. The result is very tight drag trajectory control as shown in figure 13.

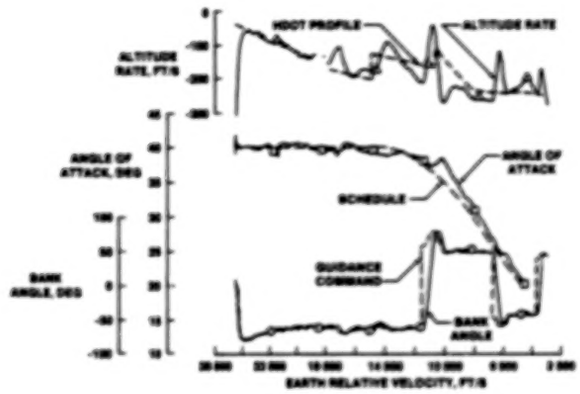


FIGURE 12.- FLIGHT DATA PARAMETERS FROM STS-5.

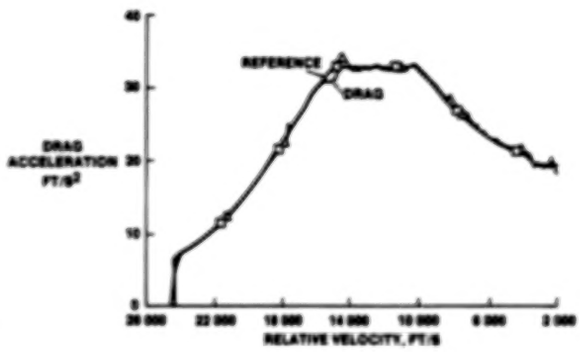


FIGURE 13.- DRAG AND REFERENCE PROFILE, STS-6.

CONTINGENCY ABORTS

The guidance, in addition to providing trajectory control for nominal and dispersed end-of-mission entries, must allow intact vehicle recovery for mission emergencies and aborts. The logic has been adapted for two contingencies: abort once around and transoceanic abort landings.

An AOA results from main propulsion system (MPS) failures during ascent which prevent nominal orbit insertion or Orbiter system failures which dictate immediate return to Earth. The latter usually involves a rather standard entry, although thermal loads may be more severe since there has been no time to dissipate ascent heating and the vehicle weight is usually higher. To compensate, the guidance drag profile is lowered. An MPS failure implies that the Orbiter may achieve entry interface with a shallow flightpath angle (perhaps necessitating entry prebank) with high heat loads resulting from the long-range, shallow trajectory. Still, the AOA falls into nearly the same region as dispersed end-of-mission entries, and no modifications to the guidance software have been necessary to support it.

A TAL is caused by one- or two-engine MPS failures during ascent and involves targeting for and flying to a downrange landing site. The TAL concept originated when flightcrews noticed during ascent simulations that entry-type energy-range conditions were often achieved. Although this observation is essentially true, the flight conditions during a TAL are similar to a very steep, low-energy entry, which would place extreme thermal stresses on the Orbiter. Figure 14 shows the vehicle drag and drag profile resulting from a TAL simulation. The entry is so steep that even lift-vector-up flight produces a large drag pulse and the associated high surface temperatures. Although this pulse is of short duration, large portions of the TPS would probably be damaged. Still, subsequent convergence to the profile is quite rapid and thus the other constraint margins can be maintained. Ranging to the new landing site is accomplished in the normal manner.

FLIGHT DECK DISPLAYS AND CREW INTERACTION

The flightcrew can monitor entry by means of computer-driven cathode-ray tube (CRT) operations displays. Figure 15 shows the configurations for the segment of flight from a velocity of 20 000 ft/s to 13 500 ft/s. The central portion of the display depicts a velocity versus range plot of the entry constraints (solid lines). From left to right, these are 2.5g load factor, nominal trajectory, equilibrium glide for 37° bank angle, and equilibrium glide for 0° bank angle. The dashed lines represent constant-drag levels with the numerical value shown above each line. The numbers in the lower section of the display are the vehicle altitude rates necessary to parallel the nominal profile. The square depicts the current guidance-commanded drag level, and the Shuttle symbol is the navigation estimate of the vehicle range to go. The dots and triangles mark the past values of these quantities snapped at 30-second intervals. In addition, reference drag command, roll command, dynamic pressure, and other guidance and flight control parameters are displayed digitally. Figure 15 represents a situation in which the Orbiter was low in drag and too far from the landing site, but has converged to

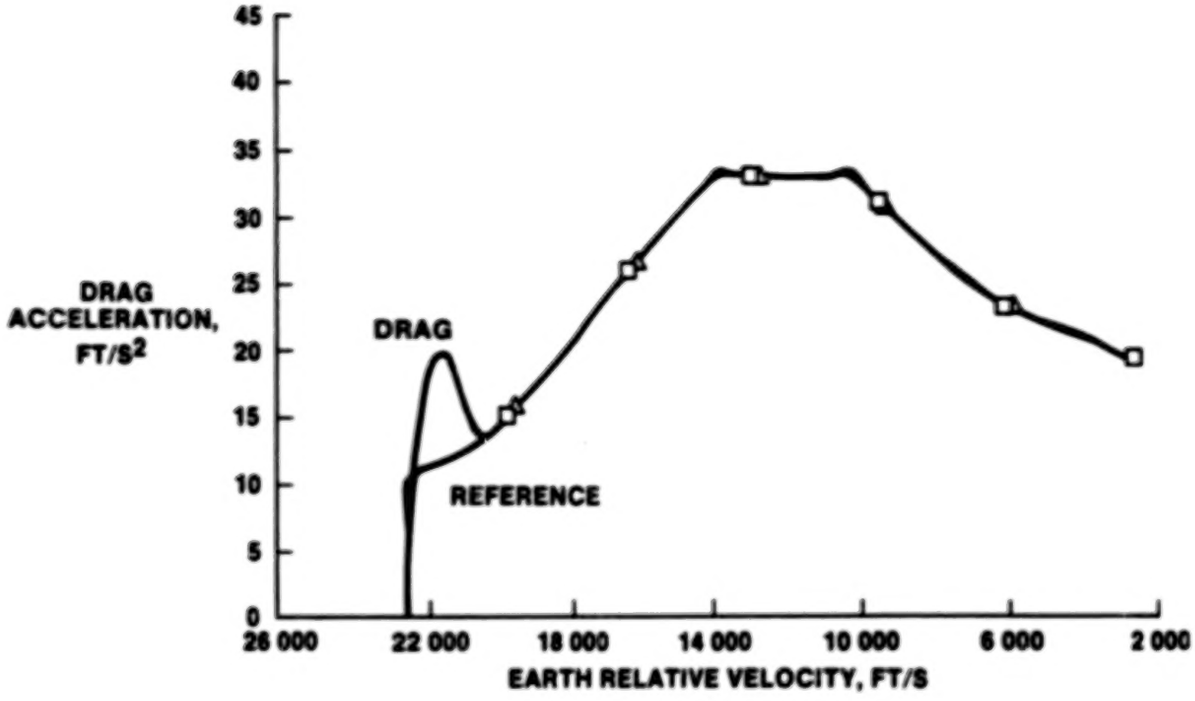


FIGURE 14.- TAL DRAG AND REFERENCE PROFILE.

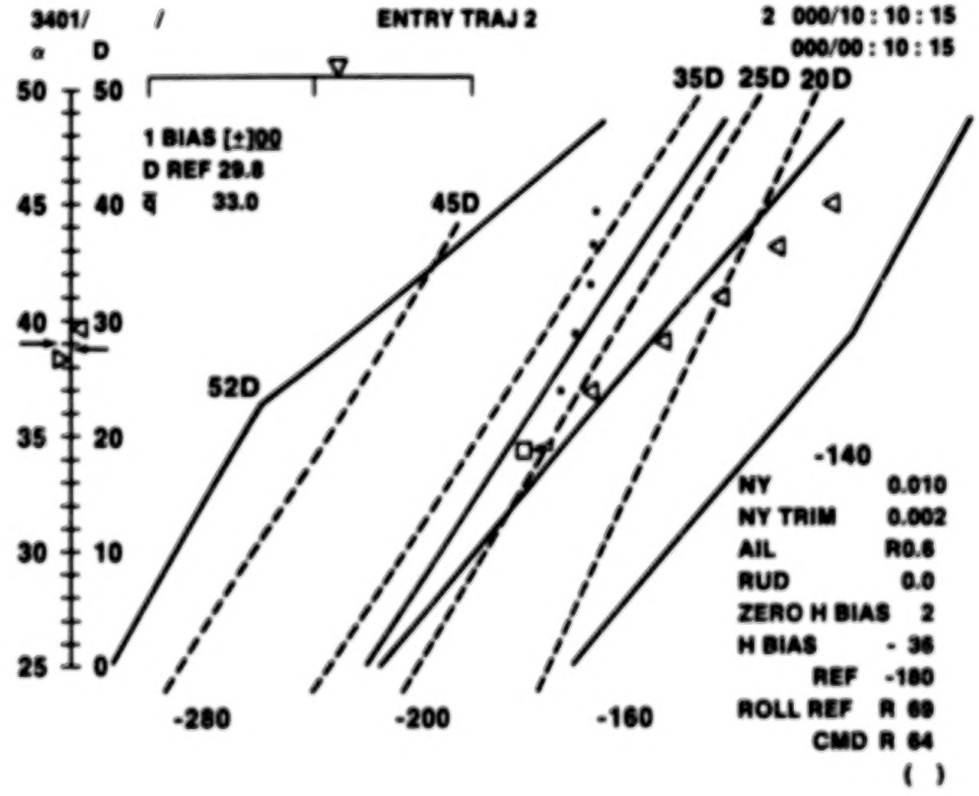


FIGURE 15.- ENTRY CRT DISPLAY.

the guidance command. In addition to the CRT's, the error needles of both cockpit attitude-direction indicators are driven by the guidance outputs.

Normally, the guidance commands are fed directly into the flight control system, but they can be interrupted if the crew enables the control stick steering (CSS) mode. In this configuration, guidance will continue to drive the flight deck displays but inputs to flight control are made by way of the commander's or the pilot's rotational hand controller.

FLIGHT RESULTS

Figures 12 and 13 represent typical flight data obtained from the onboard recorders during entry. No unexpected guidance or trajectory behavior has been seen during flight. During several entries, manual or automatic test maneuvers have been executed for the purpose of determining the Orbiter's dynamic and thermal characteristics more accurately. In all cases, the guidance system reestablished the vehicle on the proper trajectory in the predicted amount of time.

CONCLUSIONS

The Space Shuttle entry guidance meets the objectives of accommodating a large variety of mission characteristics while maintaining the vehicle within highly confining physical constraints and delivering it to the target with the required accuracy. The guidance logic and the mission planning activities are based on a reference drag profile shaped to allow for flight safety margins. Attitude commands to the flight control system are provided by correcting for deviations from this profile in a closed-loop manner. The Shuttle flight test program and subsequent operational flights have proven the soundness of interrelating deorbit targeting, guidance, mission planning, and mission design through the drag acceleration plane. No guidance-related anomalies have occurred during flight, and no modifications or improvements to the system are seen as necessary at this time.

REFERENCES

1. Shuttle Aero Sciences: Aerodynamic Design Data Book. Space Transportation System Integration & Operations Division, Rockwell International, Downey, Calif. Tech. Rep. SD72-SH-0060, 1978 (rev. 1982).

2. Graves, Claude A.; and Harpold, Jon C.: Apollo Experience Report - Mission Planning for Apollo Entry. NASA TN D-6725, 1972.

3. Mission Planning and Analysis Division: STS-1 Operational Flight Profile: Vol. 5 Descent. JSC Internal Note No. 81-FM-17, 1981.

4. Box, David M.; Harpold, Jon C.; Paddock, Steven G.; Armstrong, Neil A.; and Hamby, William H.: Controlled Reentry. Gemini Summary Conference, NASA SP-138, 1967, pp. 159-166.

5. Rogers, Joseph E.: A Performance Study of the Sundisk Reentry Guidance Program for Earth Orbital Mission. MSC Internal Note No. 68-FM-164, 1968.

6. Harpold, Jon C.: Analytic Drag Control Entry Guidance System. JSC Internal Note No. 74-FM-25, 1974.

7. Box, David M; and Harpold, Jon C.: Recommended Gemini VIII Reentry Guidance, Monitoring, and Backup Control Procedures. MSC Internal Note No. 66-FM-89, 1966.

8. Skerbetz, Frank G.: Apollo 7 Entry Postflight Analysis. MSC Internal Note No. 69-FM-89, 1969.

9. Graves, Claude A.; and Harpold, Jon C.: Shuttle Entry Guidance. In 25th Anniversary Conference, American Astronomical Society, 1978.

N85
16903

UNCLAS

D14

N85-16903

SOME EFFECTS OF DIGITAL SAMPLING ON ORBITER FLIGHT CONTROL SYSTEM OPERATION

S. V. Murray
NASA Lyndon B. Johnson Space Center
Houston, Texas

ABSTRACT

An entry dynamic stability ground test of the OV102 Space Shuttle Orbiter revealed some small amplitude oscillatory output of the flight control system which could have constrained flight of the STS-1 mission. These limit-cycle-type outputs were attributed to a combination of rigid body motion of the Orbiter on its landing gear (not a factor in flight) and some interesting effects of its digital flight control system. These effects included frequency aliasing and phenomena associated with digital quantitization of low-amplitude sensor signals. An understanding of these digital effects suggests some significant improvements possible in future designs.

INTRODUCTION

The Space Shuttle Orbiter employs a sophisticated variable gain, closed-loop, digital flight control system, designed to operate over a very wide range of flight conditions. A number of redundant sensors are used, including rate gyro assemblies (RGA's), accelerometer assemblies (AA's), and inertial measurement units (IMU's). Data from these and other sensors are processed by the digital autopilot (DAP) algorithms in the Shuttle's general-purpose computers (GPC's). Desired commands are then sent to the flight control effectors, which include main and OMS engine gimbals, elevons, body flap, speedbrake, and rudder. Unlike previous autopilot designs, the Shuttle cannot be flown open loop. Even in manual modes, the sensor-computer-effector loop remains unbroken; the control stick merely replaces automatic guidance as one of the many inputs to the control system.

In designing the DAP software for the GPC's, both the desired effectiveness of the control effector in controlling the Orbiter state and the undesired effect of effector motion feeding back through the Orbiter structure into the sensor had to be considered. For example, an abrupt movement of the elevons causes a structural vibration which produces a nontrivial feedback from the rate gyros. Designing the control system, then, required an accurate understanding of the Orbiter's structural dynamics and the incorporation of appropriate digital filters to reduce these effects.

HOT FIRE TEST

Since it is difficult to predict the structural dynamics of a vehicle to a high level of accuracy by analysis only, verifying the dynamic stability of the flight control-structural system was an obvious candidate for vehicle tests. U.S. Air Force specifications require automatic flight control systems to demonstrate a gain margin of at least 6 decibels during ground tests (ref. 1). A gain margin test was first conducted on OV102 in November 1979 as part of the APU hot fire at the Kennedy Space Center. This closed-loop test was conducted with the software in major mode 305 (terminal area energy management - from Mach = 2.5 through rollout). The forward loop gains were patched to be 6 decibels higher than nominal, and pulse-type programmed test inputs were applied. The result was a 3.6-hertz oscillation in the roll axis coupled by the first fin-bending mode through the roll rate gyro into aileron motion of the control surfaces. Amplitude was limited by the control surface rate limit in the software. It was also surprising to find that yaw rate gyros 1 and 2 were responding at 6.5 hertz and yaw rate gyros 3 and 4 responding at 3.6 hertz. Figure 1 illustrates these motions. Figure 2 shows the different mounting locations for gyro packages 1 and 2 up on the fuselage side frames. These side frames were twisting in yaw and the first wing bending mode frequency (6.5 hertz) during the coupled 3.6-hertz limit cycle. These findings resulted in changes to the Orbiter structural model, a corresponding redesign of the bending filters in the DAP software, and a relocation of RGA's 1 and 2 as shown in figure 2.

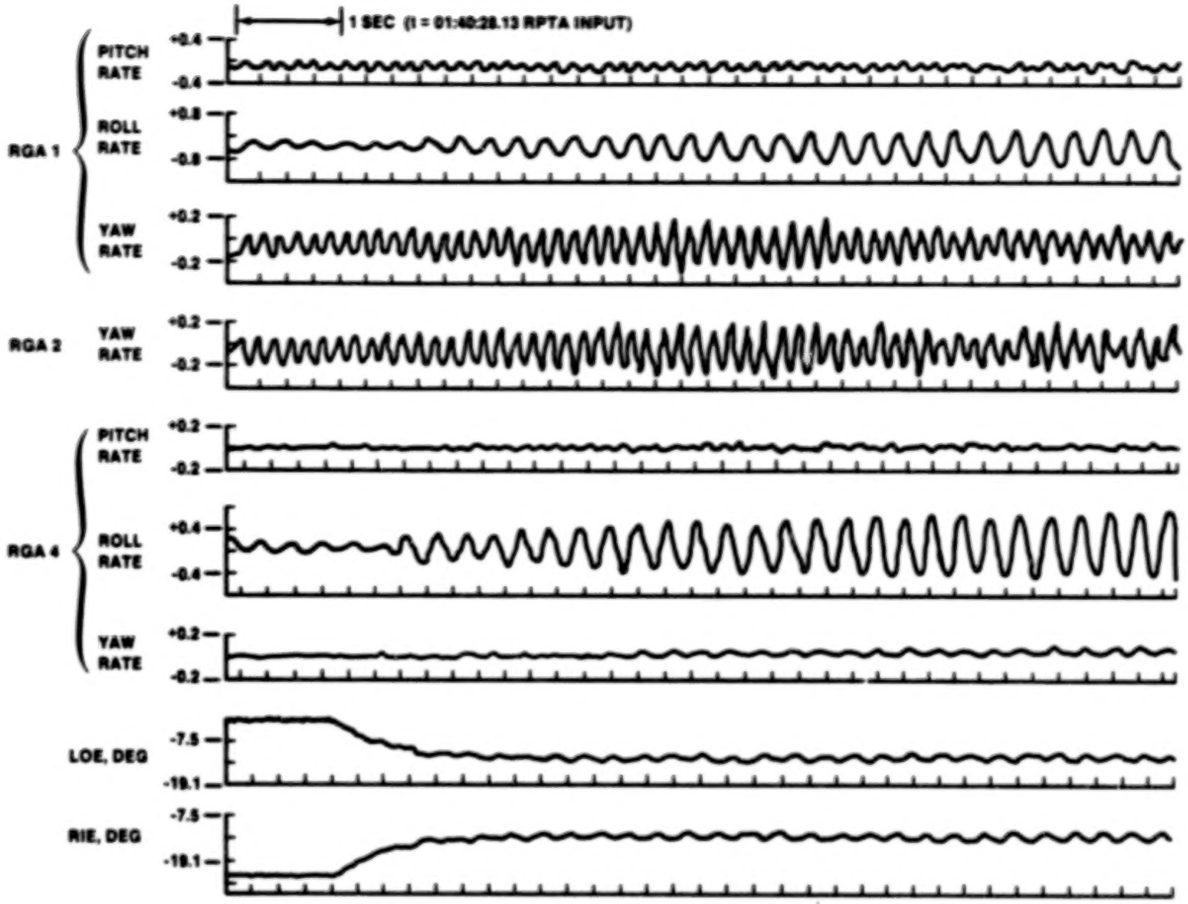


FIGURE 1.- HOT-FIRE TEST DATA (+6 dB GAIN).

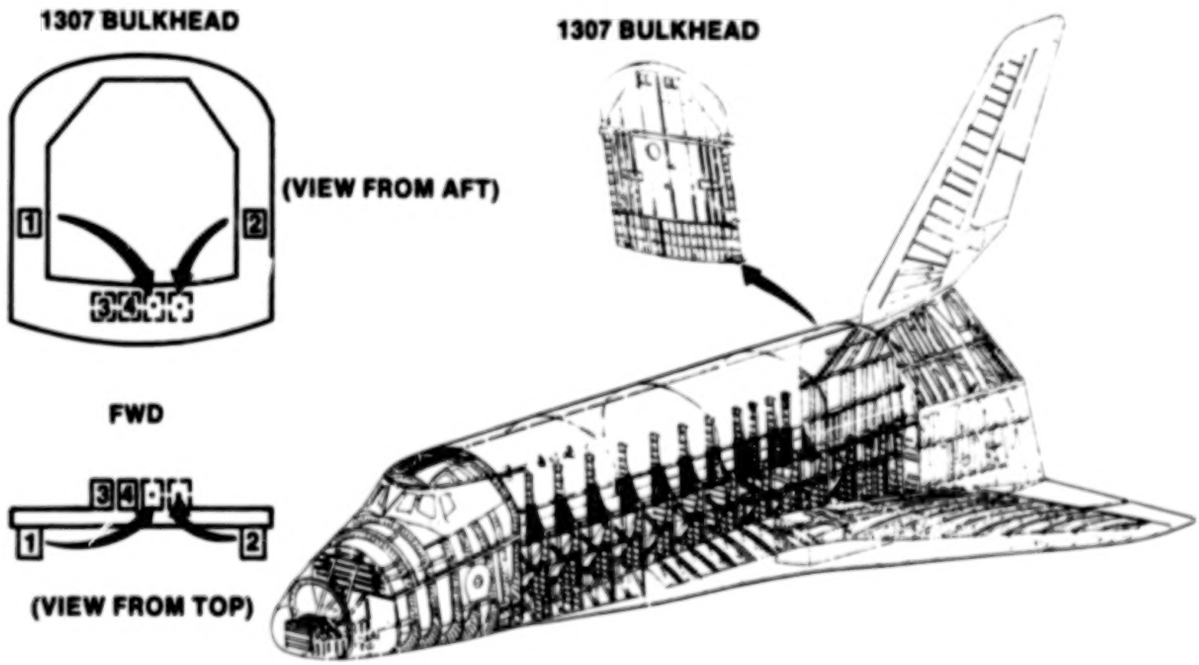


FIGURE 2.- RATE GYRO RELOCATION.

ORIGINAL PAGE IS
OF POOR QUALITY

TABLE 1.- EDST FLIGHT CONDITION IDENTIFICATION

PARAMETER	FSSR NAME	FLIGHT CONDITION		COMMENT
		CONDITION 1	CONDITION 2	
MACH	MACH	3.4	0.6	
ALT, FT	ALT	114,000	41,000	
$\bar{q}$, PSF	QBAR	85*	90	*SET TO FORCE GDQ, GDA TO LIMIT VALUE
	REL-VEL-MAG			
TAS, FPS	TAS	3535	581	
α, DEG	ALPHA	20	13.6	
θ, DEG	THETA	15.2	1.8	
ϕ, DEG	PHI	0	0	
α_c, DEG	DEFB	-7.7	-7.7	
α_{sb}, DEG	DSBC	5.0	5.0	
α_{bf}, DEG	DBFRC	0	0.0	
α_r, DEG	DROFB	0	0	
SIN α	SINALF	.34202	.23514	
COS α	COSALF	.93969	.97196	
SIN θ	SINTH	.26219	.2792	
COS θ	COSTH	.96502	.99981	
SIN ϕ	SINPHI	0	0	
COS ϕ	COSPHI	1.0	1.0	
	GDQ	5.0 (MAX)	2.06294*	*GAIN VALUE EQUIV TO "AUTO" WITH CSS OR GAIN ENABLE SELECTED
		-7.7 DEG	-7.7 DEG	
	DETRIM	0	0	
	DATRIM	↓	↓	
	DRTRIM			
	ROLLOUT			
	FLATURN			
	WOWLON			
	GROUND STEER	0	0	

ENTRY DYNAMIC STABILITY TEST

Because of this experience, a more extensive test was planned, and successful completion would be required before the STS-1 mission. Two flight conditions were examined (table 1). The first was in the entry mode (major mode 304) with the DAP patched to believe it was at Mach 3.4 and an altitude of 114 000 feet. The second was in the TAEM mode (major mode 305) with a Mach of 0.6 and an altitude of 41 000 feet. For this entry dynamic stability test (EDST), the vehicle would be resting on its landing gear with the tires deflated. Shop hydraulics would be used instead of vehicle auxiliary power units. A patched version of the appropriate flight software would be loaded, and necessary vehicle systems would be powered up. The KSC launch processing system would be used to uplink flight software patches, command step inputs, and thereby control the test. Figure 3 illustrates the vehicle configuration. The multiplexer/demultiplexer units (MDM's), in addition to their obvious function, provided the necessary analog-to-digital and digital-to-analog conversions. It will be shown that this A-D process had significant effects on the test. The Shuttle modal test and analysis set (SMTAS) consisted of special test equipment used for sinusoidal test inputs, data collection, and reduction. Step inputs would be provided to excite the system by providing torque commands, normally used only for ground checkout, to the rate gyros. In addition to the closed-loop test, an open-loop test was planned. Here, the DAP commands to the actuators were disconnected and a sine wave substituted in their place. This signal was slowly swept from frequencies of 1 to 18 hertz, which allowed measurement of the actual aerosurface command to sensor to DAP command transfer functions. This test would be useful in understanding the closed-loop response.

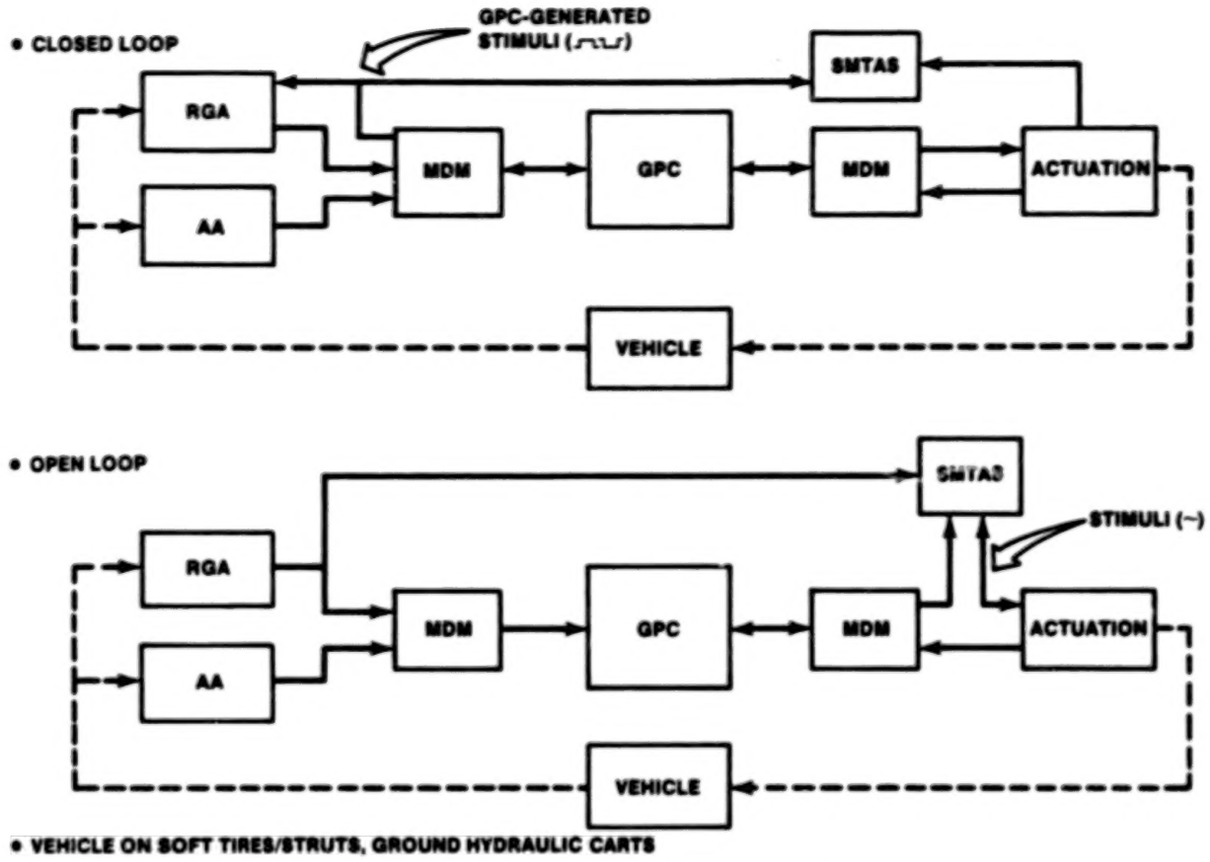


FIGURE 3.- OPEN- AND CLOSED-LOOP CONFIGURATIONS.

RESULTS

Consequently, the EDST was conducted on OV102 in August of 1982. The low-altitude (MM 305) case was stable and well damped at both nominal and +6 decibel DAP gains. The high-altitude case, at nominal gains before any test stimuli were applied, entered a sustained symmetric elevon oscillation of about 0.6 degrees peak-to-peak at 2.5 hertz. This had not been predicted pretest, but since the amplitude was small and the response to step input was damped, the test was continued.

When the gains were increased +6 decibels, an antisymmetric elevon oscillation of 3 degrees peak-to-peak at 2.5 hertz were encountered, again before any test stimuli were applied. This oscillation was a limit cycle, signifying that the elevon motion had reached the rate limit applied for hydraulic/mechanical considerations. To complete the test, the gains were backed down to +3 decibels above nominal in the roll and yaw channels, while being kept at +6 decibels in pitch. Here the oscillations continued but were symmetric, and the amplitude was limited to about 1 degree, less than the limit cycle. The response to step inputs was damped.

DISCUSSION

The results of this test caused concern about their potential impact to the STS-1 mission. Were these effects liable to appear in flight? Were they acceptable? If a significant redesign of the flight system were required, it would cause a very substantial impact to the whole STS schedule. These oscillations were attributed to two causes: (1) the interaction of the Orbiter with its suspension system (landing gear) and (2) a combination of effects unique to digital systems.

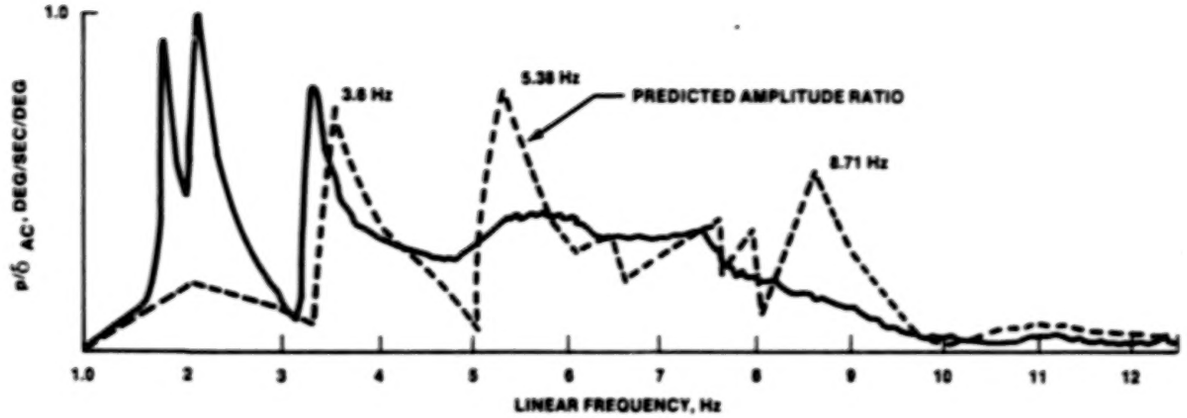


FIGURE 4.- PSA 3 ROLL TRANSFER FUNCTION PLOT
SWEEP 2-1 - AILERON ROLL.

The open-loop tests showed that the lower-frequency structural modes agreed very well with the models, but at higher frequencies they were much more heavily damped than had been predicted. The tests also showed that the rigid body mode of the Orbiter on its landing gear had a higher than predicted natural frequency, and, in the roll channel, a much higher than predicted frequency response. Figure 4 shows the predicted versus actual frequency response in the roll channel. This figure is a composite made from two frequency sweeps: one from 1 to 2 hertz, the other from 2 to 12.5 hertz. The second peak after 2 hertz is probably a start-up transient response reflecting the 1.9-hertz landing gear mode. This higher-than-predicted rigid body mode was the proximate cause for the +6 decibel antisymmetric instability. But why was this instability at 2.5 hertz instead of the 1.9-hertz rigid body mode? What caused the lower amplitude symmetric motion at the lower gains? For this, some digital effects which provided the real "lessons learned" should be examined.

These digital effects were the phenomena of frequency aliasing and the effects of digital quantitization of small amplitude signals. Frequency aliasing is caused by the fact that a digital system can sense a signal only at discrete time intervals. The sampling theorem requires that the frequency of the signal being measured be no greater than one-half of the frequency of the sampling itself. The Orbiter's RGA's are sampled at 25 hertz. Thus, the highest frequency input which could be effectively handled (or Nyquist rate) is 12.5 hertz. Signals higher than this are "folded over" around the Nyquist rate to a lower frequency. For example, a 23-hertz signal would reflect around 12.5 hertz to appear as a 2-hertz signal to the flight system. Figure 5 helps to provide an intuitive appreciation of the effect. In theory, high-frequency structural modes could be reflected down to appear to the DAP as low-frequency inputs, effectively circumventing the digital filters designed to attentuate them. Because of this concern, open-loop frequency sweeps were made during the EDST up to frequencies of 18 hertz. However, these sweeps showed that the high-frequency structural modes were much more heavily damped than predicted and should not have been important. Aliasing was important, however, but only as it was associated with some small amplitude signal quantitization effects.

The stair steps in figure 6 represent the way an analog signal from an RGA is quantitized into a digital signal in the Shuttle MDM. For normal large amplitude signals, the steps are relatively small enough to represent a straight line with a gain of unity. However, as the relative size of the signal decreases, the effective gain can increase dramatically. The small signal shown is engaging one quantitization step, and it is obvious that its gain could increase to a very high number, dependent on the bias and amplitude of the input. The output from this system would be a bit toggling square wave. Figure 7 illustrates the way a square wave can be represented in terms of its Fourier components. Consider a 7.5-hertz square wave. Its primary Fourier component would be well attentuated by the DAP bending filter. However, its third Fourier harmonic would be 22.5 hertz, which would alias to 2.5 hertz. It is also interesting that the third harmonic of 2.5 hertz is the original 7.5 hertz, thus making it possible for the signal to feed itself. In fact, there is a family of frequencies which have harmonics capable of aliasing in such a way as to reinforce themselves as shown in table 2. Factors which limit their actual impact are the DAP bending filters and the fact that for a square wave, the amplitude of the harmonic component is inversely proportional to its order.

These effects can be seen in some data taken during the open-loop test. Figure 8 is actual data taken during a frequency sweep. The first three channels are RGA inputs to the DAP. The last channel is a DAP elevon command, which was disconnected from the actuators to open the loop. On the left side, the elevons are being driven at about 7.5 hertz with the frequency slowly increasing with time.

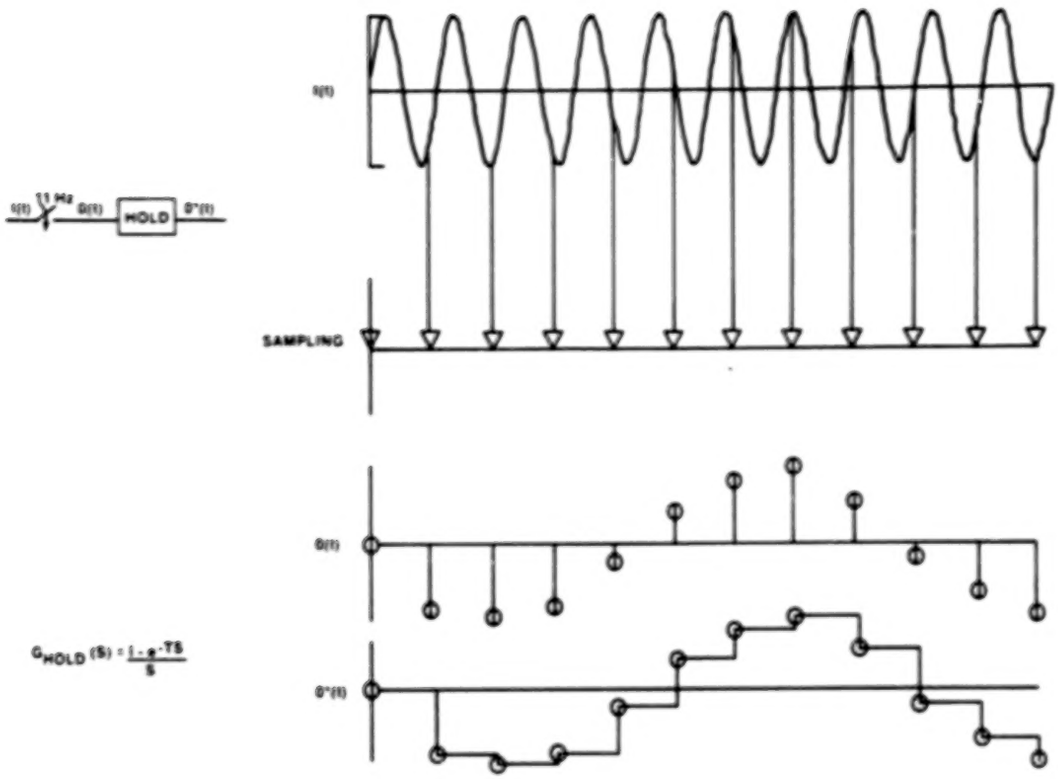


FIGURE 5.- SAMPLING/HOLD CHARACTERISTICS (ALIASING).

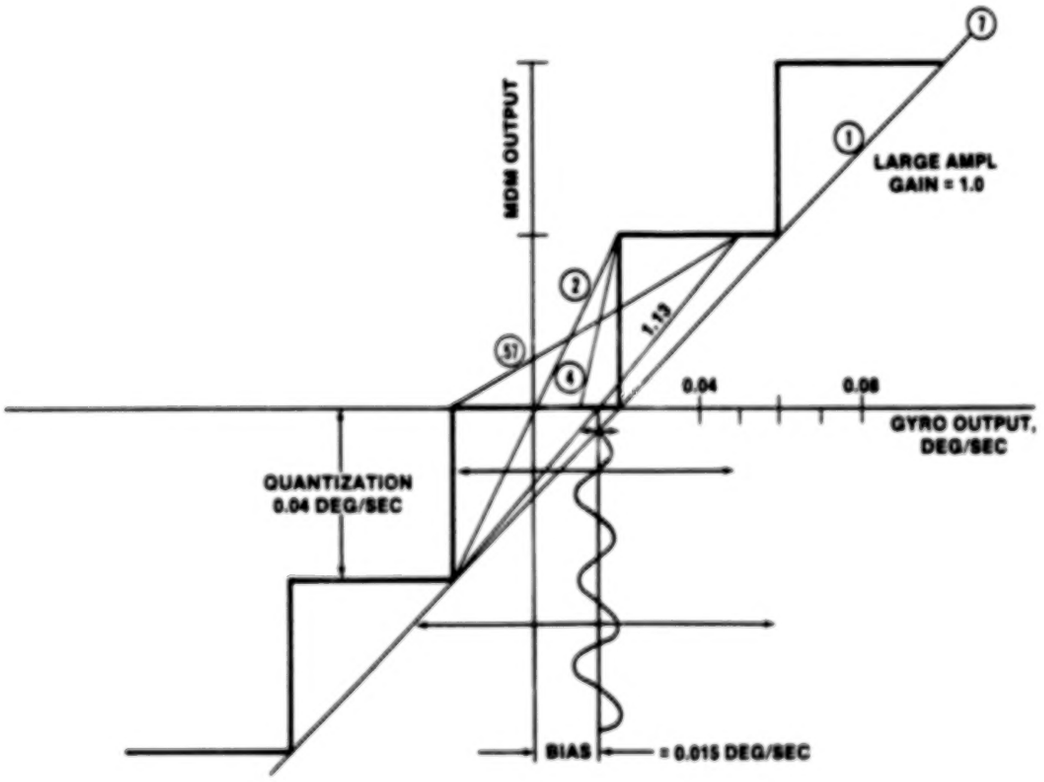
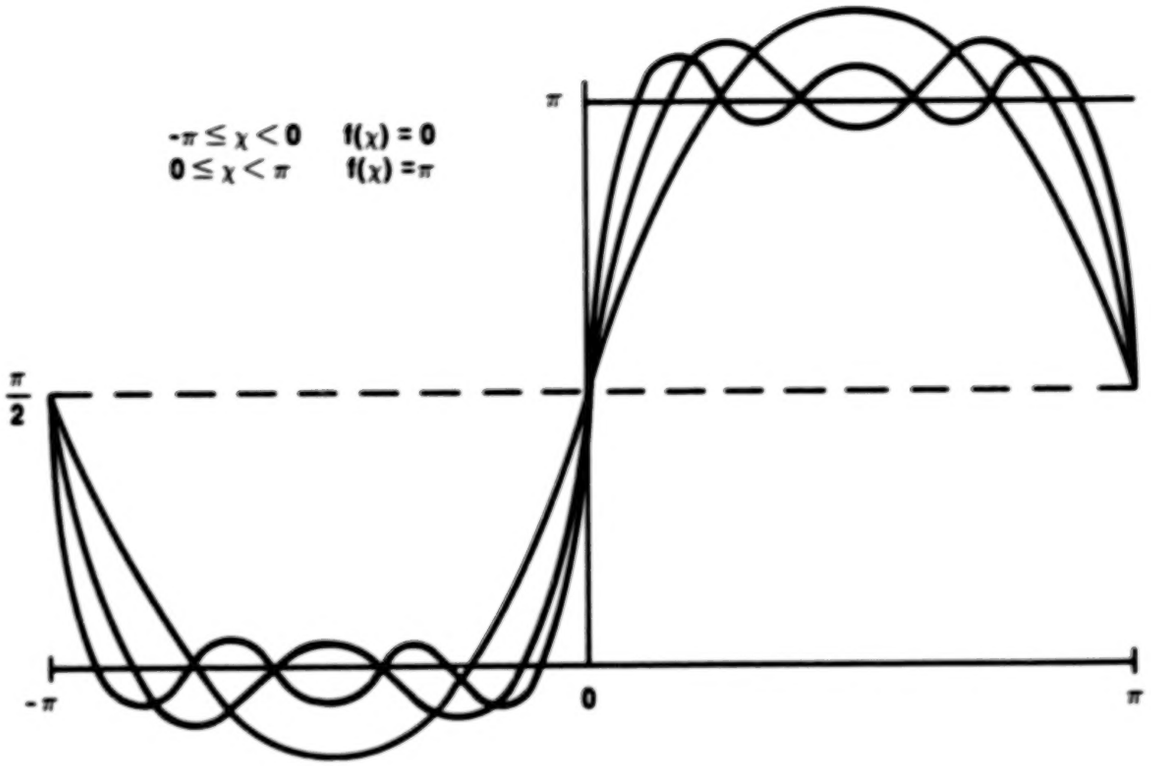


FIGURE 6.- MDM QUANTITIZATION EFFECTS.



$$f(\chi) = \frac{\pi}{2} + 2\left(\frac{\sin \chi}{1} + \frac{\sin 3\chi}{3} + \frac{\sin 5\chi}{5} + \ldots\right)$$

FIGURE 7.- FOURIER COMPONENTS OF A SQUARE WAVE.

TABLE 2.- TWENTY-FIVE-HERTZ SAMPLING CHARACTERISTICS

	FUNDAMENTAL FREQUENCY	3RD HARMONIC FREQUENCY		ALIASED FREQUENCY
3RD HARMONIC CHARACTERISTICS	6.25	18.75		6.25
	12.50	37.5		12.5
(3RD HARMONIC)^2 CHARACTERISTICS	2.5	7.5	22.5	2.5
	3.125	9.375	28.125	3.125
5TH HARMONIC CHARACTERISTICS	4.167	20.833		4.167
	6.25	31.25		6.25
(5TH HARMONIC)^2 CHARACTERISTICS	0.9615	4.8077	24.038	0.9615
	1.0416	5.2083	26.0416	1.0416
7TH HARMONIC CHARACTERISTICS	3.125	21.875		3.125
	4.167	29.167		4.167
(7TH HARMONIC)^2 CHARACTERISTICS	0.50	3.50	24.50	0.50
	.5208	3.646	25.5208	.5208

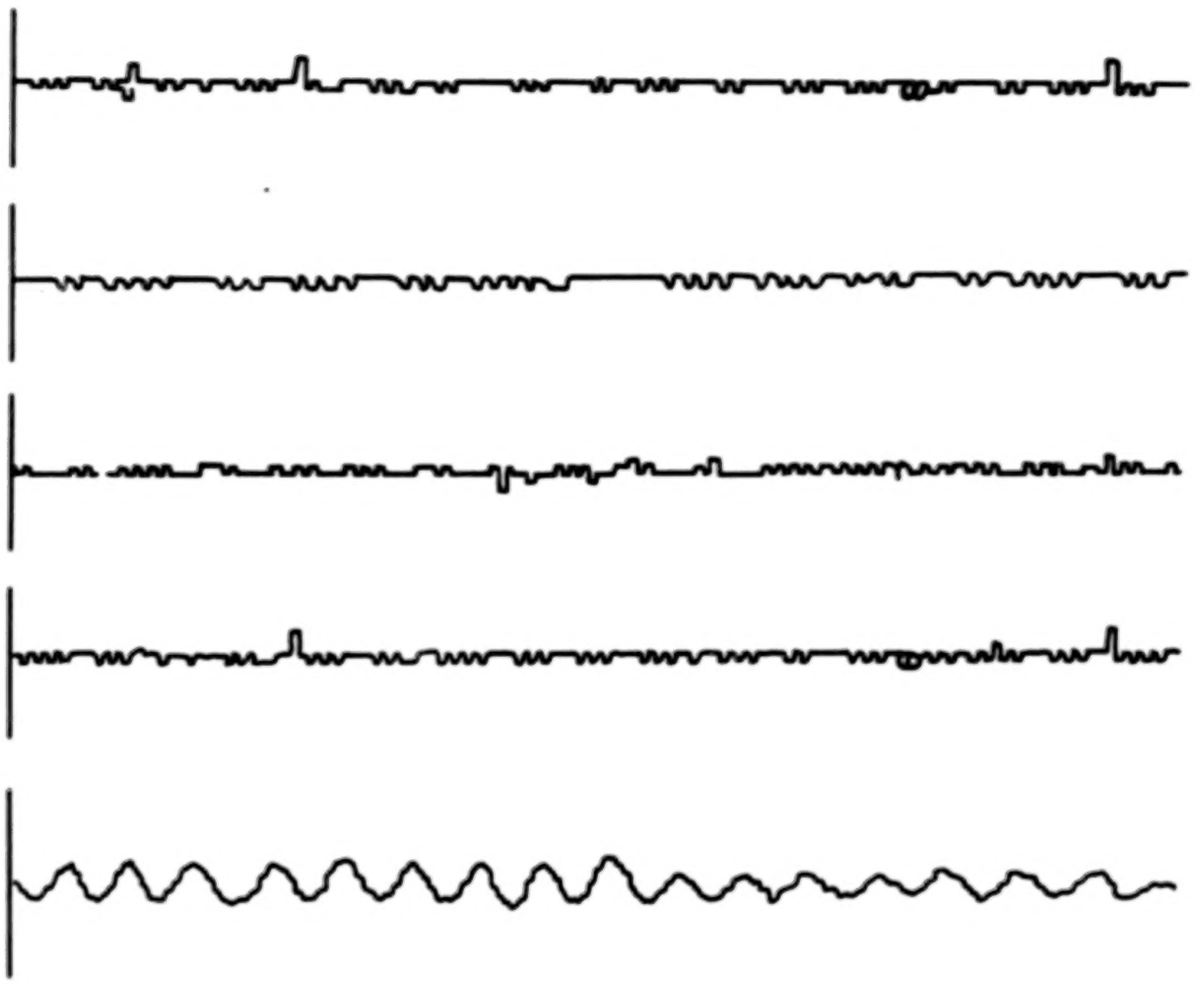


FIGURE 8.- DAP FILTER RESPONSE TO TOGGLING INPUT

The RGA's are mostly toggling 1 bit producing the small square waves discussed, only occasionally engaging a second quantitization level. Now observe the DAP command, a very significant sine wave with a frequency of about 2.5 hertz.

In looking at this type of data, other cases showed significant aliased harmonics in the output although they did not feed themselves and thus did not contribute to oscillatory behavior. The key here seemed to be whether or not the sampled, aliased harmonic had a period which was an integral multiple of the sampling period. Those which did could be expressed "cleanly" by the digital system. Those which did not experienced frequent phase shifts as the signal "beat" against the sample rate and quickly lost their significance. Table 3 shows the harmonics greater than 1.5 hertz, which meet this criterion for a 25-hertz sampling system and the inputs necessary to create them.

The driving signals greater than 10 hertz appear to be aliasing second harmonics which would invalidate our odd-only rule derived from the Fourier components of a square wave. Actually, these are fifth and seventh harmonics aliased around 50 to 75 hertz. The cases where this effect would be important would be where an open-loop "noise" source existed; e.g., an ac signal in an RGA which might alias to manifest itself in unexpected places.

As stated, only a few of these frequencies can feed back to reinforce themselves, and some of these are attenuated by the bending filter. Let's consider another effect of the bending filter. Figure 9 shows three plots. The first plot (a) is the frequency response of a zero order hold (sample and hold) with a sample rate of 25 hertz. The second plot (b) shows the frequency response of the Shuttle pitch channel bending filter. The curve between 20 and 30 hertz is obtained by

TABLE 3.- VULNERABLE FREQUENCIES IN TWENTY-FIVE-HERTZ SYSTEM

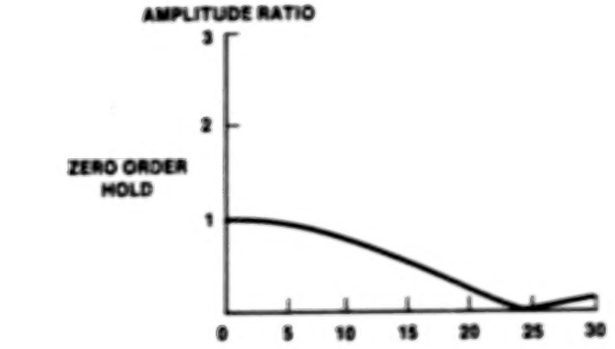
FREQUENCY OF ALIASED HARMONIC, Hz	FREQUENCY OF DRIVING SIGNALS			
5		10		
3.5714	10.714	7.1429		
3.125		9.375		
2.7778	11.1111	5.5556		
2.5		7.5		
2.2727	11.3636	9.0909	6.8182	4.5455
1.9231	11.538	7.6923	5.7692	3.8462
1.7857		8.9286	5.357	
1.6667	11.667	6.6667	3.3333	
1.5625		7.8125	4.6875	

reflecting the bending filter curve around 25 hertz and scaling it by the frequency response of the zero order hold. The third plot (c) shows this 20 to 30-hertz region increased +6 decibel. Notice how perfectly the filter tunes to 22.5 and 27.5 hertz which, of course, alias to 2.5 hertz.

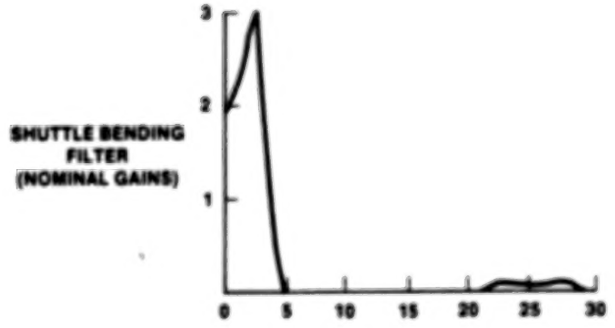
Figure 10 gives a good overview of the system with the effects discussed. It can be seen why the 2.5-hertz phenomena were encountered. The pressing question after the DST was whether or not it was safe to fly. The landing gear mode, of course, would not be a factor in flight. For landing and rollout, the DAP would be in the low-altitude flight condition, which was found to be quite stable. What about the digital effects? Could they lead to large instabilities? The answer is no because they are bounded to small amplitude. Considering figure 6, it is obvious that as the input signal increases to engage more quantitization steps, its gain rapidly decreases to approach unity. Or, using the Fourier approach, the more quantitization steps a signal engages, the more it resembles a sine wave and the weaker its harmonics become. After the DST, these effects were modeled in a time domain simulation. The results are shown in figures 11 and 12. It is obvious that while the effects are significant at low amplitudes, as either the amplitude is increased or the quantitization level is reduced, they rapidly become less important.

CONCLUDING REMARKS

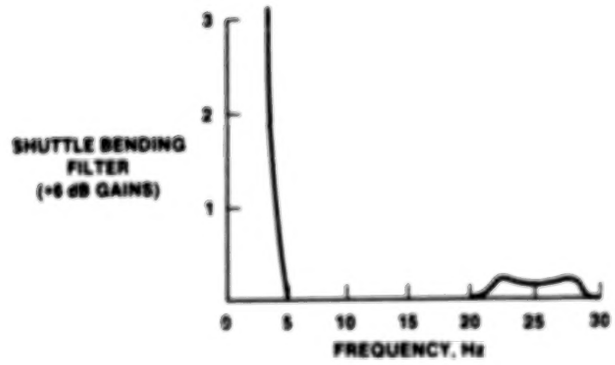
So the Shuttle is safe to fly. What can be learned from this experience that can be applied to future projects? First, this stresses the importance of a high sample rate. Increasing this rate, in addition to eliminating many other undesirable effects, reduces the number of significant harmonics which can be aliased. Second, the size of any analog to digital quantitization levels should be carefully considered in view of the application. In the case examined, the quantitization was quite appropriate for low-altitude flight. But it became inappropriate with the control system gains



(a) ZERO ORDER HOLD.



(b) SHUTTLE BENDING FILTER (NOMINAL GAINS).



(c) SHUTTLE BENDING FILTER (+6 dB GAINS).

FIGURE 9.- BENDING FILTER FREQUENCY RESPONSE.

required for flight at high altitude and Mach number. It may be worthwhile to study some new approaches, such as variable quantitization levels, as illustrated in figure 13. This would provide higher resolution around a trim point than could be provided over the whole range. In some cases, the best approach might be a hybrid system with completely analog inner loops and digitally-controlled gains. Finally, the software control laws should be designed with an appreciation of these effects. There was no hard reason for the Shuttle bending filter to peak at 2.5 hertz or to have such a pronounced peak at all. It was merely tolerated, with no appreciation of the consequences, to gain a marginally better band pass. As future control systems evolve, an understanding of these digital effects will be important for achieving optimal designs.

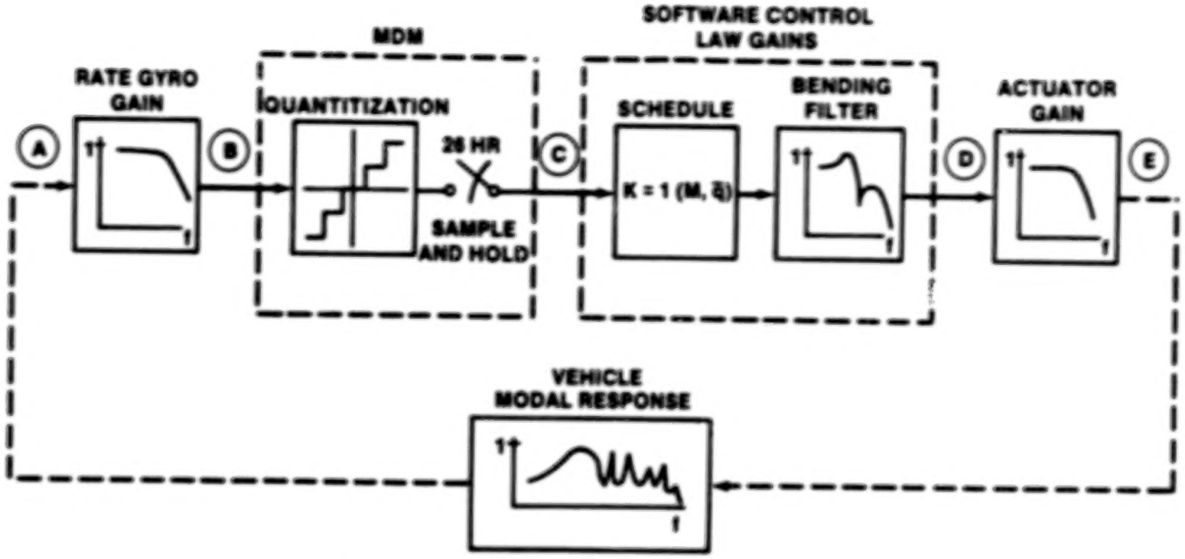


FIGURE 10.- FLIGHT CONTROL SYSTEM (FLEXIBLE-MODE-RELATED CONFIGURATION).

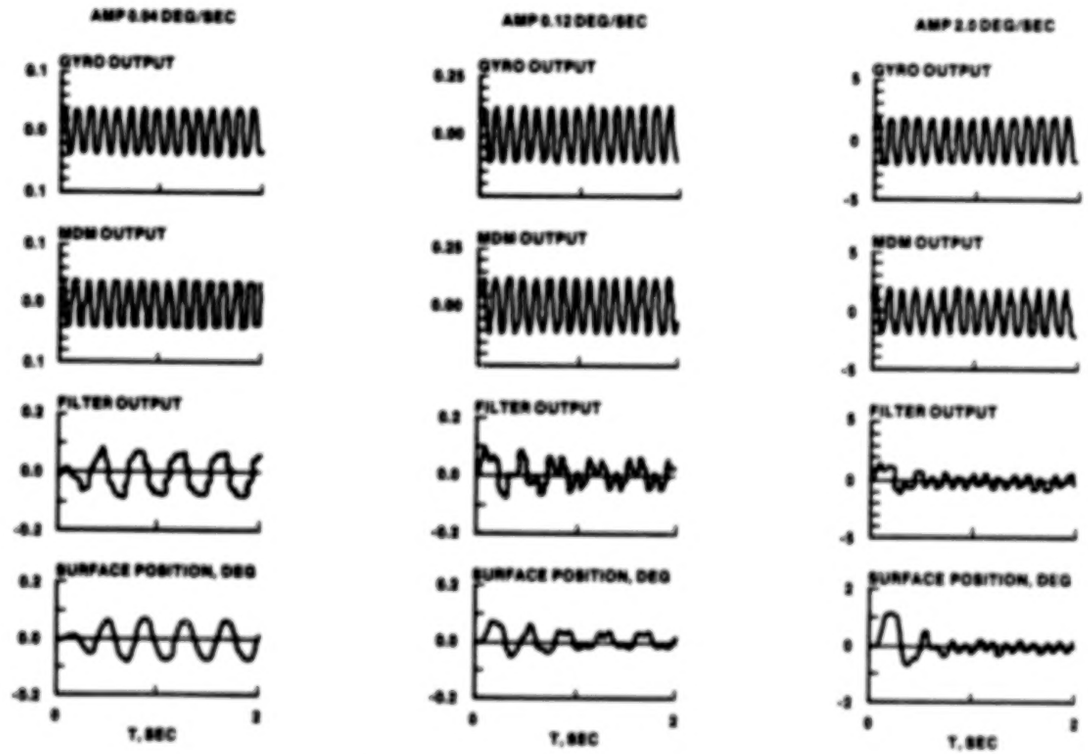


FIGURE 11.- VARIATION OF GYRO OUTPUT AMPLITUDE.

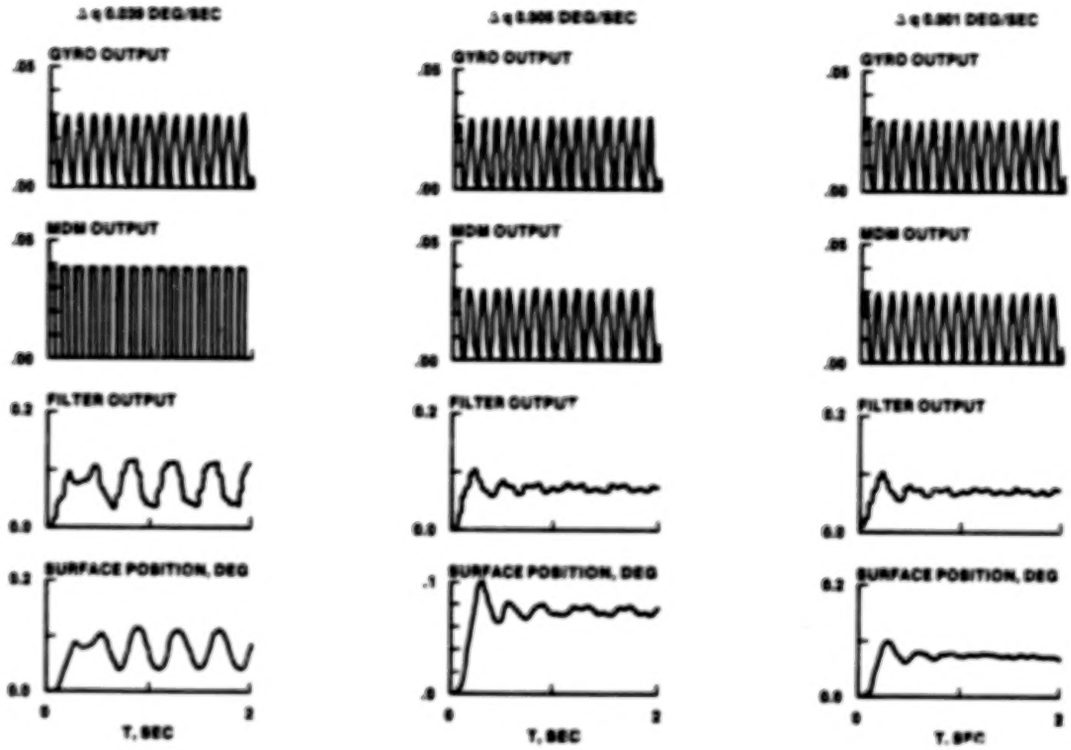


FIGURE 12.- VARIATION OF MDM QUANTITIZATION LEVEL.

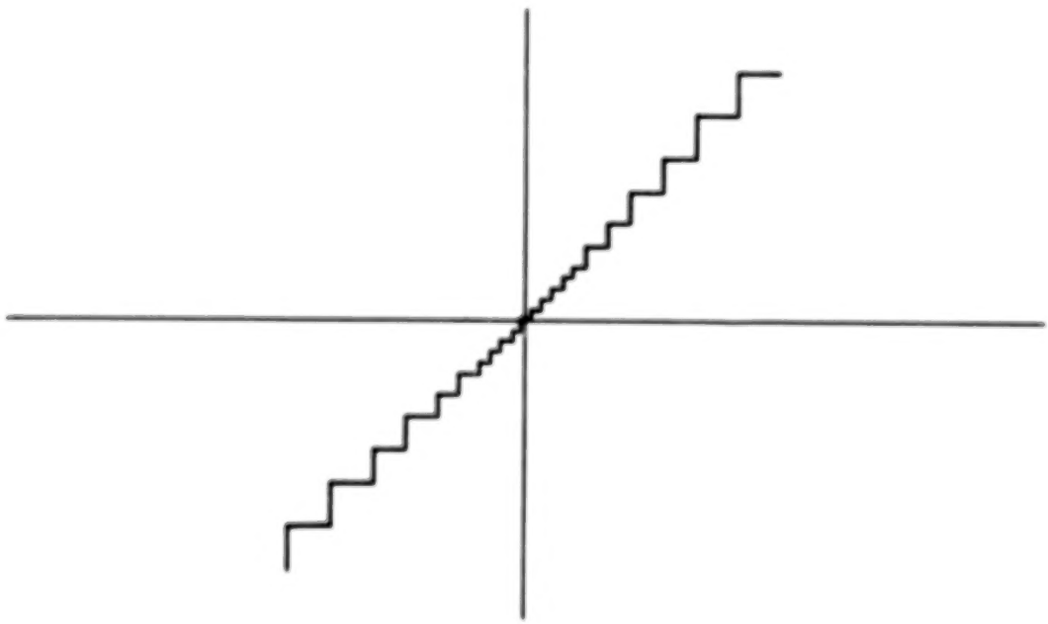


FIGURE 13.- VARIABLE QUANTITIZATION LEVEL SYSTEM.

REFERENCE

1. Background Information and User Guide for MIL-9490D - Flight Control Systems Design. General Specification for Design, Installation, and Test of Piloted Aircraft. AFFDL-TR-74-116, Jan. 1975, p. 43.

N85
16904

UNCLAS

D15

N85-16904

SPACE SHUTTLE HANDLING QUALITIES

David M. Gilbert
NASA Lyndon B. Johnson Space Center
Houston, Texas

ABSTRACT

This paper provides an overview of the initial Orbiter handling qualities requirements, their effect on the vehicle design, and how it all turned out through the first six orbital missions. Following this, there is a series of more detailed discussions of some specific areas consisting of hand controller considerations and the wheelie problem. Finally, there is a discussion which reviews the requirements for the pitch axis subsonic flight control system and provides some results of recent simulator evaluations to compare the existing system at landing with several other configurations.

THE REQUIREMENTS

The original handling qualities requirements for the Space Shuttle were written more than 10 years ago. At the time, the magnitude of the task seemed overwhelming considering the size of the flight envelope the variety of control devices, control modes and control tasks. The existing MIL Spec. and user's guide run about 800 pages. This provides the requirements for conventional aerodynamic vehicles which correspond to a small part of the Shuttle mission/flight control matrix. Table 1 attempts to illustrate this. From a flight envelope viewpoint, most conventional aircraft experience lies in the lower right corner of the entry/ aerosurface control element in table 1. What were we to do with the rest of it? As a starting point, the Space Shuttle Flying Qualities Symposium was held at what was then the Manned Spacecraft Center in Houston, Texas in January 1971.[1] This was organized by Donald C. Cheatham (NASA, retired) to solicit industry-wide opinion on the subject. It was well attended by a cross-section of the guidance, navigation, and control (GN&C) community. The coverage, however, turned out to be limited to aerodynamic control of entry through landing. While most of the problem areas were recognized and discussed and systems concepts were presented, little design criteria was proposed except in the approach and landing area. In fact, one of the participants proposed that definitive criteria were not needed. Supposedly, the contractors knew what was good and bad. The simple statement "make it good" was the only requirement needed--an interesting concept. However, the flight control system designers said they needed some response criteria because of the closed-loop, fly-by-wire control concept and the unconventional airframe characteristics. After about six months of debate, all relevant information on handling qualities for the whole Shuttle mission were incorporated into 30 pages of text.

The basic reason for the relatively abbreviated set of requirements was that it was not intended to be a generally applicable specification for manned spacecraft or define the total boundary of acceptable conditions and the ultimate limits between acceptable and unacceptable. Instead, it was intended to present conditions that were thought to be easily achievable and fall well within the acceptable boundaries for a specific vehicle and mission concept. No theoretical rationale was provided. The requirements were based on simulations of the vehicle and mission as known at the time. One underlying assumption was that there would always be active, closed-loop control of vehicle response parameters with sufficient control power and parameter adjustment capability to get any type of response desired. In most cases, all that was specified was the control power or maneuver rate, the control modes, and a transient response envelope. The response requirement format chosen allowed the requirements for the whole mission to be specified on two pages. It was all quite arbitrary. However it represented something that worked on the existing simulators and was consistent with Apollo experience where it was considered applicable.

The remote manipulator system is shown as a control effector used during onorbit payload operations. This was not addressed in the original requirements, as it is in a slightly different class. Because of the flexibility of the arm, the limited force, and variable geometry and inertia it is not a trivial matter. It is a valid man-in-the-loop handling qualities consideration for payload operations, especially heavy payloads. Handling qualities had no significant influence on the design other than control mode and controller configuration. The task now is to accommodate the result.

To provide Shuttle-type vehicles with conventional handling qualities requirements during ascent, onorbit, and early entry is a very big job remaining to be done. One might debate whether it really needs doing. The need to compromise with the ideal handling qualities requirements will be much greater for this type of vehicle because of the potential costly impact on vehicle configuration and consumables. As a result, the need to define the minimum acceptable side of the requirement is probably where the real urgency lies.

TABLE I

	Mission phase		
Control effectors	Launch and Abort	Onorbit	Entry
SRB/M.E. - TVC	First stage ascent Attitude control Fly commands	------	------
M.E. TVC	Guided ascent and Abort - fly the Commands RTLS, TAL, ADA, ATO	------	------
OMS TVC	Orbit insertion ΔV Fly commands	Orbit maneuver ΔV Rendezvous Deorbit	------
RCS	Single engine OMS Roll control Fly commands	Attitude control Stationkeep Prox OPS Payload OPS Single engine OMS Roll control	$\bar{q}$ < 2 PSF Fly commands
RCS/AERO	-----	------	$\bar{q}$ = 2 PSF → M = 1 Fly commands
Aero Surfaces	Trim for load relief	-----	M < 1 Fly commands → OTW
RMS	-----	Payload OPS	-----

RESULTS

After five approach and landing test flights and six orbital missions, a major result is that the only significant handling quality concerns have been in that little area where we have vast experience--the landing maneuver--specifically, the final flare to touchdown and the derotation to lower the nose gear. In reviewing this ironic turn of events, it appears that the reason is that in designing a vehicle that performs well in all the other mission phases where we have less experience, we have so changed the inherent vehicle characteristics, the flight control system and the flight path that it is no longer representative of the experience we do have. Efforts to make it more conventional for landing failed due to the penalties in weight, performance, and complexity imposed on some other part of the mission. The factors we were driven to accept were the following:

1. Unpowered approach and landing
2. Lack of static stability
3. Elevon controls
4. Lack of direct lift control
5. Lack canard control surfaces
6. High landing speed
7. Massive redundancy
8. Digital flight control

These factors either by themselves or combined affect the handling qualities during approach and landing. The last two contribute to additional time delays in the flight control system.

From an overall standpoint, handling qualities did not have much effect in determining the configuration of a really new first-generation vehicle, such as the Orbiter. Some of the reasons for this are the following:

1. In a radically new first-generation vehicle, the uncertainties in performance and survival far overshadow the vagaries of handling qualities requirements. In terms of urgency, compromises are not likely to be made in favor of handling qualities. In a second-generation vehicle, the result might be quite different since both handling qualities and performance capability would be better understood.

2. With the advent of fly-by-wire and digital flight control, there is a tendency to assume that any handling qualities problem can be solved with software. There is probably even a lot of truth in that but it does not follow that we are instantly smart enough to know how to do it. We still have a lot to learn about the fine points of fly-by-wire, closed-loop control of statically unstable aircraft in situations where precise control relative to another near object (a vehicle or the ground) is concerned. Even with a more favorable vehicle configuration, it would be easy to end up with poor handling qualities due to the way the control loops are designed. There are a lot more choices but we do not understand the additional set of limitations that go with them. There are more ways to go wrong. The trend in vehicle design, however, seems clearly to optimize for performance and depend more on fully active computer dependent flight control systems to make up the deficiencies. The Orbiter took a giant step in that direction.

3. These are interesting and challenging problems--the kind that engineers like to work on. Sometimes we are too willing to accept the challenge rather than argue for the tried and true. So, in a sense, we tend to invite trouble.

4. Finally, there is the fallback argument that if handling qualities become too much of a problem, the auto mode is always available. However, the auto mode must be given equal priority in the design process as it was in the Shuttle. Each control mode has its unique problems. For a really new vehicle, providing both greatly imoroves the likelihood that at least one will always be available.

The reason there have not been more problems in other mission phases might be that so far they have not really been exercised in situations that are critical from a handling qualities standpoint. All launches have been in automatic control with no launch aborts. We have not done any rendezvous, stationkeeping, or docking yet. It is the operation in close proximity to another object that tends to stress the handling qualities. For the most part, however, onorbit operations are not time critical and proceed very slowly. Some can even accommodate repeated attempts; e.g., docking. So there really is no reason for concern at this time.

During most of entry, maneuver rates are very low. Most have been flown in the auto mode. However, enough has been done to indicate the pilot has adequate control to perform the required bank reversals manually and has done some pushover/pull-up maneuvers to gather aero data. The significant issue here appears to be RCS propellant consumption not handling qualities. The auto system tends to use less. The anomalies that did occur are the result of variations in the aero data from that used to design the system and affects both auto and manual modes.

Subsonically, the pilot appears to have no problem flying the vehicle manually to perform the heading alignment maneuvers, the steep approach and preflare. From there to touchdown, it appears necessary to exercise unusual care to avoid large control inputs which tend to produce pilot-induced oscillation (PIO) in the pitch axis. More about that later. One other exception is the effect of winds aloft. Since the Orbiter is unpowered, its trajectory and energy management can be greatly affected. In three of the first six missions, there have been winds outside of the environmental design specification. Some last-minute modifications to the approach trajectory were required. There has been a continuing effort to develop ways to make the system able to accommodate a wider range of wind conditions.

SOME PROBLEMS AND CONCERNS

Several other topics warrant some further discussion with respect to handling qualities. These are hand controller configuration, the derotation control problem or "wheelie", and the pitch axis flight control system tendency toward pilot induced oscillation at landing. This section will address each of these.

HAND CONTROLLER CONCERNS

The Orbiter uses the same Apollo-type hand controller for both aero control and onorbit reaction control system (RCS) attitude control. The latter is essentially an on/off control function. Ideally it should have a different type of feel than that required for good aero control. We optimized as much as possible for good aero control and accepted the result for RCS control. As a result, it is impossible to tell by the feel force exactly when the jets fired. Consequently, there is a tendency to make sure the control input is big enough. There has been some concern, but this is apparently acceptable, although some of the more demanding tasks like docking have not been done yet. The alternative is more mechanical complexity, such as having two controllers or adjustable feel. Although this area could be developed further, it doesn't appear necessary.

Another peculiarity of this most simple fly-by-wire hand controller is the aero trim function. In a conventional mechanical system, the stick force can be trimmed without moving the stick. In the Orbiter, the manual trim signal goes into the control loop. This causes the vehicle to respond unless one backs off on the controller as the trim is applied. In general, this cannot be done perfectly but there have been no complaints. This is probably because the manual trim is hardly ever used since automatic trim follow-up is available. It would complicate the controller greatly to make the trim function appear conventional.

Controller location was also of some concern. It is in the center (not side stick) and canted some 19 degrees left to be comfortable for right-hand use. It provides better access and room for displays and switches. However, there was concern about the possibility of control cross-coupling since it is not aligned mechanically with the vehicle axes. To keep it in the center and aligned with vehicle axes would make it misaligned with natural arm motion. Either way some cross-coupling is likely. It does occur at times but not to a large degree and apparently has not been objectionable.

In the Orbiter, the hand controller is only connected to some electrical transducers and feel springs. It is easy to move the controller faster than the surface can respond without knowing it. When this happens in one control axis, a small input in the other axis will be ignored in an elevon system unless some special limiting is provided in the software. We did not have this limiting initially because it did not appear that the problem ever arose during simulations. During the last approach and landing test (ALT) flight however the situation occurred. Small lateral inputs were ignored until the pilot put in a big one provoking a lateral PIO when the vehicle suddenly responded. We subsequently added a series of limiters in the aileron/elevator/elevon mixer logic. This insured that control in one axis was never completely locked out due to rate saturation in the other.

This resulted in getting by with a very simple and light-weight hand controller configuration relative to what it might have been.

THE "WHEELIE"

The wheelie that occurred on STS-3 was a bonafide handling qualities problem even though it occurred after main gear touchdown. The external symptom was the unintended pitch up during rollout after the nose had started down. The problem is caused by the change in geometry that takes place when the vehicle touches down. The center of rotation shifts from the center of gravity to the main gear. This aft shift in the center of rotation, coupled with a vehicle that is already statically unstable, results in a rapidly increasing nose down moment as the nose is lowered. The control system configured for the inflight situation could not keep up with the rapidly changing elevator trim requirement. Nor could it provide a stable pitch rate control loop. This was recognized analytically early in the program. However there was a reluctance to accept the required switching of control system parameters at touchdown that is necessary to compensate for the change in geometry. Instead, the pilots demonstrated during simulations that they could handle the problem. The procedure was to hold the nose up at the touchdown attitude until the speed decreased to an acceptable value. Then the nose gear is let down. Pitching over can cause full-up elevator and if started at too high an airspeed can result in excessive gear loads. Once the nose starts down, the trim changes so fast that is is almost impossible to stop it without overcontrolling. That's what happened on STS-3. It was not too difficult for the lightweight ALT Orbiter. However, at today's heavier landing weight and especially combined with a forward center of gravity, the control task is considered unacceptable.

The problem was reevaluated on a fixed base simulator and several fixes were developed. They involved changing the flight control system for landing or switching parameters at touchdown. Fortunately, this problem was quite obvious on the simulator and it was also quite noticeable when an improvement was made. The simulator evaluation included a sequence where the nose was lowered then raised again to evaluate controllability under the worst weight and center of gravity conditions. We ended up choosing the fix that was simplest to implement. This consisted of switching the pitch axis hand controller output through the same signal path that the autoland system uses. It switches parameters at touchdown. Most of the software was already there.

LANDING FLIGHT CONTROL

The Orbiter pitch axis control during landing has undoubtedly been the single most worrisome handling qualities problem. The symptoms are that if the pilot attempts to take very aggressive control of the vehicle close to the ground and force it to land at a specific point, there is a tendency to get into a pilot-induced oscillation. As a result, the pilots have learned to get the approach well set up early from an energy standpoint and take unusual care to avoid large inputs close to the ground. Gusts and crosswinds could aggravate this technique, hence, the concern.

The attitude control response has been consistently reported as crisp. Consequently there is something deficient in the path control; i.e., the control of altitude rate or normal acceleration. This always leads back to the same dilemma. It is obvious that the normal acceleration (Nz) response is sluggish. To quicken it significantly requires more overshoot in the pitch rate response and the pilots always object to that. Notice that the choice of feedback parameters ($\dot{\theta}$ or Nz) is not necessarily a significant issue here. The response to command can be made the same with either feedback depending on how it is shaped. But either way, to get faster Nz response means more pitch rate overshoot. Actually, pitch rate was selected as the specified response parameter. It was well behaved with no initial reversals or dependence on sensor location as is the case for Nz. This does not inherently limit any type of control system configuration but just judges them based on the pitch rate response. Other considerations for choice of feedback parameter in the actual system are based on the response to external disturbance. For a vehicle, such as the Orbiter, with zero or slightly negative static stability, pitch rate appears the safer choice. It is less demanding on surface rate in gusts and turbulence. To rate limit under these conditions could mean loss of control.

More analytical treatments in references 3 and 4 have pointed out that the existing pitch rate control system mechanization cancels the inherent zeros in the bare airframe pitch rate transfer function and replaces them with another term that does not completely cancel the corresponding term in the flight path response like a conventional unaugmented airframe. Figure 1 illustrates this. The result shown in figure 2 is an unnatural attentuation. There is also an additional phase lag in the flight path response relative to what it would be with perfect cancelation. There are, in general, two ways to correct this. One is to reshape the pitch rate control system to preserve the bare airframe short period zero as in reference 4. The other way is to add a lead/lag filter in the hand controller output. It is tuned to cancel the existing system zero and replace it with the natural airframe value. Since this is done outside the control loop, it does not change the stability margins of the inner control loop. It only changes the handling qualities as seen by the pilot.

A recent series of fixed base simulator evaluations examined these and other variations in the pitch axis control during landing. This was done to determine if improvement is possible by changes to the software. These simulations are still in progress. A complete treatment is beyond the scope of this paper but some of the findings have been the following:

1. None of the changes made more than a 0.5 improvement in the Cooper-Harper rating or a 26 percent improvement in landing performance with respect to the existing baseline system. Twice that much would be required to consider a change.

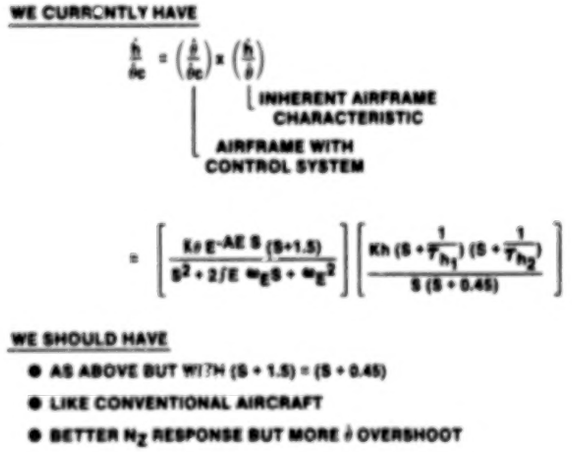


FIGURE 1.- WHAT DOES IT ALL MEAN?

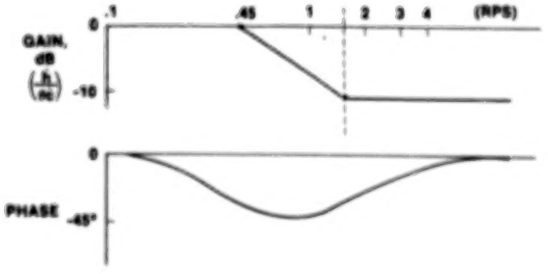


FIGURE 2.- FLIGHTPATH RESPONSE DEGRADATION WITH THE PRESENT SYSTEM.

2. The systems with the best landing performance were not rated the best by the pilots. In fact, the two systems with the best landing performances were both rated worse than the baseline.

3. The lead/lag stick filter addition to the baseline was one of the two best systems from a performance standpoint (group 1 out of 8) even though not properly implemented in detail.

4. The baseline system was in group 3 out of 8 from a performance standpoint. It was rated in group 2 out of 5 (C.H. = 3.5) by the pilots which is quite consistent.

These systems did not all have the same inner loop gain or gain margin. Consequently it is not immediately obvious what aspect of a given system caused a certain result. Also, from the pilots' comments, it is clear that there are many subtleties that affect the rating of a system. These subtleties include having to control across the hand controller detent or use push force right at touchdown. It is also clear that the pilots' first priority is attitude response. Systems with significant overshoot tended to be downgraded even though they might have better flight path response. This probably resulted from training and adjustment to accommodate the existing system. Changing the system response characterstics to achieve better landing performance would probably require a significant amount of retraining. The improvement needs to be significant enough to warrant the effort.

CONSIDERATIONS FOR NEXT TIME

It is interesting to consider what should be done from a handling qualities standpoint if a second-generation Shuttle were to be designed. There are at least two major objectives to address. First, there should be an effort to provide more definitive requirements for mission phases other than approach and landing. A significant amount of basic knowledge is available that would be useful. However, it needs to be organized and written down. The effort would probably expose holes where further activity would be beneficial. Future missions will serve to increase the understanding of these requirements and allow a more knowledgeable compromise with new vehicle configurations if available at the outset.

The other major objective should be to improve the pitch axis handling qualities for landing. First, serious consideration should be given to arrange the vehicle configuration such that fast-acting direct lift control is available for landing. This could be by means of canard control surfaces or wing flaps if it is a tail-controlled vehicle. Possibly even the reaction control system could be used if it were designed with this in mind. Secondly, there needs to be a strong influence at the beginning of the program to keep the flight control system time delays to a minimum. Additional time delays tend to creep in and this is clearly detrimental though somewhat difficult to quantify. Specific requirements should be imposed for end-to-end system response delays. In addition, the design and development effort must be monitored closely. Aggressive action should be taken where necessary to ascertain that proper attention is given to meeting the requirements. The inner flight control loops should be processed at 50 cycles/second or more for landing. The redundant actuator design should be reviewed to quantify and determine ways to minimize the response delays to small signals. Finally, a hardware feed forward provision should be implemented so that small amplitude, high passed analog signals can be sent directly to the actuators from the hand controller or sensor summing junction to bypass the digital delays and overcome the small amplitude actuator nonlinearities. These improvements are relatively easy during the design process but nearly impossible to change after the hardware is built.

REFERENCES

1. Space Shuttle Flying Qualities - Guidance and Control Division, Manned Spacecraft Center, Houston, Texas; January 20 and 21, 1971; Donald C. Cheatham

2. Flying Qualities Requirements for the Orbiter Utilizing Closed-Loop, Fly-By-Wire Control of Vehicle Response Parameters, MSC-07151; May 12, 1972; W. J. Klinar, D. W. Gilbert, C. T. Hackler, H. E. Smith, Jr., D. C. Cheatham

3. Space Shuttle Flying Qualities and Flight Control System Assessment; Myers, McRuer and Johnson, Systems Technology Incorporated (AIAA Paper 82-1608), 1982

4. Application of CALSPAN Pitch Rate Control System to the Space Shuttle for Approach and Landing; N. C. Weingarten and C. R. Chalk; CALSPAN Report No. 7102-F-1; December 1982

N85
16905

UNCLAS

D6

N85-16905

LOW-SPEED LONGITUDINAL ORBITER FLYING QUALITIES

Bruce G. Powers
NASA Ames Research Center
Dryden Flight Research Facility
Edwards, California

ABSTRACT

The shuttle program took on the challenge of providing a manual landing capability for an operational vehicle returning from orbit. Some complex challenges were encountered in developing the longitudinal flying qualities required to land the orbiter manually in an operational environment. Approach and landing test flights indicated a tendency for pilot-induced oscillation near landing. Changes in the operational procedures reduced the difficulty of the landing task, and an adaptive stick filter has been incorporated to reduce the severity of any pilot-induced oscillatory motions. Fixed-base, moving-base, and in-flight simulations were used for the evaluations, and in general, flight simulation has been the only reliable means of assessing the low-speed longitudinal flying qualities problems. Overall, the orbiter control system and operational procedures have produced a good capability to routinely perform precise landings with a large, unpowered vehicle with a low lift-to-drag ratio.

INTRODUCTION

The flying qualities task of manually landing an unpowered vehicle with a low lift-to-drag ratio (L/D) is a difficult one and has been a subject of NASA research for many years. One of the first flight programs to seriously address the problems associated with an entry from orbit was the X-15 research airplane program from 1959 to 1968. The objectives of the X-15 program included an evaluation of unpowered landings from the last part of an entry from orbit to touchdown. The program consisted of 199 flights, with routine landings made on the Edwards dry lakebed. After the X-15 program, a series of lifting body configurations, which were more representative of the aerodynamic configurations that would be required for entry, were evaluated in the terminal area and landing phases. Two landings were made during the program on the 4570-m (15,000-ft) concrete runway. These early vehicles were quite small and simple in design. The control systems generally consisted of only angular rate feedbacks since the vehicles had aerodynamic static stability. The guidance system consisted of ground controller calls based on radar tracking of the flightpath. Nonetheless, the lifting body program demonstrated the feasibility of having a pilot make a manual landing of an unpowered entry vehicle with a low L/D on a conventional runway.

From this modest beginning, the shuttle program took a bold and pioneering step to produce a vehicle that would return from orbit and land on a conventional runway. To meet this goal would require an entry vehicle with an operational capability to land day or night in all types of weather using a 4570-m (15,000-ft) runway. The low-speed longitudinal control system was further complicated by the requirement for a center-of-gravity position that ranged from statically stable to statically unstable. At the time the orbiter was designed, the flying qualities data base was limited for aircraft with advanced control systems similar to that required to meet the orbiter design requirements. Little experience existed in the use of high-gain, digital flight control systems for statically unstable aircraft, and the influence of the time delay between the pilot input and the airplane response would not be fully appreciated until much later, based on experience with the orbiter and highly augmented fighter aircraft. In general, the flying qualities design criteria reflected experience with more conventional airplanes which only required very simple control systems.

This paper discusses some of the complex challenges encountered in developing the longitudinal flying qualities required to land the orbiter manually in an operational environment. The results of tests that have led to modifications are discussed, as well as the results of some additional testing that may lead to further control system modifications. These studies have included fixed-base, moving-base, and in-flight simulation. Some of the simulation techniques required to examine the low-speed longitudinal flying qualities problems are also addressed.

OPERATIONAL TECHNIQUE FOR MANUAL LANDING CAPABILITY

The most significant task in an unpowered vehicle is that of energy management. In the terminal area phase, the orbiter's speedbrakes are used in conjunction with angle of attack and S-turns to put the orbiter in approximately the correct energy state at the start of the landing phase at an altitude of about 3700 m (12,000 ft). The first part of the landing phase (fig. 1) is devoted to the final energy management maneuver and consists of a steep glide slope (approximately 20°) with a fixed aim point relative to the runway and a constant equivalent airspeed. The objective of this phase is to reach an energy window at about 610 m (2000 ft) above the runway with the correct speed and flightpath.

Since there is no active energy management below this point, the steep glide slope maneuver becomes the critical energy management task for both the manual and automatic landings. The pitch-axis task has several levels of automation, depending on the guidance information. With the normal navigational and guidance information available, the glide slope can be tracked in the autopilot mode or the manual control mode. In the manual mode, the task consists of manually tracking the guidance command information displayed to the pilot on the flight director. If no guidance information is available, the glide slope can be established visually using a light-beam system on the ground. In all cases, the speed can be maintained by manual or automatic modulation of the speedbrakes.

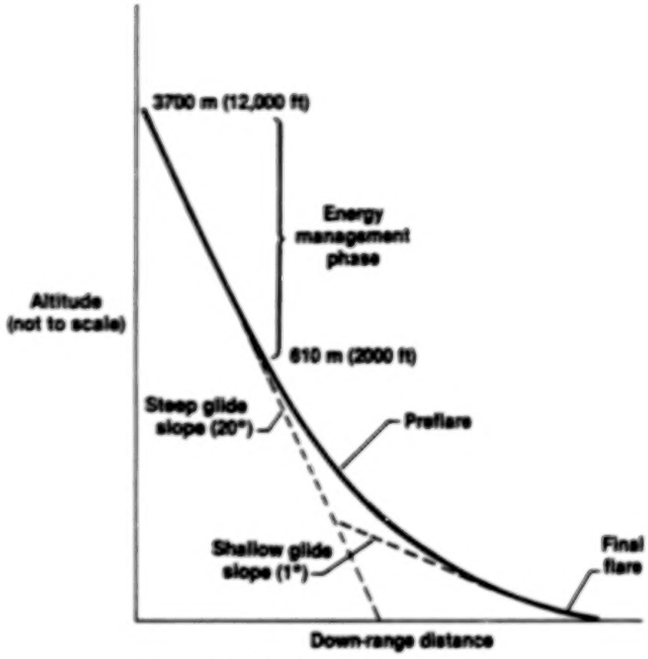


Figure 1. Landing trajectory.

Having established the proper energy, the final landing phase is begun at about 610 m (2000 ft) above the runway. Again, there are several levels of automation available: the autopilot mode; the flight director mode, which when combined with the heads-up display provides guidance information until touchdown; and the completely manual mode, in which the landing is made using the normal visual and motion references. A 1.2 to 1.5g flare is used to transition from the steep glide slope to a glide-slope angle of about 1°. In addition to the visual and acceleration cues, the pilot has cockpit displays of pitch-rate information to assist in establishing the initial pitch rate during the flare. The final glide slope is quite shallow, and a small final flare is made to reduce the rate of sink to a desirable level. The flare to touchdown is often made as one continuous maneuver without actually establishing the final glide slope. This operational technique provides an extremely versatile capability for establishing the desired touchdown conditions under all types of normal and contingency situations.

APPROACH AND LANDING TESTS

In 1977, the low-speed characteristics of the orbiter were evaluated in flight during the approach and landing test (ALT) program. The first four landings were on the Edwards dry lakebed; the fifth landing was on the 4570-m (15,000-ft) concrete runway. These tests validated the concept of landing a large, low L/D vehicle on a standard runway. In general, the flying qualities were quite good. The normal acceleration control in turns was good, although the vehicle was very responsive in pitch, which combined with the light stick forces made pitch control sensitive. The tests were not without problems, however. On the fifth flight (the concrete runway landing), a tendency for pilot-induced oscillation (PIO) in both pitch and roll was exhibited near touchdown. Postflight analysis indicated that the problem, which was primarily in the pitch axis, resulted in rate limiting of the elevons. Because of the priority rate limit logic that allocates elevon surface rate for both pitch and roll commands, the rate limiting in the pitch axis produced rate limiting in the roll axis, resulting in the roll oscillations.

Although this series of flights demonstrated the landing capabilities of the orbiter, it also indicated that additional work would be necessary to make the longitudinal flying qualities satisfactory for the manual landing task. In particular, there was a need to evaluate the cause and significance of the PIO tendencies observed in the ALT flights. In the following sections, the general nature of the longitudinal control problem is discussed, as well as some of the modifications that have been evaluated.

LONGITUDINAL CONTROL CHARACTERISTICS

The shuttle orbiter has two modes that affect longitudinal control. The first mode is pitch attitude control. A major factor contributing to pilot-induced oscillatory motions in this mode is the effective time delay between the pilot input and the airplane response. The actuators contribute a significant delay, as they do on most aircraft. The structural and smoothing filters, which are required because of the high-gain feedback control system, contribute additional significant delays. The digital control system also contributes delay because of the average sampling time and the computation time. A second factor that contributes to pitch attitude PIO tendencies is the nonlinear stick

gearing, which is a method of obtaining good sensitivity around the neutral stick position while retaining a good maximum pitch rate or normal acceleration capability. Unfortunately, in any kind of oscillatory maneuver, any divergence results in increased stick inputs, which increases the effective pilot/stick gain caused by the nonlinear stick. As a result, there is an inherent tendency for oscillations to diverge rapidly once a slight divergence occurs. In simulations of the PIO it is interesting that there were almost no instances of slowly divergent oscillations. If the oscillation began to diverge, it rapidly became a fully developed PIO, resulting in loss of control.

The second mode involved in longitudinal control is altitude or flightpath control. A primary factor that makes altitude control difficult is the loss of lift caused by elevon deflection. Because of this factor, a nose-up pitch command initially results in a downward acceleration at the center of gravity (fig. 2). At the pilot location, which is near the center of rotation, there is a delay of approximately 0.5 sec before any motion is detected by the pilot. This delay, in combination with the sluggish rise time of the acceleration to its steady-state value, makes it difficult for the pilot to accurately control altitude. The high cockpit location and poor visibility also contribute to the inability of the pilot to accurately judge altitude, especially near touchdown.

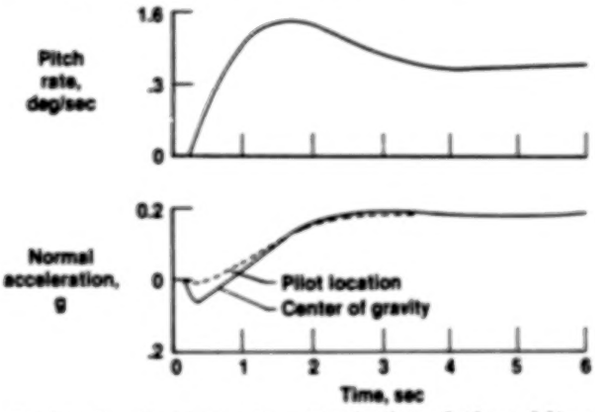


Figure 2. Response characteristics of the orbiter for a step pilot input. Airspeed = 190 knots.

These two modes have been examined in terms of a pilot closed-loop system with a pitch-attitude inner loop and an altitude outer loop (ref. 1). Regions of stability as a function of pilot gain are shown in figure 3 for several magnitudes of control input and indicate that because of the nonlinear stick gearing, stability decreases as stick deflection increases. The Neal/Smith analysis technique of reference 2 has also been used to analyze the closed-loop attitude control; the results are shown in figure 4 in terms of the amount of pilot lead and the amount of resonance experienced for various amounts of closed-loop bandwidth. As the task becomes more demanding, the pilot tries to increase the pilot-vehicle bandwidth to get better response. The pilot lead required is generally indicative of the amount of pilot workload, and the resonance is a measure of the degree of the PIO tendencies. Figure 4 shows that the

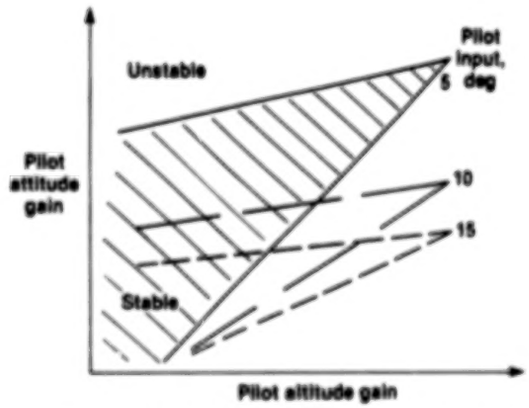


Figure 3. Effect of nonlinear stick gearing on pilot-vehicle closed-loop stability.

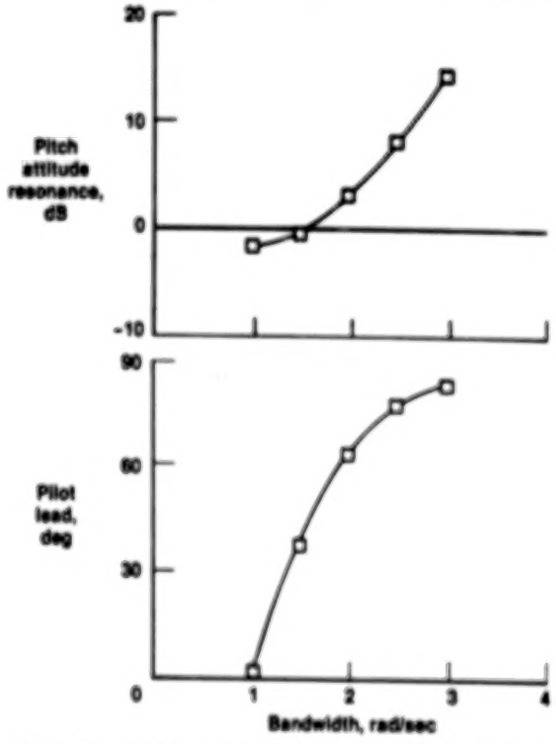


Figure 4. Pilot-vehicle closed-loop characteristics using Neal/Smith analysis of reference 2.

orbiter has reasonably good handling qualities for low bandwidths, but as the bandwidth increases, there is an increase in the pilot lead required and a sharp increase in the PIO tendency.

DEVELOPMENT OF THE STS-1 CONFIGURATION

After the ALT flights, two approaches were pursued to improve the landing characteristics. The first was to make the task easier, thus reducing the need for large values of closed-loop bandwidth; the second was to reduce the tendency toward PIO when large bandwidths were used.

TIME-DELAY AND TASK EFFECTS

One of the main causes of the pitch attitude PIO is the interaction of time delay and high-bandwidth requirements. To study this effect, a series of flights was flown using the Dryden F-8 digital fly-by-wire (DFBW) airplane (ref. 3). The two landing tasks of most interest were the high-workload case, in which the pilot was attempting to land precisely on a designated area of the runway, and the low-workload case, where the pilot was attempting to land on the runway without concern for the actual touchdown point. A steep glide slope about half that of the orbiter was used for both cases, and the high-workload case had a 46-m (150-ft) lateral offset at 30 m (100 ft) above the runway. The spot-landing case was similar to the conditions for the ALT flights. After the ALT flights, the orbiter landing task was made easier by basing the touchdown point on velocity rather than a fixed point on the runway. This technique reduced the need for high-bandwidth control and made the task more like the low-workload task evaluated in the F-8 DFBW tests.

The results of the F-8 tests are shown in figure 5 along with the results from the total in-flight simulator (TIFS) orbiter simulation. For orbiter time-delay values of approximately 235 msec, the effect of task is quite significant, and it appears that the current operational procedures for the orbiter produce a task that is between the low- and high-workload tasks of the F-8 tests. These results also indicate that time delay can cause a significant degradation in handling qualities when a high-workload task is performed. Interestingly, these same results were confirmed in a study of the standard approach task for fighter aircraft (ref. 4). This study was instigated as a result of difficulties with handling qualities in the landing phase for several of the latest generation of fighter aircraft. These aircraft have control systems similar to the control system of the orbiter, with high-gain feedback systems requiring structural bending filters and other filters that introduce significant time delays. The results for the fighter aircraft in the landing task were essentially the same as for the high-workload task of the F-8 study. These tests have contributed significantly to the understanding of time-delay effects in modern aircraft, and the results have now been incorporated into the current specifications for military aircraft.

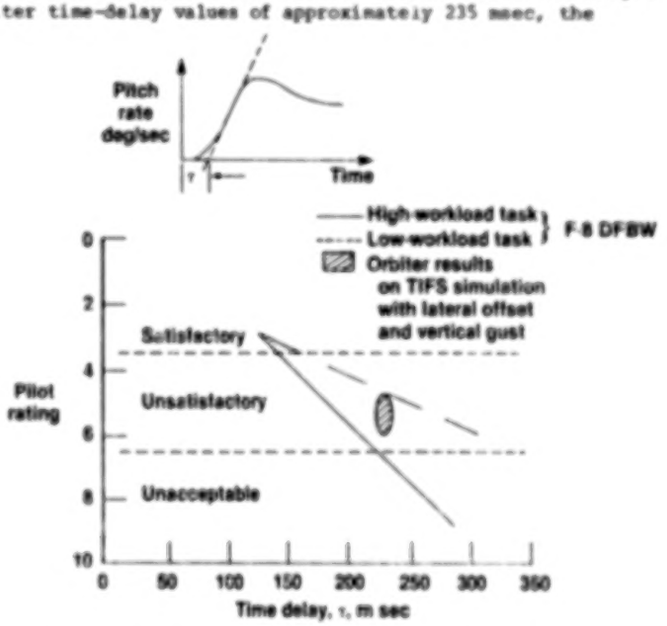


Figure 5. Time-delay effects obtained from orbiter simulations and from the F-8 flight tests of reference 1.

PIO FILTER

To reduce the possibility of developing a large-amplitude pilot-induced oscillation near the ground, an adaptive stick gain was developed (refs. 5 and 6). This system can best be thought of as a closed-loop bandwidth limiter. The relationship of resonance to bandwidth (fig. 4) shows that it would be highly desirable to restrict the pilot to bandwidths less than 3 rad/sec to avoid large-amplitude oscillations. The adaptive stick gain algorithm consists of a frequency detector combined with variable stick shaping (fig. 6). The PIO filter reduces the stick gain by reducing the parabolic portion of the stick gearing so that at its maximum amount of reduction, the stick is very nearly linear (fig. 7). By reducing the overall pilot/stick gain, the PIO tendency is reduced and, in addition, the more linear stick gain reduces the divergent nature of the PIO caused by the nonlinear stick. Tests on the TIFS demonstrated the capability of reducing the PIO tendencies of the orbiter in high-workload situations.

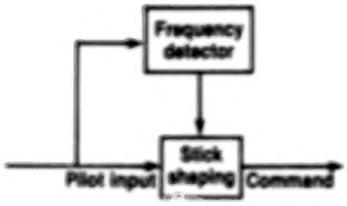


Figure 6. Adaptive stick-gearing concept to reduce PIO tendencies (ref. 6).

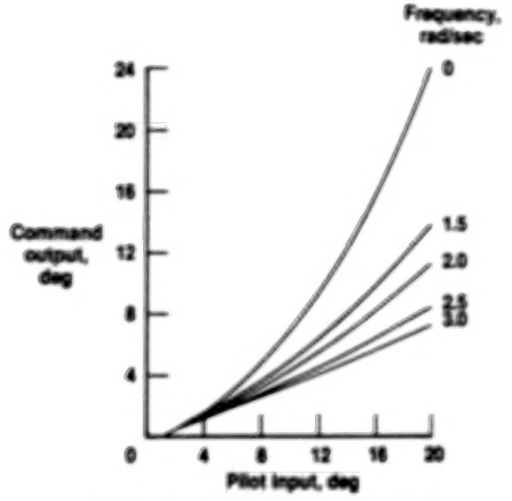


Figure 7. Example of frequency-dependent stick shaping.

The PIO filter does not significantly improve the flying qualities of the orbiter, but it does provide some protection from potentially dangerous, large-amplitude oscillations near the ground.

Another modification was to increase the stick force gradient by a factor of two. This decreased the pitch sensitivity, thus reducing inadvertent inputs. It also improved the pilot's awareness of impending PIO situations. In the orbiter, there are almost no acceleration cues because of the location of the center of rotation, and the visual cues of attitude are limited because of pilot location. As a result, the pilot would not be aware of any oscillatory motion until the amplitude grew large. With the increased stick forces, the types of inputs that generate PIOs would be more obvious to the pilot, and proper attention could be given to the oscillatory motions before they became a significant problem.

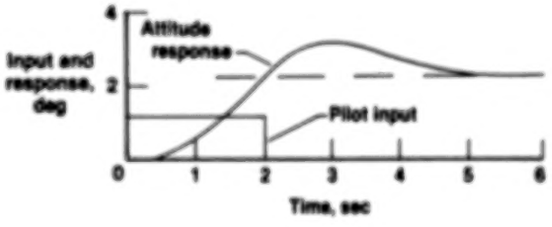


Figure 8. Orbiter attitude response for pilot pulse input. Airspeed = 190 knots.

Other changes made before the orbital flights included a change in the priority rate-limiting logic to reduce the interactions of the roll and pitch axes. In addition, the pitch attitude response was made slightly less sensitive by reducing the overall loop gains at the landing condition. The result of these changes was a high-gain, pitch-rate-command control system which was optimized to give excellent attitude control. With this type of system, the pilot can pull up to a desired attitude and release the stick, and the attitude will overshoot slightly and return to the value at which the stick was released (fig. 8). This makes it extremely easy for the pilot to establish a precise attitude without using complex pilot control techniques.

PIO TENDENCY AND SIMULATION

Analytical results can provide considerable insight into the nature of flying qualities problems, but simulation has also played an important role in the development and evaluation of the control system. Most of the early studies of the flying qualities of the orbiter during landing were performed on a fixed-base simulation with a visual display of the runway. The task was generally not very demanding, and as a result there was little indication of any PIO tendency. In 1978 after the ALT experience, the Ames Flight Simulator for Advanced Aircraft (FSAA) moving-base simulation (ref. 7) and Calspan TIFS facility (ref. 8) were used to examine the PIO characteristics of the orbiter. The FSAA is a moving-base simulator with a TV model-board visual display of a runway. The TIFS is an in-flight simulator that can reproduce cockpit motions in addition to providing the real-life visual scene. A safety pilot is used to prevent the evaluation pilot from getting into any dangerous conditions. During these evaluations, the pilots evaluated the PIO tendencies using the rating scale shown in table 1.

TABLE 1. — PIO RATING SCALE.

Rating	Description
1	No undesirable motions
2	Undesirable motions that are cured by pilot technique
3	Undesirable motions that can be cured by sacrificing the task or by increased effort
4	Sustained nondivergent oscillations
5	Divergent oscillations for abrupt maneuvers only
6	Divergent oscillations encountered in normal control

The histogram in figure 9 summarizes the results obtained. It is clear from this figure that the FSAA with limited motion and visual cues produced very little PIO tendency compared to the TIFS.

In 1979 and 1980 another series of simulations were made with the Ames Vertical Motion Simulator (VMS) (ref. 9) and the TIFS. The VMS had sufficient vertical motion to provide good vertical motion simulation, but it had the same visual display that was used on the FSAA. In both of these simulations a very demanding task was used to accentuate the PIO tendencies. A 46-m (150-ft) lateral offset was performed at 30 m (100 ft) above the runway, and a 4.6-m/sec (15-ft/sec) vertical gust was introduced at an altitude of approximately 15 m (50 ft). This produced a task that would be unlikely in real life, but it provided a situation that produced a pilot gain high enough to make the PIO tendencies of the vehicle apparent to the pilot. The results of these tests are summarized in figure 10, and a significant difference still exists between the moving-base simulation and the flight simulation. On both of these simulators, after becoming familiar with the simulator, a normal straight-in approach and landing could be made without evidence of a PIO tendency. Although the PIO tendencies were not the same for the two simulations, for tasks less demanding than those that would produce PIOs, the two simulators produced similar evaluations of the basic handling qualities. The general conclusion from these tests is that flight simulation is probably the only reliable method of evaluating the landing characteristics. The introduction of an artificial task produces pilot workload levels nearer to the workload levels that can be encountered in flight, but even flight simulation does not produce the same sense of urgency that the actual flight environment produces.

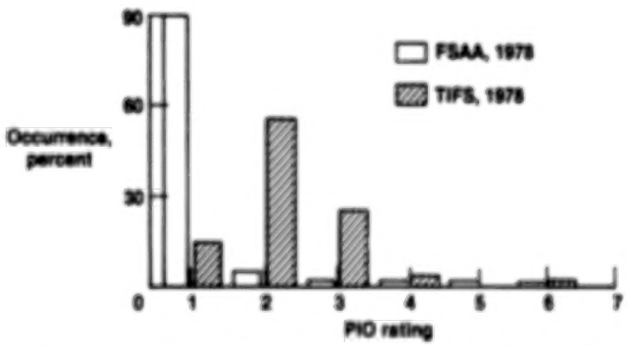


Figure 9. Comparison of PIO rating from the FSAA and TIFS simulators for the landing task with the ALT orbiter configuration.

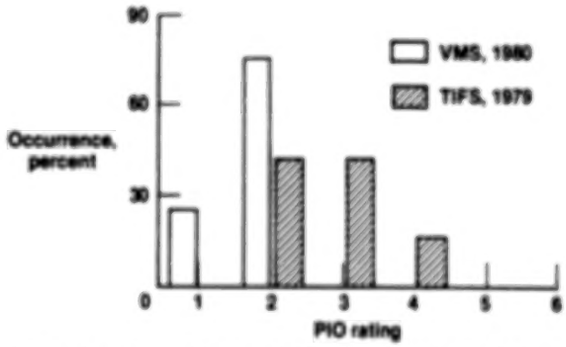


Figure 10. Comparison of PIO ratings from the VMS and TIFS simulators for the landing task with the STS orbiter configuration.

ORBITAL FLIGHTS

The first orbital flight of the space transportation system (STS), made in 1981, represented a significant event in demonstrating the feasibility of making manual landings with an entry vehicle. Subsequent flights have demonstrated a capability to land on a 4570-m (15,000-ft) concrete runway in a routine manner. In the early flights, variations in touchdown point and speed have resulted from a greater-than-predicted value of low-speed L/D. Predictions are extremely important for the landing phase because there is no energy management below 610 m (2000 ft), and increases in L/D result in higher touchdown speeds or longer landings. With the predicted data now updated with the flight results, this problem has been reduced significantly. Overall, the STS flights have demonstrated a good manual landing capability, with acceptable landings being made in a variety of wind and turbulence conditions. The capability demonstrated so far is especially impressive when one considers that each manual landing has been performed by a different pilot, thus reducing any of the pilot training advantages resulting from actual flight experience.

POTENTIAL IMPROVEMENTS

As discussed previously, one disadvantage of the current orbiter control system is the sluggish response in normal acceleration, which makes flightpath control more difficult. One maneuver that is especially difficult is leveling off near the ground (such as to bleed off speed to obtain a better touchdown velocity). This difficulty, caused by the problem with ballooning, is especially noticeable when in ground effects. Unlike a conventional transport, the orbiter has a considerable amount of excess energy at a nominal landing speed of 200 knots, but because of the rapid deceleration (4 to 5 knots/sec), any significant ballooning can result in a low-energy condition fairly rapidly. To improve the flightpath response, it is necessary to speed up the acceleration response by increasing the amount of pitch rate overshoot. The example in figure 11 shows a faster acceleration response, which results in better flightpath control, but the attitude response drops back when the stick is released, which makes accurate pitch attitude control more difficult. Simulator studies of systems of this type are currently being conducted, and an analysis of this type of system is given in reference 10. An interesting problem has developed in the effort to improve the longitudinal flying qualities. On the one hand, an effort has been made to make the landing task easier, while on the other hand, an effort has been made to improve the flightpath control at landing. These efforts have resulted in conflicting requirements for the pitch response characteristics. As the task becomes easier, it is generally performed in a more open-loop fashion and attitude becomes the primary variable to be controlled, which produces a requirement for extremely good pitch attitude control. One example of an open-loop control strategy is in the final flare and landing in which the pilot increases the vehicle attitude a predetermined amount at the final flare point and then lets the airplane land with minimal pilot inputs. Several of the landings to date have been of this type and have been quite successful. In contrast to this technique, there is the control strategy that requires a more closed-loop control of the flightpath. This technique would be especially appropriate for nonstandard landing situations, such as during recovery from an automatic landing system failure near the ground. To improve the normal acceleration response, this technique requires an increase in the pitch rate overshoot, which is in conflict with the good attitude response required with the more open-loop tasks. Further test results from both flight and simulation will be required to determine which control technique (and therefore, control system) will provide the best overall capability for the manual control task in the operational environment.

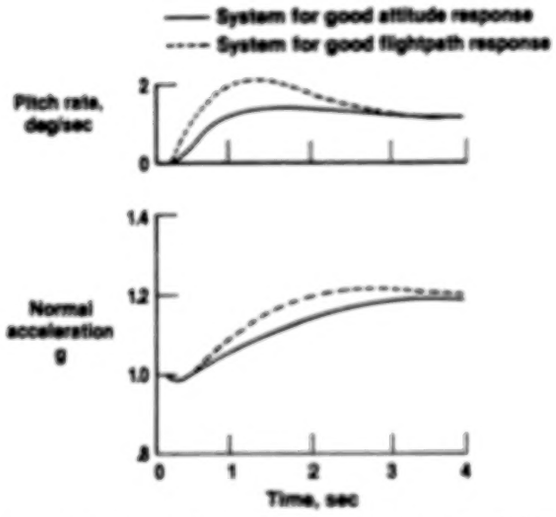


Figure 11. Comparison of response characteristics for good attitude response and for good flightpath response.

CONCLUDING REMARKS

The shuttle program was initiated as a bold and pioneering effort to develop a true spaceplane capable of returning from orbit and landing on a conventional runway. Some complex challenges were encountered in developing the longitudinal flying qualities required to land the orbiter manually in an operational environment. Approach and landing test (ALT) flights indicated a tendency for pilot-induced oscillation near landing. Changes in the operational procedures have reduced the difficulty of the landing task, and an adaptive stick filter has been incorporated to reduce the severity of pilot-induced oscillatory motions. Fixed-base, moving-base, and in-flight simulations have been used during the evaluations, and in general, flight simulation has been the only reliable means of assessing the low-speed longitudinal flying qualities problems. Some additional refinements may still be required to improve the flying qualities for the manual landing task, and two types of systems appear viable, depending on the nature of the task: one emphasizes attitude control, and the other emphasizes flightpath control. Further flight experience will contribute additional information about the manual landing task, especially in regard to the interfacing of the manual task to the automatic landing mode and the heads-up display (HUD) flight director mode in the operational situation. Overall, however, the orbiter control system design and the operational procedures have met the objective of providing the flying qualities necessary for a manual landing. An impressive manual landing capability for an unpowered vehicle with a low lift-to-drag ratio has been demonstrated, and precision landings are now being made routinely. The shuttle program has used many advanced technologies and demonstrated their application for the first time in an operational environment. In addition to providing an operational

space transportation system, the orbiter development program has also made a significant contribution to the generic flying qualities and flight control system technology for advanced aircraft.

REFERENCES

1. Teper, Gary L.; DiMarco, Richard, J.; Ashkenas, Irving L.; and Hoh, Roger H.: Analyses of Shuttle Orbiter Approach and Landing Conditions. NASA CR-163108, 1981.

2. Neal, T. Peter; and Smith, Rogers E.: An In-Flight Investigation to Develop Control System Design Criteria for Fighter Airplanes. AFFDL-TR-70-74, 1970.

3. Berry, Donald T.; Powers, Bruce G.; Szalai, Kenneth J.; and Wilson, R. J.: In-Flight Evaluation of Control System Pure Time Delays. AIAA 80-1626R, J. Aircraft, vol. 19, no. 4, Apr. 1982, pp. 318-323.

4. Smith, Rogers E.: Effects of Control System Dynamics on Fighter Approach and Landing Longitudinal Flying Qualities. AFFDL-TR-78-122, Mar. 1978.

5. Smith, John W.; and Edwards, John W.: Design of a Nonlinear Adaptive Filter for Suppression of Shuttle Pilot-Induced Oscillation Tendencies. NASA TM-81349, 1980.

6. Powers, Bruce G.: An Adaptive Stick-Gain to Reduce Pilot-Induced Oscillation Tendencies. AIAA 82-4078, J. Guidance and Control, vol. 5, no. 2, Mar.-Apr. 1982, pp. 138-142.

7. Zuccaro, J. J.: The Flight Simulator for Advanced Aircraft - A New Aeronautical Research Tool. AIAA Paper 70-359, Mar. 1970.

8. Reynolds, Philip A.; Wasserman, Richard; Fabian, Gardner J.; and Motyka, Paul R.: In-Flight Simulator (TIFS). AFFDL-TR-72-39, July 1972.

9. Jones, A. David: Operations Manual: Vertical Motion Simulator (VMS) S.08. NASA TM-81190, 1980.

10. Weingarten, Norman C.; and Chalk, Charles R.: Application of Calspan Pitch Rate Control System to the Space Shuttle for Approach and Landing. NASA CR-170402, May 1983.

N85
16906

UNCLAS

N85-16906

D17

THE SPACE SHUTTLE ASCENT VEHICLE AERODYNAMIC CHALLENGES CONFIGURATION DESIGN AND DATA BASE DEVELOPMENT

Charlie C. Dill
NASA/George C. Marshall Space Flight Center
Huntsville, Alabama

J. C. Young, B. B. Roberts, M. K. Craig
NASA/Lyndon B. Johnson Space Center
Houston, Texas

J. T. Hamilton
Rockwell International Corporation
Downey, California

W. W. Boyle
Lockheed Missiles & Space Company
Huntsville, Alabama

ABSTRACT

The phase B Space Shuttle systems definition studies resulted in a generic configuration consisting of a delta wing orbiter, and two solid rocket boosters (SRB) attached to an external fuel tank (ET). The initial challenge facing the aerodynamic community was aerodynamically optimizing, within limits, this configuration. As the Shuttle program developed and the sensitivities of the vehicle to aerodynamics were better understood the requirements of the aerodynamic data base grew. Adequately characterizing the vehicle to support the various design studies exploded the size of the data base to proportions that created a data modeling/management challenge for the aerodynamicist. The ascent aerodynamic data base originated primarily from wind tunnel test results. The complexity of the configuration rendered conventional analytic methods of little use. Initial wind tunnel tests provided results which included undesirable effects from model support structure, inadequate element proximity, and inadequate plume simulation. The challenge to improve the quality of test results by determining the extent of these undesirable effects and subsequently develop testing techniques to eliminate them was imposed on the aerodynamic community. The challenges to the ascent aerodynamics community documented in this paper are unique due to the aerodynamic complexity of the Shuttle launch. Never before has such a complex vehicle been aerodynamically characterized. The challenges were met with innovative engineering analyses/methodology development and wind tunnel testing techniques.

INTRODUCTION

During first stage flight, which for purposes of this paper corresponds to the flight regime from a Mach number of 0.60 through SRB separation, aerodynamic data bases were required to support various subsystem design studies. Over-all vehicle aerodynamic characterization was required for vehicle performance analyses, vehicle structural design analyses, and SRB separation system design studies. More detailed aerodynamic inputs were required for venting analyses, protuberance design studies, tile load studies, and the ascent air data system design study. This paper discusses the aerodynamic challenges and consequent approaches/techniques to overcome them relative to the aerodynamic characterization of the Space Shuttle launch vehicle (SSLV), its four elements in proximity (orbiter, external tank, two SRBs), and the orbiter's basic components (wing, elevons, and vertical tail). Three basic challenges are addressed in terms of an ascent launch vehicle aerodynamic data base and a SRB separation aerodynamic data base.

CHALLENGE: AERODYNAMIC OPTIMIZATION OF BASIC GENERIC CONFIGURATION

The phase B Space Shuttle systems definition studies resulted in a generic launch configuration consisting of a delta wing orbiter and two solid rocket boosters attached parallel to an external fuel tank. The evolution of this generic configuration (Fig. 1) to its present form is the result of many system and subsystem optimization studies. Preeminent among these, in the early 1970's, were performance trade studies, guidance and control design studies, and attach structure sizing studies. Because vehicle aerodynamics is a basic input to these studies, the ascent aerodynamic community was initially challenged to provide a data base that would allow configuration optimization from an aerodynamic standpoint. This challenge was met by several parametric configurational studies in the early 1970's. These studies provided a data base for determining the relative aerodynamic effect of ET and SRB nose shapes, SRB location (longitudinal and radial) on the ET, and orbiter incidence relative to the ET. The significant results of these studies (Fig. 2) showed that an ogive ET nose shape produced the least

launch vehicle drag and consequently the best aerodynamic performance; that reducing the orbiter incidence to a minimum would minimize attach structure loads by reducing the orbiter longitudinal aerodynamics; and that moving the SRBs down and aft reduced launch vehicle drag, increased stability by moving the aerodynamic center aft, and minimized aerodynamic interference on the orbiter. This movement of the SRBs also reduced the probability of contact with the orbiter wing during SRB separation. In the 1975 time frame, after the major configurational changes had taken place, additional parametric drag reduction studies were conducted to support on-going performance improvement trade studies. Innovative aerodynamic fairing designs were generated (Fig. 3) and their drag reducing potential investigated. Several configurations reduced drag (Fig. 3) and consequently improved aerodynamic performance. However, weight and manufacturing cost proved too formidable thus negating their benefits.

CHALLENGE: DEVELOPMENT/MANAGEMENT OF REQUIRED AERODYNAMIC DATA BASE

The initial concept of the launch vehicle aerodynamic data base was, relative to the final product, simple. With both the Space Shuttle main engine (SSME) and SRB nozzles having gimbal capability, sufficient control authority existed to negate using aerodynamic control surfaces during ascent. The elevons could be set in a single position for the entire ascent flight regime. Element proximity aerodynamics were considered secondary inputs to the attach structure design because thrust and inertial forces were so much larger. Therefore, the fidelity of the required launch vehicle data base was considered relatively unimportant. Even though it was understood that booster separation motors (BSM) would change the aerodynamic flowfield associated with the launch vehicle at SRB separation, the degree of change was underestimated. This was primarily due to a lack of separation system requirement definition and a lack of understanding of the criticality of controlling the nonlongitudinal aerodynamic forces to ensure no recontact.

As the Shuttle program developed and the sensitivities of the vehicle to aerodynamics were better understood the requirements of the aerodynamic data bases grew. Structural loads studies of the elevon actuator and wing structure showed capability exceedances. This dictated scheduled elevon movement as a function of Mach number (Fig. 4) to maintain actuator and wing structure within allowable limits. Because trajectory parameters affecting hinge moments would vary from flight to flight, and because of the inclusion of uncertainties on the wind tunnel derived hinge moments for any set condition, an active elevon load relief system was implemented to ensure no elevon actuator overload. This elevon movement also changed the orbiter proximity aerodynamics which had now been determined to have a significant impact to the attach structure loads. Consequently, the launch vehicle aerodynamic data base now had to include the effects of elevon movement. With the realization of the acute sensitivity of the vehicle to ascent aerodynamics, particular attention now had to be paid to the fidelity of the launch vehicle data base. That is, the seemingly minor effects of the distribution between the elements of the airload on the attach structure, the asymmetry created by the ET protuberances, and the SSME/SRB plume effects on the forebody became significant. The sensitive orbiter thermal protection tiles imposed a stringent design requirement (minimized BSM exhaust plume impingement) on the SRB separation system. This dictated high BSM thrust, over a very short burn time, and a particular orientation of the BSMs (Fig. 5). Elevated thrust was required to account for the cosine losses associated with the BSM 40 deg pitch and shallow 20 deg inboard roll angles. The combination of high thrust and forward facing jets in the SRB nose frustum greatly amplified the anticipated BSM exhaust plume effect on the vehicle flowfield (Fig. 6). This placed greater emphasis on the fidelity of the data base methodology and attached more significance to the BSM plume scaling parameters, utilized for wind tunnel testing, in the data base. Naturally, with the better understanding of the vehicle's acute sensitivity to aerodynamics, coupled with questionable wind tunnel test results (to be discussed later), the uncertainties on the aerodynamic data bases also became prominent inputs to the various discipline studies. Therefore, adequate aerodynamic characterization of the vehicle to support the various design studies exploded the size/complexity of the data bases to proportions that created a data modeling/management challenge for the aerodynamicist. However, math modeling methodology which included the effects of the potential changing vehicle parameters on aerodynamics and their associated uncertainties was developed. This modeling methodology satisfied the user discipline requirements and provided adequate aerodynamic data bases for design studies.

LAUNCH VEHICLE AERODYNAMIC DATA BASE

Aerodynamics represent external applied forces to which the vehicle as a whole and its discrete structure reacts in flight. Therefore, historically, launch vehicle aerodynamic data bases are composed of two parts: a static stability data base which constitutes the resultant three aerodynamic force and three moment coefficients, and the airloads data base which is comprised of distributed localized pressure coefficients over the geometry of the vehicle. Naturally, the integration of the airloads data base into resultant forces/moments must equal the static stability force/moment data to ensure consistency between the various system design studies relative to overall vehicle design. The Space Shuttle launch vehicle aerodynamic design data base, in this respect, is no different. The uniqueness of the Shuttle data base is that five vehicles (Fig. 7) must be dealt with in a consistent fashion — the mated vehicle and its elements (orbiter, ET, LSRB, RSRB). Since each of the elements

contribute significantly to the mated vehicle aerodynamic characteristics, none can be treated as a simple protuberance with relative minor interference effects. Each must be dealt with as an independent element in proximity to others. Additionally, the data base includes aerodynamic characterization of three orbiter components — wing, vertical tail, and elevons (inboard and outboard).

In the initial planning of the launch vehicle aerodynamic data base the aerodynamicist had to consider, along with the inherent characteristics of the basic outer moldlines of the generic vehicle, the interference effects of the ET and SRB protuberances, the airloads on the attach structure and its interference effect, and the significant effect of the SRB and SSME exhaust plumes. Consideration also had to be given to the primary source of the data base — the wind tunnel. Ideally, the aerodynamicist desired to utilize a single high fidelity model to simultaneously determine both the static stability force and moments and the distributed pressures — including plume effects. This, however, was not possible due to the physical limitations/complexity of a model to obtain the data and the interference effects of the model support system required to supply the high pressure gas for the plume simulations. Early in the Shuttle program, these considerations were hampered by a lack of knowledge of how to properly simulate the plumes and the fact that few wind tunnel facilities had the capability of supplying an auxillary high pressure air supply for plume testing. Therefore, a methodology was derived to account for these considerations and work around the problems associated with generating a consistent launch vehicle data base through combination of results from different types of wind tunnel tests.

The total coefficient (Fig. 8) is comprised of forebody and base characteristics. Furthermore, the forebody coefficients are separated into plume-off (p-off) data and plume-on (p-on) increments to account for the effects of the plumes. This formulation permitted the determination of the most significant aerodynamic characteristics, the p-off forebody data, from one test (A in Fig. 8) and the plume effects from an independent test (B in Fig. 8). This minimized the model support system effects in the data base. Plume-off base environments on the models are removed from the total measured test (A) results to create p-off forebody data. These base environments are irrelevant to the data base because of the model support system interference and the overwhelming changes created by the SRB/SSME exhaust plumes. By including the forebody plume effects as p-on minus p-off increments the effect of the model support system required for plume testing (B) is reduced to a second order effect. The base characteristics are determined from the plume test. By utilizing the measured p-on base pressures from test (B) rather than p-on minus p-off increments to be applied to the p-off base environments from test (A), the model support system effects on the base characteristics are eliminated and the effects of the plumes are adequately included in the data base. The airloads data base is formulated in much the same manner. The p-off forebody pressure coefficient distributions over the geometry of the vehicle are determined independently of the p-on pressure coefficient increments and then combined. Again, with this formulation the model support system effects are minimized.

Each of the six static stability forces and moments for the mated vehicle and its four elements are formulated in this manner. The forebody coefficients are a function of the freestream Mach number, the vehicle's orientation to the freestream flow (α,β), and the elevon deflection angles (Table 1). Math modeling of the elevon effects on the mated vehicle characteristics, using a fourth order polynomial fit, has been incorporated into the data base at the request of the trajectory and guidance/control disciplines to facilitate its use. The element data are provided for nine discrete inboard/outboard combinations. Wing and vertical tail shear, bending, and torsion and elevon hinge moments constitute the component data. These are formulated similarly to the element data. The base characteristics are formulated as forces and moments primarily as a function of altitude. This is due to their first order dependency on the plume characteristics, which, for a given nozzle and engine operating characteristics, are primarily a function of altitude. However, math modeling has been incorporated to account for the small effects due to vehicle attitude and SSME power level changes. This methodology formulation allowed, early in the Shuttle program, determination of a quality data base. Then, as forebody configurational changes took place, the plume technology data base matured, and plume-on facility testing capability developed, refinements to the data base could be effected without regenerating the complete data base.

Two types of uncertainties were generated for the launch vehicle data base — tolerances and variations. These uncertainties, although not statistically derived, were generated as three-sigma incremental values with, in general, a normal distribution about the nominal data base. The tolerances, or lower uncertainty bounds, represent a measure of the experimental wind tunnel test data scatter about the established nominal data base. Tolerances were utilized in the Shuttle program for operational subsystem design. Variations, or upper uncertainty bounds, represent the potential difference between the wind tunnel derived, experimental characteristics and the actual flight vehicle characteristics. Variations were utilized in the Shuttle program as constraints in the flight planning activities. Ordinarily variations are derived by employing the historical flight experience of a vehicle similar to the one being designed. No vehicle similar to the Space Shuttle launch vehicle has ever flown. However, vehicles such as the generic lifting bodies and high altitude/high speed aircraft are similar to the reentering orbiter. The orbiter entry aerodynamic discipline utilized the flight experience of these vehicles to derive "variations" for the orbiter entry aerodynamic data base. The ascent aerodynamic community utilized the orbiter entry variation-to-tolerance ratio along with the established

launch vehicle element tolerances to establish the launch vehicle variations. Both tolerance and variation uncertainties were generated for each totally independent forebody force, moment couple, and aerodynamic center coefficient for each component and element of the launch vehicle. This permitted determination of the total moment uncertainty for each component and element as the root-sum-square (RSS) of these three independent contributors. The mated vehicle uncertainties were established as the RSS of each element's uncertainty. The base characteristic uncertainties were likewise independent and combined in an RSS fashion with the forebody uncertainties. Analytical modeling was formulated to allow assessment of a single coefficient uncertainty or any combination of coefficient uncertainties by any subsystem discipline.

SRB SEPARATION AERODYNAMIC DATA BASE

The Shuttle Solid Rocket Boosters (SRBs) are separated at burnout from the launch vehicle by means of two basic phenomena. Longitudinal separation is achieved as a result of the higher axial acceleration of the orbiter/external tank (OET). Lateral and normal separation are achieved, however, by the application of thrust to the SRBs and aerodynamic forces. Unlike previous cylindrical launch vehicles, control of these nonlongitudinal forces is critical to assure that no recontact occurs. This criticality manifested itself in the aerodynamicist's ability to model three aerodynamic phenomena: (1) the proximity effect of one vehicle's flowfield on those of nearby vehicles, (2) the jet interaction effect of the BSM plumes on the flowfield surrounding all of the vehicles, and (3) the effect of direct BSM plume impingement on the external tank. Each of these phenomena is a function of the orientation of the OET with respect to the free stream flow and the relative displacements and orientations between the vehicles. The jet interaction and plume impingement effects are also a function of a plume scaling parameter. This knowledge defined the set of eight independent parameters, the effects of which had to be considered in deriving the separation data base (Fig. 9). The effects of Mach number and Reynolds number were found to be second order in the range of anticipated flight conditions and were thus included in the data base uncertainty. To preclude the necessity of updating the complete data base each time the vehicle outer moldline was changed, the dependent variables (aerodynamic coefficients) were formulated as BSM plume-on and plume-off proximity increments; that is, coefficient increments to be added to SRB and OET free-stream aerodynamic data. Utilizing this approach would allow the effects of minor configuration changes to be adequately reflected in updates to the isolated aerodynamics with negligible effects on the proximity increments.

It became obvious that the use of eight independent variables in the data base would present severe difficulties if a standard square grid of representation was utilized in modeling the required aerodynamic characteristics. The most obvious difficulty would be the number of data points required. The squareness of the grid in 8-dimensional space would also assure that most of the data points would be far removed from areas of interest. In fact, many data points would be required in locations that are unrealizable due to physical constraints imposed by the basic configuration. Obviously, superimposing the large matrix of proximity variables required at a large ΔX on $\Delta X = 0$ would be unrealizable since the $\Delta X = 0$ position constitutes the mated position of the SRB's where the other variables can only have the value of zero. As with the launch vehicle data base, consideration also had to be given to the wind tunnel, the basic source of the aerodynamic data. Limitations on specific combinations of the independent parameters ΔX, ΔY, ΔZ, $\Delta\alpha$, $\Delta\beta$ were imposed by physical constraints of the facility and its model mounting/sting movement capability.

These difficulties were circumvented by developing a unique data organization concept to handle the five proximity independent variables. This new approach, designated the "hypercube" format, allows data to be placed only along required separation paths. At each desired ΔX two 4-dimensional hypercubes are situated so as to encompass anticipated dispersions in ΔY, ΔZ, $\Delta\alpha$, and $\Delta\beta$. An outer cube encompasses all dispersions, including system failures, while an inner cube includes the nominal separation path with 3σ dispersions. These hypercubes are not constrained to have parallel opposite sides to that they can be shaped to match physical constraints imposed by the test facility and still provide data near the required trajectory points as determined by trajectory dispersion analyses (Fig. 10). Data points were generated at the vertices of the hypercubes. In addition, an interior point is placed within each hypercube to increase the data density in a region of interest. Typical BSM plume-on SRB trajectories through the hypercube matrix are demonstrated in Figure 11 in terms of the parameters ΔX, ΔY, and ΔZ. The ΔX values at which hypercubes are placed were selected to maintain constant time increments at the separation relative longitudinal acceleration rather than constant length increments. This increases the data density early in the motion when trends are being established.

The use of this approach has provided a much higher data density along separation trajectory paths while reducing the required number of data points by a factor of at least 20 from a square grid. A special algorithm has been developed which transforms these 4-dimensional arbitrary shapes into 4-dimensional cubes so that a low order polynominal can be easily fit to the vertices and interior point, thus providing interpolation. Interpolation in the remaining independent variables α, β, and the plume scaling parameter is handled in a similar manner, although the organization of these variables is based initially on 3-dimensional cubical shapes since there are no physical interference constraints to be taken into account.

The uncertainties associated with the SRB separation aerodynamic data base are composed of three components: an error resulting from the hypercube interpolation process, an error due to the asymmetry of the motion of the two SRBs with respect to the OET, and an error associated with scaling the BSM plumes. The uncertainty component associated with interpolation error accounts for the inability of the hypercube interpolator polynomials to exactly model the data and for the fact that the data base was generated at a constant value of Mach number. It also implicitly accounts for the random uncertainty associated with the wind tunnel data measurements/acquisition system. The uncertainty component associated with asymmetric SRB motion accounts for the error incurred in performing all plume-on testing with the SRB's in symmetric positions with respect to the OET. SRB asymmetry modifies plume-on aerodynamics by establishing unequal impingement of the BSM plumes on the external tank and by causing an asymmetric interaction of the plumes with the free-stream flow. The third aerodynamic uncertainty component results from errors in plume scaling, that is, errors incurred by using the jet-to-free stream momentum ratio rather than the momentum flux ratio as the plume simulation parameter (discussed later). The total coefficient uncertainties in the data base were obtained by root-sum-squaring the contribution of these three components.

CHALLENGE: WIND TUNNEL TESTING TECHNIQUES/IMPROVEMENTS

The primary sources of the Space Shuttle ascent aerodynamic data base are wind tunnel test results. The multibody configuration with its significant interrelated interference effects precluded using conventional analytical tools to characterize the vehicle. Initial wind tunnel tests provided results which included effects from model support structure, inadequate element proximity, and inadequate plume simulation. It became obvious, as the Shuttle program matured, that these undesirable effects were significant. The challenge to improve the quality and detail of test results by determining the extent of these effects, and subsequently develop testing techniques to eliminate them, was imposed on the aerodynamic community. In the process of establishing the ascent aerodynamic data base two basic types of wind tunnel test results were utilized. Force and moment data were obtained by using balances located in the models. Data of this type were obtained for the mated vehicle, the elements, and the components for the launch vehicle data base. Data of this type were also obtained for the SRBs and OET combination in proximity for the SRB separation data base. The other type of data obtained from testing were local pressure distributions (airloads test) over the entire vehicle. These data were obtained by locating pressure orifices on the outer moldline of the model and recording the sensed pressures. These data were utilized in formulating the airloads for the launch vehicle data base. As mentioned earlier, the physical limitations/complexity of the models did not permit simultaneously obtaining all the required data with a single model/test. Therefore, different type tests were conducted and their results combined to generate the data base. Mated vehicle/element plume-off force/moment and airloads test results were combined with plume-on mated vehicle/element airloads test results to obtain the launch vehicle data base. The SRB separation data base utilized only BSM plume-on and plume-off force-moment test results. Associated with each of the above type tests were peculiar generic problems and inadequacies that had to be resolved in order to establish a quality data base.

LAUNCH VEHICLE/ELEMENT/COMPONENT PLUME-OFF TESTS

Initial emphasis was placed on the mated vehicle force/moment aerodynamic characterization. To support generating the required data, wind tunnel tests utilizing a single sting support (Fig. 12) were conducted. The elements were rigidly mounted to each other with scaled attach structures thus preserving the required proximity. A single balance was located in the orbiter which measured the six aerodynamic forces and moments required by the launch vehicle data base. This single sting/base mounting arrangement was most practical and provided minimum sting effects on the forebody aerodynamic data.

As the Shuttle program matured emphasis shifted to defining the element and component aerodynamic characteristics. Wind tunnel tests, designated as IA81 and IA135, were conducted in the Ames Research Center Unitary Plan Wind Tunnel (ARC UPWT) to provide aerodynamic data supporting the integrated vehicle baseline characterization cycles 1 and 2 (IVBC-1 and IVBC-2). These tests, to obtain data for each of the elements and components in proximity, utilized a four-sting model support system (Fig. 13). Each element, which contained a balance for measuring the aerodynamic forces and moments, was mounted on a separate sting in proper proximity with the free-stream air off. The sting and balances were designed to minimize deflections considering model weight and aerodynamic load, yet, provide adequate measurement accuracy in terms of the expected aerodynamic loads on the model. However, with freestream air on the aerodynamic loading on each element caused excessive model separation. Thus, the proper interference effects of the elements on each other was not realized. And, furthermore, each element was at a different attitude relative to the freestream flow. Additionally, the presence of the ET sting and the sting support created an effect on the forebody aerodynamics. The presence of these effects was implicitly determined when the summation of the element did not equal the mated vehicle data obtained from other tests utilizing a single sting support system. The presence of these effects was further verified by a series of parametric tests conducted in the Marshall Space Flight Center's 14-in. Trisonic Wind Tunnel. The significance of these undesirable effects, except from a purist standpoint, were of little consequence to the aerodynamist. However, as structural load sensitivity studies developed,

significant impacts of small changes in the element/component aerodynamics on the vehicle's attach structure, wing design, and vertical tail design were realized. Obviously, the undesirable effects in the aerodynamic data base needed to be eliminated if possible, rather than incorporate them into uncertainties on the data.

To eliminate the above undesirable effects the ascent aerodynamic community and wind tunnel model designers established the "shell model" concept for Space Shuttle testing (Fig. 14). This concept offered two distinct advantages over previous model designs: (1) only a single sting support is required, thus eliminating the majority of the sting interference effects, and (2) permits measuring the element data simultaneously with the mated vehicle data, thus ensuring that the summation of the element aerodynamic data equals the mated vehicle aerodynamic data. This is achieved by utilizing a balance in each element and specific attachment of the element's outer moldline (OML) shells to each other via the scaled attach structures. This permits each balance to measure aerodynamic loads experienced by certain combinations of elements (i.e., the SRB balances measure SRB aerodynamics, the ET balance measures ET and SRB aerodynamics, and the orbiter balance measures the mated vehicle aerodynamics). Thus each element's aerodynamic characteristics are obtained directly through measurement (SRBs) or by subtracting appropriate balance results (orbiter and ET). This shell model concept was pilot tested using a 1 percent scale model in the ARC UPWT, and later utilized with a 2 percent model (Fig. 15) in the 16T Propulsion Wind Tunnel facility at the Arnold Engineering Development Center (AEDC) to provide a large part of the power-off data base for STS-1.

To eliminate the remaining potential sting interference effects on the orbiter forebody aerodynamic characteristics an additional model was designed utilizing the "shell model" concept (Fig. 16). This 3 percent scale model was supported by two stings through the base of each SRB and utilized a single balance in the orbiter to determine the orbiter aerodynamic characteristics. The orbiter was mounted as a shell model to the ET/SRB combination via the scaled attach structure. This model was also utilized to determine the power-off pressure distributions on the vehicle. The orbiter balance was removed and the complete vehicle instrumented with approximately 1,500 pressure orifices. This model was also tested at the AEDC 16T facility and the results constitute the remaining part of the power-off data base for STS-1.

LAUNCH VEHICLE/ELEMENT/COMPONENT PLUME-ON TESTS

Early in the Shuttle program it was anticipated that the exhaust plumes from the SSME/SRB engines would affect the aerodynamic characteristics of the vehicle. This was based on the history of rocket-powered launch vehicles and the resulting plume effect phenomena that was developed over the years. This phenomena is philosophically demonstrated in Figure 17. For a given engine/rocket motor operating at a fixed altitude and Mach number the exhaust plume phenomena vary with increasing rocket engine chamber pressure. The plume diameter is initially too small to significantly alter the forebody pressure. Thus, the primary effect is the entrainment of the base flow by the high velocity gases in the boundary of the plume and the subsequent reduction of power-off base pressure. As the plume grows in size, it begins to block the base and increase the base pressure. Ultimately, the boundary layer will separate, and a recirculating pattern will develop. For multiple engines, the plumes will impinge upon each other and deflect exhaust flow into the base. Three or more engines can reverse enough mass into the base to choke the volume enclosed by the engines. The effect of the plumes can actually increase base pressure above the power-off level.

To simulate the plumes and their effect in wind tunnel testing the ascent aerodynamics community had three basic design options available: (1) hot gas by combustion, (2) cold or warm/heated gas, and (3) solid body simulators. Hot gas testing was eliminated as a viable option when cost and complexity were considered. Additionally, the data quality for hot gas testing is limited extensively because of the short-duration of steady state flow. The use of a solid body simulator was also eliminated from consideration. Since the base environment was not known before testing, the configuration of the plume shape could not be determined to enable design of the solid body. Historically, cold gas testing had been used almost exclusively for launch vehicle plume simulation. A cold gas model can continuously be operated to obtain 70 to 100 data points per shift in the test facility. Therefore, the Space Shuttle Program Office chose this technique to determine launch vehicle plume effects because of cost and schedule effectiveness.

In 1972, NASA initiated the planning phase for the first wind tunnel test of the Space Shuttle launch vehicle (SSLV). At this time, the technical archives were surveyed to determine the appropriate rocket exhaust simulation techniques. The data accumulated through experience with the Saturn launch vehicle were chosen for study. A comparison of the wind tunnel predictions with the Saturn flight data indicated a deficiency in the technology at that time. The base drag was substantially overestimated by the predictions from wind tunnel testing. The surveys concluded that the simulation techniques and the simulation parameters were not well understood. Therefore, the aerodynamic community was challenged to better understand the flow phenomena and develop a set of simulation parameters for use in wind tunnel testing of the Space Shuttle launch vehicle. To this end a plume technology program was initiated by NASA.

The objective of the technology program was to determine a set of functions that would correlate base pressure data generated by wind tunnel cold gas tests with full scale flight base pressure. An empirical data base was obtained using generic models with some geometry variations to assess configuration effects on the base pressure. The key independent variables were simulated gas, nozzle geometry, and geometric configuration. Hot, warm, and cold gases were used. Simulated model nozzle area ratios and nozzle lip angles varied from test to test, assuring that internal geometry was not an explicit contributor to the correlation functions. The external configurations consisted of cone or ogive noses and cylindrical afterbodies with single or triple nozzle bases (SRB and orbiter bases respectively); and, a triple body configuration to assess the effects on a centerbody (similar to the external tank on the Space Shuttle). Because difficulties were encountered in correlating the plume technology test data due to limited variations in nozzle geometry and test conditions, analytical tools were utilized to supplement the data base.

The substantial empirical and analytical data base generated throughout this technology program was then analyzed for correlation by plotting the base pressure data as a function of reasonable candidate simulation parameters. The successful simulation parameters were those that would coalesce the base pressure data to a simple function of the assumed simulation parameter. As the technology program developed, the plume simulation correlation parameters matured from the simple parameters defining plume shape to a function based on shape and gas dynamic characteristics. The final simulation parameter developed through the technology program has the form:

$$\frac{M_j \, \delta_j}{M_{e_x}{}^{a} \, \gamma_j{}^{b}}$$

This final "winning" set of simulation parameters is demonstrated in Figure 18 along with a definition of terms. The caveat, however, is that neither the hot gas technology test nor the hot gas analytical data agree with this simulation. In other words, this simulation correlated the cold/warm gas data but an apparent temperature function, $(T_c/T_{t_\infty})^c$, needed to be included to fully correlate the data. These data came too late to impact any Space Shuttle testing prior to the first flight due to program schedule and resource restrictions. However, indications were that the exclusion of the temperature function would result in an overprediction of the flight base drag and, consequently, an underestimate of vehicle performance resulting in a conservative design. The current status of the technology program is best described as "terminated incomplete." The technology program, however, yielded substantial knowledge on how to correlate the cold gas base pressure and, therefore, advanced the state-of-the-art.

Not only did the definition of the simulation parameters have to be addressed, but also the application of the required simulation in the wind tunnel had to be established. Unfortunately, the key to the technique of base pressure correlation is that the simulation parameters are a function of the base pressure itself. For example, δ_j and M_j are dependent on the Prandtl-Meyer expansion at the nozzle lip and, therefore, proportional to the base pressure and the square root of the base pressure, respectively. Consequently, if the base pressure is not known a priori, the correct simulation in the wind tunnel is impossible to establish. The technique that evolved from the plume technology program and the early SSLV tests to circumvent this problem is as follows:

1. Model nozzles are designed, using analytical tools, to provide a range of similarity parameters for a test.

2. For a fixed Mach number, a variation of the base pressure is obtained through a variation of the model's SSME and SRB chamber pressures via the auxillary high pressure air supply.

3. The variation of the base pressure from the wind tunnel test is plotted as a function of the simulation parameter. See curve A in Figure 19.

4. A similar curve can be analytically derived for the full scale prototype by assuming a base pressure (curve B, Fig. 19). This curve represents the loci of possible values of the similarity parameters for the prototype as a function of base pressure.

5. Where the curve of prototype possibilities is equal to the wind tunnel test data, the similarity is matched, and the resulting base pressure is the design value.

The SSLV test data were acquired in the ARC UPWT. This facility developed the capability to supply secondary air flow at a rate of 1500 psi and 80 lb/sec for Shuttle propulsion system simulation. In Figure 20 the model is shown installed in the UPWT 11-ft test section. Note the model support structure required to supply the high pressure air for plume simulation and an enclosure for the instrumentation

leads from the model. As mentioned earlier, this support structure, due to its interference effects on the forebody, dictated that only incremental effects of the plumes could be utilized. Balances were utilized in the orbiter wing, elevons, and vertical tail to provide incremental force/moment data for the components. Additionally, the entire vehicle was instrumented with pressure orifices to provide the incremental plume effects on the pressure distributions. The results from this type test were combined with plume-off data, determined from other tests, providing a complete plume-on launch vehicle data base.

SRB SEPARATION TESTS

Basic wind tunnel testing of separating bodies was recognized as a complex operation early in the Shuttle program. In fact, if the bodies have significantly different flight path angles, wind tunnel testing cannot be performed to adequately simulate the combined flowfield of the bodies. This is because the wind tunnel, with its inherent axial flow, provides only a single fixed flight path angle for all bodies. The addition of booster separation motor (BSM) plume simulation further complicated the testing by providing a high energy disturbance to the flowfield. Fortunately, the SRB flight path angle was not significantly different from the Orbiter/ET flight path angle during the initial phases of separation. Therefore, the error in attitude and consequent flowfield development was small and represented no stumbling block to SRB separation testing. However, determining the correct BSM plume simulation to provide the required vehicle flowfield and plume impingement effects on the OET represented a challenge to the aerodynamicist.

The requirement of correct BSM simulation manifests itself in the need to simulate the near-field jet interaction (JI) effects on the SRB aerodynamic characteristics, and the need to simulate the far-field spacial content of the plume (jet) impingement forces on the OET (Fig. 21). Early in 1973 the planning for the first SRB separation test was initiated. At this time a literature survey was conducted to retrieve all possible information relative to the effects of jet emission normal to freestream flow. The results of the survey indicated that the similarity parameter for near-field simulation of a transverse firing single jet was the ratio of jet-to-freestream momentum flux, $\bar{q}_j/\bar{q}_\infty$. Plume interaction with a freestream crossflow, as depicted in Figure 22, was then defined by the following empirical relationship for Mach disk height:

$$h_{MD} = \left[\frac{2\left(1+\frac{\gamma_j-1}{2}M_j^2\right)}{\gamma_j^2 M_j(\gamma_j+1)}\right]^{0.25}\left[\frac{1.25(1+\gamma_\infty)\gamma_\infty M_\infty^2}{(1-\gamma_\infty)+2\gamma_\infty M_\infty^2}\right]^{0.5}\left[\frac{\bar{q}_j}{\bar{q}_\infty}\right]^{0.5}\left|\frac{d_j}{(1+\cos\theta_j)}\right|$$

The far-field jet impingement pressure similarity parameters were, intuitively, momentum flux ratio and plume diameter at the point of impingement some distance from the jet (Fig. 22).

It was also found that plume gas temperature and molecular weight affect jet/flowfield interaction by strongly influencing the external flow separation distance upstream of the nozzle for low molecular weight or high temperature transverse jets. This effect is correlated by the "RT" ratio as follows:

$$\tau = \frac{(RTo)j}{(RT)_\infty} = \frac{(To/MW)j}{(T/MW)_\infty}$$

"RT" simulation provided the rationale for using air as the injectant gas in wind tunnel plume testing. Findings from the survey indicated that "RT" effects are negligible for $\tau < 7$. Since the values for flight ($\tau = 2.91$) and test with air ($\tau = 4.6$) are below this limit, unheated air was selected to simulate the BSM exhaust product plume.

Even though these similarity parameters were developed from single jet data, they were utilized for the multijet case in the early phases of SRB separation testing. At this stage of separation system development, the BSM configuration was four motors in line rather than abreast as shown in Figure 5. The forward motors were located further aft (SRB forward skirt) and the rear motor exit planes pointed toward the orbiter body flap rather than in an aft direction. Their angular orientation directed the plumes more toward the orbiter than the final configuration shown in Figure 5 (i.e., 30 deg and 20 deg rather than 20 deg and 40 deg, respectively). Results from these tests indicated significant flowfield changes and impingement pressures on the sensitive orbiter TPS tiles. To verify and expand the findings, analytical tools were utilized to reproduce the test generated plume characteristics and a separation motor technology program was initiated at the Marshall Space Flight Center. The technology program verified the simulation parameters and added insight into the relationship between the flowfield of single jets and mutliple jets. Utilizing the developed analytical tools, sensitivity studies were

performed for various alternate BSM configurations and orientations in an effort to relieve the impingement effects on the orbiter. The final BSM orientation (Fig. 5) resulted from these studies. Along with the relocation/orientation of the BSMs their thrust was increased and burn time decreased. This reduced the time that the massive complex jet/flowfield interaction would take place and still provide adequate impulse to the SRB to avoid recontact.

As plans for testing of the final BSM configuration developed, it was realized that scaling $\bar{q}_j/\bar{q}_\infty$ was no longer possible. The increased thrust required a plume gas air supply pressure (1500 psi) that exceeded the facility's capability and the small nozzle sizes required (1/32-in. throat diameter) became prohibitive. As a result, jet-to-freestream momentum ratio (ϕ_j/ϕ_∞) was selected over $\bar{q}_j/\bar{q}_\infty$ as the plume scaling parameter. This choice preserved the geometric scaling of h_{MD} but removed any dependence on nozzle size, d_j:

$$h_{MD} = \left[\frac{2(1+\frac{\gamma_j-1}{2}M_j^2)}{\gamma_j^2 M_j(\gamma_j+1)}\right]^{0.25}\left[\frac{1.25(1+\gamma_\infty)\gamma_\infty M_\infty^2}{(1-\gamma_\infty)+2\gamma_\infty M_\infty^2}\right]^{0.5}\left[\left(\frac{4S_{REF}}{\pi}\right)\left(\frac{\phi_j}{\phi_\infty}\right)\right]^{0.5}\left\langle\frac{1}{1+\cos\theta_j}\right\rangle$$

Using momentum ratio scaling, nozzle throat size was doubled to minimize the chance of nozzle plugging (a problem encountered in early testing) and the chamber pressure was reduced to within plant gas supply limits. Model nozzle area ratio was adjusted to obtain a good match of plume cross-sectional area and hence proper simulation of the blockage associated with flowfield interaction effects. Utilizing the momentum ratio similarity parameter induced errors into the wind tunnel test results. However, an estimate of the uncertainty in SRB aerodynamic characteristics was appropriately evaluated by comparing test and flight data available from a military missile which utilized a transverse jet for attitude control. These uncertainties were included in the separation aerodynamic data base.

All testing used to define the SRB separation aerodynamic data base was conducted in the U.S. Air Force Arnold Engineering Development Center/Von Karman Facility Tunnel "A" using a 1 percent scale model of the Space Shuttle vehicle. This facility was selected because of its efficient captive trajectory system (CTS) which provides rapid computerized movement of models in the tunnel without interrupting the primary tunnel air flow.

In BSM plume-on testing, the orbiter/ET was placed on the CTS sting and the two SRBs were placed on a specially designed screw-jack adapter to the primary sting. This adapter allowed automatic movement of the SRBs in the yaw plane but required manual placement in pitch. The BSM plume-on test installation is shown in Figure 23a. Separate lines were provided to supply plume air to plenum chambers for the forward and aft nozzle clusters in each SRB. The forward clusters were fed by air flowing through the balances. Care was taken to balance the plenum chamber pressures between forward and aft jets and between left and right SRBs by means of orifice meters in the individual supply lines. In plume-on testing, previous experience has shown that it is necessary to account for SRB-to-SRB BSM plume induced flow interference as well as for the mutual coupling of the SRBs plume interference effects on the flowfield surrounding the OET. Hence, the use of both SRBs is required.

In plume-off testing, a single SRB was mounted on the CTS and moved through the hypercube matrix of points representing relative positions and attitudes of the SRB with respect to a fixed OET. The model installation is shown in Figure 23b. Although forces and moments were measured on both models, axial force and rolling moment were not measured on the SRB. The SRB model was equipped with a flow-through balance for use in plume-on testing making it impossible to measure axial force with any degree of accuracy. Rolling moment was also eliminated from the balance readings since it is negligible as a result of SRB body symmetry. Previous plume-off test experience indicated that SRB-to-SRB effects are minimal and that SRB effects on the orbiter/ET are additive, thus justifying the use of a single SRB test procedure.

The final SRB separation verification test was conducted at AEDC in March 1982 and provided the data for the current data base. This test culminated a complex wind tunnel test program to define the aerodynamics associated with SRB separation.

CONCLUDING REMARKS

The challenges to the ascent aerodynamic community documented in this paper are unique due to the aerodynamic complexity of the Shuttle's ascent flight. Never before has such a complex vehicle been aerodynamically characterized.

The initial optimization challenge was met by providing a parametric aerodynamic data base which allowed configuration optimization from an aerodynamic standpoint.

The challenge to aerodynamically characterize the vehicle with math modeling methodologies to support vehicle design and flight planning studies was innovatively met. Techniques for combining the results of several wind tunnel tests were developed which minimized model support system effects in the launch vehicle data base. A unique and effective modeling approach was developed to handle the large and complex SRB separation aerodynamic data base.

The challenge to develop testing techniques to improve the quality of initial wind tunnel test results was successfully met. Parametric wind tunnel tests and analyses were conducted to determine model support system effects on vehicle aerodynamics. The resulting optimum models and support system were designed and utilized. Comprehensive plume technology programs were conducted which established simulation parameters permitting the use of high pressure air to simulate engine exhaust plumes and high energy forward facing jet effects.

The unique and innovative engineering approaches/techniques developed to meet the aerodynamic challenges imposed by the complex Shuttle configuration and ascent flight have resulted in quality aerodynamic data bases. The success of the Shuttle ascent aerodynamic development program is exemplified by the successful STS program.

REFERENCES

1. Craig, M. K., NASA JSC; and Dresser, H. S., Rockwell International Corp.: Shuttle Booster Separation Aerodynamics. NASA Langley Research Center's Shuttle Lessons Learned Conference. 1983.

2. Roberts, B. B. and Wallace, R. O., NASA JSC; and Sims, J. L., Georgia Institute of Technology-Huntsville, AL: Plume Base Flow Simulation Technology. NASA Langley Research Center's Shuttle Lessons Learned Conference. 1983.

3. Hamilton, J. T., Rockwell International Corp.; Wallace, R. O., NASA JSC; and Dill, C. C., NASA MSFC: Launch Vehicle Aerodynamic Data Base Development and Comparison with Flight Data. NASA Langley Research Center's Shuttle Lessons Learned Conference. 1983.

4. Space Shuttle Aerodynamic Design Substantiation Report, Vol. 2 - Launch Vehicle. Rockwell International Publication SD74-SH-0206, Vol. 2K. February 1980.

SYMBOLS

A	Area
C	Coefficient
d	diameter
h_{MD}	Jet Mach disk height
M	Mach number
MW	Molecular weight
R	Universal gas constant
q	Dynamic pressure
S_{REF}	Reference area
T	Temperature
α	Angle-of-attack
β	Angle-of-sideslip
γ	Ratio of specific heats
δ	Initial expansion angle of gas
θ	Lip angle
Δ	incremental value
ϕ	Momentum

SUBSCRIPTS

A	Axial force
B	Base; bending moment
C	Chamber
E	Exit
e	Elevon
f	Forebody
H	Hinge moment
i	Inboard elevon
j	Plume boundary
l	Rolling moment
m	Pitching moment
n	Yawing moment
N	Nozzle
O	Outboard elevon
P	Pressure
S	Shear force
t	Torsion moment
V	Vertical tail
W	Wing
Y	Side force
x,y,z	Displacement of SRB from mated position
(∞)	Freestream

SUPERSCRIPTS

a,b,c	Undetermined exponents, functions of geometric configuration

TABLE 1: LAUNCH VEHICLE AERODYNAMIC DATA BASE FORMULATION

TYPE OF DATA	FORMULATION
MATED VEHICLE FOREBODY STATIC STABILITY	o MACH = 0.6, 0.8, 0.9, 0.95, 1.05, 1.10, 1.15, 1.25, 1.40, 1.55, 1.80, 2.2, 2.5, 3.5, 4.5 o α/β = -8° → +4°/-6° → +6°, Δ = 2° o ELEVON SETTINGS = MATH MODELED VIA 4TH ORDER POLYNOMIAL FIT OF DATA VARIATIONS WITH INB'D & OUTB'D SETTINGS.
ELEMENT FOREBODY STATIC STABILITY (ORB, ET, LSRB, RSRB)	o MACH = SAME AS ABOVE o α/β = SAME AS ABOVE o ELEVON SETTINGS = 9 DISCRETE INB'D/OUTB'D COMBINATIONS FOR EACH MACH.
COMPONENT STATIC STABILITY (WING, ELEVONS, V. TAIL)	SAME AS FOR ELEMENTS
POWER-ON BASE FORCE/MOMENT (ORB, ETC, LSRB, RSRB)	o ALT = 0 → = 200,000 FEET o MATH MODELING INCLUDED TO ACCOUNT FOR α/β AND SSME POWER LEVEL EFFECTS
ELEMENT/COMPONENT PRESSURE DISTRIBUTIONS	o SAME AS FOR ELEMENTS/COMPONENTS ABOVE o $C_p = f(x,y,z,\phi)$

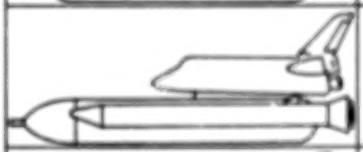
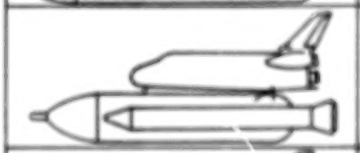
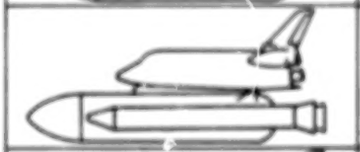
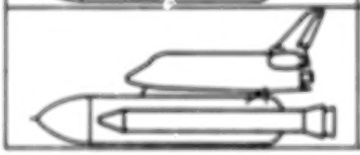
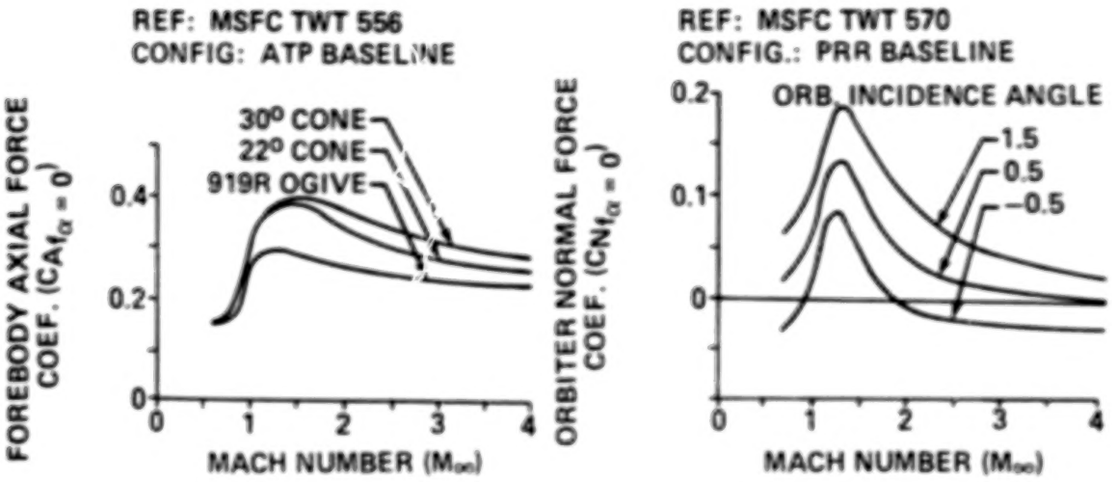
CONFIGURATION	VEHICLE	ORBITER		EXTERNAL TANK	SOLID ROCKET BOOSTERS
		LOCATION AND INCIDENCE	DESIGN EFFECTS	SIZE AND NOSE SHAPE	SIZE, LOCATION AND NOZZLE DESIGN
	ATP (3/4/72)	•972 IN. AFT OF ET NOSE •-1.2° INCID.	• STRAIGHT WING T. E.	•318 IN. DIA. •30° NOSE CONE	•156 IN. DIA. •SRB NOSE FWD OF ET SHOULDER •LARGE CANT NOZZLE •NO TVC
	PRR (10/24/72) MCR 0026	1063 IN. AFT OF ET NOSE +0.5° INCID.	• ASRMS REMOVED • OMS PODS MOVED TO SHOULDER • SWEPT T. E.	•304 IN. DIA. •OGIVE NOSE W/RETRO PKG	•162 IN. DIA. •SRB NOSE AT ET SHOULDER •PRE-CANT REDUCED •TVC ADDED
	2A (12/22/72) MCR 0074	•768 IN. AFT OF ET NOSE	• INCREASED NOSE RADIUS	•324 IN. DIA.	•142 IN. DIA. •SRB AFT OF ET SHOULDER •REDUCED AFT SKIRT FLARE •NO PRE-CANT
	3, 3A MCR 0200 (5/73)	• 680 IN. AFT OF ET NOSE	• REDUCED WING INCID. • BODY 38 IN SHORTER • DECREASED NOSE RADIUS	•324 IN. DIA. •REMOVED RETRO	•142 IN. DIA. •DECREASED AFT SKIRT SIZE •7:1 NOZZLE •INLINE SEP. MTRS.
	4, 5 MCR 3570		• BLUNT OMS PODS • UNCOVERED RCS PORTS	•333 IN. DIA. •BICONIC AADS	•ATTACH RING AREA REDUCED •ELIMINATED 2 OF THE 4 HOOP STRESS RINGS •4 ABREAST SEP MTRS

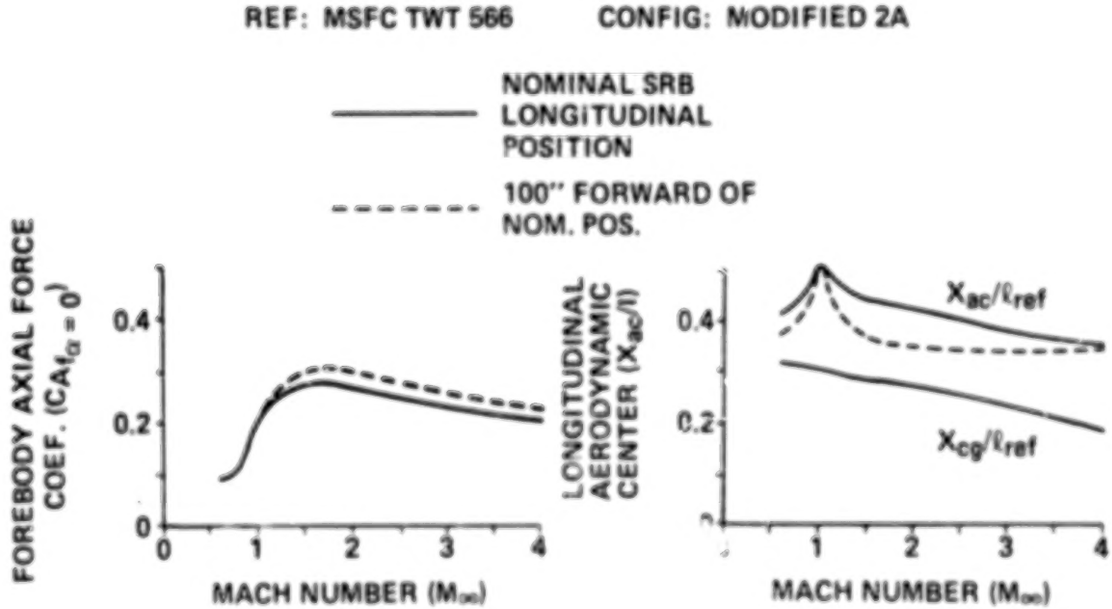
Figure 1. Space Shuttle Design Evolution.



(a) EFFECT OF ET NOSE SHAPE ON LAUNCH VEHICLE AXIAL FORCE

(b) EFFECT OF ORBITER INCIDENCE ANGLE ON ORBITER NORMAL FORCE

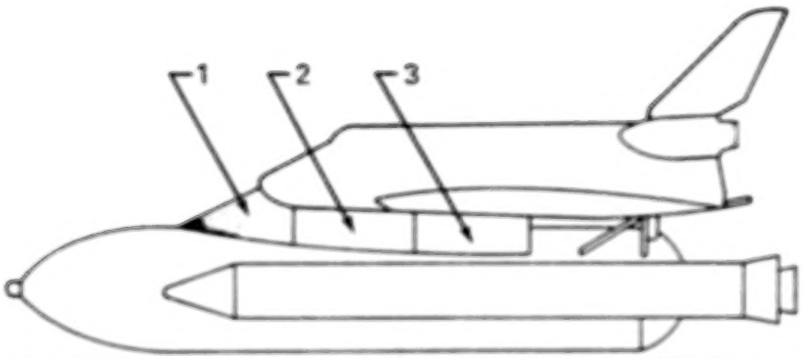
S_{ref} = 2690 FT^2
ℓ_{ref} = 1328 IN.
MRP = ORB. NOSE ON ET CENTERLINE



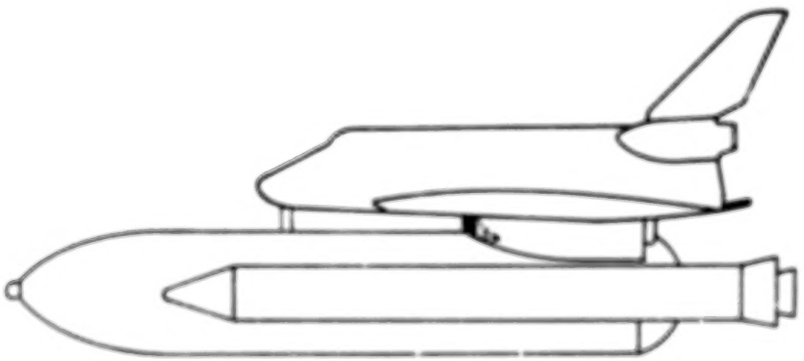
(c) EFFECT OF SRB LONGITUDINAL POSITION ON LAUNCH VEHICLE AXIAL FORCE

(d.) EFFECT OF SRB LONGITUDINAL POSITION LAUNCH VEHICLE PITCH STABILITY

Figure 2. Typical Results of Parametric Configurational Studies.

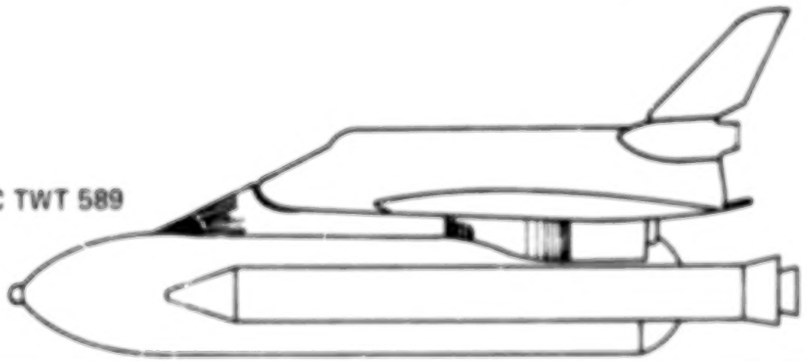


MACH NUMBER		.6	.9	1.2	3.48	4.96
% DECREASE IN FOREBODY DRAG	1	−1.0	−2.3	−1.6		
	1, 2	0	−1.0	1.3		
	1, 2, 3	9.4	7.5	5.9		



MACH NUMBER	.6	.9	1.2	3.48	4.96
% DECREASE IN FOREBODY DRAG	9.9	5.5	3.0	−1.0	0

REF: MSFC TWT 589

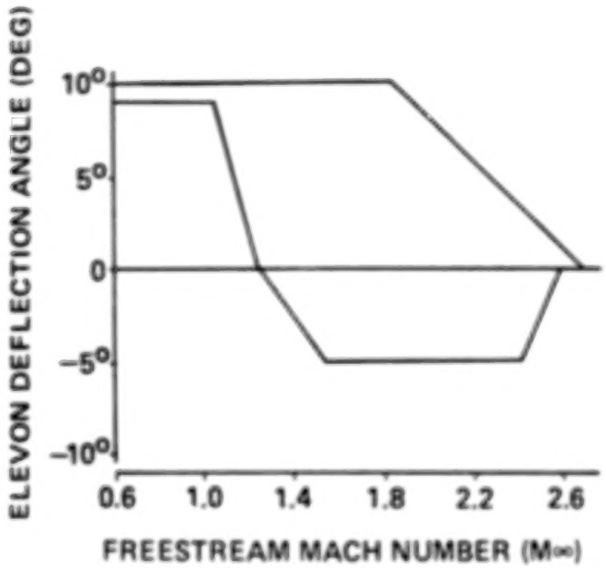


MACH NUMBER	.6	.9	1.2	3.48	4.96
% DECREASE IN FOREBODY DRAG	14.0	7.6	5.8	3.8	2.1

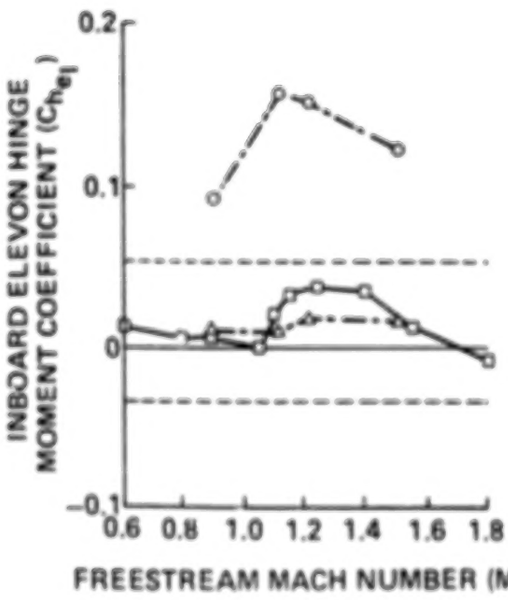
Figure 3. Aerodynamic Fairing Concepts for Launch Vehicle Drag Reduction.



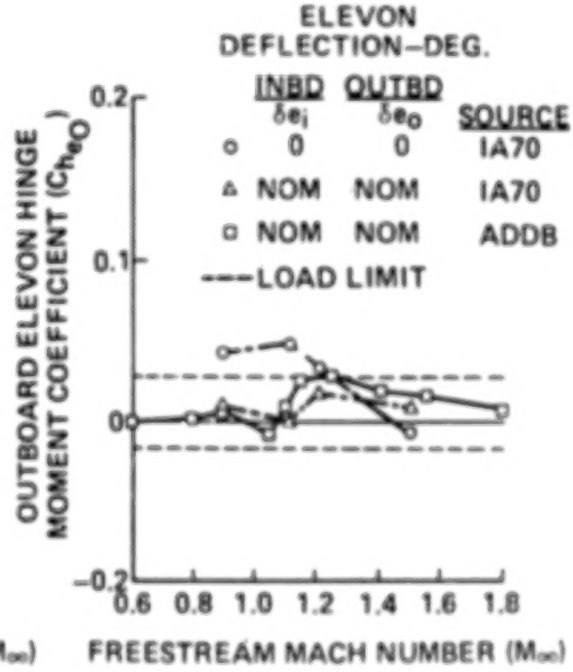
(a) SIGN CONVENTION



(b) ELEVON DEFLECTION SCHEDULE



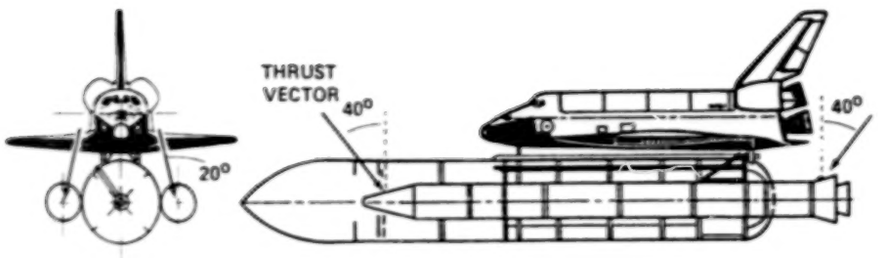
(c) INBOARD HINGE MOMENT COEFFICIENT



(d) OUTBOARD HINGE MOMENT COEFFICIENT

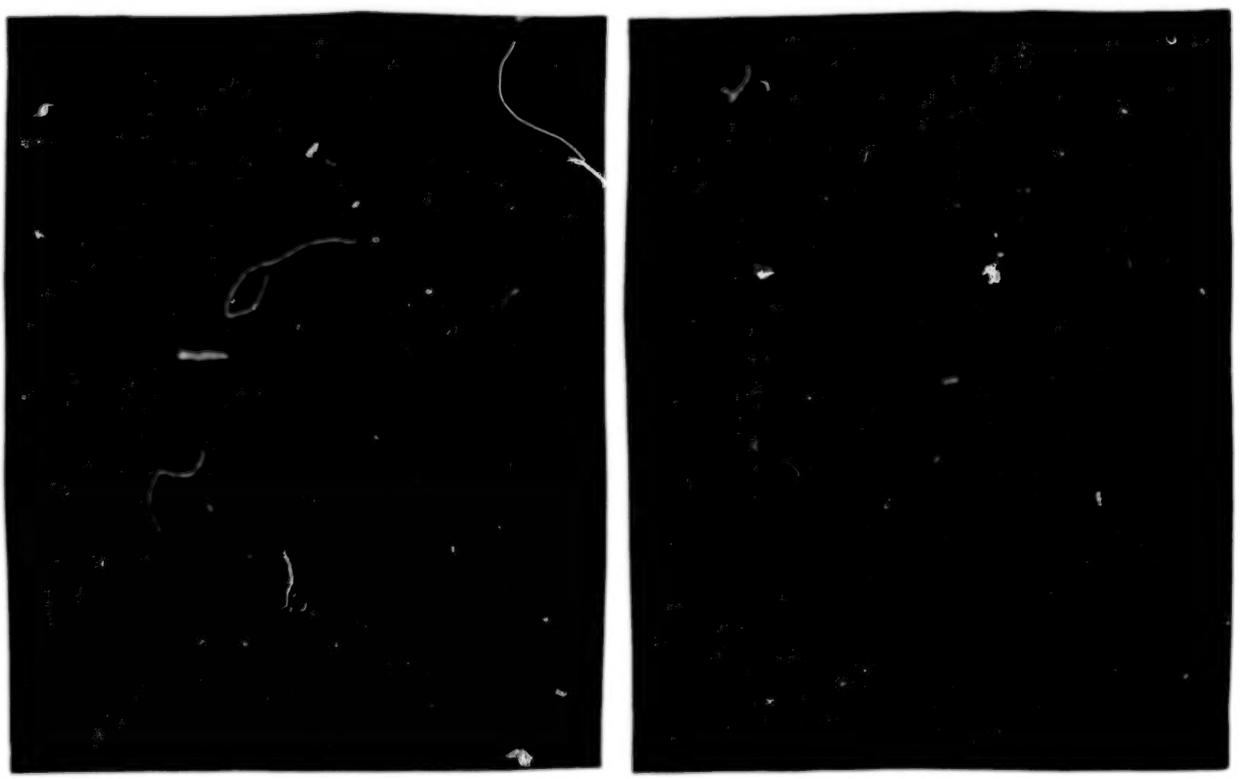
Figure 4. Ascent Elevon Deflection Schedule Requirement.

ORIGINAL PAGE IS
OF POOR QUALITY



- FOUR BSMs FORWARD AND FOUR AFT
- PERFORMANCE
  - WEB ACTION TIME ~ 0.68 SECONDS
  - VACUUM THRUST/MOTOR ~ 21,000 POUNDS
  - AVERAGE OPERATING PRESSURE = 1700 PSI

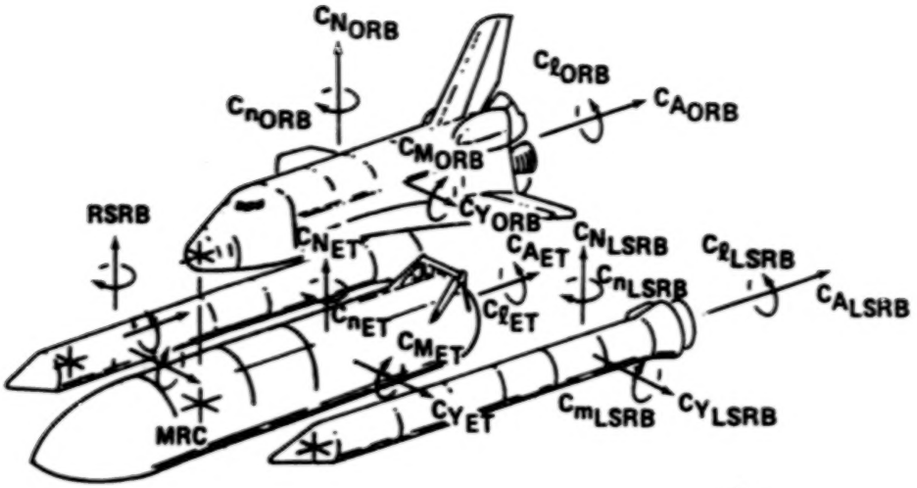
Figure 5. Booster Separation Motor Orientation.



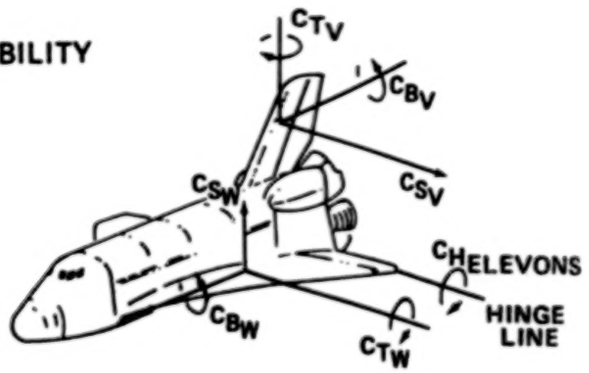
(a) BSM-Off (b) BSM On

Figure 6. Effect of BSM on Shuttle Flowfield, M_∞ = 4.5, AEDC/VKF Tunnel A.

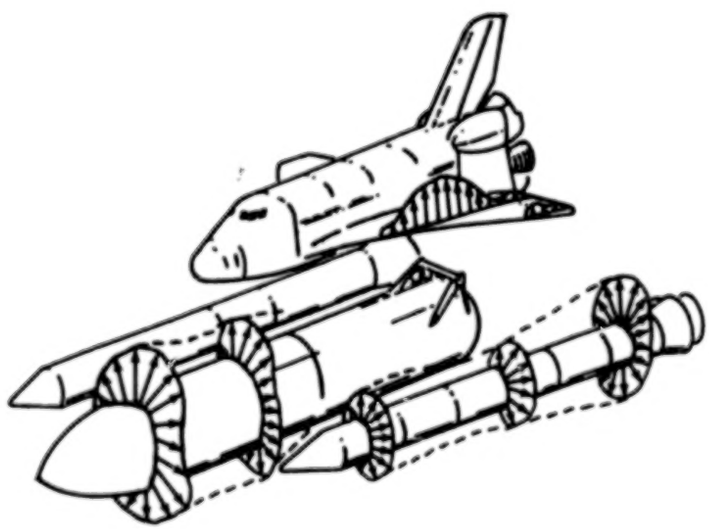
C-3



ELEMENT STATIC STABILITY

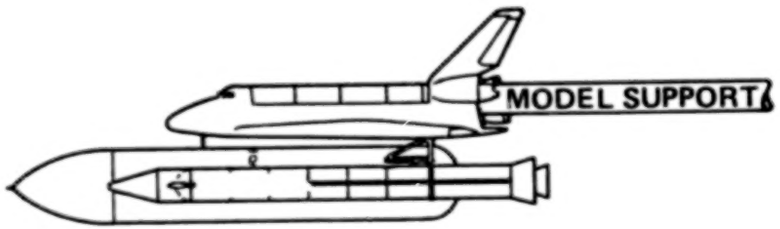


COMPONENT STATIC STABILITY

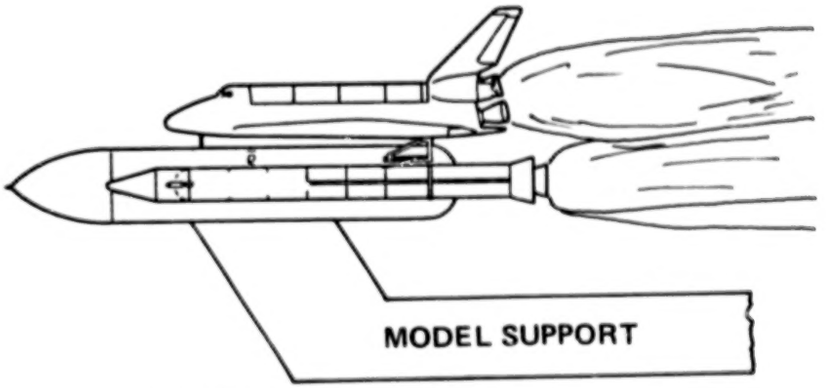


PRESSURE DISTRIBUTIONS (AIRLOADS)

Figure 7. Launch Vehicle Aerodynamic Data Base.



WIND TUNNEL TEST Ⓐ



WIND TUNNEL TEST Ⓑ

IN GENERAL,

$$C_{X_{TOTAL}} = \left(C_{X_{f_{P-OFF}}} + \Delta C_{X_{f_{DUE\ TO\ PLUMES}}}\right)_{FOREBODY\ P-ON} + C_{X_{BASE\ P-ON}}$$

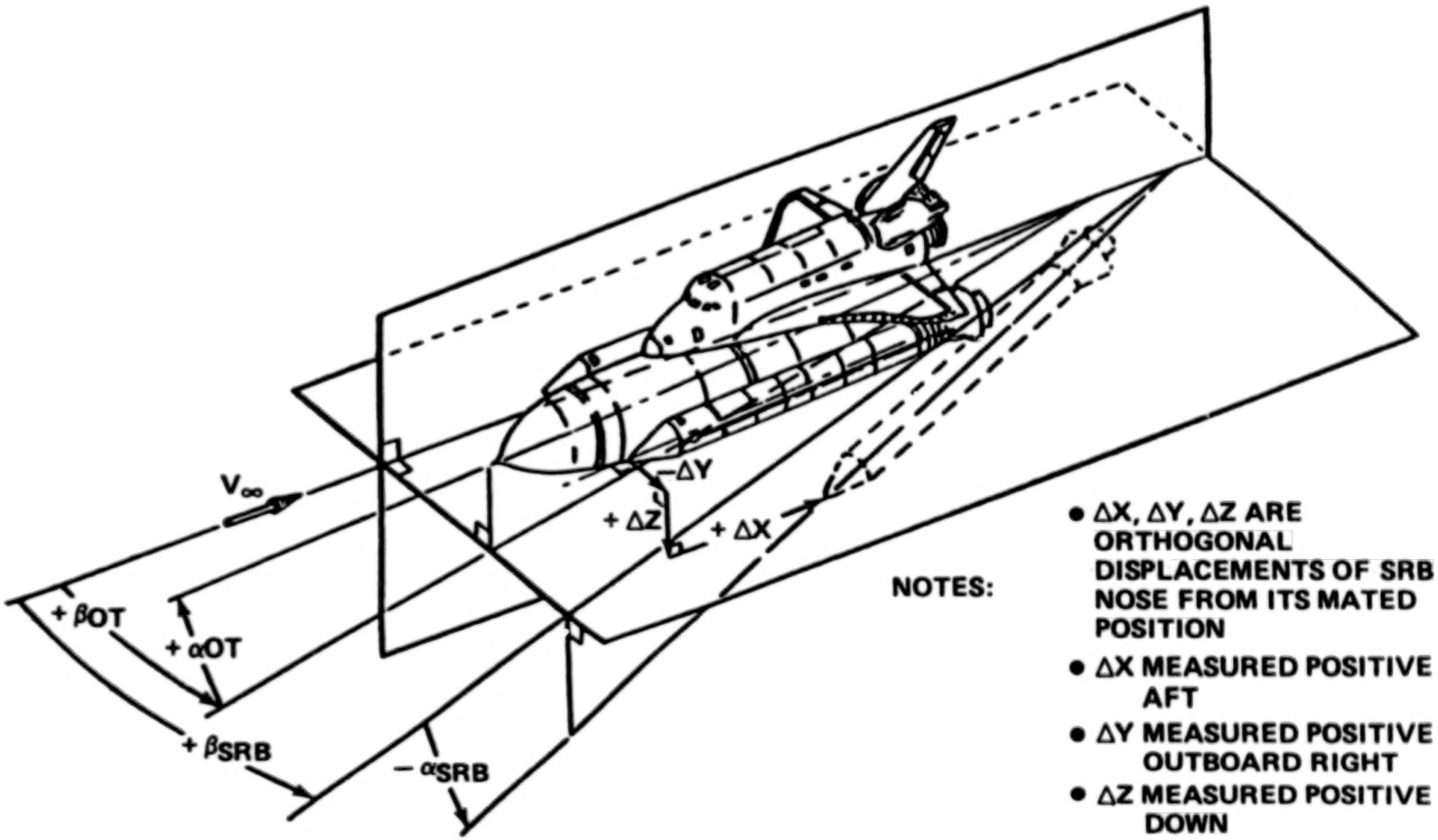
$$C_{X_{f_{P-OFF}}} = \left(C_{X_{TOTAL}} - C_{X_{BASE}}\right)_{P-OFF} \quad (\text{Ⓐ})$$

$$C_{X_{BASE\ P-OFF}} = \frac{1}{gS_{ref}} \int (P_B - P_\infty)\, d(A_B) \quad (\text{Ⓐ})$$

$$C_{X_{B_{P-ON}}} = \frac{1}{gS_{ref}} \int (P_{B_{P-ON}} - P_\infty)\, d(A_B) \quad (\text{Ⓑ})$$

$$\Delta C_{X_{f_{DUE\ TO\ PLUMES}}} = \frac{1}{q\,S_{ref}} \int (P_{P-ON} - P_{P-OFF})\, d(A) \quad (\text{Ⓑ})$$

Figure 8. Aerodynamic Coefficient Formulation.



NOTES:

- $\Delta X, \Delta Y, \Delta Z$ ARE ORTHOGONAL DISPLACEMENTS OF SRB NOSE FROM ITS MATED POSITION
- ΔX MEASURED POSITIVE AFT
- ΔY MEASURED POSITIVE OUTBOARD RIGHT
- ΔZ MEASURED POSITIVE DOWN
- $\Delta\alpha \equiv (\alpha_{SRB} - \alpha_{OT})$
- $\Delta\beta \equiv (\beta_{SRB} - \beta_{OT})$
- SEPARATION MOTOR JET–TO–FREESTREAM MOMENTUM RATIO IS ALSO INDEPENDENT VARIABLE

Figure 9. SRB Separation Aerodynamic Independent Variables.

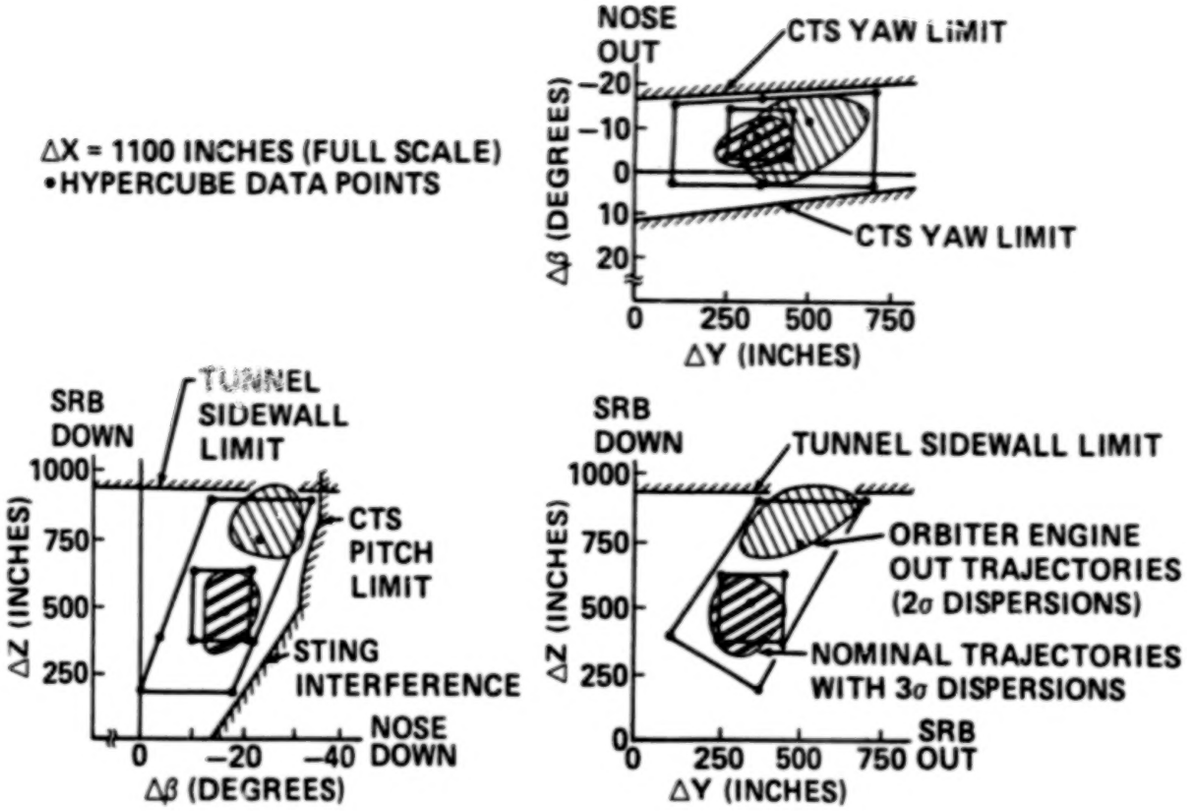


Figure 10. Trajectory Envelope Cross Section.

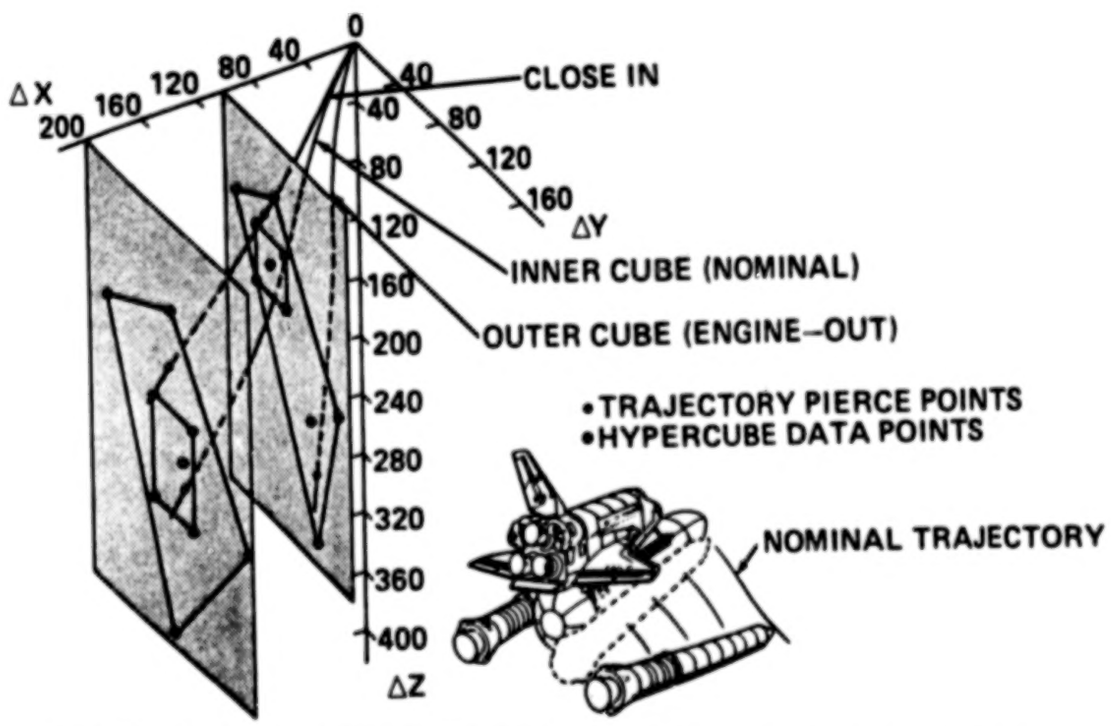


Figure 11. Typical SRB Separation Trajectories Through Hypercube Matrix (BSM Plume-On).

ORIGINAL PAGE IS
OF POOR QUALITY

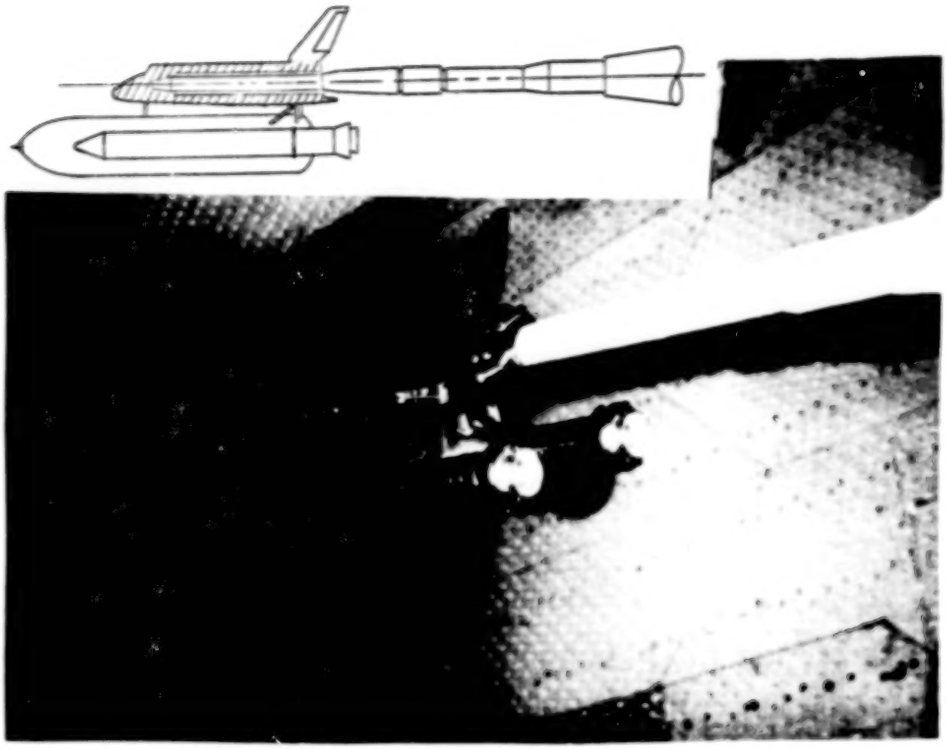


Figure 12. Single Sting/Single Balance Mounting Arrangement.

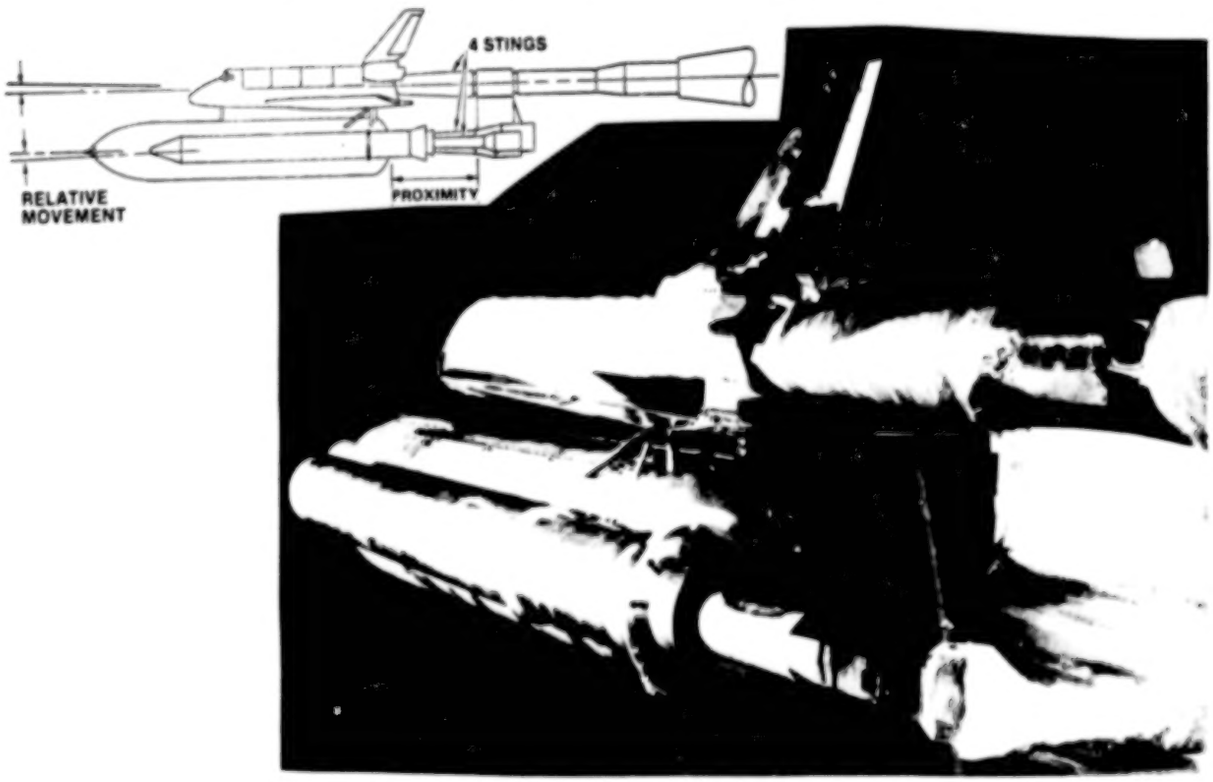


Figure 13. Model Support System for Early Element Tests.

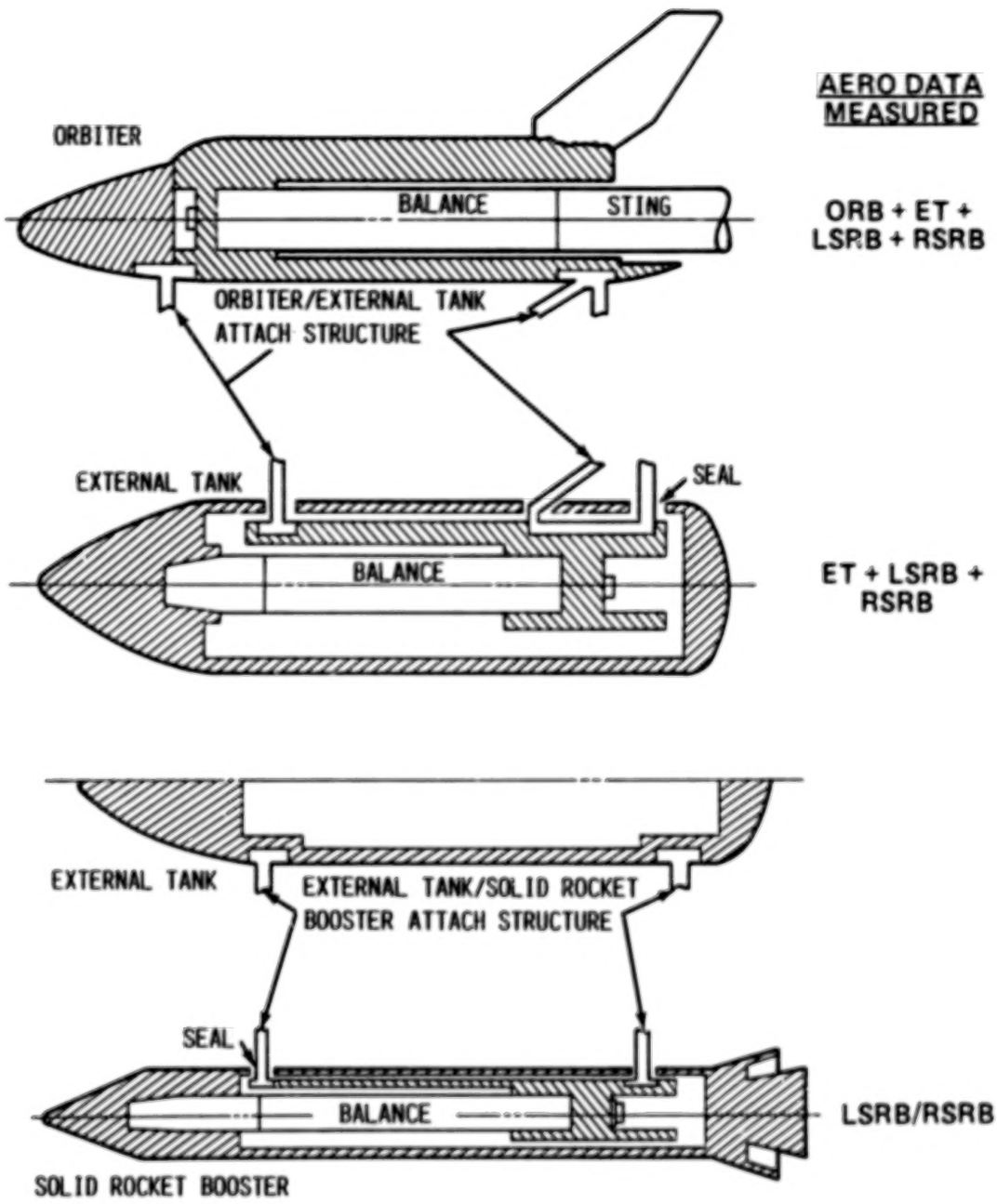


Figure 14. Single Sting/Multiple Balance "Shell Model" Concept.

ORIGINAL PAGE IS
OF POOR QUALITY



Figure 15. Single Sting/Multiple Balance Shell Model in AEDC 16T Tunnel.

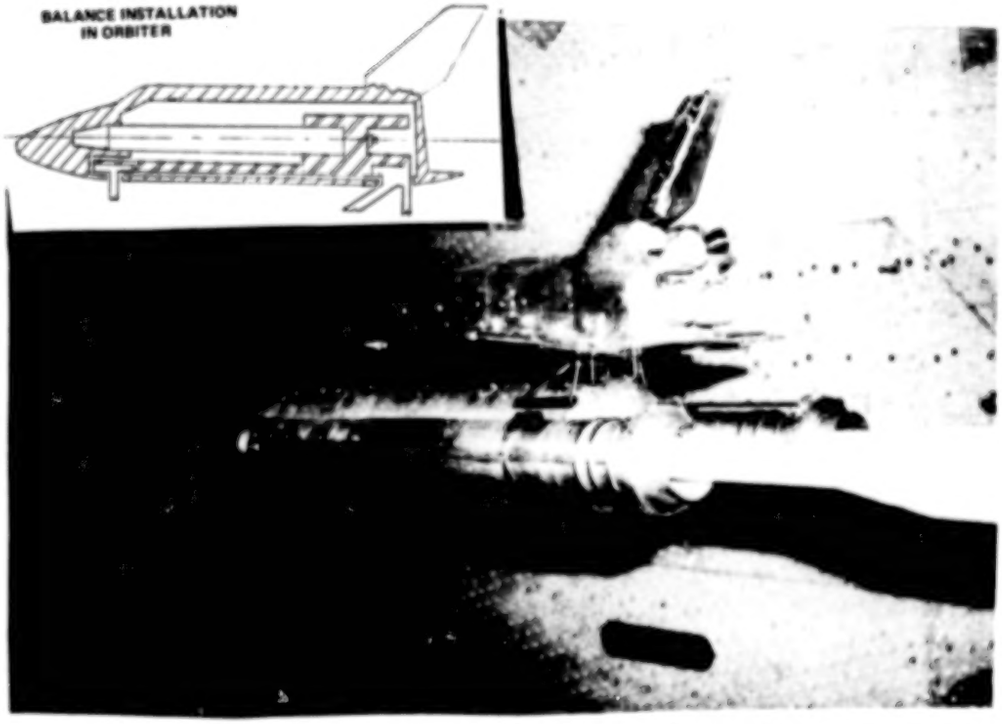


Figure 16. Dual Sting/Single Balance Shell Model in AEDC 16T Tunnel.

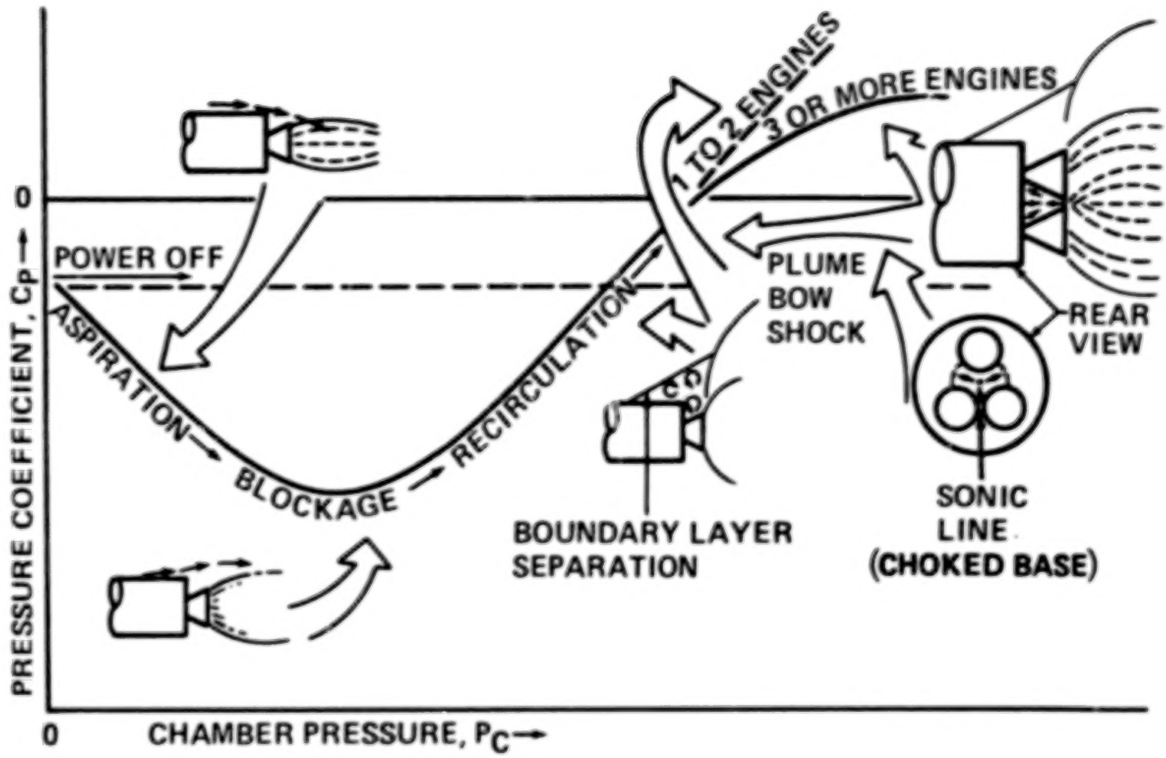


Figure 17. Base Flow-Exhaust Plume Phenomena.

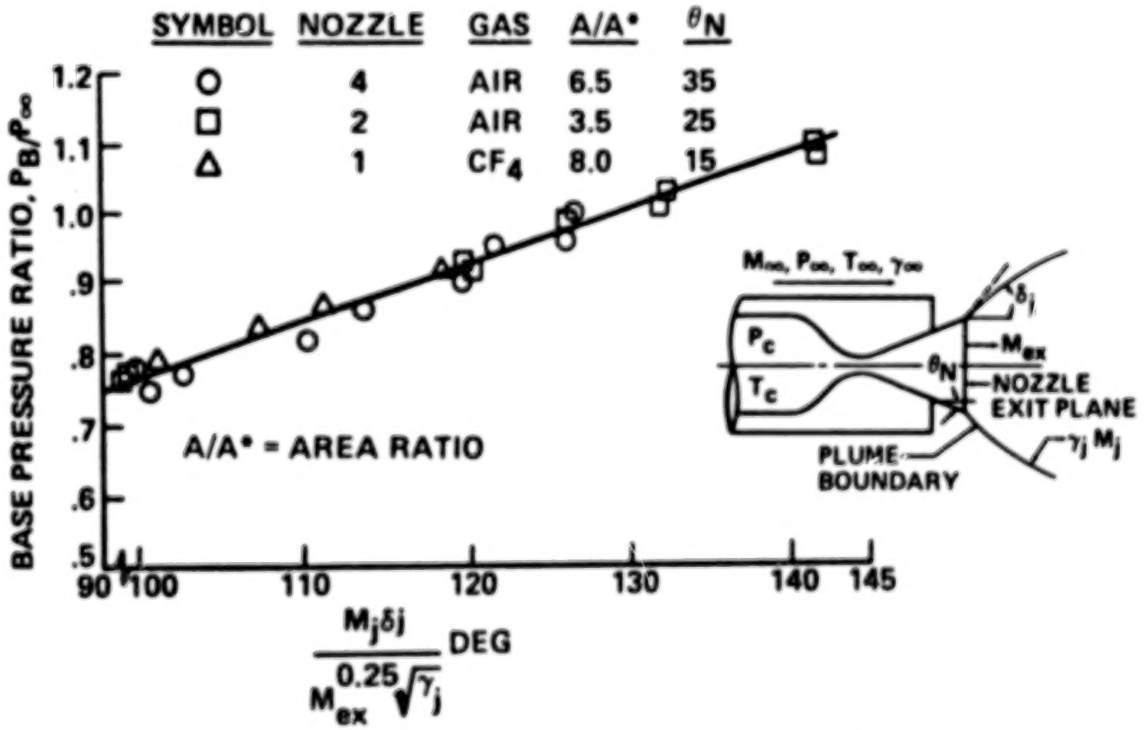


Figure 18. Example of a Successful Simulation Parameter; Cone-Cylinder Geometry.

ORIGINAL PAGE
OF POOR QUALITY

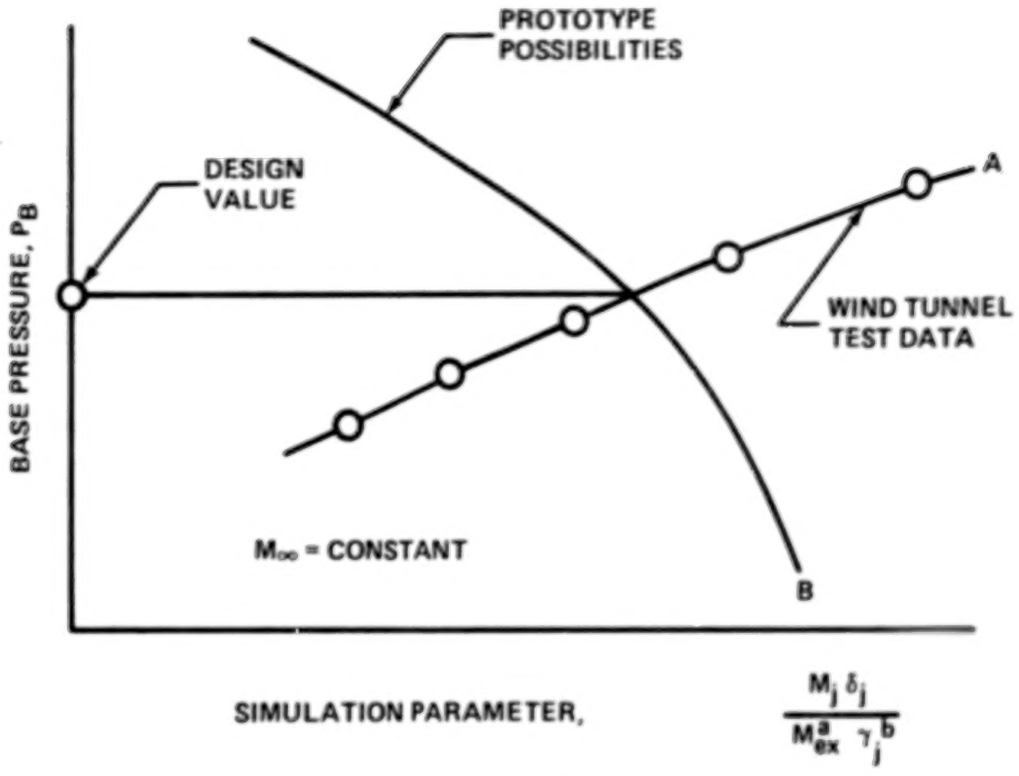


Figure 19. Application of Plume Simulation Parameters to Wind Tunnel Testing.

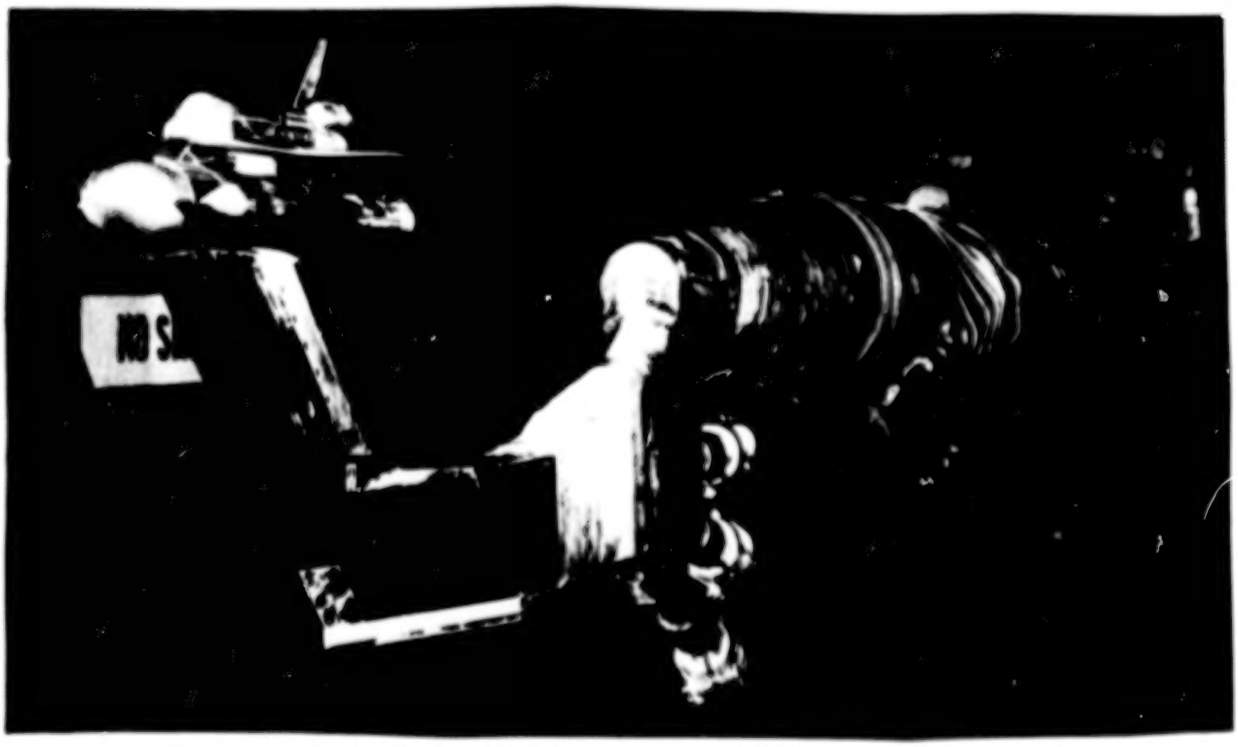


Figure 20. Launch Vehicle Plume Test Model in ARC UPWT.

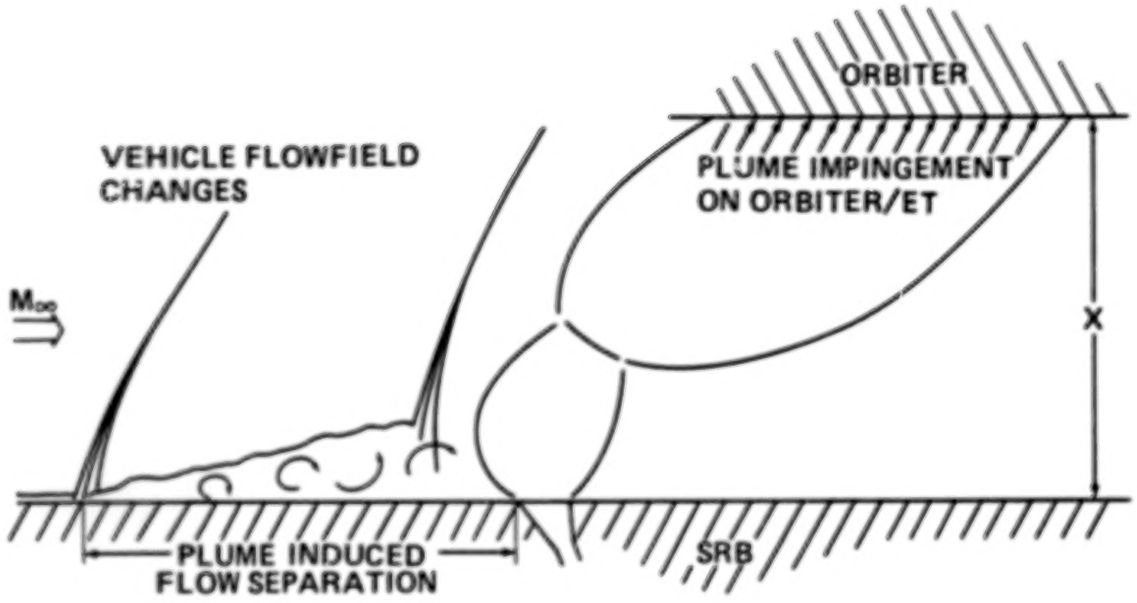
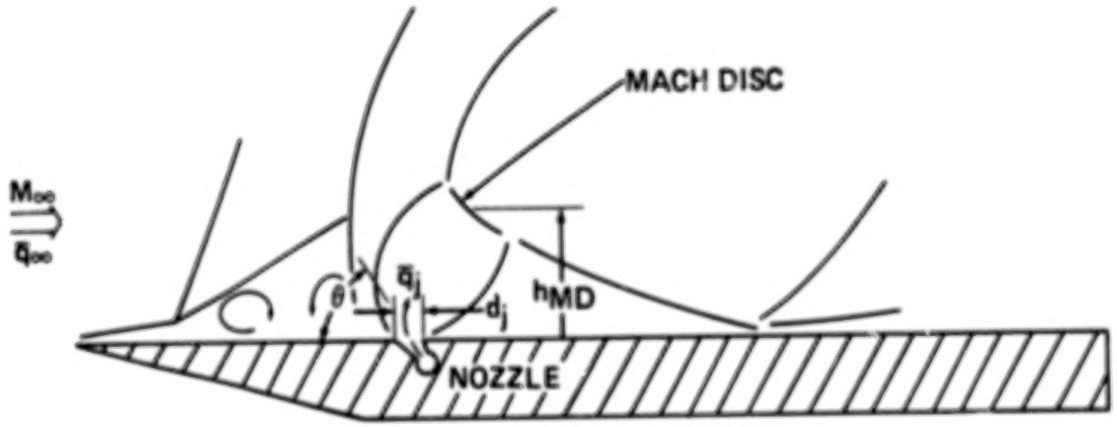


Figure 21. Schematic of BSM Plume Simulation Requirements.



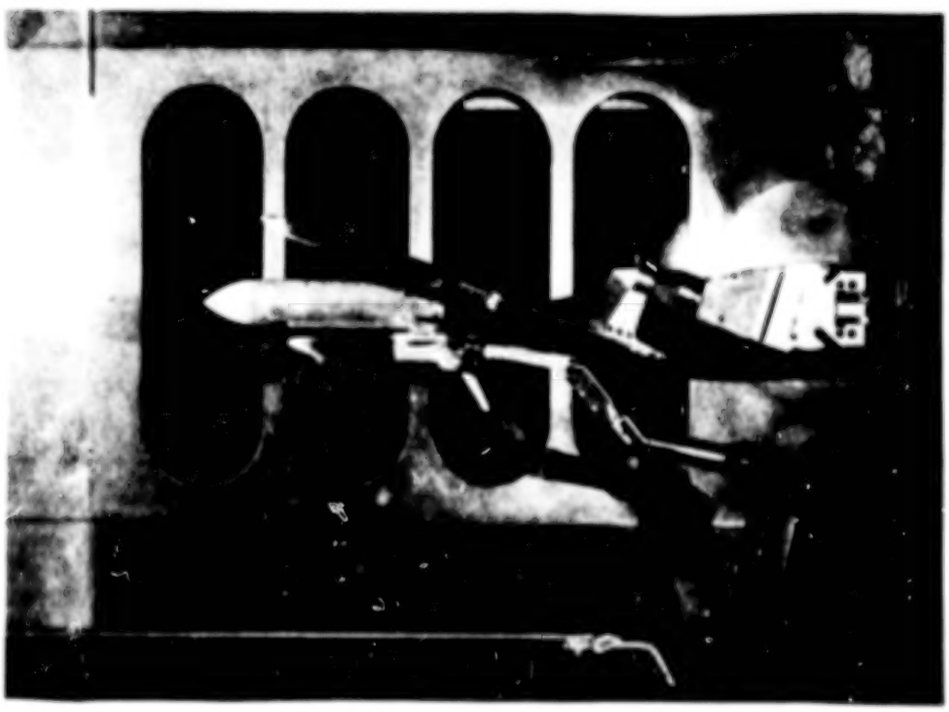
$$h_{MD}=\left[\frac{2\left(1+\frac{\gamma_j-1}{2}M_j^2\right)}{\gamma_j^2 M_j\left(\gamma_j+1\right)}\right]^{0.25}\left[\frac{1.25\left(1+\gamma_\infty\right)\gamma_\infty M_\infty^2}{\left(1-\gamma_\infty\right)+2\gamma_\infty M_\infty^2}\right]^{0.5}\left[\frac{\bar{q}_j}{q_\infty}\right]^{0.5}\left\{\frac{d_j}{\left(1+\cos\theta_j\right)}\right\}$$

Figure 22. Transverse Firing Jet Similarity Parameter.

ORIGINAL PAGE IS
OF POOR QUALITY



(a) BSM Plume-On.



(b) BSM Plume-Off.

Figure 29. SRB Separation Test Model Installation in AEDC/VKF Tunnel A.

N85
16907

UNCLAS

D18

N85-16907

THE SPACE SHUTTLE LAUNCH VEHICLE AERODYNAMIC VERIFICATION CHALLENGES

R. O. Wallace, L. D. Austin, J. G. Hondros
NASA-Lyndon B. Johnson Space Center
Houston, TX

T. E. Surber, L. M. Gaines, J. T. Hamilton
Rockwell International Corporation
Downey, CA

ABSTRACT

The Space Shuttle aerodynamics and performance communities were challenged to verify the Space Shuttle vehicle (SSV) aerodynamics and system performance by flight measurements. Historically, launch vehicle flight test programs which faced these same challenges were unmanned instrumented flights of simple aerodynamically shaped vehicles. However, the manned SSV flight test program made these challenges more complex because of the unique aerodynamic configuration powered by the first man-rated solid rocket boosters (SRB). The analyses of flight data did not verify the aerodynamics or performance preflight predictions of the first flight of the Space Transportation System (STS-1). However, these analyses have defined the SSV aerodynamics and verified system performance. The aerodynamics community has also been challenged to understand the discrepancy between the wind tunnel and flight defined aerodynamics. This paper presents the preflight analysis challenges, the aerodynamic extraction challenges, and the postflight analyses challenges which led to the SSV system performance verification and which will lead to the verification of the operational ascent aerodynamcis data base.

INTRODUCTION

The challenge of the Space Shuttle program was to develop a reusable spacecraft which would experience a conventional launch through a high dynamic pressure environment, perform an on-orbit mission and return to a conventional aircraft type landing. These requirements were satisfied by a complex configuration comprised of the first winged orbital spacecraft (Orbiter), first man-rated SRB, and external fuel tank (ET) (figure 1). During the development of this vehicle, the aerodynamics and performance communities were challenged to assure flight safety by analysis and to verify the SSV aerodynamics and system performance by flight test. Historically, flight test programs of launch vehicles have been unmanned instrumented flights. However, the Space Shuttle program management decided to perform an orbital manned mission on the first mission of the flight program. This decision was based on program mission requirements, compressed development schedules, and impact of vehicle loss.

PREFLIGHT ANALYSIS CHALLENGE

The manned SSV flight test program challenged the ascent communities to insure flight safety. Extensive preflight analyses were performed to identify the SSV system performance and structural sensitivities to potential inflight dispersions. Once these sensitivities were identified ascent trajectory profiles were designed which satisfied the STS mission requirements and maintained adequate margins of safety. Initial ascent trajectory design concepts for the SSV employed a gravity turn technique to maximize vehicle performance. This concept maintained a zero angle-of-attack ($\alpha = 0$) throughout the first stage of flight. While this design approach was found to be adequate for earlier generation launch vehicles, the resulting structural load environment for the SSV was unacceptable. Therefore, the primary challenge for the ascent community was to identify the ascent flight constraints within which the SSV trajectory profile could be designed to provide adequate margins for the vehicle structure while minimizing the impact to the STS performance capability (illustrated in figure 2 and 3). With the cooperation of the structural, aerodynamic and trajectory design communities, an approach[1] using structural load indicators was developed which modeled each of the critical SSV structural areas (see figures 4 and 5) in terms of the external forces on the element: thrust; aerodynamics; and inertia. These structural load indicator models were evaluated for various flight conditions to derive the flight constraint envelopes. To insure adequate structural margins, the structural load indicator models were evaluated using a six degree-of-freedom ascent trajectory simulation to determine sensitivities and criticality of the various indicators to potential inflight dispersions. Figure 6 illustrates the constraint envelope and inflight dispersions evaluated in terms of flight conditions. Figure 7 presents the measured wind dispersions used in figure 6 to provide protection for inflight winds

and maintain a high launch probability. Figure 8 presents the resultant flight constraint boundaries and trajectory design dynamic pressure and angle-of-attack requirements. These analyses pointed out the sensitivity of the SSV to the Orbiter aerodynamics which resulted in the requirement to extract the Orbiter aerodynamics from flight measurements.

By the mid 1970's, to provide adequate structural margins on the Orbiter wing and Orbiter/ET/SRB (element) attach struts, an angle-of-attack of -2° was required during the transonic regime of the ascent trajectory. This more negative α profile was achieved at the cost of approximately 700 pounds of payload capability relative to the initial trajectory design. In the late 1970's, the aerodynamic data base uncertainties were increased from a level which considered only wind tunnel data scatter (tolerance) to a level which also considered model scale to full scale aerodynamic uncertainties (variations). This increase was made to protect the SSV against the potential modeling and scale effect uncertainties associated with the complex SSV configuration. This change in the potential inflight dispersions resulted in an ascent trajectory profile design with $\alpha = -3^{\circ}$ and a further loss of payload capability of approximately 800 pounds relative to the $\alpha = -2^{\circ}$ design. Thus, the trajectory design for the STS-1 had protected the SSV against aerodynamic uncertainties and inflight dispersions to provide adequate performance, acceptable structural loads and to insure high launch probability.

AERODYNAMICS EXTRACTION CHALLENGE

Since the preflight analyses were based on ground test defined aerodynamics, the aerodynamics community was challenged to develop techniques to extract the aerodynamic characteristics of the SSV, elements and components from flight data. An extraction procedure was developed which substituted known or measured quantities into the equations of motion[2] and solved for the aerodynamic forces and moments. The SSV was instrumented to measure the required quantities: linear and angular accelerations, angular rates, thrust vector of each Space Shuttle main engine (SSME) and SRB (i.e., magnitude and direction), and trajectory parameters. These measurements could not be used directly to extract the aerodynamic characteristics, but required some adjustments. Analysis techniques were developed to account for vehicle characteristics, instrumentation location and instrumentation system biases. The SSME thrust vector analysis combined the elasticity of the Orbiter thrust structure and measurement of thrust vector control (TVC) actuator stroke to determine the direction of the thrust vector. Similarly, the structural characteristics of the SRB were combined with the SRB TVC actuator stroke measurement to determine the SRB thrust vector direction.

Since the center of gravity (cg) of the SSV moves during flight, techniques were required to relate the accelerometer measurements to the cg location. Acceleration measurements were taken at several locations on the Orbiter and SRB. The acceleration analysis used all compatible measurement in a least-squares procedure to define the SSV cg acceleration. Since the Orbiter is not a rigid body, accelerometer misalignment studies were required to determine the effect of body bending on the aerodynamic extraction results. These analyses indicated that the expected misalignments would not effect the aerodynamic extraction results.

Flight measurement of the SSV trajectory parameters and configuration parameters were required to relate the extracted aerodynamics to the ascent aerodynamic design data base. An air data system was designed into the tip of the ET to provide pressure measurements from which the angle-of-attack, angle-of-sideslip, dynamic pressure and Mach number could be determined (figure 9). An extensive wind tunnel calibration program was conducted to provide correlation between these pressure measurements and the required trajectory parameters.[3] Also, flight measurement of the Orbiter elevon position was required. Measurements of the elevon actuator stroke were made and converted to elevon angular position data. Also, techniques were developed to extract elevon hinge moments from actuator pressure measurements and strain gauge measurements. The flight elevon position analysis combined the position measurement, the extracted hinge moments, and the aeroelastic characteristics of the elevon support structure to determine the aeroelastic elevon position.

Since preflight analysis had identified structural sensitivities to the element (Orbiter, ET and SRB) aerodynamics, extraction procedures were developed to define the element aerodynamics. The element extraction procedure required the same measurements as previously described. However, to isolate one element from the SSV the measurement of the interface loads were required. Each Orbiter to ET strut and each SRB to ET strut (figure 4 and 5) (except the forward ball fitting) were instrumented. From the measurement of the strut loads, each body axis interface force could be determined. A precise calibration of each flight test strut assembly was performed. These calibrations were used to determine the flight measured strains. As with other measurements,

biases were required to be removed. Removal of the airload and inertial load acting on each strut was required. The initial weight of the Orbiter prior to SSME ignition was used to determine the Orbiter strut bias. A pre-ignition SRB strut bias could not be determined since a preload was present on the SRB struts on the pad which was released at lift-off. The SRB strut bias was determined by using the strut calibration zero load point and the strut measurement at SRB separation.

Prior to the first flight of the SSV the capability to extract the SSV, element and component (elevon hinge moment) aerodynamics was achieved by the aerdoynamics community. Although preflight analyses had indicated that the wing and vertical tail (components) were critical structure at some flight conditions, no procedures were developed to extract these component aerodynamics. The available strain gauge instrumentation was considered a structures community responsibility. Furthermore, the limited amount of pressure instrumentation was considered verification data and no procedures were developed to model these data.

POSTFLIGHT ANALYSIS CHALLENGES

The aerodynamics and performance communities were further challenged by the anomalies which occurred during STS-1. The first-stage trajectory was steeper than expected (lofted) which resulted in a SRB staging altitude approximately 10,000 feet higher than predicted (figure 10). Post flight extraction of the aerodynamic forces and moments revealed that significant differences existed from the baseline longitudinal forebody and base aerodynamics of the SSV and elements (figures 11 and 12).

These results challenged the aerodynamic community to understand these results and provide models of the flight derived aerodynamics. The performance communities were challenged to reconstruct the observed trajectory anomalies and verify subsystem models for trajectory design and performance prediction.

Initially, the aerodynamics community thought that the extracted aerodynamic results were incorrect because the observed discrepancies were larger than the conservative aerodynamic variations. However, preliminary trajectory reconstructions supported the flight derived aerodynamics, and extensive review of the extraction procedure, particularly thrust vectors, resulted in only minor modifications. STS-2 and -3 resulted in similar extracted aerodynamic characteristics. As the flight test program continued, the trajectory reconstruction analyses developed confidence in the trajectory design. STS-4 was designed to provide the aerodynamics community with flight data at a less negative angle-of-attack. After STS-4, gradient and intercept analyses of the derivatives ($\partial C/\partial \alpha$ and $\partial C/\partial \beta$) indicated that the wind tunnel data base derivatives and absolute levels were incorrect as shown in figures 13 and 14. These results were modeled into the present SSV and element aerodynamic data bases.

As these models were being developed, the aerodynamic community was attempting to understand the discrepancy between wind tunnel and flight aerodynamics. Center-of-pressure analyses indicated that a positive normal force increment was acting on the aft region of the SSV and primarily on the Orbiter. Assessment of limited pressure instrumentation on the Orbiter fuselage, wing and base indicated that a higher than predicted base pressure environment existed during flight which had fed forward of the Orbiter base. A review of the plume simulation used for SSV wind tunnel tests was conducted. Studies using an analytical program and flight test base pressures concluded that the plume simulation parameter (used to set test conditions) was deficient and required a temperature function to account for hot gas effects.[4] A post flight wind tunnel test was conducted to simulate the flight base pressure environment. Preliminary results seem to verify flight pressure measurements in the elevon region of the wing and aft fuselage (figure 15 and 16). Analyses of the post flight wind tunnel test are continuing and will determine what part of the observed difference was due to plume simulation deficiencies. The remaining difference is assumed to be Reynold's number effects. Since post flight wind tunnel data analyses will not be complete for some time and since only limited flight pressure data was obtained, problems in modeling the flight force and moment increments into the external pressure distributions have prevented complete verification of the ascent aerodynamic data bases.

Since the SSV pressure distributions are questionable, the day-of-launch assessment of wing loads is questionable. Wing pressure distributions are inputs to the current load indicator equations. Techniques were developed to determine the wing load distribution from flight strain gauge data. Attempts to modify the wind tunnel derived pressure distributions based on flight pressure measurements have failed to match loads data extracted from wing strain gauge data. However, the gauge data was questioned and a check calibration performed after STS-5 revealed that

several key gauges either had the wrong scaling factors or reversed polarity. After using the check calibration data, the extracted wing loads comparisons did not improve. Currently, the aerodynamics and structures communities are implementing plans to correlate calculated internal stresses using revised pressure distributions with measured flight stresses. The results of this effort will be verified SSV pressure distributions.

The performance communities' trajectory reconstruction work provided the basis for verification of the SSV system performance. The trajectory reconstruction of STS-4 using flight derived aerodynamics and post flight subsystem model updates (SSME Isp and thrust; SRB Isp and thrust; and gimbals) matched the vehicle tracking data (BET), air data system parameters, occurrence of flight events, ET propellants remaining at MECO (table 1) and attach structure loads. Figures 17, 18, and 19 present the trajectory parameter reconstruction comparisons. These reconstructions also provide load comparisons of previously critical structural loads (figure 20). The trajectory reconstruction task also produced a reassessment of trajectory design constraints. In terms of payload capability, the flight base aerodynamics increased the SSV performance approximately 1000 pounds. However, the current evaluation of wing loads reflected a need to bias the ascent trajectory profile to $\alpha = -5^{\circ}$ to maintain acceptable margins. This angle-of-attack requirement during the first stage cost approximately 1100 pounds of payload capability relative to the $\alpha = -3^{\circ}$ used during the flight test program. Figure 21 summarizes the impact of maintaining structural margin requirements as a result of changes to the aerodynamic data base on the ascent trajectory design and SSV performance from the early design phase of the SSV to the current operational baseline. Therefore, verification of SSV performance was achieved by trajectory and load reconstructions that modeled subsystem changes and accounted for as flown wind profiles.

CONCLUSION

The Space Shuttle aerodynamcis and performance communities have met the challenges of the Space Shuttle Program. From a trajectory design and performance point of view, the SSV aerodynamic characteristics and paylaod capabilities have been defined, modeled and verified. In addition the element aerodynamic characteristics have been defined and verified, which prior to STS-1 were considered most significant to the SSV structure and to trajectory design. However, the flight results changed the emphasis from the element aerodynamics to the external pressure distribution of the Orbiter wing. Because of limited external flight pressure instrumentation, flight strain gauge data must be used to extract the external pressure distributions. Attempts to model the strain gauge results failed to predict measured stresses when pre-STS-1 wing load indicator equations were used. The aerodynamics community initiated regression analyses of flight wing strain measurements to produce wing load indicators that would provide an adequate tool for day-of-launch wing load calculations to insure flight safety. Once this method was shown to provide excellent prediction capability, the structure community implemented the procedure for critical wing structure. Also, the aerodynamics community initiated a cooperative effort of the aerodynamics and structures communities to define the SSV pressure distribution through an iterative procedure of pressure distribution definition, internal loads calculations, and flight comparisons. The initial step in this effort has pointed out that the current pressure distributions are not adequate. Review of the effort to date, points out the need for the structures community to insure that the effects of fuselage torison and bending on strain gauge measurements are defined, understood and modeled. Therefore, the above cooperative effort will provide definition and verification of the ascent aerodynamics pressure distributions which will complete the ascent aerodynamics operational data base.

Finally, the efforts of the aerodynamics and performance communities to meet the Space Shuttle challenges have provided the Shuttle Program management insight to trajectory design constraints, performance improvements and limitations, effects of flight defined aerodynamics, and day-of-launch risk assessments.

REFERENCES

1. Leahy, K. S.: Techniques for Assessment of Ascent Aerodynamic Characteristics of the Space Shuttle Launch System, presented as paper at Shuttle Performance; Lessons Learned Conference at Langley Research Center, Hampton, Virginia, March 8-10, 1983.

2. Gaines, L. M.; Osborn, W. L.; and Wiltse, P. D.: Launch Vehicle Aerodynamic Flight Test Results, presented as paper at Shuttle Performance; Lessons Learned Conference at Langley Research Center, Hampton, Virginia, March 8-10, 1983.

3. Hillje, Ernest R.; and Nelson, Raymond L.: Ascent Air Data System Results from the Space Shuttle Flight Test Program, presented as paper at Shuttle Performance; Lessons Learned Conference at Langley Research Center, Hampton, Virginia, March 8-10, 1983.

4. Roberts, Barney B.; Wallace, Rodney O.; Craig, Mark K.; and Kanipe, David B.: Rocket Exhaust Plume Induced Flowfield Interaction Experiences with the Space Shuttle, presented as paper at AIAA 18th Thermophysics Conference at Montreal, Canada, June 1-3, 1983.

5. Hamilton, J. T.; Wallace, R. O.; and Dill, C. C.: Launch Vehicle Aerodynamic Data Base Development Comparison with Flight Data, presented as paper at Shuttle Performance; Lessons Learned Conference at Langley Research Center, Hampton, Virginia, March 8-10, 1983.

6. "Orbital Flight Test Aerodynamic Data Analysis, Space Transportation System Launch Vehicle, Volume 2", STS81-0558, Volume 2A, April 1982, Revision 2A-2, Space Division, Rockwell International.

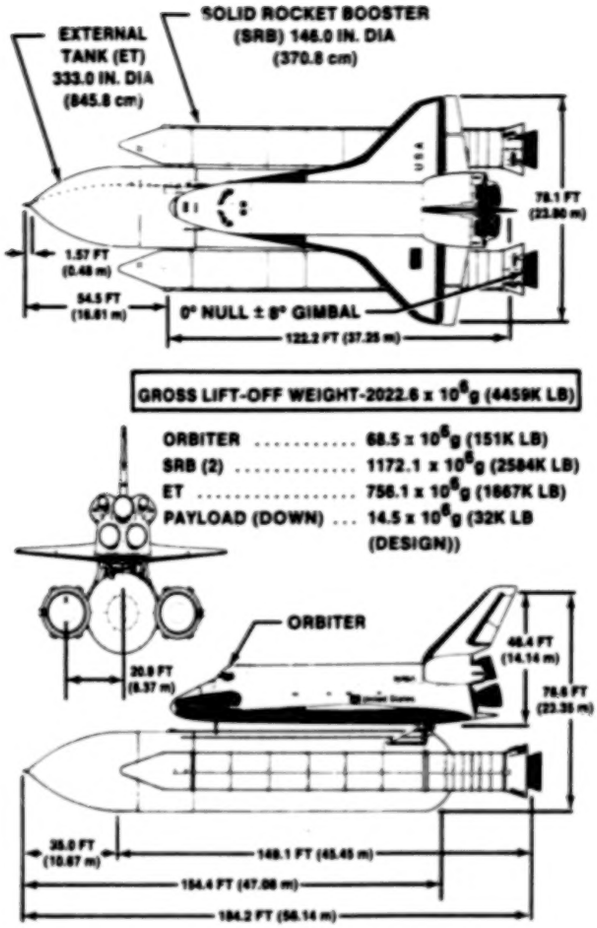


Fig. 1 Space Shuttle Launch Vehicle Configuration.

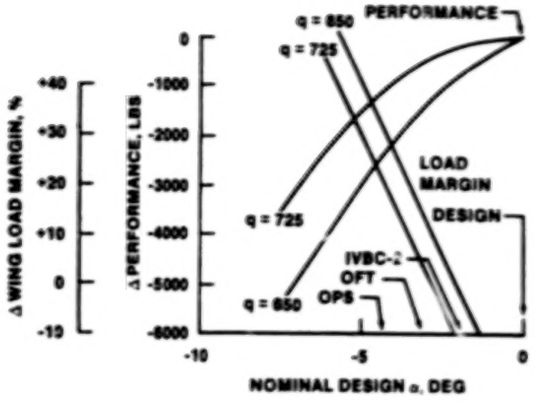


Fig. 3 Wing Load and Performance Trade Study with Angle of Attack.

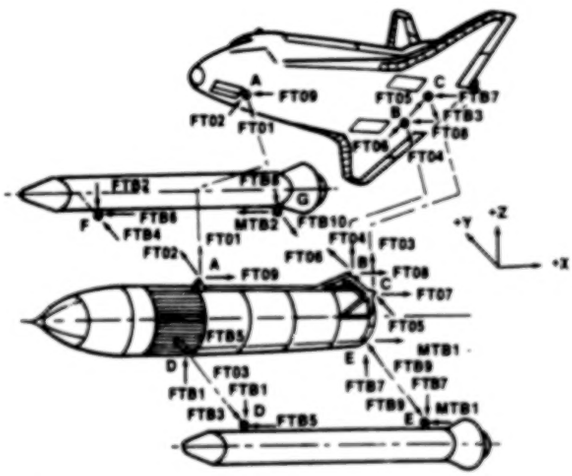


Fig. 4 Body Axis Interface Load Indicators.

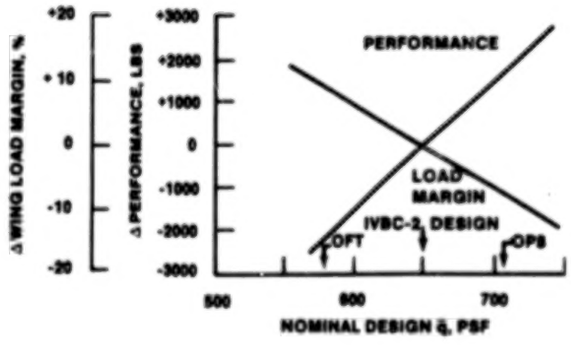


Fig. 2 Wing Load and Performance Trade Study with Dynamic Pressure.

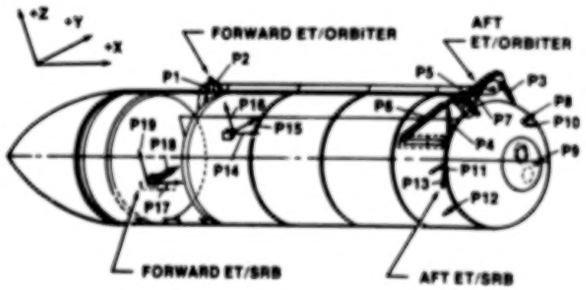


Fig. 5 Attach Strut Load Indicators

OF POOR QUALITY

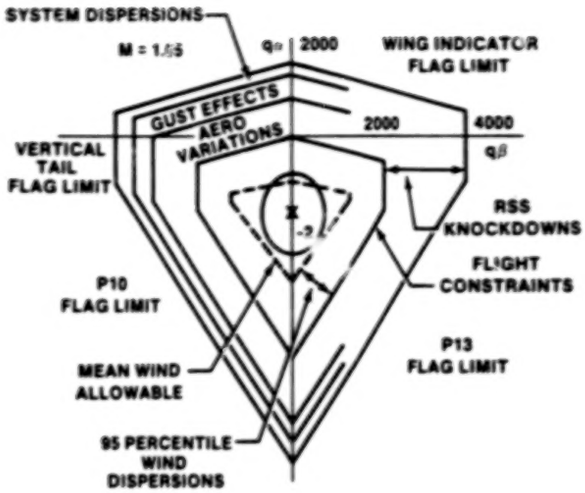


Fig. 6 Flight Constraint Envelope.

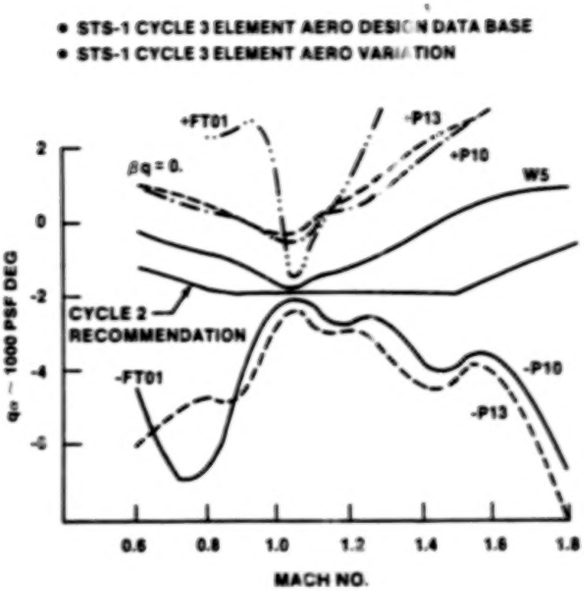


Fig. 8 Flight Constraint Boundary.

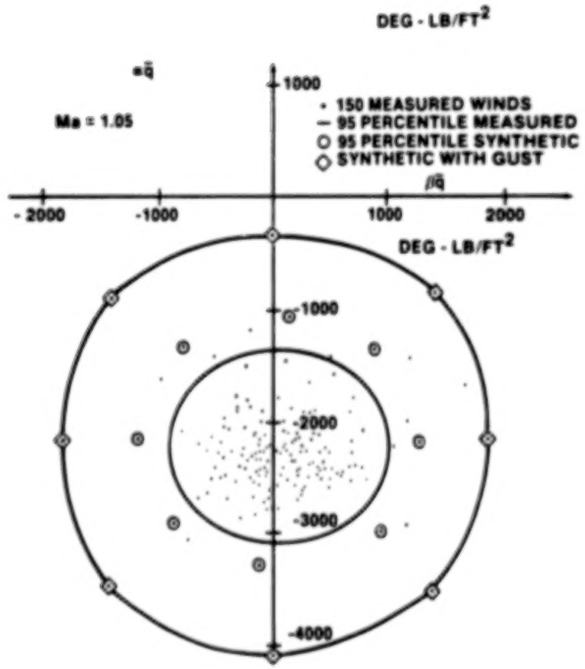


Fig. 7 SSV Response to Wind Profiles in the Pitch and Yaw Planes.

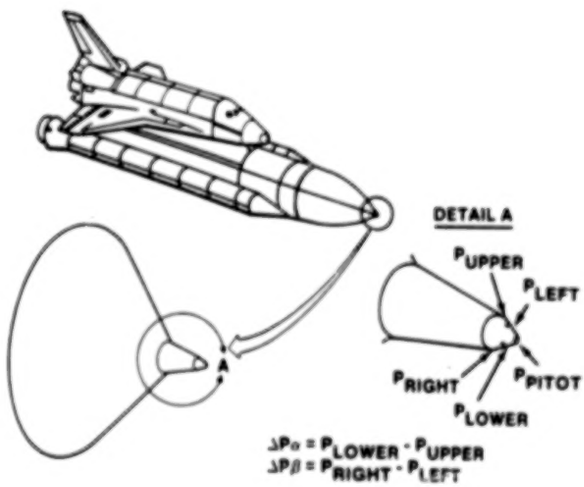


Fig. 9 Ascent Air Data System Configuration.

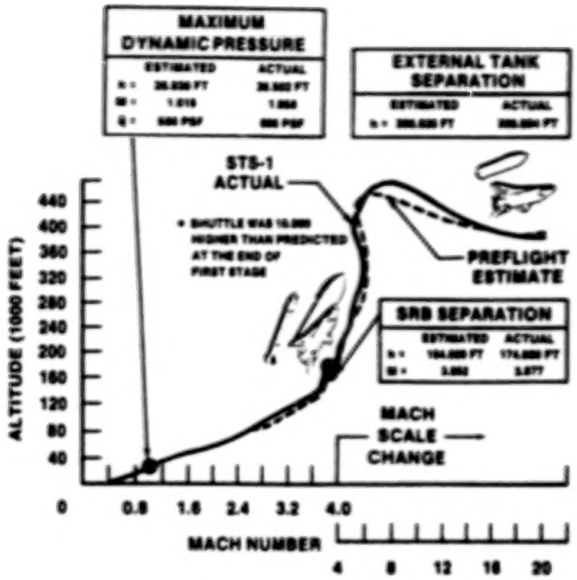


Fig. 10 STS-1 Trajectory Anomaly

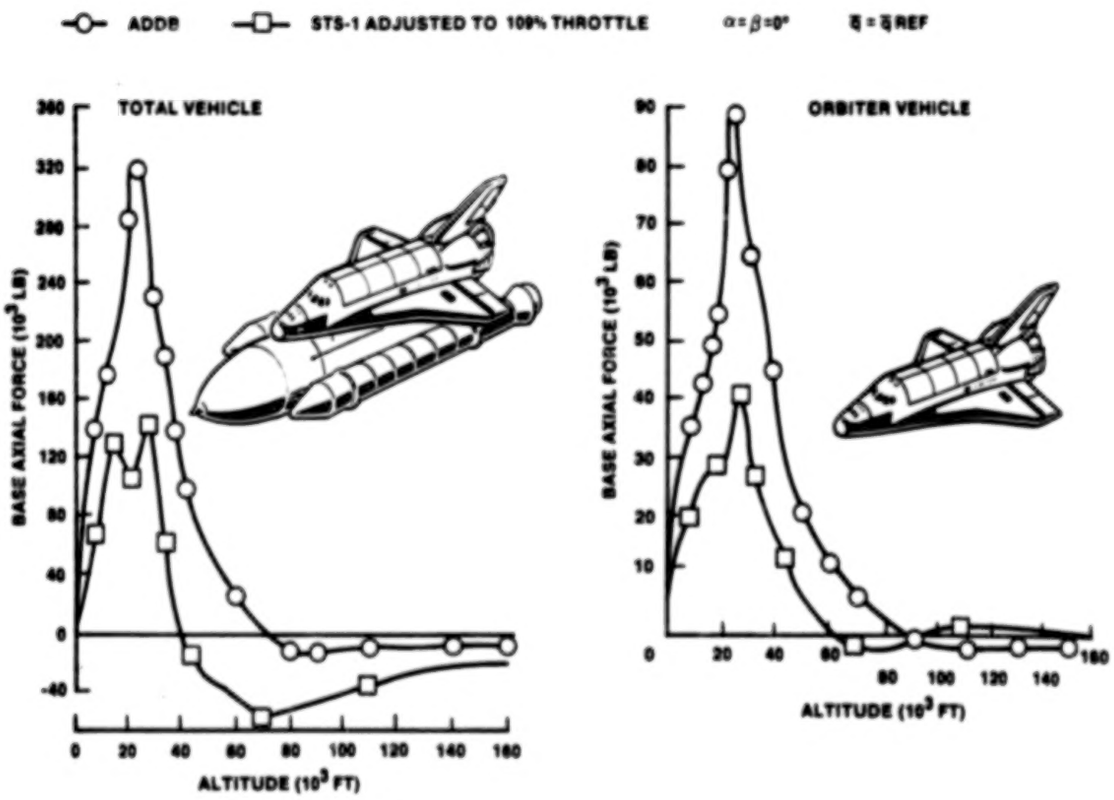


Fig. 11 Comparison of STS-1 Flight Base Axial Force and Design Data Base Axial Force.

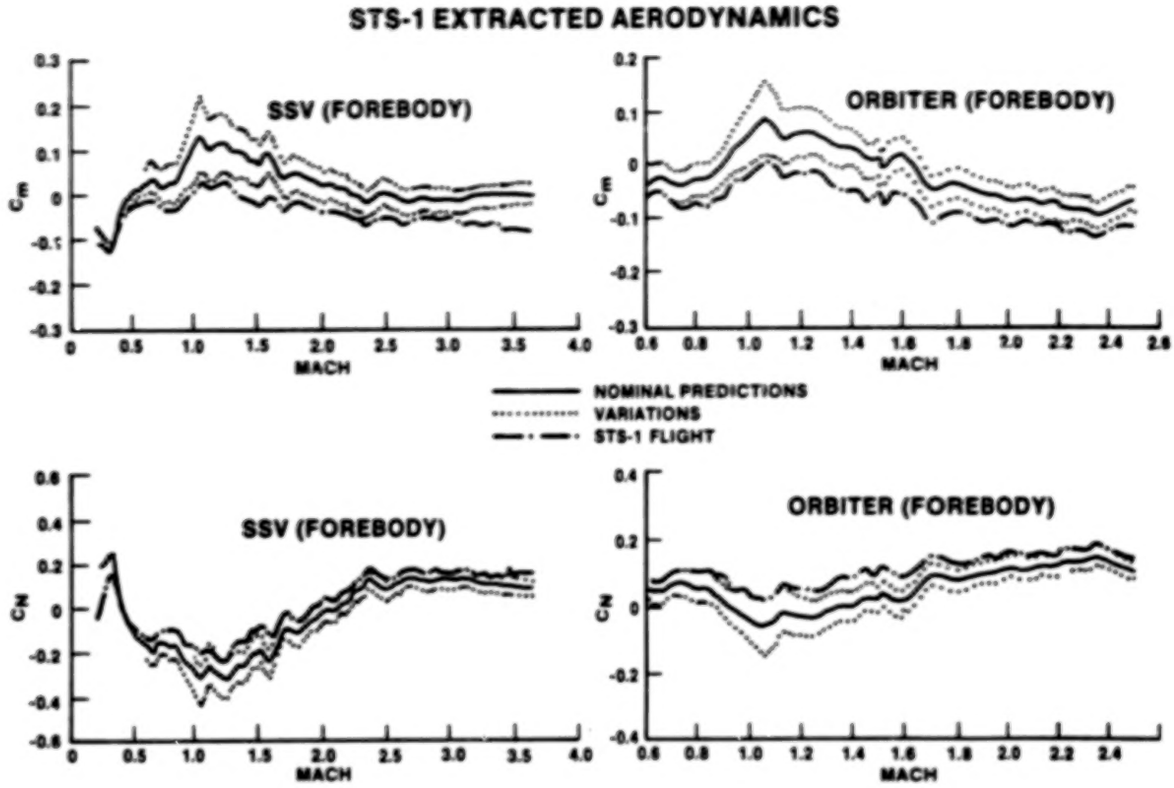


Fig. 12 STS-1 Normal Force and Pitching Moment Comparisons.

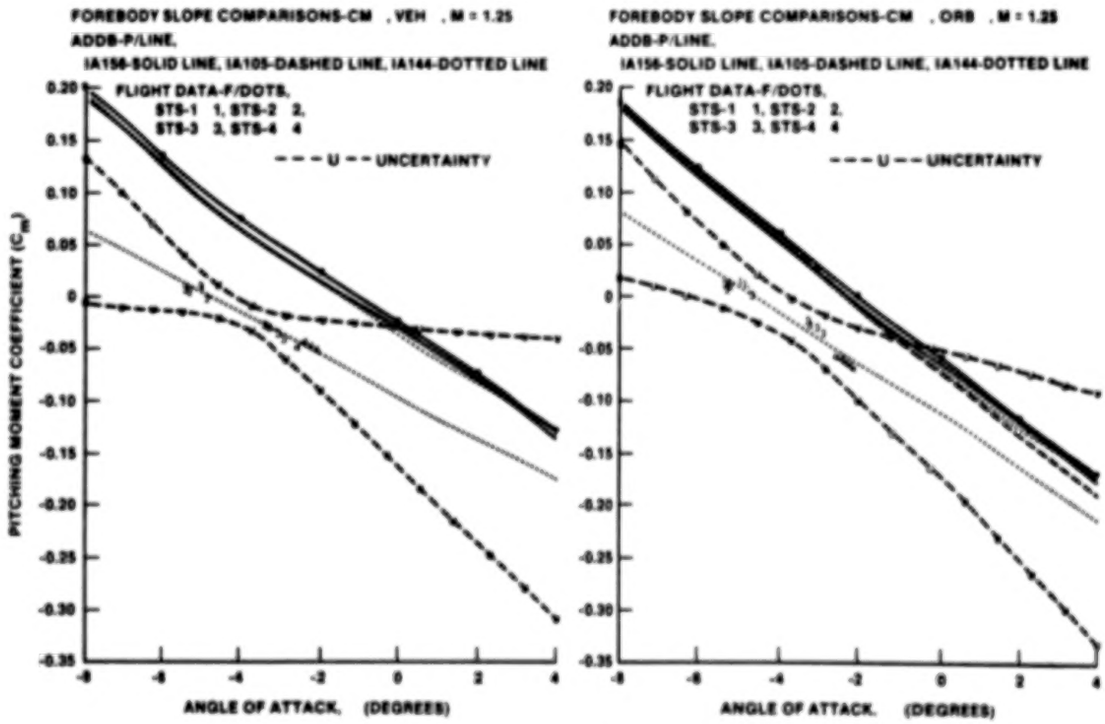


Fig. 13 Gradient Analysis of Flight Pitching Moment.

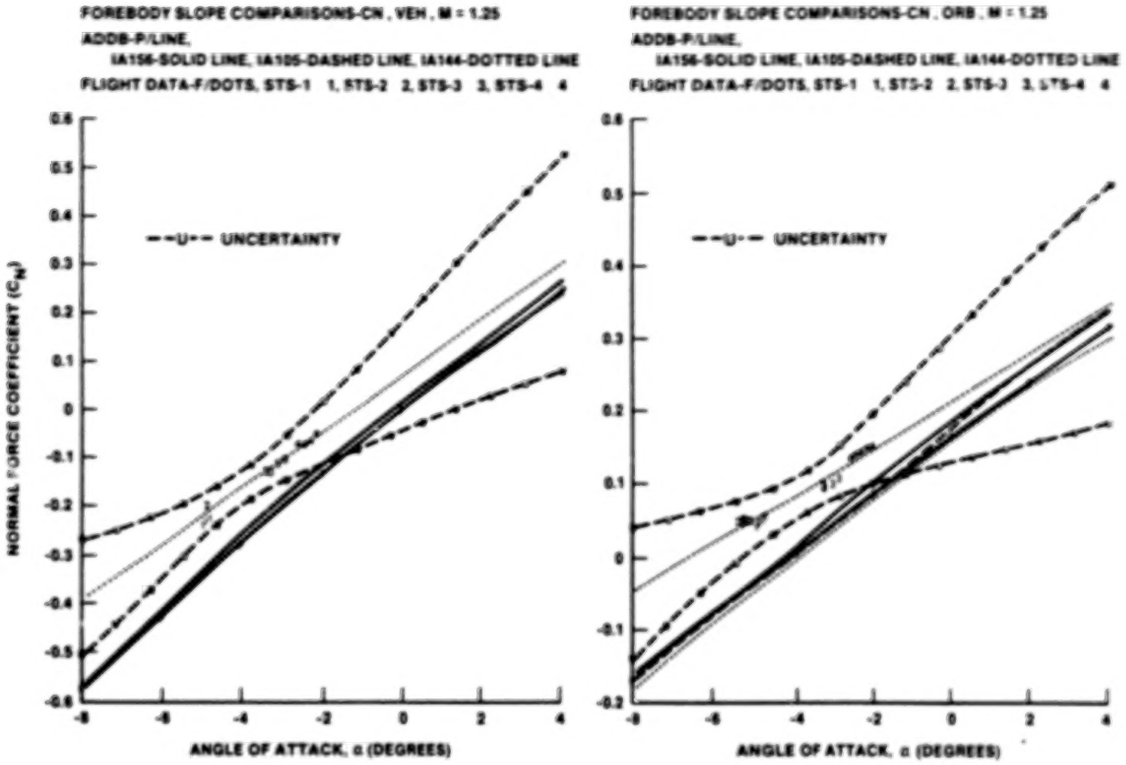


Fig. 14 Gradient Analysis of Flight Normal Force.

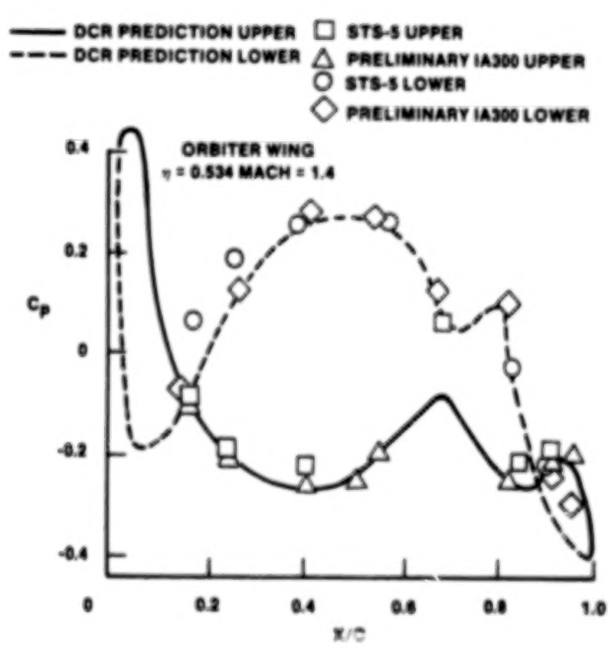


Fig. 15 Wing Pressure Distribution Comparison.

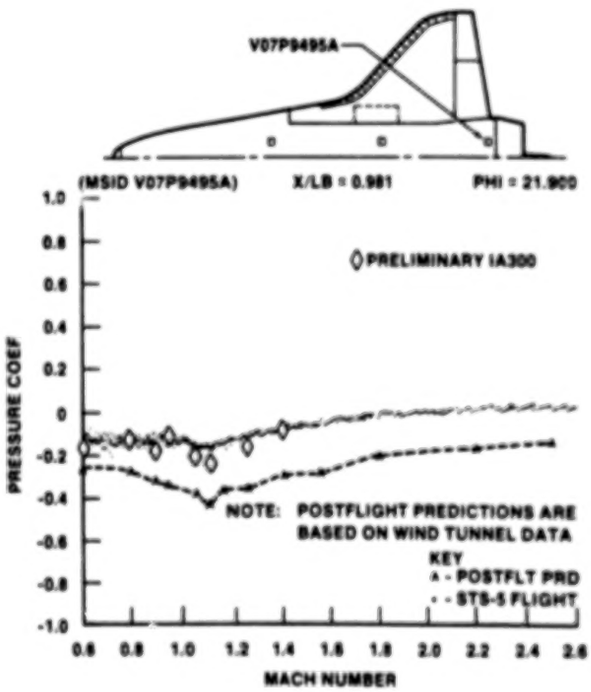


Fig. 16 AFT Fuselage Pressure Distribution Comparison.

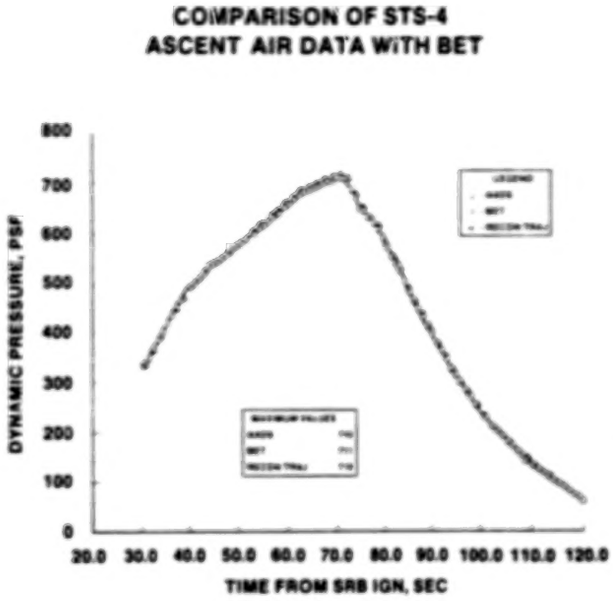


Fig. 17 STS-4 Dynamic Pressure Reconstruction.

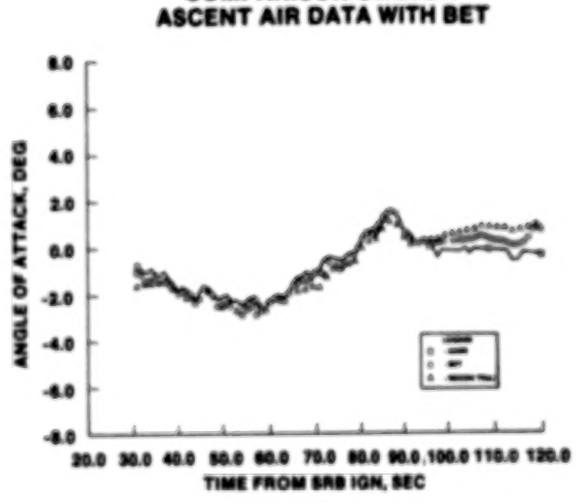


Fig. 18 STS-4 Angle-of-Attack Reconstruction.

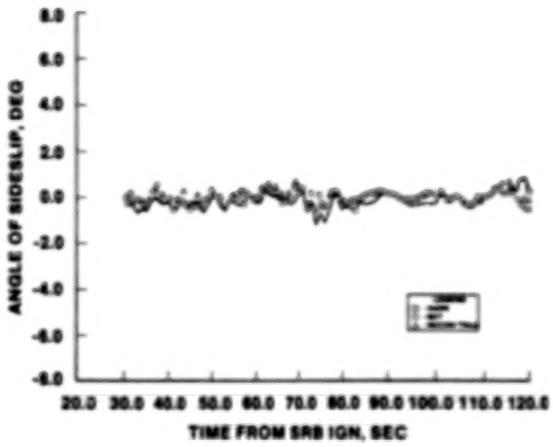


Fig. 19 STS-4 Angle-of-side Reconstruction.

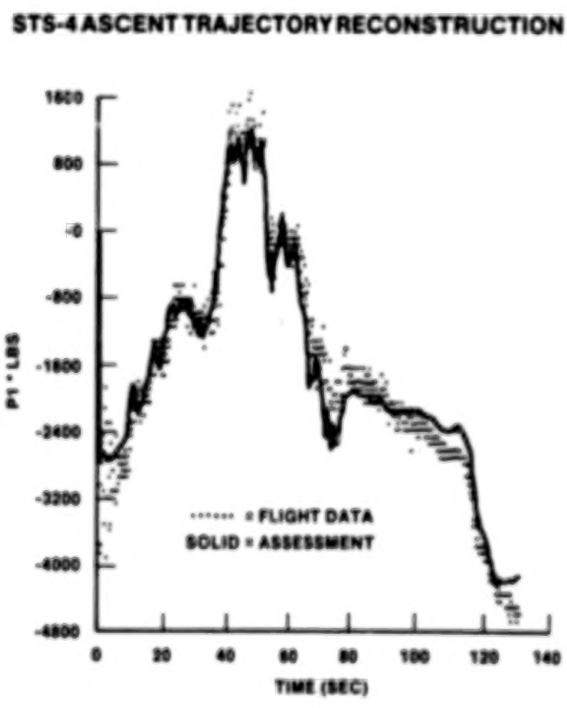


Fig. 20 STS-4 Attach Load Reconstruction.

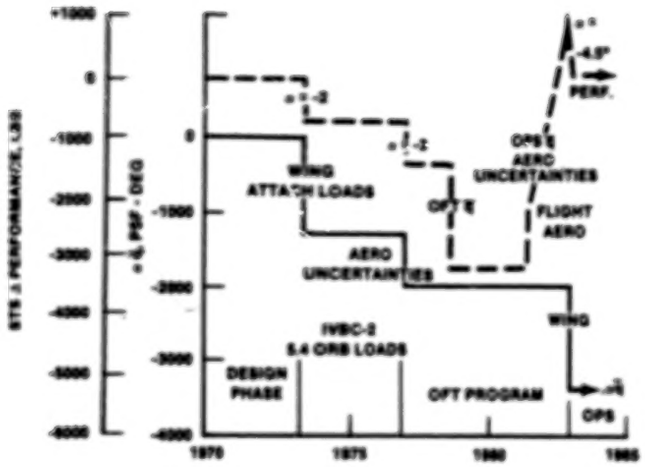


Fig. 21 Summary of System Performance Effects and Desogn $\bar{oq}$ Based pm SSV Aerodynamic History.

Table 1. Summary of STS-4 Trajectory Reconstruction.

STS-4 RECONSTRUCTION SUMMARY

PARAMETER	FLIGHT DATA	RECONSTRUCTION
MAX $\bar{q}$	711. (BET)	719.
MAX PITCH ATTITUDE ERROR	+ 3.8°	+ 3.5°
STAGING H	154,450. (BET)	154060.
STAGING V_R	4277. (BET)	4287.
STAGING γ_R	28.8	28.4
3 g THROTTLE	458.0	458.4
MECO CMD	512.7	512.5
LIQUIDS REMAINING LOX	8466.	8480.
LH_2	3013.	3540.

N85
16908

UNCLAS

D19

N85-16908

THE AERODYNAMIC CHALLENGES OF SRB RECOVERY

D. L. Bacchus and D. A. Cross
NASA/Marshall Space Flight Center
Huntsville, Alabama

and

R. D. Moog
Martin Marietta/Denver Division
Denver, Colorado

ABSTRACT

Recovery and reuse of the Space Shuttle solid rocket boosters was baselined at the initiation of the program to support the primary goal to develop a low cost space transportation system. The recovery system required for the 170,000-lb boosters was for the largest and heaviest object yet to be retrieved from exoatmospheric conditions. State-of-the-art design procedures were ground-ruled and development testing minimized to produce both a reliable and cost effective system.

The ability to utilize the inherent drag of the boosters during the initial phase of reentry was a key factor in minimizing the parachute loads, size and weight. A wind tunnel test program was devised to enable the accurate prediction of booster aerodynamic characteristics. Concurrently, wind tunnel, rocket sled and air drop tests were performed to develop and verify the performance of the parachute decelerator subsystem. Aerodynamic problems encountered during the overall recovery system development and the respective solutions are emphasized.

INTRODUCTION

At the onset of the Space Shuttle program, numerous trade studies investigated means to develop a cost effective space transportation system. One conclusion drawn from these studies was that recovery, refurbishment and reuse of the Solid Rocket Boosters (SRBs) would provide a significant cost savings over expendable boosters.[1] This conclusion was based in part on the assumption that a recovery system could be developed utilizing a current state-of-the-art design approach. This challenge was accepted by the Marshall Space Flight Center in May 1972 when this center was given overall responsibility for developing the SRB recovery system. The challenge has been successfully met as evidenced by the initial Shuttle flight verification test in April 1981 and in subsequent Shuttle flights.

Aerodynamics have played a key roll in the recovery system development. The purpose of this paper is to address some of the aerodynamic issues and trades and how various aerodynamic challenges were met through a combined conventional and innovative systematic approach aimed at providing both a reliable and cost effective system.

A trace of the historical development of the recovery system and the aerodynamic challenges encountered cannot begin without first a brief description of the SRB configuration and reentry profile. Refering to the reentry sequence in Figure 1, the twin boosters burn out and separate from the remaining Orbiter/External Tank at an altitude of approximately 150,000 ft. After reaching an apogee near 220,000 ft, the 170,000-lb spent SRBs reenter the atmosphere in a random tumbling mode. After an initial deceleration phase during which the Mach number decreases from approximately 3.0 to 0.5, the nose cap is ejected initiating the deployment sequence of the decelerator subsystem parachutes. The 54-ft drogue parachute, deployed at an altitude of approximately 15,000 ft, stabilizes the booster in a tail first attitude. The drogue is also used to deploy a cluster of three 115-ft main parachutes at an altitude near 6500 ft. The main parachute system provides the final deceleration to the nominal 87 ft/sec water impact velocity.

A schematic of the SRB illustrating the location of the recovery system major elements is provided in Figure 2. The parachutes packs, as shown, are contained in the forward portion of the booster. An 11.5-ft pilot, used to deploy the drogue, is located in the nose cap. At the proper altitude, determined by a barometric switch, the nose cap is jettisoned by firing three 30,000-lb thrusters. As shown by the sequence in Figure 3, the nose cap is connected by a three-legged bridle and riser to the pilot pack, and utilizing the drag of the cap deploys the pilot parachute.

Main parachute deployment, again initiated by a baroswitch signal, occurs when the frustum is severed by a linear shaped charge. The frustum then descends under the drogue to water impact and is recovered along with the booster approximately 140 n.mi. downrange of the launch site.

ESTABLISHMENT OF RECOVERY SYSTEM BASELINE

In the initial design definition phase of SRB recovery system development, two primary issues received the major emphasis. These were (1) how to provide high altitude booster deceleration to achieve conditions suitable for parachute deployment, and (2) how to optimize the recovery system for water impact. For both of these issues, the requirements to utilize only state-of-the-art concepts and to minimize cost and complexity of recovery eliminated some of the potential options such as the use of active stabilization or attitude control systems.

Some of the options considered for the high altitude deceleration phase of reentry are shown in Figure 4. These include the use of various drag producers such as extendable flaps, drag petals and inflatable type devices such as ballutes. However, a drawback to each of these methods is that they all tend to orient the booster centerline in the streamwise direction resulting in a tremendous decrease in SRB drag. From this standpoint, a high angle of attack or "broadside" reentry mode appeared highly desirable. In fact, the natural aerodynamic drag of the booster alone could potentially provide the deceleration required to generate the conditions needed at parachute deployment. Although the best method of achieving a near broadside reentry mode had not been determined, this reentry concept was adopted because of the numerous advantages it offered.

Concurrently, other studies were being performed to optimize the final deceleration system. One key trade considered an all parachute versus a hybrid parachute braking rocket system. The results (Fig. 5) indicated that for water impact velocities above 65 ft/sec a pure parachute system would be lighter. Studies of water impact had concluded that a 80 to 100 ft/sec tail first impact would provide a good compromise between initial impact and slap down loads. The pure parachute system was therefore baselined to provide both a lighter weight and less complex system.

With a booster recovery scheme developed, several key aerodynamic challenges remained including (1) determining the best means of achieving a broadside reentry, (2) developing an SRB aerodynamic data base, (3) establishing design requirement for the parachute system, (4) optimizing the parachute system from a design/performance standpoint, and (5) verifying overall performance through a systematic and cost effective development test program.

Since the parachute design requirements were directly dependent on the SRB initial deceleration phase, it was paramount that the initial SRB deceleration phase be investigated first. If the booster center of gravity were ideally located at approximately 53 percent body length from the SRB nose (near centroid of area) the booster would tend to trim at an angle of attack near the optimum 90-deg. The booster center of gravity at burnout, however, is 5 or 6 percent further aft which causes the booster to tend to trim in a somewhat tail first and lower drag attitude.

Early studies considered an aerodynamic "fix" to force the booster to reenter closer to 90 deg. To accomplish this several possibilities were explored. In one concept strakes were added to the fore and aft section of the SRB on opposite sides of the vehicle. The strakes would create a yawing moment sufficient to induce a flat spin. This concept, however, required a tight control of the static margin and also roll stabilization to assure that the strakes would be oriented for maximum effectiveness.

A more practical solution proposed[2] also utilized strakes but in a somewhat different manner. By adding strakes at several circumferential locations on the SRB aft skirt, an effective rearward shift in center of pressure of approximately one percent body length could be achieved.

Since the addition of strakes added weight and cost to the SRB, recovery studies continued to investigate reentry with an unmodified booster. The major concern with this approach dealt with the predictability of conditions at parachute deployment. Because of an integral effect of the phasing of the lift vector during reentry, significantly different trajectories could result from small differences in booster mass characteristics, aerodynamics, and other system uncertainties. It was difficult not only to establish a nominal reentry trajectory but also to define reasonable worst case conditions to establish design requirements for nose cap separation and drogue deployment.

The solution was to utilize a "Monte Carlo" approach to establish a set of approximately 400 possible trajectories. In each trajectory the system dispersions were selected using a random distribution for each established uncertainty. The booster aerodynamics, except for the center of pressure, were also treated in this manner. The center of pressure dispersion was fixed at the 95-percentile worse case direction (forward) to establish a set of design conditions for parachute deployment.

One result of the reentry analysis was the establishment of a booster center of gravity aft limit for recovery system design purposes. As the center of gravity moves aft, the conditions at drogue deployment become increasingly sensitive to system uncertainties and the chances of a "lock-up" to a catastrophic tail first trim more probable. The final selection of a 59-percent aft limit was a reasonable compromise between SRB weight distribution and acceptable conditions for drogue deployment.

Using the Monte Carlo trajectory set, parachute design requirements could also be traded against probability of a successful recovery to optimize the recovery system from a cost standpoint. This resulted in a design based on a 99th percentile trajectory eliminating the few cases resulting in near tail first reentries.

The primary tasks remaining were to (1) develop a valid aerodynamic data base for the final SRB baseline configuration, and (2) develop an optimum parachute system to meet the established requirements. The manner in which these tasks were undertaken will now be addressed.

SRB AERODYNAMIC DATA BASE DEVELOPMENT

The SRB reentry aerodynamic characteristics were developed primarily by a series of wind tunnel tests utilizing various size models, several test facilities and, in some instances, specialized test techniques. The data base development task was made more complex by the large test matrix required to encompass the wide range of potential reentry conditions inherent to a randomly tumbling reentry body. Other problems experienced were attributed to Reynolds number and sting interference effects.

REYNOLDS NUMBER EFFECTS

Although a major portion of the SRB reentry is supersonic, the greatest challenge in developing the data base was to obtain accurate aerodynamic characteristics in the subsonic flow regime. The reentering SRB is essentially a cylinder in crossflow type problem that is compounded by the existence of very large Reynolds numbers ($\approx 2 \times 10^7$) and SRB protuberance effects. Because of the importance of Reynolds number, every attempt to match, maximize or determine the effects of this parameter on SRB reentry aerodynamics was incorporated into each test.

Figure 6 provides a comparison between flight Reynolds number and levels obtained in wind tunnel testing. As shown, a reasonably close match was achieved with tests in the MSFC High Reynolds Number Wind Tunnel (HRWT). Reynolds numbers up to 2.0×10^6 were also obtained in large (2.8 percent) model tests in the Ames Unitary Tunnel. As expected large variations with Reynolds number were obtained.

STING INTERFERENCE EFFECTS

Although sting interference effects are present in practically all wind tunnel test results, the magnitude of the error introduced can normally be ignored. For the SRB tests, however, sizable sting effects were sometimes obvious as illustrated in Figure 7. The pitching moment coefficients presented as a function of angle of attack were obtained for identical configurations and conditions using two different model support systems; one a side mounted strut and the other a sting attached to the nose of the SRB model. The discontinuity is indicative of the presence of sting effects but not necessarily the magnitude since both sets are erroneous to some degree.

Sting interference problems have typically been associated with the testing of bodies at high angles of attack. However, in the SRB tests the problem has been amplified by the necessity to test at high Reynolds numbers where the resulting high loads dictate the use of massive model support hardware. However, even the low Reynolds number tests utilizing smaller struts demonstrated significant sting effects and made comparing data obtained from different facilities at similar conditions extremely difficult. The severity of the problem is also illustrated by Figure 7 which shows that the sting effect can have a sizeable influence on the apparent static trim angle. The 20-deg difference measured by the two systems would not be acceptable if treated as an uncertainty in developing conditions at nose cap deployment.

Because of the criticality of defining the proper reentry conditions, a special test program[3] was initiated to quantitatively determine the effects of sting interference. The goal of this program was to (1) obtain sting interference corrections for model support systems used in MSFC TWT, MSFC HRWT and Ames Research Center test results, and (2) determine the optimum sting arrangement to minimize sting effects in future tests.

The technique employed was similar to that utilized in Reference 4. That is, a dummy sting was used in conjunction with a live balance and sting to back out the sting effect (Fig. 8). Hardware was also developed to determine corrections for both the nose and side mount configurations. This provided an indication of the resulting data uncertainty, due partially to a mutual interference effect between dummy and live sting, and also the data needed to establish the best sting setup for given conditions.

A photograph of the sting interference test setup for the HRWT facility (Fig. 9) illustrates the size of the sting system relative to the SRB model. An example comparison of the sting corrected nose and side mount data with design data and large model test results (SA11F) is shown in Figure 10. In this particular case, the corrected data are to the right of both data sets. The resulting higher trim angle creates a more severe reentry environment, further illustrating the importance of these tests.

PARACHUTE PERFORMANCE DATA BASE DEVELOPMENT

The parachute system for the SRBs evolved from a systematic development/verification test program that included wind tunnel, rocket sled and air drop testing. In order to minimize development costs it was mandatory that the number of air drop tests be reduced from the thirteen originally planned to only six. This success oriented approach placed a greater burden on predrop configuration design optimization including that of the parachute deployment method and parachute configuration to achieve the desired performance.

WIND TUNNEL TEST PROGRAM

Wind tunnel tests[5,6,7] were performed for two primary purposes. One was to parametrically investigate the performance of 20-deg conical ribbon parachutes to augment the data base available. The configurations tested were appropriate for the drogue, drogue pilot and main parachute system. The second major objective was to investigate several potential deployment methods for the drogue parachute (Fig. 11). One-eighth scale models of the drogue parachute of 16- and 24-percent porosity were used for the drogue performance and drogue deployment phases of the test. Since the same parachute models were also used for the main parachute performance tests the ribbon width and spacing was geometrically scaled for the drogue parachutes only.

A photograph of the model used in the drogue deployment tests is shown in Figure 12. In these tests both the parachutes packs and the nose cap were geometrically and mass scaled to simulate the deployment dynamics. A photograph showing typical parachute models is shown in Figure 13.

These tests accomplished all of the goals established. A recommended method of deploying the drogue parachute was later adopted and proved successful. Performance characteristics were established for the SRB candidate 20-deg conical ribbon parachutes including the effects of geometric porosity, reefing, clustering, suspension line length and forebody interference. These data enabled a sound configuration selection in the early design stage that would basically remain unchanged throughout the remaining development program.

ROCKET SLED TEST

The initial phase of parachute deployment, i.e., nose cap separation and pilot parachute deployment, was considered a critical aspect of the recovery scheme. To verify that the full scale flight configuration would perform as predicted and demonstrated in scaled model tests, a rocket sled test was performed[8,9] at the Rocket Sled Test Facility at Sandia Laboratories, Albuquerque, New Mexico. This test provided a functional checkout of nose cap separation, structural verification of the nose cap/pilot chute rigging under design limit load environment and aerodynamically the dynamic behavior of nose cap separation and pilot deployment for both a worst case windward ($\alpha = 80°$) and a high alpha/high dynamic pressure (140 deg/270 psf) test condition.

The sled test was both a technically sound and cost effective alternative to an air drop for development testing this portion of the recovery system. Primarily, it provided a means of controlling the most critical test parameters such as velocity and SRB angle of attack. Figure 14 illustrates the general configuration and the test setup for the 80-deg angle-of-attack test. The configuration was comprised of a flight-type nose cap, jettisoned by firing three thrusters, and an adapter representing a small portion of the nose cap frustum.

For the 80-deg test, 16 HVAR (6500-lb thrust) rockets were used to accelerate the text fixture down the 5000-ft-long track to a peak velocity of 465 ft/sec. Following a brief coast period, the nose cap was ejected at a dynamic pressure of 197 psf. The test sequence is shown in Figure 15. No deployment problems were experienced and the cap cleared the drogue and pilot chute packs by a substantial margin.

Similar success was achieved with the 140-deg test which utilized 21 HVAR rockets. For each of the tests, film analysis and laser tracking data were used to determine nose cap ejection velocities and the cap displacement relative to the parachute packs.

AIR DROP TESTS

An important element of the SRB decelerator subsystem development program was the air drop program[10,11] performed at the National Parachute Test Range, El Centro, California. These tests were used to provide functional, structural and performance evaluation of the overall parachute system. The program consisted of six drops employing a 48,000-lb drop test vehicle (DTV) which was released from the B-52 mothership.

A schematic of the DTV configuration is shown in Figure 16. The major components include a ballast section, a flare section, an aft facing frustum and a nose cap. Three fins, not shown in this figure,

were added beginning with the third drop test to improve the DTV stability. Similar to the flight booster, the drogue and pilot chute packs are contained in the nose cap and the main parachute pack in the frustum. However, unlike the flight sequence which is initiated by ejecting the nose cap, the DTV contains a small mortar deployed vane chute which deploys a 11.5-ft nose cap extraction chute.

A comparison of the relative size of the DTV and SRB is shown in Figure 17. The significant weight difference (48,000 versus 170,000 lb) rendered it impossible to develop significant loads in more than one reefing stage of the drogue or main during a single test. Furthermore, in some cases, test peculiar reefing ratios and sequencing were required to set up the desired deployment condition. For the main chute cluster tests, the DTV deceleration was so great during deployment that it was not possible to obtain a high load condition. Single main chute tests were therefore used to evaluate the parachute structural integrity and cluster tests at flight deployment conditions used to assess the functional and performance aspects.

A matrix of the drop test program and the primary test objectives is contained in Table I. Note that in some tests planned objectives were not fully met. The reasons involve not meeting test conditions (Test 1), not attaining the desired loads (Test 2), or in having a significant failure (Test 3). The objectives were met, however, within the total drop test program.

A typical drop test sequence is illustrated in Figure 18. The test conditions for the drogue initial inflation were achieved by allowing the DTV to free-fall for a predetermined time from the drop altitude ranging from approximately 16,000 to 22,000 ft.

The measurement program consists of drogue and main chute load sensors, accelerometers, rate gyros, extensometers and a total pressure probe. Photographic coverage included two DTV onboard cameras, chase plane cameras, and ground based cameras. Space position data were obtained from the range cinetheodolite system.

A typical performance comparison between wind tunnel and drop test results[12] is contained in Figure 19. In general, the drop tests verified the predrop test performance predictions for the full open parachutes. The drop tests also permitted a refinement of the reefing line lengths to balance or optimize the loads experienced on each of the three stages for both drogue and main parachute systems.

Aside from the measured data obtained, visual coverage of the drop test program provided a significant insite into the aerodynamic behavior of the pilot, drogue and main parachute system during both the deployment process and during steady state conditions. Figure 20 illustrates some of the drogue deployment characteristics that were revealed during Test 2. As the drogue canopy emerged from the bag, the sailing lines rotated the canopy approximately 180 deg relative to the DTV. This also caused a twisting or wrap-up of the drogue suspension lines as shown. Although undesirable, no damage or appreciable drag loss resulted from this behavior. This anomaly was traced to the use of a test peculiar reefed pilot parachute which did not provide sufficient drogue pack acceleration to overcome aerodynamic forces on the lines.

Main parachute deployment has always been a major concern because the parachutes must be deployed out of a hard container (frustum) containing jagged edges at the separation plane. In Test 5 the frustum moved laterally after separating causing a skewed deployment of the three main parachutes. The cause of this is thought to be related to the dynamic motion of the DTV prior to frustum separation. Another problem experienced in single main tests is that of inflation overtake. To meet the Test 2 objective of deploying a main chute in a design limit environment, the drogue chute was reefed to 27 percent full open. Because of the resulting slow deployment velocity a phenomenon called "inflation overtake" occurred (Fig. 21). When this happens the parachute begins to inflate prior to being fully extracted from the deployment bag resulting in contact between the parachute and container. In Test 2, the result was several torn horizontal ribbons in one gore and in the vicinity of the canopy skirt.

Although many of the problems experienced were related to test peculiar conditions or configurations, a good understanding was gained relative to aerodynamic sensitivities to changes from the baseline design. This understanding has already enabled some modifications to the decelerator subsystem to accommodate unforeseeable changes in the SRB design. However, of primary importance, the drop test program established the needed confidence that the subsystem was ready for qualification testing on the actual Space Shuttle flights.

CURRENT/FUTURE CHALLENGES FOR SRB RECOVERY

'Although a recovery system has been successfully developed for the Space Shuttle SRB, both planned and proposed changes in the booster design are presenting new challenges. For instance, the reentry center of gravity has already migrated 16 in. beyond the original aft limit established for recovery system design. This movement is primarily a result of deleting development flight instrumentation,

adding approximately 1000 lb of structural reinforcement in the aft skirt region to take higher than expected water impact loads, and reducing the motor segment weight. To compensate for the hotter trajectory resulting from the more tail first reentry, some reconfiguring of the parachute sequencing and/or reefing will most likely be required.

An alternative to structurally strengthening the booster aft skirts is to reduce the water impact velocity. This approach, currently planned for the twelth Shuttle flight, will require the development of a larger main parachute.

Another major challenge will be the development of a new drogue and pilot parachute system for the planned filament would case SRB. This booster, although some 30,000 lb lighter at burnout than the current steel case SRB, will nonetheless have more stringent design requirements.

LARGER MAIN PARACHUTE

The larger main parachute system will consist of a cluster of three 136-ft-diameter parachutes of similar design and construction to the 115-ft chutes. This size parachute will provide a reduction in nominal water impact velocity from 87 to 75 ft/sec and can be contained within the volume available in the frustum.

Figures 22 and 23 provide a status of parachute system development relative to size versus peak load and dynamic pressure at deployment respectively. Included for comparison are the Shuttle drogue and main parachutes. These charts illustrate that the larger main parachute system will be stretching the boundary of parachute technology with respect to a combination of size, load, and deployment conditions. State-of-the-art design techniques can still be utilized, however, and the development risk is considered to be low.

A three-drop development test program is planned utilizing the DTV shortened by 54 in. to reduce B-52 hook loads. These tests will be performed at the Naval Weapons Centers, China Lake, California.

FILAMENT WOUND CASE PARACHUTES

The filament wound case SRB is being developed to reduce weight for high performance Shuttle missions. This booster, although externally similar to the steel case, is some 30,000 lb lighter at burnout and has a center of gravity almost 3 ft further aft. Because of the more aft center of gravity, the booster trim angle is increased about 10 deg (more tail first) causing a substantial drag loss and decrease in booster deceleration. This results in near sonic conditions at drogue deployment with dynamic pressure above 900 psf. One method available to improve the deployment conditions and currently baselined is to jettison the high performance motor nozzle extension at apogee. This provides a blunter configuration and increases reentry drag which lowers the deployment Mach number to approximately 0.95 and dynamic pressure to 715 psf.

The greatest challenge for the development of this system will be to devise a development test program that is both meaningful and cost effective which will verify that the deployment system will function properly in a high Mach, high dynamic pressure environment. A combination of rocket sled and air drop tests is currently planned to accomplish this end.

SUMMARY

The challenge of developing the recovery system for the Space Shuttle SRB has been successfully met as demonstrated by both development air drop tests and flight experience. The inherent aerodynamic characteristics of the reentering SRBs have been utilized to significantly diminish the requirements on the parachute system. The parachute system itself has been systematically optimized through wind tunnel, rocket sled and air drop tests to minimize development costs and maximize overall reliability. A similar approach using the current system data base as a foundation can now be used to develop recovery systems to meet future, more stringent Space Shuttle recovery system requirements.

REFERENCES

1. Godfrey, Roy E.: Space Shuttle Booster Recovery Planning. In Proceedings of AIAA 4th Aerodynamic Deceleration Systems Conference, AIAA Paper No. 73-441, 1975.

2. Struck, Heinz G.: Strakes, A Simple Means to Improve SRB Pitch Reentry Reentry Attitudes. NASA MSFC Internal Memorandum ED31-80-16, June 17, 1980.

3. Conine, B.; and Boyle, W.: Space Shuttle Solid Rocket Booster Sting Interference Wind Tunnel Test Data Analysis. Northrop Services TR-230-2042, 1981.

4. Dietz, W. E. Jr.; and Altstatt, M. C.: Experimental Investigation of Support Interference on an Ogive Cylinder at High Incidence. In proceeding of AIAA 16th Aerospace Sciences Meeting, AIAA Paper No. 78-165, January, 1978.

5. Bacchus, David L.; Vickers, Jack R.; and Foughner, Jerome T. Jr.: Wind Tunnel Investigation of Space Shuttle Solid Rocket Booster Drogue Parachutes and Deployment Concepts. In proceedings of AIAA 5th Aerodynamic Deceleration Systems Conference, AIAA Paper No. 75-1366, November, 1975.

6. Vickers, Jack R.; and Mickey, Fred E.: Wind Tunnel Test Report, SRB Drogue Parachute System. Northrop Corporation, Ventura Division Report NVR 74-45, 1974.

7. Vickers, Jack R.; Mullins, William M.; and Mickey, Fred E.: Wind Tunnel Test Report, SRB Drogue and Main Parachute System, Phase II. Northrop Corporation, Ventura Division Report NVR 76-24, 1976.

8. Kross, D. A.; and Webb, R. W.: Space Shuttle Solid Rocket Booster Decelerator Subsystem Rocket Sled Test Program. In Proceedings of AIAA 6th Aerodynamic Decelerator and Balloon Technology Conference, AIAA Paper No. 79-0437, March, 1979.

9. Webb, R. W.: Rocket Sled Nose Cap Ejection Test Report. Martin Mariette Report SRB-DSS-TM03-10, 1978.

10. Moog, R. D.; Sheppard, J. D.; and Kross, D. A.: Space Shuttle Solid Rocket Booster Decelerator Subsystem Drop Test Results. In Proceeding of AIAA 6th Aerodynamic Decelerator and Balloon Technology Conference, AIAA Paper No. 79-0463, March, 1979.

11. Moog, R. D.; and Sheppard, J. D.: Final Drop Test Report for Solid Rocket Booster Decelerator Subsystem. Martin Marietta Report SRB-DSS-TM11-2, 1978.

12. Moog, R. D.; Bacchus, David L.; and Utreja, Lajpat R.: Performance Evaluation of Space Shuttle SRB Parachutes from Air Drop and Scaled Model Wind Tunnel Tests. In Proceedings of AIAA 6th Aerodynamic Decelerator and Balloon Technology Conference, AIAA Paper No. 79-0464, March, 1979.

TABLE I. PRIMARY DROP TEST OBJECTIVES MATRIX

	Deployment Process		Limit Load Environment		High Q Deployment			Structural Integrity		Performance		
	Broadside	System Functional	Drogue	Single Main	Drogue	Main Cluster	Single Main	Drogue	Single Main	Drogue	Main Cluster	Single Main
Drop 1	•	●	○							●	●	
Drop 2				◒								●
Drop 3					●			○				
Drop 4						●						
Drop 5								●				
Drop 6			●				●		●			
Sled Test	●											

•Skewed deployment (α = 50°) although not objective.

○ = Objective

● = Accomplished

◒ = Partial accomplishment

ORIGINAL PAGE IS
OF POOR QUALITY

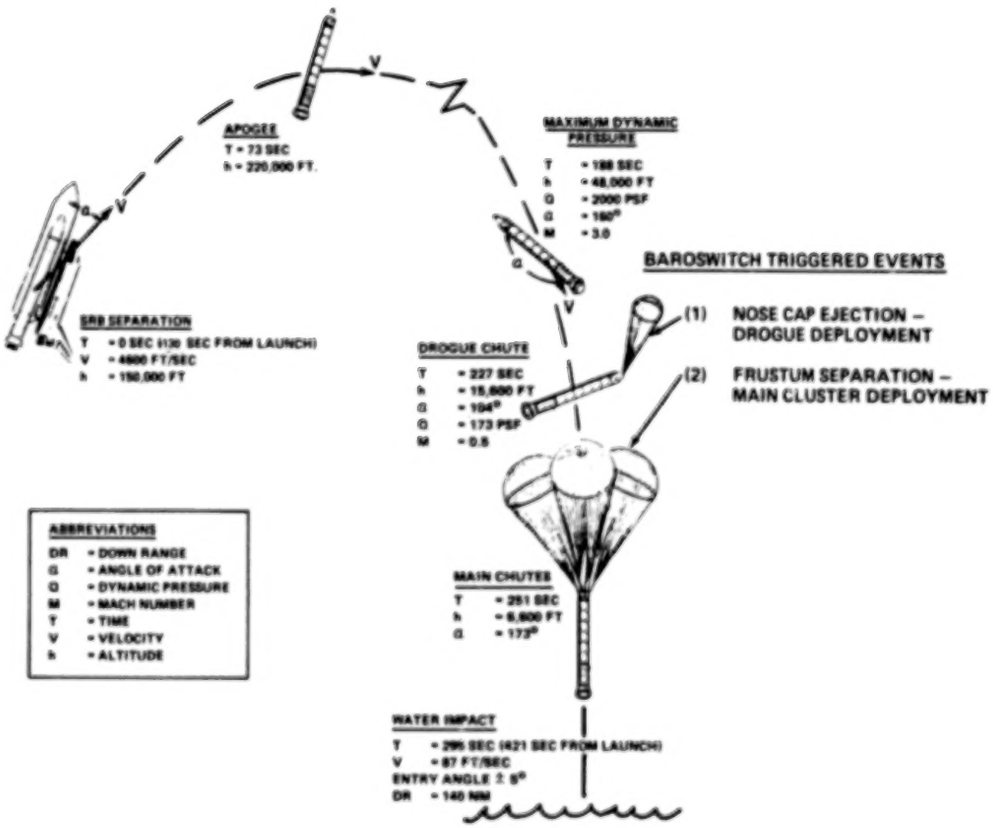


Figure 1. SRB Recovery Sequence of Events.

ORIGINAL PAGE IS
OF POOR QUALITY

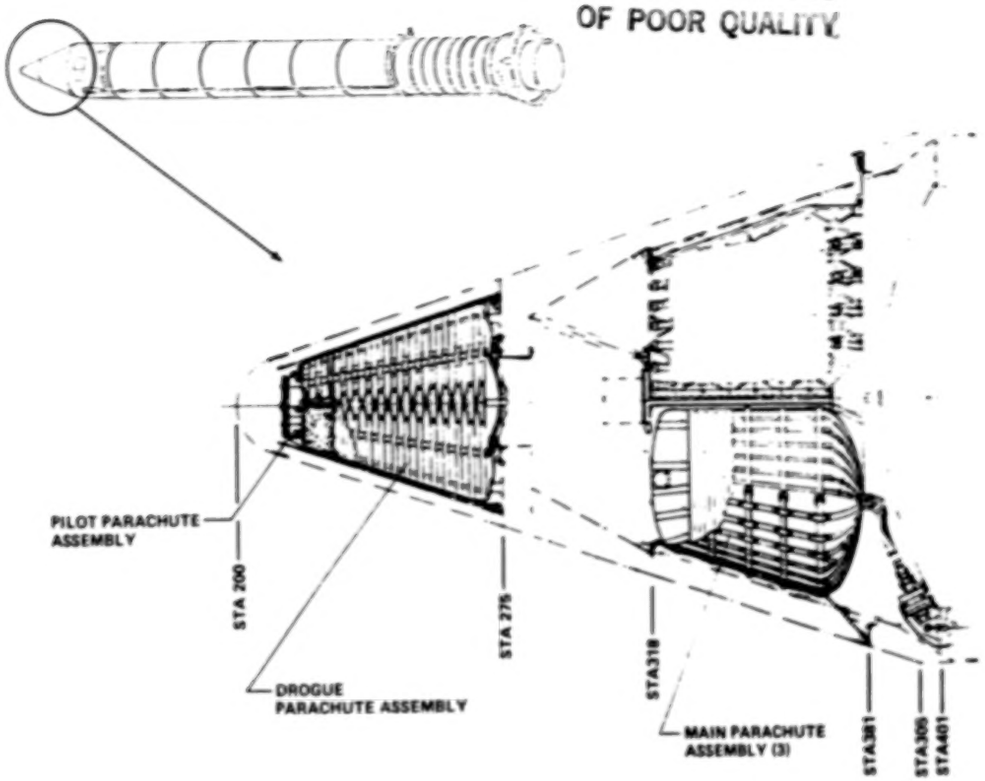


Figure 2. Parachute Locations in SRB.

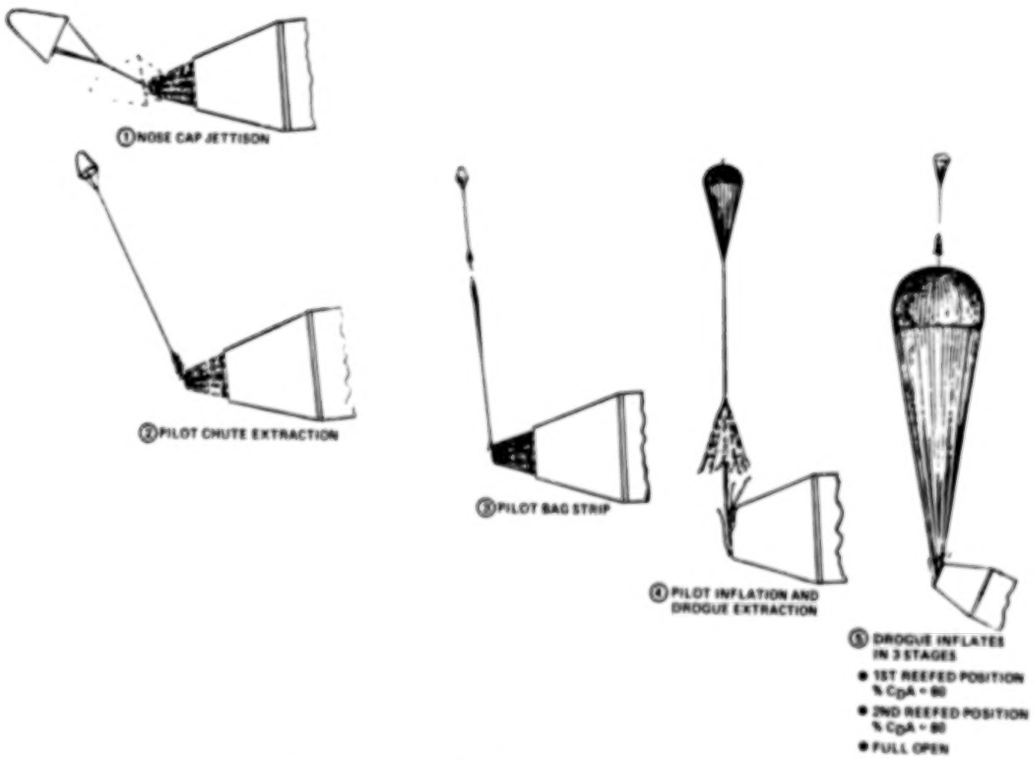


Figure 3. Drogue Deployment Sequence.

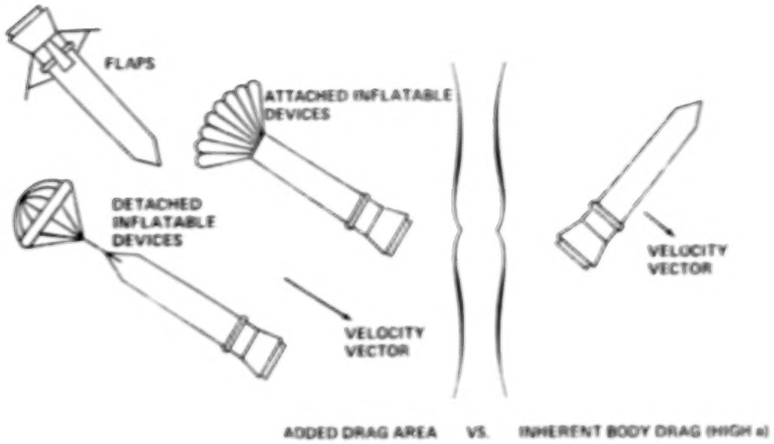


Figure 4. SRB High Altitude Deceleration Concepts.

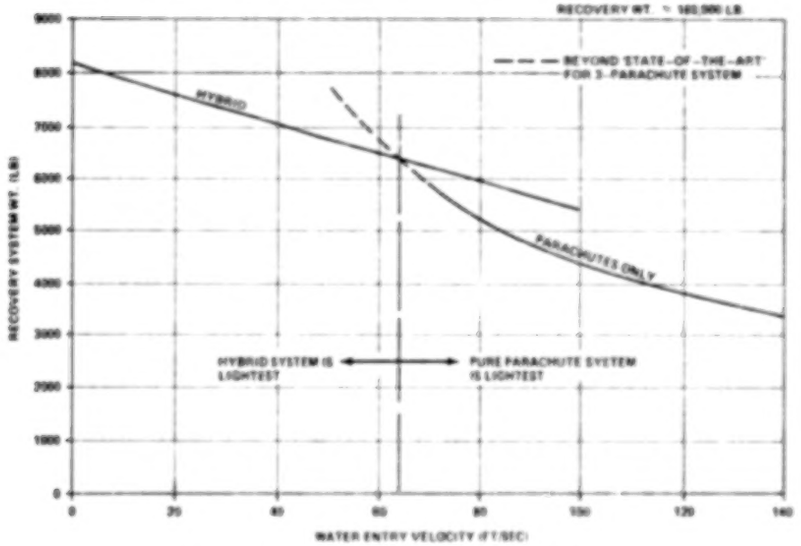


Figure 5. Deceleration System Weight.

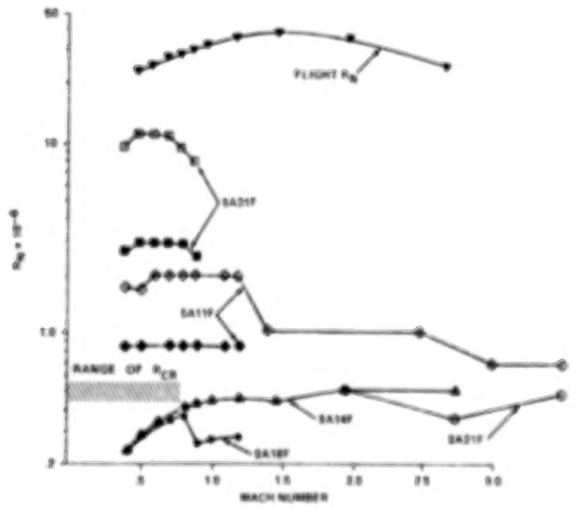


Figure 6. Wind Tunnel Versus Flight Reynolds Number.

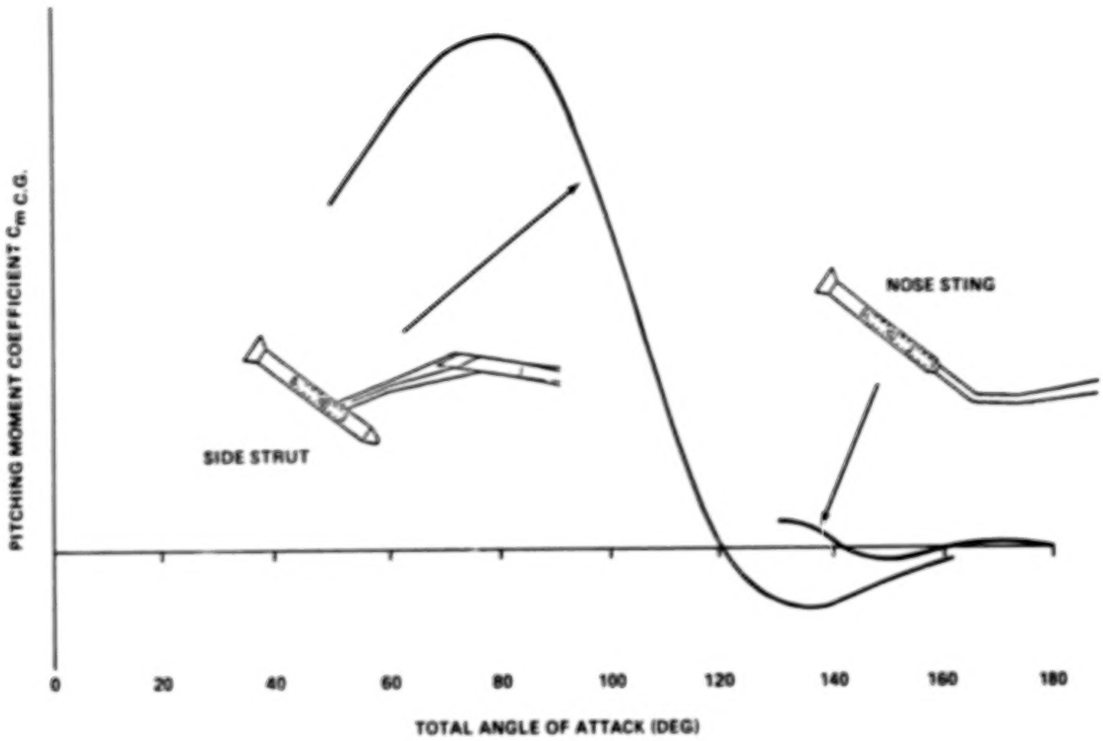


Figure 7. Effect of Model Support Method on Pitching Moment Coefficient.



a. SIDE MOUNT STRUT



b. NOSE STING WITH DUMMY SIDE STRUT



c. NOSE STING

Figure 8. Typical Sting Arrangements for Determining Sting Effects.

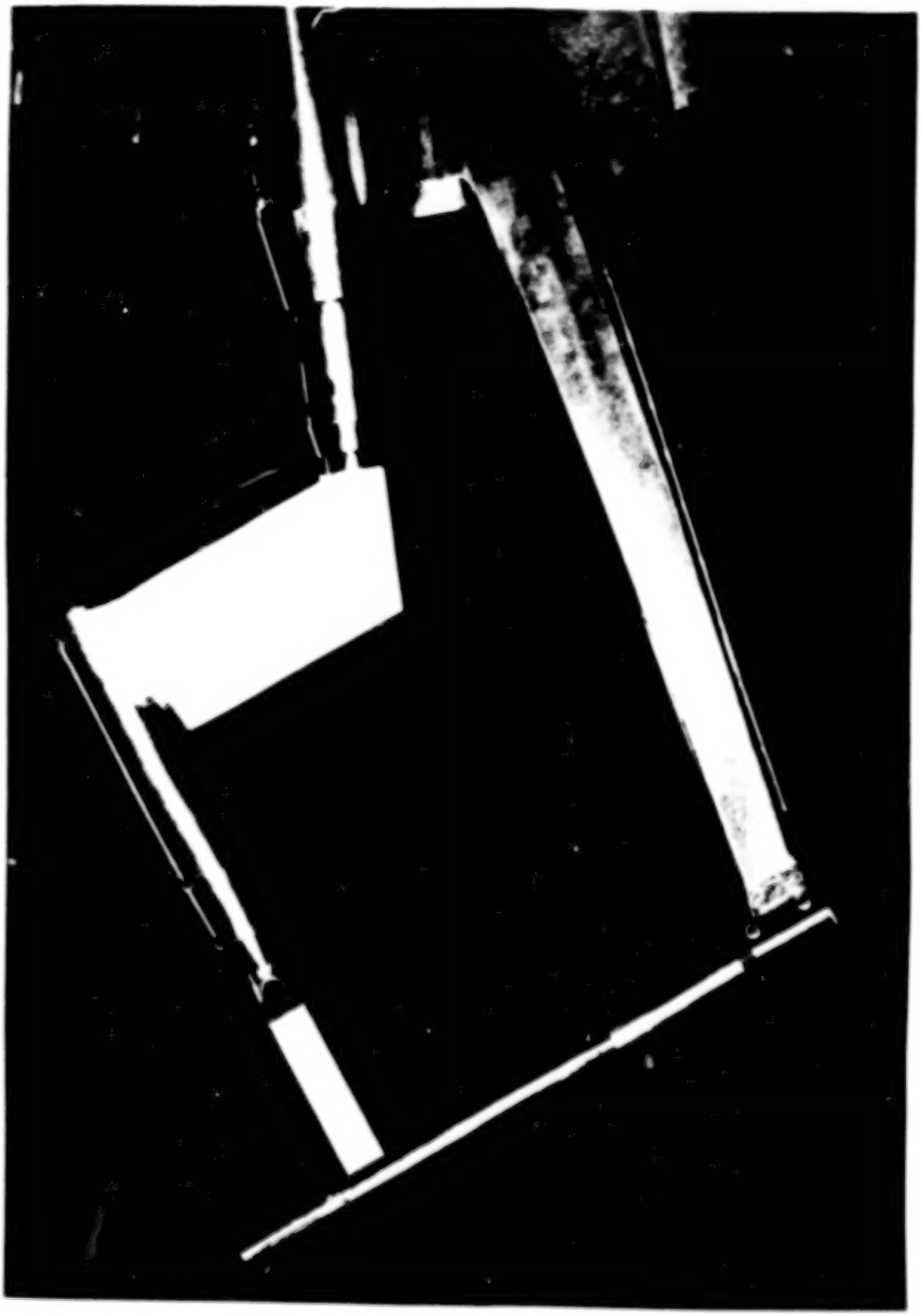


Figure 9. MSFC HRWT Side Strut With Dummy Nose Sting.

ORIGINAL PAGE IS
OF POOR QUALITY

ORIGINAL PAGE IS
OF POOR QUALITY

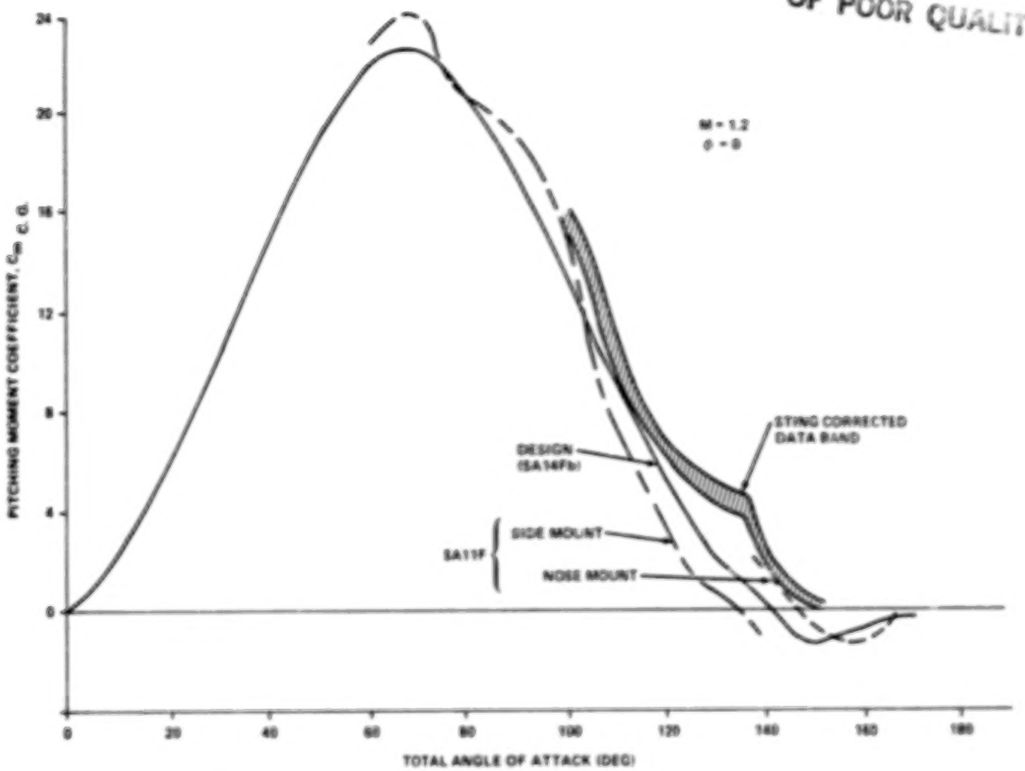


Figure 10. Sting Corrected Pitching Moment Coefficients.

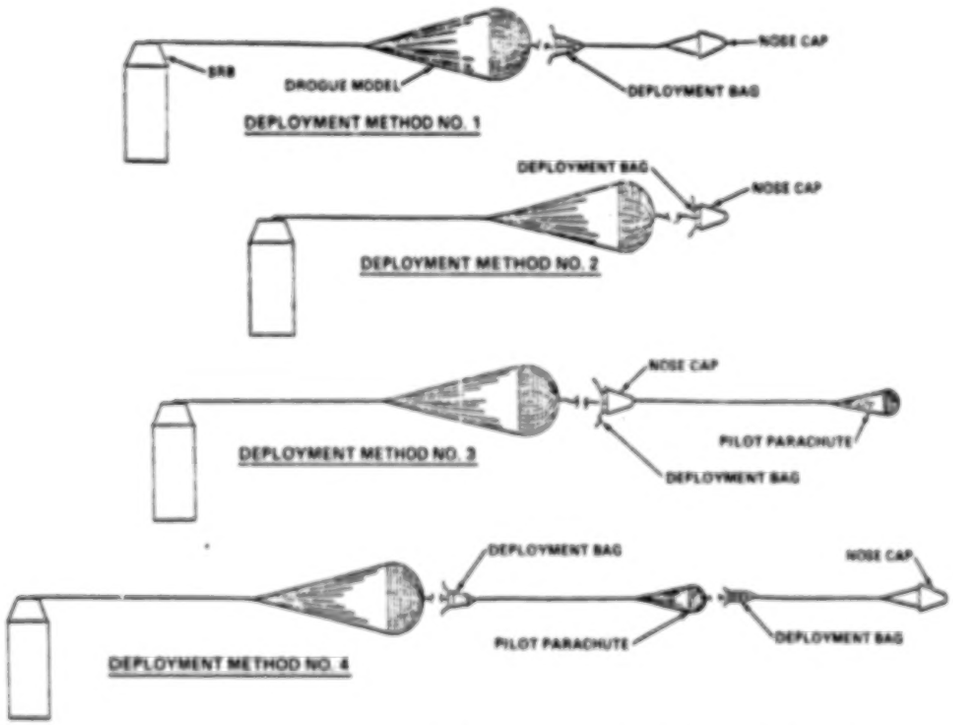


Figure 11. Candidate Drogue Deployment Methods Wind Tunnel Tested.

ORIGINAL PAGE IS
OF POOR QUALITY

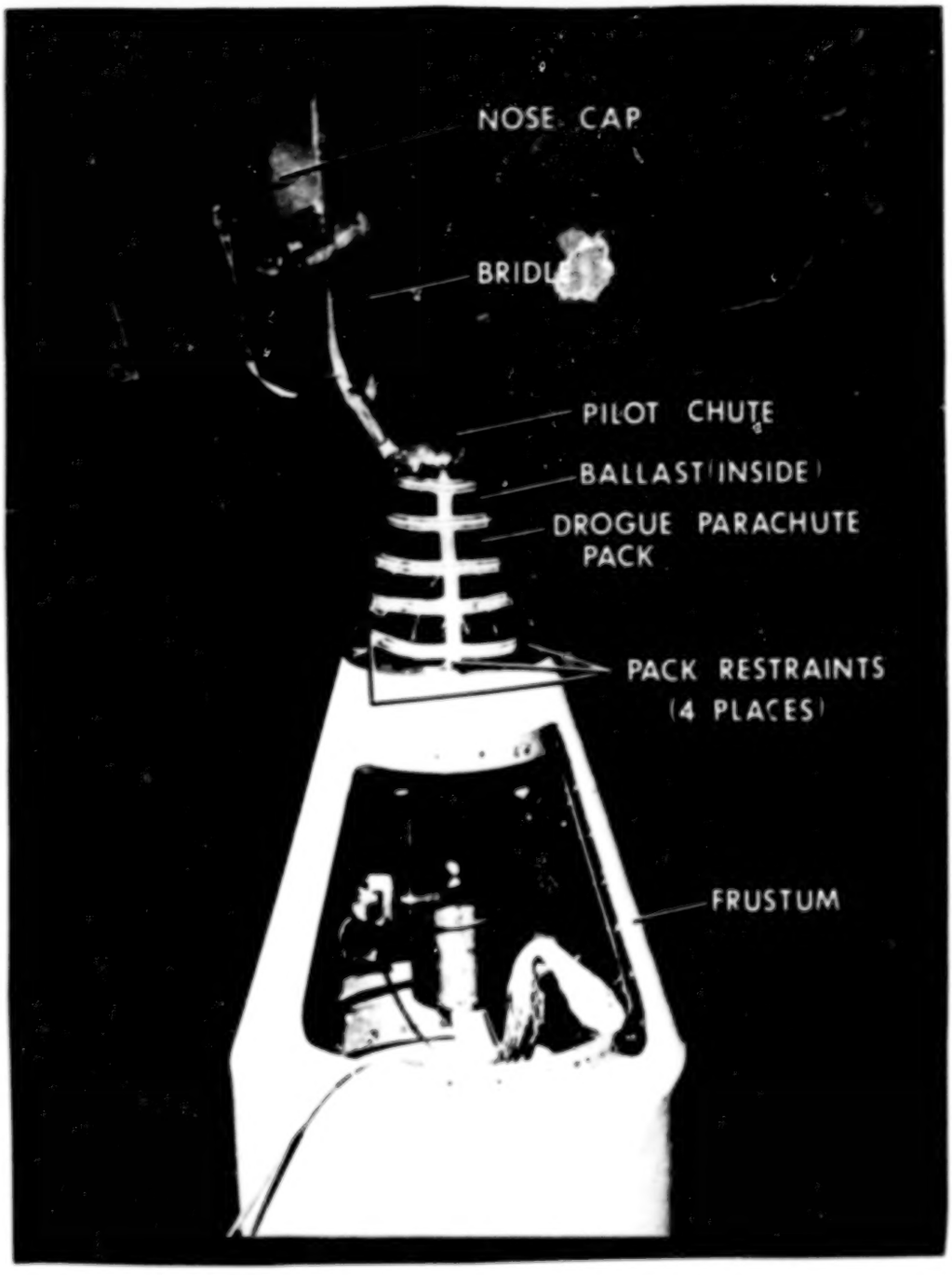


Figure 12. Drogue Deployment Test Hardware.

ORIGINAL PAGE IS
OF POOR QUALITY

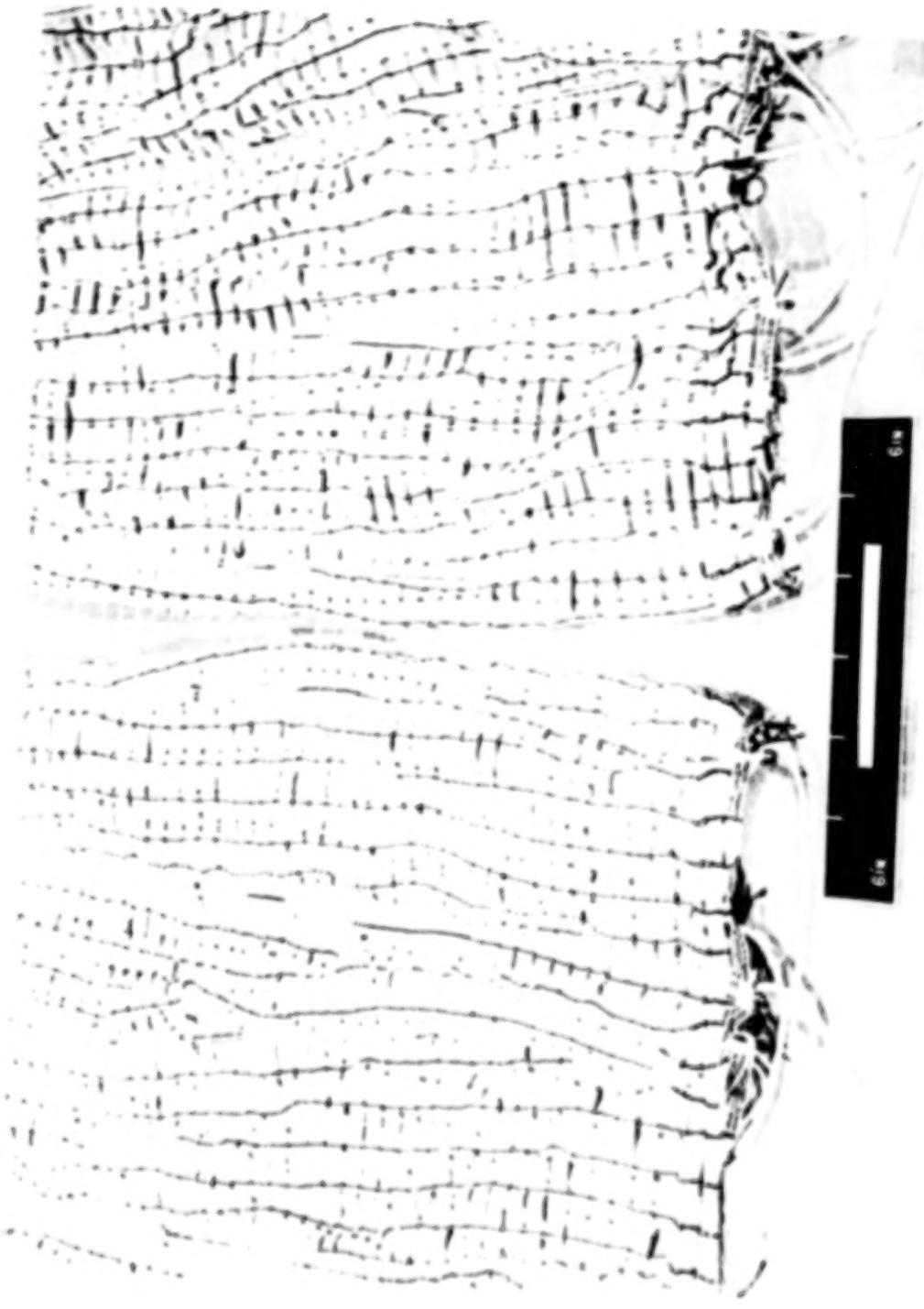


Figure 13. Wind Tunnel Test Ribbon Parachute Models.

ORIGINAL PAGE IS
OF POOR QUALITY

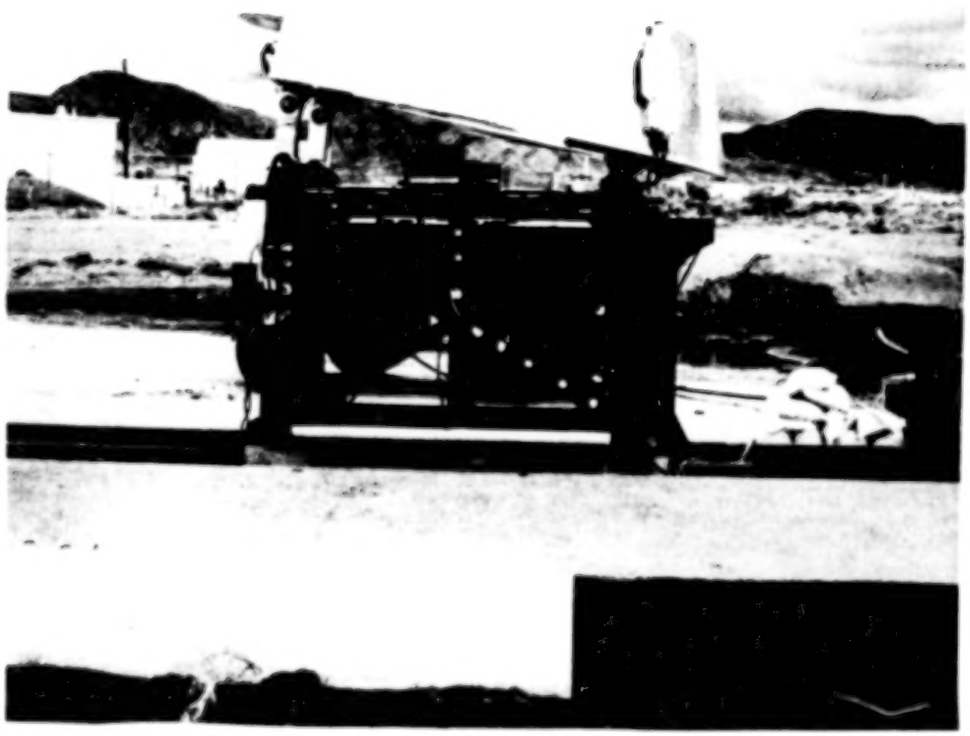


Figure 14. Sled Test Configuration (80-Degree Test).

ORIGINAL PAGE IS
OF POOR QUALITY

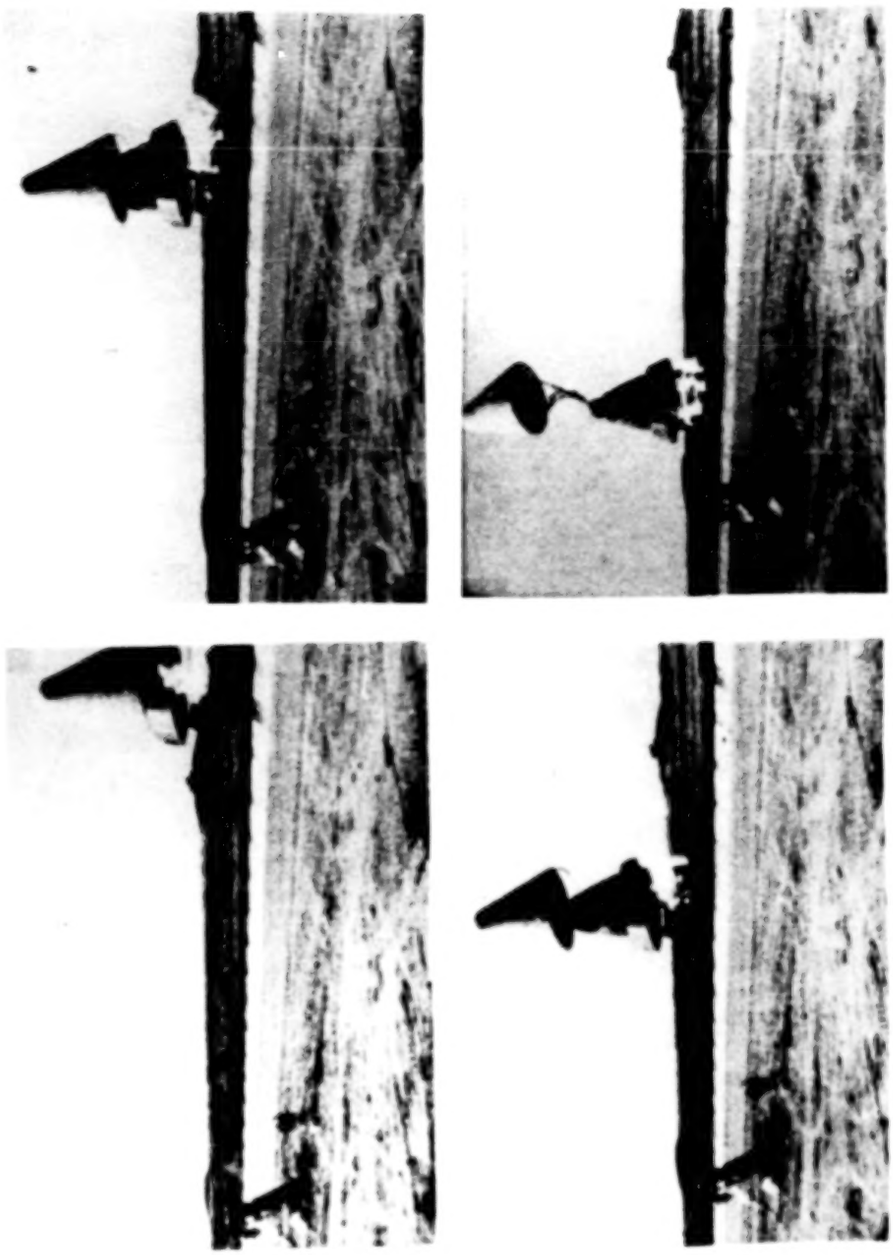


Figure 15. Nose Cap Ejection Sequence (80-Degree Sled Test).

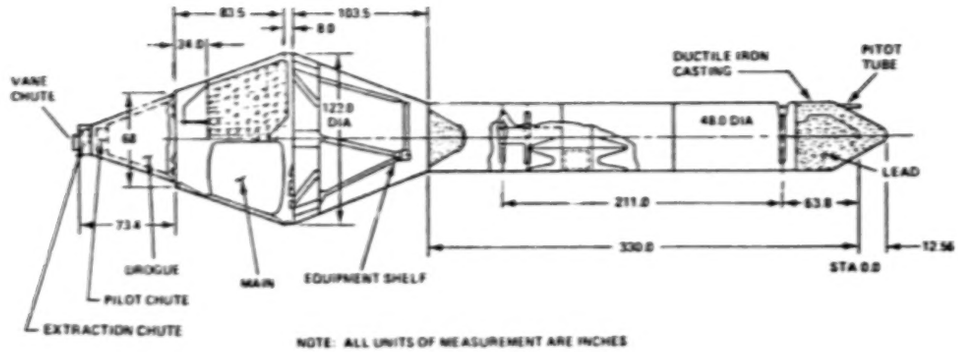


Figure 16. DTV General Arrangement.

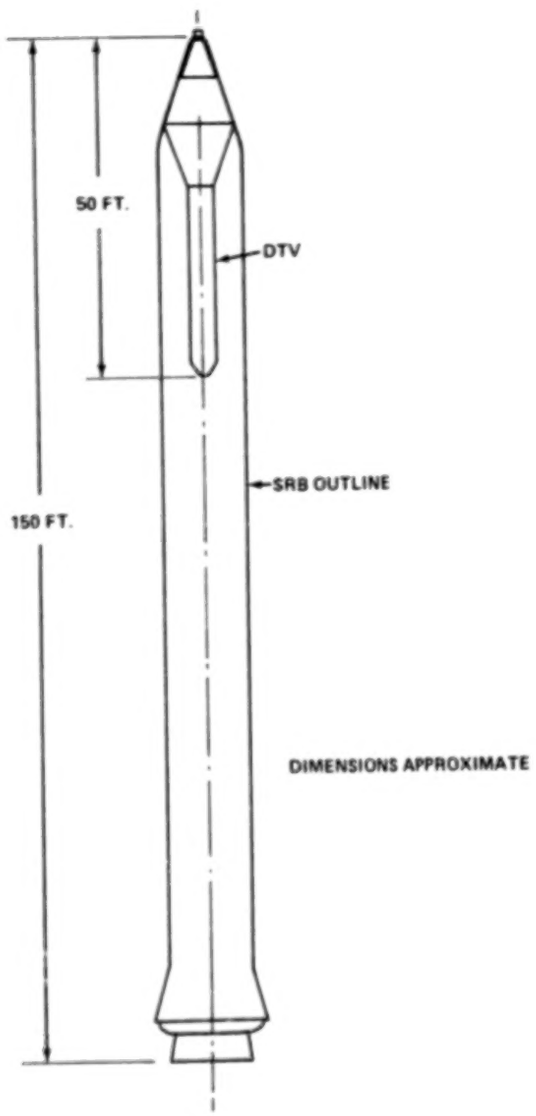


Figure 17. Comparison of DTV and SRB Size.

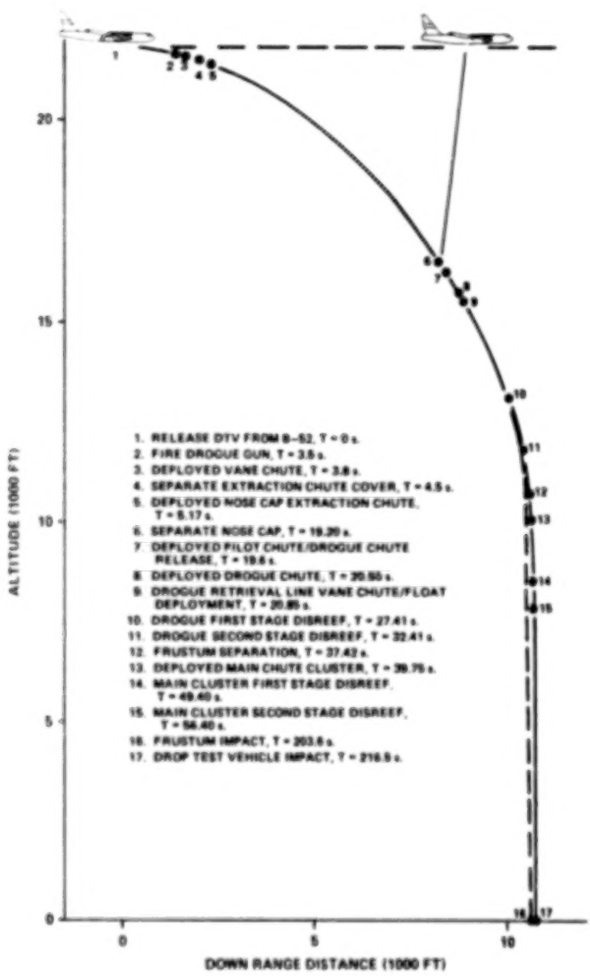


Figure 18. Typical Drop Test Sequence (Test 5).

ORIGINAL PAGE IS
OF POOR QUALITY

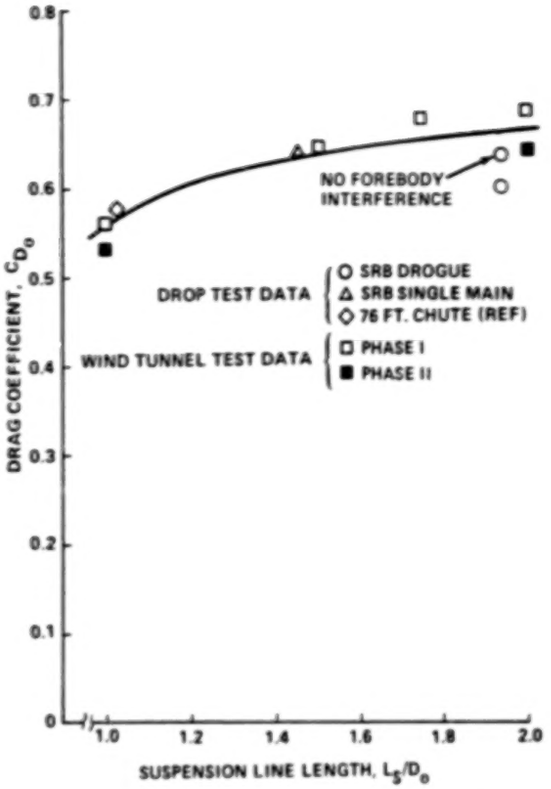


Figure 19. Drogue an Single Main Full Open Drag Performance.

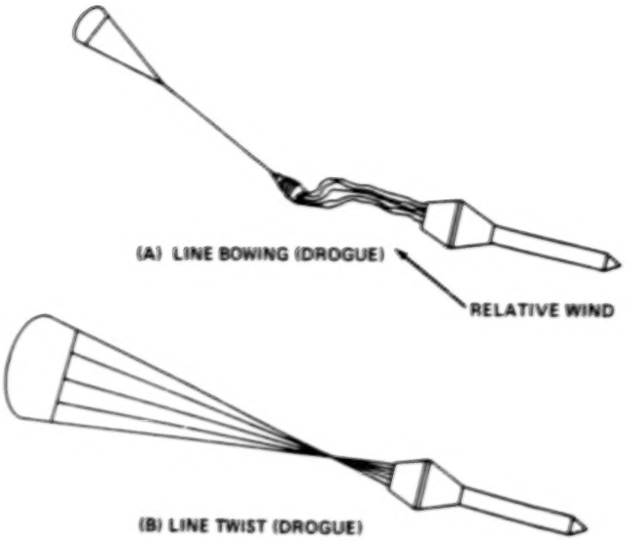


Figure 20. Drog Test Drogue Deployment Anomalies.

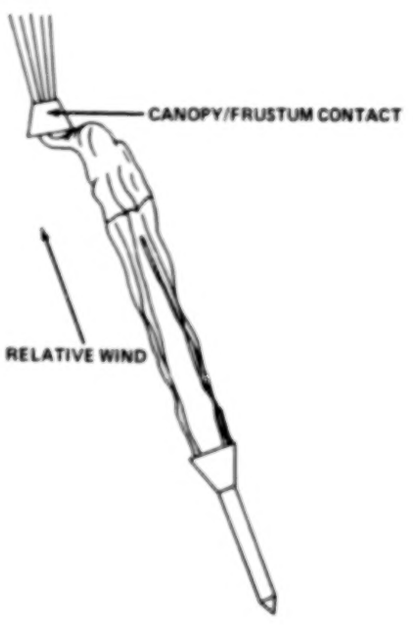


Figure 21. Inflation Overtake During Single Main Test.

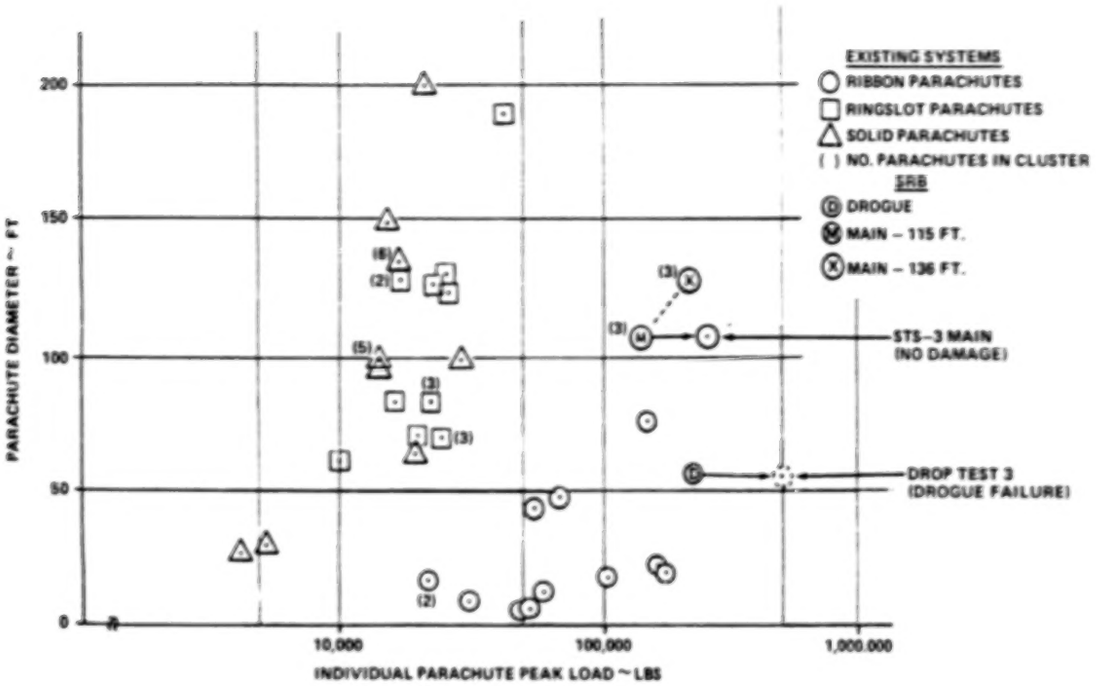


Figure 22. Parachute Experience, Peak Loads.

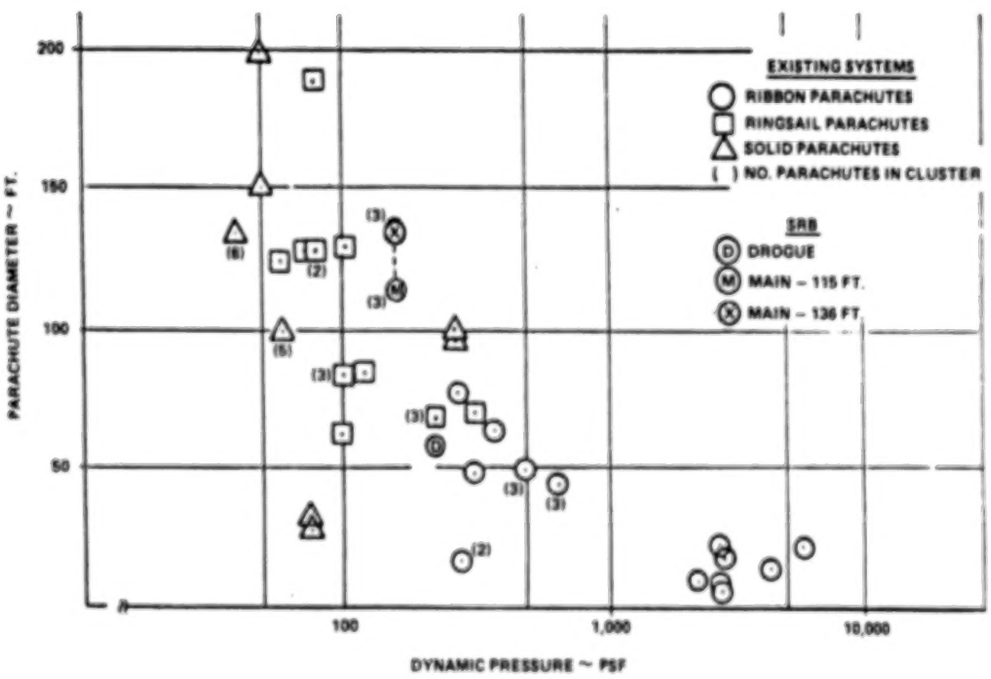


Figure 23. Parachute Experience, Deployment Dynamic Pressure.

N85
16909

UNCLAS

N85-16909

D20

THE AERODYNAMIC CHALLENGES OF THE DESIGN AND DEVELOPMENT OF THE SPACE SHUTTLE ORBITER

LEAD AUTHORS
James C. Young and Jimmy M. Underwood
NASA Johnson Space Center
Houston, TX

CO-AUTHORS
Ernest R. Hillje, Arthur M. Whitnah, Paul O. Romere,
Joe D. Gamble, and Barney B. Roberts
NASA Johnson Space Center
Houston, TX

George M. Ware, William I. Scallion,
Bernard Spencer, Jr. and James P. Arrington
NASA Langley Research Center
Hampton, VA

Deloy C. Olsen
Rockwell/Space Systems Group
Downey, CA

ABSTRACT

The major aerodynamic design challenge at the beginning of the United States Space Transportation System (STS) research and development phase was to design a vehicle that would fly as a spacecraft during early entry and as an aircraft during the final phase of entry. The design was further complicated because the envisioned vehicle was statically unstable during a portion of the aircraft mode of operation. The second challenge was the development of preflight aerodynamic predictions with an accuracy consistent with conducting a manned flight on the initial orbital flight.

This paper presents a brief history of the early contractual studies highlighting the technical results and management decisions influencing the aerodynamic challenges. The configuration evolution and the development of preflight aerodynamic predictions will be reviewed. The results from the first four test flights shows excellent agreement with the preflight aerodynamic predictions over the majority of the flight regimes. The only regimes showing significant disagreement is confined primarily to early entry, where prediction of the basic vehicle trim and the influence of the reaction control system jets on the flow field were found to be deficient. This paper concludes with an analysis of postflight results to attempt to explain these prediction deficiencies.

INTRODUCTION

A traditional phased approach was used in the programmatic design evolution of the Space Shuttle. The concept evaluation phase (Phase A) contractural studies were conducted in 1969. The Phase B concept definition phase extended over approximately 2 years beginning in mid 1970. The research and development phase (Phase C) and the production and flight test phase (Phase D) began with selection of Rockwell International as prime contractor in August 1972.

The following sections begin with background information which presents a brief review of the Phase A and B studies. The study results and management decisions which influenced the aerodynamic design are highlighted.

The remainder of the paper addresses the challenges facing the aerodynamic analyst at the beginning of Phase C & D, the approach used in attacking these challenges, and the success with which these challenges were conquered. The paper concludes with a review of the postflight analysis activity.

NOMENCLATURE

ACRONYMS

ADDB	Aerodynamic Design Data Book
AFFTC	Air Force Flight Test Center
AEDC	Arnold Engineering Development Center
ALT	Approach and Landing Test
ARC	NASA Ames Research Center
ASI	Aero Stick Input
ATP	Authority to Proceed
CDR	Critical Design Review
DFRC	Dryden Flight Research Center
EAFB	Edwards Air Force Base
ETR	Eastern Test Range
FCF	First Captive Flight
FCS	Flight Control System
FMOF	First Manned Orbital Flight
GN&C	Guidance, navigation, and control
JSC	NASA Johnson Space Center
KSC	NASA Kennedy Space Center
LaRC	NASA Langley Research Center (also LRC)
LTV	Ling-Temco-Vought Corporation
MSFC	Marshall Space Flight Center
NASA	National Aeronautics and Space Administration
OADB	Operational Aerodynamic Data Book
OFT	Orbital flight test
OML	Outer Moldline
OMS	Orbital Maneuvering System
OV	Orbital Vehicle
PDR	Preliminary Design Review
PRR	Program Requirements Review
PTI	Programmed Test Input
PWT	Propulsion Wind Tunnel
RCS	Reaction Control System
RSI	Reusable Surface Insulation
SEB	Source Evaluation Board
SRR	Systems Requirements Review
SSME	Space Shuttle Main Engine
STS	Space Transportation System
TAEM	Terminal Area Energy Management
TPS	Thermal Protection System
TWT	Transonic Wind Tunnel
UPWT	Unitary Plan Wind Tunnel
VAFB	Vandenberg Air Force Base
VKF	Von Karman Facility
WTR	Western Test Range

SYMBOLS

b	Reference wing span, ft
C_A	Axial force coefficient
C_D	Drag force coefficient
C_L	Lift coefficient
C_ℓ	Rolling moment coefficient
C_{ℓ_β}	Effective-dihedral parameter, per degree
$C_{\ell_{\delta_a}}$	Aileron roll-control effectiveness, per degree
$C_{\ell_{\delta_r}}$	Rolling moment coefficient derivative with respect to rudder, per degree
C_m	Pitching moment coefficient

C_{m_α}	Longitudinal static stability parameter, per degree
$C_{m_{\delta_e}}$	Elevon pitch control effectiveness, per degree
C_N	Normal force coefficient
C_n	Yawing moment coefficient
C_{n_β}	Directional-stability parameter, per degree
$C_{n_{\delta_a}}$	Yawing moment due to aileron deflection, per degree
$C_{n_{\delta_r}}$	Rudder yaw-control effectiveness, per degree
C_Y	Side-force coefficient
C_{Y_β}	Side-force coefficient derivative with respect to sideslip, per degree
$C_{Y_{\delta_a}}$	Side-force coefficient derivative with respect to aileron, per degree
$C_{Y_{\delta_r}}$	Side-force coefficient derivative with respect to rudder, per degree
C'_∞	Factor of proportionality in linear viscosity-temperature relation
cg	Center of gravity, inch
h	Altitude, ft
L/D	Lift-to-drag ratio
L_B	Reference body length, 107.525 ft
M	Free-stream Mach number
MAC	Mean aerodynamic chord, also $\bar{c}$, 39.568 ft
$\dot{m}$	Mass flow, lbm/sec
$\frac{\dot{m}_j}{\dot{m}_\infty}$	RCS jet mass flow ratio
n_j	Number of RCS jets firing
$\bar{q}$	Dynamic pressure, lb/ft^2
q_∞	Free-stream dynamic pressure, lb/ft^2
R_e	Reynolds number
S	Reference area, 2,690 ft^2
V	Velocity
V_D	Design touchdown speed
$\bar{V}'_\infty$	Viscous interaction parameter
x	Characteristic length, ft
$\bar{\chi}'$	Viscous interaction parameter
α	Angle of attack, deg
β	Angle of sideslip, deg
δ_a	Aileron deflection angle, (left elevon - right elevon)/2, deg
δ_{BF}	Bodyflap deflection, positive for trailing edge down, deg
δ_e	Elevator deflection, positive for trailing edge down, (left elevon + right elevon)/2, deg
δ_R	Rudder deflection, deg
δ_{SB}	Speedbrake deflection, deg
Λ	Sweep angle, deg
λ	Taper ratio
ρ	Mass density of air
ϕ	Momentum parameter (lbf)
ϕ	Bank angle, deg

$\frac{\phi_j}{\phi_\infty}$	RCS jet stream momentum ratio
X_{cp}	Longitudinal center of pressure, inch
$RM_{JI_{SFJ}}$	Rolling moment interaction due to side firing jets
$YM_{JI_{SFJ}}$	Yawing moment interaction due to side firing jets
$SF_{JI_{SFJ}}$	Side force interaction due to side firing jets
$PM_{JI_{SFJ}}$	Pitching moment interaction due to side firing jets.
$RM_{JI_{DFJ}}$	Rolling moment interaction due to down-firing jets
Δ	Incremental value

SUBSCRIPTS

j	Jet exit conditions
∞	Free-stream conditions
s	Spanwise shock location

BACKGROUND

The Space Transportation System (STS) was initiated with the "Phase A" conceptual design contracts in 1969. These contracts studied various methods of producing a completely reusable spacecraft system capable of a runway landing. A typical concept is shown in figure 1. The results of the Phase A studies led to the selection of a two-stage, completely reusable vehicle as the focus for "Phase B" contractual studies. The majority of the studies addressed a first stage manned "flyback" booster in combination with an Orbiter second stage as shown in figure 2. Subsequent to staging, the flyback booster utilized air breathing engines to return to the launch site for a runway landing. The Orbiter would continue the launch phase until low earth orbit was achieved. Following a typical on-orbit mission of 5 to 7 days, the Orbiter would re-enter the Earth's atmosphere at a high angle of attack (up to 60°), ultimately landing on a runway much like a conventional airplane. Midway through Phase B, estimates of system development costs indicated that the peak yearly funding requirements for the parallel development of two manned, fully reusable vehicles would not be a viable programmatic approach. During this time, the second stage fuel tanks were removed from the Orbiter to minimize the impact of any Orbiter weight growth during program development.

In the final months of Phase B, a parallel-burn concept was selected. This concept consisted of the simultaneous burn of both the solid rocket boosters (SRB) and the three liquid-fueled Space Shuttle main engines (SSME). The two SRBs assisted lift-off and the initial ascent flight. The SSMEs, fed by an expendable external tank (ET), continued to burn until near orbital insertion. The orbital maneuvering system (OMS) engines provided the additional delta-velocity required for orbital insertion. Figure 3 shows a Rockwell configuration, which is typical of the four parallel-burn configurations proposed for the Phase C & D contract.

As a result of the Phase B efforts, the Shuttle configuration shown in figure 4 was selected for the design and development phase. It was a partially-reusable vehicle with a parallel-burn propulsion system consisting of recoverable SRB's and an expendable ET used to supply fuel to the three main engines of the completely reusable Orbiter.

In addition to defining the concept for the Phases C & D contract, Phase B studies resulted in several programmatic decisions which significantly influenced the aerodynamic design of the Space Shuttle Orbiter.

The most significant Phase B decision was the selection of the reusable surface insulation (RSI) system rather than a hot-structure system for protection from entry heating. This RSI design dictated that the initial entry angle of attack (α) should be as high as possible (30° to 50°) to minimize re-entry heating. The U.S. Air Force requirement of a 1100-nautical mile (2037-kilometer) crossrange dictated that α be 30° or lower in order to achieve the required hypersonic L/D. To

reduce re-entry heating, thereby increasing lifetime of the RSI, an α profile of 40° was chosen for those missions not requiring the high crossrange.

Another Phase B decision affecting the future aerodynamic design was to provide for a completely computer-controlled, automated entry. This permitted the design of an entry flight control system (FCS) to artificially provide the required vehicle stability and the proper handling qualities. Traditionally, a relatively large empennage is required to provide the requisite vehicle directional stability. However, augmentation of the aerodynamic stability through the FCS permits the design of a smaller empennage, thus providing a significant reduction in vehicle weight.

Initially in Phase B there was not a design landing velocity on which to size the wing, the major weight driver of the Orbiter. As a consequence, it was difficult to make relative weight comparisons among the various contractor designs. Midway through the Phase B effort, NASA defined a subsonic "design" velocity which was to be used to size the Orbiter wing. This design velocity, later referred to as the design landing velocity, was defined as the trimmed velocity at an angle of attack equivalent to tail scrape angle at touchdown. A design velocity of 165 knots (306 km/hr) was chosen since man-in-the-loop simulations indicated this velocity produced actual touchdown velocities of 180-190 knots (334-352 km/hr). Touchdown velocities of this magnitude were well within the state of the art in landing gear systems. This criteria was used throughout the remainder of the development program.

As an end item product for Phase B each contractor was required to estimate the amount of the Phase C & D wind tunnel testing that would be required for detail design and development. In reviewing these estimates, it became obvious that the aerodynamicist would be faced with properly analyzing, verifying, and documenting the largest wind tunnel development program ever undertaken. Using these contractor estimates, NASA established the Source Evaluation Board (SEB), a total baseline wind tunnel program of 32,000 hours. Proposals of the four contractors called for programs ranging from 27,000 to 50,000 hours. The actual program ultimately accumulated 46,000 hours for the Phase C & D effort.

Although not directly related to the aerodynamic design, two program management decisions were made at the beginning of Phases C & D which significantly affected the magnitude of the challenge to the aerodynamicists. The first decision was to baseline the Orbiter systems configuration at the Authority To Proceed (ATP) milestone. Thereafter, the only design changes permitted were those which were required to fix critical system design problems. The Orbiter systems baseline included not only the vehicle outer mold line (OML) configuration, but guidance, navigation, and control (GN&C) systems and other subsystems. The second decision was to fly a manned, orbital mission on the initial flight of the Space Shuttle system. This philosophy of permitting only mandatory design changes (which became known as "make-work") significantly influenced the management of the aerodynamic and FCS development.

THE CHALLENGES

Strongly influenced by the economic and programmatic decisions previously discussed, three major aerodynamic challenges emerged.

The first challenge was the aerodynamic design of a spacecraft/aircraft that could fly through the entire atmospheric flight regime. The design had to satisfy the conflicting requirements of a spacecraft-like re-entry and a aircraft-like runway landing. It was to be the first winged vehicle to fly through the hypersonic speed regime, providing the first real test of experimental and theoretical technology of high speed flight. No design precedents existed to help establish the design requirements of such a vehicle. Yet, the design had to satisfy the conflicting aerodynamic characteristics of the various flight regimes as well as satisfying the requirements of a completely automated, multi-mode flight control system.

The second challenge was the preflight prediction of the aerodynamic characteristics of a complex vehicle with an accuracy consistent with establishing sufficient confidence to conduct the first orbital flight with a manned vehicle. This required the identification of the proper aerodynamic similarity parameters and overcoming the unknowns of the hypersonic wind tunnel facilities. It called for the efficient conduction and analysis of the most extensive wind tunnel program ever undertaken. And finally, in order to ensure consistency of design, it required careful configuration management of a continuously evolving aerodynamic data base to ensure that at any one point in time all systems and subsystems were using the same set of aerodynamics.

Finally, the third challenge was the technical management of the aerodynamic subsystem, which consisted of the following elements:

a. Integrating and focusing the efforts of a diverse number of organizations from the NASA, DOD, and industry aerodynamic communities.
b. Obtaining the support and ensuring the efficient utilization of virtually every major wind tunnel facility in the United States.
c. Ensuring the proper and timely interface with the other Space Shuttle systems and subsystems.

This paper will primarily address the first two challenges, which are technical. Although the third challenge, technical management, is indirectly addressed, more insight into this challenge may be found in reference 1.

THE APPROACH

The Approach Section reviews the rationale the aerodynamic analyst used in attempting to conquer the aerodynamic challenges. The section begins with a review of the design criteria used to configure the Orbiter. Following this initial section, the program schedule will be delineated. The section concludes with an extensive review of the aerodynamic development.

ORBITER AERODYNAMIC CRITERIA

Aerodynamic criteria[2] for the final selected configuration dictated that the vehicle perform as both a spacecraft and an aircraft during re-entry (figure 5). Accordingly, the external features must be carefully configured to (1) provide the protection and versatility required for orbital and atmospheric flight and (2) the aerodynamic performance, stability, and control necessary for an unpowered descent and landing. The aerodynamic lines must ensure acceptable performance for the hypersonic-to-subsonic speed range and provide the required crossrange and touchdown velocity.

Aerodynamic requirements, as shown in table 1, were developed from analysis of the re-entry phase of the mission. The angle of attack during initial entry was established by the RSI temperature requirement. The center of gravity (cg) requirement resulted from a NASA survey of potential payload users. Aerodynamic static stability was not required, since the design criteria permitted stability augmentation by the FCS to meet aircraft flying qualities criteria. Early entry flight simulations identified a FCS requirement for longitudinal static stability of no more than 2% L_B (5.44 % MAC) unstable at the aft cg. These requirements defined the aerodynamic design criteria for pitching moment characteristics. The subsonic lift-to-drag ratio (L/D) was set by the minimum value necessary for a safe landing.

The final Orbiter configuration, as shown in figure 6, evolved from a series of program and technical refinements directed to achieve the vehicle yielding the best combination of performance and cost. This evolution is discussed further in a later section. Figure 7 presents the general sizing criteria for the various components of the Orbiter. The double-delta wing planform, combined with a fuselage of moderately low fineness-ratio (approximately five), minimizes the interference heating effects, provides the required hypersonic crossrange, and possesses an acceptable trim and stability range over the flight Mach number range.

The subsonic design velocity was increased to 171 knots (88 m/sec) in order to reduce the Orbiter wing size thereby reducing vehicle weight. The leading edge sweep angle ($\Lambda = 45^{\circ}$) and aspect ratio (2.265) were selected on the basis of aerothermodynamic trade studies to provide the design touchdown speed for a cg at the forward limit with minimum wing size. This optimized the wing leading edge thermal protection system for a reuse cycle of 100 flights before major rework.

The fuselage was designed to accommodate a variety of payloads and to house the crew. It also was designed to contain the propulsion systems for launch and orbital maneuvering as well as provide a support structure for the main engines. The size of the payload bay was a contract specification. The size of the base of the fuselage was dictated by the packaging of the SSME's. The forward fuselage was dictated by packaging of the crew compartment. Nose camber and cross section, along with upward sloping forebody sides, were selected to improve hypersonic pitch trim and directional stability. And in conjunction with wing-body blending, to reduce entry heating on the body sides. Reaction control system (RCS) jets for entry attitude control and orbital maneuvering engines were incorporated in pods located in the aft body fairings. The orbital maneuvering system (OMS) pods

were sized for the OMS tankage. The bodyflap, originally sized to provide thermal protection for the SSME's during entry, is now also used as the primary pitch trim device.

The vertical tail was sized to provide a low speed C_{n_β} of 0.0013 at an angle of attack of 13° about a center of gravity located at the aft limit. It has a reference area of 413.25 ft^2 (38.39 m^2) including the rudder/speedbrake. The section profile consists of a 5° half-angle double-wedge airfoil. The rudder is split along the Orbiter plane of symmetry to provide directional stability augmentation in the hypersonic/supersonic flight regimes, and to apply drag modulation for the subsonic flight phase, approach, and landing.

DEVELOPMENT APPROACH

The Development Approach will initially address the development schedule followed by a review of the configuration evolution.

DEVELOPMENT SCHEDULE

Major program milestones for Phase C & D are illustrated in figure 8. They start with the ATP in August 1972 and culminate with initial operational capability in 1982. The Orbiter concept at ATP was a blended delta wing vehicle based on precontract studies and configured to meet initial Space Shuttle Program requirements. As a result of a continuing assessment of system requirements and technical refinements early in the contract, the Orbiter concept was modified to reduce weight and decrease program and operating costs.[3] Refinements in the aerodynamic configuration led to a double-delta planform incorporating a more efficient lifting surface than the blended delta. The System Requirements Review (SRR) in August 1973, finalized the technical requirements for the Space Shuttle systems (i.e., the total vehicle, its elements, and their ground systems) and approved the design approach of the vehicle and associated support equipment. The Preliminary Design Review (PDR) of the first Orbiter vehicle (OV-101) and subsystems for the approach and landing flight test (ALT) program were completed in February 1974. The PDR of the second Orbiter Vehicle (OV-102) followed in March 1975. OV-101 rollout from final assembly in Palmdale, California, took place in September 1976. The ALT Program consisted of three parts: (1) Orbiter/747 mated; (2) tailcone-on Orbiter alone; and (3) tailcone-off Orbiter alone. The vehicle was mated to the Boeing 747 carrier aircraft at the Dryden Flight Research Center (DFRC), Edwards Air Force Base, and the first captive flight was completed in February 1977. The first ALT flight of OV-101 from the Boeing 747 took place on August 12, 1977. A detailed review of the ALT program is presented in reference 4. In March 1978, OV-101 was delivered to the Marshall Space Flight Center (MSFC), Alabama, for ground vibration testing.

Fabrication and assembly of OV-102, the first orbital vehicle, began in 1975, and the Critical Design Review (CDR) was conducted in July 1977. Rollout of OV-102 was accomplished in March 1979, with delivery to Kennedy Space Center, Florida occurring a few weeks later. The first manned orbital flight was conducted in April 1981. The official Orbital Flight Test (OFT) program was established as the first four flights (STS-1 thru -4) with the initial operational capability starting with STS-5 in November 1982. However, aerodynamic flight test maneuvers are planned through STS-17.

CONFIGURATION EVOLUTION

Stability, control, and performance requirements for the Orbiter vehicle are, for the most part, established by the entry phase of the mission. On the other hand, design airload conditions are primarily driven by the ascent phase.

Design issues keyed to achieving the proper aerodynamic balance to provide stability, control, and center of gravity envelope during the entry flight regime are: (1) wing design, (2) wing-body integration, and (3) integration of aerodynamic and flight control requirements. Wing design was key because of its influence on vehicle weight, thermal environment, aerodynamic stability, buffet characteristics, and gliding and landing performance capability. Wing-body integration was important in obtaining a balanced aerodynamic configuration capable of trim and control over the entire speed range, and in minimizing thermal environment due to interference flow effects. Fuselage dimensions were largely fixed by payload size and packaging efficiency while aerodynamic and aerothermodynamic considerations established forebody shape and local contours. Integration of aerodynamic control requirements was of major importance in meeting flying quality goals in all

flight regimes, and minimizing vehicle weight as affected by control surface arrangement, size, and actuator requirements.

Prior to Shuttle Program "go-ahead" in August 1972, NASA funded extensive Shuttle System trade-off studies (Phase B contracts) to determine the following: (1) operational cost effectiveness; (2) desired configuration and geometry; (3) major subsystem definition; (4) configuration drivers consisting of landing speed, payload size and weight, and center of gravity envelope; (5) entry crossrange and aerodynamic heating; (6) stability and control requirements; and (7) flying qualities. From these studies emerged a baseline configuration at Shuttle Program ATP. Following ATP, further trade studies were conducted by JSC and the prime contractor to refine the baseline design.[5] Essentially four aerodynamic configurations were evaluated before the final baseline design was selected.

The phasing of the evolving configuration is illustrated in figure 10. The Rockwell blended delta configuration was baselined at ATP, with only "make-work" design changes permitted thereafter. The vehicle was sized for a dry weight of 170,000 lb, (77,110 kg) and landing payload of 40,000 lbs (18,144 kg). Initial wind tunnel tests indicated the ATP configuration did not meet the landing performance requirements. Wing optimization to meet these requirements led to baselining a configuration for the December 1972 Program Requirements Review (PRR).

The "make-work" philosophy was interrupted late in 1972 by a change in system requirements prompted by NASA's desire to reduce the operational cost per flight. This requirement update reduced the vehicle dry weight to 150,000 lbs (60,039 kg) and landing payload to 32,000 lbs (14,515 kg).

In addition to this requirement change, Rockwell was directed by NASA to incorporate the double-delta wing design. A year of NASA in-house study indicated the double-delta wing had exceptional landing performance. In addition the aerodynamic stability and trim could be adjusted by modifying the lightly loaded forward delta (glove). This simple control of aerodynamic features allowed the design of the main delta wing box to be frozen. Any cg or aerodynamic stability problems which might surface during program development could then be corrected by glove modification thereby minimizing program impact.

During this period, the maximum utilization of uniform dimension tiles was baselined in an attempt to minimize the RSI production and installation costs. Incorporation of this "standard" tile design, led to a vehicle whose surface was composed of large flat areas, limiting curvature to smaller areas between the flat ones.

These changes in system requirements and design led to baselining a new configuration for the March 1974 PDR. Initial wind tunnel tests of this PDR configuration indicated the configuration was not workable. Aerodynamic tests showed difficulty in providing trim capability at the forward cg in the supersonic flight regime. Aeroheating tests indicated the blunt fuselage nose resulted in early transitional flow and high temperatures along the lower body surface. Also wing incidence, camber, and thickness distributions designed for maximum subsonic performance led to local fairings on the lower wing and fuselage surfaces which caused high local heating. These findings led to a configuration modification of the Orbiter to eliminate these deficiences.

Ensuing wind tunnel tests indicated the revision of the PDR configuration was an acceptable configuration. After minor changes, such as blunting the forward portion of the OMS pod to allow the aft payload bay to open 180°, this configuration was baselined as the CDR configuration at the OV-102 PDR in February 1975.

After a flurry of configuration development activity in the first 7 months of the Phase C & D contract, the aerodynamic configuration remained relatively stable allowing the aerodynamic effort to focus on the development and verification of the preflight aerodynamic predictions.

AERODYNAMIC DEFINITION APPROACH

Conventional flight test programs call for the incremental expansion of the flight envelope to demonstrate the design capability of the aircraft. This is not feasible with the Shuttle vehicle. Once the Shuttle is launched, it is committed for flight over the complete mission profile from ascent to orbital insertion, deorbit, re-entry, and landing. Predicted flight characteristics must be based on aerodynamic data derived from theory, ground testing, and analysis. Careful attention has been given to the interactions between flight control systems design and aerodynamic characteristics. Because of these considerations great care had to be exercised in the development

of the preflight aerodynamic estimates. This section of this paper addresses the management, development and verification of the preflight aerodynamic predictions.

TYPICAL ORBITER MISSION

At an altitude of approximately 600,000 ft, the Orbiter is designed to perform an unpowered, gliding re-entry at an angle of attack of approximately 40°. The angle of attack is modulated depending upon the crossrange requirements. Downrange modulation is achieved by periodically performing bank reversals across the prescribed ground track. Figure 11 presents a typical re-entry trajectory.

Although entry interface (EI) is defined as 400,000 ft altitude, a sensible atmosphere is not reached until Mach 27 at an altitude of approximately 300,000 ft, with a dynamic pressure of 2 psf. Early entry stability and control is provided primarily by the aft-mounted reaction control system (RCS) jets, (figure 12). The forward-mounted jets are reserved for on-orbit attitude control and ascent aborts. The roll and pitch jets are active until dynamic pressures of 10 and 20 psf, respectively, are obtained, at which point the elevons are sufficiently effective to provide pitch and roll control. The yaw jets provide stability augmentation until the vehicle has decelerated to Mach 1.

A gradual pitch down is initiated between Mach 14 and 12. By Mach 2 the vehicle is flying at more conventional angles of attack from 3° to 10°. Equilibirum subsonic gliding flight is achieved at an altitude of approximately 40,000 ft. The approach and landing interface occurs at 10,000 ft, and the vehicle subsequently reaches a glide slope of approximately -19°. Nominal touchdown velocity is 195 knots with a rollout of 7,000 to 9,000 ft.

ORBITER FUNCTIONAL CHARACTERISTICS

The functional characteristics of the Orbiter are presented in figure 13. The thick, double-delta wing is configured with full span elevons, comprised of two panels per side. Each elevon panel is independently actuated. All four panels are deflected together as an elevator for pitch control and left and right elevons are deflected differentially as an aileron for roll control.

The bodyflap, originally designed as a heat shield for the SSMEs, is now also used as the primary longitudinal trim device. The elevons are programmed to follow a set schedule during entry to provide the optimum aileron effectiveness.

The vertical tail consists of the fin and a split rudder. The rudder panels are deflected together for yaw control and are separated to act as a speedbrake to provide for subsonic energy modulation. The speedbrake, initially closed upon entry interface, opens fully just below Mach 10, and then follows a predetermined schedule until Mach 0.9 is reached. The rudder is not activated for yaw control until Mach 3.5.

PREFLIGHT PREDICTION REQUIREMENTS

The preceding discussion leads to the conclusion that prediction of the basic aerodynamic characteristics of the vehicle are required from Mach 0.2 through 27, and at an angle of attack range from near 0° to 40°. Figure 14, which delineates utilization of the vehicle control effectors, shows that predictions of aileron and elevon effectiveness would be needed over the same M, α range. Rudder power needs definition below Mach 3.5. The high dynamic pressure to be encountered forced consideration of structural deformation effects on aerodynamics. Also the effectiveness of the RCS would have to be determined from on-orbit conditions down to as low as 50,000 ft (Mach 1). The RCS effectiveness is a function of jet thrust, plume impingement and the vehicle flow field/plume interaction as shown in figure 15.

PREFLIGHT WIND TUNNEL PROGRAM

Key to the Space Shuttle development has been the acquisition of wind tunnel test data to support GN&C design and evaluation by providing a continuously maturing aerodynamic data base reflecting configuration and subsystem updates. By the first orbital flight (STS-1) in 1981, approximately 46,000 total wind tunnel test hours had been conducted for aerodynamics, heat transfer, and structural dynamics, consisting of approximately 24,900 for the Orbiter vehicle, 17,200 for the mated launch configuration, and 3,900 for the carrier aircraft program, as shown in figure 16. A total of 101 models have been built: 45 aerodynamic, 34 heat transfer, and 22

structural dynamics. All wind tunnel testing was coordinated with and approved by NASA management at JSC. A detailed review of the history and management of the wind tunnel program may be found in reference 1.

Orbiter aerodynamic test hours are summarized in figure 17. Approximately 38% of the Orbiter aerodynamic test hours were utilized in the subsonic regime, 44% in the transonic/supersonic regime, and 18% in the hypersonic regime. As may be seen from figures 16 and 17, the Space Shuttle wind tunnel program was by far the largest program ever undertaken by this country. Also seen in figure 17 is an additional 10,000 hours of testing performed by Langley for special investigations requested by Space Shuttle management.

SELECTION OF SCALING PARAMETERS

In order to accurately simulate flight conditions in a wind tunnel, the appropriate similarity parameters must be matched. Traditionally, Mach number and Reynolds number are the key parameters. Problems in flow simulation[6] occur when the geometric scaling of viscous flow is important, or when coupling between the viscous surface flow and the external flow field is strong. In the first case, the boundary layer can be considered separately from the inviscid flow field, and viscous effects can be scaled. This holds for Mach numbers up to approximately 10. It is well known, for example, that skin friction varies with Reynolds number in a predictable manner and can be scaled to flight conditions from suitable wind tunnel results.

For Mach numbers greater than approximately 10, a pressure interaction results from the outward streamline deflection induced by a thick boundary layer, and the viscous-inviscid interaction must be considered. For this case, there are two classical simulation parameters commonly considered:

(1) $\bar{\chi}'_\infty$, the viscous interaction parameter introduced by Hayes and Probstein[7]

$$\bar{\chi}' = \frac{M_\infty^3 \sqrt{C'_\infty}}{\sqrt{R_{e_{\infty_x}}}}$$

(2) $\bar{V}'_\infty$, the viscous parameter introduced by Whitfield and Griffith[8]

$$\bar{V}'_\infty = \frac{M_\infty \sqrt{C'_\infty}}{\sqrt{R_{e_{\infty_x}}}}$$

where M_∞ is the free-stream Mach number, C'_∞ is the factor of proportionality in the linear viscosity-temperature relation,[9] and $R_{e_{\infty_x}}$ is the free-stream Reynolds number based on the appropriate characteristic length (x). The parameter $\bar{\chi}_\infty$ is the relevant parameter for the local effects (pressure coefficient, heat transfer, etc.) in both the strong and weak interaction cases; whereas $\bar{V}'_\infty$ is the relevant parameter in terms of overall integrated effect. For Shuttle, it has been observed that $\bar{V}'_\infty$ correlates total aerodynamic coefficients better than $\bar{\chi}_\infty$, and consequently, $\bar{V}'_\infty$ was selected as the hypersonic simulation parameter. A detailed discussion of the use of these scaling parameters for the Space Shuttle is presented in reference 10.

Figure 18 shows a comparison between flight $R_{e_{L_B}}$ and $\bar{V}'_\infty$ and the simulation capability of typical wind tunnels used to develop the Orbiter aerodynamic data base. It can be seen that the tunnel capabilities reasonably match flight conditions above Mach 3. It should be noted that although flight Reynolds number and Mach number were not simulated above Mach 15, if $\bar{V}'_\infty$ is the correct similarity parameter, the tunnel prediction of aerodynamic characteristics should be good.

One inadequacy worth noting is that at the time of the Shuttle aerodynamic development (prior to STS-1) neither experimental facilities nor theory could accurately predict real gas effects.

SIMULATION OF REACTION CONTROL JET INTERACTION

Early entry aerodynamic characteristics are highly influenced by interactions between the reaction control system (RCS) jet plumes and the local flow field over the Orbiter as shown in figure 15. The total jet effects are comprised of three factors: (1) jet thrust, (2) surface impingement, and (3) jet interaction with the flow field. Impingement and interaction effects are interrelated. Jet interaction was obtained from wind tunnel testing while surface impingement was estimated from vacuum chamber tests and theory. Coupling is present between the plume effects and aerodynamic surfaces, and between the jets themselves.

A series of scaled model RCS nozzles with different expansion ratios were employed during the wind tunnel test program. General Dynamics/Convair, under contract to the NASA (NAS9-14095),[11] developed a method whereby the experimentally-measured induced plume effect (surface impingement plus flow field interaction) could be separated into two component parts and the impingement term extrapolated to flight conditions. To obtain a correct modeling of the reaction control system plume effects in the wind tunnel, it was necessary to observe certain scaling criteria. The primary factors for consideration, aside from dimensional scaling, are plume shape, jet-to-free-stream momentum ratio (ϕ_j/ϕ_∞) and mass flow rate ratio ($\dot{m}_j/\dot{m}_\infty$). The RCS pitch jets (up and down firing jets) correlated better with momentum ratio whereas the yaw jets (side firing jets) correlated better with mass flow rate ratio.

These scaling parameters are defined as:

$$\frac{\phi_j}{\phi_\infty} = \frac{\dot{m}_j V_j}{2\bar{q} S} n_j = 7.3879 \frac{n_j}{\bar{q}}$$

and

$$\frac{\dot{m}_j}{\dot{m}_\infty} = \frac{\phi_j}{\phi_\infty} \frac{V_\infty}{V_j} \frac{1}{n_j} (\sin \theta_j)^{1/2} = 1.300 \times 10^{-3} \left(\frac{V_\infty}{\bar{q}}\right)$$

A detailed discussion of the selection of these scaling parameters is presented in reference 11.

THE WIND TUNNEL PROGRAM

The wind tunnel program can be divided into three phases. These phases are related to the development schedule as illustrated in figure 10.

The first of these phases (Phase I) was the configuration development phase. This phase, which covered the time period of ATP to SRR, addressed ATP configuration refinement, evaluation of the PDR configuration, and definition of the CDR configuration.

The prime contractor devoted the majority of their Phase II efforts to developing and verifying the aerodynamic characteristics for the ALT/carrier program although initial development testing for the OFT program was also performed. These latter development tests were directed toward establishing the basic stability and control characteristics across the Mach range; establishing control surface effectiveness and hinge moments; initial RCS testing; and viscous interaction testing. The FCS was converging on a detail design during the Phase II time period and concerns surfaced regarding the sensitivity of the FCS to nonlinear aerodynamics. In order to investigate potential nonlinearities, JSC management requested the LaRC to supplement the contractor's test program. These tests investigated the following areas: (1) non-linear aerodynamic characteristics of the basic vehicle and its control surfaces; (2) aerodynamic damping characteristics; (3) control surface interactions; and (4) high Mach/altitude simulations. In addition, the possibility of high altitude snap roll caused by asymmetric separation of the wing's leeside flow field was explored.

The final phase (Phase III) of the wind tunnel program was initiated in early 1978 to verify the predicted aerodynamic characteristics of the final vehicle configuration prior to the first orbital flight (STS-1). The objectives of this phase were to:

a. Verify and/or update the aerodynamic characteristics of the final, "as built" configuration across the Mach range of 0.2 to 15.
b. Test fine-cut (small increments) in Mach number, angle of attack, angle of sideslip, and control surface position along the nominal flight trajectory.
c. Minimize model-to-model and tunnel-to-tunnel discrepancies.

The final, preflight Aerodynamic Design Data Book (ADDB)[12] is primarily based on these verification tests. The verification phase consisted of three parts:

a. Seven initially planned verification tests.
b. Five anomaly resolution tests.
c. Five supersonic/hypersonic lateral-directional nonlinearity tests.

The complete verification phase is shown in figure 19.

Two high-fidelity wind tunnel models, of 2% and 5% scale, were designed and constructed based on the March 1976 OV-102 configuration drawings to ensure accurate modeling of all aerodynamic surfaces and simulation of all revelant cavities and protuberances as shown in figure 20. Although some minor changes to the TPS thicknesses were made after March 1976, these changes were closely monitored to ensure that there were no aerodynamicly significant differences between the wind tunnel models and the actual flight vehicle OV-102.

Part 1 of the verification phase consisted of the wind tunnel tests required for verification as it was originally conceived. These tests covered the Mach range of 0.2 to 15 using the two high-fidelity models without planned duplication of test conditions with different combinations of models and facilities. Several additional tests and considerable analyses were required to actually complete the preflight verification process. In order to acquire the highest quality data possible within time and fiscal constraints, a test team was established for each test consisting of the prime contractor, JSC, and facility engineers, co-chaired by the JSC and the prime contractor lead engineers. This team followed the test from initiation through model design and construction, test plan development, conduct of tests, and analysis of results.

The design of the verification tests drew heavily on the experience and results of a series of wind tunnel tests conducted by LaRC. These tests utilized a 1.5-scale model (OV-101/140C configuration) with remotely controlled elevons. They were conducted to investigate transonic and low supersonic lateral-directional nonlinearities and showed the importance of obtaining wind tunnel data in small increments and of utilizing remotely controlled aerodynamic surfaces.[13] Two of the major benefits of testing with remotely controlled surfaces are: (1) permits efficient acquisition of small increments of the primary variable of interest, i.e., the control surface position; and (2) permits the acquisition of more accurate data by "sweeping" the control surface position while other test variables are held constant.

The verification phase relied heavily on the NASA-Ames Research Center (ARC) wind tunnel facilities, as had the development test phase. Table 2 shows the utilization of facilities for Phase III.

Although Part 1 of the verification tests were largely successful, initial analysis of the data from these tests indicated additional wind tunnel tests were required to resolve the following test anomalies:

a. Transonic - resolve blockage and shock reflection effects.
b. Supersonic - verify relatively large facility (AEDC) flow tare corrections.

The tests shown under Part 2 in figure 19 were conducted as part of the verification tests phase to address the transonic blockage/shock reflection and supersonic tare correction problems.

The quick-look analysis of these tests still did not provide any clear-cut solutions to the original problems. Therefore, in July 1978, the Technical Panel for Orbiter Aerodynamics was formed at the request of the JSC Center Director to address these problems. The objective of the Panel was to expedite the analysis of the Orbiter aerodynamic design data to produce a mature data base that would support the launch of the first manned orbital flight planned for March 1980. This Panel was

comprised of working-level aerodynamicists representing expertise from ARC, DFRC, LaRC, JSC, AFFTC, and the prime contractor. The major functions of the Panel were:

a. Recommend and conduct wind tunnel tests.
b. Evaluate and recommend the most valid test data for use in establishing the ADDB preflight predictions.
c. Perform an independent, detailed analysis of critical areas.
d. Perform a thorough review of the proposed ADDB prior to publication and make recommendations for accceptance or change.
e. Obtain Panel consensus that the ADDB is the "best" representation of the Orbiter aerodynamics.
f. Give technical approval of the official ADDB.

The results of a wind tunnel test conducted by LaRC to assess the OV-102 configuration showed that there were no significant aerodynamic differences between OV-101 and OV-102. As a result, the large number of wind tunnel tests LaRC had conducted using the 1.5% model (OV-101 configuration) were used in developing the final fairings for the preflight ADDB. The high fidelity OV-102 model data was still considered prime and weighed the heaviest of all the data. The LaRC tests contributed significantly to filling in gaps of the OV-102 data base and to establishing model-to-model and tunnel-to-tunnel repeatability. The product of the Panel was the official Space Shuttle Orbiter ADDB published in October 1978 and revised in April 1979.[14]

Prior to the formation of the Panel, the technique of reviewing the "correctness" of the ADDB published by the prime contractor was to conduct a formal review after publication. Unless major discrepancies were identified and agreed to, no changes were usually made as a result of the formal review. Because the Panel worked closely with the prime contractor, making recommendations and changes during the development of the ADDB, a much more detailed review and refinement than by previous means of review was made possible. Almost all of the changes recommended by the Panel were accepted and implemented with minimum schedule impact. A significant amount of work by individual members was published directly in the ADDB.

After the Panel's work was complete, a minor update to the April '79 ADDB was made and the official aerodynamic data base was frozen in May 1980 to conduct final GN&C verification for STS-1. This data, the official preflight Orbiter aerodynamic data base, was published as a NASA Contractor Report in November 1980,[15] and was designated as the "STS-1 ADDB."

In January 1980, while conducting an in-house research test on high angle of attack aerodynamics, LaRC found a large difference in directional stability at Mach 6 from what the STS-1 ADDB predicted. This gave rise to some potential FCS concerns about performing a bank reversal in flight near Mach 6. An investigation of this potential problem led to Part 3 of the verification test phase: Supersonic/hypersonic lateral-directional nonlinearity tests.

It turned out that the lateral-directional characteristics are highly nonlinear with sideslip angle (β) at certain angles of attack. Further, this phenomena is not limited to Mach 6, but occurs over a Mach range of 2 to 8, at various α's. Also, nonlinearities of the sideslip derivatives with Mach, α, and speedbrake were identified that had not been observed previously. The basic problem was that the sideslip derivatives are linear only over a range of $1/2^{\circ}$ beat in some cases. The smallest tested previously was 1° and most data was at 2°. The cause of these nonlinearities is thought to be a complex vortex interaction with the vertical tail/speedbrake.

Discovery of a problem of this magnitude so late in the Shuttle program development (projected launch date of STS-1 was just over 1 year from discovery of problem) presented a schedule problem of how to acquire the necessary wind tunnel data, analyze the results, and put the data fairings in a form that was acceptable for input to the simulators so that a safety assessment could be performed prior to the STS-1.

In order to resolve the aerodynamic/FCS anomaly in time to support STS-1, a team was formed consisting of JSC, the prime contractor, LaRC, and wind tunnel facility engineers. This included aerodynamicists, flight control engineers, and simulation engineers at JSC. The wind tunnel tests conducted are shown under Part 3 in figure 19.

Detailed analysis of the test data was performed on-site during each wind tunnel test such that by the end of the test, final fairings were complete and the data had been converted into a form ready for the flight simulators. The data was then evaluated on an engineering simulator at JSC.

The results showed that the large nonlinearities with β could cause loss of control during a bank reversal when combined with certain FCS uncertainties such as winds and errors. As a result, the trajectory of the first flight (STS-1) was changed to avoid a bank reversal near Mach 6.

These new wind tunnel data were then used to produce a major update in the STS-1 ADDB, published in April 1982 as the Pre-Operational ADDB.[12] The Pre-Operational (Pre-Op) ADDB, although published after STS-1, contains no flight data (except for limited ALT results) and represents the true best estimate of preflight aerodynamics of the Space Shuttle Orbiter. Ultimately, the Pre-Op ADDB will be updated based on orbital flight test results to produce the Operational Aerodynamic Data Book (OADB) for the Orbiter. This will be the aerodynamic data base used for Shuttle operational planning such as mission planning, trajectory design, and crew training.

WIND TUNNEL DATA BASE ANALYSIS

It was a major undertaking just to collect the wind tunnel data base. The fruits of this undertaking would be meaningless unless the results of these tests could be presented to the aerodynamic analysts in a digestable form. The Space Shuttle Program management turned to the computer to facilitate this analysis. Chrysler Corporation's Space Division devised and operated a system of computer programs called "DATAMAN" to document and present test results to the aerodynamic analysts in a variety of plotted forms. The analyst could have at his disposal the data in the desired form allowing an efficient analysis to be performed. Chrysler received data tapes from the various facilities, transformed the various tapes to a common format, and used the computer program system to correlate, document, and produce data upon request to the aerodynamic analysts. A detailed review of this unique capability is presented in reference 16.

ORBITER AERODYNAMIC CHARACTERISTICS

Preflight predicted aerodynamic characteristics of the final Orbiter vehicle are summarized in this section. These characteristics derived from an extensive wind tunnel test data base adjusted for those effects which could not be simulated in the wind tunnel. Before discussing the corrections made to this data base and the actual aerodynamic characteristics, the management, control, and verification of the aerodynamic data base will be reviewed.

The challenge of the management of the aerodynamic data base falls into two areas: 1) creating and controlling a common data base for the multitude of users within NASA, and the contractors across the nation; and 2) verifying that data base. Late in Phase B, a common Orbiter aerodynamic configuration was selected as a focus for all in-house and contractor efforts. The aerodynamics for this configuration were compiled into an ADDB to be used for all computer simulations. The use of a central controlled ADDB continued into the Phase C & D time period. (An ADDB of estimated aerodynamic characteristics for the ATP configuration was submited with the Rockwell proposal.) As the configuration evolved a data book consisting of the estimated aerodynamic characteristics for each configuration was produced and subsequently verified experimentally. To further standardize the data base the process of centrally digitizing and producing computer tapes of each data book was initiated early in Phase C & D. Thus, the aerodynamic data base evolved into an ADDB and its corresponding digital computer tape, under configuration control of one of the major program panels.

ADDB verification was accomplished by a detailed technical review by NASA experts prior to each programmatic milestone until approximately 1-year before the first manned orbital flight. (The procedure used in this time frame was addressed previously in Phase III of the Wind Tunnel Section.)

WIND TUNNEL DATA BASE ADJUSTMENTS

The traditional free-stream Reynolds number was selected for the flow field scaling parameter below Mach 15, while a viscous interaction parameter ($\bar{V}_\infty'$) was utilized at higher Mach numbers. Since the test facilities were able to provide near-flight Reynolds number simulations over a large Mach number range, as shown in figure 18, no corrections to the wind tunnel results were required. At lower Mach numbers, the traditional adjustments were applied for Reynolds number effect on friction drag. Additional adjustments were applied to the profile drag to account for the added roughness of the thermal protection system tiles, and for minor protuberances, which could not be simulated on the wind tunnel test models.

In general, no attempt was made to obtain a wind tunnel measurement of the effects of structural deformation on the longitudinal aerodynamics through testing of conventional aeroelastic or deformed models. Since at higher $\bar{q}$'s these effects can be significant, some adjustment to the wind tunnel data must be made to provide adequate estimates of the flight aerodynamics. The approach used in the Shuttle Program to estimate the aeroelastic effects is thought to be unique.

First, a sensitivity analysis was performed with the aid of a structural/aerodynamic analysis computer program.[17,18] The geometry model used is shown in figure 21. This program was used to systematicly stiffen various portions of the vehicle structure to analytically evaluate the effect of the stiffness changes on the aerodynamics. The results indicated that the major longitudinal aeroelastic effects were produced by deformation of the wing back-up structure where the elevon actuator is attached, resulting in a change of the elevon position not measured by the vehicle position sensors. The effect was modeled by combining a rotary spring constant, as determined from vehicle loading tests, with wind tunnel derived aerodynamic hinge moment characteristics to determine a correction (usually less than 1°) to the rigid elevon deflection angle. The "elastic" elevon angle is used to look-up the rigid aerodynamic characteristics in determining the vehicle longitudinal aeroelastic characteristics.

The computer program indicated the major aerodynamic effect in the directional axis was the deformation of the vertical tail and the aft fuselage. Of particular concern was the predicted 40% reduction in rudder power due twisting of the vertical tail around its elastic axis. It was felt that this large effect could not be left to theoretical prediction techniques alone. After establishing the structural characteristics of the vertical tail and aft fuselage from the structural test article, an aeroelastically scaled vertical tail was constructed which simulated the root spring constant and tail stiffness distribution. It was then tested on a standard force model across the high $\bar{q}$ Mach range. The results from these wind tunnel tests were then analytically adjusted to "free" the orbiter from the sting mounting constraint necessary in the wind tunnel. The adjusted wind tunnel data are compared with the computer program predictions in figure 22 for a $\bar{q}$ of 300 psf (14,364 N/m^2). As can be seen, the correction is significant. A detailed development of this unique approach for evaluating aeroelastic effects is presented in reference 26.

AERODYNAMIC CHARACTERISTICS

The key aerodynamic parameters which have a significant influence on the Orbiter performance, and stability and control are shown in table 3. Lift, drag, and pitching moment are the primary aerodynamic parameters governing the entry trajectory and range capability. Pitching moment determines the bodyflap setting required for trim. Design areas sensitive to trim setting are elevon and bodyflap heating during initial entry, and control surface actuator stall limits at transonic speeds. In addition, there is an interaction between elevon setting and lateral-directional control capability because of the change of aileron effectiveness with elevon position. Lateral-directional trim and control capability is governed by the aileron, rudder, and sideslip derivatives. Above Mach 3.5 the aileron is used for both roll and yaw trim before the rudder becomes effective.

In the spacecraft mode of operation, bank maneuvers are initiated by the yaw jets and the aileron is used to coordinate the maneuver. Between Mach 3.5 and 1.5 the flight control system gains are scheduled to provide a transition to a conventional aircraft mode where the bank maneuvers are initiated by the ailerons about the roll axis and the rudder is used to coordinate the maneuver. Both the aileron and rudder are used for trim below Mach 3.5. The derivatives C_{n_β}, C_{ℓ_β}, $C_{n_{\delta_a}}$, $C_{\ell_{\delta_a}}$, $C_{n_{\ell_r}}$, $C_{\ell_{\delta_r}}$ were key parameters in establishing control capability, reaction control system propellant usage, and the switch-over point from spacecraft to aircraft control modes.

HIGH ALTITUDE AERODYNAMICS

Entry interface for the Shuttle has been defined as 400,000 ft (120,000 meters) altitude. In this high altitude region, rarefied gas flows are encountered by the Orbiter as it enters the atmosphere. Aerodynamic design issues in this region involve determining the effectiveness of the RCS control jets and their influence on the Orbiter flow field, in addition to defining viscous interaction effects associated with low Reynolds number/high Mach number flows.

Initial entry aerodynamic characteristics are strongly influenced by interactions between the RCS jet plumes and the local flow field over the Orbiter (figure 15). The application of the RCS data to a typical entry flight condition of $\bar{q} = 1.0$ lb/ft^2 (47.9 N/m^2) at an altitude of 260,000 ft (79,250 meters) are presented in figure 23 for three left downfiring RCS jets. The RCS impingement and flow interaction results have an adverse effect on pitch and roll control while increasing yaw control.

Viscous interaction primarily affects the shear forces with essentially no affect on normal force. Variation of $\bar{V}'_\infty$ along the nominal entry trajectory is illustrated in figure 24. High values of $\bar{V}'_\infty$ correspond to low values of Reynolds number which is associated with the thickening of the hypersonic laminar boundary layer causing increased shear on the lower surface of the Orbiter. Evidence of this is seen in figure 25 as an increase in axial force coefficient with increasing $\bar{V}'_\infty$ yields no change in normal force. There is insignificant effect of $\bar{V}'_\infty$ on pitching moment for 0° bodyflap as shown at the top of figure 26. At negative (trailing edge-up) bodyflap deflections, the movement of the bodyflap has little effect on the boundary layer on the lower surface of the Orbiter, and consequently, the effect of $\bar{V}'_\infty$ on pitching moment is similar to the 0° deflection case. However, for positive (trailing edge-down) deflections, the bodyflap control effectiveness decreases with increasing $\bar{V}'_\infty$, (figure 26). At large values of $\bar{V}'_\infty$, the correspondingly low Reynolds number results in a thickening of the boundary layer which causes the separation point to move forward with increasing control deflection. This causes the center of pressure to move forward, resulting in reduced pitching moment effectiveness with increasing $\bar{V}'_\infty$. Effects of $\bar{V}'_\infty$ on aerodynamic performance characteristics are indicated in figures 27 and 28 for a nominal entry trajectory. The decrease in L/D ratio caused by the increase in axial force is accounted for in design of the entry trajectory.

LONGITUDINAL CHARACTERISTICS

Longitudinal stability and control characteristics for low speed to hypersonic Mach numbers are illustrated in figures 29 and 30. These data are based on an extensive series of wind tunnel tests. Representative wind tunnel data are shown on the curves. The low-speed longitudinal characteristics shown in figure 29 demonstrate stall-free characteristics over operating flight conditions. The predicted characteristics are compared with test data obtained with a 0.36-scale model in the ARC 40x80-ft (12.19x24.38 m) wind tunnel. The changes in low-speed stability shown by the large changes in pitching moment at high α's are due to leeside separation on the Orbiter wing induced by vortices from the wing/fuselage junction. The leeside flow separation influences the supersonic stability characteristics also. It can be seen in figure 30 that for Mach 10 and 5, the variation of pitching moment with normal force coefficient for zero and positive elevon deflection follows the typical hypersonic pitch characteristics. This relationship between pitching moment and normal force coefficient does not follow the "sine square" variation for negative elevon deflections. The change in characteristics is due to the change in flow pattern on the leeside of the Orbiter wing as influenced by negative elevon deflections.

The surface flow patterns on the leeside of the Orbiter wing at supersonic speeds consist of three distinct flows. At low α's, the flow, which is initially perpendicular to the leading edge, is turned parallel to the free-stream by the presence of the fuselage (figure 31a). When the angle of attack is great enough to cause the wing leading edge shock to detach, the trailing edge shock will become strong enough to separate the boundary layer (figure 31b). This separation is the result of subsonic flow aft of the detached shock expanding around the leading edge and reattaching at supersonic speeds. The flow must still be turned into the free-stream direction as before. The turning is accomplished by a strong shock that causes the boundary layer to separate. The wake begins to affect the flow pattern at high angle of attack causing a secondary type of separation (figure 31c). Leeside flow boundaries at Mach 6.0 are shown in figure 32. The relationship between spanwise location of the shock induced separation, $\frac{b_s}{b}$, and Mach number was obtained from a correlation of delta wing data. The shock detached boundary was obtained from oil flow photographs.

The effect of leeside separation on wing pitching moment is shown in figure 33. The subsonic leading edge suction that occurs when the bow shock detaches results in a more stable pitching

moment slope. The change to a more stable slope is the result of leading edge suction when the wing bow wave detaches and a reduction of lift over the wing area aft of separation line. The center of pressure is more aft for the lift gain (due to leading edge suction) than for the lift loss due to shock-induced pressure aft of the separation line. The wing pitching moment becomes more stable, thus accounting for the increased stability shown in figure 30 for $+10^{\circ}$ elevon deflection.

Elevon effectiveness is also influenced by leeside separation. Loss in elevon effectiveness at high negative (trailing edge up) deflection can be attributed to the effect of back-pressure on the leeside flow field. Flap type controls will often cause boundary layer separation, especially in hypersonic low-density flows. Such back-pressure effects are of practical concern since it is desirable to control the Orbiter with leeward control deflection (trailing edge up) in order to minimize control surface heating. Figure 34 shows elevon effectiveness data obtained from the AEDC tunnel A at Mach 5 for an elevon deflection of -35°. The measured elevon effectiveness is seen to be less than shown by shock expansion theory. This is probably due to shock-induced separation. The extent of separation increases with α. After the α for shock detachment is reached, the back-pressure effect from the elevon will affect the wing flow. At high α's, the positive lift produced by the wing vortices outweighs the negative lift generated by the elevon-induced flow separation over the inner wing surface. The result is a loss of elevon effectiveness below the shock expansion value. Adjusting the theory for leeside separation results in reasonable agreement between theory and experiment.

Static trim capability for the elevon and bodyflap mentioned for trim to the forward and aft cg positions is shown in figure 35. The control schedules presented on the figure are for determining maximum obtainable cg trim limits. A reserve for maneuvering, trimming Ycg offset, manufacturing misalignments, and aerodynamic uncertainties has been added to the limits of the elevon effectiveness data to establish the limits shown on the figure. The aft cg limits are based on a positive elevon deflection of 15° for Mach numbers less than or equal to 10. A positive elevon deflection of 10° was used for Mach numbers greater than 10 due to thermal protection system design limits during maximum heating conditions. Forward cg trim limits are based on an incremental pitching moment coefficient reserve of 0.015 for Mach numbers less than or equal to 10 and 0.02 for Mach numbers greater than 10. Figure 35 indicates a slightly reduced forward cg trim margin at Mach 5.0 in the α range from 20° to 45°. This is attributed to the loss in elevon effectiveness due to leeside separation. Center of gravity trim limits for the entry α schedule are shown in figure 36. Both figures 35 and 36 indicate that a wide trim margin exists across the Mach number range.

Elevon control power, in conjunction with the bodyflap and speedbrake, provide trim capability between the design cg limits. The elevon schedule, shown in figure 37, illustrates the nominal and the most positive and negative settings for trim at forward and aft cg positions. The extreme settings account for control margin and uncertainties in aerodynamic characteristics.

LATERAL DIRECTIONAL CHARACTERISTICS

Lateral-directional stability and control characteristics for a mid cg along the nominal entry trajectory are illustrated in figures 38, 39, and 40. The Orbiter exhibits a stable dihedral effect (negative C_{ℓ_β}) across the complete Mach range during both the spacecraft and aircraft control modes (figure 38). During the spacecraft mode, and during transition to the aircraft mode, the vehicle is directionally unstable. C_{n_β} becomes positive indicating static stability in yaw between Mach 2 and 1, and remains directionally stable throughout the aircraft mode (Mach numbers below approximately 1.5). Aileron and rudder control effectiveness characteristics are illustrated in figures 39 and 40.

Early analytical studies predicted an effect of elevon deflection on the lateral-directional characteristics. Studies showed that the relatively large sized elevon in the presence of the deep, flat-sided fuselage could induce a change in the pressure distribution in the aft region of the fuselage. The change in the pressure distribution resulted in an incremental change in side force, yaw, and rolling moment when the vehicle was yawed. The effect of elevon on lateral-directional stability is illustrated in figures 41 and 42. The aileron control derivatives $C_{\ell_{\delta_a}}$ and $C_{n_{\delta_a}}$ are also affected by elevon position as shown in figures 43 and 44. The sensitivity of these derivatives to elevon position influences vehicle control boundaries.

Low-speed directional stability characteristics exhibit a strong combined Reynolds number and α effect as shown in figure 45. The figure illustrates the importance of full-scale Reynolds number testing on high α aerodynamics. Test data obtained from models tested at low Reynolds number (below 5×10^6 based on MAC) show essentially no change of directional stability with α. The early work of Polhamus[19] and Jorgensen and Brownson[20] indicated that Reynolds number and body corner radius could have a significant effect on the high α characteristics of the Orbiter. These predictions were borne out when the Orbiter model was tested at near full-scale Reynolds number in the ARC 40x80-foot (12.2x24.4 m) wind tunnel. It can be seen in figure 45 that the high Reynolds number test data show a decrease in directional stability with angle of attack which is in contrast to the low Reynolds number data which show essentially no change in stability with α.

AERODYNAMIC UNCERTAINTIES

The two program management decisions given in the Background section (to freeze the Orbiter system configuration at ATP and to fly a manual Orbital flight on the initial mission) had a significant influence on the approach selected for the aerodynamic design and verification of the Orbiter, particularly with regard to aerodynamic uncertainties. These decisions led to the development of two types of aerodynamic uncertainties: (1) Wind tunnel uncertainties, and (2) Wind tunnel-to-flight uncertainties.

WIND TUNNEL UNCERTAINTIES

The first decision baselined both the FCS and the aerodynamic configuration (as well as other systems and subsystems) in August 1972 at the ATP milestone. Thereafter, the only aerodynamic and FCS changes that were permitted were those which were required to fix critical system design problems. As evaluations of the baseline systems were conducted, it became clear that some significant changes to both the FCS and aerodynamic design would be required. This resulted in the final FCS and the aerodynamic design being conducted in parallel. This presented a problem of how to design a FCS "tuned" to the vehicle aerodynamics while the baseline aerodynamic data base was still evolving. Somehow, the FCS had to be designed to be insensitive to "reasonable" changes in the aerodynamic characteristics. This led to the requirement for a set of aerodynamic "design-to" uncertainties that would be used along with the baseline nominal aerodynamics in FCS design. These "design-to" uncertainties, designated "tolerances", were defined as the minimum error that is expected in the preflight aerodynamic predictions.

With the wind tunnel data base as the foundation for the preflight predictions, it was assumed that the minimum error that could be expected would be the ability to reproduce experimental results between various wind tunnel tests. Therefore, repeat tests were performed using various wind tunnel facilities, different models, and on occasion, different test organizations. Although the individual causes for any differences were not specifically identified, it is felt the total difference is representative of what may be expected for wind tunnel test repeatability.

As an illustration of the mechanics of this procedure, consider pitching moment coefficient, where repeat tests are presented along with ADDB estimates in figure 46. It can be seen from this figure that a 0.05 scale model (model 39-0) was tested in both ARC 11x11 foot facility, and in the LaRC 16-foot transonic facility. Similarly, a 0.015 scale model, model 44-0, was tested by LaRC in three facilities: 1) the Ling-Temco-Vought High Speed Wind Tunnel (LTV 4 x 4); 2) the LaRC 8-foot tunnel; and 3) the ARC 11x11 foot facility. In addition, the 0.02 scale model, model 105-0 was tested in the LaRC 16T tunnel. With all these potential sources of differences, a peak-to-peak repeatability in pitching moment coefficient (C_m) of approximately 0.006 was observed. This repeatability represents the combined error sources of the following: 1) the same model in several tunnels (tunnel-to-tunnel repeatability); 2) different models in the same tunnel (model-to-model repeatability); and 3) different test organizations (testing technique differences).

Based on this correlation, the difference between the wind tunnel results and the ADDB at various angles of attack were correlated with Mach number (figure 47). Tolerances (wind tunnel uncertainties) were obtained by fairing a curve through these data points using engineering judgement. The nominal flight angle of attack was given a high weighting in the fairing process. A similar process was used to develop tolerances for lift and drag coefficients, the sideslip derivatives, aileron derivatives, and rudder derivatives. Reference 21 provides a more detailed report on the development of the Orbiter wind tunnel uncertainties.

WIND TUNNEL-TO-FLIGHT UNCERTAINTIES

The second program management decision, to fly a manned vehicle on the initial orbital flight test of the Space Shuttle, raised the question of how to maximize mission safety without the benefit of conducting a graduated flight test program as is traditionally done in most aircraft development programs. This decision led to the requirement to provide a reasonable estimate of the maximum possible errors in the preflight aerodynamic predictions that might occur on the first Space Shuttle flight. These aerodynamic uncertainties were designated "variations".

In order to certify that the Space Shuttle system was ready for the first flight, a multitude of flight simulations were conducted using the aerodynamic variations, along with other system uncertainties, to "stress" test the FCS. Based on the results of these simulations, a cg, elevon schedule, and the FCS gains were selected for STS-1 which maximized the stability and control margins, thereby maximizing mission safety.

However, these "worst case" uncertainties must not be so conservative as to completely invalidate the FCS design. Since the preflight predictions were primarily based on wind tunnel tests, variations would represent the possible errors between wind tunnel and flight aerodynamics. It was felt that the most reasonable approach for the development of variations would be to analyze the wind tunnel to flight test differences of previous aircraft programs. Unfortunately, the verification of preflight predicted aerodynamics was not a major objective of most of the earlier flight test programs. This severely limited the amount of data available for conducting flight test to wind tunnel comparisons. The flight data base was further limited by restricting the comparison to those vehicles which were geometrically similar to the Orbiter.

Variations were established by fairing the differences between the flight and predicted aerodynamics as a function of Mach number. Because the selections of the configurations and the fairing process are very subjective in nature, a team of aerodynamicists from NASA Dryden Flight Research Center, NASA Johnson Space Center, Air Force Flight Test Center, and the prime contractor was formed to conduct the analysis and reach a consensus on variations.

The team's flight-to-predicted pitching moment correlation and their recommended variation fairings are presented as a function of Mach number in figure 48. As can be seen from this figure, the flight data is limited to below Mach 3. In Mach regimes where flight data was unavailable and the ideal gas assumption was justified, variations were obtained by multiplying the wind tunnel-derived tolerances by a safety factor, usually 1.5. A similar process was used to develop variations for the other aerodynamic parameters. A more detailed development of variations is given in reference 22.

A detailed investigation of the effect of real gas effects[10] was conducted in 1974 using state of the art theoretical techniques. Geometric limitation of the computer codes at that time did not lend sufficient confidence to use these results in adjusting the ideal gas wind tunnel data. Instead, a conservative estimate of the real gas effect was added to the pitching moment tolerances to estimate variation in the high altitude flight region. Presented in figure 49 is pitching moment variation as a function of the viscous interaction parameter in this flight region. The predicted real gas effects gave a more nose moment up to the basic vehicle pitching moment than ideal gas predictions. Therefore, the real gas increments were added to the positive pitching moment tolerances resulting in the unsymmetrical variations illustrated in this figure. A procedure for statistically combining these uncertainties is delineated in reference 23.

It is believed that the Space Shuttle Orbiter is the first winged aircraft/spacecraft to be designed using a systematic development and application of aerodynamic uncertainties.

THE ACCOMPLISHMENTS

The success of the first orbital flight of the Space Shuttle in April 1981 demonstrated the successful aerodynamic design and development of a vehicle configuration capable of flying both as a spacecraft and as an aircraft, and that the preflight predictions were of sufficient accuracy for a safe, manned re-entry. The question now becomes how well did the aerodynamicist do in the predictions? These preflight aerodynamic predictions[12] represent the culmination of the most intense aerodynamic development effort ever undertaken. The foundation of these predictions was an extensive wind tunnel program of more than 27,000 occupancy hours. This wind tunnel data base has been extensively analyzed by a team of aerodynamicists representing expertise from NASA, the prime contractor, and the Department of Defense. State of the art computer codes supplemented the wind

tunnel analysis. The success in predicting the flight aerodynamics represented a test of the nation's state of the art aerodynamic capability in the 1970's. For the first time in aircraft development history, the aerodynamicist was required to establish uncertainty levels (bounds) for preflight predictions. An assessment of how well the aerodynamic community performed is indicated by the ability to predict flight data within the wind-tunnel-to-flight-uncertainties (i.e. variations).

CORRELATION OF FLIGHT WITH PREDICTED

FLIGHT TEST PROGRAM

One of the major objectives of the Orbiter flight test program is the accurate determination of the aerodynamic characteristics where placards in the operational flight envelope have been identified due to possible uncertainties (variations) in the aerodynamics. For the first orbital flight (STS-1), flight test maneuvers were not conducted in order to minimize safety risks. During the second and subsequent flights, specially designed flight test maneuvers were conducted to permit aerodynamic data extraction.

Since during entry the Orbiter is in gliding flight with a relatively steep glide path slope, correlation of Orbiter flight data with predicted was somewhat more difficult than with more conventional powered aircraft. The aerodynamic analyst was faced with the dilemma of having all flight conditions varying simultaneously from entry to touchdown. Accordingly, the correlation of cause and effect was considerably more difficult.

Although a number of parameters have a significant effect on the aerodynamics, Mach number was selected as the prime correlating parameter in order to provide an overview of the entire flight. Therefore, an analysis technique must be selected to minimize the effect of the other parameters.

In order to make a meaningful correlation of data from several flights, the effect of flight-to-flight differences in the independent variables needed to be minimized. Since the same basic trajectories were flown for STS-1 thru -4, $\bar{q}$, and speedbrake setting (δ_{sb}) vary only slightly (for a given Mach number) from flight-to-flight. The most significant independent variable was elevon position (δ_e), which was progressively more positive (trailing edge down) on each successive flight. The elevon position varied from -3.5° on STS-2 to 5.8° on STS-4.

In order to correlate data over several flights, the flight minus predicted was correlated with Mach number. The predicted variations (uncertainties) are shown to gage the significance of any differences.

LONGITUDINAL PERFORMANCE FLIGHT RESULTS

In wind tunnel testing, the independent parameters are known precisely, while the accuracy of the aerodynamics is not so well known. In full scale flight testing the aerodynamics are, by definition, fully simulated and the aerodynamic forces and moments may be extracted without accurate knowledge of the flight conditions. For the Orbiter, determination of the flight independent variables particularly $\bar{q}$, with sufficient accuracy for aerodynamic correlations is very difficult. Significant correlation errors can occur when using the independent variables to non-dimensionalize the flight forces and moments and to "look-up" the corresponding predicted aerodynamic coefficients. Therefore, in correlation of flight results with predictions, analysis techniques must be selected to minimize the effect of possible errors in the independent variables.

L/D was selected for comparisons of predicted and flight aerodynamics since it is only sensitive to errors in flight accelerations and is independent of dynamic pressure. As seen in figure 50, flight results show the predicted L/D to be within variations down to near Mach 1. Subsonic L/D was underpredicted by approximately 5-10%.

The longitudinal aerodynamic center of pressure (X_{cp}/L_B), which is also independent of $\bar{q}$, was selected for trim comparisons. For a trimmed vehicle, the longitudinal center of pressure coincides with the flight cg. Figure 51 presents a comparison of the flight and predicted centers of pressure. As can be seen in this figure at Mach numbers above 10, the predicted X_{cp}/L_B is more aft than the flight value by as much as 0.7% of the reference body length (1.9% of the MAC), which is

well outside variations. As shown from Mach 3 to 10, flight results indicate that longitudinal trim was accurately predicted even though unusually high α's between 15° and 30° were flown. Although the flight results agreed with the predicted data within the variation (uncertainty) bounds, the agreement is less than satisfactory.

LATERAL-DIRECTIONAL STABILITY AND CONTROL CORRELATIONS

In order to permit the accurate extraction of stability and control characteristics, specially designed maneuvers were designed and conducted starting with STS-2.[24] The two primary types of stability and control maneuvers are: (1) Programmed Test Inputs (PTI) and (2) Aero Stick Inputs (ASI). Although both types of maneuvers are designed preflight to yield the optimum vehicle motion for data extraction, the PTIs generally result in better quality data because they are precisely executed, as designed, by the on-board computer. The ASIs are manually executed by the crew. More detailed descriptions of the flight test maneuvers, instrumentation, and data extraction techniques may be found in references 24 through 27.

Correlations of flight with predicted data are shown in figures 52 through 55 for lateral-directional stability, aileron effectiveness, and rudder effectiveness. Over the majority of the entry flight regime, flight results show good agreement with predicted data. However, at a few points during entry, both the lateral-directional stability and aileron effectiveness show differences between flight and predicted data approaching the variations level. Based on results extracted from the PTIs, rudder effectiveness appears to be well predicted throughout the flight regime.

As might be expected, the two regimes which show the largest differences between flight and predicted data are the transonic and hypersonic real gas regimes. The transonic wind tunnels have an inherent problem area of blockage and shock reflection due to tunnel walls, while at the same time having an order of magnitude lower Reynolds number than flight. And no tunnel today has the capability to truly simulate the real gas environment. In the hypersonic regime above Mach 10, the lateral stability, C_{ℓ_β}, appears to be less stable than was predicted while the directional stability, C_{n_β}, does not show any discernable trends. Flight results shown in figure 54 indicate that the elevon has a stronger effect on aileron effectiveness than was predicted.

In the transonic speed regime, the vehicle appears to be laterally more stable than predicted. However, there is considerable scatter in the flight directional stability data. Below Mach 3, the flight results indicate that the aileron is less effective in roll than predicted.

Recalling that the aerodynamic variations were derived from wind tunnel-to-flight differences experienced by previous aircraft,[22] it appears that, based on four flights, the Space Shuttle Orbiter stability and control aerodynamics were generally better predicted than most other aircraft.

RCS JET INTERACTION

The interference between the RCS jet plumes and the flow field at high altitudes is one of the more significant differences observed between flight and predicted data. The term "jet interference" is used to indicate combined jet interaction and plume impingement effects. During the first flight of the Space Shuttle (STS-1), the execution of the first bank maneuver during entry resulted in damped oscillations in sideslip angle and roll rate that were significantly larger than were predicted by preflight simulations. As shown in figure 56, oscillations up to 4° in sideslip occurred in flight whereas only 1° was predicted. Analysis of flight data indicates this was due to an overprediction of the rolling moment due to side-firing jets ($RM_{JI_{SFJ}}$) in the high Mach number, high altitude regime. As shown in figure 57, flight results obtained from PTIs conducted on STS-2, -3, and -4 not only confirm this overprediction, but also indicate that the jet interference is a function of the number of jets firing.[28] Because the $RM_{JI_{SFJ}}$ is of opposite sign and greater than the rolling moment due to direct thrust, it causes a reversal in the total rolling moment due a jet firing.

Flight results have also shown that the yawing moment jet interference ($YM_{JI_{SFJ}}$) and side force jet interference ($SF_{JI_{SFJ}}$) due a side-firing jet were underpredicted. Analysis of flight results

have also indicated that the pitching moment ($PM_{JI_{DFJ}}$) and rolling moment ($RM_{JI_{DFJ}}$) jet interference due to down-firing jets is less than predicted, as shown in figure 58. (A more comprehensive analysis may be found in reference 28.)

The flight test results obtained to-date indicate that both the side-firing jets and the down-firing jets are in general more effective than predicted.

POSTFLIGHT ANALYSIS

Several papers at the Langley "Shuttle Performance: Lessons Learned" conference[29] held in March of 1983, addressed the aerodynamic prediction deficiencies identified in a previous section.

An analysis is presented in reference 30 concludes that the underprediction of the subsonic L/D was due primarily to the over-prediction of profile drag. An over-estimate of the drag increment added for nonsimulation of the thermal protection system (TPS) steps and gaps led to this profile prediction deficiency.

Reference 30 presents an analysis of the longitudinal trim characteristics. The hypersonic pitching moment prediction deficiency is attributed to an error in prediction of the center of pressure. This is further substantiated by the good agreement between flight and predicted bodyflap and elevon effectiveness.

A possible explanation of the basic vehicle center of pressure prediction deficiency is addressed in reference 31. In this analysis, Mach, real gas, and viscous effects are incremented to Mach 8 wind tunnel data. Mach and real gas increments were obtained from computational fluid dynamic codes that were not available in the Shuttle development time frame. An estimate of pitching moment increments due to an increase in viscous shear acting on the bottom surface of the vehicle is obtained by semi-empirical means. This buildup process is presented in figure 59. Figure 60 shows a good prediction of trim bodyflap when these corrections are applied.

Finally, reference 32 concludes that the proper wind tunnel simulation parameter for RCS jet interaction still has not been identified.

CONCLUDING REMARKS

This paper has reviewed the aerodynamicists' success in conquering the challenges that were present in the Space Shuttle Program.

Apparently, the current state of the art real gas prediction techniques would properly account for the hypersonic center of pressure change encountered during re-entry of the Space Shuttle, although the quest for the proper RCS wind tunnel simulation parameter continues.

Although the flight tests for the majority of the Shuttle systems are completed, the aerodynamic flight test program is scheduled to continue through flight 17 in order to certify flight over the design cg range of 0.65 L_B to 0.675 L_B. This extended program will allow the program not only to refine the ability to predict the aerodynamics of the Orbiter, but also to provide the researcher with an extensive flight data base which should be used to improve future testing and prediction techniques.

The challenge of the future rests in the hands of the researcher and the future program analysts. That challenge is to fully exploit the methods, the information, and the experience gained from the most extensive, complicated, aerodynamic development program ever accomplished: America's Space Shuttle.

REFERENCES

1. Whitnah, A. M.; and Hillje, E. R.: Space Shuttle Wind Tunnel Testing Summary, NASA RP-TBD, 1983.
2. Rockwell International Space Division, "Aerodynamic design Data Book, Volume 1, Orbiter Vehicle," November 1977, Report No. SD72-SH-0060-1K.

3. Smith, E. P.: "Space Shuttle Orbiter and Subsystem," Rockwell International Space Division Report No. SD72-SH-0144, June 1973.
4. Hooks, I.; Homan, D.; Romere, P. O.;: Aerodynamic Challenges of ALT, NASA JSC Space Shuttle Conference, NASA CP-TBD, June 1983.
5. Surber, T. E. and Olsen, D. C.: "Space Shuttle Orbiter Aerodynamic Development," Journal of Spacecraft and Rockets, Vol. 15, No. 1, January-February 1978, pp 40-47.
6. NASA LaRC, "High Reynolds Number Research," October 1976, NASA CP-2009, pp 2-17.
7. Hayes, Wallace D. and Probstein, Ronald F.: "Hypersonic Flow Theory," New York and London, Academic Press, 1959, pp 333-345.
8. Whitfield, Jack D. and Griffith, B. J.: "Hypersonic Viscous Drag Effects on Blunt Slender Cones," AIAA Journal, Vol. 2, No. 10, October 1964, pp 1714-1722.
9. Bertram, Mitchell H.: "Hypersonic Laminar Viscous Interaction Effects on the Aerodynamics of Two-Dimensional Wedge and Triangular Planform Wings," NASA TN-D3523, August 1966.
10. Woods, W. C.; Arrington, J. P.; and Hamilton II, H. H.: A Review of pre-flight Estimates of Real-Gas Effects on Space Shuttle Aerodynamic Characteristics, NASA CP-2283, March 1983.
11. Rausch, J. R., General Dynamics Convair Division, "Space Shuttle Orbiter Rear Mounted Reaction Control Systems Jet Interaction Study," May 1977, Report No. CASD-NSC-77-003.
12. Rockwell International Space Division; Pre-Operational Aerodynamic Design Data Book, Vol. 1, Orbiter Vehicle, SD72-SH-0060-1L-7, April 1982.
13. Ware, G. M. and Spencer, Jr., B.: "Remotely Driven Model Control Surfaces for Efficient Wind-Tunnel Operations, AIAA 21st Aerospace Science Meeting, AIAA 83-0148, January 1983.
14. Rockwell International Space Division: Aerodynamic Design Data Book, Vol. 1, Orbiter Vehicle, SD72-SH-0060-1L-2, April 1979.
15. Rockwell International Space Division: Aerodynamic Design Data Book, Orbiter Vehicle, STS-1, Final Report, NASA CR-160903, Nov. 1980.
16. Kemp, N. D.: Compiling the Space Shuttle Win Tunnel Data Base: An Exercise in Technical and Managerial Innovations, NASA CP-2283, March 1983.
17. "Aerodynamic Preliminary Analysis System, Part I-Theory, "NASA CR-145284, April 1978.
18. "Aerodynamic Preliminary Analysis System, Part II-User's Manual and Program Description," NASA CR-145300, April 1978.
19. Polhamus, E. C.: "Effect of Flow Incidence and Reynolds number on Low Speed Aerodynamic Characteristics of Several Noncircular Cylinders with Application to Directional Stability and Spinning," NASA Technical Report R-29, 1959.
20. Jorgenson, Leland H. and Brownson, Jack J.: "Effect of Reynolds Number and Body Corner Radius on Aerodynamic Characteristics for Space Shuttle-Type Vehicle at Subsonic Mach Numbers," NASA TN D-6615, January 1972.
21. Young, James C.; and Underwood, Jimmy M.: The Development of Aerodynamic Uncertainties for the Space Shuttle Orbiter. AIAA Paper 82-0563, March 1982.
22. Weil, Joseph; and Powers, Bruce G.: Correlation of Predicted and Flight Derived Stability and Control Derivatives - With Particular Application to Tailless Delta Wing Configurations. NASA TM-81361, July 1981.
23. Gamble, J. D.; and Young, J. C.: The Development and Application of Aerodynamic uncertainties in the Design of the Entry Trajectory and Flight Systems of the Space Shuttle Orbiter, AIAA 9th Atmospheric Flight Mechanics Coneference, AIAA-82-1335, August 1982.
24. Underwood, J. M.; and Cooke, D. R.: Correlation of Flight with Wind Tunnel Stability and Control Aerodynamics of the Space Shuttle Orbiter, 13th Congress of the International Council of the Aeronautical Sciences, ICAS-82-3.3.2, August 1982.
25. Cooke, D. R.: Space Shuttle Stability and Control Test Plan. AIAA Paper 82-1315, August 1982.
26. Maine, Richard E.; and Iliff, Kenneth W.: User's Manual for MMLE3, A General FORTRAN Program for Maximum Likelihood Parameter Estimation. NASA TP-1563, 1980.
27. Maine, Richard E.; and Iliff, Kenneth W.: The Theory and Practice of Estimating the Accuracy of Dynamic Flight-Determined Coefficients. NASA RP-1077, July 1981.
28. Stone, J. S., and Baumbach, J. J.: Space Shuttle Orbiter Reaction and Control Subsystem Flight Data Anomalies, NASA CP-2283, March 1983.
29. Arrington, James P.; and Jones, Jim J.: Shuttle Performance: Lessons Learned, NASA CP-2283, March 1983.
30. Romere, P. O., and Whitnah, A. M.: Space Shuttle Entry Longitudinal Aerodynamic Comparisons of Flights 1-4 with Preflight Predictions, NASA CP-2283, March 1983.
31. Griffith, B. J.; Maus, J. R.; and Best, J. T.: Explanation of the Hypersonic Longitudinal Stability Problem - Lessons Learned, NASA CP-2283, March 1983.
32. Roberts, B. B.; Wallace, R. O.; and Kanipe, D. B.: "Rocket Exhaust Plume Induced Flowfield Interaction Experiences with the Space Shuttle," AIAA-82-1549, AIAA 18th Thermophysics Conference, June 1983.

TABLE 1.- AERODYNAMIC DESIGN CRITERIA

PARAMETER	VALUE
ANGLE OF ATTACK	
HYPERSONIC	25 TO 50 DEG
TRANSONIC	0 TO 15 DEG
SUBSONIC	-5 TO 20 DEG
CENTER-OF-GRAVITY RANGE	
MINIMUM TRAVEL	2% BODY LENGTH
DESIGN RANGE	0.65 L_B — 0.675 L_B
LANDING PERFORMANCE	
PAYLOAD	(14,515 Kg) 32,000 LB
LANDING WEIGHT (WITH PAYLOAD)	(85,230 Kg) 187,900 LB
MINIMUM DESIGN TOUCHDOWN SPEED, V_D	(88 m/s) 171 KNOTS
LONGITUDINAL STABILITY	
MINIMUM HYPERSONIC STATIC MARGIN	POSITIVE
MINIMUM SUBSONIC STATIC MARGIN (AFT CENTER OF GRAVITY)	-2% L_B (-5.45% MAC)
LIFT/DRAG MODULATION	
PEAK SUBSONIC VALUE (GEAR UP, δ_{SB} = 0)	NOT LESS THAN 4.4
PEAK SUBSONIC VALUE (GEAR UP, δ_{SB} = 85 DEG)	NOT LESS THAN 2.5

TABLE 2.- SPACE SHUTTLE ORBITER WIND TUNNEL UTILIZATION SUMMARY

TEST IDENTIFICATION	FACILITY	MODEL SCALE
TRANSONIC		
OA145A	ARC 11 x 11 FT	.05
OA270A	LaRC 16T	.05
OA270B	LaRC 16T	.02
LA70	CALSPAN 8 FT	.015
LA76	LTV 4 x 4 HSWT	.015
LA77	ARC 11 x 11 FT	.015
LA111	LaRC 8 FT TWT	.015
LA115	LaRC 8 FT TWT	.015
SUPERSONIC		
OA145B	ARC 9 x 7 FT	.05
OA145C	ARC 8 x 7 FT	.05
OA209	AEDC "A"	.02
LA63A	LaRC UPWT-1	.015
LA63B	LaRC UPWT-2	.015
LA75	LaRC UPWT-2	.015
LA76	LTV 4 x 4 HSWT	.015
LA101	LaRC UPWT-1	.015
LA110	LaRC UPWT-1	.015
LA114	LaRC UPWT-2	.02
LA125	LaRC UPWT-2	.02
LA131	LaRC UPWT-2	.02
LA144	LTV 4 x 4 FT	.02
HYPERSONIC		
OA113	CALSPAN HST (48 IN.)	.01
OA171	NSWC TUNNEL 9	.02
OA208	AEDC "B"	.02
OA257	LaRC 20 IN.	.01
OA258	AEDC "B"	.02
OA259	AEDC "B"	.01

ORIGINAL PAGE IS
OF POOR QUALITY

TABLE 3.- KEY AERODYNAMIC PARAMETERS

AERODYNAMIC PARAMETER	FLIGHT REGIME	WHY PARAMETERS ARE SIGNIFICANT	AERO CONCERN IN DEFINITION OF PARAMETERS
L/D, C_m, $C_{m_{\delta e}}$	ALL	• CROSSRANGE • TERMINAL AREA ENERGY MANAGEMENT • ELEVON REQUIRED TO TRIM • RCS FUEL USAGE	• VISCOUS INTERACTION EFFECTS • FLOW SEPARATION • REAL GAS EFFECTS NOT SIMULATED IN WIND TUNNEL
HINGE MOMENTS	TRANSONIC	• ACTUATOR DESIGN • DEFINES CONTROL SURFACE STALL AND RATE LIMITING CONDITIONS	• WIND TUNNEL WALL, BLOCKAGE, AND SHOCK REFLECTION EFFECTS
$C_{n_{\delta a}}$, $C_{l_{\delta a}}$	HIGH SUPERSONIC	• AILERON IS USED FOR BOTH ROLL AND YAW TRIM ABOVE MACH 3.5 BEFORE RUDDER IS ACTIVATED • RCS FUEL USAGE	• CONTROL SURFACE INTERACTION • EFFECT OF ELEVON ON AILERON EFFECTIVENESS
$C_{n_{\delta a}}$, $C_{l_{\delta a}}$, $C_{n_{\delta r}}$, $C_{l_{\delta r}}$	TRANSONIC/ SUPERSONIC	• RUDDER IS USED FOR BOTH YAW AND ROLL TRIM FOR $1.5 < M < 3.5$ • AILERON COORDINATES TURN • RCS YAW JET IS NEEDED UNTIL RUDDER IS EFFECTIVE • DEFINES SWITCH-OVER POINT FROM SPACECRAFT TO AIRCRAFT FCS MODE	• CONTROL SURFACE INTERACTION • RUDDER EFFECTIVENESS AT HIGH α AND MACH • AEROELASTIC EFFECTS • TRANSONIC WIND TUNNEL ACCURACIES

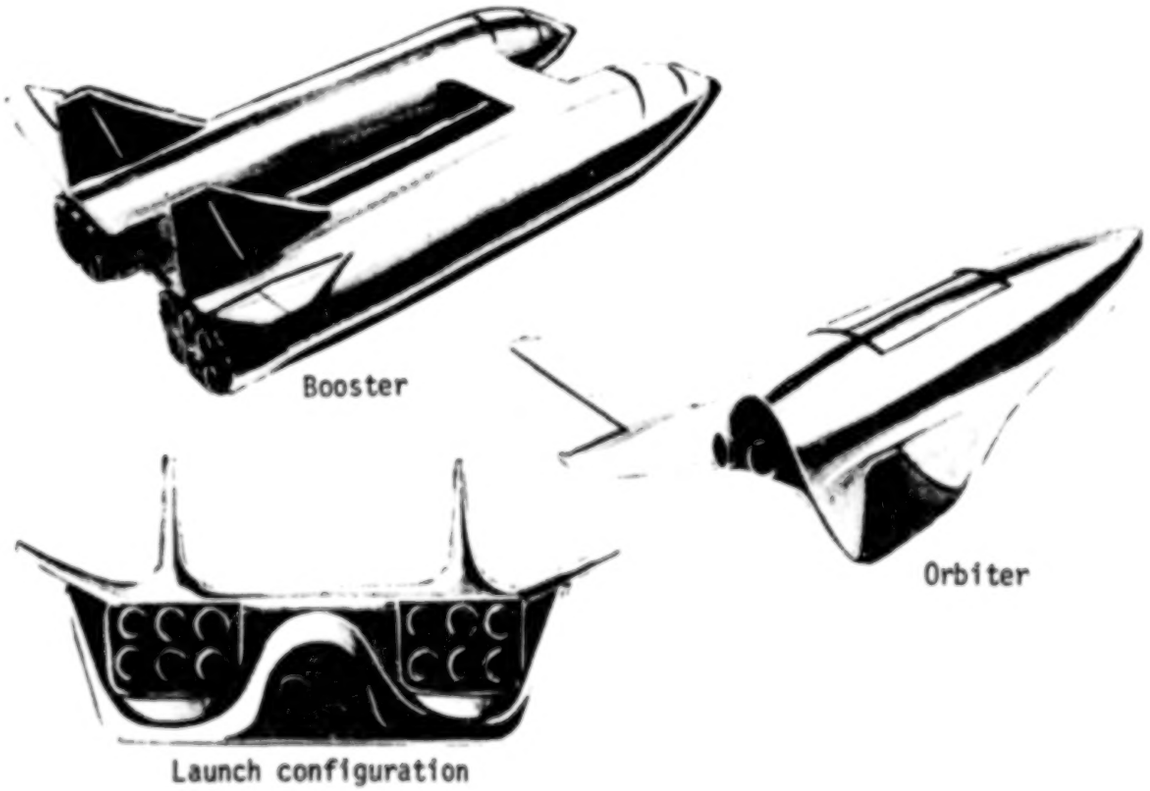
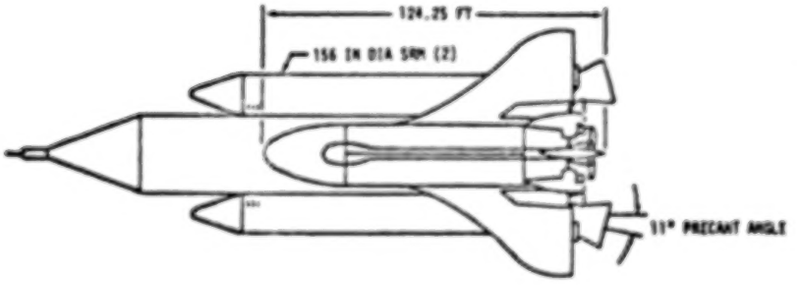


FIGURE 1.- TYPICAL PHASE A CONFIGURATION CONCEPT.



FIGURE 2.- TYPICAL PHASE B CONFIGURATION CONCEPT.



ORIGINAL PAGE IS
OF POOR QUALITY

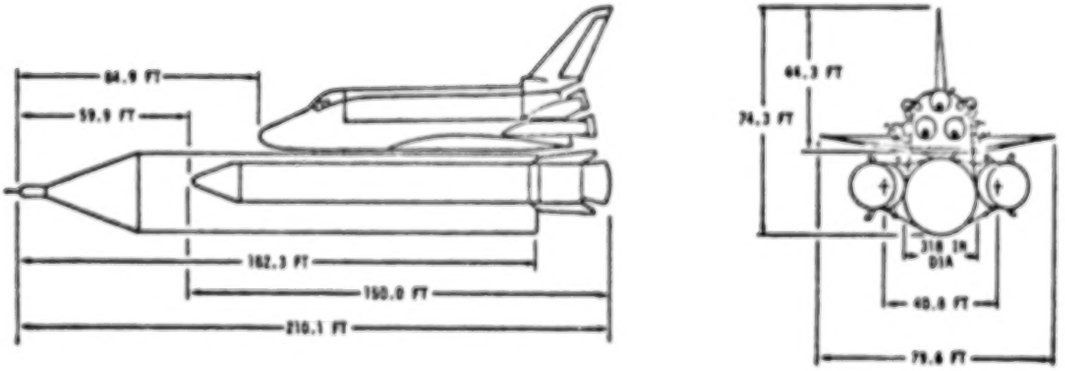


FIGURE 3.- TYPICAL PARALLEL BURN CONFIGURATION.

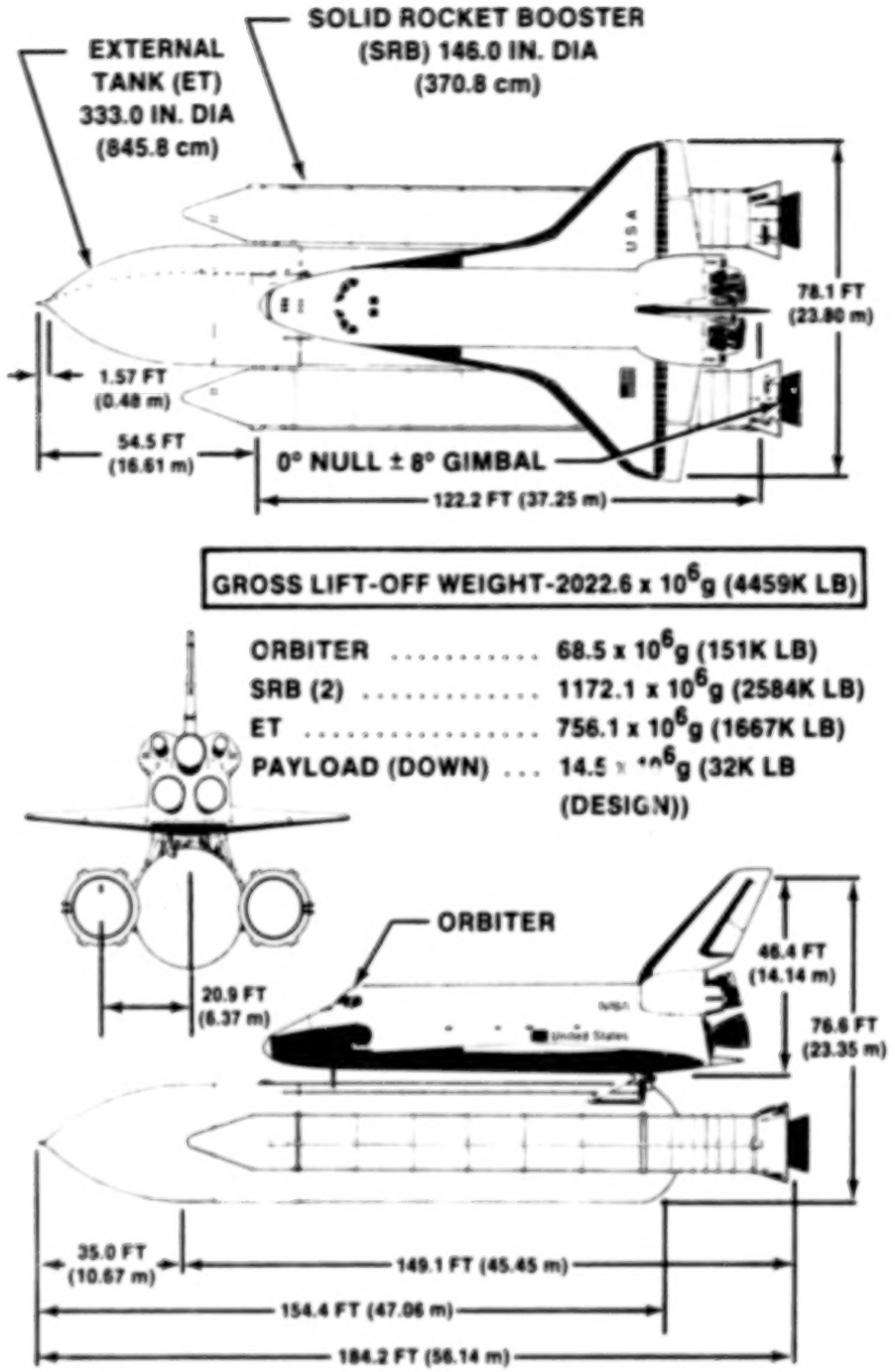


FIGURE 4.- SPACE SHUTTLE INTEGRATED VEHICLE FINAL CONFIGURATION.

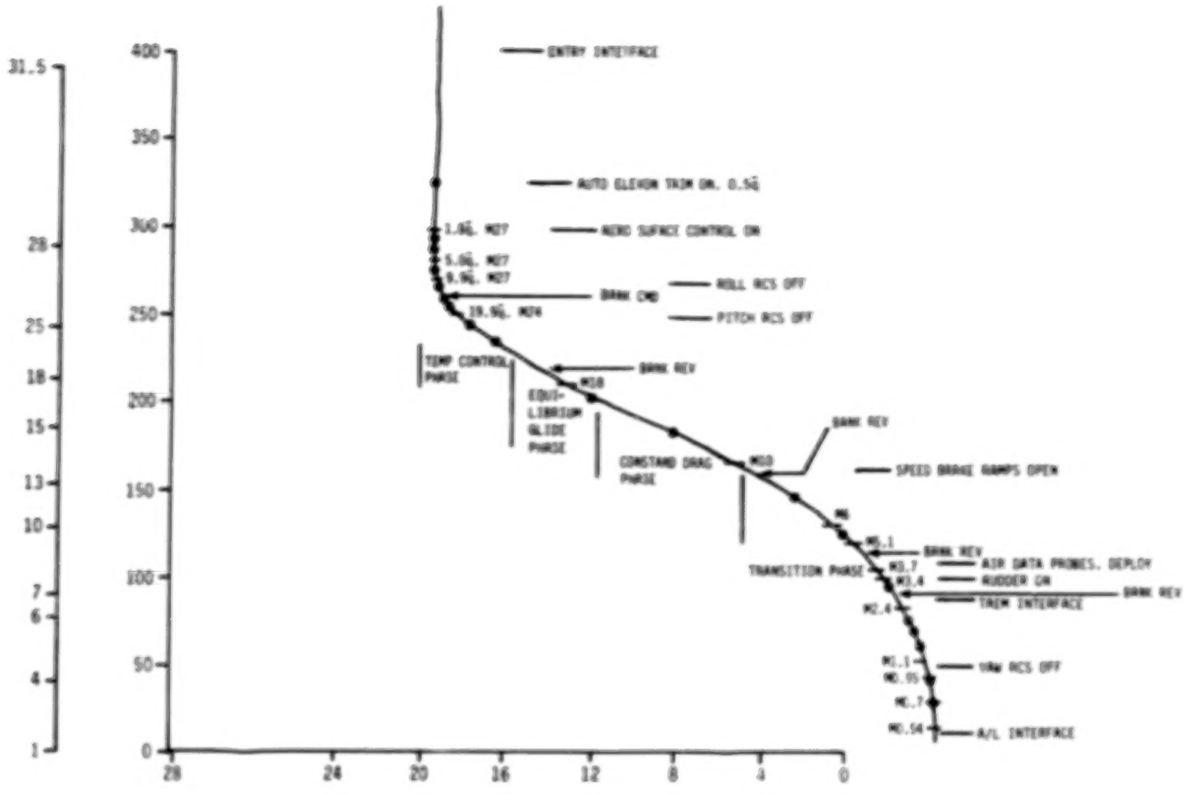
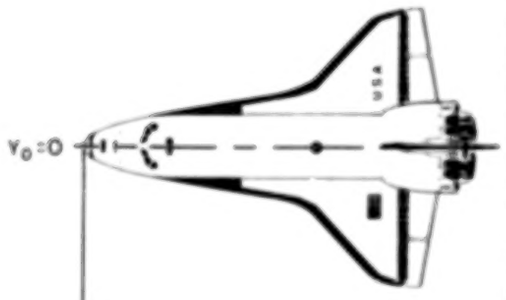
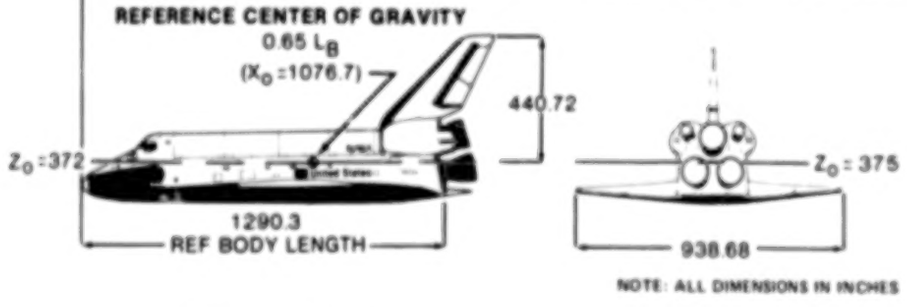


FIGURE 5.- ORBITER ENTRY PHASES.



GEOMETRY	COMPONENT	
	WING	VERTICAL TAIL
AREA	2690 FT^2	413.25 FT^2
SPAN	936.68 IN	315.72 IN
ASPECT RATIO	2.265	1.615
TAPER RATIO	0.2	0.404
SWEEP (LE)	81.45 DEG	45 DEG
DIHEDRAL	3.5	- -
INCIDENCE	0.5 DEG	- -
MAC	474.81 IN	199.81 IN

CONTROL SURFACE	AREA (FT^2)	MAX DEFLECTIONS (DEG)
ELEVON (1 SIDE)	206.57	-35 TO +20
BODY FLAP	135.75	-11.7 TO +22.5
SPEEDBRAKE	97.148	0 TO 87.2
RUDDER	97.148	-22.8 TO +22.8



NOTE: ALL DIMENSIONS IN INCHES

FIGURE 6.- SPACE SHUTTLE ORBITER FINAL CONFIGURATION.

ORIGINAL PAGE IS
OF POOR QUALITY

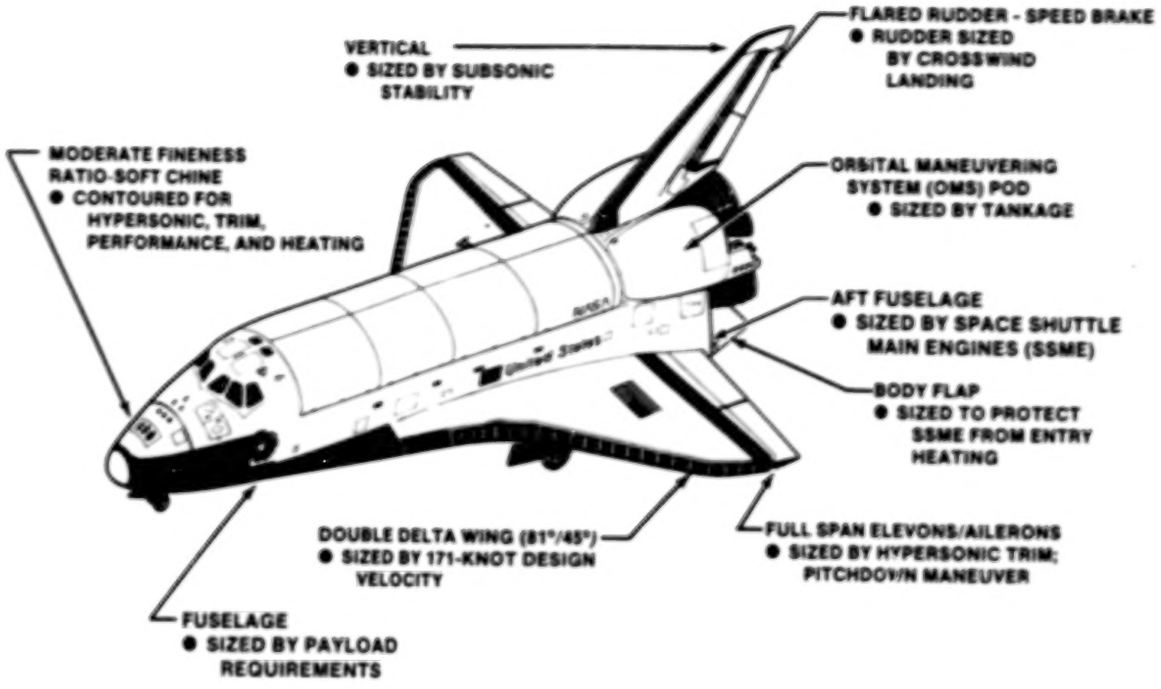


FIGURE 7.- ORBITER SIZING CRITERIA.

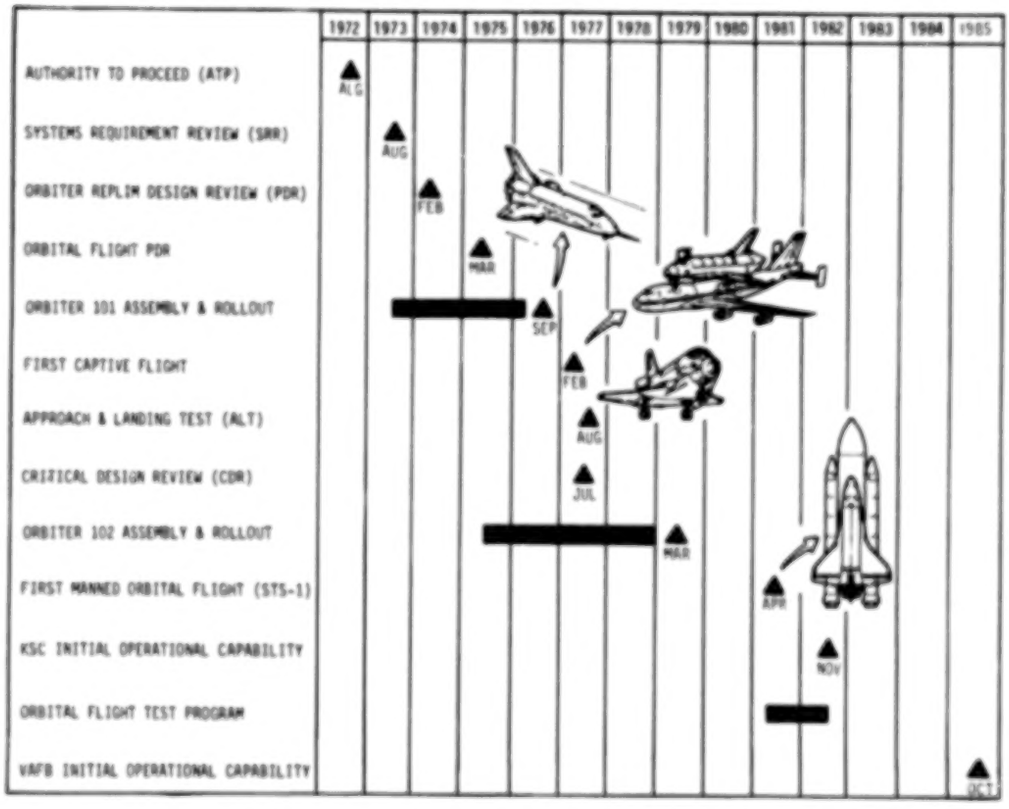


FIGURE 8.- SPACE SHUTTLE PROGRAM MILESTONES.

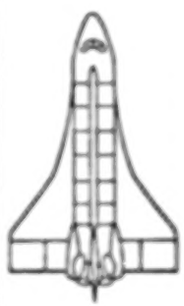
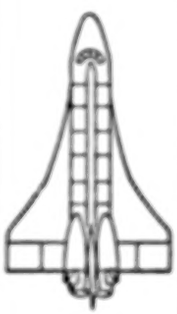
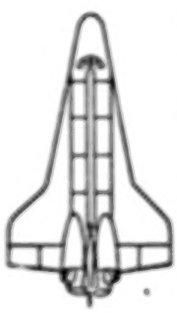
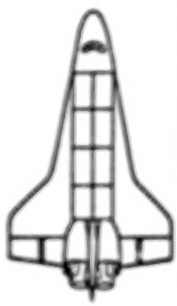
CONFIGURATION DESIGNATION	ATP	PRR	PDR	CDR
CONFIGURATION CONTROL DRAWING NUMBER	VL70 - 000001	VL70 - 000040A	VL70 - 0000658	VL70 - 000148C, VC70 - 000002
WING DESIGN	50° BLENDED DELTA	50° BLENDED DATA	45°/78° DOUBLE DELTA	45°/81° DOUBLE DELTA
WING AREA, FT^2 (m^2)	3220 (299.14)	3220 (299.14)	2690 (249.90)	2690 (249.90)
WING SPAN, FT (m)	84.0 (25.60)	84.0 (25.60)	78.1 (23.80)	78.1 (23.80)
OVERALL LENGTH, FT (m)	125.8 (38.34)	125.8 (38.34)	125.2 (38.18)	122.2 (37.25)
PLAN VIEW				
DRY WEIGHT, LB (kg)	170,000 (77,110)	170,000 (77,110)	150,000 (68,039)	150,000 (68,039)
LANDING PAYLOAD, LB (kg)	40,000 (18,144)	40,000 (18,144)	25,000 (11,340)	32,000 (14,515)
CG RANGE (% REFERENCE LENGTH)	65.0 - 68.0	65.0 - 68.0	66.0 - 68.0	65.0 - 67.5

FIGURE 9.- ORBITER CONFIGURATION EVOLUTION.

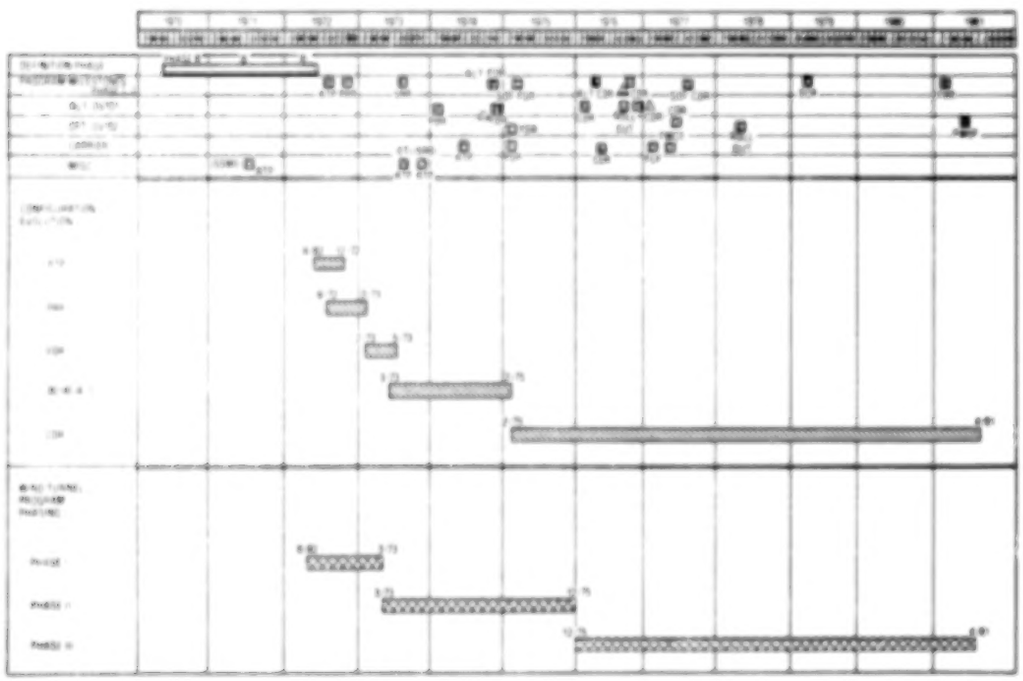


FIGURE 10.- SPACE SHUTTLE PROGRAMMATIC PHASING.

ORIGINAL PAGE IS
OF POOR QUALITY

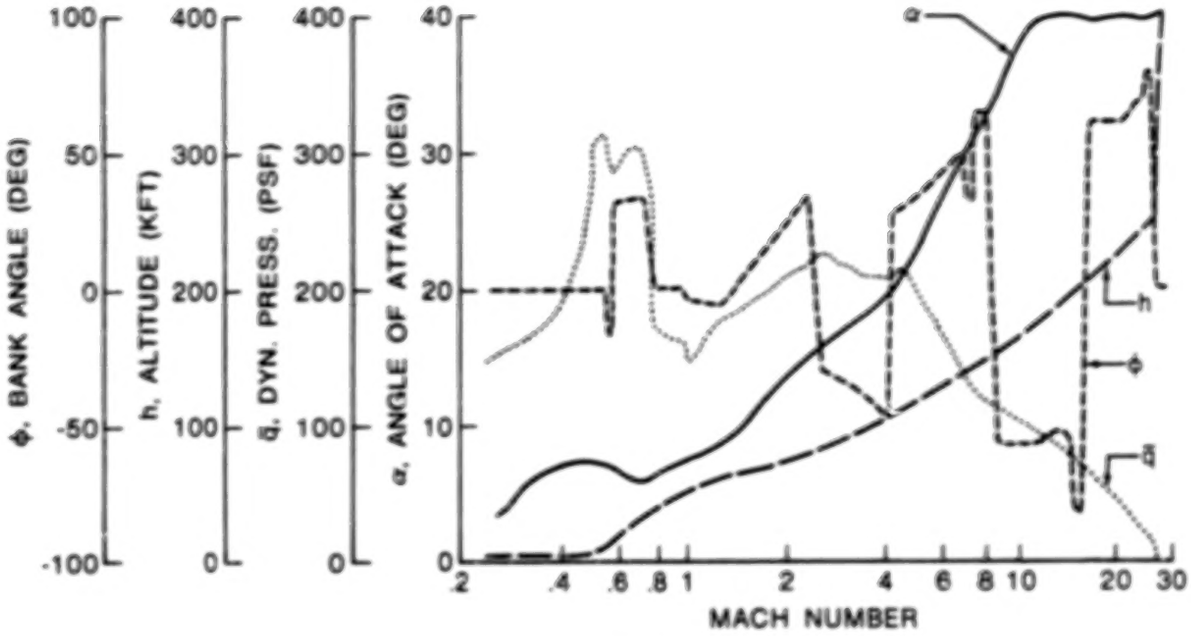


FIGURE 11.- TYPICAL ORBITER ENTRY TRAJECTORY.

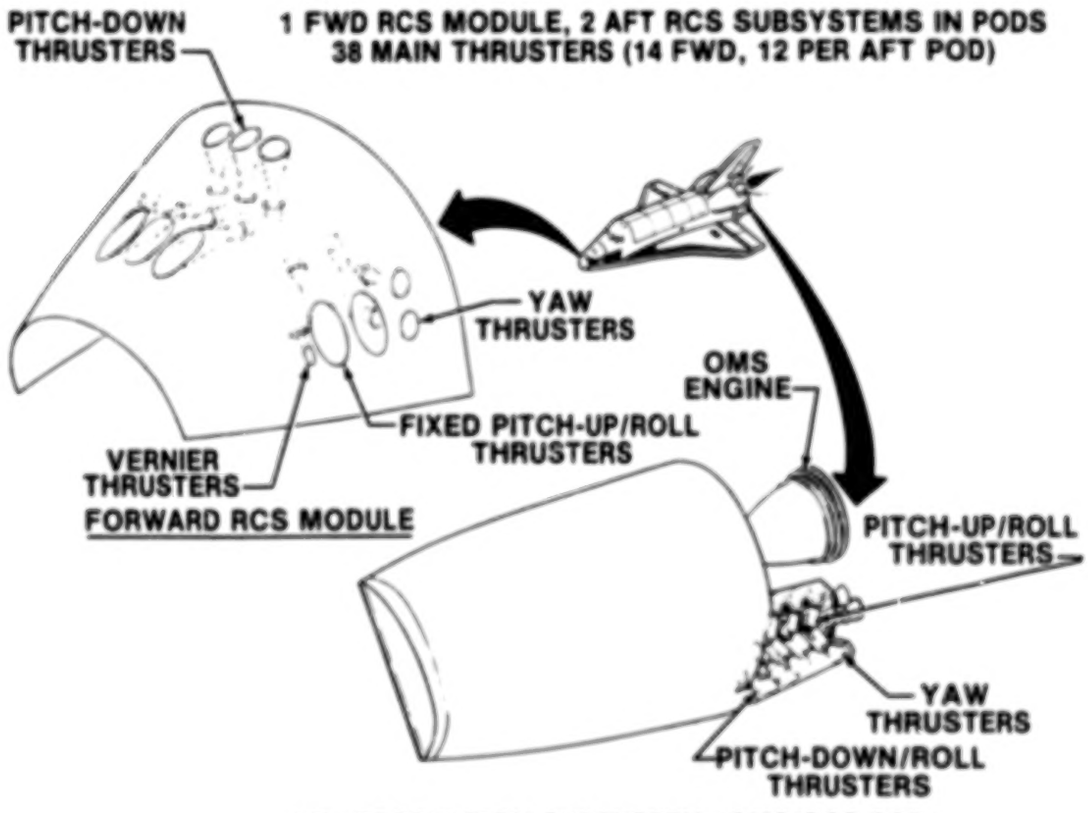


FIGURE 12.- REACTION CONTROL SYSTEM (RCS).

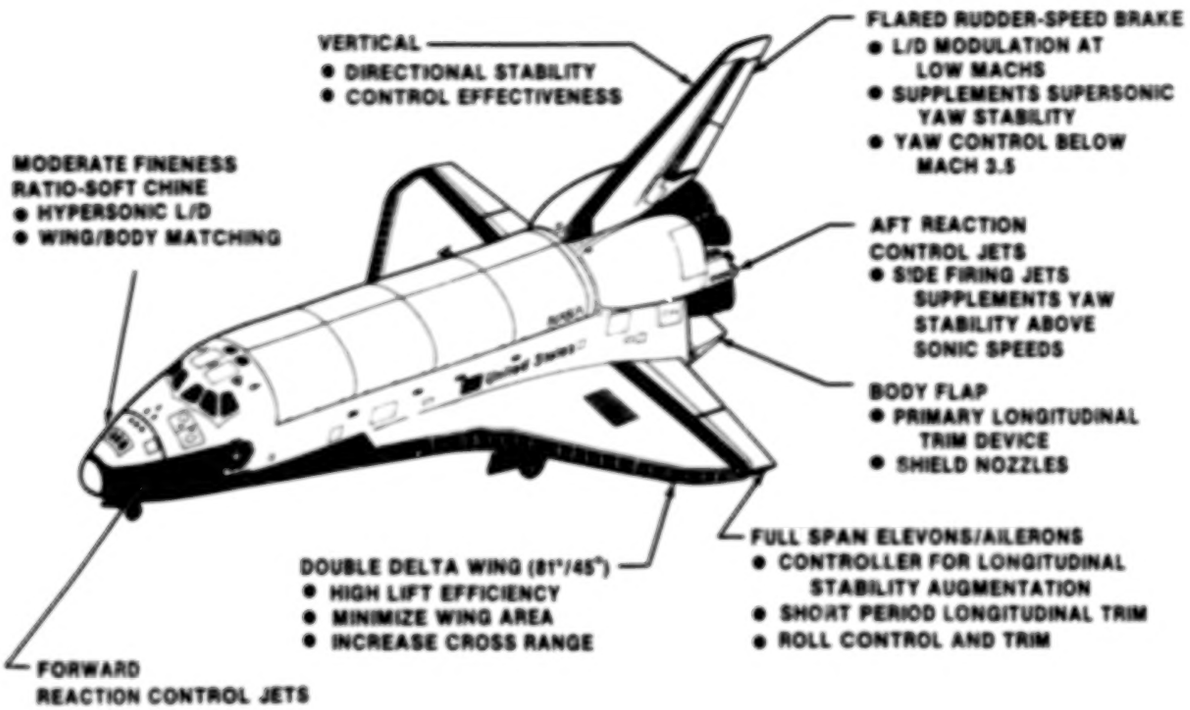


FIGURE 13.- ORBITER FUNCTIONAL CHARACTERISTICS.

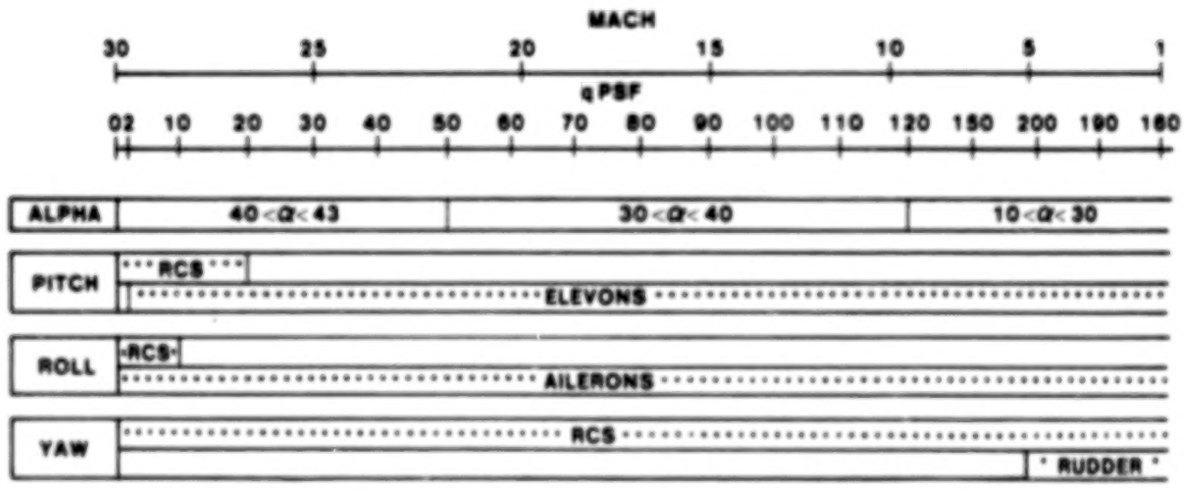


FIGURE 14.- USE OF RCS AND AEROSURFACES BY FCS.

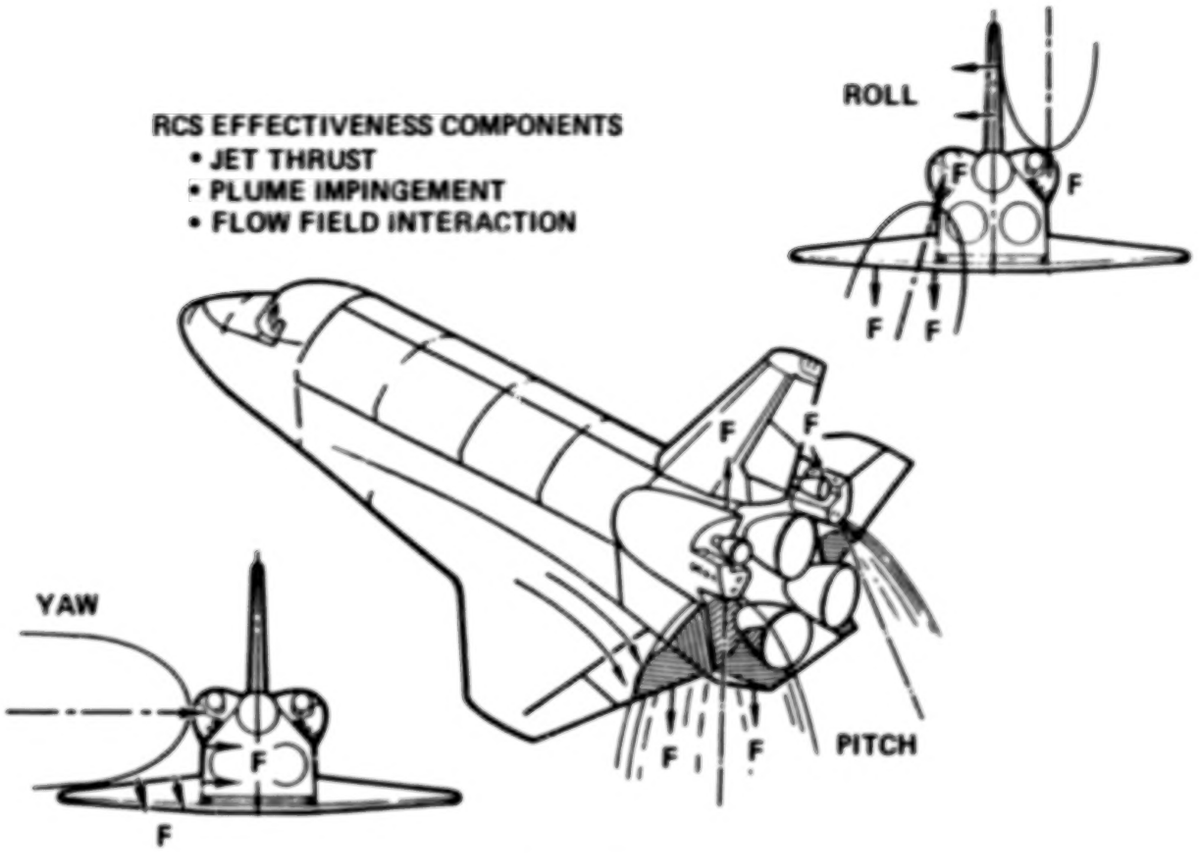


FIGURE 15.- INTERACTION OF RCS JETS WITH VEHICLE AND FLOWFIELD.

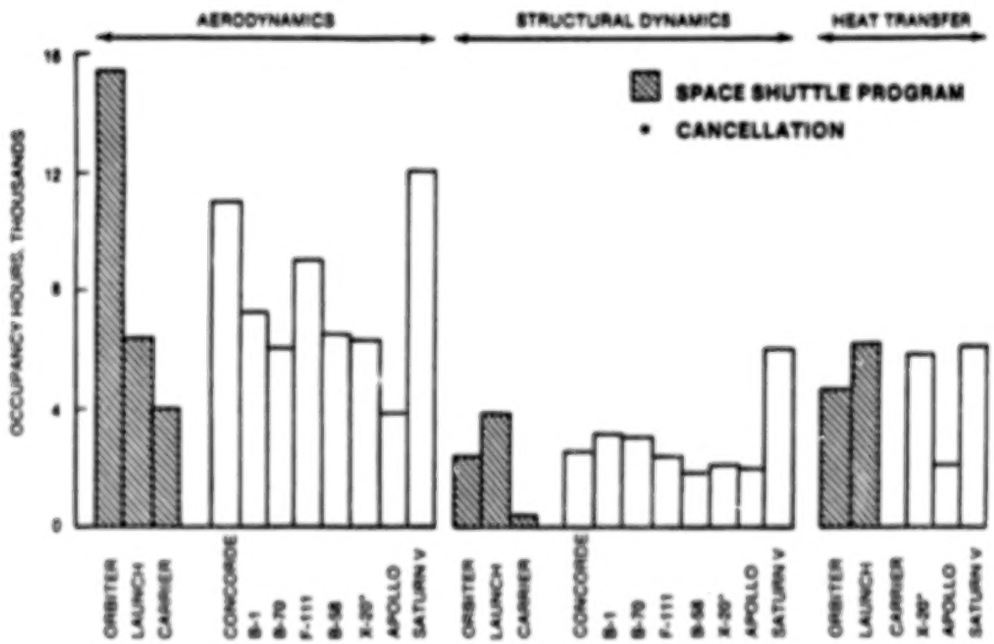


FIGURE 16.- SPACE SHUTTLE WIND TUNNEL PROGRAM.

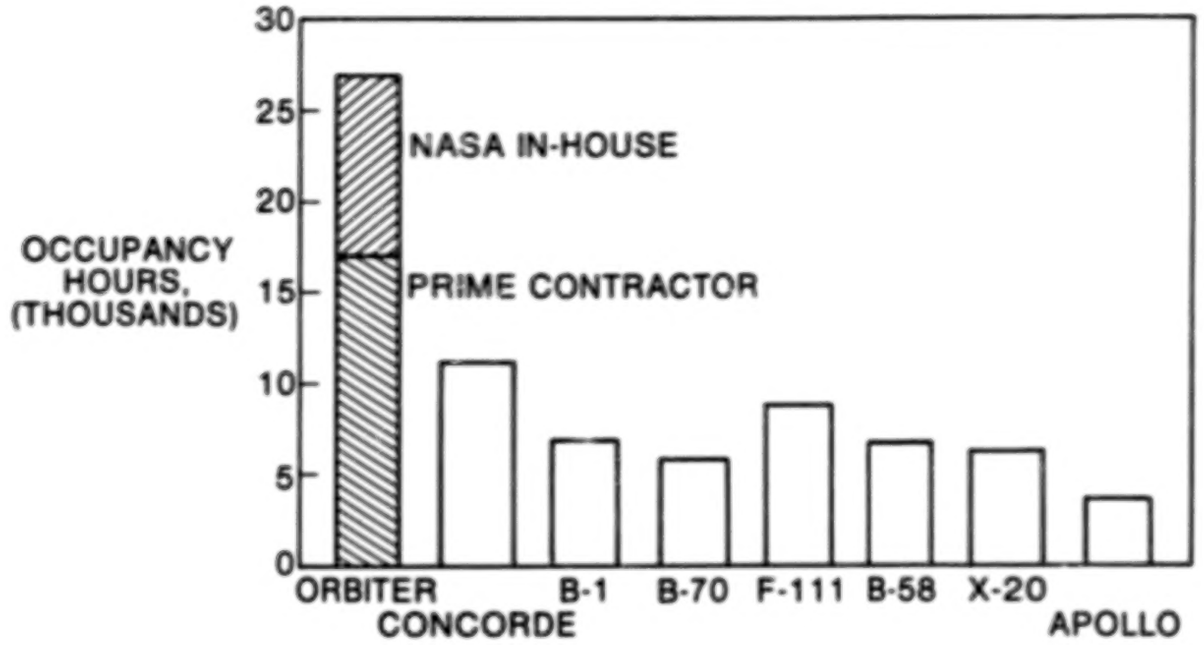


FIGURE 17.- ORBITER WIND TUNNEL PROGRAM.

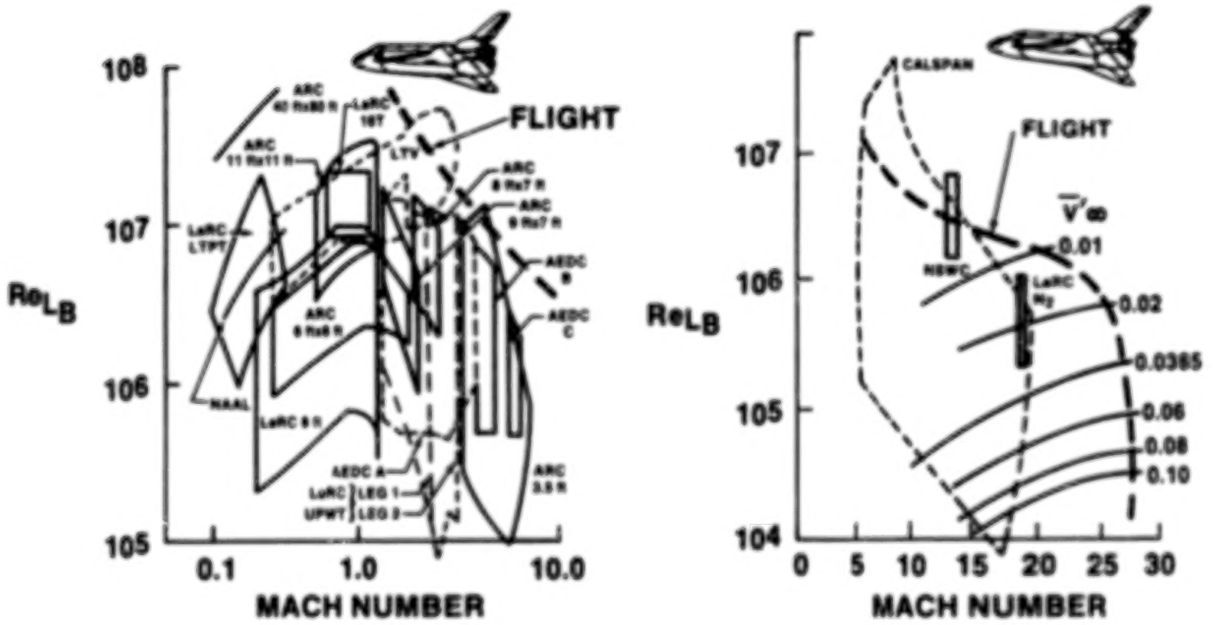


FIGURE 18.- FACILITY SIMULATION CAPABILITY.

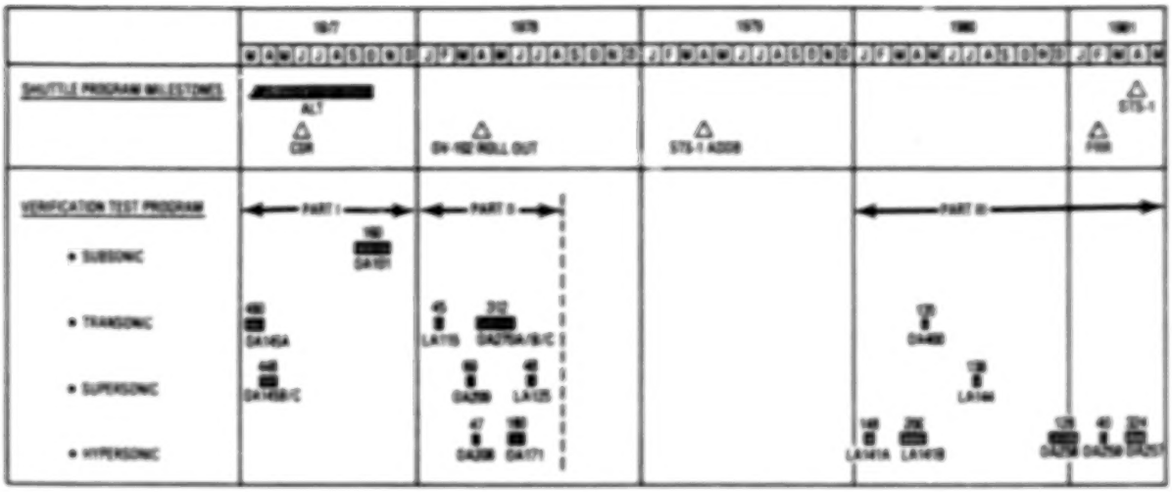


FIGURE 19.- WIND TUNNEL VERIFICATION TEST PROGRAM.

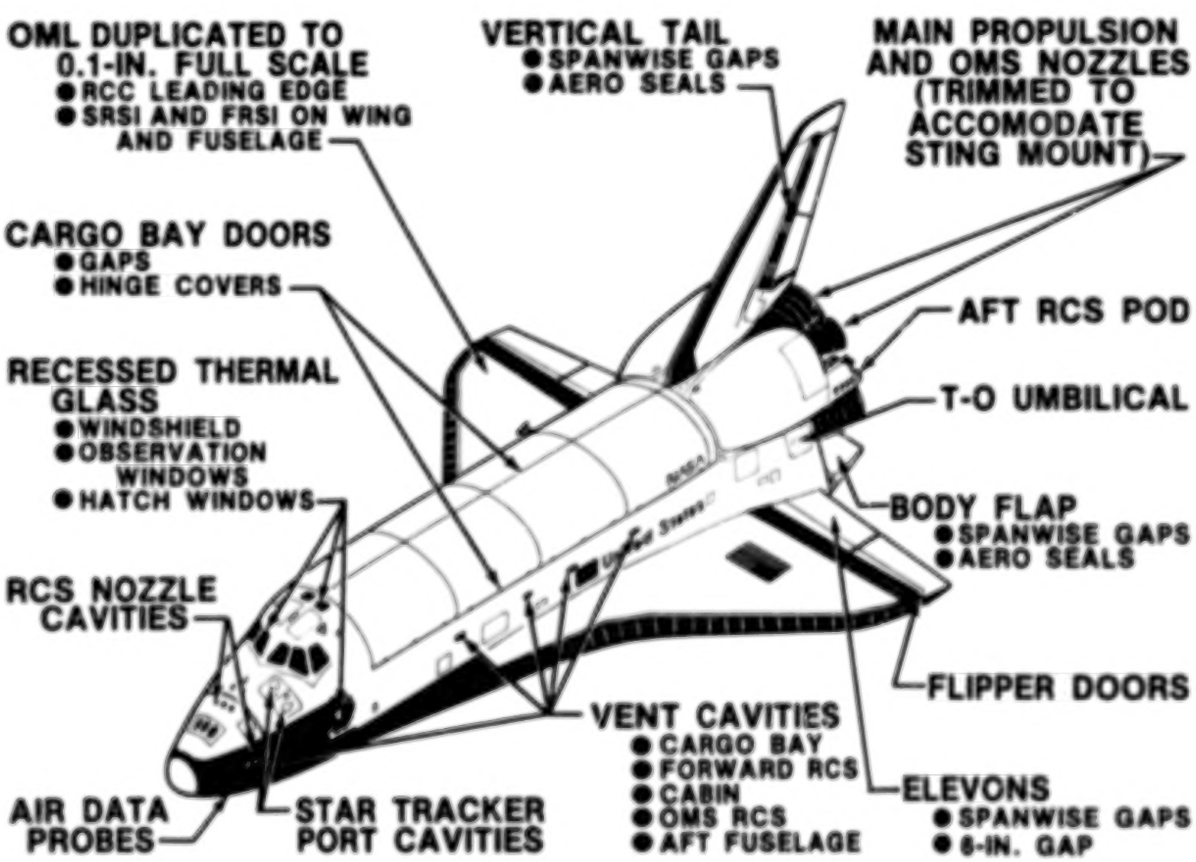


FIGURE 20.- WIND TUNNEL MODEL FIDELITY.

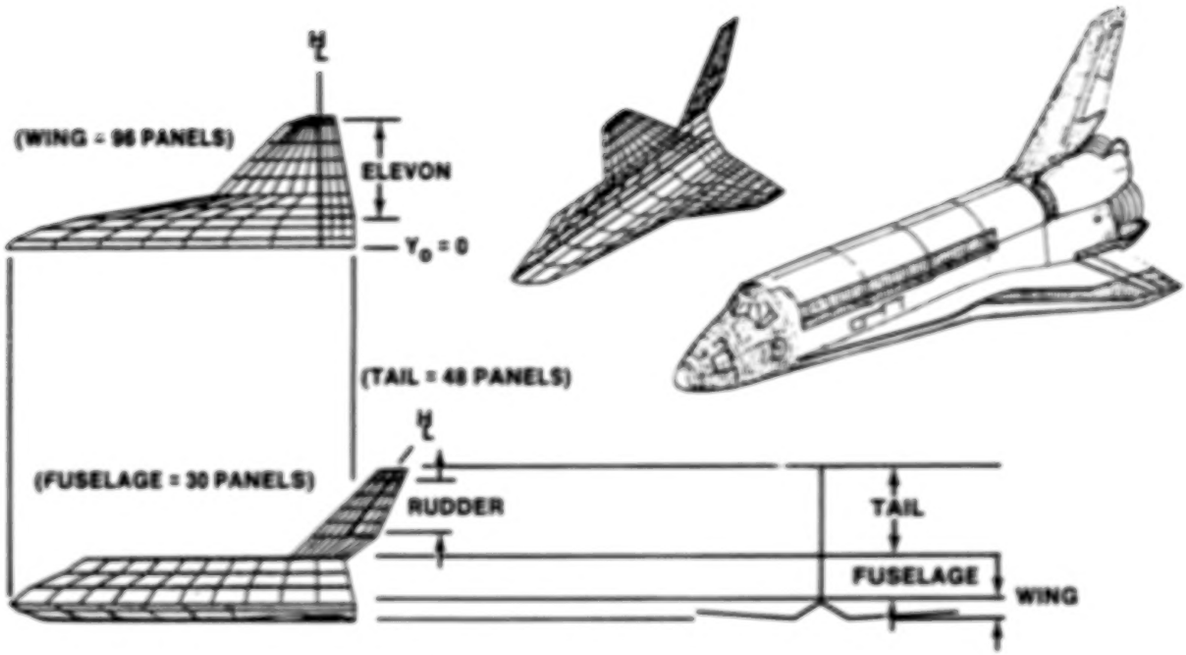


FIGURE 21.- ORBITER AERODYNAMIC PANELING.

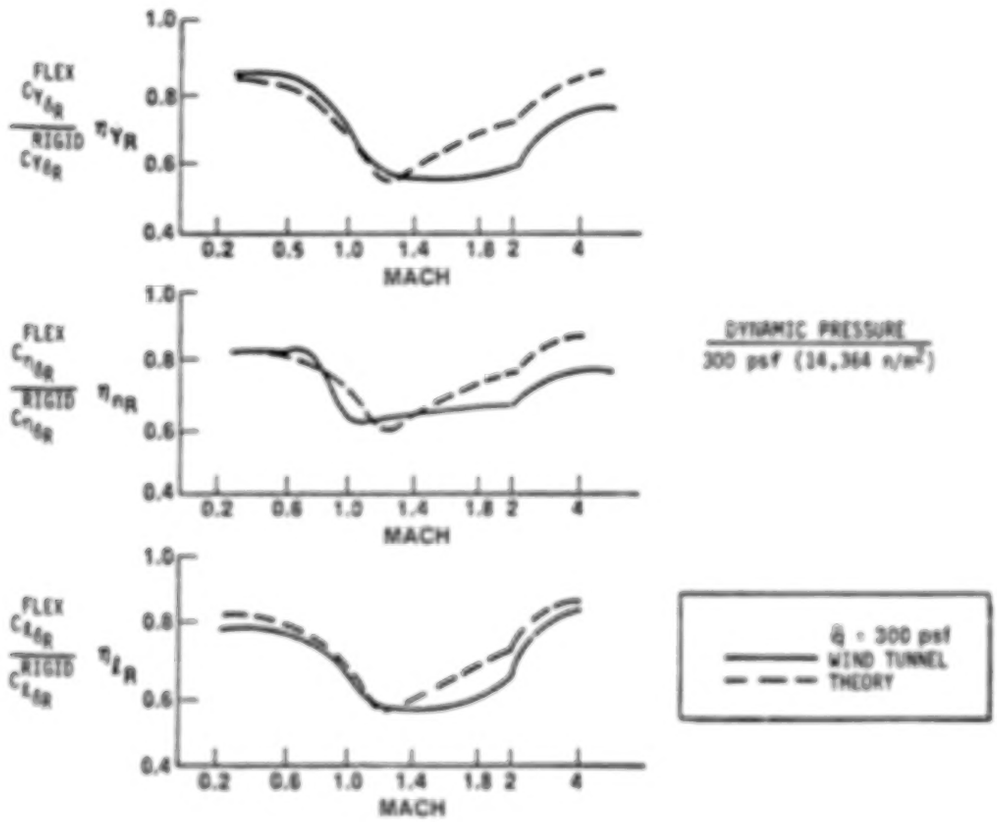


FIGURE 22.- COMPARISON OF WIND TUNNEL WITH THEORETICAL PREDICTION OF THE AEROELASTIC EFFECTS ON RUDDER DERIVATIVES.

$\alpha = 20°$ $\beta = 0°$ $\delta_E = \delta_{BF} = 0°$ $\bar{q}_\infty = 1.0$ psf (47.9 N/m^2)

CONTROL AXIS	3-JET MOMENT (N-m)	IMPINGEMENT MOMENT (N-m)	INTERACTION MOMENT (N-m)	NET MOMENT (N-m)
ROLL	+36,590	-8,030	-27,040	+1,520
PITCH	-126,600	+8,690	+43,775	-74,135
YAW	-38,300	-7,860	-4,860	-51,020

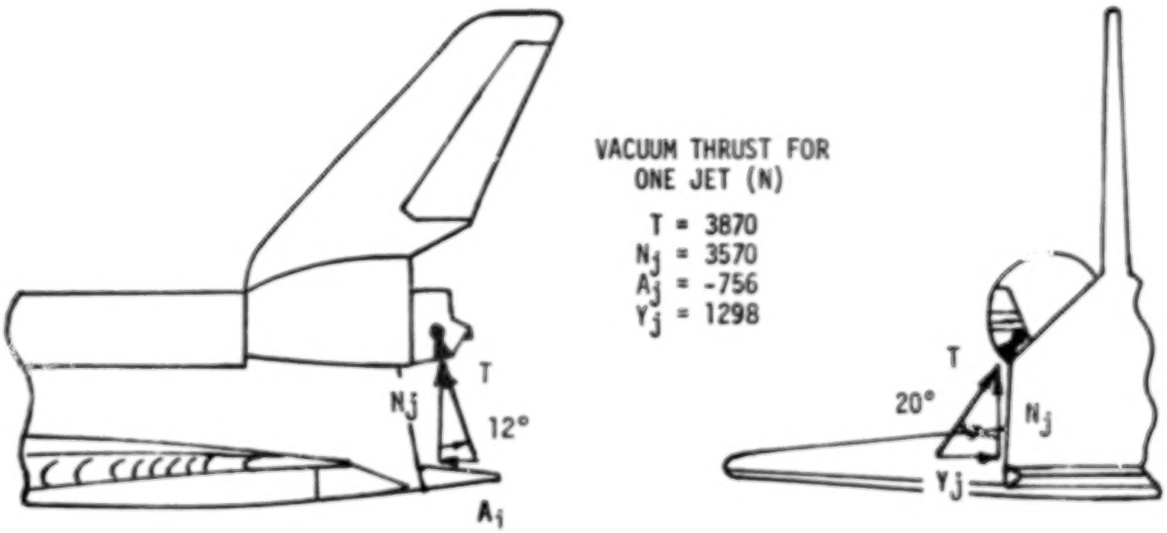


FIGURE 23.- REACTION CONTROL JET MOMENTS.

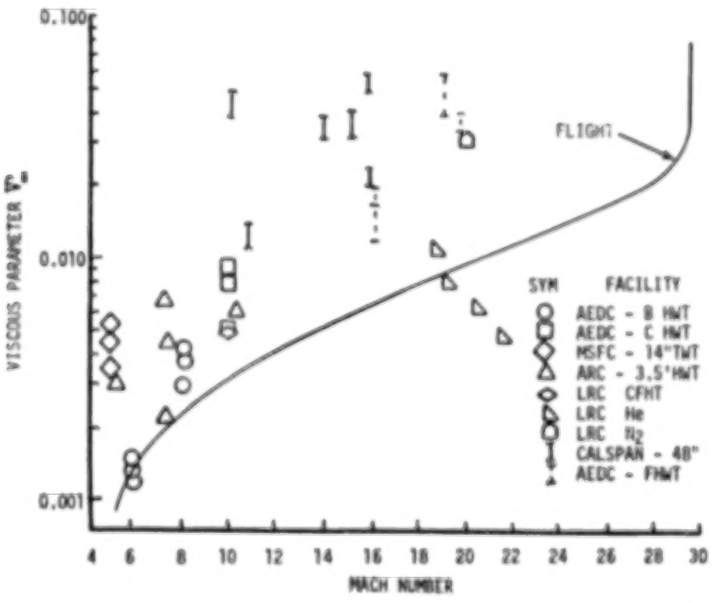


FIGURE 24.- VARIATION OF VISCOUS PARAMETER ALONG NOMINAL ENTRY TRAJECTORY.

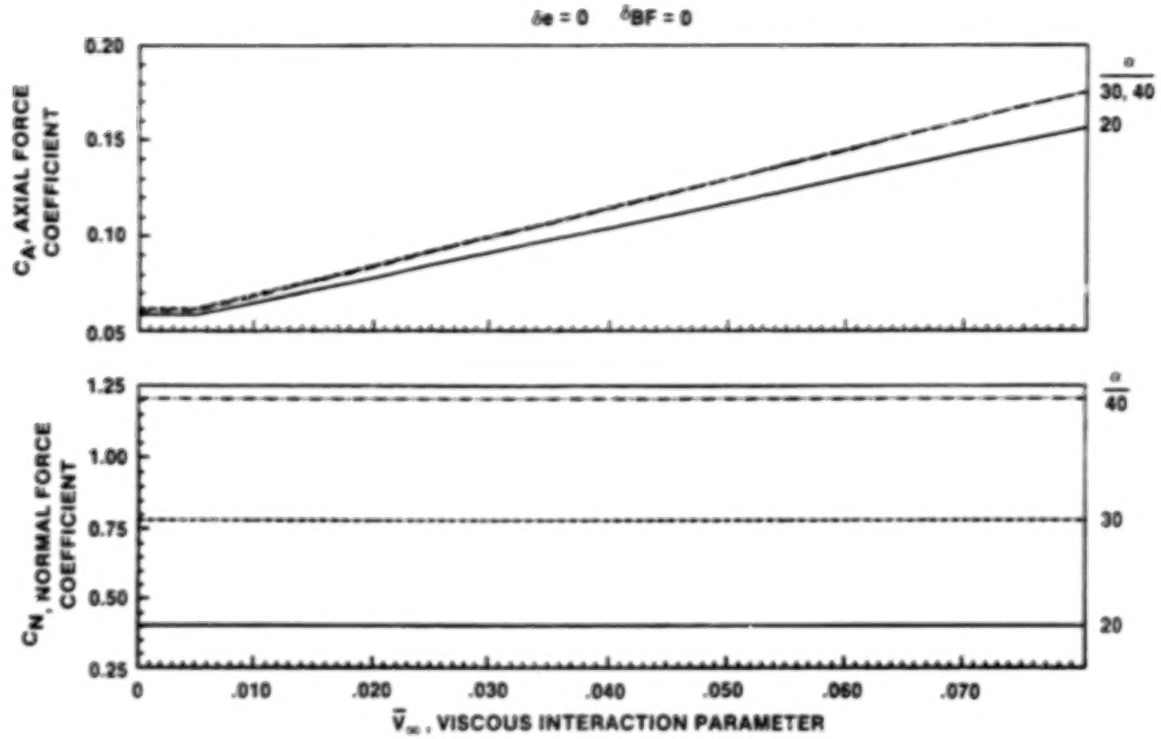


FIGURE 25.- EFFECT OF VISCOUS INTERACTION ON NORMAL AND AXIAL FORCE.

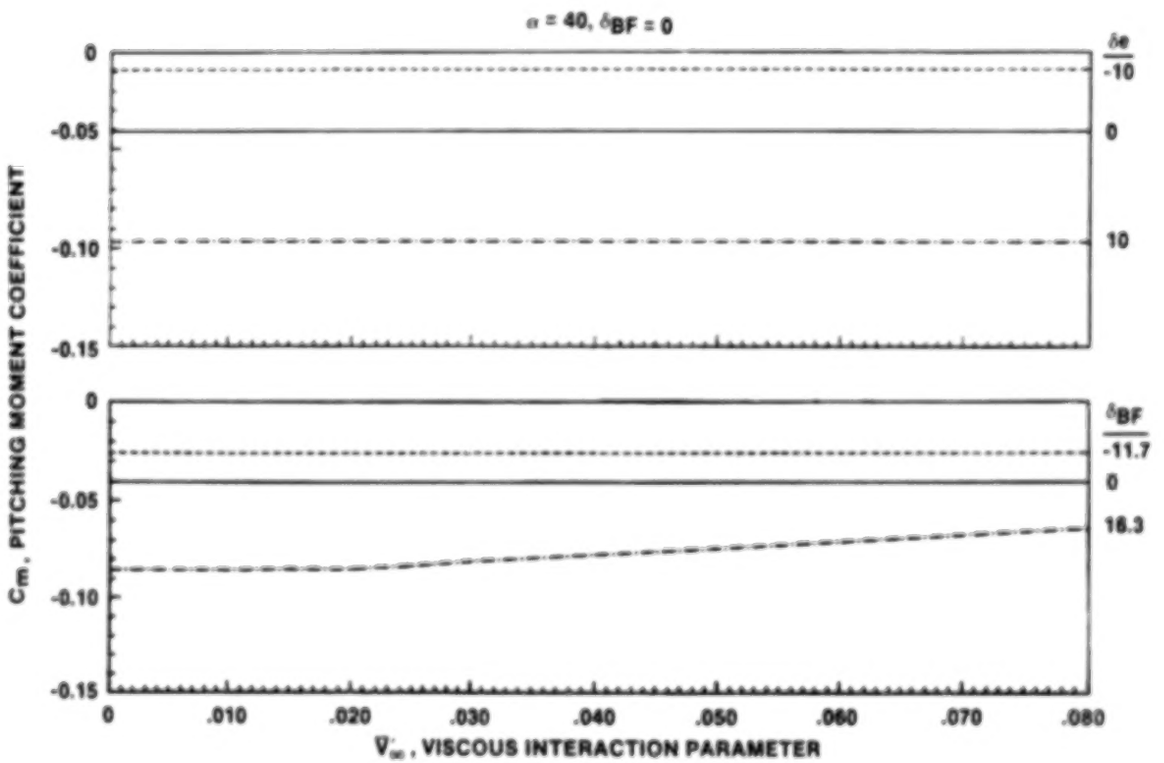


FIGURE 26.- EFFECT OF VISCOUS INTERACTION ON PITCHING MOMENT.

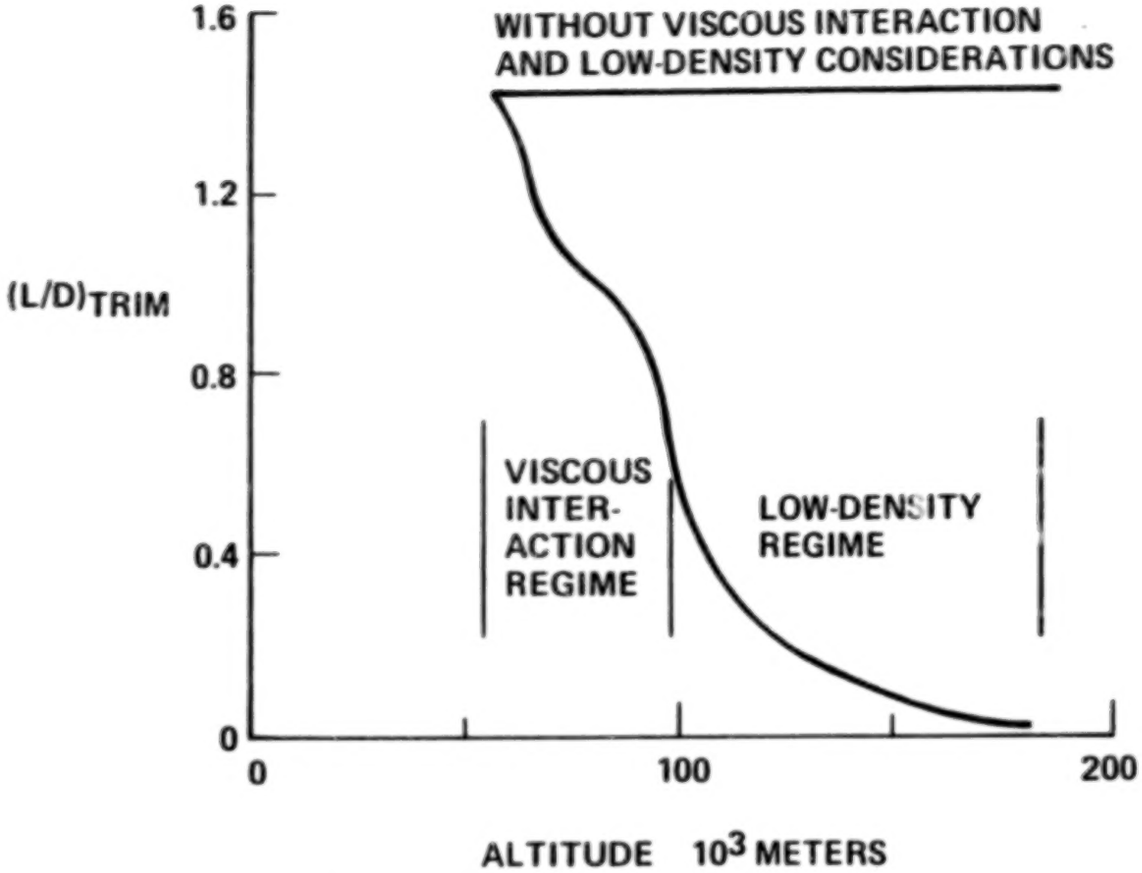


FIGURE 27.- VISCOUS INTERACTION EFFECT ON L/D.

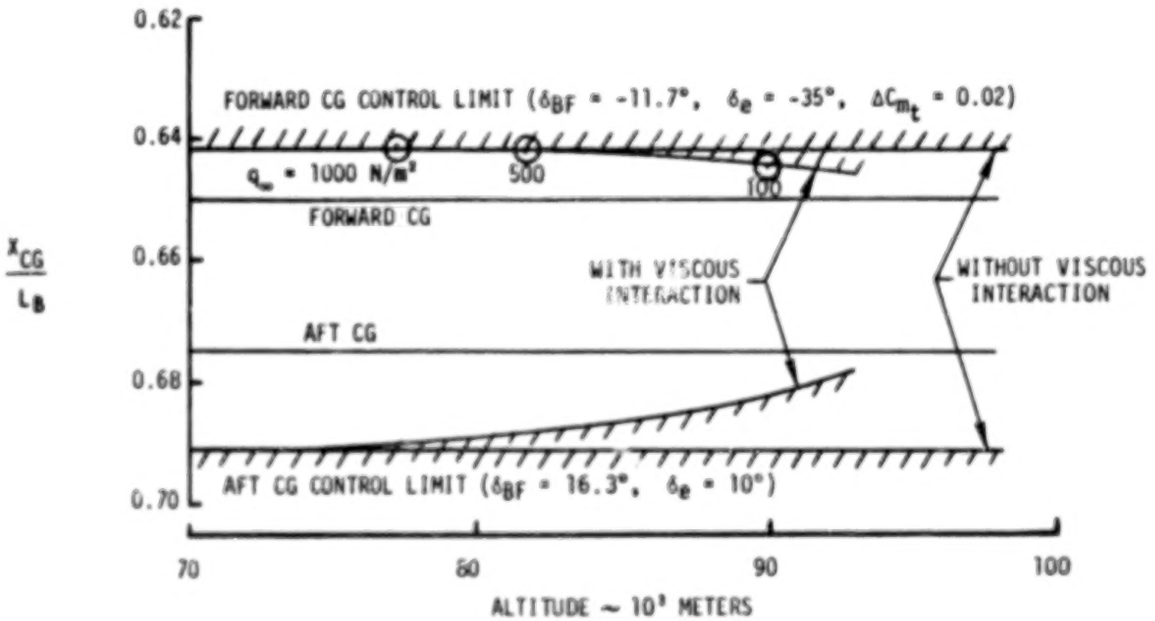


FIGURE 28.- EFFECT OF VISCOUS INTERACTION ON c.g. TRIM CAPABILITY.

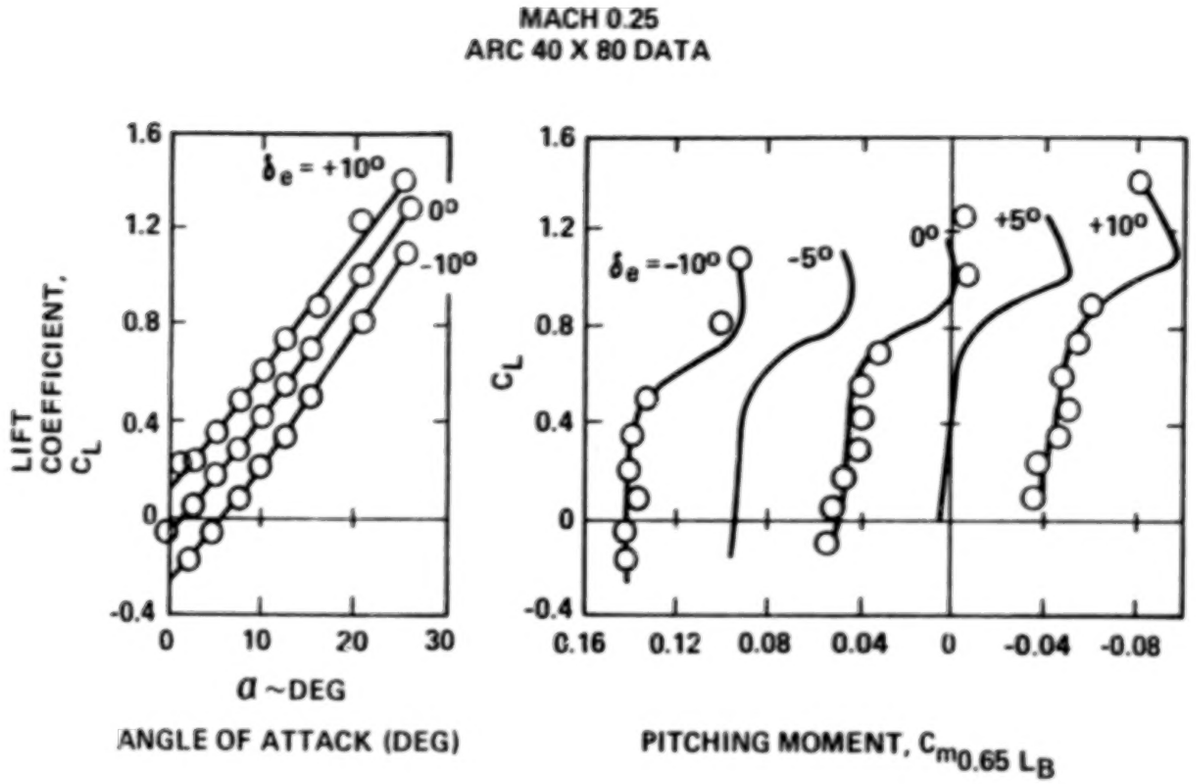


FIGURE 29.- LOW-SPEED LONGITUDINAL CHARACTERISTICS.

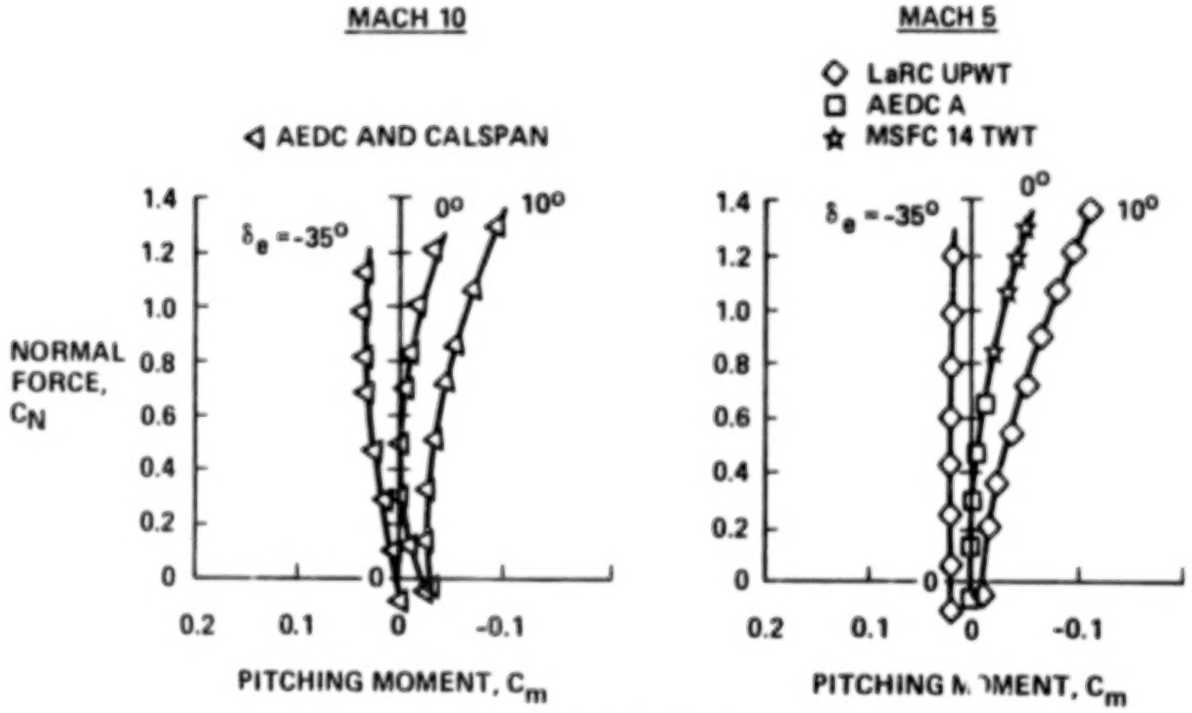
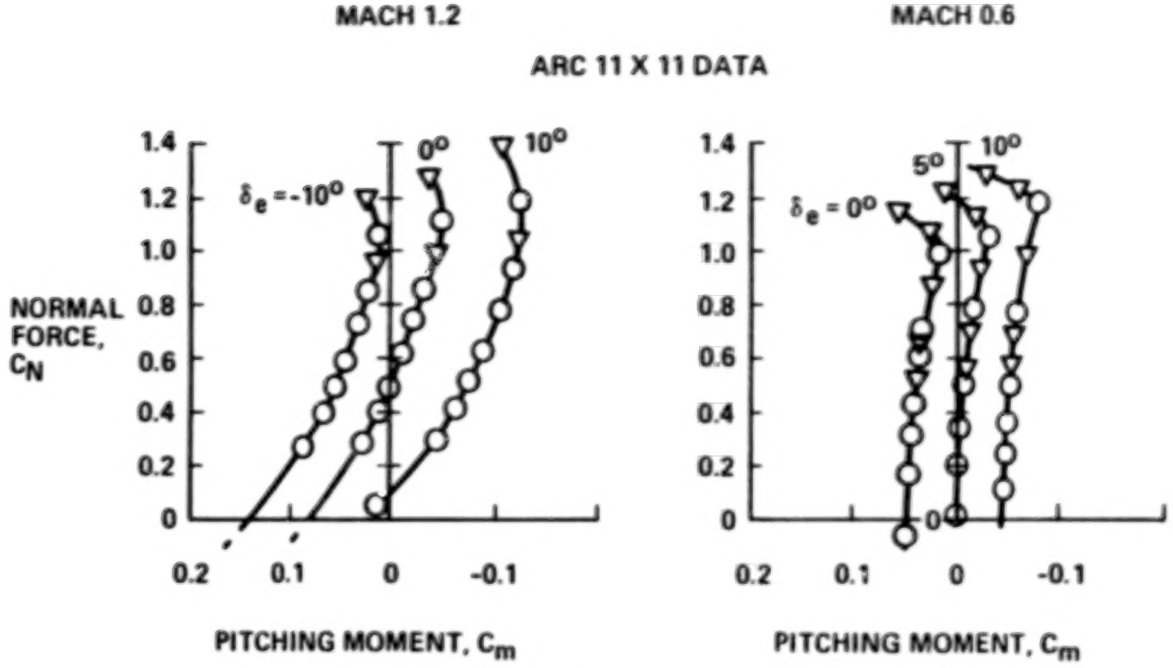


FIGURE 30.- LONGITUDINAL CHARACTERISTICS SUMMARY.



(b) SUBSONIC/SUPERSONIC.

FIGURE 30.- CONCLUDED.

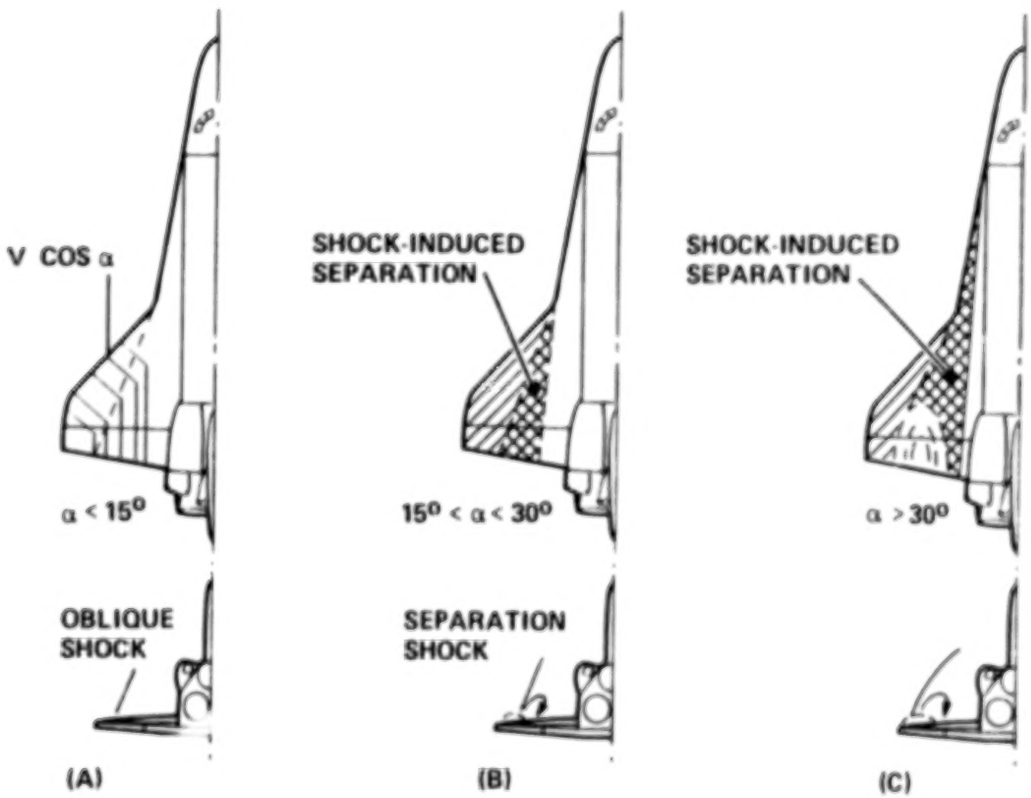


FIGURE 31.- LEESIDE FLOW PATTERNS.



ATTACHED FLOW | SHOCK INDUCED SEPARATION | LEADING EDGE SEPARATION

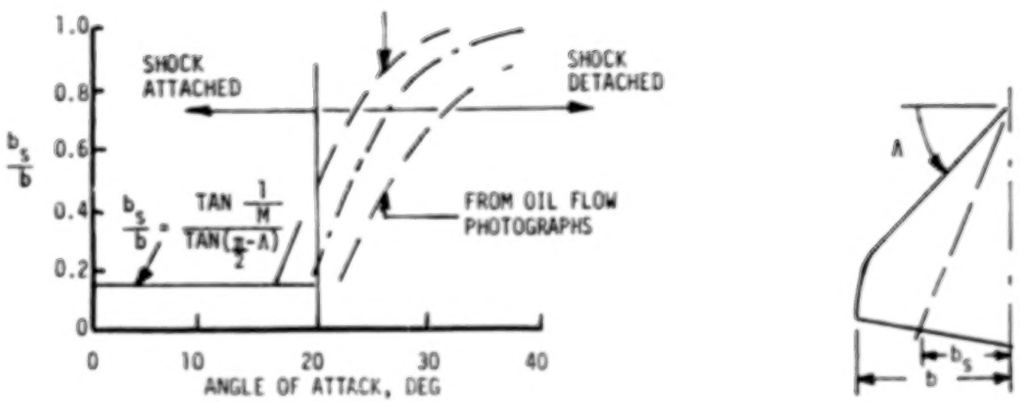


FIGURE 32.- LEESIDE FLOW BOUNDARIES.

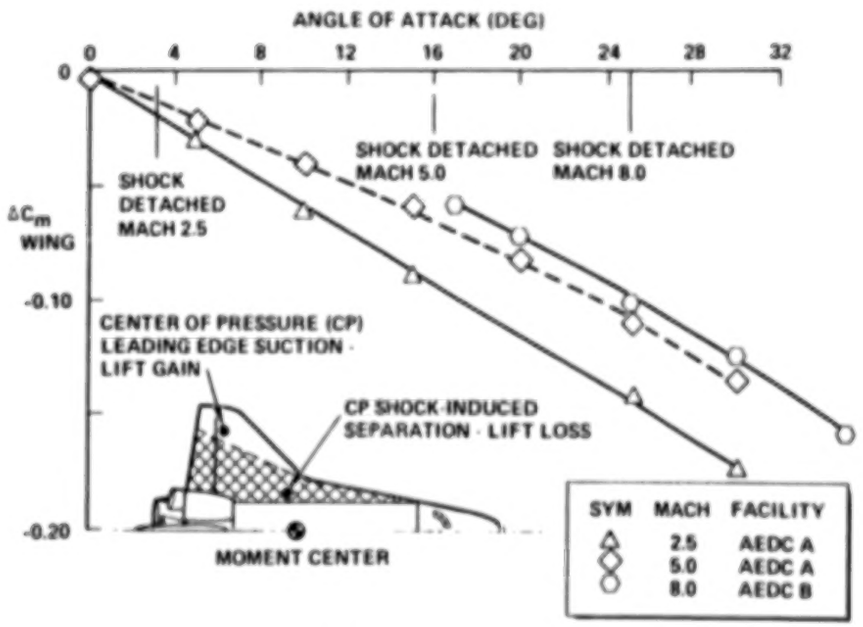


FIGURE 33.- LEESIDE FLOW SEPARATION EFFECT ON PITCH STABILITY.

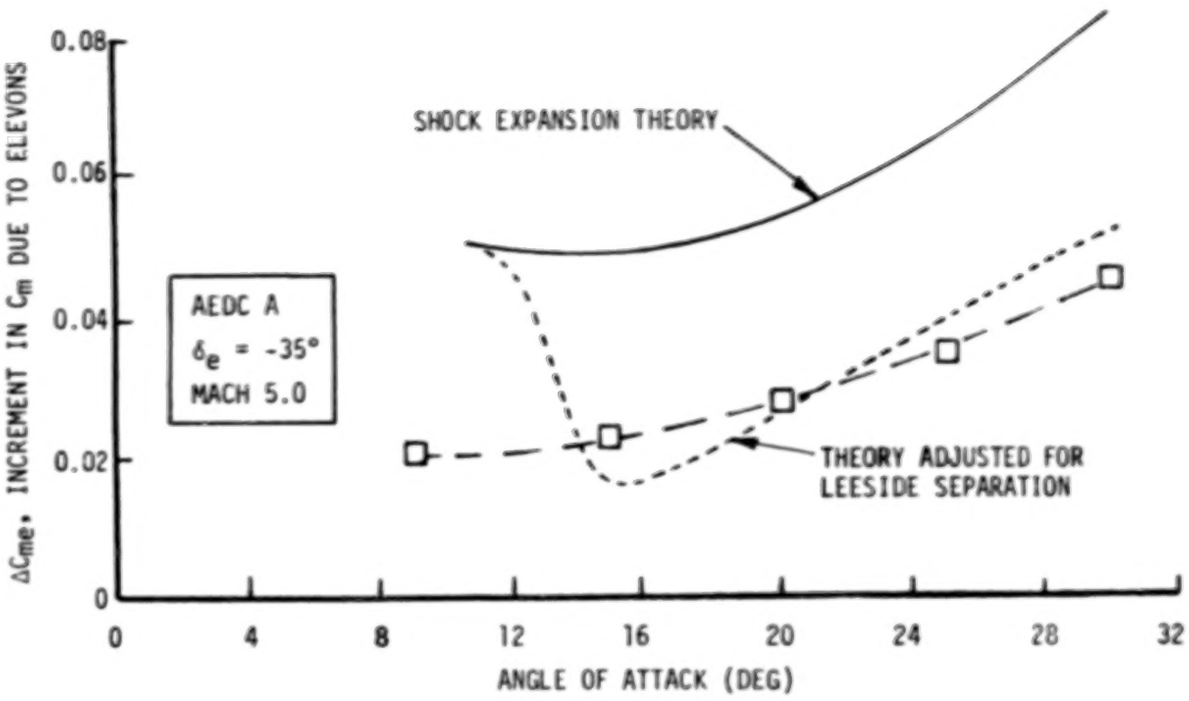


FIGURE 34.- HYPERSONIC ELEVON EFFECTIVENESS.

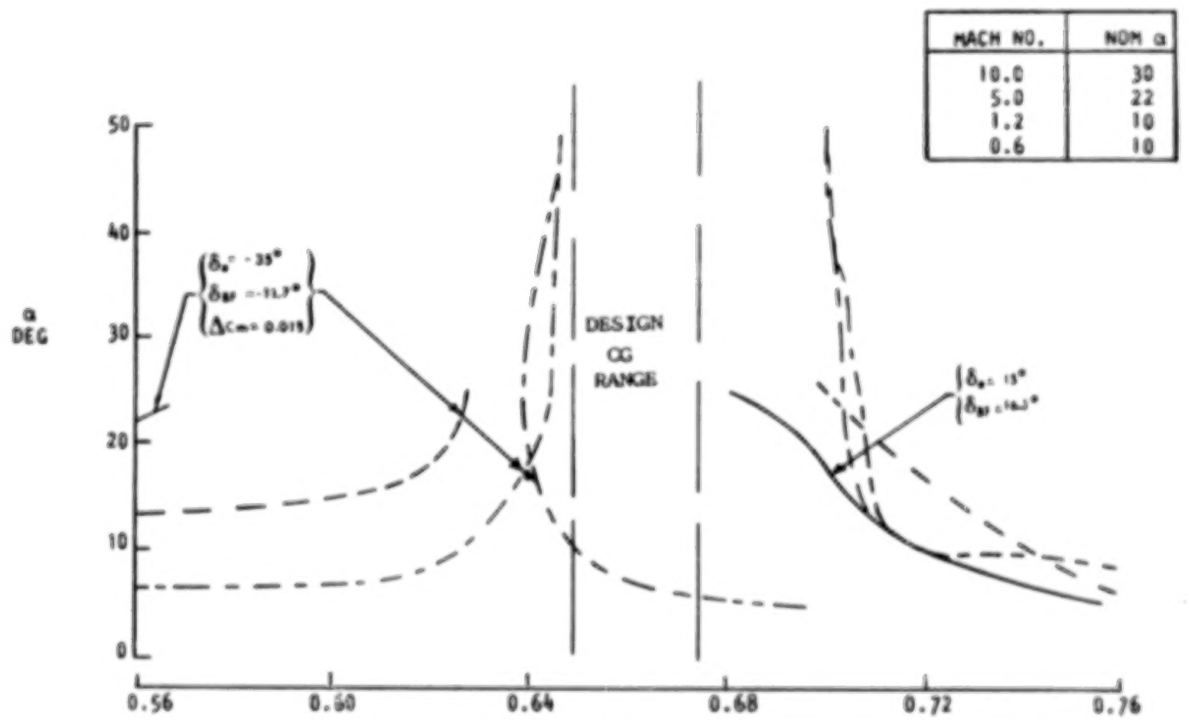


FIGURE 35.- TRIM CAPABILITY.

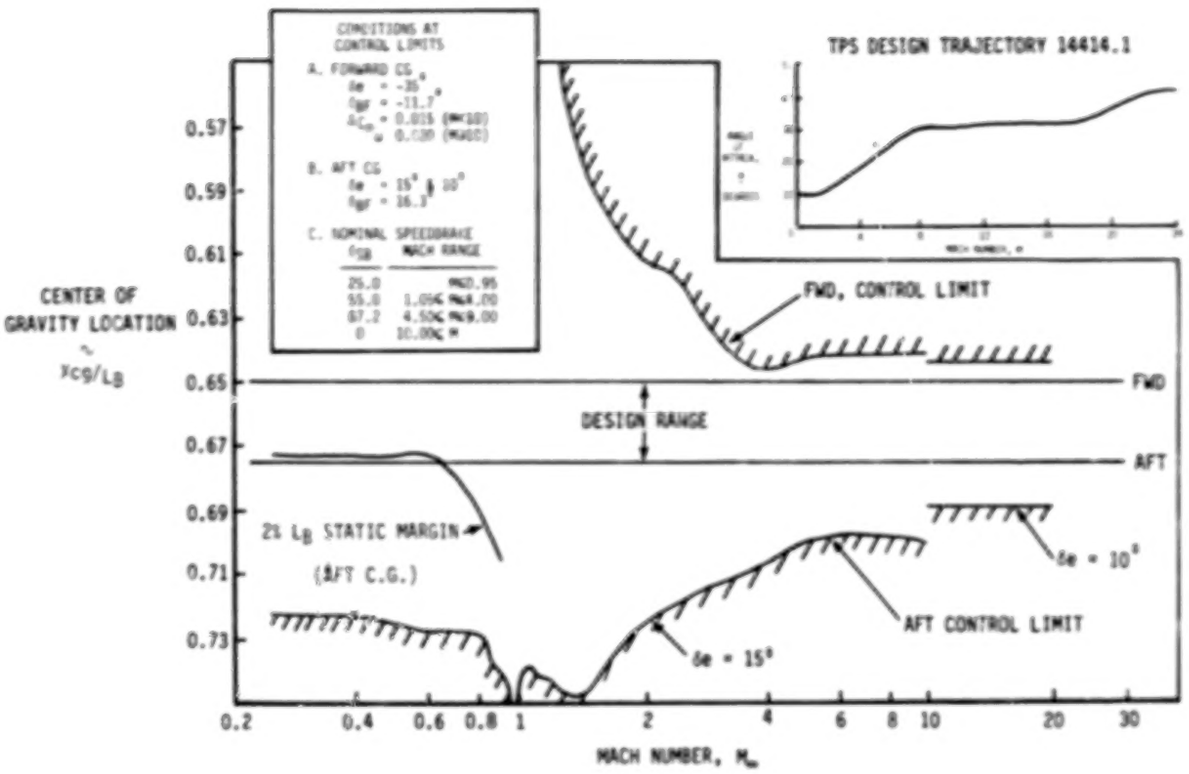


FIGURE 36.- ORBITER TRIM LIMITS.

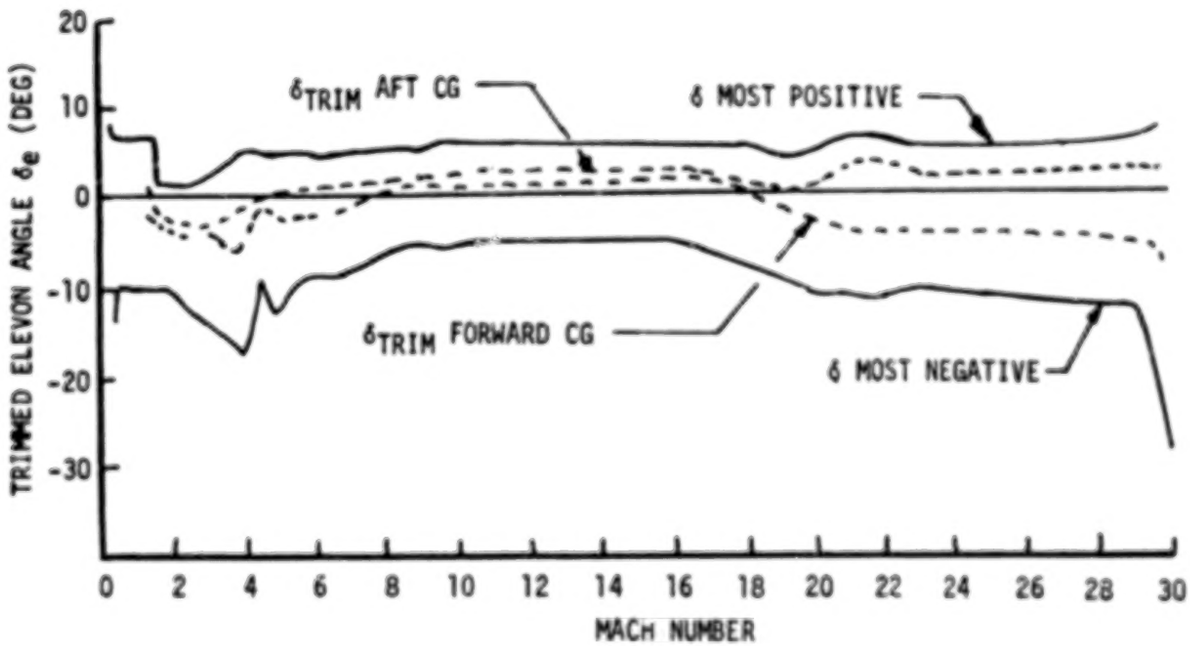


FIGURE 37.- ELEVON DEFLECTION SCHEDULE.

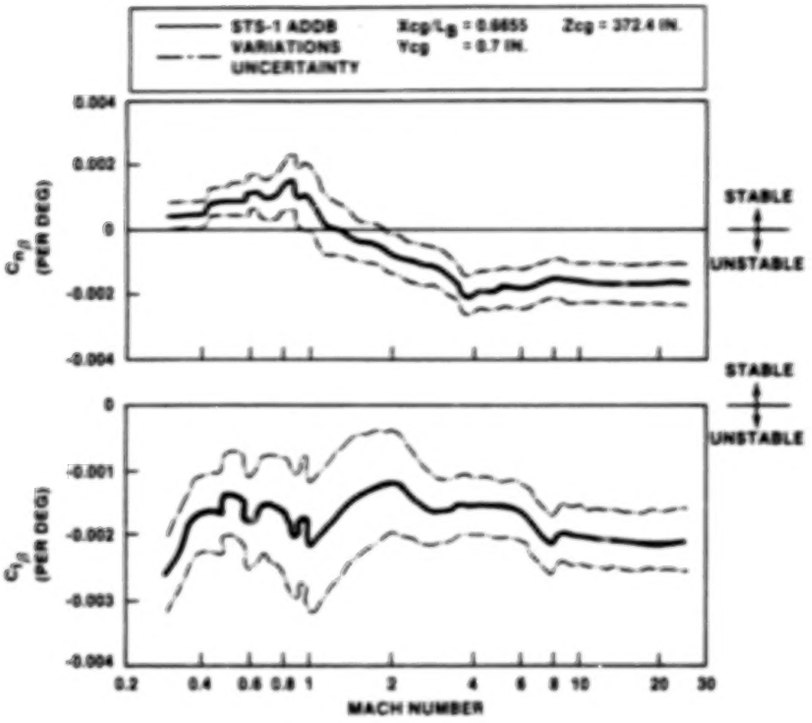


FIGURE 38.- PREDICTED LATERAL-DIRECTIONAL STABILITY.

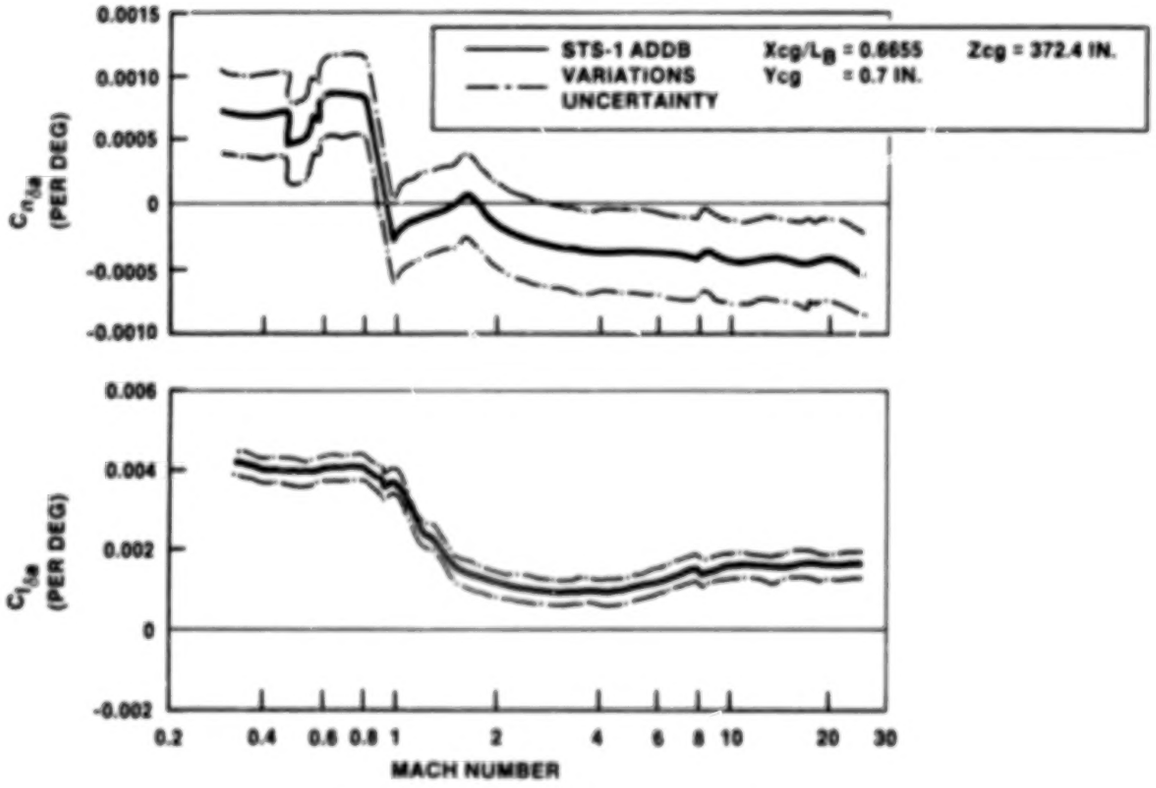


FIGURE 39.- PREDICTED AILERON EFFECTIVENESS.

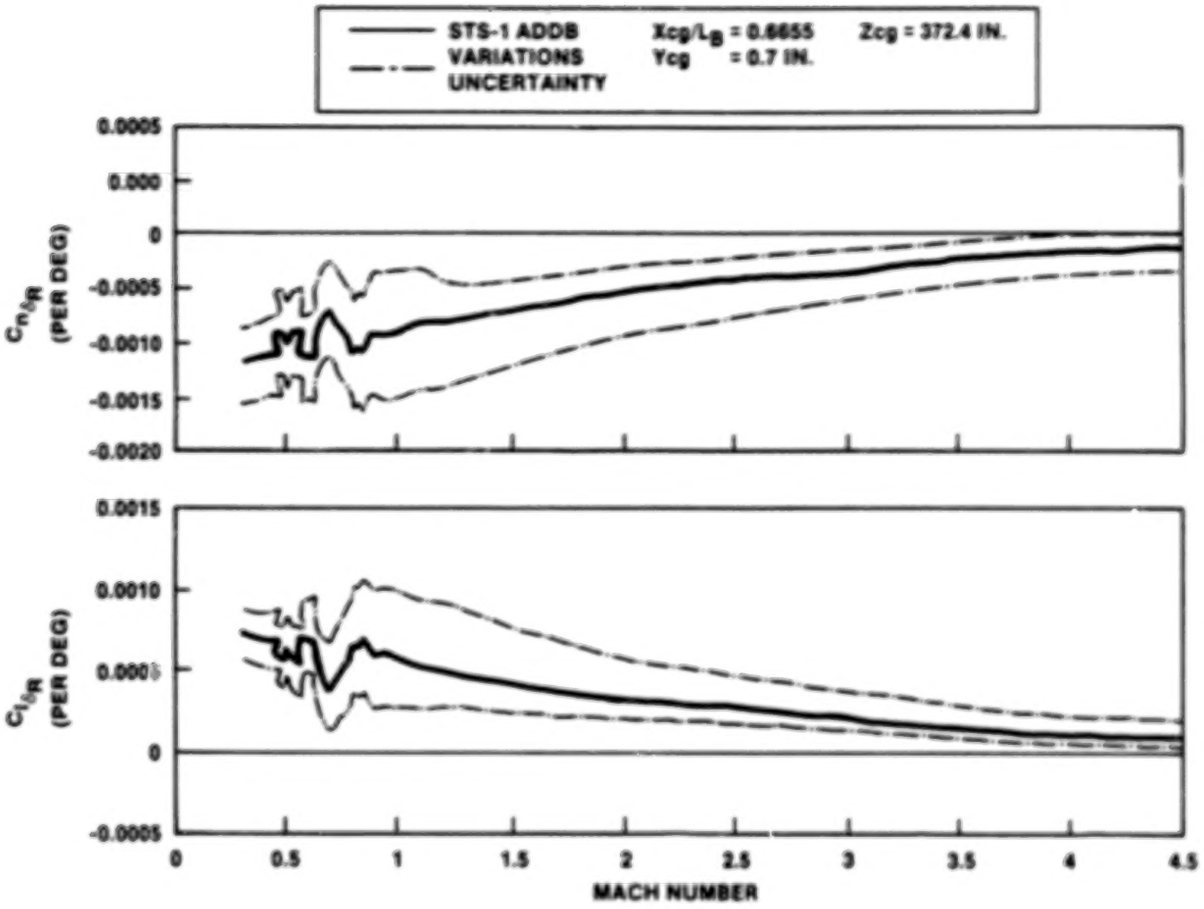


FIGURE 40.- PREDICTED RUDDER EFFECTIVENESS.

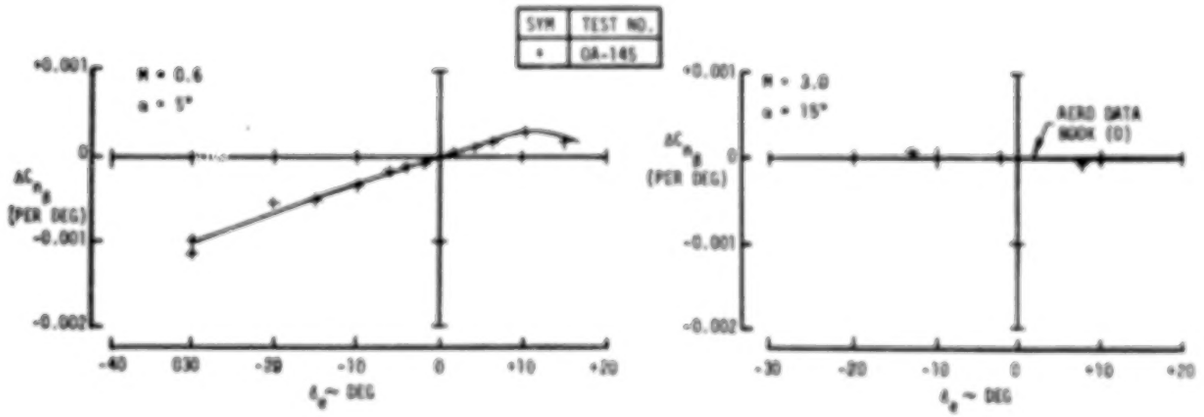


FIGURE 41.- EFFECT OF ELEVON ON DIRECTIONAL STABILITY.

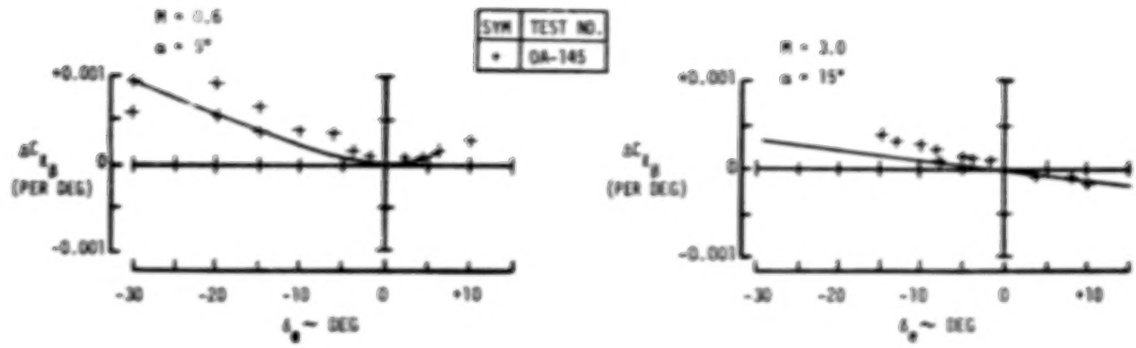


FIGURE 42.- EFFECT OF ELEVON ON DIHEDRAL STABILITY.

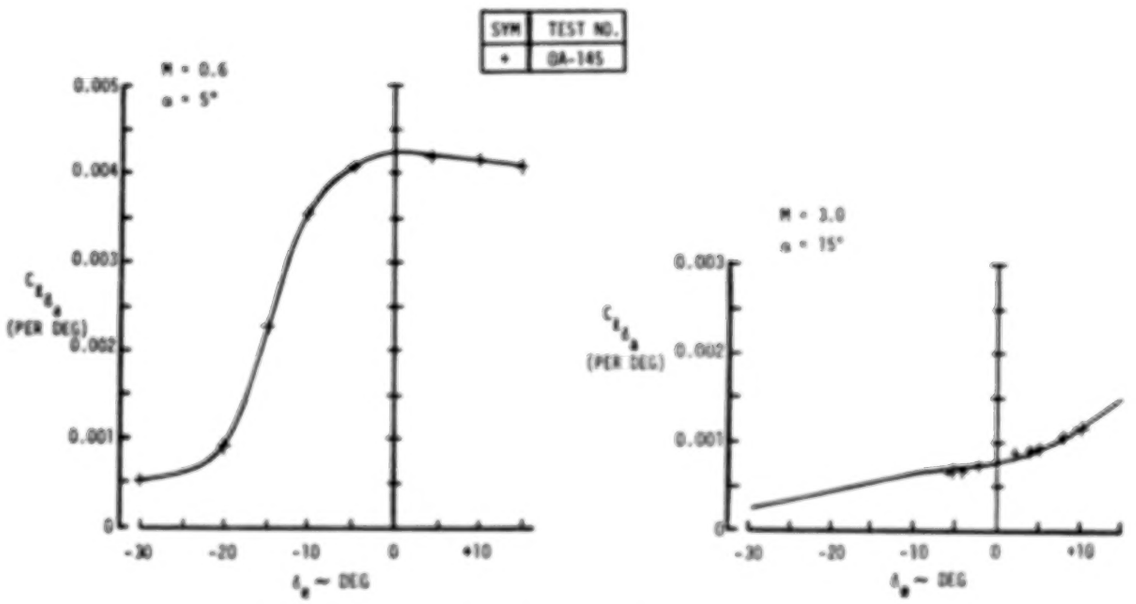


FIGURE 43.- EFFECT OF ELEVON ON AILERON ROLL DERIVATIVES.

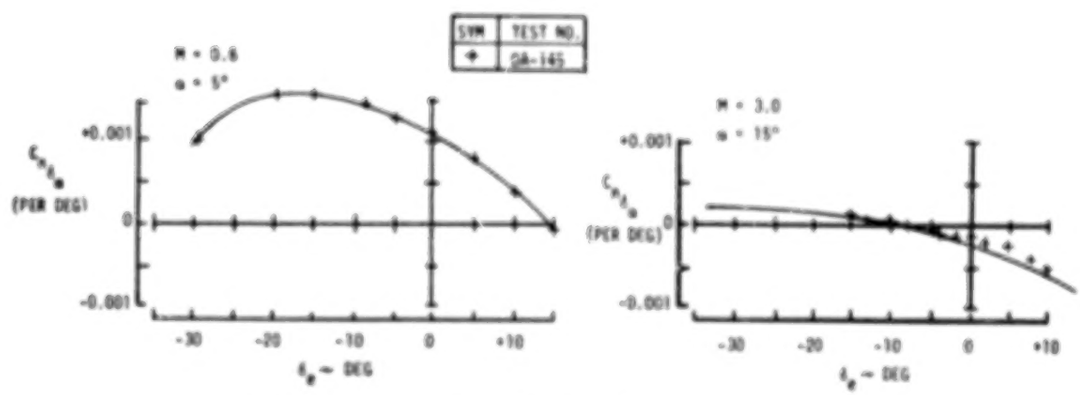


FIGURE 44.- EFFECT OF ELEVON ON AILERON YAW DERIVATIVES.

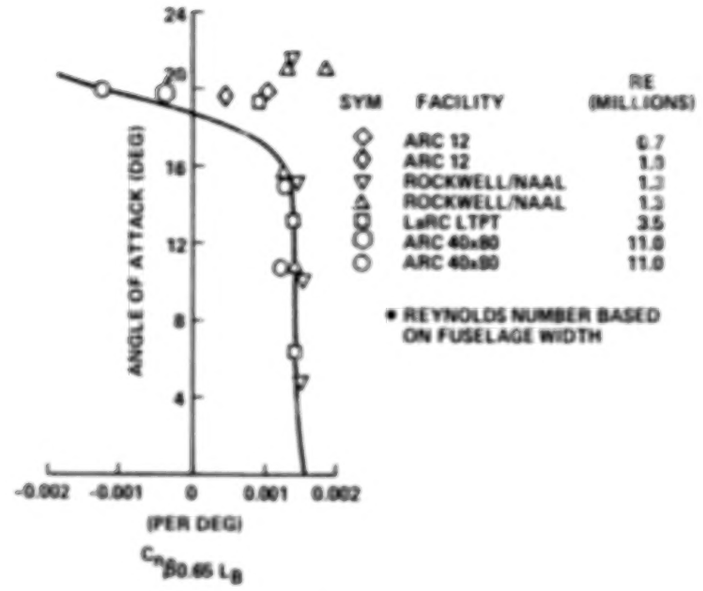


FIGURE 45.- COMBINED EFFECT OF REYNOLDS NUMBER AND ANGLE OF ATTACK ON LOW-SPEED DIRECTIONAL STABILITY.

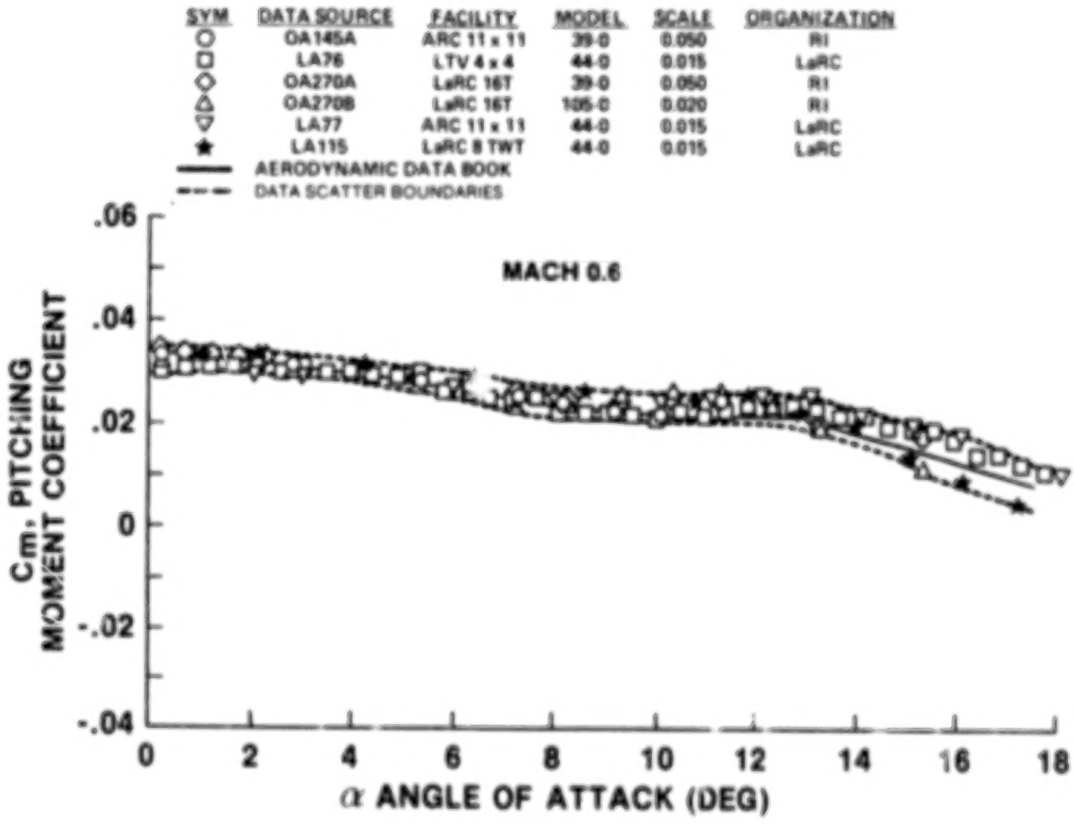


FIGURE 46.- PITCHING MOMENT DATA FOR TOLERANCES.

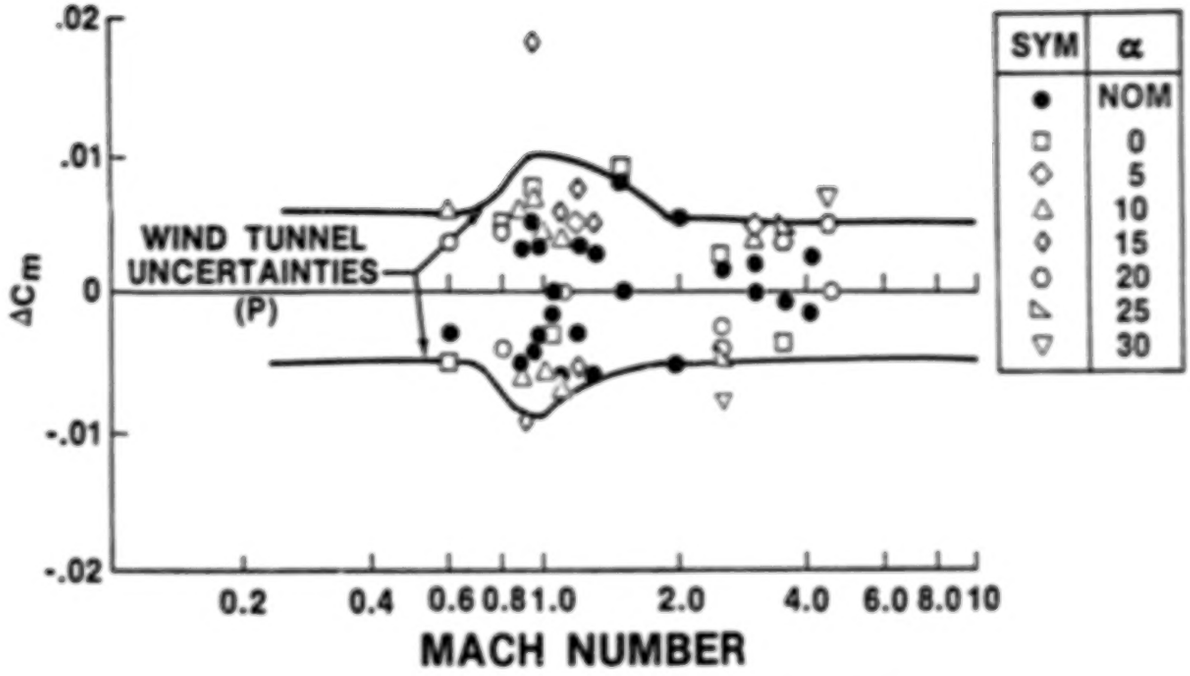


FIGURE 47.- CORRELATION OF UNCERTAINTY IN WIND TUNNEL PITCHING MOMENT WITH MACH NUMBER.

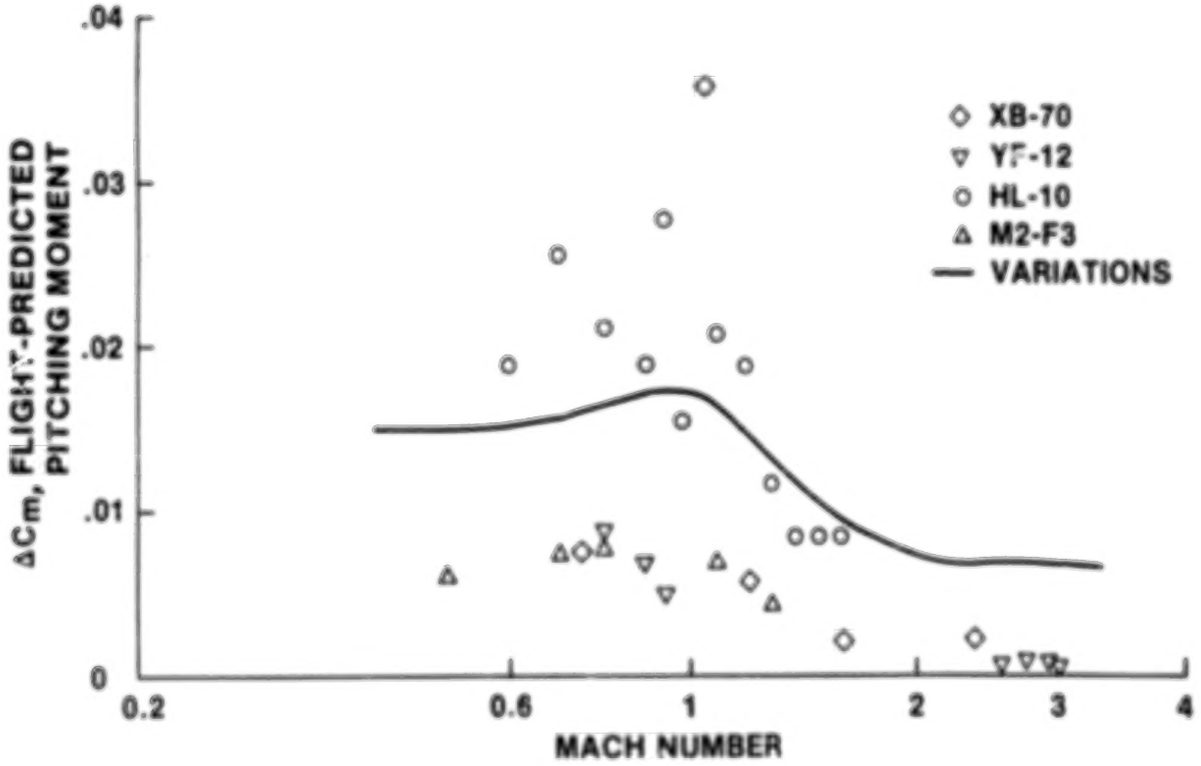


FIGURE 48.- CORRELATION OF FLIGHT AND PREDICTED PITCHING MOMENT OF PREVIOUS AIRCRAFT.

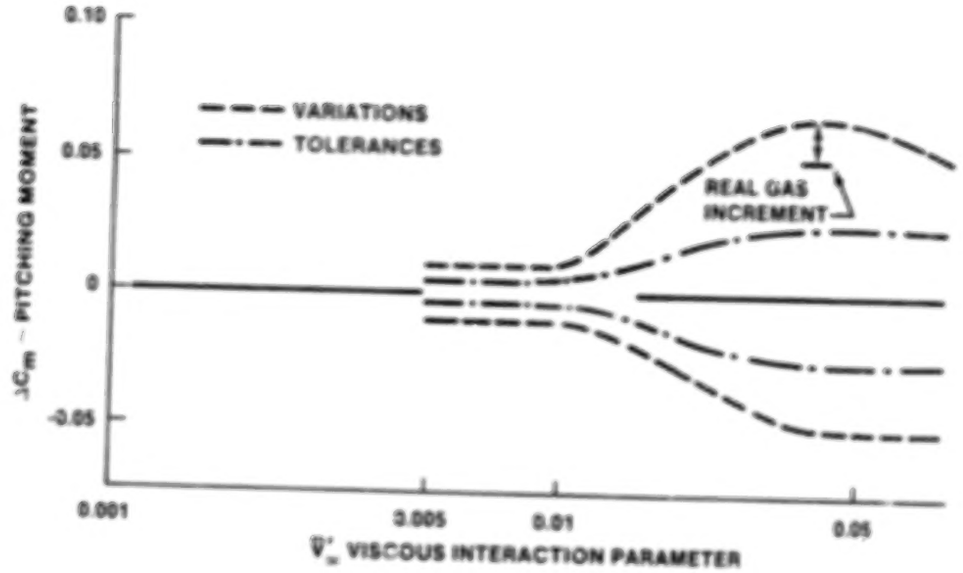


FIGURE 49.- HIGH ALTITUDE UNCERTAINTIES.

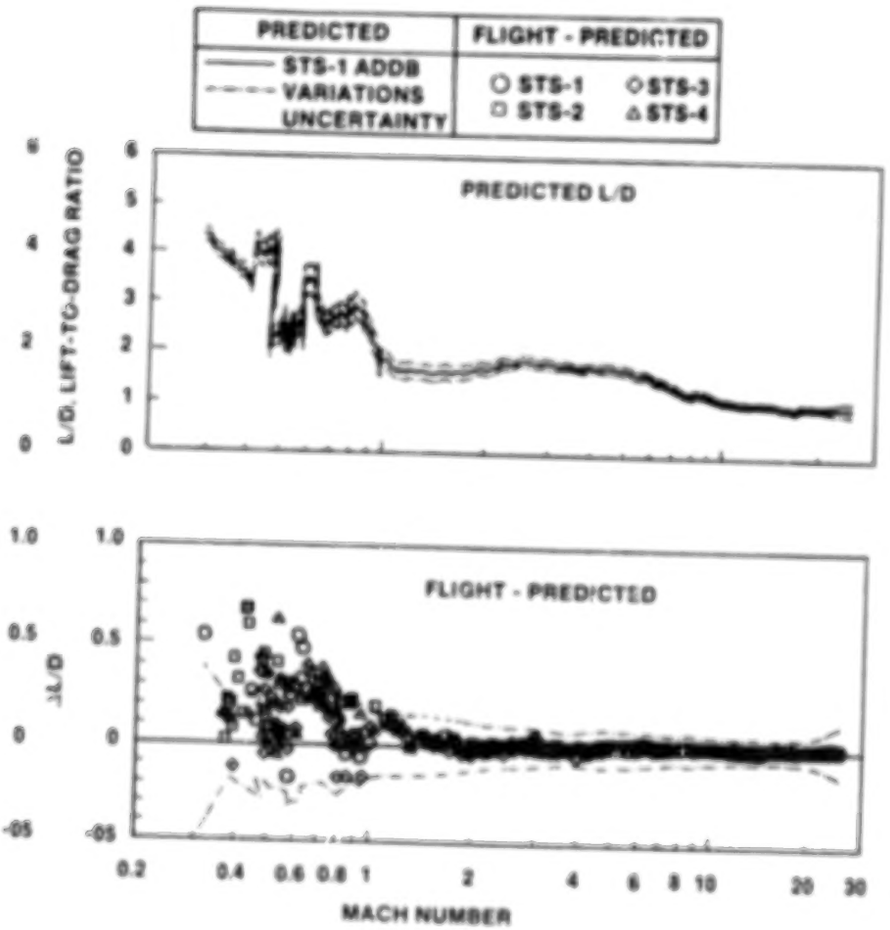


FIGURE 50.- CORRELATION OF FLIGHT WITH PREDICTED L/D.

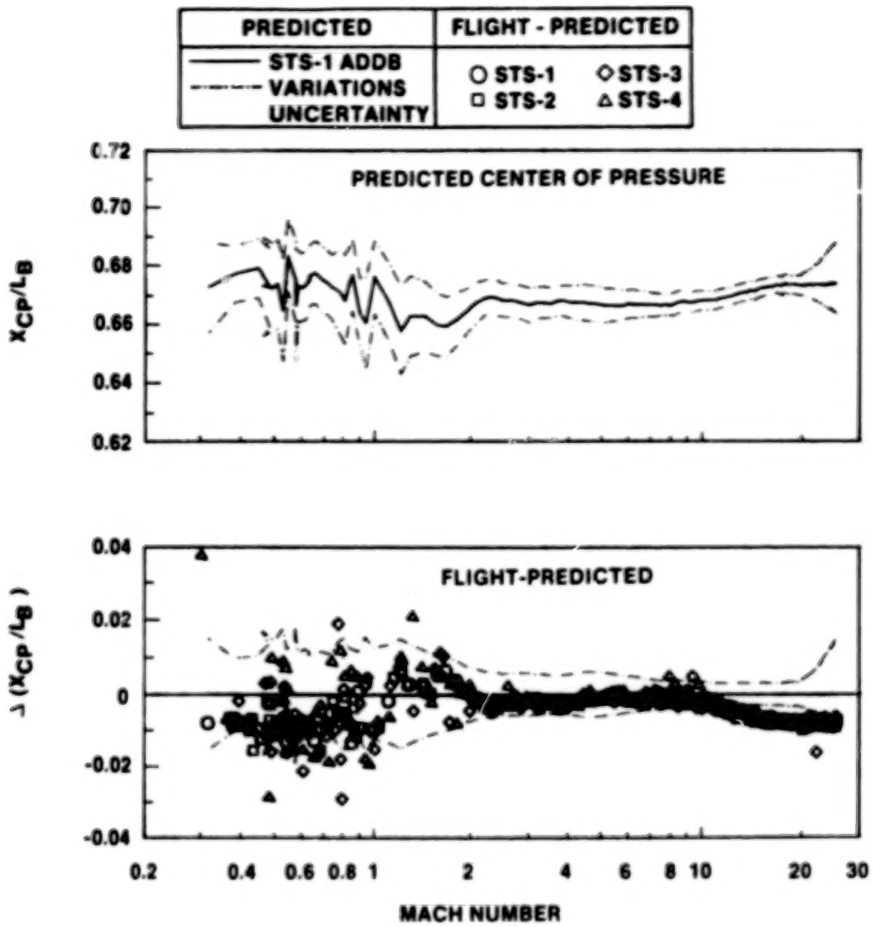


FIGURE 51.- CORRELATION OF FLIGHT WITH PREDICTED CENTER OF PRESSURE.

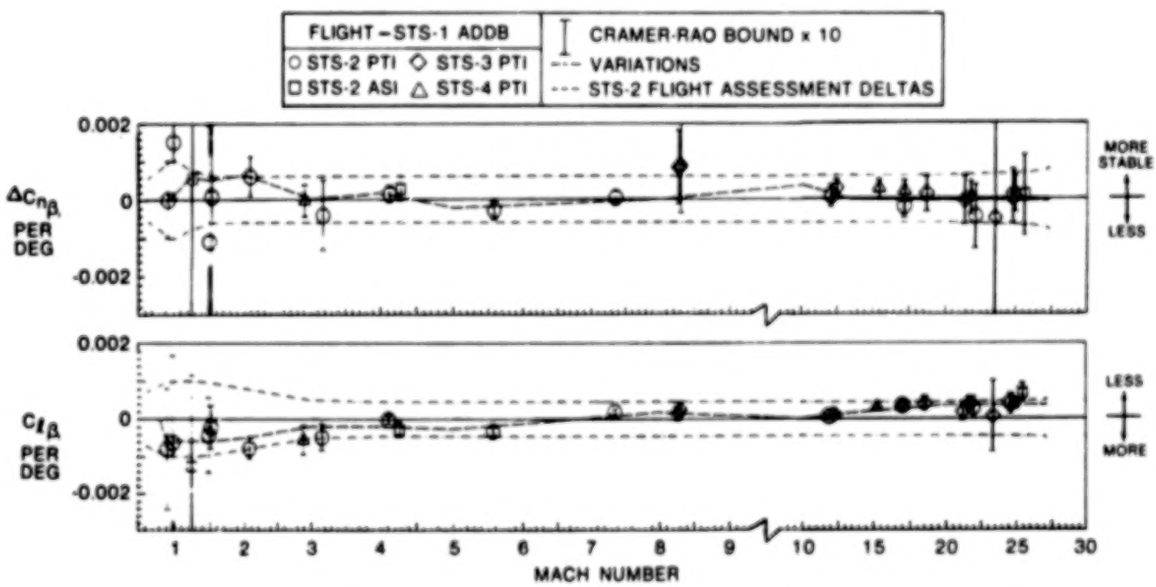


FIGURE 52.- CORRELATION OF FLIGHT WITH PREDICTED LATERAL-DIRECTIONAL STABILITY.

C-24

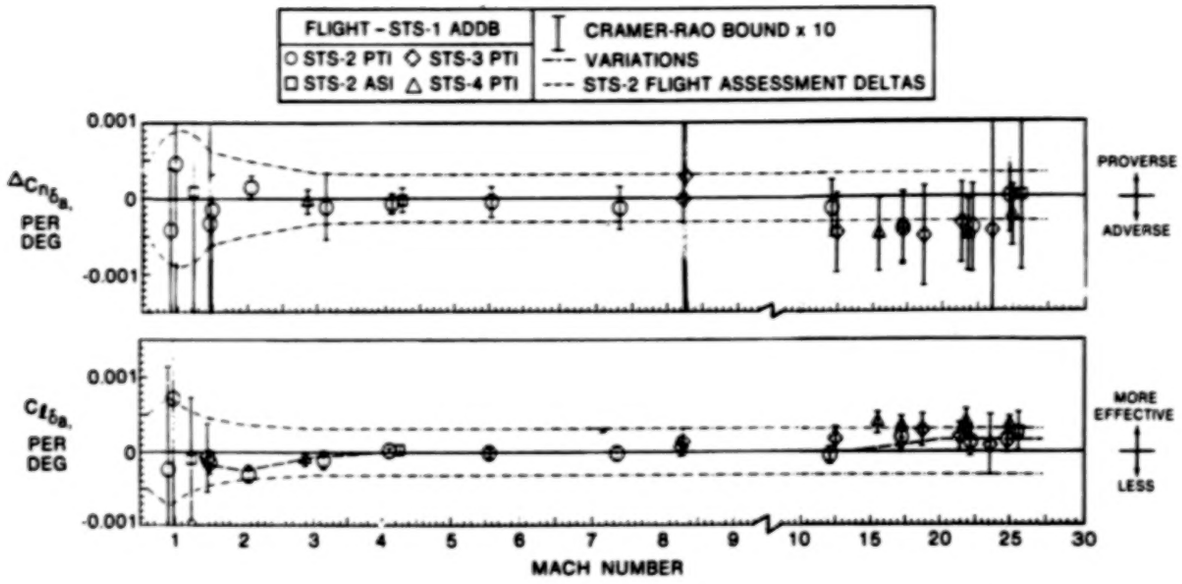


FIGURE 53.- CORRELATION OF FLIGHT WITH PREDICTED AILERON EFFECTIVENESS.

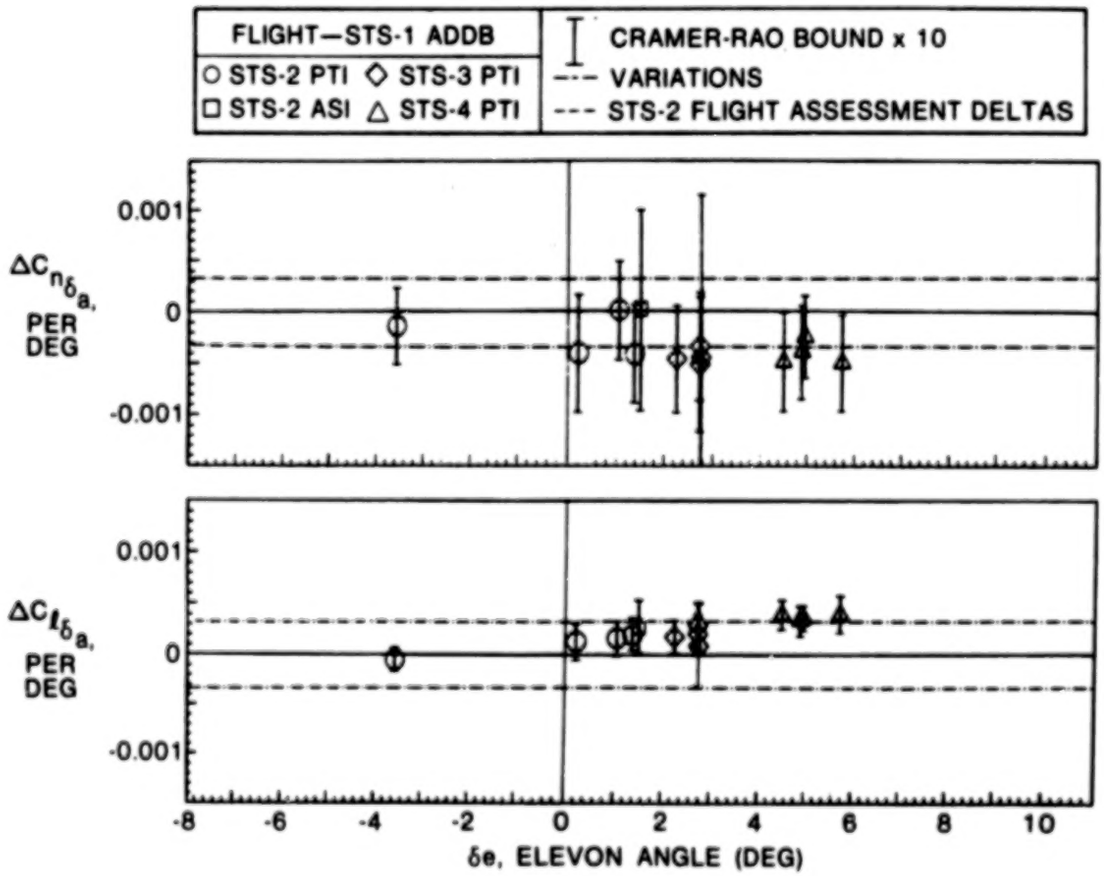


FIGURE 54.- CORRELATION OF FLIGHT WITH PREDICTED EFFECT OF ELEVON ON HYPERSONIC AILERON EFFECTIVENESS.

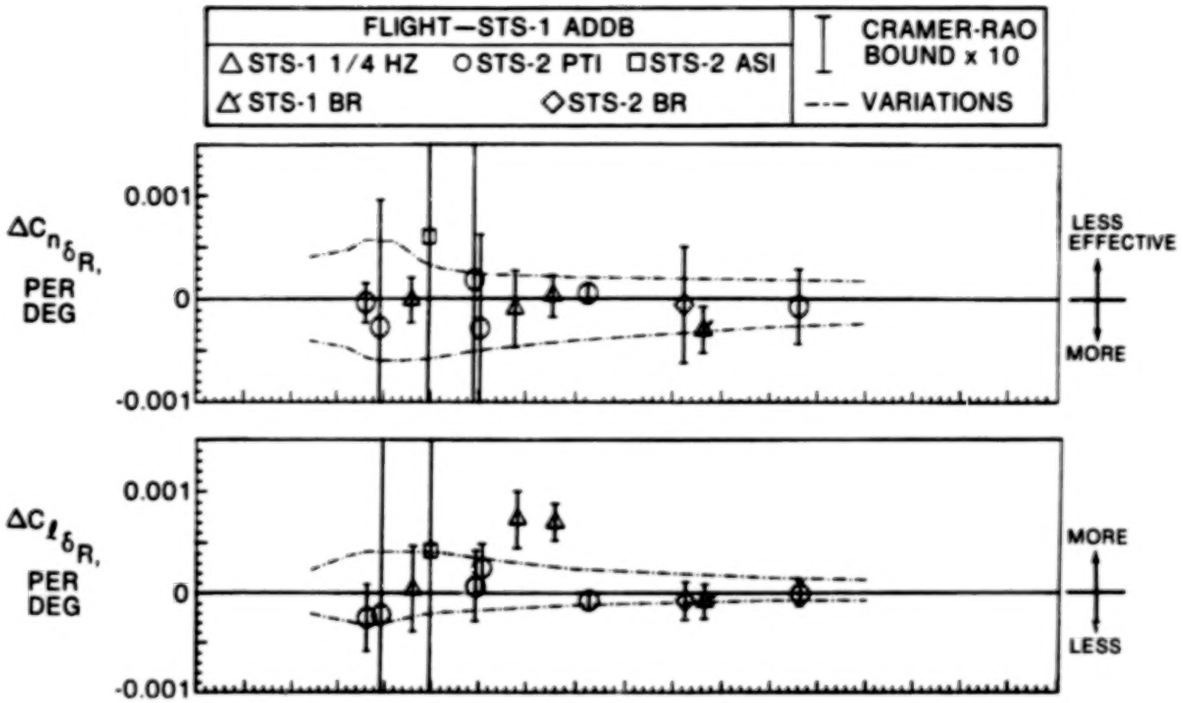
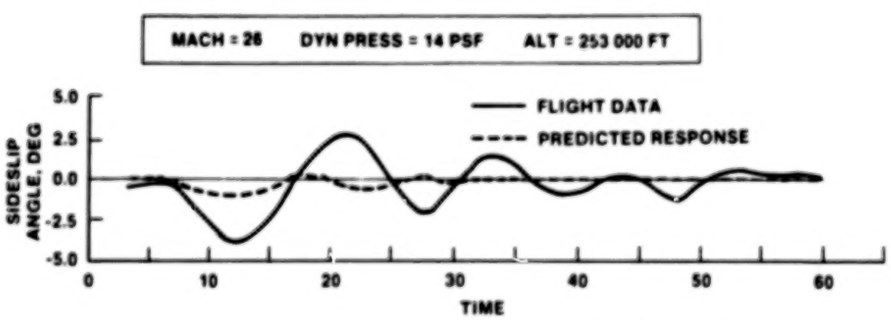
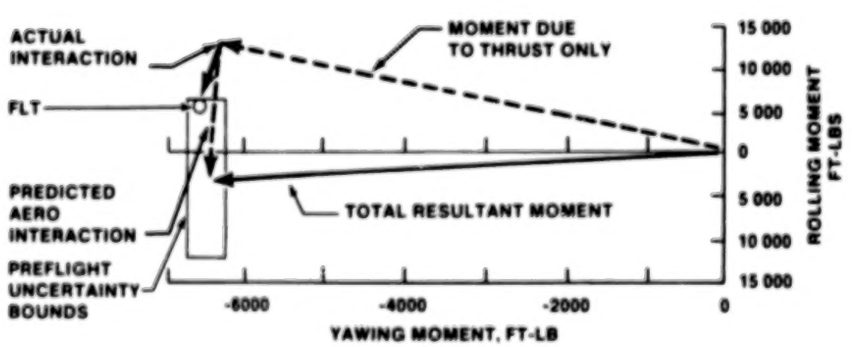


FIGURE 55.- CORRELATION OF FLIGHT WITH PREDICTED RUDDER EFFECTIVENESS.



(a) OSCILLATIONS DURING STS-1 INITIAL BANK MANEUVERS.



(b) EFFECT OF FLOWFIELD INTERFERENCE ON RCS JET EFFECTIVENESS.

FIGURE 56.- RCS JET INTERFERENCE DUE TO TWO SIDE-FIRING JETS.

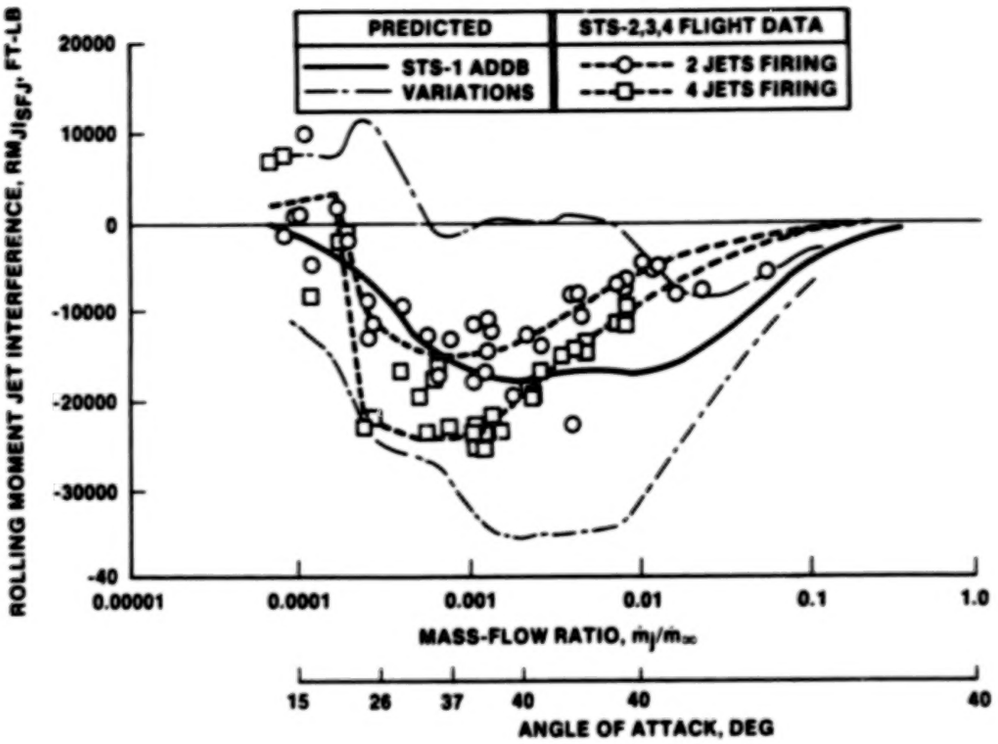


FIGURE 57.- CORRELATION OF FLIGHT WITH PREDICTED RCS SIDE-FIRING JET INTERFERENCE.

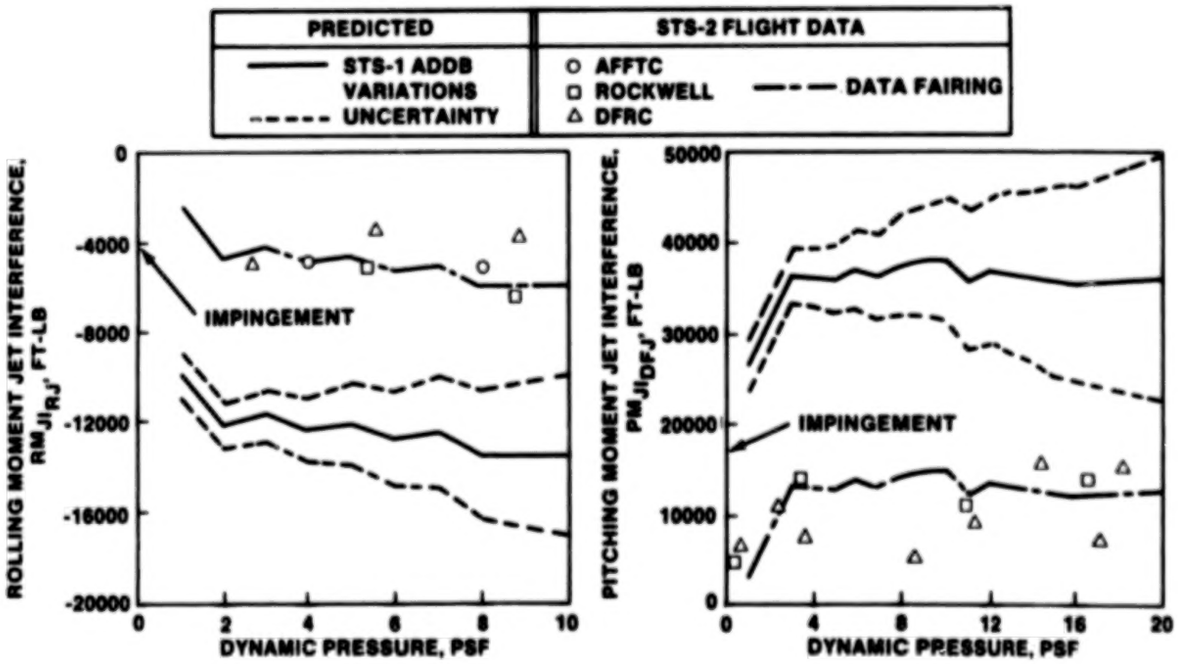


FIGURE 58.- CORRELATION OF FLIGHT WITH PREDICTED RCS JET INTERFERENCE DUE TO UP AND DOWN FIRING JETS.

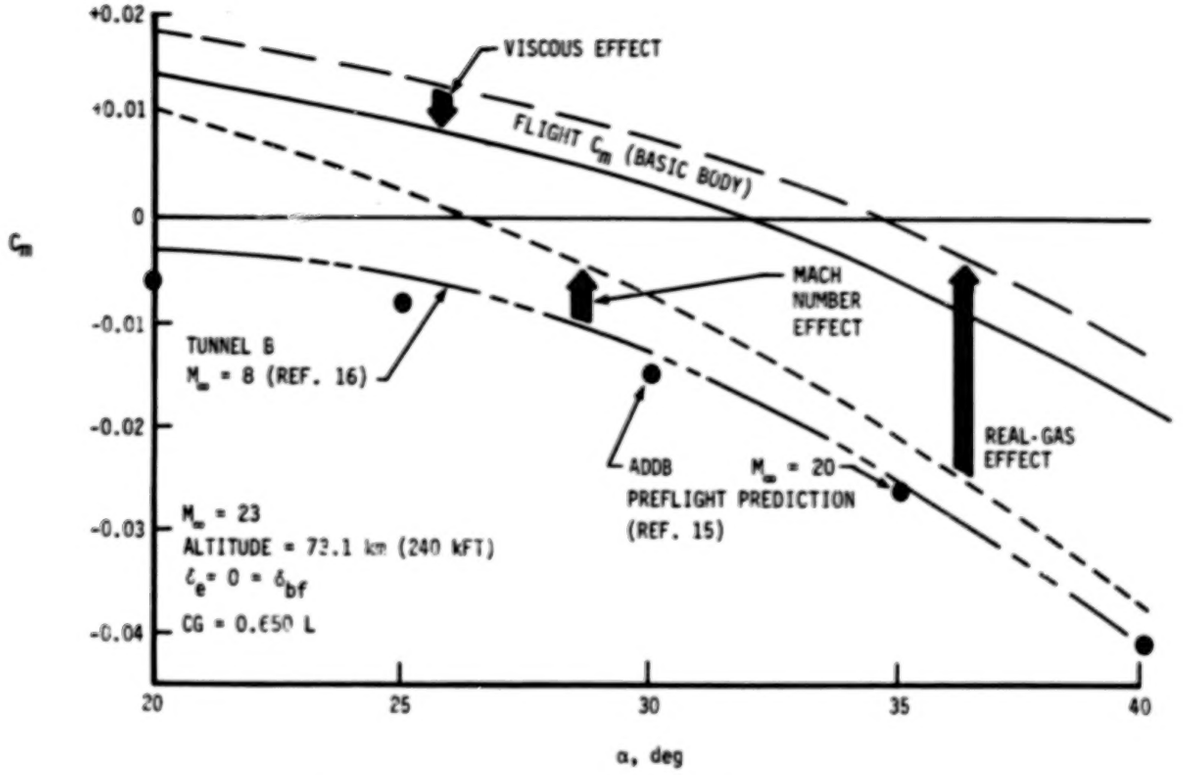


FIGURE 59.- HYPERSONIC MACH, REAL GAS, AND VISCOUS EFFECTS.

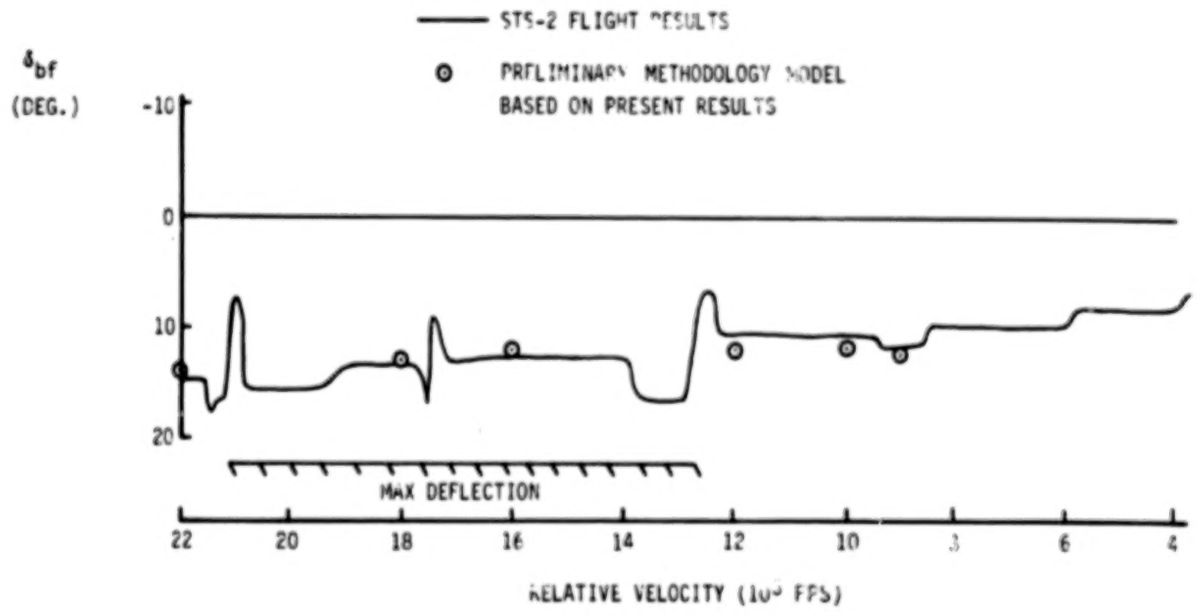


FIGURE 60.- TRIM BODYFLAP COMPARISON USING HYPERSONIC CORRECTIONS.

N85
16910

UNCLAS

D-21 N85-16910

THE DEVELOPMENT AND APPLICATION OF AERODYNAMIC UNCERTAINTIES; AND FLIGHT TEST VERIFICATION FOR THE SPACE SHUTTLE ORBITER

Joe D. Gamble, Douglas R. Cooke, Jimmy M. Underwood
NASA-Johnson Space Center
Houston, TX

Howard W. Stone, Jr.
NASA-Langley Research Center
Hampton, VA

Donald C. Schlosser
Rockwell International
Downey, CA

ABSTRACT

The approach used in establishing the predicted aerodynamic uncertainties and the process used in applying these uncertainties during the design of the Orbiter flight control system and the entry trajectory is presented. The flight test program that was designed to verify the stability and control derivatives with a minimum of test flights is presented and a comparison of preflight predictions with preliminary flight test results is made. It is concluded that the approach used for the Orbiter is applicable to future programs where testing is limited due to time constraints or funding.

NOMENCLATURE

A	Amplitude, deg/sec or g's
AN	Normal acceleration, g's
Ax	Axial acceleration, g's
Ay	Lateral acceleration, g's
C_{ℓ_β}	Coefficient of roll due to sideslip, per deg
$C_{\ell_{\delta_a}}$	Coefficient of roll due to aileron deflection, per deg
$C_{\ell_{\delta_r}}$	Coefficient of roll due to rudder deflection, per deg
C_{n_β}	Coefficient of yaw due to sideslip, per deg
$C_{n_{\delta_a}}$	Coefficient of yaw due to aileron deflection, per deg
$C_{n_{\delta_r}}$	Coefficient of yaw due to rudder deflection, per deg
$C_{N_{\delta_e}}$	Coefficient of normal force due to elevon deflection, per deg
C_m	Pitching moment coefficient
C_{m_o}	Pitching moment coefficient at 0 angle of attack
$C_{m_{\delta_{BF}}}$	Coefficient of pitching moment due to bodyflap deflection, per deg
$C_{m_{\delta_e}}$	Coefficient of pitching moment due to elevon deflection, per deg
C_{m_α}	Coefficient of pitching moment due to angle of attack, per deg
C_{Y_β}	Coefficient of side force due to sideslip, per deg
$C_{Y_{\delta_a}}$	Coefficient of side force due to aileron deflection, per deg
$C_{Y_{\delta_r}}$	Coefficient of side force due to rudder deflection, per deg

L_B	Body length, in.
L/D	Lift-to-drag ratio
M	Mach number
T	Time, sec
V	Velocity, ft/sec
X	Body axis axial coordinate, in.
Y	Body axis lateral coordinate, in.
Z	Body axis vertical coordinate, in.
α	Angle of attack, deg
β	Sideslip angle, deg
δ_a	Aileron deflection, deg
δ_{BF}	Bodyflap deflection, deg
δ_e	Elevon deflection, deg
δ_r	Rudder deflection, deg
δ_{SB}	Speedbrake deflection, deg
σ	Standard deviation
$\bar{q}$	Dynamic pressure, psf
ω_d	Undamped natural frequency of the dutch roll oscillation
ω_ϕ	Undamped natural frequency of the numerator of ϕ/δ_a transfer function

ACRONYMS

ACIP	Aerodynamic Coefficient Identification Package
cg	Center of gravity
FCS	Flight Control System
FSL	Flight Software Laboratory
GN&C	Guidance, Navigation and Control
GPC	General purpose computer
IMU	Inertial Measurement Unit
LRU	Line replaceable unit
MMLE3	Modified maximum likelihood estimator, version 3
MXRCS	RCS roll moment
MZRCS	RCS yaw moment
POPU	Pushover Pullup Maneuver
PTI	Programmed test input
RCS	Reaction control system
SPS	Shuttle Procedures Simulator
STS	Space Transportation System
STS-1	First Flight of the Space Shuttle
STS-2	Second Flight of the Space Shuttle
WOW	Worse on worse combination of errors

INTRODUCTION

The decision to perform an orbital manned mission on the first Shuttle launch presented several challenges to the entry design community. A significant challenge was presented by the question of how to maximize safety (man rate the system) on the first flight considering the parallel development of the aerodynamics and the Flight Control System (FCS). A challenge was also presented in setting up a flight test program for a vehicle that was flying through a continuously changing environment. Finally, because of cost and operational constraints, the question of how to develop an operational vehicle with a minimum flight test program became a large challenge. This paper will address how these challenges were successfully met.

AERODYNAMIC VARIATIONS DEVELOPMENT

The challenge of maximizing safety on the first flight led to development of a reasonable estimate of maximum possible errors in the preflight predicted aerodynamics which were used to certify the FCS prior to the first flight. The best approach for the development of these errors which were called variations, was concluded to be an analysis of the wind tunnel to flight test differences of previous aircraft programs. Unfortunately, the verification of preflight predicted

aerodynamics was not a major objective of most of the previous flight test programs. This severely limited the amount of data available for conducting flight test to wind tunnel comparisons. The flight data base was further limited by restricting the comparison to those vehicles which were geometrically similar to the Orbiter. Those vehicles chosen as applicable to the Orbiter are presented in table 1. Also presented are geometric factors and other considerations pertinent to the vehicle configuration choices.

Variations were established by fairing the differences between the flight and predicted aerodynamics as a function of Mach number. The selections of the configurations and the fairing process are very subjective in nature. For this reason, a team of aerodynamicists from the various NASA centers, the Air Force and the contractors was formed to conduct the analysis and reach a consensus on variations.

The team's flight-to-predicted correlation and their recommended variations fairings are presented in reference 1. A more detailed development is presented in reference 2. The development of a less severe set of uncertainties (tolerances) based on the repeatability of wind tunnel tests is also presented in reference 1.

Reaction control jet plume interaction variation development is reviewed in reference 3.

THE CORRELATION OF AERODYNAMIC VARIATIONS

A total of 9 lateral directional coefficients (3 each beta, aileron and rudder derivatives) were defined for application to the Orbiter entry FCS verification. Use of all possible combination of signs and variations for these 9 coefficients would have resulted in an impossible number of cases to analyze and simulate. Therefore, considerable attention was devoted to identifying the more critical combination of coefficient variations for use in FCS verification.

In addition, an alternative to a worse-on-worse (WOW) analysis was desirable to provide a less demanding and possibly more realistic result for formal verification. The initial step in reducing the WOW case was to define any sign correlation that might exist between coefficient variations based on the physical relation of the coefficients.

Reference 4 presents the details involved in defining the correlation coefficients. Correlations were established for the sideslip, aileron and rudder derivatives. For the correlated coefficients, 99 percentile ellipses were established from the equation

$$1 = (1 - \rho_{xy})^{-1}\left\{\left(\frac{X}{3\sigma_x}\right)^2 - 2\rho_{xy}\left(\frac{X}{3\sigma_x}\right)\left(\frac{Y}{3\sigma_y}\right) + \left(\frac{Y}{3\sigma_y}\right)^2\right\}.$$

X and Y are the correlated coefficients, σ_x and σ_y are the standard deviations and ρ_{xy} is the linear correlation coefficient which varies between zero and one. Stated from a probability standpoint there is a one chance in a hundred that a combination of errors in X and Y would lie outside the locus of the 99 percentile ellipse.

Figure 1 presents an example of correlations in the yawing moment and rolling moment sideslip coefficients. The vector from the origin represents the nominal value for C_{n_β} and C_{l_β} while the rectangle represents the 3σ variations. The different ellipses inside the rectangle show the effect of varying the correlation from 0 to a highly correlated value of .9. Results from wind tunnel tests were used to establish the correlation coefficients.

APPLICATION OF AERODYNAMIC VARIATIONS

A programmatic decision was made to use aerodynamic variations in the Orbiter FCS design evaluation and verification process. For the initial FCS design evaluation and simulation studies, a "worst on worst" combination of variations was used. For the formal entry verification at the Flight Software Laboratory (FSL) at Rockwell, variation sets were used which correlated the roll and yaw moment coefficients for the sideslip, aileron and rudder coefficients.

Because of the wide range of flight conditions the Orbiter was to encounter during the first reentry flight test, it was required to evaluate as many combinations of aerodynamic uncertainties as possible. However it was also desirable to select a more limited set of uncertainties for concentrated analysis and simulation efforts. It thus became necessary to define those aerodynamic uncertainty combinations that presented the most potential problems to the Orbiter and to make certain that the flight control system could maintain control of the Orbiter with these

combinations. In the initial FCS evaluation, a total of 26 lateral directional variation sets were evaluated in a series of almost 600 piloted simulation runs on the Shuttle Procedures Simulator (SPS) at the Johnson Space Center (JSC). These 26 cases were selected using various trim, controllability and handling qualities criteria. Based on the results of these simulation runs plus additional trim and stability analyses, a subset of 7 cases were chosen and used for the majority of the formal verification process.

Figure 2 shows a vector diagram of the aero coefficients and RCS jets for the roll and yaw axes at Mach 3.5. The numbers shown on the diagram indicate the nomenclature used for identifying the 7 cases selected for the verification process. The corners shown indicate the WOW or "rectangular" variation sets which were used in the FCS development while the ellipses represent the correlated variations. The elliptical variation sets were generally selected from points on the ellipses that were close to the rectangular counterparts. Some of the history and logic involved in the selection of the cases used for the FCS verification will now be discussed.

LCDP AND C_{n_β} DYNAMIC

A significant portion of the analysis devoted to aerodynamic variations was applied to variation sets 19 and 20. Variation set 19 represented the most severe case for the Lateral Control Departure Parameter (LCDP).[5] During the early stages of the Orbiter development, most of the reentry was performed using an all aerodynamic control concept. Prior to rudder activation which then occurred around Mach 5, the aileron was the only aerodynamic control effector for lateral directional control and trim. A reverse aileron control that required a negative value for the LCDP, $C_{n_\beta} C_{\ell_{\delta_a}} - C_{\ell_\beta} C_{n_{\delta_a}} < 0$, was utilized prior to rudder activation.[6] The lateral trim logic was also configured so that a negative value of the LCDP was required prior to rudder activation. Some of the early simulations using aerodynamic uncertainties on the aileron and beta derivatives resulted in lateral trim and controllability problems prior to rudder activation. Analysis indicated that the problem was caused by a sign change in the LCDP in the Mach 5 region. As a partial result of this problem, several changes were made to the FCS. The basic FCS design was changed from the aileron bank control to a system utilizing the yaw RCS jets to initiate bank maneuvers and the ailerons to coordinate the maneuvers prior to activation of the rudder.[7] After the rudder became active, a gradual FCS gain change produced the conventional aileron bank control with rudder coordination.

Since use of the yaw jets for trim would result in excessive propellant requirements, the aileron was still required for trim. To improve the aileron trim capability in the critical Mach region, changes were made to the angle of attack and elevon schedules. With aero variations applied, Mach 3.5 was the highest Mach number that the rudder could be considered effective and this Mach number was chosen as the activation point for the rudder. It was then considered a requirement that aileron trim be available down to Mach 3.5 with minimal yaw RCS requirements.

Figure 3 shows the sensitivity of the Orbiter LCDP to angle of attack for several Mach numbers with the worst case aero variations applied. It is obvious that in the Mach greater than 3 region an angle of attack of more then 15° is desirable in order to maintain a negative LCDP. The early flights of the Orbiter were tailored so that the angle of attack remained above 15° for Mach greater than 3.5.

Another significant factor in the LCDP is the elevon trim position. This is due to the effect of elevon position on the aileron derivatives. A desired elevon trim position of +5° (down) was eventually selected for STS-1 in the Mach 3-4 region. In the higher Mach region where elevon heating is a concern, the elevon was scheduled at -1 degree (up) and in the transonic region where there was some concern about hinge moments, a schedule close to zero was selected. The elevon position is maintained by the bodyflap through a feedback from the elevon which drives the bodyflap to maintain the pre-set elevon schedule.

Application of the LCDP in the Mach range from approximately 3-8 was a driver in the angle of attack, elevon and speedbrake schedules as well as the longitudinal cg choice for STS-1.

In the longitudinal axis the primary problem associated with aero uncertainties was the pitching moment uncertainty, C_{m_0} and its effect on elevon trim position. Figure 4 shows the pre STS-1 capability to position the elevon for the design cg body length extremes of 65 percent

(forward) and 67.5 percent (aft) with pitching moment variations and with the bodyflap positioned at its extreme limits to aid the desired trim. Also shown on figure 4 is the STS-1 elevon schedule. It is obvious that with C_m variations the Orbiter could not achieve the desired elevon schedule over the design range of cg's. Based on the desired elevon schedule and the effect of pitching moment variations, the STS-1 cg was selected at 66.7 percent body length. Figure 5 shows the elevon envelope at the 66.7 percent cg with C_m variations while figure 6 shows the effect of cg on the LCDP at Mach 3.5 for the worst case variation set. The cg envelope adopted for STS-1 mission rules is shown in figure 7.

Variation set 20 created the minimum value for C_{n_β} dynamic which is defined as C_{n_β} coan - $C_{\ell_\beta} \sin \frac{I_z}{I_x}$. C_{n_β} dynamic is the stability term for coupled lateral directional motion and it was considered a requirement to have a stable value for this parameter throughout entry. Figure 8 shows C_{n_β} dynamic in the lower Mach region for variation set 20 for 1g flight at 7.5° α. The unaugmented C_{n_β} dynamic is unstable from about Mach 1.2 to 3.2 at these flight conditions.

The Orbiter FCS utilizes a side acceleration feedback to the rudder and yaw jets to provide stability augmentation. An approximate β feedback gain to the rudder can be computed and from this gain a rudder "augmented C_{n_β} dynamic" can be calculated. For the Mach 2 region the equivalent gain for β feedback to the rudder is approximately -1.5 to -2. Additional augmentation is provided by the yaw RCS jets and although the system is nonlinear, an approximation to an augmented C_{n_β} dynamic can be obtained which is valid for sideslip angles less than that required to fire all 4 jets (approximately 1° to 2°). The effective C_{n_β} dynamic for both rudder and RCS augmentation is shown in figure 8. Very little improvement is shown for the rudder augmentation. This is due to the small rudder effectiveness which results from the aeroelasticity effects and from application of aerodynamic variations. It is evident that the RCS provides a significant improvement. However after the jets are saturated additional augmentation is not available and there is a β limit beyond which control is not possible. For STS-1, angle of attack and dynamic pressure limits were established based on the ability of 2 yaw jets to control the Orbiter at 1.5° sideslip for the worst case aero variations. Figure 9 shows the lower angle of attack boundary established for the flight rules based on lateral trim concerns above Mach 3 and C_{n_β} dynamic concerns below Mach 3. In the Mach 2 region STS-1 had a dynamic pressure limit of 250 psf programmed into the guidance laws and the trajectory was shaped to provide ample margin above the lower alpha limits.

ADDITIONAL CRITERIA

While the aero variation sets associated with the LCDP and with C_{n_β} dynamic received considerable attention during the FCS design and verification process, other combinations of variations shown on figure 2 were also extensively analyzed. Diagrams similar to figure 2 were widely used in helping to select which variation sets to use at different flight conditions. This was particularly true of cases involving co-alignment of effectors and stability derivatives. For example, with the variation set 19, the beta and aileron vectors align which corresponds to the LCDP going to zero. This results in the loss of aerodynamic lateral trim capability and would require the use of yaw jets to trim. Variation set 19 was used for the worst case LCDP analysis. Variation set 20 was used for the minimum C_{n_β} dynamic case and results in both minimum β stability and rudder effectiveness. Variation set 20 resulted in another problem at higher Mach numbers which required a change to the FCS. At the hypersonic Mach numbers and 40° angle of attack when variations were applied to 1 yaw jet, a coalignment of the jet and β vectors occurred due to a counter clockwise rotation of the jet vector. Since the bank control is achieved through the combination of jets and β, a control criteria similar to the LCDP results. The form of this criteria used for the Orbiter was $C_{n_\beta} M_{Z_{RCS}} - C_{\ell_\beta} M_{Z_{RCS}} > 0$. With one yaw jet firing a control reversal resulted which was similar to the case for the aileron control problem associated with

the LCDP. As a result of this problem, the FCS was changed so that a minimum of two yaw jets were always fired. Another case that received considerable attention was variation set 12 which is a high gain case utilizing the most stable sideslip derivatives in combination with the most effective control surfaces and jets. This case provided a balance for the low gain cases and resulted in FCS gains that covered the potential extremes in the aero variations. Case 9 was similar to case 20, but in the presence of large winds around Mach 5, a long period oscillation was observed under certain flight conditions. Offline stability analysis indicated the more negative $C_{n_{\delta_A}}$ associated with variation set 9 was resulting in a system approaching neutral stability.

In general cases 2, 11, and 23 produced less severe problems than the previously mentioned cases and were eventually dropped from the formal verification for STS-2. Case 2 was originally selected because it produced the largest value for $(\omega_\phi/\omega_d)^2$ and there was some concern about creating pilot induced oscillations (PIO) with this set of variations. However, there was no indication in any of the piloted simulations that this case produced any PIO tendencies. Case 11 was originally selected because it was thought to give the minimum value of the LCDP for the conventional aileron control mode. However, in the critical Mach region around Mach 2, case 9 usually resulted in a lower value of the LCDP. Case 23 was selected because it generated a maximum sideslip angle during the high heating region.

A problem that was observed with cases 9, 11 and 23 was an occasional tendency for the aileron and rudder to trim against each other after the rudder became active. From figure 2 it can be observed that the aileron and rudder vectors are almost co-aligned for these cases and is the probable cause for the trim problem. A procedure was utilized for STS-1 which required the crew to check the trim after the rudder became active and to trim the aileron back toward zero if a force fight resulted between the aileron and rudder.

FCS VERIFICATION PROCESS

The 570 piloted simulated runs on the Shuttle Procedures Simulation at JSC were completed in December 1977 and uncovered several significant problems when the variation sets were applied. Several changes were made to the FCS and another series of simulations were made in April and May of 1978. The modified FCS was able to maintain control of all combinations of aerodynamic variations except for one case in the Mach 6 region. This problem occurred when a variation set with minimum values of C_{n_β} dynamic was combined with large winds resulting in errors in the navigation derived angle of attack. Because angle of attack terms are present in the bank coordination logic of the FCS, errors in the angle of attack result in miscoordination during bank maneuvers and a resulting buildup in sideslip angle. If RCS jet failures occurred, control problems resulted for angle of attack errors greater than approximately 3^0. In order to accommodate this problem the flight rules for the early flights required manual bank reversals at reduced roll rates in the Mach 6 region if RCS jet failures occurred.

The formal integrated guidance, navigation and control (GN&C) verification testing began at the FSL in September 1979. A total of 35 runs were made before the simulation was suspended due to several significant problems that resulted. Forty-one flight software anomalies were identified of which 21 were related to the FCS. In general the problems occurring on the FSL had not been observed in the non integrated FCS simulations or were of a much smaller magnitude. As a result of the FSL results extensive analysis of the FCS was done to attempt to identify and correct the observed anomalies. The launch schedule slip due to the loose tile problem provided the FCS community an opportunity to perform a major review of the FCS design. Some of the problems were related to excessively large uncertainties applied to the GN&C line replaceable units (LRU) and some related to the FSL models. However some FCS changes were required to handle the aero variations and the Orbiter Software Control Board approved the change requests in April 1980.

Figure 10 shows the test matrix that was proposed for the final FCS verification.[8] The matrix includes aerodynamic uncertainties, winds, and tolerances on the GN&C LRU's. Most of the simulation runs were performed using the upper left box (nominal) and the lower right box (worst case). Figure 11 outlines the verification process that was approved by the Orbiter Configuration Control Board (CCB) prior to the final integrated verification testing at the FSL.[8]

The GN&C first was tested with nominal aerodynamics and then with the variations. If no problems occurred with worst case variations, verification was considered complete. If problems resulted with variations, the case was repeated with tolerances. If the system could not handle tolerances, a design change was required and the process repeated. A case that passed with tolerances but failed with variations resulted in a review with the aero group to discuss the validity of the specific variation case. The problem was then presented to the CCB who made the decision to either accept the risk associated with the case or to require a design change.

Formal verification was done on the FSL in August and September of 1980. The GN&C performance was greatly improved compared to the previous verification runs. A week long post simulation review by personnel from Rockwell, Honeywell, and JSC was conducted to thoroughly analyze the results of each run. A total of 16 anomalies were identified, but most of these were relatively minor and required no substantive action. The most significant problems were associated with the low C_{n_β} dynamic cases in the presence of design case winds around Mach 5. The program managers eventually accepted these cases after it was shown that the design winds for the STS-1 flight date of April resulted in less severe problems than the worst case winds used for the FSL verification. The flight rule requiring manual bank maneuvers in this Mach region following RCS jet failures also tended to alleviate the problem. Based on the results of the verification process the GN&C community had a high degree of confidence as the Orbiter entered the flight test program.

FLIGHT TESTING CHALLENGE

Stability and control testing of the Space Shuttle is driven by conflicting program desires, while limited by unique problems. Space Shuttle flights are very costly when compared with test flights of other aircraft. There is an intense desire within the program to bring the Shuttle to an operational mode, where payloads can begin to make the Shuttle cost effective. On the other hand it is important to assure the safety of entry flight and to identify the real limitations of the Shuttle through flight testing. This conflict in goals has resulted in the need for a minimum amount of highly productive testing.

Conventional flight test techniques and computer programs have formed the basis for the Shuttle flight test program. Modifications to these techniques have been necessary, however, due to the inherent constraints in Shuttle testing. Measures have been taken to ensure the quality of maneuvers and the data from them, so that the number of repeat maneuvers can be minimized.

The flight test plan developed for the Shuttle contains very few test points when compared to test programs of military aircraft. Enough maneuvers are scheduled only to verify the safety of the Shuttle entry; not enough to build a flight test data base. Where significant differences exist between the flight data and the wind tunnel data base, further test points are scheduled.

The stability and control derivatives are obtained from the onboard sensor data through the MMLE3 parameter identification program.[9] This program was developed at Dryden Flight Research Facility and is a state-of-the-art method of extracting derivatives from flight data. MMLE3 is the latest version of a program which has been used in many test programs for all types of aircraft.

Derivative deltas calculated between flight and values from the Shuttle Aerodynamic Design Data Book[10] are provided to Shuttle simulators to demonstrate the safety of further testing on upcoming flights and to assure the safety of flying cg's associated with planned payloads.

TEST REQUIREMENTS

Aerodynamic test requirements have arisen from two sources. The original source is the preflight wind tunnel data and the associated aerodynamic variations. The other source of requirements is the flight data from the initial flights, during which anomalies occurred. The types of problems identified involve either potentially excessive RCS fuel usage for longitudinal and lateral trim, or potential loss of control.

PREFLIGHT TEST REQUIREMENTS

Preflight wind tunnel data for the Orbiter is very extensive and coupled with the FCS verification process provided sufficient confidence to fly the initial missions under benign conditions and within a limited range of x cg[11]. However, at the cg extremes, analysis indicated

combinations of uncertainties in pitching moment and the stability and control derivatives resulted in potential control problems. These potential problems resulted in the establishement of the entry flight placards on angle of attack, dynamic pressure and x cg mentioned previously. Figure 12 shows the preflight areas of concern identified on a typical Mach-alpha profile.

From entry interface to a dynamic pressure of 20 lbs per sq ft, uncertainties in basic pitching moment and in pitch jet, bodyflap, and elevon effectiveness indicated a possible problem in longitudinal trim at the cg extremes. Such a trim problem would result in excessive use of RCS fuel by the pitch jets.

From Mach 7 to 3, uncertainty in the LCDP was the primary concern. Since the LCDP changes signs in this Mach region, the FCS gains were designed to provide a transition from a mode requiring a negative LCDP to a conventional aircraft control mode requiring a positive LCDP. Since the exact location of the sign change in the LCDP is unknown there is a requirement for identifying the aerodynamic coefficients in the LCDP and determining the effects of the elevon and cg position on these coefficients.

In the region from Mach 3 to 1, C_{n_β} dynamic was a concern, particularly for trajectories resulting in large dynamic pressures. C_{n_β} dynamic was also a concern in the Mach 5-8 region for high wind cases that produced an error in the navigation derived angle of attack. After the rudder becomes active at Mach 3.5, the combined lateral trim characteristics of the aileron and rudder were of particular interest.

Flight testing is planned between Mach numbers of .9 and .75 due to reduced rudder effectiveness at minimum speedbrake settings. The rudder is aft of the maximum thickness point on the vertical tail, and effects of the flow past the rudder panels become less certain with a closed speedbrake.

FLIGHT TEST REQUIREMENTS FROM FLIGHT DATA

Anomalies in the actual flight data have extended the test requirements as originally conceived. These anomalies have in some cases accentuated the need for certain data already in the flight test plan. Others have pointed to a need for more concentrated investigation of certain flight regimes. A summary of flight anomalies are shown in figure 12, items 1 through 7.

During the initial bank maneuver on flight 1, at a dynamic pressure of 14 lbs per sq ft, a large oscillation occurred in sideslip. Studies have indicated that the primary cause was a missed prediction in roll due to yaw jet firing.[12]

Another flight anomaly is a longitudinal trim difference from what was predicted. This occurs both in the hypersonic regime with a pitch up difference and in the transonic regime, where the difference is a pitch down moment.[12] Because the pitching moment anomaly causes more up (-) elevon trim transonically, the aileron effectiveness data required in this regime has become even more important. The hypersonic anomaly has caused an increased need for longitudinal stability and control data to ascertain the contributions of $C_{m_{\delta_e}}$, $C_{m_{\delta_{BF}}}$, C_{m_α}, and C_{m_o} to this problem. Figure 13 indicates the range of elevon settings required for trim based on attributing the pitching moment difference to C_{m_o} alone.

Causing additional interest in the Mach 2 to 1 regime is an anomaly which has been observed on the first five flights. The anomaly is in the form of an undamped low amplitude roll oscillation, which has a frequency of approximately 1/4 hertz. This problem has not resulted in additional test requirements, since intensive testing is already planned for this regime.[12]

Additional stability and control testing in the hypersonic regime has resulted from STS-1 data. These data indicated that lateral stability was different than expected. Specifically C_{n_β} was more (+) than expected.[11, 13, 14] In addition, aileron trim was observed to have an offset between Mach 18 and 7. This offset has been observed to change signs, indicating possible flow asymmetries.

Another important anomaly has occurred hypersonically. Above Mach 10, where the elevon schedule has been varied between -1 and +5 on flights 1-4, the flight data indicate that the aileron is more effective than predicted at positive elevon deflections. The data also indicate the effectiveness to be close to nominal at 0° elevon setting. While this is beneficial for positive deflections, the trend indicates that the aileron may be less effective at negative deflections. This accentuates the need for data which will clarify the dependence of aileron on elevon deflection.

These anomalies have not restricted the flight placards further. However, they have emphasized the need for data in certain flight regimes. They have also caused the planning of further testing in specific areas.

SHUTTLE FLIGHT TEST PROGRAM

The Shuttle test program is the product of significant planning and integration with other program requirements. The flight test requirements from wind tunnel uncertainties and flight anomalies dictated the flight conditions at which maneuvers would be done. Sufficient maneuvers were planned at nominal conditions to indicate repeatability of results. Additional maneuvers were planned over the ranges of elevon and angle of attack that will be seen operationally to check coefficient sensitivities to these parameters. The test plan has been modified to provide additional information in areas where anomalies have occurred. This is necessary to establish an understanding of the anomaly and to develop a data base for simulators in areas where the wind tunnel data is deficient.

The tests planned for each flight are limited by the nature of the Shuttle entry and by other program requirements. Only one maneuver at each flight condition is possible on a given flight, since the Shuttle glides from 400,000 ft in altitude at Mach 25 to touchdown in the span of 30 minutes. The crew has monitoring functions and other tasks during entry that also limit the number of maneuvers that can be performed. This has resulted in a limit of 8 to 10 maneuvers per flight and in a ground rule which requires that maneuvers be spaced to the satisfaction of the flight crew. Another limitation is the amount of RCS fuel available for doing maneuvers. Entry tests must compete in priority with other mission objectives for RCS fuel. This includes on-orbit activities such as rendezvous tests and payload deployment. Other entry tests such as structural flutter tests and aerothermal pushover pullup test maneuvers (POPU) have taken priority over stability and control maneuvers, because instrumentation for these tests were available on flights 1-5 only. When a conflict occurs, guidance maneuvers and guidance phase changes take priority over test maneuvers.

The flight testing has been planned to meet program objectives. The first and most important is to open the cg placards as quickly as possible in order to verify the safety of flying planned payloads. In addition, data resulting from tests are scheduled to support planned flight control system changes which will improve control where in-flight aerodynamic anomalies have occurred.

SENSOR DATA FOR TESTING

Sensor data used in stability and control analysis is obtained from two basic sources. The primary source of data is the aerodynamic coefficient identification package (ACIP), which is located in the wing carry-through structure. It was designed specifically for aerodynamic data extraction. The other source is the onboard data system, which provides real-time data for the guidance and flight control systems. The ACIP is a high quality data package recording data at 173 samples per second utilizing a 14 bit system. The onboard data system records data at 5 and 25 samples per second using an 8 bit system. A more detailed explanation of the sensor data is given in reference 12.

STABILITY AND CONTROL MANEVUERS

Maneuvers for stability and control data have been carefully developed to provide the maximum amount of information possible. It is important in this testing to excite the motion defined by the derivatives in question, so as to identify them from the flight data. Because of the limited testing of the Shuttle and the characteristics of the flight control system, precise maneuver design and execution are very important. Poorly performed maneuvers can be costly to the program in the form of further required testing.

The flight control system of the Shuttle heavily modifies inputs through the stick and is designed to damp oscillations and transients. This design causes difficulty in pulsing a control effector and allowing motion to damp as is done with most aircraft. In pulsing the Shuttle, the

control system modifies the stick input with filters, responds to rate and acceleration feedback values, and damps the response with further surface motion. In general, when the vehicle is pulsed, all control effectors available are put into action to quickly damp the vehicle motion. This can cause difficulty in separating out the effectiveness of the various control effectors. It makes it difficult to accurately identify damping derivatives.

To overcome this important problem and to provide exact designed inputs, programmed test inputs (PTI) were developed. This type of maneuver is input directly to the flight control system through onboard software. The amplitude and timing is governed by programmed variables to generate a specific input at a predesignated flight condition.

The crew involvement in the maneuvers is almost entirely a monitoring function. The maneuver sequencing is initiated by the crew before the first maneuver, and the software automatically executes the predefined maneuvers within specified windows. These windows are defined by dynamic pressure or Mach number. The software avoids executing maneuvers close to bank reversals and other guidance phase changes. The crew monitors trajectory and trim parameters and important entry flight systems to assure safe maneuver conditions. The crew can quickly stop the maneuver sequence by moving the stick or selecting the control stick steering (CSS) mode. They have full visibility into the testing status through items on their displays.

The inputs are made through the flight control system, and go to an integrator at the point where the surface deflection is commanded. The input is added to the current command. The command, a surface rate, is then processed through a maximum rate limit function. Signals can be sent to the elevon, aileron, rudder, and pitch, yaw, and roll jets. Because of the direct input capability, maneuvers are input in the automatic guidance mode. The input is in the form of a doublet. The doublet commands surface rate in one direction and then the opposite direction resulting in a pulse from the control effector. These doublets can be strung together in combinations to provide various inputs from each of the control effectors. There is a capability to define 25 PTI windows, and there are 45 doublets that can be grouped in the windows as desired.

The input from the automatic PTI is not completely free of flight control system interference, but the design does allow for enhanced maneuvers. An example of a maneuver for Mach 5.8 is illustrated in figure 14. The inputs are defined by amplitudes, times, and the effector to be pulsed. The flight control system continues to respond to the motion feedback, but direct input can be made to the control effector. In this example it is possible to make the aileron input while there are no yaw jet firings.

Direct input to the surfaces in a "bare airframe" sense is not possible in the program at present. With the basic lack of stability of the Shuttle, it would not be safe to maneuver the vehicle without an active control system. The automatic PTI design offers the most feasible alternative that is available.

Maneuvers, once designed for the optimum motion for data extraction, are assessed for flight control and guidance safety. Although potential problem areas are approached carefully, care must be taken in maneuvering not to excite an undamped or diverging oscillation. It is also important not to perturb the trajectory so as to disturb the ranging capability during the Shuttle's gliding descent.

Maneuvers are studied extensively for flight control safety. Both off-line and real-time simulators are used to study maneuvers with worst case aerodynamic uncertainty combinations. Maneuver amplitudes are increased to assess safety margins. Loss of RCS jets is also simulated. Flight test aerodynamic results are fed through this same process to verify maneuver safety margins with data that is the best possible representation of actual Shuttle characteristics.

Maneuver guidance impacts and entry timeline conflicts are assessed in a similar manner. Simulations are run to determine conflicts between stability and control maneuvers and guidance maneuvers and phase changes. Shuttle pilots assess maneuver conflicts with other important pilot functions. If conflicts arise from these studies, maneuver windows are adjusted or are deleted. In general the short, low amplitude, PTI maneuvers have a negligible impact on guidance capability, but they are studied nonetheless. When combined with other maneuver sequences, guidance impacts can occur. RCS jet fuel budgets for maneuvers are developed during these simulations to provide the pilots with fuel "red lines" that must not be violated, in order to continue initiating maneuvers. Usage of RCS fuel during maneuvers is significant. Loss of vehicle control is possible if the RCS fuel is depleted.

SHUTTLE MANEUVER TEST PLAN

The maneuvers planned or already flown on each flight are listed in figure 15. The left hand column lists the flight conditions at which the tests are planned. The other columns are labeled by flight number. Flight one had no planned maneuvers other than bank reversals required for ranging. The first entry was designed to be as benign as possible. Flight 2 had 25 maneuvers, including pitch and roll maneuvers for stability and control data, a pushover pullup maneuver, and bodyflap pulses. Subsequent to STS-2, decisions were made to reduce the number of maneuvers per flight so as to decrease crew workload during entry. As a result fewer maneuvers are shown on flights 3-17. The test program has therefore evolved from an initial 10 flights into a 17 flight program in order to obtain sufficient data. It can be observed in figure 15 that the most concentrated testing is from Mach 6 to .9. This is because it is the most critical regime with respect to potential problems in stability and control.

The test plan for stability and control data is designed to provide sufficient information to remove forward and aft cg constraints. The forward center of gravity travel is limited primarily by aileron characteristics at negative elevon settings. To verify the aileron characteristics before flying a forward cg, the vehicle trim of a forward cg is simulated by appropriate scheduling of the elevon. Elevon schedules for flights 1-17 are shown in figure 16 with the locations of the maneuvers from figure 15 superimposed. The schedules cover the range of expected values for the full range of cgs. These elevon schedules are attained during flight by onboard software programming of the elevon settings. The bodyflap is used to trim the vehicle at the given setting. The schedule shown for flight 2 is the most benign schedule and provides the most positive aileron control between Mach 6 to 1. As the flights progress and more data is obtained, the elevons are to be scheduled gradually more up (-) until the most forward cg is simulated on flights 14-17. Hypersonically, the elevon is being trimmed beyond what is required during normal entry for a forward cg (figure 13). This is due to the data already obtained which indicated anomalous aileron effectiveness as a function of elevon position. The settings shown on flights 14 to 17 should shed additional light on this problem and the results can be used to assess certain abort profiles which use more negative elevon positions for trim.

Angle of attack will be varied on a limited number of flights. Figure 17 illustrates the nominal angle of attack profiles to be flown on particular flights. Maneuvers will be executed along these profiles to verify predicted angle of attack trends in stability and control parameters. Flights 6, 8, and 12 will be flown with an elevon schedule that has been flown previously so as to vary only one parameter at a time. Flights 14, 16, and 17 will be flown with an elevon setting that represents the trim requirements for a forward cg. The symbols represent where maneuvers will occur along the profile on flights where the profile is off-nominal. Stability derivatives C_{ℓ_β} and $C_{n_{\delta_A}}$ are of particular interest as a function of angle of attack. In addition, an understanding of the possibility of aileron effectiveness being a function of the combined effects of angle of attack and elevon is to be studied. This will require deviations in both angle of attack and elevon position for various maneuver test points.

Additional factors in the planning will contribute to the necessary understanding of the stability and control characteristics of the Shuttle. Figure 18 shows speedbrake schedules for the nominal entry, and planned schedules for flights 5 through 17. With these different schedules, rudder sensitivities can be obtained. With the automatic maneuvers beginning on flight 5, a rudder pulse can be input at any point regardless of whether or not the rudder is active in the flight control system. The rudder normally becomes active at Mach 3.5. With this capability, the rudder effectiveness will be tested 1/2 Mach number higher per flight, beginning on flight 5 at Mach 4. To obtain further data on possible aerodynamic asymmetric characteristics of the Shuttle, Ycg offsets are planned through payload placement. Ycg values of .5 to .9 inches have been flown on flights 4 and 5. A Ycg value of 1.5 inches is planned for flights 7 and 11, with the sign of the offset reversing between the two flights. Although POPU maneuvers were planned primarily to obtain aerodynamic performance and aerothermal data, these maneuvers were also a valuable source of additional longitudinal stability and control data. Bodyflap pulses were flown only on STS-2. During these maneuvers the crew manually changed bodyflap trim down (+) to move the elevons up (-). A PTI was then performed. This was to provide early indications of aileron effectiveness with more (-) elevon settings.

FLIGHT DATA ASSESSMENTS

An important product of the flight test program is the confidence that is gained from flight test results, in assessing the safety of upcoming flights. Vehicle cgs associated with specific payloads must be shown to be safe. In addition, further testing in the flight test program depends on values of derivatives obtained from previous tests. For instance, it is important to

understand as much as possible about stability and control characteristics for down elevon positions, before it is safe to fly with elevons at more negative settings. To accomplish this, fairings are developed for the flight test results and are provided to the Shuttle flight control system community. These fairings or "assessment" values are incorporated into simulators which are used to verify the safety of upcoming flights. Exact maneuvers and trajectory profiles are simulated with correct cgs. In addition, stability analyses are performed using the flight derived aerodynamic data to update cg placards for the vehicle.

STS-1 THRU -4 FLIGHT ASSESSMENT VALUES

Flight test results in the form of stability and control derivatives have been output for use in simulators after flights 1, 2, and 4. Some of the most significant of these derivatives are shown in figures 19 to 24. These figures show derivative values for various types of maneuvers from flights 1 to 4. It is important to note that the highest quality maneuvers are the PTI's, which have darkened symbols. In the plots, pre-flight 1 Aerodynamic Design Data Book values (solid line) and the associated uncertainties are drawn. The abrupt changes in the data book values at some locations are due to the data being plotted for the specific flight condition and configuration where the maneuver was executed and do not represent abrupt nonlinearities in the data base. The uncertainty brackets on the derivatives are Cramer Rao bounds, which provide information on the relative accuracy of data extraction between data points.[9] Also drawn on the plots are the STS-4 assessment values. These assessment values are the fairings that have been published from flights 1 to 4 for these derivatives.

For C_{ℓ_β} in figure 19, the flight test values are shown to be significantly more positive than what was predicted above Mach 10. However, this is of no particular concern to the safety of the Shuttle through this Mach regime. Below Mach 6 the C_{ℓ_β} fairing is shown to be approximately halfway between nominal and the lower value of the uncertainties. This value of C_{ℓ_β}, by itself is not of concern for for Shuttle safety of flight, but if $C_{n_{\delta_a}}$ should become positive for more up elevon settings, the more negative C_{ℓ_β} will have an adverse effect on the LCDP.

Aileron effectiveness above Mach 10 is shown for PTI's in figures 20 and 21. These values are plotted as a function of elevon position. Because of the spread of elevon between flights 1 through 4 in this Mach regime, a difference in the effect of elevon on aileron effectivness has been discovered. Both $C_{\ell_{\delta_a}}$ and $C_{n_{\delta_a}}$ indicate increased effectiveness with down elevon deflections. The assessment values for elevon settings above 0° were set to nominal, because of the lack of data. If the trend for positive elevon deflections extend to negative elevon deflections, the aileron may be less effective than predicted. Although this difference between predicted and actual aileron effectiveness has little effect on safety hypersonically, the impact to cg placards could be important if the trend continues at lower Mach numbers. Testing on later flights, where the elevon will be scheduled with more negative settings, will provide the necessary data to determine Shuttle cg impacts. This example points out the importance of obtaining derivative sensitivities to elevon and angle of attack profiles. Between Mach 2 and 1 (figure 22) the flight values of roll due to aileron are shown to be less effective than predicted. In this region the elevon has been above 0° deflection due to overshooting the elevon schedule. Because there has been no spread in the elevon deflections on flights 1 to 4, it is not yet possible to attribute this anomaly to effectivness due to elevon position. Later flights will provide the spread necessary to determine this function.

The most significant updates in stability and control aerodynamics are the assessment values and new uncertainties for yaw jet effectiveness. Figures 23 and 24 show very consistent flight test results for RCS yaw jet effectiveness. After STS-4 sufficient data was available to update nominal values and reduce RCS jet effectiveness uncertainties from early entry through Mach 1, where the yaw jets are turned off. The jets were shown to be more effective than predicted. These results have had a significant effect on cg expansion.

CENTER OF GRAVITY EXPANSION

The primary goal of the entire data extraction effort is to open cg placards for the Shuttle, so that the full payload carrying capability can be utilized. Through the planned maneuvers, and

elevon and angle of attack schedules, sufficient data is to be obtained to verify the Shuttle operational safety during entry. The operational limits for cg have been specified to be from 65 to 67.5 percent of the reference body length. This represents a cg travel of 32.32 inches. It is the goal of the test program to relax cg placards to these operational limits. Figure 25 shows the expansion of the Xcg that has taken place as a result of flight test data from STS-1 thru -4. Opening of the aft cg boundary as well as initial opening of the forward boundary is primarily a result of the confidence that has been gained in the knowledge of the basic pitching moment of the vehicle. Pitch jet trim requirements were also determined. The most restrictive boundary is the forward cg limit, because of the critical potential problem areas between Mach 6 and 1. The most significant relaxation of this forward boundary occurred because of the yaw jet flight test results. The more effective jets along with the reduced uncertainties resulted in the change shown in the placard between STS-5 and -6. This has proved the safety of flying payloads planned for STS-7 and -9. Also shown in figure 25 are aft cg flight test limits, which must be honored in order to fly the elevon schedules planned for these flights. Relaxation of the boundary to the full forward limit of 65 percent body length will occur as a result of decreases in other stability and control derivative uncertainties by the end of the flight test program. Optimistically these data will prove that predicted potential control problems do not exist.

CONCLUSIONS

The successful flight of STS-1 in April 1981 proved that the challenge of the FCS design and verification has been met. The flight test data so far is indicating that the aerodynamic variations were not overly conservative, but are representative of the actual differences experienced in most of the aerodynamic coefficients at some point during reentry. The successful extraction of flight test data from the first four flights is proving that the challenge of developing an operational vehicle with a minimum flight test program is being successfully met.

The placards on the orbiter during entry are to be reduced after 17 flights based on high quality data from carefully designed manevuers. The approach is optimistic and ambitious but every effort is being made to insure its success through careful maneuver design, quality data and safety analysis. The experience gained and techniques employed in the Shuttle program are applicable to future flight test planning in programs where testing must be limited due to time constraints or expense.

REFERENCES

1. Young, James and Underwood, Jimmy: The Development of Aerodynamic Uncertainties for the Space Shuttle Orbiter, AIAA Paper 82-063.

2. Weil, Joseph and Powers, B. B.: Correlation of Predicted and Flight Derived Stability Derivatives with Particular Application to Tailless Delta Wing Configurations, NASA TM-81361.

3. Kanipe, David B.: Plume/Flowfield Jet Interaction Effects on the Space Shuttle Orbiter During Entry: AIAA Paper 82-1319, August 1982.

4. Gamble, J. D. and Young, J. C.: The Development and Application of Aerodynamic Uncertainties in the Design of the Entry Trajectory and Flight Control System of the Space Shuttle Orbiter, AIAA Paper 82-1335, August 1982.

5. Weissman, R.: "Status of Design Criteria for Predicting Departure Characteristics and Spin Susceptibility," J. Aircraft, Vol. 12, No. 12, Dec. 1975. pg. 989-993.

6. Kaylor, Jack T; Rowell, Lawrence F.; and Powell, Richard W.: A Real-Time Digital Computer Program for the Simulation of Automatic Spacecraft Re-entries, NASA TMX-3496, July 1977.

7. Rowell, Lawrence F.; Powell, Richard W.; and Stone, Howard W. Jr.: Development of the Re-entry Flight Dynamics Simulator for Evaluation of Space Shuttle Orbiter Entry Systems, NASA Technical Paper 1700, October 1980.

8. Bayle, G. P.: Entry Flight Control Off-Nominal Design Considerations, AIAA paper 82-1602CP, August 1982.

9. Main, Richard E. and Iliff, Kenneth W.: User's Manual for MMLE3, a General Fortran Program for Maximum Likelihood Parameter Estimation, NASA TP-1563, 1980.

10. Aerodynamic Design Data Book, Vol. 1: Orbiter Vehicle, STS-1, Final Report, NASA CR-160903, November 1980.

11. Underwood, Jimmy M.; and Cooke, Douglas R.: A Preliminary Correlation of the Orbiter Stability and Control Aerodynamics from the First Two Space Shuttle Flights (STS-1 and -2) with Preflight Predictions. AIAA Paper 82-0564, March 1982.

12. Cooke, Douglas R.: Space Shuttle Stability and Control Test Plan. AIAA Paper 82-1315, August 1982.

13. Iliff, Kenneth W.; Maine, Richard E.; and Cooke, Douglas R.: Selected Stability and Control Derivatives from the First Space Shuttle Entry. AIAA Paper 81-2451, November 1981.

14. "Evaluation of the Space Shuttle Orbiter First Flight Descent Phase," AFFTC-TR-81-21, Office of Advanced Manned Vehicles, Air Force Flight Test Center, July 1981.

TABLE 1 ORBITER CORRELATION APPLICABILITY (REFERENCE 2)

AIRCRAFT*	GEOMETRIC FACTORS					REMARKS
	Δ WING PLANFORM	WING FLAP LONG. CONTROL	WING ELEVON LATERAL CONTROL	SINGLE VERTICAL TAIL	LARGE FUSLAGE	
XB-70	√	√	√			GOOD PRED BASE, M RANGE, CANARD, LIMITED α RANGE
YF-12	√	√	√			GOOD M RANGE, LIMITED α RANGE
X-15				√	√	WIDE α, M RANGE
TACT Λ = 58°	√			√	√	ONLY LIMITED DATA CURRENTLY AVAILABLE
HP115	√	√	√	√		LOW SPEED DATA ONLY
B-58	√	√	√	√		GOOD PREDICTIVE BASE, M RANGE
YF-16 F-8SCW				√		SOURCE OF RUDDER CONTROL DATA

*SEE REFERENCE 2 FOR AIRCRAFT IDENTIFICATION

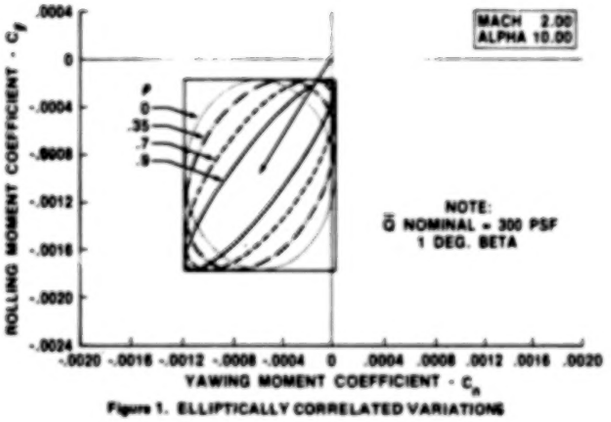


Figure 1. ELLIPTICALLY CORRELATED VARIATIONS

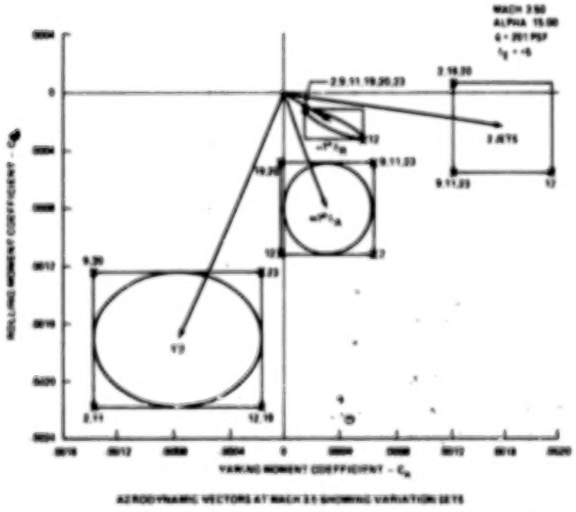


Figure 2. AERODYNAMIC VECTORS AT MACH 3.5 SHOWING VARIATION SETS

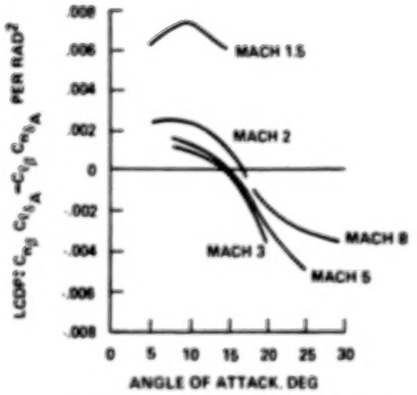


Figure 3. EFFECT OF ANGLE OF ATTACK ON LCDP FOR AERO VARIATION SET 19

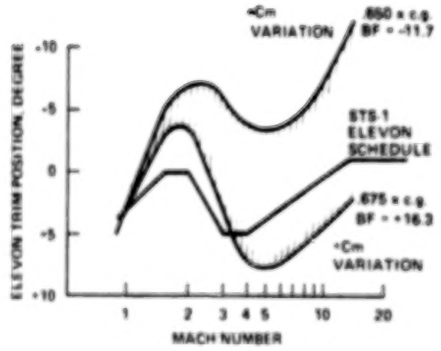


Figure 4. ELEVON TRIM ENVELOPE FOR DESIGN C.G. LIMITS WITH PITCHING MOMENT VARIATIONS

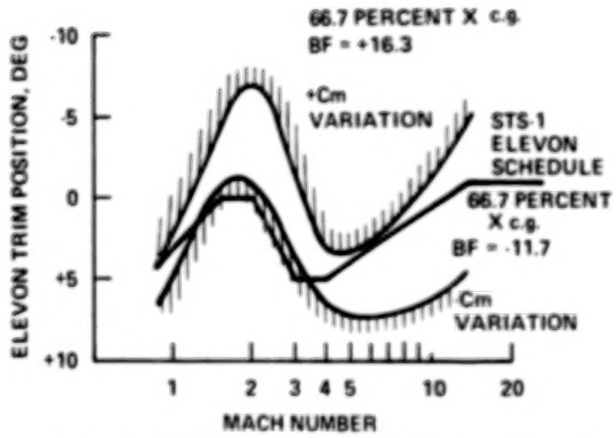


Figure 5. ELEVON TRIM ENVELOPE FOR 66.7 PERCENT L_B X c.g. WITH PITCHING MOMENT VARIATIONS.

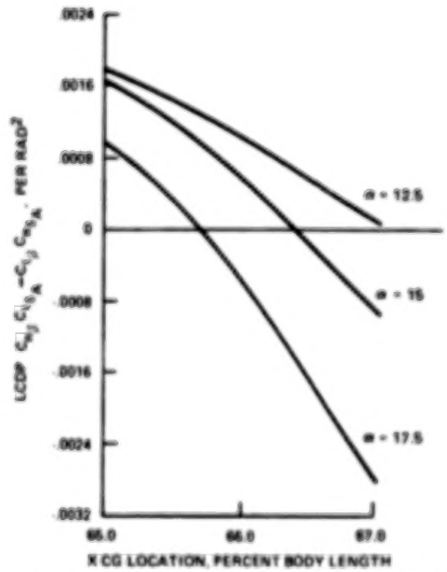


Figure 6. EFFECT OF CG, ANGLE OF ATTACK ON LCDP AT MACH 3.5 WITH AERO VARIATIONS SET 19

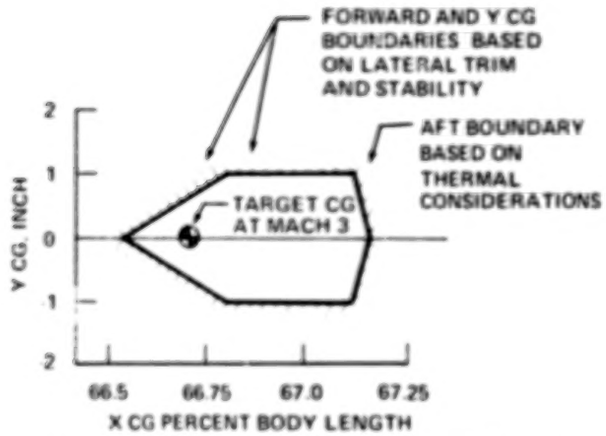


Figure 7. RECOMMENDED CG ENVELOPE CONTAINED IN FLIGHT RULES DOCUMENT FOR STS-1

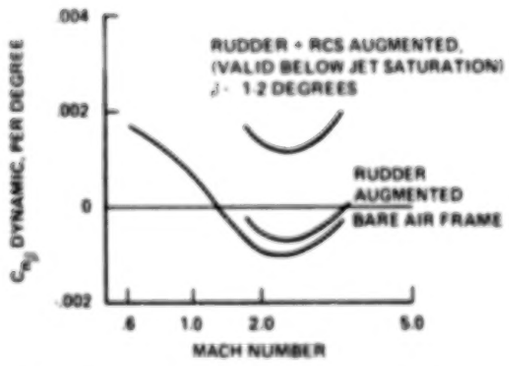


Figure 8. C_{n_β} DYNAMIC FOR WORST CASE VARIATION SET
1 g FLIGHT AT 7.5 DEGREES ALPHA

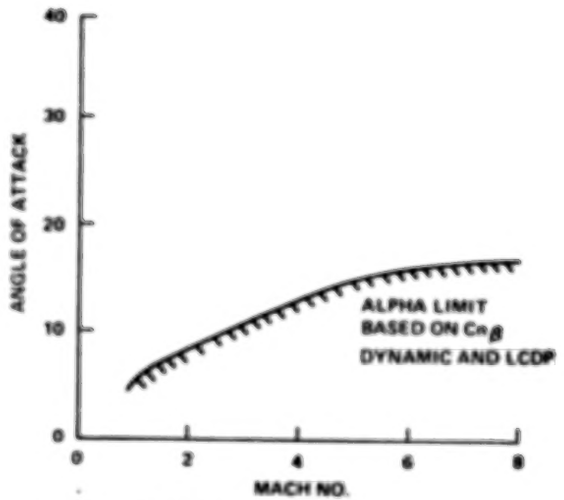


Figure 9. LOWER ANGLE OF ATTACK BOUNDARY CONTAINED IN FLIGHT RULES DOCUMENT FOR EARLY ORBITER FLIGHTS

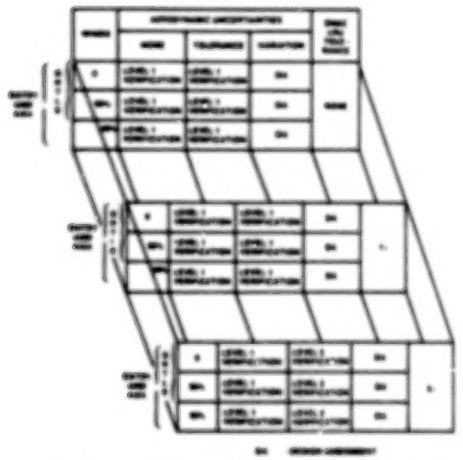


Figure 10. ENTRY VERIFICATION TEST MATRIX



Figure 11. GN&C/FCS FORMAL VERIFICATION PROCESS

PREFLIGHT TEST REQUIREMENTS AND FLIGHT ANOMALIES

PRE-FLIGHT CONCERNS AT C.G. EXTREMES

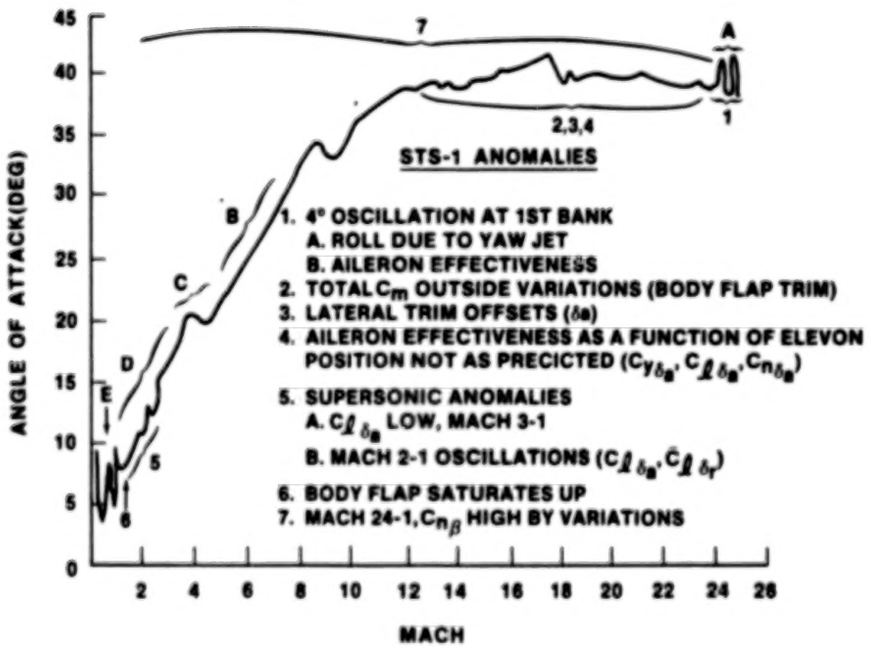
A. VISCOUS TRIM AND LONGITUDINAL CONTROL (RCS FUEL,TRIM AUTHORITY)

B. LAT/DIR TRIM WITH ADVERSE $c_{n_{\delta_a}}$ (EXCESSIVE RCS FUEL,TRIM AUTHORITY)

C. LAT/DIR TRIM, CONTROL AUTHORITY WITH UNCERTAIN AILERON, RUDDER, JETS

D. LAT/DIR CONTROL AUTHORITY WITH UNCERTAIN AILERON, RUDDER JETS

E. LOSS OF RUDDER EFFECTIVENESS AND LAT STABILITY AT LOW SPEED BRAKE SETTINGS



STS-1 ANOMALIES

1. 4° OSCILLATION AT 1ST BANK
   A. ROLL DUE TO YAW JET
   B. AILERON EFFECTIVENESS
2. TOTAL C_m OUTSIDE VARIATIONS (BODY FLAP TRIM)
3. LATERAL TRIM OFFSETS (δa)
4. AILERON EFFECTIVENESS AS A FUNCTION OF ELEVON POSITION NOT AS PRECICTED ($C_{y_{\delta_a}}$, $C_{\ell_{\delta_a}}$, $C_{n_{\delta_a}}$)
5. SUPERSONIC ANOMALIES
   A. $C_{\ell_{\delta_a}}$ LOW, MACH 3-1
   B. MACH 2-1 OSCILLATIONS ($C_{\ell_{\delta_a}}$, $C_{\ell_{\delta_r}}$)
6. BODY FLAP SATURATES UP
7. MACH 24-1, C_{n_β} HIGH BY VARIATIONS

Figure 12

ELEVON TRIM CAPABILITY

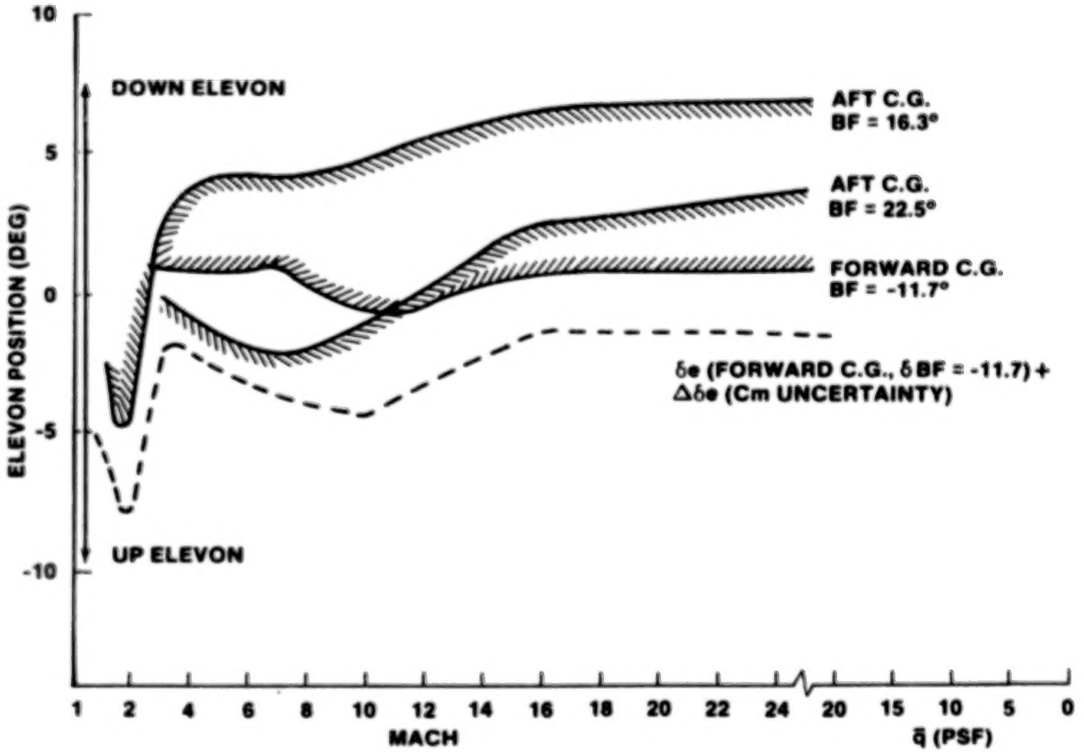


Figure 13

AUTOMATIC PTI CAPABILITY

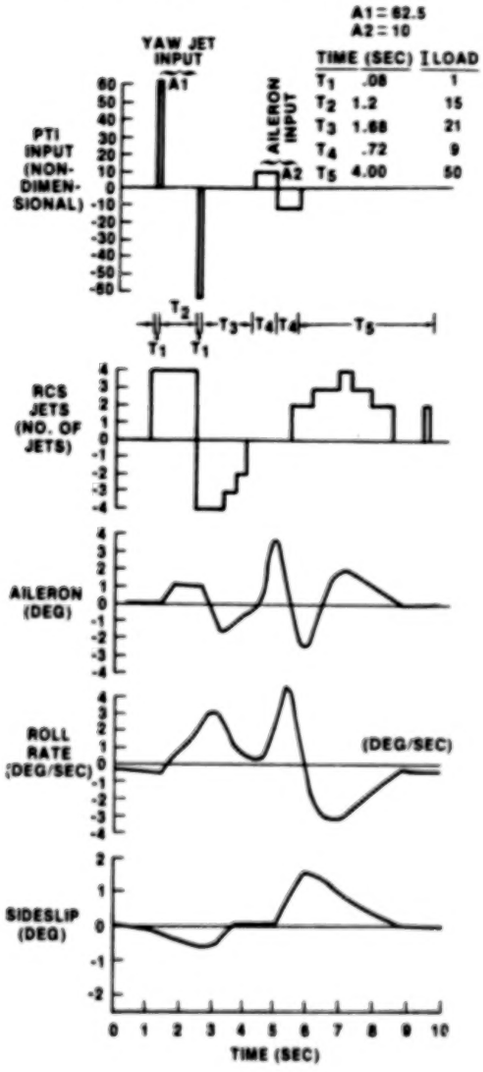


Figure 14

MANEUVER TEST PLAN

FLT COND \ FLT #	1	2	3	4	5	6	7	8	9	10	11	12	13	14	15	16	17
q = .3		P															
q = 3		P							P								L,P
q = 4		L			L		L										
q = 8		L				L				L,P	L,P					L,P	
q = 10		P															
q = 16		P			P			P		L,P		L,P	L,P		L,P		L,P
q = 18		R															
q = 22		R	L	L	L	L		L	L				L		L		L,P
M = 21.5		P,L,BF POPU	L,P	L,P	L,P		L,P	L,P		L,P	L,P	L,P	L,P	L,P			
M = 18		L,BF	L	L	POPU	L,P	L,P	L,P		L,P	L,P	L,P	L		L,P		L,P
M = 15				L					L,P					L,P			
M = 14		L,BF	L	POPU			L,P			L,P	L	L,P	L,P				L,P
M = 8.4		L	L	POPU		L,P		L,P	L,P	L,P	L	L	L	L	L,P	L	L
M = 5.8		L			L	L	L	L	L		L	L		L	L,P	L	
M = 4.0		L	L		L	L,P		L	L				L	L	L,P	L	
M = 3.2		L		L	L	L	L			L	L	L	L	L	L	L	L
M = 2.2		L	S	S			L,P	L,P	L	L	L	L	L				L
M = 1.6		L			L,P	L		L,P	L	L,P	L,P	L		L	L	L	L
M = 1.1		L				L	L		L	L	L		L	L	L	L	
M = .9		L					L,P		L			L		L		L	

P - PITCH MANEUVER
L - LATERAL DIRECTIONAL
BF - BODY FLAP PULSE
POPU - PUSHOVER - PULLUP

S - STRUCTURAL PTI
L - MANEUVER NOT EXECUTED

Figure 15

FLIGHT TEST ELEVON PROFILES

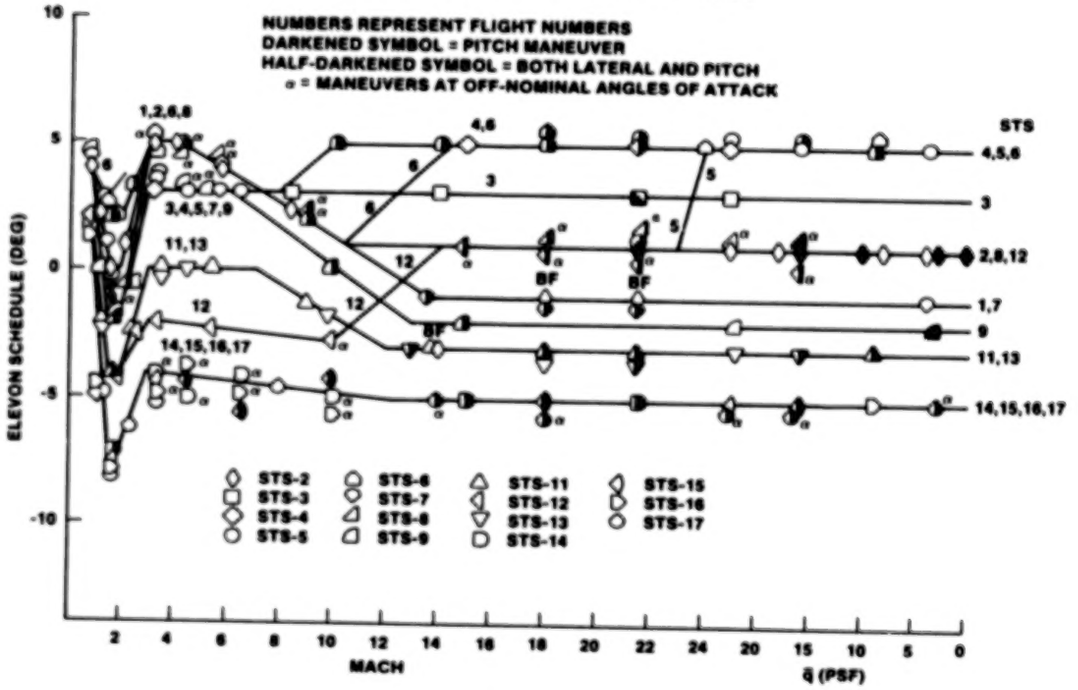


Figure 16

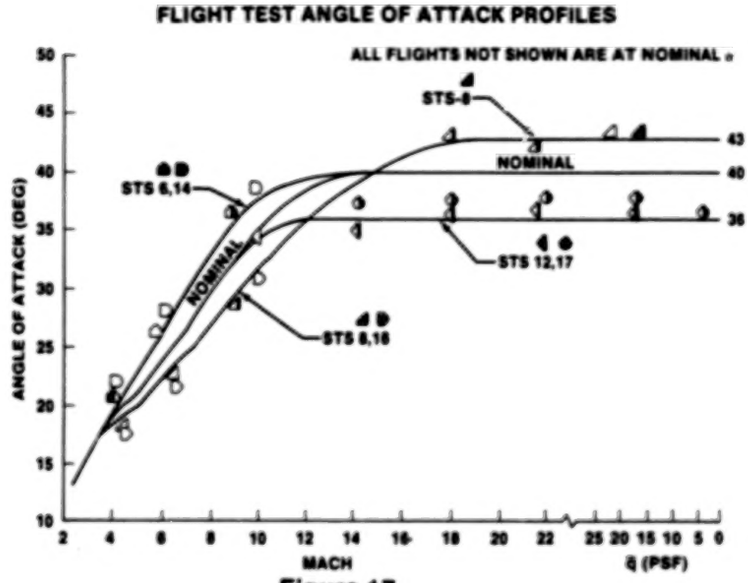


Figure 17

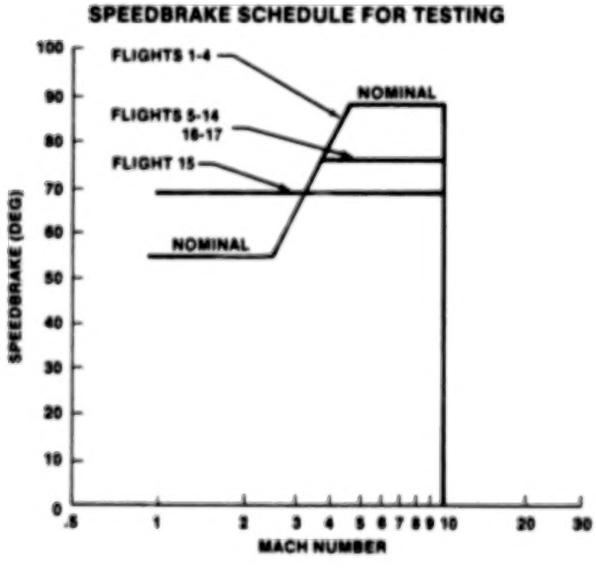


Figure 18

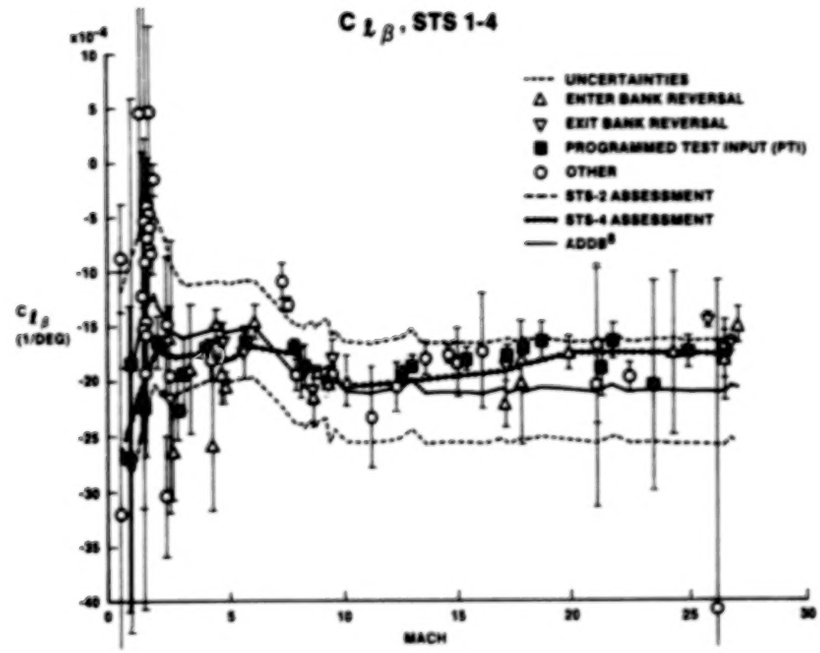


Figure 19

$C_{\ell_{\delta_e}}$ AS A FUNCTION OF ELEVON POSITION FOR M > 10, STS 1-4

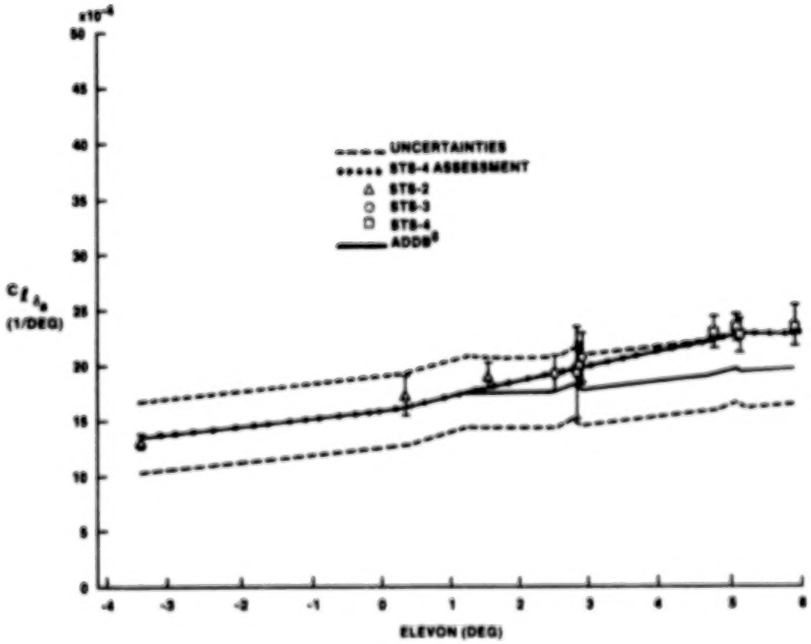


Figure 20

$C_{n_{\delta_e}}$ AS A FUNCTION OF ELEVON POSITION FOR M > 10, STS 1-4

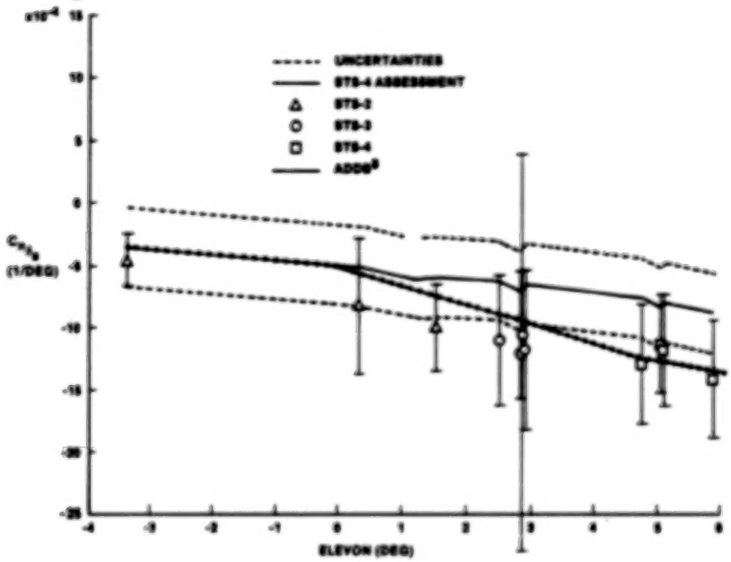


Figure 21

ROLLING MOMENT DUE TO AILERON, STS 1-4

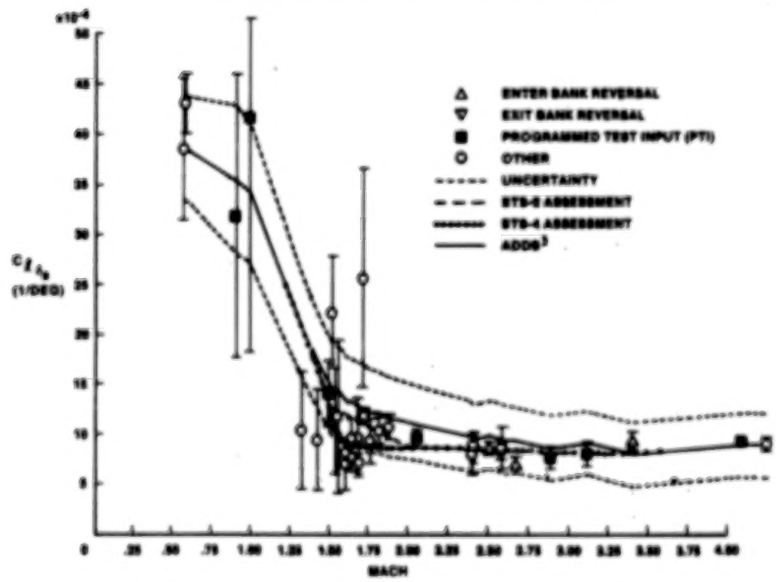


Figure 22

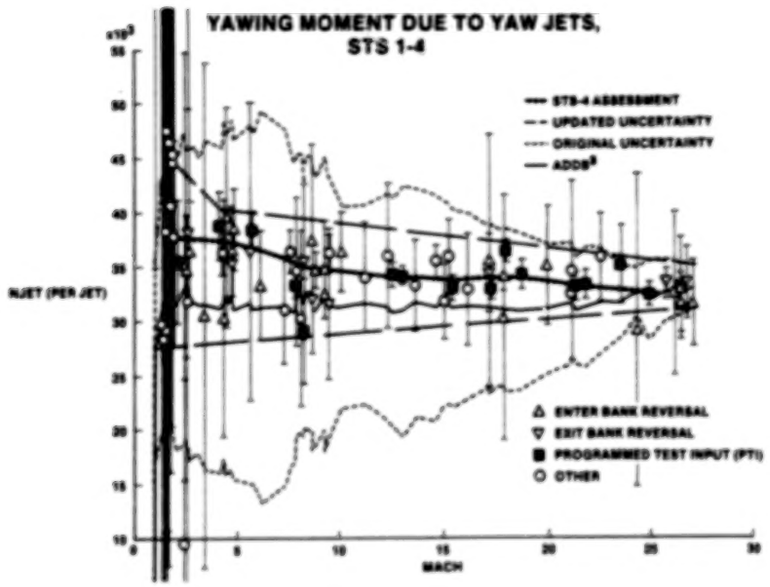


Figure 23

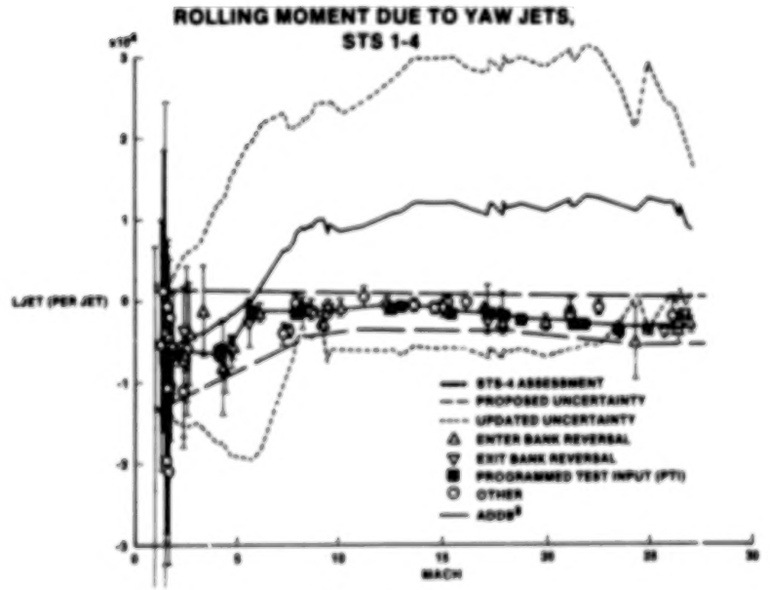


Figure 24

SHUTTLE CENTER OF GRAVITY PLACARDS (M = 3.5)

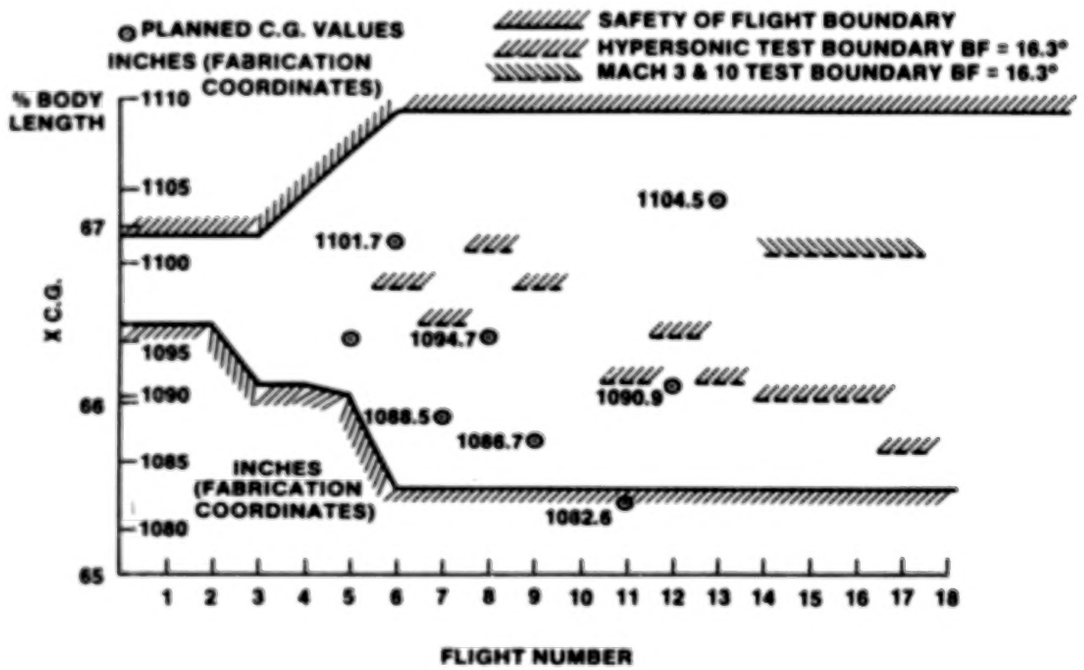


Figure 25

N85
16911

UNCLAS

N85-16911

D22

AERODYNAMIC CHALLENGES OF ALT

Ivy Hooks, David Homan, Paul Romere
NASA
Johnson Space Center

ABSTRACT

The Approach and Landing Test (ALT) of the Space Shuttle Orbiter presented a number of unique challenges in the area of aerodynamics. The purpose of the ALT program was both to confirm the use of the Boeing 747 as a transport vehicle for ferrying the Orbiter across the country and to demonstrate the flight characteristics of the Orbiter in its approach and landing phase. Concerns for structural fatigue and performance dictated a tailcone be attached to the Orbiter for ferry and for the initial landing tests. The Orbiter with a tailcone attached presented additional challenges to the normal aft sting concept of wind tunnel testing. The landing tests required that the Orbiter be separated from the 747 at approximately 20,000 feet using aerodynamic forces to fly the vehicles apart. This concept required a complex test program to determine the relative effects of the two vehicles on each other. Also of concern, and tested, was the vortex wake created by the 747 and the means for the Orbiter to avoid it following separation.

NOMENCLATURE

$\bar{c}$	Mean aerodynamic chord
cg	Center of gravity
C_D	Drag coefficient
C_L	Lift coefficient
FF	Free flight
h_w	Main landing gear wheel height above ground
IML	Interface mold line
LE	Leading edge
L/D	Lift-to-drag ratio
M	Mach number
MAC	Mean aerodynamic chord
$\bar{q}$	Dynamic pressure
X_o, Y_o, Z_o	Orbiter vehicle body coordinate system
α	Angle of attack, degrees
δ_{BF}	Body flap deflection, degrees
δ_{SB}	Speedbrake deflection, degrees

INTRODUCTION

When the Space Shuttle design was begun, in 1969, the concept included aircraft type jet engines on the Orbiter vehicle. The engines would have provided a more flexible landing operation and a means to ferry the vehicle from manufacturing or landing sites to the launch site. This design concept proved not to be feasible for a number of reasons. While the need to have engines for landing was overcome, the need to ferry the Orbiter across the country still existed. Further, most felt that the Orbiter approach and landing phase needed checkout prior to the first entry from orbit. Alternate solutions involved the use of strap-on engines to the wings and a plan to put a kit, containing both fuel and engines, in the payload bay. Neither was considered a viable concept.

At this point, NASA really had built a "boat in the basement". Not only could the approach and landing phase not be tested, but transporting the Orbiter from the manufacturing site at Palmdale, California to the Kennedy Space Center in Florida had no practical solution.

It was then suggested by John W. Kiker of the Johnson Space Center (JSC) in Houston, that the Orbiter be ferried by another vehicle in a mode similar to that used to launch the X-15 aircraft. Consideration was given to existing aircraft; ie., the Lockheed C5A and the Boeing 747, as well as to developing a new airplane for that explicit purpose. Configurations were considered with the Orbiter positioned atop and also below the carrier aircraft. Trade studies were performed which indicated that it was feasible to carry the Orbiter aboard an aircraft in a piggyback fashion. It was also believed possible to launch the Orbiter from such a position in order to do an Approach and Landing Test (ALT), and the Boeing 747 was selected as the carrier aircraft.

The solution also produced new problems. The blunt aft section of the Orbiter would produce considerable drag and create disturbances which could cause fatigue to the vertical tail of the carrier. Thus, for ferry purposes, it was concluded that an aft fairing would be required on the Orbiter. One of the first considerations was the design of the fairing, or tailcone.

Also of concern was the performance of the mated vehicle, both from a range stand point for ferry and from altitude and relative aerodynamics for separation. The primary emphasis was on the relative attitude of the two vehicles to obtain an optimum configuration for both ferry flight and separation. Restrictions included the Orbiter attach points, clearance of the tailcone, and loads on the carrier aircraft.

The need to perform an aerodynamic separation between two maneuverable vehicles required considerable aerodynamic testing and analysis. Again, other variables, originally unsuspected, arose. One example was the concern for the vortex wake produced by the carrier and the possibility of upsetting the Orbiter if it encountered the vortex wake following separation.

The Orbiter's subsonic aerodynamic characteristics required early testing and definition to allow for design of the complex flight control system. Further complicating the situation was the desire to also fly the Orbiter with a tailcone attached for the first landing. With the tailcone, the Orbiter lift-to-drag ratio was significantly improved, and it was felt that the other Orbiter systems could be tested with less risk if the initial flights were performed with the tailcone attached. Thus, the aerodynamicists were required to develop a data base for not only a basic flight Orbiter, but also an Orbiter with a tailcone attached. Similarly, the separation testing had to be done with both configurations.

The testing required to select a mated configuration and to obtain the separation aerodynamics are covered, as is the testing of the vortex wake created by the carrier. The problems associated with wind tunnel testing the Orbiter, with the tailcone attached, are discussed. Comparisons of flight test and wind tunnel-derived predicted aerodynamics are described with particular emphasis on performance, ground effects, and landing gear effects for the Orbiter, with and without the tailcone attached.

THE EVOLUTION OF THE ALT PROGRAM

The initial design of the Orbiter included jet engines to enable the Orbiter to land like a conventional aircraft. In the usual NASA manner of redundancy, it was felt that the Orbiter should be able to land safely even if the jet engines could not be started;ie, if powered flight were the nominal mode for the final landing phase, the Orbiter must be designed to fly unpowered for contingency situations. The cost of the engines was a considerable factor. In addition to the added weight penalty for the engines themselves, there were structural weight penalties for designing the wing to carry the engines. There were cost risks because of the technical unknowns of the environmental effects on the engines - the launch loads and heating, the extreme temperature environment on-orbit, and the effects of entry heating and accelerations. These concerns, and the requirement to design for an unpowered landing, led to the design modification to build an unpowered Orbiter.

This decision to design an unpowered Orbiter, for the Space Shuttle launch and entry configuration, affected two other areas. First, the need still existed to ferry the Orbiter between sites - manufacturing and landing sites to launch sites. When the Orbiter was conceived as a powered flight vehicle, it could have transported itself between sites. With the decision not to incorporate engines, the ferry technique was unresolved. Secondly, there was a plan to flight test the Orbiter in its subsonic regime. There were no unmanned flights in the program, and to have the first landing be that of the Orbiter from an entry point seemed an extreme option.

Consideration was given to engines which could be attached/removed for the purposes of ferry and subsonic testing. The cost and complexity of this system caused it to be rejected. Further, the design optimization, for the unpowered landing characteristics, resulted in an airplane which was not designed for takeoff.

It was at this time that the carrier aircraft concept was proposed. A multitude of ideas were evaluated. The extension of a large aircraft's landing gear, necessary to carry the Orbiter in an X-15 fashion seemed unreasonably complex. The idea of developing a new carrier, with the single purpose of carrying the Orbiter, was unreasonably costly. The options were reduced to carrying the Orbiter piggyback on either a Boeing 747 or a Lockheed C-5A. The technical concerns with both vehicles were related to clearances of the carrier vertical tail and relative aerodynamic effects during separation. The T-tail on the C-5A presented additional complications over the Boeing 747 aircraft. Of particular concern was the effect of the Orbiter wake on the C5A T-tail immediately following separation.

The actual decision to fly the Boeing 747 was based more on logistics than on technical rationale. The only C-5A available would have been loaned to NASA by the Air Force. Since the Air Force could recall the plane at any time, NASA would not be able to schedule operations without risk.
During the feasibility assessment, it was found that the Orbiter's blunt aft end (see Figure 1) would severely affect Orbiter/carrier performance both for climb and for ferry range. Further, it was believed that the carrier vertical tail would suffer structural fatigue due to the flow behind the Orbiter. Therefore, a drag reducing attach structure, a tailcone, was proposed (see Figure 2). This structure was to both reduce drag for performance improvements and to lessen the fatigue factor. Because the extent of these problems was not known, plans to flight test the Orbiter in its final landing phase also included retaining the tailcone.

At the time that the Orbiter/carrier aircraft program development was initiated, it was thought that nothing of this type had been attempted previously. It was as a great surprise to learn that the Europeans had flown piggyback configurations, even before World War II. The English, French and Germans each had some type of flight system which utilized two aircraft, one attached to the back of the other. The English had used their aircraft on mail runs to Greenland prior to World War II. The French, who had begun their program before the war, hid their airplanes until after the war. Films of the flight of the French configuration were made available to NASA. Of interest was the relative incidence angle, the attach structure and the pitchover maneuver to achieve separation. All were very similar to the design selected for the ALT program. Whether any wind tunnel testing was ever performed on these European airplanes is not known.

ORBITER/SHUTTLE CARRIER AIRCRAFT WIND TUNNEL TEST PROGRAM

The decision to fly an Orbiter/Shuttle Carrier Aircraft (SCA) configuration required that the precise configuration be established in a relatively short period of time. Following the selection of the Boeing 747 as the SCA, the initial wind tunnel tests were designed to gather data on proposed configurations to optimize the Orbiter/SCA with respect to both climb and separation performance. A number of drag-reducing attach structure fairings were assessed to select the tailcone configuration. The testing involved the Orbiter, with and without a tailcone, and a wide range of Orbiter incidence angles and elevon deflections. Two model scales, three facilities, and a range of Mach numbers and Reynolds numbers were tested to provide a means for correlating and abbreviating future tests throughout the program. The information gained from this series of tests led to the establishment of a mated configuration data base. One modification was made to the SCA, the addition of vertical stabilizers on the tips of the horizontal tail, to compensate for the loss of stability with the Orbiter blanketing the vertical tail.

A test was then conducted which provided performance, stability, and control data for the mated vehicle in the launch configuration. That same test was used to gather isolated SCA data and proximity data for each vehicle at the instant of separation by equipping each model with a balance. The SCA balance also read total vehicle data when the Orbiter was attached. Only the Orbiter with tailcone attached was used for this test, because at this time no tailcone-off flights were being considered. Deflections of the Orbiter elevon and body flap and the SCA stabilizer were evaluated for their effects on the proximity data. From this test came the data to establish the initial target conditions for separation and the performance estimates for the ferry flights.

A verification test was conducted on the Orbiter/SCA configuration using the same model as the test used to establish the data base, but a different facility. Runs were replicated from the earlier test to establish confidence in the data. The Orbiter, without the tailcone, was at this time incorporated into the testing, since the ALT program had been modified to include flight tests with the flight type Orbiter;ie, without tailcone. Data from these tests can be found in Ref. 1.

SEPARATION WIND TUNNEL TEST PROGRAM

The technical community expressed calm assurance that a mated flight program was a feasible undertaking. The separation of two vehicles in flight did not produce the same response. Some of the community had experienced bombs floating into aircraft after deployment, due to the influence of the aircraft on the bomb's aerodynamic characteristics. Those types of experiences and other horror stories abounded as the planning for the aerodynamic separation betwesn the Orbiter and the SCA began.

The Space Shuttle already had two parallel separations with which to contend; that of separating the solid rocket boosters from the external tank and of separating the external tank from the orbiter. Both required knowledge of the aerodynamic effects when the vehicles were in proximity, but used external forces to affect the separation. Knowledge had been gained in testing these launch separation configurations, which required supersonic test facilities. The Orbiter/SCA

separation required testing at subsonic speeds and so required that different support mechanisms, stings, and facilities be utilized.

The wind tunnel tests for separation were conducted with the Orbiter and SCA mounted on separate balances and stings. The two models were then positioned at various distances apart and at various relative incidence angles to obtain the data necessary to simulate the separation maneuver.

The amount and quality of the data obtained from these tests, and the analysis of the separation trajectory sensitivity to the data, resulted in the elimination of two complete tests scheduled in the wind tunnel test program. As an example, the analysis showed that the Orbiter elevon would be deflected only a small amount for either pitch or roll during the separation maneuver. This reduced the number of elevon positions required to be tested. The deletion of those tests and streamlining of others resulted in considerable savings to the program.

A matrix of the basic configurations tested during the ALT program is shown in figure 3. The mated Orbiter/SCA basic dimensions and configuration details are shown in figure 4.

The utilization of mated configuration, separation and isolated aerodynamic data in computer simulations provided trajectory information about the relative separation distances between the vehicles. Structural clearance was the initial concern, but this was expanded to include clearance between the Orbiter and the vortex wake of the SCA.

The problems associated with a trailing vehicle encountering the vortex wake of a large aircraft prompted concerns with the planned separation maneuver. Separation was to be accomplished by the Orbiter/SCA entering a dive maneuver to increase airspeed, followed by a reduction of power and deployment of spoilers to reduce lift and increase the drag of the SCA. Such a configuration was necessary to create the relative motion required to aerodynamically drive the two vehicles apart. This also resulted in a near maximum vortex wake condition since the SCA was now closely configured to a landing configuration.

No vortex wake test was scheduled; however, a Boeing 747 model was available in an ongoing Langley wind tunnel test. The sponsors of the test program granted JSC one evening to test the separation configuration for vortex wake information. A "wing" model was positioned in the vortex wake area behind the Boeing 747, and rolling moment induced on the wing was recorded. This information was used to define a turbulence boundary area. Design of the separation maneuver restricted the Orbiter's flight path to remain outside the area of turbulence. Figure 5 depicts the area of the vortex wake. Data from the vortex wake and separation tests are in Ref. 1.

ALT FLIGHT TEST PROGRAM OVERVIEW

The ultimate aims of the flight test program were to certify the Orbiter/SCA configuration for ferry flight and to test the Orbiter approach and landing phase. In order to flight test the Orbiter, a separation maneuver was required and an initial part of the flight test program was designed to assure that the separation was viable.

The first test of the mated vehicles consisted of taxi testing only. This was followed by flight tests of the Orbiter, unmanned and unpowered, atop the SCA. The Orbiter with tailcone attached was used for these initial flights since this was the most conservative configuration with respect to buffet on the SCA. This was also the selected ferry configuration.

A load measurement system was developed for the Orbiter/SCA to measure and record the attach forces between the two vehicles during the mated portion of each flight. Load cells instrumented to measure axial and shear forces were located on each of the three Orbiter/SCA attach struts shown on Figure 4.

Relative vertical and side forces were measured at the forward attach strut. Relative vertical and drag forces were measured at the left aft strut, while relative vertical, drag, and side forces were measured at the right aft strut. By combining these measurements mathematically, the relative normal and axial accelerations between the Orbiter and SCA and the instantaneous Orbiter pitch acceleration were determined. This data in strip chart form was utilized as quicklook information for post flight analysis and subsequently as a basis for allowing a realtime decision to separate on the initial tailcone-off flight.

A computer program was developed (Ref. 2) which could take the aerodynamic data base and flight conditions, such as airspeed, and compute the expected loads in each load cell, and conversely, could take the load cell data and extract the aerodynamic coefficients. Using the computer program and the planned flight maneuvers, a prediction of load cell readouts could be made prior to the flight. Comparison of actual and predicted load cell data could then be quickly analyzed. Further refinement of aerodynamic data was also possible from actual flight test results.

Because of the concern for the SCA vortex wake, several flight tests were made to confirm the wind tunnel test results. The initial tests consisted of a Lear jet and a T-37 flown behind the SCA. The SCA was equipped with smoke generators and the aircraft were purposely flown into the smoke area to determine the affect of the turbulence. The results clearly indicated that the Orbiter should remain clear of this area. Subsequently, an F-104 was flown with the SCA in a simulated separation maneuver. In this test, the F-104 was positioned at a point off the SCA wing, approximately one wing span away, and both vehicles flew in formation through a simulated separation maneuver. When the SCA reached its conditions for separation, the F-104 pulled away and replicated the planned Orbiter maneuver following the separation. The test confirmed that adequate clearance between the SCA vortex wake and the Orbiter flight path would be maintained.

ORBITER/SCA FLIGHT TEST RESULTS

The initial flights of the Orbiter/SCA were inert tests in that the Orbiter was unpowered and unmanned. Five flights were flown in this series. The first four flights were used to obtain takeoff and climb performance data; to investigate stability and control envelopes, flutter response, and buffet and loads boundaries; and to perform airspeed calibration checks.
The fourth flight also focused on evaluating configuration variables associated with the launch maneuver. During this flight, the SCA inflight spoilers were deployed for the first time and the aircraft performance was assessed based on the special thrust ratings on the engines. This flight provided engineers their first look at a separation-related parameter in the form of the incremental effect of the inflight spoilers on each vehicle in close proximity.

The fifth flight of the inert series obtained data during two simulated launch maneuvers starting at ceiling altitude and terminating after approximately 20 seconds of steady-state data following the "launch ready" call by the SCA pilot. Both vehicles were configured as they would be for an actual separation with the exception of the Orbiter elevon. The elevon was positioned at -1 degree for emergency jettison for these early flights.

An error in the SCA data base was discovered during these tests. The error was a result of the incorrect use of wind tunnel incremental data, and the aerodynamic data base was updated to the actual flight data. The inert tests verified that (1) the Orbiter/SCA configuration could achieve and stabilize on the separation parameters using the prescribed procedures without exceeding Orbiter or SCA constraints, (2) safe separation initial conditions could be achieved with the baseline separation configuration and airspeed, and (3) the mated configuration could recover from an aborted separation maneuver within the vehicle constraints. (Figure 6)

Three captive-active flights were then flown with the Orbiter manned. The objectives of these flights were to verify (1) the separation configuration and procedures; (2) the integrated structure, aerodynamics, and flight control system; and (3) the Orbiter integrated system operations.

The first captive-active flight was restricted in airspeed and provided no separation data. The second flight included a full separation simulation. While the SCA maintained the separation conditions, the Orbiter crew moved the rotational hand controller (RHC) full forward and full aft to obtain elevon effectiveness data. Software limits restricted the elevon to move up 1.5 degrees and down 1.5 degrees from the zero degree position for full RHC movement. Each position was held for 5 seconds to obtain steady-state data. Data from the load cells during this flight test were processed through the computer program to assess the elevon effectiveness. The results indicated a shift between the predicted values and the flight test data; equivalent to an approximately -1 degree bias in the Orbiter elevon position. Otherwise, the effectiveness of the elevon was in excellent agreement with preflight predictions.

The third captive-active flight was a dress rehearsal for the actual separation. The elevon was moved from the climb position (-2 degrees) to the separation position (0 degrees) during the maneuver. The elevon bias did not appear during this test. This gave rise to questions regarding data repeatablility and elevon position calibration accuracy. Fortunately, the first two separations were relatively insensitive to small elevon dispersions;ie. the one degree uncertainty still provided an adequate separation window. During the pre-separation maneuvers on these flights, more data could be obtained regarding the elevon bias for use in establishing separation conditions for more sensitive separations.

To design the separation maneuver, off-line simulations were run to evaluate clearances and sensitivities. Manned simulations, for crew training were made for the Orbiter and the SCA. In these manned simulations, the trainer vehicle, either Orbiter or SCA, was modeled to reflect the proximity aerodynamics. The SCA was modeled as the mated vehicle until separation and then was influenced by predefined proximity aerodynamic effects as it was flown away from the Orbiter. The

Orbiter flew a predefined profile to the separation point. After separation, predefined proximity aerodynamics were applied while it was under the influence of the SCA.

While the designers felt comfortable with their work, upper management was still concerned. To better represent the separation to management, off-line simulations were run and coupled with computer graphics to provide a moving picture of how separation would be accomplished. After the film was shown, no one questioned the separation maneuver.

To assess the performance of the first separation, the off-line simulation was used to recreate the flight conditions, using load cell, downlist, and recorded data from the flight. The maneuver differed from planned due to a larger than expected Orbiter pitch up rate immediately following separation. This was probably due to the fact that an onboard computer failed at the instant of separation and distracted the crew. Comparison of the off-line simulation, using the flight conditions and the aerodynamic data base, closely paralleled the flight results. A discrepancy in the SCA normal load factor following separation was attributable to the difference between the post separation steering maneuver used by the SCA pilots and that programmed into the off-line simulation. The elevon bias was not evident on this flight.

The second separation of the Orbiter with tailcone attached also confirmed the preflight predictions. On this flight, the Orbiter pitch up acceleration was as planned.

The third flight in this series had the Orbiter ballasted to a more negative center of gravity. To compensate, the elevon at separation was set at 2.5 degrees and the airspeed at separation was decreased to prevent overloading the Orbiter during the pitch up maneuver following separation. The comparison of off-line to flight results was again in close agreement. (Figure 7)

The Orbiter without the tailcone attached presented two major problems with the separation phase of flight. First, the increased buffet level could possibly result in an SCA cockpit environment that would make it impossible for the SCA to attain the specified target conditions. Second, with the removal of the tailcone, the change in Orbiter pitching moment required +7 degrees of down elevon, which was well outside the elevon range tested in the preceding flights. The SCA tail loads and climb performance degradation created by the increased buffet and drag levels, respectively, were also unknowns. A fourth captive-active flight was originally planned to investigate the flight envelope of the tailcone-off configuration but was deleted. The objectives of the canceled captive-active flight were combined with free flight 4 and were evaluated in the first half of the flight. The optimum incidence for tailcone off was 5 degrees as opposed to the 6 degrees for tailcone attached. However, to reduce the number of variables, it was decided to leave the incidence angle at 6 degrees.

The first portion of the flight was dedicated to a realtime assessment of the buffet-induced loads and verification of the separation configuration and target conditions. A realtime GO/NO-GO decision for separation was based on load cell data telemetered to the ground and displayed on strip-charts in the Dryden Flight Research Center control room.

The buffet levels were determined to be acceptable from takeoff to maximum airspeed and a separation rehearsal maneuver was initiated. Had the data not matched the preflight predictions, a second rehearsal would have been flown to obtain elevon effectiveness over the untested range. The data in the first rehearsal, with the elevon deflected to +7 degrees, confirmed the preflight predictions and all parameters were within the acceptable separation window. A realtime decision was made to continue with the actual separation maneuver. Again, post flight analysis in off-line simulations agreed well with actual flight data.

The fifth flight of the free flight series was a duplicate of the first from the separation viewpoint. Again, the trajectory reconstruction showed excellent agreement between flight data, including photographic time histories, and off-line simulation data. (Figure 7)

DEVELOPMENT OF ORBITER TAILCONE-ON AERODYNAMIC DATA BASE

The decision to fly the initial ALT flights with the tailcone on the Orbiter was made approximately one year prior to the scheduled flight dates.The short lead time to acquire a preflight tailcone-on aerodynamic data base prompted a flurry of wind tunnel testing over the ALT flight regime of Mach 0.8 down to touchdown. Due to the shape and location of the tailcone, much of the testing involved evaluation of various model support systems such that a primary support system could be selected. This testing also involved evaluation of alternate support systems such that tares on the primary support system could be determined. A summary of the support systems evaluated is presented in figure 8.

Following the decision to utilize a sting as the primary support system, sting tares were determined in a subsonic wind tunnel test while supporting the model with wing tip mounted dual

struts, as shown in configuration 6 of figure 8. Those tares were applied to the test results for the Mach 0.4 to 0.8 regime, assuming Mach effects to be negligible. Further testing utilizing support configuration 5 of figure 8 provided verification of the validity of that assumption.

Wind tunnel testing at Mach 0.20 to 0.25 was not only accomplished through use of the previously mentioned wing tip mounted dual struts and sting support systems, but involved utilization of a triple-strut mounted 0.36-scale model, figure 9, in the Ames Research Center 40x80-ft facility. Previously determined triple-strut tares from Orbiter tailcone-off testing were utilized during the 0.36-scale tailcone-on test.

ORBITER AERODYNAMIC PERFORMANCE COMPARISONS

Orbiter flight test data from the ALT program were obtained from both quasi-steady state and dynamic flight test conditions. Flight data utilized herein was determined from references 3, 4, and 5. The dynamic test maneuver occurred with tailcone off and consisted of a pushover-pullup maneuver providing an angle of attack range from 2 to 16 degrees in a relatively short time. Mach number was virtually unchanged during the maneuver.

The predicted data used for comparison with the flight test data was determined from the Aerodynamic Design Data Books (ADDB), references 6 and 7, using given flight attitudes, Mach numbers, and control surface deflections. Aerodynamic "tolerances" and "variations" shown on the performance comparison figures were also obtained from the referenced ADDB's. "Variations" were derived utilizing past flight test experience from many representative aircraft and represents an uncertainly between wind tunnel-derived and flight-derived aerodynamic coefficients. "Tolerances" represent only the uncertainty related to the wind tunnel predictions due to data scatter and scatter resulting from testing with various models and in various wind tunnel facilities.

The aerodynamic analyst is faced with a dilemma in the comparison of preflight predictions and flight test data. In wind tunnel testing, which is the basis of the preflight predictions, the independent parameters are known precisely while the aerodynamics are questionable. In flight testing, the aerodynamics are known exactly, by definition, but the accuracy of the independent parameters may be in question. To minimize the impact of this dilemma, the aerodynamic comparisons were selected such that errors in the flight-independent parameters are minimized. Thus, lift-to-drag ratio (L/D) was selected for comparisons of predicted and flight aerodynamic performance, since it is independent of flight dynamic pressure ($\bar{q}$).

Tailcone-on L/D, illustrated in figure 10, indicates a slight reduction in flight data relative to the predictions. The lift and drag coefficients presented in figure 11 indicate that at the same lift coefficient, drag coefficient from flight is slightly higher than that predicted, thus reducing L/D from the predicted levels. It should also be noted that both lift and drag coefficients are well within the predicted tolerance and variation limits indicated.

Figure 12 presents tailcone-off L/D at an average Mach number of 0.4. The maximum flight L/D is approximately the same as predicted; however at the lower values of lift coefficient the flight L/D is slightly higher than predicted. As seen in figure 13, both lift and drag coefficients as a function of angle of attack are slightly less than predicted, although the flight lift curve slope is very close to predicted. Comparison of drag coefficient at the same lift coefficient does indicate that flight drag coefficient is slightly less than predicted, thus the slight increase in flight L/D. Again, both lift and drag coefficients are well within the predicted tolerance and variation limits indicated.

An area of concern which has been verified by the flight test data is ground effects, which were primarily confined to main gear wheel heights (h_w) of less than twenty feet, as illustrated in figure 14. For both tailcone-on and tailcone-off configurations, the flight incremental lift due to ground effects compared well with predicted data. The ground effect on drag coefficient is negligible and, therefore, is not presented.

Estimates of flight landing gear axial force and drag indicate that the incremental effect of landing gear was over predicted, due probably to not correcting the low-speed, low-Reynolds number wind tunnel test results to flight Reynolds number. A post flight wind tunnel test was conducted utilizing a large (0.05-scale) high fidelity model at a high Reynolds number. The results of that test are shown in figure 15 and agree quite well with the landing gear axial force and drag coefficients as derived from the flight tests.

CONCLUSIONS

The analytical prediction techniques and mathematical modeling incorporated in the design of the separation procedures for the Orbiter/SCA were based on scale-model wind tunnel test data. These techniques proved to be extremely accurate and useful throughout the Approach and Landing Test Program.

The load measurement system installed aboard the SCA provided a means for extracting the proximity aerodynamics and was a reliable source for making realtime assessments of separation and loads parameters. The load measurement system also allowed some wind tunnel tests to be deleted form the program, with actual flight data completing the aerodynamic data base. The Orbiter separated from the SCA, successfully and as predicted, five times during the ALT program

During the Approach and Landing Test Program the Space Shuttle Orbiter was flown as both tailcone-on and tailcone-off configurations. Due to the shape and location of the tailcone on the Space Shuttle Orbiter, much of the initial wind tunnel testing required to support the Approach and Landing Test Program requirement to fly some flights with the tailcone on involved evaluation of various model support systems. From these tests a primary support system consisting of an aft mounted sting was selected. Support systems consisting of both wingtip mounted struts and lower forward fuselage strut were utilized to evaluate and verify sting tares.

Comparisons of predicted and flight test performance data indicate that lift-to-drag ratio, lift coefficient, and drag coefficient were well within predicted tolerance and variation limits for both tailcone-on and tailcone-off. The flight incremental lift due to ground effects also compared well with predicted data.

The flight-derived axial force and drag indicate that the incremental effect of the landing gear was over predicted, due probably to not correcting the low-speed, low-Reynolds number wind tunnel results to flight conditions. A post flight high-Reynolds number wind tunnel test confirmed the flight test results.

REFERENCES

1. Orbiter/747 Carrier Separation Aerodynamic Data Book-SDM Baseline. SD75-SH-0033C, Rockwell International Space Division, Nov. 1976.
2. Homan, D.J.; Denison, D.E.; and Elchert, K.C.: Orbiter/Shuttle Carrier Aircraft Separation: Wind Tunnel, Simulation, and Flight Test Overview and Results. NASA Technical Memorandum 55223, May 1980.
3. Romere, P.O.; Eichblatt, D.L.; Underwood, J.M.; and Howes, D.B.: The Space Shuttle Orbiter Approach and Landing Tests - A Correlation of Flight and Predicted Performance Data. Presented as paper 78-793 at AIAA 10th Aerodynamic Testing Conference, San Diego, CA, April 19-21, 1978.
4. Romere, P.O.; Eichblatt, D.L.; Underwood, J.M.; and Howes, D.B.: Orbiter Approach and Landing Tests Correlation of Flight and Predicted Performance Data. AIAA Journal of Aircraft, Volume 16, Number 4, April 1979, pp. 233-238.
5. AFFTC Evaluation of the Space Shuttle Orbiter and Carrier Aircraft, NASA Approach and Landing Test, AFFTC-TR-78-14, May 1978.
6. Aerodynamic Design Data Book, Orbiter 101, SD72-SH-0060, Volume IV, Rockwell International, Space Division, Downey, CA, Revision 2, May 31, 1977.
7. Aerodynamic Design Data Book, Orbiter Vehicle, SD72-SH-0060-1J December 1975 plus Revisions 1 through 6, Rockwell International, Space Division, Downey, CA.

GEOMETRY	COMPONENT	
	WING	VERTICAL TAIL
AREA	2690 FT^2 (249.9092 m^2)	413.25 FT^2 (38.3922 m^2)
SPAN	936.68 (23.8425)	315.72 (8.0193)
ASPECT RATIO	2.265	1.675
TAPER RATIO	0.2	0.404
SWEEP (LE)	81/45 DEG	45 DEG
DIHEDRAL	3.5	— —
INCIDENCE	0.5 DEG	— —
MAC	474.81 (12.0602)	199.81 (5.0752)

NOTE: UNLESS OTHERWISE NOTED, ALL DIMENSIONS ARE IN INCHES (METERS)

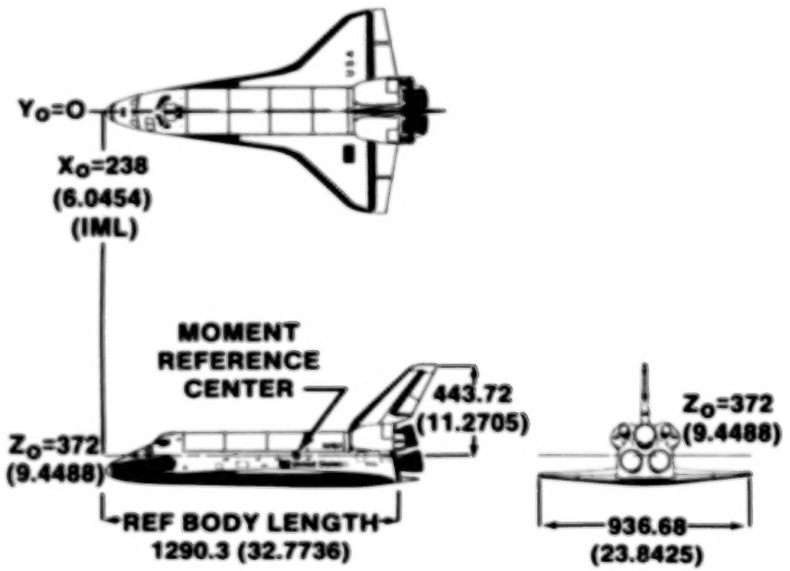


Figure 1. Space Shuttle Orbiter Tailcone-off Configuration.

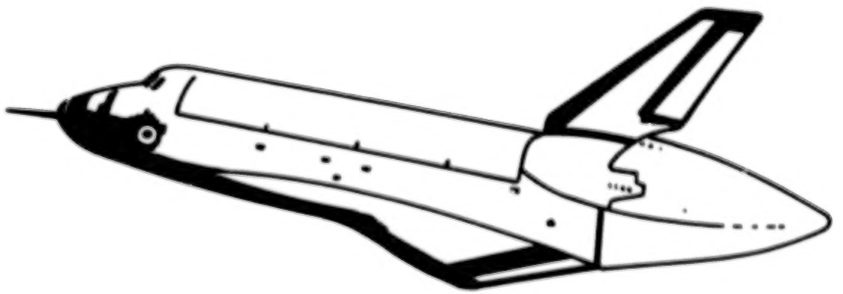


Figure 2. Space Shuttle Orbiter Tailcone-on Configuration.

TEST CONFIGURATION	1974												1975												1976											
	J	F	M	A	M	J	J	A	S	O	N	D	J	F	M	A	M	J	J	A	S	O	N	D	J	F	M	A	M	J	J	A	S	O	N	D
									11	1, 16	18			6			8	5		20			7				12	1		18					12	
ISOLATED CARRIER									CA 5	CA 20			CA 23A					CA 23B																		
ISOLATED ORBITER									CA 5	CA 20							CA 6						CA 14A													
MATED (TAILCONE ON)									CA 5								CA 6						CA 14A				CA 13								
MATED (TAILCONE OFF)									CA 5	CA 20			CA 23A				CA 6										CA 13								
SEPARATION n										CA 20								CA 23B	CA 20																	

Figure 3. Ferry and Approach and Landing Test Program Wind Tunnel Configuration Matrix.

MEASUREMENT	SCA			ORBITER	
	WING	VERTICAL	HORIZONTAL	WING	VERTICAL
AREA, m^2	511	77.1	136.6	249.9	38.4
SPAN, m	59.8	9.8	21.9	23.8	8
ASPECT RATIO	6.96	1.25	3.60	2.265	1.675
TAPER RATIO	0.356	0.340	0.250	0.200	0.404
SWEEP, DEG	37.5 (1/4 c)	45.0 (1/4 c)	37.5 (1/4 c)	[a]45	[a]45
DIHEDRAL, DEG	7.0	—	7.0	[b]3.5	—
INCIDENCE, DEG	2.0	—	+5 TO -10	0.5	—
MAC, [c]m	8.3	8.5	6.9	12.1	5.1

[a]LEADING EDGE.

[b]TRAILING EDGE.

[c]MEAN AERODYNAMIC CHORD.

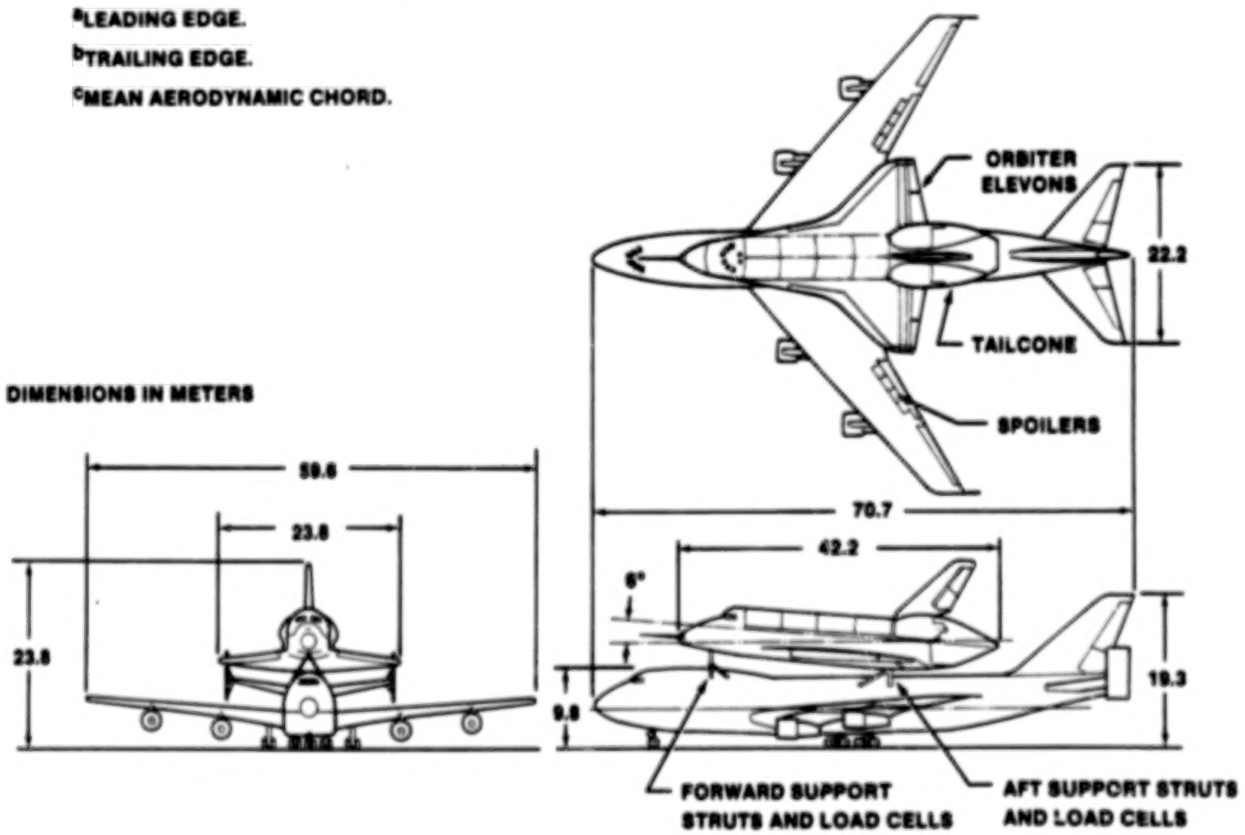


Figure 4. Mated Space Shuttle Orbiter/Carrier Aircraft Configuration.

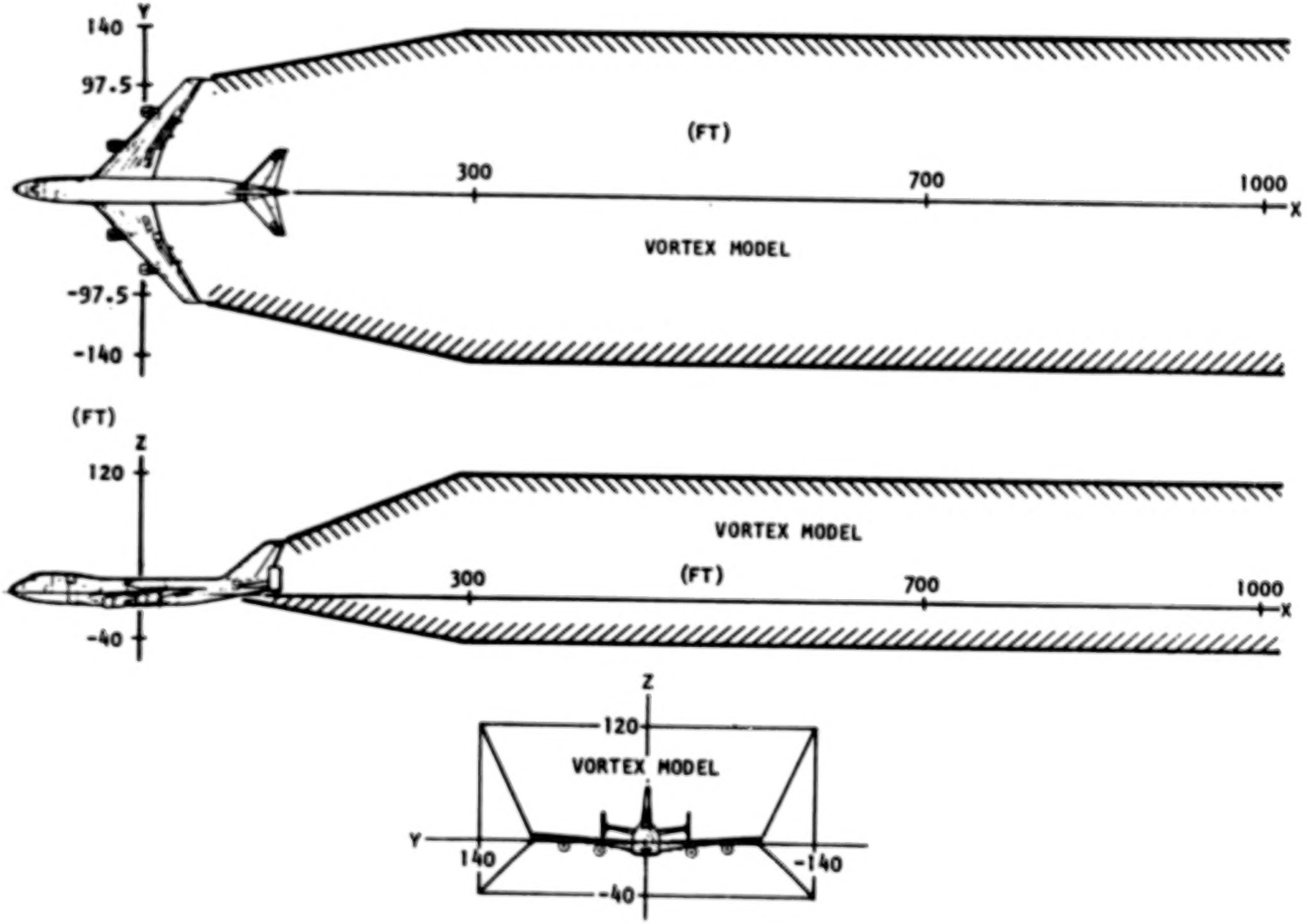


Figure 5. SCA Vortex Wake Definition.

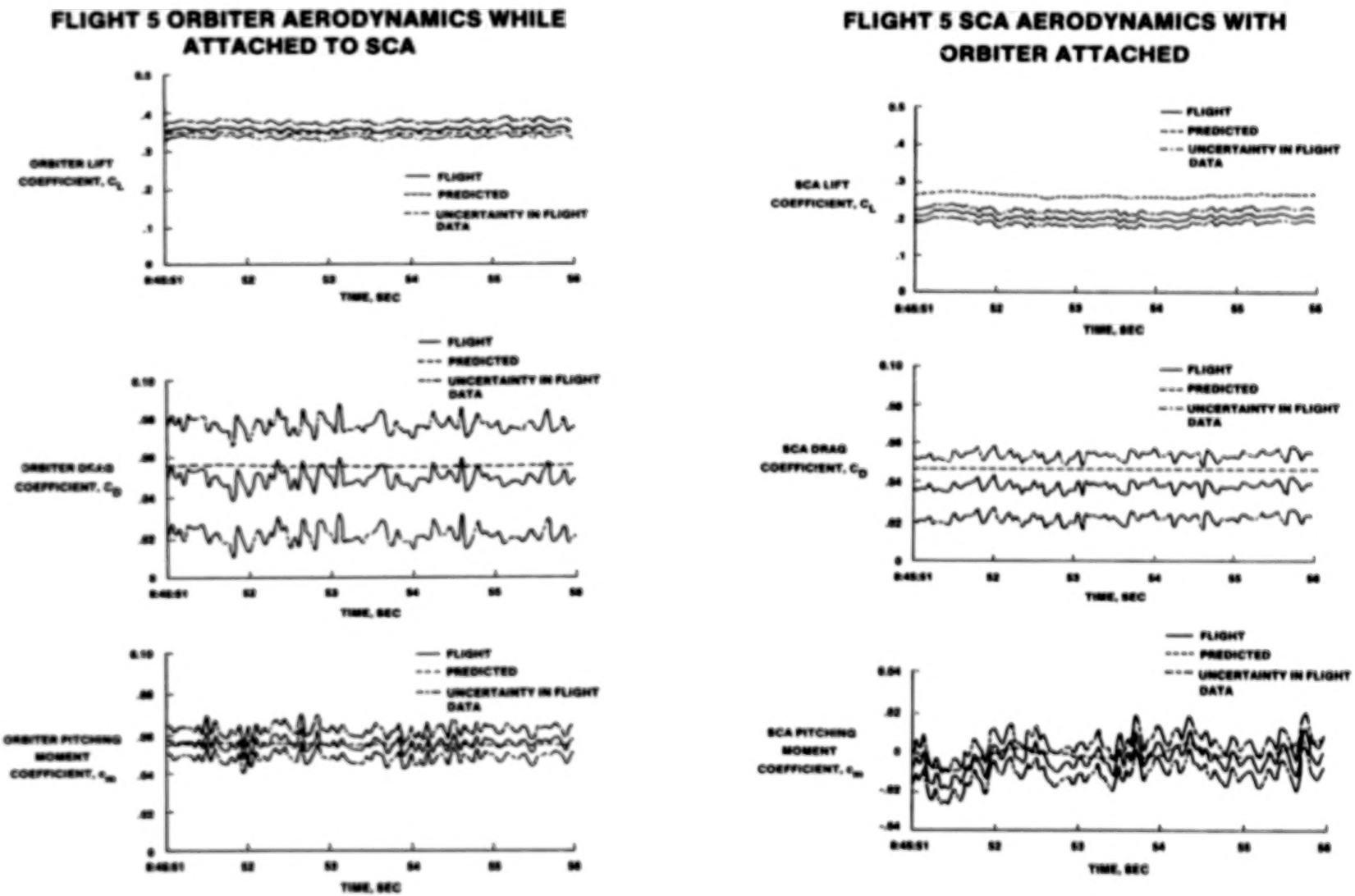


Figure 6. Inert Flight 5: Flight Test Data Compared to Off-Line Simulations.

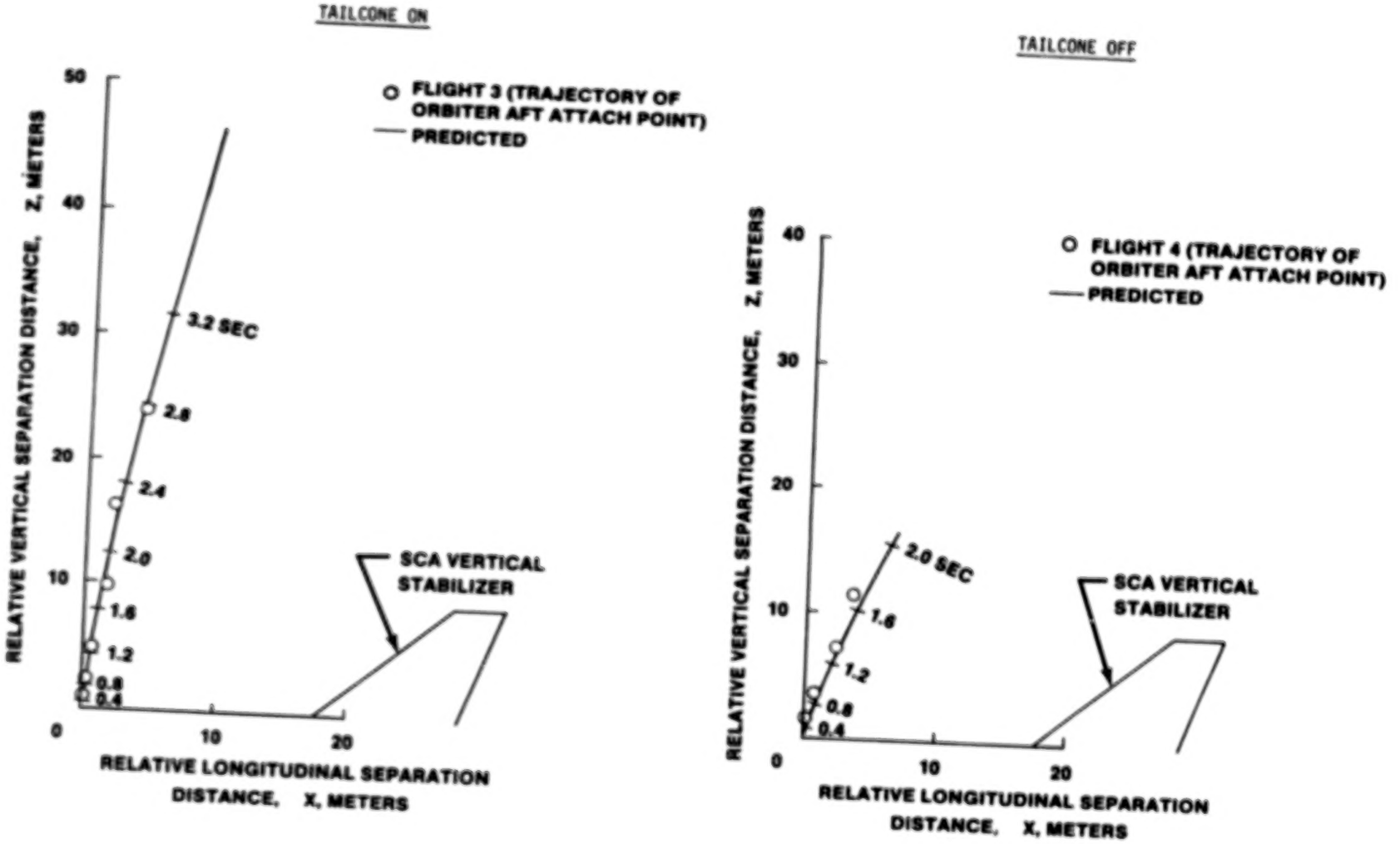


Figure 7. Comparison of Separation Clearances Between Flight Test and Predicted Data

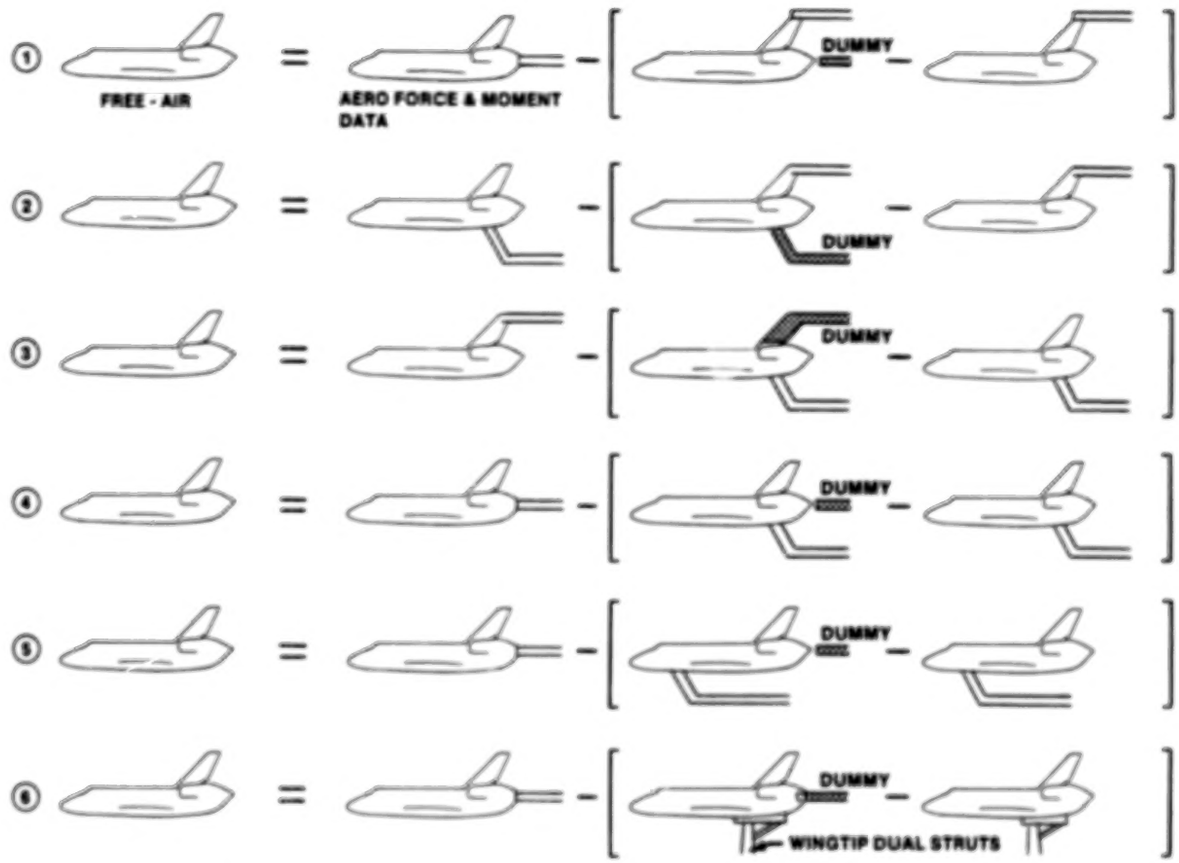


Figure 8. Model Support Systems Evaluated during Tailcone-on Wind Tunnel Testing.

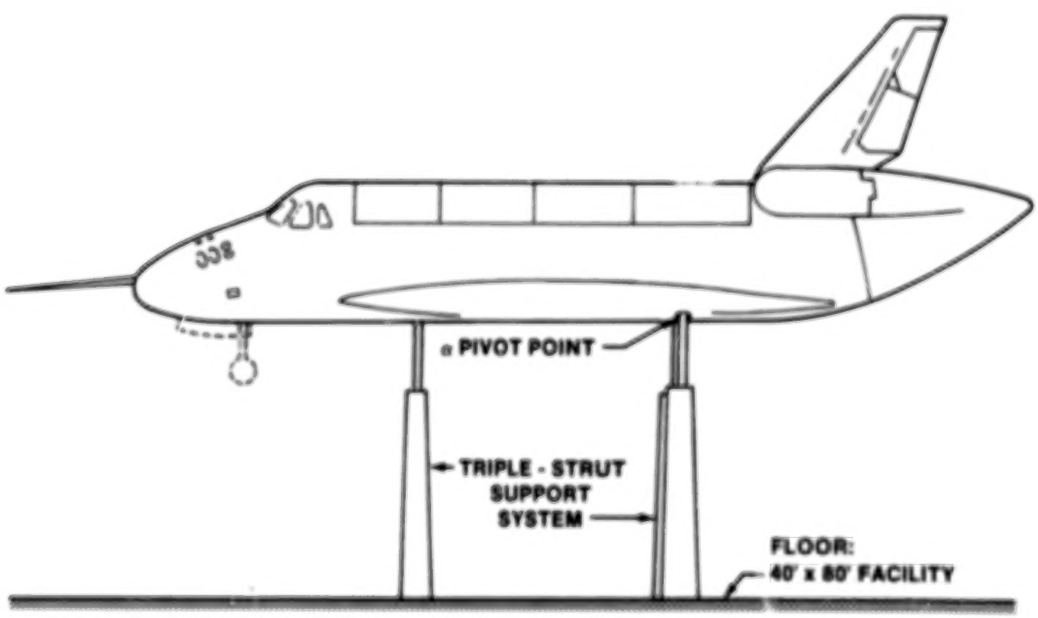


Figure 9. Triple-Strut Support System Utilized with the 0.36-scale Model Orbiter.

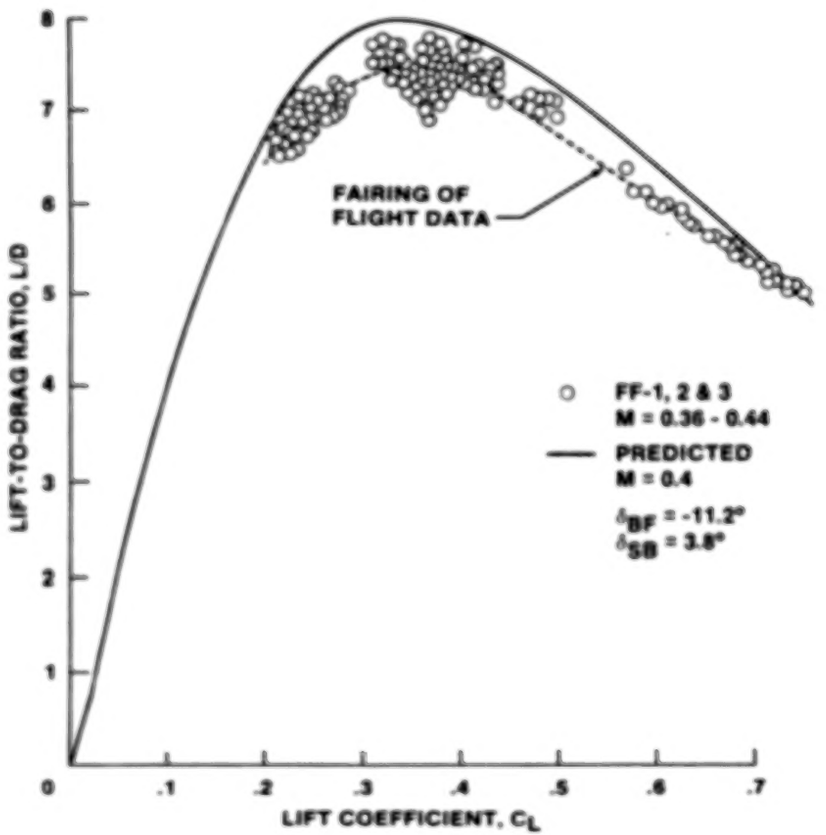


Figure 10. Tailcone-on Performance Comparisons of Flight Test and Predicted Data.

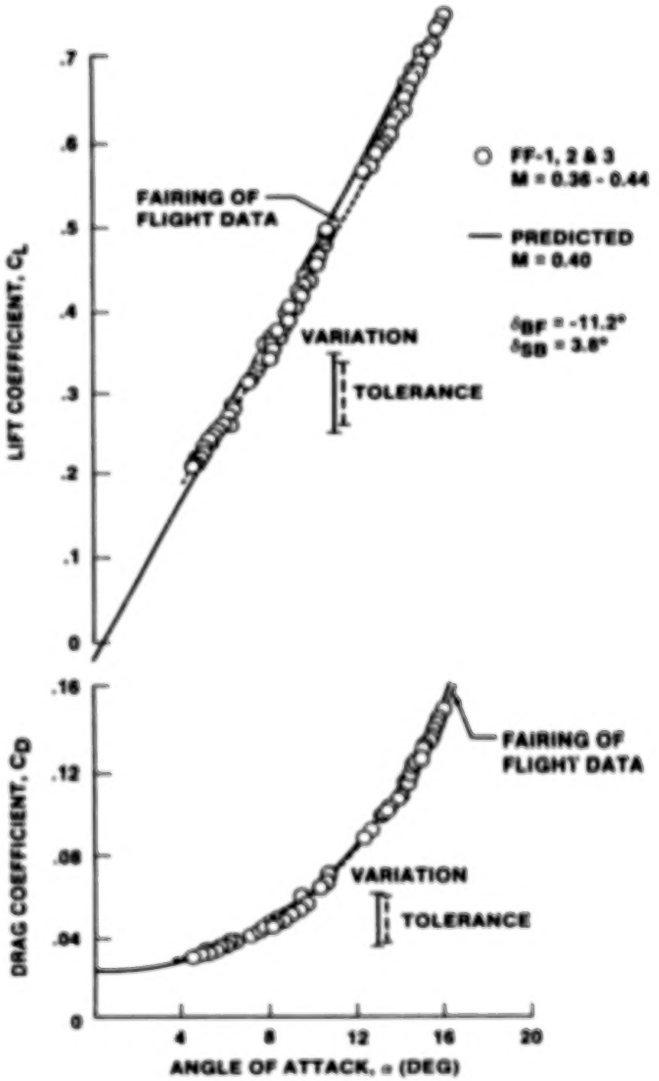


Figure 11. Tailcone-on Lift and Drag Coefficient Comparisons of Flight Test and Predicted Data.

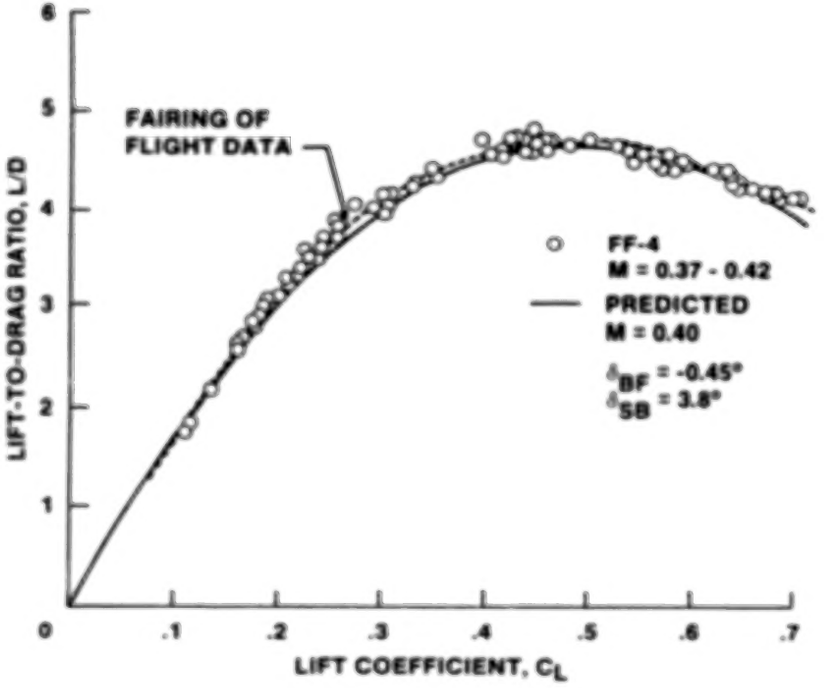


Figure 12. Tailcone-off Performance Comparisons of Flight Test and Predicted Data.

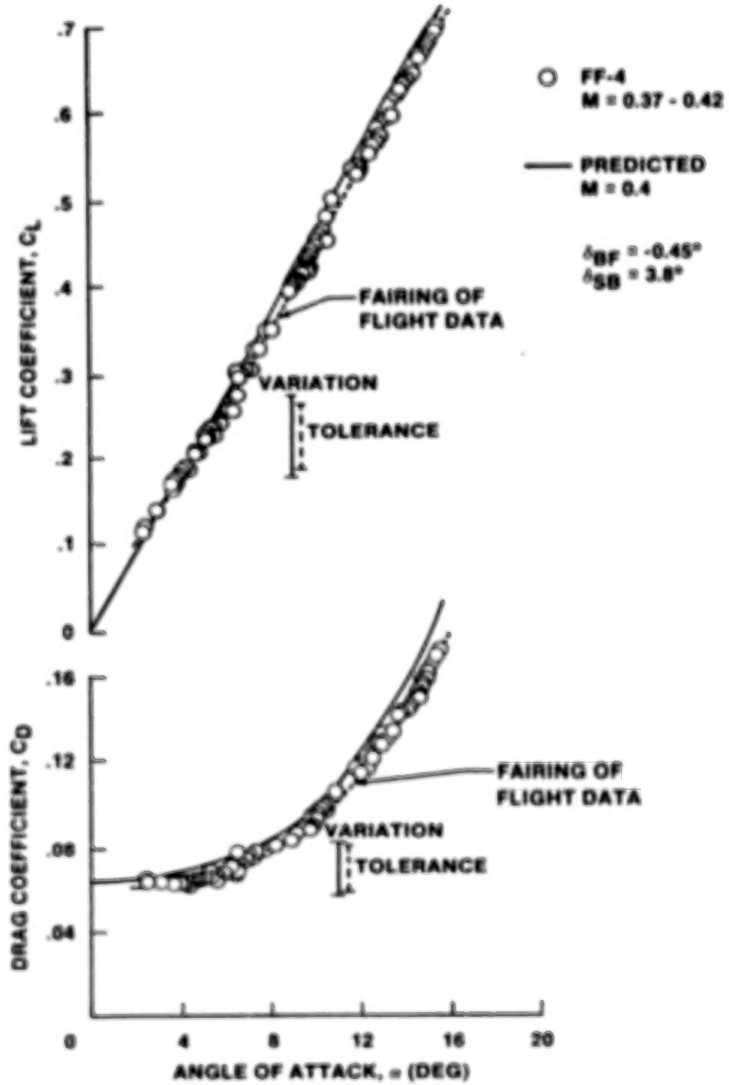


Figure 13. Tailcone-off Lift and Drag Coefficient Comparisons of Flight Test and Predicted Data.

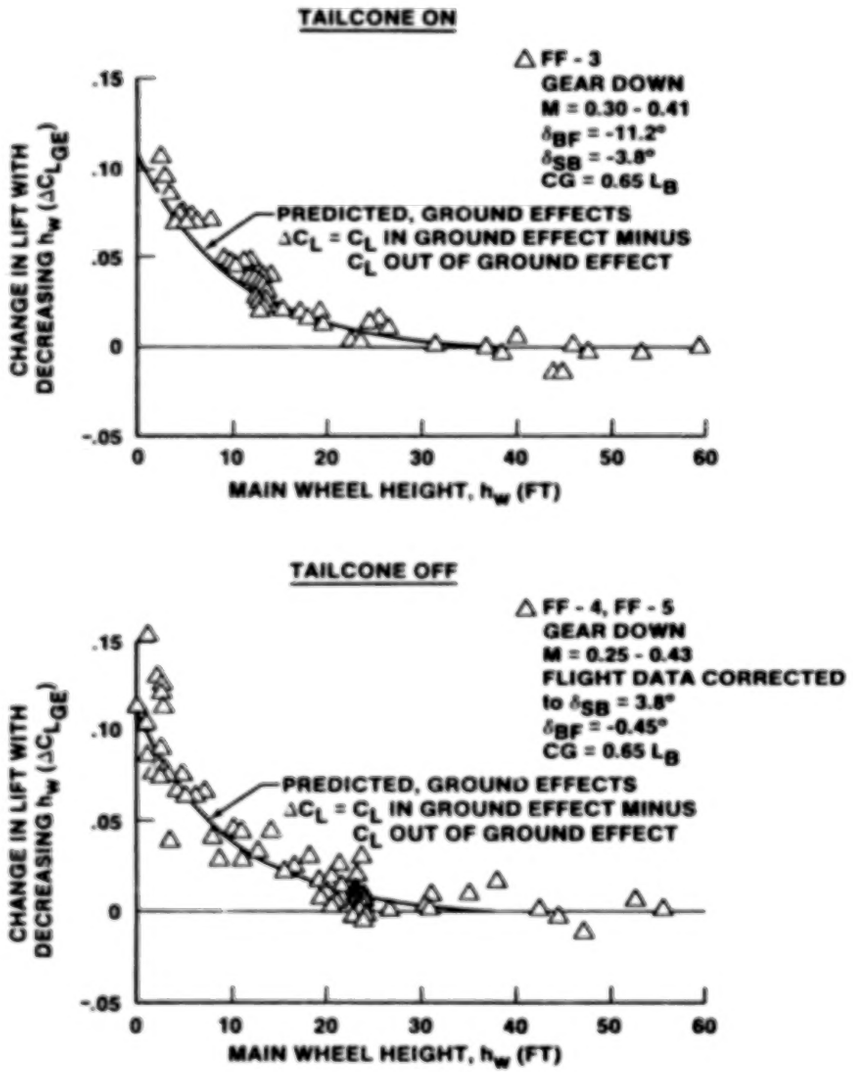


Figure 14. Incremental Lift Coeffiecient due to Ground Effect.

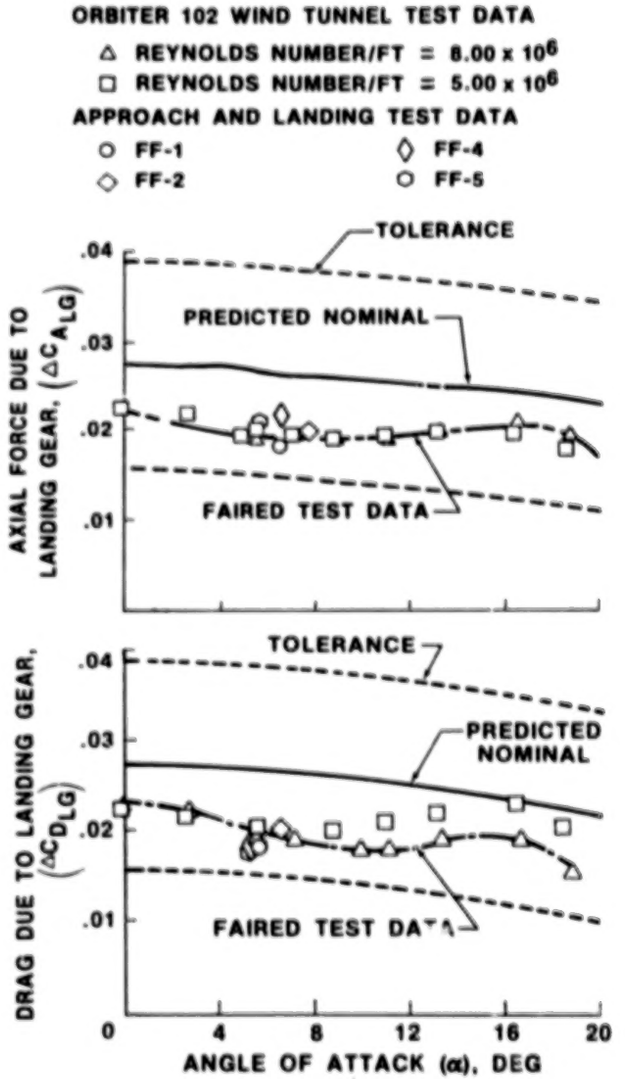


Figure 15. Incremental Axial Force and Drag Coefficients due to Landing Gear Deployed.

N85
16912

UNCLAS

N85-16912

D23

THE ORBITER AIR DATA SYSTEM

Ernest R. Hillje
NASA-Johnson Space Center
Houston, TX 77058

ABSTRACT

Air data parameters are required during Orbiter atmospheric entry for use by the auto-guidance, navigation, and flight control systems, and for crew displays. Conventional aircraft calibrations of the Orbiter air data system were not practicable for the Space Shuttle, therefore extensive wind tunnel testing was required to give confidence in the preflight calibrations. Many challenges became apparent as the program developed; in the overall system design, in the wind tunnel testing program, in the implementation of the air data system calibration, and in the use of the flight data to modify the wind tunnel results. These challenges are discussed along with the methods used to solve the problems.

NOMENCLATURE

SYMBOLS

C_{P_s}	Static pressure coefficient
M	Mach number
P_C	Center port (pressure)
PL	Lower port (pressure)
PM	Measured static pressure
PS	Static pressure (port)
PT	Total pressure (port)
PU	Upper port (pressure)
$\bar{q}$	Dynamic pressure
T_T	Total temperature
X	Orbiter vehicle X-station
Y	Orbiter vehicle Y-station
α	Angle of attack
β	Angle of sideslip

SUBSCRIPTS

C	Calibration-corrected value
CAL	Calibration parameter value
m	Measurement by air data probe
WT	Wind tunnel
∞	Free-stream value

ACRONYMS

ADS	Air data system
ADTA	Air data transducer assembly
ALT	Approach and landing test
A/L	Approach and landing
ARC	Ames Research Center
FRL	Fuselage reference line
FS	Fuselage X-station
FTB	Flight test boom (flight test probe and mast)
GN&C	Guidance, navigation and control
GPC	General purpose computer
IMU	Inertial measurement unit
LaRC	Langley Research Center
LeRC	Lewis Research Center
MS	Model X-station

NAAL	North American Aerodynamics Laboratory
NASA	National Aeronautics and Space Administration
OA	Orbiter aerodynamics test series
OFT	Orbital flight test
OML	Outer mold line
STS-1	First space transportation system flight (OFT)
TAEM	Terminal area energy management
TPS	Thermal protection system
WL	Fuselage water line
WP	Fuselage water plane

INTRODUCTION

The NASA Space Shuttle is designed as a reusable transportation system to near Earth orbit. The prime element of the total Space Shuttle configuration is the payload - carrying Orbiter. Subsequent to launch and orbital operations the Orbiter must be able to negotiate the critical entry portion of the flight and land safely on a conventional runway. During the entry phase, the Orbiter configuration must maintain stability and control as well as a required trim attitude, for large center of gravity position changes and a large angle of attack span (the latter from heating and ranging considerations). Mach number varies from 28 at initial entry to approximately 0.25 at landing, and the angle of attack varies from 40 degrees to 0 degrees. During entry to touchdown, the automatic flight control system passes through three distinct phases: entry, terminal area energy management (TAEM) and approach and landing (A/L). Each of these phases has established requirements for processed air data, such as angle of attack, altitude, Mach number, etc., from the Orbiter air data system (ADS) for the conditions shown in table I.

In many ways, the Orbiter ADS is a typical ADS. It uses two fuselage-mounted probes to measure local flow conditions. Freestream conditions, such as Mach number, angle of attack, and altitude are computed using previously derived calibration algorithms. The freestream conditions are used by the guidance, navigation and control (GN&C) system and are also displayed to the crew. In addition, air data are used extensively during the postflight aerodynamic analyses.

In terms of obtaining accurate preflight air data calibrations for the Orbiter there existed a somewhat unique situation. The typical aircraft flight calibration was not practicable (i.e. tower flyby, pacer aircraft, etc. type testing was not compatible with any sustained Orbiter test flight conditions). In addition, the blunt nose of the Orbiter causes large "position errors" that must be accounted for in the calibration. Because of all the aforementioned conditions, an extensive wind tunnel calibration program was required. The approach and landing test (ALT) phase of the flight test program had a conventional flight test boom (FTB) installed in the nose of the Orbiter for the purpose of evaluating the subsonic wind tunnel calibration of the ADS. The wind tunnel data were merged with data obtained during the ALT program to produce an on-board calibration for orbital flight test (OFT) and a more accurate calibration for the postflight aerodynamic analyses. Results from the OFT program indicated that the on-board calibration easily met the specified requirements. These results were also used in an extensive effort to refine the postflight calibration in order to provide the best possible data for the postflight aerodynamic analyses.

SYSTEM DESCRIPTION

A sketch of the Orbiter ADS probes illustrating their location on the Orbiter nose is shown in figure 1. There are two probes, one on either side of the vehicle. They are secured to rotating doors that allow them to be stowed (and thus protected) during ascent, orbit, and initial re-entry. The probes are deployed during re-entry when the Orbiter has slowed to approximately Mach 3.5. Each probe includes a semispherical head with three pressure measurements. The center port (P_C) gives an indication of total pressure (P_{T_m}), and senses local total pressure when the probe is aligned with the local flowfield. The upper and lower ports (P_U and P_L) are sensitive to local flow angle. In addition, several static pressure ports (P_{S_m}) are located aft on the probe shaft, and a total temperature (T_T) sensor is located at the rear. The probes are connected to four air data transducer assemblies (ADTA's), redundant pairs per side, through pneumatic lines. The ADTA's house pressure transducers that convert the probe-measured pressures to electrical signals. Using the ADS calibrations, the general purpose computer (GPC) processes the ADTA signals to provide the basic air data parameters: static pressure, total pressure, and angle of attack. From these basic parameters, Mach number, dynamic pressure, pressure altitude, equivalent airspeed, and true airspeed are computed.

The ADS calibration relates a set of conditions that cannot be measured directly during flight (i.e., Mach number, angle of attack, etc.) to a set of parameters that can be measured (i.e., probe total, static, upper and lower pressures, and total temperature). In the wind tunnel, specific freestream conditions (i.e., static and total pressure, angle of attack, and Mach number) are known to a relatively high degree of accuracy. During a wind tunnel test these conditions are held constant, while the probe pressures are carefully measured and recorded. A schematic depicting the relationship between wind tunnel and flight measurements/calibration is shown in figure 2. The flight probe measurements are channeled through the calibration software to calculate the air data parameters as shown in figure 3.

Some of the more obvious "system" challenges for the Orbiter ADS were deployment/storage capability and system redundancy. A definition of when ADS deployment would occur depended on a trade between the high heat environment that occurs early in re-entry and where ADS information is needed to increase the GN&C system performance levels. From heating information and entry simulations a value near Mach 3.5 was agreed on. In actual practice the ADS parameters are computed in the GPC, compared with other available sources, as well as with the redundant air data sources, then if deemed good data, used at Mach 2.5 and below.

Redundancy was built into the system by having two probes (right and left) and two separate ADTA's for each pressure measurement. Because of this redundancy four sets of air data parameters were produced and a rating system was used for selection of the "best" data. A more detailed assessment of the ADS estimated performance and the system definition can be found in references 1 and 2.

WIND TUNNEL TEST PROGRAM

The ADS wind tunnel calibration development program initially consisted of one low subsonic calibration test of a complete 0.36 scale Orbiter with 0.36 scale side probes; one transonic test, one low supersonic test, and one high supersonic test of a 0.10 scale forebody model with 0.20 scale side probes. Because of physical size limitations, for the transonic and supersonic tests the smallest side probes that could be tested with at least pitot-static instrumentation or upper and lower pressure instrumentation in each probe, was 0.20 scale. The largest model size that could be tested without introducing significant blockage was 0.10 scale, resulting in a model-scale, probe-scale difference. Due to test data problems related to the scale difference the wind tunnel test program was expanded in the Orbiter aerodynamics (OA) series to that shown in table II.

Prior to wind tunnel model design and testing philosophy many compromises had to be decided upon. The full-scale Orbiter vehicle is over 107 feet long and the side probes are approximately 1 foot long. Testing facilities have model size constraints that were pushed to the limit. There were no model scaling problems with the 0.36 scale Orbiter. There were however, problems retaining the configuration fidelity on the 0.10 scale forebody model. In this case the model had to be shortened and was boat-tailed in the region of fuselage station 670 (full-scale) as shown in figure 4. In addition, as previously mentioned, the side probes were 0.20 scale in order to get two of the four pressure lines in one side probe (for PU and PL), and two in the other probe (for PS and PT). As much geometric similarity as possible was retained in the region of the side probes. For determining probe scale effects, the static pressure port standoff distance (Y_{PS}) and X-model station location (X_{PS}) were correctly simulated. For total pressure and angle of attack measurements, the 0.20 scale probe was moved aft such that the probe tip X-station corresponded to a 0.10 scale probe tip X-station. Further model/configuration duplication problems resulted because only a portion of the wing root could be retained. The effects of all of these model/full-scale vehicle differences on the probe measurements were investigated. In addition, differences in the vehicle outer mold line (OML) between the initial lines and the final configuration lines were assessed. The solution to these model scale and model fidelity problems was to use theoretical calculations where possible and run supplementary tests otherwise. Potential flow calculations were used to determine the effects of afterbody closure (boat-tail), model/probe scale mismatch, and OML duplication. Effects of the wing root/leading edge exclusion was measured in test OA-22. The results, in the form of pressure increments, were added to the basic data and an estimated uncertainty added in the accuracy analysis.

Data problems that resulted later during the actual testing were: facility reference static pressure differences, effects of model/probe scale mismatch (for the 0.10 scale forebody model), OML differences, and wind tunnel blockage effects. Facility reference conditions are dependent on when and how each facility performs their calibrations. The reference conditions were investigated by testing several standards and calibration devices that were available and comparing these with a slender cone-cylinder probe furnished by the manufacturer of the side probes. The results indicated differences from the reference probe from +1.0 percent to -1.5

percent of $\bar{q}$. During the later ascent air data system wind tunnel calibration program similar procedures were used.[3] These corrections were applied to all data used in subsequent analyses. The effect of model/probe scale mismatch (subsonically) is detailed in reference 2. Basically a larger effect was found from that estimated earlier by the theory, particularly at angles of attack where the theory assumes zero angle of attack. The effect of OML changes is also delineated in reference 2. Here, because of quite drastic configuration modifications in the nose area a new 0.10 scale forebody was constructed. Blockage effects were also determined by testing. Test OA237 was conducted using the smaller (0.10) scale model and the results were compared to the larger (0.36) scale model that was tested previously is this same facility. All of these aforementioned testing problems are discussed in more detail in reference 4.

CALIBRATION FORMULATION/IMPLEMENTATION

The development of the ADS calibration involved deriving a set of calibration parameters that relate the freestream conditions to the probe-measured conditions, using the wind tunnel derived data base. From the freestream conditions, the various air data parameters (Mach number, altitude, etc.) can be computed using basic aerodynamic equations. Analysis of the static pressure coefficient with Mach number indicated a "Mach Jump" region of extremely non-linear data. As the free stream Mach number increases to 1.0 and greater, a bow shock is formed that stands off the Orbiter nose. The bow shock delays the local Mach number at the side probe from reaching sonic speeds until the free-stream Mach number is in the range of 1.2 to 1.4. When the local flow reaches sonic speeds a very large rise in measured static pressure occurs and is referred to as the static pressure "Mach Jump". Figure 5 shows the variability of static pressure coefficient with Mach number. To avoid the extreme non-linearities in the onboard software implementation, static pressure is derived from a GPC stored standard atmosphere model for Mach numbers from 0.9 to 1.6.

Analyses of the wind tunnel data calibration parameters resulted in a set of polynomial equations with over 600 coefficients. For the on-board calibration, software storage limitations dictated 200 or less coefficients. Studies to reduce the number of coefficients indicated that by fitting the polynomials to concentrate on nominal trajectory conditions the number of coefficients could be reduced to 196.

Another potential error source was the on-board initialization of the calibration. The system begins with the previous Mach number (initially an assumed Mach number) to enter the calibration equations, but does not iterate with a corrected Mach number. Prior to STS-1, it was analytically shown that the rate of change of Mach number, and/or the calibration coefficients, was low enough to preclude a significant error. This analysis has been verified by flight results.

FLIGHT DATA ANALYSES

Post flight data from the ALT series were used to adjust the ADS calibrations in the subsonic flight regime. Data from the OFT series was used to adjust the ADS calibrations at the higher Mach numbers, where much smaller modifications were required.

APPROACH AND LANDING FLIGHT DATA

The ALT phase of the flight test program had a conventional flight test boom (FTB) installed in the nose of the Orbiter for the purpose of evaluating the subsonic wind tunnel calibration of the ADS using data from the FTB as a reference. In addition to FTB data, ground data in the form of radar and phototheodolite tracking, combined with weather balloon data, were used to verify the FTB. In order that the FTB data be used to correct the wind tunnel data, all potential sources of error had to be eliminated or accounted for. Adjustments and compensations were made to the FTB attitude data for the following effects: aerodynamic flowfield upwash and offset, FTB incidence and mounting misalignment, change in the aerodynamic flowfield due to vehicle pitch rate, and FTB structural deflections due to normal acceleration, pitch acceleration, and airloads. Pressure coefficients from the FTB were seen to be very accurate, with no calibration required for total pressure and only small adjustments for static pressure. The resulting flight data from the ALT series was used with the transonic and supersonic wind tunnel data to formulate the calibration for the OFT series.[5]

ORBITAL FLIGHT TEST DATA

The ADS calibration for OFT proved to be adequate for on-board use (see table I). For post-flight aerodynamic analysis, however, further refinements were developed from the flight programs to produce the best possible air data parameters for postflight analysis work. From Mach 3.5 to Mach 0.6, the meteorological static pressure was substituted for that derived by the ADS. From Mach 0.6 to landing gear deployment, corrections derived from a regression analysis technique were applied to angle of attack, static pressure, and total pressure. The resulting ADS calibration has generated air data that has been used in conjunction with flight-derived aerodynamic data to evaluate the performance of the Orbiter during re-entry.[6]

SUMMARY

The Shuttle ADS calibration was difficult to obtain because of the Orbiter unique flight regime, configuration, and operational characteristics. System challenges involved when to deploy the ADS probes to avoid reentry heating and how to handle the ADS redundancy requirement. During the wind tunnel calibration data discrepancies surfaced, with the major problems identified as: facility reference pressure, model/probe scale differences, OML changes and blockage effects. Calibration implementation challenges were "Mach Jump", on-board software limitations and air data calculation initialization. Each of these problems was surmounted by careful analysis of the existing data and by thorough design of supplementary testing to resolve the data discrepancies. Testing hardware and techniques were modified for on-going testing as required. The resulting preflight calibrations were modified using the ALT data (subsonic flight) to formulate the OFT calibration. Post-flight comparisons of OFT data showed the calibration to be adequate for operational flight. Further refinements were made, however, to assist in the evaluation of the aerodynamic characteristics of the Orbiter.

REFERENCES

1. Anonymous: Orbiter Air Data System Substantiation Report. Rockwell International, Space Transportation and Systems Group, SD75-SH-0038, Rev B, Dec. 1978.

2. Hillje, Ernest R.; and Tymms, David E.: Wind Tunnel and Flight Calibration of the Shuttle Orbiter Air Data System, AIAA Paper 78-792, April 1978.

3. Hillje, Ernest R.; and Tymms, David E.: The Ascent Air Data System for the Space Shuttle, AIAA Paper 80-0422, March 1980.

4. Tymms, David E.; and Hillje, Ernest R.: Calibration of the Orbiter Air Data System for Space Shuttle Orbital Flight Testing, presented at the 1980 Air Data Systems Conference, USAFA, Colorado Springs, CO, May 1980.

5. Tymms, David E.; and Hillje, Ernest R.: Subsonic Flight Calibration and Performance of the Space Shuttle Orbiter Air Data System, presented at the 1978 Air Data Systems Conference, USAFA, Colorado Springs, CO, May 1978.

6. Dean, Alden S.; and Mena, Arthur L.: The Calibration and Flight Test Performance of the Space Shuttle Orbiter Air Data System, presented at the NASA-Langley Conference on "Shuttle Performance: Lessons Learned", March 1983.

Table I. Orbiter Air Data System Parameter Requirements.

AIR DATA PARAMETER	SYMBOL	UNITS	FLIGHT PHASE UTILIZATION	SYSTEM REQUIREMENT		CREW DISPLAY
				RANGE	ACCURACY (% OF READING UNLESS NOTED) (3σ)	
GEODETIC ALTITUDE (PRESSURE ALTITUDE CORRECTED FOR NON-STANDARD ATMOSPHERE)	h_{pc}	FT	ENTRY & TAEM	10K TO 100K	±10%	YES
PRESSURE ALTITUDE RATE (SINGLE PROBE OPERATION ONLY)	$\dot{h}$	FPS	TAEM	0 TO -600	±10 FPS OR ±5% W/E IS GREATER	YES
			A/L	0 TO -250	±2 FPS OR ±5% W/E IS GREATER	
DYNAMIC PRESSURE	$\bar{q}$	PSF	TAEM & A/L	90 TO 375	±10%	NO
MACH NUMBER	M	—	TAEM	0.6 TO 2.5	±10%	YES
			A/L	0.25 TO 0.6	±10%	
TRUE AIRSPEED	V_T	FPS	TAEM	600 TO 2500	±10%	NO
			A/L	250 TO 600	±10%	
EQUIVALENT AIRSPEED	V_e	KTS	TAEM & A/L	160 TO 335	±5%	YES
		FPS	A/L	112 TO 270	±5%	
ANGLE OF ATTACK	α	DEG	TAEM & A/L	-4 TO +20	$\pm 2^0$	YES

Table II. Orbiter Air Data System Wind Tunnel Program

TEST	MODEL SCALE		MACH RANGE	FACILITY	PURPOSE
	ORBITER	PROBE			
OA-22	0.03	None	0.6 → 1.5	ARC 11x11, 9x7	Pressure survey
OA-143	0.03	None	0.25	Rockwell NAAL	Pressure survey
OA-100	0.36	0.36, FTB	0.25	ARC 40x80	Development
OA-164	0.36	0.36, FTB	0.25	ARC 40x80	Development (Contd.)
OA174	0.36	0.36	0.25	ARC 40x80	Verification
OA-161A,B,C	0.03	None	0.6 → 3.5	ARC 11x11, 9x7, 8x7	Pressure and local survey
OA-220	0.10 (forebody)	0.20, FTB	0.3 → 1.1	ARC 14x14	Development
OA-224	0.10 (forebody)	0.20	0.2 → 1.3	LaRC 16-ft transonic	Verification
OA-228	0.10 (forebody)	0.20	0.25	Rockwell NAAL	Static pressure comparison
OA-237	0.10 (forebody)	0.10, 0.20	0.25	ARC 40x80	Scale and blockage
OA-232	0.10 (forebody)	0.10, 0.20	0.2 → 1.3	AEDC 16T	Scale and blockage
OA221B,C	0.10 (forebody)	0.20	1.5 → 3.5	ARC 9x7, 8x7	Development
OA-234	0.10 (forebody)	0.10, 0.20	2.0 → 3.5	LeRC 10x10	Verification
OA-238	0.10 (forcbody)	0.10	0.25	Rockwell NAAL	Scaled probes
OA-251B,C	0.10 (forebody)	0.10, 0.20	1.5 → 3.5	ARC 9x7, 8x7	Verification
Other tests:					
OA-236	Tunnel Calib. Probes		0.25	Rockwell NAAL	Facilities calibration comparison

ARC=Ames Research Center, NAAL=North American Aero. Lab., LaRC=Langley Research Center, LeRC=Lewis Research Center

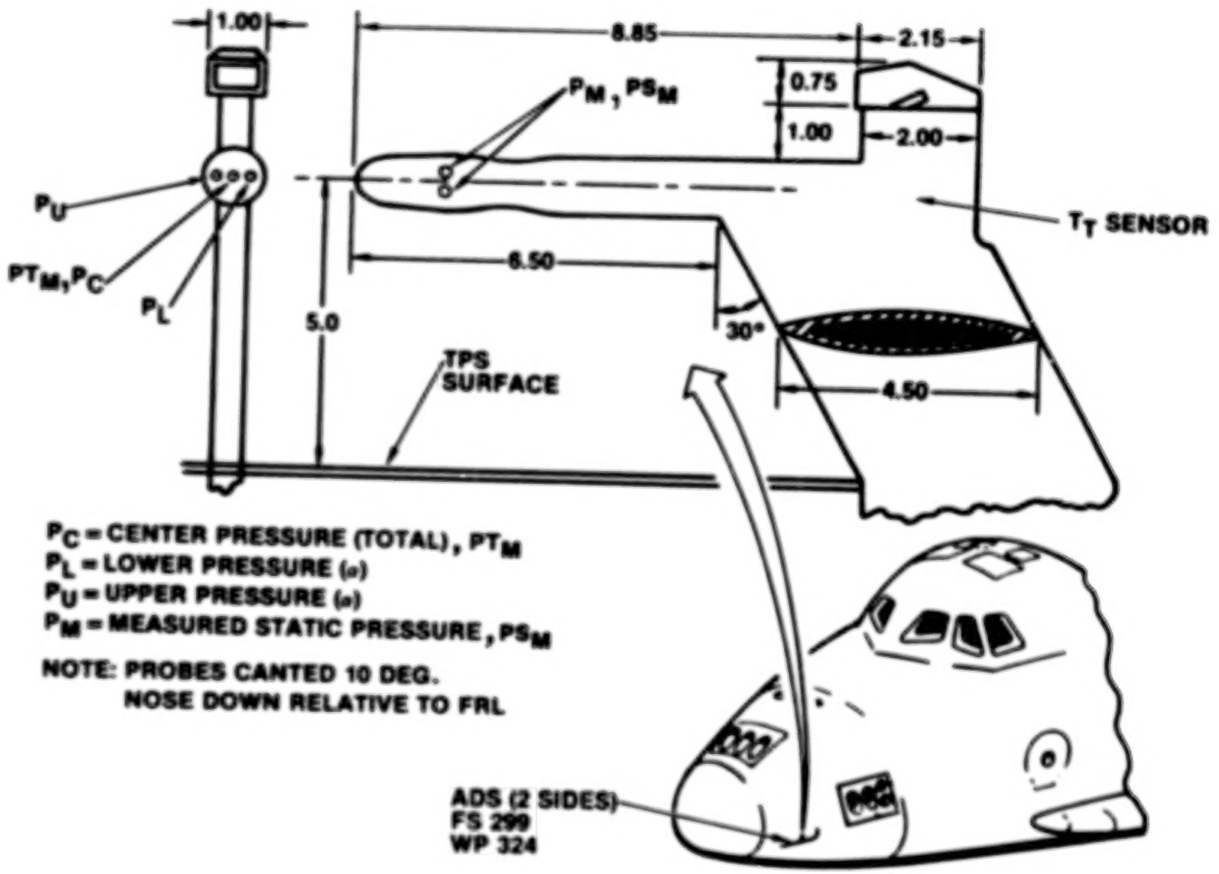


Fig. 1 Orbiter ADS Probe Geometry (All Measurements In Inches)

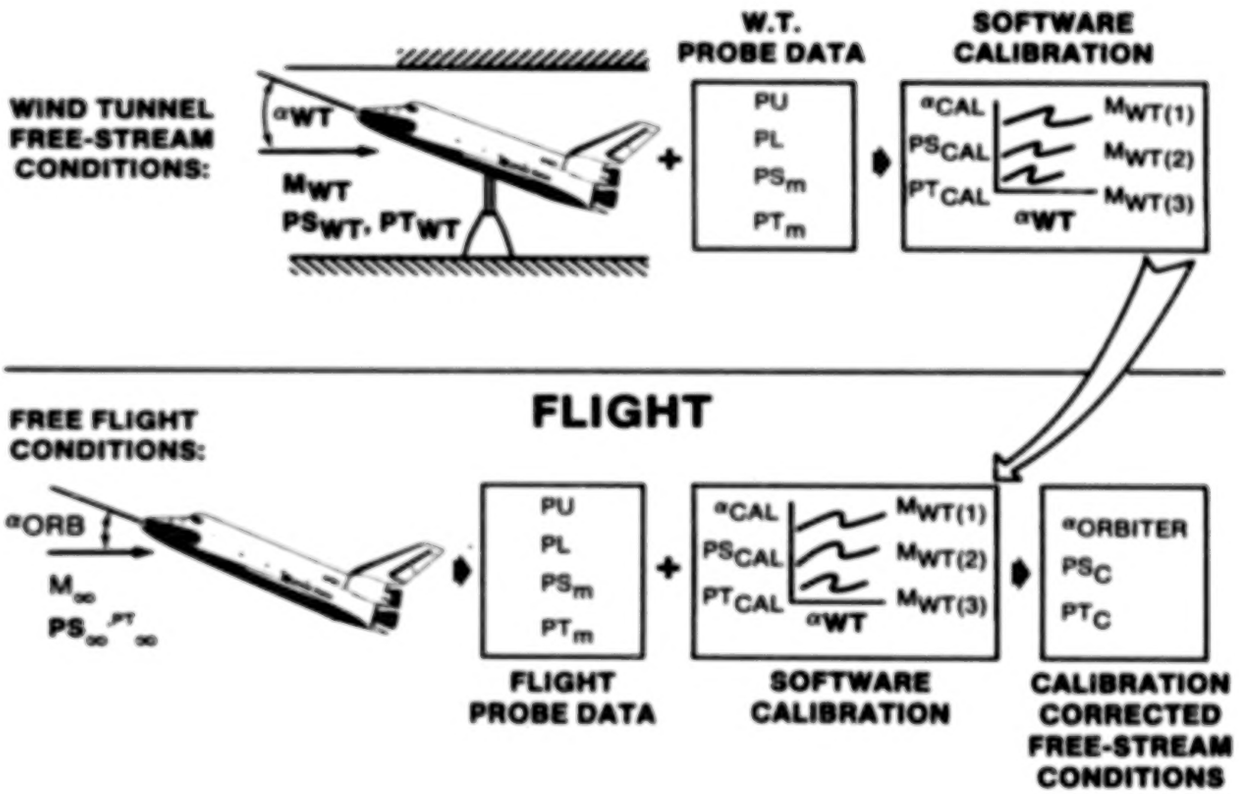


Fig. 2 Wind Tunnel ADS Calibration/Flight Usage

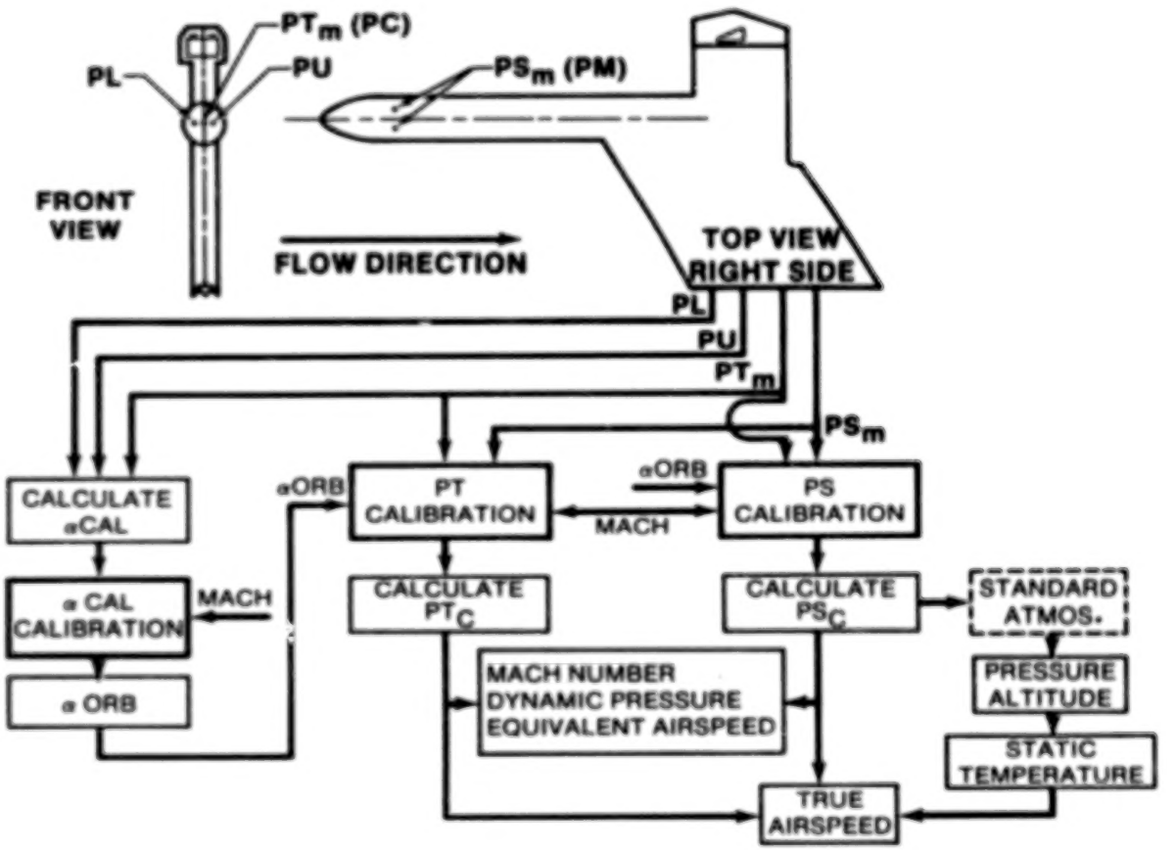


Fig. 3 Operational ADS Software Calculations

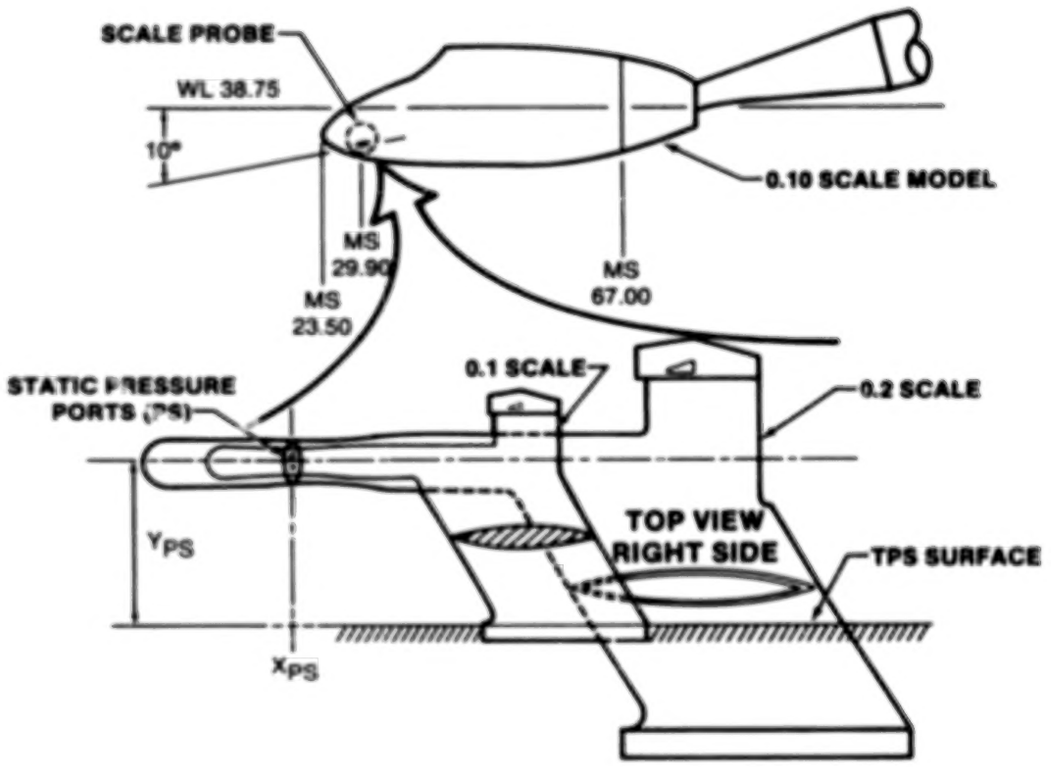


Fig. 4 Side Probe/Model Scaling Compromises

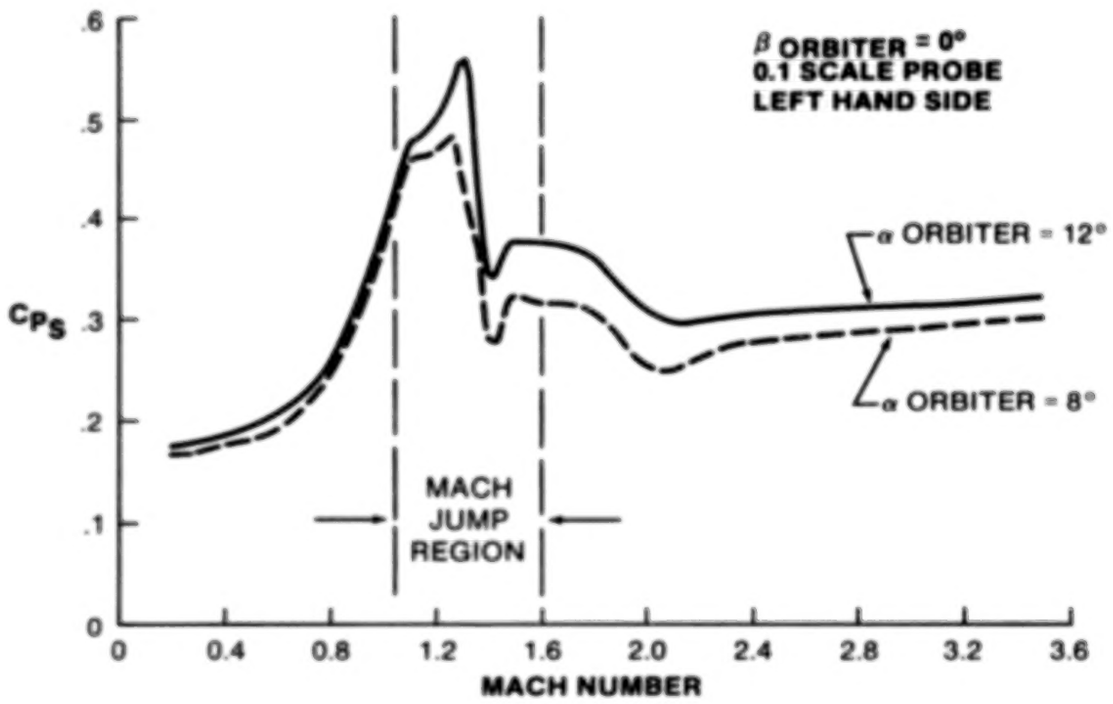


Fig. 5 Variation of Static Pressure Coefficient with Mach Number

N85
16913

UNCLAS

N85-16913

SHUTTLE STRUCTURAL DYNAMICS CHARACTERISTICS, THE ANALYSIS AND VERIFICATION

C. Thomas Modlin, Jr., and George A. Zupp, Jr.
NASA Lyndon B. Johnson Space Center
Houston, Texas 77058

INTRODUCTION

The building and operation of the Space Shuttle represents a milestone in the U.S. space program. The Shuttle is the first manned spacecraft to be reusable; on its first flight on April 12, 1981, it successfully carried astronauts and a payload into Earth orbit.

Up to this point in space exploration, a launch vehicle had to successfully complete an extensive and comprehensive flight test program before being man rated. The Shuttle program philosophy, on the other hand, was to use key element testing and verified analytical models to certify the reliability of the Shuttle launch configuration.

Several engineering disciplines relied heavily on verified analytical models of the Space Shuttle, i.e., the disciplines of structural dynamics, pogo, and flutter. The verification of these models employed laboratory control testing to develop data critical to math model verification. The basic philosophy was to correlate analysis and testing to an acceptable degree of accuracy and infer from this that the launch vehicle dynamics could be predicted with the same accuracy.

During the phase B period of the program, analytical studies pointed up unique dynamic characteristics of the parallel burn configuration, in particular, a very high modal density with 200 structural modes below 20 hertz in combination with a wide spectrum of conditions involving a wide variety of dynamic problems (fig. 1). Studies conducted at the NASA Langley Research Center (LaRC) on a 1/8-scale dynamic model reinforced these concerns, and the results indicated the substantial influence of element interface stiffness on the primary low frequency modes of the system.

Immediately after approval to proceed with the Shuttle, particular emphasis was placed on developing a technical plan of action that would ensure early resolution of the key issues in the structural dynamics area. The testing portion of the verification plan that evolved consisted of three major parts: the 1/4-scale dynamics model program to provide early data, tests of full-scale elements, and a full-scale mated vertical ground vibration test (fig. 2). In the development of the 1/4-Scale Model Program, emphasis was placed on investigating enough propellant conditions to adequately represent the flight configurations from lift-off to end burn and to minimize the requirements for full-scale testing.

Further attention was directed toward planning analytical activities to support hardware development and ground testing. User requirements for structural loads, flight control, pogo, and flutter were identified and, where required, specific models were generated to meet the discipline's need.

The plan established the mechanics for generating and updating the structural dynamic math models. Each element contractor was responsible for generating and updating the models of his elements, and the system contractor was responsible for identifying requirements to the element contractor and for integrating the complete model. The objective of this system was to require each contractor to be responsible for the element-unique models and their verification. Schedules were established for the development of the structural math models to support the Shuttle program milestones, the element milestones, and the ground vibration test program.

Extensive testing was also conducted to support the verification of the pogo and flutter forcing function models. Since each of these disciplines utilizes the structural dynamic model, the testing verification was oriented toward defining the associated closed-loop forcing function. In the case of pogo, where pogo suppressors on the Space Shuttle main engines (SSME's) were baselined early in the program, the testing primarily addressed the SSME dynamics and suppressor characteristics. This was accomplished through the pulsing of the oxygen feed system to the main engines and measuring the attenuation or amplification of the pulse signal through the system. From these data, the system characteristics were extracted and used in the pogo stability analysis. The flutter models were verified using the same philosophy. Flutter testing was extensive, using wind tunnel testing with aeroelastically scaled models.

The final verification procedures of these models did require an assessment of flight data, with the bulk of these data being developed from STS-1 to STS-5. Approximately a thousand developed flight measurements were involved.

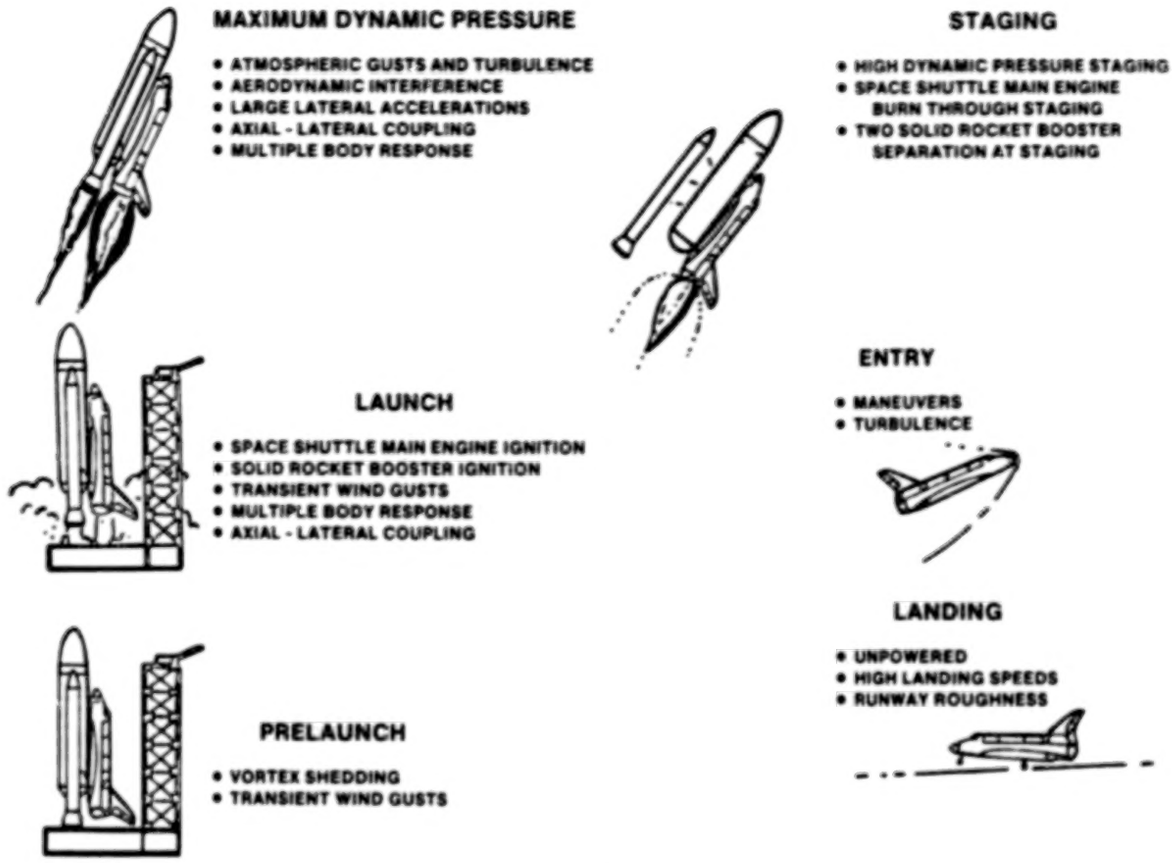


FIGURE 1.- SPECTRUM OF SHUTTLE DYNAMIC CONFIGURATIONS.

STRUCTURAL DYNAMICS

The Space Shuttle introduced a new dimension in the complexity of the structural dynamics of a space vehicle. The four-body configuration exhibited structural frequencies as low as 2 hertz with a model density on the order of 10 modes per hertz.

The structural dynamic mathematical models are derived from the "stress model," which is a detailed finite-element model of the Space Shuttle structure. The stress model has approximately 50 000 degrees of freedom (fig. 3). The dynamic models were derived from the stress model by various reduction techniques, and each has on the order of 1000 degrees of freedom.

The degrees of freedom that are retained in the dynamic models are designed to satisfy user requirements, i.e., disciplines such as pogo, dynamic loads, flutter, and flight control. For example, in the pogo structural models, a finer grid is retained in the Orbiter thrust structure and in the liquid oxygen (LOX) feed system. Since the hydrodynamics of the propellant are important to the pogo stability analysis, a hydroelastic model of the external tank (ET) is employed. Similar fidelity is preserved in critical areas of the vehicle as defined by the disciplines of dynamic loads, flutter, and flight control.

One prime driver in the degree of reduction of the model is the economy of computer operation. By virtue of the limits on computer size and speed, the eigen solutions of the reduced model will be small in comparison to the stress model. Therefore, it is of paramount importance that the frequencies and mode shape that are critical to the user are preserved to an acceptable accuracy during the reduction process.

In the verification process, certain mode shapes and frequencies were identified by the users as more important than others and, as such, the test objectives were oriented toward experimentally extracting those modes and frequencies for analysis and test correlation purposes. To provide the necessary experimental data, a series of ground vibration tests (GVT's) was conducted using test articles ranging from the 1/4-scale structural replica of the Space Shuttle to the full-scale vehicle.

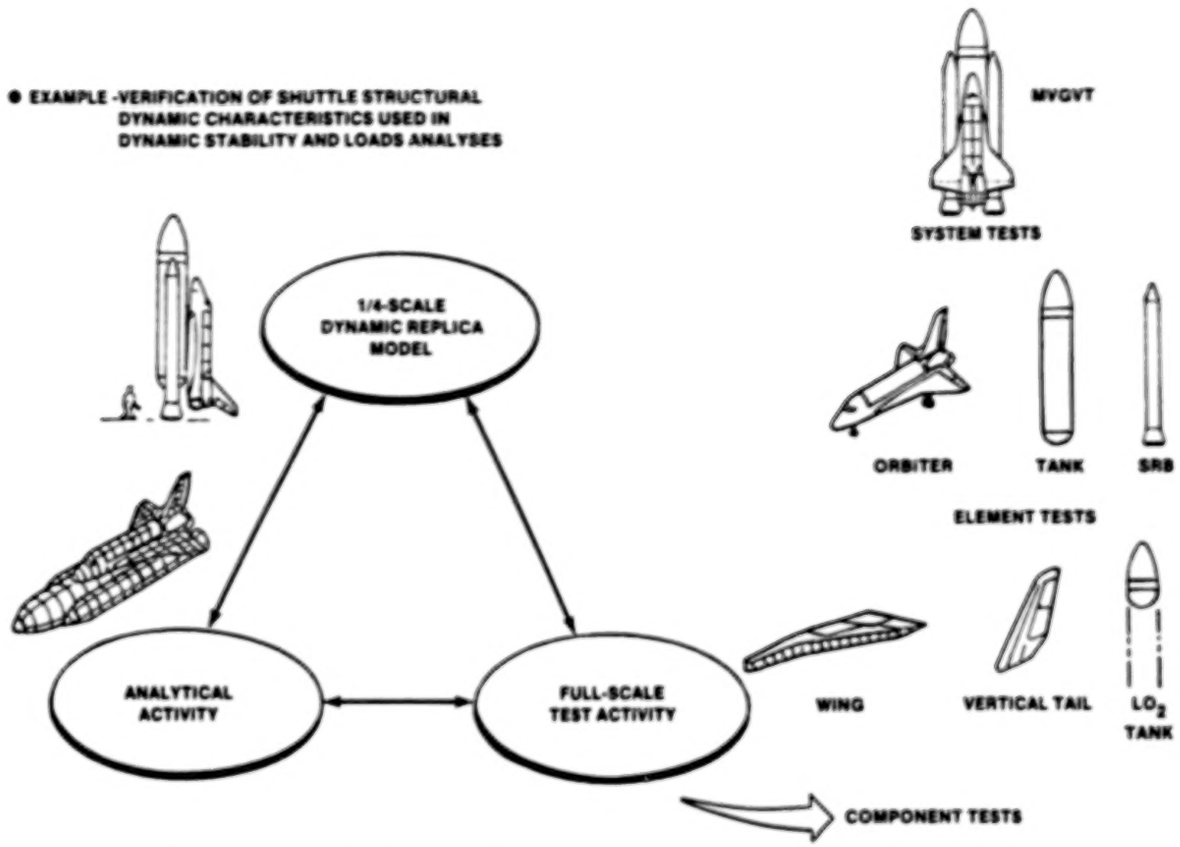


FIGURE 2.- "BUILDING BLOCK" APPROACH TO AN UNDERSTANDING OF SHUTTLE STRUCTURAL DYNAMICS.

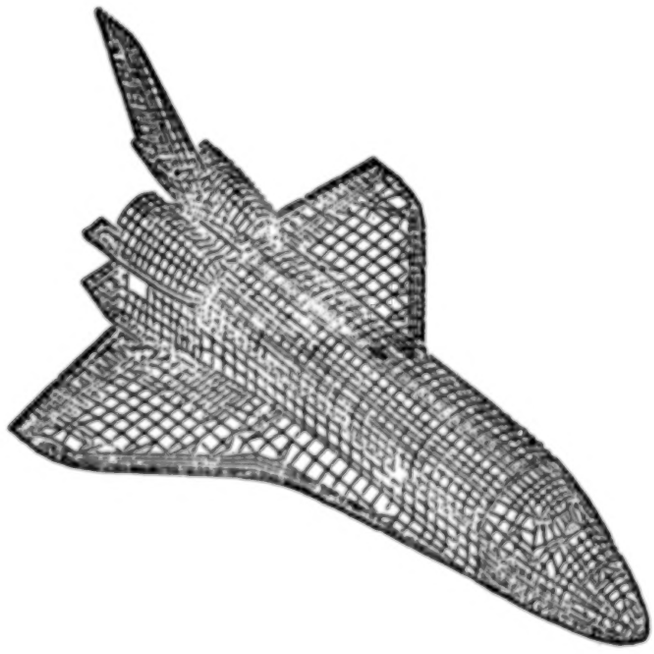


FIGURE 3.- OVERALL VIEW OF STRESS FINITE-ELEMENT MODEL.

GROUND VIBRATION TESTING

The Space Shuttle GVT program was designed to provide structural dynamic data early in the program so that if problems did occur, the solutions could be implemented with a minimum of program cost and schedule impact. The Langley Research Center was the first to start a vibration test program using a 1/8-scale structural model (refs. 1 and 2). Although the model replication was coarse, the overall configuration was representative of the Space Shuttle. The early LaRC data indicated the presence of low frequency structural modes associated with the four-body configuration and the importance of the interface stiffness on these modes. Also of concern was the lack of a verificd analysis of the ET hydroelastic characteristics.

To develop the necessary experimental data for math model verification, three basic GVT programs were baselined in the Shuttle development schedule. These were the horizontal ground vibration test (HGVT), the 1/4-scale model GVT, and the mated vertical ground vibration test (MVGVT). The test and analysis schedule spanned the years from 1974 to 1981 (fig. 4).

In all major GVT programs, shakers were used to excite the structure and accelerometers were used to measure the structural response. A system known as the Shuttle Modal Test and Analysis System (SMTAS) was used to control and process the test data. The excitation was in the form of sine dwells, and sine sweeps. The frequency range of excitation was from 1.5 to 50 hertz. The test articles were usually instrumented with more than 300 accelerometers, of which about 60 accelerometer channels would be processed simultaneously during a dwell period. The vehicle instrumentation philosophy assumed that the vehicle was symmetric about the longitudinal axis, and, as such, the modal extraction would be either a symmetric or an antisymmetric mode. In selected cases, asymmetric modes were extracted. The test system, SMTAS, has an illustrative feature that computes the orthogonality between a test mode and an analytical mode. The mass matrix, [m], in this calculation was derived from the analytical model and reduced to the appropriate accelerometer grid locations. The test, Φ_{test}, and analysis, $\Phi_{analysis}$, mode shapes were normalized in such a manner that for a perfect mode shape correlation

$$\Phi^{T}_{test} \; [m] \; \Phi_{analysis} = 1$$

This feature gives a quantitative measure of the quality of the mode shape comparison between test and analysis. Judgment has to be exercised in the interpretation of the cross orthogonality calculation because of inherent error due to coarse gridding and reduction of the mass matrix to the test grid location.

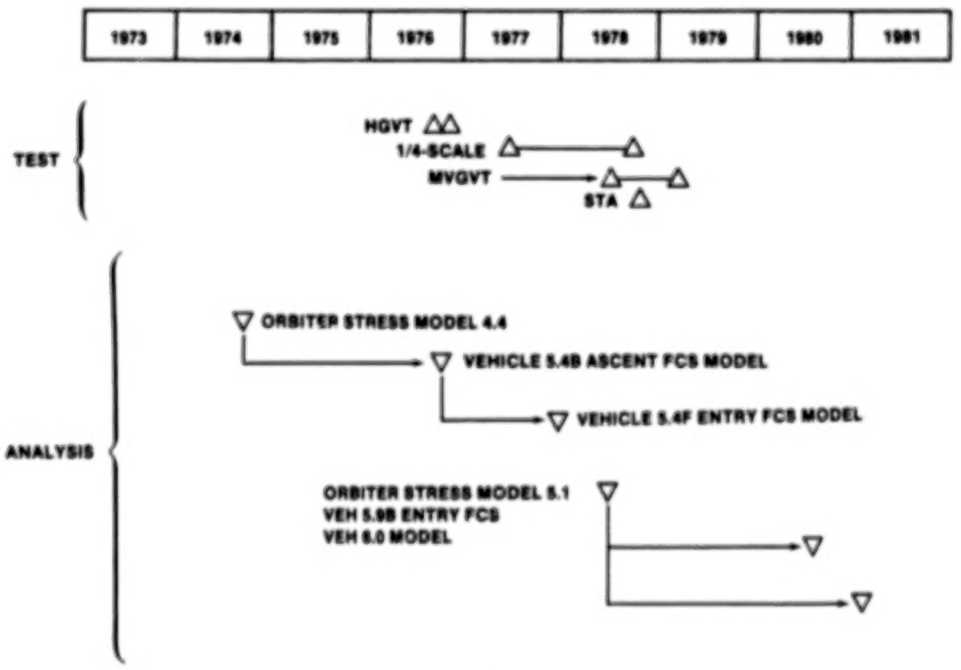


FIGURE 4.- CHRONOLOGY OF THE SHUTTLE STRUCTURAL MATH MODEL AND GROUND VIBRATION TESTS.

HORIZONTAL GROUND VIBRATION TEST

The HGVT article was the Orbiter 101 (OV-101) vehicle (the Orbiter used in the Approach and Landing Test (ALT)). These tests were conducted in the summer of 1976 at Palmdale, California. This was the first opportunity to get quality structural dynamic data for math model verification. Although OV-101 was not identical to the Orbiter 102 (OV-102) vehicle (the Orbiter used in the first Shuttle launch), the differences were accounted for in the structural math model. The primary differences were in the areas of the OMS pod (OV-101 did not have OMS pods but these were simulated by a "boiler-plate" cover), the thrust structure (the thrust structure was not boron epoxy as it was in the case of OV-102), and the vertical fin (the vertical fin was made up of a skin and stringer configuration vs. integrally machined for the OV-102 flight vehicle). The payload in the Orbiter during testing was the Development Flight Instrumentation (DFI) package, which weighed approximately 10 000 pounds.

There were two basic test configurations: the Orbiter supported in a "free-free" condition to simulate the entry and landing configurations, and the Orbiter rigidly attached to the ground at the ET/Orbiter interface to simulate the boost configuration (figs. 5 and 6). Ferry locks also secured the control surfaces during testing. The test objectives were to determine experimentally selected mode shapes, frequencies, and modal damping in the frequency range from 0.5 to 50 hertz, and to acquire frequency response data at the Orbiter guidance and control sensor locations. Table 1 is a comparison of analysis frequencies and test frequencies for the free-free, or soft mount, configuration. As the analysis indicates, the structural mode shapes are quite complicated and are not generally amenable to classic descriptions, but the modal descriptions noted in table 1 are the areas of primary motion in the noted mode.

The major results from these tests were (1) the identity of friction in the payload bay door shear pins, which had the effect of increasing the pitch bending stiffness of the fuselage, (2) the modal damping, and (3) the lack of analytical correlation of the center-mounted rate gyros on the 1307 bulkhead. The modal damping data extracted from these tests were invaluable to flight controllers in the final verification of the entry flight control stability assessment. For a detailed comparison between test and analysis, refer to reference 3.

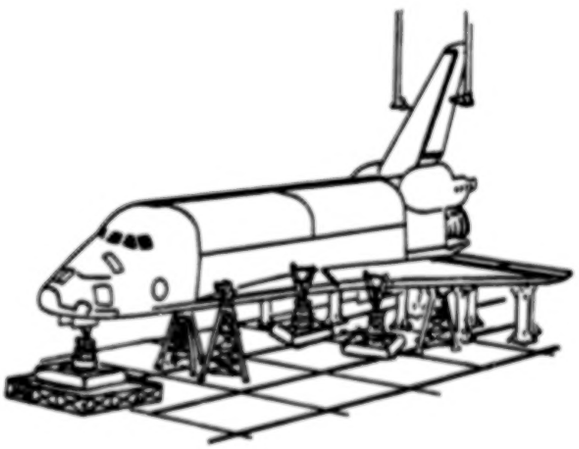


FIGURE 5.- SOFT HORIZONTAL GROUND VIBRATION TEST ARRANGEMENT.

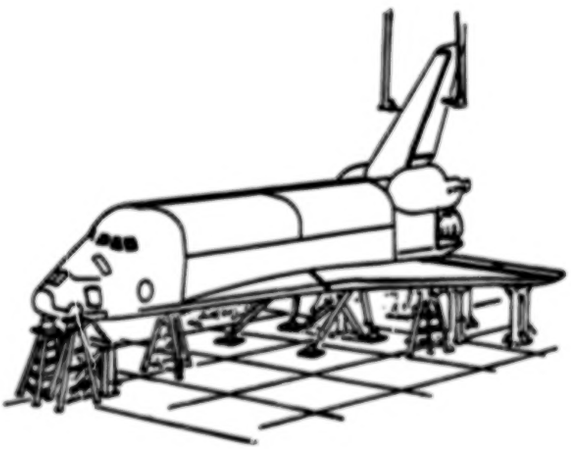


FIGURE 6.- RIGID HORIZONTAL GROUND VIBRATION TEST ARRANGEMENT.

TABLE 1.- COMPARISON OF TEST AND ANALYSIS FREQUENCIES FOR THE FREE-FREE, OR SOFT MOUNT, HGVT (10^{K} PAYLOAD)

Modal description	Analytical frequency, Hz	Test frequency, Hz
First fuselage bending (X-Y plane)	5.09	5.97
First wing bending (Y-Z plane)	7.86	7.31
First vertical fin bending (Y-Z plane)	4.15	3.80
First vertical fin torsions	17.20	14.27

QUARTER-SCALE STRUCTURAL MODEL

The 1/4-scale model program was started in early 1975 for the purpose of developing high-quality structural dynamic data early in the Shuttle program that would be representative of the first Shuttle flight configuration. The structural model was a high-fidelity replication of OV-102, the standard ET, and three flight configurations of the solid rocket booster (SRB) (ref. 4). The 1/4-scale program was the most comprehensive element in the Shuttle GVT program. Of the test articles used in the vibration test program, the 1/4-scale model was structured most like the flight hardware.

The 1/4-scale vibration test configuration included the following.

1. Orbiter/ET/SRB configuration (with 45^k "rigid" payload)

    a. Lift-off
    b. Maximum dynamic pressure
    c. Pre-SRB separation

2. Orbiter/ET configuration (with 45^k "rigid" payload)

    a. Start boost
    b. Mid boost
    c. End boost

3. Orbiter element (with and without 45^k "rigid" payload)

4. ET element, 13^o tilt

5. SRB element

During testing, water was used to simulate the LOX in the ET and the weight and hydroelastic effects of the liquid hydrogen (LH) in the hydrogen tank were neglected. This procedure was also used in the MVGVT.

To complement the vibration test program, load-deflection tests were conducted on the SRB and the ET. The load-deflected tests were designed to provide data that could be used to resolve anomalous or unexplained vibration test data. Primarily, the load-deflection data supported the verification of the stiffness matrix in the idealized structural model.

At the start of the 1/4-scale program, there were several areas that presented problems in structural dynamic modeling. These were the ET hydroelastic analysis, the interface stiffnesses between the elements, the SRB propellant and internal pressure effects on the system structural modes, and the payload bay door effectivity in the Orbiter fuselage pitch bending stiffness.

Because of the pogo requirements for a high-fidelity hydroelastic analysis, the hydroelastic model of the ET was of particular concern in the early stages of the program. The lack of correlation between test and analysis with LaRC data indicated that the same deficiency could be expected from the hydroelastic analysis of the ET; therefore, several 1/4-scale tank configurations were selected for testing. In parallel, the Martin Marietta Company was developing a new hydroelastic analysis which became available before 1/4-scale testing. The quality of correlation between the upgraded hydroelastic analysis and the ET vibration data was judged excellent and provided the confidence in the analysis that allowed a reduction in scope of the ET vibration testing. Generally, the analysis frequencies were higher than the test frequencies. These differences were attributed to internal pressure effects in the LOX tank and the LH tank.

The Orbiter test verified the presence of friction in the payload bay door shear pin sufficient to effectively increase the pitch bending stiffness at low excitation levels. This increase in stiffness increased the bending frequency above that of the predicted value. The use of higher excitation forces on the structure overcame the friction in the shear pins and thereby allowed relative motion between the door bays and consequent reduction of the bending stiffness and frequency. The reduction in frequency was consistent with pretest analysis.

Several Orbiter configurations were tested that addressed the effects of payload weight on the Orbiter vibration characteristics. Ground vibration tests were also conducted with payload bay doors opened to simulate the on-orbit configuration.

The SRB tests identified several areas in the math model that required additional study. These were (1) the ET/SRB interface, which required additional detail in the finite-element model, (2) the incorporation of a representative shear modulus for the propellant, and (3) the incorporation of the internal pressure effects on shell stiffness. The posttest analysis incorporated changes in the math

model that corrected some of these deficiencies. The internal pressure effects on the shell stiffness were handled emperically; the shear stiffness effects of the propellant were still in a state of iteration at the time of MVGVT. Comparisons of the test and analysis frequencies for the Orbiter test and the Orbiter/ET/SRB lift-off test are presented in tables 2 and 3, respectively. A detailed presentation of 1/4-scale model test data and analysis can be found in reference 5.

TABLE 2.- COMPARISON OF TEST AND ANALYSIS FREQUENCIES FOR THE "FREE-FREE" 1/4-SCALE ORBITER GVT (45^k PAYLOAD)

Modal description	Analytical frequency, Hz	Test frequency, Hz
First fuselage bending (X-Y plane)	4.6	4.8
First wing bending (Y-Z plane)	7.0	6.6
First vertical fin bending (Y-Z plane)	3.9	3.6
First vertical fin torsion	14.0	12.8

TABLE 3.- COMPARISON OF TEST AND ANALYSIS FREQUENCIES FOR THE "FREE-FREE" 1/4-SCALE ORBITER/ET/SRB LIFT-OFF CONFIGURATION (45^k PAYLOAD)

Modal description	Analytical frequency, Hz	Test frequency, Hz
SRB roll (antisymmetric)	2.0	1.8
SRB roll (antisymmetric)	2.0	2.0
First vertical fin bending (Y-Z plane)	3.7	3.4
First wing bending (X-Z plane)	6.3	6.4

MATED VERTICAL GROUND VIBRATION TEST

The MVGVT was the final major test program in the structural dynamic model verification plan. These tests were conducted between the summers of 1978 and 1979 at the NASA George C. Marshall Space Flight Center (MSFC) in Huntsville, Ala. The primary objectives of these tests were to experimentally obtain full-scale structural mode shapes, frequencies, damping data, and transfer functions at selected flight control sensor locations. The test configurations (figs. 7 and 8) were as follows.

1. Orbiter/ET/SRB configuration (payload 10^k)

    a. Lift-off
    b. Pre-SRB separation

2. Orbiter/ET configuration (payload 10^k)

    a. Start boost
    b. Mid boost
    c. End boost

The modal data extracted from these tests compared favorably with the modal data derived from 1/4-scale model testing when the known configuration differences were considered. Presented in table 4 is a comparison between test and analysis frequencies and the associated modal damping presented as percent of critical damping for the MVGVT lift-off configuration.

The major result of these tests was the identification of local resonances in the area of the SRB rate gyro locations. These resonances had the effect of corrupting the sensor signals, which, if occurring in flight, would have the effect of a lost sensor. Other anomalies were also noted on the Orbiter side-mounted rate gyros.

The issue raised during 1/4-scale testing concerning SRB propellant stiffness was not resolved. Because of the nonlinear viscoelastic properties of the SRB propellant, the eventual resolution of

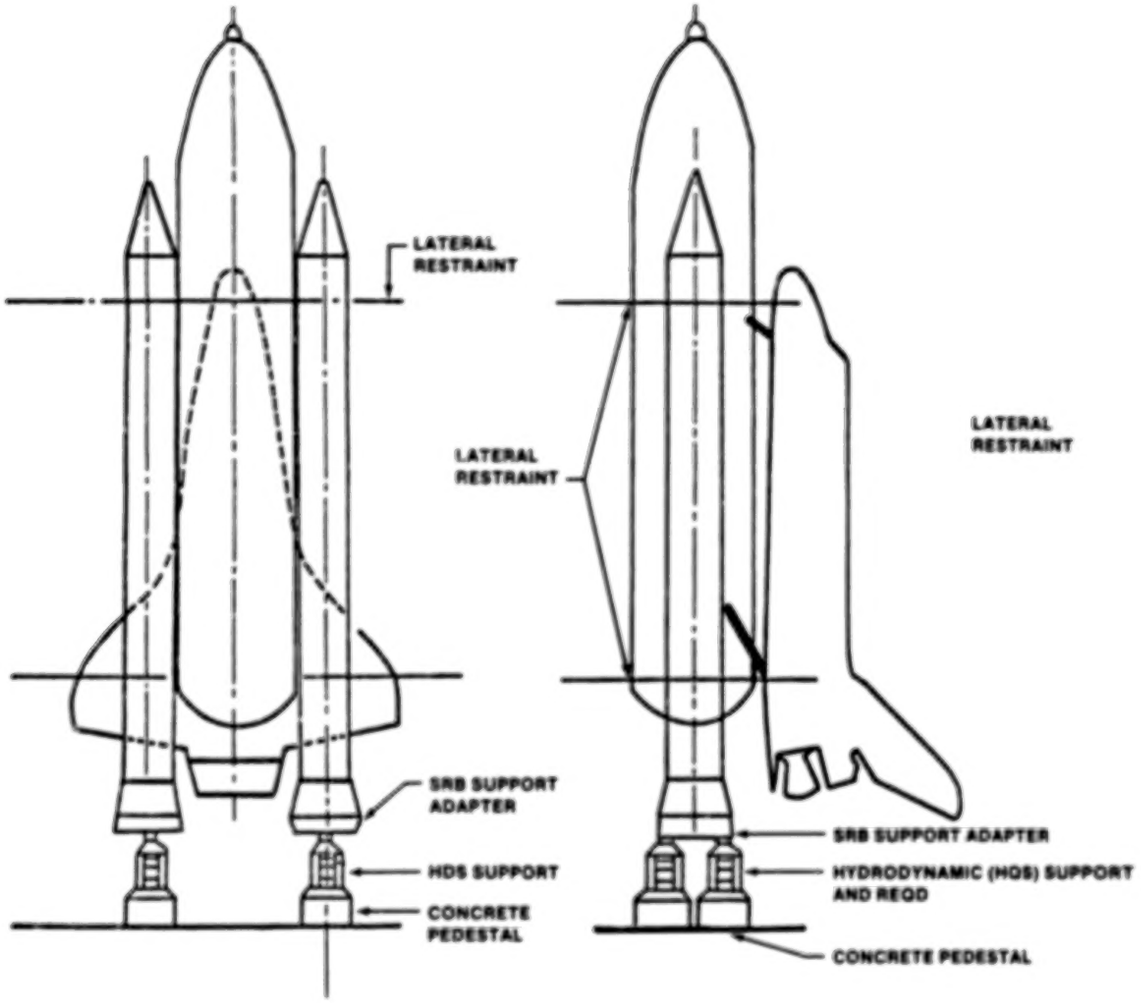


FIGURE 7.- SUSPENSION SYSTEM FOR THE SPACE SHUTTLE (FOUR-BODY CONFIGURATION).

this problem was through adjusting the analysis via the propellant shear stiffness to agree with test data. Fortunately for the users of the structural dynamic models, the structural modes with significant SRB propellant motion had relative high damping and were not significant in the performance of the various user disciplines.

The structural damping data extracted from these tests ranged from a low of about 0.1 percent for the modes with significant fluid motion to more than 10 percent for certain "local" modes. The average modal damping ranged from 1 to 3 percent. The damping data were extremely valuable in the final certification of the flight control stability margins in that measured damping values in the critical flight control modes were higher than the initial baseline of 0.5 percent.

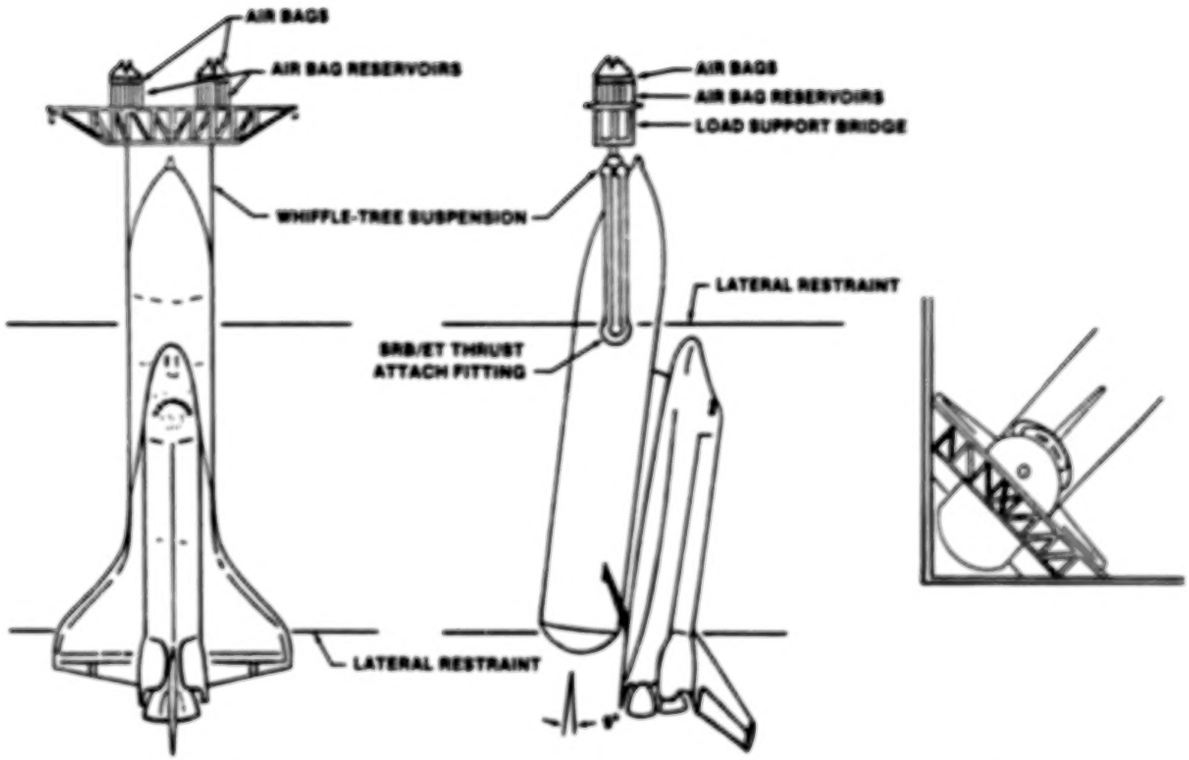


FIGURE 8.- SUSPENSION SYSTEM FOR THE ORBITER/ET CONFIGURATION (TWO-BODY CONFIGURATION).

TABLE 4.- COMPARISON OF TEST AND ANALYSIS FREQUENCIES FOR THE "FREE-FREE" MVGVT LIFT-OFF CONFIGURATION (10^K PAYLOAD)

Modal description	Analytical frequency, Hz	Test frequency, Hz	Damping c/cc
SRB roll (antisymmetric)	1.88	2.08	0.01
SRB roll (symmetric)	1.90	2.05	.013
First Orbiter bending (Y-Z plane)	2.97	3.24	.01
First wing bending (Y-Z plane)	6.70	6.43	.037

SUMMARY

The advent of the Space Shuttle presented unique challenges to the structural dynamics analyst in the sense that the analytical models had to be verified to an acceptable accuracy before a manned launch. This objective was accomplished in the Shuttle program by an extensive vibration test analysis program. The three main vibration test programs were MGVT, 1/4-scale model GVT, and the MVGVT. Significant analytical effort was committed to modeling the test configuration. The correlation of these results provided a foundation for model certification.

The structural dynamic model used provided an invaluable input into the certification process by defining the structural dynamic elements and modes that were critical to the discipline analysis. For example, to improve the accuracy of predicting the dynamic response of Orbiter payloads during landing and lift-off, increased fidelity in the modeling of the Orbiter longerons and payload interfaces was required.

Generally, the vibration test and analysis program revealed that the mode shapes and frequency correlations below 10 hertz were good. The quality of correlation of modes between 10 and 20 hertz ranged from good to fair and that of modes above 20 hertz ranged from poor to good. Since the most important modes, based on user preference, were below 10 hertz, it was judged that the Shuttle structural dynamic models were adequate for flight certifications.

REFERENCES

1. Blanchard, U. J.; Miserentino, R.; and Leadbetter, S. A.: Experimental Investigation of the Vibration Characteristics of a Model of an Asymmetric Multielement Space Shuttle. NASA TN D-8448, 1977.

2. Pinson, L. D.; and Leadbetter, S. A.: Some Results from 1/8-Scale Shuttle Model Vibration Studies. J. Spacecraft & Rockets, vol. 16, Jan.-Feb. 1979, pp. 48-55.

3. Bejmuk, Bohdan: Space Shuttle Vehicle and System Dynamics Data Book, vol. 1A, Orbiter 101 Horizontal Ground Vibration Test Data Book, Rockwell International SD-75-SH-0032, Dec. 1976.

4. Emero, Donald H.: The Quarter-Scale Space Shuttle Design, Fabrication, and Tests. J. Spacecraft & Rockets, vol. 17, no. 4, July-Aug. 1980.

5. Ujihara, B. H.; Guyan, R. J.; et al.: Baseline Quarter-Scale Ground Vibration Test. Rockwell International STSB0-0187, July 1980.

6. Ujihara, B. H.; Jennings, S. J.; Guyan, R. J.; and Barrett, J. R.: Mated Vertical Ground Vibration Test Engineering Analysis Report. Rockwell International STSB0-0038, Mar. 1980.

7. Bugg, Frank: Viscoelastic Propellant Effects on Space Shuttle Dynamics. NASA TM-82403, Mar. 1981.

N85
16914

UNCLAS

D25

N85-16914

STRUCTURAL LOAD CHALLENGES DURING SPACE SHUTTLE DEVELOPMENT

Alden C. Mackey
NASA Lyndon B. Johnson Space Center
Houston, Texas 77058

Ralph E. Gatto
Rockwell International
Downey, California 90241

ABSTRACT

The challenges that resulted from the unique configuration of the Space Shuttle and capabilities developed to meet these challenges are described. Discussed are the methods and the organization that were developed to perform dynamic loads analyses on the Space Shuttle configuration and to assess dynamic data developed after design. Examples are presented from the dynamic loads analysis of the lift-off and maximum dynamic pressure portion of ascent. Also shown are Orbital Flight Test results, for which selected predicted responses are compared to measured data for the lift-off and high-dynamic-pressure times of ascent.

INTRODUCTION

The challenge of the Space Shuttle was to develop a system which had optimum structural weight, structural integrity, and the operational flexibility to carry a wide variety of payloads to Earth orbit. The Space Shuttle structural system, which had a unique combination of configuration, environments, and operating procedures, represented the greatest challenge to the dynamic loads analyst in the history of space vehicle design. This configuration had four bodies connected in parallel, whereas all previous space vehicle configurations were axisymmetric (sometimes with strapped-on motors). The Orbiter had wings and a vertical tail, whereas no previous configurations had aerodynamic surfaces. Three of the four bodies had thrust forces in the millions of pounds. The winged Orbiter configuration and the proximity of the external tank (ET) and the solid rocket boosters (SRB's) resulted in complex and difficult to define forces and pressure distributions on all of the bodies, whereas previous space vehicles had the relatively clean aerodynamic configuration of an axisymmetric vehicle. The structure that connected the elements of the Shuttle was very sensitive to the external forces applied to any element. A small change in aerodynamic force or a small change in thrust or thrust direction was magnified into a large percentage of change in the interface struts and backup structure. Therefore, during all ascent loading, balance had to be maintained between the vehicle elements during periods of transient thrust, such as lift-off, and during the period of high aerodynamic loading.

To meet the challenge of developing a structural system that would meet the Space Shuttle program overall goals, new capability had to be established in both the analytical and organizational areas. In the analytical area, the capability to evaluate the variables that would affect the vehicle loading and response was required. Typical of these variables are thrust and thrust transients, winds and gusts, and mass variations. Analytical tools had to be developed to assess each effect that could contribute to the vehicle loading. In addition, lines of communication had to be established between the structural loads analysis community and each group or organization that had the responsibility for definition of all effects that should be considered in the dynamic loads analysis.

The interactions among vehicle systems and environmental effects are shown schematically in figure 1. The flow of design data for vehicle structural design is shown by the arrows. In some cases, the events or effects from the different disciplines can interact and result in changes from the original definition of the effect. The Space Shuttle design conditions included all significant loading events. These were prelaunch, lift-off, maximum dynamic pressure, maximum load factor during SRB boost, SRB staging, and Orbiter/ET ascent with Space Shuttle main engine (SSME) burn.

In this paper, two analysis conditions that presented the greatest challenge to the vehicle loads and dynamic analyst are discussed. The first is the lift-off event, which was chosen because of its extremely transient nature in which engine ignitions, overpressure waves, release of holddown constraints, and winds must all be considered. The second is the high-dynamic-pressure (high q) region of ascent. It is chosen because of the complexity of the aerodynamic environment and the concept developed to define high-q loading conditions for vehicle design. Other conditions, such as staging, that have been so important in transient loads analysis in previous space vehicle designs are quite benign for the Space Shuttle and will not be addressed here.



FIGURE 1.- VEHICLE SYSTEMS AND ENVIRONMENT INTERACTIONS.

LIFT-OFF

The lift-off event, because of its extremely transient nature, represented the greatest challenge to the analyst in predicting the overall elastic-body dynamic response of the Space Shuttle. The effects that were of greatest concern were the ability to simulate the SSME and SRB ignition characteristics and the longitudinal expansion of the SRB motor case, accurate inclusion of the SRB ignition overpressure environment, and the physically accurate simulation of the constraint force release between the vehicle and the launch facility.

Developing the capability to make realistic predictions of vehicle lift-off loads and to satisfy all the pre-analysis concerns was the challenge. Three areas of development had to be completed for a prediction of lift-off loads for design or design certification. These were:

1. Development of a structural dynamic mathematical model
2. Development and definition of the variables or the effects significant to the lift-off event
3. Development of the structural design criteria and load analysis procedures

SPACE SHUTTLE STRUCTURAL DYNAMIC MATHEMATICAL MODEL

The Space Shuttle structural dynamic mathematical model development presented several challenges. These were:

1. The coupling of four large bodies and payloads into the math model

2. Accounting for temperature effects on the stiffness characteristics of the solid rocket motor propellant

3. Consideration of pressurized and nonpressurized SRB's

4. Requirement for many degrees of freedom in the model, typically in the range of 1000 (Previous space vehicles had degrees of freedom in the range of 500.)

A comprehensive discussion of math model development is given in reference 1.

EFFECTS SIGNIFICANT TO THE LIFT-OFF EVENT

The number of effects and their variations that were significant contributors to the analysis of lift-off are as follows.

1. Structural dynamic mathematical model
   a. SRB propellant stiffness (hot or cold)
   b. Effects of external tank cryogenic-induced shrinkage (preloads at base)
2. SSME thrust characteristics
   a. Buildup rate (fast or slow)
   b. Thrust misalinement (±pitch, ±roll, ±yaw)
   c. Dispersion on start time (simultaneous or 333-millisecond delay)
   d. Ignition overpressure
   e. Failure case (loss of thrust on one SSME)
3. SRB thrust characteristics
   a. Buildup rate
   b. Thrust level (high or low performance)
   c. Mismatch (symmetric or unsymmetric thrust buildup)
   d. Thrust misalinement (inboard, outboard, ±pitch, ±yaw, ±roll)
   e. Ignition overpressure (magnitude, frequency, and timing)
4. Winds
   a. Direction and speed
   b. Gust wave length and timing
   c. Asymmetric vortex-shedding
5. Timing of events - Nominal timing and dispersions
6. Sudden release of reaction forces at vehicle base

The challenge in properly assessing these effects was getting each effect defined in a manner which was applicable to the structural load analysis and combining the effects to define a structural limit load for the lift-off event.

STRUCTURAL DESIGN CRITERIA AND LOAD ANALYSIS PROCEDURES

The lift-off dynamic loads event that is initiated with the start of the SSME's is shown schematically in figure 2. This event involves the general dynamic response of the Space Shuttle when attached to the mobile launch platform (MLP) and when free from the MLP. The challenge to the structural loads analyst is to evaluate this sequence of events for structural loading. Shown in figure

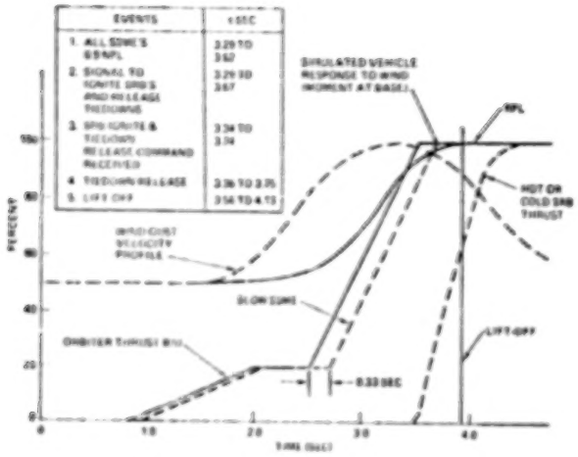


FIGURE 2.- LIFT-OFF SEQUENCE.

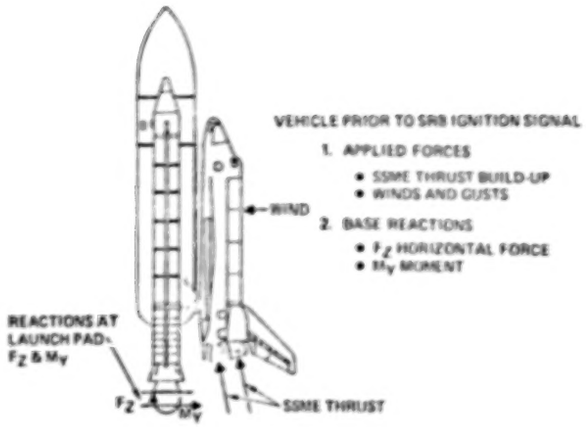


FIGURE 3.- LIFT-OFF CONFIGURATION AND APPLIED FORCES.

3 is the Space Shuttle and the external forces acting on the vehicle just before SRB ignition and holddown release. The effects that are applied in the lift-off simulations are combined to yield an engineering approximation of an overall 3σ event.

The SSME engines are ignited and build up to 100 percent of rated power level. The design-level winds, including gusts, are applied. When all three engines are at 90 percent thrust or greater, a signal is given to ignite the SRB's and release the vehicle. Before release, the horizontal forces and overturning moments are reacted at the base of the vehicle by the launch pad. At the time of release, a significant moment has built up at the base of each SRB to counteract the wind and SSME forces. In figure 4, the left side shows the deflected shape of the SRB's just before release, and the middle shows the deflected shape just after lift-off. The forces at the base of the SRB's decay rapidly to zero at the time of lift-off since there are no reacting forces once the vehicle leaves the pad. This rapid decay of base forces and change in deflected shape represents a shock input to the structure. The shock excites, or "twangs," the vehicle and causes it to vibrate significantly, mainly in its lower frequency structural modes. The right side of figure 4 shows a time history of the base moment.

An update to the lift-off analysis data base was conducted in 1977 in support of the Shuttle critical design review. This analysis resulted in a marked increase in dynamic loads, notably in the region of the Orbiter/ET forward attachment structure. Although the analysis included updates to all areas of the data base, the increase in dynamic loads was primarily attributed to refinements in the stiffness characterization of the SRB's. Changes were made in the treatment of the stiffness properties of the solid propellant and in the stiffening effect of internal pressure. Among the measures considered to alleviate the loads were:

1. Lift-off with a lower thrust level on the SSME's
2. Lift-off with one engine out
3. Tilting the vehicle on the launch pad
4. Devising a controlled release for the base restraints
5. Introducing a time delay for SRB ignition and vehicle release

A study of these options showed that most of them were either ineffective or unfeasible, or introduced undesired risks. Option 5 proved to be both effective and easy to implement.

A time history of the base-bending moment of the vehicle and the time of nominal release are shown in figure 5. It is known that if the magnitude of the base-bending moment at the time of release could be reduced, the subsequent twang loads would also be reduced; thus, it was proposed that the time of the lift-off be delayed past the time of peak moment until the vehicle has rebounded and the bending moment is in the trough. The delay chosen was 2.7 seconds. The effect of this time delay is to reduce the critical twang load in the forward attachment structure by 25 percent. The effect of the SRB ignition delay on payload capability (a loss of 600 pounds) is considered acceptable, and the effect on the acoustic life of the structure is negligible.

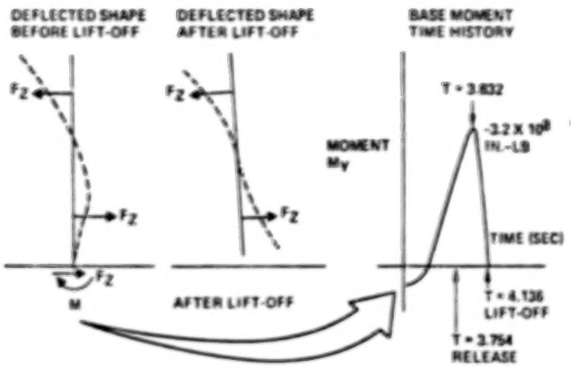


FIGURE 4.- LIFT-OFF TWANG EFFECT.

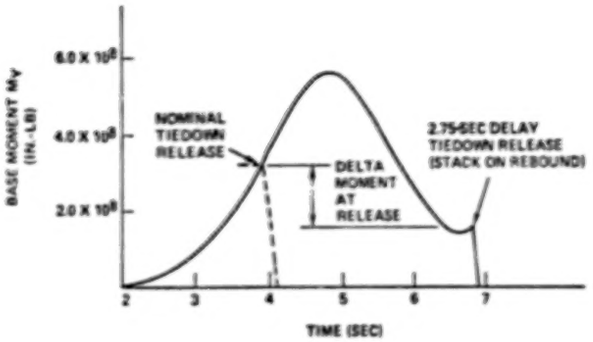


FIGURE 5.- DELAYED SRB IGNITION BASE M_Y VERSUS TIME.

The implementation of the 2.7-second SRB ignition delay required assurance of the ability to accurately predict the cantilevered dynamic characteristics of the vehicle, i.e., the time and extent of the rebound. Full-scale dynamic testing was conducted using SRB's bolted to the launch pad. Final verification was obtained from the flight readiness firing of the Shuttle engines before STS-1. Figure 6 is a time history of the strain in the tiedown bolts between the SRB's and the launch pad. This strain is a measure of base-bending moment. The predicted optimum time for lift-off coincided precisely with the time of minimum strain in the bolts. The 2.7-second SRB ignition delay is now the baseline procedure in the Shuttle lift-off sequence.

HIGH-q BOOST - GENERAL DESCRIPTION

The second ascent event presenting significant challenges in loads analysis is high-q boost. As shown in figure 7, the time of high dynamic pressure (i.e., greater than 400 psf) is approximately 30 seconds to 90 seconds flight time, which corresponds to a Mach number range of 0.6 to 2.7. These values will vary from flight to flight, being dependent on specific trajectory design and dispersions such as winds. Features, some new or unique, of the high-q boost event are as follows:

1. Vertical ascent through wind shears and gusts

2. Throttling of the three main engines to as low as 65 percent of rated power to limit the value of maximum dynamic pressure

3. Movement of the elevons through a predetermined deflection schedule to limit airloads on the elevons

4. An active load-relief control system providing commands for gimbaling the three SSME's and the two SRB's in response to wind shear and gust

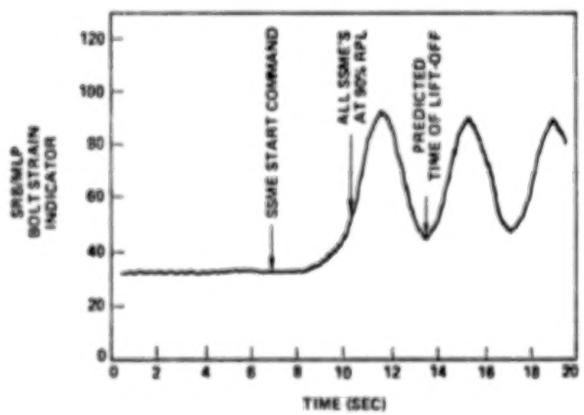


FIGURE 6.- FLIGHT READINESS FIRING TIEDOWN BOLT STRAIN.

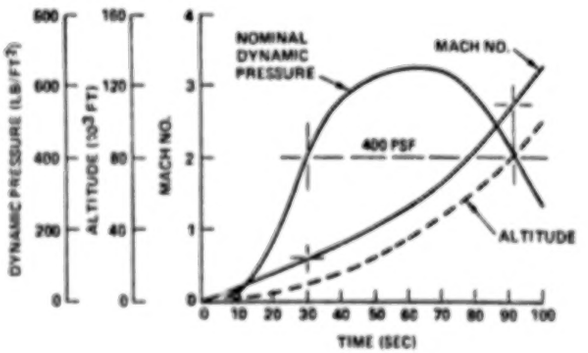


FIGURE 7.- TYPICAL HIGH-q BOOST TRAJECTORY DATA.

HIGH-q BOOST LOADS SURVEY

In early Shuttle load studies, full dynamic simulations were made of the elastic vehicle transient response. Approximately 20 cases were run in a typical loads survey; however, it was apparent that the Shuttle configuration (i.e., winged vehicle with parallel staging) made it more sensitive to wind azimuth and system dispersions than was an axisymmetric vehicle such as Apollo/Saturn. This difference is illustrated in figure 8. The structural loads survey considered dispersions on parameters such as:

1. SSME thrust level and thrust vector alinement
2. SRB thrust level and thrust vector alinement
3. SRB thrust mismatch
4. Trajectory differences for the various design missions
5. Variations in rotational accelerations
6. Tolerances in aerodynamic coefficients
7. Loss of thrust of any one SSME.

A calculation technique was required to provide a more rapid and cost-effective means of surveying all combinations of flight time, wind azimuth, and systems dispersions. Expanded use of full-transient-response simulations would be time-consuming and expensive; thus, a new technique based on the use of weighting factors applied to unit sensitivity load cases (load partials) was devised to identify the critical combinations of dispersions. These selected critical cases were then evaluated to obtain balanced distributed loads.

The focus of the load survey was the q-alpha versus q-beta flight envelopes called "squatcheloids." The squatcheloid provides a means of defining the pertinent flight dynamics parameters such as dynamic pressure (q), angle of attack (alpha), angle of sideslip (beta), and the rotational accelerations (p, q, and r). An example is shown in figure 9. The inner A squatcheloid is based on nominal wind criteria as noted. The B squatcheloid is based on the full design wind criteria; i.e., 99 percentile wind shear and 9 m/sec gust, reduced by a multiplying factor of 0.85 to account for a statistical combination of shears and gusts. The A1 squatcheloid includes the effects of system dispersions such as thrust variations and accelerometer alinements. The load increments between the B and A squatcheloids and between the A1 and A squatcheloids are treated as dispersions and are combined appropriately with other dispersions in the loads calculation process. Such a methodical treatment is necessary because of the sensitivity of the Shuttle configuration to dispersions in vehicle and environmental data.

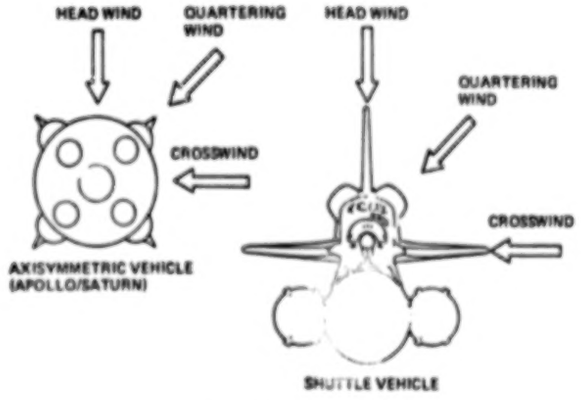


FIGURE 8.- CONFIGURATION DIFFERENCES.

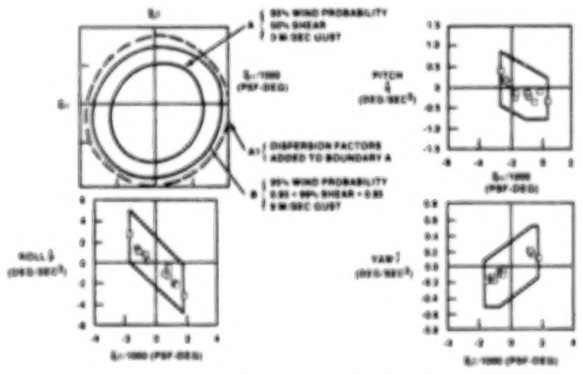


FIGURE 9.- EXAMPLE OF SQUATCHELOID FOR MACH 1.05.

Squatcheloids are developed for each of several Mach numbers of interest in the high-q regime for both no-failure and one-engine-out conditions. The high-q loads analysis then becomes the methodical survey of the squatcheloids, including consideration of all pertinent deterministic and random dispersions in the data base. The method for handling dispersions is as follows.

$$L_{max} = L_A + \Sigma \text{ (deterministic load increments)} + \text{RSS (random load increments)}$$

where L_{max} is the maximum load for survey and L_A is the baseline load (Mission 3; A squatcheloid). The load increments are defined as follows.

1. Deterministic load increments
   a. Portion of SRB thrust dispersion
   b. Effect of SSME throttling
   c. Missions other than Mission 3
2. Random load increments
   a. SRB thrust misalinements
   b. SRB thrust mismatch
   c. Rotational acceleration dispersions
   d. Elevon deflection dispersion
   e. Effect of maximum wind shear and gust (squatcheloid B minus squatcheloid A)
   f. Effect of flight control dispersions (squatcheloid A1 minus squatcheloid A)
   g. Aerodynamic tolerances
   h. Portion of SRB thrust dispersion

Using the load partials, the effects of deterministic dispersions are combined directly, whereas the effects of random independent dispersions are combined by root sum square (RSS). The load survey is conducted by calculating loads for approximately 30 places on the vehicle including the wing, the vertical tail, and the interface structures between the Orbiter and the ET, and between the SRB's and the ET. Computer programs have been developed for the rapid and inexpensive survey of load cases using rigid-body calculation techniques. When the critical cases have been identified, balanced distributed load cases are developed including the loads caused by elastic-body response.

At the time of the Shuttle critical design review, the methodology described was used to survey approximately 65 000 load cases in the high-q boost regime. Of these, approximately 50 cases were selected for final distributed loads. Figure 10 illustrates a typical distribution of critical cases on the squatcheloids, wherein each data point represents a maximum load on the wings, the vertical tail, or the interface structure. The squatcheloid survey technique has proved to be an efficient method for the survey of all Shuttle system dispersions.

ORBITAL FLIGHT TEST PROGRAM RESULTS

In this paper, several challenges to the structural load analysis discipline resulting from the unique Shuttle vehicle configuration are discussed. In the case of lift-off, changes to the characterization of the vehicle dynamic properties, SSME and SRB thrust buildup data, and ignition overpressure data all posed threats to the structural design during Shuttle development. Similarly, for high-q boost, updates to aerodynamic characteristics and the advent of higher performance trajectories also had the potential to impact the structural design. After years of analysis and re-analysis, the final verification of structural design load adequacy was to come from data obtained during the Orbital Flight Test (OFT) program. The OFT program consisted of the first four Shuttle flights, STS-1 through STS-4. On these flights, as well as on STS-5, development flight instrumentation collected data for the postflight reconstruction of the loads. In both lift-off and high-q boost, there was general verification of the design data base; however, some surprises also occurred.

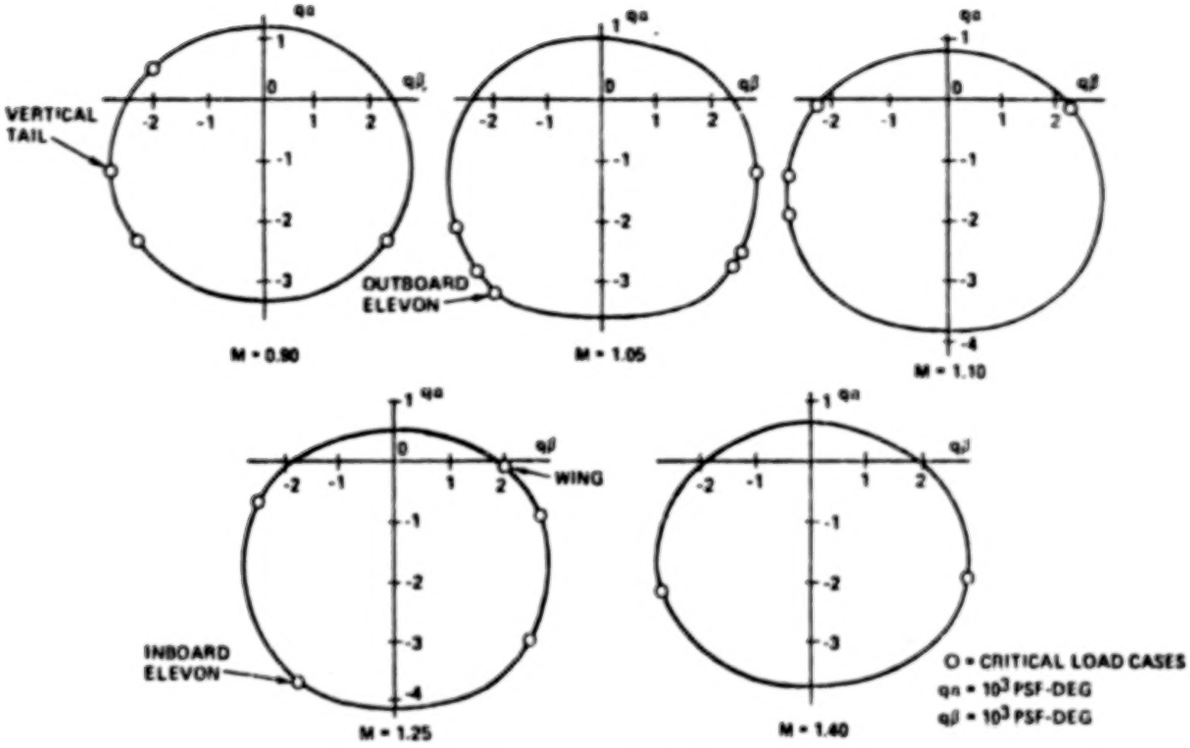


FIGURE 10.- SQUATCHELOIDS WITH CRITICAL LOAD CASES.

LIFT-OFF FLIGHT TEST RESULTS

The most notable result pertaining to lift-off occurred on STS-1. The ignition overpressure wave from the SRB's was much more severe than predicted. The resulting transient loads caused damage to a strut supporting a tank in the Orbiter forward reaction control system. The subscale model testing that had been used to predict the overpressure environment was deficient in predicting the full-scale pressure wave. After STS-1, additional modified subscale testing led to modifications to the launch pad to attenuate the overpressure wave. These steps were strikingly successful in eliminating overpressure as a contributor to dynamic loads. In all subsequent flights beginning with STS-2, nominal lift-off loads that are well within design limits have occurred. Shown in figure 11 are examples of the generally excellent correlation between the analytical reconstruction and the measured flight data.

HIGH-q BOOST FLIGHT TEST RESULTS

An unanticipated result during high-q boost also occurred on STS-1. The trajectory was "lofted"; i.e., the flightpath deviated from the planned trajectory. In postflight evaluations, this phenomenon was attributed to a discrepancy in the aerodynamic data pertaining to interactions with the rocket plumes. In the design data base, the aerodynamic interaction with the plumes was based on subscale wind-tunnel tests. In the following flights in the OFT program, adjustment of the aerodynamic data for consistency with flight measurements effectively eliminated the lofting phenomenon. These adjustments were also included in postflight reconstructions of the structural loads. Some examples are shown in figure 12. In the lower portion of the figure, the correlation of an interface load between the Orbiter and the ET illustrates the generally good correlation of total vehicle characteristics; i.e., aerodynamics, thrust, and mass properties. In the upper portion of the figure, the correlation of a wing load indicator illustrates an area in which further update is required in the local pressure distributions.

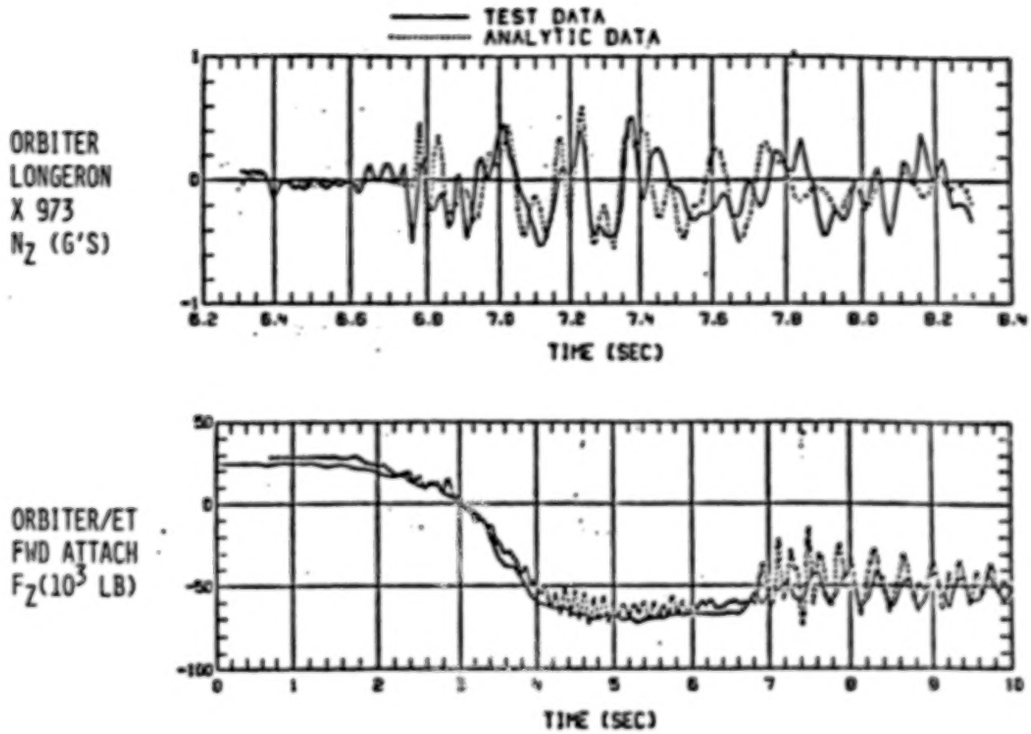


FIGURE 11.- STS-2 LIFT-OFF MEASURED LOADS VERSUS RECONSTRUCTION.

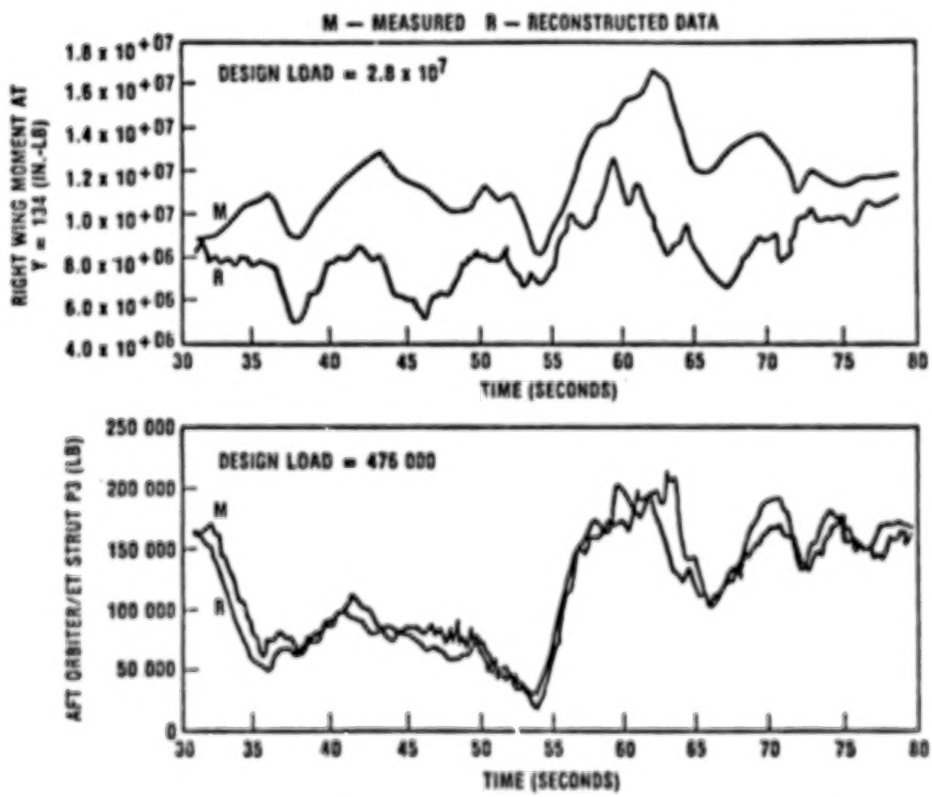


FIGURE 12.- HIGH-q BOOST LOADS, MEASURED LOADS VERSUS RECONSTRUCTED LOADS.

CONCLUSIONS

Because of its sensitivity to changes in environmental data, the Shuttle configuration presented unique challenges to the structural loads analyst. Results of the Orbital Flight Test program have generally verified the design analysis. However, subscale testing was found to be deficient in predicting full-scale results in two areas: the ignition overpressure at lift-off and the aerodynamics/plume interactions at high-q boost. In these areas, the results of the flight test program have been accommodated with no impact to the vehicle design. The challenge of developing a structural system which meets the Shuttle program goal has been met. The analytical tools and data which accrued during Shuttle development remain as significant contributions to structural analysis technology.

REFERENCE

1. Modlin, C. Thomas, Jr.; and Zupp, George A., Jr.: Shuttle Structural Dynamics Characteristics -- The Analysis and Verification. Space Shuttle Program Technical Conference, Johnson Space Center, Houston, Texas, June 28-30.

N85
16915

UNCLAS

N85-16915

ORBITER STRUCTURAL DESIGN AND VERIFICATION

Philip C. Glynn and Thomas L. Moser
NASA Lyndon B. Johnson Space Center
Houston, Texas 77058

ABSTRACT

The Space Shuttle development program provided the opportunity to challenge many of the established practices and approaches used in prior manned-space-flight programs. The most significant accomplishments and resulting precedents which emerged during the structural development of the Space Shuttle and the Space Shuttle Orbiter are reviewed. Innovations in criteria, design solutions, and certification are highlighted, and brief comments on the lessons learned are included.

INTRODUCTION

As the final Space Shuttle concepts matured, the new challenges offered by the Shuttle main engines, the Orbiter thermal protection system (TPS), and the Orbiter avionics systems became clearly visible. The engineering challenges faced by designers of the primary structural system were created by features for which no precedent existed and thus provided the momentum for creative and innovative criteria, approaches, and hardware features. Simply stated, the reusability and mission flexibility of the vehicle, the weight sensitivity of the Orbiter to the mission requirements, and the cost consciousness of the project provided the constant pressure for innovative design challenges. Although the expertise of NASA and the supporting aerospace team had been focused on high-reliability single-use boosters and spacecraft, early studies identified no significant technology issues with structural reusability. As engineering concepts emerged, it became more obvious that a considerable change in the size and design life of the spacecraft would force the emergence of new concepts and precedents.

DEPARTURE FROM FULL-SCALE TEST SIMULATION

Previous experience had led to complete spacecraft vibration and acoustic testing as well as complete entry vehicle thermal testing. Initial proposals emerged for subjecting forward and aft sections of the Orbiter to vehicle-level acoustic tests. After detailed technical and programmatic examination, the differences with the past precedents became clear. Secondary structure and installations were to be designed in accordance with life requirements for the Orbiter. Generic installation concepts would evolve throughout the vehicle and would require additional development and verification. Prevention of acoustic fatigue of the primary structure emerged as a serious requirement (fig. 1). This factor complicated the structural reliability since extensive coverage of the Orbiter with external TPS tiles plus internal insulation made regular inspection much more costly and impractical. The technical issues associated with the complexity of the environmental simulation, the remaining unanswered structural and systems issues, the availability of the Main Propulsion Test Article (MPTA) to aid in vibration and acoustic development, and, of course, the significant saving in test article and development test cost led to the challenge of developing the reusable Orbiter structure without the full-scale spacecraft vibroacoustic test articles. This challenge was addressed in the structural and system acoustic fatigue program and is discussed herein.

The large-scale transient thermal response of the entire Orbiter was also recognized as a significant challenge for the structural discipline. Efforts and approaches such as those implemented by the British Aircraft Corporation for development of the Concorde were technically and programmatically evaluated. The Concorde approach was to convectively heat the entire airframe using a special shroud and heating facility while applying mechanical loads simulating the in-flight load spectra. In this program, creep and fatigue issues for steady-state flight conditions were addressed. The Orbiter design was sensitive to the peak combined transient thermal stress as it related to out-of-plane deflection of the airframe and to airframe panel stability. Full- and quarter-scale airframe test programs were evaluated to address the challenge. This challenge was finally addressed through a combined program of criteria, structural testing, and flight testing. The resulting precedents are discussed herein.

DEPARTURE FROM ABORT AND TRAJECTORY UNIQUE DESIGN

Pre-Shuttle NASA experience had been focused on clearly defined mission models and reference trajectories. Abort scenarios would emerge as the most demanding structural event, and complexity, cost, and weight would be designed into the spacecraft. As the flexibility of the Shuttle was exam-

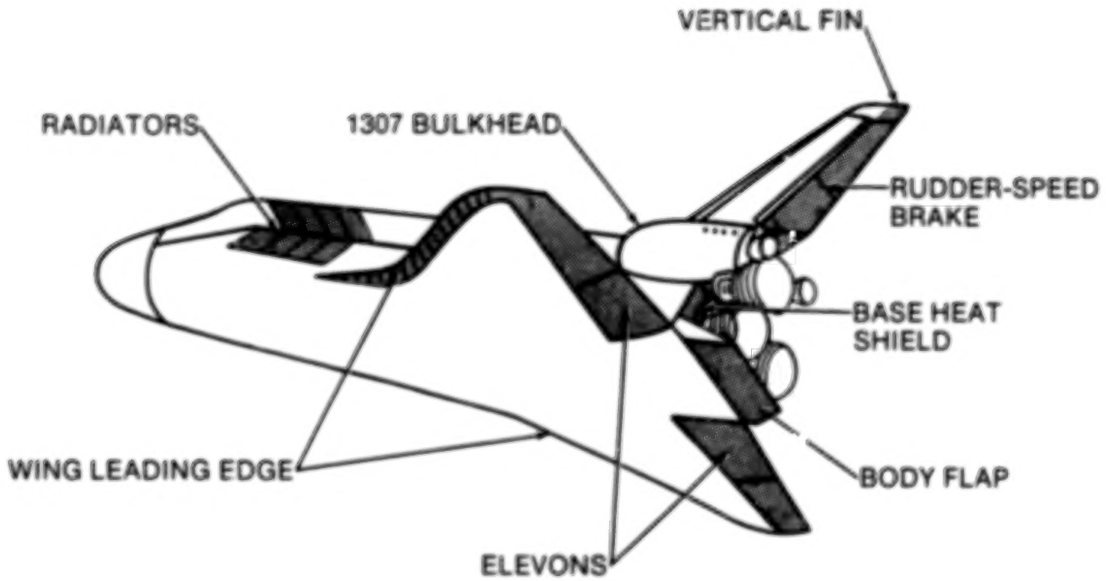


FIGURE 1.- PRIMARY STRUCTURE AREAS SUBJECT TO ACOUSTICS.

ined, it became clear that, as the performance parameters of payload weight, orbital inclination, and orbit altitude were varied over feasible ranges, the flexibility available through use of the engine throttles led to a myriad of variations not easily examined using direct trajectory simulation for design. Concurrently, the required system redundancy specified and the Orbiter weight sensitivity led to the design philosophy of minimum design impact for abort requirements. Such an early NASA design approach was unprecedented. The direct impact to the hardware structural weight was minimized by design conditions for loss of only one main engine using rational statistics to avoid the worst possible case. Descent operational maneuver and landing placards were specified for the resulting heavyweight entry and landing. This approach, of course, put exceptional pressure on the abort planners to invent concepts which would "stay within" the operational capability - an effort achieved with commendable expertise.

SERIAL DESIGN EVOLUTION OF AIRFRAME DESIGN LOADS

Results of early Space Shuttle studies had shown a clear performance benefit with increasing dynamic pressure (q) and minimum throttling. A conscious design decision was made to limit the maximum dynamic pressure to 650 psf nominal and the maximum longitudinal acceleration to 3g axial. The desired effect was to limit the q-sensitive parameters such as peak differential pressure, buffet intensity, aerodynamic noise, aerodynamic loading, control authority, and flutter requirements within manageable bounds. The constant weight sensitivity and development of the emerging flexible capability of the Space Shuttle continued and resulted in changes to the ascent loading requirements late in the design cycle. Changes to the detailed structural criteria were necessary to minimize the impact of updated ascent configurations and the serial update of the required data bases. Although Columbia and Challenger were designed to an early data base designated the 5.1 loads data base, it was clear that a later certification to a 5.4 loads data base would have to be incorporated. The separate certifications of OV-101, MPTA, and OV-102 to different requirements with different data bases and criteria were a significant challenge. Resource pressures forced a serial approach. The Enterprise was certified by analysis and placarded to 80 percent of limit load. The MPTA was certified by analysis. The Columbia was certified by analysis and testing to the 5.4 loads data base following partial modification performed in the field. Further, the Columbia was restricted to a reduced operational envelope before final modification. The Challenger was structurally tested and returned to the fleet. This approach is unprecedented in NASA experience and is discussed further herein.

SERIAL DESIGN OF AIRFRAME AND TPS INTERFACE

The classical design process dictated an early definition of the structural moldlines and structural details before the integration and final sizing of the TPS. Early sensitivity of the TPS to short wavelength, out-of-plane deformations led to the selection of a nonbuckled external skin design. Since the TPS thickness was not defined and would vary depending on final requirements and

aerodynamic moldlines, a significant challenge was an adequate but minimum weight definition of three-dimensional temperature gradients and stresses. Detailed attention to the thermal stress additions which would contribute to skin buckling was also required. The approach to design definition and resulting performance was a worthy challenge and is discussed further herein.

CRITERIA INNOVATIONS

DEFINITION OF DESIGN LOAD ENVELOPES

As the critical loads analysis studies progressed, it became obvious that trajectory simulation of high-q ascent and descent was sufficiently cumbersome to prevent surveying the entire flight envelope for hardware design cases. For ascent, an entirely new precedent, which was analogous to the airframe V-n (velocity versus load factor) diagram and was named the squatcheloid, emerged. The detailed implementation of this approach is discussed in reference 1. Because this concept preceded the development of the ascent control system as well as the multimission and real-wind trajectory simulations, the criterion generated much debate. There was genuine concern that the criterion would force the vehicle to fly through a "tube" of $q\alpha/q\beta$ versus Mach number values which, at that date, the ascent control community had serious reservations about the control system capability to handle. After numerous reviews, the weight penalty and the credibility of the load survey associated with any other alternative resulted in the adoption of the squatcheloid; thus, a new precedent was set and design surveys could proceed.

The impact of this innovation was readily obvious. The Shuttle vehicle loads analysis was capable of surveying hundreds of potential design conditions within the flight envelope. Load surveys and indicators were evaluated even though the trajectory surveys had not been performed. The thrust structure could be designed for compatible engine deflections, consistent with the control system and engine mixing logic rather than with a worst case geometric mix. This criterion also became an active system integration tool. It allowed the performance, flight control, and structure disciplines to work in parallel rather than in the serial manner required with trajectory simulations and evaluations.

A similar situation existed with respect to descent maneuver loading requirements since only nominal trajectory-based data had emerged. Early ballistic trajectories did not require any significant maneuvers and did not provide any meaningful "design to" envelopes of control surface constraints required for load surveys. The initial maximum speed was defined as that required to stall the actuators. The structural criterion was baselined using Mach-number-dependent V-n diagrams illustrated in figure 2. The maximum speed, equivalent to 375 psf, was derived from upsetting the nominal trajectory and recovering and was tempered with understanding of the entry control system limits. Modifications to aircraft maneuver requirements such as limiting the maximum yawing load factor to 3/4g were also derived. Envelopes for the control surface were generated so that a complete loading survey could be performed. Since no deterministic flight conditions to justify the myriad of descent cases existed, this criterion also generated serious review. The criterion was found to be the logical alternative and set a precedent of deviating from deterministic ballistic load definition.

DEFINITION OF COMBINED STRESS CRITERIA

Once the trade-off studies showing the relative insensitivity of the unit weight of structural effective thickness plus TPS unit weight to maintain a temperature of 350° F (fig. 3) were performed, the decision to preclude buckled external skin became the baseline approach. Using techniques such as those documented in reference 2, the frame and rib spacings were set for minimum structural weight. As [illegible]esign concepts evolved, it became apparent that the local skin deflections amplified by the beam column effect over relatively short wavelengths were important to the induced through-the-thickness stresses in the TPS. A consistent approach to and method of combining the stresses were needed to assure adequate and uniform specification of skin peak stress. The criterion of figure 4 was specified after some debate and trade-off study. This level of specified combined stress criterion was unprecedented for design of manned spacecraft. As weight-saving pressures mounted, the assurance provided by the criterion contributed to further sophistication in the skin deformations. The post-heating criterion on skin buckling was relaxed from no buckling at 115 percent of limit load to 100 percent limit load.

EMPHASIS ON FRACTURE, LIFE, AND ALLOWABLE DEFORMATIONS

Studies were performed to assess the approach to implementing fracture control on the primary airframe. Fracture control plans were generated by the contractors and approved. The importance of the fracture requirement, the life requirement of the structure, and the ratio of yield to ultimate

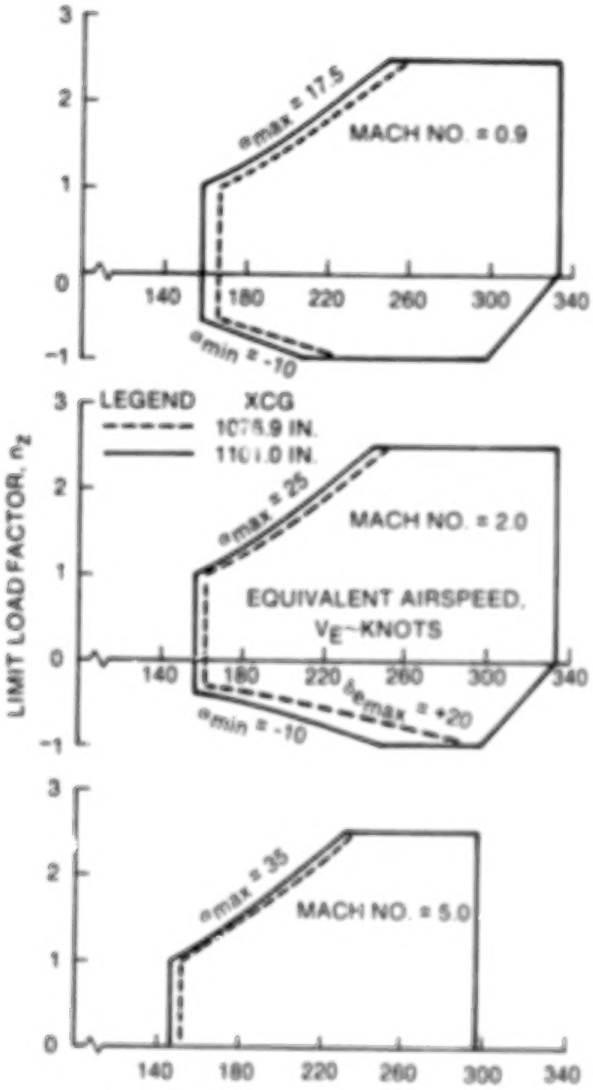


FIGURE 2.- DESCENT V-n CRITERIA.

stress of modern materials led to the unprecedented approach of not specifying a yield factor. It was shown that a yield factor could be misinterpreted during preliminary design and that the preferred approach was to focus on the deformations and on fracture and life requirements.

DEFINITION OF FEASIBLE CREW CABIN WEIGHT

As the crew cabin design evolved, it was noted that the specific design missions compared to the available volume resulted in considerable opportunity for weight growth. Apollo command module volumetric stowage densities were reviewed. The result was that the structural design of the crew cabin was performed using a value of 30 000 pounds even though specific mission requirements could not define weights above 27 891 pounds. This provision proved to be well worth the minor scar weight of approximately 57 pounds and allowed very flexible mission planning with non-weight-limited stowage volumes used for payload and mission integration.

DEFINITION OF DESIGN BUDGET FOR THERMAL STRESS

Results of early studies had not revealed the complexity of defining design-case thermal stresses. With the extreme pressure of "designing out" Orbiter structural weight, redesign to desen-

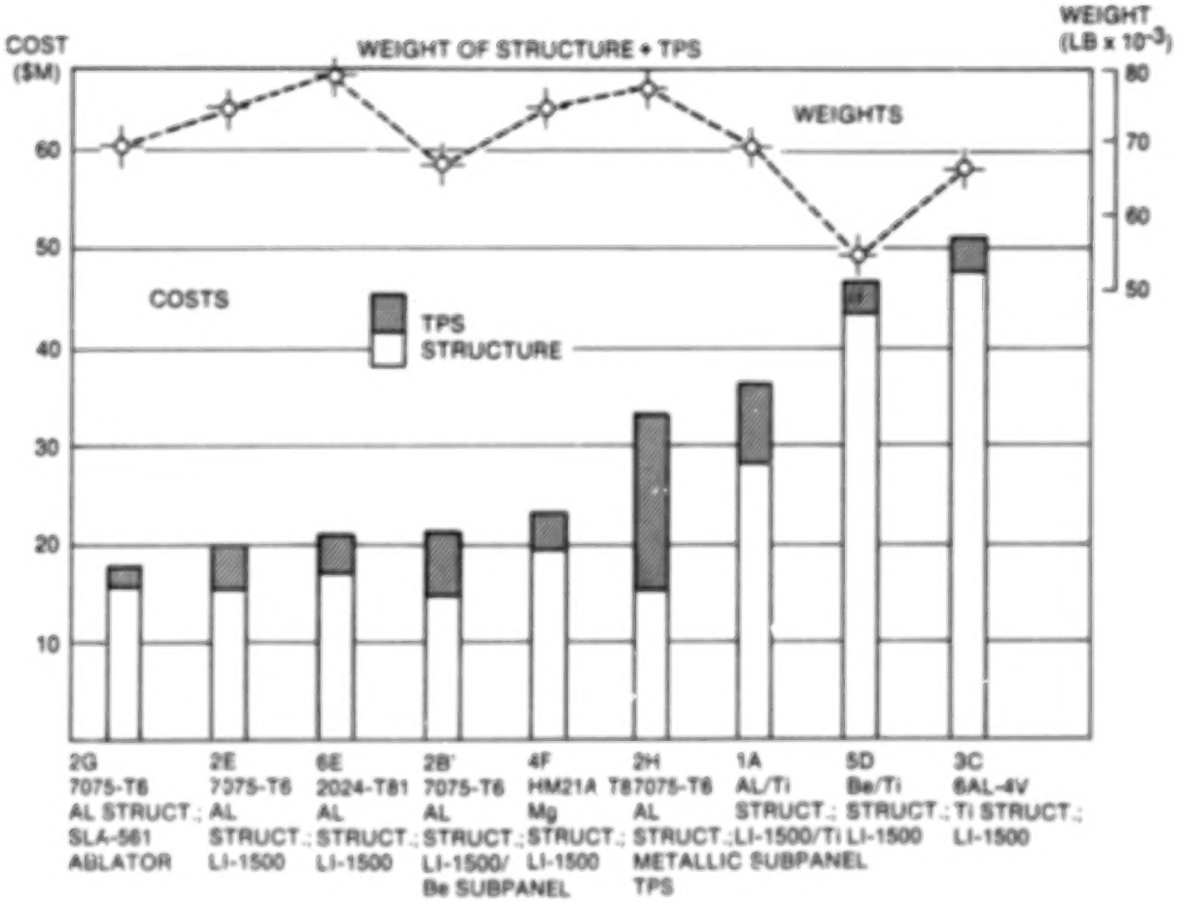


FIGURE 3.- ORBITER STRUCTURE/TPS FIRST UNIT COST COMPARISON.

3.2.2.2.6 ULTIMATE COMBINED LOADS. THE MECHANICAL EXTERNAL, THERMALLY INDUCED, AND INTERNAL PRESSURE LOADS SHOULD BE COMBINED IN A RATIONAL MANNER ACCORDING TO THE EQUATION GIVEN BELOW TO DETERMINE THE DESIGN LOADS. ANY OTHER LOADS INDUCED IN THE STRUCTURE, E.G., DURING MANUFACTURING, SHALL BE COMBINED IN A RATIONAL MANNER. IN NO CASE SHALL THE RATIO OF THE ALLOWABLE LOAD TO THE COMBINED LIMIT LOADS BE LESS THAN 1.40

K_1L EXTERNAL + K_1L THERMAL + K_2L PRESSURE, $\geq 1.40 \Sigma L$

K_1 = 1.4 WHEN THE TERM IS ADDITIVE TO THE ALGEBRAIC SUM, ΣL

K_2 = 1.5 FOR TANKAGE WHEN THE TERM IS ADDITIVE TO THE ALGEBRAIC SUM, ΣL

K_1, K_2 = 1.0 WHEN THE TERM IS SUBTRACTIVE TO THE ALGEBRAIC SUM, ΣL

FIGURE 4.- COMBINED LOADS CRITERIA.

sitize the minimum weight concepts from thermal stresses was not practical. Also considered was the concept of a tolerance on the thermal gradients. Although seemingly logical, a three-dimensional finite-element model was not suitable for a consistent combination approach. An automated worst case would have inferred different temperatures at the same node point. This conflict implied inconsistent added weight, and the concept was rejected. Results of studies performed showed the sensitivity of the initial conditions achieved on orbit. These data showed that approximately 30 percent of the total stress could be attributed to that "locked in" at entry interface.

Tail Sun, top Sun, side Sun, and nose Sun attitudes and initial conditions from a once-around mission were chosen as design initial conditions. Theoretical thicknesses of TPS tiles were specified for approximately 100 three-dimensional models. The gradients were assessed and several time points were selected for detailed analysis. These data were then hand-faired and extrapolated to the entire finite-element grid. This procedure involved judging the temperatures to about 100 times the resolution of the thermal analysis. This experience demonstrated the technology weakness of determining the design-case transient thermal stress for large three-demensional structures. The design was frozen to this budget of thermal stress. It remains for operational planners to ensure that the operational envelope stays within the budget.

MATERIAL BASELINE OF THE PRIMARY STRUCTURE

In selecting the materials for the "airframe" of the combined airplane/spacecraft Orbiter, the conventional trade-off studies, considering the costs to produce the first unit and the weight, had to accurately reflect the compatibility requirements imposed on the structure by the external TPS. The very low strength, brittle TPS tiles, which were to be bonded to the skin of the Orbiter, required that the skin not buckle when exposed to 115 percent of maximum expected loads (limit load) during ascent and 100 percent of the maximum expected load during atmospheric entry. From a weight standpoint, this skin-buckling requirement made aluminum and titanium equivalent since the ratio of the compression modulus to density is approximately the same for both materials ($E_c/\rho = 10 \times 10^7$ inches). The structure of the Orbiter, sized by flight loads where the material could be worked to high stresses, favored the high-strength materials such as titanium. The third general category considered in the structural material selection was the heat capacitance and the strength at elevated temperatures. When considering the requirements of buckling for TPS compatibility, strength, heat capacitance, conductance, and a few other factors, the combined weight of the structure and the TPS was approximately 15 percent less for titanium than for aluminum as the primary structure; however, the cost for the titanium structure was approximately 300 percent greater than that for aluminum. The much higher production cost and the higher production development risk for titanium and the system performance studies resulted in selection of aluminum for the basic primary structure.

There were two major areas of the primary structure for which aluminum was not selected - the payload bay doors and the main engine thrust structure. The payload bay doors were designed for maximum reliability in opening and closing in space. To help achieve this reliability, the doors were designed so they could be "zipped" up during closure. This zipping capability dictated that the doors be flexible and have large clearances between door segments and surrounding structure. To help meet these requirements, the Orbiter primary structure was designed so that the doors were not affected by fuselage bending (only by pressure and torsion loads). The large, flexible payload bay doors, which had very few TPS tiles, were then optimized for weight, thermal distortion, and cost. Graphite epoxy was selected as the material.

The thrust structure reacts 1.5 million pounds of Space Shuttle Main Engine thrust load and distributes the vertical stabilizer loads and external tank aft attachment loads into the fuselage. The material selected for this highly loaded structure was titanium. For long truss members that were compression/buckling critical, the weight was reduced by overlaying longitudinal strips of boron epoxy. The thermal expansion compatibility between the titanium and the boron epoxy permitted this composite system. The system reliability was increased by sizing the titanium structure so that limit load could accommodated on any structural member even if a segment of the boron epoxy became debonded.

The general arrangement of the Orbiter primary structure and the materials used is shown in figure 5.

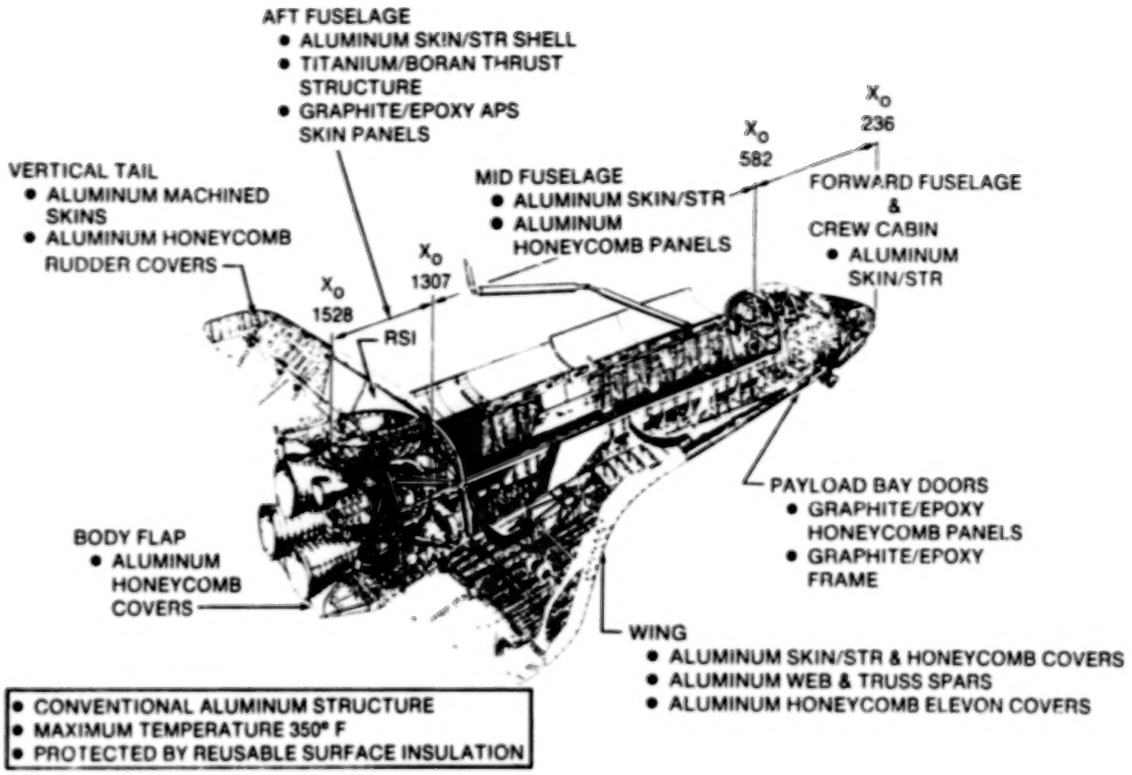


FIGURE 5.- ORBITER STRUCTURE.

DESIGN INNOVATIONS

ORBITER WINDOW SYSTEM

The Orbiter window system shown in figure 6 represents a significant and unheralded achievement in glass structural technology. The Corning Glass Company agreed to produce the windows as a national service. Fracture mechanics criteria were used to design the untempered 1200 pounds of fused silica glazings. Sustained load flaw-growth requirements set the proof test requirement at 8600 psi to screen a flaw of 0.0018 inch. Initially, serious technology reservations were expressed because of the "mass effect" of the large boules weighing approximately 2000 pounds each. Development of the processes and coating verification required 2 years of challenging engineering. Because of changes in aerodynamic data and lessons learned from the flight data, critical inspection and polishing of the operational windows are necessary to asssure the life of the window.

MAJOR STRUCTURAL CONCEPT STUDIES

Several major studies were performed to define the minimum-weight structural concepts. These studies had been identified as a result of the phase B options that had been proposed. Trade-off studies were performed by the contractor and by in-house NASA engineering groups. For example, it was shown that a space frame concept for the thrust structure would save approximately 1730 pounds as compared with a competing plate girder concept. Similarly, it was shown that integration of the aft carrythrough spar with the 1307 bulkhead would save approximately 450 pounds compared to a floating carrythrough and would require a corrugated bulkhead web to limit the stress concentrations. A single-point drag attachment between the Orbiter and the external tank was studied since it achieved a statically determinate interface. It was found to be heavier and more difficult to integrate with the natural load paths from the thrust structure. Results of other studies confirmed the weight effectiveness of the separate crew module as compared to an integrated fuselage and crew module. The requirement for the payload bay doors to react body torsion while precluding vehicle bending was confirmed. Weight and cost studies led to the selection of the composite material systems used in the payload bay doors, the Orbital Maneuvering System (OMS) pod external shell, frame and rib tubes, and the thrust structure. These concept selections resulted from penetrating engineering trade-off

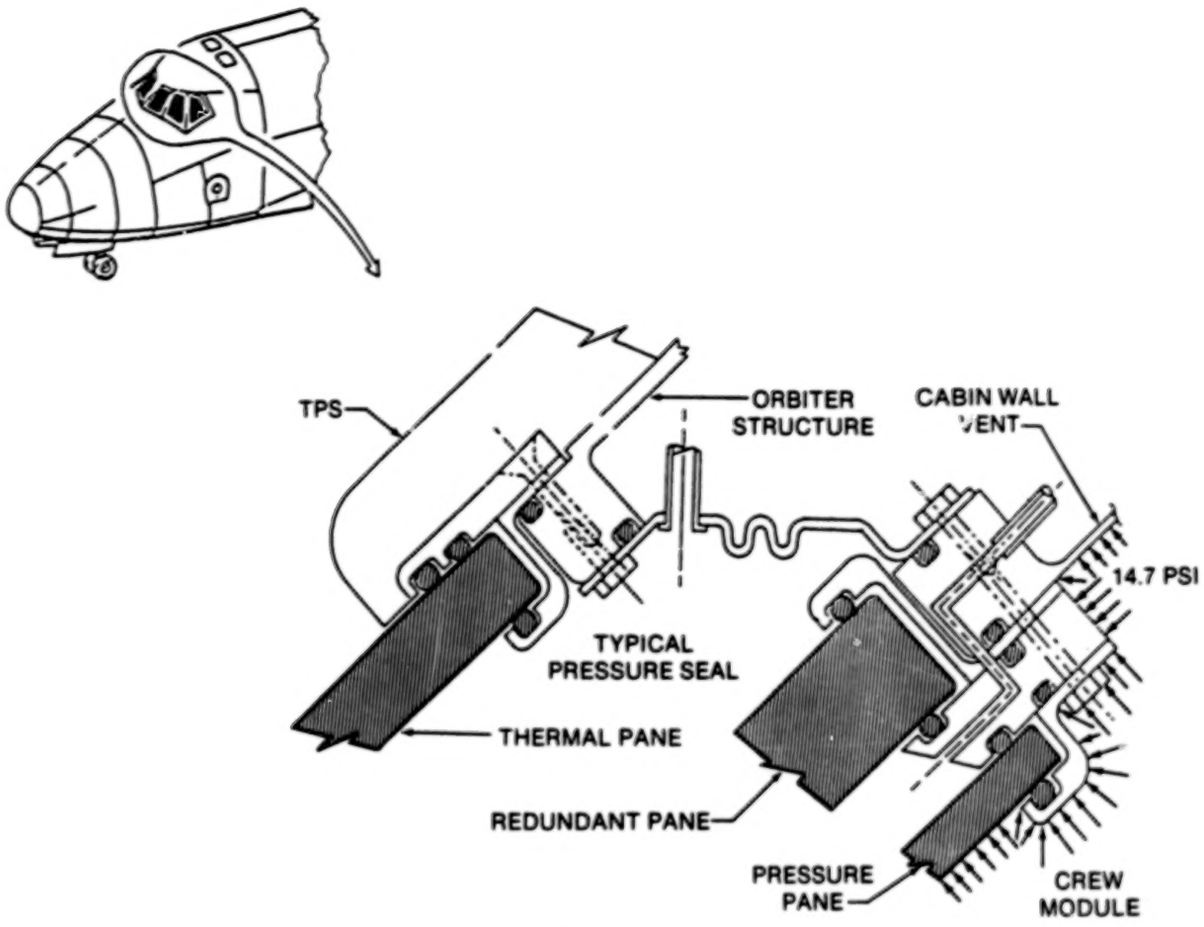


FIGURE 6.- TYPICAL ORBITER WINDSHIELD CONFIGURATION.

studies. The weight "scraping" which followed was the next significant milestone as the loads matured. Significant weight reduction was achieved on Orbiter vehicles OV-103 and OV-104. Attention to detail, with the successful development period confirming the stress distributions, led to structural weight reduction of approximately 1000 pounds.

ORBITER VENTING SYSTEM

Design of the Orbiter venting system involved challenges not previously encountered. Previous spacecraft experience dictated a design which would have connected the entire volume and vented it through base vent areas. Because of the requirements of contamination and cleanliness of the payload bay and the potential hazards of hydrogen concentrations, a multicompartment scheme of self-vented, passively vented, and controlled venting compartments evolved. This arrangement required the vent areas to be distributed around the vehicle and required that they be placed and sized so as to accommodate significant variations in pressure coefficient at the vent. The definition of design differential pressures across the internal bulkheads required extensive analysis to identify the critical combination of venting parameters. The resulting design and performance are discussed in reference 3. Overall, the system performed as designed, is tolerant of failures and variations, and has adapted well to changes in design data and initial requirements. Although it has been largely unnoticed, it represents an outstanding example of a thorough, innovative design achievement.

ACOUSTIC FATIGUE

Fatigue of the Orbiter structure was considered by many engineers and managers to be inconsequential since the design life was for 100 missions and only a few hours of flight in the atmosphere. By comparison to the classical airplane ground-air-ground leading cycles for a 20 000-hour airframe, the Orbiter did have reduced requirements; but, when considering the high acoustic levels (fig. 7), high cycle, low-stress fatigue could not be ignored.

The challenge was in certifying this large, complex, multimaterial, multiconfiguration, multimanufactured source structure for multicombinations of loads for the high acoustic levels. The obvious solution was to certify by testing as is done for airplanes - apply a spectrum of flight loads to a dedicated test airframe for as many as four times the number of expected load cycles. The Concorde airplane, which was designed for elevated temperatures (200° C), was fatigue-tested in the classical manner while simultaneously being convectively heated. Such a test program for the Orbiter would have required a dedicated structural test article (costing approximately $100 million), a nonexistent acoustic facility, and a method of imposing rapidly changing temperatures on the structure. The cost, schedule, and technical capability were out of reach.

The acoustic fatigue certification program established was truly innovative. The concept was to test representative structure of various forms, materials, and construction in a representative acoustic environment until the test article failed. (The regions to be tested are shown in fig. 8.) This procedure would result in establishing an acoustic fatigue damage allowable for each type of material and construction. The allowable damage would then be reduced analytically to account for the damage induced by the flight loads and elevated temperature. The test articles were sized so that only one-third of the specimen was the test region - the remaining two-thirds of the specimen was compromised because of the boundary conditions. Several of the test articles are shown in figures 9 to 11.

This approach was modified for some test articles like the payload bay doors, which have great fatigue durability because of the graphite epoxy construction. The compromise consisted of not testing to failure but instead of analytically modeling the structure and correlating with strain measurements from the test. The test articles were then used as flight hardware.

Additional acoustic fatigue certification objectives relative to secondary structure, system installations, and TPS were also accomplished on many of the test articles. This additional hardware was "piggybacked" on the test articles.

STRUCTURAL TEST APPROACH

Detailed planning of the structural test conditions was well underway for a classical static test program followed by fatigue investigations when a new opportunity emerged. The Orbiter structure had evolved under such weight-saving pressure that virtually all the primary structure had a significant thermal stress component. Attempts to factor mechanical loading into equivalent thermal loadings resulted in inconsistent stress distributions which were not meaningful simulations. Thus, it became clear that the classical demonstration of design ultimate strength was not feasible without a thermal simulation. Such a simulation was not practical and probably not possible for the transient cases of interest. The objective of the test then had to emphasize the correlation of the stress analysis with the measured strain data. It also became evident that a test to ultimate load (1.4 times limit) would not achieve design ultimate stresses but would probably result in deformations and strains to render the airframe unusable for flight. At the same time, it became clear

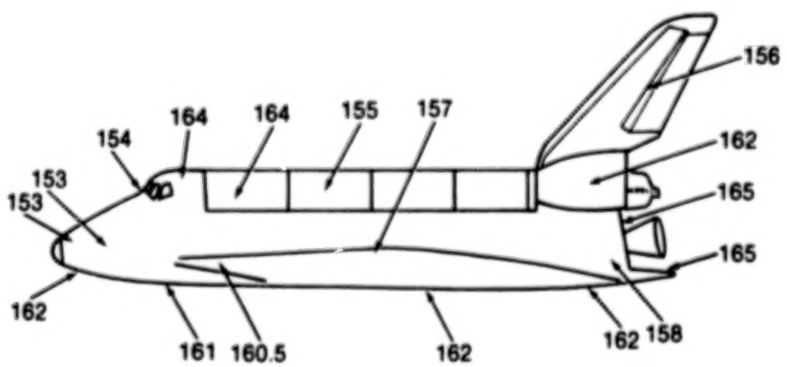


FIGURE 7.- ORBITER AERODYNAMIC-ACOUSTIC NOISE LEVELS.

ORIGINAL PAGE IS
OF POOR QUALITY

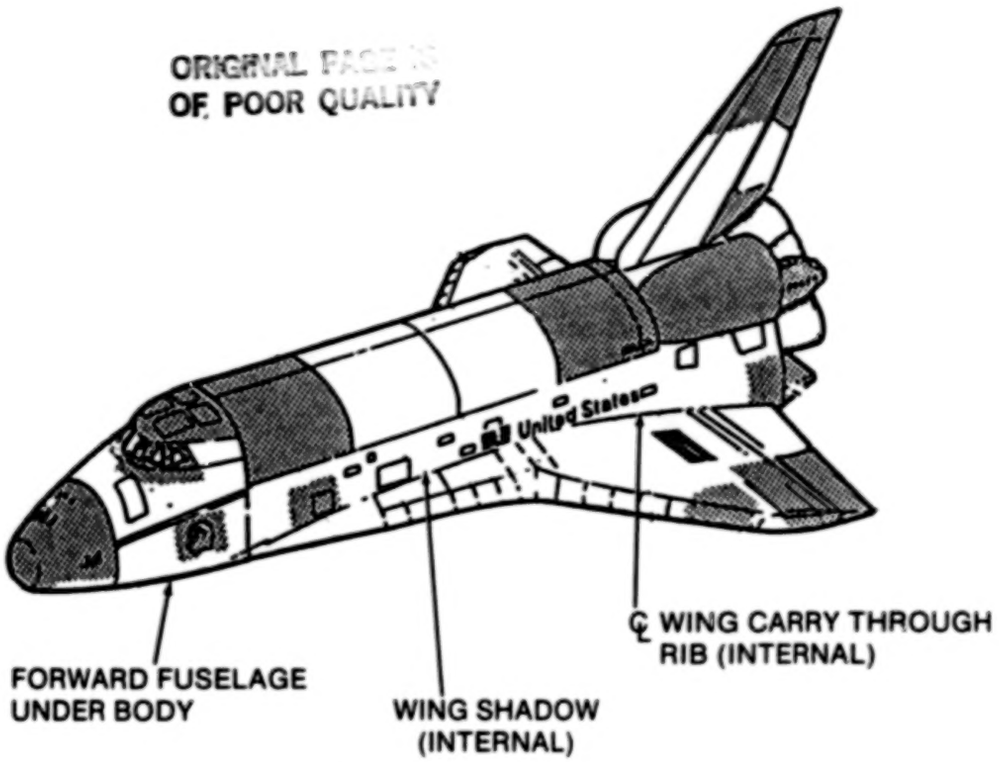


FIGURE 8.- ORBITER ACOUSTIC FATIGUE TEST ARTICLES.



FIGURE 9.- NOSE CAP TEST ARTICLE.



FIGURE 10.- VERTICAL STABILIZER TEST ARTICLE.

ORIGINAL
OF POOR QUALITY

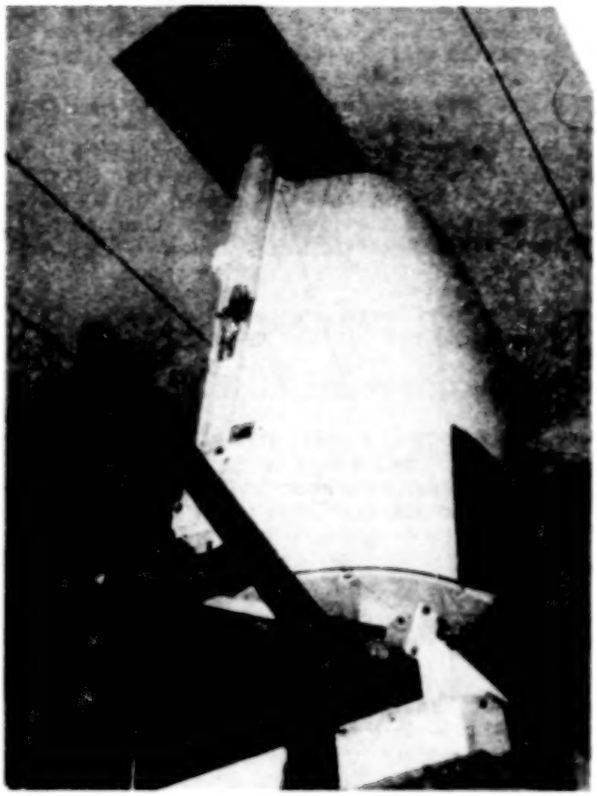


FIGURE 11.- OMS POD TEST ARTICLE.

that the structural test article (OV-099) had to be proved acceptable with the 5.4 loads data base even though it had been designed for the 5.1 data base. From this situation emerged a precedent-setting proposal: (1) test to 1.2 times the 5.4 loads, (2) require detailed stress analysis of each test condition, (3) include unit load test evaluations where required, (4) perform a combined thermal and mechanical test of the forward fuselage, (5) instrument sufficiently to compare with analysis and identify peak critical stresses, (6) perform additional component test investigations for ultimate strength and fatigue of identified critical interface hardware, (7) perform and document a critical post-test inspection, and finally, (8) refurbish the airframe structure for use as a flight vehicle. Daring as this proposal initially sounded, the technical detail and innovative imagination was sustained through complete management review as well as special technical review teams.

The test was a remarkable accomplishment. Thirty-nine test conditions simulating 32 critical design conditions were used. The engine thrust loads required innovative design concepts to accurately position the engine thrust vector. A typical test involved control of 256 jack loads which were distributed over 836 load application points. Because of lack of agreement with analysis, a complete influence test program was performed on the thrust structure; this program resulted in a high-fidelity empirical math model. Partial influence coefficient tests were performed on the payload reactions. The thermal test was accomplished on the forward fuselage by heating the external skin with external resistive blankets controlled in six zones. Cooling was provided by gaseous purge of the internal frame caps. When the test temperatures and gradients had been achieved, mechanical loading was applied to simulate the nose gear impact inertial loads.

The results of the testing were quite impressive and may be summarized as follows. The stress distributions in the critical test regions compared within 10 percent of the analysis with few exceptions. Exceptions were noted in the external tank forward and aft fittings and support structure, in the distribution of reaction between the front and aft spars of the vertical stabilizer, and in the y-load distribution of the main gear reaction. Supplementary instrumentation and component test articles were defined to fully instrument and certify these regions. The thermal test measured stresses compared well (10 percent) with those measured on the frames and internal structure. The skin stresses in the circumferential directions were considerably less (30 percent) than predicted analytically and in good agreement longitudinally. Hardware modifications resulting from the test data were identified. The forward reaction control system tank support structure, which failed in

test because of inadequate lateral stiffness, was redesigned, retested, and implemented. The empirical load distribution between front and aft spars of the vertical stabilizer resulted in drag angle modifications, which were implemented after component retest. The lateral load sharing of the main gear reaction was used to define the shimming and rigging specifications. The deflections measured around the nose landing gear door were used to define the rigging requirements.

The proof test concept used on the Challenger vehicle continues to achieve significant cost savings as it has been applied to several Space Transportation System (STS) payloads. This concept is a recognized verification concept for payloads as specified in JSC-14046. It is emphasized that use of this approach requires detailed engineering with attention to the structural details, sufficient instrumentation, and rigorous post-test inspection.

LESSONS LEARNED

THERMAL STRESSES

Mathematical surveys of peak transient thermal stresses were not technically feasible using the operational tools of the early 1970's. Technology and computational capacity are now available to perform integrated thermal/thermal stress surveys analogous to those used to identify the critical aerodynamic loading conditions. These analysis tools should be exercised and tested against flight data. Such studies would determine the criteria, extent, and accuracy of the methods before their use on the next major program.

GRAPHITE EPOXY MOISTURE

Graphite epoxy structure will absorb moisture by diffusion and will degrade in strength properties at temperatures above 250° F. It should also be noted that the honeycomb configurations can absorb enough moisture to be susceptible to failure by vaporization of the moisture and rupture of the honeycomb panel. Flight data appear to indicate that the thermal conductivity of such panels is complex. During the STS-1 mission, vaporization at a temperature exceeding 250° F caused the failure of a portion of the OMS fairing.

WINDOW STRUCTURE

Window design stress and sustained load flaw-growth parameters are sensitive to detailed knowledge of the loading environment, and the windows are susceptible to damage in flight as well as on the ground. Future technology thrusts are warranted to develop high-temperature glazings which are effectively tempered, perhaps by preloading concepts rather than conventional techniques. Annealed glazings should be used with comfortable conservative margins.

STRUCTURAL INSPECTION

Detailed routine structural inspection of large spacecraft will continue to be laborious and costly because of the required insulation systems. Technology advances are required to identify structural damage without requiring removal of the thermal systems. An innovative technique could be effectively tested and implemented during the STS operational era.

REFERENCES

1. Mackey, A.; and Gatto, R.: Structural Load Challenges During Space Shuttle Development. Paper presented at Space Shuttle Program Technical Conference, Lyndon B. Johnson Space Center (Houston, Tex.), June 28-30, 1983.

2. Emero, D. H.; and Spunt, L.: Wing Box Optimization Under Combined Shear and Bending. AIAA J., vol. 3, no. 2, 1966. pp. 130-141.

3. Lutfi, J. S.; and Nieder, R. L.: Space Shuttle Orbiter Venting - OFT Lessons Learned. Structures Branch Report, Lyndon B. Johnson Space Center (Houston, Tex.), Mar. 1983.

N85
16916

UNCLAS

D27

N85-16916

SPACE SHUTTLE EXTERNAL TANK PERFORMANCE IMPROVEMENTS – THE CHALLENGE

Harold R. Coldwater
NASA/MSFC, Huntsville, Alabama

Richard R. Foll, Gayle J. Howell, and Jon A. Dutton
Martin Marietta Aerospace
New Orleans, Louisiana

ABSTRACT

The External Tank (ET) has been actively involved in performance improvements since the inception of the program, primarily by weight savings. Weight savings were realized on the first block of flight articles [Standard Weight Tank (SWT)]. With a need for further performance improvements, the ET Program Office was requested to develop a program to reduce tank weight an additional 6000 lb and schedule delivery of the first lightweight ET (LWT) for June 1982.

The weight savings program was accomplished by (1) a unique approach to use of factors of safety, (2) design optimization, and (3) redesign of structures with large margins of safety which resulted in an actual weight savings of 7294 lb. Additional studies have identified further weight savings which will be implemented at appropriate times in production flow. Examples are an improved TPS system for the LH_2 tank aft dome and reduction of slosh baffles in the LO_2 tank based on flight data. All performance improvements were compared and selected based on non-recurring and recurring cost and technical risk.

INTRODUCTION

The primary method of ET participation in Shuttle performance improvement is weight savings. Weight savings were realized in the first block of flight articles (ET-1 through ET-6) as all had actual weights less than specification (Fig. 1). This was attributed to having to establish the specification weight using the high side of tolerance bands for metal and thermal protection system material thicknesses, whereas, the actual thicknesses were less than nominal.

Because the ET is the structural backbone of the Space Shuttle, load paths are complex, making weight reduction a difficult task (Fig. 2). With the challenge to reduce the weight of the basic design by 6000 lb to improve Shuttle performance and since the ET is the only expendable element of the Shuttle, economics of saving weight was extremely important. The weight savings were achieved for only $75/lb/flight increase in 1978 dollars (Fig. 3).

An initial list of 30 weight-saving candidates was identified with a potential saving of 7500 lb, providing a 20% contingency to assure the required 6000 lb. A screening process was established based on recurring and non-recurring costs as discriminators using a 1978 dollar base. The recurring cost screen was selected at $75/lb for welded aluminum fabrication and the non-recurring cost was $15,000/lb based on removing the same weight from the Orbiter. Since it was difficult to mix the Standard Weight Tank (SWT) and the Lightweight Tank (LWT) across the same tools, a single production line concept was used to minimize total costs.

WEIGHT SAVINGS PROGRAM

The weight-savings program was focused primarily on structural components and was accomplished by using the SWT and optimizing that design for LWT loads and environments to arrive at the LWT design. Additionally, all excessive margins of safety were reduced and a unique approach to factors of safety was applied. This approach was tailored to repeatability and predictability of loads. The standard factor of safety (F.S.) of 1.40 was applied to all aerodynamic and dynamic loads; whereas, a F.S. of 1.25 was applied to all well-defined loads, i.e., thrust loads, internal pressure, inertia loads (Fig. 4). The resulting combined equation,

$$F.S. = \frac{(1.25\ S/S + 1.40\ DYN.)}{S/S + DYN}$$

yields a factor of safety between 1.25 and 1.40.

- S/S = Steady State Loads (well-defined)
- DYN = Aerodynamic and Dynamic Loads

As the result of applying these factors to redesign and optimization, a total weight saving from the SWT to LWT of 7294 lb resulted.

DESIGN OPTIMIZATION

Most of the significant design optimization candidates not only saved weight (2748 lb), but also resulted in lower recurring cost. The major weight saving items are the antigeyser line deletion, crossbeam depth increase, LH_2 tank stringer removal, Fire-Retardant Latex (FRL) costing deletion, and changing interface hardware fitting material to Ti-6Al-4V (Fig. 5).

Antigeyser line deletion (Fig. 6), replaced by helium (H_e) injection in the main feedline to prevent geysers, took four years to develop through extensive flow testing in a lox feedline simulator and system testing on the Main Propulsion Test Article at NSTL. Main feedline injection is possible because helium rising in the feedline provides transpiration cooling to keep the liquid below saturation temperature, thus precluding formation of vapor which causes geysering. The change eliminated expensive propulsion hardware and a TPS ablator strip along most of the length of the LH_2 tank with more efficient packaging of the propulsion lines (GH_2 pressurant line moved to former location of the antigeyser line). The total weight savings of this change was 666 lb.

The ET/Orbiter aft crossbeam height was deepened and chord thickness was reduced providing increased structural stiffness with a resulting weight saving of 91 lb (Fig. 7). The ET/Orbiter aft crossbeam is limited by its proximity to the Orbiter. A flow restrictor attached to the top of the aft crossbeam was eliminated to allow increased height. This structure is an attractive candidate for composite construction.

A net savings of 235 lb was achieved by deletion of some of the stringer and Z-frames (Fig. 8) in the LH_2 tank, optimization of design of the Station 2058 frame and several intermediate frames, and operational optimization for loading the LH_2 tank. Dutailed finite element structural analyses in conjunction with cryogenic structural tests of the SWT LH_2 tank at MSFC showed that many of the integral stringers on the -Z axis (side away from Orbiter) and the intermediate Z-frames in five locations could be eliminated. Originally, the stringers and Z-frames were designed in to make as many of the LH_2 tank parts common to each other as possible for low cost. The 2058 frame was optimized by reducing backup fittings and reconfiguring stiffener design. Operational optimization was required to allow the LH_2 tank to be loaded without preload to assure no bulkhead buckling. Additional material was added to the aft LH_2 bulkhead to assure no buckling.

Since operational ET's will not be exposed for long periods on the pad, TPS top coat (Fire-Retardant Latex) could be eliminated over most of the acreage. The rind of the as-sprayed CPR-488 Spray-On Foam Insulation (SOFI) provides adequate protection from the elements for short periods of time (11 weeks). Areas where rind has been removed require painting with matching color top coat. Over 580 lb were saved by elimination of the top coat.

Major interface fittings were changed to more efficient and available materials. All titanium alloy fittings at the SRB/ET interfaces were changed from Ti-5Al-2.5 Sn to more widely used Ti-6Al-4V because of higher strength (Fig. 9). Most of the ET/Orbiter interface hardware (thrust struts, vertical struts and diagonal struts) had material change from 7075-T73 to 7050-T73 to take advantage of the 10 percent strength increase. The total weight savings from all these changes was 379 lb.

Other weight savings attributed to design optimization include miscellaneous hardware in the Intertank, using an integrated receiver/decoder in the range safety system, miscellaneous electrical wiring changes and deletions of development flight instrumentation and Thermal Protection System (TPS) thickness optimization on the LO_2 and LH_2 tanks. These savings totaled 797 lb.

MARGINS OF SAFETY REDUCTIONS

Structural margins-of-safety were reduced by changing design criteria (LH_2 proof test) and tailoring the structure to specific internal loads (Fig. 10). Commonality was reduced resulting in most margin reduction items increasing recurring costs. Those selected met the $75/lb criteria. Total weight saved by margin reduction amounted to 3244 lb.

The LH_2 tank proof test was originally based on a relief pressure of 37 psig. This was changed to a maximum operating pressure basis of 34 psig for LWT. This change makes the LH_2 tank a fail-safe

structure; like the fail-safe approaches used for the rest of the Space Shuttle. This change realized a weight savings of 500 lb.

Significant weight savings were also realized in the tank major frames, especially in frame 2058 in the LH_2 tank. Excellent correlation between structural testing data and analysis allowed this to happen. Intertank areas that were tailored to specific internal loads include all skin panels, frames, and the SRB crossbeam. Primary methods of reduction include skin panels reduced in thickness, stringers reduced in thickness and chem-milled; main frame chords machined down to tailor them for specific loads and intermediate frame chords were reduced in thickness.

The LH_2 tank structural changes included added machining of skin panels, especially on the -Z side, increasing the number of different panel types from 21 to 30. Also, two massive LH_2 thrust longerons were redesigned to eliminate unnecessary stiffeners. Elimination of the stiffeners reduced weight, improved producibility and improved the difficult weld of the longeron into the tank, our most difficult weld. Total weight savings of all these items is 1918 lb.

Significant weight reduction was also realized in the hardware at the ET/Orbiter interface (struts and fittings). Margin reductions amounted to a savings of 166 lb. Additional weight reductions occurred in the Intertank skin-stringer panels and frames. Thicknesses were reduced, resulting in a savings of 660 lb.

FACTOR OF SAFETY APPROACH

Structure designed by highly transient flight events (lift-off and high "q") will have a factor of safety of 1.40. Those structures designed by steady state events (max SRB acceleration, post SRB staging, end burn) will have a factor of safety of 1.25. Structures designed by a combination of the above will have safety factors between 1.25 and 1.40. Most of the 1312 lb saved by utilizing this approach came from reducing the material thickness of the Intertank thrust panels, crossbeam, thrust fittings, reinforced skin panels and struts, where 556 lb were removed. The LH_2 tank barrel skins and frames were reduced in thickness, and thrust longerons were redesigned and lightened resulting in a savings of 618 lb. Interface hardware (struts and ball fittings) were reduced in weight by 138 lb.

STRUCTURAL VERIFICATION PROGRAM

The primary ingredient in making the LWT performance improvements work was the unique approach to structural verification for the LWT. It was established that no full-scale, flight type structure would be provided for ultimate load testing, as the structural design approach was essentially the same as for the SWT. This, of course, drove the LWT program to heavy dependence on analytical techniques to verify designs.

STANDARD WEIGHT TANK (SWT)

Early in the SWT program, it was recognized that if extensive and continuing structural testing was to be avoided, it would be necessary to:

1. Establish ultimate strength capability for flight certification
2. Do sufficient testing to validate internal load distributions
3. Do influence coefficient testing to validate math models for analysis
4. Generate a data base to handle future load increase and margin assessments.

The SWT test program was established and completed successfully in late 1979. In all the tests, major emphasis was placed on determination of internal loads through extensive use of strain instrumentation, supplemented by deflection and thermal measurements. The total number of instrumentation channels used during the test program was in excess of 7000. Test data were essentially linear to ultimate load levels and provided satisfactory correlation with analytical predictions. With only minor adjustments based on test data, the analytical tools were verified for use in design of the LWT.

LIGHTWEIGHT TANK (LWT)

Upon undertaking the LWT program, a major effort was made in using SWT data to reduce test requirements necessary for LWT certification. Retests were necessary only in areas where there was a significant configuration change. Wherever configurations were similar with only dimensional changes, the design was supported by the verified analytical methods.

For LWT the only components requiring additional validation tests were:

1. The LH_2 tank - significant configuration changes in some barrel panels and the STA 2058 frame

2. The aft Orbiter/ET interface hardware - material changes and significantly reduced margin of safety.

Major changes in the LWT LH_2 tank consisted of removal of stringers in all 4 barrel panels adjacent to the ±Y axes and reduced margins of safety in the inner chord of STA 2058 frame to levels below those demonstrated on SWT.

A series of development tests was identified where the existing SWT tank could be modified structurally to simulate the LWT configuration in the barrel 4 area. Stringers were removed to test various stringer spacing effects on unpressurized panel stability. Out-of-plane stiffness of the LWT design STA 2058 frame was simulated by material removal of the inner chord. Wherever possible, original SWT instrumentation locations were utilized for correlation. Ultimate load test data indicated all structure responded linearly and good correlation was achieved with predictions further verifying the analytical allowables.

As a final step in the certification of the LWT, the first two LWT LH_2 tanks were subjected to a series of special tests in the Proof Test Facility at MAF.

LWT-1 was instrumented with deflection gages to support influence coefficient tests to verify modeling of the reduced stiffness STA 2058 frame.

LWT-2 was instrumented with nearly 500 strain gages to support limit load testing. Tests were conducted to verify performance of barrel panels having wide stringer spacing and reduced skin thickness, to verify analysis and performance of the longeron, barrel panel 2 in compression and STA 1871 frame; and to validate the redesigned STA 2058 frame. All measurements during these tests were linear and agreed very well with predictions.

Maximum utilization has been made of test data generated during the SWT and modified SWT structural test programs, and coupled with judiciously selected limit load testing on flight hardware has provided verification of the structural modifications made to establish the LWT and realize and exceed the goal of 6000 lb of performance improvement.

IMPLEMENTATION STATUS

All engineering has been released; preliminary design reviews, critical design reviews, and design certification reviews have all been completed. The first Lightweight Tank was delivered to the Kennedy Space Center in August 1982, and was flown successfully on STS-6 in April 1983.

ET IS ALREADY ACTIVE IN SHUTTLE PERFORMANCE IMPROVEMENT:

STANDARD WEIGHT ET

	ET-1	ET-2	ET-3	ET-4	ET-5	ET-6
Specification Weight	78,278 LB	78,581 LB	77,789 LB	77,902 LB	77,362 LB	77,457 LB
Actual Weight	77,099 LB	77,249 LB	75,770 LB	75,895 LB	75,172 LB	75,453 LB
Performance Improvement	-1,179 LB	-1,322 LB	-2,019 LB	-2,007 LB	-2,290 LB	-2,004 LB

LIGHTWEIGHT ET

	LWT-1	LWT-2	LWT-3
Specification Weight	71,278 LB	71,173 LB	71,144 LB
Actual Weight	66,824 LB	67,009 LB	66,809 LB
Performance Improvement	-4,454 LB	-4,164 LB	-4,335 LB

Figure 1. Performance Improvements.

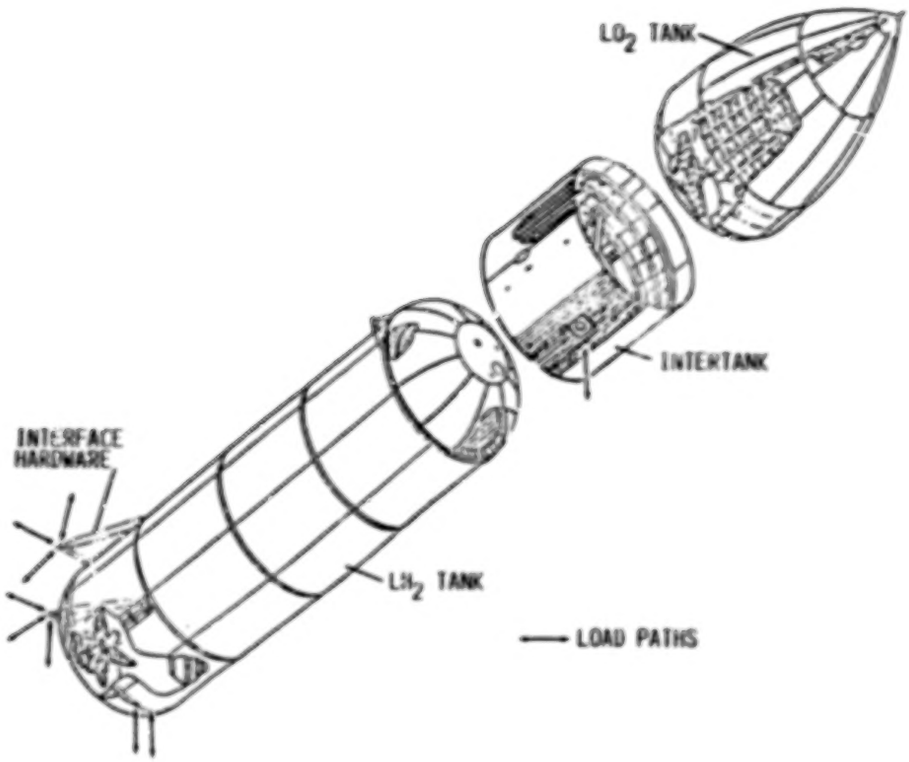


Figure 2. ET General Arrangement.

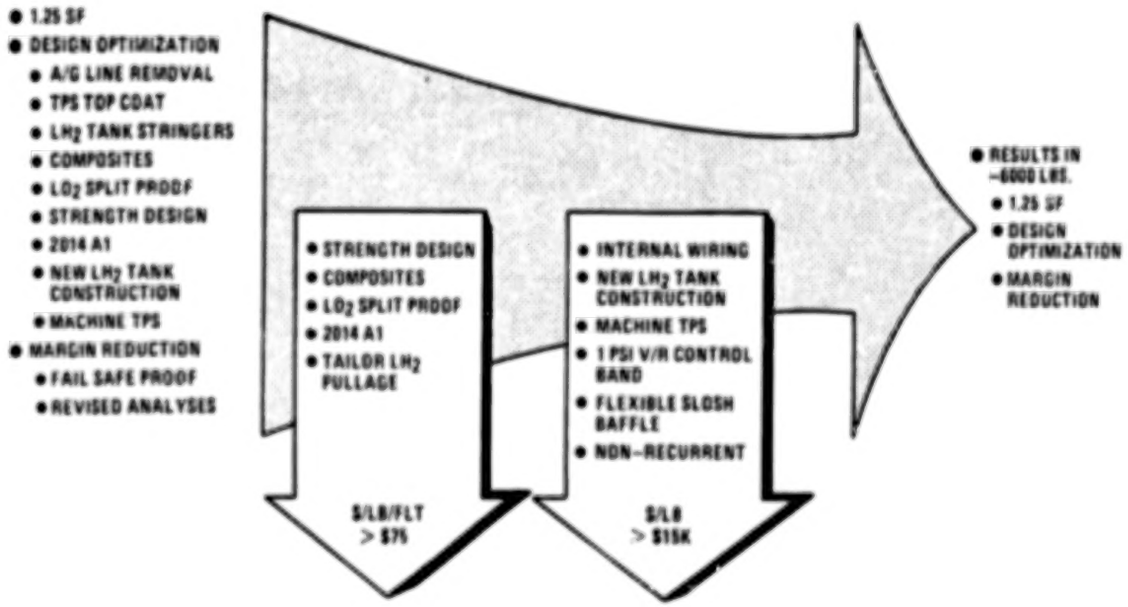


Figure 3. Weight Savings Screening.

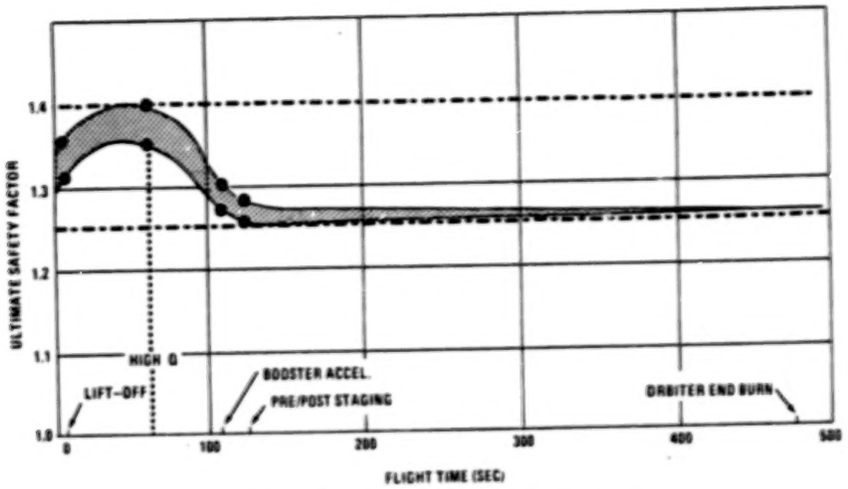


Figure 4. A Different F.S. Approach.

- MAIN FEEDLINE GHe INJECTION (ANTI-GEYSER LINE DELETION)
- EFFICIENT CROSSBEAM IN INTERTANK
- LH_2 TANK STINGER/Z-FRAME REMOVAL
- DELETE FIRE-RETARDANT LATEX PAINT ON TPS.
- NEW MATERIALS
- MISCELLANEOUS HARDWARE

Figure 5. Design Optimization Within Design-To-Cost Goals.

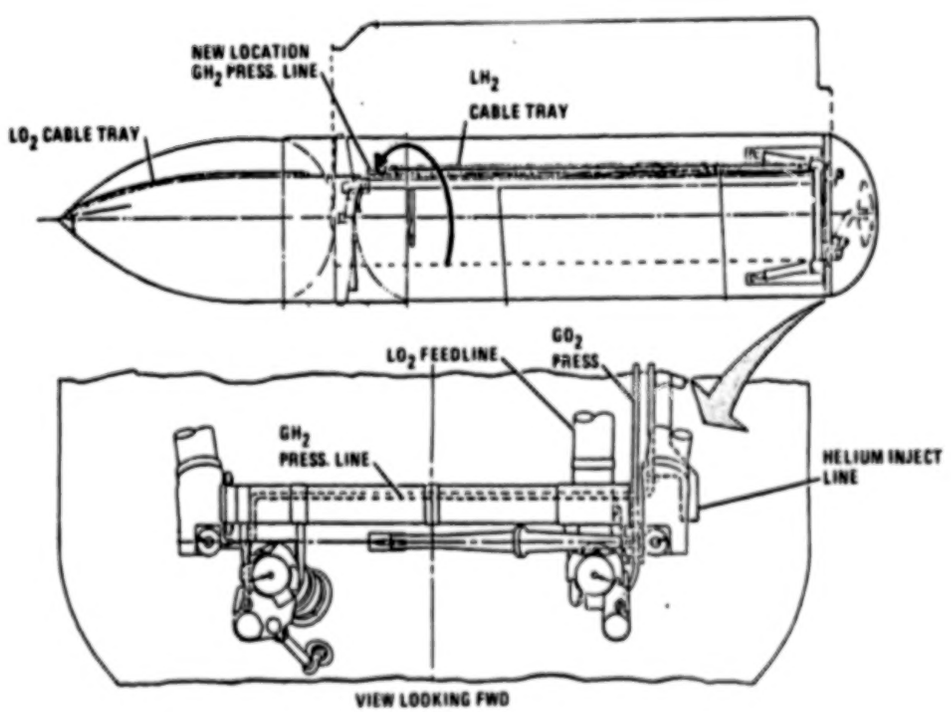


Figure 6. Main Feedline Injection Saves Weight and Dollars.

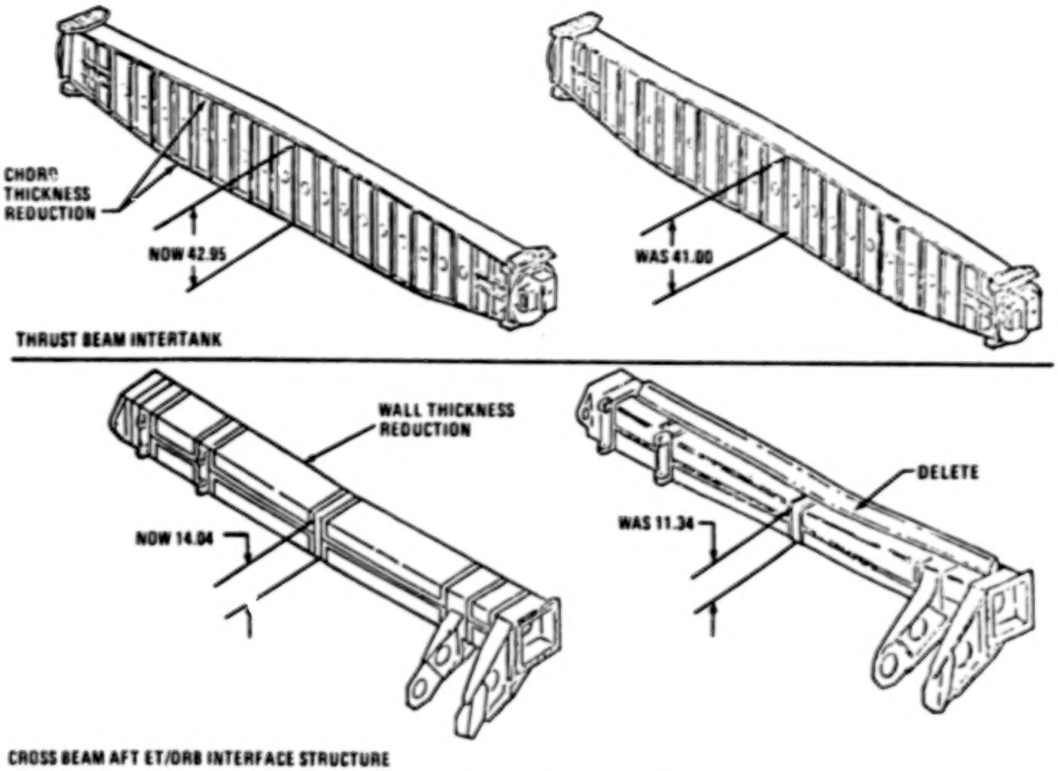


Figure 7. More Efficient Crossbeams.

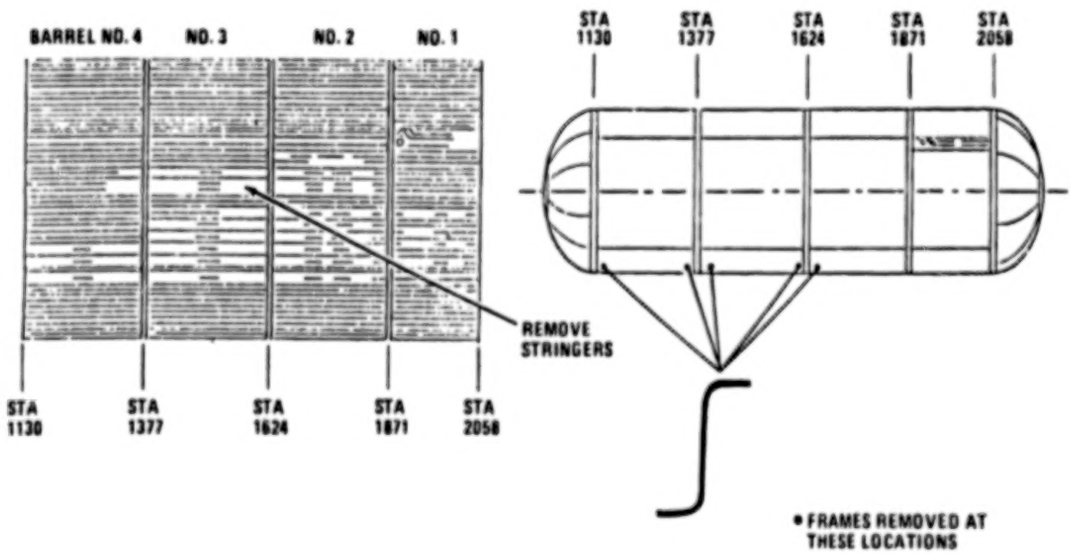


Figure 8. LH_2 Tank Selected Stringer and Z Frame Removals.

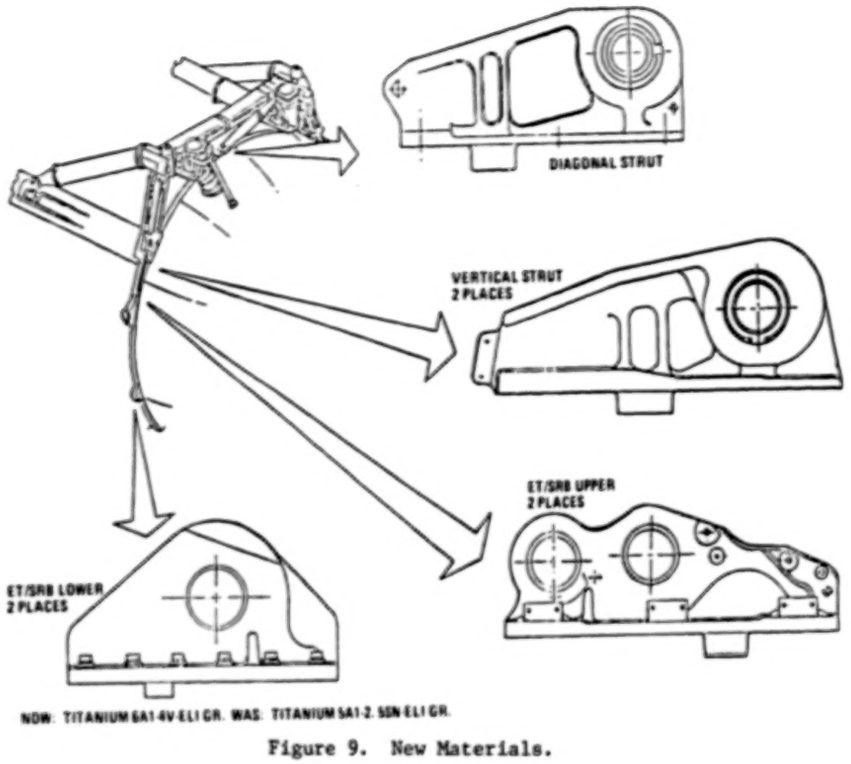


Figure 9. New Materials.

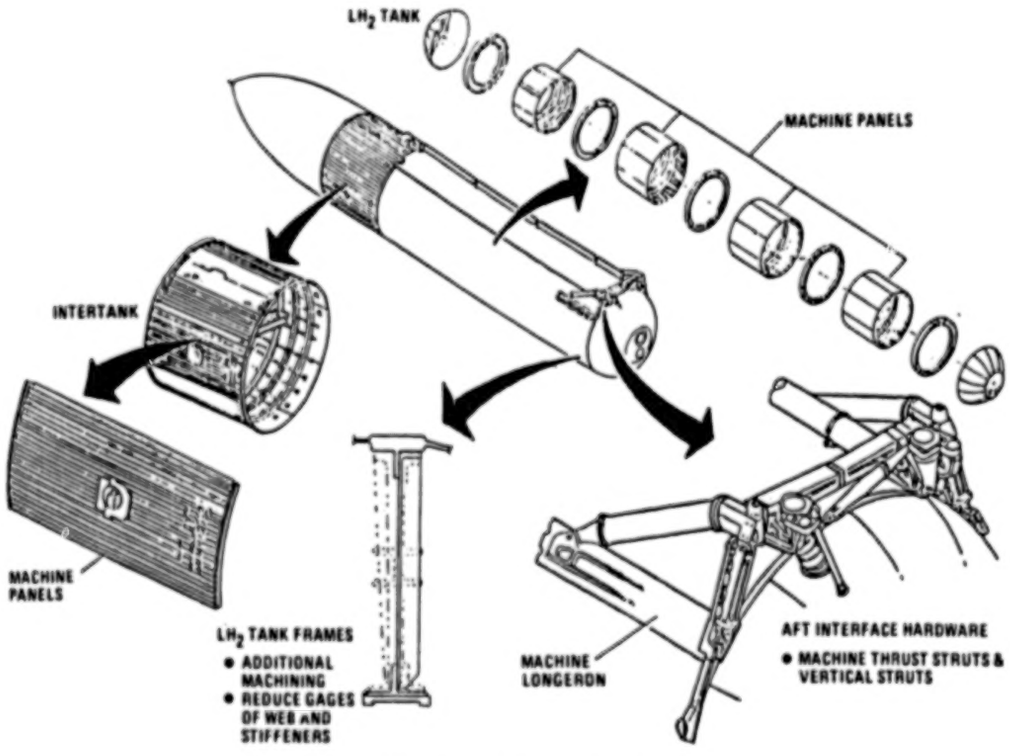


Figure 10. Margin Reduction Areas.

ORIGINAL PAGE IS
OF POOR QUALITY

N85
16917

UNCLAS

N85-16917

STRUCTURAL AND MECHANICAL DESIGN CHALLENGES OF SPACE SHUTTLE SOLID ROCKET BOOSTERS SEPARATION AND RECOVERY SUBSYSTEMS

William R. Woodis
Martin Marietta Corporation
Denver, Colorado

and

Roy E. Runkle
Structures and Propulsion Laboratory
Marshall Space Flight Center, Alabama

ABSTRACT

The design of the Space Shuttle Solid Rocket Booster (SRB) subsystems for reuse posed some unique and challenging design considerations for the engineers at Marshall Space Flight Center, Alabama. The separation of the SRBs from the Cluster (Orbiter and External Tank) at 150,000 ft when the Orbiter engines are running at full thrust meant the two SRBs had to have positive separation forces pushing them away. At the same instant, the large attachments that had reacted launch loads of 7.5 million pounds thrust had to be severed. These design considerations dictated the design requirements for the pyrotechnics and separation rocket motors. The recovery and reuse of the two SRBs meant they had to be safely lowered to the ocean, remain afloat, and be towed back to shore. To safely lower a 150-ft long, 85 ton, steel cylinder to the ocean from a 220,000-ft free fall was a design challenge in every sense. It meant the development and testing of the largest parachute recovery system in use in the free world. The parachutes are capable of withstanding loads of 300,000 lb and slowing the SRBs, that would impact at 500 to 600 ft/sec to 85 to 95 ft/sec.

INTRODUCTION

The Space Shuttle concept was based on the idea of reducing the launch costs associated with putting a payload into space. One means of reducing launch costs is to return as much of the launch vehicle as practical for a safe Earth landing to be recycled for another launch.

NASA has achieved this objective by having the Orbiter "fly" back to Earth from orbit, land like an airplane, and be refurbished for future launches. Further, NASA decreed, from the onset of the Space Shuttle Program, that the Solid Rocket Boosters would also be recovered and reused after each launch. Early cost trades showed that this approach would be cost effective over the old Saturn throwaway booster concept.

This SRB reuse concept and the "piggy back" Space Shuttle design posed many unique and challenging design considerations for the engineers at Marshall Space Flight Center. The SRB reuse concept meant that a recovery system had to be developed that would safely lower the free falling SRB to an ocean landing at an acceptable impact velocity. The "piggy back" Space Shuttle design imposed special design requirements on the pyrotechnic separation systems that were to be used on the Solid Rocket Boosters (SRBs).

This paper will discuss some of the structural and mechanical challenges posed by the design of the pyrotechnic and recovery subsystems of the SRBs to the engineers and designers at Marshall Space Flight Center, Alabama.

PYROTECHNIC SEPARATION SYSTEMS

The pyrotechnic separation systems and the recovery subsystems are closely interrelated in that most of the separation systems' functions are necessary in order for the recovery subsystem to perform its function. Figure 1 shows a typical launch and recovery sequence of the Space Shuttle SRBs. At approximately 150,000 ft altitude, the three struts, which fasten the aft end of the SRB to the ET/Orbiter combination, and the separation bolt, which fastens the forward end of the SRB to the External Tank (ET)/Orbiter combination, are separated (by pyrotechnics). At the same time, four Booster Separation Motors (BSMs) in the frustum and four BSMs in the aft skirt of each SRB fire to push the SRBs away from the accelerating ET/Orbiter. Figure 2 shows the relative location of these separation systems on the SRB.

After the SRBs have coasted up to an apogee of 220,000 to 250,000 ft, they free fall back to Earth. At approximately 16,000 ft altitude, a high-altitude baroswitch closes which fires three nose

cap thrusters which push the nose cap off the frustum. This event initiates the parachute sequence which will be discussed later. At approximately 9,000 ft altitude, a low-altitude baroswitch closes which fires a linear shaped charge that cuts the frustum free of the SRB. This action allows deployment of the main parachutes out of the frustum.

At approximately 1,000 ft altitude, a timer in the forward Integrated Electronics Assembly (IEA) fires an LSC which separates the aft 60 in. of the nozzle (nozzle extension) from the nozzle. At water impact, a "G" switch in the forward IEA senses 7.5 to 8.5 "g's" and fires six separation nuts which release the three main parachutes from the SRB.

SEPARATION BOLT

The forward SRB separation bolt is shown in Figures 3 and 4. The bolt is fabricated of 4340 steel heat treated to 180 to 200 ksi ultimate tensile strength and nickel plated. It is approximately 3 in. in diameter and 2 ft long. Launch and flight loads dictate that the bolt withstand 189,000 limit tension loads a bending end moment of 55,344 in.-lb. The bolt is torqued to 900 to 1,100 ft-lb of torque. The bolt has redundant pressure cartridges. At SRB burnout, redundant separation signals are sent to each of the two pressure cartridges. The pressure generated by each cartridge acts against a primary piston. This force is amplified through compression of a soft lead coupling and is transmitted to the secondary piston. The force generated by the secondary piston reacts against the secondary piston of the redundant side. This force causes the bolt housing to fail in tension at a pre-machined fracture groove. The sudden release of tension plus the extra margin of force/piston overstroke accelerates both ends of the bolt to approximately 100 ft/sec. The bolt ends are contained by crushable honeycomb installed in the SRB thrust fitting and the ET bolt catcher.

SRB/ET STRUTS

The aft SRB/ET attachment/separation system posed a unique design challenge in several areas. The strut design had to accommodate 5 to 6 in. of relative longitudinal motion between the SRB and ET, be able to transmit axial loads of 393,000 lb, transmit commands from the Orbiter/ET to the SRB, and be able to separate in a maximum of 0.010 sec. The struts had to be able to accomplish these tasks in severe flight environments. Figure 5 shows the orientation of the three strut assemblies on the SRB. All three terminate in the ET attach ring of the SRB. The lower strut and the diagonal strut are virtually the same design and could be interchangeable while the upper strut is considerably more complex because it carries the command and instrumentation signals across the ET/SRB interface.

During the stacking operation at KSC, the ET is lowered between the two vertical SRBs. The two diagonal struts (two SRBs) are pre-adjusted in length (although all three struts have adjustment capability) and are the first to be fastened to the ET when it is resting on the forward thrust posts of the two SRBs. The upper struts are the next system to be attached to the ET. At KSC, the diagonal and upper struts are premated to the SRB and swung back out of the way in low bay. The lower struts are the third and final SRB aft attach system to be mated to the ET in the high bay. They are brought into the high bay as a separate piece of hardware and mated to the "stack" at both ends — the SRB on one end and the ET on the other end.

During the initial mate, all three strut systems must rotate aft (or down) 9.5 deg. to support the ET and Orbiter (Orbiter and ET weight is supported by the forward thrust post). However, when the ET is loaded, the cryogenic temperatures of the fuel and oxidizer shrink the ET to 5.5 to 6 in. and all three strut systems swing up to a near or slightly above horizontal position. The upper strut, in addition to accommodating these initial "stacking operation" motions, must be able to rotate 18 to 20 deg (11 to 12 in.) further forward. This additional movement allows the seven electrical connectors to be separated by a more axial tensile force than sheared off by the wiping motion of the ET passing by the SRB (the strut separation planes are normal to the relative motion of the SRB/ET). All three strut systems have covers which protect the NSI cables that connect to the pressure cartridges. Figure 6 shows the cover configuration for the lower and diagonal struts. This cover is oriented on the aft side of the struts and protects the NSI cable from aerodynamic forces and heating during Space Shuttle ascent. The NSI cables cross the separation plane and are physically pulled apart by the motion of the SRB leaving the ET. It requires approximately 140 lb of pull to break the NSI cables on the lower and diagonal struts. The upper strut NSI cable crosses the separation plane through one of the seven electrical connectors (mentioned earlier) (Fig. 7).

Because of the need to protect all the electrical cables passing over the upper strut, the upper strut cover completely encapsulates the strut (Fig. 7) and is more complex than the small covers on the lower and diagonal struts. The large motion requirements of the struts, especially the upper strut, caused considerable difficulty in designing a Thermal Protection System (TPS) for the Orbiter command wiring and NSI cables. The TPS had to accommodate the motion and still prevent hot gas from reaching

the cables. No mechanical transition sections from the strut to the ET ring could be designed that was rigid enough to withstand aerodynamic forces and yet flexible enough to accommodate the large angular excursions of the strut. The TPS system, finally derived for this area, is basically a "bandade" approach. The wires are wrapped with blast tape, then PR 855 foam is used to fill in between the wires. To protect the foam, it is covered with a silicon rubber and finally with three to five layers of EPDM rubber. It is desirable to accomplish the TPS closeout with the struts in the launch position (relative to the ET ring). However, this is not possible because this only occurs after ET fueling at the launch pad. Therefore, as much of the PR 855 foam and silicon rubber are pushed into the cavity as possible in an effort to allow the foam to expand and fill the gap left by the upward motion of the struts during ET filling. The whole TPS closeout process on the struts is extremely time consuming and cumbersome and will undoubtedly become an assembly "tent pole" as Shuttle launch rates increase.

SEPARATION MOTORS

Each SRB has eight Booster Separation Motors (BSMs) which fire, simultaneously, with the thrust post bolt and the strut separation initiators. These separation motors (four aft and four forward) fire for a nominal 0.7 sec and produce 20,000 lb thrust each (Fig. 8). The four forward BSMs are mounted in the frustum and canted inward toward the Orbiter and have their nozzle pointed forward (upward when sitting on the launch platform), their thermal shield design is rather complex. The thermal shield is required to insure that, during ascent, no hot gaseous flow funnels down the nozzle and impinges on the propellant. If this were to happen, the motor could be auto-ignited by this phenomena. Also, because of the possible Orbiter debris problem, the forward BSM thermal shield design had to insure that no debris would be generated at the time of BSM firing. This problem does not exist with the aft BSMs because they are aft of the Orbiter and pointed away from the Orbiter wings/tiles. The thermal shield design for the forward BSMs looks and functions like a hinged cover or door. The hinge pin is actually yielded in torsion by the opening of the door. In this way, the kinetic energy of the door is changed into heat energy by the yielding of the hinge pin (Fig. 9). Thus, the door is retained (i.e., no debris). Further, a ratchet latching mechanism insures that the door will not inadvertently swing closed after opening. The aft BSM thermal shields (covers) are not nearly as complex and are blown off at BSM ignition (Fig. 10). Because of the location of one of the skirt support posts, it was necessary to place one of the four aft BSMs by itself on the opposite side of the post structure (Fig. 11). The separation motor system and the structural separation system are initiated simultaneously. Redundant separation signals to the forward and aft separation motor systems initiate redundant NSI detonators. The detonation shock from the NSI detonators propagates through two CDF manifold and eight CDF assemblies to eight CDF initiators mounted in the separation motors (Fig. 12).

NOSE CAP THRUSTERS

The nose cap separation system is activated by the high baroswitch at approximately 16,000 ft. Because the nose cap encapsulates the drogue parachute/pilot parachute packs, the nose cap must be pushed off with a minimum of 80 ft/sec to clear the parachutes during nose cap deployment. The thruster (Fig. 13) consists of a small piston inside a cylinder that, using the gaseous pressure produced by the pressure cartridge, produces a 30,000-lb thrust over a 6-in. stroke. At the end of the 6-in. stroke, the piston rod separates from the piston and is ejected with the nose cap. Since the nose cap separation system is not man rated (i.e., is not required to function during ascent for mission success), it is a simplex system (Fig. 14). The thruster serves a dual purpose in that a 0.5-in.-diameter bolt screws into the piston body to fasten the nose cap structure to the frustum. To achieve this purpose, the thruster has a shear flange that will withstand a static tension load of 10,000 lb applied through the 0.5-in. nose cap holddown bolt's longitudinal axis prior to actuation. The thruster will also withstand a torque of 1,000 in-lb applied to the 0.5-in. holddown bolt. The shear flange is sheared by the upward movement of the piston during actuation. The majority of the thruster components (body, piston, piston rod, etc.) is 4340 steel.

SRB/FRUSTUM SEPARATION RING

The frustum separation system consists of one NSI detonator, one CDF assembly, and one frustum separation assembly (Fig. 15). During descent, as the SRB passes through approximately 6,000 ft, the low altitude barometric switch sends a fire command to the frustum separation pic. The pic initiates an NSI detonator located in the top ring of the forward skirt. The output of the detonator is propagated through the CDF assembly which detonates the Linear Shaped Charge (LSC) in the detonator block assembly. The detonator block assembly LSC detonates the LSC in the frustum separation assembly. The 30 grains/ft HMX Jetcord detonates at 7,000 m/sec and severs the 0.215 thick 2219 aluminum separation ring and releases the frustum from the forward skirt/SRB.

MAIN PARACHUTE SEPARATION NUT

The main parachute separation system consists of six separation nuts (Fig. 16) which are mounted to the underside of the forward skirt 401 ring. A 1.25-in.-diameter bolt fastens the main parachute attach fitting to the upper side of the 401 ring, passes through the ring, and threads into the separation nut.

At splashdown, a "G" switch located in the forward IEA of the SRB closes which issues a fire command through the recovery logic to the main parachute disconnect pic. The pic ignites an NSI detonator (Fig. 17) whose detonation is propagated through a CDF manifold, and six CDF assemblies to six CDF initiators installed in each of the six separation nuts attaching the three main parachutes to the SRB (there are two separation nuts per main parachute). When fired, these initiators pressurize the separation nut causing the case/collet ring to slide back opening the collet and releasing the main parachute attach bolt (Fig. 18). The attach bolt is ejected from the separation nut by the ejector piston and the tension in the main parachute links. The separation nuts are presently designed for a parachute bolt tension of 135,000 lb and a bolt torque of 750 to 800 ft-lb.

RECOVERY SUBSYSTEM

Each SRB contains a Recovery Subsystem which consists of five parachutes and associated support/attachment and deployment hardware (Fig. 19). All of the parachutes are ribbon construction made of nylon webbing, are 20 deg conical geometry, and have 16% geometric porosity. All five of the parachutes are contained in the SRB nose cone. The nose cone consists of a 75-in. tall nose cap forward section and a 120-in. tall frustum aft section. The nose cap houses the pilot and drogue parachutes while the frustum contains the three main parachutes. The frustum also contains the high and low altitude baroswitches described earlier. As might be expected of a Recovery (parachute) system that is designed to decelerate an 85-ton 150-ft-long cylinder, that is falling at about 600 ft/sec, all of the parachutes are of heavy duty construction. The pilot parachute is 11.5 ft in diameter and has a design limit load of 14,500 lb. It has a 50-ft trailing distance. It is deployed by the nose cap which has been ejected from the SRB by three piston thrusters at 80 to 90 ft/sec. The pilot parachute has 16 gores (i.e., 16 suspension lines), weighs 42 lb packed, and is attached to the top of the drogue parachute pack.

The drogue parachute is 54 ft in diameter and has 60 gores. It has two reefing stages (i.e., reefing lines) with two reefing cutters placed 180 deg apart on each reefing line. The design limit load of the drogue is 270,000 lb and its construction is massive. A few design details will illustrate this as follows: The radials are made of 4 plies of 4,000-lb strength nylon webbing, the 60 suspension lines are each made of 1 ply of 150,000-lb webbing, the reefing lines are made of 3 plies of 12,000-lb webbing, the horizontal ribbons are 1,000-, 1,500-, and 2,000-lb webbing, etc. The drogue parachute pack weighs 1,270 lb. The function of the drogue parachute is to rotate the descending SRB into a tail first orientation so that the cluster of three main parachutes can be deployed and the risks of their entanglement are minimal. The drogue parachute slows the SRB, and, when the low altitude baroswitch closes, provides the necessary force for main parachute deployment. The drogue parachute canopy trails the SRB by 105 ft and, when the frustum is released from the SRB, extracts the main parachutes (lines first) out of their deployment bags.

Each main parachute is 115-ft in diameter and has 96 gores. Like the drogue, they have two reefing stages (i.e., reefing lines) with two reefing cutters placed 180 deg apart on each reefing line. The design limit load of each main is about 174,000 lb. The radials on each canopy are made of two plies of 3,000-lb webbing, the 96 suspension lines are made of 6,000-lb webbing, each reefing line is made of two plies of 9,000-lb webbing, and the risers and dispersion bridles consist of 6 plies of 15,000-lb webbing. Each main parachute pack weighs about 1,700 lb. The function of the three main parachutes is to decelerate the SRB to an acceptable water impact terminal velocity (about 85 to 90 ft/sec) and then release from the SRB and be retrieved from the ocean by retrieval vessels.

PARACHUTE DEPLOYMENT SEQUENCE

The typical deployment sequence is shown in Figures 20 and 21. At approximately 16,000 ft the sequence is initiated by the high baroswitch as discussed earlier. The nose cap deploys the pilot chute whose function it is to deploy the drogue parachute. Early studies concluded that the nose cap did not have sufficient energy to deploy the drogue under all deployment conditions. After the pilot bag has moved about 8 ft, zero time delay cutters (100 msec) are initiated to release the drogue pack restraint straps. The pilot parachute inflates and pulls the drogue bag from the SRB. The drogue parachute is then deployed lines first. The pilot parachute and drogue bag are one-use items and are not recovered.

At drogue deployment, the angle of attack of the SRB is between 80 and 140 deg. The function of the drogue is to rotate the falling SRB into a tail first orientation and reduce its velocity so that the cluster of three main parachutes can be deployed with minimum risk of deployment damage, entanglement or excessive loads. The drogue also provides the force required to deploy the main parachutes liner first from the frustum. After the main parachutes are stripped from their deployment bags, the drogue parachute, frustum and main parachute deployment bags continue to water impact and are retrieved for reuse.

The function of the three main parachutes is to decelerate the SRB to an acceptable water impact velocity of 85 to 90 ft/sec. In the initial concept, the main parachutes were released from the SRB at water impact to facilitate retrieval of both the SRB and the main parachutes.

The large recovery weight (160,000 to 170,000 lb) and the ocean landing of the SRBs posed some interesting design challenges for the Recovery Subsystem designers. A list of a few of these design challenges is as follows:

Pilot/drogue deployment.

Drogue loads measurement.

Main parachute flotation/energy absorbers.

Main loads measurement.

Each of these "design challenges" will be briefly addressed in this paper.

PILOT/DROGUE DEPLOYMENT

As stated earlier, because of the need of deployment condition flexibility (deployment dynamic pressure of 127 to 340 lbs/ft^2, SRB pitch attitudes of 70 to 140 deg, and SRB roll rates of 0 to 135 deg/sec), the decision was made to use a pilot parachute to insure a repeatable, orderly, drogue parachute deployment.

Figure 20 shows the deployment sequence of the nose cap pilot/drogue. The pilot bag is connected to the base of the nose cap by a three-legged bridle system. In order to limit the loads into the nose cap interface attach point and the pilot parachute bag, a method of absorbing the shock caused by the relative velocity between the nose cap and pilot parachute had to be devised.

Rip stitch type energy absorbers (Fig. 22) were developed by which shock loads could be controlled by varying the number of piles and the stroke of the energy absorbers could be controlled by varying the number of bight elements. After many static and dynamic development tests using various parent material fabrics, stitch patterns, thread strength and material, the selected configurations consist of 6,500 lb strength nylon MIL-W-4088 TY XIII with a modified six-point stitch using eight cord thread. Initially, we experienced problems of the parent material failing rather than the stitches failing. We noted that if the first stitch failed, the remainder failed in an orderly fashion with minimal damage to the parent material, the desired result. Initial test success was achieved by simply cutting the first stitch in each point of each bight. Later it was determined that the same results could be obtained by lifting the needle on the sewing machine at the end of each point stitch pattern and moving it laterally a small amount before returning back along the bight. The selected configuration produces 730 ± 230 lb per ply and 1 ft of stroke per bight. A three-ply, 10-bight configuration is used to connect the nose cap to the pilot parachute bag (Fig. 23). A 12-ply, 8-bight configuration of the same basic design is used to connect the main parachute floats to the apex of the main parachutes (discussed later). The momentum/aero drag of the nose cap provides the force necessary to break the cotton ties that fasten the pilot bag to the top of the drogue bag. As the pilot bag leaves the drogue pack, cotton ties break allowing the pilot to deploy lines first out of the bag. A drogue bag restraint loop passes through loops in the end of six drogue bag restraint straps and through two redundant reefing cutters. The other end of the six restraint straps attach to ratchet fittings on the frustum top deck to hold the drogue pack onto the frustum (i.e., SRB) until the restraint loop is cut by either of the two cutters. The two cutters are zero time cutters, i.e., they fire within 100 msec after their firing pin is pulled. The first 8 ft of motion of the pilot bag provides this pulling motion. A lanyard from the pilot bag is fastened to the firing pin of the cutters. As the pilot bag leaves, the lanyard becomes taut and pulls the cutter firing pins. We recognized a potential problem: after the two cutters had performed their function (i.e., they had cut the restraint loop), they would be unrestrained and flying freely. Because of their size and mass (2 lb), they would be potential "bullets" and could pass through the drogue canopy. If they severed a major structural member (vent line, radial, or suspension line), total loss of the SRB could result. This potential problem was averted by providing another lanyard to assure that the cutters would remain attached to the drogue deployment bag.

DROGUE DECK FITTING/LOAD PINS

At the time of drogue deployment, the SRB may at any angle of attack from 80 to 140 deg with pitch and yaw rates of 15 deg/sec and a roll rate up to 135 deg/sec. The deck fittings therefore must accommodate loads in any direction and allow changes in direction as the SRB is stabilized in a nozzle-first attitude. A double clevis arrangement shown in Figure 24 shows the selected configuration. Twelve of these fittings (each holding five suspension lines) react the drogue loads into the frustum.

At the high roll rates possible at drogue deployment, the possibility of the suspension lines twisting into a node and causing them to rub against each other as the SRB swings back and forth (pitch and yaw) was of some initial concern. A swivel attachment between the drogue and SRB was considered. However, the physical size required to react 270,000 lb, plus the tendency of bearings to lock up due to rapid load onset and the large increase in loads to individual fittings resulting from a confluence point in the drogue suspension lines caused the swivel concept to be discarded. Also, analysis showed that the rubbing force of the suspension lines, the relative velocity between suspension lines and the small number of cycles were all low enough to present a low risk. To date, after six drop tests and six Shuttle flights (12 SRBs), no suspension line damage due to twisting has been observed. The first development air drop test gave an indication of significant galling at the point contact of the 4340 steel clevises. An application of dry film lube on the rubbing surfaces has eliminated this problem.

The requirement to measure drogue loads during both development air drop tests and the first six Space Shuttle flights presented a unique challenge. Because of the symmetry of the twelve drogue attach points and the limitation of data channels, six of the fittings were instrumented. The concept of standard load cells placed in the suspension line was discarded because of the difficulty of assuring that they would not "bang" into each other during deployment and possible twisting of the lines and the expected problems of protecting the wires leading from the load cells to the frustum deck. The severe rotation and chafing environment of the clevises precluded putting strain gages on the fittings and there were not enough data channels available to instrument the four bolts on each fitting. The obvious choice remaining was the pin that fastens the drogue suspension line spool to the deck fitting shackle. Several instrumentation personnel advised against instrumenting a pin in bending because of lack of repeatability due to pin clocking and fulcrum shift during loading. The final load pin design is shown in Figure 25. Strain gages are applied to the machined "neck" of the pin. Collars are then pressed on to each end with a tolerance of ± 0.0002 in. The spacing between the ends of the upper shackle is controlled by placing a spreader tube between the clevis legs. Clocking accuracy (and pin retention) was accomplished by drilling the flange at one end of the pin and fastening it to the shackle by a screw. Once the unit is calibrated to a load of 35,000 lb, the shackle, pin and spreader tube remain as a unit until flight, so that the configuration flown is identical to the one calibrated. These drogue pins have proven very reliable and accurate. Only three drogue load measurements out of 72 pins have been lost on the first six Shuttle flights (no measurements were available from STS-4 due to SRB loss, but the retrieved drogue load cells were intact). Load accuracy of ±3% with 1% repeatability have been achieved.

MAIN PARACHUTE FLOTATION/ENERGY ABSORBERS

The expense of the large heavy duty parachutes dictated that they be retrieved for reuse. The original End Item Specification stated that access to the parachute apex be provided because riser-first retrieval causes the parachute to inflate under water and act as a sea anchor. The drogue parachute remains attached to the frustum. Access to the apex is provided by a long (175 ft) retrieval line supported by a small peanut float for easy location and retrieval.

The initial recovery concept called for the main parachutes to separate from the SRB at water impact and therefore had to be self supporting. Floats (Figs. 26 and 27) were attached to the apex of the main parachutes through 12-ply 8-bight energy absorbers (discussed earlier). The load from the floats acquired limiting for two reasons: (1) to avoid structural damage to the float bags and main parachute vent lines and (2) to limit the acceleration of parachute location aid (PLA) that was originally to be housed in the float. The PLA was never developed. The development air drop program confirmed our concern that retaining the flotation/PLA system in the dynamic environment of main parachute deployment would be difficult. During the first three drops, the PLA mass simulator nor the flotation foam could be retained. After redesigning the float and float bridle, the floats on drop tests 4, 5, and 6, with various degrees of float bag damage, were retained. Due to the uncertainty of PLA requirements and the limitation of funds for the drop test program, only one parachute on drop No. 5 tested the actual configuration used on the Shuttle flights. On the first Shuttle flight, two parachutes sank because of loss of flotation foam. On the second Shuttle flight, no parachutes were lost even though no design change was made. Examination of the float bag revealed the marginal nature of the bag design. Before flight three (STS-3) the float bag was strengthened. During STS-3, the floats of two chutes became entangled causing the failure of one chute. A program decision was then made to leave the parachutes attached to the SRB. On STS-4, the separation nut on one of two main

chute attach fitting was deactivated. Due to premature activation of the active separation nuts, both SRBs were lost. On STS-5 and STS-6 and for the forseeable future, the main parachutes will remain attached to the SRB until the retrieval crew detaches them. If an improved separation nut design and software is developed, a deck-mounted flotation system will be developed to again allow separation of the main parachutes at impact.

MAIN PARACHUTE LOAD MEASUREMENT

Each of the three main parachutes are attached to the SRB at two attach points. The total of six attach points are equally spaced around the circumference of the forward skirt. Load measurement for the main parachute attach fitting presented a different challenge. These fittings were designed for a load of 125,000 lb. Since the SRBs might still be rolling and swinging at main chute deployment, and to accommodate changes in pull angle resulting from the different inflated stages of the main parachutes, the fittings were required to articulate in two planes to assure pure tension measurements (Fig. 28). Radial articulation was provided by means of a yoke attached to the fixed portion of the fittings bolted to the SRB. Tangential articulation was provided by pinning to the upper portion of yoke, the two plates that carried the loads from the four bolts through the risers to the yoke of the deck fittings. Since these plates are the only component reacting pure parachute riser tension loads, this was the logical place to locate the load cells. In order to control the attitude and restrict the motion of the articulated attach fittings, shear bolts were placed through the yoke and fixed deck fittings and tangs on the plates were forced against the fixed fittings. This approach held the total assembly rigid until the bolts were sheared at main parachute line stretch. In order to avoid bending stresses in the instrumented plates, the four bolts that pass through the spreader plates and spools were carefully torqued and a feeler gage measurement was made between the plate and spools. Also, once the unit was calibrated, all components remain together. A standard load cell was considered for this application, but 125,000 lb capacity load cells are quite large and supporting any hardware from the SRB forward skirt dome was not allowed. Therefore, the problem of cantilevering such large load cells from the deck fittings was avoided by using the selected configuration.

The main parachute attach fittings, the drogue load pins and the drogue deck fittings were all initially intended for single usage. The drogue deck fittings have been tempered from a maximum tensile strength of 180,000 lb to 160,000 lb and are certified for multiple reuse providing they pass proof test and magnetic particle inspections. The main chute deck fittings and drogue load pins have been refurnished and certified for a second use.

CONCLUSION

This paper has discussed some of the more significant design challenges raised by the initial specification requirements. Now that the developmental flights (STS-1 through STS-6) have flown, how well these challenges have been met can be assessed.

In general, both the pyrotechnic and recovery subsystems have met or exceeded design requirements. In twelve vehicles, there has only been one instance where the pyrotechnic system has failed to function properly. That was on STS-4 when a 7.5 g "G" switch sensed the design 7.5 g's from the pyrotechnic shock propagated by the frustum/SRB linear shaped charge and fired the main parachute separation nuts and released the parachutes before they could function. Since STS-4, the parachutes have been attached to the SRB's by structural nuts.

The recovery subsystem has had some anomalies occur because of the requirement for the parachutes to be separated from the SRB at water impact and be self floating. This buoyancy requirement requires flotation be added to the parachutes. This flotation has caused the following anomalies: On STS-1, two parachutes "drowned" because the flotation was torn off during parachute deployment and the parachutes sank. On STS-3, the floats of two parachutes became entangled and caused the failure of one of the parachutes. Since STS-4, the decision was made to leave the parachutes attached to the SRBs, and we have had no parachute failures since. The drogue parachute has always been subjected to loads above design limit on each Space Shuttle flight, and no major structural damage has been noted. One of the two remaining STS-3 main parachutes saw loading 34% above design limit and again no major structural damage was noted.

Presently, larger main parachutes (136-ft-diameter) are under development to slow the SRBs to 75 ft/sec to lessen water impact damage. We expect no major problems with this development based on our experience with the existing design.

ORIGINAL PAGE IS
OF POOR QUALITY

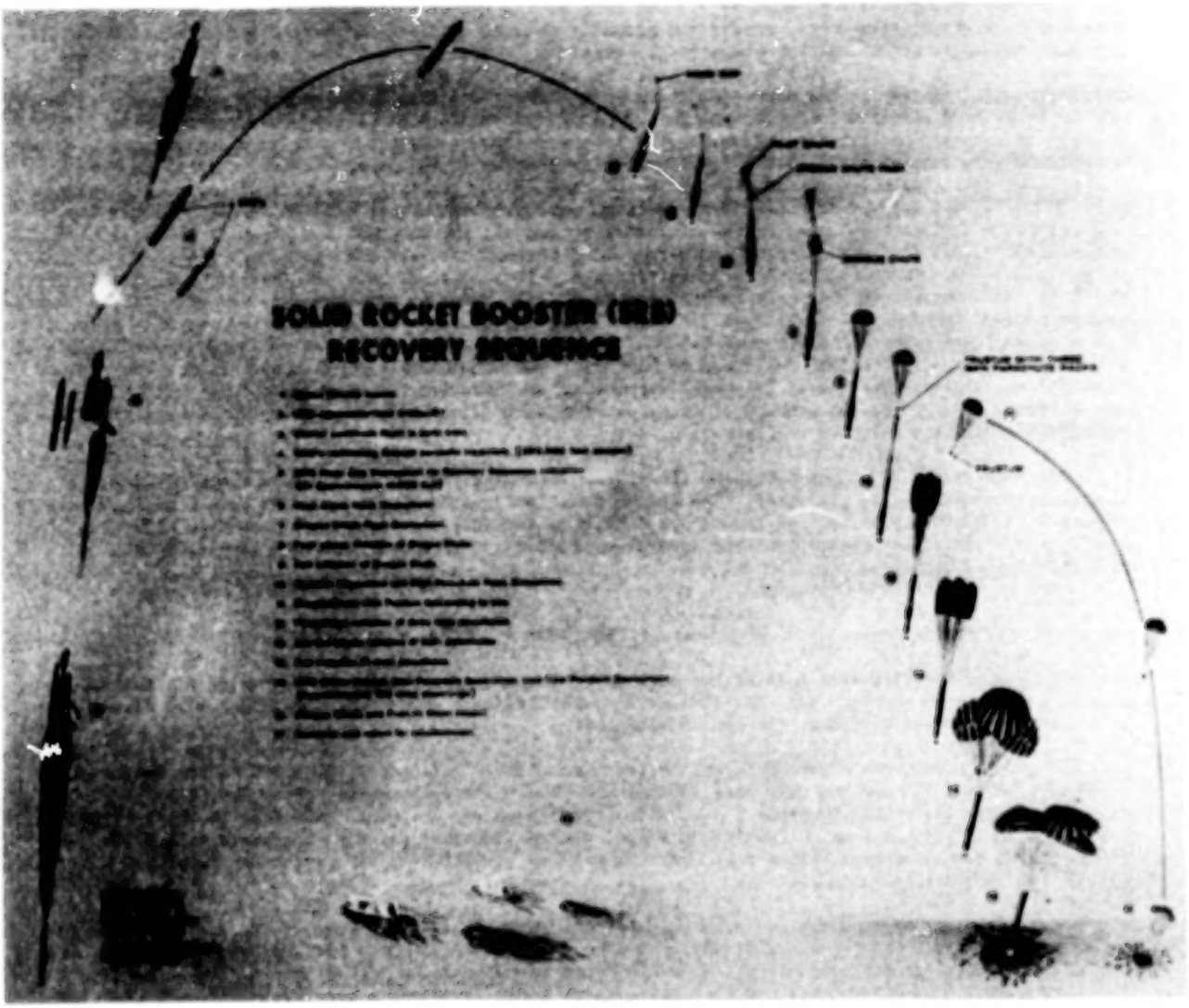


Figure 1. Solid Rocket Booster Recovery Sequence

ORIGINAL PAGE IS
OF POOR QUALITY

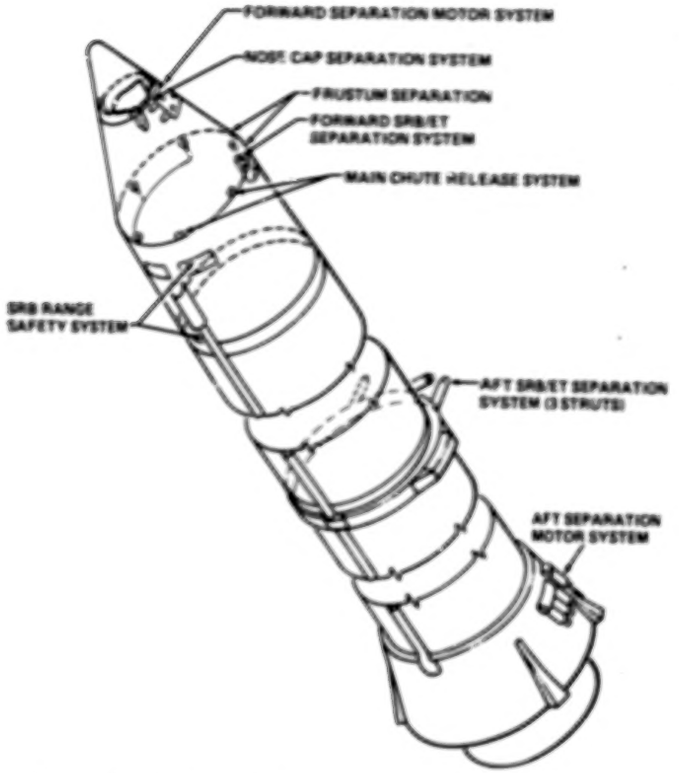


Figure 2. SRB/ET Separation and Recovery Systems.

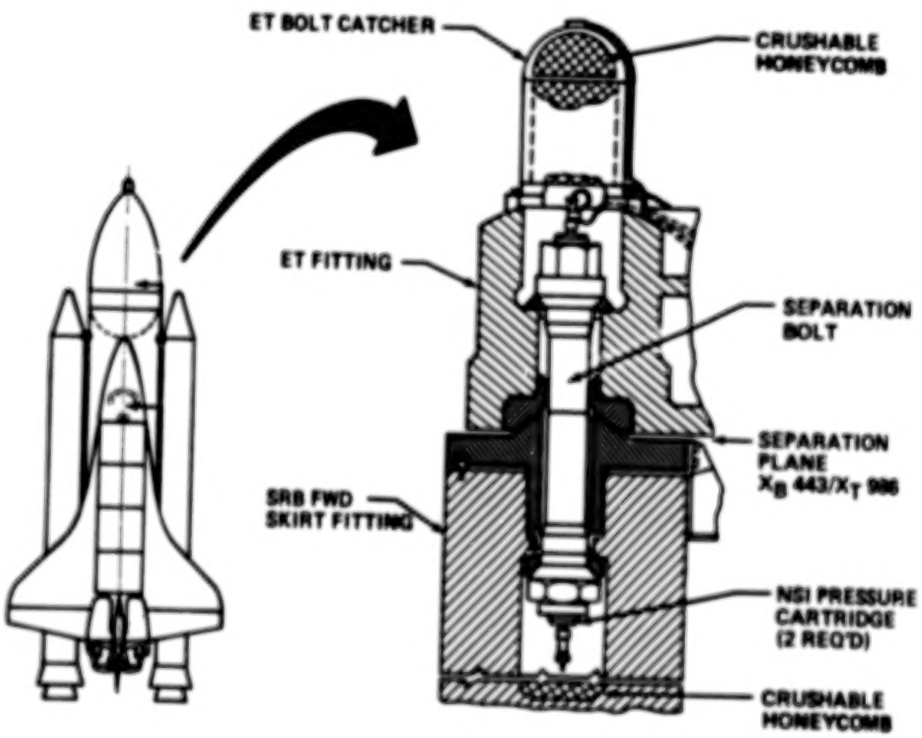


Figure 3. Forward SRB/ET Separation System.

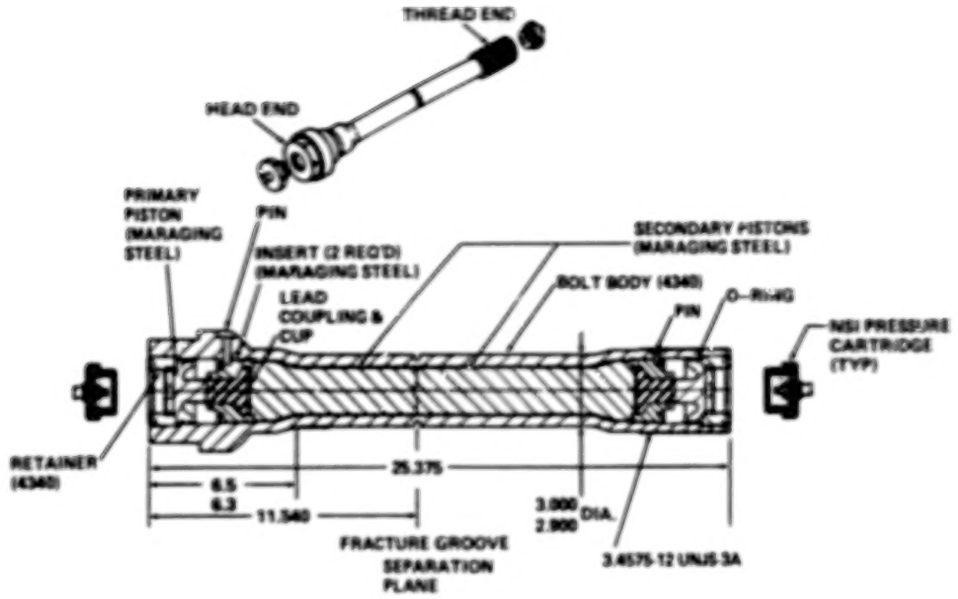


Figure 4. Forward SRB/ET Separation Bolt.

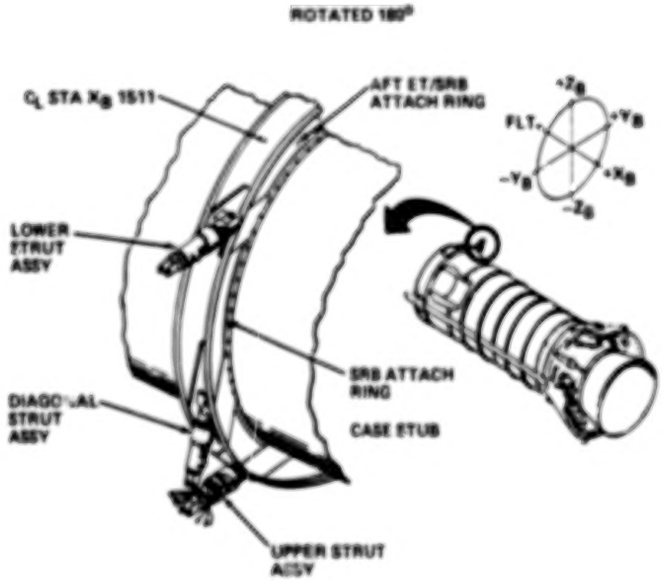


Figure 5. Aft Separation Strut Assemblies.

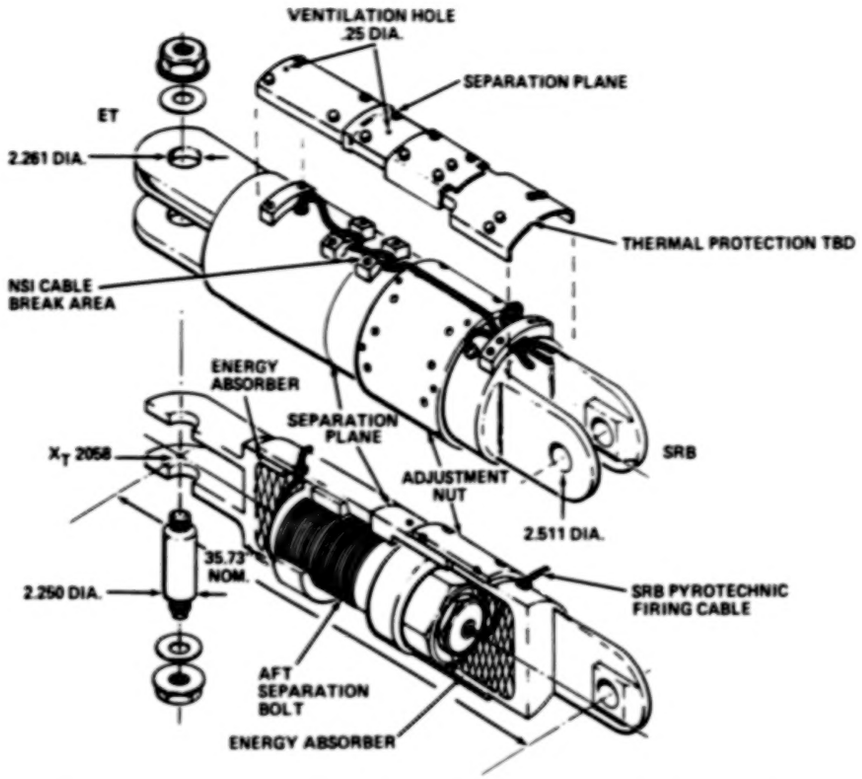


Figure 6. SRB/ET Aft Separation System, Lower and Diagonal Struts.

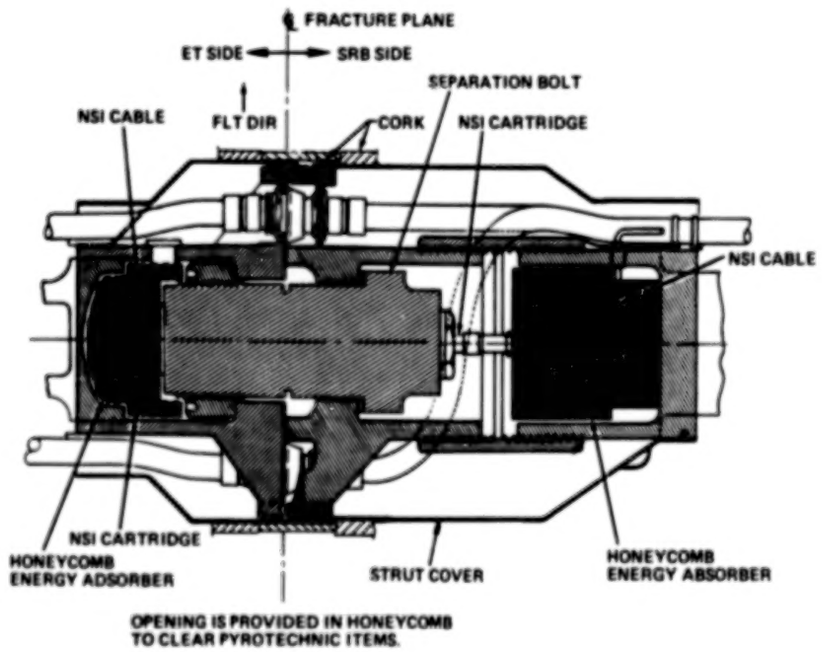


Figure 7. SRB/ET Aft Separation System (Upper Strut).

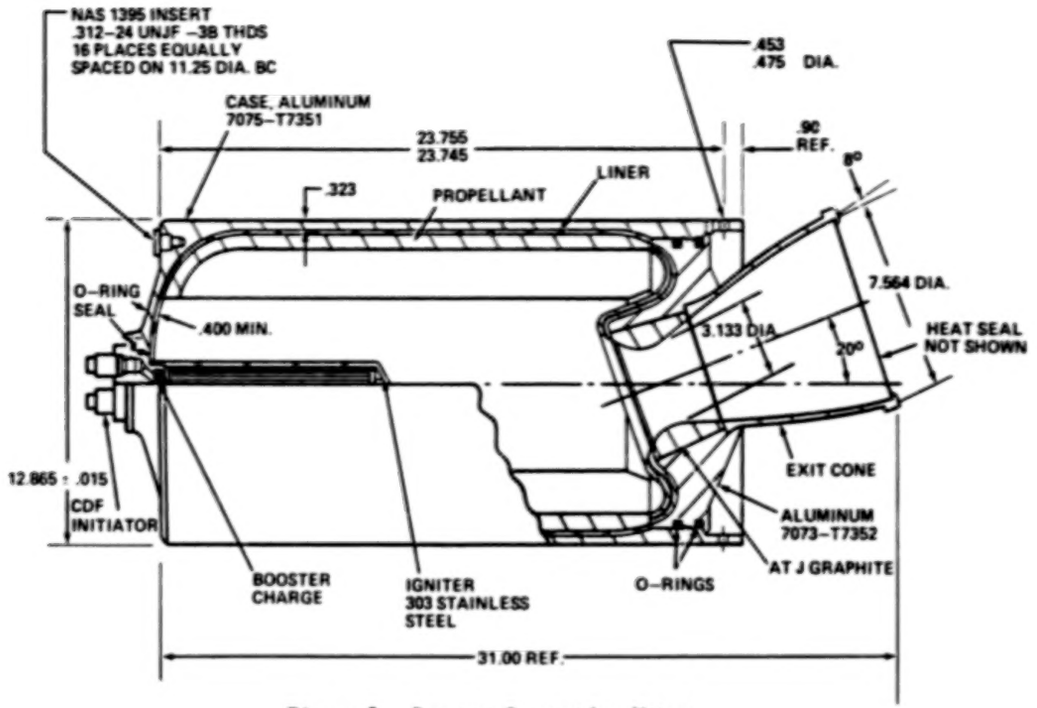


Figure 8. Booster Separation Motor.

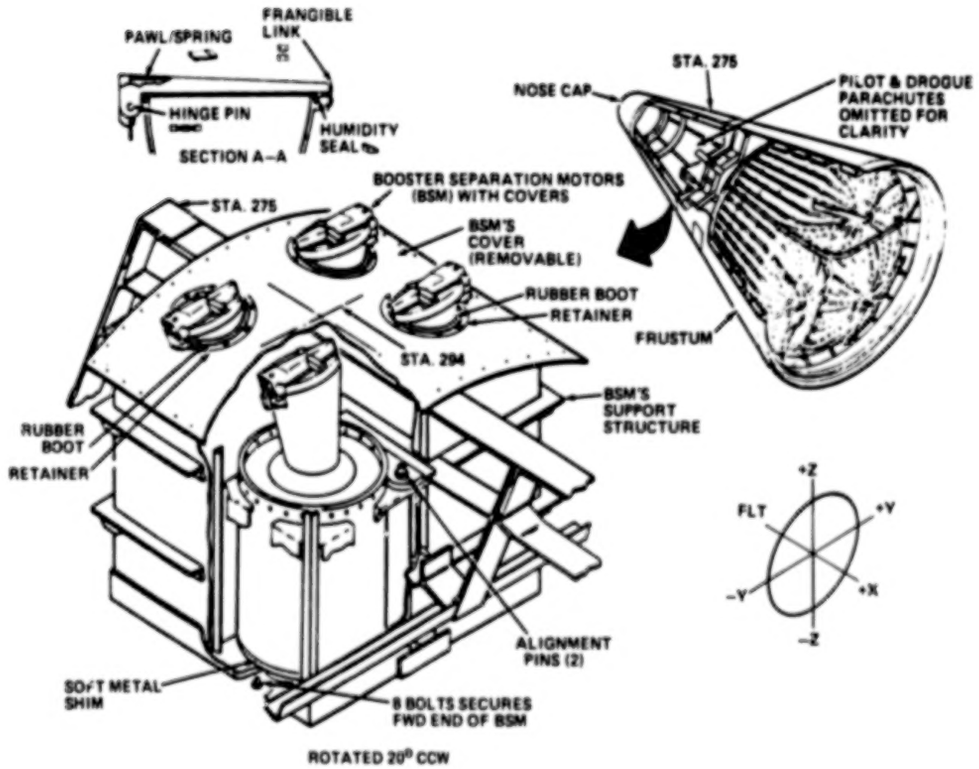


Figure 9. SRB Forward Booster Separation Motors.

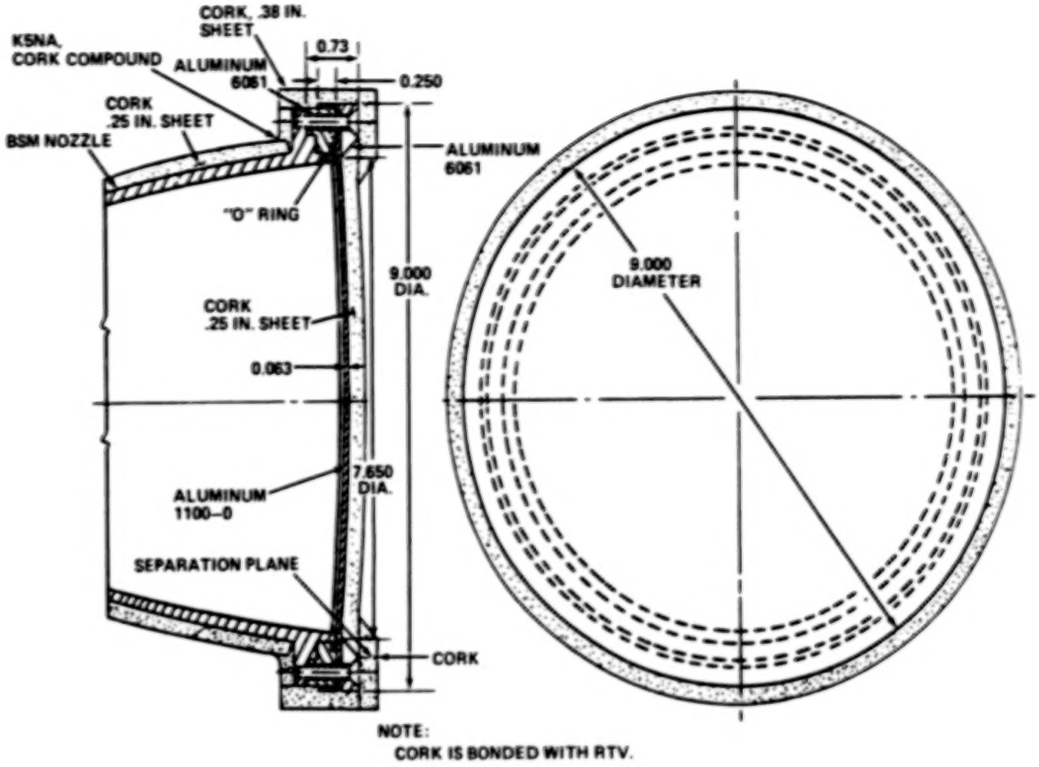


Figure 10. SRB Aft BSM Heat Seal.

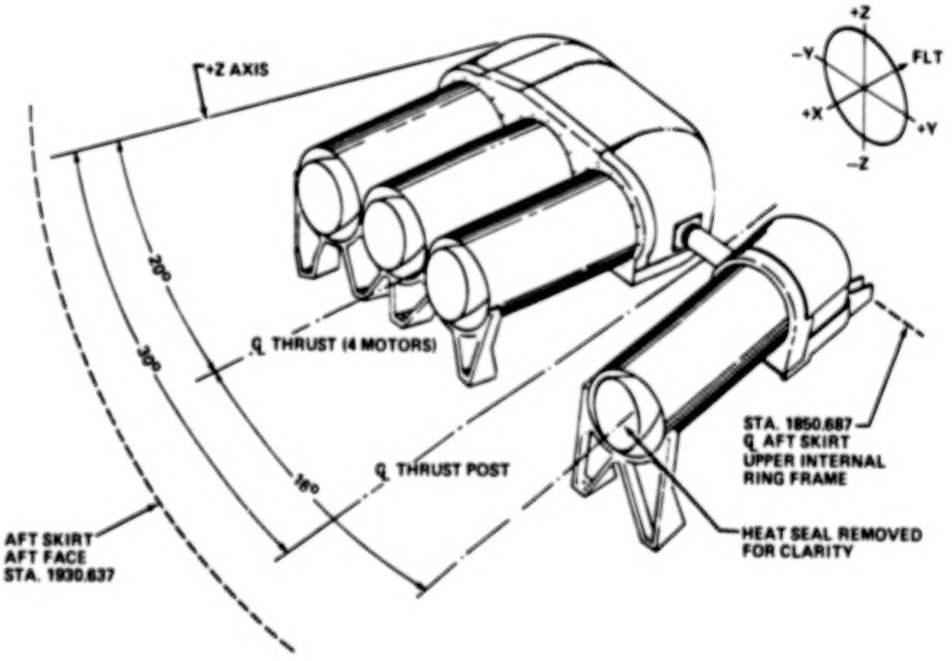


Figure 11. SRB Aft Booster Separation Motors.

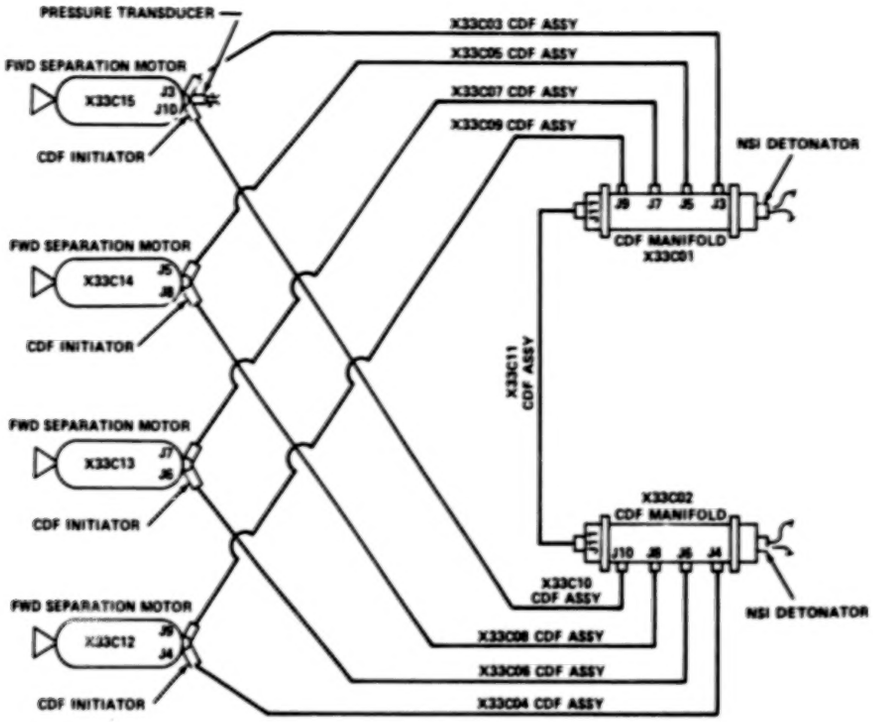


Figure 12. SRB Forward Booster Separation Motor (BSM) Ignition.

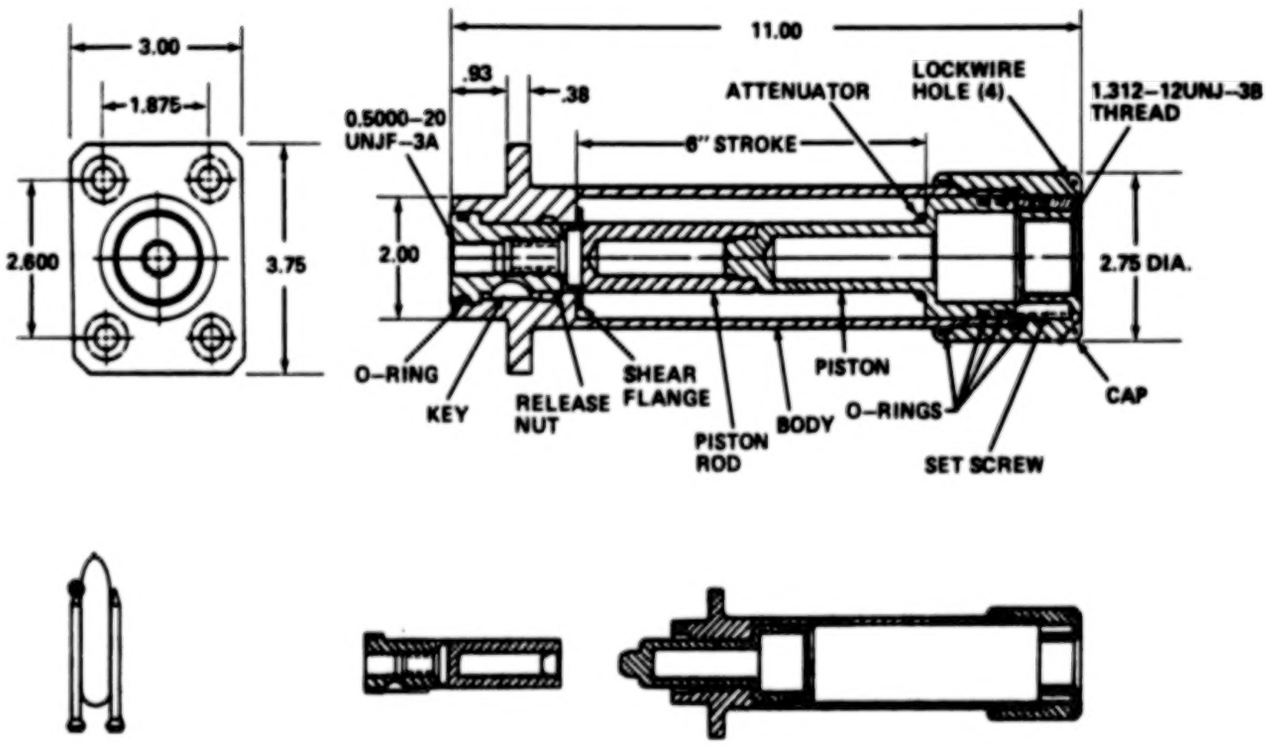


Figure 13. Nose Cap Separation Thruster.

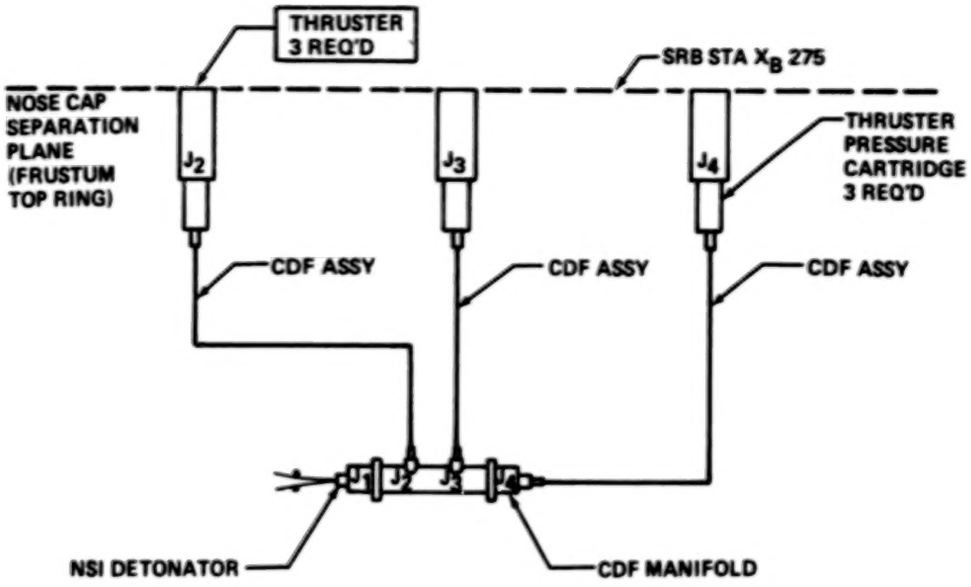


Figure 14. SRB Nose Cap Separation.

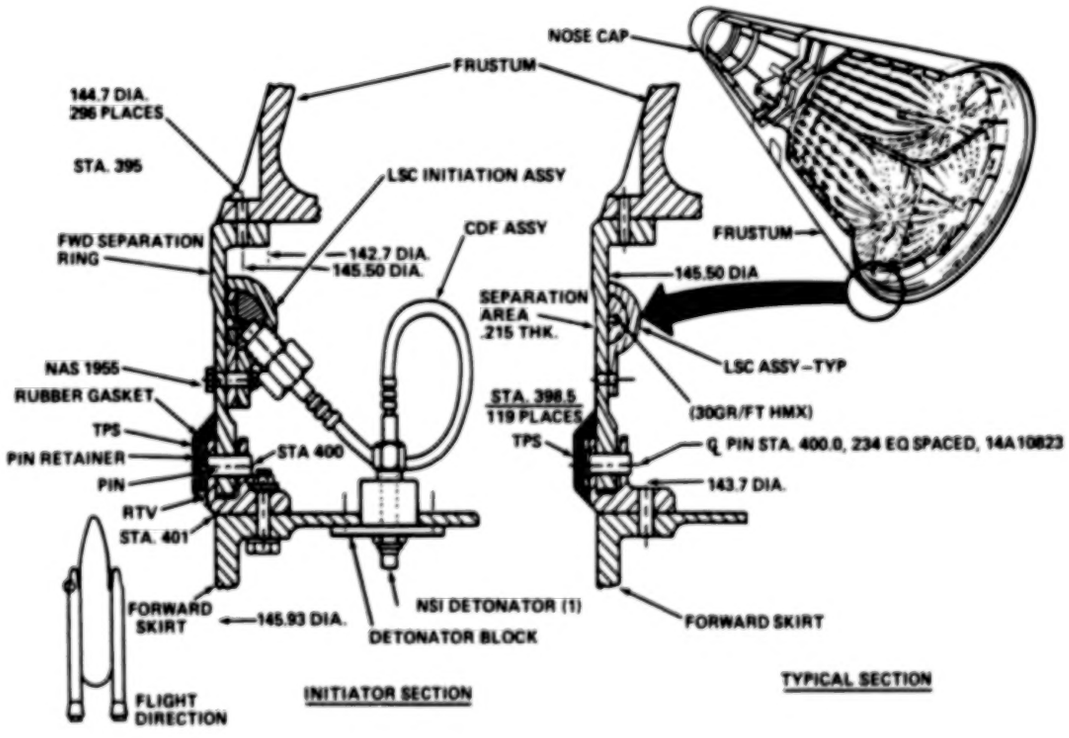


Figure 15. SRB Forward Separation Ring Cross Section.

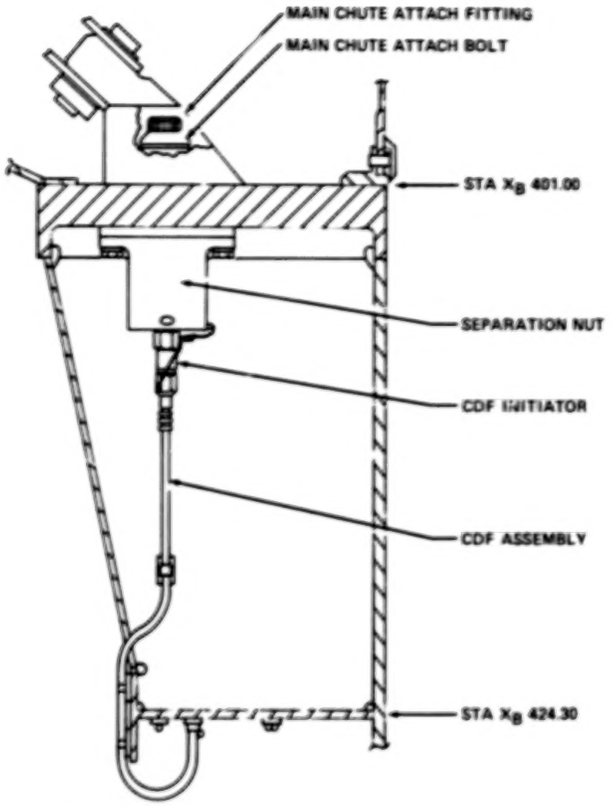


Figure 16. Main Parachute Release System.

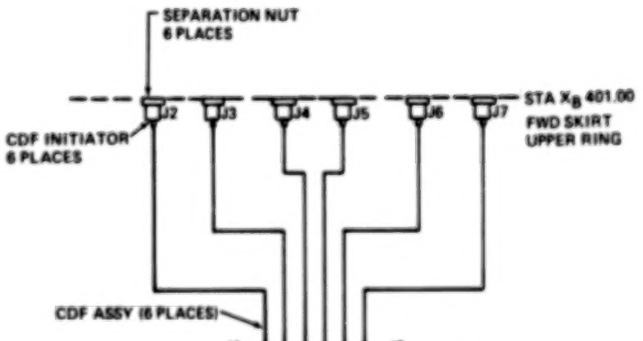


Figure 17. Main Parachute Release System

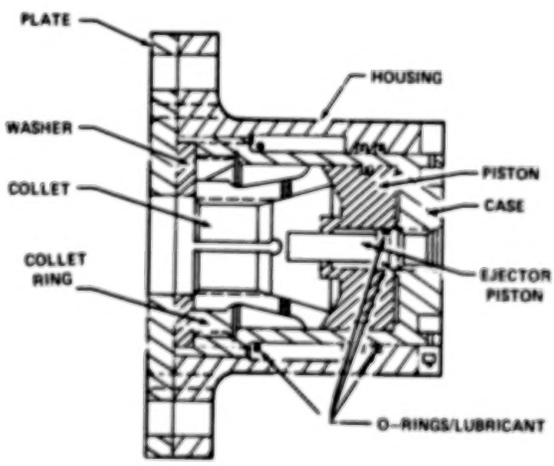


Figure 18. Separation Nut, Main Parachute Release.

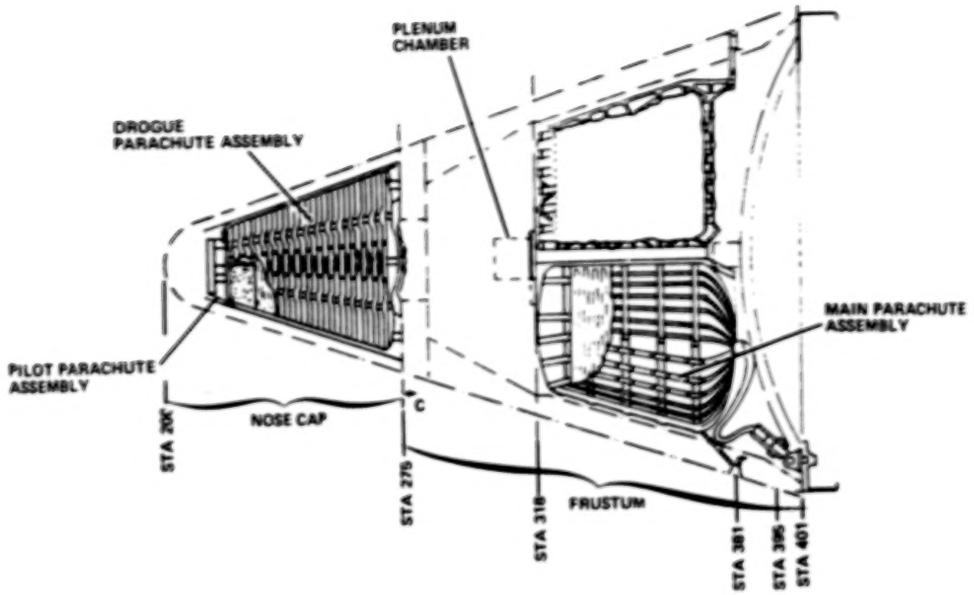


Figure 19. SRB Decelerator Subsystem Installed.

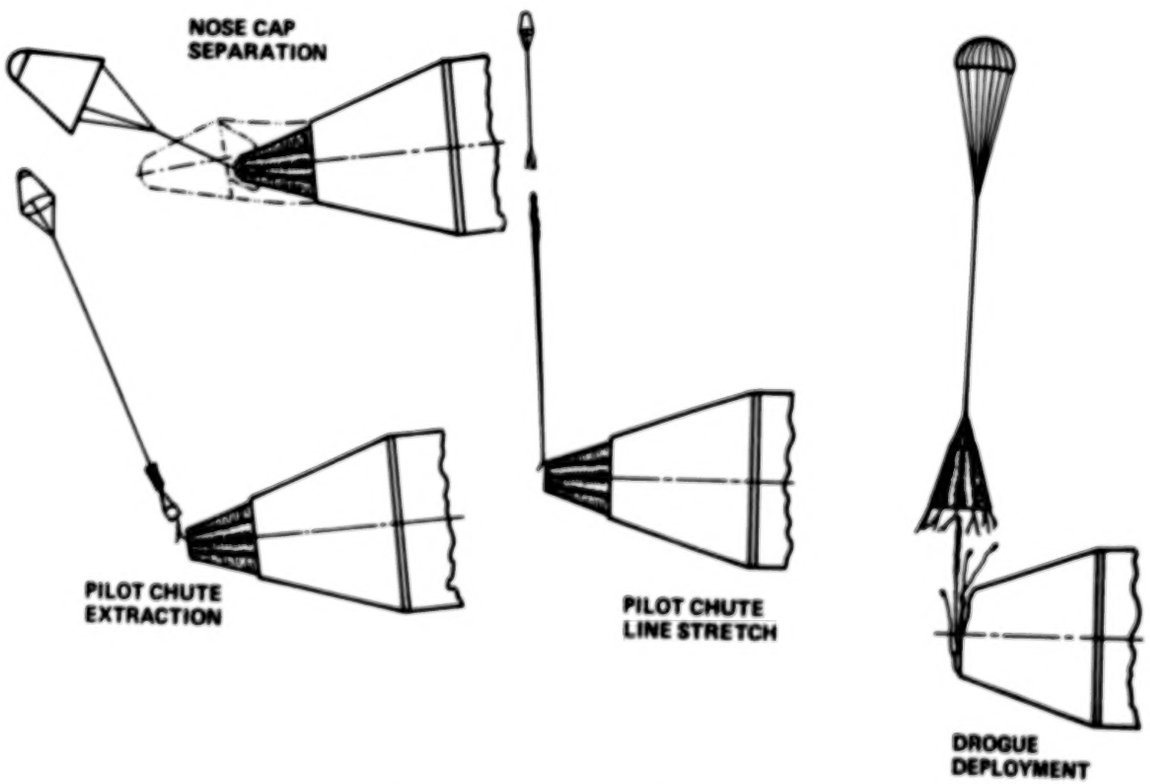


Figure 20. Deployment Sequence, Pilot Chute.

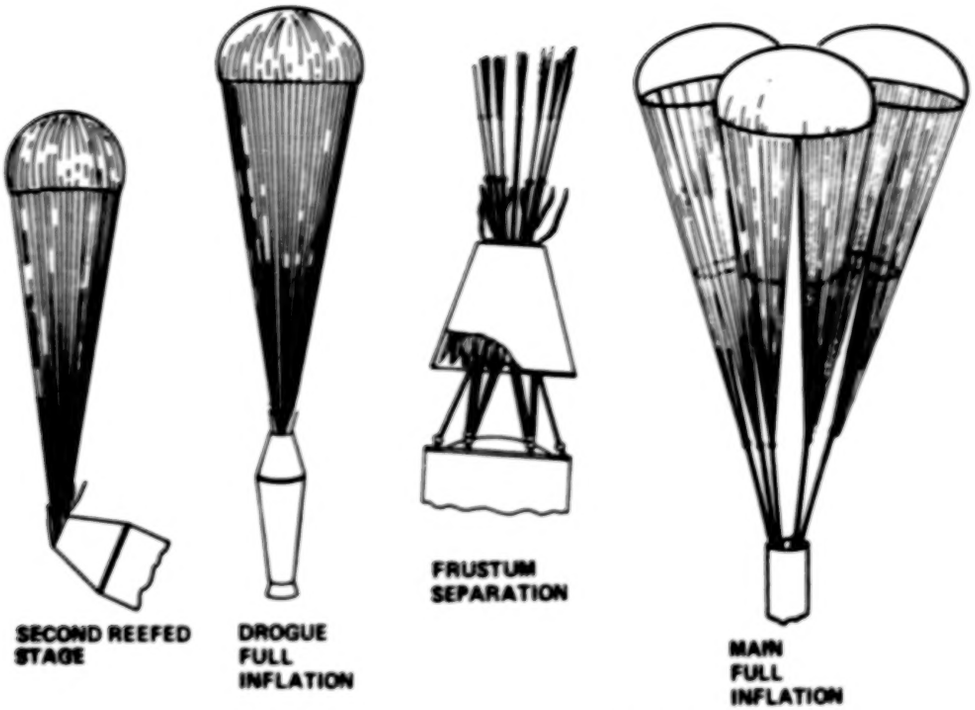


Figure 21. Deployment Sequence, Drogue/Main Chute.

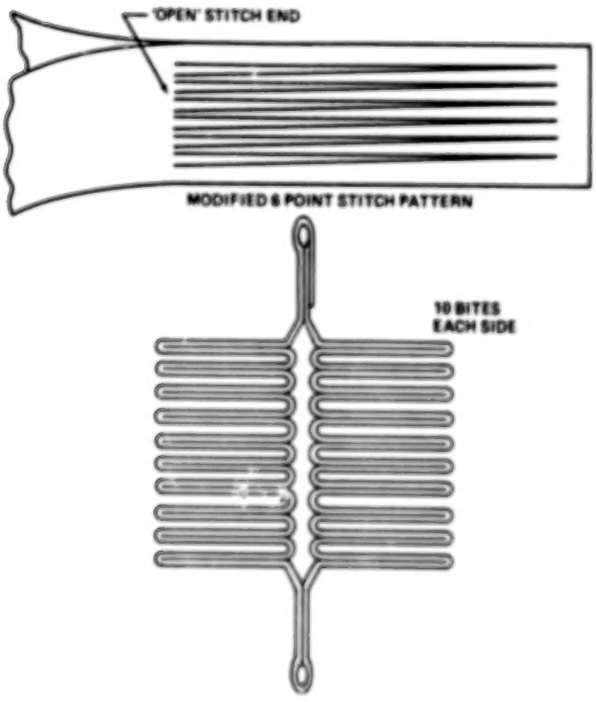


Figure 22. Energy Absorber Pretest Configuration.

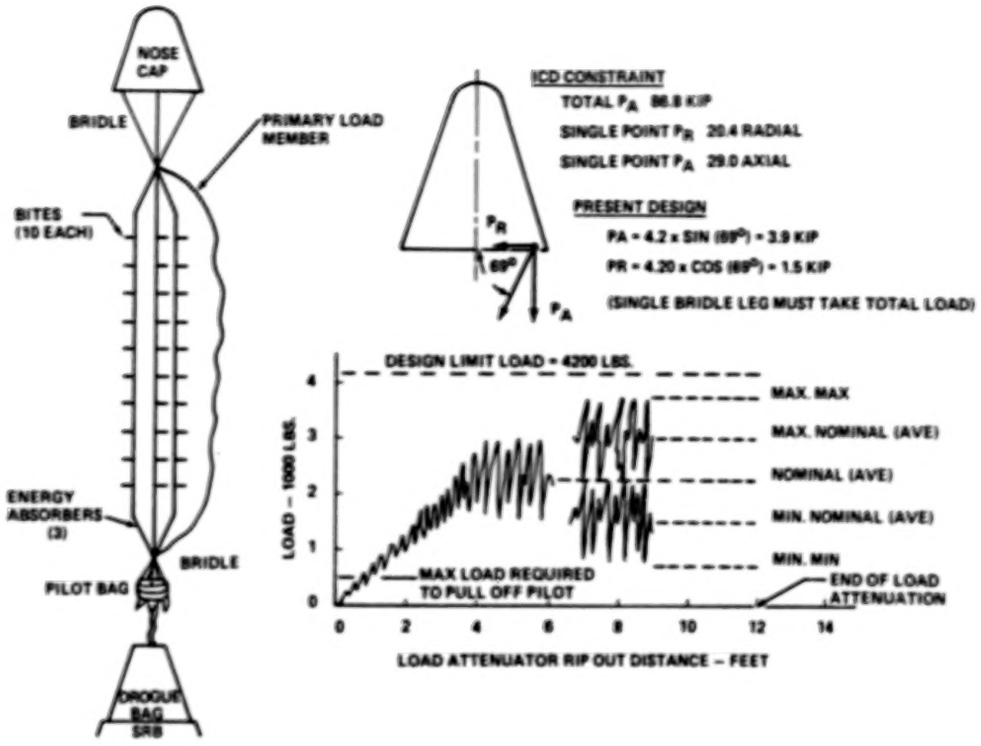


Figure 23. Nose Cap/Pilot Chute Load Attenuator.

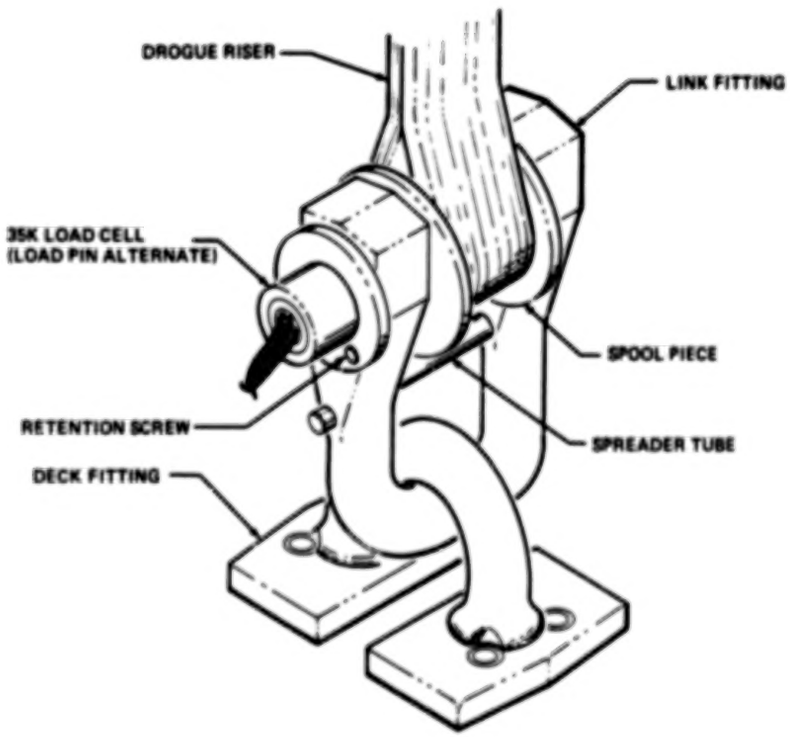


Figure 24. Drogue Riser Attach Fittings.

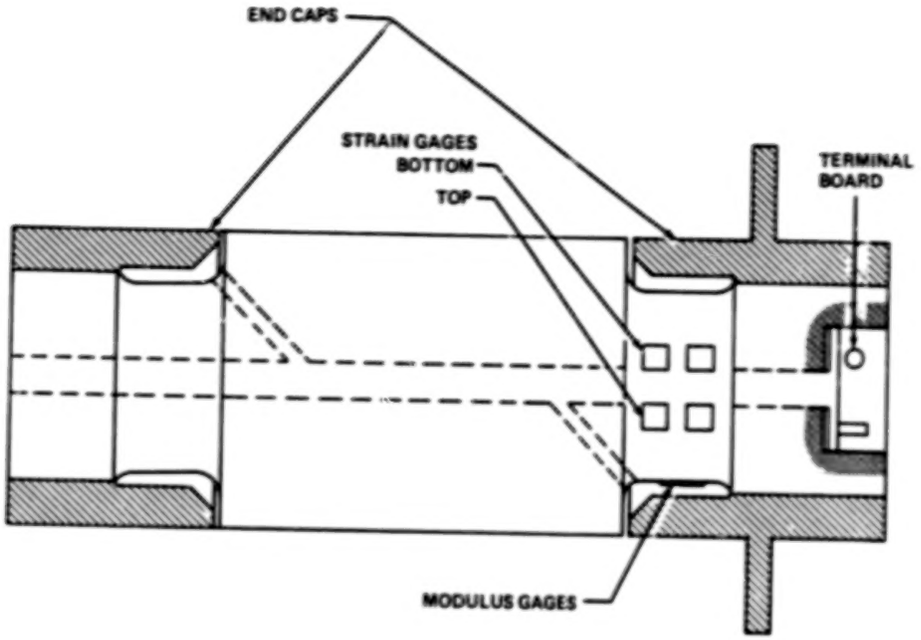


Figure 25. Drogue Load Cell.

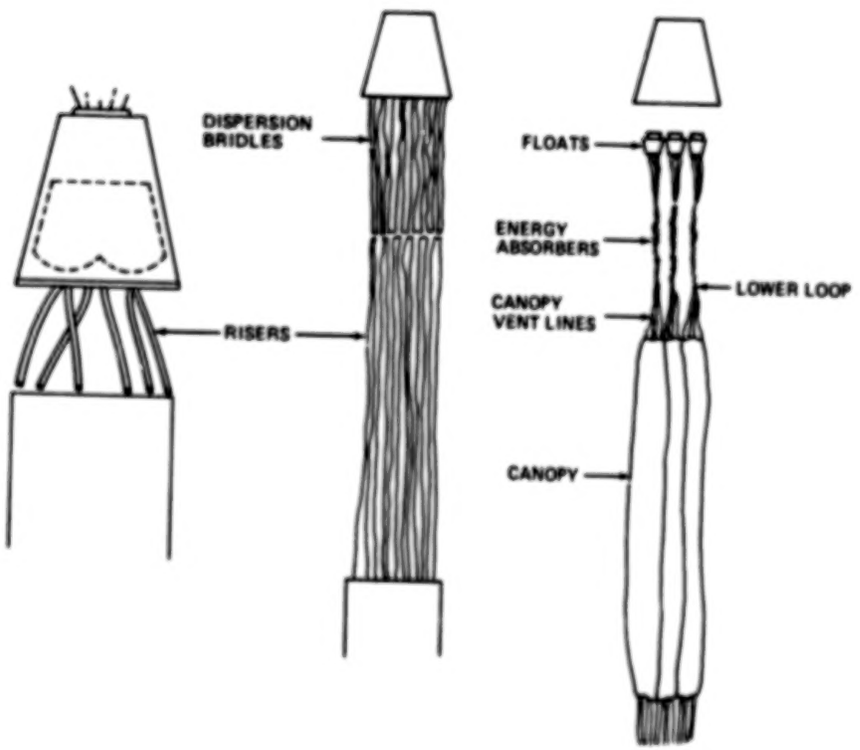


Figure 26. SRB-DBS Main Chute Deployment Sequence.

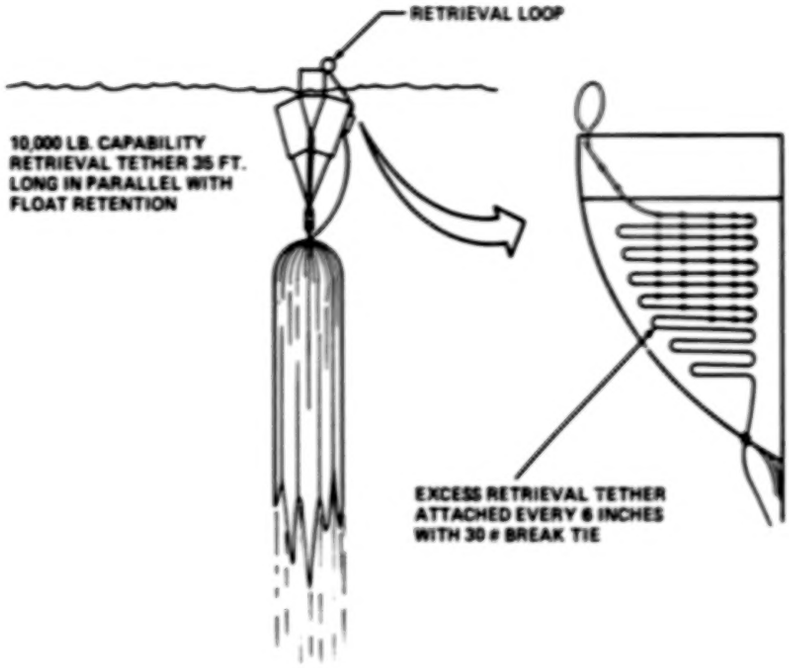


Figure 27. Main Parachute Float and Retrieval Provisions.

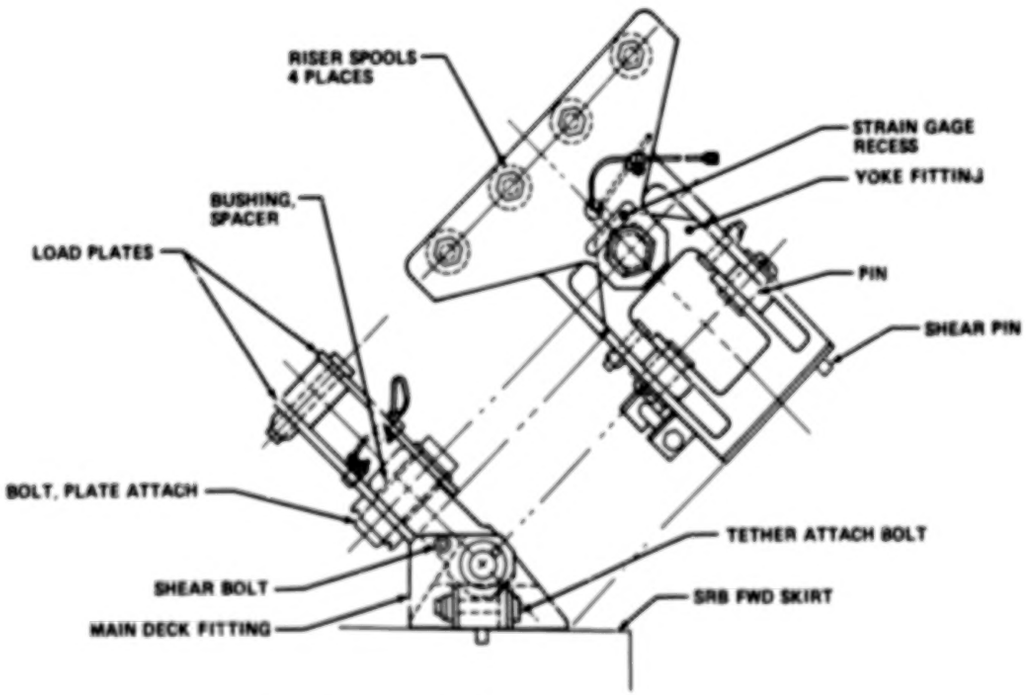


Figure 28. Main Riser Attach Fitting.

N85
16918

UNCLAS

D29 N85-16918

SSME LIFETIME PREDICTION AND VERIFICATION, INTEGRATING ENVIRONMENTS, STRUCTURES, MATERIALS; THE CHALLENGE

Robert S. Ryan, Larry D. Salter, George M. Young, III, and Paul M. Munafo
Marshall Space Flight Center
Huntsville, Alabama

ABSTRACT

The planned missions for the Space Shuttle dictated a unique and technology-extending rocket engine. The high I_{sp} (performance) requirements in conjunction with a 55-mission lifetime, plus volume and weight constraints, produced unique structural design, manufacturing, and verification requirements. Operations from earth to orbit produce severe dynamic environments, which couple with the extreme pressure and thermal environments associated with the high performance, creating large low cycle loads and high cycle alternating stresses above endurance limit which result in high sensitivity to alternating stresses. Combining all of these effects resulted in the requirement for exotic materials, which are more susceptible to manufacturing problems, and the use of an all-welded structure. This paper discusses the challenge of integrating environments, dynamics, structures, and materials into a verified SSME structure to meet a 55-mission lifetime while producing unprecedented performance. Included also are the verification program and developmental flight results. Rocketdyne Division of Rockwell International Corporation, under contract to Marshall Space Flight Center, is the prime contractor for the development of the Space Shuttle Main Engine (SSME).

INTRODUCTION

The Space Shuttle mission requirements and the resulting propulsion system requirements have led to very stringent and technology-extending structural design, verification, manufacturing, and operational approaches. Being a manned vehicle, Space Shuttle dictated that the engine be of the highest possible reliability (References 1 and 2).

The Space Shuttle missions require the engine to have high performance I_{sp} of 455 seconds, a thrust of 375,000 pounds (sea level), long life (55 missions), minimum maintenance, and to be achieved within stringent weight and volumetric constraints. These concepts and requirements led to a new approach, "line replaceable units (LRU's)," that could be installed either in the field or factory. Acceptance and/or verification of LRU's are accomplished separately from the engine system (Reference 3).

In order to achieve the high performance (I_{sp}), a two-stage pump system is used in conjunction with preburners which burn the fuel rich, furnishing the power for the pumps. This extremely hot fuel rich gas feeds the main combustion, efficiently developing the engine thrust. This system results in unprecedented operating regimes of temperatures, pressures, and rotating machinery speeds. The high rotary speeds and the combustion processes create mechanical, acoustical, and fluctuating pressure environments. Figure 1 is a schematic showing typical pressures and temperatures. The volumetric and weight constraints drive the design toward a high concentration of energy and minimum structure sizing (thickness, etc.). The energy concentration can be illustrated by observing the size of the high pressure fuel pump, which generates 70,000 horsepower within an envelope 18 inches in diameter by 30 inches long and rotates at speeds up to approximately 40,000 rpm (References 1, 2, 4, 5, 6, 7, 8, and 9).

The structural design problem is further complicated by the multivaried operating regime (throttling to 65%) and the requirement to gimbal the engine ± 10 degrees at a 10 degree/second rate for vehicle control authority. The engine starts on the ground, operates in the atmosphere and then in a vacuum, and shuts down, producing large thermal and pressure cycles for each burn. Since the nozzle expansion ratio is a key parameter to high performance, a compromise between atmosphere and vacuum is required, leading to a very complex, additional set of environments during ground start.

Volumetric and weight constraints introduce designs which create additional fluctuating environments. For example, curved ducts, bellows, valves, and changing duct/valve diameter create higher velocities, unsteady flow environments, and acoustic pressures which are additive to the normal turbine fluctuating pressures and combustion induced noises.

Combining all of these environments leads to three classical design problems, (1) strength - pressures, thermal loads, and inertial loads; (2) low cycle fatigue - pressure and thermal cycles associated with each firing that is unprecedented in rocket engine design, and (3) high cycle

ORIGINAL PAGE IS
OF POOR QUALITY

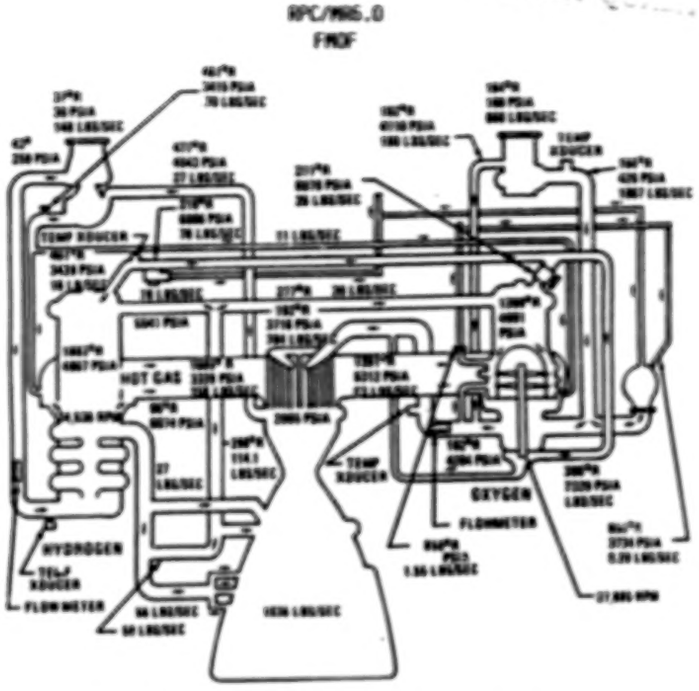


FIGURE 1. SSME PROPELLANT FLOW SCHEMATIC

fatigue/fracture mechanics - flow, combustion, and mechanically induced. Strength and low cycle fatigue problems have been solved by material selection and design considerations, leading to an all-welded design using exotic materials. The other major challenge was high cycle fatigue and fracture mechanics. The SSME operating conditions generate environments where many parts are operating at or beyond their endurance limits, producing a limited lifetime. The design point on the SN curve is very flat, making lifetime very sensitive to small changes in alternating stresses (5% alternating stresses change lifetime up to an order of magnitude), manufacturing errors, and material deterioration (see Figure 2).

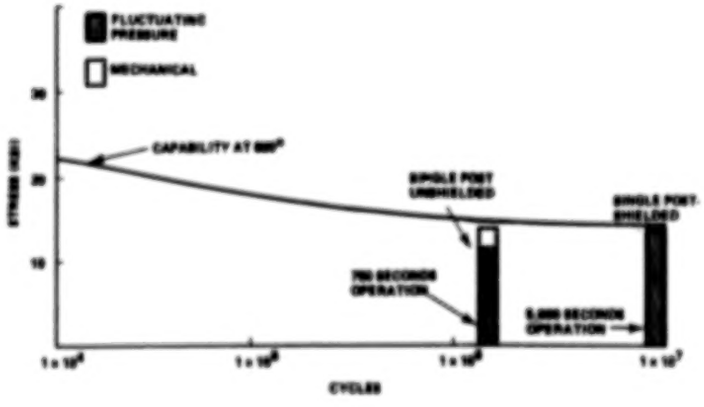


FIGURE 2. ALTERNATING STRESS VERSUS LIFETIME

Taking the above-mentioned considerations, integrating them into a structural design, manufacturing the design, and final verification of an acceptable product results in a very compelling program. This was the challenge of the SSME Program. The requirements of this program where each are subsets of the challenge are:

1. Develop and characterize special materials.

2. Develop accurate environment predictions and verification techniques.

3. Develop accurate structural dynamic and stress models and their verification.

4. Develop a fracture mechanics and nondestructive evaluation (NDE) program.

5. Develop extensive verification procedures (DVS).

   - Analysis.
   - Test.
   - Hot firing instrumentation.

6. Develop accurate and technology-challenging manufacturing and quality control procedures.

Design adequacy is assured through implementation of a Design Verification Specification (DVS), which is a detailed set of well-documented tasks with government/industry verification with complete signoff on each. Tasks are broken out in terms of engine systems, valves and ducts, rotary machinery, combustion devices, and controller. The tasks are all inconclusive in terms of analysis, tests, and hot firing verification. Each discipline and subsystem maintains current documentation of all analyses and test procedures and results keyed to the DVS. In addition to the DVS, many system requirements are placed on total engine verification accomplished in single and multi-engine ground firings.

The approach used in meeting the design challenges in the areas of strength, low cycle fatigue, high cycle fatigue, manufacturing, and material processing followed classical techniques. Figure 3 shows this approach where environments are predicted, models developed, loads calculated, material properties determined, and design stresses developed. As a result of tests, component firings, engine developmental firings, and DVS, the design verification cycle becomes one of iteration where changes in each discipline are made as additional information and design deficiencies are uncovered. As a result of following this approach, no major failure has occurred during SSME developmental firing for parts that could and did go through the rigorous 7½ hours, each axis, vibration testing. Failures have occurred but only in those areas not amenable to total lifetime testing as components.

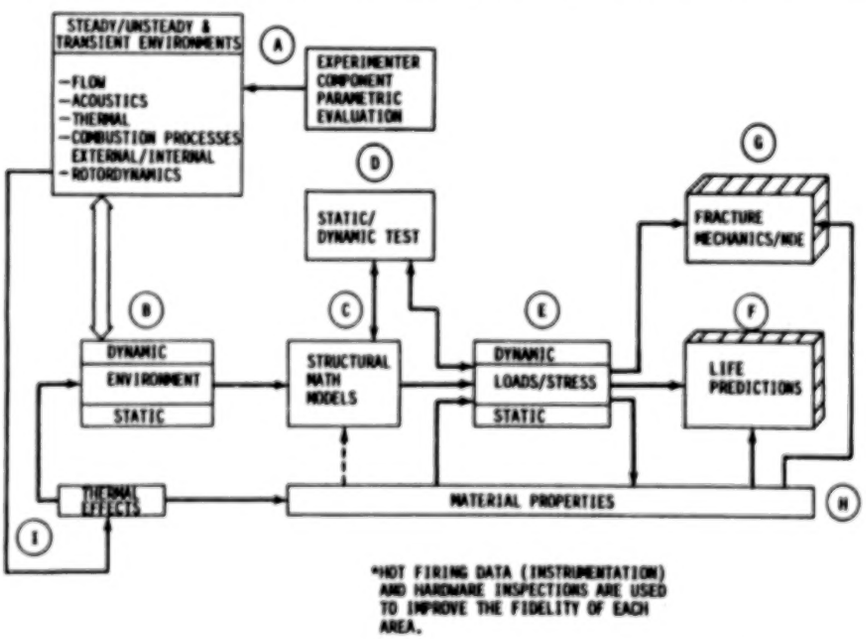
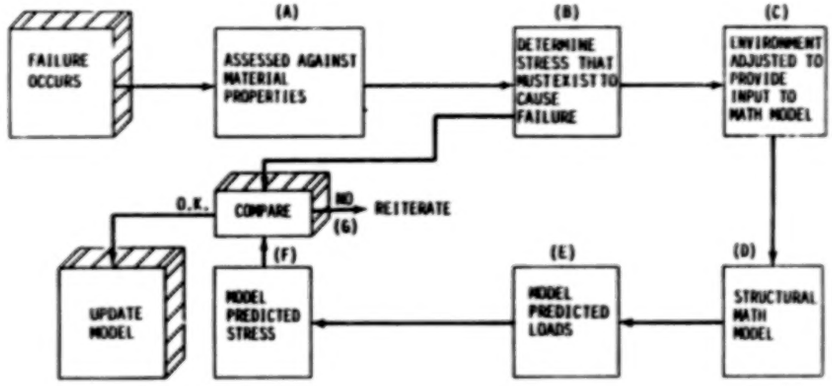


FIGURE 3. CLASSICAL DESIGN/ANALYSIS FLOW SCHEMATIC

The major challenge that faced SSME design was those parts which were sensitive to flow environments and not amenable to DVS testing. Analytical procedures were not, in general, accurate enough to predict environments and the engine could not be penetrated in all areas to measure the environments (References 10-15).

The criticality of the lifetime of certain engine components and the complex environment prediction problem have led to an alternate approach for determining high cycle fatigue limits, see Figure 4. A component failure is used as an empirical failure reference point, determining the stress level required for failure from the SN curve (minimum properties, maximum predicted temperature and pressures). The environments are "backed out" of these empirically derived data using the analytical dynamic model. The environments thus derived serve as a means of evaluating new designs and higher engine performance levels, as well as determining life limits.

The challenges of each of the major disciplines will be discussed. How these techniques were applied to the challenge of three typical design problems associated with lox posts, nozzle, and turbine blades will be illustrated.



(1) EMPIRICALLY UPDATED MODEL CAN BE USED TO PREDICT REDESIGNED CONFIGURATION CAPABILITY.

(2) THE INPUT ENVIRONMENTS ARE NOT ACCURATELY CHARACTERIZED

(3) RESULTS ARE WELL ANCHORED BUT ARE ONLY RELATIVE IN TERMS OF ANY GIVEN ELEMENT DATA BASE.

(4) ANALYSES AND TEST ARE BEING USED TO UPDATE AND IMPROVE FIDELITY OF ENVIRONMENTS (C)

FIGURE 4. SSME LIFETIME VERIFICATION ANALYSIS FOR SPECIAL PROBLEM AREAS

ENVIRONMENTS

The key to meeting the challenge of SSME design for lifetime prediction and verification is an accurate determination of the static and dynamic environments. As discussed previously, in the high pressure and high temperature regimes and in rotating machinery, large mean stresses exist which drive the accuracy requirements higher for both static and dynamic environments. Classically, these environments fall into the categories of thermal, mechanical, flow, and acoustics.

THERMAL ENVIRONMENTS

Definition of SSME component thermal environment is required to determine material properties, structural loads due to thermal gradients, and component performance. The challenge of this requirement is characterized by the following:

- Temperature extremes from -420°F to 1800°F.
- Complex fluid flow patterns.
- Intricate geometrical shapes.

- Exotic superalloy materials.
- Transient as well as steady-state phenomena.

This challenge was met by instrumentation at critical locations, analytical extrapolation of measured temperatures, and calculation of temperatures at internal locations inaccessible to instrumentation. In many cases, post-test hardware inspection revealed evidence that resulted in additional instrumentation and revision of models used in the initial characterization.

Instrumentation techniques vary from externally attached thermocouples and "plug in" type resistance thermometers to specially assembled "one of a kind" instrumentation systems for high response, wide range, transient measurements, such as that installed to assess high pressure fuel turbopump turbine inlet conditions. Special test fixtures and experimental models representing engine hardware were also used in instances where instrumentation of actual engine operation could not be effectively accomplished. This was necessary for thermal assessment of shields for the main injector lox posts. In addition, limited use of thermal coatings, temperature sensitive paints, and even metallurgical evaluation of metal discoloration contributed to establishing the limits of SSME thermal environments.

Analytical models of SSME components were used to evaluate temperatures at locations other than those discretely measured. In general, thermal models must interface with analyses of fluid flow fields to achieve boundary conditions and with structural analysis tools for meaningful evaluation of thermal effects on SSME capability and life. Examples of computer analysis codes employed in SSME thermal analysis are SINDA, NASTRAN, BLAYER, and TSONIC.

Analysis results are evaluated and updated by comparison to periodic inspection of actual SSME hardware. The spectrum of models utilized ranges from one-dimensional, constant property, steady-state hand calculations of average material temperatures to integrated three-dimensional, variable property, transient thermal/stress analysis of fatigue life.

Frequently, evaluation of test anomalies and/or component failures requires rapid assessment of component temperatures at specified locations. These analyses are performed with small special-purpose computer programs or hand calculations. Important hypotheses or conclusions reached in this manner are generally verified with more comprehensive analysis or by testing.

MECHANICAL VIBRATION ENVIRONMENTS

Mechanical environments are design drivers for many components, such as valves, ducts, and bellows. The sources of these vibration environments are rotating machinery, combustion, shock, valve actuation, etc. Figure 5 depicts the approach for working these environments. Initial design values were scaled from previous engine programs, such as H-1 and F-1. A comprehensive hot firing measurement program was developed for updating these predicted environments during the developmental firings. Vibration criteria have been gathered and put in statistical form for all major components at each power level. These data were statistically evaluated and stored in data banks.

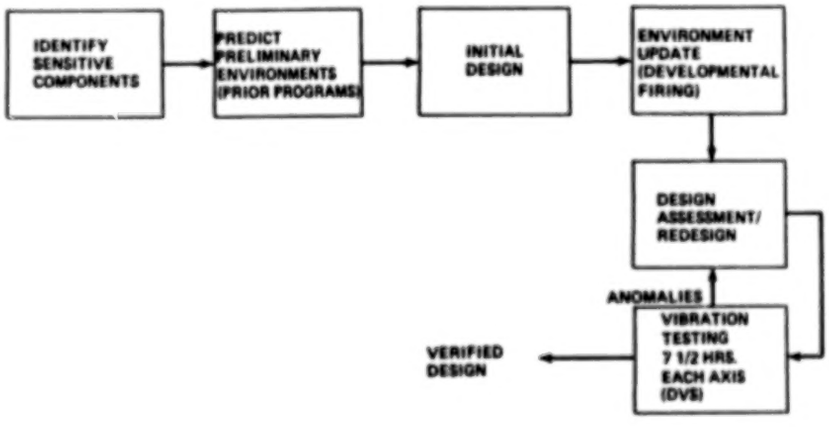


FIGURE 5. SSME VIBRATION ENVIRONMENT AND COMPONENT RESPONSE PROCEDURE

These vibration data serve as the criteria for vibration testing the components 7½ hours in each axis. This is a very comprehensive data base and has resulted in no major component failure of any parts that have passed vibration testing (not all components are amenable to vibration testing). In many cases, this testing showed design flaws that were corrected with the components subsequently passing the vibration testing. The combination of hot firing data acquisition and the DVS testing using these data solved the challenge associated with design and verification against vibration environments.

FLOW ENVIRONMENTS (FLUCTUATING PRESSURES)

As discussed previously, the sensitivity of the lifetime of SSME parts to alternating stresses places a demanding challenge on environment predictions, both static and fluctuating. The sources of these fluctuating pressures are blade pass from rotating machinery, acoustical resonances, turbulent flow, and flow instabilities. The challenge was met using previous engine test data, standard flow data from flow in ducts and bellows, etc., one- and two-dimensional codes, instrumentation during engine development hot firings, and special component flow tests. In all cases, the predicted environments were anchored using hot firing data, since predictions inherently have uncertainties incompatible with design accuracy requirements. Limited instrumentation access to the engine flow areas has restricted the amount of hot firing data that could be acquired. Data have been acquired in the hot gas manifold near the lox post, in the pump discharge areas, and in certain valves. Development of special instrumentation was required in the turbines and hot gas manifold. Stringent requirements exist for design, development, and verification of this instrumentation. As a result, an alternate approach was used for component failure cases by backing the environments out from the level of alternating stresses required to produce failure. The basic requirements for defining fluctuating environments have been met for the current engine. Challenges still exist in this area for 109% power level verification and upgrading to higher power levels. In the examples given later, some of these approaches will be briefly discussed.

DYNAMICS

Conventional state-of-the-art finite element structural modeling and response techniques have been used for the SSME to predict design and verification data. The challenge has been the choice of elements, material properties, and boundary conditions which are key since each component was analyzed as a unit. Two- and three-dimensional models were used throughout the program. Analysis of the total engine system has been limited since local conditions drive the individual component design with small influences from system dynamics. The basic approach has been to 1) develop finite element models of each component or subsystem; 2) construct generalized force distribution of the environments: flow, fluctuating pressures, thermal, mechanical vibrations; 3) determine resulting loads in order to arrive at design loads for strength, cyclic loads (low and high cycle) for lifetime predictions, see Figure 3.

Analytical models have been anchored using special dynamic test using sine sweep, modal dwell, and random testing techniques. Further verification has been obtained from developmental firing instrumentation in terms of strain gauges and accelerometers. Special dynamic tests have been run for total engine system, powerhead, lox post, nozzle, main fuel and oxidizer valves, and high pressure lox and fuel pump cases and rotors. Dynamic models have been adequate in all cases to define dynamic responses.

STRUCTURAL ANALYSIS

Stress, fracture mechanics, and strength analyses and tests, their accuracy and efficiency, and choice of design criteria are key elements in meeting the design challenge of the SSME to meet the mission, lifetime, refurbishment, and operational requirements. Conventional state-of-the-art stress analysis techniques were utilized throughout the design and development of the engine components. In the preliminary design phase, hand analysis solutions and selected finite element models were utilized to size the structure. As the program progressed and the design became more solidified, the majority of the critical components were analyzed through the use of either two-dimensional or three-dimensional finite element models, as applicable. In many cases, common models were used for both the dynamic and stress analyses, and, in some instances such as the turbine blades, the same model was used for detailed dynamic, thermal, and stress analyses. The finite element models included both elastic and plastic solutions as required. The design margins or factor of safety requirements utilized in the engine design were:

- Factor of safety on ultimate = 1.50 pressure only.
- Factor of safety on ultimate = 1.40 combined loads.

- Factor of safety on yield = 1.10.
- Factor of safety on low cycle fatigue = 4.0.
- Factor of safety on high cycle fatigue = 4.0 or 10.0, depending on adequacy of SN curve data base.
- Factor of safety on creep = 10.0.

The overall design goal was infinite life with at least a factor of 1.0 on the endurance limit, except for the rotating components in the turbomachinery where the factor of safety of 1.4 was used. When other design constraints prohibited meeting this design goal, the safety factors on life were utilized. Miner's rule for accumulated damage was generally used for assessing components subject to the combined effects of low cycle, high cycle, and creep damage. The majority of the engine components subjected to high cycle fatigue environments operate on the flat or close to the flat portion of the SN curve due to the combination of the 27,000-second life requirement and the operating frequency of the component, see Figure 2. This contributed to several high cycle fatigue failures during the research and development phase of the program, for example, the main injector lox post, which experienced several failures. In retrospect, it could be questioned whether it would have been prudent to design all life sensitive components to a higher factor against the endurance limit, such as 1.25, rather than 1.0. The larger factor would result in tradeoffs between weight, reliability, development costs, and performance.

The early design phase was further complicated by the lack of complete characterization of material properties for all of the extreme temperatures and environments. Much of the early analyses had to be accomplished with estimated properties until adequate characterization could be completed when all environments were finalized and schedule and cost permitted.

The structural reliability (ultimate load and life capability) was verified by such methods as hot firing developmental and certification testing, component static structural tests, proof tests, and laboratory vibration tests. These tests were utilized to verify the structural reliability of the critical components. Appropriate instrumentation, pressures, temperatures, environments, loads, cycles, etc., were utilized where applicable and practical for this accomplishment.

FRACTURE MECHANICS ANALYSES

The objective of the fracture mechanics analyses was to assess the flight engines fracture critical components for flightworthiness based on fracture mechanics logic and nondestructive inspection history. Fracture critical components were selected using the following guidelines:

1. Components made of Inconel 718 and whose operating conditions involve exposure to gaseous hydrogen temperatures which are determined to result in accelerated flaw rates.
2. All shrapnel-producing hardware such as turbine disks, pump inducers, or impellers.
3. Major structural elements loaded in tension or bending.
4. All turbopump housings.

Engineering judgment was applied with consideration of component function, failure effects, design complexity, and known material characteristics. The above selection logic resulted in approximately 300 fracture critical locations involving approximately 60 components on the engine. Figure 6 is a flow diagram of the fracture mechanics verification analysis procedure.

The application of fracture mechanics for the engine components was based on the following simple logic:

1. Determine the maximum size of any undetected flaw that may be present in the subject structure at the time it enters service.
2. Based on the results of 1., calculate the number of service loadings that will cause the undetected flaw to grow to critical size, thereby precipitating failure.
3. Compare the predicted number of service loading cycles before failure with the design requirements.

The information necessary to perform step 1. may be obtained from either proof testing or the inspection procedure used to detect flaws. When proof testing is used to determine the maximum

undetected flaw size, the analysis is called proof test logic. The stresses imposed during proof testing are related to the material fracture properties through fracture mechanics formulas which predict the maximum undetected flaw that would not precipitate proof test failure. When proof testing does not provide adequate structural assurance, NDE is used and based on the undetectable flaw size.

The preferred method for determining the maximum undetected flaw is the proof test logic approach, but due to the characteristics of the materials (tough ductile materials that exhibit stable flaw growth), this approach was only applicable to a few aluminum components. The NDE approach was, therefore, utilized extensively through the engine, both on the fracture critical and nonfracture critical components. It was the general policy to proof test all pressurized hardware, where feasible and practical, to a proof factor of 1.20 times limit design operating pressure, for 5.0 cycles to assure good quality hardware and a measure of structural integrity.

A program has been baselined which subjects high time hardware to teardown inspections periodically throughout the program to verify the fracture mechanics/NDE logic approach. As a result of these inspections, adjustments will be made to the procedure as required.

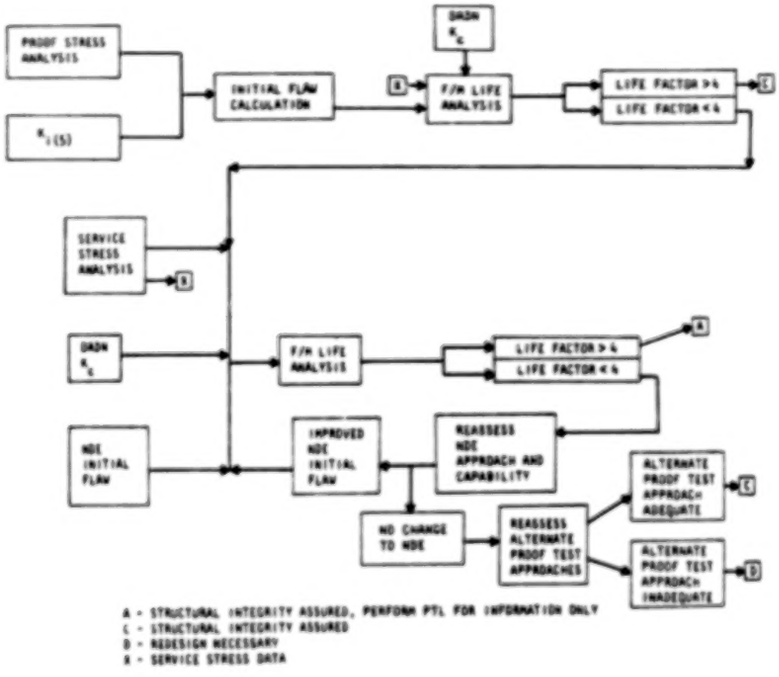


FIGURE 6. VERIFICATION ANALYSIS PROCEDURE

MATERIALS

The combination of design envelope requirements, complex service environments, and severe load conditions described in the preceding sections led to material performance criteria that were different from those normally encountered in high performance engine systems. Resistance to time-dependent, steady-state load conditions (i.e., creep and stress-rupture strength) were of minor importance due to the short operating lifetime of the SSME. Classical stress corrosion, while a consideration in material selection, was not encountered during the test and operational phases. Even the traditional material design allowables, ultimate and yield strength, within obvious limits would be viewed as having a relatively minor impact on the SSME design. Material considerations of major importance included high cycle fatigue (HCF), low cycle fatigue (LCF), and hydrogen environment embrittlement (HEE). Fracture mechanics/flaw growth characteristics had to be determined under conditions of HCF, LCF, and HEE (References 16 and 17). Finally, there was the extremely critical ability of the material to be "forgiving" with respect to unusual or unplanned manufacturing practices; this property will be loosely referred to as "fabricability" in the following discussion.

HIGH CYCLE FATIGUE

Although the life of the SSME is short in terms of operating time, high frequency vibrations and pressure fluctuations drive many of the structural components into the HCF-critical regime. A major deficiency existed in the HCF data base, due to the need for special-purpose materials that were not characterized in existing material properties manuals. This was compounded by operating conditions and temperatures which had major effects on HCF properties, often making it necessary to generate additional HCF properties for materials that were covered in the design literature. Synergistic effects of residual stress from transient loads and the relaxation of residuals during mainstage operations could only be measured in the laboratory. The effectiveness of standard HCF control procedures, such as shotpeening and stress relief, had to be confirmed under the operating environments of the SSME. The result was a long and continuing process, as follows:

1. Define the operating conditions.

2. Develop design criteria using available data and (conservative) rules for lower-bounding HCF behavior.

3. Fill the required need for additional data in the laboratory.

4. Check the validity of the assumptions made in 2.

The process is continuing, e.g., the turbine blade material, directionally-solidified MAR-M-246(Hf), has been evaluated for at least eight operating temperatures, five stress ratios ("R"), six test frequencies, and under numerous empirical conditions simulating turbine operating conditions. Figure 7 shows some of the data, addressing the question of test frequency effects. The evaluation of the HCF behavior of the turbine blade material is still in progress.

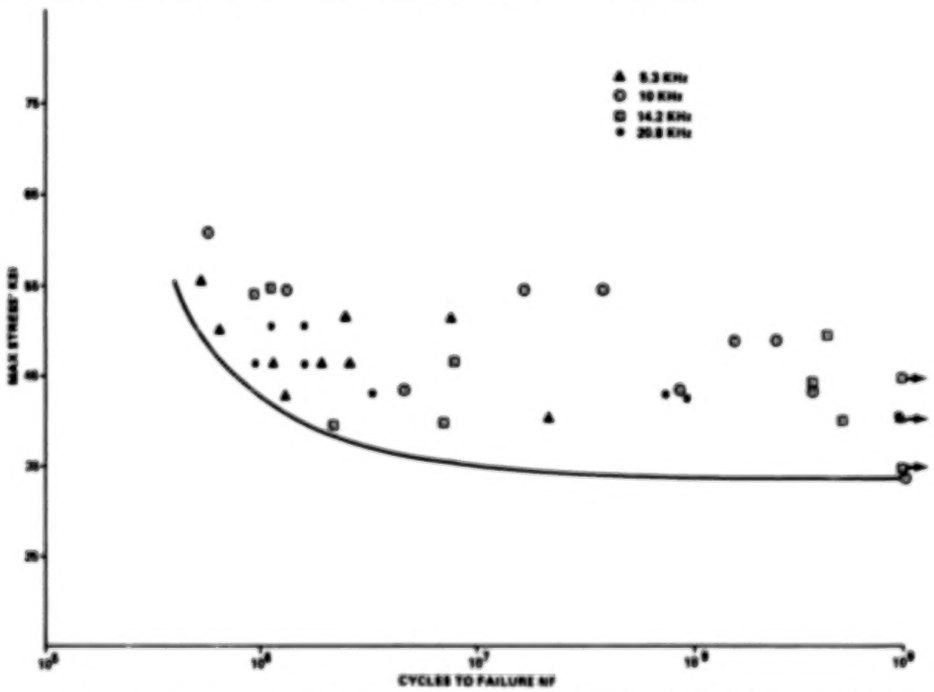


FIGURE 7. HIGH CYCLE FATIGUE DATA FOR MAR-M-246(Hf) DIRECTIONALLY SOLIDIFIED TURBINE BLADE MATERIAL, GENERATED AT ULTA-HIGH FREQUENCIES

LOW CYCLE FATIGUE

Many areas in the SSME experience LCF conditions, loosely defined here as cyclic strain in the inelastic range. LCF level strains occur during transient startup and shutdown conditions, or as a result of thermal deformations during mainstage. Generally, one or two LCF cycles are applied per operating cycle, but the strain levels are very high, well in excess of the engineering yield strain. LCF data were obtained for all of the structural materials on the SSME and were used to develop design modifications to ensure adequate LCF life. This process is continuing; many SSME components are LCF-life limited.

HYDROGEN ENVIRONMENT EMBRITTLEMENT

Not to be confused with classical hydrogen embrittlement, HEE refers to the real-time effect of hydrogen on ductility and strength. It is generally limited to certain alloy systems operating in the inelastic strain range, but one of the affected material systems is the nickel-based alloys, which include the major structural material in the SSME, Inconel 718. HEE does not usually occur at cryogenic or elevated temperatures; it is only a design consideration at temperatures that would otherwise be considered benign, close to room temperature. A thin layer of nonsusceptible material is an adequate shield against HEE, hence control measures frequently include electroplating of copper, gold, and other materials. In cases where the area in contact with gaseous hydrogen is the underside of a closeout weld and is inaccessible for plating, welding techniques have been developed and characterized which involve an underlay and root pass made from a nonsusceptible material, see Figure 8. When possible, design modifications have been made to eliminate the conditions that cause HEE, such as stress concentrations (e.g., inelastic strains). Non-traditional concepts of materials usage have emerged in the control of HEE. For example, one common procedure involves modifying the operating temperature to move it out of the HEE range.

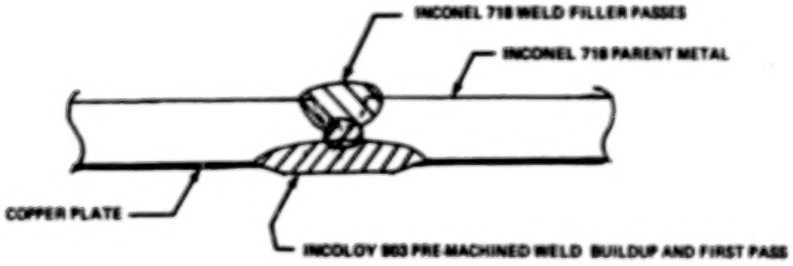


FIGURE 8. SPECIAL WELD UNDERLAY CONFIGURATION FOR CLOSEOUT WELDS IN HYDROGEN SYSTEMS

FABRICABILITY

Building an SSME is a sequential operation involving expensive, long lead items, usually joined by welding. Manufacturing discrepancies are inevitable, and it would not be feasible to scrap an assembly each time a major discrepancy occurred. Perhaps more than any other characteristic, "forgiveness" with respect to repairs and unconventional processing is a major consideration in material selection. For example, despite being susceptible to damage from a hydrogen environment, as noted above, Inconel 718 is the major structural material of the SSME. Laboratory tests have shown that the weld tensile and HCF properties are unaffected after as many as sixteen repairs in the same location. Solutionizing and aging times and temperatures can be varied over a wide range, with little effect on mechanical properties, so that furnace brazing and heat treatment can be accomplished in one operation. Undercuts due to mismatching are routinely filled in by welding and fairing, and the part is restored to design material requirements by heat treatment. Inconel 718 can be structurally welded to a large number of dissimilar materials by a number of welding processes, using many different filler materials. All of the preceding fabricability-related characteristics have been evaluated in the laboratory, and the resulting material design allowables have been documented. Additional requirements will develop as the SSME design continues to evolve in the direction of increased performance.

TYPICAL EXAMPLES

Typically, SSME lifetime problems have been characterized and solved in a unique manner. The large sensitivity of lifetime to small changes in alternating stress, temperatures, etc., moves beyond fluid flow analysis accuracy capability dictating that lifetime be determined from hot firing data in conjunction with analysis (Reference 10). The approach was discussed previously, see Figure 4. Using this approach in conjunction with the LRU concept has produced an acceptable solution to the challenge. Examples are now given of how the challenge was met.

LOX POSTS

The main injector is part of the hot gas section, which is the heart of the SSME. It includes a hot gas manifold, primary and secondary face plates, a lox dome, and 600 lox posts or feed tubes between the lox dome and the primary injector plate. Figure 9 shows a top plane view of the lox post array with the three transfer tubes from the hydrogen preburner and the two transfer tubes from the lox preburner.

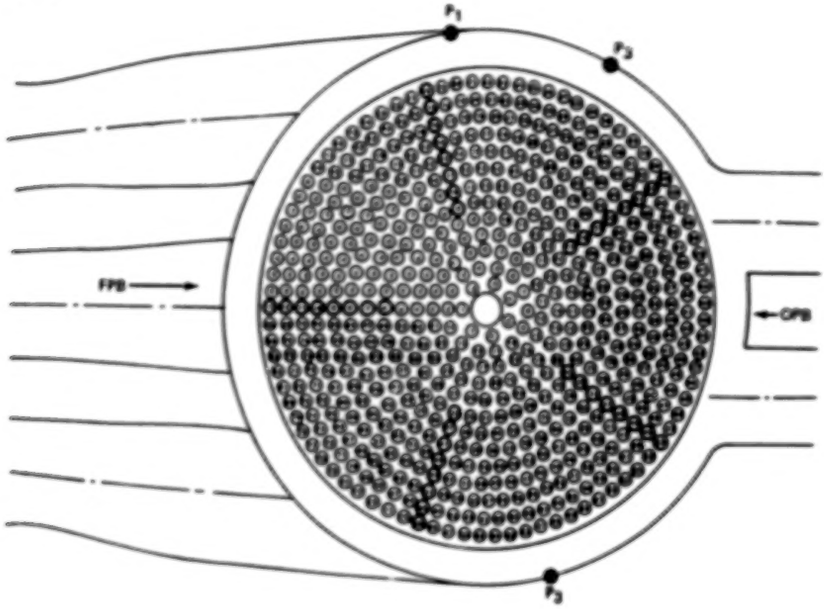


FIGURE 9. TOP PLANE VIEW OF LOX POST ARRAY

High velocity gas at a temperature of approximately 1800°F flows through the injector, then through the gap at the base of each post and around the tip of the injector plate, where it mixes with the liquid oxygen flowing down the center of the post. This flow environment, coupled with mechanical vibrations and variable dynamic characteristics, produces severe high cycle fatigue loading on the lox posts. This is augmented by high static stresses resulting from the thermal and static pressure loads. Flow shields (see Figure 10) have been added to the outermost row, but the posts are still high cycle fatigue life limited, and there have been two related engine failures during demonstration firings.

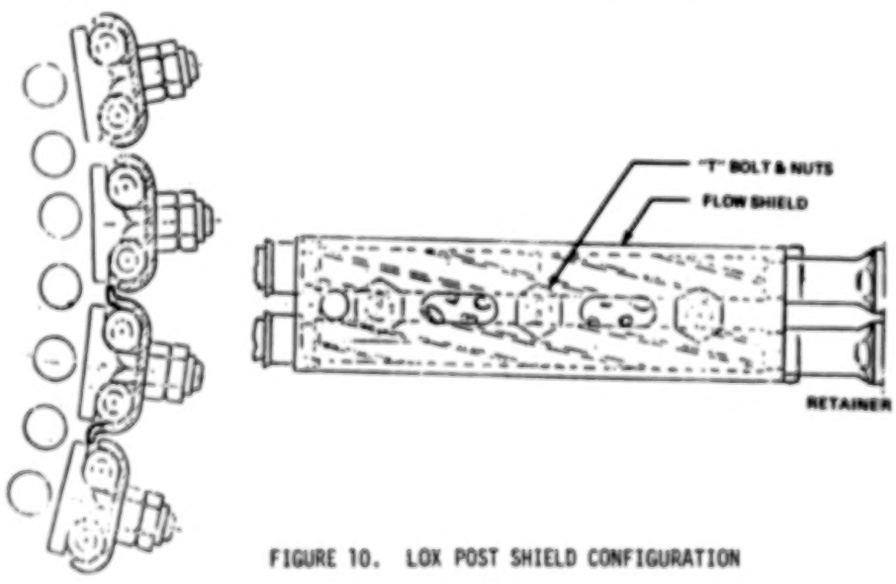


FIGURE 10. LOX POST SHIELD CONFIGURATION

Metallurgial analysis determined that the failure mechanism was high cycle fatigue, initiating in the threads of the face plate retainer. Sources of alternating stress at that point are mechanical oscillations, vortex shedding, and fluctuating pressures (flow and acoustics). Static loads arising from thermal gradients and internal flow induced pressures are superimposed as a high mean stress to the alternating loads. Despite the presence of the flow shields, the highest fatigue loads and most frequent occurrence of fatigue cracks are in the outermost posts, row 13.

The approach used to rationalize the hypothesized failure mode was the approach shown on Figure 4. Certain aspects of the problem can be handled analytically with good success. For instance, the analysis has shown a mechanical and fluctuating pressure environment in the 1200 Hz regime, which couples with and drives the modes (natural frequencies) of the posts; these analytical modes have been verified experimentally and by instrumented lox posts in hot firings. Cold flow tests of the hot gas manifold, powerhead, and lox post were used as a test bed for flow characteristics.

Demonstrated lifetimes from single engine firings have been combined with analytical data to arrive at lifetime predictions. Figure 2 is a plot of alternating stress capability versus number of cycles, taking into account static loads and temperature effects. Two empirical data points have been assumed: 1) a 750-second failure time for a single post, as observed in one engine test, and 2) the 5,000-second cracked post case demonstrated for shielded posts. The first bar is the alternating stress for the single post mode (750 seconds) showing the combined stress induced by mechanical and fluctuating pressure. The analysis was adjusted to predict high cycle fatigue failure in 750 seconds using mechanical and fluctuating pressure forcing function ranges based on best estimates from hot firing measurements. The second bar is the two-post flow shield predicted alternating stresses for mechanically and flow-induced oscillations using a model adjusted in the same manner (Reference 10). The model has been used to redesign the posts to assure long life and to increase engine performance from shield removal. The redesign involves a two-phased approach. Phase 1 is a change of material from CRES 316L to Haynes 188S (used in FPL engine configuration), raising the alternating stress allowable by approximately a factor of two. The second phase is a heavier post, which will further increase the alternating load capability.

TURBINE BLADES

The high pressure fuel turbopump (HPFTP) is a three-stage centrifugal pump that is directly driven by a two-stage hot-gas turbine. The turbine is powered by hot gas (hydrogen rich steam) generated by the fuel preburner. Hot gas enters the turbine and flows across the shielded support struts, through the first and second stage nozzles and blades, and is discharged into the hot gas manifold. Requirements for high performance within a restricted envelope have led to a complex, cyclic-load-producing configuration of 13 struts, 41 first stage nozzle vanes, and 59 second stage turbine blades. There have been numerous instances of cracking in both the first and second stage turbine blades at the locations shown in Figure 11. Although none has precipitated an engine failure, turbine blade life improvement remains a major goal in the SSME Program.

Loads analysis and lifetime prediction for the HPFTP turbine blades have presented problems similar to those encountered in the lox posts. Major problems have included environment definition, dynamic modeling, and static and alternating stress distribution. The environment definition is extremely complex for both the thermal and fluctuating pressure standpoints. The blades are near the preburner and use the hot preburner gas as the source of their power (flow forces). These environments are not uniform due to baffle posts, struts, etc., and the blade geometry. Fluctuating pressures present the same problem, plus the clear introduction of harmonics due to the struts and the multiblade passages. Dynamic modeling is complicated by the basic geometry, hot surface, boundary conditions at the wheel, and special dampers for reducing blade response. Stress is composed of static centrifugal force, power bending, steady-state thermal, cyclic thermal (start and shutdown transients), and fluctuating pressure components. Significant factors in the alternating stress are 1) tuning of strut wakes with blade lower modes, 2) multiblade relative motion of adjacent blades, 3) variable damping coefficients and lockup, 4) changes through engine operating range, and 5) startup and shutdown thermal and pressure cycles.

Each instance of blade cracking has been addressed using an analytical/empirical approach similar to that described for the lox posts; loads and stresses are calculated by analysis, and the models are adjusted as required to be compatible with observed phenomena. A detailed finite element model has been generated for the blades. Detailed definition of the forcing functions has been accomplished by accurate modeling of the strut/nozzle/blade configuration, and the output has been matched to results obtained from special air rig and "whirlygig" tests. Basic material strength and fatigue data have been obtained over a range of operating stresses and temperatures. Figure 12 shows the form of the engineering solution with all of the data taken into consideration, including the observed frequency of the particular blade cracking incident under investigation. Curve 1 is for rated engine

power level (RPL) assuming 5,000 seconds of life. Curve 2 is full or maximum engine power level (FPL) and 5,000 seconds of life, while curve 3 is the same power level assuming 2,500 seconds of life. The mean stress for RPL is 46 Ksi, and for FPL, it is 55 Ksi. The blade operating temperature is in the 1,600 to 1,700 degree range, resulting in a low allowable alternating stress.

At the present time, there are no serious blade cracking problems. Each instance of blade cracking has been solved by material-related improvements or environment modifications. Periodic inspections are required, however, and the average blade changeout interval of 3,000-5,000 seconds is far short of the design goal of 27,000 seconds. Studies for long-term improvement in blade life are in progress. Improved materials are being considered, including advanced superalloys in the single crystal form, and environment reduction techniques are under study.

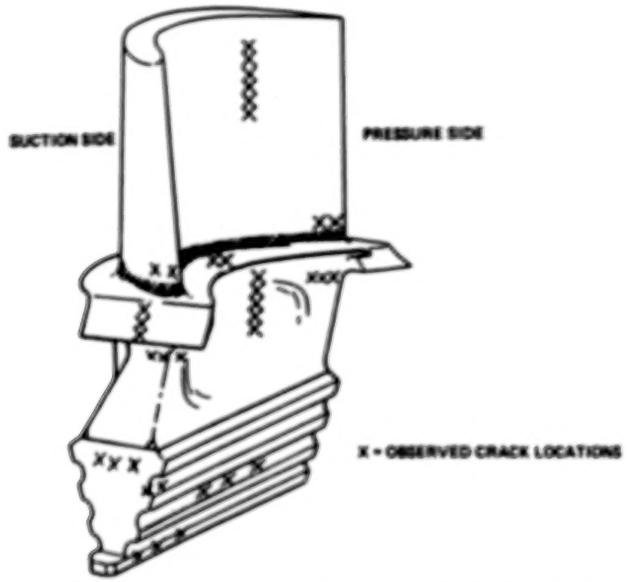


FIGURE 11. AREAS OF HIGH STRESS AND OBSERVED CRACK FORMATION

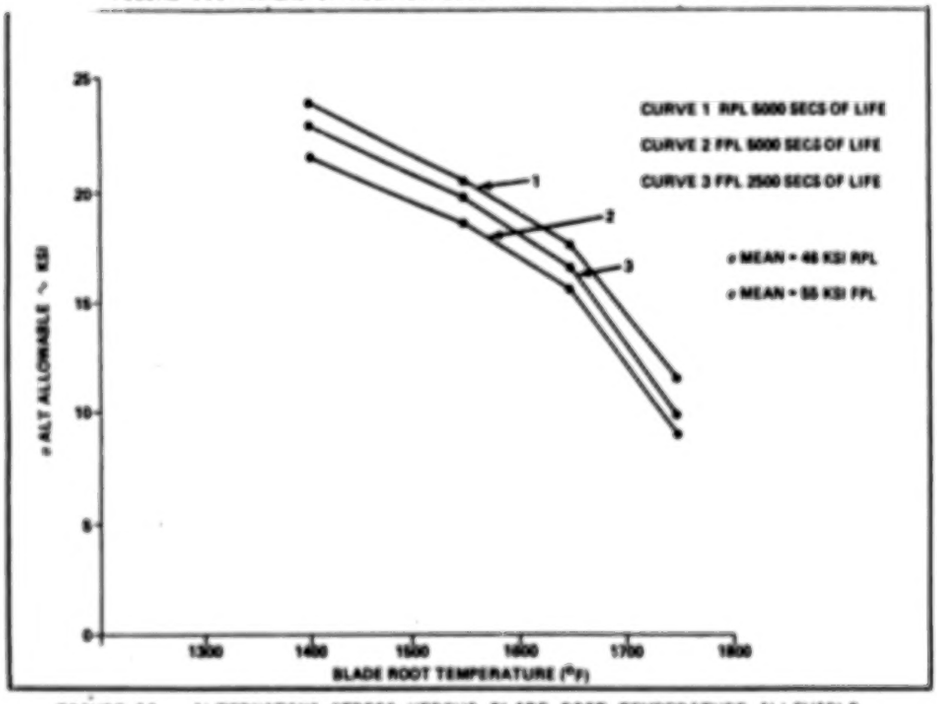


FIGURE 12. ALTERNATING STRESS VERSUS BLADE ROOT TEMPERATURE ALLOWABLE

NOZZLE AND STEERHORN ENGINE SIDE LOADS

The SSME nozzle has three engine downcomer coolant lines that take hydrogen from the main fuel valve to the aft nozzle manifold. The aft nozzle manifold feeds the coolant tubes which in essence is the engine nozzle. Two of these coolant lines have failed during hot engine firings due to high cycle fatigue. Figure 13 gives the basic configuration, showing the downcomer line (steerhorn). A history of cracking nozzle tubes has also plagued the engine.

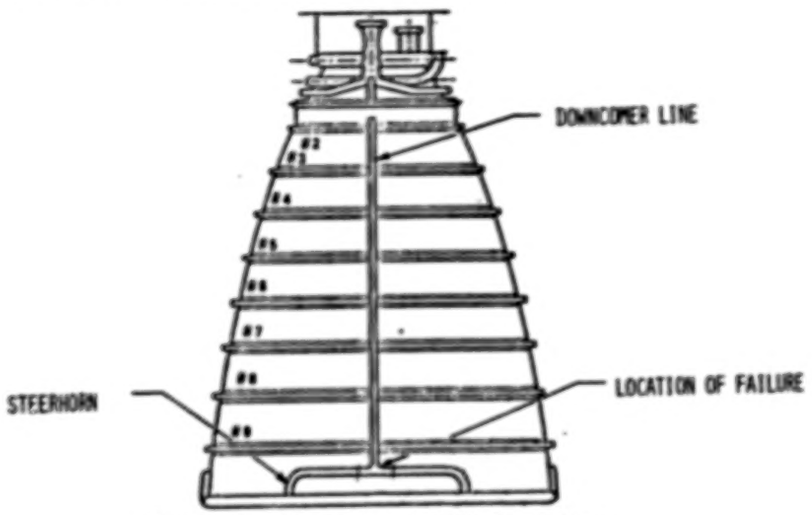


FIGURE 13. DESCRIPTION OF NOZZLE SYSTEM

The loads on the line nozzle system arise from firing of a high-expansion-ratio nozzle under ground atmospheric conditions. The plume does not fill the nozzle until the internal pressure is greater than atmospheric pressure. As the nozzle plume flow velocity increases, it passes through a region where a Mach disc or cone exits the nozzle. Two distinct phenomena occur during this thrust buildup phase. The first occurs around 600 to 700 psia chamber pressure. In this case, the plume is basically cylindrical in nature and is directionally unstable, moving around radially within the nozzle. The loads induced by this case drive the actuator design. The second occurs around 1,200 psia where the Mach cone leaves or enters the nozzle, creating high local shock loads. Figure 14 shows a typical thrust buildup and shutdown curve and stress response measured on the nozzle steerhorn. The side loads response is clearly shown in this figure. The large strain amplitude occurs due to the excitation of the n = 0 (expansion mode) and the n = 6 (shell mode). Notice that the response is very sharp and around 250 Hz (the insert shows a blowup of the response) (References 10, 13, 14, 15, and 18).

Figure 15 depicts the n = 6 shell mode on the right-hand side. The left-hand side of the figure shows the shell mode frequencies as a function on n-number. At the bottom of the figure is a spectrum of the measured acceleration of the engine nozzle aft manifold showing presence of all n modes but by far the larger peak occurring for the n = 0 and n = 6 modes.

The presence of this large load at the discrete frequency of 250 Hz (near resonance with nozzle modes) created many engine design and program problems, particularly during the developmental firing program. Two things had to be accomplished. The underdesigned steerhorn had to be fixed so that firings could continue, and the steerhorn had to be redesigned for operational flights. Since initially an internal nozzle pressure forcing function was not available, it was decided to take the hot-firing measured accelerations at the aft manifold and use these to base drive a dynamic model of the steerhorn. The first major result obtained was that just thickening the tube helped the problem. The increased mass offsets the increased stiffness so the frequency stays the same. The nozzle-induced driving force is not changed; therefore, the increased mass increases the steerhorn loads proportionally to the mass increase. As a result, a sensitivity analysis and redesign matrix was pursued as a means of obtaining a solution.

The conclusion of this study was that the horizontal run of the steerhorn must be fixed to the nozzle stiffness ring to reduce loads. This meant that a steam loop had to be incorporated above the hatband to take out thermal induced expansion loads. The other main result was that for the T area (original design) a nickel-plating would provide adequate life for developmental engine firings and first Shuttle flights. The redesigned steerhorn was incorporated on the FPL engines.

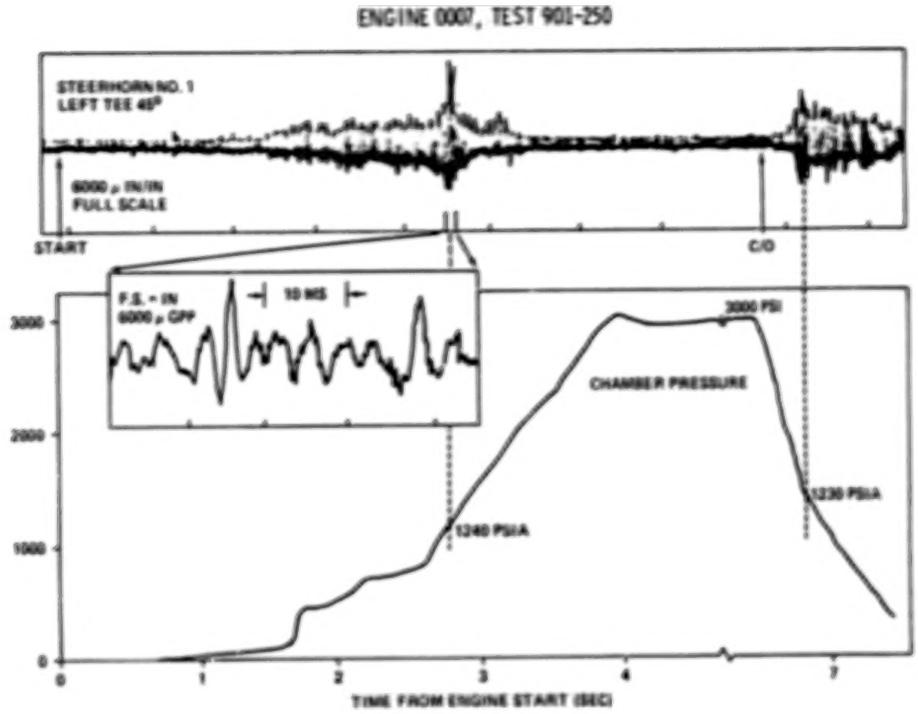


FIGURE 14. STEERHORN STRAINS IN TRANSIENT OPERATION

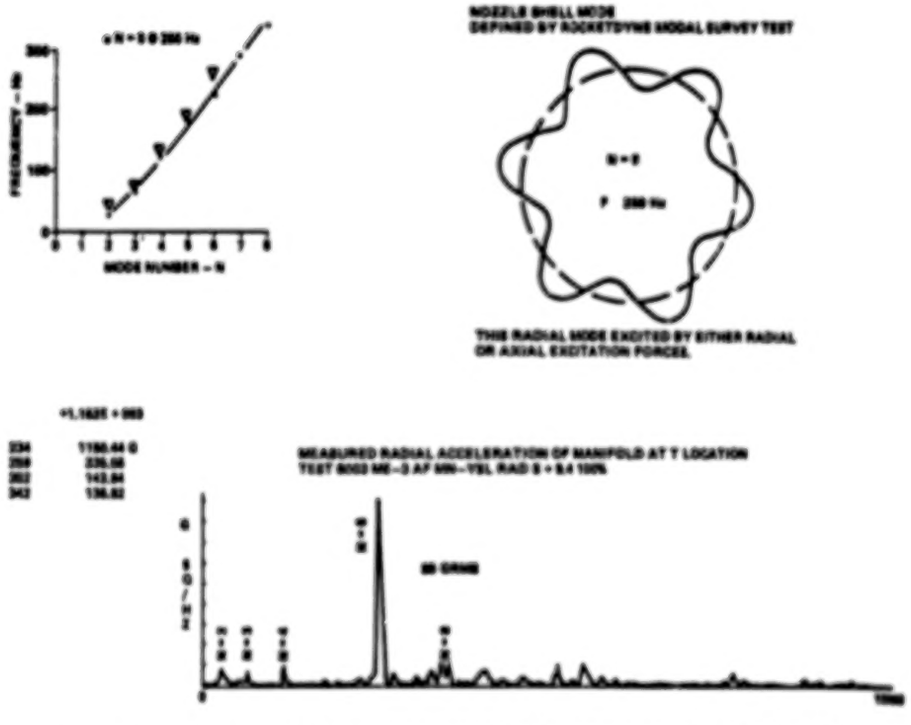


FIGURE 15. NOZZLE SHELL MODE DEFINED BY ROCKETDYNE MODAL SURVEY TEST

Two test programs were instituted to finalize these loads and the redesign: Scale model engine cold-flow test and full-scale flight nozzle dynamic test. The dynamic model used in this analysis was verified in a full-scale dynamic test. Analytical modes had good agreement with test modes. The cold-flow model test varied the flow rate, etc., and determined the forcing functions. A full set of pressure gauges was mounted so that the force distribution could be determined. These results were scaled to full scale.

Using these test-derived forcing functions, a dynamic response analysis was made for both the original design and the redesigned steerhorn configurations (steam loop). Good agreement with hot-firing data was obtained. The reduction in loads is approximately 40 percent for the redesigned case, providing infinite life. Table 1 is a summary of stresses measured in hot-firing data for the nonsteam loop configuration.

TABLE 1. HOT-FIRING DATA SUMMARY

DATA BASE	STRAIN AT T LOG DISTRIBUTION*			
	START		CUTOFF	
STAND	MEAN	3σ	MEAN	3σ
A1 (14 TESTS)	3,262	10,537	5,033	15,642
A2 (20 TESTS)	3,876	16,503	1,636	6,529
MPT (3 TESTS, 7 ENGINES)	6,270	20,685	4,916	12,088
MPT & A1	4,064	18,469	4,938	13,552
COMBINED ALL STANDS (41 TESTS)	3,954	17,084	2,722	21,528
COMBINED ALL STANDS ALL MEASUREMENTS ALL EVENTS 41 TESTS		19,053		

*CONTAINS NO EXTRAPOLATED DATA.

Test stand A-2, which has a simulation for altitude (reduced pressure), showed different characteristics from the other stands. Based on this analytical work and the statistics of the hot-firing data, a lifetime prediction of the redesigned steerhorn was accomplished verifying a redesign that would meet the 55-mission lifetime requirement.

CONCLUSIONS

The design, manufacturing, and verification of the SSME has been one of the major challenges in obtaining an operational Space Shuttle. Basic problems have been met with a high performance engine and acceptable refurbishment requirements. Additional efforts are required for efficient refurbishment regimes and to have the potential for higher performance to meet future Shuttle mission requirements.

The first six Shuttle flights had engine performance as predicted with no failures. Using the LRU concept, some pumps were changed out as planned. The engine system has met the basic design challenges.

REFERENCES

1. Thompson, J.R.: Space Shuttle Main Engine. In 14th Space Congress, April 27-29, 1977.

2. Colbo, H.I.: Space Shuttle Main Engine - The Liquid Rocket Engine Technology Leader. AIAA Student Journal, vol. 17, 1979-1..., pp. 22-26.

3. Dankoff, Walter; Herr, Paul; and Nailwain, Melvin: Space Shuttle Main Engine (SSME) - The "Maturing" Process. Aeronautics and Astronautics, January 1983.

4. Rocketdyne Report: Space Shuttle Technical Manual, SSME Description and Operations. Report RSS-8559-1-1-1 E4100, January 15, 1981.

5. Sanchini, D. J. and Colbo, H. I.: Space Shuttle Main Engine Development. AIAA Paper No. 80-1129, 1980.

6. Colbo, H. I.: Development of Space Shuttle Main Engine. AIAA Paper No. 79-1141, 1979.

7. Thompson, J. R., Jr.: Space Shuttle Main Engine. In 17th Space Congress, April 30-May 2, 1980.

8. Edgar, R.: Prime Power for the Shuttle. Spaceflight, vol. 17, February 1975, pp. 70-73, 80.

9. Johnson, J. R. and Colbo, H. I.: Space Shuttle Main Engine Progress Through the First Flight. In AIAA, SAE, and ASME 17th Joint Propulsion Conference, July 27-29, 1981.

10. Ryan, R. S., et al.: Systems Analysis Approach to Deriving Design Criteria (Loads) for Space Shuttle and Its Payloads. NASA TN 1949, December 1981.

11. Ryan, R. S., et al.: Mechanism Associated with the Space Shuttle Main Engine Oxidizer Valve Duct System, Anomalous High Amplitude Discrete Acoustical Excitation. In AIAA/ASME/ASEE/ ATTS Structural Dynamics and Materials Conference, May 1980.

12. Ryan, R. S., et al.: Elimination of Discrete Frequency Acoustical Phenomenon Associated with the Space Shuttle Main Engine Oxidizer Valve-Duct System. In 50th Shock and Vibration Symposium, October 1979.

13. Kiefling, Larry: Space Shuttle Main Engine Nozzle-Steerhorn Dynamics. In AIAA Dynamics Specialists Conference, April 6-8, 1981.

14. Larson, E. W.: Investigation of the Fuel Feedline Failures on the Space Shuttle Main Engine. In AIAA/SAE/ASME 16th Joint Propulsion Conference, June 30-July 2, 1980.

15. Ryan, R.; Jewell, R.; Bugg, F.; Ivey, W.; McComas, R.; Kiefling, L.; and Jones, J.: Dynamic Testing of Large Space Systems. NASA TM-78307, September 1980.

16. Schwinghamer, R. J.: Materials and Processes for Shuttle Engine, External Tank, and Solid Rocket Booster. In Internat'l Astronautics Federation, IAF Paper 76-202, October 10-16, 1976

17. Schwinghamer, R. J.: Materials and Processes for Shuttle Engine, External Tank, and Solid Rocket Booster. NASA TN-D-8511, 1977.

18. Johnston, G. D.: SSME Steerhorn and Nozzle Assembly Test, Phase III, SSME Nozzle Dynamic Test Plan. Marshall Space Flight Center, DST-SSME-TIP-001, December 19, 1979.

19. Nave, L. H. and Coffey, G. A.: Sea Level Sideloads in High-Area-Ratio Rocket Engine. AIAA Paper No. 73-1284, 1973.

20. Fenwich, J.; Jones, J.; and Jewell, R.: Space Shuttle Main Engine (SSME) Pogo Testing and Results. In 52th Shock and Vibration Symposium, October 1981.

21. Lewis, Jack R.: Materials and Processes for Space Shuttle's Engines. Metal Progress, vol. 107, March 1975, pp. 41-43.

N85
16919

UNCLAS

D30

N85-16919

THE CHALLENGING "SCALES OF THE BIRD" (SHUTTLE TILE STRUCTURAL INTEGRITY)

William C. Schneider and Glenn J. Miller
NASA Lyndon B. Johnson Space Center
Houston, Texas 77058

INTRODUCTION

The launch and landing of the U.S. Space Shuttle Orbiter has now become almost routine. The development of such a highly successful vehicle involved the resolution of many challenging problems. One problem area where the challenges to creativity, inventive design, and analytical understanding were particularly demanding involved the structural integrity of the thermal protection system (TPS). The problems associated with these tiles were resolved in the unfavorable engineering environments of tight schedule, budget constraints, and high public visibility. The successful resolution of these problems is evident with each landing of the Shuttle (fig. 1).



FIGURE 1.- OV102 COMES HOME.

The Orbiter is essentially a conventional skin stringer aluminum structure with some limited usage of graphite epoxy for the cargo bay doors and orbital maneuvering system (OMS) pods. The properties for these materials dictate a maximum structural temperature of 350° F. The reusability goal of 100 missions necessitates a lightweight nonablative TPS that protects the structure and withstands the thermal and environmental loads of space flight. The TPS material selected (LI900) was developed by Lockheed Missiles and Space Company and is an exceptional thermal insulator. This ceramic material is highly brittle and has a low coefficient of thermal expansion. Therefore, any contraction of the aluminum skin to which the tiles are directly bonded would cause the reusable surface insulation (RSI) to fracture. To minimize in-plane incompatibility, a felt strain/isolator pad (SIP) was bonded between the tiles and the structure (fig. 2).

In addition, the plan form dimensions for most lower surface tiles were on the order of 6 inches or less. The 6-inch dimension was computed so as to meet the requirement that the tile gaps should be no less than 0.010 inch. This occurs during entry (when the structure is still cold from deep-space radiation) as the tiles become hot. The stiffness and dimensions of the SIP were designed to minimize the stresses induced into the brittle tile material from deformations predicted for the aluminum structure. Initially, the stresses expected in the TPS were well within the strength of the RSI, but as the design of the Orbiter progressed, mission requirements became firmer, and load predictions became refined, it became clear that the TPS would have to withstand loads higher than originally anticipated. Additionally, stress concentrating stiff spots were found to exist in the SIP (fig. 3). These stiff spots (caused by needling) decreased the allowable system strength to 6 psi in-

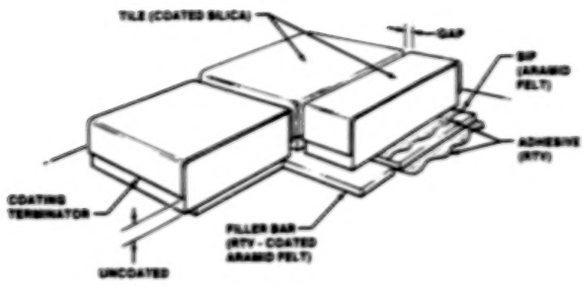


FIGURE 2.- SYSTEM DESCRIPTION.

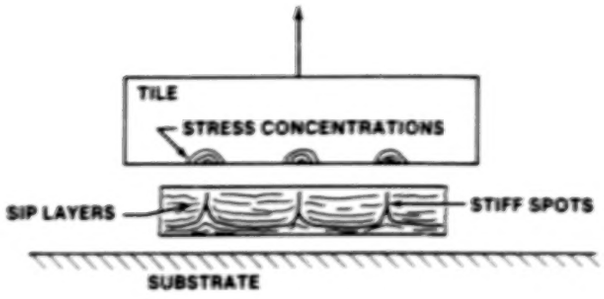


FIGURE 3.- STIFF SPOTS EFFECT ON LOCAL TILE STRESS.

stead of the 13 psi originally used for the tile strength. This caused negative structural margins of safety to exist over large areas of the structure and, in certain areas, the TPS was computed to be inadequate to survive even a single mission.

This paper will cover the principal design issues, tests, and analyses required to solve the tile structural integrity problem and performance based on the recent flight test program.

PROOF TESTING INSTALLED TILES

Because of the cost and schedule limitations imposed on the Orbiter project, it was necessary to begin fabrication and installation of the tiles long before the final loads and stress analysis had been completed. When large numbers of tiles were found to have inadequate structure margins, the Orbiter had just been delivered to Kennedy Space Center (KSC) with all but 6000 of the 33 000 tiles already installed. It seemed that there was no alternative but to remove every tile and start over (seriously impacting schedule and cost) with some new (as yet undeveloped) stronger tile system. The challenge was clear: to salvage the majority of the installed tiles while ensuring sufficient structural margin for a safe flight. The approach devised to overcome this almost insurmountable challenge was the so-called Tile Proof Test. The proof test involved the application of a load to the installed tile so as to induce a stress over the entire footprint equal to 25 percent above the maximum flight stress experienced at the most critical point on the tile footprint.

To fully appreciate the value of this proof test, it is necessary to understand the stress-inducing environments taken into consideration when computing structural margins. In addition to the local flight-induced loads (caused by aerodynamics, vibrations, and acoustic noise) and local substrate displacements (structural response to pressure differential and acoustic noise), a value of 0.019 inch (maximum allowed by installation specification) of tile/structural mismatch is assumed to exist at the point of maximum stress (fig. 4). Also, since this brittle TPS material has a large scatter in the strength data, the low 99-percent value was used in computing margins of safety.

Because most of the installed tiles would be stronger than the statistically derived low strength value, and since most of the tiles would realistically not have the maximum mismatch, it became clear that if the tiles were proof tested, most of them would successfully pass. Therefore, this approach could potentially salvage thousands of installed tiles and only a small percentage would fail and have to be replaced. The tiles that would fail would be replaced with tiles that had been densified on the inner moldline surface. The device used for this proof test (fig. 5) employs a vacuum chuck to attach to the tile, a pneumatic cylinder to apply the load, and six pads attached to surrounding tiles to react the load.

Since any appreciable tile load may cause some internal fibers to break, it was essential to develop a means of evaluating the residual strength of a tile after the proof test had been performed. During the actual proof testing, acoustic sensors (fig. 5) placed in contact with the tiles were used to monitor the acoustic emissions from any internal fiber breakage. A large-scale laboratory program was initiated to arrive at a failure criteria. The program consisted of acoustically monitoring many tiles during the proof loading and subsequently inducing cyclic loads (simulating flight values) until failure occurred or an equivalent of 100 missions was reached. A pass/fail criterion was established from the acoustic signatures of the tiles both failing and passing the laboratory tests. The proof testing of installed tiles was incorporated and not only salvaged tens of thousands of installed tiles but also revealed those tiles (13 percent failing proof test) with inadequate flight strengths.

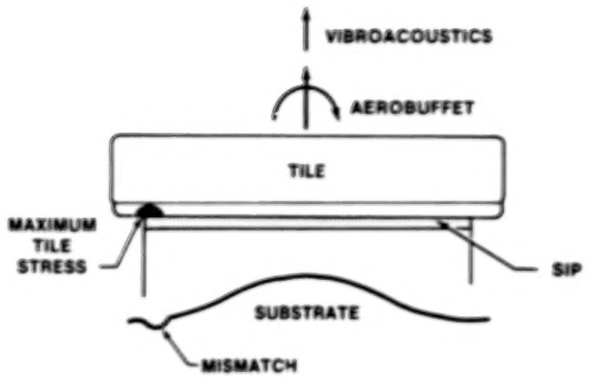


FIGURE 4.- TILE LOAD SOURCES.

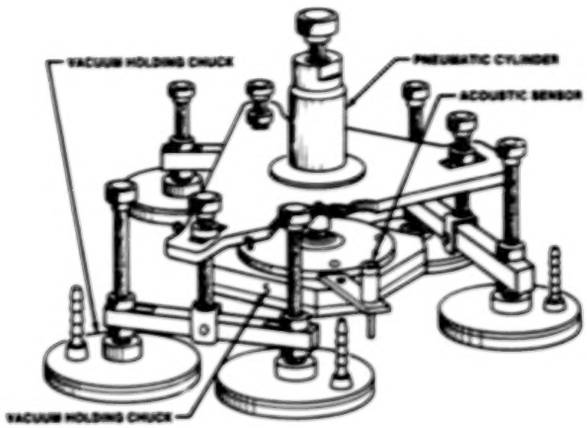


FIGURE 5.- PROOF TESTING DEVICE.

LOAD/DEFLECTION ALLOWABLE

If a tile were to fail during the proof test, it would be removed, the bottom of the tile would be densified (with a coat of colloidal silica particles), and the newly densified tiles reinstalled on the Orbiter. This densified layer, serving the function of a stiff plate on the tile bottom, eliminates the effect of local stiff spots in the SIP and thus increases the tile/SIP system strength from 6 to 13 psi (fig. 6).

However, there existed a large number of tiles where the combined loads were so high that even this doubled system strength was theoretically not adequate. The clear challenge was to exploit any additional densified tile strength not accounted for in the analysis. This challenge was successfully met by the incorporation of the so-called Stress versus Delta (displacement) allowable curves. This idea was conceived by realizing that the combined stresses could be classified into those induced by external loads (aerodynamics, vibrations, acoustics) and those induced by displacement (mismatch, structural out-of-plane displacement existing under the tile). It is the displacement-induced stresses that could possibly be reduced because the densified layer, being stiff, would resist bending and thus not transmit the total displacement stress to the virgin RSI material. This hypothesis was supported by extensive finite element analysis (fig. 7). The solid element models used in this analysis indicated a significant reduction of peak stresses in the virgin RSI material just above the densified layer.

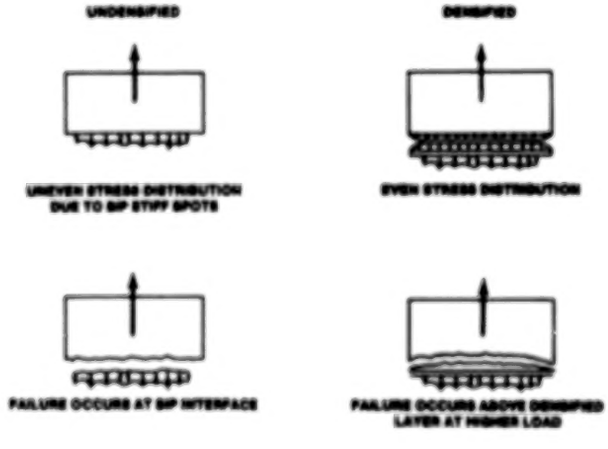


FIGURE 6.- EFFECT OF TILE DENSIFICATION.

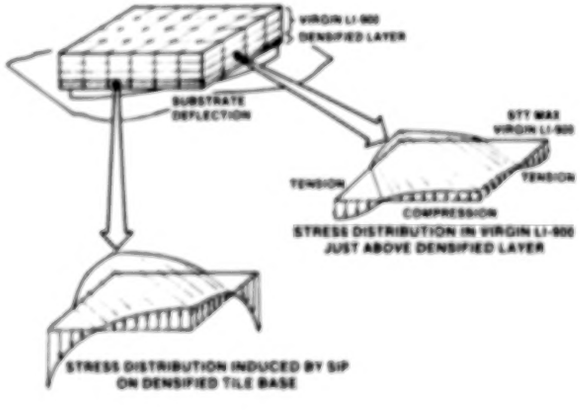


FIGURE 7.- TYPICAL ANALYSIS SHOWING HOW DENSIFIED LAYER REDUCES STRESS INDUCED INTO RSI.

ORIGINAL PAGE IS
OF POOR QUALITY

With this information in hand, a test program was initiated to test numerous densified tiles to failure for various combinations of structural displacement and external loads. The test arrangement is shown in figures 8 and 9.

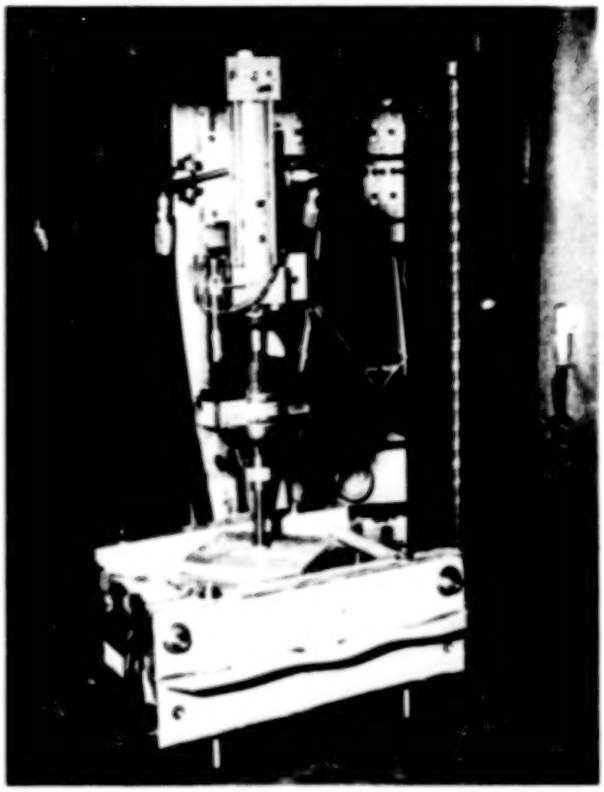


FIGURE 8.- TEST SETUP FOR LOAD/DISPLACEMENT ALLOWABLES.



FIGURE 9.- TILE SHOWING FAILURE SURFACE DURING LOAD/DISPLACEMENT TESTING.

The average external stress level (P/A) at which each densified specimen failed was then plotted against the displacement (Delta) imposed under the tile. A bounding curve for densified tiles was then drawn on the Stress versus Delta plot. The results are shown in figure 10 together with similar data for undensified tiles.

The results obtained provided a method by which externally applied stresses and displacement-induced stresses could be realistically combined. The conservatism of simple addition of all stresses was eliminated and the full capability of densified tiles could be used to replace thousands of highly stressed undensified tiles.

AIRFLOW TEST OF SPECIAL TILES

During both ascent and entry, the TPS is subjected to numerous loadings from a severe aerodynamic environment including shocks and pressure gradients. Through development testing of RSI material, a basic load diagram was constructed for each of these conditions (fig. 11). These free-body diagrams make the analysis of square or rectangular (acreage) tiles relatively straightforward. However, most of the tiles adjacent to tile boundaries (such as the wing leading edge, windshield, landing gear doors, etc.) do not have such simple geometry. These special tiles are often located in a very complex flow field and because of their unique geometry create various intricate venting paths that can not be easily analyzed. Therefore, the challenge presented was to ensure the structural integrity of these special tiles and to gain a better understanding of the local flow conditions around such tiles. To meet this challenge, a combination of flight and wind tunnel testing was initiated. Locations (fig. 12) from several of the most complex flow fields and tile geometries were chosen to be tested.

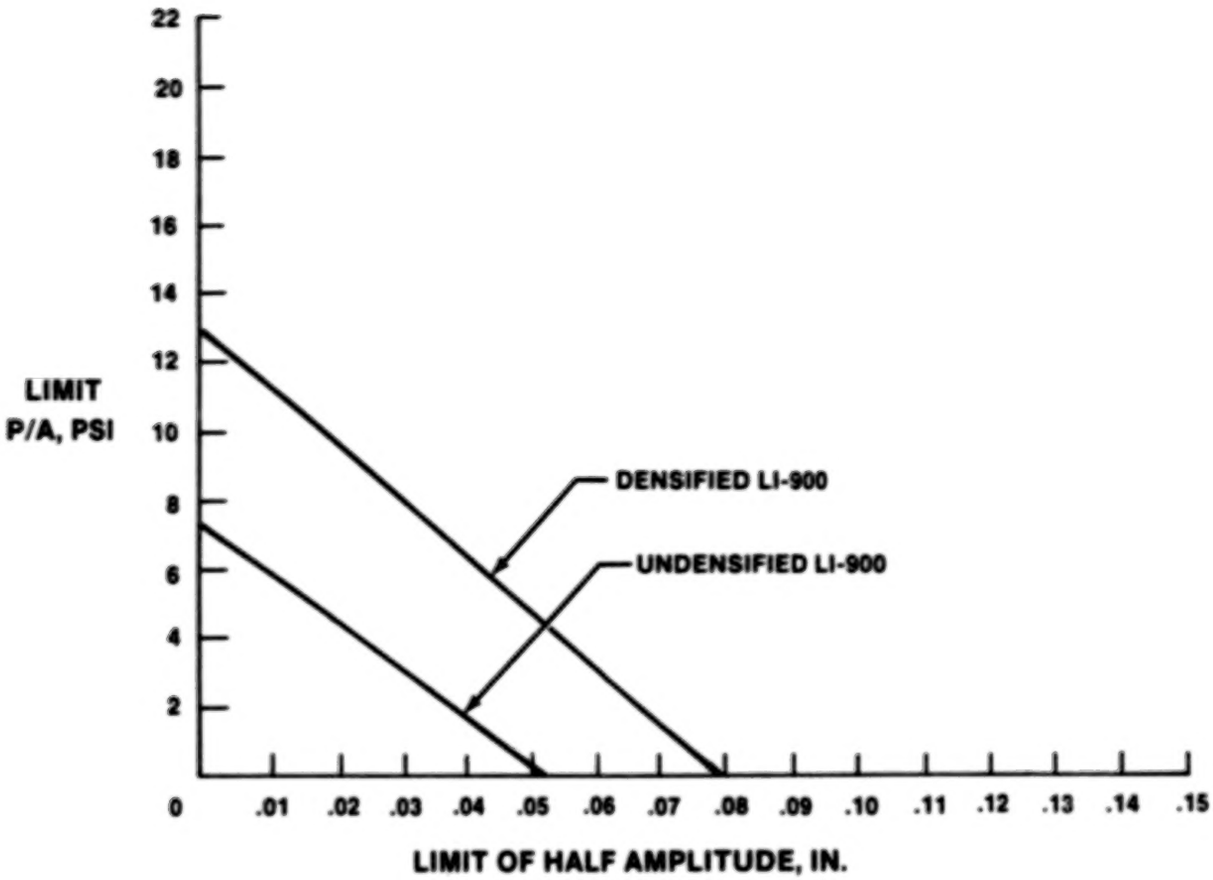


FIGURE 10.- ALLOWABLE FWT IN PRESENCE OF SUBSTRATE DEFLECTION.

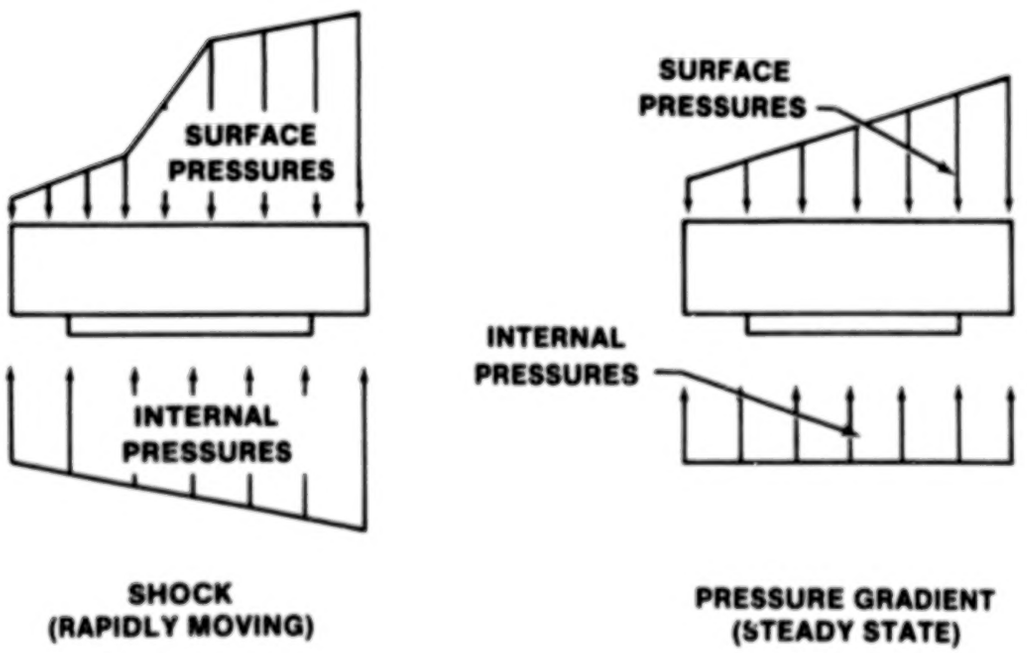


FIGURE 11.- BASIC LOAD DIAGRAM.

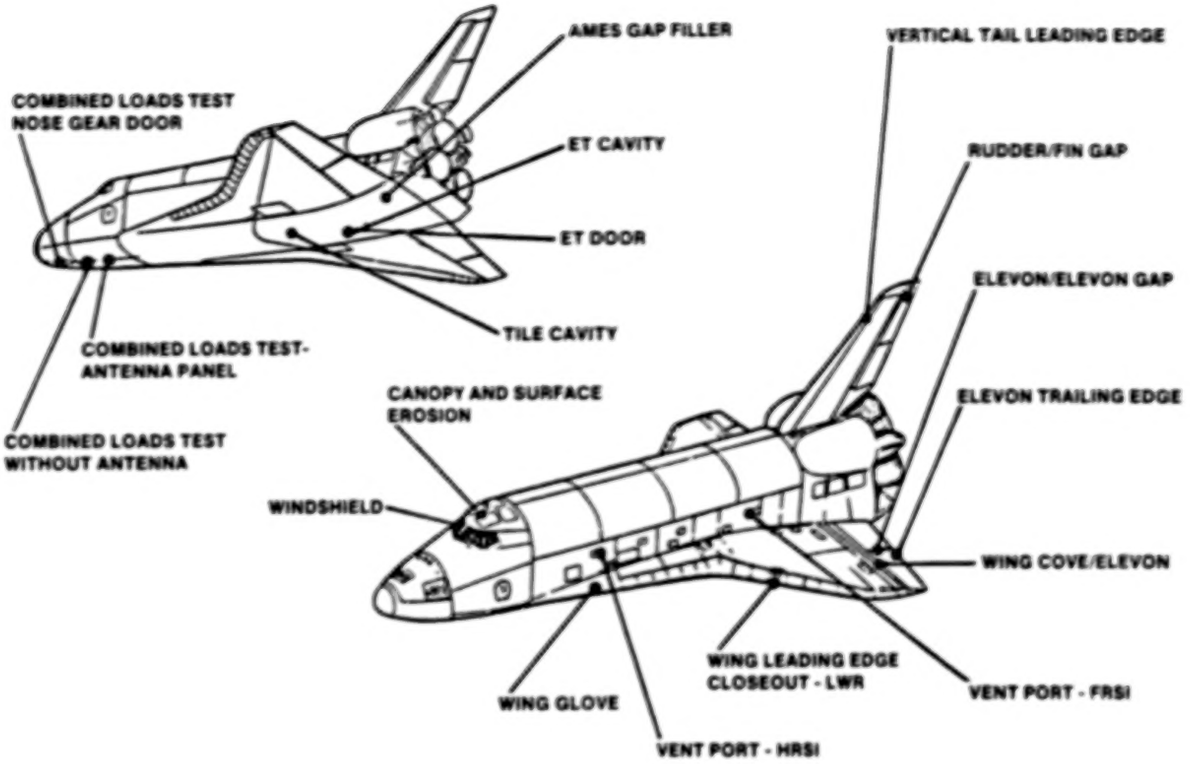


FIGURE 12.- TPS FLOW PROGRAM TEST ARTICLE LOCATIONS.

In each case, the local aerodynamic environment of the Shuttle (obtained from wind tunnel testing of scale models) was correlated to a similar flow field existing at some point on the surface of a high-performance aircraft or in a wind tunnel cross-section. All test articles were constructed to simulate the local Orbiter geometry. The tiles were heavily instrumented to ensure that test conditions achieved were within the predicted aerodynamic regimes (fig. 13).

A partial summary of these test conditions and results is shown in table 1. The tests not only demonstrated the structural integrity of each tile tested but increased the knowledge of flow around, under, and through the TPS. A more detailed treatment of tile flow tests may be found in reference 1.

This test program provided a unique solution to the challenge of aerodynamic loads on special tiles. The program increased confidence in TPS design by identifying design deficiencies which were corrected and retested to ensure their reliability during future flights.

SPECIAL PROBLEM TILES

Late in the certification program, it became apparent through analysis and tests that a few unique tiles had high stress levels that could result in low margins of safety and/or failure. Each of these tiles represented a special challenge since most were already installed on the Orbiter and their removal or redesign could severely impact a tight launch schedule. Development of timely resolutions to these special tile problems presented an immense challenge.

Several examples of the challenges met and the techniques used are described in the following sections.

WINDSHIELD TILES

During ascent, the tiles bordering the Orbiter windshields are subjected to high stagnation pressures (fig. 14) which tend to lift the tiles. Analysis indicated that these pressures could drive

ORIGINAL PAGE IS
OF POOR QUALITY



FIGURE 13.- TYPICAL AIRFLOW TEST PANEL ON F-15 AIRCRAFT.

the SIP bondline stresses above the RSI material allowables. This predicament presented a clear challenge; to increase the strength capability of these tiles while maintaining the substructure at an acceptable temperature.

The windshield tiles (like all Orbiter tiles) are machined from blocks of RSI material such that the layers of silica material run in a direction generally parallel to the Shuttle skin. This parallel grain orientation is a thermal requirement to minimize the conduction of heat from the outer moldline (OML) to the inner moldline (IML). However, this grain orientation causes a reduction of strength (through the thickness) because of the relatively low number of vertically running fibers between the silica layers. It is these vertical fibers that transfer loads to the structure. A possible solution was envisioned where the tiles directly around the windshield could be machined with their grain running perpendicular to the Orbiter skin. This would provide twice the strength but would create the possibility of overheating the structure. Accordingly, a thermal analysis was performed with tiles whose grain was oriented in a direction perpendicular to the Shuttle skin. In this configuration, more heat reached the aluminum skin as expected, but the heavy framing around the windows acted as a large heat sink that prevented unacceptable temperatures.

As a result of this analysis, the tiles around the windows were remachined so that the grain ran perpendicular to the Shuttle skin. While this significantly increased the strength of the tiles, an adequate margin of safety was not quite achieved. A further improvement was obtained by bonding the RSI material that overhung the window glass to the glass itself (fig. 14). This extra area, in combination with the grain orientation, provided acceptable margins of safety for flight.

INSTALLED TILE DICING

The curved forward section of the orbital maneuvering system (OMS) pod is covered with thin 8- by 8-inch tiles (fig. 15). Shortly before the first flight of Columbia, it was discovered that the

TABLE 1.- SUMMARY OF AIRFLOW TESTS

Description	Test facility	Test conditions	Results
Elevon trailing edge	F-104	Max Q = 455 psf	No anomalies.
ET umbilical cavity	AEDC[a] 16 ft	Max Q = 900 psf	Thermal barrier frayed, tiles under crossbeam loosened, and baggie retainer cord damaged tile outer moldline (OML). Redesigned hardware tested with no anomalies.
Canopy diced tile	Ames 11 ft	Max Q = 750 psf	Three tiles came off and several loosened. Pretest OML damage did not propagate. Re-test with mini tile edges bonded to filler bar was successful.
Wing leading edge closeout	F-15	Max Q = 1140 psf	Gap filler (horsecollar) migrated beyond OML and tiles showed excessive deflection. Redesigned horsecollar and tile support successfully tested.
Wing [illegible]	F-15	Max Q = 1140 psf	No gap filler migration and tile step and gap change less than predicted. Test successful.
ET umbilical door	AEDC 16 ft	Max Q = 800 psf	Flow restrictors failed in initial test. Redesign successful.
Vent port - FRSI	Ames 11 ft	Max Q = 970 psf	No anomalies.
Vent port - HRSI	Ames 11 ft	Max Q = 970 psf	Limit and ultimate load portion complete. After ultimate condition was reached, portion of aft tile came loose. Life testing to continue.
Windshield closeout tiles	F-15	Max Q = 1140 psf	Initial tests indicated high net airloads. Redesign tested. No anomalies.
Wing cove/elevon	F-104	Max Q = 1125 psf	No anomalies.
Shaved tile/ mini gap fillers	Ames 11 ft	Max Q = 650 psf	No anomalies.
Vertical tail leading edge	F-15	Max Q = 1140 psf	No anomalies.
CLOT - forward fuselage acreage-calibration panel	LaRC[b] 8 ft	Over 90 min of shock from bipod	No anomalies.

[a]Arnold Engineering Development Center.
[b]Langley Research Center.

revised combined loads on the OMS pod structure would produce considerably higher deflections than previously anticipated. Since thin tiles are relatively weak under a bending load, the increase in predicted deflections could cause these fragile tiles to fracture and possibly separate from the OMS pod. The challenge then became how to reduce the effect of these increased deflections on tiles already installed without requiring their removal. The approach pursued was to develop a vehicle dicing procedure (fig. 16) whereby the larger 8- by 8-inch tiles were cut into smaller pieces which could more easily accommodate the high structure deflections.

Dicing had previously been used to reduce deformation-induced stress and to aid in the installation of thin tiles but the tiles were always diced before installation. To perform the operation on the Orbiter, special tools were developed and the cutting carefully monitored to ensure the desired cuts were made without damage to tile or substrate. This procedure was successfully performed on the OMS pod and later in other areas of the vehicle thus providing a timely solution to a challenging problem and salvaging hundreds of tiles.

AUGER

During the calculation of flight stresses for the body flap tiles, it was determined that the trailing edge corner tiles did not have adequate margins of safety for the predicted vibration and acoustic loads during lift-off (fig. 17). This was later confirmed during the acoustic testing of the body flap when both corner tiles (weighing approximately 6 pounds) failed within seconds of start-up. These LI2200 corner tiles are overhung in two directions, thus creating a large overturning moment on a small SIP area and correspondingly high tension stress. But even more significant than the stress levels was the inability of the SIP to withstand this high cyclic loading. The challenge therefore became twofold: (1) how to prevent failure caused by high RSI tensile stress, and (2) how to prevent the SIP from failing because of the high values of cyclic loading experienced on the body

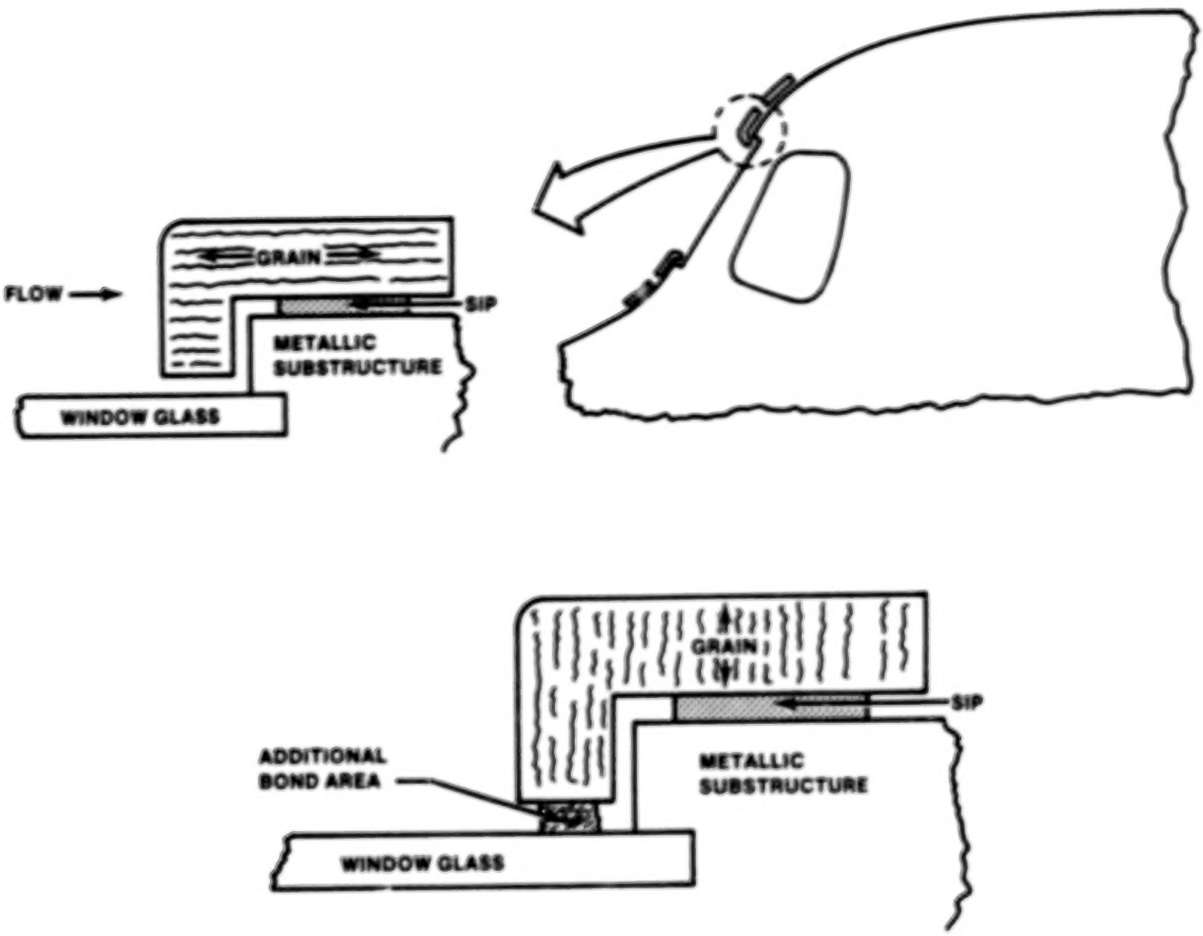


FIGURE 14.- WINDSHIELD TILES.

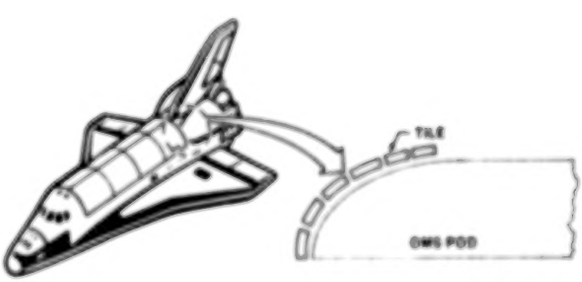


FIGURE 15.- OMS POD TILES.

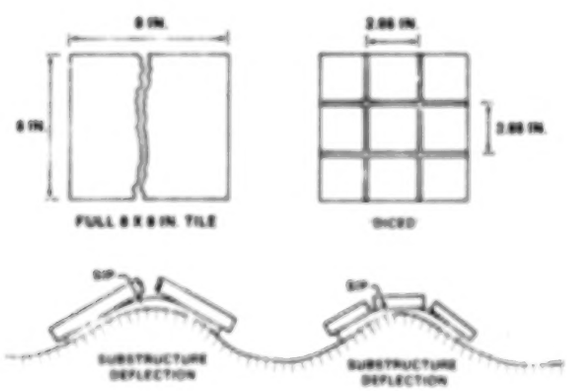


FIGURE 16.- EFFECTS OF DICING.

flap. To increase the capability of the corner tile for high oscillatory load, a mechanical attachment developed earlier called the Auger was considered. The auger system (fig. 18) is twisted into a tile and then attached to the substructure by bolts.

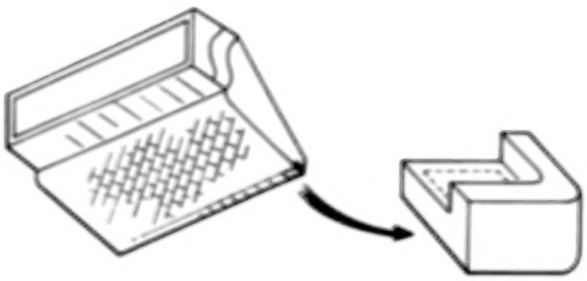


FIGURE 17.- BODY FLAP CORNER TILE.

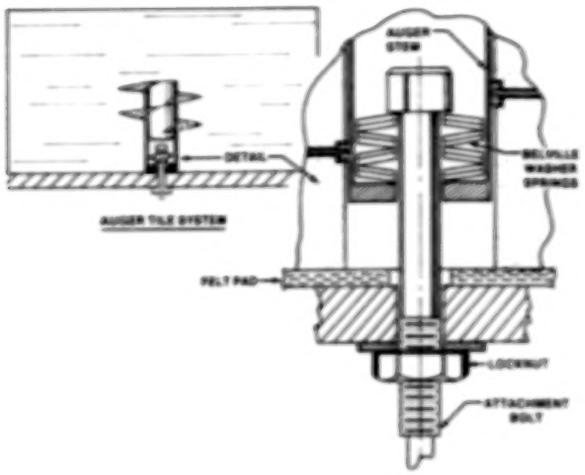


FIGURE 18.- AUGER TILE ATTACHMENT.

The key component of this system is the use of Belville washers to preload the auger itself with a tension load while at the same time inducing a compression stress in the SIP. The preloaded washers (acting as a soft spring) and the compressed SIP (acting as a stiff spring) then worked together as a parallel spring system. The stiff SIP, since it is greatly compressed, takes most of the external cyclic loading, while the Belville washers help prevent significant cyclic loads from being induced by the auger into the intolerant RSI material. The auger system is preloaded to a high enough level that the SIP remains in compression throughout the flight environment, and the tension sensitive bondline is prevented from experiencing a high tensile loading (see load diagrams in figures 19 and 20). The auger system has been fully certified by test for 100 missions and has flown successfully on both OV102 and OV099.

GAP FILLERS AND FILLER BAR BONDS

Two other on-the-Orbiter techniques were developed to meet the challenge of salvaging tiles with high shock-induced stresses in a timely manner. One of these "fixes" involved thick tiles (usually on the lower surface) with a relatively small footprint. As shocks sweep over these tiles, they would tend to rotate inducing high stresses at the SIP/tile bondline (fig. 21). To reduce this shock-induced overturning moment, gap fillers were installed. Once contacted by the rotating tile, a gap filler will create a horizontal reaction that acts against the overturning moment and reduces bondline stresses.

However, for thin tiles (usually found on the upper surface) a gap filler "fix" would not efficiently reduce a shock-induced stress to acceptable levels. Therefore, a second on-the-vehicle technique was developed in which the filler bar surrounding the SIP was bonded to the tile. This was done by inserting a crooked needle into the tile-to-tile gap and depositing RTV on top of the filler bar where the additional bond area is desired (fig. 21). This extra bond area significantly increases the total bonded footprint and decreases the effects of a shock-imposed overturning moment.

Both of these techniques have been selectively implemented where analysis indicated shock-induced stresses were exceeding allowables and needed to be reduced significantly.

The special tiles examples presented in these sections affected very few tiles but their resolution contributed greatly to the highly successful Shuttle flights.

CONCLUDING REMARKS

A wise man once stated, "It is better to attempt a gigantic endeavor but fall slightly short than to attempt very little and be highly successful." The Space Shuttle and indeed the development of the TPS tiles was such a gigantic endeavor but it was almost flawlessly achieved. In this paper, the focus was on the challenges and technical resolution of the tile structural integrity; however, it should be emphasized that the challenges were resolved in an environment of tight cost, tight schedule, and high public visibility. This environment necessitated the practical resolution

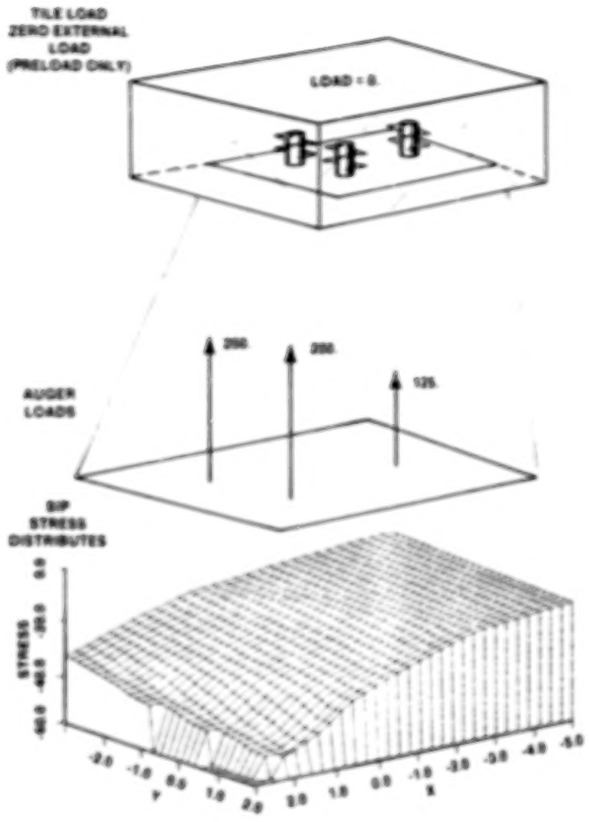


FIGURE 19.- FREE-BODY DIAGRAM OF HIGHLY LOADED AUGER TILE.

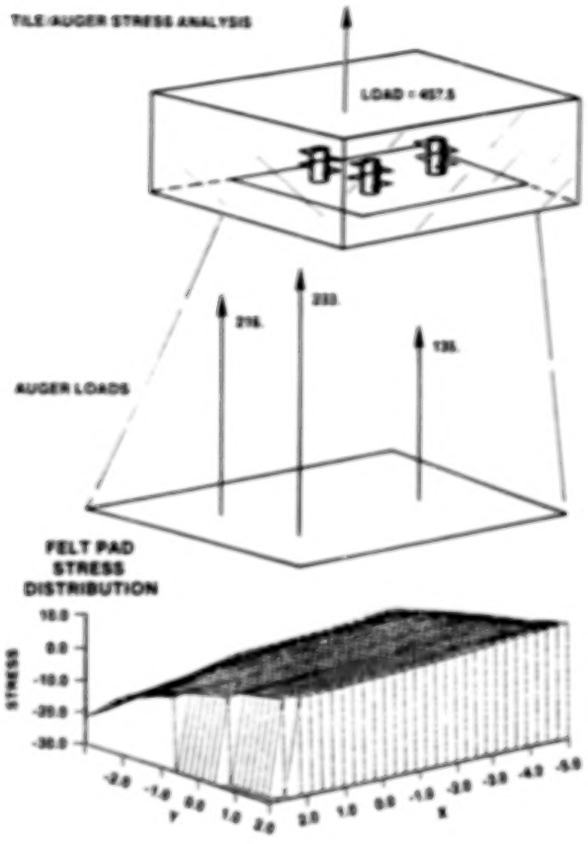


FIGURE 20.- FREE-BODY DIAGRAM OF HIGHLY LOADED AUGER TILES.

afforded first by the Proof Test (affecting tens of thousands of tiles), later by the Load versus Delta curves (affecting thousands of tiles), and the Airflow Tests (affecting hundreds of tiles), and finally by the Special Tile Fixes (affecting small numbers of tiles). It is in this emphasis on the most timely resolution of the tile structural challenges that the program should feel much pride.

REFERENCE

1. Barneburg, Jack: Inflight Aerodynamic Load Testing of the Shuttle Thermal Protection System. AIAA 81-2468.

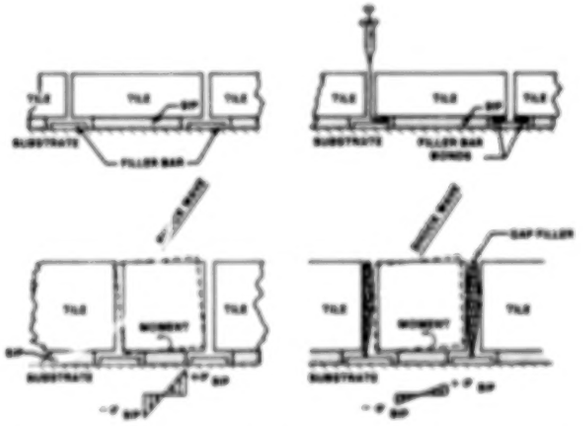


FIGURE 21.- SCHEMATIC OF A TILE AND GAP FILLER INSTALLATION.

N85
16920

UNCLAS

D31. N85-16920

CHALLENGES IN THE DEVELOPMENT OF THE ORBITER ATMOSPHERIC REVITALIZATION SUBSYSTEM

R. Norman Prince
NASA Lyndon B. Johnson Space Center
Houston, Texas 77058

Joe Swider, John Wojnarowski, and Angelo Decrisantis
Hamilton Standard
Windsor Locks, Connecticut 06096

George R. Ord and James J. Walleshauser
Moog Inc., Carleton Group
East Aurora, New York 14052-0028

John W. Gibb
Rockwell International
Downey, California 90241

ABSTRACT

The Orbiter atmospheric revitalization subsystem provides thermal and contaminant control as well as total- and oxygen partial-pressure control of the environment within the Orbiter crew cabin. Challenges that occurred during the development of this subsystem for the Space Shuttle Orbiter are described in this paper. The design of the rotating hardware elements of the system (pumps, fans, etc.) required significant development to meet the requirements of long service life, maintainability, and high cycle-fatigue life. As a result, a stringent development program, particularly in the areas of bearing life and heat dissipation, was required. Another area requiring significant development was cabin humidity control and condensate collection. The requirements for this element of the system include long life, ease of maintenance, and bacteria growth control. These were combined with the requirement to handle a wide range of operating conditions in the zero-g environment. Innovative solutions required to resolve problems that arose during design and qualification of the pressure control system include a vibrating wire and associated electronics to quantify the rate of cabin pressure change; magnets and electronics to accomplish noninvasive valve-position indication; power-saver electronics for hold-open solenoids combined with a failed-closed capability upon loss of power; oxygen-compatible, high-pressure, motor-operated latching valves using pressure-balancing metal bellows; a five-way, two-position manual valve to protect the cabin pressure regulator from ascent-induced vibration; high-accuracy, long-life oxygen partial-pressure sensors; and accurate oxygen/nitrogen flow sensors.

INTRODUCTION

The environmental control systems (ECS's) for Project Mercury and the Gemini and Apollo Programs were all designed for single-mission use. Although high reliability of this hardware was essential, the requirement for multimission use was not a principal design consideration. In contrast, the Orbiter design requirement is for an extended multimission capability, which requires the combination of the high-reliability technology developed during the preceding programs with the capability to withstand the induced and operational environments of the Shuttle Orbiter to produce an ECS with 100-mission life. These requirements resulted in several interesting challenges to be solved during the design, development, certification, and final verification of the various elements of the Orbiter atmospheric revitalization subsystem (ARS).

ORBITER ARS COMPONENT DEVELOPMENT

ROTATING ELEMENTS

The design of the rotating elements contained in the Shuttle Orbiter ARS was considered quite sensitive to this unique concept of multiple mission use. The specific requirements and problem areas that had an impact on the design of the fans, the pumps, and the water separator were as follows.

1. Long-term operating life - 10 000 hours for the bearing system

2. High environmental load levels - as much as ±25g vibration

3. High cycle-fatigue life - approximately 10^6 cycles

4. Minimum weight

5. Thermal environment

6. Maintainability

7. No external liquid leakage

8. Corrosion considerations (galvanic and/or environmental compatibility)

9. Self-generated and system-borne contamination

10. Fluid properties

ORIGINAL PAGE IS
OF POOR QUALITY

Motors

The impact of the design requirements affected the design of the electric motors that power the fans, the pumps, and the water separator as applied to the electric motor efficiency and shaft bearing life. Motor efficiency is improved as the gap between the rotor and the stator is reduced. Motor manufacturers try to optimize the combination of shaft size, manufacturing tolerances, and shaft stiffness to achieve best overall efficiency. The unusually high environmental loads (shock and vibration) induced by the Orbiter required close attention to reducing shaft deflection and manufacturing tolerances to meet the minimum motor efficiency target (η = 60 percent).

The long-operating-life requirement coupled with the high-level environmental loads made the bearing selection a very critical design task. To maximize bearing life, choice of the bearing type and the lubricant required close cooperation between the various suppliers and a carefully conceived development program. The bearings as finally selected are precision, deep-groove, angular-contact ball bearings that are sealed and lubricated with Andok C grease. The success of the bearing design is proven by the fact that there have been no flight failures and fans have demonstrated operating lives far in excess of the design requirement. A cabin fan has accumulated in excess of 56 000 hours of operation and an avionics fan in excess of 28 000 hours. The cross section in figure 1 is typical for the various electric motors used in the Shuttle Orbiter ARS.

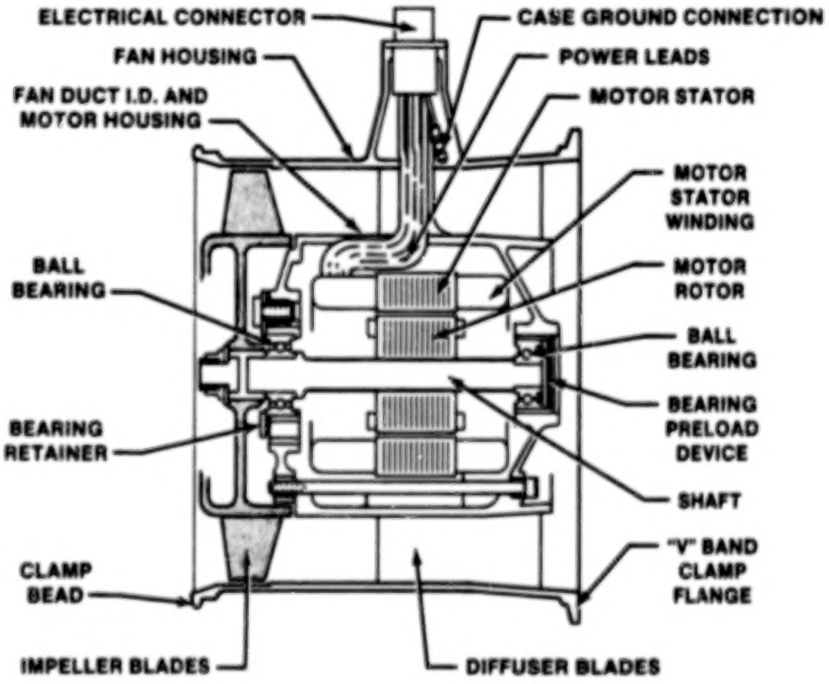


FIGURE 1.- CABIN AIR FAN MOTOR.

Pumps

Design of the fluid pumps was severely impacted by the Space Shuttle requirements. The restriction on external leakage, the long operating life, and the short turnaround time between launches precluded the use of a dynamic shaft seal between the motor and the pump. The choice was immediately reduced to either a magnetic-coupling pump drive or an immersed motor. The flowthrough (immersed) motor design was selected after a trade-off study revealed the following.

1. The magnetic coupling is more costly.

2. The magnetic-coupling configuration is heavier.

3. The magnetic-coupling drive results in a lower operating efficiency.

4. The immersed motor uses the pumped fluid for its coolant, whereas the magnetic-coupling design effectively insulates the motor and thereby accrues substantial weight penalty in providing a conductive heat path to a thermal ground.

The immersed motor uses hydrodynamic sleeve bearings because antifriction (ball) bearings when running immersed develop excessive friction, which shortens life. A second consideration that reinforced the use of sleeve bearings was the lubrication properties of the operating fluid, water. Water is not a good lubricant. However, carbon-sleeve bearings can even be run dry without galling, chipping, or spalling. The performance of antifriction bearings is degraded by operation in water.

Even though carbon-sleeve bearings have desirable properties, the actual design of the bearings was complicated by the conflicting bearing requirements. The bearings must operate with minimum friction in a zero-g environment and in a very high g-level vibratory environment and must not sustain vibration damage when not operating in the very high g-level environment. The bearings that finally evolved are high-precision parts for which very close control of the bearing/journal clearance (i.e., radial clearance is 0.0004 to 0.0008 inch) is maintained to (1) prevent overloading during high-g operation, (2) prevent the development of the self-destructive half-speed shaft whirl while operating in zero g, (3) prevent impact damage during nonoperating vibration periods, and (4) allow minimum armature/stator clearance for maximum motor efficiency. (The overall pump efficiency is approximately 36 percent.)

Combating the effects of fluid contamination was a very important consideration. The steps taken to reduce the potential wear problems include the following.

1. Precision clean the pump as a detail item.

2. Install "last chance" filters to prevent the ingestion of foreign particles during handling.

3. Adjust operating clearances to minimize pump sensitivity to contamination.

4. Provide a fine-level, high-capacity filter in the pump package on the inlet side of the pump.

The design adequacy of the various pumps and motors was demonstrated by successful performance in passing development and qualification testing, in ground operation, and, ultimately, in actual mission operation. A water pump (fig. 2) has accumulated 42 000 hours of ground test operation, which demonstrates the capability of the fluid pump design.

Water Separator

The water separator is also a Shuttle generation device with little or no previous flight history. It is constructed of two primary components: a fan/separator and a pitot pump. Although a rotary separator and pitot pump assembly was flown on the Apollo lunar module, it was a freewheeling turbine-driven device. The Shuttle separator is driven by an eight-pole, 400-hertz, three-phase synchronous electric motor, which also drives the fan on the same shaft.

The motor-driven system is superior to the turbine separator. Startup is a matter of turning a switch to initiate suction at the slurper, and the humidity control system is ready to function. The turbine separator was dependent on airstream energy to develop adequate power to drive the turbine. This dependence required oversizing the air recirculation fan and motor. If this approach were taken with the Orbiter, the total power consumption would increase significantly since a turbine would impose a significant additional pressure drop. The unique concept of the Shuttle separator is removing condensate with only 2 to 2.5 percent of the airstream flow rate. Figure 3 illustrates the fan/separator.

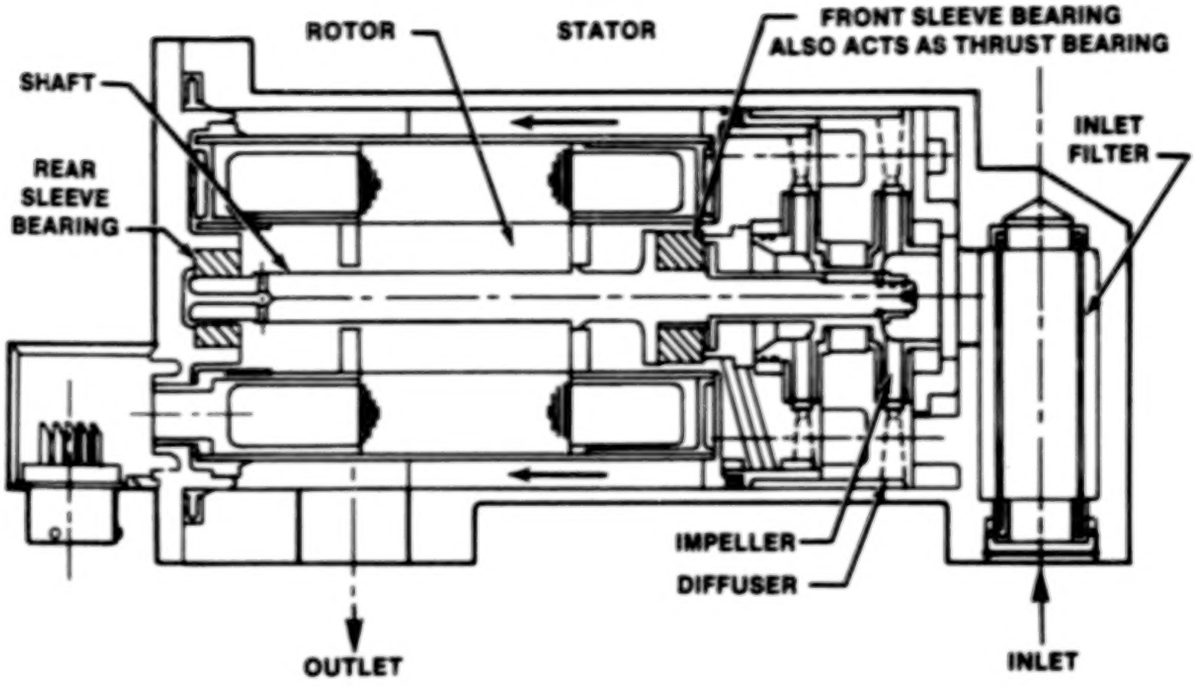


FIGURE 2.- SPACE SHUTTLE PUMP.

After the condensate is centrifugally separated from the return air to the cabin, a pitot pump is employed to pump the fluid into the wastewater tank. At a speed of approximately 5900 rpm, the pitot pump generates 38 to 40 psi at a flow rate of 3.5 to 4.0 lb/hr. The pitot pump has been used extensively in previous programs because it is conducive to these pumping conditions. The pump must overcome the pressure drop of two ball relief check valves and the plumbing to the waste tank. These check valves prevent the backflow of wastewater into the cabin and provide sufficient backpressure on the pitot pump to prevent the pumping of gas into the waste system.

Redundant fan separators are used on the Shuttle; one operates at all times both on the ground and in flight. This continuous operation gives the cabin environment a reliable humidity control system.

HUMIDITY CONTROL SYSTEM

Humidity control for manned spacecraft is a necessary part of the total environmental control and life support system. Proper atmospheric water content is required for crew comfort, for protection of avionic and other electronic equipment, and to prevent the growth of fungi and bacteria. In addition, high humidity levels can result in annoying problems such as condensation on windows, walls, and optical equipment. Compared to dehumidification systems for aircraft, design of a humidity control system for spacecraft is more challenging because of the absence of gravitational force. Condensate removal and storage requires the use of capillary devices and/or rotating machinery to produce artificial gravity.

The advent of the Shuttle Program necessitated longer life and lower maintenance equipment. Rapid turnaround of the Orbiter following each mission was a prerequisite. These requirements prompted the need for an improved humidity control subsystem.

The humidity control system is composed of three essential elements: a condenser, a water collector, and a separator/pump assembly. A plate-fin heat exchanger was selected for the condenser with a four-pass, cross-counterflow coolant loop. The plate-fin design provides excellent performance and lightweight. To improve temperature distribution and provide a free core face for condensate collection, a cross-counterflow approach was necessary. This arrangement also increased coolant velocity, which minimized flow diftribution problems and resulted in more uniform core temperatures.

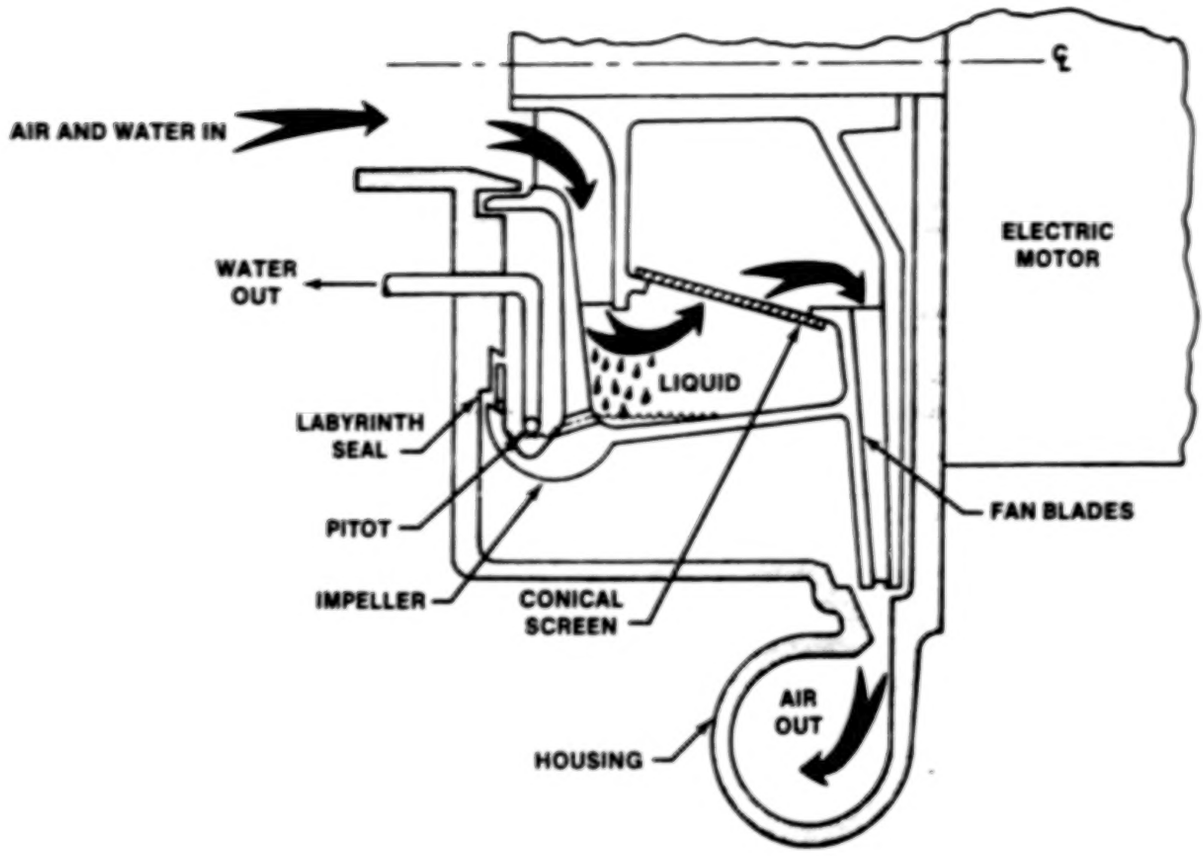


FIGURE 3.- SCHEMATIC OF ROTARY SEPARATOR.

Condensate collection was achieved with the use of a slurper bar (fig. 4). The slurper is the heart of the system, and, although it had never been flown before the Shuttle Program, the slurper concept was selected over two other methods that had been successfully flown previously.

One of the options available was the "elbow separator and scupper," which collects water downstream of the core in the main airstream outlet duct. The advantages of the elbow and scupper were ease of maintenance, simplicity, and freedom from wicks. Wicks are undesirable for any long-term use since they are susceptible to contamination. Disadvantages of the "elbow/scupper" concept are high pressure drop, which results in increased fan power, and inadequate handling of surges. Surges of condensate are released from the condenser at intervals when sufficient core-pressure drop has developed to overcome the capillary head-pressure rise of the fin passages. As one section of the core is "blown" free, another section is undergoing the condensation process and buildup of water. Deficiency of the scupper in handling surges results in some carryover into the cabin airstream.

A second option is the use of a wick at the face of the condenser to draw away the water from the airstream. The advantages of a wick are low pressure drop and, in the case of an integral wick, lower probability of surge occurrence. A disadvantage of the wick concept is the need for some type of startup procedure by which the wick is prewetted. This requirement is inconsistent with Orbiter operating philosophy.

In view of these considerations, the slurper becomes an attractive device. It incorporates the advantages of the other systems and minimizes or eliminates the disadvantages. With a suction of 2 to 2.5 inches of water provided across the slurper holes by the fan/separator unit, the slurper can separate as much as 3.5 to 4.0 lb/hr of condensate. The slurper has the advantages of a wick in terms of pressure drop and surge protection. A hydrophilic coating on the surface surrounding the 0.020-inch-diameter holes provides a wettable surface, which has "wicking" capability to draw water into the holes. Main airstream pressure drop is not affected, and only 2 to 2.5 percent of the airflow rate is bled from the stream by the fan/separator and is returned to the cabin after condensate

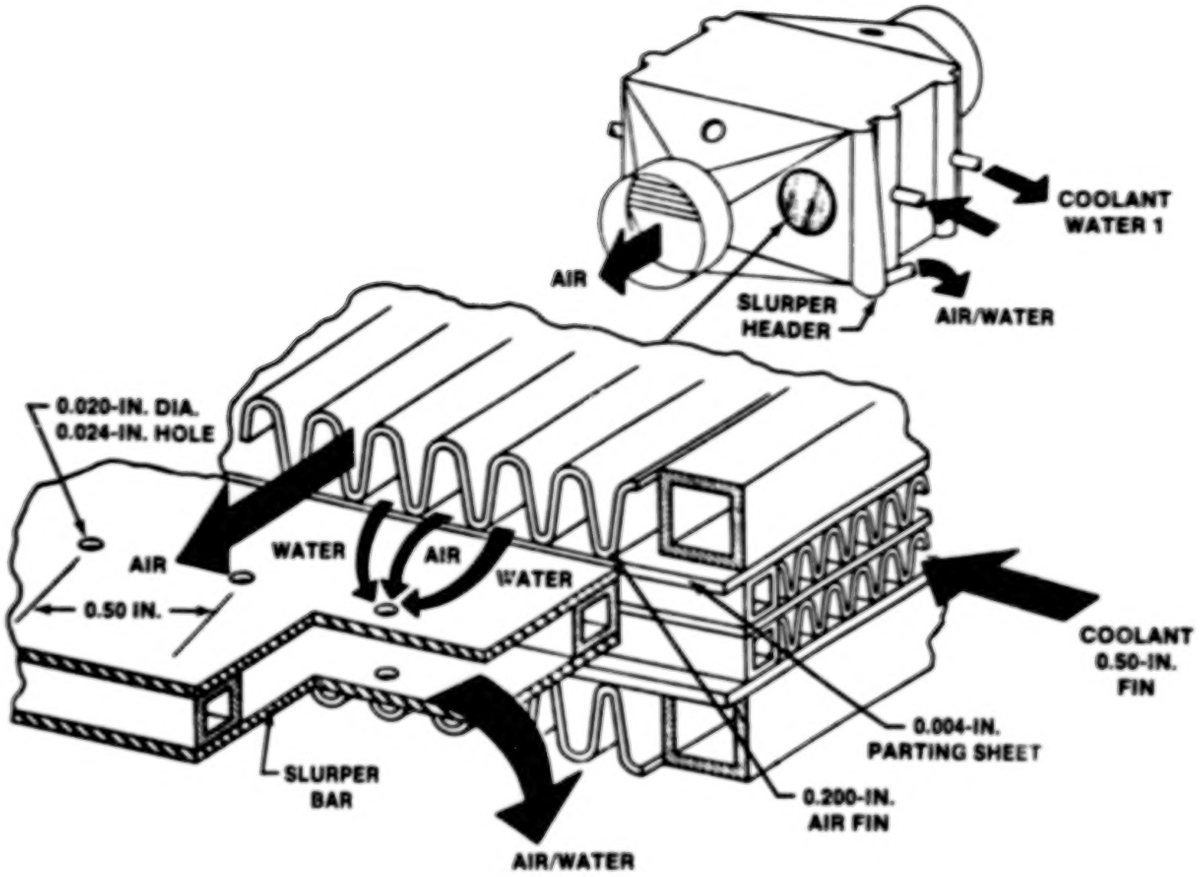


FIGURE 4.- DETAIL VIEW OF SLURPER.

removal. The slurper capability to handle the transient condensation process has been demonstrated in testing and in six Shuttle flights.

Incorporation of the slurper into a heat exchanger is illustrated in figure 4. The slurper is purely an extension of the coolant passage closure bar and, in this location, has the advantages of a face wick. The slurper requires minimum maintenance. It was discovered during the first Shuttle flights that a considerable amount of lint and fibers did plug many of the holes. Backflushing was required to clean the holes and some vacuuming to remove the contamination. If a wick were present, it definitely would be rendered useless since the lint fibers would have penetrated deep into the wick matrix to create a difficult and time-consuming cleaning process.

PRESSURE CONTROL SYSTEM

Rapidly increasing or decreasing pressure within the atmosphere of the Space Shuttle Orbiter is often indicative of a malfunction that may endanger the crewmembers or the mission. A ruptured pneumatic line (pressure increase) within the flightcrew compartment or a puncture in the compartment's pressure barrier (pressure decrease) are extreme examples of such malfunctions. The need for a device capable of providing a warning, in "real time," as contrasted to a graph that provides historical data of events that have previously transpired is obvious. Such a device should also relieve crewmembers of constant visual monitoring and interpretation of graphs.

Pressure Decay Sensor

The pressure decay sensor produces an electrical signal that accurately represents the actual instantaneous pressure change in the cabin. The electrical signal produced by the pressure decay

sensor is visually displayed and is interfaced with caution and warning devices that alert crewmembers to the necessity of immediate corrective measures. This same electrical signal is telemetered to Earth monitoring stations.

The natural resonant frequency of a fine wire varies with the tension on the wire. The wire is driven by an oscillating current in the wire acting in a permanent magnetic field. The wire is part of the electrical driving circuit; therefore, the circuit oscillates at the resonant frequency of the wire. The cabin atmospheric pressure acting upon a metal bellows aneroid varies the wire tension and thus the frequency becomes a function of the atmospheric pressure. The cabin pressure rate of change is continuously calculated from the frequency and expressed as an output voltage.

The electronic circuit boards that comprise the rate electronics portion of the decay sensor must withstand exposure to the cabin environmental conditions of relative humidity as great as 100 percent, salinity of 1 percent by weight, temperatures of -12^{0} to 120^{0} F, and pressure from 4.8 psia to 15 psig. These circuit boards are therefore mounted in a sealed, anodized aluminum enclosure that is vented through a water-shedding surfactant filter. Additionally, each circuit board is protected by a coating of approved silicone rubber. Unit interfacing is accomplished through two hermetically sealed electronic receptacles. The pressure transducer portion of the decay sensor, except for the pressure port, is hermetically sealed. The pressure port is open to the vibrating wire through a surfactant filter that protects against moisture and contamination. Unit venting through surfactant filters coupled with the hermetic seals incorporated in the design of the decay sensor also protect the unit from sand and dust.

Specified g-levels corresponding to specific phases of Shuttle operation were 3.3g in the longitudinal axis and 2.8g in the vertical axis. Through testing, it was determined that the pressure transducer anvil transmits the force of the aneroid to the vibrating wire. The mass of the anvil was reduced and thereby the effects of the specified g-loadings were minimized. Additionally, the least sensitive axis of the pressure transducer was oriented in the atmospheric revitalization pressure control system (ARPCS) control panel to aline with the Shuttle axis subject to the greatest g-level. Each circuit board in the rate electronics portion of the decay sensor is fully supported; thus, flexing at the g-levels specified is eliminated.

The suspended (free) portions of the pressure transducer (aneroid, vibration wire, and anvil) have been designed for high strength-to-mass ratio to maximize resistance to the rectangular pulses of various g-levels, in the minus-Z direction, experienced during landing. The initial design change called for tapered ends on the vibrating wire, appropriate configuration of the anvil, and minimal aneroid size without affecting sensitivity. During testing, however, it was discovered that the tapered ends of the vibrating wire tended to fracture. The new configuration calls for a chemically machined, square wire with wide ends and narrow center section. Testing has proven this configuration to be the best suited to rectangular pulses.

Required operating life is a minimum of 20 000 hours over a 10-year period. Early decay sensor designs encountered problem areas. Small fractures in the vibrating wire were observed at the vibration nodes, and cracks were observed at the welded seam joining the two formed disks of the sealed bellows. The new chemically machined, square-cross-section vibrating wire with wider ends eliminated fractures in the vibrating wire. Brazing replaced welding of the two formed disks of the sealed aneroid bellows. This change resulted in lower residual stress and reduced contamination in the axis of attachment. The insulator at the electrically insulated end of the vibrating wire was also changed from fired lava to machined alumina, which resulted in improved resistance to fatigue stress, enhanced dimensional stability, and relief from low-rate, continuous drop in resonant frequency. In addition, the anvil mass was redesigned to the absolute minimum and the assembly technique incorporated an adjustment to establish "zero" inherent twist in the vibrating wire. These measures eliminated all extraneous modes of vibration except for the desired mode.

Pressure-Balanced Latching Valve

The pressure-balanced latching valve is used to control the combined flow of oxygen (O_2) and nitrogen (N_2) at a pressure of 3300 psi. During the Skylab Program, a solenoid valve that weighed 4.35 pounds was used for a similar requirement. Weight limitations imposed in the Space Shuttle Program required a much lighter valve. The Skylab valve solenoid coils accounted for a majority of this weight. The Shuttle version, which has an overall weight of 1.5 pounds, incorporates an electric motor drive and screw arrangement.

The latching function of the pressure-balanced latching valve is provided by a bistable Belleville spring. The electric motor drives the valve stem and the Belleville spring in the same direction. After actuation from either stable region (open or closed), the spring "snaps through" and retains the valve in the selected position. The Belleville spring provides a positive mechanical latch that is unaffected by vibration and shock conditions.

As its name indicates, the latching valve is pressure balanced. Simply stated, the force required to either actuate or deactuate the valve is not affected by the level of inlet or outlet pressures controlled by the valve. This pressure balancing is accomplished by making the effective areas of both the bellows and the orifice identical. Valve reliability has been greatly increased by the employment of a triple-wall, electrodeposited nickel bellows. This bellows configuration eliminates the necessity of dynamic seals. The O-ring seals used on the pressure-balanced latching valve are secondary seals only.

Power Saver

Two large nonlatching, normally closed, solenoid-operated valves are used in the N_2/O_2 control panel. Design parameters dictate that these two valves "fail safe" in the closed position in the event of power failure. Hence, mechanical or magnetic latching is not feasible. These valves require two distinct operating power levels: the "actuating" level and the "holding" level. The actuating level requires high power to overcome friction and move the armature or valve stem to the operated position; the holding level requires 10 to 25 percent of the power needed in the actuating level to maintain the valve in the operated position. Although the holding power level is greatly reduced from the actuating level, the power drain is still significant. The holding power must be applied on a continuous basis because the valves do not have mechanical or magnetic latching devices.

Two basic methods are commonly employed to maintain a non-latching-type solenoid valve in the operated position. The first method is the continuous application of power at the actuating level. This method tends to cause serious overheating and power requirement problems. An alternate method is the use of an additional switch and resistor circuit. The overheating of the solenoid coil is eliminated; however, the heating problem is now switched to the resistor.

The power saver is an alternative to the two previously applied methods. The power saver is connected between the solenoid valve and the power source, and automatically sequences power to the solenoid without the use of resistors. Hence, excessive overheating and excessive power loss due to increased line resistance is eliminated. Upon solenoid circuit initiation, power from the power source passes through the power saver and is applied to the solenoid valve at the actuating level. After actuation (usually 1/2 second or less), the power saver automatically reduces applied power to the holding level.

Initially, the power saver provides full actuating power to the solenoid coil from the power source. This full power is supplied until the power saver senses some preset current level in the solenoid coil; application of power is then discontinued. Discontinuation of power allows the current in the solenoid coil to decay through a "freewheeling" diode. When the current in the solenoid coil has decayed to some preset level, as sensed by the power saver, full power is once again applied to the solenoid coil. The averaging of these two preset current levels produces the holding power level.

The power saver is completely solid-state; thus, the unit is compact, dependable, and durable. All switching operations occur without inducing line voltage spikes from coil induction and without introducing electromagnetic interference (EMI) from the changing current rates. The switching points for actuation and holding levels are absolute values and are not affected by changes in line voltage, ambient temperature, or coil warmup temperatures. The power saver has met all operating parameters imposed and has a rated minimum useful life of 20 000 hours.

Valve-Position Indicator

Several inherent shortcomings of standard mechanical switches has led to the development of the solid-state valve-position indicator. This position indicator employs two samarium-cobalt magnets attached to the valve stem and a Hall-effect transducer to accurately indicate the relative position (on/off) of a given valve within a sealed housing. This valve-position sensing technique is accomplished without penetration of the valve pressure wall. Mechanical switches require a portion of the valve stem to extend through the pressure wall. Valve stem penetration of the pressure wall necessitates additional dynamic seals at the point of penetration and thus increases friction and potential leakage points. In the case of the valve-position indicator, a magnetic flux, developed by the samarium-cobalt magnets, passes directly through the pressure wall to operate the Hall-effect transducer (fig. 5).

The new valve-position indicator technique results in a reduced hysteresis (differential travel) distance. Mechanical switches require a minimum of 0.010 inch of travel between the on and off switching positions. The magnet and Hall-type transducer combination is capable of discerning movements as small as 0.003 inch. This value is less than one-third previously required travels; thus, lower valve flow settings are obtainable.

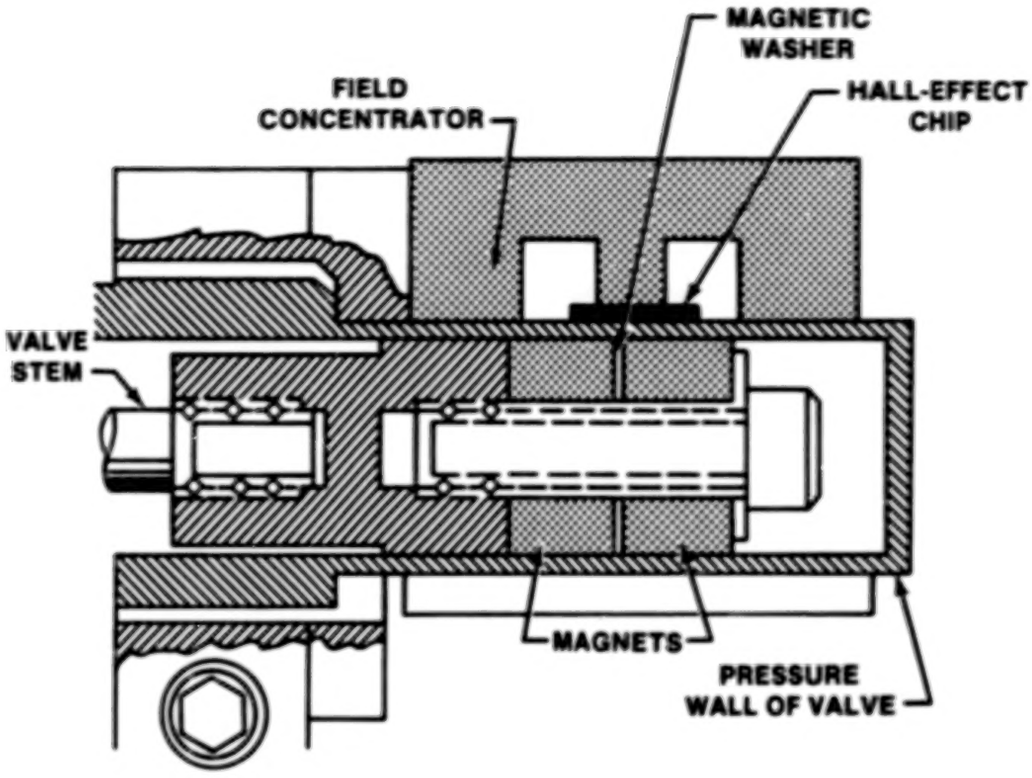


FIGURE 5.- SOLID-STATE VALVE-POSITION INDICATOR.

The absence of moving parts completely eliminates wear-related failures and ensures infinite cycle life. Mechanical switches are subject to breakdown due to excessive flexing, which results in deterioration of hermetic seals. Mechanical switches are also subject to contact erosion with resulting increases in circuit resistance; additionally, contact-point bounce produces unwanted EMI. The output signal of mechanical switches is of poor quality and may result in a sensitive indicator or recorder producing erroneous data. This valve-position indicator is free of these mechanical impairments and consistently produces "clean" signals in less than 0.5 millisecond.

Vibration has no effect on the valve-position indicator. The sensing element (Hall-type transducer) is rigid with no moving parts, and the magnets are rigidly attached to the valve stem.

A minimum of 5 ounces of actuation force is required to operate the most sensitive mechanical switches; many switches require 10 to 20 ounces actuation force. The valve-position indicator requires only 4 ounces of force to operate. Additionally, no preloading of the valve stem and no retention force is required to maintain the Hall-type transducer in the actuated position. Since no mechanical linkage is made with the switching portion arrangement in the valve-position indicator, overtravel problems are nonexistent.

Flow Sensor

Two flow sensors are used in each of two redundant systems in the cabin pressure control panel: one for oxygen at 900 psi and the other for nitrogen at 200 psi. Each flow sensor is calibrated to read mass flow rates between 0 and 5.0 lb/hr using the appropriate gas and pressure. Flow-rate displays are provided for the crew, and data are telemetered to monitoring stations on Earth. Caution and warning signals alert the crew if flow rates exceed 4.9 lb/hr.

The flow sensor consists of a relatively large, straight-through, cylindrical passage with several thicknesses of woven stainless steel wire filter mesh located approximately midway across the passage. A parallel flow path bypasses the filter by way of a capillary tube the ends of which are just upstream and downstream of the filter. The purpose of the filter is to produce a pressure drop across the ends of the capillary tube and thereby to induce a small flow through the capillary tube.

The flow sensed is flow that bypasses the main stream by way of this small-diameter tube. A layer of thermally conductive, electrically insulating material is deposited on the outside of the capillary tube. Two separate coils of very-small-diameter resistance wire are closely wrapped, one after the other, around the capillary tube. Each of these resistance coils is one leg of an electrical bridge.

The determination of flow rate is based on the difference in temperature of these adjacent resistors as a result of flow. The resistance of the wire varies with the wire temperature so that the bridge bias that exists at zero flow is upset. The degree of upset is sensed, amplified, temperature compensated, and linearized to compensate for nonlinear pressure differential across the aforementioned layers of filter screen. The result is an analog voltage output that varies from 0 to 5 volts direct current as the mass flow rate varies from 0 to 5 lb/hr.

The basic design approach remained the same during development and qualification. However, satisfactory implementation of the design proved troublesome. In retrospect, the solutions seem obvious. At the time, each anomaly seemed mysterious and required careful investigative work. One frustrating example was originally thought to be a matter of test equipment and test procedure differences between the manufacturer and the receiving inspection. Identical test masters for both stations were calibrated at the same time. The same gage facility and test equipment was duplicated; test procedures were standardized to no avail. Test results still differed. It was finally discovered that the manufacturer, to assure an optimum degree of cleanliness, was flushing the unit with cleaning fluid after his acceptance tests. Unfortunately, the cleaning fluid used was badly contaminated. This in turn partly clogged the internal filters, used to create a controlled pressure differential, and altered the heat-transfer characteristic of the flow-sensing capillary tube. The solution was clean fluid and the addition of a finer convoluted wire mesh filter at the unit inlet.

The need for additional diodes was revealed by EMI tests. Finding space for the diodes and providing mechanical support to withstand launch vibration required additional time to work out and prove.

Another problem was that some flow sensor elements could not be trimmed and adjusted within the range of the electrical elements designed to accomplish this function. The defect was traced to a partial breakdown of electrical insulation between the capillary tube and the wrap of resistance wire around the tube. Triple electrical insulation coatings are now used. This modification resulted in a reduction of flow sensor sensitivity due to the thermal insulating effects of the electrical insulation layers. To compensate, the electronics components were changed to supply more power so that the necessary degree of sensitivity could be returned.

One final undesirable characteristic of the flow sensor remains. Flow rates greater than 5.0 lb/hr are not displayed; caution and warning signals occur at 4.9 lb/hr. As the flow rate increases, the two adjacent legs of the resistance bridge, wrapped around the flow-sensing capillary tube, move closer to each other in temperature and resistance because the limited power available to the bridge is overcome by the increased heat dissipation of the higher flow rate. At some flow rate, the display starts to reverse with additional flow-rate increases until an indication approaching zero may be shown.

Oxygen Partial-Pressure Sensor

The oxygen partial-pressure (pO_2) sensor (refs. 1 and 2) has an impressive operational record including thousands of hours of flight time accumulated during the NASA Skylab and Apollo-Soyuz missions. In the Shuttle, the sensor performs the same function as in the Skylab application - providing the control signal to maintain proper oxygen levels in the two-gas (O_2/N_2) cabin atmosphere. The oxygen sensor has evolved into a device suitable wherever continuous, real-time monitoring of oxygen is critical and has been successfully adapted to a wide range of man-rated environmental control systems in addition to that of the spacecraft cabin oxygen monitor described previously.

The sensor is a self-contained, self-powered electrochemical cell, which generates a millivolt signal as a function of the O_2 partial pressure in the environment being monitored. The millivolt signal generated automatically compensates for temperature and is compatible with end-item telemetry and instrumentation systems. The sensor uses the controlled conversion of chemical energy to electrical energy to provide a direct measure of oxygen partial pressure. This function is accomplished by immersing a pair of electrodes, as shown in figure 6, in an electrolyte retained within a bladder and a gas-permeable membrane.

Oxygen contained in the atmosphere to which the sensor is exposed permeates the membrane to the gold sensing electrode serving as a catalyst to ionize the oxygen molecule. The electrolyte, an alkaline solution, provides a conductive path for ionized O_2 to the metal counter electrode to form a

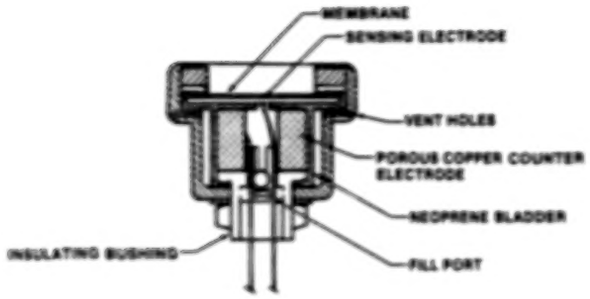


FIGURE 6.- CUTAWAY VIEW OF THE OXYGEN PRESSURE SENSOR.

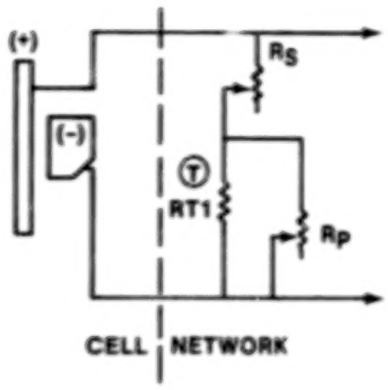


FIGURE 7.- SENSOR SCHEMATIC.

metal oxide. This oxidization involves a release of electrons, which flow through an external resistance (fig. 7) to provide the sensor output signal.

The current/partial-pressure relationship is constant for a specific electrode configuration and constant temperature. For changes in temperature, the absolute permeability of the membrane varies and thus produces a change in the output current. The change in permeability (hence current) is a first-order change increasing logarithmically with increasing temperature. Dependence on temperature is essentially eliminated from the sensor output signal by matching the cell to a resistive load including a temperature-sensitive component (fig. 7). The component, a thermistor, is trimmed with series and parallel resistances to provide a network temperature coefficient which is equal in magnitude but negative with respect to the temperature component of the membrane permeability.

The theoretical sensor life is readily determined by electrochemical relationships. The copper counter electrode is the consumable and is depleted at a rate which is related directly to the electrical current generated by the sensor. Actual life of a specific sensor will vary with average operating temperature and oxygen partial pressure as well as with thickness of the diffusion barrier (membrane).

Required calibration frequency is a function of system accuracy constraints and sensor drift. Initial calibration upon installation will hold for the life of the sensor. Results of recently completed tests indicate average sensor drift during operation to be -0.23 mmHg pO_2 per month. When compared to the Shuttle oxygen monitor accuracy requirement of $\pm$7.75 mmHg pO_2, it is clear that an initial calibration should hold. Required operating life is 6236 hours at 297 K and 165 mmHg pO_2.

The sensor is not affected by background gases normally found in a habitable atmosphere. A shift in calibration with total pressure would therefore be attributed to a physical change within the sensor, specifically to a change between the diffusion barrier and the sensing electrode. A shift of this nature is prevented by (1) the flexible bladder referenced to sample pressure and (2) the front-end design for which a unique process has been developed to integrate the membrane and sensing electrode into a stable one-piece assembly.

Sensor response rate is a function of temperature, film thickness, and thickness of the goldplate applied to the sensing electrode. Film and goldplate thickness have evolved to satisfy the maximum number of applications and to idealize overall performance. Rate of output response for the standard sensor at 298 K is to within 90 percent of a step change in pO_2 in 30 seconds or less.

Early sensor configurations employed a stainless steel rigimesh substrate sensing electrode. A gold-plated, sintered nickel sensing electrode was substituted to enhance performance, through greater active surface area, and to eliminate sensitivity drift during storage. Additionally, the sintered nickel disk provides a more uniform sealing surface and an increased film support area and permits spotwelding of leads. Newer sensor configurations also employ a gain adjustment within the amplifier portion of the transducer to facilitate field adjustment. This gain adjustment replaces the previous method of individually adjusting the potentiometers within the sensor and eliminates the possibility of unbalancing the sensor temperature compensation circuit.

Cabin Pressure Regulator

The cabin pressure regulators and the oxygen partial-pressure sensors together maintain the crew compartment atmosphere at 14.7 ± 0.2 psia total pressure and 3.20 ± 0.25 psia oxygen partial pressure (ref. 3). The function and accuracy of the oxygen partial-pressure sensors are unaffected by vibration, acceleration, and shock once their elements are adequately supported to withstand the resultant dynamically induced stresses. However, cabin pressure regulators depend on the positional interaction of internal mechanical elements. Close-tolerance pressure regulation required, ±1.36 percent, necessitates a design sensitive both to the crew compartment pressure feedback control and to the externally imposed dynamic environment.

Qualification testing showed the 14.7-psia pressure regulators to be sensitive to the random vibration spectrum of the Shuttle launch environment. The level of regulation exceeded Shuttle specification limits during launch vibration. Since their operation during launch is unnecessary, this deviation might have been countered by closing the unit's manual on-off valves before launch and opening them when in orbit. However, two other problems occurred as a result of 100-mission random vibration testing: (1) after vibration, the pressure regulation level decreased as much as 0.25 psi and (2) internal leakage increased greatly. Short vibration time qualified the ARPCS N_2/O_2 control panel for use on the first Shuttle development flights. Nevertheless, extending the vibration duration to encompass 100-mission-life simulation showed that the cabin pressure regulator performance degraded sufficiently to require further corrective action.

The control pressure sensed by the cabin pressure regulators during launch is only a little higher than the 14.7 psia that they are set to control. This means that the springs and the pressure-sensing device are practically in balance so that any disturbing force, such as imposed vibration, causes these internal elements to react rather violently. The movement thus induced causes accelerated wear. Damage to the pressure regulator seats caused excessive internal leakage and pressure regulation shifts. The most effective and uncomplicated way to immobilize the unit internally was to close the port where the regulator senses the crew compartment pressure and, at the same time, raise the pressure that the regulator sensing element sensed internally. This raised pressure must be high enough to force the metal bellows pressure-sensing element back against its internal parts to achieve the desired results. The source selected to backpressurize the cabin regulators was the nitrogen regulator normally used to pressurize the water tanks.

The cabin pressure regulators already had manual toggle-operated on-off valves. The cabin pressure regulators were redesigned in such a way that a single action of the toggle could accomplish the required functions simultaneously. The resultant multifunction toggle valve is a two-position, five-way valve. Two poppet/seat combinations have been added to accomplish the desired backpressure function. Nitrogen from the 16-psig water pressurization regulator is fed to the appropriate port of the designed valve to act as the backpressure source. Reversing the toggle position closes the poppets that were open and opens those that were closed so that normal crew compartment pressure control can resume.

REFERENCES

1. Rudek, F. P.; and Fuller, J. D.: O_2 Sensing for Environmental Control and Monitoring Systems. Paper presented at 10th Intersociety Conference on Environmental Systems, July 14-16, 1980.

2. Fuller, J. D.: Proposed Flight Transducer Modifications. Memorandum, General Electric Company, Valley Forge Space Center, Mar. 5, 1980.

3. Walleshauser, J. J.; Ord, G. R.; and Prince, R. N.: Space Shuttle Orbiter Atmospheric Revitalization Pressure Control Subsystem. SAE Paper 820882, 1982.

N85
16921

UNCLAS

D32

N85-16921

CHALLENGES OF DEVELOPING AN ELECTRO-OPTICAL SYSTEM FOR MEASURING MAN'S OPERATIONAL ENVELOPE

Barbara Woolford
Experiments and Operations Support Division
NASA Lyndon B. Johnson Space Center
Houston, Texas

ABSTRACT

In designing work stations and restraint systems, and in planning tasks to be performed in space, a knowledge of the capabilities of the operator is essential. Answers to such questions as whether a specific control or work surface can be reached from a given restraint and how much force can be applied are of particular interest. A computer-aided design system has been developed for designing and evaluating work stations, etc., and the Anthropometric Measurement Laboratory (AML) has been charged with obtaining the data to be used in design and modeling.

Traditional methods of measuring reach and force are very labor intensive and require bulky equipment. The AML has developed a series of electro-optical devices for collecting reach data easily, in computer readable form, with portable systems. The systems developed, their use, and data collected with them are described.

INTRODUCTION

THE CHALLENGE

The Space Shuttle program brought a challenge to spacecraft designers to accommodate comfortably and efficiently a much larger portion of the population than had been considered previously. The Shuttle was to be operated by persons ranging in size from the fifth percentile female to the ninety-fifth percentile male, a range of approximately a foot in height.

Providing suitable work stations and living quarters for humans operating in a zero-g environment requires consideration of many new phenomena (refs. 1 to 3). For example, the body changes in size and shape: the torso stretches as much as 2 inches and the waist may shrink a similar amount. The natural comfortable posture in space is very different from the normal posture on Earth. Specifically, the legs and arms bend forward from the torso rather than hanging straight down; they are flexed at the elbows and knees. The head tilts downward, lowering the line of sight. In order to produce any effective force, the astronauts must be restrained in some way or they will simply move themselves.

To develop work stations, plan tasks, and design habitable areas, quantitative data are required on the anthropometric characteristics of users in zero g. These data can be collected in various ways: measurements may be taken in one g and extrapolated to zero-g conditions; they may be taken in simulated zero g, as in the Weightless Environment Training Facility; or they can be determined from data collected on Skylab or the Shuttle. No matter how the data are obtained, they should be made available to designers in the early stages of the design process.

Specific measurements desired are the sizes of body components (height, arm length, leg length, chest circumference, etc.), the reach capabilities, the strength that may be applied at various positions, and the time it takes to perform a given motion.

THE APPROACH

The approach to this challenge has been to build an Operator Station Design System which includes a computer-aided design (CAD) system and the Anthropometric Measurement Laboratory. The development of PLAID (Panel Layout Automated Interactive Design), the CAD system, started in 1976 (ref. 4). At the same time, development of automated equipment to collect anthropometric data was begun (ref. 5). The emphasis has been to use computer technology, from a VAX 11/780 computer to a Rockwell 6502 microprocessor, to collect data, process the data, present data to the design engineers, and provide design tools for the engineers. The goal, not yet achieved, is to provide dynamic models of human activities in candidate work areas and habitations. These models would ideally take a task description or checklist, translate it into desired movements, simulate those movements for bodies described in the anthropometric data base, and report to the engineer on such

issues as inability to reach items, collision with other bodies or with spacecraft furnishings, the time to perform the actions, the strength required, and other design concerns.

BACKGROUND

ANTHROPOMETRIC MEASUREMENT SYSTEM

The first step in developing an automated anthropometric measurement system for range of motion data was the design and development of a video-based system for joint angle measurements. This device, called a goniometer, and the subsequent anthropometric measurement systems were developed by Southwest Research Institute of San Antonio, Texas, under the guidance of Dr. W. E. Thornton of the JSC Astronaut Office (ref. 6). To measure joint range of motion, a bar with incandescent bulbs on each end is attached to the limb to be moved. The limb is positioned in a neutral, 0^{o} position. The two lights are alternately blinked on and off several times under microprocessor control. The position of the lights is sensed through a video camera and a line is fitted to the two points by the microprocessor. The limb is then moved to an extreme position, the lights are activated, a second line is fitted, and the angle between the lines is displayed on a digital readout.

The goniometer was a first step, a feasibility test, of the possibility of measuring motion through video tracking of point sources of light. The goniometer was a two-dimensional device: the person being measured had to sit or stand so that the axis of rotation was perpendicular to the camera image plane. The total errors achieved during testing did not exceed $\pm 4^{o}$ at a distance of 8 feet from the camera; the average error was about 2^{o}.

The next step was the development of a three-dimensional tracking system. This anthropometric measurement system (AMS) locates positions in three dimensions by triangulation. Three video cameras are positioned on three corners of a rectangle. Two small incandescent bulbs, which are to be tracked, are attached to the person, for example, on the fingertips for collecting reach data. Figure 1 illustrates the arrangement of cameras, equipment, and subject. The room is very dimly illuminated. A

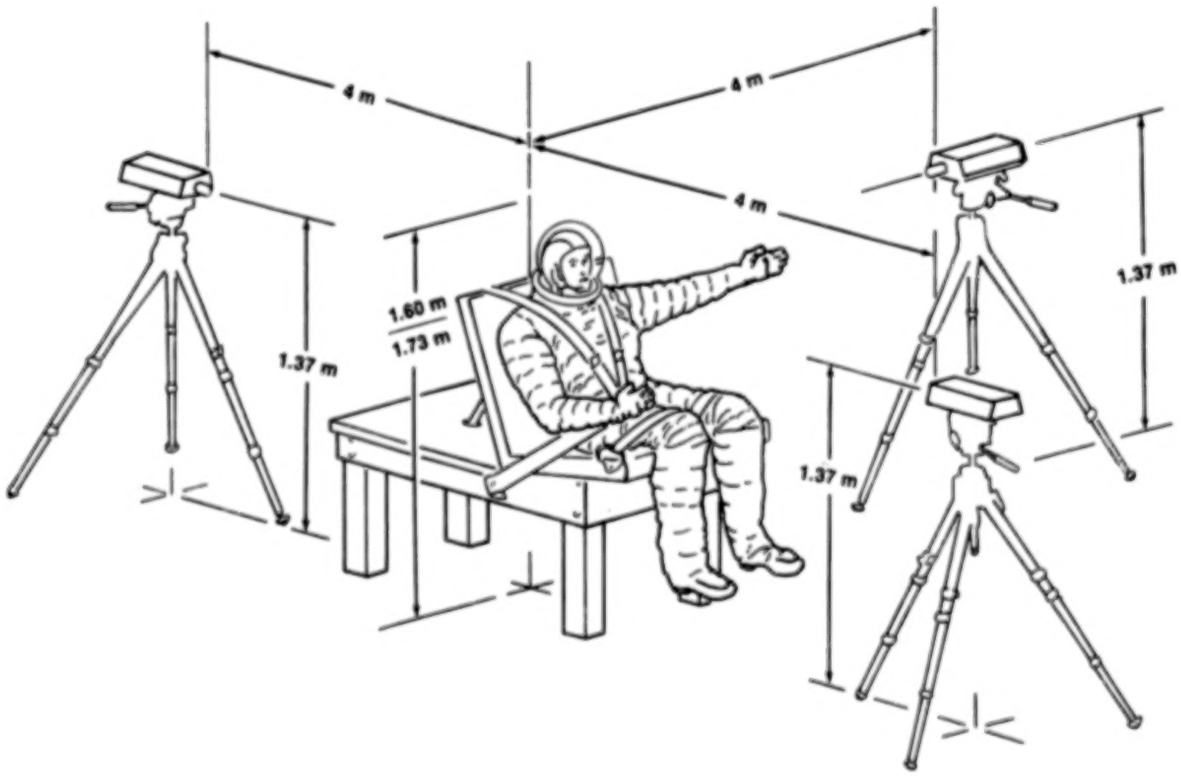


FIGURE 1.- THREE CAMERAS ARE USED TO TRACK A LIGHT ON THE CREWMEMBER'S HAND.

microprocessor turns on one light, analyzes a video scan for the peak brightness, digitally records its position in the video image plane, then sequentially analyzes the video scans from the other two cameras in the same manner. If no signal rises above a preset threshold value, a "no data" flag is stored for that camera, for that scan. The first light is then turned off, the second lit, and the process proceeds. Because of the video processing and the inherent limitations of incandescent bulb cycling, the data rate is about 10 points per second.

The digital data are stored on a floppy disk during the test. Data analysis is performed after the test. The position of a point in three-dimensional space is determined from the camera coordinates (two dimensions) from two non-colinear cameras. With three cameras, 180° coverage is possible.

The AMS also has provisions for force data collection. A commercially available Cybex dynamometer with a special pulley arrangement is connected to the AMS so that force is digitally recorded with corresponding position data.

Development of PLAID began in 1976 (ref. 7). This project was intended to provide a powerful design tool for spacecraft design engineers. Standard CAD features in PLAID include composition of primitive objects to form complex assemblies, data entry through cursor, digitizer, or keyboard, display in wireframe or with hidden line removal, and viewpoint position and orientation specified by user. This capability was developed for JSC by Rothe Development, Inc., of San Antonio, Texas, with the guidance of J. L. Lewis, J. W. Brown, and M. M. Thomas of the Engineering and Development Directorate of JSC.

The extensive use of PLAID in Shuttle operations planning has been reported by J. W. Brown (ref. 8). The conflict detection algorithms permit fit checks to be made early in the design process rather than in mockups. Through viewpoint specification, the areas in sunlight or earthshine can be displayed by specifying the viewpoint to be at the Sun or the Earth. A variable lens focal length feature allows assessment of camera fields of view. Previously, all of these tests had to be conducted with models and mockups, with a high cost in materials and manpower.

The initial human modeling capabilities of PLAID were limited. Bodies had to be constructed in pieces and assembled into the desired position by specifying the angle of each limb to another body part. Digitized data describing one human body in detail were obtained from the Institute for Biomedical Engineering Research at the University of Akron.

An early feature of the system was the REACH module, which provided for the use of data collected with the AMS. The AMS data consisted of a collection of points in three-dimensional space indicating those areas which the subject could reach. Figure 2(a) is an elapsed time photograph taken during the collection of reach data in a pressurized suit. To make use of this, provisions exist for examining one horizontal (or vertical) "slice" of some given thickness and drawing closed contours enclosing the points. Figure 2(b) shows a "slice" of reach points with the boundaries drawn in. The contours could be smoothed, and the sequential contours joined together to form a three-dimensional solid object. This process is illustrated in figure 2(c). The resulting object could then be positioned by PLAID, and its intersection with such elements as work stations, controls, and surfaces to be reached displayed. This capability was used extensively in analysis of thermal protection system repairs before the STS-1 mission. Figure 2(d) shows the model of an astronaut with reach envelope attached for use in evaluating reach capabilities.

THE EVOLUTION

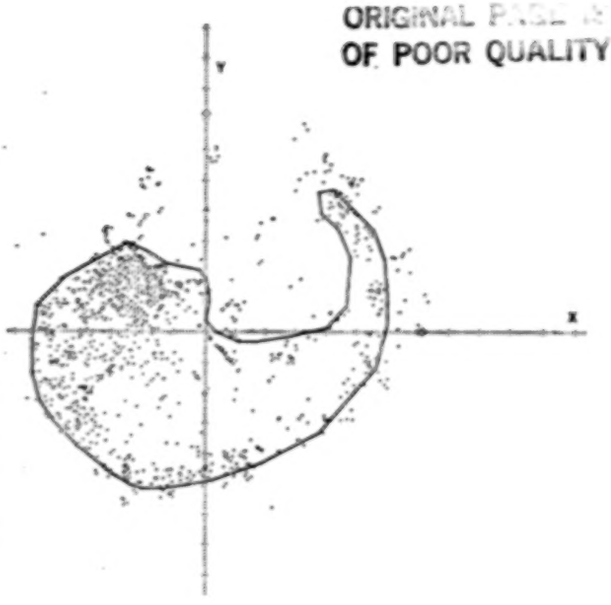
The limitations of the AMS prototype were the data rate, the number of points tracked, and the requirement for low light levels. A high-speed AMS (HAMS) was developed to surmount these difficulties (ref. 9). The HAMS is based on the commercially available SELSPOT system, which permits tracking up to 30 separate points at rates up to 300 hertz. The SELSPOT used infrared emitting diodes (IRED's) to provide the fast switching rates and to provide a signal in a radiation wavelength not strongly generated by normal room lighting. The light detection is done by a photosensitive plate which generates currents in its "x" and "y" axes in proportion to the location of the center of intensity. The image is focused on the plate by Canon lenses. The output consists of two analog signals (x, y position) which are digitized and initially processed by the SELSPOT control hardware.

The SELSPOT system was originally designed to feed raw data into a computer at high rates. To provide portability, the unit was coupled with a microprocessor-controlled recording and playback unit in its implementation at JSC. The resulting system can be loaded on a laboratory cart

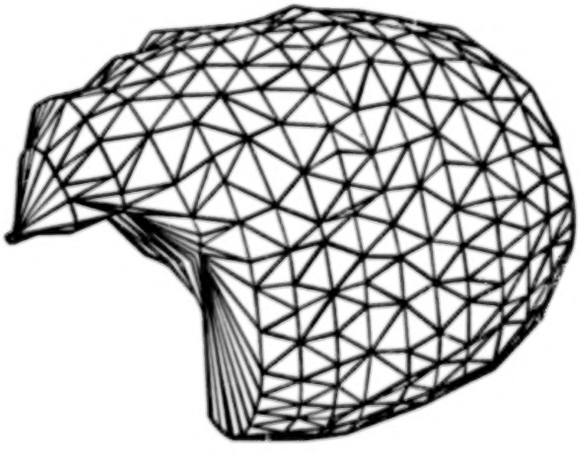
ORIGINAL PAGE IS
OF POOR QUALITY



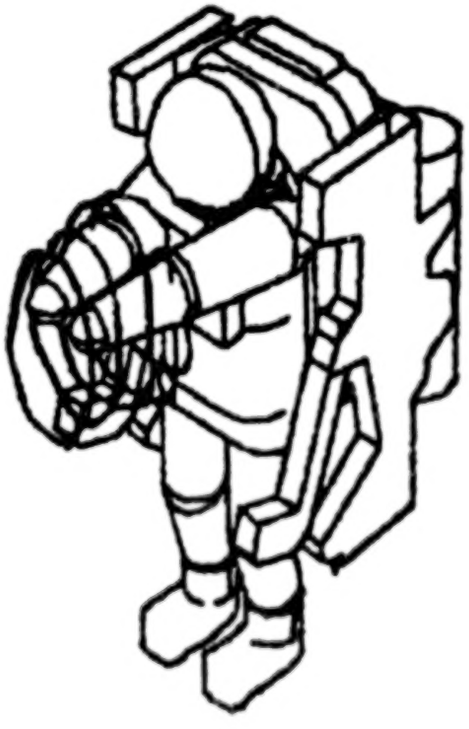
(a) DATA ARE COLLECTED FOR REACH RANGE IN A PRESSURIZED SUIT.



(b) REACH DATA ARE PLOTTED, AND CONTOURS INDICATING THE REACH RANGE ARE DRAWN BY THE INVESTIGATOR.



(c) CONTOURS FROM DIFFERENT HEIGHTS ARE CONNECTED TO FORM A THREE-DIMENSIONAL SOLID.



(d) A PLAID RECONDITION OF A SUITED CREWMEMBER WITH THE TWO-HANDED REACH ENVELOPE ATTACHED FOR INSPECTION.

FIGURE 2.- STEPS FOR COLLECTING REACH DATA.

and transported to any desired location to collect data. After the test, the system is transported to the computer room to dump the raw digital data to computers for processing. The interface to PLAID through REACH is maintained.

This system has been used to collect range of motion data for use in evaluating alternate joint designs for an 8-psi space suit. Besides its use for collecting reach data, it has been used to replace the goniometer and generates images of the arcs swung by a distal limb when a joint is rotated. Figure 3 shows arcs from two different suit designs generated by movement of the shoulder joint.

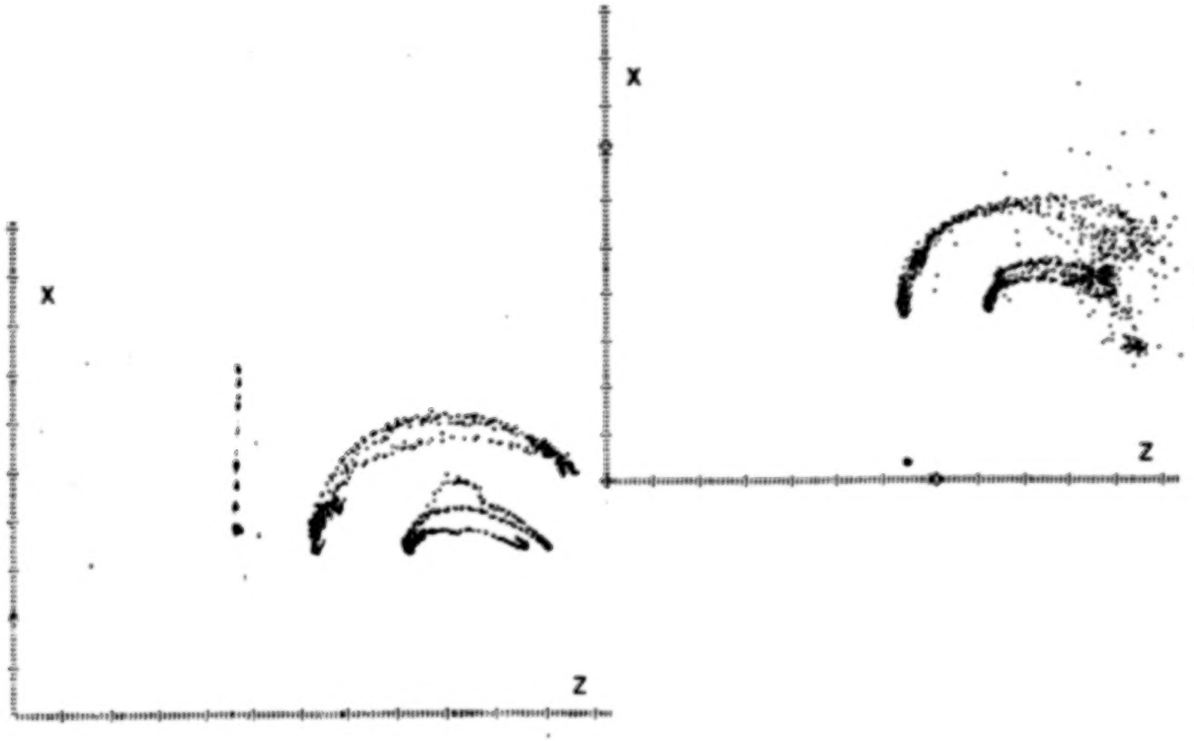


FIGURE 3.- SHOULDER ROTATION ARCS IN TWO PROTOTYPE SUITS. IRED'S WERE ATTACHED TO THE UPPER ARM AND ELBOW.

PLAID is undergoing development in two directions. The graphics capabilities are being extended, and the man modeling capabilities are being increased. Additions to the graphics include generation of raster output, the use of color and shadowing, and the use of hardware and firmware implementations of hidden line removal to increase the speed of the output by orders of magnitude.

Man modeling has been an active research area in computer science. One model, "Bubbleman," developed by Dr. Norman I. Badler and his colleagues (refs. 10 and 11), is being integrated with PLAID and the model extended significantly. Figure 4 shows a typical "Bubbleman" standing up. Special features of this model include the ability to select or build a body by specifying a few parameters rather than generating complex solids, and the ability to position a body by specifying a few key points rather than every angle and distance. The current model is a kinematic model. When given a starting position and a desired ending position, the model can generate the intermediate steps necessary to transition from one to the other. This animation technique provides a very helpful tool for the design engineer in checking reachability for detecting possible collisions between one body and another or between a body and surrounding crew station surfaces.

ORIGINAL PAGE IS
OF POOR QUALITY

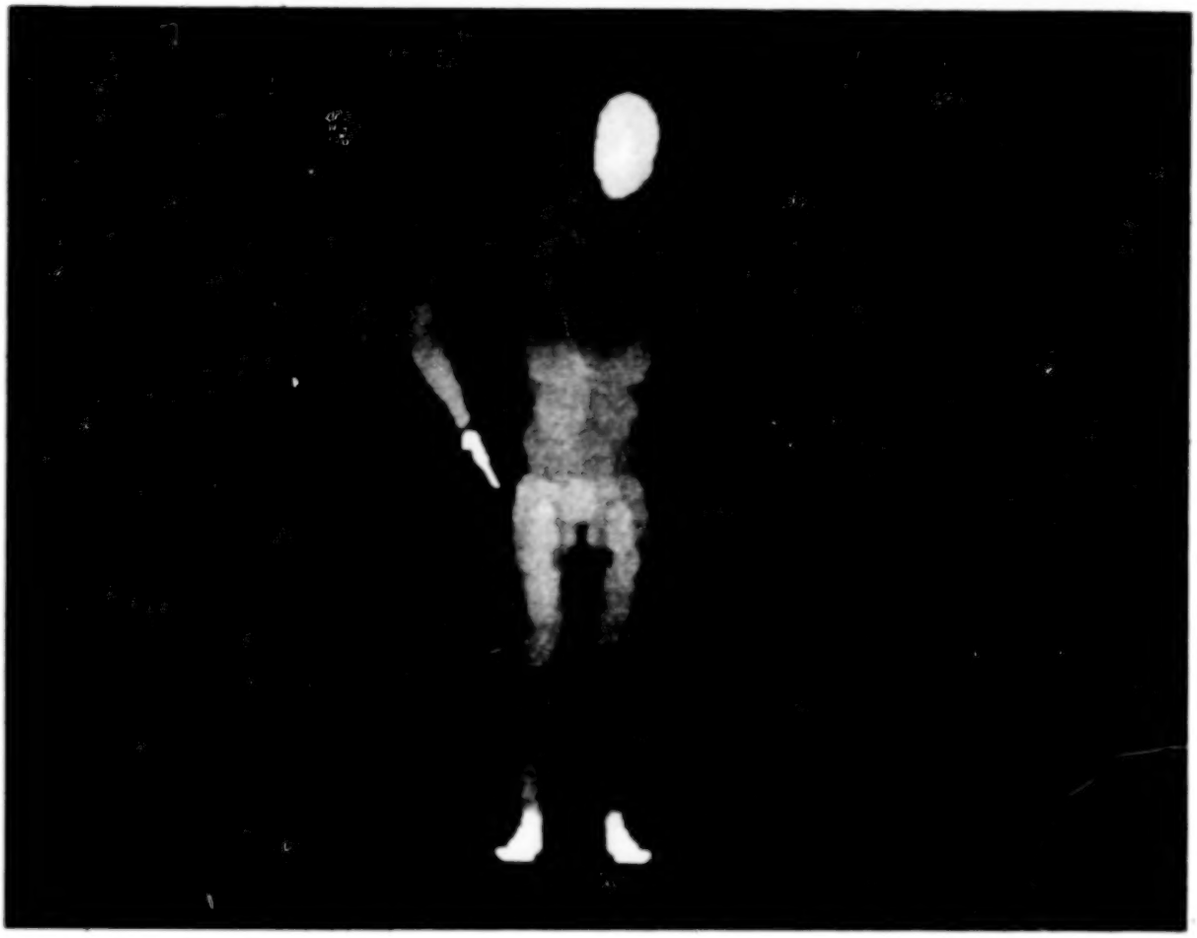


FIGURE 4.- BUBBLEMAN IN A STANDING POSITION.

CURRENT PLANS

SURFACE MAPPING

Further developments of the anthropometric measurement system and of PLAID are planned.

The next stage of the Anthropometric Measurement Laboratory is to develop a technique for mapping the entire body surface. Current techniques for obtaining a digital representation of the surface of a human body are based on manually picking points from stereophotographs. This is an error-prone and laborious method. In conjunction with Wright Patterson Air Force Base (WPAFB), a laser-based anthropometric measurement system (LAMS) is being designed and built. The principal investigator is Dr. Bruce R. Altschuler of WPAFB. The design of this system is described by M. Altschuler (refs. 12, 13, and 14).

The principle involved is again triangulation. In this application, rather than having data from two video cameras or two electo-optical devices, there is an "active" camera and a "passive" camera. The passive camera is indeed a sensitive video camera. The "active" camera is a rectangular array of discrete beams of light which are projected on the object to be measured. Multiple exposures are used to give a position code for each beam position. Figure 5 shows the beam array projected on a model spaceman. There are 128 columns of beams; in this exposure, every other 8 columns are blanked out. Thus, for an array of 128 by 128 beams (more than 16 000 points), there must be a minimum of 8 exposures ($\log_2 N + 1$) to permit a binary coding of the location of the column from which

ORIGINAL PAGE IS
OF POOR QUALITY

the beam originates. Each exposure currently takes one-thirtieth of a second, because of the limiting factor of video scan rate. Thus, to obtain eight exposures requires approximately one-third of a second. This is adequate for cooperative, stationary objects but is limiting for collection of velocity data.



FIGURE 5.- BEAM ARRAYS PROJECTED ON MODEL ASTRONAUT. THERE ARE 128 COLUMNS OF BEAMS. IN THIS PICTURE, THE PATTERN IS 8 COLUMNS OFF, 8 COLUMNS ON.

The design goal is to be able to collect all necessary exposures within 100 milliseconds or less, to permit mapping motion data for kinematic and dynamic models. Two items are currently limiting: the light modulator and the camera. There are several technical challenges in developing a surface mapping system. One is development of an adequately fast "shutter," which is actually not a mechanical shutter but a light modulator whose transparency or opacity is determined by an electric current. The first-generation light modulator was developed by Sandia Laboratory; a second-generation one with lower power requirements and higher speed is under development. Design of a CCD camera with parallel outputs to cut data acquisition time from one-thirtieth of a second to milliseconds is proposed. The multiple-exposure beam position coding technique, the implied algorithm for decoding the beam position, and the calibration procedures in which calibration is performed by viewing an object of known size and shape are technical problems under investigation.

The applications for this device are varied. The project was initiated to map the surfaces of teeth for automatic crown development. NASA applications require a system which can be used (1) to

map large objects at long ranges, such as antennas; (2) to map human-sized objects at medium ranges to collect motion data; and (3) to map smaller objects, such as limbs or torso to determine physiological changes caused by fluid shifting and other zero-g effects.

DYNAMIC MODELING

The ultimate goal of the Operator Station Design System is to permit simulation of individual crewmembers or of statistical samples from a specified population performing complex tasks. The simulation would model the motions and the information processing that takes place and would report impossible or very difficult actions, percentage of population capable of performing an action, times of performance, and a measure of workload or fatigue.

The immediate goal is to add enhanced graphics, motion models, and strength models. Graphic enhancements include modeling reflectance properties, modeling multiple light sources, and increasing the speed of the system. The strength and motion models will drive the graphics displays to show how a specific point might be reached (translation, rotation, limb movements, etc.) and how much force can be brought to bear on the object of the task.

CONCLUSIONS

Computerized models and data collection techniques provide a means of placing man in the loop early in a design cycle, saving time and money over the techniques which rely on mockups. With the extensive data base now built that describes the Shuttle, payloads, and workstations, and with the anthropometric data base, operations can be planned and examined for fit, visual access, and physical access without recourse to mockups. Further automation of this process is under development.

REFERENCES

1. Thornton, W. E.: Anthropometric Changes in Weightlessness. Anthropometric Source Book, Vol. I, Ch. 1. NASA RP-1024, 1978.

2. Thornton, W.; Hoffler, G. W.; and Rummel, J.: Anthropometric Changes and Fluid Shifts. Biomedical Results from Skylab, NASA SP-377, 1977.

3. Jackson, J.: Neutral Body Posture in Zero-G. JSC-09551, 1975.

4. Lewis, J. L.: Computer Aided Crew Station Design for the NASA Space Shuttle. NATO Symposium on Anthropometry and Biomechanics, Cambridge, England, July 1980.

5. Woolford, B. J.; and Lewis, J. L.: Applications of Digital Image Acquisition in Anthropometry. Proceedings of the SPIE Technical Symposium East, vol. 283, 3-D Machine Perception, Washington, D.C., Apr. 1981.

6. Thornton, W. E.: Dynamic Anthropometry. Proceedings of the American Institute of Industrial Engineers, Houston, Tex., Fall 1979.

7. Lewis, J. L.: Operator Station Design System: A Computer Aided Design Approach to Work Station Layout. 23rd Annual Meeting of the Human Factors Society, Boston, Mass., Oct. 29, 1979.

8. Brown, J. W.: Using Computer Graphics to Enhance Astronaut and Systems Safety. 33rd Congress of the International Astronautical Federation, Paris, France, Sept. 27 to Oct. 2, 1982.

9. Stramler, J. H., Jr.; and Woolford, B. J.: Measurement of Reach Envelopes With a 4-Camera Selective Spot Recognition (SELSPOT) System. 26th Annual International Technical Symposium in Instrument Display of SPIE, Biostereometrics '82, San Diego, Calif., 1982.

10. Badler, N. I.; and Smoliar, S. W.: Digital Representation of Human Movement. Computing Surveys, vol. 11, no. 1, Mar. 1979, pp. 19-38.

11. Badler, N. I.; O'Rourke, J.; and Kaufman, B.: Special Problems in Human Movement Simulation. Computer Graphics (Proc. Siggraph '80), vol. 14, no. 3, July 1980, pp. 189-197.

12. Altschuler, M. D.; Altschuler, B. R.; and Taboada, J.: Measuring Surfaces Space-Coded by a Laser-Projected Dot Matrix. Proceedings of the Society of Photo-Optical Instrumentation Engineers, Apr. 19-20, 1979, Washington, D.C.

13. Altschuler, M. D.; Posdamer, J. L.; Frieder, G.; Altschuler, B. R.; and Taboada, J.: The Numerical Stereo Camera. SPIE, vol. 283, 3-D Machine Perception, Apr. 1981.

14. Altschuler, M. D.; Altschuler, B. R.; and Taboada, J.: Laser Electro-Optic System For Rapid Three-Dimensional Topographic Mapping of Surfaces. Optical Engineering, vol. 20, no. 6, Nov./Dec. 1981, pp. 953-961.

About the Author

Barbara Woolford, manager of the Anthropometric Measurement Laboratory, has been at JSC for 7 years. She received a B.A. in psychology and an M.A. in mathematics from Arizona State University. Ms. Woolford is a member of the ACM, the AIAA, and the IEEE Computer Society.

N85
16922

UNCLAS

N85-16922

CHALLENGES IN THE DEVELOPMENT OF THE SHUTTLE EXTRAVEHICULAR MOBILITY UNIT

Harold J. McMann and James W. McBarron II
NASA Lyndon B. Johnson Space Center
Houston, Texas 77058

ABSTRACT

The development of the Shuttle extravehicular mobility unit (EMU) has required significant technology advances in the design of the astronaut life support system and space-suit assembly. For the first time in U.S. manned space flight, the life support system and space-suit assemblies are integrated into a single system and optimized for the primary function of supporting astronaut extravehicular operations. Rather than accommodating a limited, male-only astronaut population, the EMU must satisfy size requirements for both males and females with a minimum of sized parts. In addition, the Shuttle EMU has been designed to implement Space Shuttle Program philosophy of long operating life and mission reuse capability to minimize program lifetime cost.

INTRODUCTION

The advancement in life support system and space-suit technology achieved by the development of the Shuttle extravehicular mobility unit (EMU) shown in figure 1 is best illustrated by comparison with the requirements for and the design features of the Apollo EMU shown in figures 2 and 3. This comparison is relevant because of the excellent performance of the Apollo EMU demonstrated during 162 man-hours of astronaut lunar surface exploration and scientific task accomplishments. The same basic Apollo EMU space-suit design was again successfully demonstrated during the Skylab Program, when an additional 81 man-hours of astronaut extravehicular activity (EVA) tasks were performed.

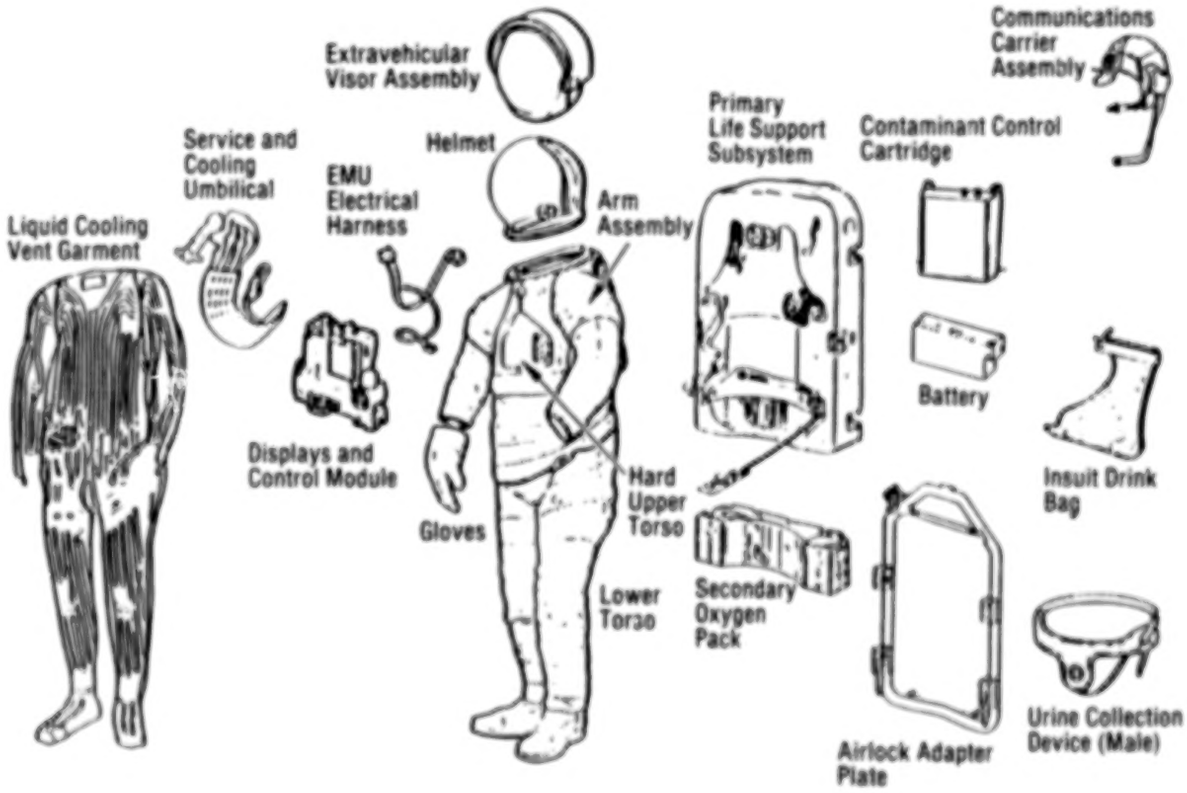


FIGURE 1.- SHUTTLE EMU COMPONENTS.



FIGURE 2.- SIGNIFICANT REQUIREMENT DIFFERENCES BETWEEN SHUTTLE AND APOLLO EMU'S.



FIGURE 3.- DESIGN DIFFERENCES BETWEEN SHUTTLE AND APOLLO EMU'S.

The two major challenges met in the development of the Shuttle EMU are

1. Enhancement of astronaut EVA operations
2. Capability for multiple mission reuse by male and female astronauts

The design approaches and problems experienced in meeting these challenges are presented in this paper.

ENHANCEMENT OF ASTRONAUT EVA OPERATIONS

LIFE SUPPORT SYSTEM AND SPACE-SUIT INTEGRATION

Elimination of the requirement that the space suit be compatible with the Orbiter life support system for astronaut protection in the event of loss of cabin pressure provided the first opportunity in U.S. manned-space-flight history to optimize the EMU design solely for EVA operation. Deleted were design-compromising interface requirements between the space suit and the crew station, the couches, and the vehicle life support system. Operating with these requirements necessitated assembly and disassembly of the Apollo EMU in flight, and attachment and removal of the portable life support system while the space suit was worn. This approach required separate portable life support system attachment straps and mounting brackets, with multiple hoses and connections for ventilation oxygen, emergency pressurization, and cooling water. Electrical cables had to be connected and checked out before EVA. The optimization of the Shuttle EMU for EVA operations shown in figure 4 was accomplished by completely integrating the life support system and its controls and displays into the upper torso portion of the space suit.

ORIGINAL PAGE IS
OF POOR QUALITY

ORIGINAL PAGE IS
OF POOR QUALITY

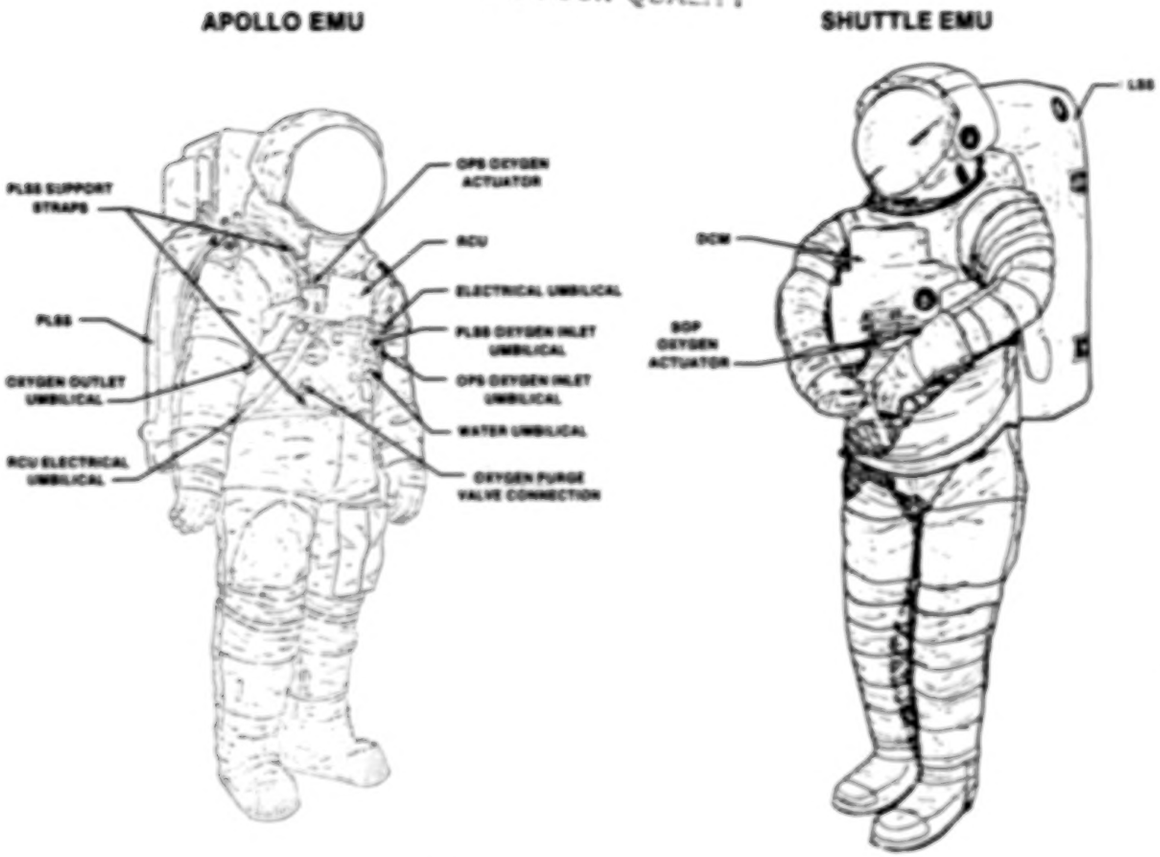


FIGURE 4.- PLSS/DCM TO SPACE SUIT ATTACHMENT METHODS.

HARD UPPER TORSO CONFIGURATION

A rigid aluminum, formed upper torso that conformed to the shape of the body was initially selected to provide a dimensionally fixed life support system mounting structure. This hard upper torso (HUT) design provided the capability to incorporate shoulder bearings, which significantly increased astronaut arm mobility. This configuration was changed, however, after excessive difficulty in donning and doffing satisfactorily was revealed during development testing.

The donning and doffing problem caused by the aluminum HUT and shoulder bearing configuration was solved by incorporating gimbaled shoulder bearings which pivoted at the hard upper torso, with a laminated fabric bellows interface for pressure integrity. This design increased upward movement of the upper arms during donning. The complex geometry of the shoulders and neck area resulting from this design change made aluminum forming of the HUT undesirable. Fiberglass material was then selected. This material permitted molding of the shell and the integral layup and bonding of the gas ventilation and cooling water ducting into the upper torso structure and, thus, provided a smooth and more comfortable internal profile.

LIFE SUPPORT SYSTEM DESIGN APPROACH

A closed-loop life support system similar to the configuration developed for the Apollo Program was selected for Shuttle use, as shown schematically in figure 5, rather than the umbilical-type systems used during the Gemini and Skylab Programs. The closed-loop concept is superior for the Shuttle application since vehicle dependency is minimized and astronauts are freed from managing bulky umbilicals.

ORIGINAL PAGE IS
OF POOR QUALITY

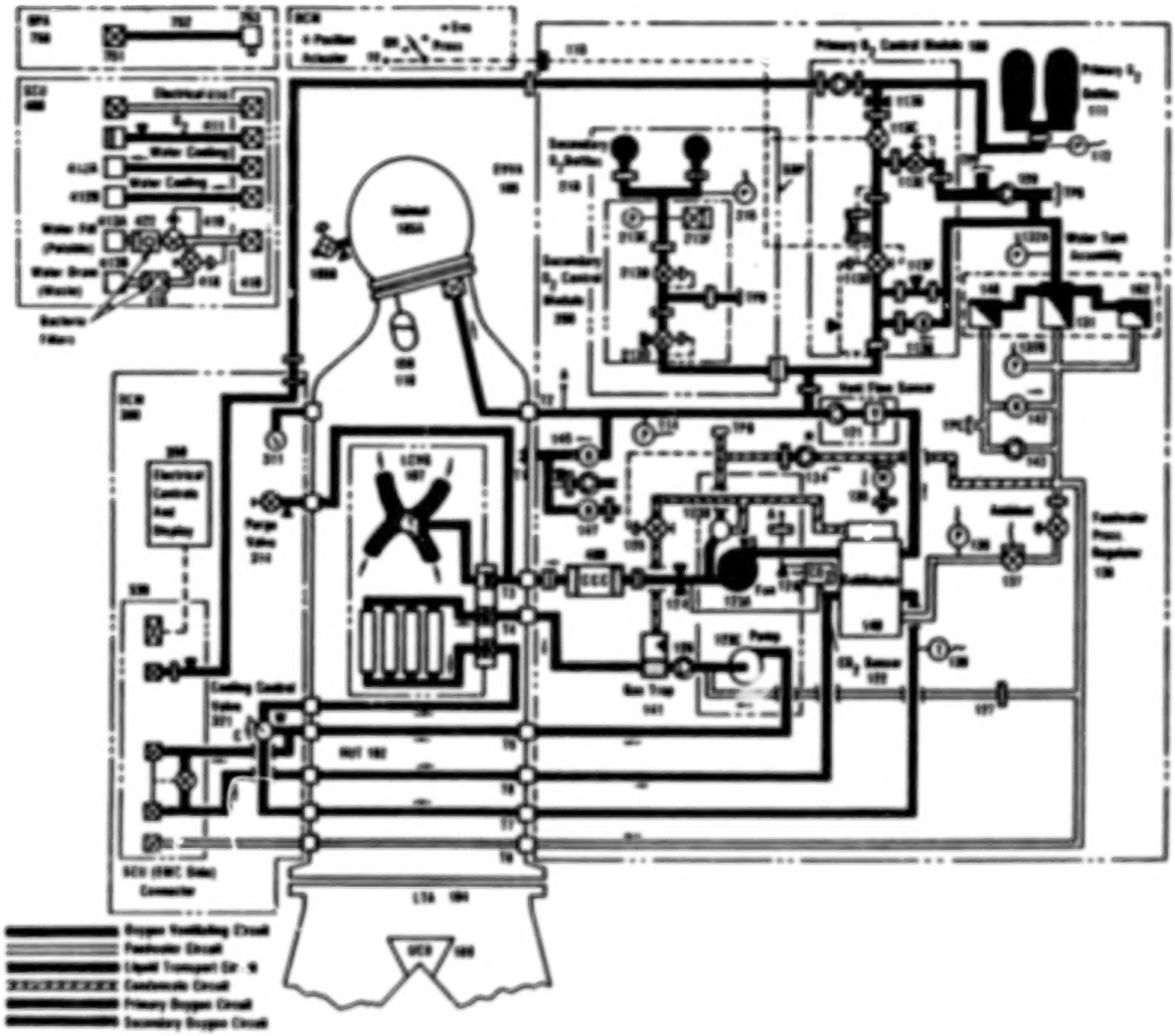


FIGURE 5.- SPACE SHUTTLE EMU SCHEMATIC.

The primary life support system (PLSS) of the Shuttle EMU provides cooling of the astronauts by the circulation of cool water through small-diameter tubes contained in the liquid cooling and ventilation garment. A water sublimator and heat exchanger, similar in concept to that of the Apollo unit, is used to cool the water and also to cool and dehumidify the oxygen in the recirculating ventilation loop. As in the Apollo EMU, lithium hydroxide and charcoal are used to remove carbon dioxide (CO_2) and odors from the oxygen gas stream of the Shuttle EMU.

Makeup oxygen is regulated to 4.3 psi from twin 1000-psi PLSS storage tanks shown in figure 6. A secondary oxygen package (SOP) located below the PLSS provides 30 minutes of emergency purge flow from two 6000-psi spheres. The SOP is brought on standby just before EVA, using the valve actuator shown in figure 7, and provides flow automatically any time suit pressure drops below 4.0 psi. Controls and displays are located on the displays and control module (DCM) (fig. 8), which is mounted on the front of the HUT. A silver oxide/zinc battery provides power for the radio, the caution and warning system, and the fluid circulation equipment.

ORIGINAL PAGE IS
OF POOR QUALITY

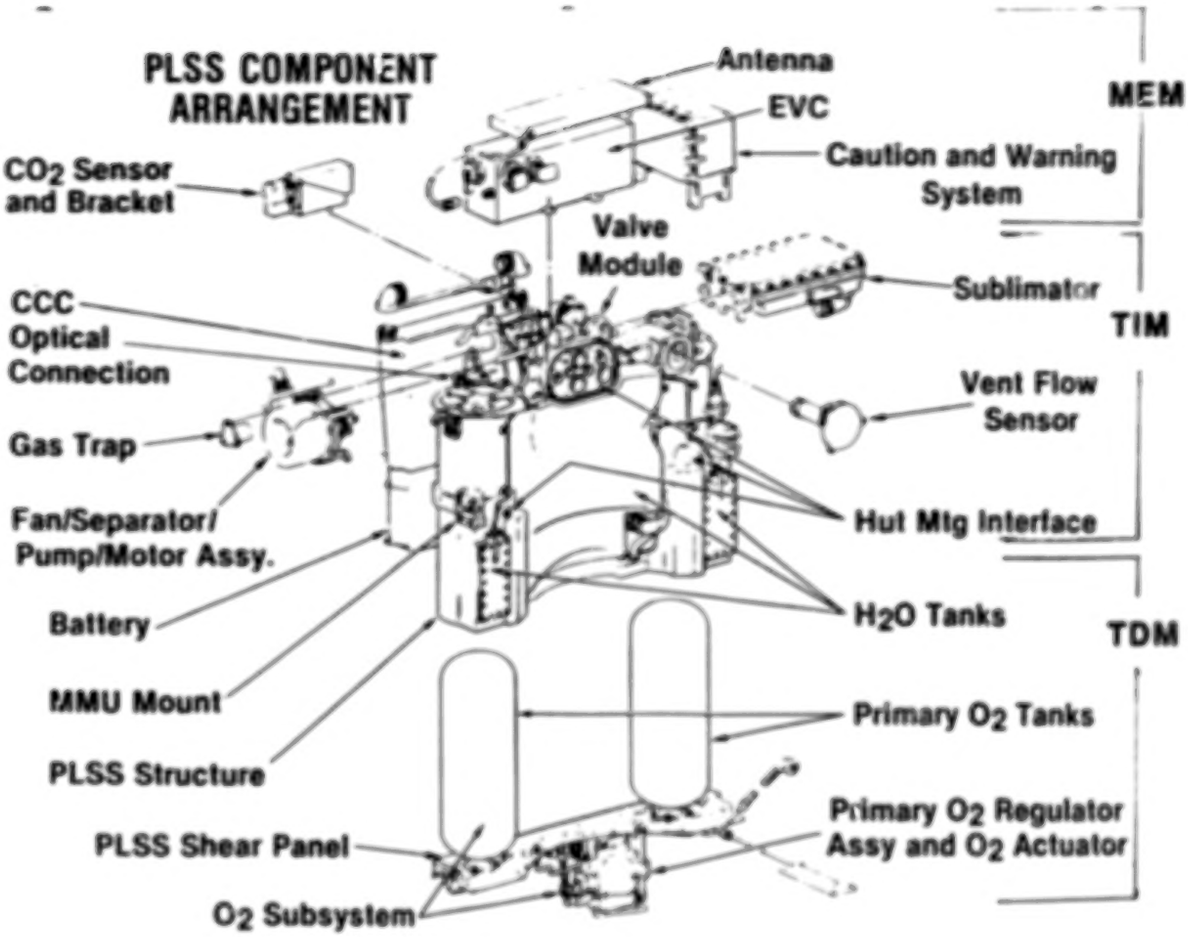


FIGURE 6.- SHUTTLE EMU PLSS.

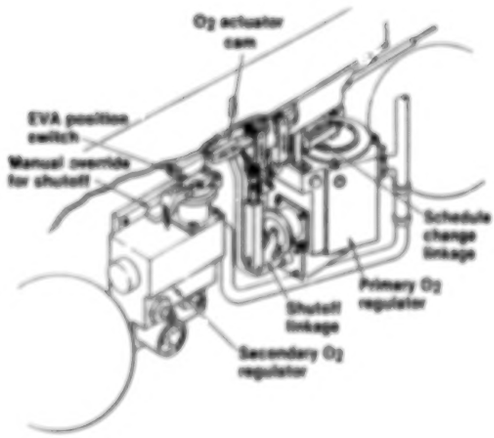


FIGURE 7.- SOP WITH FOUR-POSITION ACTUATOR VALVES AND LINKAGE.

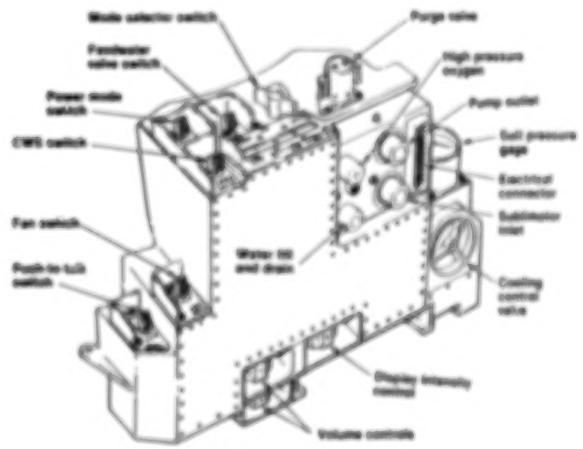


FIGURE 8.- DCM FRONT VIEW.

ORIGINAL PAGE IS
OF POOR QUALITY

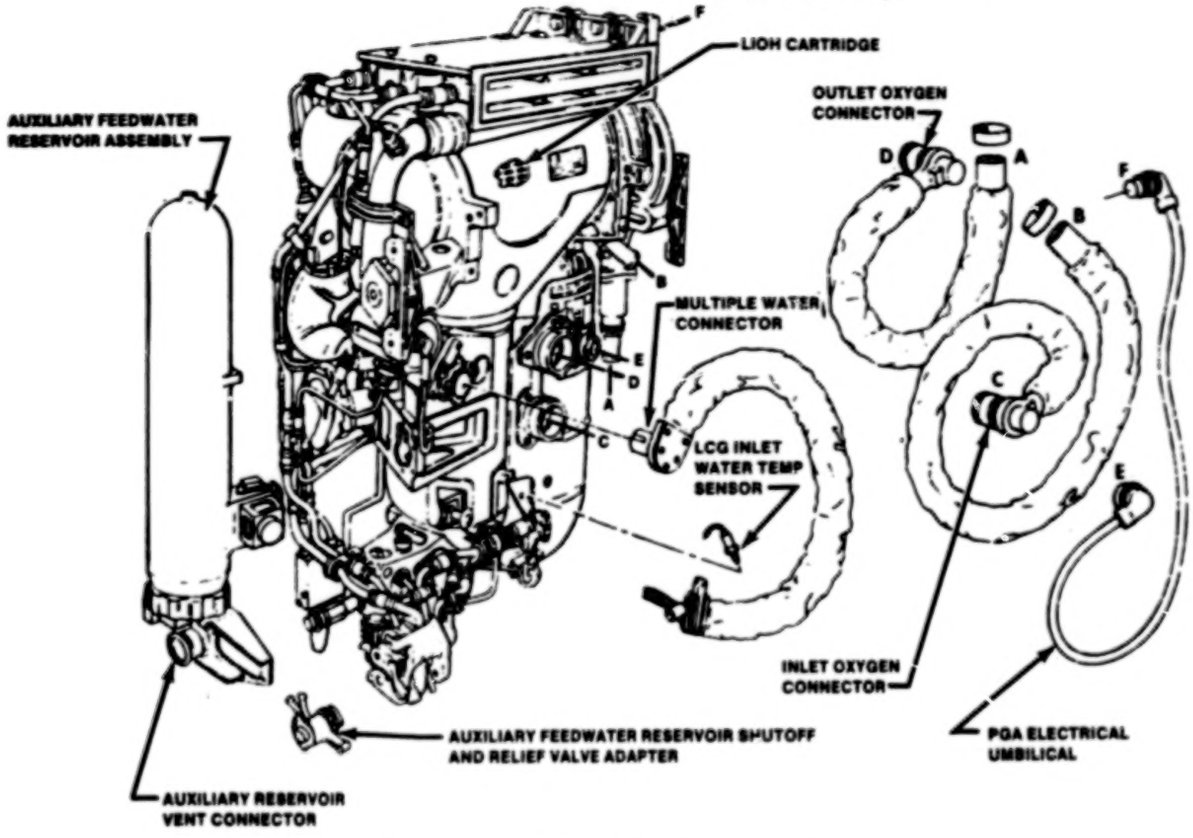


FIGURE 9.- APOLLO EMU PLSS FLUID HOSES.

EMU FRONT-TO-BACK DIMENSION

Shuttle EMU designers found that the Orbiter interdeck hatch passthrough requirement imposed a front-to-back dimensional constraint which ruled out conventional plumbing methods for coupling the components and subsystems of the EMU. Figures 9 and 10 show the various runs of tubing and hoses required for the Apollo life support system. Selection of this approach for Shuttle would have increased the envelope size to unacceptable dimensions, because of not only the physical size of the hoses and fittings involved but also the space required for tool insertion in assembly and disassembly.

The approach selected to solve this problem was modularization of the entire life support system. The Shuttle PLSS is divided into the following three modules (fig. 6).

1. Time dependent module (TDM)

2. Time independent module (TIM)

3. Major electronics module (MEM)

The TDM consists of components the physical size of which is a function of mission time or total metabolic load or both. These components are the water tanks, the battery, the contaminant control cartridge (CCC), and the oxygen subsystem. The water tanks are shaped to conform to the contour of the back of the HUT and, in combination with protective shrouds around the oxygen tanks, form an integrated structure for the PLSS. This structure provides attachment points for the airlock adapter plate (AAP), used for flight stowage and as a holding fixture for donning and doffing, and for the manned maneuvering unit (MMU). The CCC and the battery are nested together in a rear cavity of the PLSS; this configuration provides easy access for recharge and maintains a dense package.

The TIM consists of a valve module, which provides internal connecting water and gas lines, plus provisions for mounting cartridge-type valves, transducers, a sublimator, and rotating machinery.

C-6

ORIGINAL PAGE IS
OF POOR QUALITY

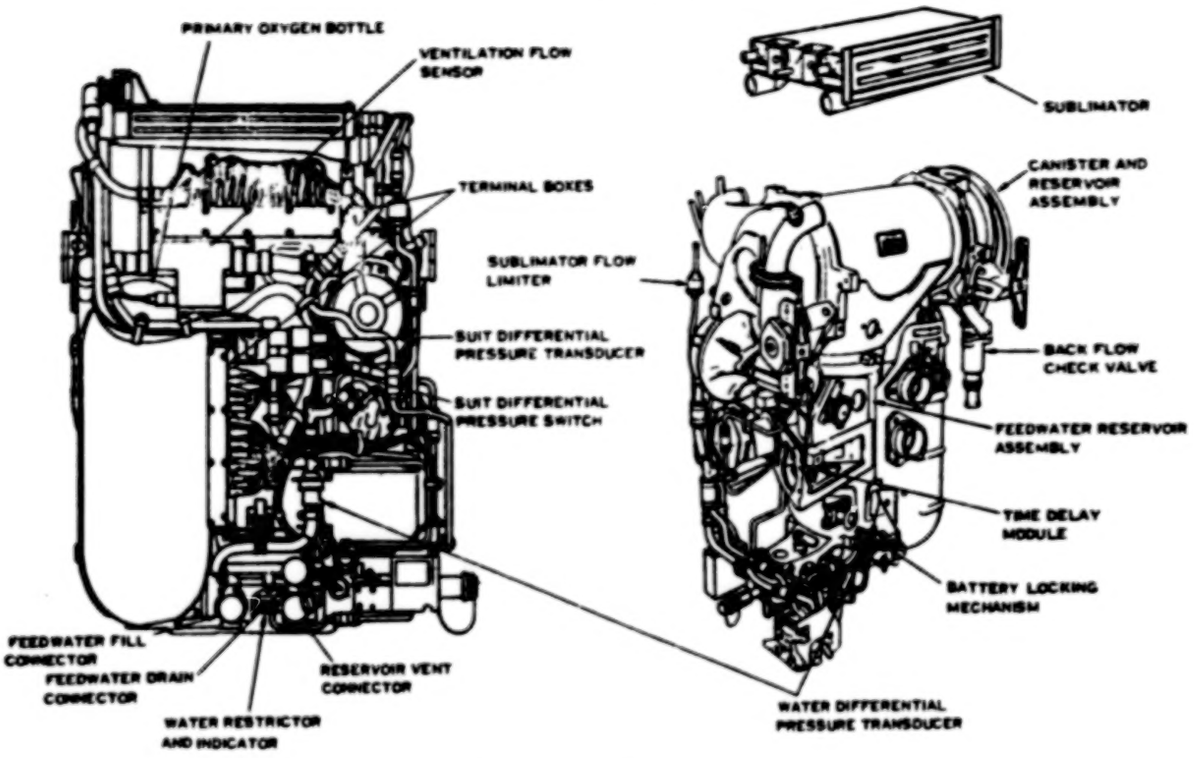


FIGURE 10.- APOLLO EMU PLSS COMPONENT LAYOUT.

The MEM components, which are mounted on top of the TIM, consist of the caution and warning system, the extravehicular communications radio, and a CO_2 sensor. The SOP fits snugly at the bottom of the PLSS.

The packaging density achieved in the Shuttle life support system is 80 percent, compared to 40 percent for the Apollo life support system.

ELIMINATION OF EXPOSED OXYGEN VENTILATION HOSES

By flange mounting the PLSS and the DCM to the HUT as shown in figure 1, designers not only enhanced Shuttle EMU packaging and met the 19-3/4-inch front-to-back dimensional requirement, they also solved one of the most worrisome problems of the Apollo EMU design - exposed ventilation hoses. Rupture or severe damage to the Apollo PLSS hoses could have had catastrophic results, since severe loss of pressure integrity could easily have exceeded emergency oxygen system capability.

ASTRONAUT MOBILITY

One of the more important requirements for efficient performance of EVA tasks in the zero-g environment is astronaut upper body mobility. Shuttle EMU upper body mobility is superior to that of the Apollo EMU as a result of incorporating gimbaled bearing shoulder joints, a gimbaled wrist joint in each glove, and a waist bearing. This configuration resulted in the increased mobility ranges shown in figure 11.

The objective to increase lower torso mobility for the Shuttle EMU was initially considered but was not implemented because of the lack of a walking requirement in zero g and the disadvantages of additional design complexity, weight, and increased development and manufacturing costs. As a result, the lower body mobility of the Shuttle EMU is less than that of the Apollo EMU.

The flat patterned fabric joints shown in figure 12 were selected for the Shuttle EMU because of their increased flexure cycle life and reduced manufacturing cost.

UPPER BODY MOBILITY JOINTS	MOTION	SHUTTLE EMU	APOLLO EMU
● SHOULDER	LATERAL-MEDIAL	206°	130°
	FLEXION	186°	158°
	ADDUCTION-ABDUCTION	123°	101°
● ELBOW	FLEXION	133°	137°
● WRIST	ADDUCTION-ABDUCTION	148°	128°
	FLEXION-EXTENSION	111°	92°
● WAIST	ROTATION	212°	49°
LOWER BODY MOBILITY JOINTS			
● WAIST	FLEXION	162°	112°
● HIP	FLEXION	63°	90°
● KNEE	FLEXION	82°	106°
● ANKLE	FLEXION-EXTENSION	162°	103°

FIGURE 11.- SPACE-SUIT MOBILITY-JOINT RANGE COMPARISON.

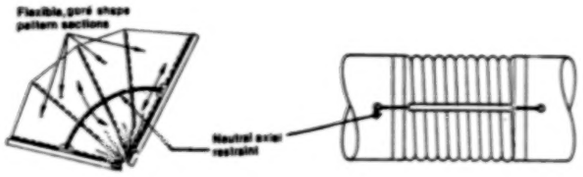


FIGURE 12.- SPACE-SUIT MOBILITY-JOINT DESIGN APPROACHES.

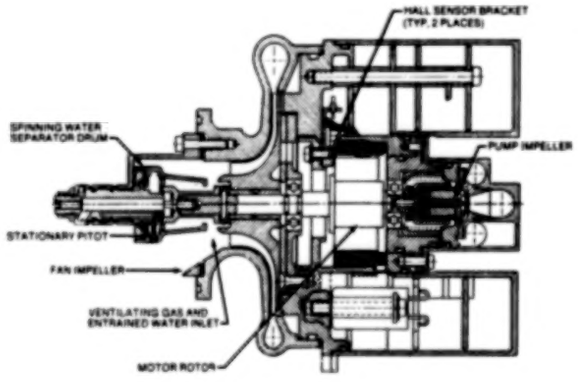


FIGURE 13.- FAN/PUMP/SEPARATOR ASSEMBLY.

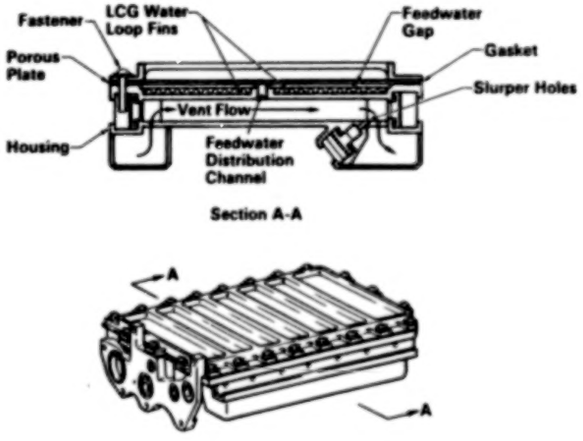


FIGURE 14.- SUBLIMATOR.

FAN OPERATION AT SEA-LEVEL ATMOSPHERE

The Shuttle EMU provides astronaut ventilation during a 3-1/2-hour oxygen prebreathe period at sea-level pressure followed by airlock depressurization to vacuum and suit pressure control at 4.3 psia. In Apollo missions, the 5-psia, 100-percent oxygen lunar module cabin atmosphere eliminated the need for prebreathing and reduced the fan design-load requirements. The requirement for Shuttle EMU fan operation over a wide range of pressures was solved by the development of a motor with speed limiting circuitry so that virtually all operating conditions are met within speed variations of less than 15 percent. To sense rotor position, two Hall-effect electromagnetic sensors shown in figure 13 are used for commutation, and power input is "chopped" at the lower pressure during EVA to control speed and decrease power consumption. The Apollo EMU fan was limited to momentary operation at sea-level pressure to prevent overheating of its motor winding.

PLSS OPERATION IN ZERO g

Separation and removal of humidity in the PLSS ventilation loop occurs in two stages. First, the gas stream is cooled in the sublimator and the resulting condensate spreads over fins coated with a hydrophilic substance. It is then transported by pressure differential through holes into a collection manifold, called the "slurper" (fig. 14), where the mixture of ventilation oxygen and water enters a rotating drum and stationary pitot assembly. The drum is mounted to the motor shaft at the fan inlet shown in figure 13, and the driving force for the slurper is the fan pressure rise. When spinning at about 19 000 rpm, the tapered drum slings the water droplets to the periphery of the housing, where the water stream contacts a stationary pitot tube. As much as 25 psid pressure can be developed in this manner, and the water is pumped either into the EMU water storage tanks or directly to the sublimator for immediate heat-rejection use. The water-free oxygen stream is returned to the fan inlet. Thus, unlike the Apollo EMU wherein condensate was stored and dumped at the end of an EVA, the Shuttle EMU makes use of metabolically generated water and thereby allows a reduction in stored water requirements. This approach aided in the attainment of the compact PLSS packaging.

The tasks of ventilation at various system pressures, water circulation, and moisture removal from the ventilation loop are accomplished by the integrated fan/pump/separator assembly shown in figure 13. The high efficiency of this assembly is illustrated by noting that the Shuttle water pump consumes only 2 watts, compared to 10 watts for the Apollo pump.

In addition to water in the gas stream, the opposite problem also exists - the presence of as much as 30 cubic inches of unwanted gas bubbles in the cooling water loop. These bubbles are produced by (1) attachment of a liquid cooling garment partly filled with water or (2) evolution due to the system pressure reduction during depressurization. In Apollo missions, lunar 1/6-g force provided the means of separation and the loop was periodically "burped" to remove gas. In the Shuttle EMU, a fine mesh (18 micrometer) cylindrical screen shown in figure 15 receives the full 240-lb/hr cooling loop waterflow, delivered by a centrifugal pump magnetically coupled to the motor shaft. The screen has a very low flow resistance to water and a very high (comparative) resistance to gas flow so that water flows radially outward, and gas bubbles and a small flow of water are carried out through the exit orifice and into the water separator described previously.

IN-FLIGHT CHECKOUT AND STATUS MONITORING

During Apollo missions, the EMU was donned and checked following a written checklist, and EMU performance during EVA was monitored by ground controllers using telemetry, which required an extensive real-time EVA support team. In addition to an oxygen pressure tank "gas gage," the Apollo EVA astronaut had a suit pressure gage and five electromechanical warning flags to alert him of EMU system malfunctions.

The Shuttle EMU caution and warning system shown in figure 16 uses a microprocessor and slightly more than 5 kilobits of memory to provide the user with procedures to be used during checkout, to allow tracking of limiting consumables during EVA, and to provide notification of out-of-limit conditions with appropriate corrective actions. This approach puts the information directly at the point where action can be taken - with the user. Continuing the effort to make the EMU "user friendly," all controls and displays are located on the DCM shown in figure 8. By contrast, the Apollo PLSS had the suit cooling water control valve, the sublimator on/off valve, and the primary oxygen supply valve located on a remote lower corner of the backpack, which was difficult to reach.

IN-FLIGHT RECHARGE

In-flight recharge of water, oxygen, and electrical power is accomplished through a common connector located on the DCM shown in figure 8. One connection accomplishes the same task as several connections made separately on the Apollo backpack. The service and cooling umbilical (SCU), which mates to the common connector, also allows the recirculation of water for cooling the astronaut during suited operations before airlock depressurization using the PLSS pump and an Orbiter heat exchanger. The Apollo EMU had no such PLSS capability. Removal of the CCC involves unzipping a flap on the PLSS thermal cover, releasing two latches, and pulling out the expended can, with a reversal of steps to install a new one. The battery can also be replaced instead of being recharged in place to expedite reuse. Total recharge time is about 1 hour if the battery is replaced rather than being recharged. Battery recharge takes approximately 19 hours.

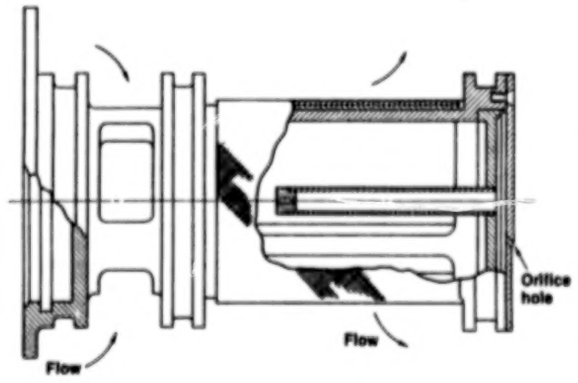


FIGURE 15.- GAS TRAP.

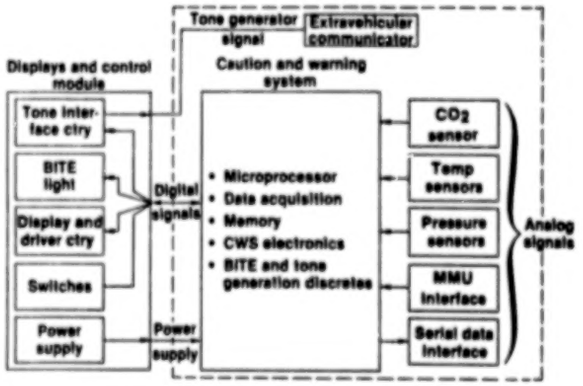


FIGURE 16.- CAUTION AND WARNING SYSTEM BLOCK DIAGRAM.

SPACECRAFT UMBILICAL OPERATION

Although umbilicals have appreciable drawbacks from the crew handling aspect, there are cases in which umbilical EVA capability might be useful. For example, consider a payload benefiting from EVA but with a sensitivity to water vapor contamination. Use of the standard Shuttle EMU would not be appropriate because of the EMU sublimator exhaust, but water vapor emission could be avoided by using suit cooling water chilled by the vehicle's radiator-based heat-rejection system and circulated by the PLSS pump. Another instance might require that an astronaut plan to extend an EVA past the expendables limits. By using an extended length SCU with its water circulation, power, and oxygen lines, the Shuttle EMU will provide this capability.

CAPABILITY FOR MULTIPLE MISSION REUSE BY MALE AND FEMALE ASTRONAUTS

SPACE-SUIT SIZING TO ACCOMMODATE FEMALES AND A LARGE SIZE POPULATION OF ASTRONAUTS

The large number of planned Shuttle missions results in a large astronaut size population to be accommodated with correctly sized and fitted space suits. The scope of the requirement to satisfactorily fit both female and male Shuttle astronauts whose body dimensions vary from 5th percentile female to the 95th percentile male is shown in figure 17. The design approach to meet this large variation in body dimensions was to use a modular system of interchangeable, standard-sized components shown in figure 18. Unlike the Apollo approach to manufacture custom-sized suits using individual astronaut's measurements, the Shuttle suit design approach provides the capability to "custom-assemble" previously manufactured and "on the shelf" standard size components. After mission use, the Shuttle suit is disassembled and components are made available for subsequent mission use by another astronaut. The critical design feature necessary to allow for the modularity of the standard size components was the flange mounting of fabric restraint and bladder components to joint bearings and disconnects shown in figure 19. By removing a series of circumferentially spaced screws and a mounting ring, different standard-sized fabric components can be interchanged easily. Pressure integrity between the fabric bladder material and the bearing or disconnect is assured by use of an O-ring seal. The Apollo suit design approach used adhesive bonding of the fabric bladder to hardware with a cord overwrap to provide adequate structural integrity. Removal of either side of this interface was difficult and required considerable time and effort since adhesive removal, surface cleaning, and long adhesive cure times were necessary.

Figure 20 shows the different standard-sized suit components required for the pressure retention portion of the Shuttle EMU space suit. Standard sizes of thermal micrometeoroid garment components,

CRITICAL BODY DIMENSIONS	5TH PERCENTILE FEMALE, IN.	-TO-	95TH PERCENTILE MALE, IN.	MAX. SIZE VARIATION, IN.
CHEST BREADTH	9.9		14.5	4.6
CHEST DEPTH	8.2		10.9	2.7
CHEST CIRCUMFERENCE	32.4		43.2	10.8
SHOULDER CIRCUMFERENCE	36.7		50.6	13.9
SHOULDER BREADTH	15.2		18.4	3.2
SHOULDER HEIGHT	48.4		61.7	13.3
FINGERTIP SPAN	60.0		77.0	17.0
TORSO LENGTH	22.1		27.7	5.6
HIP BREADTH	12.4		15.3	2.9
CROTCH HEIGHT	26.8		36.8	10.0
KNEE HEIGHT	15.0		21.3	6.3
STANDING HEIGHT	59.9		74.3	14.4

FIGURE 17.- SHUTTLE EMU SPACE SUIT ASTRONAUT SIZE REQUIREMENTS AND VARIATION.

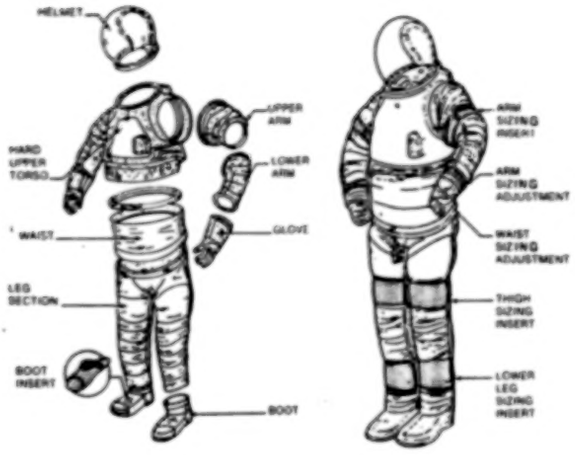


FIGURE 18.- SHUTTLE EMU SPACE-SUIT COMPONENT MODULARITY AND LENGTH SIZING ADJUSTMENTS.

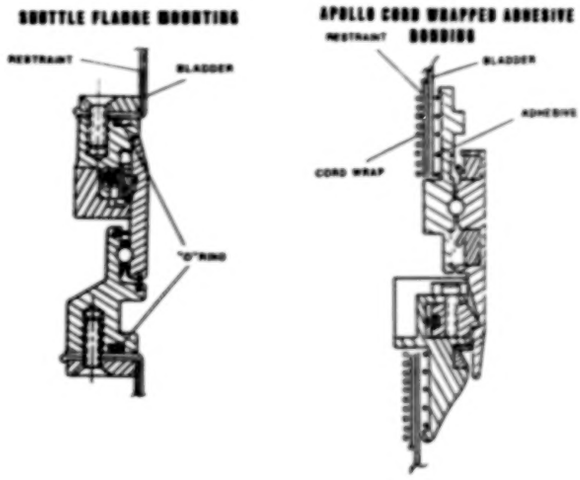


FIGURE 19.- SPACE-SUIT PRESSURE RESTRAINT AND BLADDER TO HARDWARE ATTACHMENT METHODS.

liquid cooling ventilation garment, and communication carrier are also necessary. The quantity of possible size combinations of each major component of the space suit is also identified.

AGE AND OPERATING LIFE

The Shuttle EMU is designed for multiple mission reuse, as compared to the single mission use required for the Apollo EMU. This design resulted in increased age and operating life requirements for the Shuttle EMU space-suit assembly and life support system.

Space-Suit Assembly

To accomplish multiyear, multimission capability for the suit, a requirement for 6 years age life for nonmetallic materials and 15 years for metallic hardware was implemented. This compares with the 4-year age life capability of the Apollo EMU suit design. The 6-year age life requirement resulted in the selection of polyurethane-coated nylon fabric for the Shuttle suit pressure bladder in lieu of the neoprene-coated nylon fabric and the combination neoprene and natural rubber convolute compound used in the Apollo suit. The 6-year life requirement resulted in a 462-hour manned pressurized operating lifetime requirement as compared with the 105-hour capability of the Apollo EMU suit design.

Low endurance life components used for the Apollo suit had to be replaced as a result of this longer life requirement. These included the Apollo suit pressure-sealing slide fastener used for donning and doffing. This component was found to be life limited to approximately 50 opening and closing cycles, with an average of 3 replacements required in each Apollo flight suit before launch. The Shuttle suit design uses an oval-shaped metal disconnect to attach the hard upper torso to the lower torso assembly, and the device is not cycle life limited.

To increase the reliability of the suit for multiple mission use, a redundant axial load restraint design shown in figure 21 was incorporated into all fabric pressure restraint elements. This design consists of independent webbings, sewn together to maintain joint stability, which have separate hardware attachment brackets. In the event of a primary restraint webbing failure, the redundant restraint webbing and brackets are capable of maintaining suit pressure integrity to enable completion of three 7-hour EVA's on a mission with minimum effect on astronaut mobility.

Figure 22 shows the different bladder seam design approaches used for the Shuttle and Apollo EMU suits. The heat-sealed bladder seam design was selected for the Shuttle suit to reduce seam leakage, which was a recurring problem with the Apollo suits, and also to reduce manufacturing time and cost.

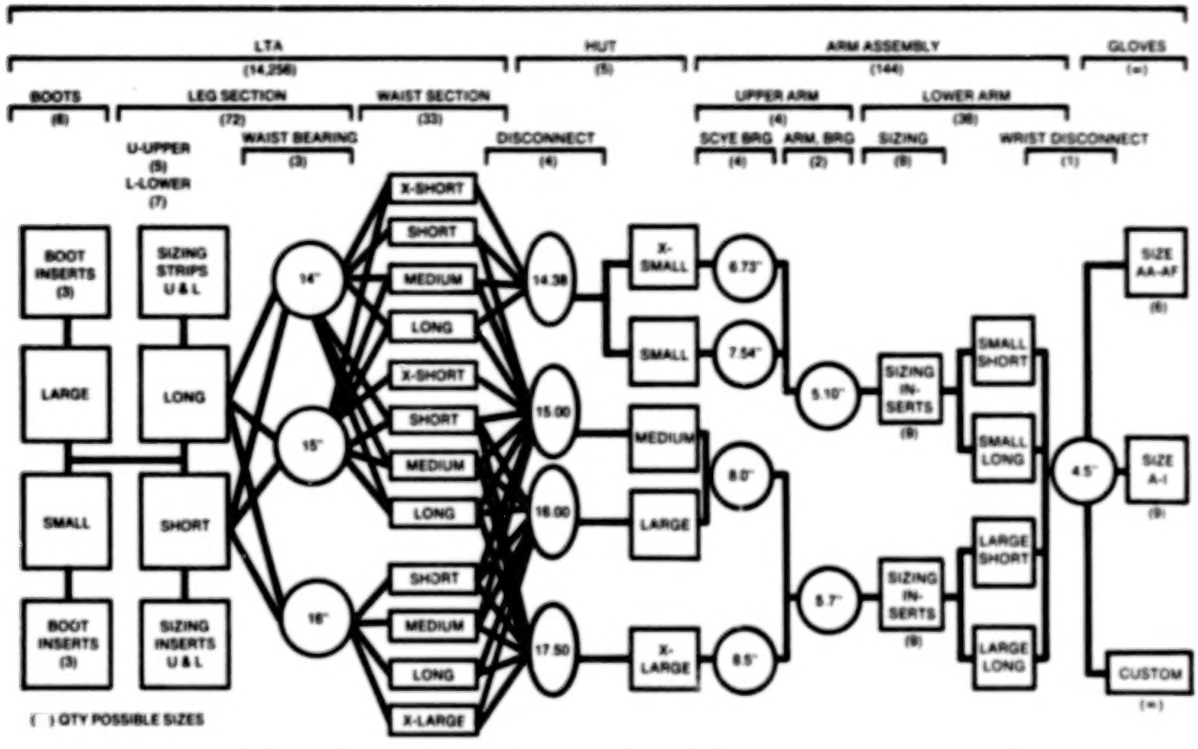


FIGURE 20.- SHUTTLE EMU SPACE-SUIT SIZING SYSTEM - PRESSURE RETENTION ASSEMBLY.

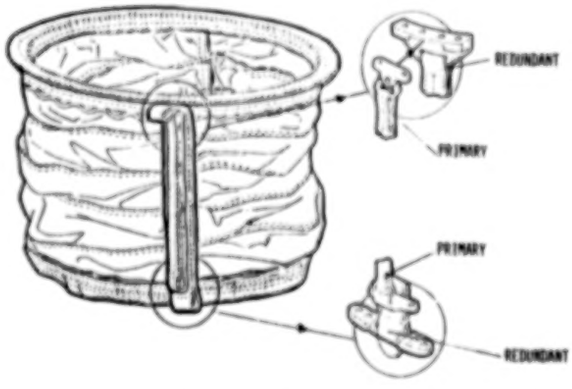


FIGURE 21.- SHUTTLE SPACE SUIT REDUNDANT AXIAL LOAD RESTRAINT DESIGN.

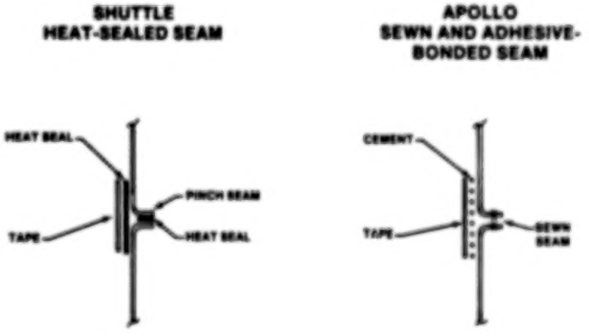


FIGURE 22.- SPACE-SUIT BLADDER SEAM DESIGN APPROACHES.

Life Support System

The Apollo backpacks were left on the lunar surface following their final EVA mission use. As a result, required operating lifetime was low, and there was no requirement for mission reuse capability.

The goal of 15-year service life for the Shuttle life support system with mission to mission reuse was approached by determining from the mission model and required hardware turnaround time the number of units required and, then, certifying for the required number of operating hours and cycles. For example, a typical EMU fan motor can be expected to operate for slightly more than 1500 hours from STS-11 through fiscal year 1995, and the DCM status switch can be expected to undergo about 145 000 cycles.

Naturally, a considerable amount of ground maintenance will be necessary over this long time period. The modular accessible design shown in figure 6 enhances rapid replacement of components. For example, 13 components plug, cartridge fashion, into the valve module.

The Shuttle EMU aluminum porous plate sublimator is much smaller (one-sixth the plate area) and much lighter (3.2 pounds compared to 7.7 pounds) than the Apollo EMU unit. Its small size helped in achieving the reduced Shuttle EMU envelope. Significantly less plate area is required, and a single porous plate, which is bolted to one side of the unit, is used. Since it is removable, it may be cleaned and/or replaced.

CONCLUDING REMARKS

The majority of the operational EVA experience planned for the Space Shuttle lies ahead. However, the success of the EVA demonstration conducted during the STS-6 mission is significant. Also, although the actual Shuttle EVA mission time to date is relatively small (fig. 23), the Shuttle EMU has already exceeded EMU time at vacuum (fig. 24) for the total Apollo Program, principally because of the 15-year-life certification and chamber training of astronauts conducted for each Shuttle mission. Figure 25 shows the accumulated manned operating pressure time of the EMU space suit, including operating time in which only life support system mockups are used, such as for underwater neutral-buoyancy training. Based on this impressive accumulation of EMU system operational time, the current indications are that the EMU development challenges are being met.

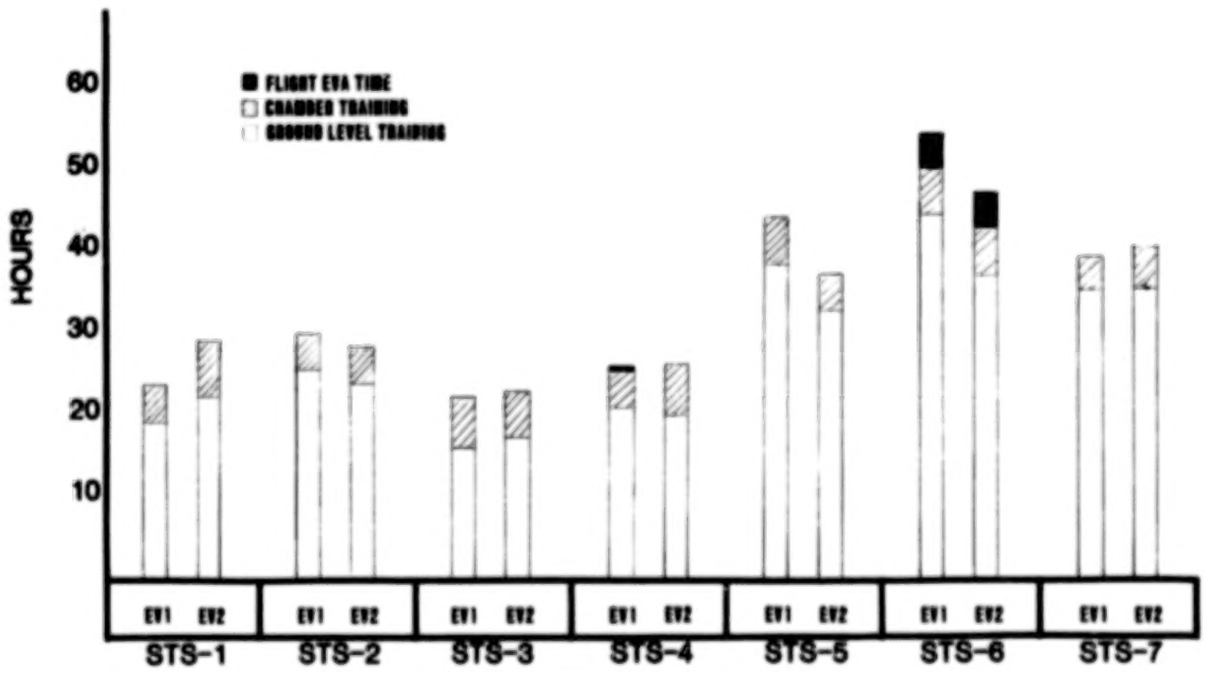


FIGURE 23.- SHUTTLE EMU SUITED HOURS OF USE.

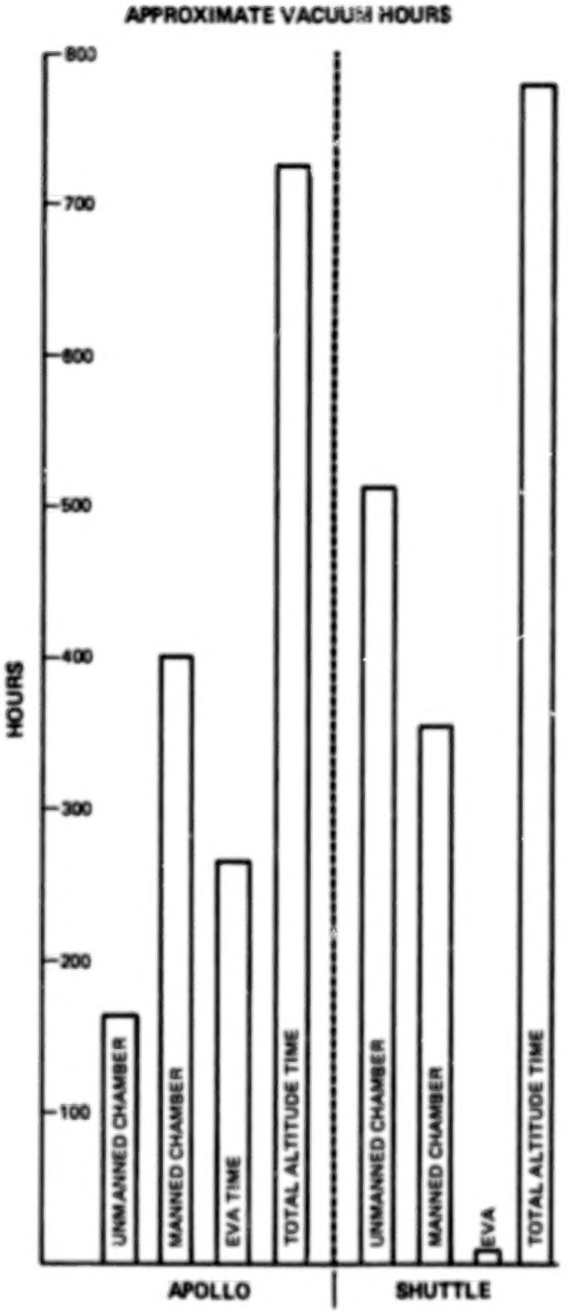


FIGURE 24.- COMPARISON OF APOLLO AND SHUTTLE EMU HOURS AT VACUUM.

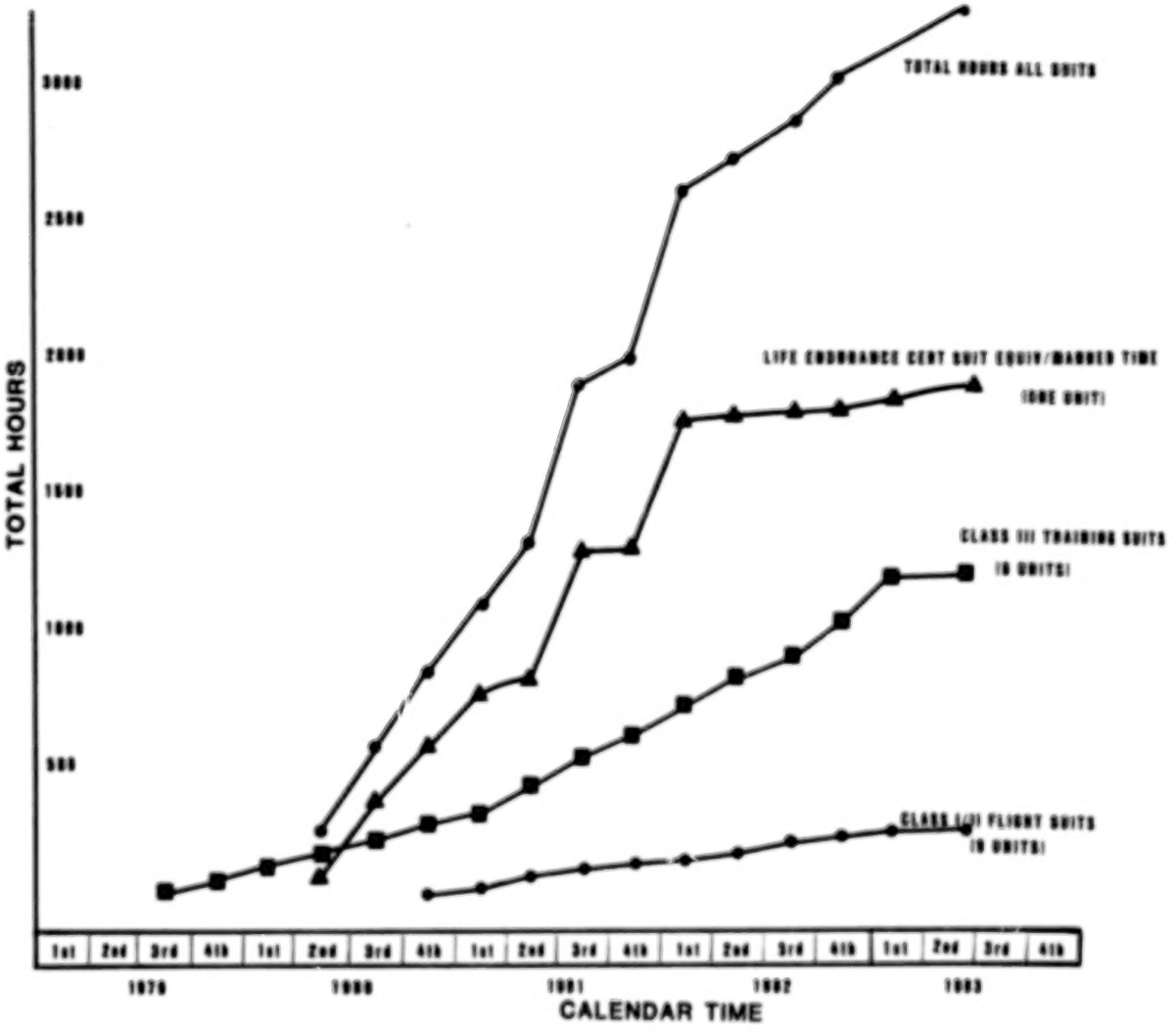


FIGURE 25.- SHUTTLE EMU SPACE SUIT ACCUMULATED MANNED OPERATING PRESSURE TIME (AS OF JUNE 1, 1983).

ACKNOWLEDGMENTS

The authors acknowledge the contributions of the following Shuttle EMU program personnel who provided technical suggestions and data for this paper: James Clougherty, Bill Maas, and Joe Whitman of ILC Dover, and Steve Krasinski, Fred Goodwin, and Phillip Heimlich of the Hamilton Standard Division of United Technologies Corporation. In addition, appreciation is extended to Cathy Kramer, Ann Marie Hoffman, and Deborah Poinsett of the Hamilton Standard JSC Field Support Office, who assisted in the preparation of the numerous draft revisions of this paper.

N85
16923

UNCLAS

D34

N85-16923

CHALLENGES IN THE DEVELOPMENT OF THE ORBITER ACTIVE THERMAL CONTROL SUBSYSTEM

Author:

John R. Nason
Senior Analytical Engineer
United Technologies Corporation
Hamilton Standard Division
Windsor Locks, Connecticut

Contributing Authors:

Frederic A. Wierum
Professor of Mechanical and Aerospace Engineering
Rice University
Houston, Texas

James L. Yanosy
Analytical Engineer
United Technologies Corporation
Hamilton Standard Division
Windsor Locks, Connecticut

ABSTRACT

A number of major challenges were faced in the design and development of the Orbiter Active Thermal Control Subsystem (ATCS). At the system level, the initial challenges were to define an approach that would interface dual Freon coolant loops with multiple coolant loops from other vehicle subsystems with the lowest weight penalty to the Orbiter; and to provide highly responsive vehicle heat rejection throughout all of the Orbiter mission phases.

Optimized heat exchangers, representing an advance in the state-of-the-art in heat exchanger design, were developed to transfer heat between the orbiter Freon coolant loops and five other vehicle systems. The heat exchangers interface four or five separate coolant loops in a single unit while maximizing performance and minimizing weight, volume and coolant loop pumping power. This paper includes a description of the various heat exchanger configurations, optimization techniques used in their design and performance characteristics realized during testing and flight operations.

Flash evaporation was selected as a highly efficient and responsive means for cooling the Orbiter Freon loops during ascent and entry. It also provides supplemental cooling on-orbit. The Flash Evaporator Subsystem (FES) utilizes cyclic water spray cooling in a chamber maintained at or below the water triple point pressure. Because of the dynamic nature of the flash evaporation process, challenges were faced in hardware and control scheme development and in performance verification testing of the subsystem under flight simulated conditions. This paper includes a summary of the basic heat transfer research conducted by Rice University to identify the fundamental heat transfer processes involved in water spray cooling in support of the FES design. Also included is a discussion of the high fidelity dynamic analytical model of the FES that was generated to aid in the design of control logic, evaluate performance and simulate ground test and flight anomalies. A description of the FES and Integrated ATCS testing conducted in the SESL chamber A at NASA-JSC is also presented.

NOMENCLATURE

$M_f(i)$	=	mass of Freon in core wall segment "i", lbm
C_{pf}	=	specific heat of Freon, Btu/lbm-°F
$T_f(i)$	=	average temperature of Freon in core segment "i", °F
t	=	time, sec
$\dot{m}_f$	=	Freon flow, lbm/sec
$T_{fin}(i)$	=	inlet Freon temperature at segment "i", °F
$T_{fout}(i)$	=	exit Freon temperature at segment "i", °F
h_f	=	Freon film coefficient, Btu/hr-ft²-°F
$A(i)$	=	heat transfer area between Freon and core wall, ft²
$T_w(i)$	=	wall temperature of core segment "i", °F
$M_w(i)$	=	mass of core wall segment "i", lbm
C_{pw}	=	specific heat of core wall metal, Btu/lbm-°F
C	=	conductance between core wall segments, Btu/hr-°F
$T_w(i-1)$	=	wall temperature of core segment "i-1", °F
$T_w(i+1)$	=	wall temperature of core segment "i+1", °F
$Q_e(i)$	=	heat loss from wall segment "i" to evaporate water, Btu/hr
β	=	water spray angle
$f(\beta)$	=	cumulative mass of water sprayed into core up to angle β as a fraction of the total
ϕ	=	curve fit constant equal to the water spray angle at $f(\beta) = 0.5$
n	=	curve fit constant equal to the slope of $f(\beta)$ at $f(\beta) = 0.5$

INTRODUCTION

Because the nature of the Space Shuttle mission is different from previous spacecraft, new challenges were faced in the design and development of the Orbiter Active Thermal Control Subsystem (ATCS). Hardware weight and volume have always been of paramount concern in spacecraft design. However, they take on added importance for the orbiter since it is reusable and every pound of hardware weight must be launched to low earth orbit a maximum of 100 times during the life of the vehicle. Economics also had a stronger influence on the orbiter hardware design than on previous spacecraft. Every pound of orbiter equipment displaces a pound of payload and the revenue that could be realized from that payload.

Reliability, ground maintenance and turn-around time also were strong considerations in the system design phase. In order to provide an economically viable Space Transportation System, the Shuttle must be kept flying with a maintenance philosophy approaching that of a commercial airline.

These design drivers made it doubly important to optimize the ATCS from a performance, weight and volume standpoint, while providing sufficient redundancy and flexibility to accommodate failures during flight without adversely affecting the mission or ground turn-around time.

Extensive system engineering optimization studies, a basic research program, sophisticated dynamic computer analyses and extraordinary testing were used to meet the ATCS challenges.

Both system and component level challenges were encountered during the design and development phases of the Shuttle ATCS program. Some of the most challenging areas are discussed in the following sections.

SYSTEM DEFINITION

Providing the desired flexibility at minimum weight and volume was the biggest challenge at the system level. The ATCS performs the following three basic functions:

- Cools or heats other subsystems through interface heat exchangers.
- Transports heat from sources to sinks by means of dual Freon coolant loops.
- Rejects heat by various means dependent on mission phase.

A functional block diagram of the subsystem is shown in Figure 1.

ORIGINAL PAGE IS
OF POOR QUALITY

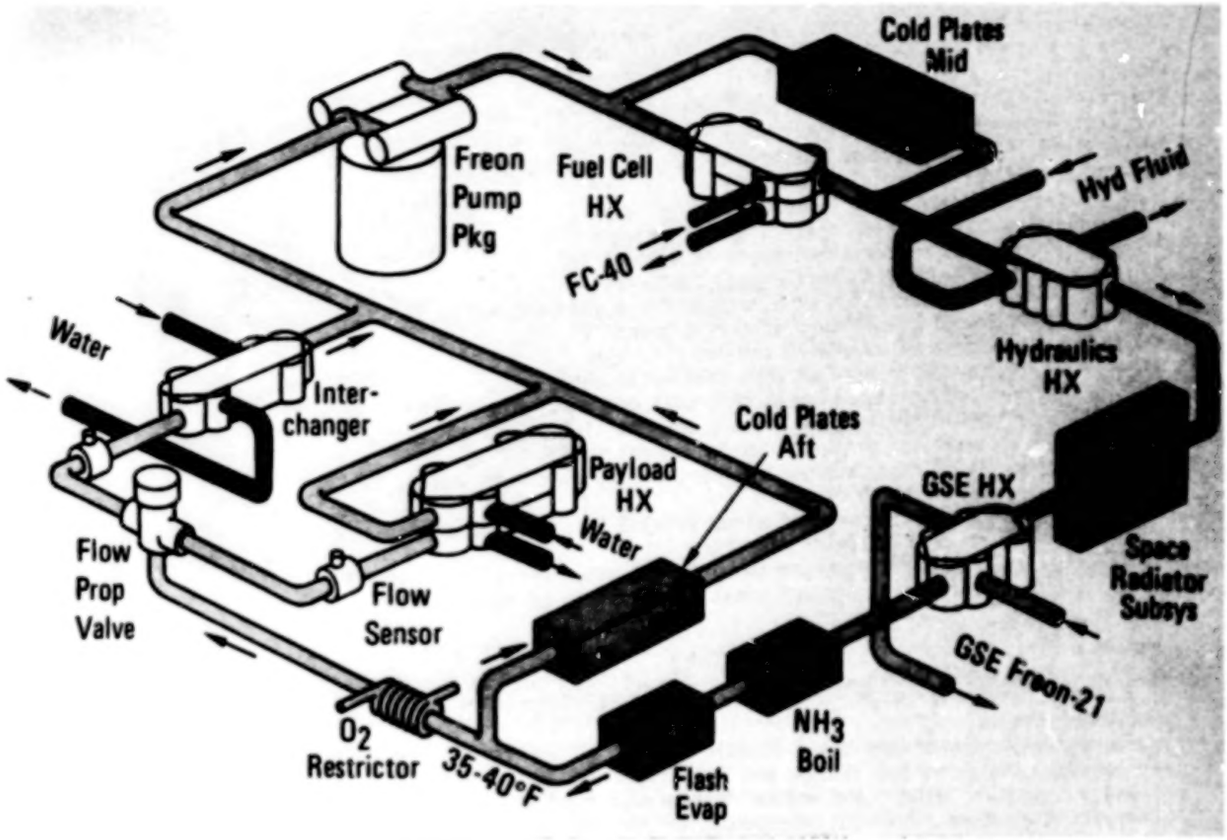


FIGURE 1 FREON COOLANT LOOP SCHEMATIC

Other equipment cooled or heated by the ATCS includes:

- o Cabin Atmosphere Revitalization Subsystem - two redundant water coolant loops.
- o Fuel Cell Power Systems - three separate FC-40 coolant loops.
- o Payloads - two separate payload coolant loops using either Freon or water.
- o Hydraulic Systems - three separate hydraulic fluid loops.
- o Cold Plate mounted electronic equipment.

(Only one each of the interfacing coolant loops is shown in Figure 1.)

Heat transport from heat sources to heat sinks is provided by dual Freon-21 coolant loops (only one loop is shown in Figure 1). Extensive trade-off studies were performed during the shuttle definition phase to arrive at the optimum mode of operation. The mode selected was that of operating both Freon loops normally with single loop operation only in a failure mode providing on-line redundancy rather than standby redundancy. This approach saved considerable fixed weight and power over an approach where a single loop provides total cooling during normal operation with the second redundant loop on standby. The dual loop approach does require redundant pumps in each loop and a reduction in heat load (power usage) from normal when only one loop is operating. This, however, was deemed acceptable in a failure case and does not adversely affect the safety of the crew and vehicle.

Heat rejection must be provided during a number of vastly different mission phases by different means. Trade-off studies during the shuttle definition phase resulted in the need for four different heat sink devices to provide heat rejection during all of the mission phases. The major mission phases and the type of heat rejection provided are:

- o Prelaunch/Postlanding - ground support equipment cooling
- o Launch - thermal inertia
- o Ascent/Entry - water evaporation
- o On-orbit - space radiation with supplemental water evaporation
- o Landing - ammonia evaporation

Prior to launch and at some time after landing, cooling is provided by a ground cart refrigeration system. A trade-off study was conducted that resulted in the use of a permanently installed Ground Support Equipment (GSE) heat exchanger in the orbiter cooling loops to interface with the ground cooling loop. Cold Freon is supplied to the vehicle through fly-away quick disconnects. The high GSE Freon flow and cold temperature minimize heat exchanger size and weight. Although a small weight penalty results because the unit must be carried into orbit every mission, isolation is provided between the vehicle and ground loops resulting in a much safer and more reliable design.

Heat rejection during the on-orbit mission phase is provided by radiation to space. This was an obvious choice over expendable evaporation. If water was used as an evaporant, approximately 16,400 lb would be required for a seven day mission (maximum payload heat load) while the fuel cell would produce only 2400 lb (available for heat rejection). The difference (14,000 lb) would have to be carried to orbit resulting in a tremendous weight penalty.

Water evaporation was the choice, however, for heat rejection following launch until the space radiator is deployed and during entry after the radiator is stowed inside the payload bay doors. These mission phases are relatively short and the launch weight penalty is small. Water is used as the evaporant because it has a latent heat of vaporization double that of any other potential evaporant, and it can be replenished on-orbit by the fuel cells.

The water evaporation pressure (saturation pressure) and corresponding saturation temperature must be maintained at low enough levels (less than 0.1 psia and 35°F) to cool the Freon loops to 40°F. An altitude above approximately 140,000 ft must be reached before the desired ambient pressure is attained. For this reason water is not an acceptable evaporant for launch and landing.

Prior to launch, cooling is provided by ground support equipment. It takes the shuttle slightly over two minutes to reach an altitude where water evaporation becomes effective. There is sufficient thermal inertia in the system to limit the Freon loop temperature rise that active heat rejection is not required for the first two and a half minutes of launch.

An ammonia boiler is used to provide cooling during the last ten minutes of flight and until ground support equipment is connected (about 10 to 15 minutes following landing). This 20 to 25 minute period is too long to rely totally on thermal inertia. Ammonia, although toxic, is the most efficient evaporant with the exception of water, having a latent heat of vaporization about half that of water. But, because of the short time period involved, the quantity of ammonia required is small.

SYSTEM LEVEL CHALLENGES

An integral part of the system level trade-off studies and one of the greatest ATCS challenges was defining an efficient means for interfacing the two Freon coolant loops with the multiple cooling loops from other systems. The result was an innovative heat exchanger design approach that allows heat transfer between four or five separate cooling loops in a single unit. Another major challenge resulting from the system level studies was the design and development of a highly responsive, long life, low maintenance water evaporator that operates over a large range of heat loads with a gravity range from 0g to 3g's. Both of these component challenges are discussed in detail in the following sections.

INTERFACE HEAT EXCHANGERS

Optimization of the Orbiter ATCS required advances in the state-of-the-art of compact heat exchanger design and manufacture. In the areas of fin density, flow configuration and headering, the heat exchanger designs have gone beyond anything previously manufactured for the space program.

The design of these heat transfer devices was approached with a concentrated effort to minimize weight, volume and power impact on the vehicle.

Fin Optimization

Optimization studies concluded that, to a practical limit, the highest density design yields the lightest and smallest unit. A measure of the compactness of a heat exchanger, both from a weight and volume standpoint, is the term (A/V), heat transfer area divided by core volume. This term is plotted against fin height and number of fins per inch (FPI) in Figure 2.[1] Fin heights ranging from 0.010 to 0.200 inches and FPI ranging from 8 to 48 were investigated. The obvious conclusion is that denser fins yield higher values of A/V.

The shorter more dense fins give the added advantages of higher fin efficiency, improving heat transfer performance and the ability to use thinner parting sheets reducing weight. Smaller core sizes also result in smaller, lighter headers, lighter core bands, passage closure bars and mounting feet and less fluid weight.

Prior to the shuttle program, the densest fin configuration successfully manufactured by Hamilton Standard in stainless steel was a fin height of 0.050 in. and 24 FPI. After reviewing manufacturing limitations it was concluded that fin heights as small as 0.020 in. and FPI as high as 32 could be manufactured with some development and this fin configuration was selected for use on the orbiter. They resulted in a 55% improvement in A/V.

In order to size and predict the performance of heat exchangers with the selected fin density, existing fin data for Coburn and friction factors had to be generalized and extrapolated to fin heights 40% less and FPI 33% greater than that for which data was available. A number of manufacturing challenges were also faced. Techniques for manufacturing the dense fin material were refined. New techniques for fixturing and brazing cores were developed. Techniques were also developed to seal minute leaks at closure bars and between layers in order to meet the extremely low leakage rate required by the Orbiter ATCS.

In optimizing a design for a given set of requirements, total equivalent weight including heat exchanger, fluid and power equivalent weight must be considered. Figure 3[1] presents an example of this trade-off for the Interchanger that cools the cabin water loops.

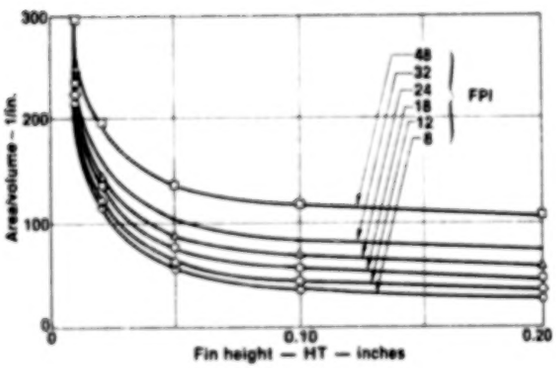


FIGURE 2 FIN OPTIMIZATION

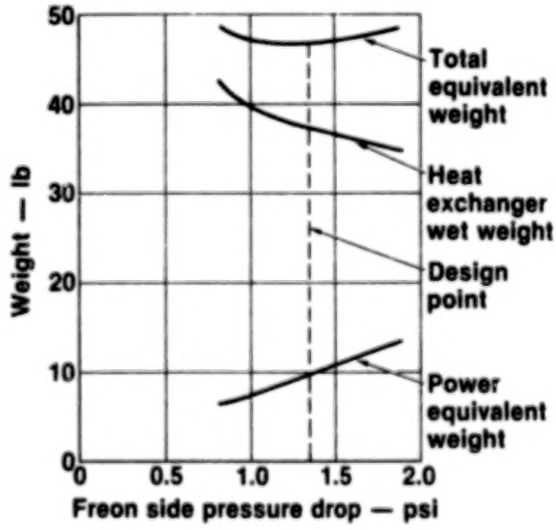


FIGURE 3 INTERCHANGER OPTIMIZATION

In all cases except the Hydraulics heat exchanger the optimum fin configuration was a height of 0.020 inches and 32 FPI. Because of the very viscous hydraulic fluid, that heat exchanger optimized at a fin height of 0.050 inches and 32 FPI.

Configuration Optimization

In each of the five different ATCS applications (coolant loop interfaces), various heat exchanger system configurations or arrangements are possible. Two of the applications will be discussed as examples. Figure 4 shows three of the configurations considered for the Interchanger. Both the 4 two-fluid and 2 three-fluid heat exchanger configurations proved to be heavier in total equivalent weight than the single four-fluid unit. In addition, a single heat exchanger shows a considerable cost advantage over multiple heat exchangers.

Even though one of the ARS water loops is not operating normally, very little performance is lost in the four-fluid heat exchanger because of the way in which the layers are arranged. Figure 5 shows this arrangement. Each active water loop layer has an active Freon loop layer on either

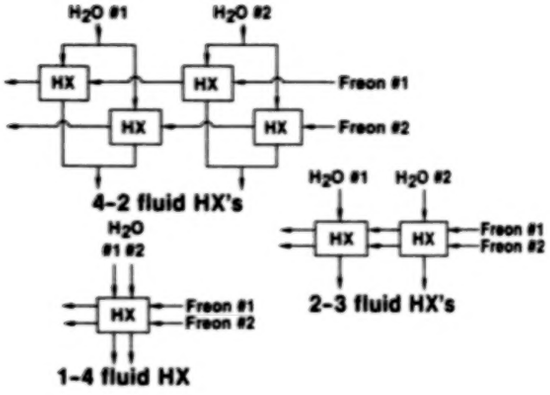


FIGURE 4 INTERCHANGER CANDIDATE APPROACHES

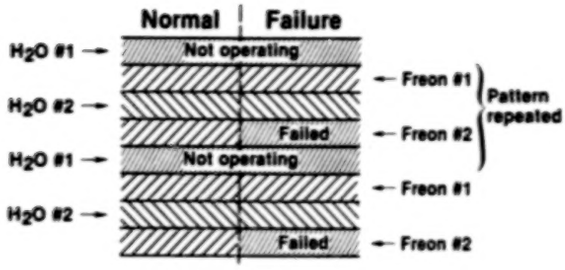


FIGURE 5 INTERCHANGER LAYERS

side resulting in high performance. The only performance difference over a two-fluid heat exchanger is that the effective fin height of the Freon layers is doubled resulting in a slight loss of UA. However, with the short fins the performance degradation is small. In the event one of the two Freon loops fails, each active water layer still has an active Freon layer on one side but must conduct heat through two dead layers on the other side. Again, because of the short fin height the performance degradation is minimal due to a loss of UA.

The second example of a system configuration trade-off is for the fuel cell heat exchanger. In this case, the interfacing of five coolant loops must be accomplished. Figure 6 shows the options considered, a 6 two-fluid, 3 threefluid, and a single five-fluid heat exchanger approach. The single five-fluid unit is actually 2 four-fluid heat exchangers manufactured in a single stack. Trade-off studies showed the single five-fluid heat exchanger to be lightest in total equivalent weight.

A refinement of the selected approach was effected by building up the two heat exchanger cores in a single stack making one unit with appropriate headering. This again shows a cost advantage over multiple units.

A different layer arrangement was required for the fuel cell heat exchanger from that presented for the Interchanger. This is shown in Figure 7. Any one, two or three fuel cell loops can be effectively cooled by either or both Freon loops.

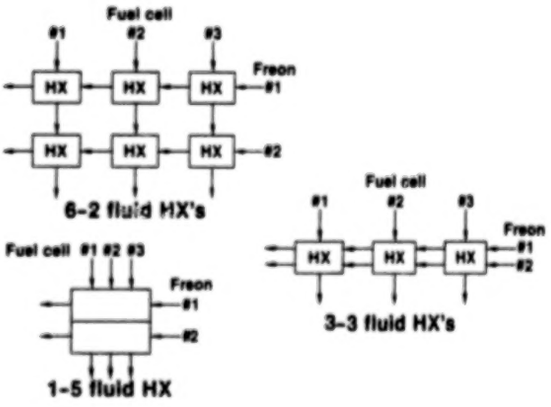


FIGURE 6 FUEL CELL HEAT EXCHANGER CANDIDATE APPROACHES

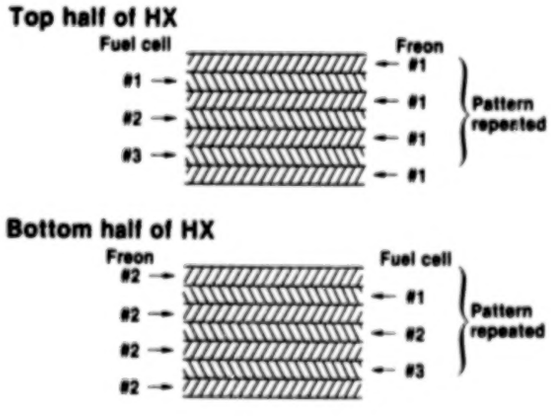


FIGURE 7 FUEL CELL HEAT EXCHANGER LAYERS

Headering

In order to achieve high performance, counterflow within the heat exchanger core is desired. When flowing four separate fluid loops through the same core efficient headering is difficult. A novel combination of internal and external headers was devised that provides counterflow through most of the core. Figure 8 presents two layers of a typical heat exchanger showing the semicircular external headers and the flow distributing internal finned headers. The triangular ends of the core are called "tent tops". One of the fluids enters the core on the end of the tent top, flows the length of the core and exits on the opposite side of the other tent top. The other fluid enters at the side of the core in the tent top area, flows the length of the core in the other direction and exits on the opposite side. As can be seen most of the core is counterflow. The internal header finned sections are well slotted to aid in flow distribution. Poor flow distribution that adversely affected thermal performance was observed during initial development testing of an Interchanger. Tolerance studies indicated that fin passages near the edge of the core could be blocked. A computer flow distribution analysis was conducted that defined the slotting required in the inlet sections to properly distribute flow. Subsequent units exhibited no maldistribution or performance deficiencies.

The final configurations for the Interchanger and fuel cell heat exchanger are shown in the photographs of Figures 9 and 10.

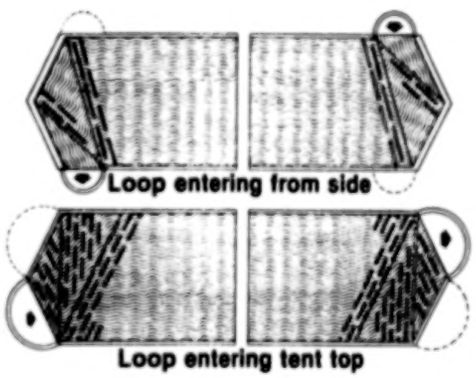


FIGURE 8 TYPICAL HEAT EXCHANGER FIN CONFIGURATION



FIGURE 9 FUEL CELL HEAT EXCHANGER



ORIGINAL PAGE IS
OF POOR QUALITY

FIGURE 10 INTERCHANGER

WATER EVAPORATION

Water evaporation was selected as a heat rejection means for the following reasons:

- o Water is the best evaporant from a weight standpoint since it has the largest latent heat of vaporization of any candidate fluid. This minimizes the evaporant weight penalty for cooling required during launch and an abort following launch.
- o A large quantity of excess water is produced by the fuel cell power system. Although not nearly enough water is produced for total heat rejection during the entire mission, water is available for supplementary heat rejection on-orbit when the vehicle attitude reduces the radiator capability.
- o A water evaporator can be used to expel excess water as steam when the water storage tanks reach maximum capacity. The steam can be expelled at high velocity through a nozzle and directed away from the vehicle to reduce contamination of the environment in the immediate vicinity.

Previous spacecraft used water evaporators for heat rejection. Mercury, Gemini and the Apollo command module used wick-feed boilers and the Lunar Module, Saturn V and Apollo space suit used porous plate sublimators. All of these devices have response, heat load range and life limitations. Early in the shuttle program, NASA concluded that a new concept for water evaporation would be advantageous and the flash evaporator evolved.

Flash evaporation involves spraying water on the walls of a chamber that is heated by Freon coolant. The spray chamber is maintained at a pressure (saturation pressure) low enough for the water to evaporate at a temperature below the desired Freon outlet temperature. Since a Freon outlet temperature of 40°F maximum is required, the chamber pressure must be maintained at or below about 0.1 psia (35°F saturation temperature). In flash evaporation, it is imperative that all of the water that reaches the wall be instantly evaporated to prevent excessive carryover or flooding and eventual freezing causing failure of the device.

The low evaporation pressure is maintained on-orbit by venting the steam generated overboard to space vacuum through a sonic nozzle. As the heat load is reduced, the pressure will fall because of reduced steam flow and may drop below the triple point aggravating the potential freezing situation.

In the flight unit, water is introduced into the chamber in a pulsing manner for temperature control reasons. This causes the chamber pressure to fluctuate during each cycle with minimum pressures below the triple point. A detailed description of the Flash Evaporator Subsystem and a discussion of its flight performance are presented in Reference 2 and 3 respectively.

Because of the potential freezing problems and the dynamic nature of flash evaporation, it was necessary to perform extensive analyses and to conduct basic research on flash evaporation to thoroughly understand the process and aid in the design of the flight system.

Three typical areas of investigation concerning the design and development of the flash evaporator are detailed in the following sections:

- o The basic research program conducted at Rice University to better understand the process.
- o The analytical effort in the form of a thermal math model performed during the design and testing phases.
- o Flash evaporator and integrated ATCS testing conducted at NASA-JSC.

In addition to the above, significant effort was expended in developing the desired hollow cone water spray distribution and droplet size distribution and in analyzing the steam flow pattern and velocities within the evaporator using finite element techniques to predict water droplet carryover.

FES Description

A brief description of the flash evaporator subsystem is in order before the details of its operating characteristics are discussed. A more detailed description can be found in Reference 1 and 2.

The FES (Figure 11) contains two evaporators, three controllers (two primary and one secondary), two sets of feedwater spray valves, nine temperature sensors and thermostatically heated exhaust steam ducts. Figure 12 presents the FES schematic. Freon flows in two loops through both evaporators in series - first, through a "high load" unit, then through a "topping" unit. Both evaporators operate during launch and entry but only the "topper" operates in orbit.

ORIGINAL PAGE IS
OF POOR QUALITY

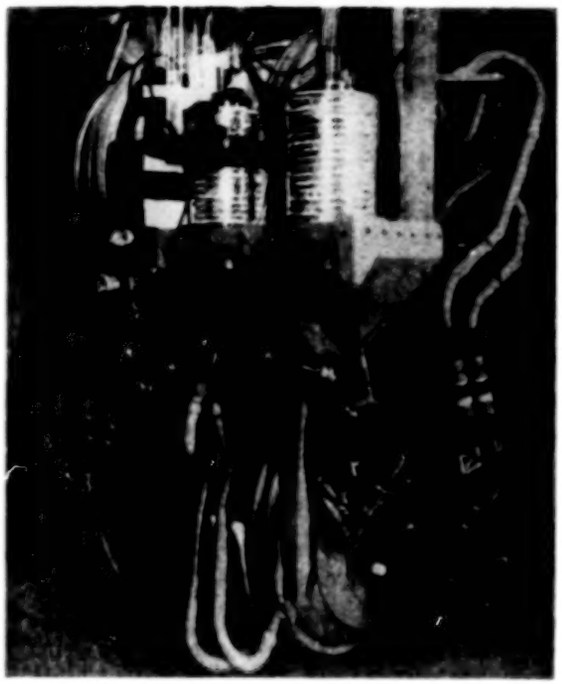


FIGURE 11 FLASH EVAPORATOR PACKAGE

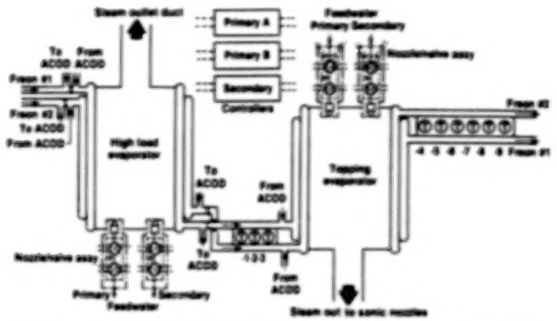


FIGURE 12 FLASH EVAPORATOR ASSEMBLY SCHEMATIC

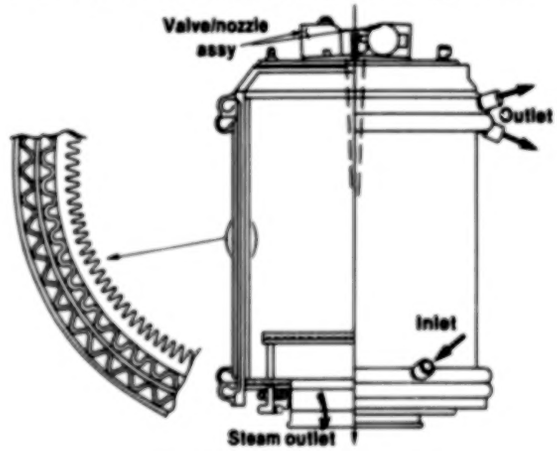


FIGURE 13 SHUTTLE EVAPORATOR

Each evaporator consists of three basic parts made of aluminum alloy: the evaporator core, the spray valve/nozzle mounting plate, and the anti-carryover device (ACOD). The cylindrical core contains the primary heat transfer surface area. At one end of the core, the valve plate provides a heated mounting surface for the spray valves. At the opposite end of the core, the anti-carryover device aids in evaporating any water carried by the steam flow before it leaves the evaporator.

In order to enhance the evaporative heat transfer area and water retention, the internal surfaces of the cores are grooved in an axial direction as shown in Figure 13. Two concentric annular finned passages carry the dual Freon loops longitudinally within each core from the anti-carryover device to the valve plate end.

Each valve/nozzle assembly contains an isolation valve, pulser valve, and spray nozzle. The spray nozzle distributes feedwater over the evaporator heat transfer surface. The pulser valve is pulsed open for 200 msec at a variable frequency to meter feedwater flow. The isolation valve provides redundant sealing of the feedwater line during quiescent periods and isolation of the feedwater following failure of a pulser.

Three temperature sensors monitor Freon midpoint temperature (between evaporators) and six monitor Freon outlet temperature. The three midpoint sensors and three of the outlet sensors are used by the control sections of the three controllers, and the remaining three outlet sensors are used by the three shutdown sections of the controllers.

Once activated, FES startup and shutoff is programmed as a function of midpoint Freon temperature. Freon outlet temperature is maintained within a band of 39 $\pm$ 1°F by one of the redundant primary controllers.

Circuitry in the secondary (abort) controller is similar to the primary controllers, except the control set point is 62 $\pm$ 2°F.

Each controller has a shutdown section physically isolated from the control section. Each shutdown section monitors the performance of the controller through a Freon outlet temperature sensor. If temperature or rate of change limits are exceeded the FES is shut down.

There are two separate steam ducts. The high load duct is relatively short (7.5 ft) with few bends. The topping duct exhausts overboard through two thrust balancing nozzles, one on each side of the vehicle. The distance from the evaporator to each nozzle is approximately 21 ft.

Basic Research Program

A spray cooling research program was initiated by Rice University, Houston, Texas, under NASA Grant NAS 9-65274. Results were reported to NASA-JSC in three separate reports during 1979 and also documented in Reference 4.

The purpose of the research, summarized in this section, was to identify the fundamental heat transfer processes involved in spray cooling, to provide experimental data useful to the design engineer, and to add to the general understanding of the overall spray cooling process. Secondarily, the effect of grooving the heat transfer surface was also evaluated.

Three distinct operating modes of spray cooling have been identified. The first is the case in which the surface vaporizes all of the impinging spray. This is called the "dry-wall" state, and the heat transfer process in this mode is called "spray evaporative cooling". The second operational mode is that in which the spray forms a thin liquid film upon the surface. This is referred to as the "flooded" state and "spray film cooling" is the name given to the associated heat transfer process. The third operational mode is that in which the liquid droplets are deflected from the surface by a thin vapor film which forms on impact. This is called the "Leidenfrost" state and heat transfer. A number of studies of these heat transfer processes has been reported in the literature. A listing of the references can be found in Reference 4.

The research conducted at Rice was primarily concerned with the dry-wall state and with the transition from it to the flooded state. The crux of the experimental investigations was determining, for spray evaporative cooling, the locus of flooding points -- that is, determining the wall temperature and corresponding heat flux at which the dry-wall to flooding transition occurs. This yields the maximum possible heat flux for each surface temperature during dry-wall operation.

The influence of various parameters upon this flooding locus was investigated. The effects of surrounding pressure, from atmospheric to just below the triple point of water were studied. The influence of a grooved surface compared to a smooth polished surface was studied. The influence of feedwater temperature and the influence of an intermittent-pulsing spray were also investigated.

The heat flux (q) during dry-wall operation is directly related to the impinging spray mass flux ($\dot{m}$). Assuming no superheating of the departing vapor

$$q = \dot{m}[\lambda + C_p(T_s - T_o)] \qquad (1)$$

where λ is the latent heat of vaporization of the spray liquid, C_p is its constant pressure specific heat, T_s is its saturation temperature, and T_o is its supply temperature. What is of interest is the wall temperature (T_w) and corresponding heat flux (q) range over which the dry-wall mode of operation may exist for a given spray mass flux.

In dry-wall operation, the wall temperature and heat flux adjust so that all the impinging spray evaporates without accumulation on the surface. If the surface temperature is lowered, with the spray unchanged, a point is reached where the droplets no longer evaporate as fast as they arrive, and liquid will begin to accumulate on the surface. This flooding point is the lower limit for spray evaporative cooling (dry-wall mode). The transition to the flooded state will be a gradual, progressive change when T_w is greater than the nucleate boiling temperature T_b of the thin liquid film. The transition is sudden, or catastrophic, when T_w is less than T_b.

Experimentally the two primary quantities to measure are the surface temperature and the heat flux through the metal surface upon which the water spray is impinging. The technique employed was to measure the axial temperature profile along an insulated aluminum cylinder heated on one end and cooled by the water spray on the other end. From this temperature profile, both the heat flux through the surface and the surface temperature were readily determined. The liquid spray was directed at the sample surface from a nozzle located above the sample; the mass rate of impingement of spray on the surface was not measurable. For a given spray mass flux, steady state operation was achieved with a temperature feedback control circuit to adjust electrical power to the heater. The entire assembly was placed in a bell jar in which the pressure was controlled by exhausting through an orifice to a liquid nitrogen cold trap by means of a vacuum pump.

Beginning with the surface in a dry-wall state, the set point to the temperature controller was lowered gradually until the surface just began to flood. At this point data was recorded. It

should be noted that "flooding" was a subjective visual determination based upon the experimenter's evaluation that the surface was just on the verge of flooding, small pools just beginning to form. For the smooth polished surface this was fairly straight forward. For the grooved surface, however, flooding was a bit more difficult to define. It was chosen as the point where some water could be standing in the grooves, but never enough to allow spanning of the grooves.

Using distilled water at 25°C sprayed from a 0.40 mm dia., 90° included angle, full-cone nozzle located approximately 45 cm above the surface, the flooding locus was determined for a smooth 6061-T6 aluminum surface at atmospheric pressure, and at average pressures of about 19, 6.76, and 4.56 mmHg. These flooding locus curves are shown in Figure 14 (data points have been eliminated for clarity).

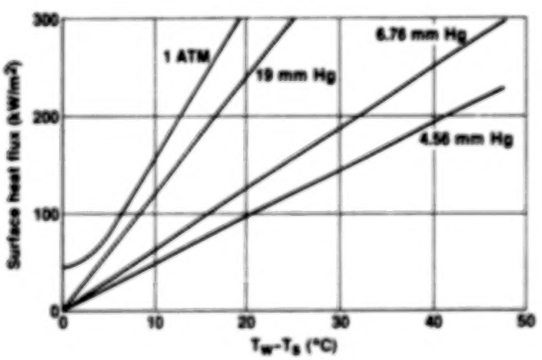


FIGURE 14 FLOODING LOCUS

For a grooved aluminum surface, the flooding locus was determined at atmospheric pressure, and average pressures of about 20.18, 7.11, and 4.51 mmHg. It was found that grooves on the surface had no apparent effect on the flooding locus or dry-wall operation. However, based on testing conducted at Hamilton Standard, grooves do improve water retention and help spread unevaporated water to less stressed areas in a flight evaporator configuration.

Knowledge of the flooding locus is particularly important for operation at pressures below the triple point of water (4.587 mmHg). At such pressures, excess water on the surface creates the potential for freezing. For both surfaces studied, at pressures below the triple point, it was observed that for values of $T_w - T_s$ less than about 15°C, freezing would begin at the interface of the heated surface and the surrounding Teflon insulation (the coolest points on the surface). The ice formation then moved rapidly inward above the surface and formed an ice cap over the entire surface. Once formed, increasing the heating rate through the surface would not stop the ice growth (the surface just got hotter). The only way to halt the growth of the ice cap was to raise the pressure to a value above the triple point. On doing so, melting began immediately. Increasing the pressure proved to be the only effective means of controlling ice formation. A procedure for doing this on the flight unit was developed during testing at NASA-JSC.

Water freezing and accumulating on poorly heated surfaces was also experienced on the flight configuration evaporator. Great care was exercised in the design of the core to assure that all areas receiving spray would be heated sufficiently to prevent ice formation.

Testing was conducted using a pulsing-intermittent rather than a steady state spray at low pressure. A nozzle with a solenoid valve was operated with a fixed "on-time" of 200 msec and an on-off pulsing frequency variable between 0 and 4 hz, thus allowing the spray "duty cycle" to be varied. Tests were run at 7.11 mmHg and at atmospheric pressure. Attempts were made to operate at pressures below the triple point, but at these low pressures the accumulation of water on the nozzle negated proper spray operation. This accumulation of water on the nozzle at very low pressures is thought to be associated with solenoid operating in the nozzle; it was not observed at pressures above the triple point or for continuous operation. A great deal of development effort was spent on the flight configuration spray valves to reduce the valve "dribble volume" and prevent valve freezing.

The results obtained suggest that with pulsing duty, the spray evaporative cooling process is not basically different from that with continuous duty. The flooding locus is the same in either case; it occurs, for a given wall temperature, at a heat flux lower than continuous duty by the ratio of the duty cycle of the pulsing spray.

A number of measurements were attempted at low pressures using feedwater at temperatures greater than 25°C. It was found that for water temperature greater than about 40°C, the water droplets leaving the nozzle "instantaneously" evaporated -- flash evaporation -- particularly in the interior of the spray. The large vapor plume so formed negated a reasonably steady spray reaching the heated surface in the apparatus used. It was concluded that for a given system operating pressure, there is an upper limit on the feedwater temperature above which the effectiveness of the spray evaporative cooling process is negated because of the spray flashing directly to vapor before reaching the surface to be cooled.

All of the flooding locus data obtained in the experiments at Rice University may be summarized, as shown in Figure 15, by defining a "flooding coefficient"

$$h^* = q^*/(T_{flood} - T_s) \qquad (2)$$

which is simply the slope of each flooding locus, and is dependent upon the operating pressure, or perhaps more conveniently the saturation temperature of the liquid spray. For the designer, the variable of interest is the wall temperature T_w rather than $(T_w - T_s)$. Figure 15 could be used to determine the best operating pressure (saturation temperature) to yield the largest attainable heat flux without flooding.

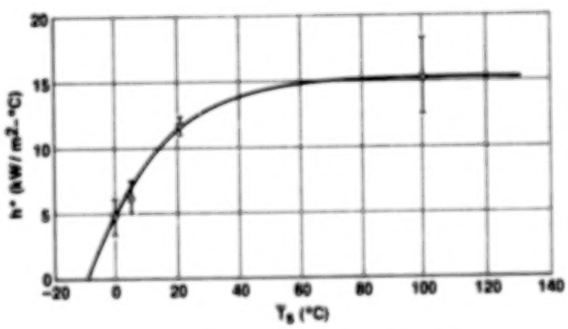


FIGURE 15 FLOODING COEFFICIENT

The linear flooding loci determined experimentally suggest that a conduction-controlled droplet evaporation model might serve as an adequate analytical model for predicting the flooding coefficient h*. Such a model was developed and documented in reports to NASA-JSC under the previously mentioned NASA grant. Agreement of the analytical results for atmospheric pressure with those obtained from experiment are close enough to give confidence in the model and suggest that further study might yield fruitful results.

FES Thermal Model

A computer model of the FES was written to study and predict its dynamic behavior. This model includes the effects of water spray distribution on the core walls, dual Freon loops at varying inlet conditions, cyclic steam pressure resulting from a pulsing water spray and steam exhaust duct flow characteristics and the control laws that modulate spray pulsing to control Freon outlet temperature. The highly dynamic nature of the FES results from the short 200 millisecond pulses of water sprayed onto the core at controlled intervals and the low thermal inertia of the evaporator. These pulses of water are rapidly evaporated upon contacting the hot core walls heated by the Freon. Steam pressure quickly builds up in the core as the water evaporates and then rapidly decays as the pulse of water spray ends and the steam exits from the duct. In the subsystem, the important dynamic parameters are the Freon temperatures, the amount of water sprayed into the core and evaporated, the steam pressure in the core, and the controller signals to modulate the short 200 millisecond pulses of water.

Freon temperatures are calculated throughout the subsystem. The evaporator is divided into an Anti-Carryover Device (ACOD) zone, a core wall zone, and a valve plate zone as shown in Figure 16. In the evaporator core wall zone where the temperature distribution is crucial to determine the amount of water evaporation, as fine a division of the core wall into segments as desired can be made. Figure 17 shows one of these segments as used in the computer model. Any loss of heat from the Freon to the core wall results in a decrease in Freon temperature; this is modeled for each Freon segment by applying the First Law of Thermodyanmics as follows:

$$M_f(1)C_{pf}\frac{d\bar{T}_f(1)}{dt} = \dot{m}_f C_{pf}[T_{fin}(1)-T_{fout}(1)]-h_f A(1)[\bar{T}_f(1)-T_w(1)] \qquad (3)$$

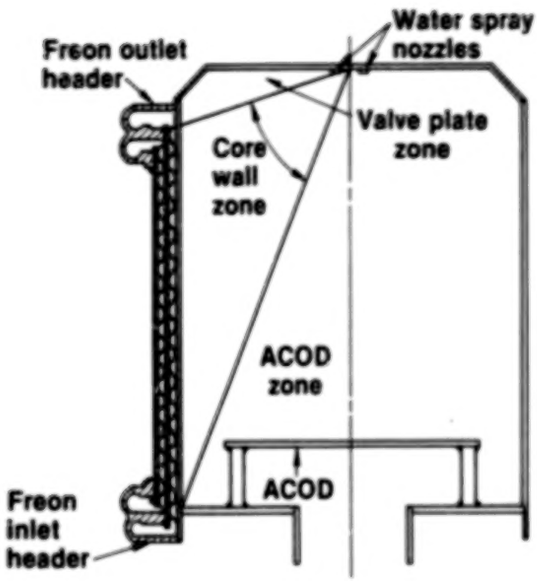


FIGURE 16 SPRAY ZONES

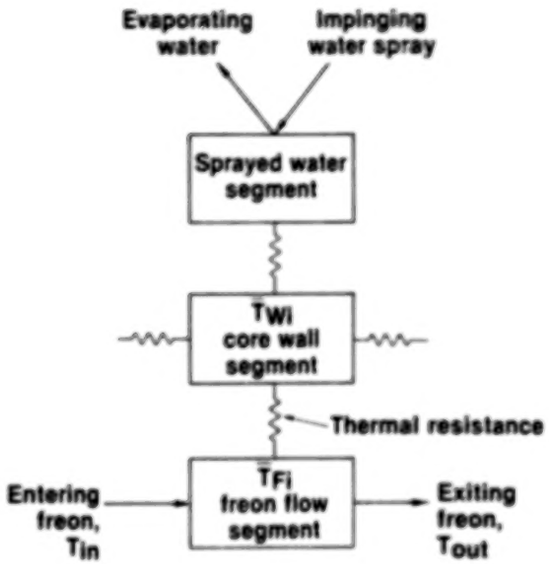


FIGURE 17 THERMAL MODEL

A similar energy balance is applied to the evaporator core wall whereby its temperature changes whenever an unbalance exists between the heat input from the Freon and the heat loss to the impinging water spray:

$$M_w(i)C_{pw}\frac{dT_w(i)}{dt} = C[T_w(i-1)-T_w(i)]-C[T_w(i)-T_w(i+1)]-Q_e(i)+h_f A(i)[\bar{T}_f(i)-T_w(i)] \quad (4)$$

The thermodynamics and heat transfer on the water spray is the most dynamic and the most challenging to model. The water leaving the nozzle impinges on the various zones and segments of the core in different amounts. This distribution varies with feedwater temperature and pressure and is different for the high load and topping evaporators. A spray distribution factor was defined and correlated to test data to arrive at the following expression which gives the general shape of all spray distributions:

$$f(\beta) = 0.5\{1 + \tanh[m(\beta - \phi)]\} \quad (5)$$

The factors ϕ and m are functions of feedwater temperature and pressure. A typical cumulative spray distribution is shown in Figure 18.

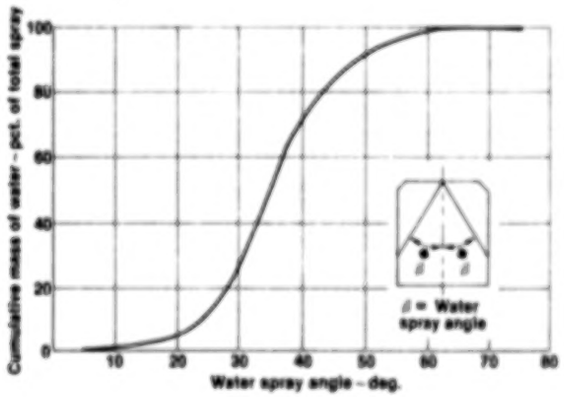


FIGURE 18 SPRAY DISTRIBUTION

The water impinging on a segment of the core is then evaporated at a rate dependent upon the difference in temperature between the wall and the temperature of the steam in the core. The temperature of the steam is at the saturation temperature corresponding to the pressure in the core. As the steam evaporates, the pressure and therefore the temperature rises in the core until the spray stops. Then, the pressure and temperature decrease as the steam exits the core. Steam pressure is a function of the flow characteristics of the exhaust duct system. Depending on the rate of evaporation, all the water impinging on the core may not evaporate before the beginning of the next spray pulse. The division of the core into segments permits the calculation of the precise spot where this buildup of water may occur. Division of the core into fewer segments would average over this spot and would not predict any water buildup when there actually may be one. This highly dynamic rising and falling of the steam temperature and pressure is therefore coupled in the model with the spray and wall temperature distributions to determine the amount of impinging spray that is evaporated in the core and thereby the heat removed from the Freon.

The pulsing of the spray is regulated by the controller to cool the freon to an outlet temperature of 39°F. To model the controller, the actual electronic circuitry was analyzed. As in the controller, the computer model translates the incoming temperatures into voltages and applies the control laws. The control includes a combination of proportional, integral and differential gains with lead-lag compensation. When the control law output voltage reaches six volts, a 200 millisecond spray pulse is initiated; and the control law output voltage is reset to zero. In addition to the control laws, the shutdown logic and the control laws for the secondary controller are included in the computer model.

Modelling the Flash Evaporator Subsystem on a digital computer presented a major technical challenge. More than twenty simultaneous partial differential equations with time constants sometimes orders of magnitude different had to be solved. The Gear Method,[8] which is a multistep predictor corrector method whose order and time increments are automatically chosen as the integration proceeds, was used effectively to produce computer running times as low as 1/3 of real time.

In spite of the inherent difficulty in modelling the highly dynamic FES, the computer program has been used successfully to predict test data, to establish acceptance criteria for controller operation, and to simulate ground test and flight operation.

FES Testing

The FES presented a performance verification challenge. Because of the size of the steam exhaust ducting, the actual flight configuration could not be tested at a commercial facility. FES performance testing was conducted using a duct simulator. The simulator consisted of a short duct section, a large diameter volume and adjustable exit orifice. The large volume was necessary to simulate the volume of the flight duct configuration. The orifice was adjusted to give the same steady state evaporator pressure as the flight configuration when operated in the Hamilton Standard chamber. Chamber pressure could not be maintained at space vacuum levels and reached 1 mmHg at maximum steam flow.

In order to fully qualify the FES for flight, it was deemed necessary to test the flight configuration under expected flight conditions. Two series of tests were conducted in the Space Environmental Simulation Laboratory (SESL) at NASA-JSC. It was necessary to use the large chamber A for these tests.

The first series of tests (OFEST) was conducted with a flight configuration FES as the only test hardware. Testing included:

- o Simulated launch and entry ambient pressure transients.
- o Simulated Freon inlet temperature transients.
- o Steady state performance limits.
- o Testing to help size the orifice in the duct simulator used at Hamilton Standard.
- o Steam exhaust plume evaluation.

The second series of tests (Integrated ATCS Tests) was conducted with a flight configuration FES plus additional ATCS hardware, including a space radiator panel, in an integrated system test. Testing included:

- o Actual system transient performance
- o Evaluation of failure conditions
- o Radiator panel performance

A major accomplishment of the testing relative to the FES was the establishment of a cleanout or thawing procedure in the unlikely event of a freeze-up on-orbit. Following the intentional flood-

ing of the evaporator, the secondary controller that controls Freon outlet temperature to 62°F was used to raise the evaporator steam pressure above the triple point. Under these conditions, thawing of ice accumulated in the core occurred quite rapidly and completely.

CONCLUSIONS

The major ATCS challenges were met using a combination of established system engineering techniques, basic research, sophisticated analytical techniques and extraordinary testing. In the process, advances in the state-of-the-art of heat exchanger design and manufacture were effected. These advances resulted in significant weight and particularly volume reductions over what were previously typical spacecraft heat exchanger configurations. In order to realize these gains, it was necessary to perform extensive system level optimization trade-off studies, extrapolate existing sizing techniques to much denser fin configurations and develop improved manufacturing techniques. All of the heat exchangers in the ATCS met or exceeded predicted performance during ground test and flight.

Flash evaporation at pressures below the triple point had never been attempted previously in spacecraft heat rejection. In fact, it was not a well understood process. A system, based on basic flash evaporation research and extensive analytical modeling, was developed that met all of the high response, high heat load range and long life requirements of the orbiter. The FES also can be considered an advance in the state-of-the-art in spacecraft expendable heat rejection. During the development process, basic knowledge of the spray evaporation process and how to control it was gained. With the exception of some minor temperature sensor anomalies on the first two shuttle flights, the FES has performed flawlessly.

REFERENCES

(1) Trusch, R. B., Nason, J. R., "Compact Heat Exchangers for the Space Shuttle", 75-ENAs-54, American Society of Mechanical Engineers publication, presented at the 5th Intersociety Conference on Environmental Systems, San Francisco, California, July 21-24, 1975.

(2) Nason, J. R., Decrisantis, A. A., "Shuttle Orbiter Flash Evaporator", 79-ENAs-14, American Society of Mechanical Engineers publication, presented at the 9th Intersociety Conference on Environmental Systems, San Francisco, California, July 16-19, 1979.

(3) Nason, J. R., Behrend, A. F., Jr., "Shuttle Orbiter Flash Evaporator Operational Flight Test Performance", 820883, Society of Automotive Engineers publication, presented at the 12th Intersociety Conference on Environmental Systems, San Diego, California, July 19-21, 1982.

(4) Grissom, W. M., Wierum, F. A., "Spray Cooling of a Heated Surface", published in the International Journal of Heat and Mass Transfer, Vol. 24, pp. 261-271, 1981.

(5) Gear, C. W., "DIFSUB for Solution of Ordinary Differential Equations", published in the Communications of the ACM, March 1974, Vol. 14, Number 3.

N85
16924

UNCLAS

D35

N85-16924

OTHER CHALLENGES IN THE DEVELOPMENT OF THE ORBITER ENVIRONMENTAL CONTROL HARDWARE

John W. Gibb and
M.E. McIntosh
Rockwell International
Downey, California

Steven R. Heinrich
Fairchild Control Systems Co.
Manhattan Beach, California

Franz Schubert, E.P. Koszenski, and R.A. Wynveen
Life Systems, Inc.
Cleveland, Ohio

Emory Thomas and Mike Steele
Defense Division
Brunswick Corp.
Costa Mesa, California

R.W. Murray, J.D. Schelkopf, and J.K. Mangialardi
Space Division
General Electric Co.
Valley Forge, Pennsylvania

ABSTRACT

Development of the Space Shuttle orbiter environmental control and life support system (ECLSS) included the identification and resolution of several interesting problems in several systems. Some of these problems occurred late in the program, including the flight phase. This paper addresses problems and solutions related to the ammonia boiler system (ABS), smoke detector, water/hydrogen separator, and waste collector system (WCS).

ABS problems were concerned with:

- Inducing vortex flow in the heat exchanger to improve heat transfer
- Accumulating contamination from ammonia as a result of evaporation in the heat exchanger
- Excessive carbon content, which developed while redrawing tubes to size resulting in corrosion and leakage
- Slower control system response to changes in temperature as a result of redesign to inhibit moisture entering the outlet temperature sensors

Smoke detector problems and solutions resulted in:

- Changing from a quartz crystal microbalance (QCM) sensing concept to an ionization sensor
- Understanding ion sensor operation during altitude changes
- Changing air pump design
- Revising pump motor design
- Modifying electronics hybrid design

Water/hydrogen separator problems and challenges included:

- Revising flow path lengths to meet pressure drop requirements
- Increasing H_2 removal efficiency by adding flow turbulators
- Techniques of welding tubes into a thin header plate
- Bundling of tubes to withstand shock and vibration environments

Waste collector system problems encountered and resolved during the orbiter flight test program involved:

- Restraint systems
- Last drop of urination removal
- Urine cap evaluation

AMMONIA BOILER SYSTEM

During the Space Shuttle orbiter entry mission phase at altitudes below 120,000 feet, the ammonia boiler system (ABS) provides a means for rejecting waste heat loads into the atmosphere. The ABS also provides cooling on the ground between postlanding but before the ground support cooling equipment is connected. Heat loads generated by Shuttle orbiter systems are transported within the vehicle by two separate and independent Freon 21 loops. When the ABS is operating, heat is transferred from the Freon 21 by evaporation of anhydrous ammonia, which is then vented overboard. The ABS is a completely self-contained system that uses a small amount of electrical power as its only outside supply requirement, and can transfer heat at a rate in excess of 120,000 Btu's per hour.

HEAT EXCHANGER DESCRIPTION

The ABS heat exchanger consists of four separate shell-and-tube modules. Figure 1 shows the tube bundle used in each module, the internal baffles, and the tube sheets. Each bundle contains 77 tubes that have an outside diameter of 0.093 inch and transport the ammonia internally. Each tube expands into each of the baffles to prevent flow bypass and to secure the tubes during vibration. The tubes are brazed into the tube sheets and the tube sheets are brazed into the shell to form a module. The Freon 21 makes five passes through the tube bundle in each module. Each of the tubes in the two ammonia outlet modules contains a spinner, which is a twisted metal ribbon divider that forms two spiral paths to impart a vortex-like flow to the ammonia in order to help increase the rate of heat transfer. The ammonia circuit, which consists of two modules, was sized to bring the superheated ammonia exhaust gas to within 10 °F of the inlet Freon temperature. All of the heat exchanger parts are fabricated from stainless steel and either brazing or welding is used to join parts in order to minimize weight.

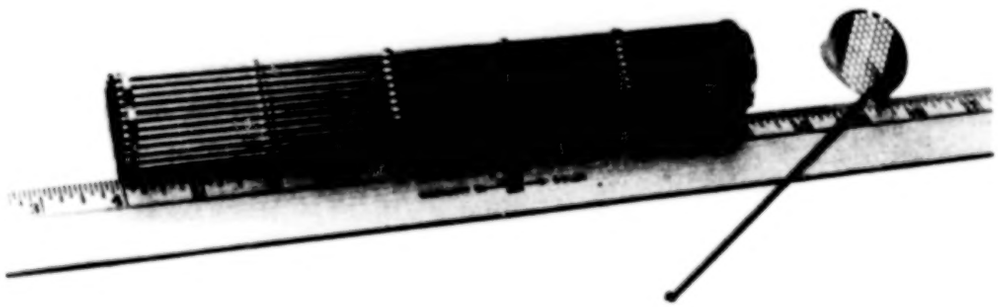


FIGURE 1. HEAT EXCHANGER MODULE TUBE BUNDLE

HEAT EXCHANGER DEVELOPMENT TESTING

In order to confirm the heat transfer and pressure drop characteristics of the heat exchanger, a simplified development unit was built early in the program. The unit consisted of two modules welded together with one counterflow Freon circuit. This configuration would normally be used to cool a single Freon loop. At the ammonia exit there was a long duct containing a bundle of 77 spinners that could be inserted into various positions in the ammonia tubes. The spinner was fabricated by twisting a flat piece of stainless steel to form a helix with about six turns per inch.

During the design phase, it was believed that the spinners would improve the low velocity heat transfer rate at the ammonia inlet end of the tubes by rotating the flow and throwing liquid droplets outward to the warmer tube wall. Initial test results were unusual and it was quickly determined that the best heat exchanger performance was achieved when the spinners were located in the downstream portion of the tubes where the ammonia was being superheated. Figure 2 shows some of the test data and the final spinner placement. When the spinners were inserted further upstream into the mixed (vapor/liquid) region, the liquid droplets probably gathered toward the center of the spinners and traveled down without the normal boiling that would occur when the liquid droplets contact the tube wall. The result was a loss of superheat in the ammonia discharge and a reduction in heat exchanger effectiveness.

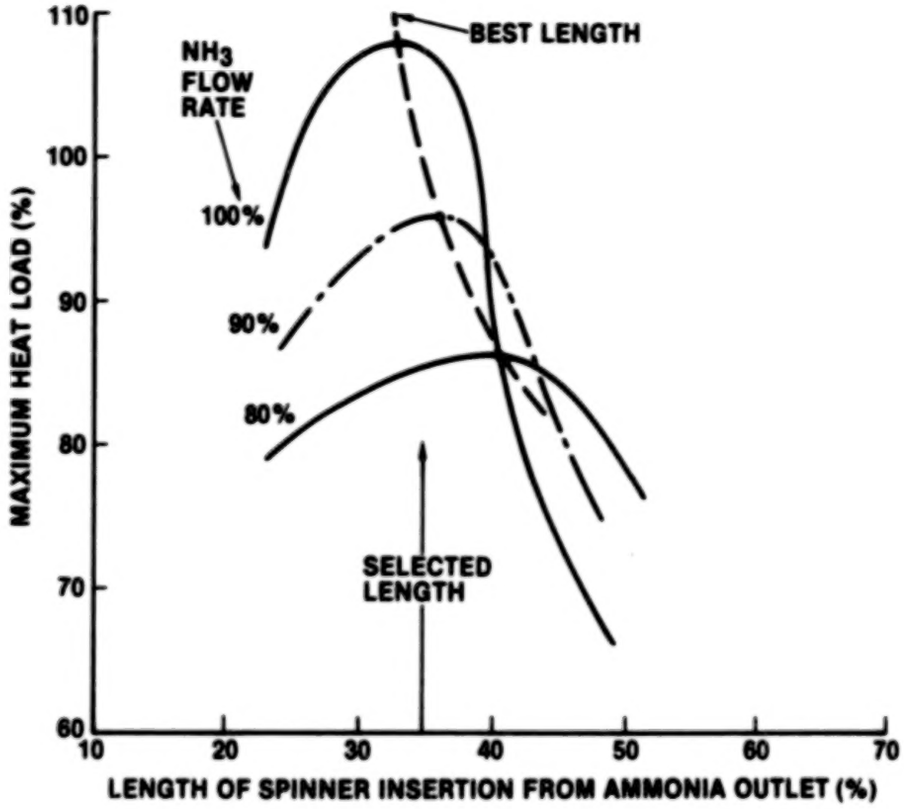


FIGURE 2. EFFECT OF SPINNER LOCATION ON PERFORMANCE

HEAT EXCHANGER CONTAMINATION

During development testing of the full-size heat exchanger with the spinners correctly placed, a loss in superheat was observed with some cold liquid ammonia droplets in the exhaust after considerable operating time. The degradation in performance, which resulted in an increase in ammonia flow rate to absorb the required heat load, was caused by the accumulation of oil in the ammonia tubes. A clean heat exchanger will transfer about 90 percent of the total heat load in the upstream module, but after only about 2 hours of operation, the heat transfer in the upstream module would be about the same as in the downstream module. It was apparent that the transition to dry vapor, which separated the boiling and superheat regions in the heat exchanger, was moving down the ammonia tubes toward the exit with operating time. After about 10 hours of operation, the ammonia side of the heat exchanger was flushed with a solvent. Analysis of the nonvolatile solvent residue disclosed that it contained 4 to 5 cubic centimeters of oil. Subsequent heat exchanger flushing operations that were performed after operating periods in excess of 10 hours indicated that a self-cleaning process limited the amount of oil that could accumulate.

After noticing the accumulation of oil in the heat exchanger, the oil content in the ammonia was monitored. Although the ammonia procurement specification required a 5-ppm maximum oil content and the supplier certified that the ammonia conformed to the specification, actual analysis showed approximately a 30-ppm content. An investigation of ammonia manufacturing, storage, and delivery systems revealed that the 5-ppm oil content limitation is not realistic for ABS operation. A 10-ppm limit appears to be more practical, but it is anticipated that periodic flushing of the heat exchanger will still be necessary for removing oil accumulation and restoring the desired heat transfer effectiveness level; however, instead of specifying a fixed operating time interval between flushing operations, the need for such cleaning on the orbiter will be established by monitoring the ammonia vapor discharge temperature to detect loss of superheat.

CORROSION OF HEAT EXCHANGER TUBING

At the conclusion of the qualification test program, it was determined that there was excessive leakage from the Freon side to the ammonia side of the heat exchanger. The areas were located that were leaking and metallurgical examination with a scanning electron microscope revealed a pitting corrosion attack on the stainless steel 3/32-inch diameter tubing. In the leaking areas, the corrosion had progressed through the 0.008-inch thick tubing wall.

Tubing for the development heat exchanger and for the assembly installed on Orbiter 101 for the approach and landing test program had been specified to be made from 347 CRES material. But delivery schedule problems caused a change to 304L CRES material to meet the manufacturing schedules for the test heat exchanger.

Although the specification for this material allows a maximum carbon content of 0.03 percent, chemical analysis of tubes showed that the actual carbon content was about 0.07 percent. The use of 304 series stainless steel with a carbon content greater than 0.03 percent is not recommended for brazing because of carbide precipitation, which occurs during cooling and results in a loss of corrosion resistance.

Since it was suspected that the tubing vendor had used the wrong material to redraw the tubing to its proper final size, additional tubing was ordered from a different vendor. This time, several samples were chemically analyzed prior to redrawing and found to have a carbon content of about 0.025 percent. After redrawing, chemical analysis of several samples showed a carbon content of about 0.07 percent.

Redrawing of the tubing to the proper final size (3/32-inch outer diameter, 0.008-inch wall thickness) requires multiple draws. Typically, hydrocarbon greases are used to help draw the tube through the dies. After each draw, the tubing is cleaned and annealed to soften the material prior to the next draw. As the tubing diameter becomes smaller, cleaning the grease from the tubing becomes more difficult. Apparently, the small residue of hydrocarbon grease that remained in the tubing after cleaning resulted in carburization of the tubing during the annealing process.

In order to prevent the carburization from recurring, two changes were made. First, after conducting an industry survey to determine practical tube cleaning procedures, a detailed procedure was prepared. Second, the tube material was changed back from 304L CRES to 347 CRES. Although the 347 CRES can also be carburized, substantial amounts of stabilizing elements (columbium and tantalum) make carbide precipitation less likely if a small amount of carburization takes place. Additional tubing was procured from a vendor who followed the recommended cleaning procedure. Samples taken before and after redrawing showed that no carburization had taken place and subsequent usage of this tubing has been successful.

TEMPERATURE SENSOR MOISTURE PROBLEM

Each Freon outlet loop has three surface-mounted platinum resistance temperature sensors to maintain the outlet temperature at a nominal 35 °F, based on a change in sensor resistance with changes in temperature. One sensor controls temperature through the primary control system. The second sensor controls temperature through the secondary control system, which duplicates the primary control system and is used only in the event of a primary control system failure. The third sensor is monitored by circuitry that switches control from the primary to the secondary control system if the Freon outlet temperature is excessively low for an extended period of time. All three sensors are identical in design and each is surface-mounted on the Freon line. The mounting surface of each sensor is coated with a thin film of thermal conducting grease to provide quick response from the sensor to changes in Freon temperature.

After the qualification test program during field operation, there were several temperature sensor failures. These failures were caused by moisture penetration into the porous ceramic insulating material between the platinum element and the metal-mounting baseplate. The ceramic exhibited very high bulk electrical resistivity when dry, but this resistance dropped rapidly when the smallest amount of moisture was absorbed.

The sensor assembly incorporates a fiberglass-reinforced silicone rubber cover to seal the platinum element from the ambient environment. Water immersion testing performed on this design showed a rapid degradation in insulation resistance between the element and the mounting base. Impregnation of the rubber cover with a silicone gel, which was previously used for moisture resistance in similar applications, decreased the rate of moisture penetration through the cover, but the bond between the rubber cover and the silver baseplate was not an adequate moisture seal. Attempts to improve this bond by roughening the silver plate surface and adding room temperature vulcanized (RTV) type silicone rubber were not successful.

In order to provide adequate resistance to moisture penetration, it was decided that the rubber cover should be replaced by a thin metal cover and soldered to the baseplate with multiple rubber seals where the lead wires extend through the cover. Because of the additional mass of the metal cover, it was anticipated that the time response of the sensor to temperature changes might be longer, and, therefore, result in system instability. Water immersion testing of this configuration showed no significant loss in insulation resistance after an extensive length of time; however, the results of system response testing were somewhat surprising. Although the response of the sensor was slower, there was no apparent effect on system stability. Instead, the slower response of the primary control sensor (RT_1) resulted in a longer temperature undershoot during start up. This increased time, monitored by the control transfer (RT_3) sensor, resulted in a transfer of control from the primary to the secondary system.

In order to solve this problem, the length of time required to transfer from primary to secondary control could have been increased, but this would have required an expensive change in the electronic controls. Instead, the thermal conducting grease under the RT_3 sensor was replaced by a silicone grease with a much lower thermal conductivity. The effect was to further slow down the time response of the RT_3 sensor to compensate for the slower time response of the RT_1 and RT_2 sensors.

SMOKE DETECTOR

Brunswick fire detectors are used in the avionics bay enclosures and the crew compartment in conjunction with a Halon suppression system to provide early warning and contain any potential hazards. Figure 3 shows their locations. To better understand the design problems and how they were solved, a brief description of the detector operation follows.

This device is an active instead of a passive ionization detector and continuously samples the surrounding air for detection of submicron pyrolitic matter, which is associated with the early (incipient) stage of fire. Figure 4 shows a sectional view of the unit. The sample air flow drawn into the detector is divided between two paths: one goes through the ionization sensing chamber and the other bypasses the chamber and goes directly to a rotary vane positive displacement pump. The pump is driven by an ac synchronous motor powered by a 28 Vdc dc-to-ac converter motor controller hybrid.

The two-path air flow scheme provides for aerodynamic separation of particles entering the unit and prevents all large particles not associated with a hazard from entering the sensor and creating false alarms. Submicron particles in the air sample combine with charged particles created by a radioactive source of Americium 241, which reduces the ion current produced within the ionization chamber. The resulting change in current is proportional to the concentration of particles. This current is converted to a voltage through a high impedance resistor network, and is processed through a voltage-to-frequency converter hybrid for evaluation by a large-scale integrated circuit (LSI). The LSI measures the frequency and rate of change and triggers an alarm signal when the appropriate threshold values are reached.

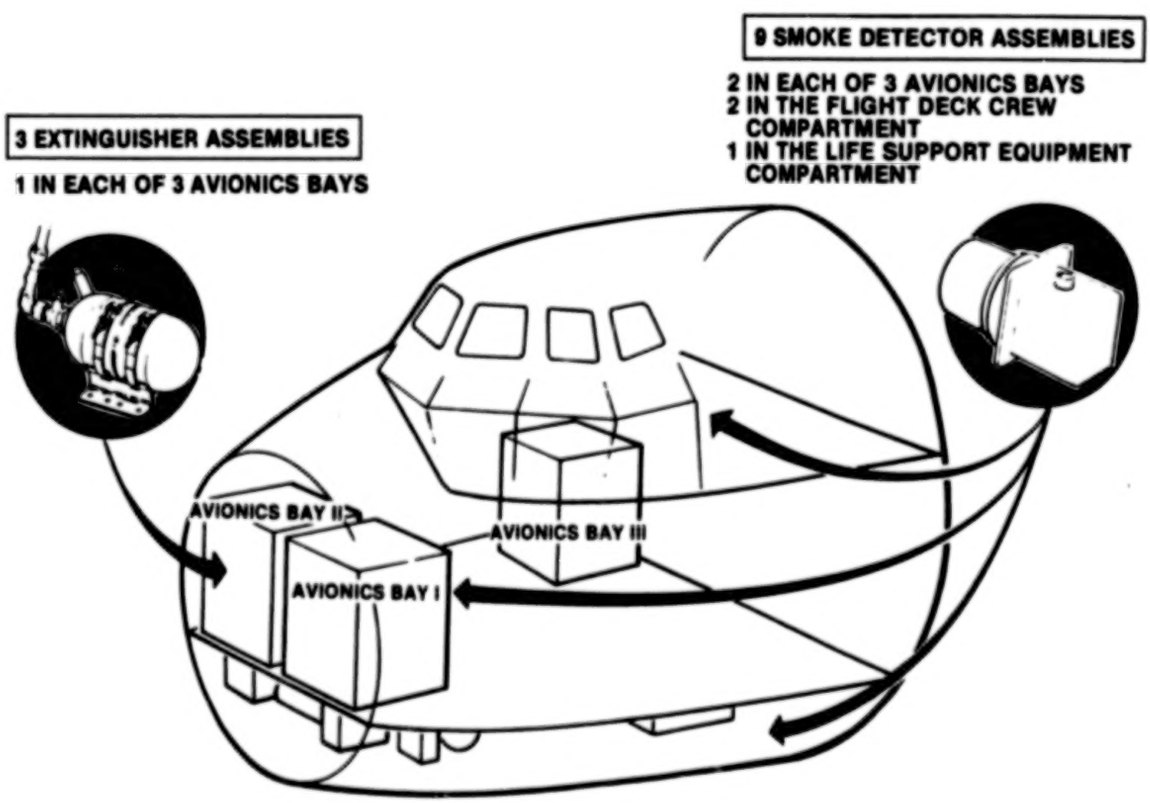


FIGURE 3. SPACE SHUTTLE ORBITER FIRE PROTECTION SYSTEM

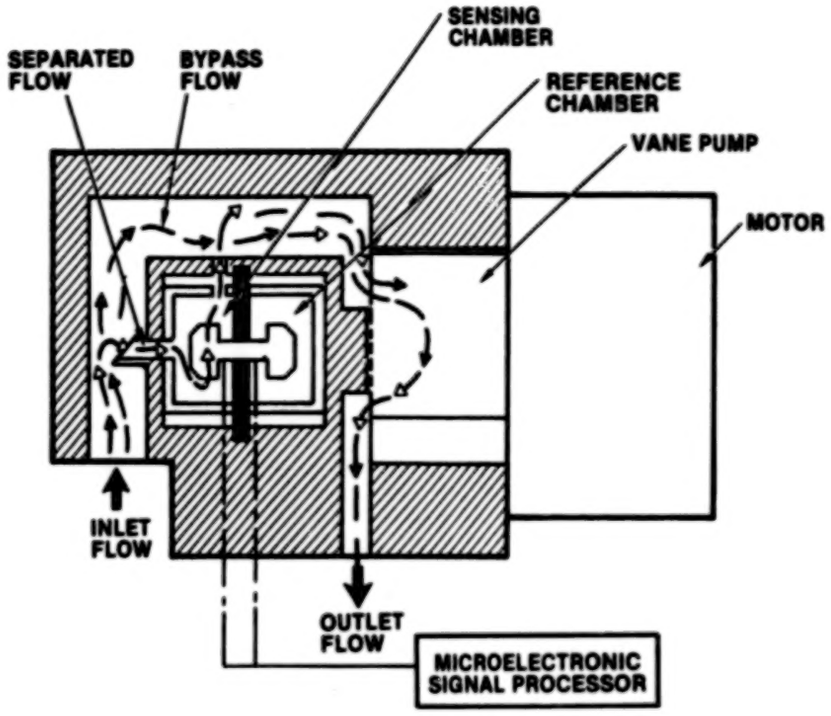


FIGURE 4. SMOKE DETECTOR AIR FLOW DIAGRAM

DESIGN PROBLEMS AND SOLUTIONS

The design problems encountered after the detector basic concept was proven involved meeting the operational life requirements of the orbiter. The problems and their solutions are as follows.

Quartz Crystal Microbalance (QCM) Sensor

The original design used a QCM as the sensing device to measure the rate of mass change that was collected on the crystal, which was the signal generator of an alarm. The problem with this system was in providing adequate crystal life to meet the design goal. Even in a clean environment, constant particle collection was enough to saturate the crystal within a relatively short time. Attempts to regenerate the crystal remotely were cumbersome and required considerable development. At this time, the use of an ionization chamber as a substitute for the QCM was introduced. This chamber's life was a function of the radioactive source's longevity (half life equals 458 years). This substitution did not jeopardize the program objectives and solved the sensor life problem.

Ionization Chamber Altitude Operation

The ionization characteristics of a low-energy alpha source vary with the density of the surrounding air. In order to provide signal compensation for minor changes in the ambient atmosphere, this detector contains two low-energy sources in its sensing and reference chambers, as seen in Figure 4. The orbiter altitude pressure requirement for this system is 8 psia (16,000 feet) and is tested to 7.3 psia to provide margin. During altitude testing of the sensors, a large signal shift in some units and no shift in others (up to 50,000 feet) was observed. It was concluded that there had to be differences in the two ionization sources to create the unbalance in the electrical current that was generated between the two chambers. The two parameters controlling the source characteristics are energy level (mean electron volts [MEV]) and activity (microcuries). If these characteristics are matched, the sensor signal will remain balanced; however, this is not easy to accomplish.

A series of matrix-oriented tests were conducted to pinpoint the characteristic that most affected the signal shift. The most effective results were first obtained by maintaining one source as a constant and varying the second. Through extensive analysis and testing, the upper and lower limit values that produced the desired results were determined for both activity and energy levels. These values were then used to pair the sources before being installed in the sensor. This selection process doubled the number of acceptable sensors; however, manufacturing assembly techniques still create source characteristic changes that prevent 100 percent of acceptable units even after selection.

The importance of this solution is that it determined how to minimize the sensor signal from shifting during changes in ambient air density.

Air Moving Pump Design

Two problems were encountered during the development of the rotary vane air moving pump: one involved the material used to make the vanes and the second involved contact friction between the rotor and the mating end surface during vibration testing. This design is shown in Figure 5.

The original vanes were made from a graphite-impregnated resin material that, by design, deposits a thin layer of resin on the housing wall to improve pump efficiency. Unfortunately, this deposit also increases the friction forces because the graphite does not form a perfect lube surface and, therefore, the motor torque requirements are higher. To overcome this would have meant increasing the motor power to an undesirable value. Various materials were tested that showed high-pressure velocity (PV) characteristics, but only one passed the design criteria. That material is a cadmium oxide impregnated Teflon called Fluoroloy D and it has successfully operated in excess of 12,000 hours without appreciable wear.

The contact friction problem during vibration testing was solved by designing the small diameter rotor retainer such that it always protrudes above the rotor face. This means that only it can contact the mating surface, thus preventing contact with the entire diameter of the rotor face. Also, the retainer was made of heat-treated 17-7 Ph and the mating surface was finished with a Class I anodize so that any contact between them involved two very hard surfaces.

Pump Driving Motor Design

The major problem in the design of the pump motor was the selection of dry lube bearings in order to minimize the power consumption. This type of bearing did not provide the expected motor life. A design change to wet lube bearings required an increase in power to overcome the higher friction load; however, it was possible to reduce the motor speed to increase its driving torque without exceeding the allowable power consumption. This change resulted in a 20,000-hour operational life motor.

Because of the lower motor speed, the lower pump flow had to be compensated for in order to maintain the same sensor performance. This was accomplished by a size change to the orifice that controls the flow split through the sensor.

Electronics Hybrid Design

When the previously discussed motor speed change was made, the motor controller hybrid, which supplies the correct driving frequency to the motor, required a new design. It was a straightforward change to provide the new frequency.

Another function of this hybrid is to supply the self-test signal that verifies the running condition of the motor. The original design measured the running current to determine either a stalled or open-winding condition. The current window available to make this determination was very narrow because of the hysteresis effect on the current, and, consequently, a false not-running condition would occasionally be indicated. A new self-test circuit design was introduced to eliminate this problem.

The new self-test circuit examines the motor current wave-form frequency instead of current level to determine an open winding, thereby making this function independent of normal running current changes. Since this eliminates the aforementioned current window, it allows setting the stall point indicator very close to the actual stall value, which maximizes the most self-test life.

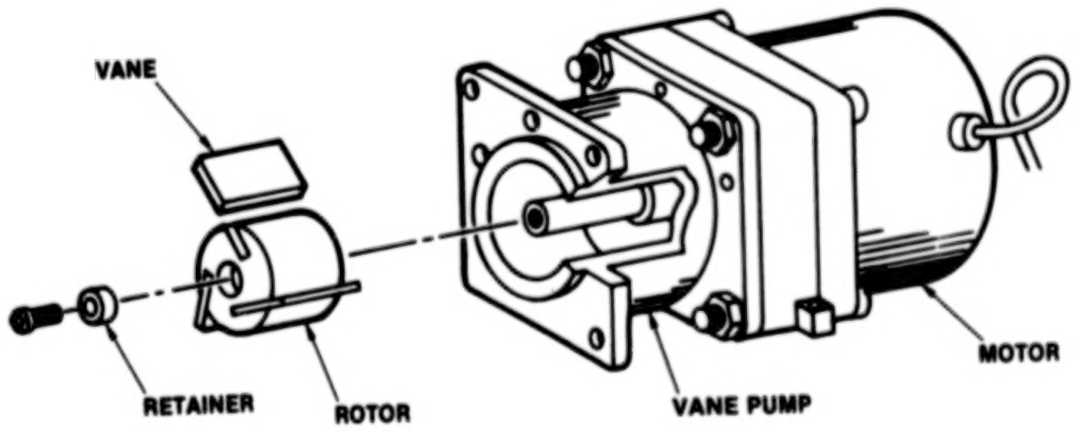


FIGURE 5. PUMP/MOTOR ASSEMBLY

REMOVAL OF HYDROGEN FROM FUEL CELL PRODUCT WATER USING LOW TEMPERATURE CATALYZED METAL TUBES

The water management system (WMS) of the Shuttle orbiter relies upon the water produced by its fuel cells to replenish that water used for either metabolic consumption by the crew or in the Shuttle's flash evaporator. However, the water produced by the fuel cells is saturated with hydrogen (H_2) at the operating conditions of the fuel cell (150°F, 60 psia), which results in 0.066 cubic centimeter of hydrogen being dissolved in every cubic centimeter of water produced. In the process of water storage and consumption, hydrostatic pressure is decreased, which causes the dissolved hydrogen to come out of solution and revert to the gaseous phase unless provisions are made to remove a major portion of it from the water. The technique that has been selected for removal of hydrogen from the fuel cell generated water is based upon the use of catalyzed palladium/silver (Pd/Ag) tubes operating at ambient temperature. Fuel cell product water flows on the inside of the tubes while space vacuum is applied to the outside tube surfaces causing the hydrogen to pass through the solid metal tubes to space vacuum. This hydrogen removal concept was first qualified aboard Apollo spacecrafts; however, to satisfy the removal requirements for the Shuttle orbiter the hydrogen separator was required to demonstrate an absolute hydrogen removal capacity of approximately ten times that of units built for the Apollo spacecraft. In addition, reductions in relative weight and volume were required.

The challenges of developing such a lightweight, high performance hydrogen separator for the Shuttle orbiter were successfully met, but not without development hurdles and problems that required timely and creative solutions. The following discusses the major development challenges and problems encountered and how their solutions were implemented.

PROBLEMS AND CHALLENGES

The major challenge of the hydrogen separator development can be summarized in one statement: reduce size by a factor of three (compared to Apollo hardware) and increase capacity by a factor of ten.

Specifically, the requirements that had to be met were a hydrogen removal rate equal to or greater than 70 percent with product water flowing at 23 pounds per hour at ambient temperature (70°F ± 2), without inducing a pressure drop of greater than 0.7 psid. Maximum allowable hydrogen separator weight was 5 pounds.

PROBLEM RESOLUTIONS

Performance Enhancement

Calculations and experimental data indicated that to remove a minimum of 70 percent of the dissolved and/or free hydrogen from water flowing at a rate of 23 pounds per hour and at ambient conditions would require a total water flow path length in excess of 900 inches. The calculations were based on catalyzed Pd/Ag tubes optimized at a 0.125-inch diameter and a wall thickness of 0.010 inch. Since a single 900-inch path length would exceed the allowable ΔP of 0.7 psid and internal catalyzation of the tube would be impractical, a technique for manifolding the hydrogen-saturated water flow into a combination of shorter series/parallel lengths was devised. This manifold technique permitted the use of 16 Pd/Ag tubes, with each tube having a path length of 57 inches. This series/parallel configuration permitted the fuel cell product water to enter eight inlet tubes simultaneously (Figure 6) and flow through these tubes in parallel; exit from the initial eight tubes and simultaneously enter into a set of four parallel outlet tubes manifolded in series with the initial eight inlet tubes. The water then exited the first four outlet tubes and simultaneously entered a second set of four parallel outlet tubes manifolded in series with the first set of four outlet tubes. The product water passing through the second set of four tubes then exited into a common water outlet port. This series parallel manifolding technique divided the tubing into catalyzable lengths, met the required pressure drop, and still maintained sufficient residence time within the catalytic Pd/Ag tubes to meet the hydrogen removal requirements.

While the calculations predicted satisfactory performance, initial verification testing with the development unit showed less than the calculated 70 percent removal efficiency. Through a series of bench top experiments, the reduced removal rate was traced to the final 10 percent through 15 percent length of each flow path, i.e., where only dissolved (as opposed to free) hydrogen exists with the water. Since flow is laminar in these regions, dissolved hydrogen near the center of the tubes reaches the walls only by diffusion.

The solution to enhancing the removal rate in the diffusion-only regions consisted of developing small turbulators inserted into the last 10 inches of each tube path of the first set of four outlet tubes and into the first and last 10 inches of each tube path of the second set of four outlet tubes (12 turbulators). These thin, spiral-like metal turbulators were designed to break up or turbulate the laminar flow characteristics of the water. This allowed hydrogen trapped at the center of the water column to reach the catalyzed tube surfaces and thereby enhance its removal.

PACKAGING

The use of 16 separate tubes proved feasible from a performance standpoint. The need for creative solutions to the inherent challenge of packaging 16 tubes, each 57 inches long, into a package weighing 5 pounds or less remained to be solved. First, a technique had to be devised for bending the tubes into a double-U configuration with each tube having three 180-degree bends. To achieve a compact configuration, an extremely small bend radius was desired, smaller than standard (0.50 inch) bend radii normally associated with 0.125 inch diameter tubing. Since the Pd/Ag tubes were of such a small diameter and thin-wall construction, bending the tubes in a very tight radius by using conventional techniques resulted in crimping or collapsing the tube. To resolve this, the Pd/Ag tube (in its initial 60 inches of straight length) was sealed at one end (crimped shut) and carefully filled with a nonabrasive, nontoxic water-soluble packing. Once the tube was filled, the open end of the tube was crimped shut. Bending of the tubes to a 0.31-inch radius was then successful and reproducible. Once the tubes were bent, the crimped ends were cut off and water was flushed through the tubes to remove the water soluble packing.

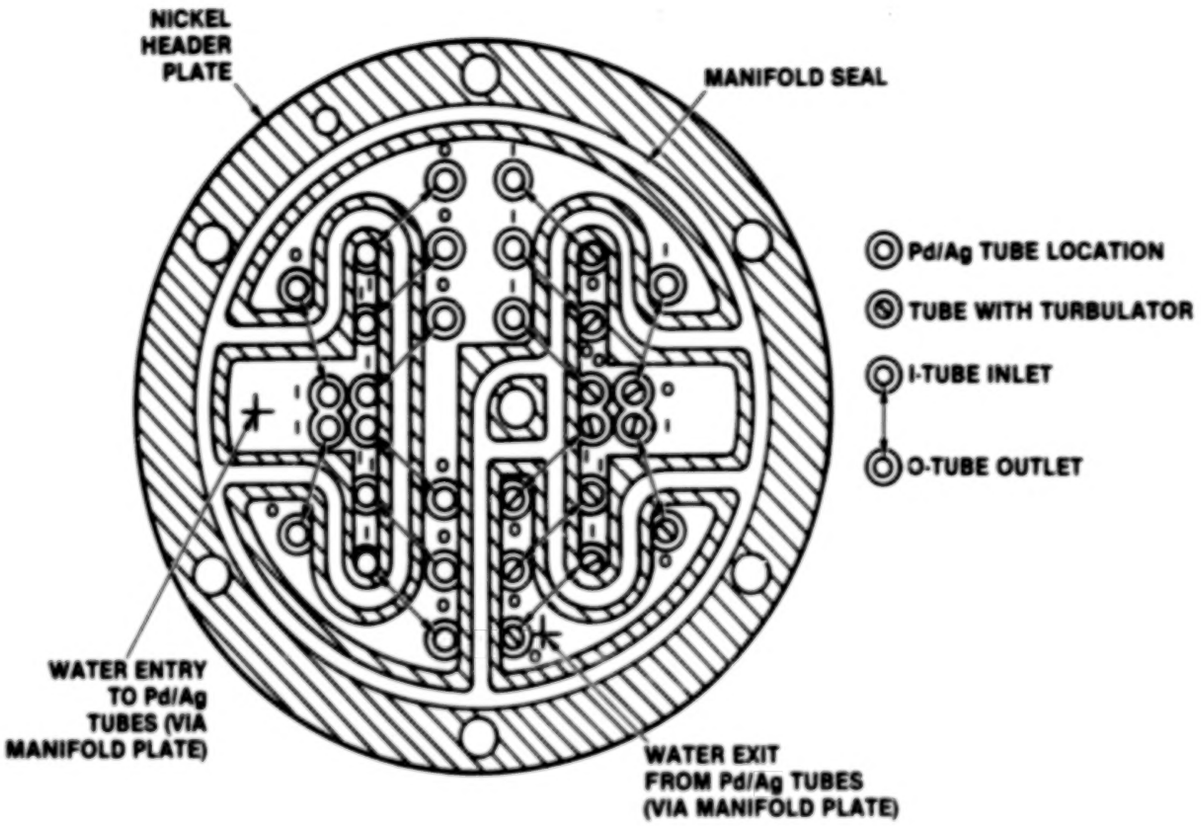


FIGURE 6. HEAD PLATE SHOWING Pd/Ag TUBE LOCATIONS AND MANIFOLD SEAL CONFIGURATION

Locating the tubes into a common header plate posed the problem of performing 32 separate welds (one weld for each end of the 16 Pd/Ag tubes) in a nickel plate designed to be 3.5 inches in diameter and 0.110-inch thick. Heli-arc welding techniques were examined and rejected since the heat generated could warp the thin header plate and the potential for welding error and subsequent increased scrap rates was high. Electron beam (EB) welding was selected as a viable technique to secure the tubes into the header plate. A treepan-type weld (Figure 7) was initially considered but was rejected when calculations showed that stress on the weldment of the treepan-configured joint was too severe. Additionally, reproducibility of an EB weld using a treepan joint was suspect. An EB weld technique using a butt-weld configuration between the Pd/Ag tubes and the header plate (Figure 8) was developed and qualified for weld integrity, structural strength, and reproducibility.

In order for the tube bundle of the welded Pd/Ag tube and header assembly to withstand the shock and vibration conditions experienced aboard the Shuttle orbiter, a technique for forming a tube bundle was devised. The technique allowed for tube growth (about 0.375 inch for the 16-inch lengths) characteristic of Pd/Ag metal exposed to hydrogen. A porous Teflon cord was selected for the tube tie-down and support technique. The Teflon cord was laced through the tubes in a braiding fashion, with the ends of the Teflon cord tied together to form a secure lace through the tube bundle. This Teflon cord braiding at various locations on the tube bundle secured the tubes of the bundle to resist the effects of shock and vibration and at the same time minimize cover up of the catalyzed outside surface of the Pd/Ag tubes, which could result in reduced separator performance and allow adequate tube growth.

Photographs of an assembled hydrogen separator and its components are presented in Figures 9 and 10, respectively. Key features and components are identified.

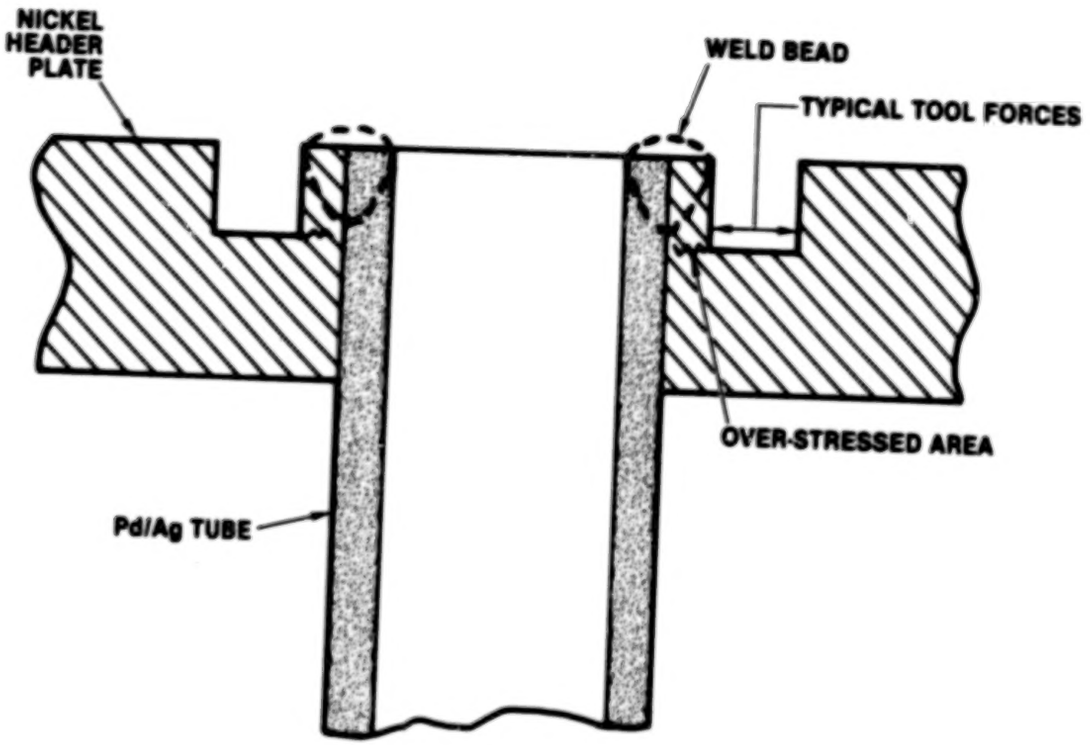


FIGURE 7. CROSS SECTION OF A TREEPAN WELD

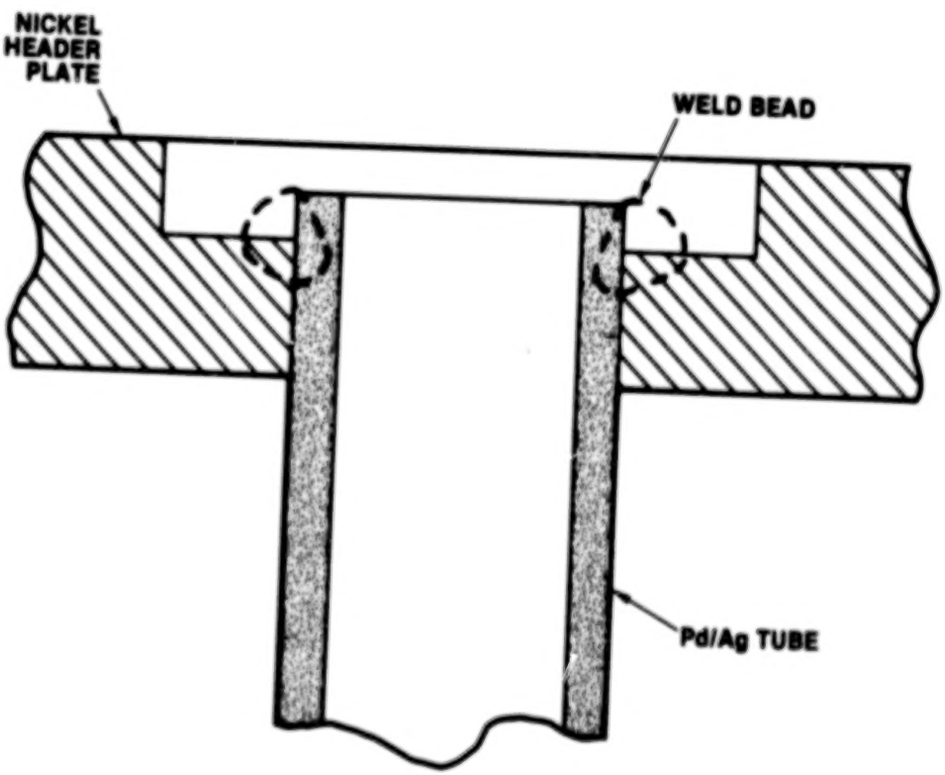


FIGURE 8. CROSS SECTION OF PRESENT WELD JOINT

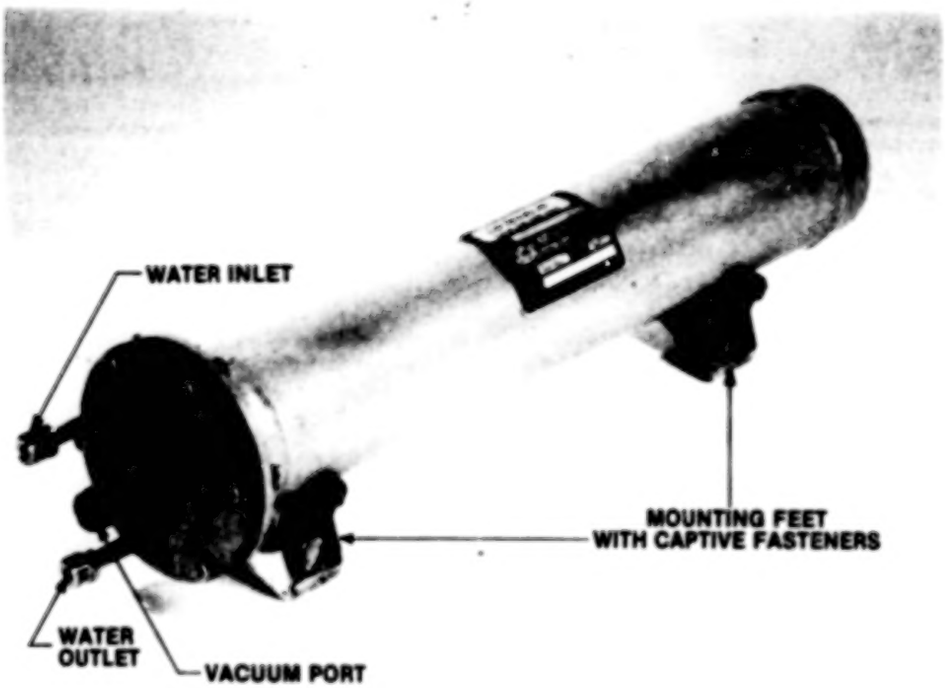


FIGURE 9. ASSEMBLED H_2 SEPARATOR

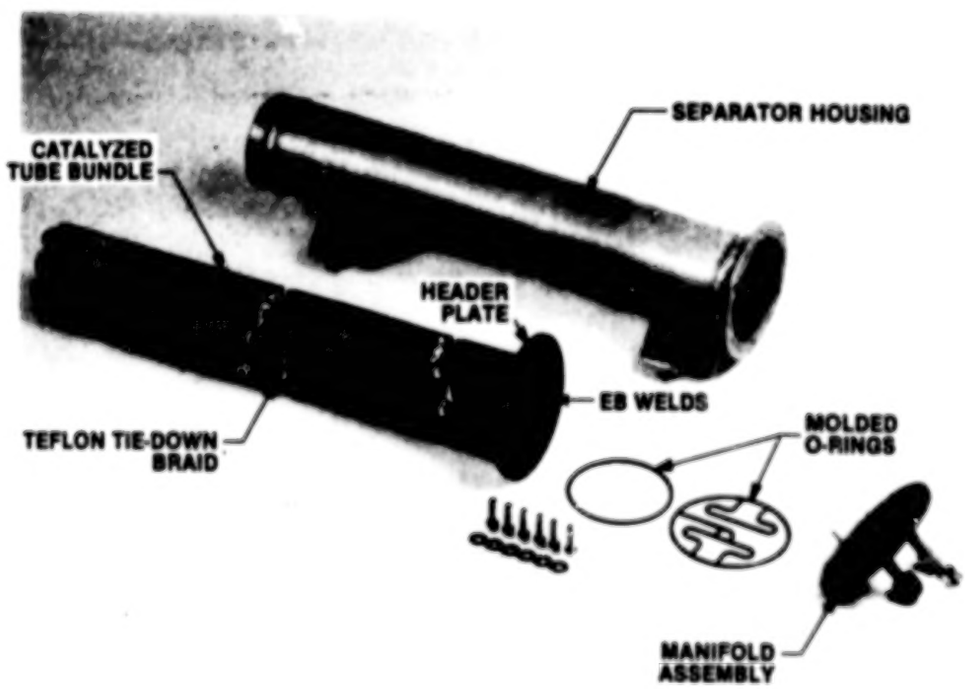


FIGURE 10. H_2 SEPARATOR COMPONENTS

ORIGINAL PAGE IS
OF POOR QUALITY

FLIGHT EXPERIENCE

Shortly after STS-2 was launched, a high PH alarm occurred, which indicated potassium hydroxide (KOH) in the fuel cell produced water. The supply water system was configured to isolate the contaminated water from the drinking supply. The problem fuel cell was shut down and the mission was successfully completed. After this problem, the crew reported gas in the drinking water. It was suspected that the KOH had poisoned the separator catalyst. The following actions were undertaken:

- Hydrogen separator performance was tested at Life Systems, Inc.
- Water dispenser servicing techniques were reviewed.
- Drink bags were tested for residual gas.

Tests on the separator showed that the KOH had not affected its performance; however, servicing procedures used for the water dispenser could have trapped air in it, which was later displaced during the mission. Also, the water drink bags, which were serviced by evacuation were determined to be slightly permeable to air. It was concluded that the last two conditions were the cause of the problem.

To minimize recurrance on future flights, water dispenser procedures have been changed to preclude air entrapment. Water bags are evacuated as late as possible to minimize air permeation. No change was necessary for the separator.

CONCLUSIONS

Solution to key challenges in performance and packaging resulted in the successful development of a hydrogen separator that was capable of removing greater than 70 percent of the dissolved hydrogen from the fuel cell product water at ambient temperatures and at a flow rate of 23 pounds per hour within the specified pressure drop of 0.7 psid. The compact unit had a total length of 16.8 inches, an outside diameter of 3.5 inches, and not only met the 5-pound weight goal but beat it by 34 percent, weighing only 3.3 pounds.

WASTE COLLECTOR SYSTEM (WCS)

The major achievement of the WCS was to focus the problems of waste management into one integrated multifunction assembly (Figure 11). The WCS collects and processes human wastes, wash and extravehicular mobility unit (EMU) dump water, and trash vent gases in a sanitary and odor-free manner. Specific challenges were to simplify user procedures while minimizing weight, power, and volume requirements. There were significant achievements in several areas, including:

- Zero gravity operation
- Valve design
- Liquid/gas separation
- Corrosion protection

ZERO GRAVITY OPERATION

Simplified operational mechanisms and procedures for crew accommodation and restraint systems were developed through the use of past history, neutral buoyancy tests, and aircraft tests of many concepts. Final proof was obtained during STS flights where sufficient zero gravity time was available for full evaluation.

RESTRAINT SYSTEM

Prior to STS-5, the WCS restraints relied on a seat belt and a fixed-foot support. STS-1 through STS-4 data indicated that these methods were inadequate for reliable user positioning and restraint. A number of options were evaluated on STS-5 and several became operational.

Spring-loaded thigh bar restraints are self-stowing, easily positioned for use, permit a no-hands required retention of the user, and offer the user additional handholds for zero-gravity locomotion in the stowed position. No actions are necessary for stowage for launch and entry.

Foot restraints, consisting of a heel cup and toe straps, were added to an adjustable foot support for additional user restraint and height adjustment, if desired.

A user-adjustable toe bar was also added to provide a restraint means for standing micturations in the zero-gravity environment. The toe bar is used with the footrest in the stowed position. Restraint systems are shown in Figure 12.

URINAL CAPS

Prior to STS-5, a common urinal cap was utilized for both males and females. The STS-4 crew reported urine migration under the cap in the unsealed area between the urinal and the cap. This open area had been provided for proper air flow when the cap was used by a female. In addition, the crew also reported the last-drop problem.

ORIGINAL PAGE IS
OF POOR QUALITY



FIGURE 11. WCS ASSEMBLY



FIGURE 12. THIGH BAR AND FOOT SUPPORT WITH HEEL CUP, TOE STRAPS, AND TOE BAR

Several revisions were made to the caps for a male-only design. The mating area between the urinal and the cap was sealed by addition of a rubber gasket. This directed all air through the top opening only, which increased the effective air velocity and eliminated a leakage path.

There were several options for the cap opening to support in-orbit testing. The cap variations included the large rectangular opening (the common male-female cap with rubber gasket added), a centered hole opening, and an off-set hole opening, as shown in Figure 13. The smaller opening area of the latter two versions increased the air velocity at the collection point to aid in last-drop removal.

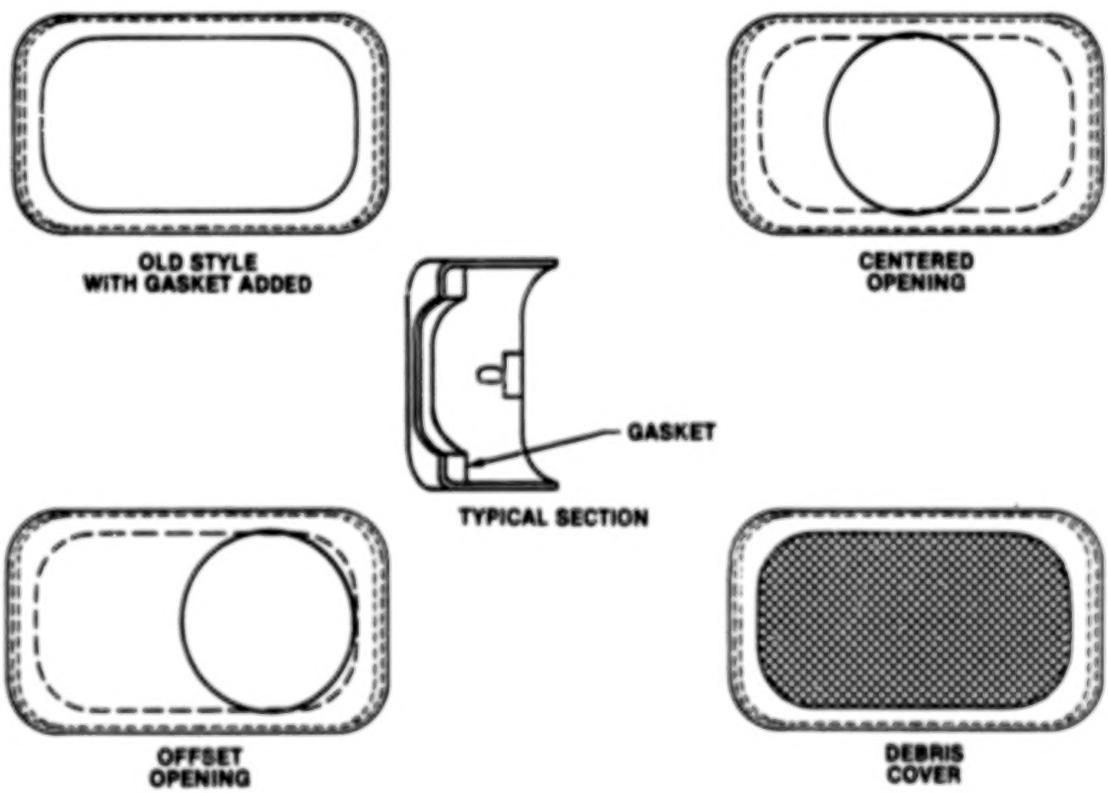


FIGURE 13. URINAL CAPS

In-flight testing of these three male-only caps was limited to the off-set hole version by the STS-5 crew, as it was very effective. No reports of liquid migration were received with the new cap. In addition, when combined with the pinch valve urinal, collection of the last drop ceased to be a problem.

In order to limit debris accumulation in the urinal, a cap with a debris screen was provided to cover the urinal when not in use. This was effective in preventing ingestion of cabin debris.

URINAL DEBRIS PROBLEM

STS-1 revealed problems related to unexpected amounts of cabin debris. During operation of the WCS, cabin air (8 scfm) is drawn into the urinal for liquid transport. After the STS-1 flight, when tested in a dry condition, the urinal screen was found to be nearly blocked with lint and debris. When wetted with liquid in zero gravity, the urinal air flow was further impaired such that the clogged screen acted as a liquid/gas separator.

Because of the suction of the fan-separator, the liquid thus tended to collect downstream of the screen in large liquid slugs with small pockets of air. This is compared to normal operation where only small slugs of liquid are separated by relatively large pockets of air. The result was an excessive instantaneous urine flow to the fan separator, which overwhelmed the centrifugal phase separator and carried over to the fan, which forced the urine with the air to the odor filter.

The problem was solved by adding a single filter, called a prefilter, to the urinal, as shown in Figure 14. The prefilter is easily changed on a daily basis to prevent debris buildup. Subsequently, the WCS operated successfully to confirm the postulated cause of the problem. Because of excessive debris collection in the urinal, the urinal prefilter will continue to require periodic replacement in flight.

VALVE DESIGN

Manual operation of control valves was dictated by the weight and power limitations and the complexity of the interlocking and sequencing of functions. As a consequence, the valves typically required low operating forces for the required large orifices. The large 4-inch sliding gate valve that opens the commode for defecation is also a vacuum seal. The pressure differential on the gate is relieved prior to opening to minimize operating force and structural weight.

Conversely, the pressure differential on the floating gate is used to achieve sealing pressure against a simple O ring when the commode is closed for vacuum drying of the solid wastes.

Similarly, a three-way 1-1/2 inch ball valve used for air flow control and vacuum sealing utilizes a floating seal design to achieve sufficient pressure for sealing while operating at a low torque of less than 25 inch-pounds.

A third unique valve design developed for the WCS was a simple pinch valve for air flow control in the urinal, as shown in Figure 14. An air flow of 8 scfm is used to entrap the urine and convey it through a funnel to a liquid/gas separator. The last drop of urination is often as large as a tablespoon of liquid, which has always been a disposal problem in zero gravity. For the WCS, this is collected by diverting the suction air flow to a port at the top of the collection funnel, which is achieved by squeezing a rubber tube at the base of the funnel, stopping the main flow air, and causing a small amount of suction flow at the top port. The user merely touches the drop to the port and the liquid is drawn into the system.

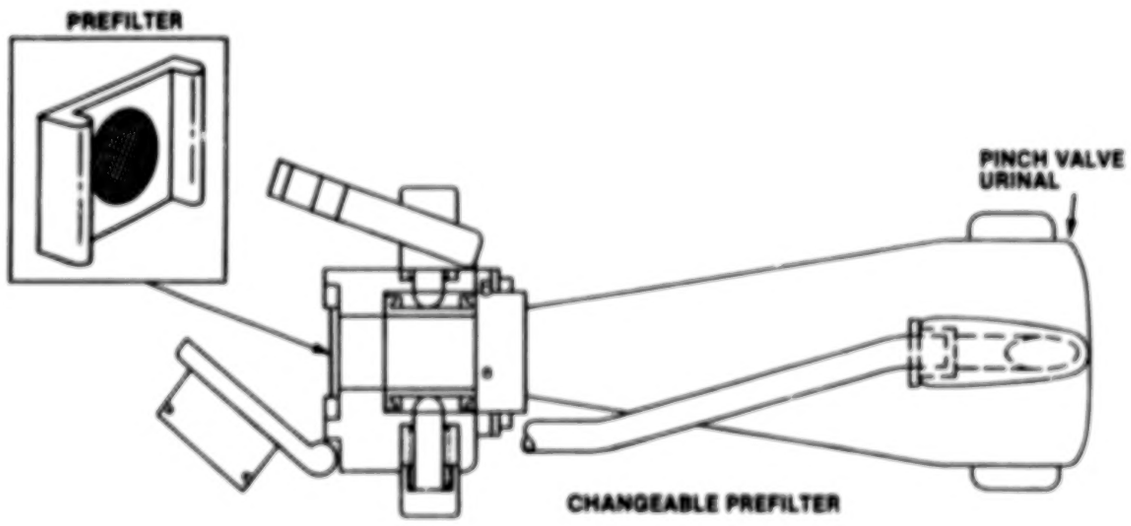


FIGURE 14. URINAL/PINCH VALVE ASSEMBLY

LIQUID/GAS SEPARATION

Separation of urine and other waste liquids from the transport air presented a number of design challenges. Foremost was the need to achieve reliable phase separation at minimal weight and power consumption. One method used to accomplish this goal was the integration of three functions into the fan separator (Figure 15): liquid/gas phase separation, liquid pumping, and air flow pressurization. Power requirements were further reduced by eliminating high friction dynamic seals and maintaining proper pressure differentials at required seal locations. By properly designing the flow paths for the commode and urinal air flows, it was possible to maintain a lower internal pressure in the rotating bowl than that between the bowl and the external housing. This condition prevents any liquid leakage out of the bowl and eliminates the need of a seal, which would add a significant cost in power, complexity, and reliability.

When the liquid/air mixture reaches the fan separator, the liquid is centrifugally separated from the air and pumped out of the unit through a stationary pitot tube in the separator. The fan separator is designed to produce sufficient air flow for the operation of the urinal and the commode. Since the commode is not necessarily used during micturition, a ballast air flow of approximately 30 cfm enters the system via a particulate filter, a calibrated orifice, and valve. The air mixes with the urine transport air flow in the fan separator to assure that moisture in the warm urine transport air does not condense in the cooler outlet line.

CREW TRAINING

Crew comments during flight debriefing indicated that considerable difficulties were being experienced in obtaining the proper position. As a result, a special training aid was designed, utilizing a television camera to assist the crew in obtaining proper positioning. In addition, the WCS development was utilized during flight simulations by the flight crew. Comments from crew personnel who have utilized the training aid indicate that it is very effective.

CONCLUSIONS

The greatest challenge in developing the WCS was integrating multiple waste management functions into a single flight assembly. In addition to the typical flight constraints of minimal power, weight, and volume, other requirements imposed on the WCS included ease of operation, user acceptance, liquid/gas separation performance, and satisfactory materials protection against the various waste products.

Flight experience has confirmed the basic design integrity of the WCS and that the principles of operation in zero gravity were correct. Modifications that have been incorporated have improved positioning and restraint methods utilizing user-accepted systems.

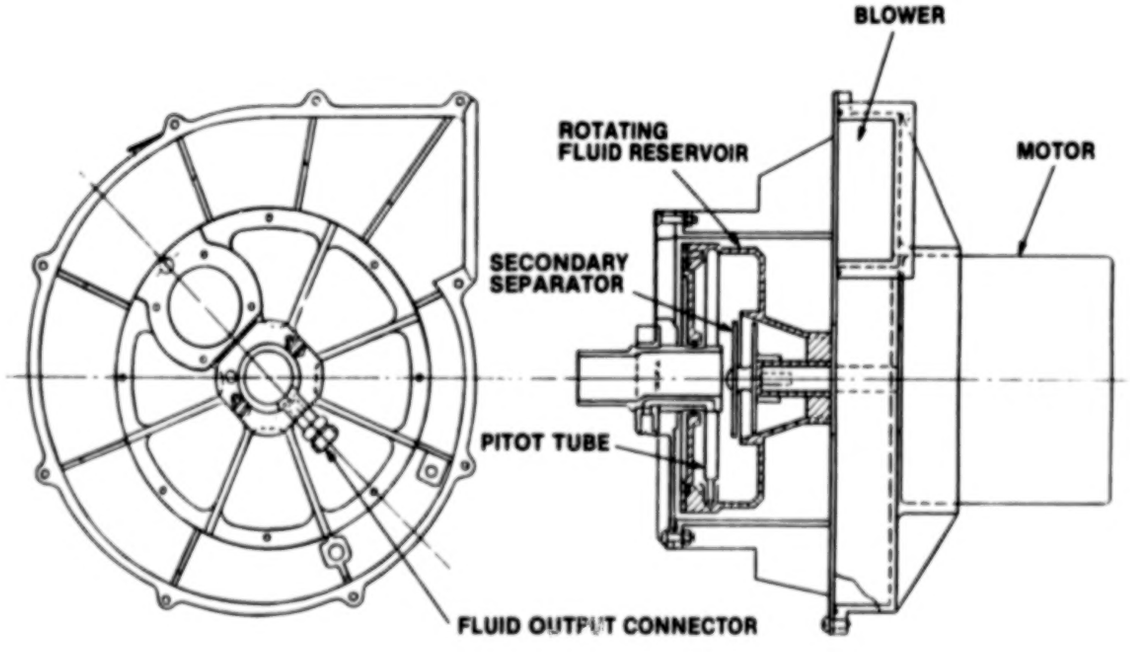


FIGURE 15. FAN SEPARATOR ASSEMBLY

N85
16925

UNCLAS

D36

N85-16925

CHALLENGES IN THE DEVELOPMENT OF THE ORBITER RADIATOR SYSTEM

J. L. WILLIAMS
LTV Vought, Dallas, Texas

M. F. MODEST
U. of So. Cal., Los Angeles, California

J. A. OREN
LTV Vought, Dallas, Texas

H. R. HOWELL
LTV Vought, Dallas, Texas

ABSTRACT

This paper describes major technical challenges which were met in the design and development of the Space Shuttle Orbiter Radiator System. This system rejects up to 30 kW of waste heat from eight individual radiators having a combined surface area of 175m^2. The radiators, which are deployable, are mounted on the inside of the payload bay doors for protection from aerodynamic heating during ascent and re-entry. While in orbit the payload bay doors are opened to expose the radiators for operation. An R21 coolant loop accumulates waste heat from various components in the Orbiter and delivers the heat to the radiators for rejection to space. Specific challenges included high acoustically induced loads during lift-off, severe radiating area constraints, demanding heat load control requirements, and long life goals. Details of major design and analysis efforts are discussed. The success of the developed hardware in satisfying mission objectives showed how well the design challenge was met.

INTRODUCTION

The Space Shuttle Orbiter offered a significant challenge to radiator designers since the high reentry heat flux preludes the use of conventional externally mounted radiators. Mounting the radiators on the inside of the payload bay doors provided a solution to this problem. The doors provide reentry thermal protection to the radiators, and there is no disadvantage associated with having the doors open while the radiators are in operation. This placement solved a difficult problem, but it created several challenges in radiator design which are discussed in this paper. These challenges are primarily related to the radiating area and attachment limitations inherent in the payload bay door mounting scheme, the launch vibration environment, the wide operating temperature range (-130°C to 120°C) and stringent heat transfer and coolant pressure drop constraints. A systems engineering approach was applied universally to design parameters because of the unusually close (for a radiator system) interrelationship of the parameters. The final radiator design will be discussed briefly, and then some of the major challenges associated with the Shuttle Orbiter radiator design will be addressed.

SYSTEM DESCRIPTION

The Orbiter radiator system is described in detail in Reference [1] and flight performance is described in Reference [2]. Briefly the radiator system consists of eight radiators which are evenly divided between two independent Refrigerant 21 (Freon 21) flow loops. Figure 1 shows the routing of one R21

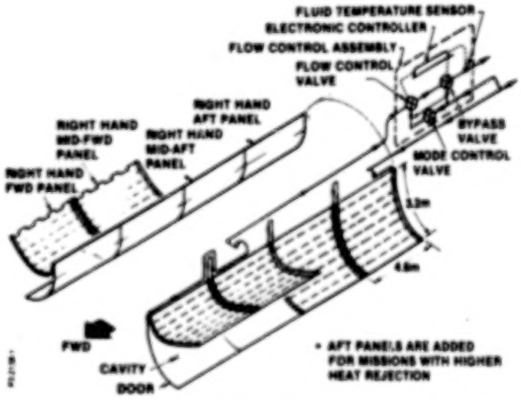


Figure 1 RFCA System Flow Schematic

loop through the four radiators mounted on one side of the payload bay door. Radiator outlet temperature control is achieved by simply bypassing hot R21 around the radiators in the proper quantity such that the mixed temperature of the hot bypassed flow and the cold flow from the radiator is at the desired control point, as shown in Figure 2.

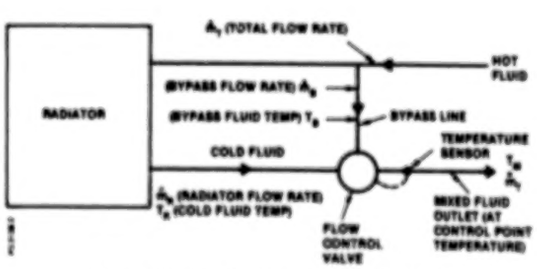


Figure 2 Radiator Temperature Control Approach

The eight radiators are curved to conform to the payload bay doors. Each radiator is about 3.2 m along the curved section by 4.6 m in the longitudinal axis, as shown in Figure 3.

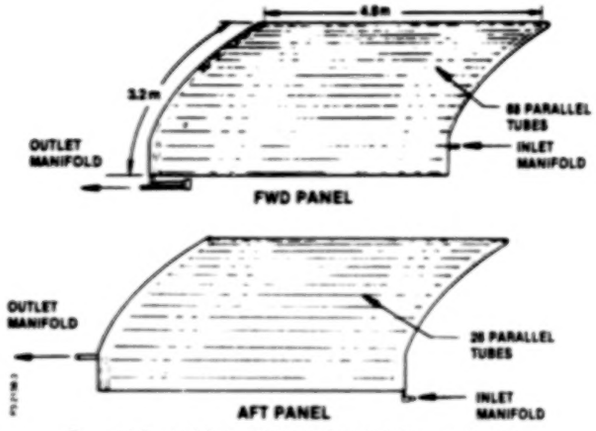


Figure 3 Typical Radiator Panel Physical Characteristics

The forward two radiators, which may be deployed from the door to increase radiator area are each about 2.3 cm thick, while the aft two radiators on each side are about 1.3 cm thick. The radiators are made of bonded aluminum honeycomb structure with tubes attached to the facesheets as shown in Figure 4.

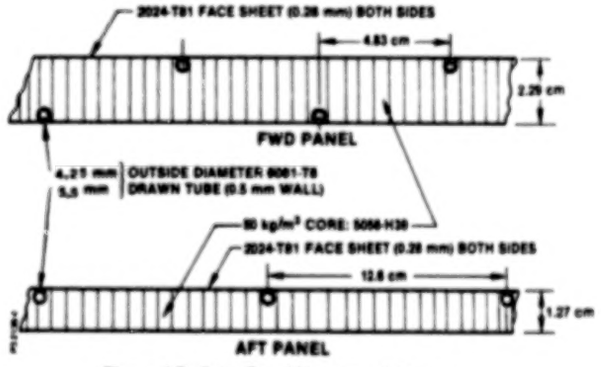


Figure 4 Radiator Panel Honeycomb Layup

HEAT REJECTION OPTIMIZATION

The limited heat transfer area of the inside of the payload bay doors, which represents about 118 sq.m., proved to be inadequate for the required heat rejection of about 20 kW_t in the popular flight attitude of payload bay toward the earth. This made it necessary to deploy the forward radiators away from the doors, as shown in Figure 1, creating a cavity into which additional heat is radiated from the underside of the radiators. Evaluating heat transfer performance gain provided by the cavity was difficult due to the specular silver-backed Teflon surface coating on the inside of the door and radiators. The radiators had to be optimized for maximum heat radiating efficiency rather than minimum weight and an effective means of applying a long lasting optical solar reflection coating to the radiator had to be devised. These challenges are discussed in the succeeding subsections.

PAYLOAD BAY DOOR-RADIATOR CAVITY ANALYSIS

In order to accurately predict the heat rejection rates from the door-radiator cavity by thermal radiation, radiative exchange factors from surface-to-surface, from surface-to-space, and from sun-to-surface must be determined. The calculation of radiant interchange is commonly performed under the assumption that the participating surfaces are diffuse emitters and diffuse reflectors of radiant energy. Experimental investigations, however, have shown that real surfaces can depart substantially from this model, particularly in the case of smooth and/or metallic surfaces. Extreme examples are deep cavities exposed to incoming radiation (e.g., solar) or outgoing radiation (e.g., heat rejection into space), as are encountered in the Space Shuttle payload bay door-radiator configuration.

Two different methods of calculating radiation exchange factors in complex geometries with complex surface characteristics are possible: the statistical approach (usually called the Monte Carlo method), and the analytic approach, solving a set of simultaneous integral equations numerically. The different approaches require different definitions for the radiative exchange factors. Any numerical method including three-dimensional effects will be complex and computer time-consuming, even if idealized surface properties are assumed. Extremely complex cases such as the payload bay door-radiator cavity with its curved surfaces and its non-ideal surface characteristics are an ideal application for the Monte Carlo technique, which was employed here.

Heat Transfer Relations

Assuming that the door-radiator cavity can be broken up into J isothermal subsurfaces (strips) as shown in Fig. 5, the net heat flux for any strip i may be calculated from

$$Q_i = \int_{A_i} q_i \, dA_i = \epsilon_i \sigma T_i^4 A_i - \sum_{j=1}^{J} \epsilon_j \sigma T_j^4 A_j \mathcal{F}_{j-i} - q_{ext} A_s \mathcal{F}_{s-i} \qquad [1]$$

$1 \leq i \leq J$

where $\mathcal{F}_{j-i}$ = radiative exchange factor from strip j to strip i,

q_{ext} = external energy entering through the opening of the enclosure,

A_s = area of the opening irradiated from external sources,

A_i = strip surface area,

T_i = strip temperature,

ϵ_i = total hemispherical emissivity of strip.

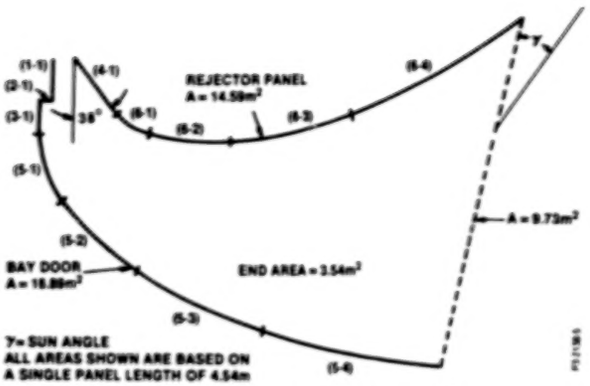


Figure 5 Bay Door/Rejector Panel Cross Section

Although heat fluxes Q_i can be calculated directly by the Monte Carlo method, it is of advantage to instead determine the exchange factors: although the Q_i's depend on all surface temperatures in the enclosure, the $\vartheta_{i\to j}$'s either do not (gray surfaces) or depend only on the temperature of the emitting surface (nongray surfaces).

If a large statistical sample of energy bundles N_i is emitted from surface A_i, and if the N_{ij} becomes absorbed by surface A_j after direct travel or after any number of reflections, then the exchange factor may be calculated from

$$\vartheta_{i\to j} = \lim_{N_i\to\infty}\left(\frac{N_{ij}}{N_i}\right) \approx \left(\frac{N_{ij}}{N_i}\right)_{N_i>1} \qquad [2]$$

Surface Properties.

The accurate calculation of radiation exchange factors requires an extensive knowledge of surface property data. In general, the spectral directional emissivity and absorptivity as well as the bidirectional reflectively must be known for the material for all wavelengths, directions (incoming and/or outgoing solid angles ω), and temperatures; i.e.,

$$\alpha'_\lambda = \epsilon'_\lambda = f(\lambda, \omega, T) \quad \rho''_\lambda = f(\lambda, \omega_{in}, \omega_{out}, T) \qquad [3]$$

These surface properties must be determined from experiment and/or electromagnetic wave theory. No complete set of surface property data was avilable for silver-backed Teflon, in particular as far as bidirectional reflectivity ρ''_λ is concerned.

For the cavity analysis the following assumptions were made:

1. The properties α'_λ, ϵ'_λ, and ρ''_λ are independent of temperature (this has been shown by experiment to be an accurate assumption for most materials).

2. For infrared wavelengths ($\lambda > 2.5$ μm) and for solar irradiation wavelengths ($\lambda < 2.5$ μm) spectral directional values for emissivity may be calculated from simple correlation formulas, which were based on electromagnetic wave theory combined with available experimental data (an example is shown in Figure 6).

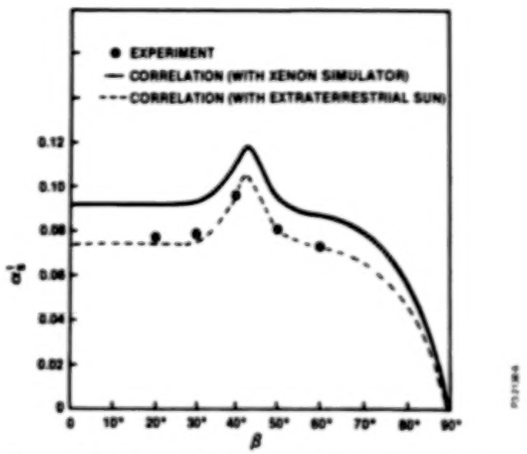


Figure 6 Total Directional Solar Absorptivity of Silver/Teflon

3. The surfaces are smooth and isotropic, so that the bidirectional reflectivity has its maximum in the specular direction and diminishes monotonically for directions farther and farther away.

Surface Description and Ray Tracing

In the computer program all surfaces are described in vectorial form (Reference [3]), where the vector components are polynomials in either one of two perpendicular surface parameters. This description allows for curved or flat "quasi-three-dimensional" surfaces; i.e., surfaces for which there exists a plane such that the projection of the surface on this plane is a (curved or straight) line.

The emission and tracing of energy bundles was carried out by using standard techniques; i.e., by comparing random number with probabilities for emission location, wavelength, and direction, as well as for absorptivities and reflectivities. In order to minimize the required computer time, a number of timesavers were devised, tailored especially to the payload bay door-radiator cavity, which are reported in greater detail elsewhere (Reference [4].)

Results

In order to calculate net heat rejection rates from the deployed panels of the Space Shuttle Orbiter while it is in orbit around the earth, the exchange factors in Eq. (1) must be determined; i. e., the absorbed fractions of (infrared) emission from all subsurfaces and of

solar and planetary irradiation entering the cavity through the openings. For comparison with limited experimental data (Reference [5]) the cavity was broken up into a relatively small number of isothermal strips, as shown in Figure 5.

Table 1 Radiative Exchange Factors s_{i-j} between Zones of Panel/Door Cavity (Emitting Zone at 80°F)

From strip no. / to		(1-1)	(2-1) + (3-1)	(5-1)	(5-2)	(5-3)	(5-4)	(4-1)	(6-1)	(6-2)	(6-3)	(6-4)
Space												
Experiment (EX)		0.298	0.306	0.421	0.397	0.422	0.481	0.185	0.168	0.245	0.480	0.799
Monte Carlo (MC)		0.295	0.288	0.397	0.414	0.454	0.519	0.184	0.178	0.277	0.495	0.801
TRASYS		0.181	0.421	0.438	0.441	0.473	0.552	0.158	0.210	0.321	0.527	0.819
(1-1)	EX	–	(0.019)[a]	(0.013)	(0.015)	(0.013)	(0.009)	0.324	(0.018)	(0.002)	(0.001)	(0.002)
	MC	0.013	0.003	0.008	0.016	0.016	0.011	0.296	0.018	0.000	0.000	0.000
(2-1) + (3-1)	EX	(0.025)	–	(0.043)	(0.036)	(0.020)	(0.012)	0.164	0.090	(0.002)	(0.001)	(0.002)
	MC	0.004	0.191	0.049	0.044	0.024	0.017	0.135	0.077	0.003	0.000	0.000
(5-1)	EX	(0.021)	(0.054)	–	(0.032)	(0.020)	(0.013)	0.217	0.224	(0.042)	(0.002)	(0.003)
	MC	0.017	0.065	0.019	0.018	0.014	0.014	0.202	0.229	0.039	0.003	0.000
(5-2)	EX	(0.037)	(0.068)	(0.049)	–	(0.019)	(0.013)	0.143	0.285	0.180	0.035	(0.003)
	MC	0.041	0.080	0.027	0.010	0.010	0.009	0.126	0.293	0.200	0.031	0.003
(5-3)	EX	(0.045)	(0.053)	(0.042)	(0.027)	–	(0.019)	(0.028)	0.127	0.306	0.170	0.026
	MC	0.060	0.069	0.030	0.012	0.010	0.009	0.027	0.138	0.294	0.179	0.028
(5-4)	EX	(0.045)	(0.045)	(0.039)	(0.026)	(0.026)	–	(0.005)	(0.033)	0.130	0.274	0.139
	MC	0.059	0.060	0.039	0.018	0.013	0.011	0.008	0.031	0.150	0.266	0.154
(4-1)	EX	0.518	0.204	0.214	0.093	(0.013)	(0.002)	–	(0.021)	(0.006)	(0.001)	(0.000)
	MC	0.490	0.162	0.194	0.079	0.011	0.002	0.021	0.003	0.000	0.000	0.000
(6-1)	EX	(0.024)	0.091	0.178	0.151	0.047	(0.009)	(0.017)	–	(0.012)	(0.004)	(0.001)
	MC	0.023	0.081	0.184	0.159	0.050	0.008	0.003	0.012	0.010	0.002	0.000
(6-2)	EX	(0.005)	(0.004)	(0.059)	0.166	0.200	0.061	(0.008)	(0.021)	–	(0.013)	(0.004)
	MC	0.000	0.002	0.053	0.183	0.194	0.072	0.000	0.017	0.013	0.007	0.002
(6-3)	EX	(0.004)	(0.003)	(0.004)	0.048	0.165	0.191	(0.003)	(0.009)	(0.019)	–	(0.007)
	MC	0.000	0.000	0.001	0.045	0.165	0.192	0.000	0.005	0.011	0.010	0.006
(6-4)	EX	(0.010)	(0.007)	(0.007)	(0.005)	0.033	0.129	(0.001)	(0.003)	(0.007)	(0.009)	–
	MC	0.000	0.000	0.000	0.002	0.040	0.138	0.000	0.000	0.004	0.008	0.007
Sum of experiment		1.032	0.854	1.069	0.996	0.978	0.939	1.095	0.999	0.951	0.990	0.986

[a]Values in parentheses were obtained from TRASYS (Reference [6]).

Table 1 shows a comparison of calculated exchange factors between strips with experimental data. In both cases the emitting strip was assumed (or held) at the constant temperature of 27°C (80°F). The exchange factors from strips to space are the fractions of emitted energy that leave the cavity through all openings, front, rear, and sides. Also included in Table 1 are values for the exchange factors to space as obtained by the TRASYS computer code (Reference [6]), which assumes plane strips with gray, diffuse surface characteristics. In general, the agreement between the experimental exchange factors and the results obtained by the Monte Carlo method is excellent, in spite of the fact that only scarce surface property data were available. Much of the small discrepancies may be attributed to experimental inaccuracies. For small exchange factors the experiment became too unreliable, so the TRASYS data were used. The experimental uncertainty is illustrated by the last row in Table 1, which shows that the sums of the experimental exchange factors do not add up to unity as they should, indicating at least a 10% error margin. (The error is larger in the case of strip (2-1) + (3-1) because of significant self-irradiation, which the experiment neglects.) Not surprisingly, the TRASYS results are also fairly accurate for infrared emission, as the reflectivity of the silver-backed Teflon coating is low in this wavelength range. In the Monte Carlo calculations, an average of about 20,000 energy bundles were traced from each emitting strip. Duplicate runs with different sets of random numbers showed that the results can be assumed accurate to ± 0.005, well within experimental accuracy. With such a tolerance it took approximately 1 min. to calculate the exchange factors from one strip to all strips and openings, using a Univac 1110 computer. This amount of computer time compares favorably with the time used by the less sophisticated TRASYS program, which employs fourth-order integration.

A summary of solar irradiation exchange factors is shown in Figures 7 and 8. In these calculations it is assumed that the sun rays are parallel to the sides of the cavity (i.e., perpendicular to the Shuttle axis) so that all insolation enters through the front openings. The solid lines show exchange factors calculated with absorptivities obtained from the previously discussed correlation and bidirectional reflectivities that direct about 99% of all reflected energy into a cone of 3° half-angle around the specular direction, as indicated by a few experimental data for silver-Teflon. The agreement with experiment is fairly good,

especially if one considers that the high

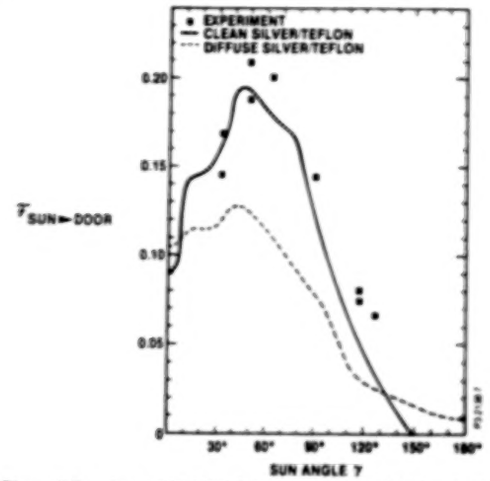


Figure 7 Fractions of Incident Solar Flux Absorbed by Bay Door

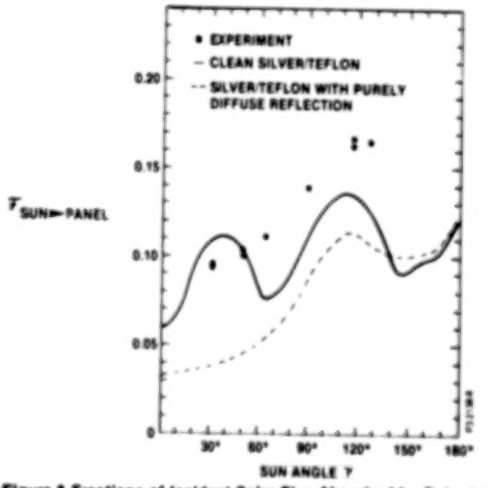


Figure 8 Fractions of Incident Solar Flux Absorbed by Rejector Panel

reflectivity of the surface (≈ 90%) tends to amplify small inaccuracies in the data for reflectivities and geometry. It is interesting to note what happens to the values of the exchange factors if the surface is a purely specular of a purely diffuse reflector. In the case of purely specular reflection the results practically coincide with the actual reflection pattern, and are therefore not displayed separately. For purely diffuse reflection the absorption rates are reduced, as is the dependence on solar incidence angle. This is shown by the dashed lines. The experimental data seem to follow a diffuse reflection pattern, but with higher absorptivities. This suggests that in the experiment (Reference [5])not enough care was taken to keep the surfaces free of dust or other contaminants, which would tend to increase absorptivity and make reflection more diffuse. In the Monte Carlo calculations about 10,000-20,000 energy bundles were traced for each solar incidence angle. Computer time on the Univac 1110 was again on the average about 1 min. for each incidence angle.

RADIATOR FIN OPTIMIZATION

The radiator panel design is primarily based on design criteria other than thermal. Structural requirements dictate a panel face sheet and honeycomb thickness greater then would be required for weight optimum heat rejection. The coolant loop hydraulic requirements limit the allowable panel pressure drop and hence set the tube size. The only variable available for weight optimizing heat rejection is the tube spacing or number of tubes on the panels. The forward panel (radiation from two sides) tube arrangement also presents an opportunity for optimizing heat rejection. As shown in Figure 4, the tubes on opposite face sheets are staggered to allow heat transfer from the tube through the honeycomb to the opposite face sheet. This effectively increases the radiation fin efficiency by raising the average radiation temperature.

Tube Spacing

The tube spacing or number of tubes on the panel determines the radiation fin effectiveness. As the number of tubes is increased, the fin effectiveness and hence heat rejection are increased but panel weight is also increased. Radiation fin effectiveness of the forward and aft honeycomb layup fin was determined from a two dimensional thermal model which considers heat transfer perpendicular to the tube direction and between the face sheets. The thermal models were verified by element and full scale prototype test data. Figures 9 and 10 show the variation in fin effectiveness with the number of tubes.

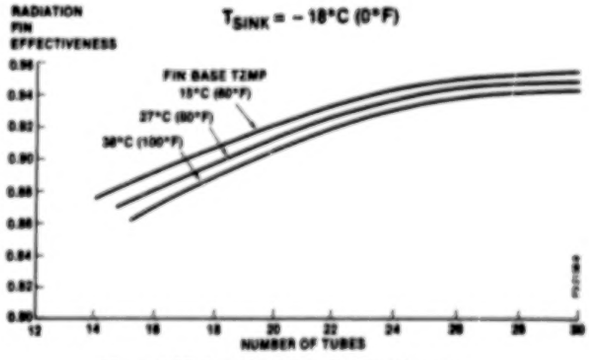


Figure 9 Aft Panel Radiation Fin Effectiveness

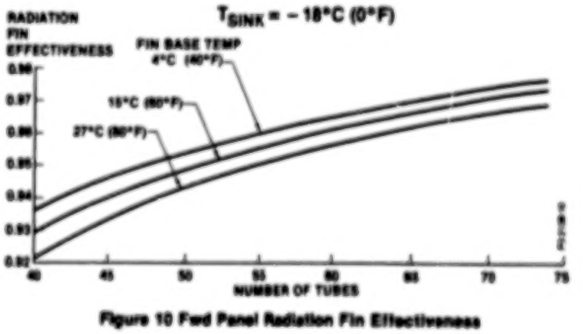


Figure 10 Fwd Panel Radiation Fin Effectiveness

Tube Size

The radiator tube size is selected to meet the panel pressure drop requirements and to provide a minimum temperature drop between the fluid and the tube. Due to the relatively low thermal conductivity of R-21, the flow must be in the turbulent region to provide adequate heat transfer coefficients. Figure 11 shows the

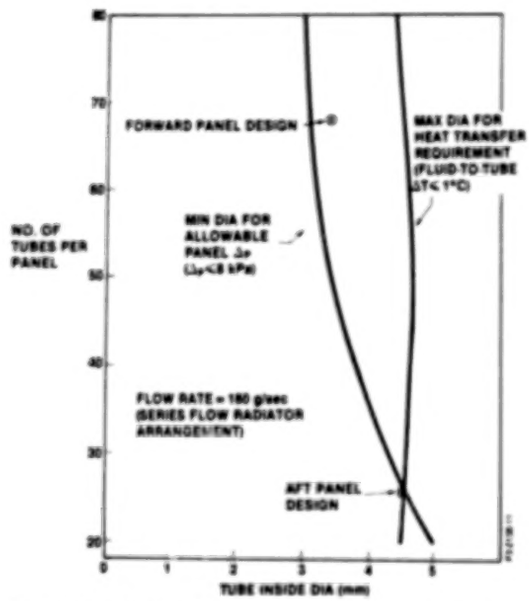


Figure 11 Number of Radiator Tubes versus Allowable Inside Diameter

allowable tube diameters as a function of the number of radiator tubes. A somewhat arbitrary criteria of a 1°C temperature difference between the fluid and tube is used in this analysis. As indicated, the range of allowable diameters is narrow, and at least 26 tubes are required to meet both the pressure drop and heat transfer criteria. For the heat rejection optimization study a baseline design was established and variations were considered to determine their effect on weight and performance. The relationship between pressure drop, tube diameter and number of tubes is given by:

$$\Delta P = f\left[\frac{w^{1.75}}{D^{4.75}}\right] = f\left[\frac{1}{D^{4.75}}\right]\left[\frac{1}{N^{1.75}}\right] \qquad [4]$$

where ΔP = tube pressure drop
w = tube flow rate
N = number of tubes
D = tube diameter

The fluid to tube area for heat transfer times the convection heat transfer coefficient (hA) is a function of the number of tubes to the 0.2 power and the inverse of the tube diameter to the 0.8 power,

$$hA = f\left[\frac{N^{0.2}}{D^{0.8}}\right] \qquad [5]$$

for turbulent flow. Thus the effect of the number of tubes on hA is found by finding the tube diameter from the pressure drop relationship and the change in hA from the above relationship.

Heat Rejection

A system thermal model that had been verified by correlation with test data was used to optimize the tube spacing. Appropriate fin effectiveness and hA products for various tube spacings were input to the model to determine system heat rejection. Panel weight variations with the number of tubes were used to determine the heat rejection rate per unit weight (BTU/hr-lb). Both 6 panel and 8 panel systems were considered. The heat load and orbital attitudes were chosen such that the heat rejection requirement exceeds the system capacity. This prevents radiator bypass and provides heat rejection optimization under conditions which require maximum radiator performance.

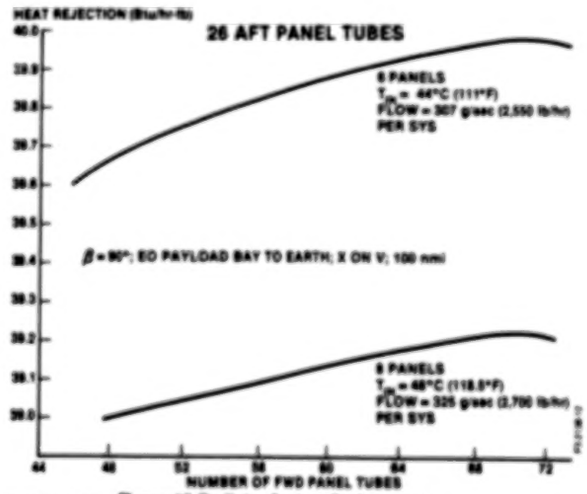


Figure 12 Radiator System Performance

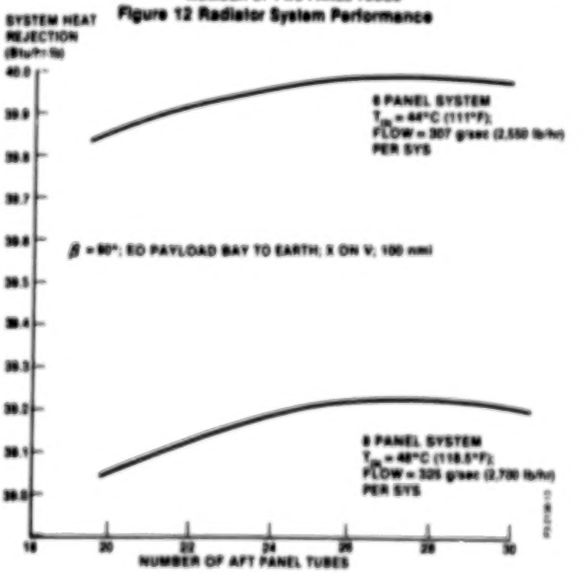


Figure 13 Radiator System Performance

Figures 12 and 13 show the system heat rejection per unit weight as a function of the number of tubes on the forward panel and aft panel respectively. It is seen that for both the six panel and eight panel systems the optimum number of forward panel tubes is 70. However, the use of 70 tubes required a non-standard tube inside Diameter of 3.269 mm (0.1287 in). A 68 tube forward panel allows the use of a stock 4.7625 mm OD tube with 0.71 mm wall thickness (3/16 x .028 in) and provides a near optimum design. The cost and schedule aspects of using stock tubing overrides the slight performance gain of the optimum design panel, thus the 68 tube forward panel design was selected.

The aft panel optimization (Figure 13) indicates optimum performance in the range of 26 to 29 tubes. Again, based on the criteria of using stock tubing (6.35 mm OD with 0.889 mm wall thickness) (1/4 X .035 in.) a 26 tube aft panel design was selected. It should be noted that both the forward and aft panel stock tubes are chemically milled to the outer diameters shown on Figure 4 as a weight savings measure.

SYSTEM PERFORMANCE

Performance of the radiator system can be predicted with a high degree of accuracy using large scale computer routines. Results from the foregoing analysis were used to develop a thermal model of the radiator system which includes Orbiter structure with which the radiators interchange energy by thermal radiation. The techniques used and the results of these analyses are reported in detail by Benko (References [7] and [8]) and Howell and Williams (Reference [2]).

Temperature Control

Each of the two R-21 flow loops in the Orbiter contains a Flow Control Assembly (FCA) which performs temperature, fluid flow, pressure drop control and fault detection functions. Incorporating all of these control requirements, some of them quite unusual was a major challenge in hardware design. One such function: temperature control of the coolant is accomplished by simple bypass of the radiators, as shown schematically in Figure 2. Electronic controllers regulate the Flow Control Valve position to maintain the mixed outlet temperature at either 3.3 $\pm$ 1°C or 14.4 $\pm$ 1°C, as selected by the crew. Specifically, the temperature control approach is a closed loop control system with velocity damping. The flow control valve is driven by a stepping motor with approximately 2200 steps from the full radiator flow to full radiator bypass positions. The stepping rate to the valve motor is a function of the temperature error and the rate of change of the temperature error as given by the equation:

$$P = Ge\ Te + Gr\ \frac{d(Te)}{dt} \qquad [6]$$

where P = the pulse rate or stepping rate, pulses/sec.
Ge = The temperature error gain
= 11 Steps/sec-°C (6 steps/sec-F) nominally
Gr = The temperature rate of change gain
= 25 Steps/°C (14 steps/ °F nominally
Te = The sensed temperature error
= Tsen-Tset
Tsen = Sensor temperature,
Tset = The set point temperature, 3.3°C or 14.4°C (38°F or 57 °F) by crew selection

The pulse rate has the limitations of 24 pulses per second maximum and a dead band of zero pulses per second when a pulse rate of less than approximately 1.0 pulses per second is called for. The rate of change term, Gr, was added to the control function when the requirement was imposed to maintain the sensor temperature, Tsen, above the fault temperature of 0.6 $\pm$ 0.3°C (33 $\pm$ 0.5°F) when a rapid decrease in bypass temperature, T_B (see Figure 2) occurs. This rapid decrease in the bypass temperature could be as high as 1.4°C/sec (2.5°F/Sec) given by the following relation

$$T_B = T_{BO} - 20\ (1-e^{-t/8}) \qquad [7]$$

where T_B = radiator inlet temperature during downramp, °F.
T_{BO} = Radiator inlet temperature at start of downramp, °F.
t= time from start of downramp seconds.

This severe transient requirement also imposed restrictions on two other components in the control circuit. The flow control valve was designed to counter the nonlinear variations of the system flow characteristics to provide a linear flow split that is within a band of 15% of full flow and with a local slope of one half to twice the linear slope. In addition the temperature sensor, shown in Figure 2 was required to have a low time constant. The temperature sensor is mounted in a dry well (could be removed without fluid loss) which is filled with thermal grease (Eccotherm TC-4). The resulting time constant has been estimated by correlating test data to be 2.74 seconds for the time constant following a 1.13 second time delay for the fluid temperature change at the control valve to reach the temperature sensor.

There are two valves in each FCA in addition to the Flow Control Valve. The Bypass Valve is plumbed in parallel with the Flow Control Valve with the Bypass Valve in the dominant position. During launch and re-entry the bypass valve is manually activated by the crew to divert flow around the radiator subsystem. The mode control valve is a pre-launch, ground operated hand activated on-off valve which is used to set the pressure drop characteristics of the flow control valve bypass line according to whether six or eight

radiators are being used (to satisfy a requirement that the R21 loop flowrate be lower for eight panels than for six). The pressure drop requirements are shown in Table 2 for the six panel and eight panel system configurations.

TABLE 2 ALLOWABLE FCA PRESSURE DROP

MODE	FLOWRATE g/s(lb/hr)	ΔP ACROSS FCA - kPa(psi) MAX	MIN
6 PNLS	283 (2350)	186 (27.1)	69 (10.0)
6 PNLS	307 (2550)	219 (31.9)	89 (13.0)
8 PNLS	301 (2500)	137 (20.0)	62 (9.1)
8 PNLS	325 (2700)	160 (23.3)	72 (10.4)
BYPASS	331 (2750)	21 (3.0)	-

The Flow Control Valve also required special flow/pressure drop characteristics to meet the system pressure drop needs. Figure 14 shows the valve pressure drop versus valve position designed into the valve by shaping of the poppet to provide the pressure drop control.

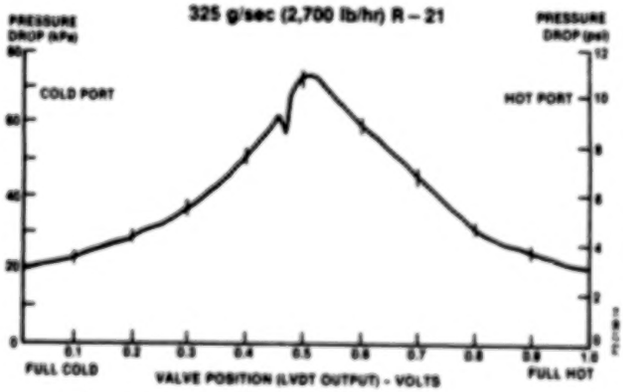


Figure 14 Development Flow Control Valve Acceptance Test Data

The fault detection system on the FCA monitors the temperature of the controlled outlet fluid temperature and automatically switches the bypass valve to full bypass if the temperature goes below 0.6 ± 0.3°C (33 ± 0.5 °F). The FCA also provides for performance monitoring which supplies an electrical signal proportioned to the FCA outlet temperature. The signal is a DC voltage which is zero VDC at -1°C (30°F) and is 5 VDC at 18°C (65°F) The bypass valve positions are also indicated by the performance monitoring system.

FLOW TUBE/STRUCTURE/THERMAL CONTROL COATING INTEGRATION

Thermal control coating selection is a significant challenge for Space Radiators. The desired charactertics for a space radiator coating are high energy emission (low reflectance) in the infrared (or low-temperature) spectrum while being highly reflective in the solar spectrum. The coating also needs to be unaffected by the space environment.

The two general types of coatings used for space radiators are white paints and optical solar reflectors. At the time of the Orbiter radiator development, the optical solar reflector silver-backed Teflon was selected as the best available coating considering thermal performance, maintenance, weight, life, and life cost. A major development program was required to find an adhesive which would satisfactorily bond silver-backed Teflon to structure over the required temperature range of -200°C to 100°C. The selected adhesive was silicone based Permacel 223. An autoclave cure process was developed for using the silver-backed Teflon's P223 adhesive to aluminum. The process will keep P223 bonded to aluminum over a temperature range of -300°C to 120°C in a vacuum.

While thermal studies were showing the need for adhesively bonded silver-backed Teflon, structural analyses were indicating the need for a fatigue resistant structure such as bonded honeycomb. It quickly became apparent that adhesively bonding silver-Teflon to radiators having closely spaced tubes on the outside of the conductive fin, as would be required on the two-sided forward radiators, would be particularly time consuming and conducive to unsatisfactory workmanship. Thus a scheme was developed for embedding the tubes inside the radiator honeycomb layup to provide the smooth surface for silver-Teflon application shown in Figure 4. The smooth exterior surface permits the use of vacum bagging to maintain pressure on the silver-Teflon during the adhesive cure process.

It was found that using conventional raidator tubes with a flange which bonds to the radiator skin was difficult when the tube is embedded in the honeycomb core. Analyses showed that standard round tubes could be used if the bond line between the tube and the skin could be sufficiently reduced and a conductive adhesive was used. A technique was developed for bonding the radiators so the tube-to-skin bond line thickeness would be 0.08 mm or less. This gives a tube to skin temperature drop of 0.5°C, under maximum heat rejection conditions. This compares favorably to other radiator tube-to-fin attachment configurations.

The conductive adhesive, Metlbond 329-7, is loaded with aluminum powder to increase its thermal conductivity. This provides another plus for the radiator honeycomb structure since the aluminum powder loading makes the adhesive's thermal expansion coefficient more nearly match that of aluminum. This permits the structure to operate over a temperature range of -200°C to +175°C without delamination due to thermally induced stresses.

FLUID SYSTEM SEALING

The Orbiter radiator system has a maximum allowable leakage rate of 0.03 scc per second (0.0011 lb/hr). Loss of fluid is to be avoided for the obvious reason that carrying make-up fluid is expensive, and the leaked-out fluid may contaminate other Orbiter systems or payloads. All welded construction was desirable for the Orbiter radiator system to eliminate leakage.

FLANGE JOINTS

Welding was not practical for the connection of the aluminum radiators to the stainless steel flex hoses between radiators as shown in Figure 15. Flange joints were selected

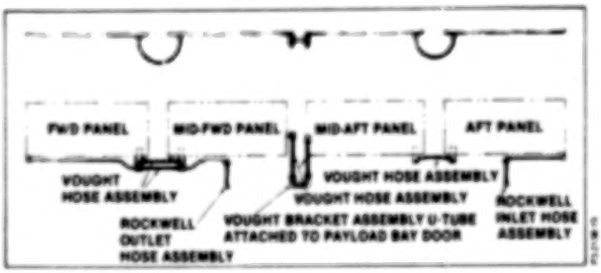


Figure 15 Radiator Interpanel Plumbing

for this joint because effective dissimilar metal corrosion protection is easily provided for them. The aluminum flange is anodized and the stainless steel flange is passivated, and both are coated with super Koropon except on the flange face. When the joint is made, RTV is applied to the interface region.

Obtaining a seal was a more formidible challenge because of the wide temperature range of the radiators (-130°C to 120 °C), and the material compatibility problems associated with R-21. Teflon is the material of choice for R-21 seals; however, it is not satisfactory in O-ring form for the radiator temperature range. Teflon omni-seals were selected because the spring in these seals keeps the seal lips in place over the desired temperature range. In order for the Teflon omni-seal to form a leak-tight seal, it was found that the flange faces should be finished with a tool that has a rotary motion, and that the finish should be in the range of 32-63 -in. RMS. Smoother finishes, or those in which rotary motion of the tool was not used were found to be prone to leak.

MANIFOLD WELDS

The numerous tubes in each radiator are welded into manifolds at each end as shown in Figure 16. The flow tubes are 6061-T6 Aluminum Alloy to provide the yield strength required due to bending of the radiators. Welding of the flow tubes into the manifolds produced "hot short" cracks in the manifolds with all manifold materials and welding techniques tried. Finally a suitable material, Aluminum Alloy 5083, was

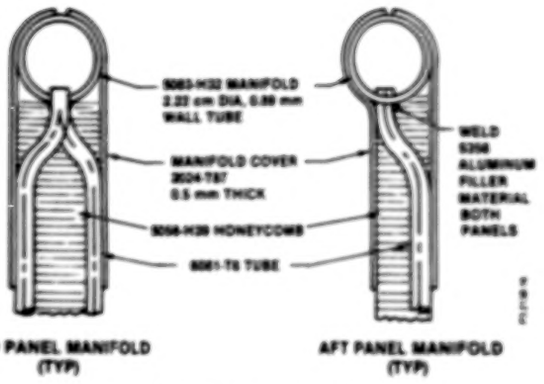


Figure 16 Radiator Manifold Details

found. However, 5083 is not commercially available in seamless tube form. And, while it generally has excellent corrosion characteristics, it is susceptible to stress corrosion if improperly thermally conditioned. Vought bought a billet of 5083 and had it processed into 2.22 cm (7/8-inch) O.D. manifold tubing (Reference [9]). This tubing completely eliminated welding problems throughout the program.

LEAKAGE DETECTION

Proving that leakage of the radiators was within the allowable range was a significant challenge. Halogen detectors are used with great success to verify there is no leakage from the flange joints; however, it is difficult to obtain a quantifiable leakage rate from a large structure such as the radiators with this technique. Vought developed a technique for measuring leakage from an entire radiator. This was done by calibrating a gas Partial Pressure Analyzer reading with a known R21 leak rate within the thermal-vacuum chamber used for radiator acceptance testing (Reference [10]). Most of the radiators have a leakage rate below the minumum detectable level of 10^{-4} scc/sec.

LOADS AND STRESS ANALYSIS

The Orbiter lift-off acoustic noise environment has unusually high energy levels at low frequency; in the 10-20 Hz range in which the large radiators are highly responsive. Determining the loads and stresses on the radiator was a major challenge involving state-of-the-art finite element computer analysis which is beyond the scope of this paper to describe. However, The importance of this challenge was of such magnitude that it must be mentioned in any compilation of Radiator Design Challenges.

Dynamic response models of the entire Orbiter (generated by Rockwell International) were combined with models of the radiators to determine radiator loads. These loads were then used to size radiator structural components. These are reported in References [11] and [12],

and and to very limited extent in Reference (2). The work of Mr. Ron Ott (deceased,1981), was particularly significant in the structural design of the radiator systems.

CONCLUSIONS

The Orbiter radiator system has performed flawlessly as expected during the first six Shuttle flights. During execution of the program all major milestones and all hardware deliveries were met on schedule. In addition, the program was completed under the planned budget. This factor, when considered together with those technical challenges discussed herein, illustrates the extent to which the challenges of Space Shuttle Orbiter Radiator design were satisfied. The well-conceived and executed space radiators research and development programs carried out in the late 1960's and early 1970's provided the basis for the success of the Orbiter Radiator program.

REFERENCES

(1) Williams, J. L. ; and French, R. J.: Space Shuttle Orbiter Radiator System. Seventh Intersociety Conference on Environmental Systems, ASME paper 77-ENAs-33, 14 July 1977.

(2) Howell, H. R.; and Williams, J. L. : Qualification of the Space Shuttle Orbiter Radiator System. Eleventh Intersociety Conference on Environmental Systems, SAE Paper 820886, 21 July 1982 (to be published in SAE Proceedings).

(3) Modest, M. F.; and Poon, S. C.: Determination of Three-Dimensional Radiative Exchange Factors for the Space Shuttle by Monte Carlo; ASME Paper 77-HT-49, 1977.

(4) Modest, M. F.: Three Dimensional Radiative Exchange Factors for Nongray, Nondiffuse Surfaces. Numerical Heat Transfer, Vol. I, 1978. pp.403-416.

(5) Scheps, P. B. ; and Howell, H. R.: The Effect of Radiation Trapping within the Cavity Formed by the Shuttle Forward Radiative and Payload Bay Door. ASME paper 76-ENAs-55, 1976.

(6) Thermal Radiation Analysis System (TRASYS), Martin-Marietta, Contract NAS9-13033, 1973.

(7) Benko, D. J.: Combined Radiator and Payload Bay Door Thermal Analysis. Vought Report 224RP0100, 22 Dec 1977.

(8) Benko, D. J.; Postflight Radiator Performance Assessment for STS-4 Mission. Vought Report 2-53200/3DIR-014, 10 May 1983.

(9) Vought Specification 207-2-407; Tube, Aluminum Alloy, Drawn, Seamless, 5083; 12 Nov. 1976.

(10) Vought Specification 205-24-019C; Acceptance Test Specification for Radiator Kit, No. 2BB, 11 Nov. 1980.

(11) Ott, R. E.; Radiator Structural Dynamics Report. Vought Report 224 RP 0113A, 16 March 1981.

(12) Payne, C. W. ; Space Shuttle Radiator Stress Analysis, Vought Report 224 RP 113 C, 23 Sept. 1981.

N85
16926

UNCLAS

D37 N85-16926

OVERVIEW OF STS GROUND OPERATIONS/ORBITER TURNAROUND STS-1 THROUGH STS-7

Richard Schwartz*
Rockwell International
Shuttle Launch Operations Division
Kennedy Space Center, Florida

ABSTRACT

A review of STS-1 processing is presented as a reference for Shuttle processing time and the magnitude of the associated modifications, discrepancies, technical requirements, and ground systems activities. STS-1 processing provided the basis from which a plan to perform operational turnaround was established. Turnaround processing for Launch and Landing are treated separately to depict more clearly the progress made to reduce turnaround time and manhours expended.

Turnaround time was reduced from 187 days for STS-2 to 60 days for STS-7 and landing turnaround was reduced from 14 days to 5 days. Modifications were reduced from 114 to 51. Requirements changes for launch readiness verification were reduced from 536 to 107. Special tests or inspections were reduced from 292 to 52. Anomalies resolved concurrent with processing were reduced from 13,000 to 4,000.

While total turnaround time was reduced, the relative time spent in the Orbiter Processing Facility (OPF) continue to be one half of the turnaround. Integration in the Vehicle Assembly Building (VAB) is about 10 percent of the flow, and Launch Pad operations comprise 40 percent of the turnaround.

As turnaround operations matured, the volume of work and turnaround time steadily decreased. The work force has matured and has demonstrated the capability to perform planned and contingency operations. The turnaround program is fast approaching the goal of becoming operational. The challenge ahead is to transition from a development-dominated operation to a production oriented operation.

INTRODUCTION

In the last two decades many major technical projects have been designed concurrent with the planning of their operational phases. The Space Shuttle program exemplifies the challenge of concurrency, which is management of a project while significant factors are very dynamic. Ground operations for the Shuttle Orbiter flight test program were planned during the design and build phases of both the flight and ground systems. This planning of ground operations before the flight systems design certification and qualifications were completed later necessitated changes to insure compatibility. Facilities and support equipment were constructed before flight hardware had been completely defined, and later required changes as well.

Our progress toward achieving a repetitive operation with reduced turnaround time is easily traced. The approach was founded in the proven techniques of airline maintenance and aircraft fabrication. Maximum effort has been expended to establish a standard processing flow cycle that is repeated on each flight, while still dealing with the peculiar features of payloads or flight anomalies. To accomplish this, we have carefully evaluated requirements reductions, efficiency improvements, and design changes that could shorten the turnaround and reduce the cost per flight. Each of these improvements has been carefully analyzed to assure there is no degradation in safety and to assure mission success.

Requirements for ground processing are prepared by the design centers and levied on the operational center by the Operations and Maintenance Requirements Specification Document (OMRSD). These requirements have been carefully analyzed for reductions by the design and operational centers starting with STS-1.

Important among these reductions has been the retention of hypergolic propellants on the vehicle. Implemented only after a careful review by safety system engineers, hypergolic retention has saved significant time in the processing flow. No significant safety issue has occurred due to this operational improvement.

*Vice President & General Manager, RI-KSC

Excellent progress has been made in firming processing procedures, and this has provided greater ground crew proficiency and efficiency. Procedures have been subjected to post-test critiques with both engineering and operations personnel. These critiques have improved operational sequences and eliminated unncessary steps.

Improvements have also been made in simplifying the work documents from which the technician must work, allowing him to spend more time on the job and less time obtaining related instructions. Another improvement is the provision of parts and tools to the work areas on a planned schedule.

These improvements, enhanced by the constant attention to bettering the operational turnaround, have resulted in a great reduction in the expended manhours per flight. Figure 1 shows the reduction in turnaround days and Figure 2 the reduction in manhours per flow. Continued application of these techniques and improvements will allow the Shuttle program to achieve and exceed its cost per flight objectives.

STS-1 PROCESSING

One of the major challenges of the Design, Development, Test and Engineering phase of the Space Shuttle Program was to develop the basic ground operations techniques which will be the cornerstones for the operational era ground processing methods. Two major criteria must be satisfied: fulfillment of the technical requirements of this highly complex spacecraft to certify its flightworthiness and accomplishment of major processing milestones that had been scheduled some months in advance. Ground operations are conducted to support a traffic model of 24 to 30 annual launches from the Kennedy Space Center and 6 to 10 launches from Vandenberg Air Force Base, California by 1990. These criteria must be met while still maintaining a high degree of flight safety and systematically reducing the cost per flight.

The ground operations effort for STS-1 cannot be assessed as a measure of Orbiter turnaround since these activities focused almost entirely on certifying Orbiter 102 for its maiden flight. Orbiter 102 arrived at KSC on March 25, 1979 and launched on April 12, 1981 - 744 days after its arrival. During this two-year period, 340 modifications were made to the Orbiter. In addition to these modifications, approximately 24,000 thermal protection system tiles (over-thirds of the total number of tiles which comprise the outer mold line of the Orbiter) were removed, densified, and reinstalled. This period also saw a tremendous effort in the development, evaluation, and changing of Operations and Maintenance Requirements Specifications and the development of Operations and Maintenance Instructions (OMI's) to implement the requirements. One thousand four hundred thirty-three (1,433) OMI's were developed to process STS-1. These procedures contained almost 250,000 pages of detailed processing instructions, special instructions such as operational and safety notations, data sheets, and emergency procedures. Formal approval of 2,373 Requirement Change Notices (RCN's), as well as numerous operational and safety requirements, resulted in virtually all of the OMI's for STS-1 being revised prior to or during their use. The STS-1 task was further complicated by the parallel efforts of modification of Apollo program facilities and ground support equipment, and new design, construction, and activation to support the STS-1 flow. As an indication of this effort, 9,273 design/modification packages were released to support the initial ground processing of the Space Shuttle vehicle.

Operational concepts on how to process a reusable spacecraft were developed, tested, and modified, and eventually resulted in vastly improved ground operations. New and modified processing and launch facilities were evaluated. A vast majority of the written processing procedures were developed and improved to support future Space Shuttle missions. Basic methods of doing business were developed into plans and detailed into implementing instructions implemented, and modified, as required, to streamline operations. The major benefit derived from this flow was the invaluable training the processing team gained in this first processing effort. The actual "hands-on" experience is resulting today in continuing processing improvements and lower cost per flight of operational Shuttle vehicles.

This massive effort culminated on April 12, 1981, at 0700:03.9834 EST when the Columbia, with Astronauts John Young and Bob Crippen aboard, lifted off from Launch Complex 39A and inaugurated a new era in manned space flight. During its planned mission of 54.5 hours, the Columbia completed 36 orbits of the Earth and landed at the Dryden Flight Research Facility at Edwards Air Force Base, California at 1022 PST on April 14, 1981. After the flight crew egressed, the Orbiter was towed to the mate/demate device for safing of systems, reconfiguring for transportation, and mating of the Orbiter to the Shuttle Carrier Aircraft (SCA). Ferry operations began on April 27 with SCA takeoff occurring at 1016 PDT. After an overnight SCA refueling stop, the Orbiter returned to KSC on April 28; just 16 days after launch. This successful landing and ferry operation completed the last phase of the STS-1 ground operations.

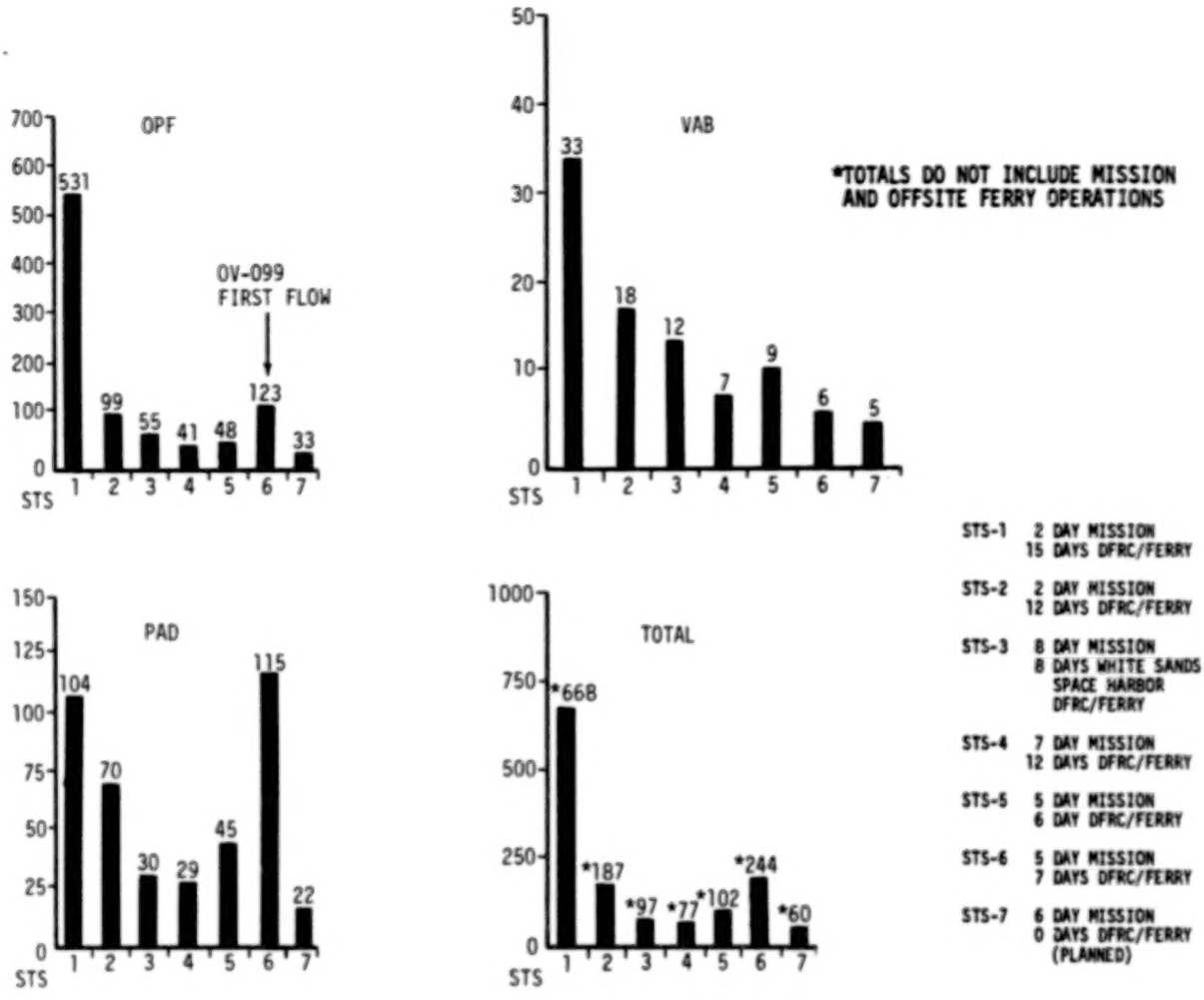


Figure 1.- STS Processing Times (Working Days).

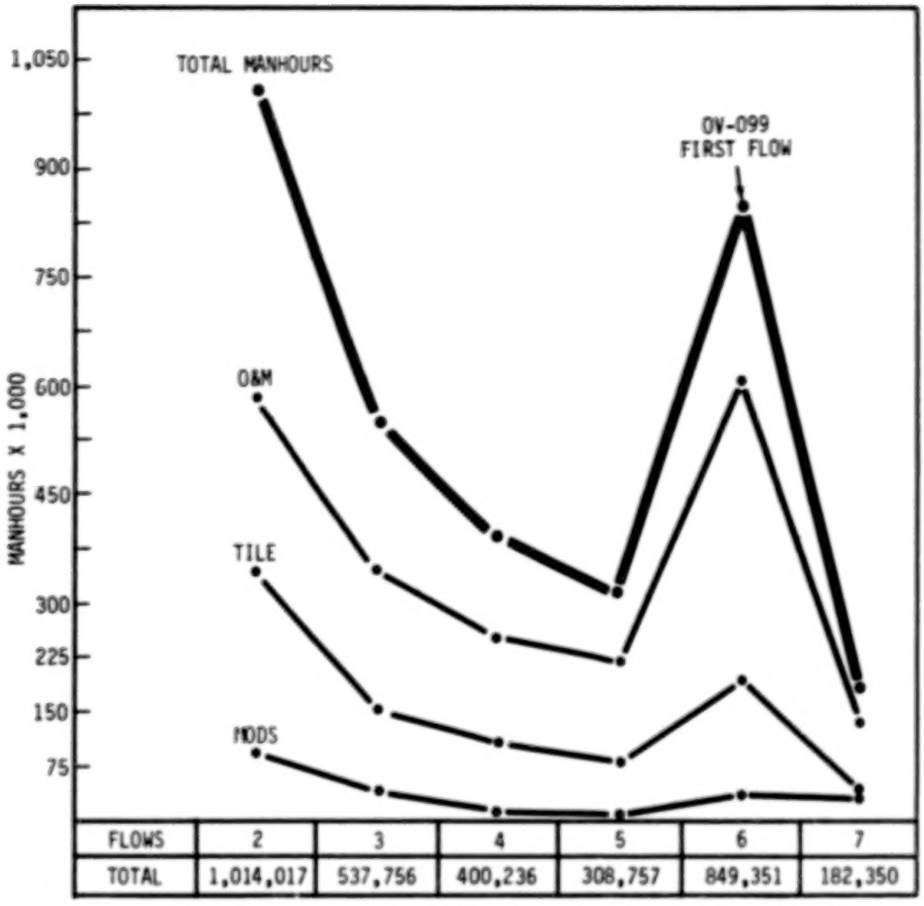
MATURATION OF SHUTTLE PROCESSING

The ground operations for STS-2 constituted the first Orbiter turnaround processing. It is from this processing flow that we have developed the data parameters to measure our performance toward our goal of processing Orbiters more efficiently at reduced cost.

The best measure of turnaround time is the actual number of working days required to process each flow. In examining the number of work days to process each STS flow, it is obvious that the data trend indicates a continuous improvement in each succeeding turnaround (Figure 3). The apparent exceptions to this trend is the number of days required to process STS-5 and STS-6. On these flows, the Orbiter spent more time in ground processing than for STS-3 and STS-4. On STS-5 this was due mainly to the first cargo installation with the vehicle on the launch pad. STS-6, of course, was the first flight of OV-099.

The trend in the reduction of turnaround time is continuing on subsequent operational flights. The total processing time for STS-7 was only 60 working days, with the processing time for STS-8 projected to be approximately 50 working days.

The continuing decrease in processing time can be attributed to the maturing of the flight hardware, decrease in the number of requirements and procedure changes, and an increased proficiency of the processing team. For turnaround flows for STS-2 through STS-7, the data indicate a continuing decrease in the number of Revision Change Notices, Master Change Records, Engineering Orders, and Work Volume Indicators worked for each flow. The total number of Work Volume Indicators includes Discrep-



FLOWS	2	3	4	5	6	7
TOTAL	1,014,017	537,756	400,236	308,757	849,351	182,350

Figure 2.- Total Manhours per Flow.

ancy Reports, Problem Reports, Interim Problem Reports, Operations and Maintenance Instructions, and Test Preparation Sheets. A massive reduction in the total number of work items performed is shown. Figure 3 illustrates these trends.

Some of the major requirement reductions and procedure changes that contributed to reduced turnaround time are: retention of residual OMS/RCS hypergolic propellants on-board the Orbiter; parallel loading of OMS, RCS, Orbiter APU and SRB APU propellants; reduced flight control system testing; deletion of dynamic integrated tests in the OPF and VAB; deletion of wet countdown demonstration tests; and improved propulsion system leak check methods.

In addition, a major contributor to the reduction in Work Volume Indicators and in processing time is the drastic reduction in tile work. The data indicate a progressive trend in decreasing tile repair with the exception of Flow 5 (Figure 4). A slight upturn of the trend is due mostly to a large number of tiles suffering minor damage in a hail storm just prior to the launch of STS-4, with this damage being repaired during the STS-5 flow.

An important indicator of the relative processing cost of each flow is the total manhours worked per flow. Figure 2 shows the total number of manhours charged against each flow, with each flow being less than the preceding flow. Also indicated is the consistent decrease in the percentage of total manhours devoted to modifications and tile work along with the corresponding manhours spent in Operations and Maintenance effort. This favorable trend is the key to accurate cost estimates for each flight in the operational era.

Recovery and ferry operations to return the Orbiter from the landing site to KSC have continuously shown the same favorable data trend as the KSC turnaround (Figure 5). The data show an upturn in manhours to recover STS-3, but it must be remembered that the STS-3 landing was moved from DFRF to White Sands Space Harbor, New Mexico, neccessitating transporting ground support equipment and personnel from California to New Mexico in a relatively short time.

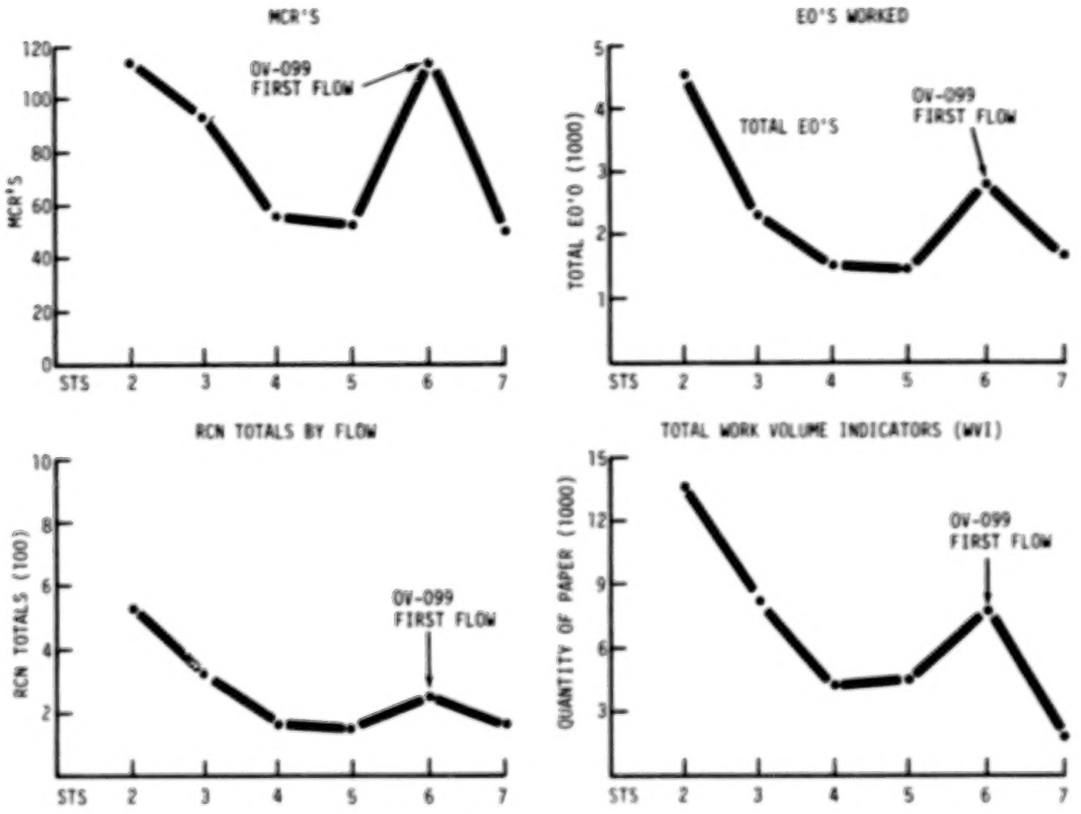


Figure 3.- Total Requirement Trends.

Flight safety has been outstanding, as indicated by the fact that of the six flights completed as of this writing, only STS-2 did not complete its intended mission duration. The anomaly on that mission, a malfunctioning fuel cell, was not related to ground operations, and did not jeopardize the safety of the crew or the vehicle.

In summary, the overall trend has been to perform each ground turnaround flow in fewer working days and with significantly fewer manhours expended during each successive flow. This overall reduction in time and cost has also been accompanied by a consistently decreasing number of in-flight anomalies (Figure 6). The increase shown in flight 6 anomalies is due to the fact that the flight was the first of OV-099. This indicator is indicative of flight hardware maturity, higher quality of workmanship, and increased understanding of the operation of the flight hardware.

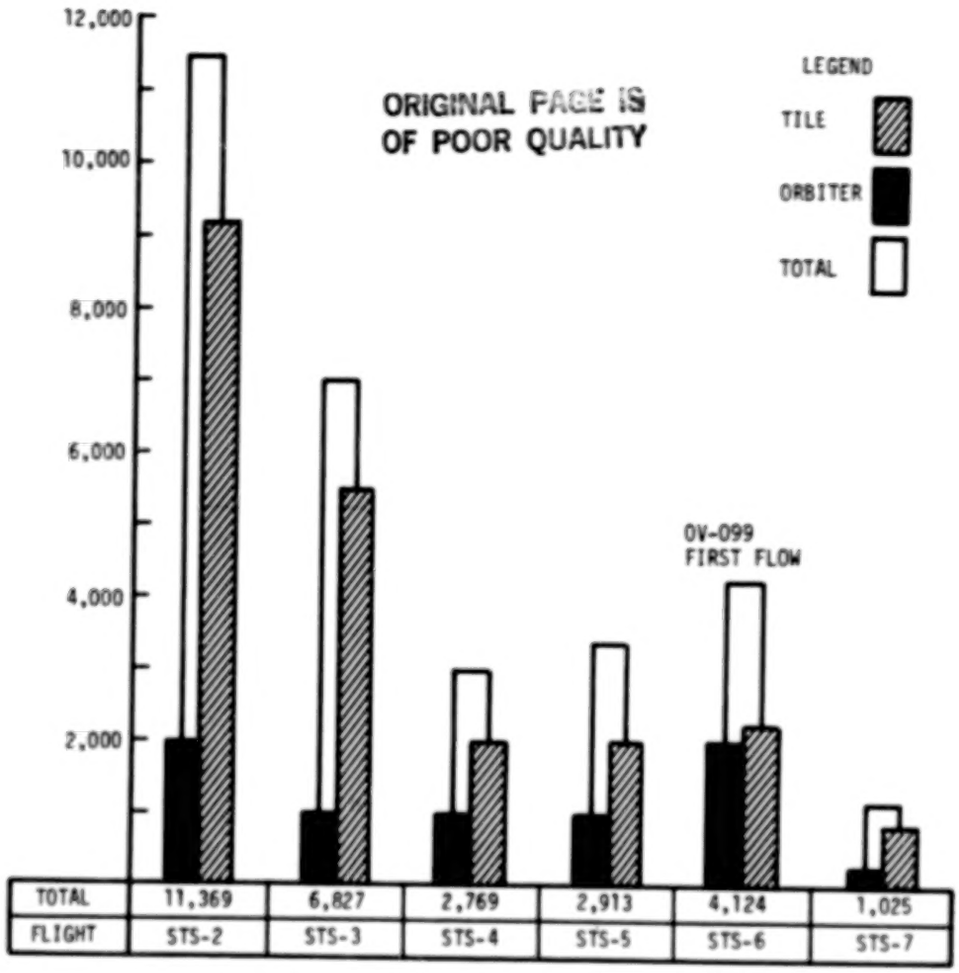
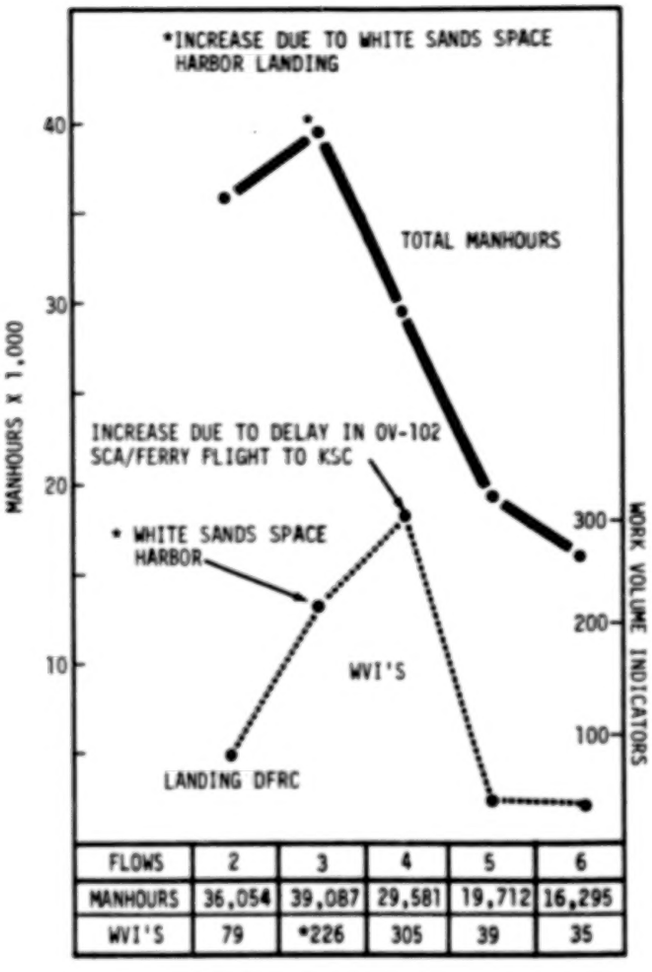


Figure 4.- Vehicle Problem Reports by Flight.



FLOWS	2	3	4	5	6
MANHOURS	36,054	39,087	29,581	19,712	16,295
WVI'S	79	*226	305	39	35

Figure 5.- Orbiter Off-Site Recovery Data.

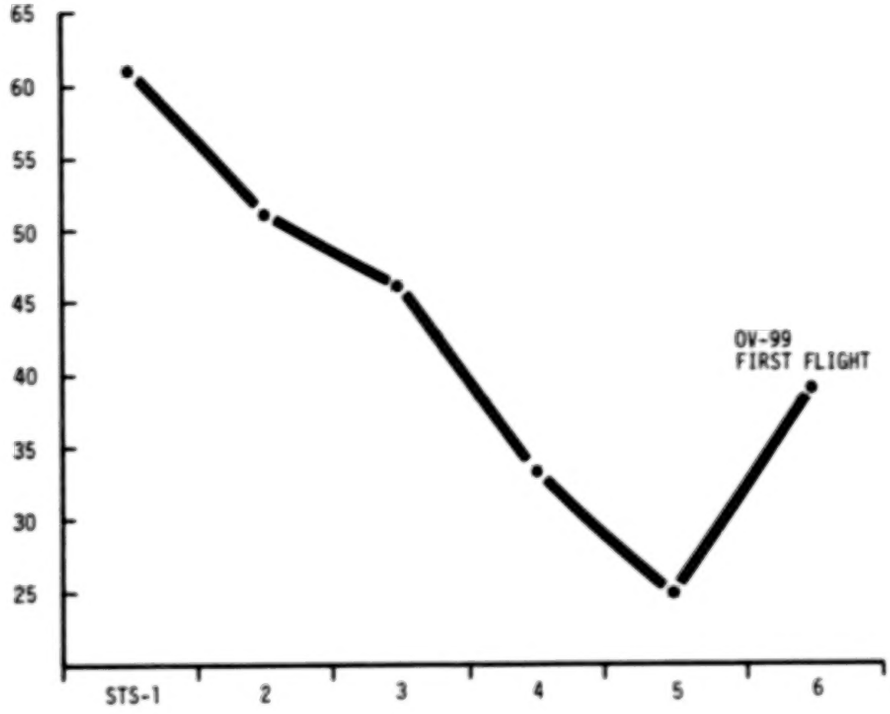


Figure 6.- In Flight Anomalies.

N85
16927

UNCLAS

D38. N85-16927

EXTERNAL TANK PROCESSING FROM BARGE TO PAD

J. E. Carpenter*
Martin Marietta Corporation
External Tank Operations
Kennedy Space Center

ABSTRACT

The External Tank (ET) is off-loaded at the KSC Barge Turning Basin and towed to the Vertical Assembly Building (VAB), High Bay Transfer Aisle. It is erected vertically and placed in the ET Checkout Area of High Bay 2 or 4 for standalone checkout. At the completion of checkout the ET is transferred to storage or to the Integration Area of High Bay 1 or 3 for SRB and Orbiter Mate. A Systems Intergration Test is performed with the Orbiter and SRBs. Final movement is to the Launch Pad for final checkout and launch.

INTRODUCTION

The External Tank serves a dual role: to provide the structural backbone of the space Shuttle during launch operations and to contain and deliver liquid hydrogen (LH2) and liquid oxygen (LO2) propellants for the Orbiter's three main engines. The External Tank is 153.8 feet long and 27.6 feet in diameter (Figure 1). It weighs approximately 69,000 pounds empty and when loaded with propellants weighs approximately 1,660,000 pounds. The External Tank must accomodate the complex stresses created by its own weight and that of the Orbiter prior to launch. The flow of operations for the External Tank requires the precise accomplishment of delivery and launch readiness events in unison with other space Shuttle elements and the Orbiter turnaround schedule.

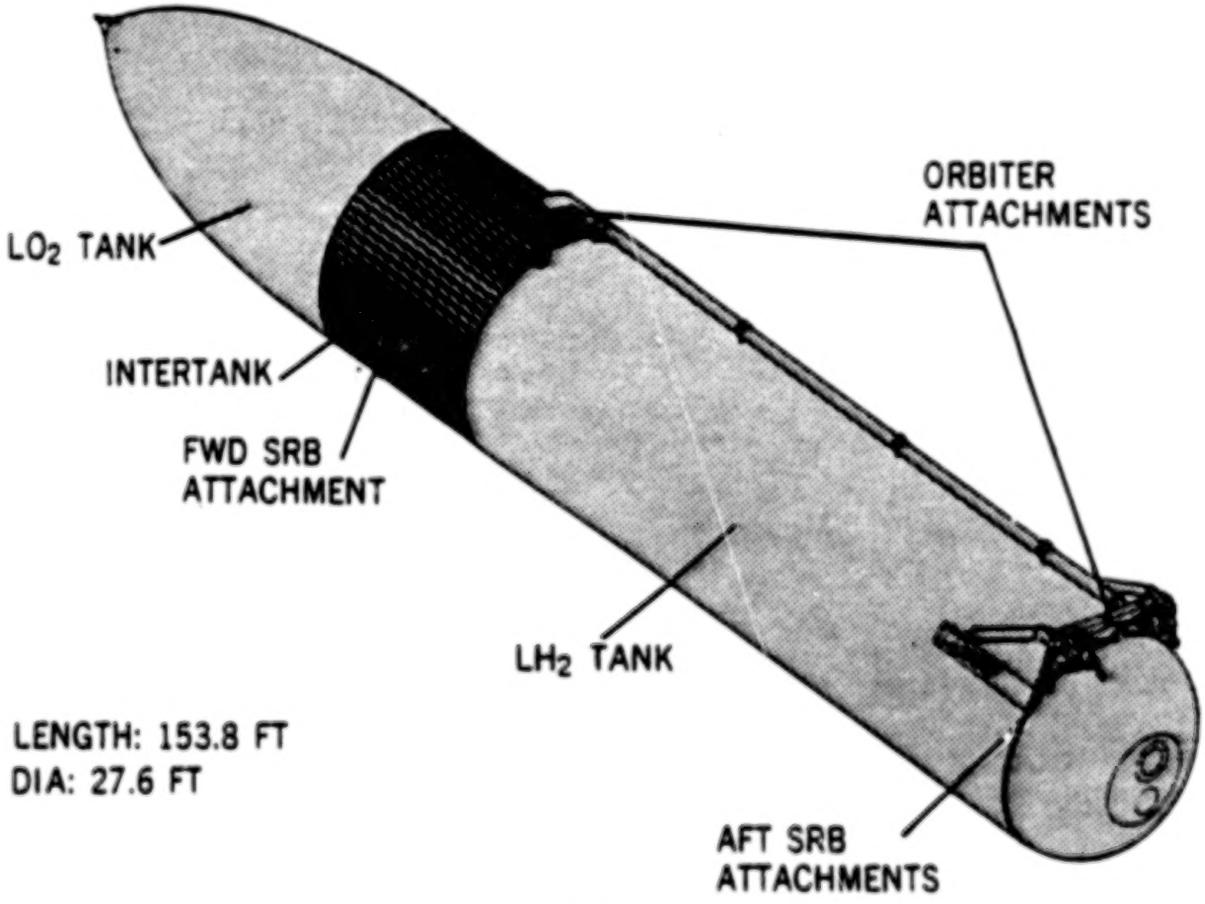


Figure 1.- External tank.

*Manager Shuttle Processing, MMC-KSC

ASSEMBLY AND DELIVERY

The External Tank is manufactured, assembled and given final acceptance testing at the NASA Michoud Assembly Facility (MAF) in New Orleans, Louisiana. The ET is mounted on an eight-wheeled (Modified Saturn SI-B) transporter at the Michoud Assembly Facility (Figure 2). This transporter serves as the means of moving the ET system to and from various points of activity during delivery, and remains with the system until it is moved into the VAB at KSC.

The ET and transporter are secured on a barge at Michoud Assembly Facility for delivery to KSC. The barge transportation system was developed to deliver NASA Saturn Stages to KSC, and has been modified for ET delivery. The ET is monitored during transportation by a sensitive instrumentation system. This system monitors the ET for pressures, humidity and acceleration.

Upon arrival at the KSC Barge Turning Basin the barge is secured and ballasted to dock level. The barge doors are opened and the ET and transporter are prepared for towing to the VAB. The transporter is secured for sea by four pedestals and tie down chains to the barge deck. After removal of the above and overall visual inspection of the ET and transporter for any apparent damage, the ET system is towed to the VAB and made ready for ET transfer into a checkout or storage cell.

ET SUB-SYSTEM CHECKOUT

Operations for erecting the ET in the High Bay begins with positioning of mobile access platforms to facilitate visual inspection, disconnection of special shipping instrumentation, and attaching forward and aft hoist slings. The ET will be hoisted from its transporter by the 250 ton and 175 ton High Bay cranes and rotated to vertical for translation into a storage or checkout cell.

In the checkout cell, a complete receiving inspection is made of all Thermal Protection System (TPS) surfaces, the intertank and nose cone interiors, and all ground umbilical connections. Ship-loose items and Ground Support Equipment (GSE) and Launch Processing System (LPS) are connected.

ELECTRICAL SYSTEM CHECKOUT

The electrical system provides the Operational Instrumentation (OI) which includes instrumentation sensors, heaters, a tumbling subsystem and Range Safety System (RSS) (Figures 3-5). The electrical system also includes the ET cabling, Orbiter/SRB cabling, electromagnetic compatibility, and lightning protection. Electrical checks consist of installation of the RSS flight equipment, continuity and isolation checks, system power on, and an end-to-end systems test using the LPS to simulate Orbiter interfaces. This makes the checkout period as short as possible through the automated use of display consoles, computers, data transmission systems and associated computer programs.

PROPULSION SYSTEM CHECKOUT

The propulsion system serves the primary function of delivery oxidizer and fuel to and from the propellant tanks and Orbiter interface through 17 inch feedline disconnects. The complete system is comprised of LO2 feed system, LH2 feed system, LO2 and LH2 tank pressurization, vent/relief and tumbling system, intertank and tank environmental control systems, and ET intertank carrier plate assembly. Propulsion system checkout consists of tank and feedline leak checks, relief and vent valve checks and tank purge and environmental checks.

THERMAL PROTECTION SYSTEM (TPS) CHECKOUT

The External Tank Thermal Protection System is to maintain the primary structure and subsystem component within temperature limits during pre-launch and ascent phases. It serves the following functions: maintains LO2 and LH2 boil-off rates below the vent valves capabilities, contributes to loading accuracy and increased propellant densities, insures LO2 and LH2 specified temperatures at the Orbiter interface, minimizes air liquefaction on the LH2 tank, minimizes air formation on the ET surface and minimizes hard debris during ascent heating environment. Normal work on the above system at KSC is limited to closeout operations and minor repairs, although major modifications of repairs can be performed as necessary. Checkout cell TPS closeouts consists of the following: transporter attachment point, leak check ports, nose cone installation and closeout and Orbiter bipod jack pad closeout.

With the completion of the above subsystems checkouts, the ET is removed from the checkout cell using the forward sling and the 250 ton crane, and is transferred to the storage or integration cell (Figure 6).

ORIGINAL PAGE IS
OF POOR QUALITY

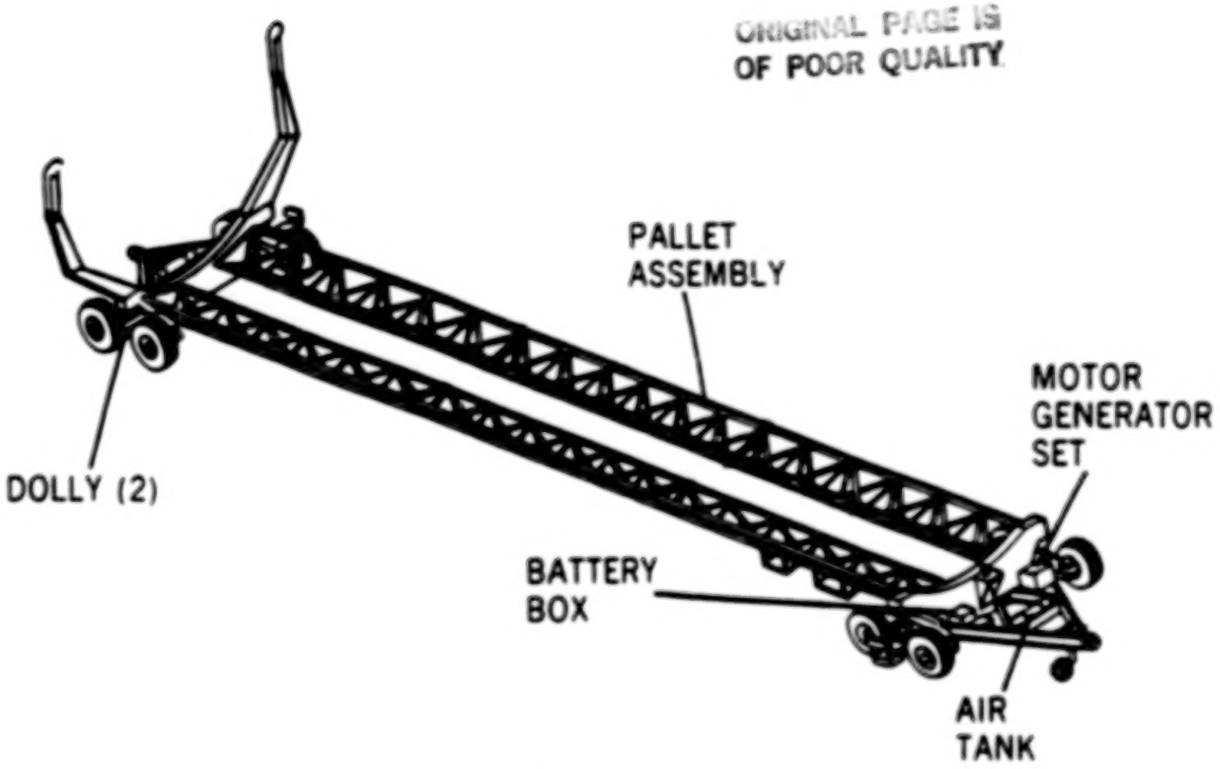


Figure 2.- ET assembly transporter.

ET TO SRB MATE

Upon transfer to the Integration cell, the External Tank is lowered into position for securing the ET/SRB forward support fittings (Figure 7). The ET is then lowered onto the SRB forward fittings. GSE guides and pins are used to facilitate final seating alignment, and are then replaced by the flight frangible bolt/nut assembly. At this point the ET is suspended entirely from the two forward attach points. When the forward fittings have been secured, the sequence of attaching the aft ET/ERB stabilizing struts begins. It begins with the attachment of the right and left diagonal struts to the ET upper fittings. One strut is preadjusted to length, the other is adjusted to fit. The upper lateral struts are assembled to the SRB's, adjusted to fit, and attached to the upper ET fittings. The lower struts are then similarly attached to the SRB's adjusted to fit, and bolted to the ET lower fittings. The ET/SRB mate is completed by mating the electrical pull-away connectors located on the two upper lateral struts, and by completing the electrical connections to the forward attach point frangible bolt.

With the completion of ET/SRB mechanical and electrical mate the upper lateral strut and forward attach point cable fairings are installed and TPS closeouts begin. TPS closeouts consist of TPS spray on the aft cable fairing and the associated area around the aft fairing area.

ET/ORBITER MATE

The Orbiter is erected and vertically aligned with the ET by means of a sling set and jacks attached to the Orbiter. The two aft ET/Orbiter structural interface points are attached first. Both attachment points are hemisphere (ET) to socket (Orbiter) interfaces with concentric, retaining bolt/frangible nut assemblies. The right interface is a fixed reference point; the left ET attach point is free floating laterally once the Orbiter socket has captured the ET hemisphere. Prior to this a temporary adjustable support strut is used to hold the left attach point in position. The two Orbiter supplied interface bolts are installed, but final torquing is deferred until the forward attachment is complete. Mating of the forward interface occurs by drawing the Orbiter, via the ET provided yoke fitting, onto the pivotal bipod. The strut flanged joints are then bolted together. One strut has an adjustable sleeve that is used to obtain the required lateral alignment tolerance (Figure 8).

ORIGINAL PAGE IS
OF POOR QUALITY

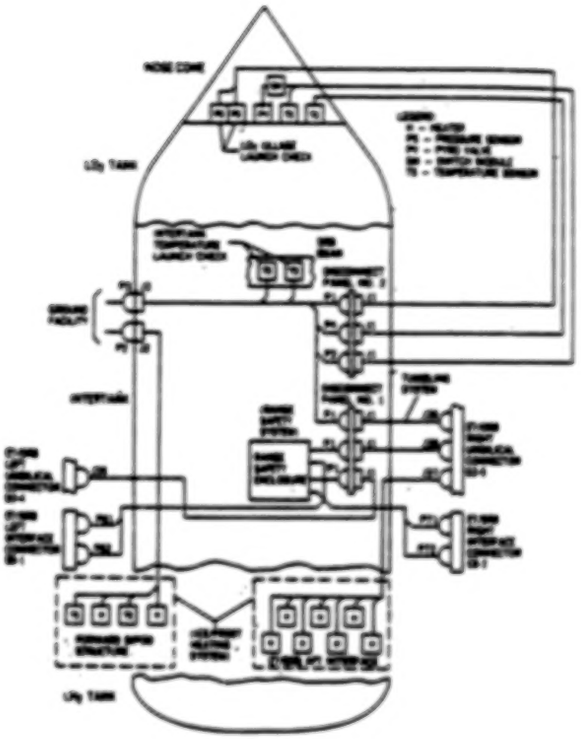


Figure 3.- Operational instrumentation systems components.

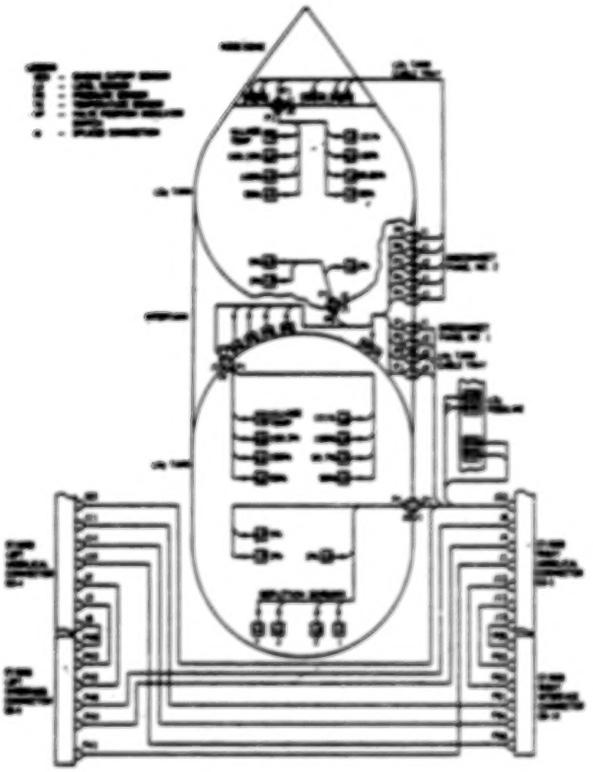


Figure 4.- Operational instrumentation sensors and switches.

With the completion of mechanical mate the ET/Orbiter aft umbilical disconnects containing the electrical, pneumatic and fluid interfaces are mated. Interface protective covers are removed from the disconnect halves. The Orbiter halves of the umbilical plates are extended from their retracted position and aligned with the halves. They are secured using three flangible bolt/nut combinations per assembly.

At the completion of mechanical/electrical pneumatics and fluid mate, a leak check is performed on the pneumatic and fluid systems and a system integrated test is performed. The STS is now ready for pad roll out.

LAUNCH OPERATIONS

The complete Space Shuttle vehicle is moved from the VAB to the Launch Pad on the Mobile Launch Platform (MLP). The MLP is connected to the Launch Pad and its interfaces verified. Concurrently, facility interfaces are mated through the ET intertank Ground Carrier Plate Assembly (GUCA). The GUCA having been installed on the intertank during ET checkout, remains with the ET throughout the vehicle integration flow. Six fluid transfer lines, an electrical grounding cable, two disconnect lanyard cables, and two support lanyard cables emanating from the launch complex are permanently attached to the GUCA. The facility LO2 and LH2, and both ET tanks are purged with helium and sampled to assure an inert atmosphere for propellant loading.

FINAL COUNTDOWN

The Space Shuttle terminal countdown sequence begins at T-5 hours. Propellant loading is accomplished with vent valves open, loading from the facility through the Orbiter into the ET. Both LO2 and LH2 are loaded simultaneously, starting with a slow flow rate to precondition the lines, tanks and engines. The slow flow is continued until the 2% level is reached, at which time the flow rates are increased to the maximum of 12,000 gpm for LH2 and 5,000 gpm for the LO2 until each of the tanks contains 98% of its capacity. The flow rates are then reduced to provide a topping flow rate to 100% capacity, followed by a still slower replenish flow continues until the automatic sequence starts at T-9 minutes.

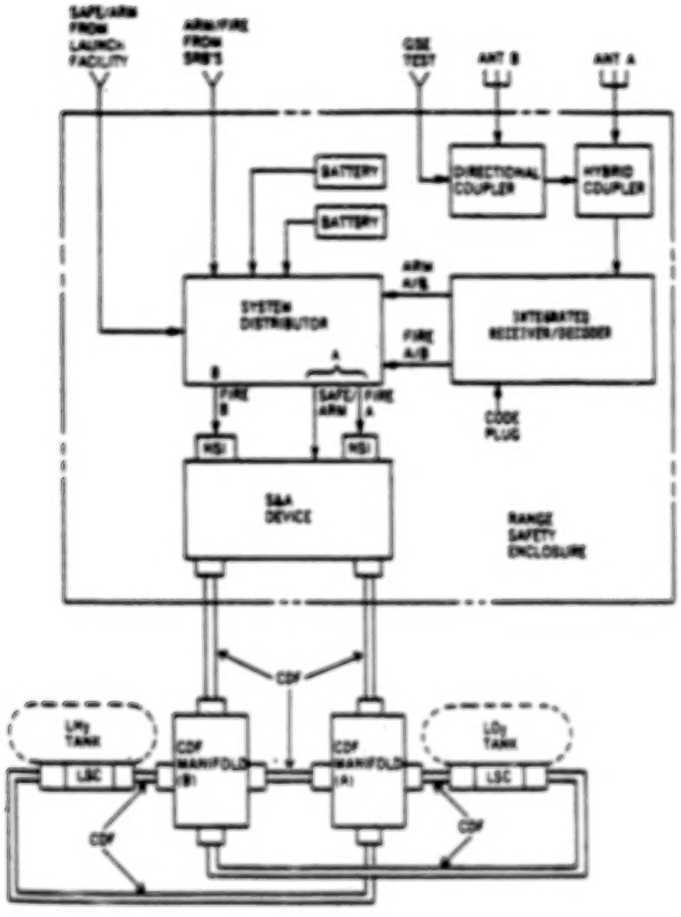


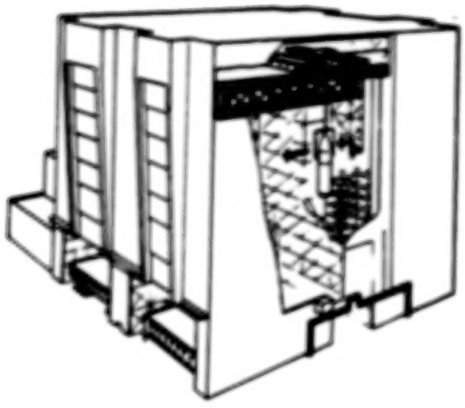
Figure 5.- Range safety system block diagram.

The LO2 vapors generated during the loading and conditioning process are vented through vent louvers in the nose cone and facility line carrying GO2 to the umbilical tower. LH2 vapors are vented directly to a burn pond through a ET/facility vent system via the intertank ground umbilical carrier assembly. This assembly also provides connections to the pneumatic lines for conditioning the nose cap and intertank cavity, monitoring the hazardous-gas detection system, and for the actuation of the vent valves. The LO2 and LH2 tanks are then pressurized, with pressurization occurring for the LO2 tank at T-155 seconds and at T-106 seconds for the LH2 tank.

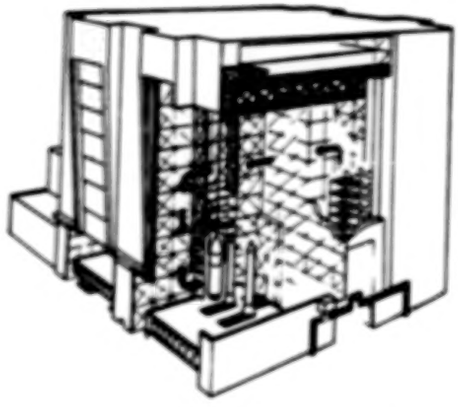
REFERENCES

1. Manual — System Definition Handbook, Space Shuttle External Tank, MMC-ET-SE25-0, August 1980.

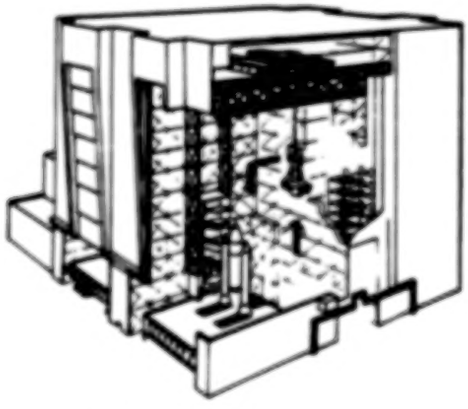
ORIGINAL PAGE IS
OF POOR QUALITY



ET leaving checkout cell



ET mating integration cell



Orbiter mating operation

Figure 6.- ET leaving checkout cell.

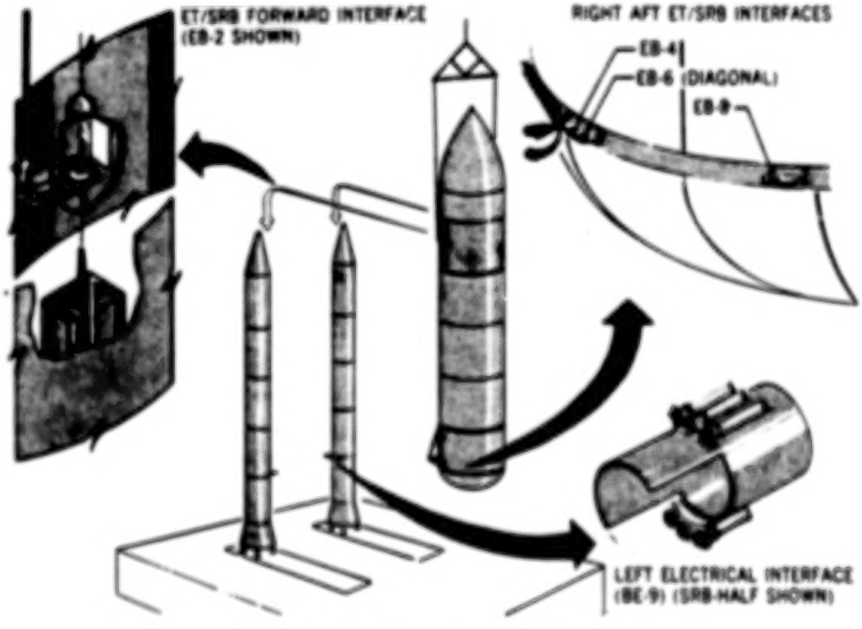


Figure 7.- ET/SRB integration.

ORIGINAL PAGE IS
OF POOR QUALITY

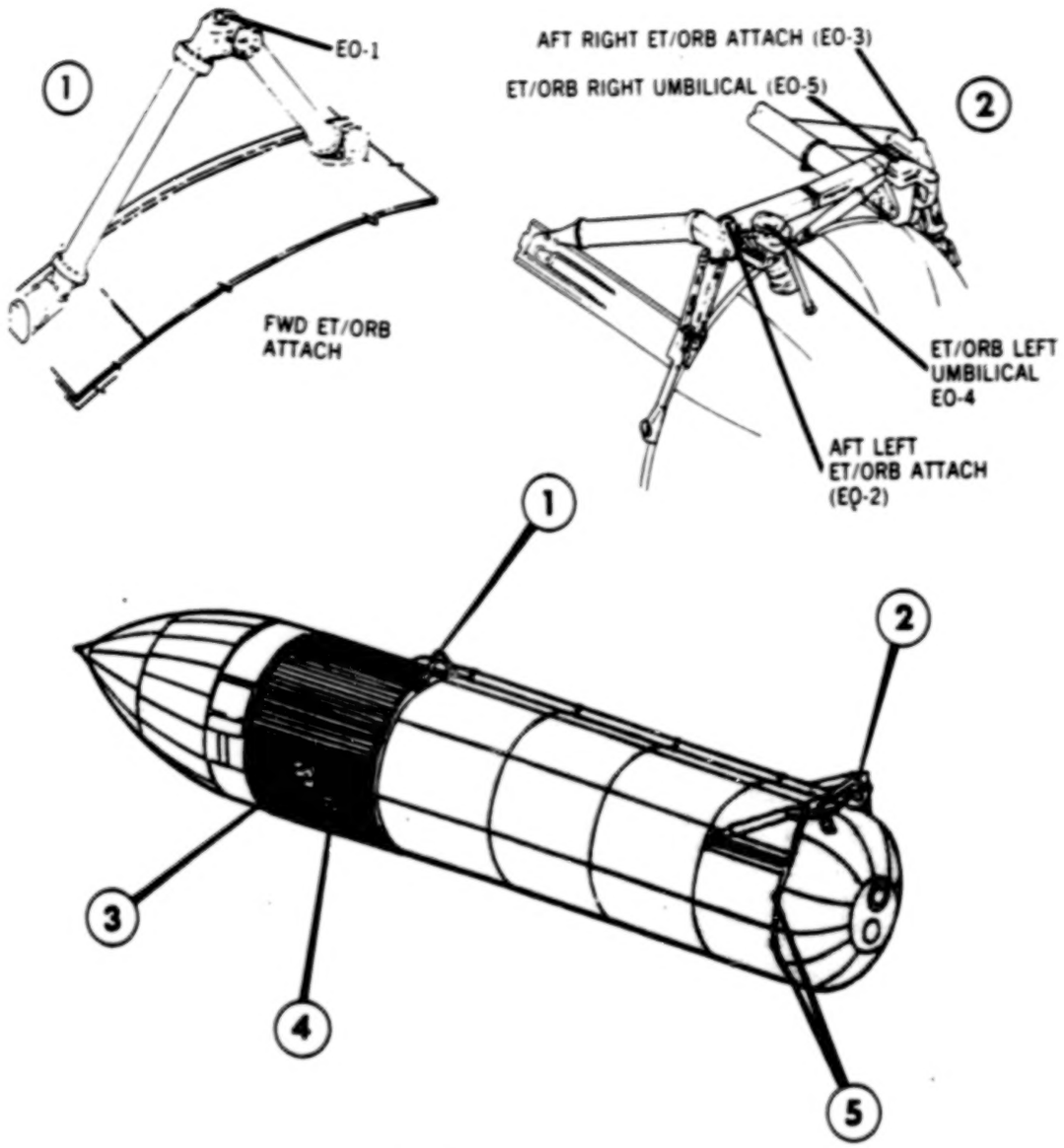


Figure 8.- ET interface configuration.

N85
16928

UNCLAS

N85-16928

D39

SOLID ROCKET BOOSTER RETRIEVAL OPERATIONS

Anker M. Rasmussen*
United Space Boosters
Kennedy Space Center

ABSTRACT

The Solid Rocket Booster Retrieval Program operates with one primary objective, the recovery of expended boosters and associated hardware without damage attributable to retrieval procedures. This is accomplished by a retrieval force consisting of ship's personnel and retrieval team members, each of whom has been trained and is highly skilled in multi-faceted operations. The retrieval force is equipped with two specially-built, highly maneuverable ships outfitted with parachute reels, retrieval cranes, towing winches, large volume-low pressure air compressors, SCUBA diving gear, inflatable boats with outboard motors and diver-operated SRB dewatering devices.

The two ships are deployed in sufficient time to conduct an electronic and visual search of the impact area prior to launch.

Upon search completion, each ship takes station a safe distance from the predetermined impact point initiating both visual and electronic search in the direction of flight path, ensuring SRB acquisition at splashdown. When safe, the ships enter the impact area and commence recovery of all floating flight hardware which is subsequently returned to the Disassembly Facility for refurbishment and reuse.

INTRODUCTION

NASA's commitment to Retrieval Operations began with and paralleled Shuttle development. Several feasibility studies were conducted after which contracts were initiated for Solid Rocket Booster Retrieval System final design concept. The following extracts, NUC TN 1822, describe the final design concept.

*The Naval Undersea Center, San Diego, and the U.S. Navy Supervisor of Salvage formulated and developed the final design concept.

For each flight mission there will be a total of fourteen elements subject to retrieval consisting of: two SRB casings, six main parachutes, two frustums, two drogues and two pilot parachutes. Each of these elements is equipped with location aids such as flashing lights, acoustic pingers and radio-frequency beacons, or are attached to elements equipped with these devices. All of the elements impact in a tear-shaped footprint 62 nautical miles long by 16 nautical miles wide.

Retrieval vessels will be stationed outside the impact area until splashdown. Following splashdown two fully-equipped vessels will deploy and transit to the impact area. These vessels will be oilfield tug/supply vessels with all retrieval equipment installed. The vessels will be at least 170 feet long with a beam of not less than 30 feet and engines that will develop at least 3500 h.p., twin screws and a bow thruster for station-keeping.

The first items to be retrieved will be the main parachutes. The retrieval vessel will capture the satellite float and apex float of the parachute. A line will then be attached to the apex of the parachute and the parachute will be reeled aboard the retrieval vessel by a hydraulically operated power block with a power grip. The power block and grip will be suspended outboard of the retrieval vessel from the boom of a deck-mounted crane. The parachutes will then be reeled onto stowage reels, one main parachute per reel. The stowage reels will be covered to protect the parachutes from sunlight.

The drogue and frustum will be retrieved next. The retrieval vessel will snare the pilot parachute and attach a line to the apex of the drogue. The drogue will be brought onboard the retrieval vessel using the power block and grip and stowed on the remaining parachute stowage reel. The frustum will be lifted from the water by the drogue suspension lines; the crane boom will then be swung to position the frustum over dunnage on the deck of the retrieval vessel. The frustum will be lowered onto the dunnage and secured to cleats on the deck.

The last items to be retrieved are the SRBs.

*Manager, Marina Operations, USBI-RP-2

A Nozzle Plug (NP) is used to dewater the SRB casing so that the casing will float in a log mode, after which it can be towed to port by the retrieval vessel. The NP is an unmanned, umbilical-cable-controlled submersible vehicle and is controlled from a console located aboard the retrieval vessel. The NP is launched by the deck-mounted crane.

The NP docks with the SRB and is locked into place by three locking arms. Dewatering of the SRB is accomplished when air from the retrieval vessel is forced through the pneumatic hose of the umbilical into the SRB. The air pressure forces the water out through the SRB nozzle (past the NP). When sufficient water has been removed from the SRB, the booster will become unstable and float in a log mode.

An inflatable bag on the NP will be inflated, once the SRB assumes a horizontal mode and a dewatering hose will be deployed. Additional air is then forced into the SRB to achieve a pressure differential which will force the remaining water out of the SRB through the dewatering hose. The umbilical is then detached prior to towing operations. A towline is attached to a towing pendant on the nose of the SRB and transit to the refurbishment site is begun."

STS-1 flight delay allowed delivery of specially built retrieval vessels and provided time to fully evaluate final design concepts. Extensive training resulted in a cohesive retrieval organization which immediately demonstrated Shuttle cost effectiveness.

It must be noted that the first retrieval mission paid for the Parachute Development Program, SRB Water Impact Testing and cost of two retrieval vessels. Replacement value of hardware retrieved from STS-1 thru STS-5 would exceed $216,000,000.00. (Table 1)

RETRIEVAL SHIP OPERATIONS

Effective ship operations require proper interfacing of ship, ship's crew, retrieval team members and procedures bonded through extensive training and observance of safety procedures.

The dedicated retrieval vessels with controllable pitch propellers, transverse bow and trainable stern thrusters afford unmatched maneuverability and station-keeping accuracy. The vessels were constructed and documented in accordance with strict U.S. Coast Guard, American Bureau of Shipping and Federal Communications Commission regulations. The vessel crews are dictated by the U.S. Coast Guard and must possess appropriate licenses demonstrating proper experience and education levels. Basic ship handling techniques require fine honing to provide station keeping and close in maneuvering expertise essential for safe, efficient retrieval activities.

The camaraderie between ship's crew and retrieval team members, created by individual respect and personnel cross-utilization, has instilled a 'team' spirit. This 'team' spirit has provided a broad information exchange system providing coordinated operational inputs. The retrieval force operational capabilities are clearly illustrated by success rates under diversified conditions.

RETRIEVAL EQUIPMENT IMPROVEMENTS

Retrieval Operations have undergone rapid change. The major changes have occurred in the area of equipment improvements and as a result, technical developments have enhanced overall mission effectiveness.

Prior to STS-1

Prior to STS-1, the final design concepts were thoroughly tested during at-sea training using a full scale Ocean Test Fixture simulating the SRB, a full scale model frustum, and full sized parachutes. During these at-sea training missions, procedures were developed to retract the frustum location aid antenna, thereby eliminating the large wooden beams (79K12931 - KSC DWG) which were provided to eliminate antenna damage. Plywood was substituted as a base in frustum landing area which substantially eliminated potential frustum damage. The parachute retrieval concept required use of two heavy idler rollers (79K12922 - KSC DWG). Parachute retrieval operations demonstrated that a parachute slide (nylon) on the deck could be utilized effectively, thereby eliminating personnel handling hazards. The Ballast Aerating Retrieval Boom (BARB) (79K20974 - KSC DWG) was developed for use if SRB nozzle damage prevented use of the NP and associated telescopic harpoon. Additionally, the BARB could be utilized in a dual role for open nozzle towing. The BARB is a simple, efficient device constructed from aluminum pipe and tubing. The main member is 20 feet long and 1 1/4 inches in diameter. The upper end is fitted with an aluminum cap and "O" ring seal. The lower end is threaded to accept a 2 inch ball valve and 1 1/2 inch quick-disconnect fitting. The cross member is 10 feet long, 2 inches in diameter with welded ends. The units are attached with a swivel fitting, approximately 5 feet from the main member upper end. Bungee cord is secured around the swivel

fitting placing the unit under tension when the cross member is parallel to the main member. A cable lanyard attached to the main member cap and cross member retains the device in a cocked position.

Air applied through the ball valve deploys the main frame cap allowing the tensioned cross member to re-position perpendicular to the main member, effectively retaining the unit in the SRB nozzle.

Prior to STS-2

The nozzle plug (79K15557 - KSC DWG) failed to operate satisfactorily during STS-1 operations. From a conceptual viewpoint, the remote-control plugs designed and constructed for NASA fulfilled the requirements for a positive and hazard free retrieval of SRBs from the ocean. In actual use the plugs proved to be maintenance intensive, hazardous to launch, and unreliable in performance. Close tolerance, interlocking segments and general 'layer cake' design prevented minor maintenance unless the total system was desegregated. The basic design would not lend itself to adjustment or modification that would allow for tracking the learning curve; therefore, the nozzle plugs remained inflexible from intended design use and application. Based upon this conclusion, the Ballast Aerating Retrieval Boom and divers were baselined for SRB dewatering. Additionally, an in-port Diver Operated Plug was developed and brought into service to provide final SRB dewatering at Port Canaveral, thereby facilitating transit through the Banana River to the refurbishment facilities. The frustum landing area was modified and standard dunnage (double thickness 2 x 12 planks) installed.

Prior to STS-3

Considerable problems had been encountered with the final concept design weak link (79K19967 - KSC DWG), which was placed in series between the SRB and towing vessel alleviating damage to the forward skirt. NASA analyzed the problem area and designed a weak link that would fail in tension and bending modes while providing higher breaking strength, ease in handling, and low maintenance.

Prior to STS-4

Evaluation of parachute retrieval operations clearly illustrated that the existing parachute deck edge roller (79K12922 - KSC DWG) caused additional and unnecessary damage to the parachutes. At this time, the deck edge roller was replaced with a permanent deck edge guide consisting of a 3/4 round stainless steel pipe with vertical guides. This resulted in a drastic reduction in damage and provided for an overall smoother, safer parachute recovery. Decelerator sub-system problems required parachute flotation removal; therefore, procedures were developed for detaching main parachutes from the SRBs at the 40 foot release links. To aid divers with detaching, two Avons, rigid hull inflatable boats and five diver propulsion vehicles were added to the retrieval equipment inventory. SRB and frustum location aids had proved to be marginally effective or had intentionally been deactivated; therefore, 12 commercial emergency radio indicator beacons with lights were purchased for severe weather and night station-keeping operations. The accelerated use of divers required by BARB and parachute operations mandated additional safety equipment. A recompression chamber was obtained from the Navy and installed on-board one retrieval vessel for use in the event of diving accidents. At-sea operations in various weather conditions had demonstrated the concept design hawser was of insufficient length creating situations that could potentially impart snap loads upon the SRB forward skirt. After careful evaluation, the nylon tow hawsers were replaced with 2000 foot plastic covered tow wire. These provided a longer life use cycle, catenary in the tow line to eliminate snap loads and additional safety to deck personnel.

Prior to STS-5

Projected SRB modifications and future filament wound casing information indicated the center of gravity would shift aft on the casing necessitating at-sea dewatering capabilities. Response to future requirements resulted in design and construction of an at-sea prototype Diver Operated Plug. The prototype utilized a smaller, less expensive bag seal, check valves in the mandrel and was streamlined to facilitate diver handling. In-water testing verified bag seal design and provided sufficient information to verify check valve utilization.

RETRIEVAL TECHNIQUE DEVELOPMENT

Retrieval techniques have evolved in parallel with equipment and flight hardware configuration changes. Additional changes have been initiated to improve personnel safety.

Prior to STS-1

Prior to STS-1, extreme emphasis was placed upon crane operations training. This was mandated

by the requirement to develop safe procedures for deploying the nozzle plug and to develop operator techniques which would preclude damage to the frustum during retrieval operations.

At this time, it became evident that a diving contigency would be desirable. To this end, a basic five-man dive team was formed, trained and with the advent of the BARB, developed preliminary insertion techniques.

Prior to STS-2

NASA's decision to suspend NP operations on STS-2 placed heavy emphasis on additional diver training and BARB techniques had to be fully operational. STS-1 operations demonstrated that the SRB would return to the spar mode in various sea states. To eliminate this potential hazard in shallow waters, an astern air supply technique was developed and utilized. Upon initi l rotation to the semi-log mode, the SRB air hose was disconnected and capped 200 feet aft of the BARB. Additionally, a 100 foot positively buoyant polypropylene line was attached to the free end. This allowed a retrieval vessel to work astern of the distressed SRB, retrieve the airline and resupply air without interrupting the tow of either vessel.

Prior to STS-3

Towing procedures had proven to be a continuous problem. Elimination of these problems was analyzed with subsequent equipment change. The final design concept H-Bitt and capstan towing equipment was removed allowing the towline to be deployed directly from the towing winch. This change required two seamen versus five for handling the towline and eliminated towline chafing problems. It also allowed for easy variance in towline lengths as dictated by changing sea states.

Prior to STS-4

Decelerator subsystem problems necessitated removal of the parachute flotation which, in turn, mandated that parachutes remain attached to the SRB. Various parachute removal techniques were investigated and detachment at the 40 foot release links was elected as the preferred mode.

Parachute removal utilizing this mode requires the attachment of two 180 pound positive floats to each leg of the parachute. This is accomplished by divers passing a nylon line through the center of four dispersion bridles above the 40 foot release links. The line is attached to the floats effectively transferring the parachute weight from the SRB to the floats allowing the divers to disassemble the release links. Once released the parachute floats free and vessel retrieval can commence.

When parachutes are detached in this mode, the apex is approximately 200 feet beneath the ocean surface. Parachutes can be retrieved in three basic modes, i.e., apex first, one leg or two leg. Retrieval and refurbishment operations prefer the apex first recovery, sea conditions permitting. This is accomplished by towing the parachute, with one leg, into the current until the apex is floating 15 to 25 feet below the surface. Divers from a following boat enter the water and attach a nylon messenger line through the apex suspension lines. This messenger is passed to the retrieval vessel and the parachute is reeled onboard.

Prior to STS-5

Extensive testing of the prototype At-Sea Plug was conducted in a water environment. Divers established handling and docking techniques which impacted design criteria.

PLANNED FUTURE DEVELOPMENTS

At-Sea DOP development has continued on schedule with the first devices to be operational for STS-7. The device will be inserted manually at depth, permit SRB dewatering to the full log mode, thereby improving towing characteristics and subsequently reducing corrosive in-water time.

The DOP's primary structure element is constructed from 12' of 10" diameter aluminum pipe. It contains a one-way valve and has an "O"-ring seal and end cap at each end. The forward half of the pipe houses an 8" diameter dewatering hose. A sliding collar is fitted outside the forward end of the pipe which moves three folding arms into open or closed positions. A 1/2" ball valve penetrates this pipe forward of the one-way valve and is used to add ballast water on the surface, and equalize the pipe after the DOP is locked into place at depth allowing the two end caps to fall free.

A 52" diameter mandrel is flanged around this pipe with an inflatable neoprime bag seal bolted around the rim. Three hinge points are welded to the top outer edges of the mandrel as supports for the three folding arms. The bag air supply and valve are attached to the lowerside of the mandrel. Three attachment points are welded to the bottom of the mandrel supporting three rigid legs that are

welded to the after 10" pipe section.

The DOP utilizes a chain and cable system for opening and restraining the locking arms during insertion. A rod, chain and ratchet system closes and locks the arms after docking.

A 1 1/2" pipe with a quick-disconnect and check valve passes through the mandrel and is attached to each end of the 10" pipe providing a means for pressurizing the SRB.

Plans are currently being formulated to establish procedures, equipment and time lines required to support retrieval operations in the Pacific area.

This author believes labor intensified diving requirements and increased launch rates will require a review of the original baselines; i.e., remote-controlled dewatering devices and detached parachute with subsequent reduction of diver requirements.

TABLE I.- RETRIEVED FLIGHT HARDWARE - REPLACEMENT COSTS*

MISSION STS	SRB		MAIN PARACHUTES								FRUSTUM		
	RIGHT	LEFT	1	2	3	4	5	6	RIGHT	LEFT	RIGHT	LEFT	
1	25M	25M	65K	65K	65K	65K	—	—	50K	50K	1.5M	1.5M	53.36M
2	25M	25M	65K	65K	65K	65K	65K	—	50K	50K	1.5M	1.5M	53.425M
3	25M	25M	65K	65K	65K	65K	65K	—	50K	50K	1.5M	1.5M	53.425M
4	—	—	—	—	—	—	—	—	50K	50K	1.5M	1.5M	3.1M
5	25M	25M	65K	65K	65K	65K	65K	65K	50K	50K	1.5M	1.5M	53.49M
TOTALS	100M	100M	260K	260K	260K	260K	195K	65K	250K	250K	7.5M	7.5M	216.8M

* COST DATA PROVIDED BY MSFC, APRIL 1983

REFERENCE MATERIAL

Technical Report - Naval Undersea Center, San Diego, California:
Solid Rocket Booster Retrieval System Final
Design Concept. NUC TN 1822, 1977.

N85
16929

UNCLAS

D-10

N85-16929

SPACE SHUTTLE FLIGHT READINESS FIRING DRESS REHEARSAL FOR STS-1

Lt Colonel Warren L. Riles
HQ Space Division/YOO
Los Angeles AFS, CA

ABSTRACT

As we approached the first space Shuttle launch, the tension and excitement increased with each passing day. The dedication and resolve of the joint government/contractor team was also increasing as we approached the Flight Readiness Firing (FRF) test. The FRF test afforded us an opportunity to assess the readiness or the integrated systems to support the STS-1 launch and flight. The assessment included the following integrated systems: Structures and mechanics; thermal design integration; propulsion and power; avionics and software; guidance, navigation, and control; mechanical systems; communications and tracking; an integrated ground systems.

The Space Shuttle Flight Readiness Firing was also an excellent opportunity to exercise the operational capability developed for STS-1 at a time when test teams, facilities, plans and procedures were in a flight ready condition.

To ensure that we were prepared to function effectively as an integrated team for STS-1, we conducted a simulation of the pre-mission activities, countdown and launch operations, and post-mission activities associated with STS-1 in conjunction with the Space Shuttle Flight Readiness Firing. The exercise involved all STS-1 management and operations elements functioning as they would for STS-1 launch to the degree that was practical and productive.

INTRODUCTION

The final step in the Space Shuttle system verification network prior to the first DDT&E flight was a static firing of the Space Shuttle main engines using mated flight vehicle elements in as near as possible flight configuration, on launch pad 39A at KSC. The flight readiness firing (FRF) was conducted as part of the countdown demonstration test (CCDT) for the first Shuttle manned flight.

In previous space and missile programs, static firing and integrated flight control and propulsion tests were conducted at a test site prior to the vehicles arriving at the launch sites. However, due to the unique design and multi-elements of the Shuttle, all flight systems (propulsion, flight control and avionics) were not integrated until mated at the launch site. Although each element and subsystem of the Shuttle goes through development and verification test, including a main propulsion system test (MPT) utilizing a flight ET or Orbiter aft fuselage with SSMEs, the total integrated system was not available until the vehicle was mated at the launch pad. Two other important factors necessitated a flight readiness firing: (1) the Shuttle program had no unmanned flights scheduled and (2) no facility checkout vehicle. Specific system objectives realized from the FRF were:

a. First verification of the flight MPS and associate subsystem structural integrity and performance during SSME firing (exact launch conditions up to SRB ignition).

b. First verification of the adequacy of flame and heat protective shielding for SRBs and ET during SSME pre-liftoff firing and simulated launch abort shutdown.

c. First integrated avionics/MPS test (SSME control and monitoring with Orbiter avionics).

d. First integrated APU/hydraulics/SSME/flight control functional test.

e. Additional verification of prelaunch servicing procedures and countdown timelines.

f. Additional SSME cluster firing data to verify first flight vehicle MPS predicted performance.

The FRF was conducted with an unmanned Orbiter. Additional switch control functions had been provided in the Orbiter for ground control through the launch processing system (LPS) that would not have been required for a manned FRF. These additional ground control functions, plus a modified flight software program, allows the Shuttle main propulsion system (MPS) to be tested at the launch pad with the vehicle configured for flight. The solid rocket boosters (SRB) flight control systems were not activated for the FRF; however, SRB ignition commands and SRB holddown release signals were verified. The Orbiter T-0 umbilicals and the external tank liftoff umbilicals remained connected dur-

ing the 2-second firing of the MPS. The Orbiter Orbital maneuvering systems (OMS) and the forward and aft reaction control systems (RCS) were not activated during the FRF. Orbiter flight control commands were exercised during the 20-second firing. At the termination of the 20-second firing, the three SSME's were sequentially shut down simulating a prelaunch shutdown. Following the post firing securing, a vehicle inspection and data analysis were conducted and the vehicle was reconfigured and prepared for the first STS launch.

REQUIREMENTS

Test Philosophy

Wet CDDT/FRF was a detailed practice run for the STS-1 launch and, as such, identified any failure or weaknesses in any systems or operating conditions not occurring during pretesting. All conditions were identical to or as close to the actual STS-1 timelines and launch preparation as possible.

This was a one-time-only test on Orbiter vehicle 102 and was preceded by a tanking and detanking checkout of the Orbiter, external tank, and ground systems/facilities. The FRF-unique and piggyback software tests at the Shuttle Avionics Integration Laboratory at Johnson Space Center (JSC) were completed and instrumentation for special test installed, characterized, and calibrated. All facility and servicing equipment was operationally ready to support FRF countdown. The Space Shuttle main engines (SSME) hardware backup shutdown capability checkout was completed. The crew cabin was not manned once propellant loading started and those Shuttle subsystems that required operational control after that time was configured for and had ground remote control capability. The T-0 umbilical interfaces were maintained through the FRF along with general purpose computer/launch processing system (GPC/LPS) polling command capability.

The FRF firing duration was limited to approximately 20 seconds of main stage operation. SSME start was identical to STS-1 launch: The engines were tested at 94 percent and 100 percent rated power level (RPL) with shutdown occurring from 100 percent RPL (launch abort). SSME gimbaling was performed at both power levels. See Figure 1 and 2 for FRF thrust profile and FRF gimbaling profile.

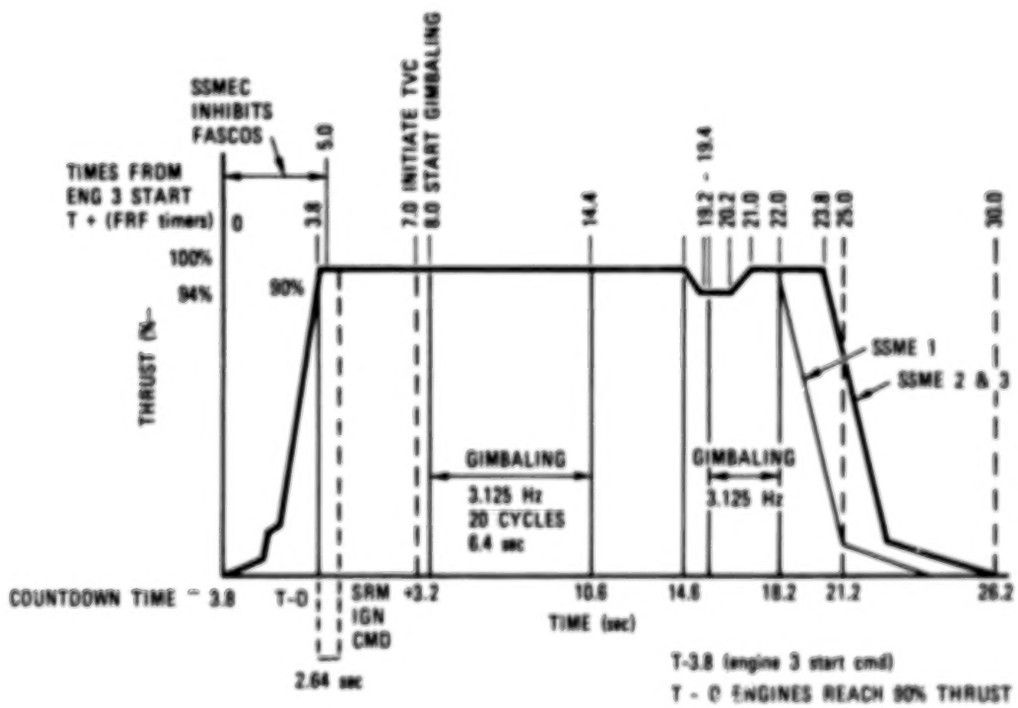


Figure 1.- FRF thrust profile.

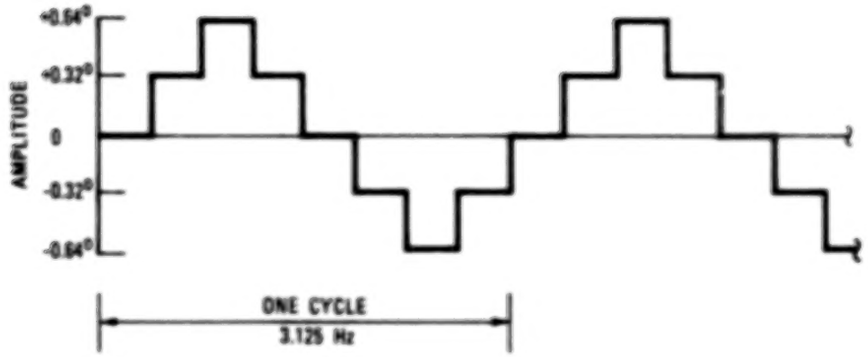


Figure 2.- FRF gimbaling profile.

The flight and ground software were structured to maintain the launch processing system (LPS) contact with the vehicle throughout the test and preclude the flight software from progressing to major mode 102 (ascent). Redundant set launch sequence (RSLS) flight software operated in major mode 101 (prelaunch) and controlled the functions of the Orbiter systems and issued commands to the rest of the Shuttle vehicle from T-35 seconds until approximately T+26 seconds for FRF. The time from T-20 minutes to T-0, was identical to STS-1 countdown. The time from T-0 to approximately T+26 was FRF test software control. This test verified that the Shuttle vehicle was ready for launch.

The various phases of the wet CDDT/FRF were:

- o Pre-FRF started with power up for the CDDT/FRF simulated run just prior to the actual test
- o Wet CDDT/FRF began with the launch countdown type of action starting at T-53 hours with call to station from OMI S0014 and verification of configuration of all elements ready for the test
- o FRF ended with the last cryogenic liquid out of the vehicle, which was the beginning of post-FRF activities
- o Post-FRF ended with the completion of all FRF-unique objectives, closeout of the test discrepancies affecting configuration, and the OMRSD requirements being met

TEST OBJECTIVES

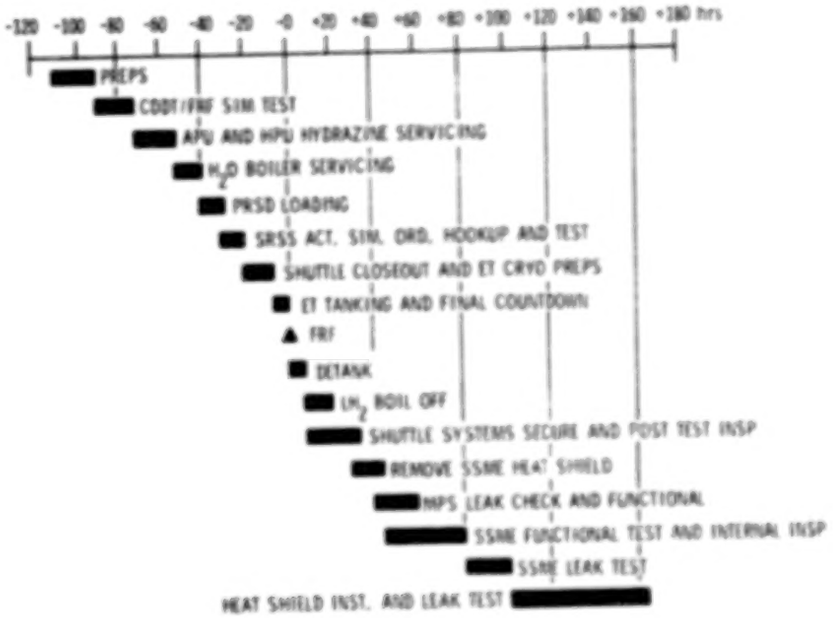
FRF provided the only opportunity to subject the Space Transportation System (STS) to the launch environment without concern for ascent transition. The test provided confidence that the STS was fully integrated in the critical functions where elements have not been tested together in the launch environment. The primary test objectives to be accomplished during this test were:

- o Exercise all elements of the STS, including personnel, facilities, vehicle, and software in a real-time launch countdown culminating in a SSME firing and simulated launch to ensure proper integration prior to STS-1 flight
- o Verify the capability of the launch facility to provide propellants to the Shuttle at specified conditions (i.e., subjecting the external tank (ET) and Orbiter elements to the same thermal environment as STS-1 and to maintain pressure in the ET from the ET/SSME and main propulsion system (MPS) control during SSME firing)
- o Verify the functional performance of the integrated auxiliary power unit(APU)/hydraulic/flight control system during simultaneous engine gimbaling and throttling
- o Load and operate the power reactant supply and distribution (PRSD) system in the Orbiter with cryogenic reactants for the first time
- o Verify the predicted performance of the ET-SSME-MPS interfaces and systems, including software and the capability of the avionics equipment to effectively monitor and control the active vehicle under dynamic prelift-off vibroacoustic conditions
- o Verify that LPS/GPC control of launch countdown sequencing can be performed down to T-0 along with simulated launch abort shutdown and securing in post T-0 time
- o Verify compatibility of the Shuttle avionics equipment with the launch radio frequency environment
- o Provide data to verify the validity of modeling techniques to extend dynamic and vibroacoustic analysis from previous test to KSC conditions
- o Assess the "twang" effects of the SSME: in the start position at ignition, and on the STS flight vehicle without SRM ignition
- o Exercise the data acquisition system, data reduction methods, and data analysis documentation methods to be used for launch

ORIGINAL PAGE IS
OF POOR QUALITY

SEQUENCING

The sequence of operations between T-52 hours and T+160 hours are summarized in Figures 3 and 4.



CDDT/FRF S-0004

Figure 3.- CDDT/FRF timeline flow.

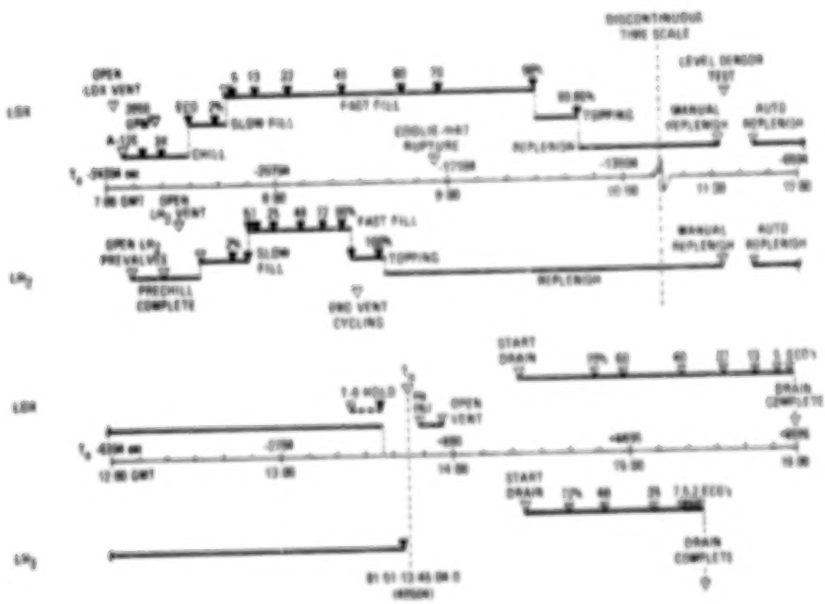


Figure 4.- FRF loading timeline.

THE CHALLENGES

ORBITER SSME WATER DELUGE SYSTEM

DESCRIPTION

SSME post-shutdown after-burning had occurred on several occasions on the MPTA at NSTL. Program concern was expressed that a similar condition would occur during FRF or during a pad abort.

A study was made by the integration contractor to determine thermal effects on the most sensitive vehicle hardware (engine mounted heatshield) and to evaluate and recommend an effective means of protecting the vehicle against the potential from an engine shutdown/abort as mentioned above.

A facility system with a series of water spray nozzles mounted around the periphery of the MLP opening and directed to impact discrete areas of the Orbiter aft heatshield structure was recommended and approved by the Level II PRCB. As designed, the system is tied to the MLP fire system to be activated manually from the LCC after detection of a potentially damaging afterburning condition.

POTENTIAL PROBLEMS

1. Damage to TPS. - Potential damage to TPS by direct impact of the water spray was a primary concern of the proposed system. To answer this question a special water spray impact test was carried out at the integration contractor's laboratory and test facility in Downey, CA. Results of the test demonstrated that TPS would not be damaged with the planned application of the nozzles. Also, characteristics of the nozzle spray plume (throw distance and diameter vs. pressure) were determined to verify proper nozzle selection/application.

2. Dedicated Spray System - The requirement of a fully independent water supply for the Orbiter-SSME deluge system could not be met on STS-1. This was due to the fact that the existing 6" diameter supply line is flow limited and can serve only one of the three major Orbiter protective spray systems at any given time.

For STS-3 this condition will be eliminated by the replacement of the 6" supply line with a 12" line, permitting full flow to all of the protective systems simultaneously, if necessary. Incorporation of the 12" supply on MLP-1 for STS-1 was delayed until STS-3 due to the high potential for impacting FRF and the STS-1 launch schedule with the significant construction effort required on the MLP.

3. Automatic vs. Manual Spray Actuation - Initial system requirements specified that the Orbiter-SSME deluge system be initiated by automatic control in the event of a planned or aborted SSME shutdown to minimize the reaction time for flow of the protective spray.

Due to potential vehicle launch schedule impact in the event that water sprays were activated needlessly (without significant afterburning) following engine shutdown, direction was given by the PRCB that the system would be manually activated. As planned, control of the system will be under the cognizance of an operator in the LCC augmented by UV sensors viewing the SSME nozzles and observation of the vehicle through closed circuit TV.

4. Alignment Verification of Spray Nozzles - During the nozzle alignment procedure prior to FRF it was determined that four of the spray nozzles on the north side of the MLP would impact directly on the trailing edge of the Orbiter body flap. To avoid the potential of TPS damage those nozzles were changed to fog jet nozzles which produce a "softer" spray with less impact energy at the tile surface.

5. Water Contamination of OMS Nozzles - The use of fly-away-throat plugs for the OMS engines was deemed unacceptable to the Program and will not be used on STS-1 and subs. To minimize the possibility of direct spray entering the OMS engines, two water nozzles were re-aimed. This request was initiated through a formal Engineering Service Request (ESR) as a manadatory requirement prior to STS-1 and has been accomplished.

6. Water Flow Test - A full deluge test with the vehicle in place was deemed not feasible due to potential schedule/cost impact to FRF/STS-1. In lieu of this final vertification test the following procedures were approved by the Program as an acceptable means of determining adequacy of the system:

a. Analysis of A&E calculations for flow-pressure.

b. Alignment of water spray nozzles using a light source to assure that spray impact areas were in accordance with the design drawings.

Results

All of the potential problems associated with Orbiter-SSME deluge system have been resolved as noted. Completion of the ESR for re-aiming at water nozzles has been implemented for STS-1.

HYDROGEN BURN-OFF SYSTEM

Description

A detailed assessment of main engines ignition overpressure data from MPTA Static Firings in early 1980 revealed the necessity of a hydrogen burn-off system at the launch pad to avoid potentially damaging overpressures caused by ignition of the SSME fuel lead of hydrogen gas at engine start.

Due to the limited time available prior to STS-1, a NASA/Contractor working group was established to expedite the design, development, delivery, and verification of the burn-off system.

After evaluation of alternate methods including an engine mounted fly-away system, a pyrotechnic initiated, facility ground system was baselined by the PRCB. This concept utilized an "off-the-shelf" igniter to minimize delivery time and provide greater assurance of supporting STS-1 with a functionally qualified system.

In addition, the development of a second pyrotechnic device (the long throw igniter) was approved as a backup to the baselined unit. In concept, this unit offered distinct advantages over the baselined short throw igniter.

a. It could be mounted on the tail service masts thus eliminating the need for cumbersome pylons required to support the short throw igniters.

b. Avoided interference/operational contraints with engine access platforms.

c. Eliminated handling and maintenance of pylons.

d. Enhanced safety.

e. It delivered a high density pattern of ignition particles under the entire area of the SSME nozzle.

The major disadvantage of this device was the limited time available to accomplish the full development and qualification program that would be required prior to STS-1.

An Integrated Vertification Plan was formulated for the candidate pyro devices which included the orderly progression from single engine testing at SSFL leading to cluster engine testing on the MPTA at NSTL.

Problems

The subsequent implementation of this plan, and the problems encountered, resulted in the timely evolution of the preferred long throw igniter:

a. Analyses in support of testing revealed that the short throw igniter could be adversely affected by wind. Conversely, the long-throw igniter was relatively insensitive to the wind. (This was later confirmed by wind tests conducted at the vendor's facilities).

b. On Static Firing 12, data acquired on the first usage of the long throw igniters revealed high overpressure levels associated with engine E-1. The baseline design provided igniters for E-3 and E-2 only, for both MPTA at NSTL and OV-102 at KSC. This was due to difficulties involved in mounting short throw igniters near Engine 1 and the belief that E-1 hydrogen would be ignited by E-3 and E-2 burning. MPT SF12 demonstrated the necessity of igniters on all three engines.

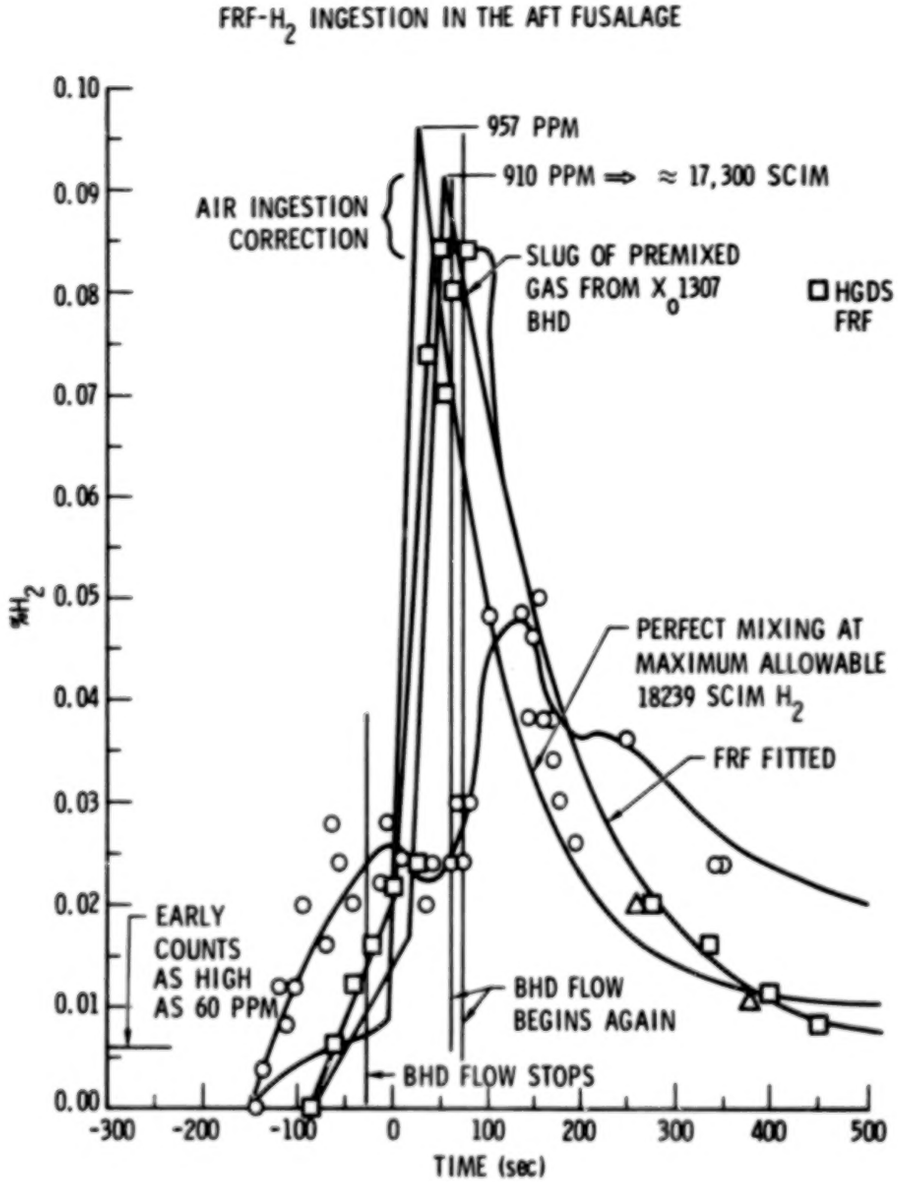


Figure 5.- FRF--H_2 ingestion in the aft fuselage.

Results

Inherent throw capability of the long throw igniter and simplicity of the mechanical installation on the TSMs made it feasible to add the additional igniters for Engine 1 at KSC. This was accomplished with no impact to the FRF schedule.

Review of FRF data has indicated an effective burn-off system that limited the SSME overpressure to less than 0.1 PSID. The Hydrogen Burn-Off System was now qualified to support STS-1.

FLIGHT READINESS FIRING (S0014)

Overall Objective

Provide final verification of critical integrated systems (i.e., main propulsion system, etc.).

Dry CDDT Objectives

a. Interface the flight crew and launch test team in a count rehearsal.

b. Demonstrate the sequence of operations required to prepare Shuttle for launch.

c. Evaluate timelines established for launch countdown.

Problems

The FRF countdown went very smoothly. There were a total of 151 Interim Problem Reports (IPRs) written against the test of which 13 affected the ground equipment. Of the 13 IPRs the following five were considered to be significant:

PRSD Sampling Results (IPR-017). During the ground servicing of the PRSD system, samples of the reactant gases failed to pass the sample test. The H_2 contained a high percentage of GHe and the O_2 contained a high percentage of GN_2. It has been determined that this was caused by a ground procedure problem during the pulse purging of the ground system. This problem was corrected prior to STS-1 launch.

Water Leaking at OAA/Orbiter Interface (IPR-038). During the FRF countdown, rain water was leaking past the dock seal of the OAA white room at the Orbiter moldline when the RSS was retracted. Prior to this time, the item of GSE which prevents water from entering the crew hatch was not installed. The GSE model A70-0643-3 is a Fiberglass scupper that fits over the crew hatch to direct water away from the hatch. Without this GSE installed, water was allowed to enter the crew module. A significant amount of water had to be removed after FRF.

This problem was resolved prior to launch in that the GSE (A70-0643-3) was installed around the crew hatch.

GOX Vent Hood. During the tanking test prior to FRF it was noted that GOX vapors were leaking from the GOX vent hood during loading of the ET LOX tank. It was determined that the leakage was past the seal where the seal interfaces with the ET tank SOFI. This GOX leakage past the seal caused erosion of the SOFI on the ET.

Pressure was increased on the seal for FRF but the seal ruptured on the South side of the ET tank just below the louvers. The tank was approximately 12-14 percent full and it was decided to retract the hood at that time and proceed with the LOX loading. The seal on the North side operated properly.

Subsequent to FRF a series of tests were run at LETF to evaluate the problem. It was found that replacing the orifice configuration from a standard orifice to a cruiciform orifice lowered the pressure on the louvers and evenly distributed the pressure on the louvers. The pressures on the North and South seals were now essentially the same.

Subsequent to FRF an evaluation of the location of the GOX vent arm indicated that the seal may have been slightly out of position and on one corner of the louvers rather than on the SOFI. This would have contributed to the failure. Steps have been taken to accurately position the seal around the louvers.

On March 9, 1981, the Level II PRCB decided to install the cruciform orifice on ET-1 based on the LETF tests. Starting March 13, 1981, a series of tests were conducted on the LETF with an improved seal design and cruciform orifice. The tests were successful.

Hypergolic Storage Tank. An incident occurred prior to the FRF countdown involving the hypergolic storage tank located on the perimeter road around the pad. During hypergolic servicing, the heater in the storage tank failed. Servicing continued, resulting in a failure of the storage tank. A new heater has been installed in the tank and a constraint has been added that use of the tank when the heater is off is prohibited.

Pressure Spike LOX Fill and Drain System. A pressure spike of approximately 150 psig occurred on the ground side of the LOX fill and drain line during detanking. The pressure on the Orbiter side of the interface did not exceed the proofpressure of the line. Preliminary indications revealed that this problem can be corrected procedurally by refilling the ground system up to the vehicle interface prior to initiating LOX tank drain. This was not implemented until STS-2.

Results

In summary, the ground systems performed exceptionally well. All test objectives were met and the ground systems were ready to support launch.

WET CDDT/FRF TEST RESULTS

The Wet CDDT/FRF test was very successful. We increased our knowledge about the integrated Shuttle MPS system. All the SSMEs will leak some hydrogen. The SSME joints will leak hydrogen and oxygen below specification levels. MPS leak tests procedures in the OPF should be improved. The STS-1 tests procedures were for joints only and the pressure was at 25 PSI. The leak checks procedures that are a part of the SSME second E&M at NSTL should also be improved. THE MPS FRF objectives were satisfied and Tables I and II summarizes the problems and discrepancies encountered during the FRF test.

TABLE I

SUMMARY OF MPS FAILURES, ANOMALIES, DEVIATIONS, AND RECOMMENDED ACTIONS

SUBSYSTEM/COMPONENT	PROBLEM DESCRIPTION	PROBLEM CLASSIFICATION	RECOMMENDED ACTION
GO_2 PRESSURIZATION • FCV-1	LOW GO_2 PRESSURANT FLOW FROM FCV-1 DOWNSTREAM OF ORBITER/SSME INTERFACE WHEN FCV CYCLED OPEN	ANOMALY	FLY STS-1 AS IS • FAILURE INVESTIGATION DID NOT DISCLOSE SOURCE OF RESTRICTED FLOW • ANALYSES INDICATE 2 VALVE FAILURES IN FLIGHT ACCEPTABLE
HAZARDOUS GAS DETECTION	H_2 AND O_2 CONCENTRATIONS APPEAR HIGHER THAN EXPECTED DURING ENGINE FIRING	ANOMALY	DETERMINE EXPECTED TRANSIENT CONCENTRATION LEVELS FOR FRF • COMPARE WITH KSC FRF LEVELS EVALUATE KSC POST FRF LEAKAGE TEST RESULTS ASSESS LEVELS DURING SPECIAL TANKING TESTS INITIATE CORRECTIVE ACTION IF REQUIRED
EXTERNAL TANK • LH_2 TANK	ABILITY TO MAINTAIN FLIGHT MASS IN LH_2 TANK MARGINAL • ATTRIBUTED TO FLOW RESTRICTION DUE TO WATER ENTERING VENT MANIFOLD AT BURN POND	ANOMALY	RESOLVE FACILITY PROBLEM AT KSC; EVALUATE FIXES ON SPECIAL TANKING TESTS • KSC MODIFICATION COMPLETED BY TANKING TEST • TANKING TEST RESULTS WILL BE EVALUATED
LO_2 PROPELLANT FEED SYSTEM • LO_2 PREVALVE-1	CLOSING TIME MARGINALLY FAST COMPARED TO COMPONENT SPECIFICATION	ANOMALY	FLY STS-1 AS IS • SSME ASSESSMENT INDICATES TIMING ACCEPTABLE FOR IN-FLIGHT SHUTDOWN • CONTINUE EVALUATION OF PRE-VALVE TIMING ON SPECIAL TANKING TESTS
SSME	ME-1 AND 3 MR APPEARS HIGH BY 0.02 UNITS • ATTRIBUTED TO CONTROLLER	DEVIATION	PROVIDE UPDATED MR TAGS FOR STS-1 PERFORMANCE ASSESSMENT PROPULSION PERFORMANCE PANEL (PPP) REVIEW CONTROLLER LOGIC FOR MR CONTROL ON STS-2
	GO_2 PRESSURANT SUPPLY TEMPERATURE NOT AS PREDICTED • HIGHER TEMPERATURES ATTRIBUTED TO MR SHIFT • LOWER TEMPERATURE ATTRIBUTED TO HEAT EXCHANGER REORIFICE	DEVIATION	PROVIDE UPDATED GO_2 PRESSURANT SUPPLY TAGS FOR STS-1 PERFORMANCE ASSESSMENT PPP ESTABLISH METHOD FOR UPDATING ENGINE TAGS WHEN HARDWARE CONFIGURATION CHANGES

TABLE 2

MPS FRF OBJECTIVE AND ACCOMPLISHMENT SUMMARY

OBJECTIVE	OVERALL OR PRIMARY	DEGREE OF ACCOMPLISHMENT	DISCREPANCIES/COMMENTS
VERIFY SATISFACTORY INTEGRATION OF ALL SHUTTLE FLIGHT SYSTEMS IN A TYPICAL TERMINAL COUNTDOWN CULMINATING IN SSME FIRING	OVERALL	FULLY COMPLETED	
VERIFY FUNCTIONAL PERFORMANCE OF THE INTEGRATED ET/SSME/APU/ HYDRAULIC/FLIGHT CONTROL SYSTEMS IN THE FLIGHT CONFIGURATION	OVERALL	PARTIALLY COMPLETED • HAZ GAS OPEN	GO_2 FCV-1 APPARENT RESTRICTED FLOW JUST AFTER T_0 • FAILURE INVESTIGATION DID NOT DISCLOSE PROBLEM • ACCEPTABLE FOR STS-1 HIGHER THAN EXPECTED H_2 AND O_2 CONCENTRATIONS IN AFT FUSELAGE DURING ENGINE FIRING • INITIAL RESULTS SHOW CONCENTRATIONS BELOW ALLOWABLE LIMITS • EVALUATION CONTINUING LO_2 PREVALVE-3 CLOSING TIME MARGINALLY FAST • COMPONENT TIMING ACCEPTABLE FOR SSME IN-FLIGHT SHUTDOWN • ACCEPTABLE FOR STS-1 ME-1 AND 3 MR APPEARS HIGH BY 0.02 UNITS • ATTRIBUTED TO CONTROLLER • ACCEPTABLE FOR STS-1
VERIFY THE CAPABILITY OF THE LAUNCH FACILITY TO PROVIDE PROPELLANTS TO THE SHUTTLE VEHICLE AT SPECIFIED CONDITIONS	PRIMARY	FULLY COMPLETED	ABILITY TO MAINTAIN LH_2 FLIGHT MASS MARGINAL • ATTRIBUTED TO KSC FACILITY DRAIN LINE • FLIGHT MASS ACHIEVED FOR FRF • ACCEPTABLE FOR STS-1
VERIFY PREDICTED PERFORMANCE OF THE INTEGRATED MPS AND INTERFACE COMPATIBILITY WITH ASSOCIATED FLIGHT AND GROUND SYSTEMS	PRIMARY	FULLY COMPLETED	SSME RECONSTRUCTED TAGS NOT AS PREDICTED • ME-1 AND 3 MR 0.02 UNITS HIGHER • GO_2 PRESSURANT SUPPLY TEMPERATURES DIFFERENT BY -100 TO +60° RANGE
DEMONSTRATE THE HYDRAULIC WARRANT FLOW CAPABILITY	PRIMARY	FULLY COMPLETED	
VERIFY INTEGRATED APU/HYDRAULIC SYSTEM OPERATION DURING SIMULTANEOUS SSME GIMBALLING AND THROTTLING	PRIMARY	FULLY COMPLETED	

GUIDANCE, NAVIGATION, AND CONTROL

Integrated Guidance Navigation and Control (IGN&C) FRF Test Objectives

The prime FRF test objectives of a total GN&C system integration nature included: (a) demonstration of capatible initialization of TVC actuator commands for hydraulics application, engine start, run and shutdown positions, (b) the ability to perform the prelaunch gimbal slew checks, (c) compatibility of the Orbiter avionics/software with the SRB thrust vector control system, (d) confirmation that the dynamic response of the SSME TVC system, in the "near flight" configuration, was comparable with that obtained from MPTA test results, and (e) provision of a test data point on analytically predicting elastic body response to a control effector command.

IGN&C Data Assessment - The first objective was accomplished successfully, although the yaw actuator on SSME I had drifted to -1.04 degrees (from the desired value of zero degrees) prior to Orbiter APU start. This was expected due to a non-zero plumbing torque on the nozzle at zero deflection. The second objective was accomplished with no anomalies; i.e., the slew checks were performed

successfully on all actuators, even though the SRB HPUs were shut down prematurely prior to completion of the SRB nozzle slew. There was adequate kinetic energy in the turbine to permit slew completion. Ability of the Orbiter to properly orient the SRB nozzles was demonstrated with no anomalies.

This FRF test provided significant and substantial information relative to the flight readiness of STS-1 in areas pertinent to the general technical discipline of GN&C. This was in the form of assurances that: (a) the prelaunch procedure successfully prepared avionics, propulsion and hydraulic subsystems for launch, (b) the LPS was properly integrated with the on-board avionics, and (c) in the limited scope of the test, the individual GN&C elements (consisting of sensors, data processing, and control effectors) performed their required functions.

SRB THRUST VECTOR CONTROL

All four of the Auxiliary Power Units (APU) in the SRB Hydraulic Power Units (HPU) were shutdown prematurely. The scheduled operation of the APUs was to be activated at T-25 seconds and terminated at T+22 seconds. However, at T-19 seconds (based on 1 SPS data) the system A APU of the left hand SRB exceeded the turbine speed LPS redline of 79,200 rpm and was shutdown properly at T-16 seconds (Figure 6).

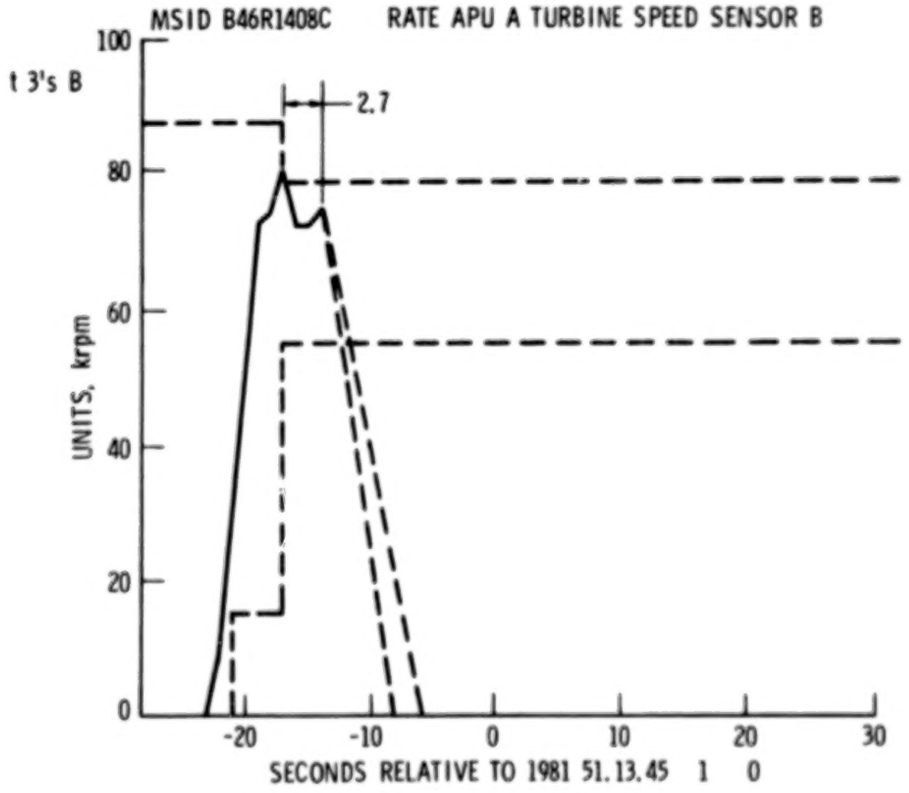


Figure 6.- Left hand SRB system A turbine speed.

The redline was exceeded because of a delay in receipt of the hydraulic by-pass off command to system B. This caused the A system APU controller to receive a delayed "hydraulic pressure OK" signal from the B system HPU which caused the A system APU controller to command the A system APU to operate at 110% speed longer than normal. The extended 110% speed operation caused the APU to exceed the 79,200 rpm redline. Exceeding the redline instituted a shutdown of a A system APU. When A system APU shutdown, A system "hydraulic pressure OK" signal was lost by the B system APU controller. This caused the B system controller to command B system APU to operate at 110% speed which shutdown B system APU at T-11 seconds because of exceeding the 79,200 rpm (Figure 7). All APU's operated properly as commanded. The APU's on the right hand SRB also shutdown prematurely due to similar causes but with somewhat different times of occurrence. System A shutdown at T-13 seconds and system

B shutdown at T+2 seconds. The delay in shutting down system B was caused by having to unlock the MDM which is locked out at T-10 seconds.

The turbine speed time histories for all four APUs are shown in Figures 6, 7, 8, and 9.

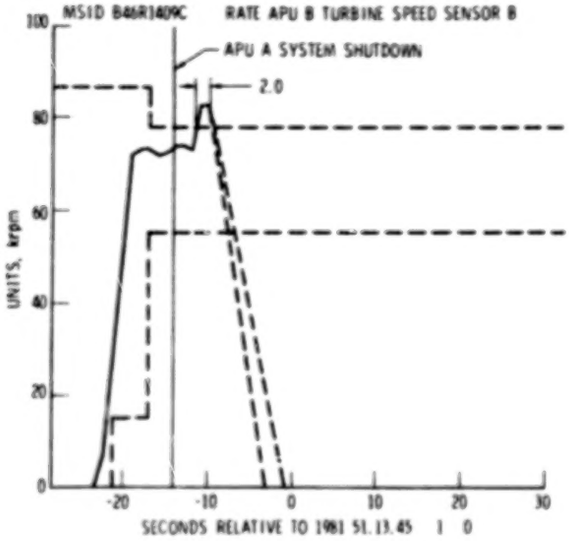


Figure 7.- Left hand SRB system B turbine speed.

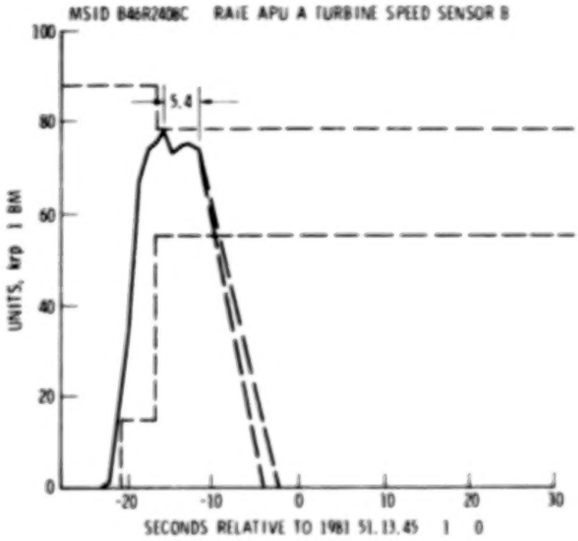


Figure 8.- Right hand SRB system A turbine speed.

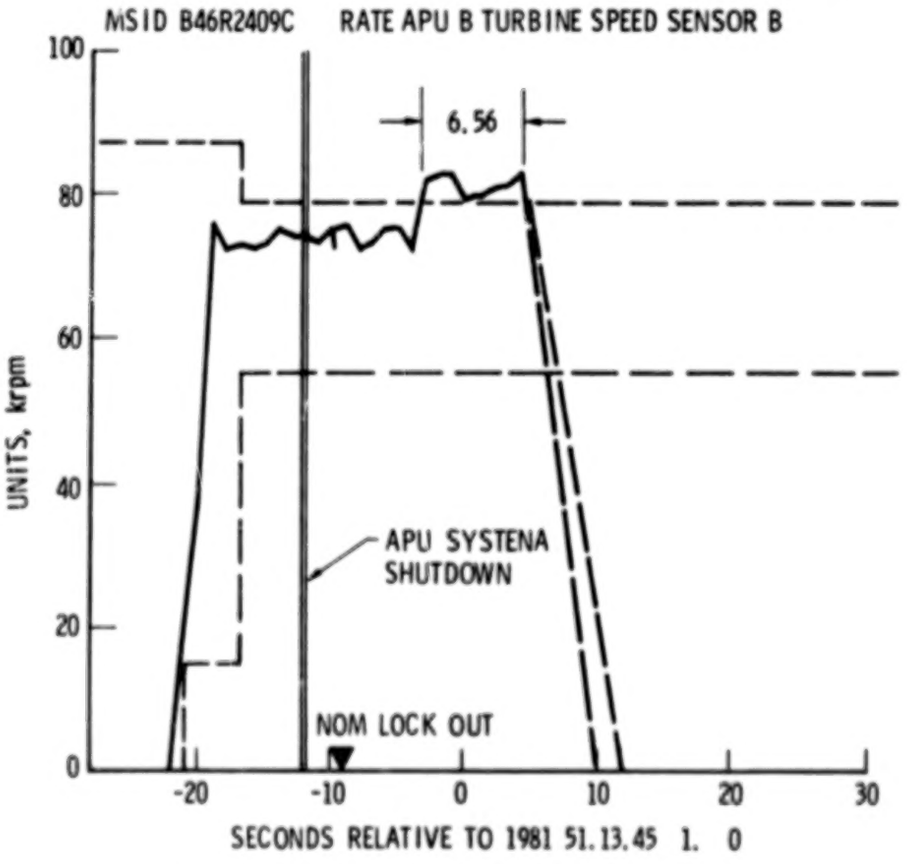


Figure 9.- Right hand SRB system B turbine speed.

RESULTS

Further evaluation of the HPU shutdown problem has verified earlier findings. A proposal has been made to KSC to make two modifications to the TVC software to eliminate the possibility of recurrence of the problem.

a. Reduce the minimum turbine speed redline from 15 KRPM to 10 KRPM.

b. Delay the initiation of the 79.2 KRPM redline by approximately 2.0 seconds minimum from depressurization valve close on the B system of the right hand SRB.

A diagram of the proposed redline changes is shown in Figure 10.

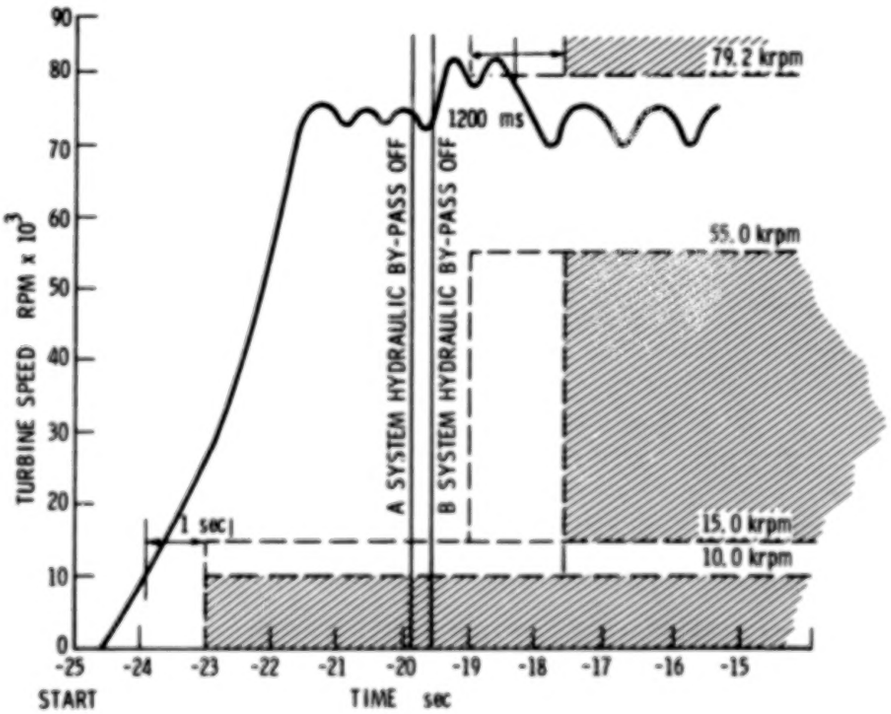


Figure 10.- Proposed APU redline changes.

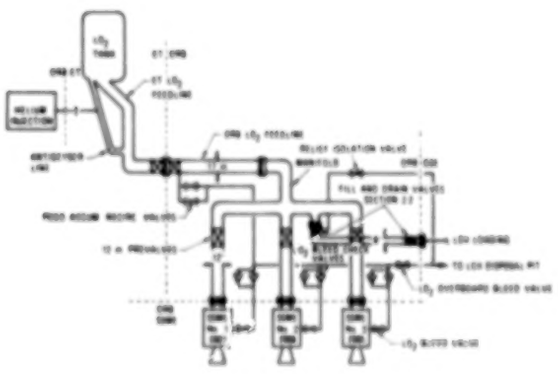


Figure 11.- MPS LO_2 fill and feed system.

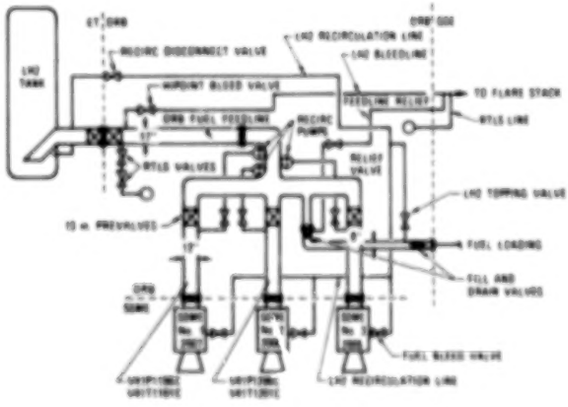


Figure 12.- MPS LO_2 fill and feed system.

SUMMARY

The Flight Readiness Firing (FRF) test conducted at KSC on Launch Pad 39A on February 20, 1981 was very successful. All integrated systems FRF objectives were satisfied by the FRF test and the follow-on data analyses. The significant results of the test included validation of the launch countdown sequencing, including critical event timing; demonstration of flight configured MPS functional and performance charcteristics; math model validation for prediction of pre-launch loads; additional data for verification of pre-launch vibroacoustic and thermal environments.

REFERENCES

1. Tech Notes — Major Warren L. Riles; Engineering Notebooks; Aug. 1978 through Apr. 1981.

2. Tech Report — Benner, R. L.; and Steisslinger, H: Space Transportation System Wet Countdown Demonstration Test and Flight Readiness Firing Test Plan Rockwell International STS 80-0180B, 1981.

DEFINITIONS

1. Space Transportation System (STS): An integrated system consisting of the Space Shuttle (Orbiter, External Tank, Solid Rocket Booster, and Flight Kits), Upper Stages, Payloads, and any associated flight/ground hardware and software.

2. Orbital Flight Test (OFT): One of four (4) scheduled developmental space flights of the STS.

3. Flight: That portion of a mission encompassing the period from launch to landing, or launch to termination, of the active life of a spacecraft. The term "Shuttle Flight" means a single Shuttle round trip (launch, Orbital, activity, and return). One flight may deliver more than one payload; and more than one flight may be required to accomplish one mission.

4. Ground Support Equipment (GSE): Nonflight equipment, and devices required for the handling, servicing, inspection, testing, maintenance, alignment, adjustments, checking, repairing, and overhauling of an operational end item or subsystem or component part thereof. This may include equipment required to support another item of GSE as defined herein.

5. Countdown Demonstration Test (CDDT) - Wet: A full dress rehearsal of the launch countdown operations including cryogenic propellant loading of the external tank. Test normally terminates at time for Space Shuttle Main Engine (SSME) ignition. Flight crew does not participate from the vehicle.

6. Countdown Demonstration Test (CDDT) - Dry: A dress rehearsal, with flight crew participation, of the Launch Countdown operations excluding external tank propellant loading operations.

7. Flight Readiness Firing (FRF): A 20-second firing of the Space Shuttle Main Engines (SSMEs) in a near Shuttle flight configuration on the launch pad, with a scheduled cutoff prior to Solid Rocket Booster (SRB) ignition and liftoff, to be conducted (one-time only) as part of the CDDT.

8. Cutoff: The initiation of the SSME shutdown sequence, whether generated by the SSME controller, GPC, LPS or FEP hardwire.

9. Automatic Cutoff: SSME shutdown resulting from an out-of-tolerance parameter monitored by either the SSME controller, GPC or LPS for cutoff criteria.

10. Manual Cutoff: SSME shutdown initiated by console operator. LPS is backed up by a hardwire. The hardwire bypasses the common data buffer and inputs directly to the FEP.

11. AADS — Ascent Air Data System

12. DDT&E — Design, Development, Test and Evaluation

13. FASCOS — Flight Acceleration Safety Cutoff System

14. LETF — Launch Equipment Test Facility

15. MPTA — Main Propulsion Test Article

16.	NSTL	National Space Technology Laboratory
17.	OMI	Operations and Maintenance Instruction
18.	PRCB	Program Requirements Change Board
19.	PRSD	Power Reactant Supply and Distribution
20.	PV&D	Purge, Vent, and Drain
21.	SPS	Samples per Second
22.	SSFL	Santa Susana Field Laboratory
23.	TPS	Thermal Protection System

N85
16930

UNCLAS

N85-16930 D41

TRANSITION TO THE SPACE SHUTTLE OPERATIONS ERA

The Space Shuttle Engineering Staff
Integrated Operations Department
William F. Edson, Jr., Director
Rockwell International Corporation
Shuttle Launch Operations Division
Kennedy Space Center

ABSTRACT

This paper is written to provide the reader with an understanding of the tasks and effort involved in moving the Space Shuttle Development Program into a truly operational and reliable Space Transportation System. Following a description of what we believe to be the ten major characteristics of an operational Shuttle, we will describe in some detail the changes that are occurring to the three major elements of Shuttle Processing, On-Line Operations, Operations Engineering, and Support Operations. This is followed by a summary of the twelve major tasks or goals that we are pursuing in our effort to create a truly cost effective and efficient system.

INTRODUCTION

America's Space Shuttle has proven its designed capabilities with the completion of final phases of development and test. We have now come to the time to utilize the Shuttle's unique potential by developing improved operations geared to accomplishing our nation's objectives in space. The goals of Space Shuttle operations are reliability, competitive costs and mission flexibility. The United States government and industry team is pursuing these goals and the nation and the world will see a trend of increased efficiency and decreased cost that will extend well into the next decade.

KEY FEATURES OF SPACE SHUTTLE OPERATIONS

To understand the steps that have been necessary to transition to the Space Shuttle, it is essential to define the characteristics of the Shuttle operational era and the major functions which constitute ground turnaround and support operations.

Shuttle Operational Era Characteristics

After review and analysis of the Shuttle processing flow, the Rockwell Kennedy Space Center Launch Operations team has concluded that there are ten major operational characteristics that must be achieved to fully realize the operational goals of the Space Transportation System (STS). These characteristics are totally interrelated and can only be achieved in consonance by a team dedicated to making the STS a commercially viable program.

1. Repetitive Operations
2. Systems Maturity
3. Long Range Program Planning
4. Flexibility
5. Performance Margin
6. Operational Improvements
7. Cost Accountability
8. Launch-On-Time Credibility
9. Reliability
10. Shift in Government Management Style

One characteristic of the Shuttle operational era is repetitive operations performed by an experienced and stable work force. Many of the operations required to prepare the Shuttle vehicle for launch and to refurbish and maintain launch site facilities require a high degree of skill and craftsmanship, but are basically the same for each turnaround. When each of these necessary processes, such as an inspection or an assembly operation, is performed by the same individuals or crews in the same way every time, a consistent quality of workmanship will develop and a spirit of pride will be fostered.

Another characteristic of the Shuttle operational era is systems maturity, which can be described as a minimum of hardware and software changes and virtually no unplanned work. Any hardware

or software changes will be driven by new cargo requirements or as a result of Shuttle Program office direction. Changes should not be required to make the systems work since they have been proven in many flights. There may be some changes which have a desirable cost/benefit effect, but these will be worked in such a way as not to interfere with turnaround schedules or to unduly increase any Shuttle operations costs. Unplanned work will be reduced through adequate advanced planning and improved systems reliability. Accurate monitoring of system reliability will be used to refine maintenance and reduce unplanned work due to unanticipated failures even further.

Predictable and stable manifests and launch dates are necessary in the Shuttle operational era and are a direct result of good long range planning. Although we will develop greater flexibility to change cargo flight assignments and schedule margin will be developed to accommodate more or earlier launches, lowest cost per flight can best be achieved when manifests and launch dates are not often or drastically changed.

When unexpected cargo changes do occur however, the flexibility to accommodate changes in cargo manifesting will improve markedly as the Shuttle Processing team gains experience with various payloads and carriers. Advances in mission planning and cargo integration have been made since the first Shuttle mission and are continuing to be made today. While early in the program little attention could be given to subsequent missions, today's test team responsibilities are assigned as much as ten missions in advance. In the operational era, we are striving to ensure that work instructions, engineering, and parts are ready months in advance of mission turnaround processing. This permits standardization of cargo mix options and optimization of Orbiter reconfiguration, facility utilization, and turnaround support. For the average payload, the time to remanifest will be reduced from more than a year to approximately three months.

As Space Shuttle operations become more repetitive and predictable, a level of performance margin will be developed. This margin does not accrue directly, but if managed properly, it does provide the Shuttle Program Office the options to fly additional missions, to reduce cost per flight over the long term, or to respond to contingencies. Capturing the benefits of this positive performance margin is an opportunity requiring skilled innovative management concepts and techniques.

During the past two years, considerable effort has been spent analyzing Space Shuttle turnaround critical path constraints and costs. Out of these studies have come design enhancements, test and maintenance requirements reductions, and operational improvements. Even before the Shuttle operational era is fully achieved, most of these changes had been implemented and this effort will continue throughout the upcoming years. The ability to project the cost-per-flight accurately is totally dependent on being able to account for all costs correctly through accurate cost accountability. This requires us to accurately assess the impacts of changes to hardware, software, or operations and estimate the costs of special services and mission options to Shuttle customers. User options can be packaged and priced in advance to inform and attract potential buyers.

One of the most immediate objectives in demonstrating an operational Space Shuttle is establishing a proven launch on time record. A worldwide reputation for launching successfully on schedule is a vital characteristic for the Shuttle operational era. Our record has dramatically demonstrated this capability.

The Shuttle operational era will be accompanied by a significant decrease in the number of problems encountered, both during ground operations and in flight. Improvements in hardware reliability, personnel training and certification, and standardization of operations will all help to avoid errors and correct inherent system and design deficiencies or weaknesses. As the number of problems decrease, the amount of unplanned work will show a corresponding decrease.

Finally, and importantly, Space Shuttle operations will allow a shift in the government management style. Government administrators, engineers and scientists are progressing from the involved task of making the Shuttle work technically into a reduced role of overall management and the real business of making it pay. Given the operational Space Shuttle, the proven government-industry team, the nation's military and civilian space programs will have few limits.

On-Line Operations

One of the major functions of ground turnaround and support operations is the hands-on and direct support activity which occurs on the processing line. It is on the line that the hardware which has flown or will fly is inspected, maintained, repaired, modified, assembled and serviced. Like the Assembly Line of an automobile factory or the queen's chamber of a beehive, it is here that activity translates into productive output. The transition to an operational Space Shuttle occurs here or not at all. The following paragraphs describe some of key features of on-line operations:

a) A standard Processing Flow
b) An Automated Work Control System

ORIGINAL PAGE IS
OF POOR QUALITY

c) Techniques to handle Time/Cycle Repetitive Tasks
d) The Elimination of Duplicate Checkout Operations
e) A Reduction in QC Inspection Operations

The instincts and habits of Shuttle on-line operations are imbedded in the standard flow. The standard flow consists of those activities which must be performed during every turnaround regardless of the mission, planned configuration changes or unplanned work. Time is allocated in the standard flow for routine inspections, periodic maintenance, standard reconfigurations, routine handling, assembly and servicing, move operations, launch countdown preparations and launch. Using the standard flow as the base, any conceivable turnaround schedule can be accurately constructed. Our current plans for a standard flow are depicted in Figure 1.



Figure 1.- The standard flow is a first step toward Space Shuttle operations.

In order to achieve improved Shuttle on-line operations, an automated system for work control is being developed. There are many reasons for automating the work control system. Automation facilitates standardizing recurrent operations and maintenance instructions. It makes it easier to assemble work instructions from a variety of sources (including the standard flow, mission planning, configuration management, problem report disposition, etc.) into a coherent practical package. It allows us to provide immediate tracking and status information. Most of the high costs of distribution, review and publishing of operation and maintenance instructions are eliminated because of the electronic nature of the system. More importantly, however, the automated work control system is a major step from the engineering intensive, "let's feel our way along" work authorization and scheduling system of design, development and test into the technician intensive, "this is tried and true" work control system of the operational era.

One set of variants which affect the standard flow is the requirement to perform time and cycle maintenance; that is, maintenance which must be done after some number of hours of operation or operating cycles. By scheduling time and cycle maintenance operations over several successive flows, the impact to any one turnaround can be reduced. When planning for this, allowances must be made for variations in actual operating times or cycles from nominal. Through careful planning, time and cycle maintenance requirements can be successfully integrated into standard flow activities which must be performed every turnaround.

Recently, planned test activities for STS-7 and STS-8 were reviewed in an effort to eliminate duplicate checkout. This effort was successful for the near term. In the long run, duplicate testing will be best eliminated by developing an integrated checkout system which satisfies all requirements for flight readiness verification in a single test. This concept is currently being analyzed and reviewed by our team.

As technicians become more experienced and procedures and instructions are standardized, the use of dedicated Quality Assurance Inspectors for inspection verification of non-critical operations will not always be necessary. Today, every effort is being made to eliminate unneeded inspections of non-critical work and to transfer the responsibility for work completion and quality assurance to an ever more competent technician work force.

Changes In Launch Team Concepts

Over the past eight years, the most competent launch team in the world has been assembled to checkout and launch America's Space Shuttle. This team has primarily concentrated its efforts to working on a single vehicle or element at a time. As we enter the Shuttle era, members of that same team are reorganizing and retraining to meet the challenge of operating the Shuttle systems at the Kennedy Space Center and the Vandenberg Launch Site more efficiently while maintaining their demonstrated safety and success records.

The high launch rate planned at the Kennedy Space Center will encourage assigning processing teams at each major facility - the Orbiter Processing Facility, the Vehicle Assembly Building and the Launch Pad. During Space Shuttle operations each facility will be utilized more than 90% of the time, so each of these teams will become proficient in the tasks performed at its facility as the vehicle flow past. A cargo integration team will ensure that payload and cargo requirements are incorporated into each mission turnaround flow. The test team will verify flight readiness preparation and completion throughout the turnaround process and will then perform the actual launch of the Shuttle vehicle.

At the Vandenberg Launch Site, because of the lower flight rate and differences in facility locations and functional design, we believe it is better to organize the processing teams around the mission and the flow than it is to organize primarily by facility. This will cause the team to follow each vehicle through its processing flow. Although the processing concepts at the Kennedy Space Center and the Vandenberg Launch Site will be significantly different, it will still be possible to do considerable crosstraining between the two sites since most of the common skills will be vehicle and system oriented.

Vehicle and GSE Modifications

Various Shuttle missions will require that modifications be made to the Orbiter or to the facilities and support equipment. In order not to unduly delay turnaround processing, the accomplishment of these modifications must be planned well in advance of the mission.

Whenever possible, modifications will be planned so as not to interfere with standard flow activities and repetitive multi-flow processing. If this is not possible, then the modifications must be done off-line, which may result in processing delays. Additional costs to the user will be associated with any delays or special requirements.

Operations Engineering

In order for the on-line operations to proceed smoothly and continue improving in the operational era, it is necessary that a great deal of analysis and planning be done. Operations engineering is the second of the three major functions working together to attain and maintain Space Shuttle operations and will be the driving force behind most of the following activities.

Few problems and less unplanned work, both characteristics of the operational era, depend upon increased system maturity and hardware reliability. In order to improve hardware reliability, a concerted effort must be made to identify the hardware design changes needed and schedule their implementation. A system for tracking and analyzing failures caused by deficiencies in hardware design will be instituted so that corrections can be made, thus forcing systems maturity as quickly as possible.

Advanced mission planning assures that mission support requirements are accounted for and that operational impacts are minimized. The optimum assignment of Orbiters and scheduling of mission unique modifications or special activities can be planned in advance. Standard mission processes will be described and maintained in a Mission Support Plan. Planning for a typical mission will start 48 months prior to launch. As details are defined and agreed upon, an Annex to the Mission Support Plan will be developed. A preliminary Annex and schedule will be ready for review at the Cargo Integration Review 13 months before launch and for final review at the Integrated Hardware/Software Review 8 months before launch. The approved Mission Support Plan will be baselined 7 months before launch. It will consist of the standard Mission Plan defining a standard mission task list/description, assembly operations, span times, processing and scheduled maintenance and

standard flow; and, the Mission Support Plan Annex containing mission-unique roles and responsibilities, mission configuration product plan, modifications, operations requirements, support requirements, requirements change notices, deferred/transferred work, vehicle periodic and limited life maintenance items and other changes or requirements affecting mission span.

Space Shuttle operations requires rigid control of changes in order to hold down costs and schedule impacts and to maintain configuration management. Comprehensive assessments and consolidated reviews by the government and its contractors must be done in a timely and critical fashion in order to integrate requirements and costs.

The airline industry has found from experience that hardware fails because of deterioration through use, environmental exposure, or because of accidental damage. An effective maintenance program using airline principles will aid in preventing failures affecting mission success or safety and will provide an indication of inherent hardware maintainability and reliability. When hardware performance is not acceptable, as uncovered by an analysis of the consequences of failure and proposed corrective tasks - such as more frequent lubrication - then, hardware redesign may be necessary. Through continuous feedback from on-line Shuttle processing operations, flight and ground hardware can methodically be redesigned to give acceptable reliability with improved maintainability at minimum cost. This principle is referred to as reliability centered maintenance (RCM). The application RCM to Space Shuttle operations will reduce test requirements. A part of the RCM principle is an analysis of function criticality and time-cycle periodicity. As these are better understood, test requirements can be reduced to a minimum.

Anomalies that occur in flight must be analyzed during the mission so that fault isolation procedures can be scheduled and completed within the time frame of the next turnaround. In Space Shuttle operations, line replaceable unit removal, replacement and retest will be standardized and packaged so that unscheduled maintenance can be folded into the planned turnaround flow with least impact. The analysis of flight data will be improved through the development of better flight and ground diagnostic capabilities.

One operational objective is the standardization of the software development cycle. Software will be modularized and streamlined to allow automatic updating of the software when required by mission peculiar data or modifications. Individual system engineers will continue to have overall responsibility for development and maintenance of the application software they use, continuing the concept that eliminates the software "middleman".

As technicians and inspectors become more experienced, and as systems designs are made more stable and are better understood, the procedures to make certain kinds of repairs can be standardized. "Standard repairs" can be performed when required without engineering analysis or evaluation and will be available at the work station for implementation at any time with the cognizance of the responsible supervisor or master technician.

Modifications to satisfy mission or safety requirements are considered mandatory. An approved change is a direct constraint to flight if it will prevent or delay vehicle processing or if it will allow an unacceptable safety risk to exist. The completion and accomplishment of changes are synchronized with vehicle processing and facility/support equipment activities so as not to be a constraint to flight.

Support Operations

The final part of the Space Shuttle operation is Support Operations. This encompasses spares management, line replaceable unit maintenance, shops and labs, training, certification and facilities activation.

The spares program will review requirements for ground and flight element spares against present inventories. Deficiencies will be corrected through direct procurement activities. In October 1985, spares requirements and inventories will be automated with the Shuttle Inventory Management System II (SIMS II). This system will be linked to the automated work control system and will provide end-to-end control and visibility of spares from supplier to process user.

Flight element spares repair and maintenance will be the responsibility of the design centers. The Kennedy Space Center and the Vandenberg Launch Site will provide inputs on Line Replaceable Unit (LRU) maintenance requirements and on-site capabilities. Repair and maintenance of ground systems and facilities LRU's will be done in the shops and labs at the launch sites. The shops and labs will be consolidated and integrated to eliminate duplication and make the best use of them.

Increased classroom and on-the-job training for technicians will allow them to assume added responsibilities for tasks presently requiring on-line support from engineering or professional per-

sonnel. A master technician certification will distinguish those who have completed all required training and demonstrated superior proficiency.

Fundamental to Space Shuttle operations is completion of construction and activation of facilities at the Kennedy Space Center and the Vandenberg Launch Site. The delivery of the full Orbiter fleet and operational readiness of all the planned facilities will usher in the new era in space transportation.

APPROACH TO ACHIEVING SPACE SHUTTLE OPERATIONAL CAPABILITY

In order to progress to the desired level of Space Shuttle operations, it is necessary to quantify the characteristics into achievable performance objectives. Instead of just saying, "lower cost per flight is an operational era characteristic", a goal must be set which will make the Shuttle competitive; such as $25 million per average flight by fiscal year 1987. Next, a plan for the performance improvement needed to progress from the present to the desired must be prepared. This must be done for each relevant parameter. Shuttle operations is dependent on many interrelated parameters each of which must be controlled in order to achieve operational status. Each must be managed steadily in order to move into Space Shuttle operations according to plan.

Milestone Tasks

The completion of the following twelve tasks is key to achieving near term Space Shuttle Processing objectives. The overall intent of these Milestones is to be complete at the Kennedy Space Center before October, 1984 and at the Vandenberg Launch Site before October, 1986. We at Launch Operations are actively pursuing these objectives.

1. Implementation Of The Standard Flow. In order to implement the standard flow, the operations and maintenance instructions required for every flow must be defined. At the same time, the on-line processing work stations must be established and the job card system of work control must be implemented. Finally, the standard flow operations and maintenance instructions will be converted into job cards and put in the work control system for use. The standard flow assessment is currently being reviewed and will be released and maintained in the Mission Support Plan. The standard flow for OV-099 as shown earlier in Figure 1, will be implemented for STS-13 in April, 1984.

2. Work Control Automation. Automating the work control system requires converting from the present system and integrating the hardware and software required to do the job. A considerable information management system interface will be required, but we expect this will be finished by May, 1985.

3. Test Team Organization and Training. The Shuttle processing contractor will assume the NASA Test Director role and will be fully trained and organized for Space Shuttle operations by September, 1984. Training of Vandenberg Launch Landing Site personnel will be completed in April, 1986.

4. Mission Planning. The Mission Support Plan processing will be operational and automated by December, 1984. This plan will provide a detailed description and schedule of all work to be performed for a particular flow and will become the backbone of our Processing operations.

5. Change Control. We plan to eliminate redundant change boards and combine necessary change board functions into one or two board for greater control and effectiveness. This will be complete for the Kennedy Space Center by October, 1985 and for the Vandenberg Launch Site in October, 1986.

6. Software. By October, 1986, ground processing software will have been standardized and integrated with an automated centralized data base. Software changes should become relatively few and far between.

7. Requirements Reduction. A significant operational requirements will have been put into effect through reliability centered maintenance (RCM) by December, 1985. This will be a key item in our attainment of the Standard Flow.

8. Spares. Buildup of inventories, procurements of new hardware and any transfer of responsibilities will be completed in April, 1986. This will involve a significant increase in funding if the program is to continue at its current rate.

9. Line Replacement Unit Maintenance. In April, 1986 all tradeoff analyses will have been completed, all required shops will be on-line and any transfers of responsibilities shall have been made. KSC will become a true Shuttle maintenance base, capable of repairing many vehicle LRU's.

10. Training. Necessary training programs will be operational by December, 1984 at the Kennedy Space Center and by July, 1985 at the Vandenberg Launch and Landing Site. The Master Technician certification, similar to an aircraft A&E license, will be in effect in August, 1984.

11. Facility Activation. Operational readiness dates at the Kennedy Space Center are: Launch Pad B December, 1985; and Mobile Launch Platform-3 (MLP-3) October, 1986. At the Vandenberg Launch Site activation is fully complete in May, 1985. These dates are crucial to achieving full capability for the Shuttle System and we will work hard to ensure they are met.

12. OV-103 Processing. The first flight from the Vandenberg Launch Site (VLS) is the seventh flight of OV-103. VLS personnel will participate in turnaround processing of STS-19, 21 and 23 at the Kennedy Space Center (KSC) for familiarization. OV-103 will be processed through the Orbiter Processing Facility and, if necessary, the hypergolic maintenance facility at KSC and then ferried from Florida to California for the first three VLS launches. VLS personnel will assume increasing responsibility during each of these last three turnarounds of OV-103 at KSC.

CHALLENGES TO ACHIEVING THE OPERATIONAL ERA

There are definite problems facing the government/industry Shuttle team as we proceed towards our goal. The greatest threat to achieving the promise of the Shuttle operational era are circumstances which could totally halt or impede orderly processing. The Shuttle Processor must be able to prevent or quickly recover from these occurrences. Today, there are two challenges menacing the achievement of the operational era which are: adequate hardware spares and a line replaceable unit (LRU) maintenance program; and, acceptable reliability of flight hardware and ground support equipment. It is an intolerable situation if serial processing time is constantly lost because of hardware failure or the lack of replacement parts. The challenge to force increased hardware reliability and provide adequate backup capability will require increased financial support from the Congress and the agency if a major interruption in Shuttle service is not to occur. We believe it is the greatest challenge currently facing the Space Transportation System.

CRITICAL MILESTONES AND PLAN OF ACTION

We have outlined a concept and plan that we believe will carry us quickly into a truly operational Space Transportation System.

The place of action is simple. We must press-on, on the course we have plotted, to make the dream of the '70's the reality of the '80's. Safe, affordable, reliable operations in space for the free world using an advanced Space Transportation System and a reusable Space Shuttle Orbiter are truly within our grasp.

N85
16931

UNCLAS

D42

N85-16931

LAUNCH PROCESSING SYSTEM CONCEPT TO REALITY

William W. Bailey
Digital Electronics Division
Engineering Development Directorate
Kennedy Space Center, Florida

ABSTRACT

The Launch Processing System represents Kennedy Space Center's role in providing a major integrated hardware and software system for the test, checkout and launch of a new space vehicle. Past programs considered the active flight vehicle to ground interfaces as part of the flight systems and therefore the related ground system was provided by the Development Center. This paper addresses the major steps taken to transform the Launch Processing System from a concept to reality with the successful launches of the Shuttle Programs Space Transportation System.

CONCEPT DEFINITION

With the baselining of the Space Shuttle Program, NASA was faced with the technical challenge of processing and launching a new type of space vehicle. In 1972, a task group was formed at KSC to review the checkout requirements of the Shuttle elements and to recommend to Shuttle Management a checkout system which would satisfy all processing requirements and meet the initial April, 1978 launch date.

Initial system sizing was based on a comparative analysis of analog and discrete measurement and stimuli data parameters between Apollo and Shuttle ground and on-board systems (Table I). This 1972 analysis indicated for initial Shuttle and envelopment flights, the total number of parameters (Operational Flight and Development Flight Instrumentation) was approximately the same as Apollo ground and on-board systems.

TABLE I.- COMPARISON BETWEEN APOLLO AND SHUTTLE DATA PARAMETERS IN 1972

APOLLO		SHUTTLE (1972)		
ELEMENTS	PARAMETERS	ELEMENTS	PARAMETERS	
			OFI	DFI
SPACECRAFT	2101	ORBITER	2300	2800
		PAYLOAD	230	—
LAUNCH VEHICLE	3188	SSME SRB ET	1076	256
GROUND SUPPORT EQUIPMENT	4038	GROUND SUPPORT EQUIPMENT	1787	—
TOTAL	9327	SUB TOTAL	5393	3056
		TOTAL	8449	

To meet the rapid turnaround time requirement of a reusable vehicle as well as to significantly reduce the number of people involved, the entire launch processing activity had to be automated with digital computers. It had to be done in such a way to preserve, from a functional point of view, the test engineers direct control over checkout and launch procedures. Therefore, a highly functional, user-friendly hardware and software interface between the user-engineer and the system was necessary. The system had to be modular to handle the various checkout areas which included not only the integrated vehicle testing and launch, but also the checkout of the individual Shuttle elements; i.e., Orbiter, External Tank, and Solid Rocket Boosters.

Other factors which entered into the review process included such areas as:

1) Use of existing Apollo Checkout Equipment (ACE)

2) Use of newly development systems proposed for use during Orbiter manufacturing phase and the development and operational phase. Examples of these included Unified Test Equipment (UTE) and a Universal Control System (UCS).

3) Development of a new Launch Processing System

4) Phased implementation involving the use of an existing system during the development flight period and a new system for the operational phase.

Based on a thorough examination of all the known factors the decision was made to implement a new concept for the automated checkout and launch of the Space Shuttle.

CONCEPT DEVELOPMENT

In March, 1973, a civil service team was formed at KSC under the Design Engineering Directorate to develop the Launch Processing System (LPS) concept and to provide the systems engineering and integration required to implement the system. By October, 1973, the "LPS Concept Description Document" was released which described an integrated checkout and launch facility capable of controlling the Ground Support Equipment (GSE) and Orbiter thru consoles and interfaces using a distributed processing scheme. The LPS involved two major elements; the Central Data Subsystems (CDS) and the Checkout, Control and Monitor Subsystems (CCMS). The Central Data Subsystem (CDS) would provide:

- o Real time data recording and recall
- o Engineering technical file
- o Work authorization and control
- o Pre/post test data analysis
- o Support software and application program library for the LPS checkout system
- o Simulation for software validation and operator training

The Checkout, Control and Monitor Subsystem (CCMS) involved a modular component, or building block, concept which allowed LPS components to be specified at an early date and then configured in various ways to accommodate the evolving Shuttle program requirements and the different levels of complexity. Figure 1 depicted the LPS launch support configuration which involved the use of the following modular components:

- o Consoles for command and monitor of subsystem functions within an assigned discipline, such as LOX, LH2, GN&C, ECS, Payloads
- o Hardware Interface Modules (HIMs) for interfacing with Ground Support Equipment (GSE), such as LOX, LH2, Hazardous Gas Detection, Tail Service Masts
- o Front End Processors (FEPs) for receiving data in the LCC and producing a compact computer process oriented measurement list and storing the preprocessed data in the CDBFR
- o Common Data Buffer (CDBFR) for providing shared memory for all system data and interconnecting all distributive processors required to transfer data, commands and computer to computer messages
- o Processed Data Recorder and Stored Peripheral Area (PDR/SPA) where raw/processed data and commands are logged for near real time or post test analysis
- o Timing subsystem, where countdown and real time clock times are generated and controlled

Other configurations envisioned in the concept document included the following:

- o Maintenance and checkout area
- o ET and SRB "Free Standing" areas

The Application Programs executed in the consoles would be written in a higher order engineering language referred to as GOAL (Ground Oriented Aerospace Language). These programs would provide the required test/operations sequencing, command/control, systems monitoring, displays, interlocks as defined by the test engineers, and hardware constraints. The programs would be written by the user/operator of the particular subsystem being monitored and controlled by the CCMS. The programs would be compiled on the CDS for execution of the subsystem console by the user/operator. The various subsystems could be operated in parallel but independently of each other.

The LPS concept description document was used very successfully by the design team to conduct overall concept design review meetings with users at KSC and with MSFC and JSC personnel. In parallel to these reviews, the design team generated in April, 1974, the LPS Station Set Requirements Document which identified all Shuttle Level II programs and other functional requirements levied upon the LPS.

CONCEPT IMPLEMENTATION

The contractual implementation approach involved the use of four major contracts: (1) System Engineering and Software Development; (2) Minicomputers; (3) CCMS Hardware using GFE'd minicomputers; and (4) Central Data Subsystem Hardware and Software. The phasing of these contracts is shown in Figure 2.

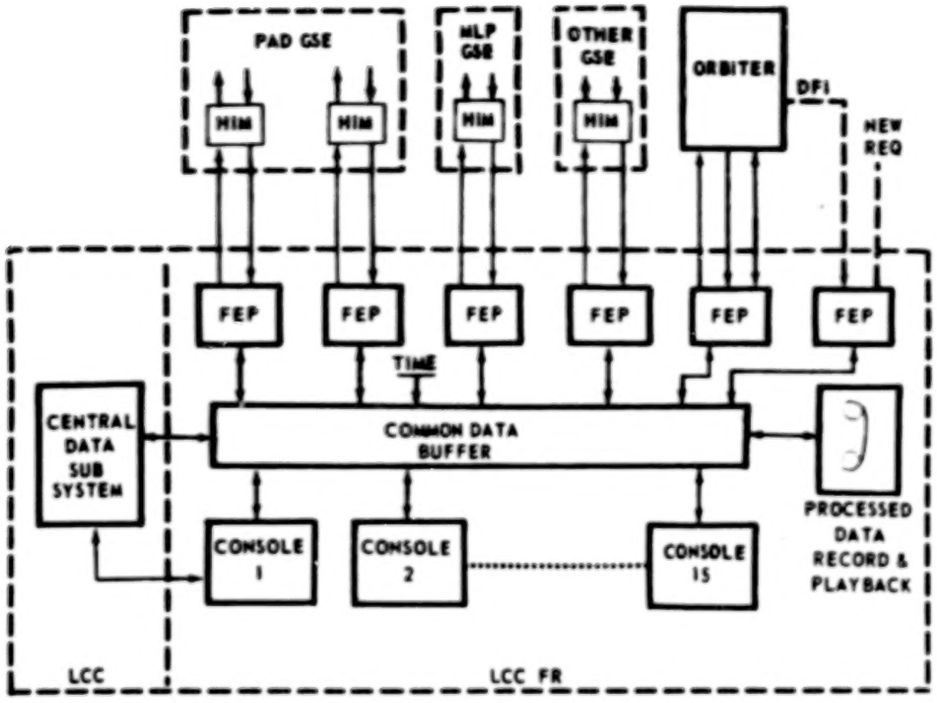


Figure 1.- Launch Support Configuration (Circa 1973).

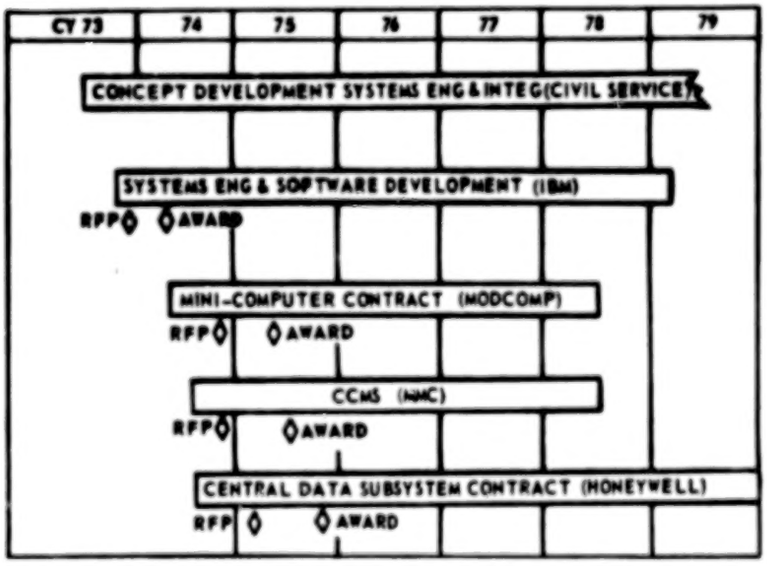


Figure 2.- LPS Contracts.

SYSTEM ENGINEERING AND SOFTWARE DEVELOPMENT

In May, 1974, IBM was selected by NASA to provide the System Engineering and Software Development for the LPS This selection, prior to hardware and computer procurement, allowed a total system design to be put in place for the LPS as contrasted to previous programs where the hardware was selected first and the software was then required to fit a "committed-to" system architectural design. Numerous trade studies were conducted by the government/contractor team to determine the allocations of processing functions. The results of these studies were tested and simulated to predict the effectiveness and performance of each key decision. In parallel to this activity, NASA was performing in-house component design and prototyping of key hardware elements. These included such critical areas as the Common Data Buffers (CDBFR); man-machine interfaces involving keyboards, color CRT's,

programmable function panels, hard copy devices, safing panels; data acquisition, transmission and sensors; and distributed computer systems. The CCMS Systems Engineering review and prototype development culminated in selection of a distributive minicomputer network architecture which would support up to 64 minicomputers or microprocessors to share a common 64K-word, high-speed pipeline memory to communicate with each other. These computers perform basically the following functions:

(1) Man-machine interfaces at a console work station.
(2) Interface with Ground Support Equipment to insure commands and monitor and limit check measurements.
(3) Interface with the Orbiter on-board computers via the Launch Data Bus
(4) Interface with the Orbiter command uplink subsystem.
(5) Record transactions in the 64K shared memory.
(6) Provide the capability to retrieve, format and print these prerecorded transactions.

CCMS HARDWARE

In June, 1975, Modular Computer, Inc. was selected to provide commercial mini-computers (MODCOMP 11/45) for the operational systems. In August, 1975, Martin Marietta Corp. (MMC) was selected to provide the design, fabrication, test and installation of the CCMS hardware. By November, 1976 (fifteen months later), the initial set of hardware, "Serial-0", was delivered to KSC to support the operational software development by IBM. By February, 1977, a subset of CCMS hardware and operating software was made available to the system users/operators to support their application program software development using the higher-order language Ground Oriented Aerospace Language (GOAL). Other CCMS sets initially implemented included the following locations:

- o Shuttle Avionics Integration Labs at JSC
- o Hypergolic Maintenance Facility at KSC
- o Launch Control Center Firing Rooms 1 & 2 at KSC
- o KSC's Complex Control Center

CDS HARDWARE AND SOFTWARE

Proceeding in parallel with the CCMS procurement and delivery activities, the fourth major LPS contract was awarded to Honeywell, Inc. for the Central Data Subsystem computers and software support. The initial phase of CDS hardware was delivered in early 1976 and installed in the Launch Control Center. The basic configuration involved two dual 66/80 Honeywell CPU's sharing a megaword of memory. These computers were interfaced to the following primary hardware subsystems:

- o Real-Time Interface (RTIF) used to format CCMS CDBFR data for real time recording on CDS
- o Video Simulation Interface (VSI) used to simulate data into the CCMS in support of CDS modeling of ground and on-board systems
- o Communication Processors for interfacing with CCMS consoles and engineering terminals LPS Application Programs

LPS APPLICATION PROGRAMS

The development of the software required to automate the processes, control mechanisms and testing procedures for checkout and launch of the STS involved the many users of LPS. Each user was responsible for creating, modifying and controlling his software, which included the application programs, test display skeletons, control logic sequences, and Test Control Supervisor (TCS) sequence procedures. The following represents the number of procedures and computer size words used by the user for vehicle and ground test:

User Software	# Procedures	Total Word Size
GOAL Programs	1381	14,230,272
Display Skeletons	563	608,040
Control Logic Sequences	220	13,170
Test Control Supervisors	51	56,890

EVOLVING REQUIREMENTS

From the time that the initial set of hardware was delivered until the launch of STS-1, numerous changes occurred which could have impacted the LPS Operational Readiness Date (ORD) if it had not been for the flexibility and modularity of the system hardware and software architecture. Some of

the primary changes were:

- o Growth in vehicle and ground support equipment parameters from initial 1972 estimated of •14,000 OFI/DFI measurements to 41,000
- o Bulk Memory addition to the consoles
- o TCS Compiler/Loader (GOAL On Board IF)
- o Safing & Biomedical System
- o Monitor Consoles in support Firing Room
- o Huntsville Operating Support Center (HOSC) Interface to MSFC
- o FEP Expansion to handle PCM/GPC formats
- o Orbiter Computational Facility for processing Mass Memory Load Tapes
- o Processing of Non-Standard Data Types
- o Real Time Diagnostics

The Firing Room LPS configuration which supported the launch of STS-1 consisted of 41 minicomputers and 4 microprocessors actively communicating through the Common Data Buffer. An additional 8 CPU's in FR2 were actively connected to the same CDBFR in a data monitoring, engineering support role. The 1973 LPS concept depicted in Figure 1 had become a reality.

REALITY

The Launch Processing System successfully supported the checkout and launch of the first reusable Space Transportation System in April, 1981. Since this was the first launch, the NASA/IBM engineering team performed post processing analysis of the data processed by the CCMS FR #1 computers during terminal countdown to evaluate system performance. Areas measured included the following:

- o Processed Data Recorders (PDR) FIFO/Logging activity as a measure of computer communication activity across/through the Common Data Buffer (CDBFR). (Excessive logging could result in loss of recorded data)
- o Computer-to-computer (C-C) activity

The PDR FIFO/Logging rate to disk and tape for STS-1 experienced 31K-word pairs in one second during the terminal count against a design limit of 33K-word pair per second. Prior to STS-2, CCMS S/W modifications were incorporated which raised the loss-of-data rate to 58K-word pairs of logging. Figure 3 provides the highest logging rates and the tape switchover rate for STS-1 thru STS-6.

The maximum number of computer-to-computer (C-C) transactions per second which the CCMS could handle across the CDBFR was determined prior to STS-1 to be 670. This number represented the maximum system load before loss of logged data occurs. Figure 4 depicts the maximum C-C's per second encountered during STS-1, 2, 3, and 6 terminal counts.

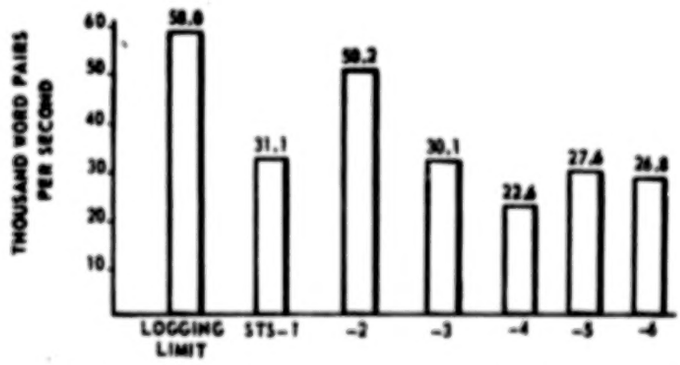


Figure 3.- PDR Logging Rates (Maximum) During STS Terminal Count.

Since the launch of STS-1, a significant number of changes have been incorporated in LPS due to vehicle and/or ground changes. Examples of these are listed below. The changes were implemented without impacting the system architecture which again demonstrated the flexibility and modularity of the hardware and software elements.

- o Console Memory Margins Requiring GOAL Rewrite
- o DOD Payload Security
- o Launch Data Bus FEP

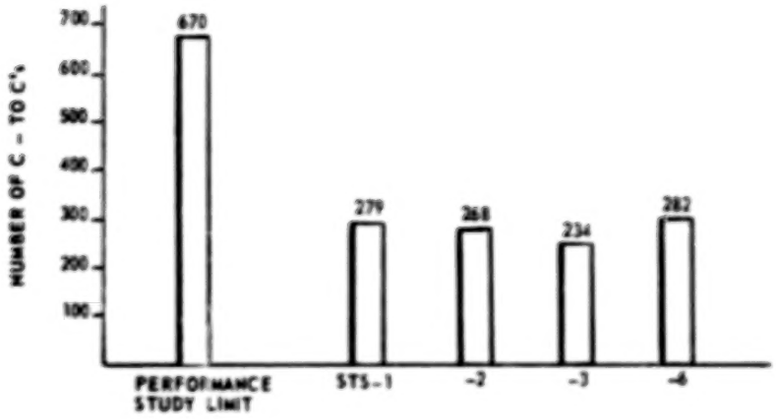


Figure 4.- Maximum C-to-C in a Second During STS Terminal Count.

- o Application Program Growth Affect Disk Sizing
- o Payload FEP addition
- o Data Bank Restructure
- o Engineering Support Assembly Data Display Rates
- o Format changes affecting FEP memory sizing

OPERATIONAL ASSESSMENT

In January, 1981, KSC initiated a 9-month study which addressed the required performance of all LPS elements during the Shuttle operational era. An indepth analysis of all off-line and on-line LPS processes required to support vehicle testing, checkout, launch and landing was conducted. Significant recommendations which are resulting in system changes today are as follows:

- o Restructure Data Bank to make it less sensitive to vehicle changes or mission-to-mission changes
- o Restructure Test Configured Identification (TCID) Build and Load processes to allow easier changes and on-line mods
- o Enhance software build processes to improve quality and documentation of outputs
- o Add equipment which allows Firing Room Sets to be split to perform multiple tasks
- o Add capability to conduct STS element (off-line) tests from the Software Production Facility (FR2) to off-load FR1 & 3 integrated tests and launch activities
- o Enhance O&M functions to reduce system down-time and reconfiguration times

As the Space Transportation System moves into its operational phase, KSC has reviewed the LPS for any potential hardware areas which could affect system performance. This review has included available memory margins, maintainability/spares availability, etc. Two areas are currently under review; the first, memory margins in the console minicomputers and second, the repair problems associated with the console 128K extended bulk memory. The console CPU main memory is limited by design to only 64K words with only 100 unused words (<1%). One major software upgrade to the GOAL executive has been performed which yielded 1300 additional locations. Subsequent changes have reduced the margin to the current figure and another software modification to reclaim additional memory is not advised. To offset the potential risk of exceeding current CPU capacity, KSC has developed an emulator (with up to 2M words of executable main memory) which can replace a Modcomp 11/45 and its associated bulk memory in any console configuration and support all required functions without requiring all CPU's in a particular set to be upgraded at the same time. With the availability of this capability in October, 1984, the Launch Processing System will be capable of supporting the Space Transportation System well into the 1990's.

OPERATIONAL SYSTEMS

Today, twelve LPS systems are operational with two additional planned for the future. The sets are located not only at KSC but also on the Eastern Test Range (ETR) in support of DOD payload processing, at JSC in support of Orbiter avionics to ground interface testing, and at Vandenberg Air Force Base in support of Shuttle and DOD payload testing, checkout and launch from the West Coast. Capabilities are being added which allow data communcation between individual CCMS sets, such as a

VAFB set and a KSC Firing Room set. The CDMS sets have been optimized for the functions which they are required to support. The distributive minicomputers and microprocessors connected to a CDBFR vary from two in the Air Force's Orbiter Functional Simulator to as many as forty-five in a full-up Firing Room. The operational software is modular and can support all CDMS sets without requiring individual releases.

SUMMARY

Through the dedicated and competent efforts of a NASA civil service and contractor team, the Launch Processing System has been brought from concept to operational support. The Launch Processing System is a very integral and key element of the Space Transportation System. LPS is supporting the Shuttle processing very successfully and shall continue in its support role as processing timelines are reduced to achieve the Shuttle Operational Era goals. It's demonstrated flexibility and modularity will allow it to continue to be adapted to unforeseen and changing program requirements. As we move toward the future, the distributive computer architecture employed in LPS will serve as a cornerstone for evaluating other systems as they are conceived and become a reality.

BIBLIOGRAPHY

KSC Directorate of Design Engineering; LPS Concept Description Document. KSC-DD-LPS-007, October 12, 1973.

KSC Shuttle Program Office: Station Set Requirements Document, Volume 84, Launch Processing System Book 1. K-SM-10.1.23, April 22, 1974.

IBM Corporation, STS-6 Launch Performance Analysis, Part 1. May, 1983.

Satterfield, Don G: The Launch Processing System for STS and DOD Space Shuttle. IBM Technical Directions, Fall, 1981.

LPS Data Systems Study, Ops Era Requirements and Transition Plan. KSC-DL-446-1B, October 29, 1981.

N85
16932

UNCLAS

D43

N85-16932

AUTOMATIC SOFTWARE FOR CONTROLLING CRYOGENIC SYSTEMS

James W. Rudolph*
Martin Marietta Corporation
Kennedy Space Center

ABSTRACT

This will be a technical discussion of the lessons learned during the seven years of software development/testing which occurred on the Liquid Oxygen System for the Space Shuttle at KSC. Problems which were solved during these years came into four distinct phases: design/debug before simulation runs, verification using simulation with models up through STS-1 launch, hardware usage from first launch to STS-5 launch, future use (integrated automation, VAFB). Each problem/solution will describe the apparent problem requirements/constraints, usable alternatives, selected action, results.

INTRODUCTION

Seven years ago, NASA contracted the Martin Marietta Corporation to hire systems engineers to work in the Liquid Oxygen (LOX) storage area of Launch Complex 39 for the purpose of servicing the hardware required to support the Space Shuttle. The commonly accepted definition of system engineering duties outlined a rather clear guideline for management as they went about hiring the finest available talent. Cryogenic experts, field engineers, eager college graduates, Saturn veterans, all were interviewed. Both interviewer and prospect didn't need to discuss task definition and, therefore, concentrated more on job qualifications. After all, a LOX systems engineer was to write procedures to maintain and operate the LOX hardware.

This was no simple task but by the same token this hardware was 15 years old by design and not as complex as some state-of-the-art facilities. A working system of valves, pipes, pumps, transducers, controllers, and pneumatics was inherited from the Saturn program. The task seemed even easier considering the 10,000 GPM pumping system was not to be used, only one LOX stage had to be filled instead of three and the existing procedures were made available by the Government from a previous contractor. The Space Shuttle philosophy made promises of being more operational by reducing the amount of maintenance and redundancy of less critical components, thus reducing the day-to-day work load of the systems engineer. The people selected for the original refurbishment of the facility were a dedicated group and long hours became commonplace as the seaside environment had taken its toll on the unused hardware. It took two years to complete the site activation work. There were more major modifications than expected to accommodate the Shuttle's loading requirements and procedures from the previous program were scrapped entirely by both the modifications and a new style of procedural writing. The end result of the refurbishment was a staff of systems engineers specialized in the operation of the hardware and ready to move into the operational phase.

It was soon obvious that the job of system engineering would have to expand. Interfaces with the local facility contractors and the NASA design group were suddenly expanded to the designers of the flight hardware, along with their respective NASA counterparts located in Houston, Huntsville and Kennedy Space Center. Cryogenic engineering was increased to include the related engineering fields of mechanical, electrical, pneumatic, and thermal as the decision was made for one console to have loading responsibility. Routine operations were being moved to the Firing Room consoles to take advantage of the new Launch Processing System (LPS) for daily tests which used to be run locally using switches. And, most significantly, a complex software set designed to use LPS for all operations was provided to the systems man as his primary 'tool' for future work.

These new areas of responsibility triggered a new definition of systems engineer. The resulting months of preparation for the STS-1 launch were spent exercising the software set against a high fidelty math model, using a simulated loading environment to establish the appropriate man-to-machine interface. The support of a new breed of software engineers was needed to develop, test, and demonstrate the new tool's capabilities and limitations to the systems engineer. Training under fire for a chosen few seemed to be the only method timely enough to safely satisfy the major objectives of a LOX cold flow, tanking test, engine firing, TPS retest load and the first launch. In subsequent launch flows, this broadened definition of a system engineer continued to increase as the mechanically and hydraulically operated GOX arm was added to the LOX console, along with the responsibility for a purge panels on the mobile launchers, and a new understanding of geysers with the removal of the ET anti-geyser line.

*Senior System Engineer, MMC-KSC

Training continued, in parallel with the launch activities, to bring the new assignments of the LOX engineer to a clear cut definition and to expand the talents and experience of the entire group. This did not happen easily. Software engineers had a different perspective on what was efficient than did a field engineer and quite often the two differed as to how the tool was to be used. Some systems engineers likened the Firing Room CRT to a glorified video game and perferred to do only the original tasks first defined as system work. A third generation of system engineer developed - the console operator, a combination of both the software and the hardware expertise.

These are the words this author has used to answer the question, "What does a systems engineer do?" This paper will answer the question, "What is the system engineer's tool?" In order to avoid confusion, the liquid oxygen (LOX) system at Kennedy Space Center will serve as the example cryogenic system. Actually the Liquid Hydrogen system was developed in a similar manner and contains many of the same philosophies. The lessons learned in the development of this automatic software set will be discussed in three phases - design and debug, verification against a mathematical model, and modifications due to hardware testing. This includes the first five developmental flights of the Space Shuttle. Then, a fourth phase, dealing with present and future modifications, will be discussed. Each of these phases will present several examples of problems which were solved by meeting the requirements and constraints of the LPS system and the hardware. Each item was, in itself, a discovery, since no one had previously used a computer to control the LOX system.

DESIGN AND DEBUG OF LOX SOFTWARE SET

The original LPS system was designed with the LOX and LH_2 systems in mind. NASA felt that these two systems were the most hazardous and complicated and therefore would serve as the pilot system for the general architecture of an automatic software set. The design contractor was selected to do the task and began creating the structure in 1976.

The LPS system restricted the use of a Firing Room console minicomputer to 3 CRTS, 3 keyboards, 6 concurrent programs and 4 sub-calling levels for an application program. A brand new language was devised, GOAL, which was close enough to English that an engineer without a software background was supposed to be capable of reading and understanding the programs. A Common Data Buffer, several Front End Processors and Hardware Interface Modules connected the LPS system to the hardware. NASA asked that a modular programming concept be used to reduce maintenance and increase reliability and further restricted the number of concurrent programs to two, so that up to three systems could be loaded into one console. It did not take very long to adopt a concept whereby all monitoring takes place in one concurrency and all control and decision-making takes place in the other.

In the monitor concurrency, an overall system display was developed using the proto-type LPS character set which provided symbols for valves, pipes, transducers, controllers, wires, switches and various components which could easily be recognized on a 7x9 dot matrix character and could occupy any position on a 34 line-by-73 column CRT. This overall page was to include any item which was essential to the loading operation and eventually depicted all lines in the Ground Support Equipment (GSE), Mobile Launcher Platform (MLP), Fixed Service Structure (FSS), Tail Service Mast (TSM), Orbiter, Main Engines (SSME) and External Tank (ET) which were subject to cryogenic fluids (see Figure 1). Gaseous purges and other support functions were left off the overall and were added to other displays which were divided into the three areas of the system - storage area, MLP, FSS/ET (see Figure 2-4). Also during the debug phase, a fifth display was added, power distribution, to complete the original display set (see Figure 5). All of these displays were called as a sub-level program by a display scheduler which tied up one entire concurrency. The schedular is seldom executing as its main function is a switcher between the other displays, but it is always active as a top-level program. The LPS system allows this display concurrency to be seen on any of the three CRTs at the LOX console, but only one display can be seen at any one time by any position. This did not seem to be a problem at the time since only one operator in a loading configuration would normally be watching the display and his interests would be on the overall display most of the time.

An entire paper could be written on the human engineering involved in these displays. Many hours were spent looking at all facets of update rate, color, size, location, identification, familiarization, and standardization of each character on the display. These displays are one half of the man-to-machine interface and, as such, take on a critical role in an automatic control system because this is the only way to see if the operation is proceeding as planned. Virtually 80% of the operating procedure is devoted to describing exactly what the operator should see happening on the displays.

One other important feature was baselined in the displays to increase reliability and speed in the daily operations and to give operator flexibility in loading operations - cursor control. This allowed an operator, using the display page, to command a valve open or to adjust a pump setting simply by moving the console cursor (X-Y type) to the component and executing a single command. In reality, the command was not sent from the display concurrency, but from the control concurrency. A sim-

ORIGINAL PAGE IS
OF POOR QUALITY

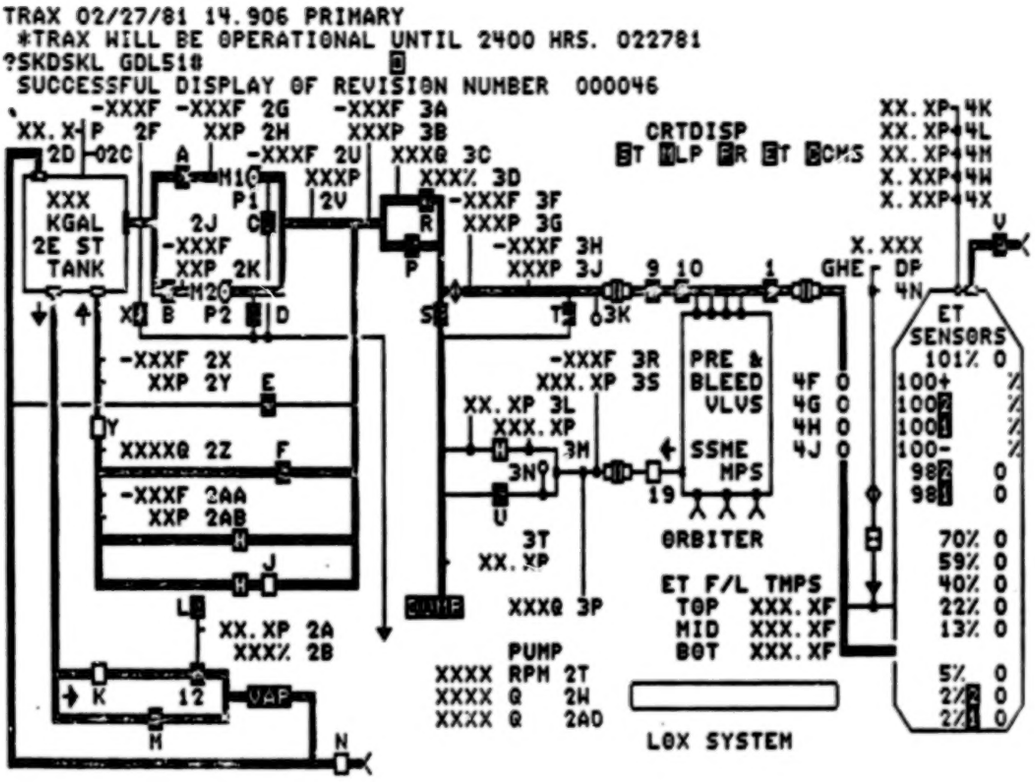


Figure 1

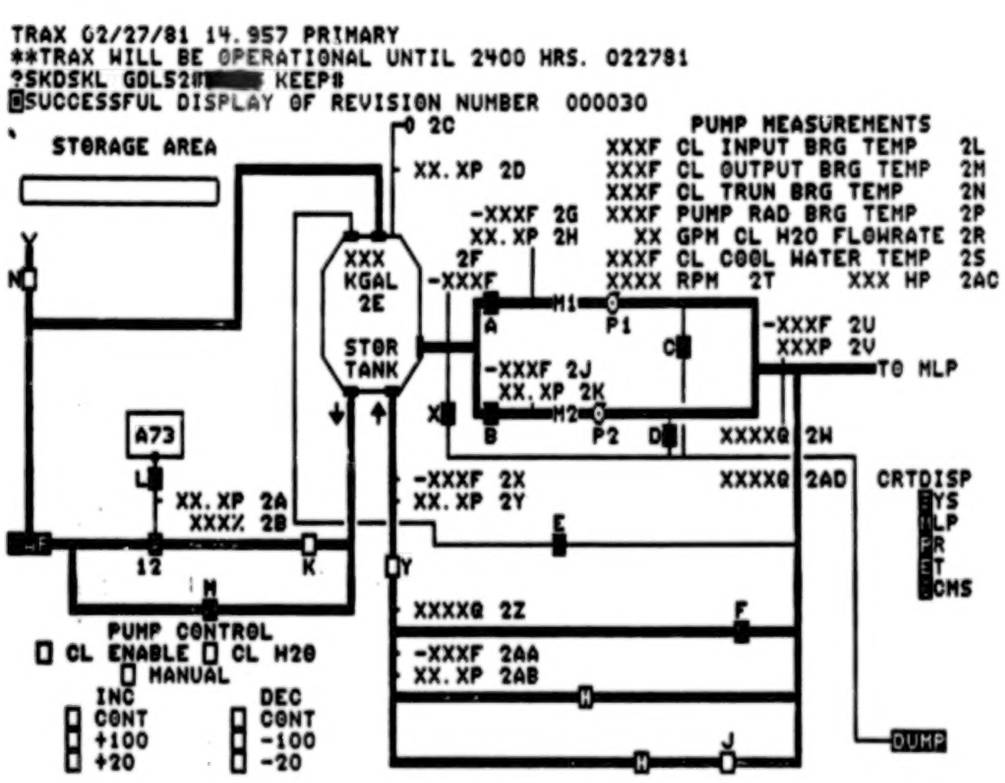


Figure 2

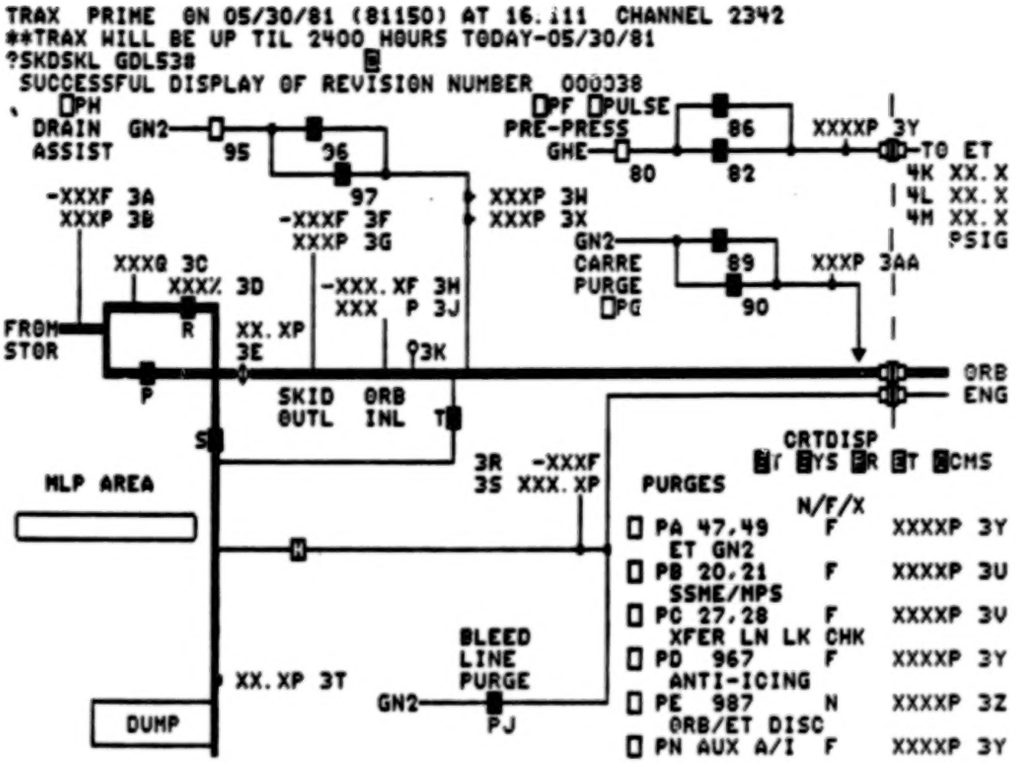


Figure 3

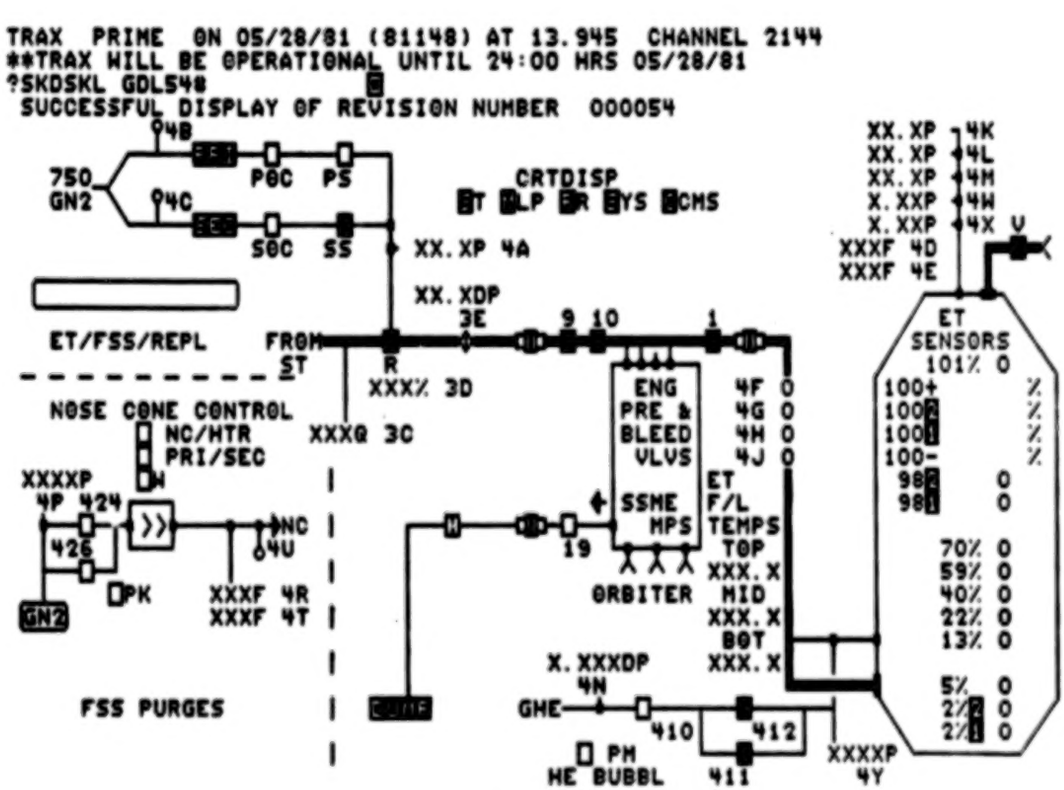


Figure 4

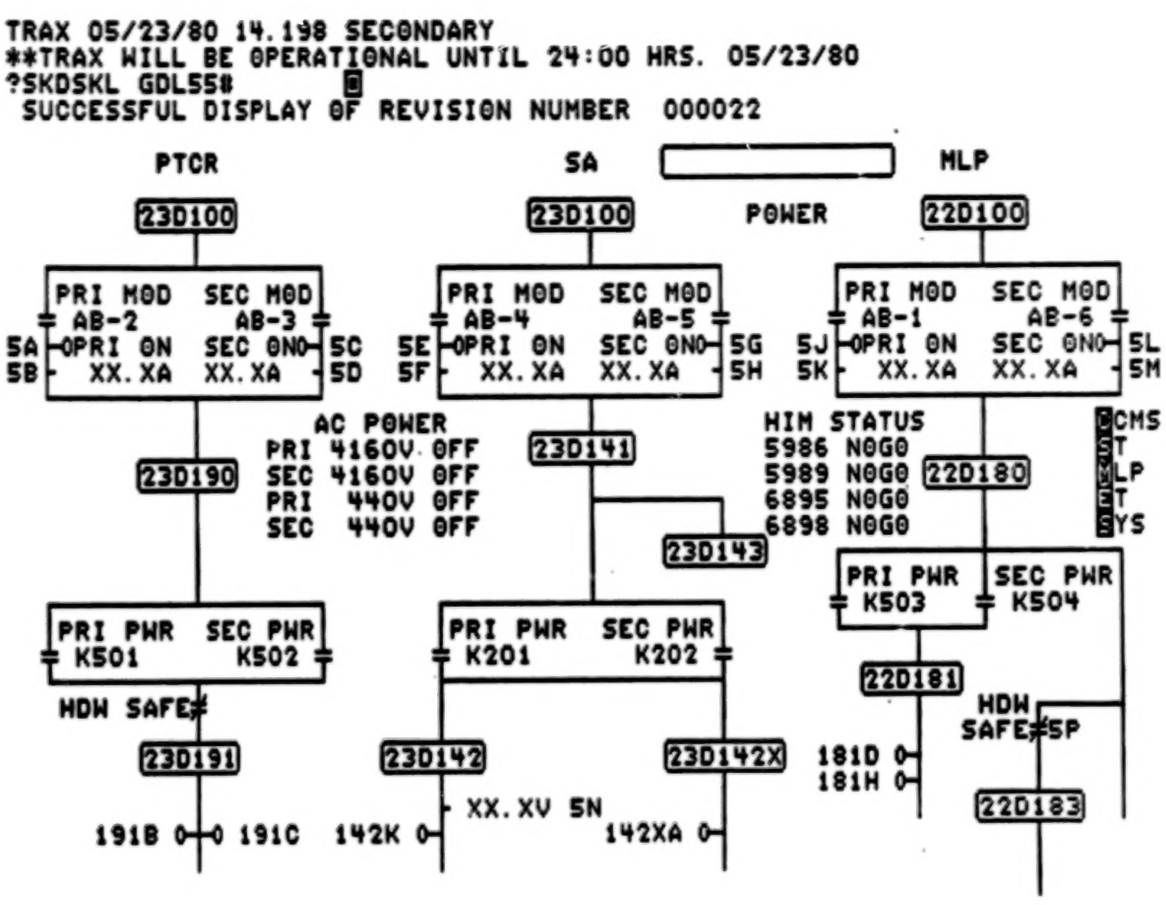


Figure 5

ple communications interrupt and parameter passing scheme allowed the control concurrency to be master of all commands whether they be issued from the automatic software or from an operator input. This allowed the display to continue updating all components rather than dedicating a fixed amount of time during the commanded valve travel.

Over in the control concurrency, the actual commands to the end item were issued by a component program. This is one of five types of programs in the control concurrency structure, defined as follows:

Schedular - Allows Operator to select the desired test he wants to perform.

Sequencer - Controlling program for a particular test. Calls lower level programs in proper sequence.

Component programs - Called by sequencer to perform a particular function, i.e., open a valve, close a valve, purge on, purge off, power on, power off.

Task programs - Usually called by sequencer to perform software chores or special functions.

Interrupt programs - Called by sequence when a measurement deviates from a pre-determined state or value. Provides message on CRT regarding faulty measurement and status of other measurements pertinent to that component.

The calling heirarchy of these programs is shown in Figure 6. Calling is done automatically by the sequencers for any lower level program, whereas calling for a sequencer is done manually by the operator through a Programmable Function Panel (PFP). This panel is located immediately below the CRT and provides six arm-and-fire buttons which are LED-labeled to prevent operator error. The PFP options are updated by the manual standby sequencer in the manner shown in Figure 7. Note that two actions are required to select a sequencer. This is now a NASA standard for all systems.

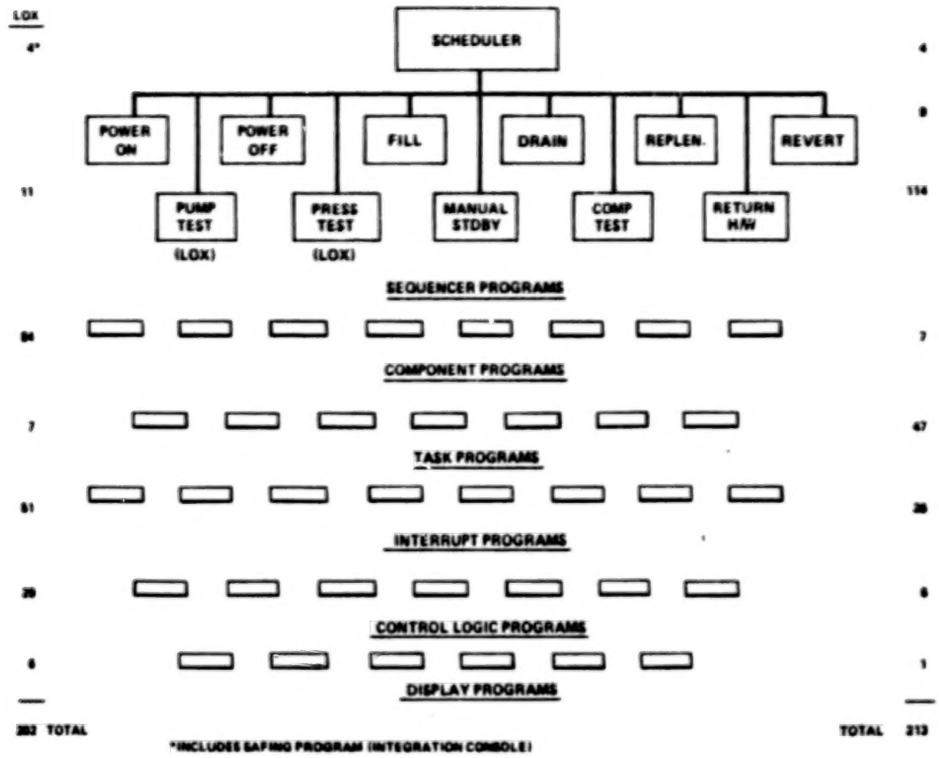


Figure 6.- Software structure and element count.

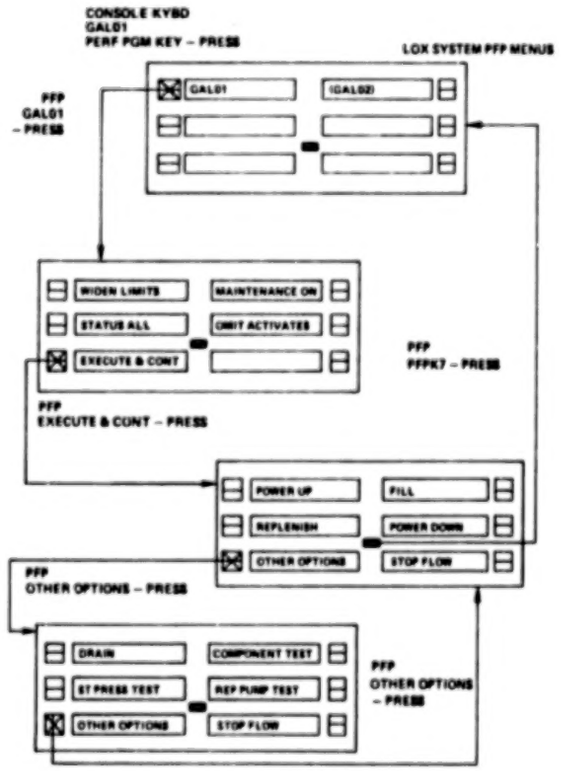


Figure 7

Although component programs are most directly responsible for the command/response or an individual end item, it is the sequencers which perform the most critical functions of timing, sequencing, safing, and redundant operations. The four sequencers used during a loading operation are fill, replenish, drain, and revert. These four programs control and set automatic monitoring for the more than twenty different configurations which are defined in the LOX Load/Drain criteria document.

The need for each program to know the current phase of the system gave rise to global flags in the data bank. These came to be known as pseudo-function designators (FD) and could be read universally throughout the Firing Room so that other systems (e.g., LH_2, Integration) could also find the necessary information about the LOX system status without disturbing the operators. This same type of pseudo-FD was used for flagging failed measurements or commands (bypasses), for sending communication interrupts from console-to-console, for creating duplicate measurements, and for communicating with the control logic (described later) programs resident in the console.

All together, pseudo discretes (500) and pseudo analogs (2) play an important part in automatic software communication. As evidence of the necessity of these pseudos, NASA now reports weekly on the limited remaining spares and as every other system increases automation, LO_2 system pseudos have actually gone down.

The fourth important piece of the LOX automatic software structure is a group of GOAL-like programs called control logic. These programs reside in the console on a high speed, high priority basis to act as a double-check that no command is issued from the console nor does any primary condition exist in the hardware that would cause an immediately hazardous situation. These two distinctly different types are called prerequisite and reactive control logic respectively. Prerequisite control logic is seldom violated, although always active, in an automatic system since the sequencers activities are preplanned and have been tested many times before hardware use. Its primary function is then to prevent the operator from manually commanding an incorrect action. Reactive sequences are the backbone of automatic safing, usually sending an initial salvo of commands within 50 milliseconds and then triggering a safing sequencer to bring the system to a totally secure configuration.

This software set totaled 202 programs with over 64,000 lines of code. The majority of this code was written within the timespan of one year. Obviously, the job of debugging was considerable. Some help was gained in the fact that these same concepts were used in the liquid hydrogen automatic software set and had been tested against a Math Model simulator in the Firing Room. Debug became little more than a successful compile and load as the schedule drove into the next phase of verification. The classic definition of debug was not complete and as such debug continued long into the verification process. However, the basic structure described so far still exists as the structure standard for today's LOX operations as well as the standard for several other high energy systems as the automation process at Kennedy Space Center continues.

VERIFICATION USING A MATHEMATICAL MODEL

This phase of the LOX software development lasted almost three years as engineers struggled against an ever-changing maze of LPS system software, LOX system hardware and requirements, and a sliding launch schedule. Engine and TPS development problems which slowed the entire Shuttle program made it difficult to predict when this new set first would be used against the hardware. Firing Room time was hard to get as everyone wanted to checkout the new LPS capabilities. Manpower was limited, at first, because the complications of an automated control system required software engineers to aid systems engineers in creating the automatic set.

Despite these complications a great deal was accomplished during this phase. The greatest 'aid' of all, the SGOS Math Model, was in the final stages of development and provided a high-fidelity simulator to respond to the application set. This high-fidelity modeling is essential to the verification of any hazardous software set. A great deal of timing problems was found simply because some commands responsed in milliseconds and others would see no appreciable change for up to one minute. Operator training became important and if a perspective operator watched the model respond incorrectly to a given situation, it would be sheer guesswork to estimate the effect of an incorrect real-time reaction. Details of the LOX model will not be discussed in this paper, but can be found in "Mathematical Models For Space Shuttle Ground Systems" by E. G. Tory.

The second major accomplishment of this phase was the establishment of software verification procedures (SVP). This was a configuration - controlled document which listed the exact steps required by an engineer to effectively test <u>every</u> line of code against the Math Model. Both NASA and contractor management could not justify the risk of leaving out unlikely branches of code from the verification, so rather than accepting an improbable failure, a 12-volume, 7,000-page set of SVPs was developed and executed. This, of course, required numerous informal runs before running the official test with the signature authorities present. To this day, maintenance of the SVP is a task equal to

the effort required to maintain the code. Many problems were found as the SVP sought to run all code over and over again in different configurations to really provide all aspects were covered.

The third major accomplishment was the development and use of simulated loadings. Over thirty simloads were performed before the first Shuttle tanking test at KSC, enough to try over 100 different hardware 'failures'. This procedure, with over twenty different operators working together in the same Firing Room configuration, using the same consoles and communications channels as a normal launch day, was also used for almost 1000 man-hours of informal engineering runs. Once again, the Math Model proved to be the tool capable of simulating realistic failures or anomalies, and then responding to the workarounds initiated by the operator. Many a vehicle was "damaged" as the simloads exercised the developing software set.

The verification process also brought some significant changes to the actual coding design. A new flag for maintenance operations was invented as a way to short-circuit control logic which was always active but was designed with a loading day configuration in mind. An emergency button was added to the PFP that could call a revert and bypass all control logic so that an operator would have total cursor control capability. A hardwire panel was added to the console to provide control in the event of a LPS failure and a hardwire recovery sequencer was coded to provide a faster recovery from such an event. Every component program was rewritten to suspend interrupt processing during 'valve in transition' when the first valve cycling test against hardware showed two interrupts for every valve indicator in motion. Measurement sampling rates were increased from 1 sample per second to 100 sps while a valve was in transition and then returned to 1 sps so that accurate data was automatically recorded.

A significant change to the control logic design had to be found when ten prerequisite sequences exceeded the size limitation of 256 bytes. The coding had already been written in the most streamlined fashion so the only alternative seemed to be a streamlining of the requirements. Deleting some requirements seemed too risky since control logic is the last line of defense and the impact to the LPS to upgrade the size limitation was severe. The solution seemed to be to find a way to consolidate a block of 'pump off' code which was common to all ten prerequisite sequences. Since subroutines were not possible in control logic, this block of code was made into a reactive control logic sequence which was always active and whose primary function was simply to set the correct state of a 'pump off' pseudo discrete flag. Now the ten prerequisite sequences only had to status the one flag thus reducing all the programs to less than 256 words. This became known as a "pseudo reactive sequence" because it issues no commands and performs no safing and, as such, is treated differently than all other reactive control logic programs.

Control logic also provided the best technique for a new vent valve cycling requirement which came into effect a few months before the first launch. Simply stated, the ullage pressure in the External Tank (ET) must be maintained above 1.7 psig when the liquid level is greater than 2%. A new set of two low pressure measurements with a range of 0-5 psig were installed on the ET along with the three original 0-30 psig high range instruments. Since this requirement applied to four different sequencers and must be active during all transitions between loading and drain phases, interrupt processing alone was determined to be risky in view of the likelihood of tank damage as a result of a pressure undershoot. So three control logic programs were created as follows: one to open the vent valve on the high limit of 8.0 psig based on any of the high range transducers, another to close the vent valve when the primary low range transducer reached 2.2 psig using the primary command, and the third to close the vent if the secondary low range transducer reached 2.0 psig using the secondary command. These trigger points were selected to allow adequate response time for the pneumatically operated vent valve (2 seconds) and the control logic sequence (50 milliseconds). This concept featured a pair of totally redundant circuits on the low side which precluded any single-point failure from threatening vehicle damage. Math model testing, SVP, and simloads were used to verify the process and the decision was made to use this technique for the first loading with no other hardware testing.

MODIFICATIONS DUE TO FIRST FIVE LAUNCHES

The LOX loading for the first space Shuttle launch on April 12, 1981 went extremely well. This turned out to be the sixth loading that would be performed using the baseline STS-1 software set as a launch scrub and two TPS tanking tests were added to the planned loadings. These loadings were far from 'automatic' though as operators learned to manually adjust their new tool to the first-time anomalies as they occurred.

The two biggest problems were two long-term control loops which had to be done manually and in parallel by the same operator. The nose cone purge was designed for a hardware controller to maintain 55 to 110 degrees in the nose cap, but failed to respond fast enough to the cooling effects of the vent valve cycling. This required the operator to manually adjust both the set point and the heater panel output temperature and to constantly monitor for further adjustments throughout the six hour

countdown. Also, the replenish control loop coded into the software failed to achieve the stabilized values which had been seen during testing at the National Space Technology Laboratories. So the same operator for the final three hours of the countdown had to manually monitor and adjust the replenish valve to maintain a steady flight mass on-board.

The other operator was constantly occupied with the steady stream of interrupts, exception monitoring and anomaly messages generated as a result of several blueline measurements being set too tight to allow momentary spikes or glitches to pass through the wary eye of the computer. Limit setting during debug and verification had not seen the kind of 'noise' and transducer inaccuracies which were within specifications and acceptable for a loading environment.

Other annoyances came from the slower than expected update rate of the displays. It took fifteen seconds for an initialization each time the operator changed pages and then ten seconds for each subsequent pass through the loop. Some measurements unexpectedly, needed to be constantly monitored such as the nose cone temperatures and the pump bearing temperatures, but were not available on the overall display. When the operator switched to a detailed area, say the storage area to check a pump reading, there was a total loss of visibility to the rest of the entire system. Application programs had no way of knowing when control logic programs had interceded, forcing the operator to presume that his invisible safeguard was in operation. Communications between LOX automatic software and Ground Launch Sequencer (GLS) automatic software were operational for a normal countdown, but incomplete as far as handling some abort and recycle conditions. Interfaces with GOX arm and ET power operators cluttered the communications net and seemed to indicate a need for greater software automation in those areas.

Most of these items were corrected by the STS-2 launch in November, 1981, however two major projects were put in motion on the second software set which would take until the last developmental flight (STS-5) to complete. Several years had passed since the original displays were built and the addition of new items late in the development left some areas terribly crowded and other areas totally blank. Display and color standards had been adopted by NASA, but had been waived to avoid impacting existing displays, so there were several obvious items of non-conformance. Update rates, limited visibility, and the status of related systems became a concern as described in the previous paragraph. All these became of more concern when the decision was made to move the GOX arm system into the LOX console and to absorb their software and displays. Clearly, a new display structure was needed. Secondly, a top level decision to remove the LOX anti-geyser line, as a weight-saving measure, created a much tighter set of temperature requirements in all phases and meant a totally new loading procedure.

Returning first to the display problems, it seemed certain that the learning experience of the first six loadings should allow the console operators to redesign the overall layout so that it could be made more compact. If this was done so as to create enough room to have a breakdown area included in a split-screen effect, then each area could be seen without loss of visibility to the overall and redundant displaying of items on more than one screen would be unnecessary. Pursuing this path soon led to a single display with three sections - the top half was the overall, the bottom right quadrant was the GOX arm system, and the bottom left quadrant was a selectable area which could show either the storage area, MLP, FSS, Power, or the new LPS status page (see Figure 8). By adding in the new color and display standards, the LOX loading displays took on an entire new look on the outside, but that did not complete the job.

On the inside, a brand new structure was required to cyclically update the selectable quadrant as a sub-level program from the overall, rather than directly from the schedular. Voting logic from each valve with multiple indicators and bypasses was streamlined to be unanimous or show an undetermined state rather than projecting a best guess to the operator. Code to determine significant change from the previous reading on analogs was dropped as bit toggling was handled by a simple formatting change. Console disk files were used as an innovative method for saving valve states while bouncing between displays. Initialized displays stayed in an undetermined state until one pass through the update loop to prevent the operator from quickly reporting an erroneous state. If several measurements could be interpreted and condensed to one signal, this was done in the software and shown on the display as one data point. New coding techniques got the loop update rate down to three seconds and initialization time down to three seconds on sub-levels, with no initialization time for the overall since it was displayed constantly. This entire project was phased in over three loadings (STS-2 to STS-4), and resulted in a total achievement of the previously mentioned objectives.

During the same loadings, the loading criteria was rewritten for Orbiter chilldown and slow fill phases. Test data from STS-1 showed sufficient cooling of the facility to allow the anti-geyser line to take away any excess heat which may cause a geyser in the 120-foot long 17" feedline during slow flowrates. But with the anti-geyser line removed for STS-5, temperatures were several degrees above saturation. At first, a 2-minute hi-speed flush of the transfer line was tried. This took enough heat out of the facility but could not relieve the latent heat of the Orbiter and engines. On the next loading, the flush was followed by a low flow load to the engine cut-off sensors (ECO) with a

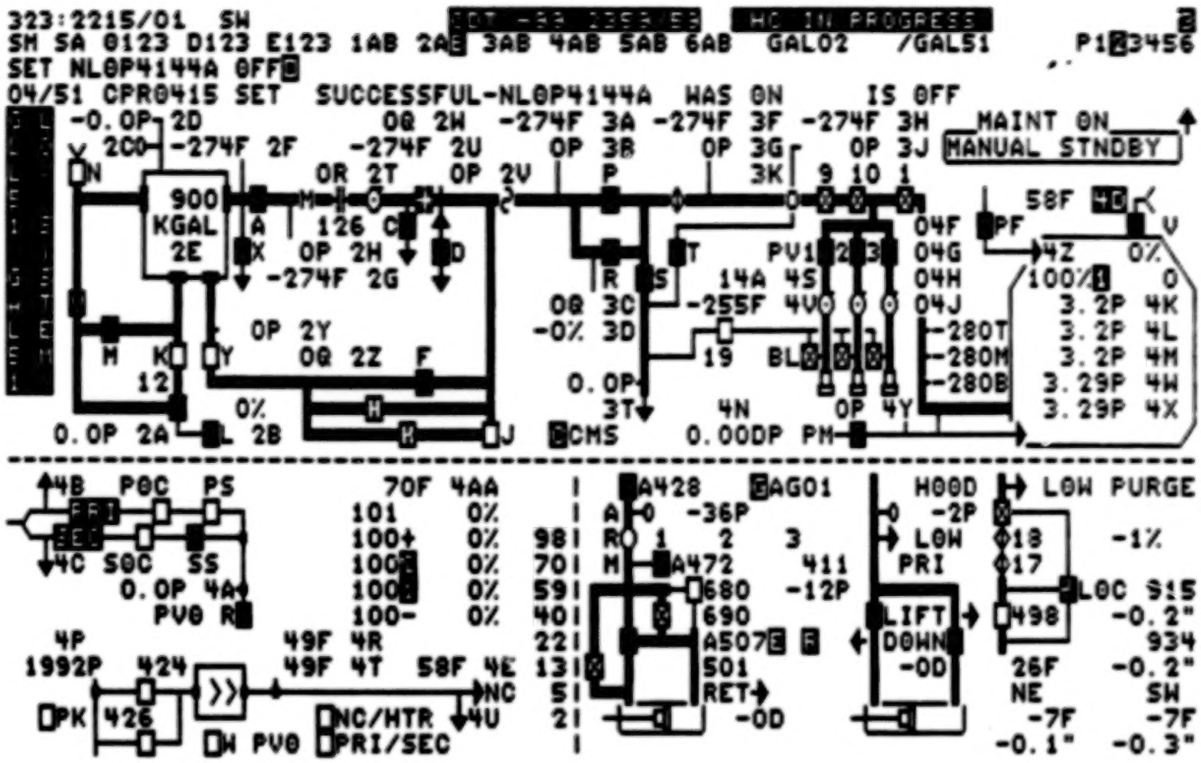


Figure 8

5-minute drain back through the engine bleeds. Each loading changed the valve actions, timers, and redlines such that the same software was never used, yet each time the automated sequencer had the flexibility to safely provide the required LOX on time to support launch for STS-5. Several modifications had to be made to the terminal count, abort and recycle operations to support the warmer LOX coming down the main feedline prior to engine start. Good planning and the conscientious efforts of the entire propulsion community, made the STS-5 tanking test and the subsequent loading for launch the first truly automatic loadings of the LOX system at KSC. All of the procedures, requirements, criteria, software, displays, and hardware modifications had come together in a way as to allow the auto fill sequencer to be initiated at T-7 hours and automatically continue through post-launch securing.

THE FUTURE OF AUTOMATIC SOFTWARE

The future of automatic software is now! Based largely on the remarkable success of the LOX and LH_2 systems, NASA and the operations contractors have formed an automation sub-panel which has established the automation goals of every console in the Firing Room. It is important to realize that while every system suffers the risk and effort that is required to leap from a cursor-controlled, manually-operated software set to a fully automated one, the LOX system must continue to improve. Software decays! It becomes outdated as the world of hardware, requirements and LPS changes around it.

For STS-6, for example, a new lightweight ET, a new Orbiter, and a new MLP meant the operation of configuration flags which a single sequencer could use so that it was capable of loading to any configuration. Representatives from Vandenberg Air Force Base are part of the automation sub-panel and, as part of developing their LOX software set, have submitted an idea for parameter-passed component programs which this author believes will save maintenance costs over the life of the Shuttle program. LPS is scheduled to provide more coding capabilities which will allow the continued development of fault isolation and correction programs. The integration console is designed for the day when a top-level manager program, communicating through linkers to all consoles, can kick-off the entire 72-hour countdown with one button.

ORIGINAL PAGE IS
OF POOR QUALITY

Other changes to software, not driven by improving automation, but by improved hardware, will be required. Already approved and in the working stages are a new chilldown sequence for STS-7, a requirement to delete vent valve cycling and maintain sub-cooled LOX for STS-8, an increase of the vent valve stroke limiter to 1.5" on STS-10, and the removal of the 2% liquid sensors on STS-13. Eventually there will be two launch pads, three MLPs, and four Orbiters being processed in parallel.

Controlling these cryogenic systems and other hazardous systems must be accomplished with automated software for the Shuttle program to meet the turnaround time objectives. Systems engineers will continue to be essential to perform the classic functions of design, test, and maintenance of the hardware and procedures, but we must also take an active part in design, test, and maintenance of our most valuable tool - the software set.

N85
16933

UNCLAS

D44 N85-16933

MATHEMATICAL MODELS FOR SPACE SHUTTLE GROUND SYSTEMS

Edward G. Tory*
Martin Marietta Corporation
Kennedy Space Center

ABSTRACT

MATH MODELS are a series of algorithms, comprised of algebraic equations and Boolean Logic. At Kennedy Space Center, math models for the Space Shuttle Systems are performed utilizing the Honeywell 66/80 digital computers, Modcomp II/45 Minicomputers and special purpose hardware simulators (Micro-Computers). The SGOS (Shuttle Ground Operations Simulator) operating system provides the language formats, subroutines, queueing schemes, execution modes and support software to write, maintain and execute the models.

Ground systems presented here consist primarily of the Liquid Oxygen (LO_2) and Liquid Hydrogen (LH_2) Cryogenic Propellant Systems, as well as LO_2 External Tank (ET) Gaseous Oxygen Vent Hood/Arm and the Vehicle Assembly Building (VAB) High Bay Cells.

The purpose of math modeling is to simulate the ground hardware systems and to provide an environment for testing in a benign mode. This capability allows the engineers to check out application software for loading and launching the vehicle, and to verify the Checkout, Control, & Monitor Subsystem (CCMS) within the Launch Processing System (LPS). It is also used to train operators and to predict system response and status in various configurations (normal operations, emergency and contingent operations), including untried configurations or those too dangerous to try under real conditions, i.e., failure modes.

INTRODUCTION

LAUNCH PROCESSING SYSTEM (LPS)

The Launch Processing System (LPS) at KSC consists of three primary subsystems: The Checkout, Control and Monitor Subsystem (CCMS), the Central Data Subsystem (CDS), and the Record and Playback Subsystem (RPS), (Figures 1 and 2).

CDS consists of four large Honeywell 66/80 Digital Computers (Systems A, B, C and D). Systems A and B are designated as Set 1 and C and D as Set 2. Set 1 and Set 2 are identical.

Within a Set the systems share mass storage and memory. The purpose of this is to facilitate switchover. Switchover is designed so the primary can switch to the secondary in case of a system failure (only during launch operations) utilizing the Real Time Data Management System (RTDMS).

Each system has dual processors and each processor can handle 1.2 million instructions per second. Each system has a mos memory of 1.5 million (36 bit) words and within a Set share an additional 1 million (36 bit) words of memory. Each set also shares 64 disk packs containing a total of over 12 billion (36 bit) words of storage.

SHUTTLE GROUND OPERATIONS SIMULATOR (SGOS)

Three operational modes exist for SGOS on CDS: (1) Real-time, (2) Remote Batch, and (3) Remote Terminal.

Real-time mode operates with any of the three Launch Control Center Firing Rooms. FR-2 is normally configured as the Ground Software Production Facility (GSPF), where model performances correspond to actual real world timing of events. It is here that GOAL Programs are de-bugged and verified, and engineering evaluation and training take place.

Remote Batch mode is initiated from a user's remote terminal. There is no interaction between the model and user once the "job" is submitted, and processing occurs at a much faster rate than real-time rate. All timing, however, is relative and kept consistent with real world activity. For example, in filling a tank with liquid in real time it may take 30 minutes, but in Batch Mode this time may be shortened to 1 minute, while preserving consistency throughout the entire model. Output from a Batch run can be printed or saved in mass storage.

(*Senior Field Engineer, MMC-KSC)

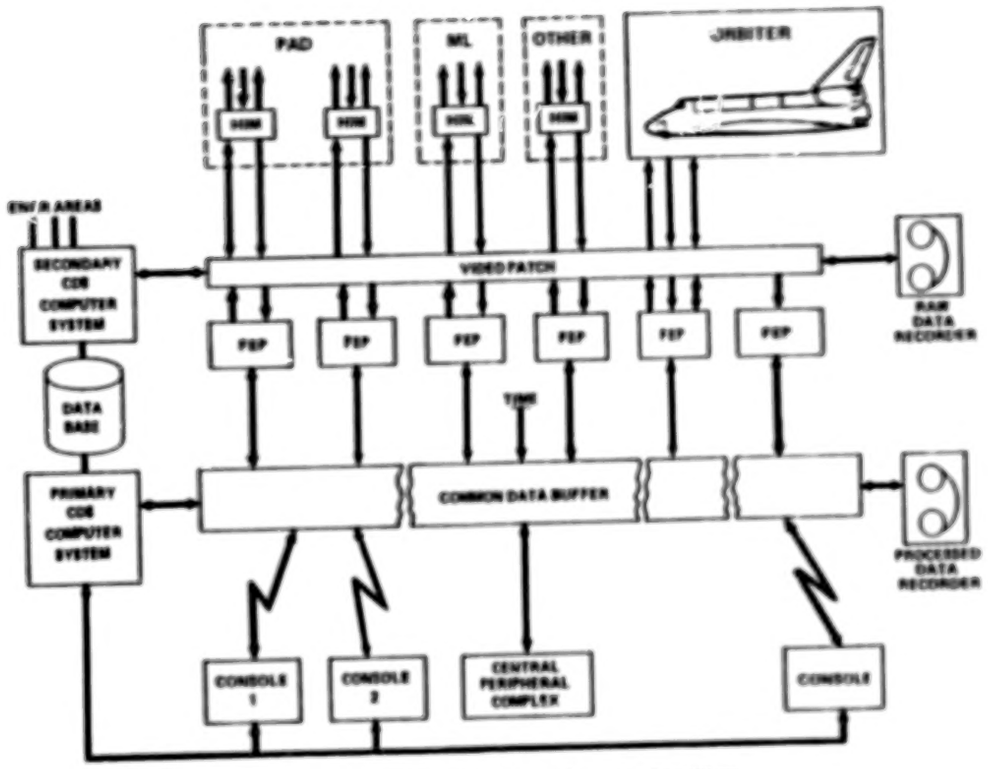


Fig 1.- Hardware relationships for LPS/CCMS.

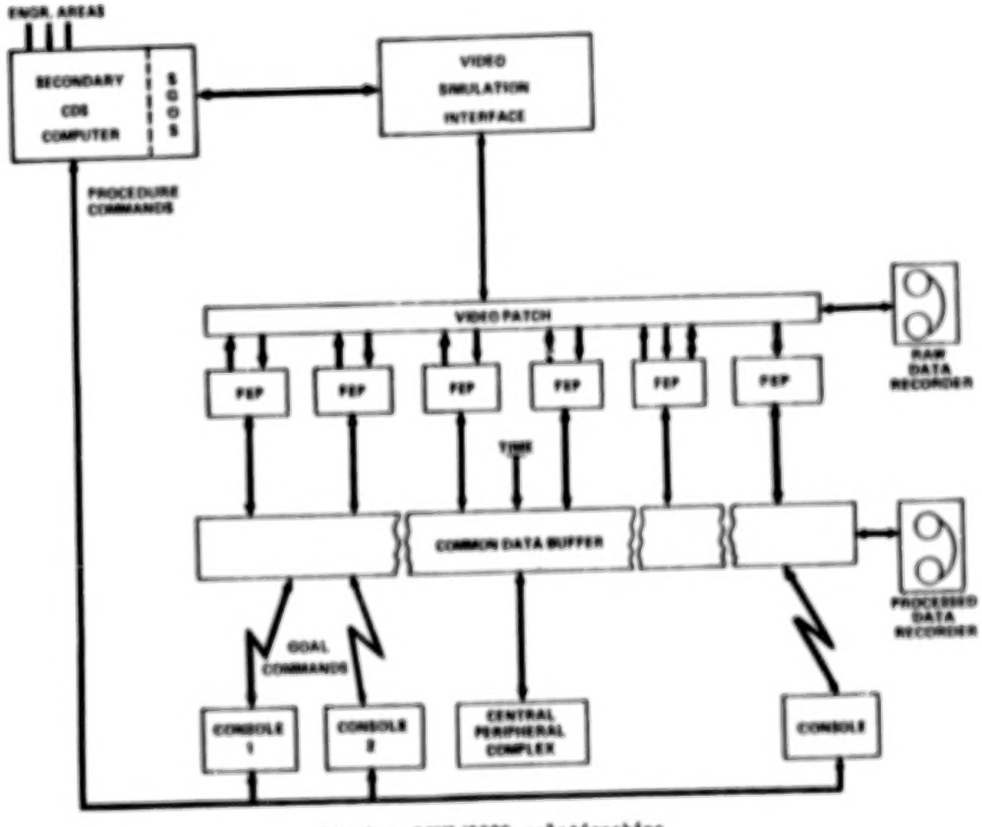


Fig 2.- CCMS/SGOS relationships.

Remote Terminal Mode (non-real time) is used for creating source files of models, procedures, and data banks. Compilation of models and procedures is done via Terminal Mode. The model can also be executed in Terminal Mode, but the output is directed back to the user's terminal, where an interactive session can occur.

Engineering Displays, Full Trace, and selected Variable Column Trace and Plotting are available in both Terminal and Batch modes.

Real-time also supports a logging capability similar in nature to the non-real time Full Trace, recording every change that occurs within the model, i.e., every calculation which produces a change in value or external stimuli which produces a change.

SYSTEMS MODELED AND PURPOSE

The types of systems involved in KSC Ground Math Models at LC39 are:

1. Cryogenic Fluid Networks (LO_2 and LH_2)
2. Electrical Power Distribution Systems
3. Mechanical Devices, GOX Vent Arm and Hood
4. Pneumatic Actuators and Gaseous Supply Pressures and Purges

Areas Modeled are:

1. Vehicle Assembly Building (High Bays)
2. Mobile Launch Platform (MLP)
3. Pad Terminal Connection Room (PTCR)
4. Launch Pad 39, Storage Areas and Burn Pond

An End-to-End Nodal Analysis is necessary for modeling the cryogenic fluid networks, therefore, the LO_2 and LH_2 External Tank and Flow Path through the Orbiter are also modeled as part of the Ground System Models.

The main purpose of the math models at KSC is the checkout and verification of the Ground Operations Aerospace Language (GOAL) programs[5] designed to automatically load and launch the Space Shuttle. The programs must control and respond to the math model exactly as they would to the real hardware.

At this point it would be helpful to discuss model fidelity. Model fidelity is the degree of accuracy and completeness with which a model simulates the real world. There are, then, two distinct model forms, namely: imitators and predictors.

An imitator is a model which is as complete as it must be, but is blind to any other conditions or anomalies. Coding in this fashion allows for computer processor efficiency, faster-running models, use of less file space, and easier maintainability. The main drawbacks are its limited scope and flexibility. An imitator is based mainly upon empirical data.

A predictor is a model which can be written using (in addition to empirical data) real physical equations relating flows, pressures, temperatures, etc. Coding in this fashion is usually more difficult, and in most cases requires more computer time. The obvious benefits are accuracy and flexibility in testing new operational techniques, and accurate predictions of system response in abnormal and failure mode configurations.

As it turns out, KSC models are a hybrid of these two forms, stressing predictive qualities in areas of fluid networks and associated calculated phenomena, and an imitative analysis in areas such as electrical power and pneumatics, where exact replication is unnecessary.

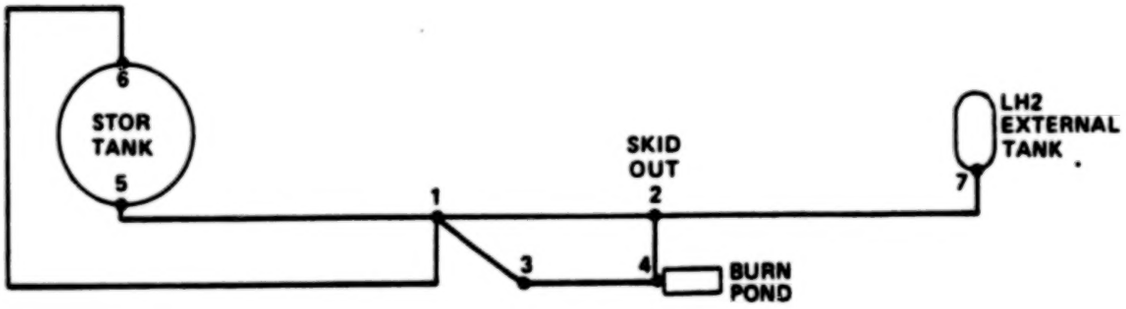
MODELING TECHNIQUES

FLUID NETWORKS

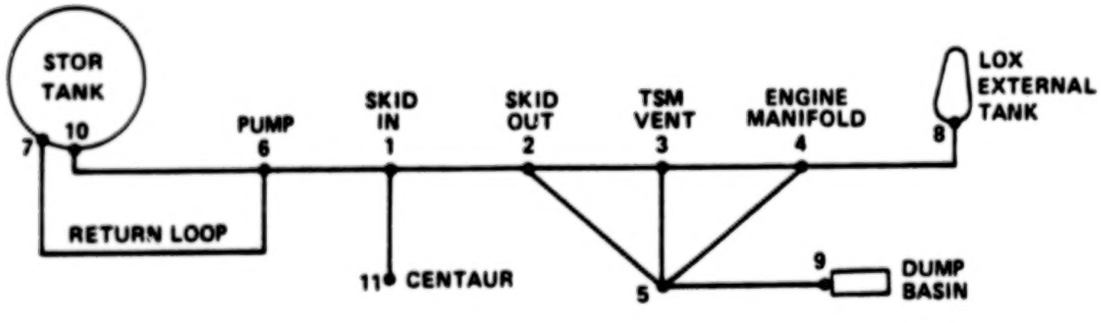
FLows and Pressures

Accurate modeling of fluid networks has proven to be essential for cryogenic propellant loading. The fluid network shown in Figure 3 is for LH_2 and LO_2. This is known as a nodal analysis, in which a node represents an exterior source or sink point, and interior points (points at which there is a fluid branch). The theory behind a nodal analysis is conservation of mass, or continuity, in which the sum of the flows into an interior node equals the sum of the flows out of that node. The boundary conditions must be known or calculated, and the internal admittance between nodes must also be known or calculated. A series of n simultaneous equations in n unknowns can be generated. The unknowns we are solving for are the pressures at the nodes. The flows are the dependent variables, and once the pressures are solved for the flows are calculated. IN SGOS, the "CALL FLOW" statement provides the format for easily setting up and solving any fluid network. Specifically, at boundaries where a source or sink exist, a pressure must be input at that node. The interior admittances, called G-numbers or Flow Constants, follow the inverse rules as electrical resistances where admittances in series sum as:

$$1/G^2_t = 1/G^2_1 + 1/G^2_2 + 1/G^2_3 \text{ --- } + 1/G^2_n$$



LH2 NODAL ANALYSIS



LO2 NODAL ANALYSIS

Fig 3.- LH2 and LO2 fluid network nodal analysis.

and admittances in parallel sum as:

$$G_t = G_1 + G_2 + G_3 + \text{---} G_n.$$

However, the larger the value of the G-Number, the greater the flow. The flow constant was initially based on historical data and design information. It is simply a constant that is a function of the C_v of the valve, the density of the fluid flowing through it and admittance of the plumbing between nodes. Originally the solution for flows and pressures was obtained by using an iterative calculation similar in nature to the Runge-Kutta method. First a nodal analysis of the network is drawn, then the pressures at the ends or boundaries are calculated. The G-numbers are calculated along with the head pressures between the internal nodes. Once all the known quantities are computed, the flow rates are calculated using the flow equation:

$$Q = G\sqrt{P_2 - P_1 - HP_{21}}$$

where Q = Flow rate in gal/min
G = Flow constant
P_2 = Upstream pressure
P_1 = Downstream pressure
HP_{21} = Head pressure between P_2 and P_1

The flows are iterated to increment the pressures to that the sum of the flows into each interior node equals the sum of the flows out. This method used enormous amounts of CPU time and the accuracy was very limited.

SGOS developed the "Call Flow" routine in the Spring of 1981. This new method of computing flows and pressures used the same basic flow equation and nodal analysis as before as well as the Law of Conservation of Mass.

Given boundary conditions of known pressures, and interior G's and head pressures, solve (iterate) for the pressures at the interior nodes first and then compute the flows. The method of computing these interior pressures uses a piecewise linear approximation for the vector square root function. Convergence is achieved in one (50 millisecond) model cycle as opposed to hundreds of cycles before which at best only approached convergence.

The Flow Solver is processed in the SGOS executive, and is done with maximum efficiency, rather than having all the calculations performed in the model itself. The ease of formatting the fluid network and the reliable accuracy the flow solver achieves, has made true predictors out of the LO_2 and LH_2 models.

During actual vehicle loadings, Flows, and Pressures were recorded. This data was used to recompute more accurate flow constants, which then reflected all the dynamics in the system. Typical items that contribute to the flow constant between two nodes are: valves, orifices, pipes and plumbing, filters, and the fluid medium itself (viscosity/density). One additional consideration, vitally important, to be calculated and input to the fluid network calculation is the fluid head pressure.

Head Pressure in the format for the "CALL FLOW" is input as a negative number when computing Flow from a lower elevation to a higher elevation. Knowledge of the system in terms of elevations of various nodes must be known, as well as the volume of liquid contained in various segments of pipe between nodes. This is necessary when filling or draining segments of pipe to allow realistic head pressure rise rates as the pipe fills up. When flowing "downhill" head pressure is added to the nodal pressure, and will increase the flow rate. When flowing "uphill" the head pressure is added to the nodal pressure and is used to reduce the flow rate.

There are several limitations to the SGOS CALL FLOW statement which can be treated "outside" of the general matrix of simultaneous equations. These limitations are: fluid inertia, water hammer, non-continuous fluid networks (as when a segment of the network is drained), isolated interior networks, check valves and one-way flow, and pumps between interior nodes. Detailed discussion of these items is outside the scope of this paper; however, these problems have been overcome in the cryogenic models.

Volumes

Volumes of tanks, canisters, and pipes are needed in order to provide a realistic and accurate model. The volume of liquid in a tank at a source or sink node is computed by integrating, using a time constant, the net volume that exists in the tank - beginning with its initial volume and incrementing by adding or subtracting the flow rate from that node. The SGOS "CALL INTGRL" statement is very useful for this purpose. "CALL INTGRL" provides the format where an integrand can be summed to at a fixed but selectable rate of from 10 times per second to once every 10 seconds. A one second update is normally used, but a number of special cases need faster or slower iteration rates.

Volumes of pipes between nodes can be computed based on segment length and diameter, that fill and drain based on flow rates. Imaginary or pseudo wet/dry liquid sensors at each node triggers the calculations.

Temperatures

In most instances, temperature dynamics is done mostly for display purposes. A stagnant or empty segment of the fluid network will start off at an ambient temperature of 73^{0} F. As cryogenic fluid enters a segment of the network, rapid boiling occurs and gaseous propellants will move downstream, causing a pre-chilldown. At this point, we start calculating temperatures colder until actual liquid (based on tests) would reach the location of a temperature probe. When the liquid volume reaches a probe, the temperature is assumed to be that of LO_2 or LH_2 at the Boiling Point. Very little change in temperature will occur thereafter. When the line is drained, the temperature will begin to rise. This rate may be rapid, unless the line is vacuum-jacketed.

One notable exception where temperature fluctuations are pronounced, dynamic and critical is the feedline temperature in the LO_2 system, which forewarns a geyser condition if redline criteria are exceeded. Due to head pressure in the feedline, this creates a very dynamic temperature profile during loading.

ELECTRICAL SYSTEMS

Power supplies are usually modeled in discrete terms. Power is either on or off, and sub-busses automatically receive power when the supply is turned on. Fuses are not modeled, but, in certain instances, circuit breakers are. Voltages and currents are assigned as constants based upon hardware data. These systems are handled rather simply, with very little dynamics involved. Every Function Designator will have a power bus assigned to it, and when the power is off that "FD" will read its powered-off value. Back-up batteries are also modeled, along with a limited amount of dynamics involved with threshold Zener Diode Systems.

PNEUMATIC, GASEOUS SUPPLIES AND PURGE SYSTEMS

Gaseous supplies are treated as inexhaustable reservoirs which supply GN_2 or Helium. Generally, these supplies are for purge systems and pneumatically actuated values. Modeling of these systems typically uses discrete logic, depending upon whether supply valves are open or closed. Dynamics are involved when a regulator is modeled using the line pressure as a feedback to the regulator to provide more or less regulator opening. Another case involving dynamics is when a purge flows through a heater where heater temperature is a function of a cool purge flowing through it. All pneumatic values are modeled to require a specified minimum supply pressure to operate. Helium bubbling in the LO_2 feedline is modeled to provide a realistic temperature gradient profile. This will influence the head pressure in the feedline.

It is noteworthy to mention that for the LH_2 system, helium is always used when cryogenic hydrogen may be present, due to the fact that the boiling point of helium is lower than that of LH_2. If GN_2 were used in contact with LH_2, the nitrogen would form GN_2 ice. In the LO_2 system both GN_2 and Helium can be used since GN_2 stays gaseous at liquid oxygen temperatures. For economy, GN_2 is generally used with LO_2.

MECHANICAL SYSTEMS

The ET GO_2 Vent system consists of a heated purge and a hinged cantilevered truss assembly supporting a conical shaped plenum chamber (which also is hinged). It is moved to a docking position with the ET nose cone to provide an environment for warming the nose cone while venting GO_2, which prevents ice build-up on the ET. The simultaneous motions of the arm and hood, primary and secondary drives, presented an interesting challenge in designing the math model.

MODEL DEVELOPMENT

DATA COLLECTION: FEEDBACK TO MODEL THROUGH STS-1

Sources for model data include:

1. The original schematics and specifications

2. Discussions with engineers about operating parameters

3. Consulting with vendors on specific hardware items, and actual test data during system operation. After a hardware test (such as a tank loading) or an actual launch, a quantitative analysis is done on the data collected, and is compared to model output. From this analysis we can provide accurate empirical data and write more comprehensive equations for further model development. When new operating techniques are employed during a simulated loading, model predictions can also be verified by test data later.

ADVANCED DEVELOPMENT: STS-2 THROUGH STS-5

Advanced development has included continual feedback from hardware testing and launch data. Hardware modifications have also been fairly regular throughout each flight, and model dynamics have been heavily impacted. A "New Standards and Guidelines for Math Models" (KSC-80K00009) has instituted numerous convention and fidelity conformities. This was necessary in order to coordinate and make common, models written by all KSC and Vandenberg Air Force Base contractors. This has also specified the identification of all Ground and Vehicle interfaces, and all system interfaces to be recorded in the "Math Model Interface Definition Document" (MMIDD).

FUTURE DEVELOPMENT: STS-6 AND BEYOND

Model enhancements will dominate this effort, along with sustaining engineering for hardware modification. The most significant hardware change was the development of the Martin Marietta Light Weight External Tank. STS-6 was launched April 4, 1983, with the first lightweight tank. At the time of this writing, STS-7 is scheduled for launch in mid-June and will have successfully completed its mission a week before this conference.

Future plans include the installation of a Centaur stage in the Orbiter cargo bay, which will be fueled with LO_2 and LH_2 simultaneously with the External Tank. This will present a new challenge for modeling as the LO_2 and LH_2 fluid networks will be modified to accommodate this space vehicle. At present, the first Centaur launch, STS-38, is scheduled for May, 1986.

Study plans are under way at Martin Marietta for Shuttle derived vehicles, Advanced Space Transportation System (ASTS), which include an aft cargo carrier (ACC) or shroud on the External Tank, with a cargo carrying volume greater than that of the Orbiter Cargo Bay.

Launch Complex 39B should be in operation by January 1, 1986, and the first launch will be STS-36, in February, 1986. Pad-A & B at KSC will be very similar, requiring only slight model changes. Mobile Launch Platforms (MLP) 1 and 2 are in use now with some hardware differences, and MLP-3 is being processed at this time.

Vandenberg models were patterned after KSC models, with some hardware differences inherent to VAFB. Their first launch (1V) is scheduled for October, 1985. Plans are for KSC to operate with OV99, OV102 and OV104 and VAFB to operate with OV103.

The next major event for math models at KSC will be in June, 1983, with the implementation of the expanded model capability project also known as BIG SIM. Currently, the largest master model which can be built is approximately 227K words. It may be possible that BIG SIM will expand that size 2 or 3 times. This new capability will allow for an integrated test of a launch countdown model with all consoles supporting. Also this will greatly increase GSPF support time by allowing more users to operate the model simultaneously (restricted only by the processor's capability). This will greatly reduce the GSPF's down time, because at present each of several smaller master models must be loaded, which can take several hours, during which time there is no model support. Once a large 700K master model is loaded and running, it can support continuously, with changes necessary only to update the master model. Changes will not be necessary for scheduling purposes.

With the large master models it will be necessary to streamline all existing models, to write more efficient code, and to understand how model segments are ranked, queued and executed. Caution should be exercised in attempting to make a model segment run faster, while at the same time, not adding more of a burden to the model executive processing.

CONCLUSION

Math modeling presents a unique opportunity to intimately blend engineering/hardware knowledge with computer technology. Since a model must perform identically as the hardware, a very broad knowledge is gained by the modeler in both the hardware and the software. Within the environment of operations and maintenance, this author has found model research and development to be challenging and satisfying.

In closing, I would like to quote from Kenneth P. Timmons, Michoud Division Vice President and General Manager, at an address to 300 members of the Louisiana Tech University Engineers Association in Ruston, Louisiana, March, 1983:

[3]"In your generation, which saw polio conquered and man landing on the Moon, I believe the greatest advance is the ability to model events, states and phenomena and to process these models in small fractions of seconds in large capacity computers.

Engineers have contributed to these achievements and will continue to make us part of the technological triumphs - such as the Space Shuttle - today."

REFERENCES

1. Manual — Shuttle Ground Operations Simulator User's Reference Manual, KSC-LPS-UM073, February, 1983
2. Manual — LPS User's Manual, Volume II: Hardware, KSC-LPS-OP-033-2, Revision F
3. Periodical — Mission Success Bulletin, April, 1983, Volume 2, No. 3, MMC, Michoud
4. Tech Notes — Dr. Dick Ingle (CSC & West Georgia College) to SGOS Math Model Team, KSC
5. Tech Report — Rudolph, James W.: Automatic Software for Controlling Cryogenic Systems, JSC Conference June 28-30, 1983

N85
16934

UNCLAS

D45

N85-16934

MANAGING COMPUTER - CONTROLLED OPERATIONS

John B. Plowden*
Shuttle Launch Operations Division
Rockwell International
Kennedy Space Center, Florida

ABSTRACT

A detailed discussion of Launch Processing System (LPS) Ground Software Production is presented to establish the interrelationships of Firing Room resource utilization, configuration control, System Build operations, and Shuttle Data Bank management.

The production of a Test Configuration Identifier (TCID), will be traced from requirement generation to program development, Data Bank update, GOAL program debug and verification to release thru Configuration Management for use in processing flight hardware.

The challenge of the Operational Era will be to implement fully automated utilities to interface with a CDS resident System Build Requirements Document to eliminate all manual intervention in the System Build operations. Automatic update/processing of Shuttle Data Tapes will enhance operations during multi-flow processing.

INTRODUCTION

Ground Software Production for processing and Launch of the Shuttle Vehicle begins with the generation of requirements for a specific mission. The changes that effect ground software can be a hardware modification, flight software modification, measurement change, or a checkout requirements change.

Requirements are processed through the Configuration Control Board where impacts are determined to effect OMI's, application software, etc. Based on approval, updates to the effected elements are scheduled. Automated tracking systems are maintained to provide visibility of open work items to support software planning, scheduling, and engineering open item reviews.

These automated tracking systems are the cornerstone of an automated Configuration Management (CM) system that efficiently tracks software requirements from identification through completion. The CM system deletes manual intervention by interfacing directly with the System Build process. The software selects the approved programs and console locations based on Vehicle (099, 102, 103), Site (OPF, VAB, PAD) and Facility (MLP1, MLP2, HB1). Additionally the CM system generates a computer maintained work authorizing document for Firing Room verification supporting real-time Quality Assurance buy-off, automated library updates and Release Notice generation.

The System Build operation utilizes the TCID in the compilation and translation of all application software elements into a controlled application library resident on the Central Data Subsystem (CDS). The following elements are included in a TCID: (1) Flight Format Files (defines valid Pulse Code Modulation formats), (2) Function Designator Directory (FDD) Build (selects from CCMS on-line data bank), (3) Front End Processor Table Build (constructs tables from FDD and Flight Format File data describing FEP data processing), (4) Application Software Configuration (selects application software from the library, updates interpretative code from the FDD, resolves and links all external references), (5) Installation (collects all TCID elements, formats data for CCMS and write data to CDS tapes for tape to disk generation in CCMS or real time CDS to CCMS data transfer) (50KBS).

A Master Math Model Build is also performed to provide simulation capability in the debug and verification process. The Master Model Build selects system models from the model library and creates simulation tables from the FDD. These models interface with CDS resident simulation software for ground software development activities.

The Software debug and verification process is performed in the Ground Software Production Facility (Firing Room 2). Firing Room 2 can be divided into three sets so that multiple TCIDs can be processed concurrently. The three sets are flexible in configuration to allow a various number of Consoles and Front End Processors to be used. System configuration ties the Firing Room sets to simulation models residing in the CDS computers via Video Simulation Interfaces.

Following software verification, Software Assurance and Configuration Management provides quality control verification and assures compliance with all effective approved engineering requirements.

*Manager, Ground Software/LPS Operations, RI-KSC

Additionally, this function provides verification of all open items and the generation of Release Notices reflecting the configuration of application software packages prior to the package being used for hardware processing.

SYSTEM BUILD OPERATIONS

The System Build function is the compilation and translation of all application software elements into a controlled applications library resident on CDS. An Applications TCID can be divided into the following categories to support testing and Vehicle processing: (1) Support Equipment Site Activation and Revalidation, (2) STS Element Test, i.e., Orbiter, SRB, ET, Cargo, (3) STS Integrated Processing.

Ground software types included in a peculiar TCID include: (1) (GOAL) Ground Operations Aerospace Language programs, (2) Control Logic sequences, prerequisite and reactive, (3) Display Skeletons, and (4) Test Control Supervisor sequences.

Management of the System Build process is controlled by the System Build Manager (SBM). The System Build Manager is a controlled, interactive, real-time software tool for initiating and executing all TCID build functions. The SBM software was generated to remove manual intervention in the build process, to avoid mistakes and to create a repetitive process. The SBM software assures that (1) The build function being initiated is authorized, (2) Only approved application program revisions are included in the build, (3) Application software compiler release effectivity is correct and (4) Application software console assignments are made. The SBM generates a log for historical record data for inclusion into the Software Release Notice.

The System Build process is controlled by Operating Maintenance Instruction (OMI) V9025. This OMI is broken up into Mini OMI's for individual repetitive execution of standalone tasks. It defines Software Assurance check points and minimizes the opportunity for human error.

This System Build process is depicted in Figure 1.

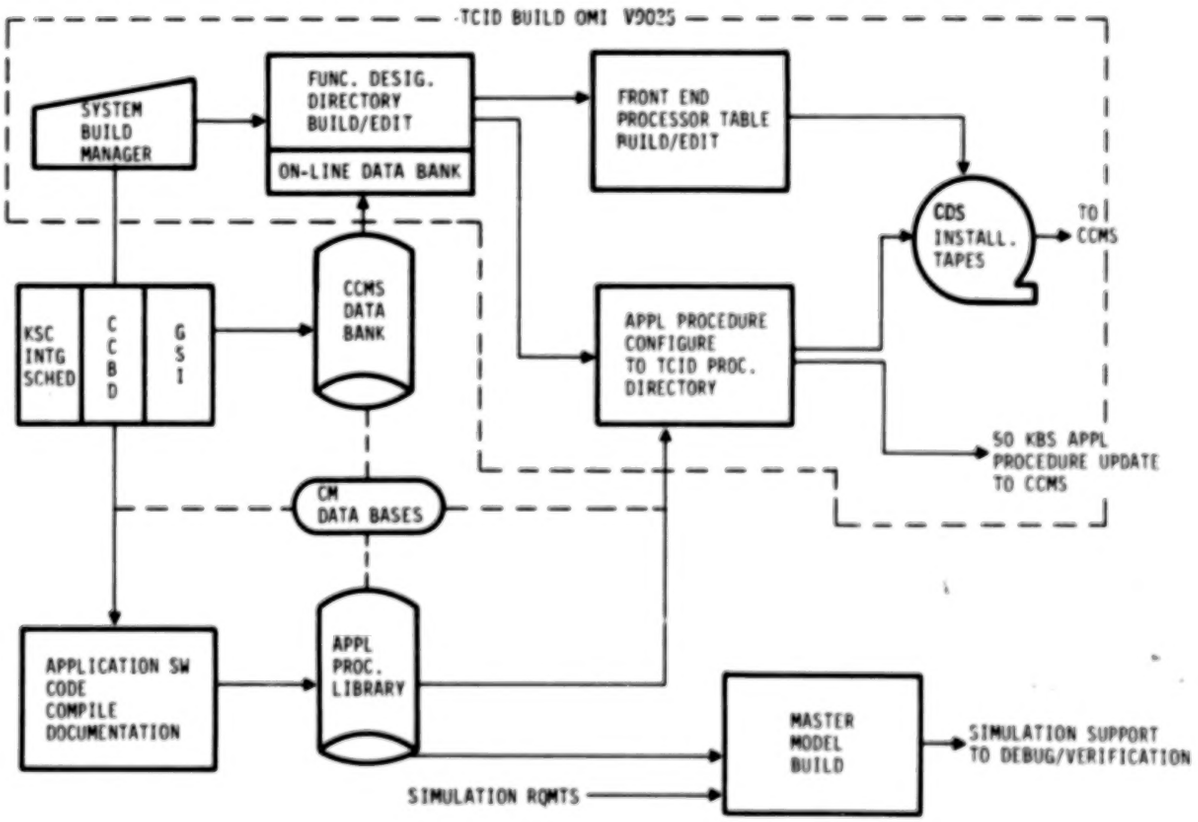


Figure 1.- System build.

To meet the challenge of the Operational Era, software development techniques are evolving to allow more automated utilities to control the System Build function to eliminate errors and provide software for multi-flow operations.

A "System Build Requirements Document" concept is presently in development. This document will contain a complete set of hardware and software policies, responsibilities, configuration and interfaces as well as any unique support requirements for each Checkout Control and Monitor Subsystem (CCMS) set.

The System Build Requirements Documert will consist of the CCMS data which will control the LPS System Build process. The software configuration (Function Designator Directory Build requirements, table build requirements and application software) and interfaces will be stored on CDS for an Automated TCID Build Process.

Automated utilities will be developed to be initiated by the operator for access to the System Build Requirements Document on CDS to produce a Function Designator Directory Build input deck, a table build input deck and a baseline of application programs to support that TCID.

The intent is to use the System Build Requirements Document to control the LPS System Build process from start to finish by utilizing this Document as well as Automated Software Utilities to fully implement an approved set of requirements. This concept is depicted in Figure 2.

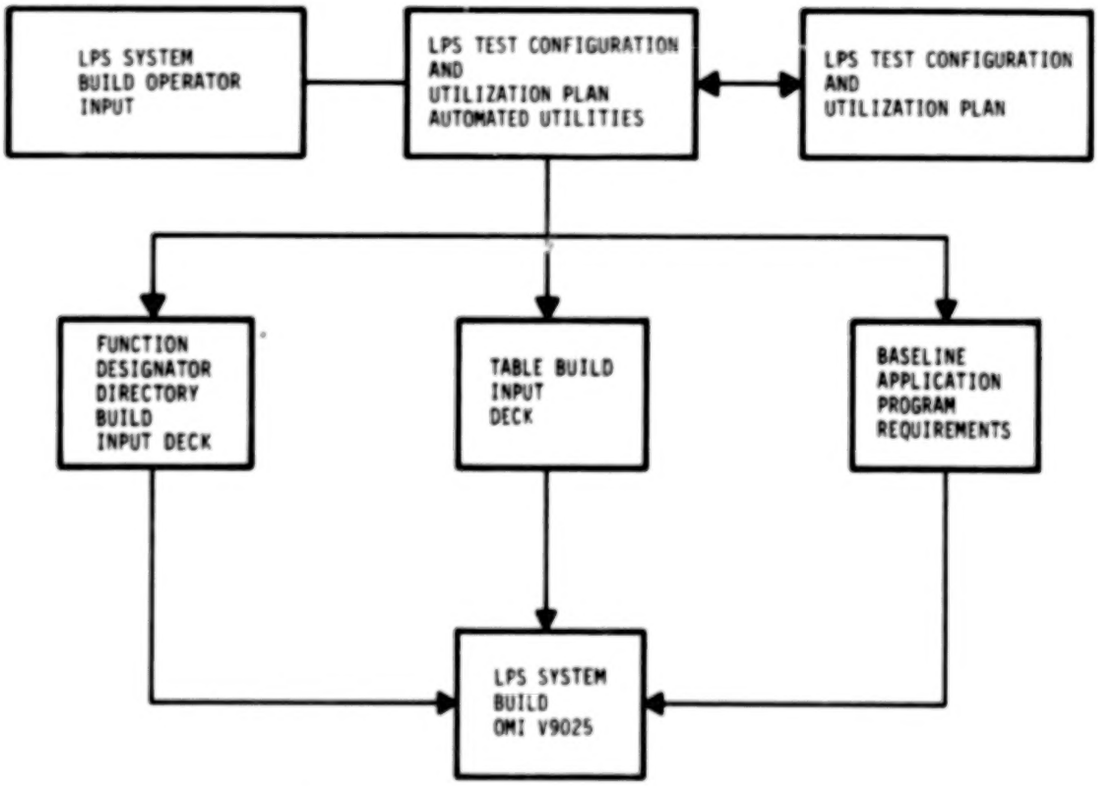


Figure 2.- System build requirement document.

SHUTTLE DATA BANK MANAGEMENT

The Shuttle (CCMS) Data Bank is a large, structured, disk file residing in the Central Data Subsystem. The Data Bank contains all the information on measurements, stimuli, and system parameters needed for the operation of CCMS support software. Among other data, the CCMS Data Bank contains function designator data for each measurement and stimulus of the Shuttle Vehicle. The function designator data consists of the Measurement/Stimulus Identification (MSID) number, name, range, dimensional units and other such characteristics.

The CCMS Data Bank is maintained in three sections on a common disk including a section for Space Shuttle Vehicle (SSV), for Ground Support Equipment (GSE), and one for Cargo/Payloads. KSC is the design agency for the GSE section. JSC, MSFC and Rockwell/Downey are responsible for SSV and Cargo/Payloads.

The use of function designators (FD) is a fundamental GOAL concept that allows/requires the GOAL Programmer to specifically designate the function and destination of external references. Approximately 50,000 FD's reside in the CCMS Data Bank, broken down as follows: (1) Orbiter - 24,000, (2) SSME - 1400, (3) ET - 500, (4) SRB - 1100, and (5) GSE - 23,000. Each FD requires approximately 55 pertinent pieces of technical data for a total of 2.7 million data elements for a single mission.

A Shuttle Data Tape (SDT) supplies the measurement/stimulus data from the design agencies to the LPS for the generation of CCMS Data Bank field data.

The Shuttle Data Tape Processor is a unique software component that forms the repository of Shuttle information required in the CCMS Data Bank under control of the CDS Operating System.

From the raw SDT, the Processor generates a file of card-image updates for the Shuttle associated function designator in the CCMS Data Bank. This update file, along with other required data, will be used to update the CCMS Data Bank. Typical flow of SDT to Data Bank updating process is shown in Figure 3.

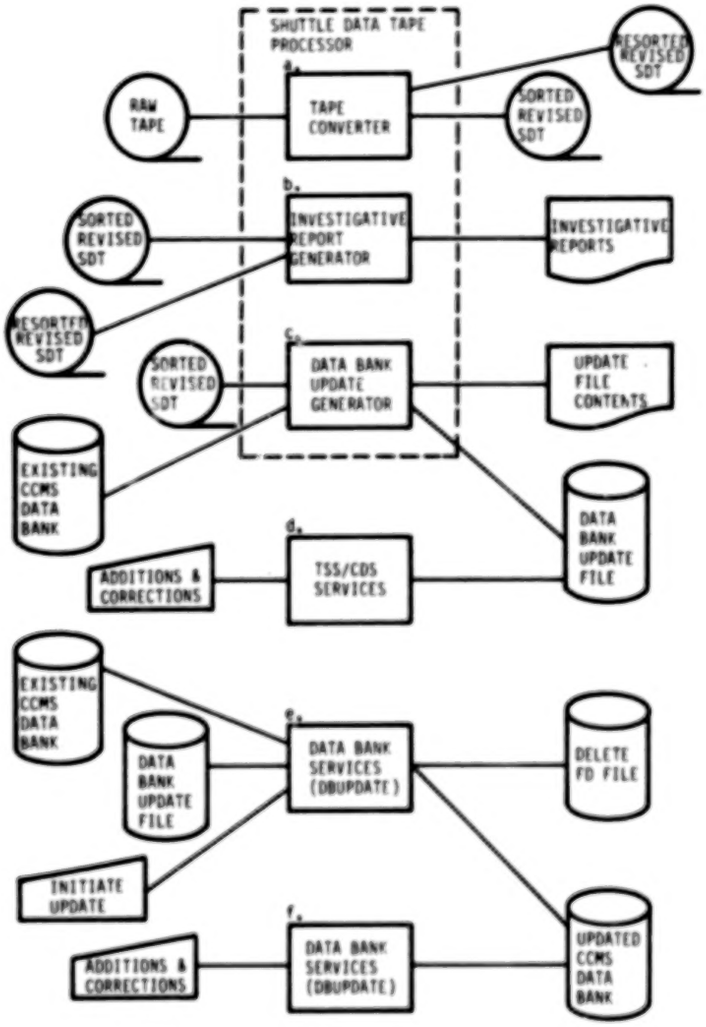


Figure 3.- Typical SDT-to-DB updating process.

Data Bank Services functions are utilized to add, modify, delete, copy transfer, and receive the various types of records in the Data Bank. The Data Bank Update Generator portion of the SDT Processor builds compiler and hardware records according to data link, data type and on-board sources and destination. These records are compared to current records in the Data Bank. Following these comparisons, the Data Bank Generator provides update data for the Data Bank reflecting new or modified data fields from the SDT. Data Bank update change approval flow is shown in Figure 4.

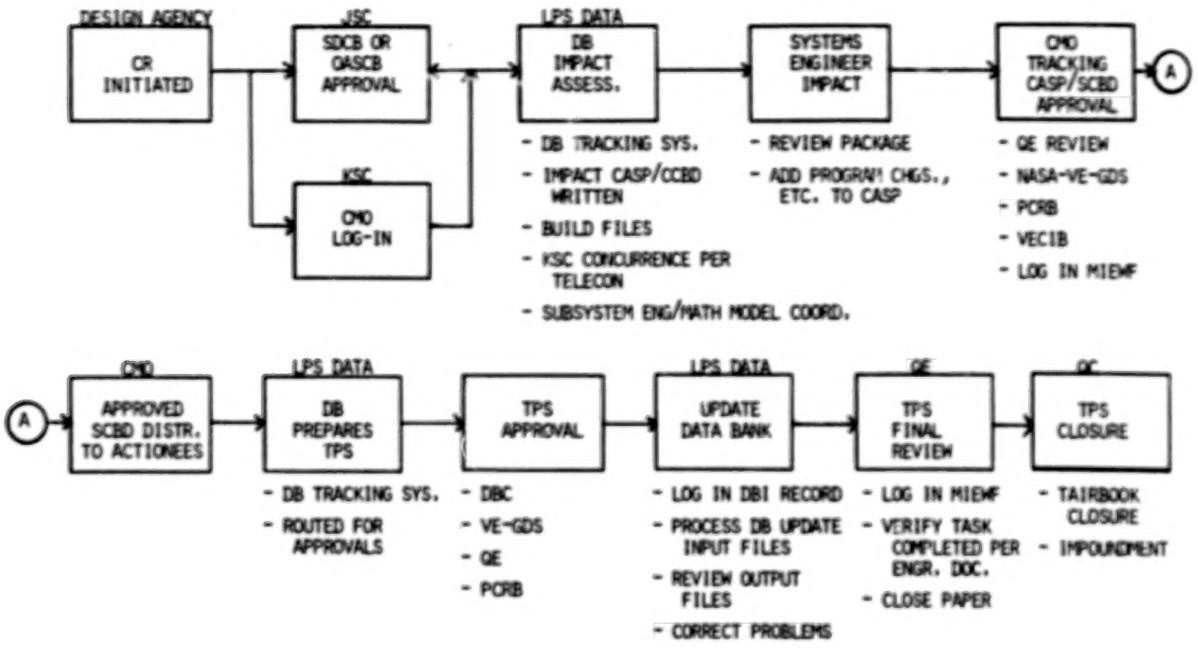


Figure 4.- CCMS data bank update.

FIRING ROOM UTILIZATION

To meet the challenge of the Operational Era, efficient utilization of Firing Room resources will be mandatory to manage multi-flow schedules. Presently, three Firing Rooms are available at KSC for Vehicle processing and software development activities. Firing Room 4 is presently under construction.

Firing Room 2 at KSC has been designated as the Ground Software Production Facility (GSPF). The GSPF has been divided into three sets for maximum resource utilization and allowing multiple software TCIDs to be processed concurrently. Reference Figure 5 for Software Development Configuration.

The three sets are very flexible in order to allow a varying number of Consoles and Front End Processors to be used. The configuration ties the Firing Room sets to simulation models residing in the CDS computers via "Video Simulation" interfaces. Software is executed from the consoles with responses from the system models in the debug/verification process. The system models are controlled from a console in the CDS set. Verification of application programs are performed per approved Software Verification Procedures (SVP's).

Software planning and resource utilization control is managed by software planning and utilization scheduling. The Software Integrated Support Schedule is updated weekly and shows the complete software development cycle from Data Bank, System Build, debug, verification and release to hardware testing.

The STS/Payload 72 Hr/11 Day Operations Integration Schedule is updated via daily meetings to reflect the Day to Day schedule and set utilization. The Software Test Conductor who coordinates the GSPF activity has the authority to make real time schedule adjustments to meet changing real time requirements.

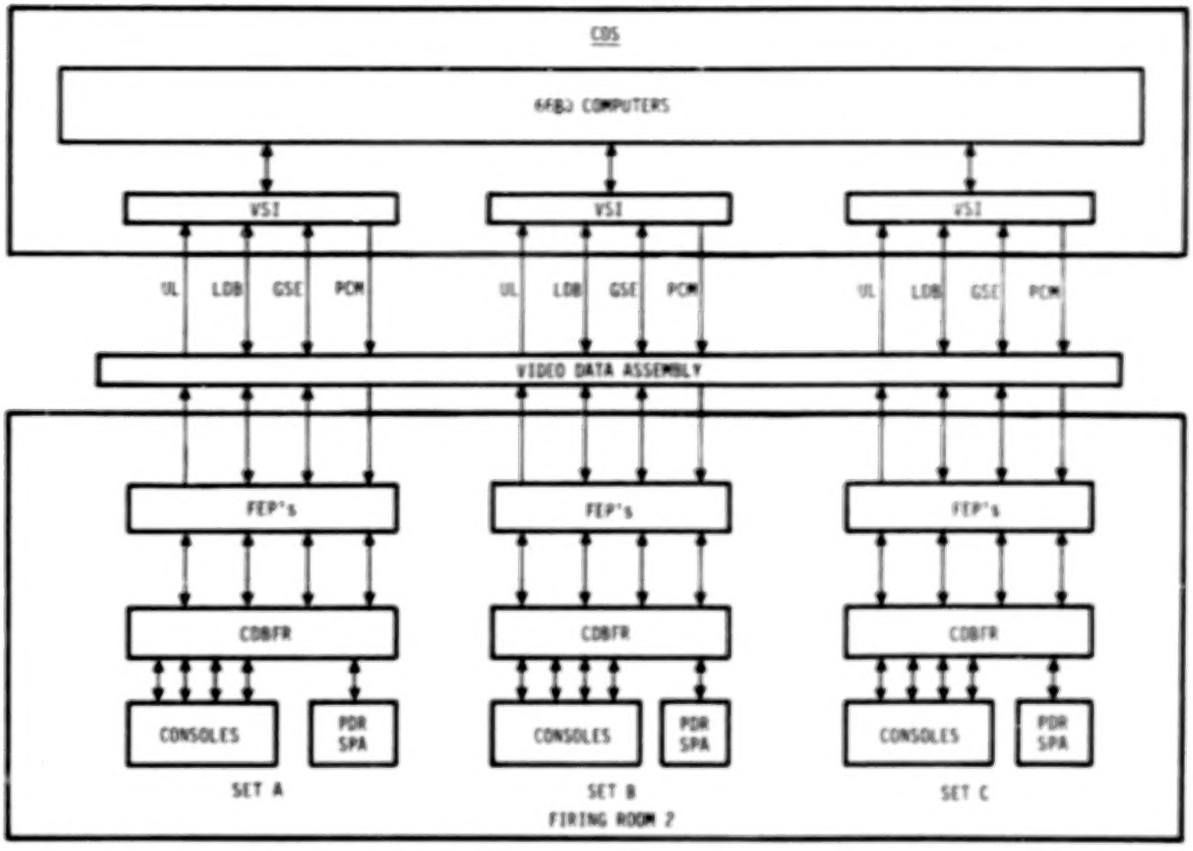


Figure 5.- Software development configuration.

The Software Development/Release process through the Ground Software Production Facility is shown in Figure 6.

Change control, use of automated utilities and configuration management are essential keys to efficient software production operations to meet the challenges of the Operations Era.

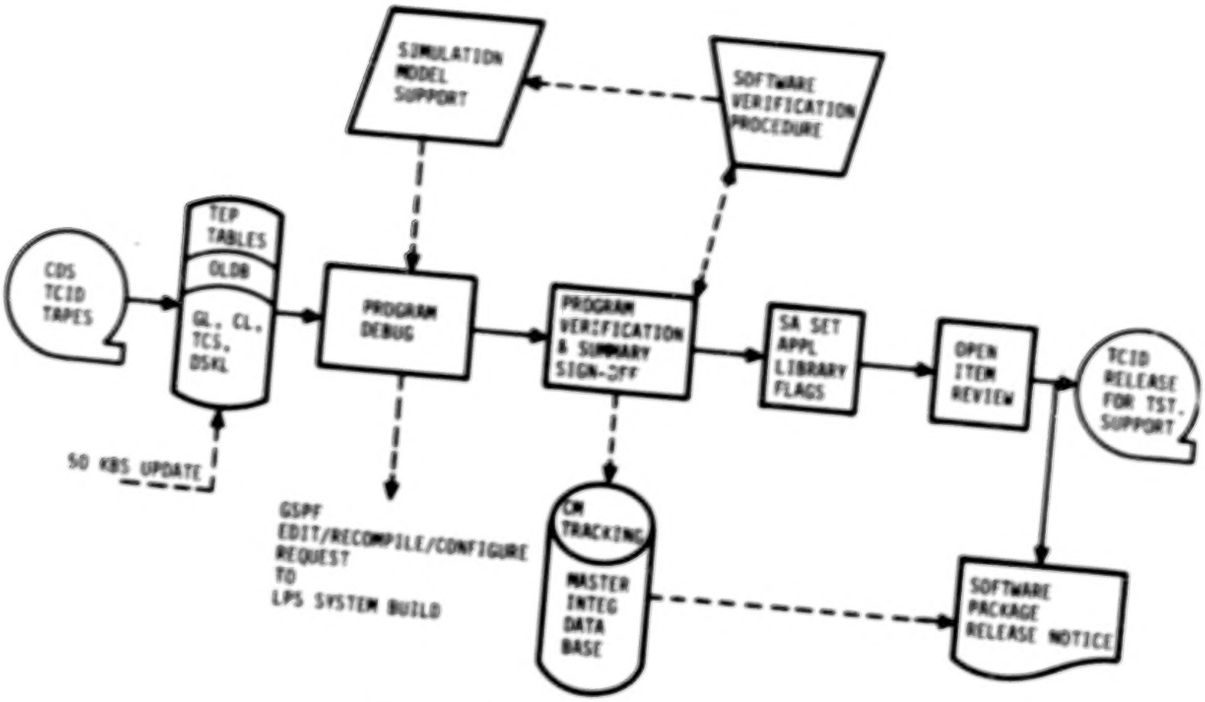


Figure 6.- S/W development/release.

N85
16935

UNCLAS

N85-16935 D46

SUPPORT SYSTEMS DESIGN AND ANALYSIS

Robert M. Ferguson*
DL-NED-2
NASA, Kennedy Space Center

ABSTRACT

The integration of KSC ground support systems with the new Launch Processing System and new Launch Vehicle provided KSC with a unique challenge in system design and analysis for STS. Approximately 70 support systems were to be controlled and monitored by the Launch Processing System. Typical systems are Main Propulsion Oxygen and Hydrogen loading systems, Environmental Control Life Support system, Hydraulics, etc. An "End-to-End" concept of documentation and analysis was chosen and applied to these systems.

Unique problems were resolved in the areas of software analysis, safing under emergency conditions, sampling rates, and control loop analysis. New methods of performing "End-to-End" reliability analyses were implemented. This paper discusses the systems design approach selected and the resolution of major problem areas.

KSC SYSTEMS PROBLEM IN SHUTTLE ACTIVATION

The integration of ground support systems with the new sophisticated Launch Processing System (LPS) presented KSC with a unique challenge in system design and analysis for STS.

It was the intent that the LPS would be used to control and monitor approximately 70 support systems. An applications software set would be developed for each system. Examples of these systems are: Fuel Cell Servicing System, Hypergol Loading System, Main Propulsion Oxygen and Hydrogen Loading systems, Environmental Control System, Orbiter/SRB (Solid Rocket Booster) Hydraulics, Environmental Control Life Support, etc. The challenge was to develop methods to document, define software requirements, and assure a "fail safe" design for these systems.

A system usually consists of many components which have been designed by KSC and other NASA Centers. A multitude of different design disciplines are involved. (See Figure 1). There existed a need to tie these diverse elements together in a systematic manner to define an end-to-end system.

THE SYSTEM DESIGN APPROACH SELECTED

In reviewing existing KSC design, documentation and reliability analysis procedures at the time, it became apparent that new and innovative approaches were needed to design, document and analyze software controlled systems. The system design approach was to bring together some quality engineering talent who were familiar with total system requirements and assign them the job to integrate fluids, electrical, LPS, controls, and sensor designs into an end-to-end system design. The design process selected is shown in Figure 2. Some of the unique elements in this process are the SMS/EMCD (System Mechanical Schematic/Electro-Mechanical Control Diagram), and the Operating Criteria. The SMS/EMCD (see Figure 3) was developed as a new drawing to aid designers, operators, and application software programmers, to understand a system end-to-end. The SMS/EMCD depicted a system from the GSE thru the Orbiter/SRB/ET (External Tank) showing those elements on board the vehicle that function as part of Ground System Operation. In addition, the SMS/EMCD showed all commands and monitors with their function designators to aid the system software programmers. The Operating Criteria explains the step by step operation of a system; for instance, in Main Propulsion Lox, these are such things as set-ups, chill down, slow fill, fast fill, topping, and replenish. This document had been used previously by KSC, but it was expanded to provide additional information for the software programmer. As an example, a section was added to satisfy control logic software interlocks. The intent was that with the SMS/EMCD, Operating Criteria, and Electrical Schematic systems operating personnel would have all information needed to develop software flow diagrams, and code the application software. Referring to Figure 2, many other documents are needed, but the key documents are the SMS/EMCD, Operating Criteria, and Electrical Schematic. With this documentation it is also possible to provide an end-to-end system assurance analysis which will be addressed later. To implement the system design process at Kennedy, System Integration teams were formed consisting of designers, operators, safety, and reliability personnel. The teams met on a regular basis to review and assure that all necessary requirements were incorporated into the system design.

*Chief, Systems Design Branch

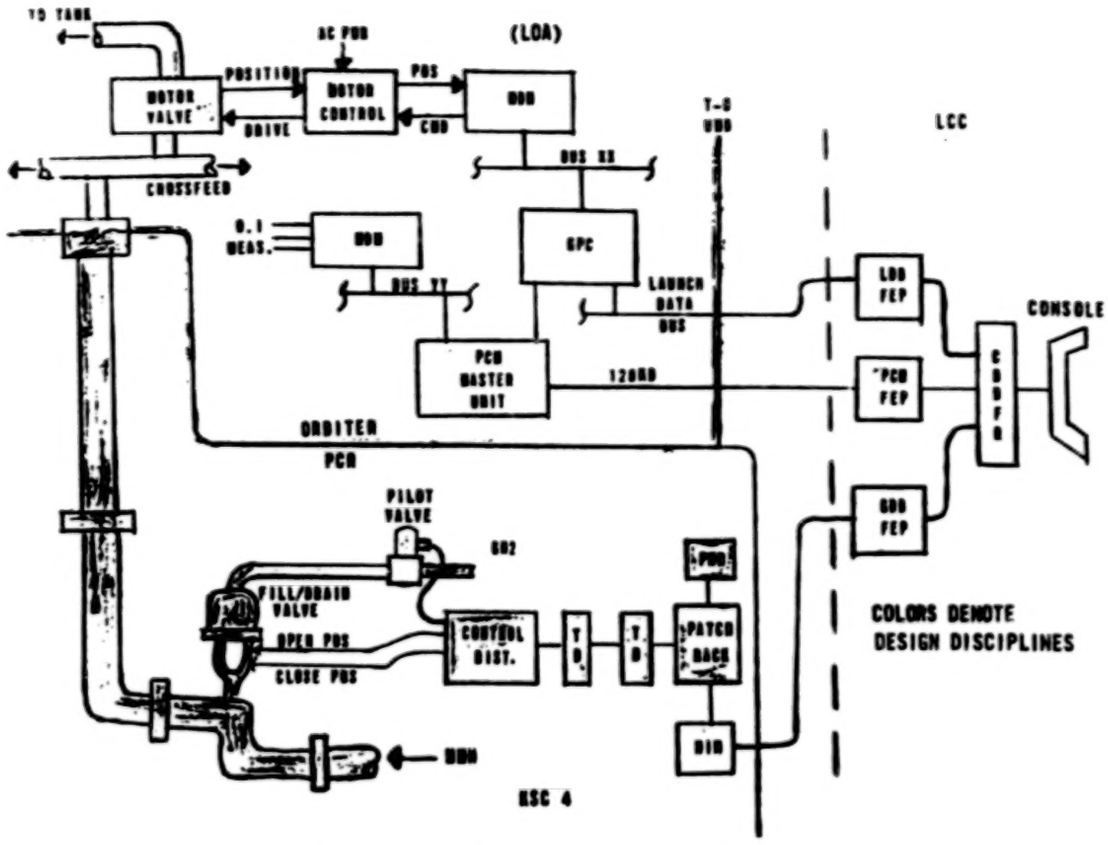


Figure 1.- Typical valve control/monitor.

SPECIAL PROBLEMS

Software would have to be analyzed to satisfy an end-to-end system assurance analysis. The amount of software and changes to software would be of such a tremendous quantity that it would be impossible to analyze the software and maintain the analysis current. To circumvent this problem, it was decided that critical interlocks would be placed in the control logic portion of the application software set (See Figure 4). By doing this, the amount of software to be analyzed would be highly restricted, making it practical to perform a software analysis. The objective achieved was to place GOAL applications programs under Operations control and Control Logic programs under Design control. Criterias were structured so that each system control logic requirement was spelled out. To analyze these hazardous situations the requirements were stated in the Operating Criteria and the implementing software was written in control logic, making it relatively easy to perform a software analysis.

Emergency Safing took on a new meaning when coupled with the new LPS. While the LPS was designed to have a standby console, it would take approximately 15 or 20 minutes to bring the redundant console on line and, if a hazardous propellant loading were in process at the time, the vehicle could be left in a hazardous condition during this transition to another console. Another example is a failure mode in the LPS common data buffer which stops processing of all LPS information. To circumvent these situations and others of this nature, an emergency hardwire safing system was implemented. This system bypasses the LPS system from a control panel located in each LPS console which is used to place the system in a safe condition until the LPS has regained control (see Figure 5). For example, in Main Propulsion Lox, if an LPS failure occurs, the integration console assumes the safing function; if the integration console has also failed, the Emergency Safing system commands the pumps to stop, opens the vehicle vent valves, and leaves the system in a safe stand by condition. Further, if the problem were of an extreme nature, the Emergency Safing system can be used to drain liquid oxygen and liquid hydrogen from the vehicle. Systems other than MPS, LOX and LH2 (such as Hypergols, Fuel Cells, etc.) fail to the Emergency Safing as back-up. Thru STS-6 there has been only one usage of the Emergency Safing System which attests to the reliability of the LPS.

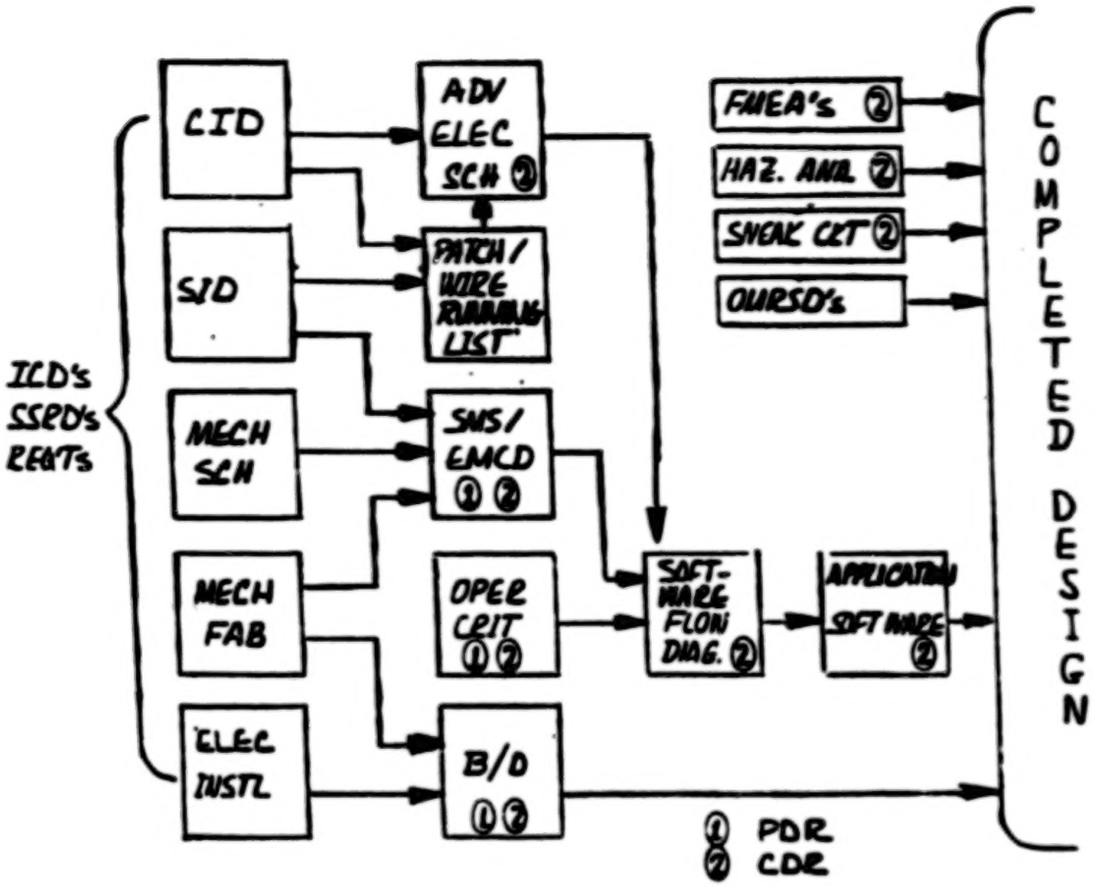


Figure 2.- DE systems design process.

Since sample rate is of prime importance for proper utilization of a computer control system, a basic requirement was levied on designers to use a sampling rate of one sample per second for all commands and monitors, and that higher sampling rates would require special approval. This did not preclude that during an operation the samping rate could be raised at the time a higher sampling rate was required. The sizing of this task is better understood by the fact that 6500 commands and monitors are used in the launch configuration.

Analysis was performed on the control Loops of a higher complexity first; and, then as time allowed, this analysis was extended to less complex situations. As a result of control loop analysis, problems were uncovered on propellant replenish and hypergol loading.

RELIABILITY ANALYSIS

Previously at KSC, reliability analysis had been performed in piece parts. There was a mechanical systems analysis for the Lox system and an electrical systems analysis for the LOX system. In addition, there was a vehicle analysis for the Lox system. These analyses were not tied together end-to-end. The SMS/EMCD was made to depict an end-to-end system with the onboard vehicle components that function as part of the GSE operations. In the KSC System Assurance Analysis four areas (see Figure 6) were analyzed to assure that the analysis was end-to-end: These areas were:

1) The KSC GSE system (electrical/mechanical/electronic).

2) The control logic software.

3) The LPS CCMS hardware and Executive software.

ORIGINAL PAGE IS
OF POOR QUALITY

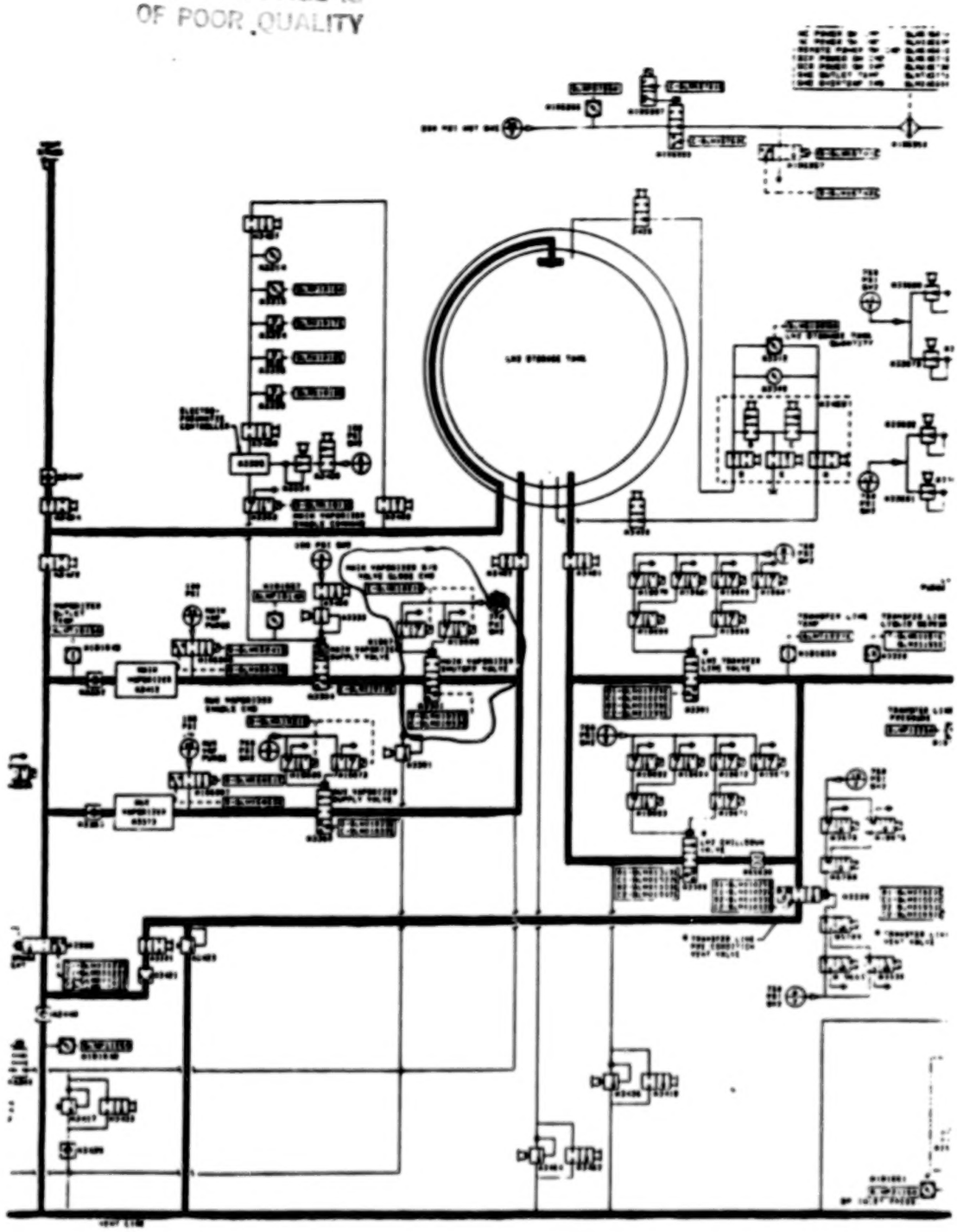


Figure 3-1

4) Other Center Analyses. A review was made of the analyses provided by other Centers of the on board vehicle components. When problems were uncovered in analyses from other Centers, these problems were presented to other Centers as "Items of Concern". Several "Items of Concern" were identified, due to the fact that other Centers used different analyses techniques, and that their analyses addressed the flight configuration instead of the ground servicing configuration. An example of one of these Items of Concern was a failure to the closed position of the LOX Inboard Fill Valve during GSE loading operations. This was not addressed in the Orbiter FMEA (Failure Mode Effect and Analysis). This failure mode was classified hazardous as a result.

ORIGINAL PAGE IS
OF POOR QUALITY

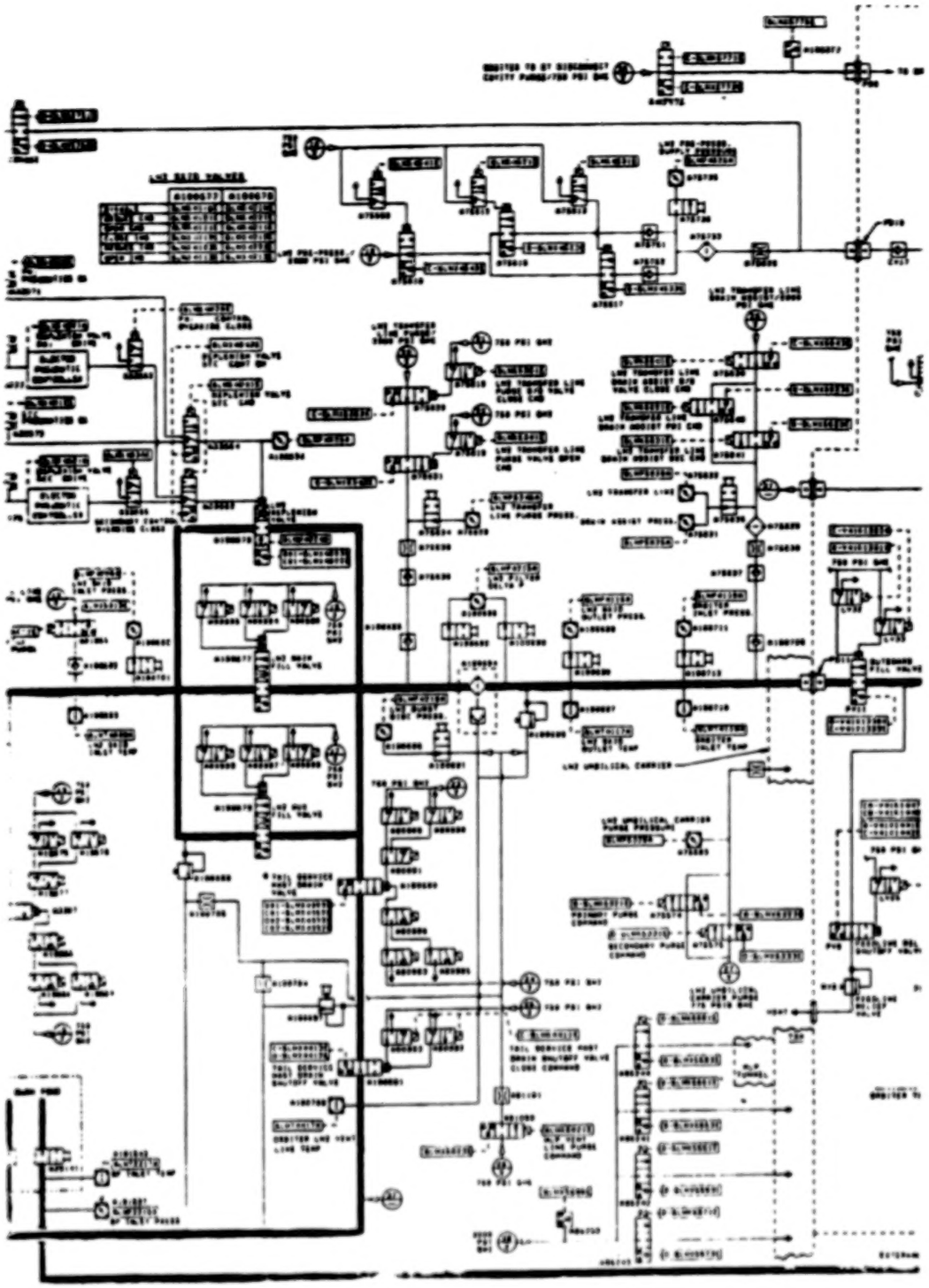


Figure 3-2

The Shuttle program offered many challenges to system designers at KSC. The implementation of the LPS for control contributed to the expansion of the system design function. The methods that have been developed as being refined and applied to such current programs as Centaur and the nuclear power control field. These methods have produced reliable systems for STS and will serve well in the operations era.

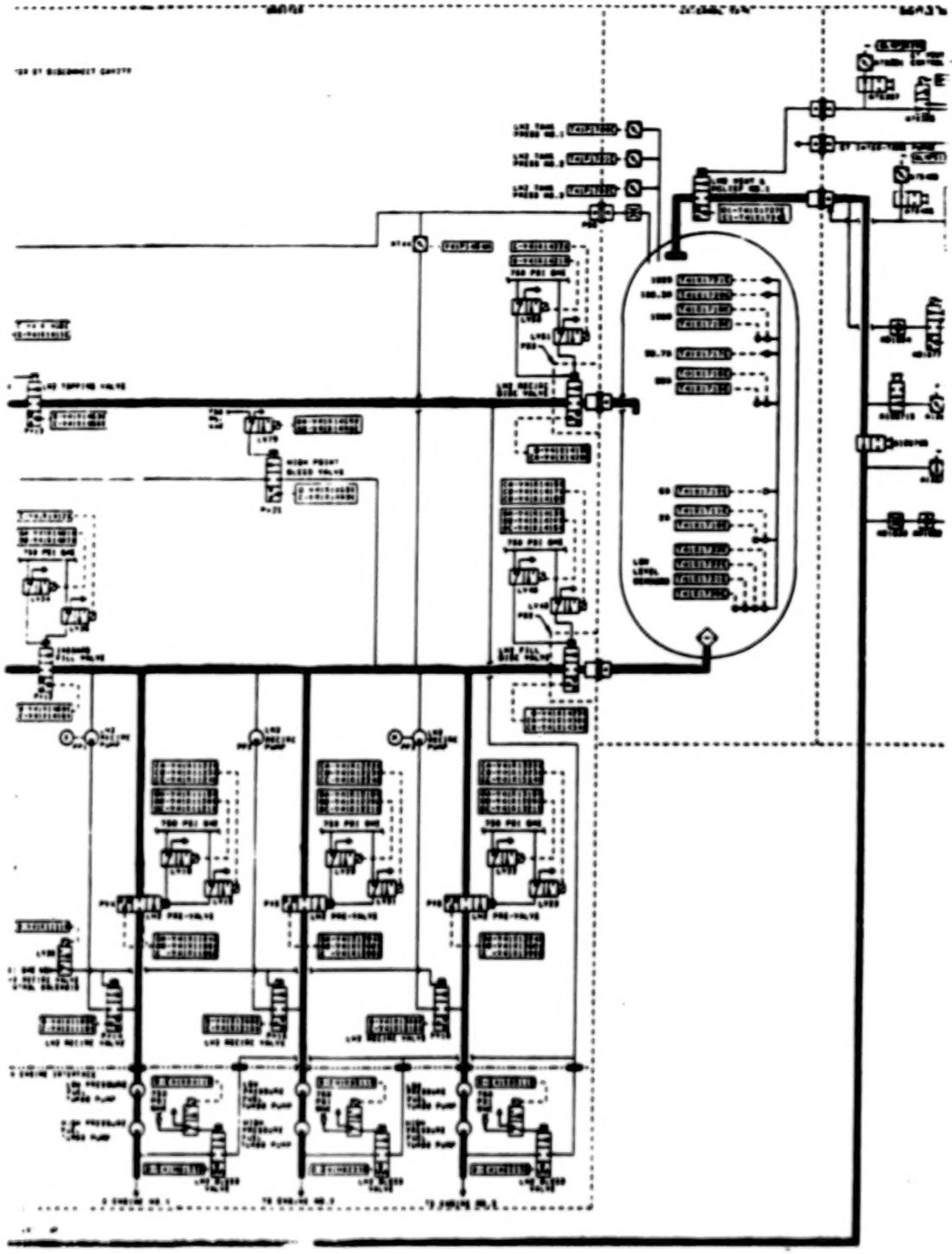


Figure 3-3

ORIGINAL PAGE IS
OF POOR QUALITY

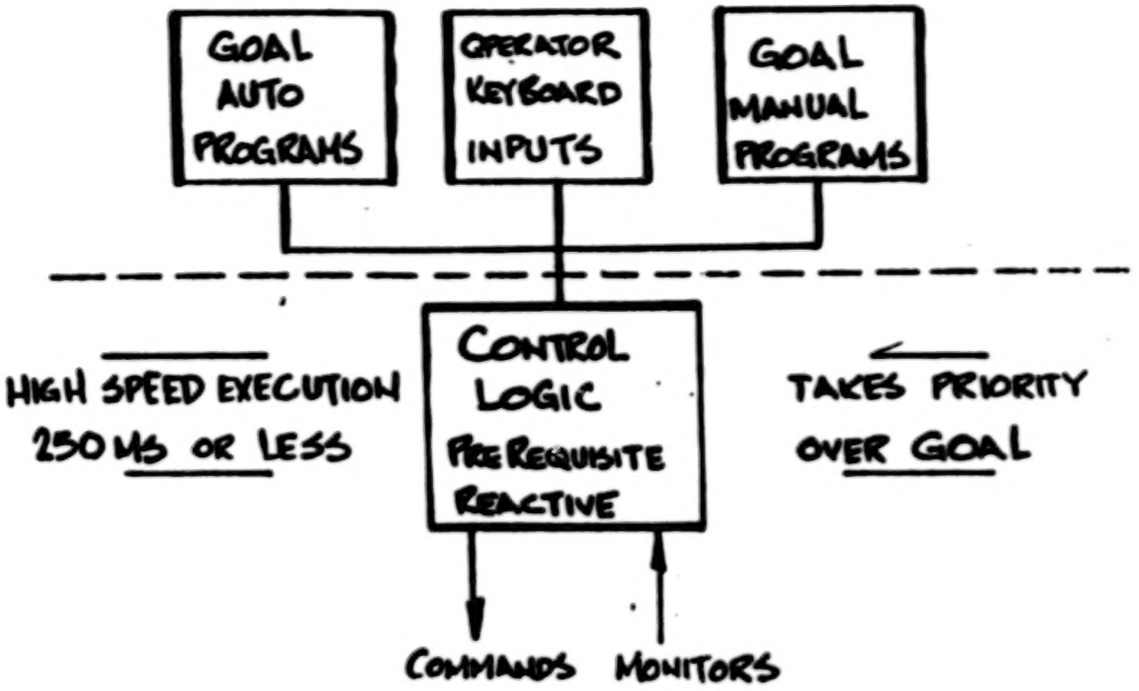


Figure 4

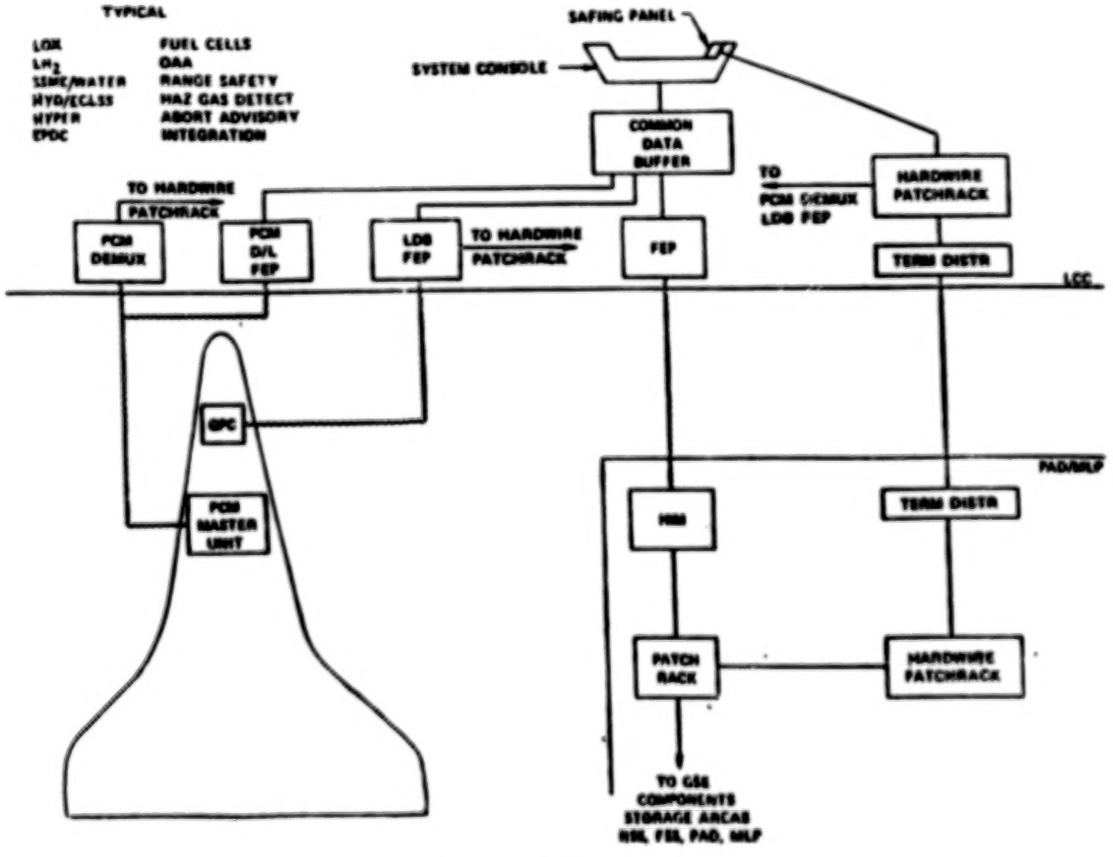
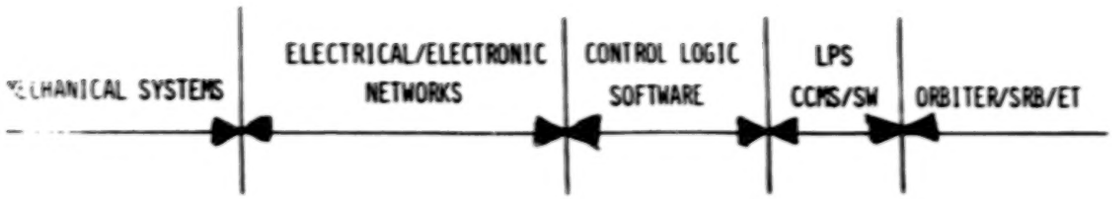


Figure 5.- Emergency safing system.



CATEGORY I HAZARDS -- LOSS OF LIFE/LOSS OF VEHICLE

CATEGORY II HAZARDS -- LOSS/DAMAGE OF VEHICLE SYSTEM

Figure 6.- Reliability analysis.

N85
16936

UNCLAS

D47

N85-16936

HISTORY, DESIGN AND PERFORMANCE OF THE SPACE SHUTTLE HAZARDOUS GAS DETECTION SYSTEM

William R. Helms
NASA, Engineering Development Directorate
John F. Kennedy Space Center, Florida 32899

ABSTRACT

Large quantities of hazardous cryogenic propellants are loaded aboard the Space Shuttle prior to launch. The Hazardous Gas Detection System is designed to detect leaks which could result in pre-launch or in-flight fires or explosions.

This paper describes the historical development, design, anJ performance of the HGDS. Data for response time, detection limits, accuracy, and drift are presented. Finally, present and future applications are discussed, and some general conclusions are drawn.

INTRODUCTION

Over 1.5 million pounds of liquid oxygen and liquid hydrogen are pumped onto the Space Shuttle during final countdown. Leaks, either during pre-flight preparations, or in-flight could result in a fire or explosion which would endanger the Space Shuttle and its crew. The Hazardous Gas Detection System (HGDS) is designed to detect the presence and measure the concentration of hazardous gases within the Space Shuttle.

The HGDS is located inside the Mobile Launch Platform and consists of three subsystems. The sample delivery subsystem draws samples from four Space Shuttle compartments surrounding propellant tanks and engines, and provides calibration gas samples. These compartments are the External Tank Intertank Area, the Orbiter Aft Fuselage, Payload Bay, and Midbody. All are purged with gaseous nitrogen during propellant loading. The mass spectrometer measures the samples from these areas qualitatively and quantitively for specific compounds. These are hydrogen, oxygen, helium, argon, and up to four others. The control and data subsystem controls the entire system, and provides operator interface for local setup via keypads and a display panel. Once this setup is complete, control is transferred to the Firing Room in the Launch Control Center. All measurement and control during propellant loading is handled through the Launch Processing System. The Firing Room console operator controls the system and warns propellant loading and test management personnel of leaks which might endanger the Shuttle or the astronauts.

HISTORY

The Hazardous Gas Detection System was first used in the early Saturn program. A need to detect leaks in the Saturn I Launch Vehicle was recognized in 1964. The first HGDS was a modified magnetic sector residual gas analyzer. It was brought from Huntsville for each launch, set up, and operated by a chemist from Marshall Space Flight Center.[1] As Figure 1 shows, it was crude, and could only measure hydrogen, but it demonstrated the potential of mass spectrometry as applied to space vehicle leak detection.

The system was gradually improved until, by the first Saturn V flight, a stable design configuration was reached. A valve manifold was added to allow sampling from four areas and from a calibration gas cylinder. Packaging was improved and a peak selector was added to allow measurement of hydrogen, oxygen, nitrogen, helium, and argon.[2] The Saturn V configuration is shown in Figure 2.

The Saturn HGDS produced reliable data throughout the program. It never failed to operate when needed; however, it required time consuming maintenance and calibration. The operator interface was anything but simple. System operation was slow, requiring eight minutes to survey the entire space vehicle. For the Space Shuttle program, a faster, more operator-friendly system was needed, while still retaining the sensitivity and flexibility of a mass spectrometer.

SHUTTLE HGDS DESIGN

A set of design goals was established to guide the development of the Shuttle HGDS.
- Fast response (2 minutes to survey the entire Shuttle)
- Accurate (+/-5% of reading)
- Automatic calibration and operation

- Flexible, to meet changing requirements
- Rugged, to meet the launch vibration environment



Fig 1.- Saturn I HGDS.

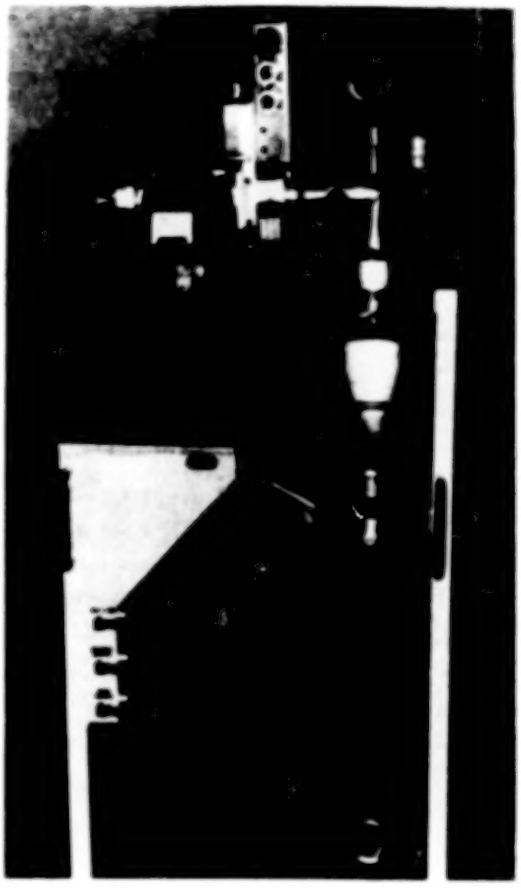


Fig 2.- Saturn V HGDS.

In order to demonstrate these concepts, a prototype system was constructed and tested by the Design Engineering Directorate at Kennedy Space Center. It was sent in 1977 to the National Space Technology Laboratories in Bay St. Louis, MI, for Main Propulsion Test Article static firings. Experience from KSC and MPTA testing was used to formulate the specifications for operational systems.

The prototype HGDS has been described by Helms and Raby.[3] The sample subsystem consists of five sample lines, each continuously pumped, plus zero and span gas. The zero gas is ultrapure nitrogen, and allows measurement and subtraction of background gases within the mass spectrometer. The span gas consists of precisely known amounts of each gas to be measured, to allow generation of calibration (sensitivity) coefficients. The mass spectrometer is a commercial quadrupole type, with automatic pumpdown, shutdown, and bakeout, and a mass range of 0-300 AMU. The digital logic controller is built of individual integrated circuit chips, some 250 in all. The operator selects up to eight gases to be measured, and up to five sample lines to be automatically scanned. The system is capable of performing an automatic self-calibration on operator command. Drift and measurement error over an eight-hour period are typically less than five percent (5%) of the reading. Correlation against simulated leaks is better than 0.99.

The operational Hazardous Gas Detection System for the Shuttle program (shown in Figure 3) was designed and built by UTI Instruments, Inc., Sunnyvale, CA. The first of four units was delivered to NASA/KSC in December, 1979. The design has been described in papers by Bunyard et. al.,[4] and Wells.[5] It consists of the same mass spectrometer used in the prototype, and a similar sampling system. These are depicted in Figure 4. However, the digital logic controller is replaced by three

ORIGINAL PAGE IS
OF POOR QUALITY

Zilog Z-80A Microprocessors. One controls the sampling system, one the mass spectrometer, and one acts as overall system controller. All programs are contained in EPROM read-only memory. Extensive health-check instrumentation is included to warn the operator of failures which might invalidate the data. This includes sample selector valve and sample transfer pump failures, analog pressure and flow measurements on both the sample subsystem and the mass spectrometer, and various fault indications on the vacuum system, mass spectrometer, and microprocessors.

The operator interface is extremely user-friendly. Guided by "prompt" messages on the local control panel, the operator enters the mass-to-charge ratio, the measurement range, and the calibration gas concentration for each gas to be measured. The system performs an automatic calibration by locating the mass peaks, and generating background (zero) and sensitivity coefficients for each gas. The operator can check or refresh the calibration at any time.

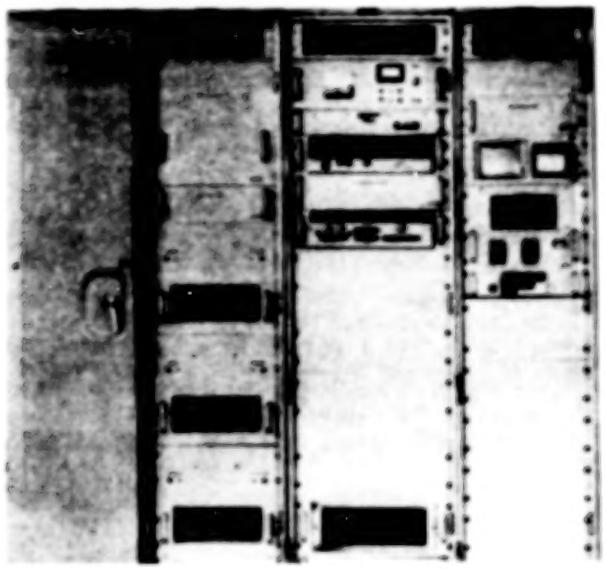


Figure 3.- Space Shuttle HGDS.

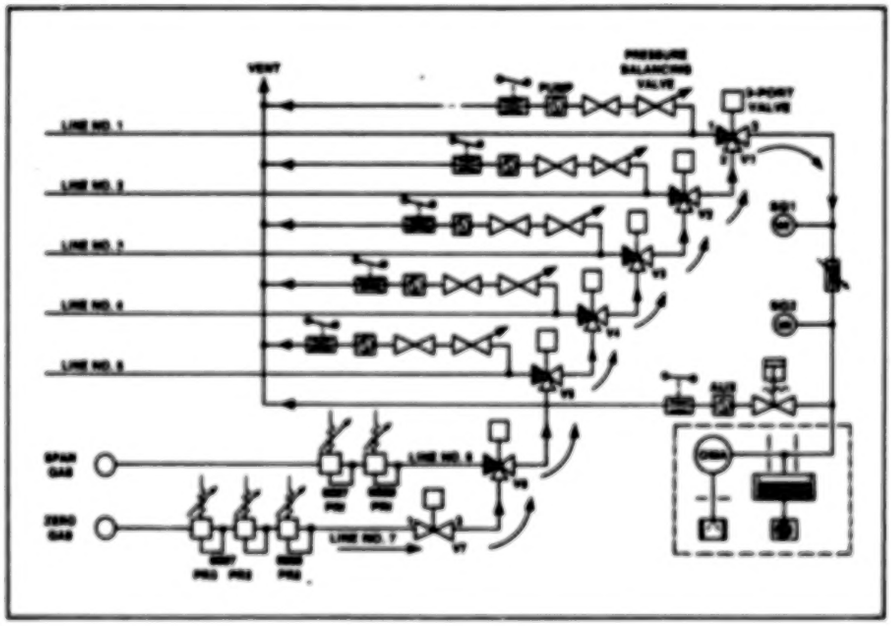


Figure 4.- HGDS schematic.

HGDS PERFORMANCE

Among the most important measures of performance for any analytical instrument are speed of response, detection limit, accuracy, and stability. The HGDS has, in general, met or exceeded its performance design criteria. Initial acceptance tests and periodic performance tests are run to assure optimum performance of the system.

RESPONSE TIME

THE HGDS draws samples from the 200 foot Orbiter sample line in less than twelve seconds, and from the 400 foot External Tank Intertank Area sample line in less than twenty seconds. The design goal was 30 seconds or less. Response at the instrument is virtually instantaneous. The system responds to 50% of a change in concentration in one second, and 90% of a change in two seconds. The HGDS samples up to eight different gases, one each second. In addition, there is a one-time 20 second delay prior to analysis each time a new sample line is selected, to assure adequate purge of the previous sample. With the 20 second delay plus 8 seconds of measurement time for each of four lines, the HGDS can sample all four areas of the Shuttle in 1 minute, 52 seconds, well within the design goal of 2 minutes. Considering a maximum sample transport time of 20 seconds, plus up to eight seconds to analyze all gases, changes in concentration for any one area on the Shuttle can be sampled, analyzed, and reported in 30 seconds or less.

DETECTION LIMITS AND ACCURACY

Detection limits are primarily a function of the precision (repeatability) of a measurement system. A detailed study of both the accuracy and precision of the HGDS was undertaken. Data for hydrogen and oxygen are shown in Table 1 and 2, and in graphical form in Figures 5 and 6. Similar studies, albeit less detailed, were conducted for helium and argon with similar results. From these data, it can be conservatively stated that the HGDS accuracy is +/-5% of the reading or +/-20 ppm, whichever error is greater. Furthermore, using twice the standard deviation as a criterion, the detection limit for hydrogen is 40 ppm, and for oxygen, helium, and argon, less than 10 ppm.

TABLE 1. HGDS ACCURACY AND PRECISION FOR HYDROGEN

Theoretical Concentration	HGDS Reading (Average)	Error (Average)	Standard Deviation	Number of Samples
4040 ppm H_2	3971 ppm	-69 ppm	29 ppm	6
1060 ppm H_2	1037 ppm	-23 ppm	25 ppm	8
491 ppm H_2	511 ppm	+20 ppm	22 ppm	25
250 ppm H_2	258 ppm	+8 ppm	13 ppm	25
100 ppm H_2	96 ppm	-4 ppm	23 ppm	25
50 ppm H_2	55 ppm	+5 ppm	22 ppm	25
24 ppm H_2	27 ppm	+3 ppm	11 ppm	25

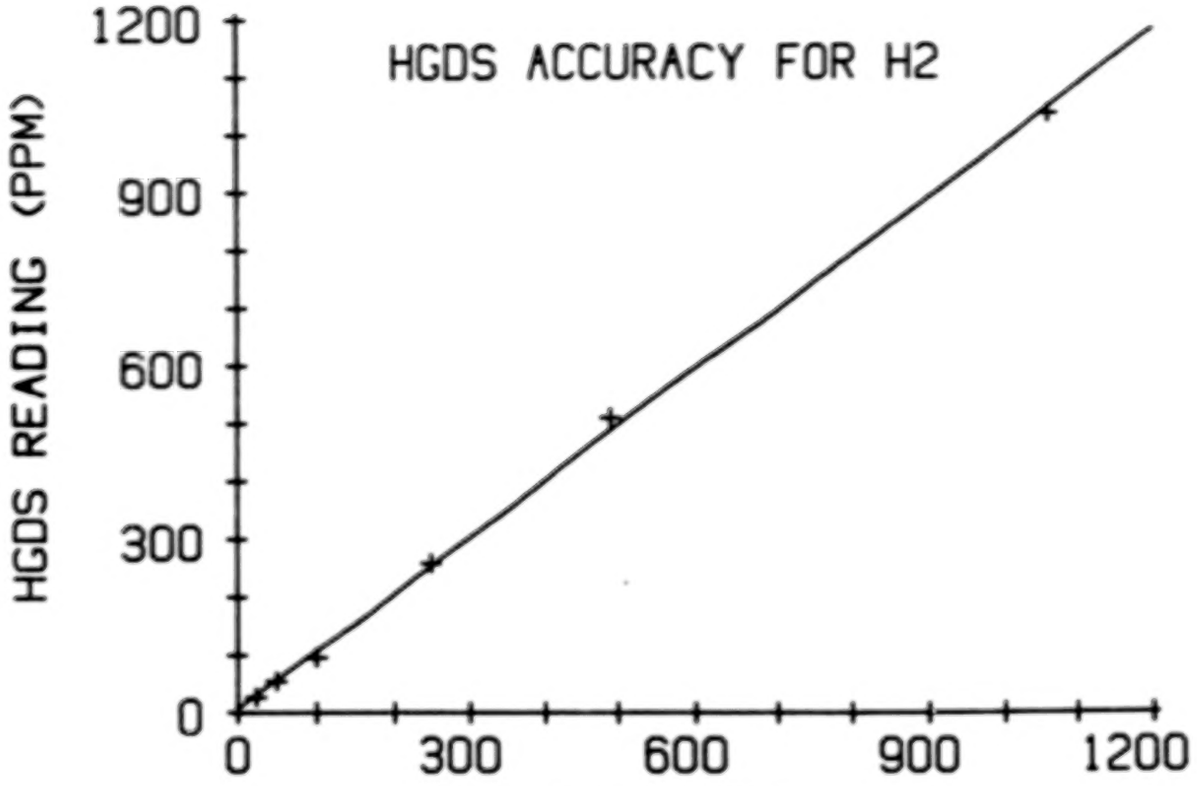


Figure 5.- Input H_2 conc. (PPM).

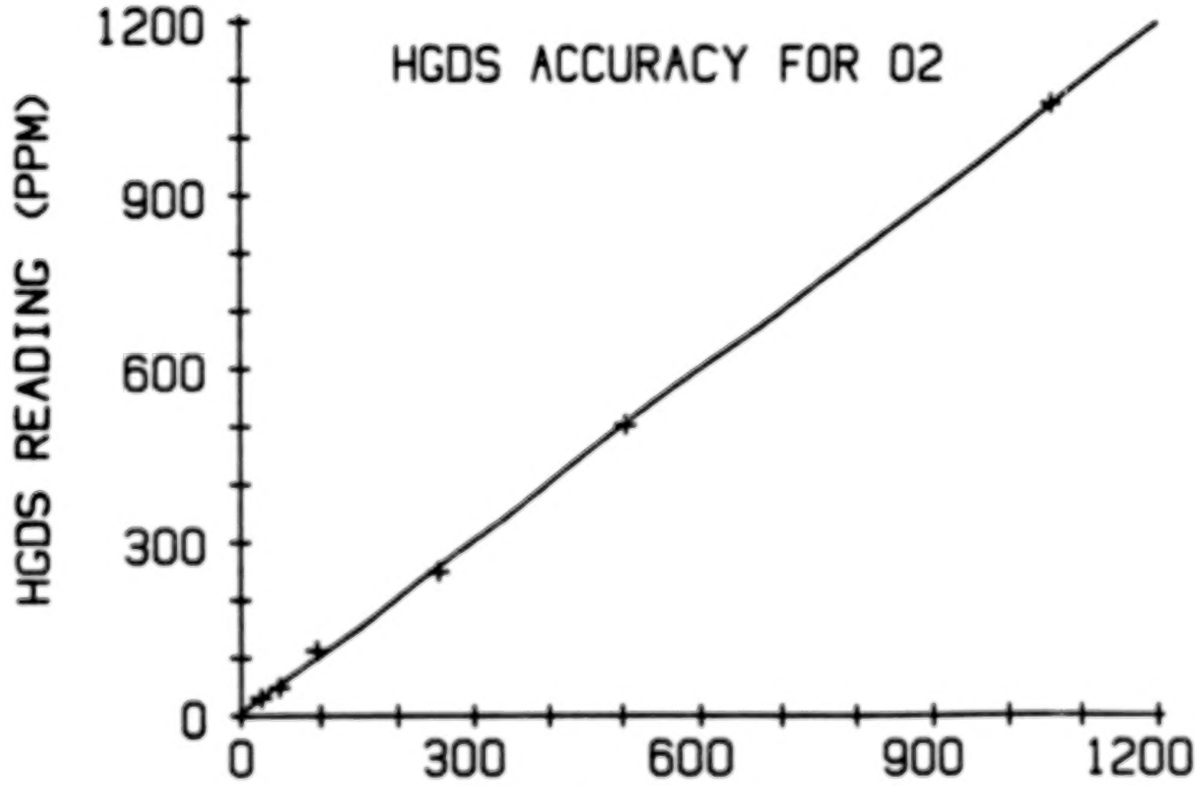


Figure 6.- Input O_2 conc. (PPM).

TABLE 2. HGDS ACCURACY AND PRECISION FOR OXYGEN

Theoretical Concentration	HGDS Reading (Average)	Error (Average)	Standard Deviation	Number of Samples
364Ø ppm O_2	3696 ppm	+56 ppm	13 ppm	6
1Ø6Ø ppm O_2	1Ø56 ppm	-4 ppm	23 ppm	8
5Ø5 ppm O_2	5Ø2 ppm	-3 ppm	8 ppm	16
255 ppm O_2	249 ppm	-6 ppm	9 ppm	19
96 ppm O_2	113 ppm	+17 ppm	3 ppm	19
49 ppm O_2	49 ppm	Ø ppm	2 ppm	16
26 ppm O_2	31 ppm	+5 ppm	3 ppm	2Ø

DRIFT

The HGDS was operated without operator intervention for 12 hours. Data was read hourly. The system alternately sampled a test gas cylinder and a zero gas (pure GN_2) cylinder. Worst case peak to peak drift for any one-hour period, and for the entire test, are reported in Table 3, and shown in Figure 7.

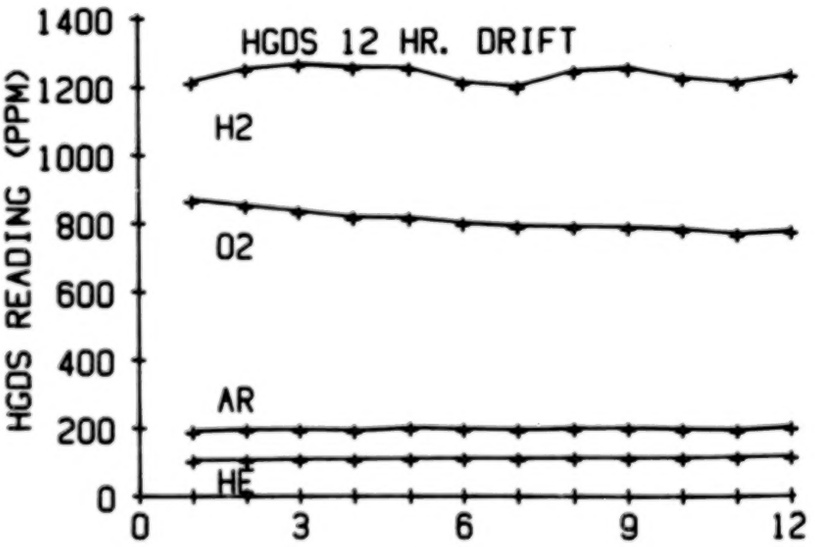


Figure 7.- Time (hours).

TABLE 3.

Gas	Test Gas Concentration	1-Hour Drift	12-Hour Drift
H_2	1Ø6Ø ppm	44 ppm	66 ppm
He	1Ø5 ppm	2 ppm	1Ø ppm
O_2	1Ø6Ø ppm	17 ppm	95 ppm
Ar	196 ppm	7 ppm	1Ø ppm

DESIGN IMPROVEMENTS

Like many computer-based systems, the HGDS has suffered from AC power line noise. Due to excessive noise on the Mobile Launcher Uninterruptible Power System (UPS), the HGDS was placed on a dedicated mini-UPS, which solved the power related problems.

The HGDS uses an ion pump to achieve the requisite vacuum of one-billionth of an atmosphere. This type of pump is susceptible to eventual hydrogen saturation and subsequent spontaneous, periodic elution, called "burping". This causes a degradation of measurement precision. The only solution is replacement of the ion pump. A recent modification has made this a simple, risk-free, one-hour procedure.

Several minor microprocessor firmware "bugs" have been identified and corrections are in work. Component faiures have been within acceptable limits.

APPLICATIONS

The HGDS is used to make critical go - no go decisions during the Space Shuttle countdown. The Launch Commit Criteria Document specifies the maximum allowable limits. A concentration of 8ØØ parts per million of hydrogen or oxygen is considered unacceptable for flight. Leakage of this magnitude at preflight propellant pressures could indicate a leak which would create flammable conditions when the propellants are at the much higher flight pressures. A concentration of 1Ø,ØØØ parts per million of hydrogen or oxygen (25% of the lower flammable limit) is considered an immediate on-pad hazard.

The most notable success of the HGDS was the detection of hydrogen leaks on two of Challenger's main engines during the STS-Flight Readiness Firings, as shown in Figure 8. In the ensuing investigation, incipient leaks were found in the third Challenger engine, and in a spare engine. All three engines were ultimately removed and repaired, thus avoiding a potential catastrophe.

As a result of lessons learned during the STS-6 hydrogen leak investigation, the accuracy and sensitivity of the HGDS is now used to perform an in-place end-to-end helium leak check on the entire Orbiter Main Propulsion/Engines system. In addition, the HGDS will be used to leak check the ground-to-Orbiter hydrogen and oxygen umbilical disconnects. It replaces a laboratory gas chromatograph and operator which were previously flown in from California before each launch to perform the leak check.

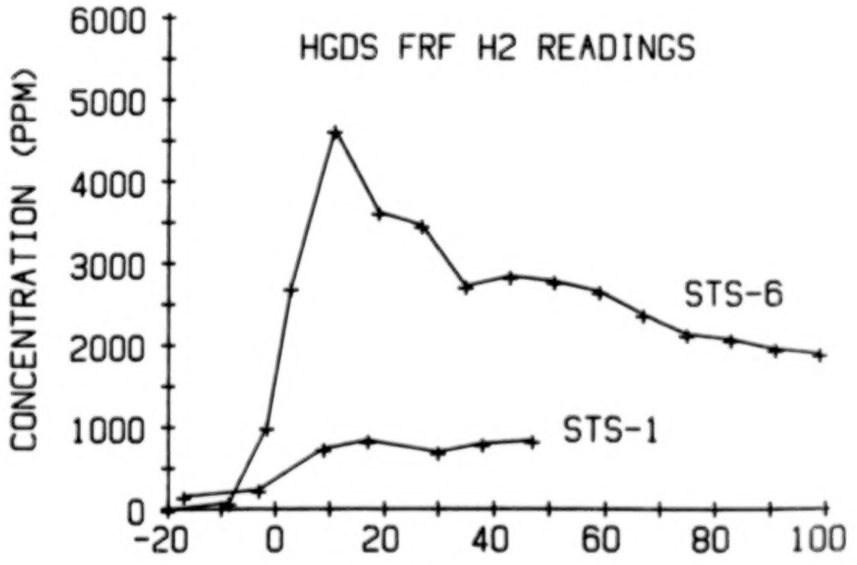


Figure 8 T-time (seconds).

CONCLUSIONS

The HGDS is an accurate, stable, and sensitive analytical instrument. It can make reliable measurements of a variety of gases at a few parts per million. Launch vibration has caused only one minor failure in six launches. Calibration can be verified and refreshed in real time, thus allowing high confidence to be placed in the data. It has demonstrated its importance to the Space Shuttle program by detecting leaks which, if uncorrected, could have caused a catastrophe. With the advent of cryogenic payloads such as Centaur within the Space Shuttle Payload Bay, that importance can only increase.

REFERENCES

1. Perry, C. L., Personal Communication

2. Perry, C. L., Krupnick, A. C., and Harwell, R. J.: Design and Development of the Hazardous Gas Detection System for Launch Vehicle Propellant Loading and Checkout. NASA TM X-53720, 1968.

3. Helms, William R. and Raby, Bruce A., "a Prototype Hazardous Gas Detection System for NASA's Space Shuttle", 26th Annual Conference of American Society for Mass Spectrometry, St. Louis, MO, May, 1978.

4. Bunyard, G. B., Wells, P., Jewhurst, F., and Raby, B. A., "Hazardous Gas Detection System for Space Shuttle", Instrument Society of America National Conference, Chicago, IL, 1979.

REFERENCES (CONT)

5. Wells, P., "A Microprocessor-Controlled Hazardous Gas Monitor", UTI Journal, Vol, 3, No. 2, 1980.

INDEX

Abner, Charles A., 81
Anderson, Judith A., 97
Arrington, James P., 209
Austin, L. D., 177

Bacchus, D. L., 189
Bachtel, Frederick D., 1041
Bailey, William W., 532
Batson, Bartus H., 767
Binkley, William H., 972
Blackmon, F. Herb, 76
Blevins, Donald R., 656
Boggs, Clifton R., 910
Boykin, Jack C., 1
Boyle, W. W., 151
Braun, Walter R., 798, 804
Bromley, Linda K., 831
Burghduff, Richard D., 47

Campbell, Carlisle C., Jr., 850
Carpenter, J. E., 498
Carsley, Renton B., 872
Cassisi, Vincent, 961
Chase, Charles A., 628
Chevers, Edward S., 30
Coldwater, Harold R., 357
Cole, Timothy W., 585
Cooke, Douglas R., 264
Craig, M. K., 151
Crump, John M., 920
Curry, Donald M., 1062

Davis, Richard M., 986
Decrisantis, Angelo, 414
Dessouky, Khaled, 815
Dill, Charlie C., 151
Doetsch, K. H., 892
Donahue, Michael E., 952
Dotts, Robert L., 1062
Dutton, Jon A., 357

Edson, William F., Jr., 525
Eggers, D. S., 720
Ehlers, H. K. F., 1082

Felder, G. L., 857
Ferguson, Robert M., 565
Fisher, Robert R., 1030
Foll, Richard R., 357
Foster, Lee D., 1022
Fouts, W. B., 64

Gaines, L. M., 177
Gamble, Joe D., 209, 264
Gatto, Ralph E., 335
Gibb, John W., 414, 465
Gibson, Cecil R., 639
Gilbert, David W., 137
Glassburn, Charles W., 942
Glynn, Philip C., 345
Godfrey, Robert D., 787
Gray, Carroll, 1041
Greenwood, Terry F., 1022
Griffin, J. W., 757

Hamilton, J. T., 151, 177
Hampton, P. W., 54
Haratunian, Michael, 935
Hardee, J. H., 883
Heinrich, Steven R., 465
Helms, William R., 573
Henderson, John, 656
Henderson, O. L., 19
Hendrickson, Kenneth O., 97
Herr, Denver W., 821
Hillje, Ernest R., 209, 313
Hohmann, Carl, 656
Homan, David, 295
Hondros, J. G., 177
Hooks, Ivy, 295
Howell, Gayle J., 357
Howell, H. R., 480
Hughes, Robert W., 690
Humphrey, Terry D., 35
Humphries, Clarence, 639
Huth, G. K., 757

Jacobs, Steve, 1082
Jamieson, John R., Jr., 585
Joosten, B. Kent, 113

Karakulko, W., 656
Kelley, J. S., 757
Kilminster, Joe C., 618
Koch, John C., 986

Koszenski, E. P., 465
Kross, D. A., 189

Lak, Tibor I., 585
Lance, Renee, 673
Lee, Dorothy B., 1022
Leger, L. J., 1082
Lenett, S. D., 720
Lewis, James L., Jr., 47
Lewton, W. A., 720
Lindsey, William C., 810

Mackey, Alden C., 335
McBarron, James W., II, 435
McCarty, John P., 600
McIntosh, M. E., 465
McKenzie, Teresa M., 798, 804
McMann, Harold J., 435
Mangialardi, J. K., 465
Mesmer, J., 64
Miller, Arthur J., 972
Miller, E., 1082
Miller, Glenn J., 403
Miller, John Q., 618
Mitchell, Walter T., 38
Modest, M. F., 480
Modlin, C. Thomas, Jr., 325
Moog, R. D., 189
Moser, Thomas L., 345
Munafo, Paul M., 386
Muratore, John F., 87
Murray, R. W., 465
Murray, S. V., 125

Naber, Ruth A., 905
Nason, John R., 450
Novosad, S. W., 720

Olsen, Deloy C., 209
Ord, George R., 414
Oren, J. A., 480

Patterson, William J., 1030
Pawlowski, J. F., 720, 767
Plowden, John B., 558
Porter, J. A., 720
Powers, Bruce G., 143
Price, Charles R., 35
Prince, R. Norman, 414

Rasmussen, Anker M., 505
Reichle, Garland E., 942
Ried, Robert C., 1051
Riles, Warren L., 510
Ripley, John G., 861
Roberts, B. B., 151, 209
Romere, Paul O., 209, 295
Rudolph, James W., 539
Runkle, Roy E., 365
Ryan, Robert S., 386

Salter, Larry D., 386
Scallion, William I., 209
Schelkopf, J. D., 465
Schiesser, Emil R., 102
Schlosser, Donald C., 264
Schmidt, Oron L., 767
Schneider, Henry E., 1
Schneider, William C., 403
Schubert, Franz, 465
Schwartz, John J., 777, 821
Schwartz, Richard, 490
Searle, Richard F., 38
Seibert, W. W., 720
Seyl, J. W., 720
Simon, William E., 702
Smith, Gerald W., 628
Smith, H. E., 64
Spearing, Robert, 777
Spencer, Bernard, Jr., 209
Steele, Mike, 465
Steiner, A. W., 757
Stoker, C. Jack, 831
Stone, Howard W., Jr., 264
Stuckey, James M., 1041
Surber, T. E., 177
Swider, Joe, 414

Taeuber, Ralph J., 656
Tatem, Bemis C., Jr., 961
Taylor, J. Thomas, 995
Teasdale, William E., 767
Thibodaux, Joseph G., Jr., 581
Thibodeau, Joseph R., 1
Thomas, Emory, 465
Tillian, Donald J., 1062
Tory, Edward G., 550
Townsend, Don H., 81

Underwood, Jimmy M., 209, 264
Ussher, T. H., 892

Vang, H. A., 720, 757
Vaniman, Jerold L., 1030, 1041
Vick, H. G., 54

Wallace, R. O., 177
Walleshauser, James J., 414
Walvis, Dirk J. M., 821
Ware, George M., 209
Weary, Dwayne P., 673
Weinberg, Aaron, 777, 821
Whitcomb, Kathy K., 87
Whitnah, Arthur M., 209
Widofsky, Bernard, 1041
Wierum, Frederic A., 450
Williams, J. L., 480
Wojnarowski, John, 414
Wood, Byron K., 600
Woodis, William R., 365
Woolford, Barbara, 426
Worlund, Armis L., 585
Wynveen, R. A., 465

Yanosy, James L., 450
Young, George M., III, 386
Young, J. C., 151, 209

Zrubek, W. E., 757
Zupp, George A., Jr., 325

END

DATE

FILMED

APR 2 1985